SANDIA REPORT

SAND2010-6109—Revised
Unlimited Release
Printed September 2010—Reprinted December 2010

PAT-1 Safety Analysis Report Addendum

Docket No. 71-0361

Revision 1, Final, December 2010

Prepared by:
Sandia National Laboratories
Albuquerque, New Mexico 87185

Sandia National Laboratories is a multi-program laboratory managed and operated by Sandia Corporation, a wholly owned subsidiary of Lockheed Martin Corporation, for the U.S. Department of Energy's National Nuclear Security Administration under contract DE-AC04-94AL85000.

Approved for public release; further dissemination unlimited.

Issued by Sandia National Laboratories, operated for the United States Department of Energy by Sandia Corporation.

NOTICE: This report was prepared as an account of work sponsored by an agency of the United States Government. Neither the United States Government, nor any agency thereof, nor any of their employees, nor any of their contractors, subcontractors, or their employees, make any warranty, express or implied, or assume any legal liability or responsibility for the accuracy, completeness, or usefulness of any information, apparatus, product, or process disclosed, or represent that its use would not infringe privately owned rights. Reference herein to any specific commercial product, process, or service by trade name, trademark, manufacturer, or otherwise, does not necessarily constitute or imply its endorsement, recommendation, or favoring by the United States Government, any agency thereof, or any of their contractors or subcontractors. The views and opinions expressed herein do not necessarily state or reflect those of the United States Government, any agency thereof, or any of their contractors.

Printed in the United States of America. This report has been reproduced directly from the best available copy.

Available to DOE and DOE contractors from
U.S. Department of Energy
Office of Scientific and Technical Information
P.O. Box 62
Oak Ridge, TN 37831

Telephone: (865) 576-8401
Facsimile: (865) 576-5728
E-Mail: reports@adonis.osti.gov
Online ordering: http://www.osti.gov/bridge

Available to the public from
U.S. Department of Commerce
National Technical Information Service
5285 Port Royal Rd.
Springfield, VA 22161

Telephone: (800) 553-6847
Facsimile: (703) 605-6900
E-Mail: orders@ntis.fedworld.gov
Online order: http://www.ntis.gov/help/ordermethods.asp?loc=7-4-0#online

DISTRIBUTION		
1	NRC Document Control/ Max Barela	U.S Nuclear Regulatory Commission Washington, DC 20555-0001
1 and 1 (electronic copy)	NNSA/Max Barela	NRC Review Team NZ/Building 382-1 P.O. Box 5400 Albuquerque, NM 87185-5400
2 and 1 (electronic copy)	NNSA/PCD	NZ/Building 382-1 P. O. Box 5400 Albuquerque, NM 87185-5400
1 and 1 (electronic copy)	NNSA/Paul Mann	NA-172.1/Building 382-3 P.O. Box 5400 Albuquerque, NM 87185-5400
2 and 1 (electronic copy)	Energy Solutions/Scott Shiraga	2345 Stevens Dr Suite 240 Richland, WA 99354
2 and 2 (electronic copies)	Michael L. Caviness	LANL NPI-1, Technical Area 55, Building 313, MS E513 Los Alamos, NM 87545
1 and 1 (electronic copy)	MS0718	David Miller
10 and 10 (electronic copies)	MS0718	Richard Yoshimura
1 (electronic copy)	MS0899	Technical Library

Sandia National Laboratories

SAND2010-6109—Revised
Unlimited Release
Printed September 2010—Reprinted December 2010

PAT-1 Safety Analysis Report Addendum

Docket No. 71-0361

Revision 1, Final, December 2010

P.O. Box 5800
Sandia National Laboratories
Albuquerque, NM 87185

Author: Richard H. Yoshimura, David C. Harding, Lili A. Akin, Robert J. Kalan, Carlos Lopez, Perry L. Jones, David R. Miller, David T. Schmale, Gerald A. Knorovsky, Charles W. Morrow, and Ruth F. Weiner

Contributors:
Don Mueller (ORNL), Bryan Broadhead (ORNL), Richard E. Mason (LANL), Stephen P. Willson, LANL), Jim Rubin (LANL), Michael L. Caviness (LANL), and Monty L. Goins (Y-12)

Abstract

The Plutonium Air Transportable Package, Model PAT-1, is certified under Title 10, Code of Federal Regulations Part 71 by the U.S. Nuclear Regulatory Commission (NRC) per Certificate of Compliance (CoC) USA/0361B(U)F-96 (currently Revision 9). The purpose of this SAR Addendum is to incorporate plutonium (Pu) metal as a new payload for the PAT-1 package. The Pu metal is packed in an inner container (designated the T-Ampoule) that replaces the PC-1 inner container. The documentation and results from analysis contained in this addendum demonstrate that the replacement of the PC-1 and associated packaging material with the T-Ampoule and associated packaging with the addition of the plutonium metal content are not significant with respect to the design, operating characteristics, or safe performance of the containment system and prevention of criticality when the package is subjected to the tests specified in 10 CFR 71.71, 71.73 and 71.74.

This page intentionally left blank

TABLE OF CONTENTS

1. GENERAL INFORMATION 1-1
1.1 Introduction 1-1
1.2 Package Description 1-2
1.2.1 Packaging 1-2
1.2.2 Contents 1-5
1.2.3 Special Requirements for Pu 1-15
1.2.4 Operational Features 1-15
1.3 Appendix 1-16
1.3.1 References 1-16
1.3.2 Drawings 1-16
1.3.3 Specifications 1-43
1.3.4 Justification for Exclusion of the TB-1 Elastomer O-ring for Plutonium Metal Shipments 1-43
1.3.5 PAT-1040 Titanium and O-Ring Materials and Component Fabrication Specification 1-44

2. STRUCTURAL EVALUATION 2-1
2.1 Description of Structural Design 2-1
2.1.1 Discussion 2-3
2.1.2 Design Criteria 2-4
2.1.3 Weights and Centers of Gravity 2-10
2.1.4 Identification of Codes and Standards for the Package Design 2-11
2.2 Materials 2-12
2.2.1 Material Properties and Specifications 2-12
2.2.2 Chemical, Galvanic, or Other Reactions 2-12
2.2.3 Effects of Radiation on Materials 2-13
2.3 Fabrication and Examination 2-23
2.3.1 Fabrication 2-23
2.3.2 Examination 2-23
2.4 General Requirements for All Packages 2-23
2.4.1 Minimum Package Size 2-23
2.4.2 Tamper-Indicating Device 2-23
2.4.3 Positive Closure 2-24
2.5 Lifting and Tie-Down Standards for All Packages 2-24
2.5.1 Lifting Devices 2-24
2.5.2 Tie-Down Devices 2-24
2.6 Normal Conditions of Transport 2-24
2.6.1 Heat 2-24
2.6.2 Cold 2-26
2.6.3 Reduced External Pressure 2-26
2.6.4 Increased External Pressure 2-26
2.6.5 Vibration 2-26
2.6.6 Water Spray 2-27
2.6.7 Free Drop 2-27

2.6.8 Corner Drop 2-27
2.6.9 Compression 2-27
2.6.10 Penetration 2-27
2.7 Hypothetical Accident Conditions 2-27
2.7.1 Free Drop 2-28
2.7.2 Crush 2-29
2.7.3 Puncture 2-29
2.7.4 Thermal 2-29
2.7.5 Immersion – Fissile Material 2-30
2.7.6 Immersion – All Packages 2-30
2.7.7 Deep Water Immersion Test (for Type B Packages Containing More than 105 A2) 2-30
2.7.8 Summary of Damage 2-30
2.8 Accident Conditions for Air Transport of Plutonium 2-31
2.8.1 Discussion 2-31
2.8.2 Full Package Validation Model 2-33
2.8.3 Impact Test and Material Failure 2-33
2.8.4 NCT, HAC, and High Velocity Impact Analyses 2-34
2.8.5 Bolt Analysis 2-41
2.8.6 Summary 2-42
2.9 Accident Conditions for Fissile Material Packages for Air Transport 2-43
2.10 Special Form 2-43
2.11 Fuel Rods 2-43
2.12 Appendix 2-43
2.12.1 References 2-43
2.12.2 Full Model Validation Analyses 2-45
2.12.3 Impact Test and Material Failure Criterion 2-61
2.12.4 Material Data 2-90
2.12.5 Component Analyses Using Complete Model 2-105
2.12.6 Bolt Analysis 2-368
2.12.7 Sample Input 2-369
2.12.8 Design Pressure Calculations for the T-Ampoule (in Accordance with Section VIII Division 1 of the ASME Boiler and Pressure Vessel Code 2-389

3. THERMAL EVALUATION 3-1
3.1 Description of Thermal Design 3-1
3.1.1 Design Features 3-2
3.1.2 Decay Heat of the Contents 3-2
3.1.3 Summary Tables of Temperatures 3-4
3.1.4 Summary Table of Maximum Pressures 3-4
3.2 Material Properties and Component Specifications 3-5
3.2.1 Material Properties 3-5
3.2.2 Component Specifications 3-6
3.3 Thermal Evaluation under NCT 3-7
3.3.1 Heat and Cold 3-10
3.3.2 Maximum Normal Operating Pressure 3-15

3.4 Thermal Evaluation under HAC 3-16
3.4.1 Initial Conditions 3-21
3.4.2 Hypothetical Accident Conditions (HAC) 3-21
3.4.3 Maximum Temperatures and Pressure 3-25
3.4.4 Maximum Thermal Stresses 3-27
3.4.5 Hypothetical Accident Conditions for Fissile Material Packages for Air Transport 3-28
3.5 Appendix 3-30
3.5.1 References 3-30
3.5.2 Viton® O-Ring Technical Information 3-31
3.5.3 Eutectic Analysis of Ti-6Al-4V with Plutonium and Copper 3-47
3.5.4 Determination of Most Damaging Package Orientation for HAC Analysis 3-63

4. CONTAINMENT 4-1
4.1 Description of the Containment System 4-2
4.1.1 Special Requirements for Plutonium 4-6
4.1.2 Plutonium Metal Contents 4-8
4.2 Containment under Normal Conditions of Transport (NCT) 4-11
4.3 Containment under Hypothetical Accident Conditions (HAC) 4-12
4.3.1 Containment under Plutonium Air Transport Fire Test 4-12
4.4 Leakage Rate Tests for Type B Packages 4-13
4.5 Appendix 4-13
4.5.1 References 4-13
4.5.2 PAT-1 Contents 4-14
4.5.3 Helium Generation 4-21
4.5.4 O-Ring Decomposition 4-28
4.5.5 Determination of A2 for the PAT 1 Package with Plutonium Contents 4-39
4.5.6 Calculation of the PAT-1 Containment Vessel's Regulatory Reference Air Leakage Rates 4-44
4.5.7 References for Sections 4.5.5 and 4.5.6 4-61

5. SHIELDING EVALUATION 5-1
5.1 Description of Shielding Design 5-1
5.1.1 Design Features 5-1
5.1.2 Summary Table of Maximum Radiation Levels 5-2
5.2 Source Specification 5-2
5.2.1 Gamma Source 5-3
5.2.2 Neutron Source 5-3
5.3 Shielding Model 5-4
5.3.1 Configuration of Source and Shielding 5-4
5.3.2 Material Properties 5-6
5.4 Shielding Evaluation 5-7
5.4.1 Methods 5-7
5.4.2 Input and Output Data 5-10
5.4.3 Flux-to-Dose-Rate Conversion 5-11
5.4.4 External Radiation Levels 5-11

5.5 Appendix 5-15
5.5.1 References 5-15
5.5.2 Summary of Source Bounding Analyses 5-15
5.5.3 Analysis of Pu/Be Source Contents 5-19
5.5.4 List of Various Code Inputs 5-24

6. CRITICALITY EVALUATION 6-1
6.1 Description of Criticality Design 6-1
6.1.1 Design Features 6-1
6.1.2 Summary Table of Criticality Evaluation 6-2
6.1.3 Criticality Safety Index 6-2
6.2 Fissile Material Contents 6-3
6.2.1 Plutonium Metal – General Form 6-3
6.2.2 Plutonium Metal – Pu/Be Sources 6-4
6.3 General Considerations 6-4
6.3.1 Model Configuration 6-4
6.3.2 Material Properties 6-11
6.3.3 Computer Codes and Cross-Section Libraries 6-16
6.3.4 Demonstration of Maximum Reactivity 6-17
6.4 Single Package Evaluation 6-39
6.4.1 Configuration 6-39
6.4.2 Results 6-40
6.5 Evaluation of Package Arrays under Normal Conditions of Transport 6-40
6.5.1 Configuration 6-40
6.5.2 Results 6-40
6.6 Package Arrays under Hypothetical Accident Conditions 6-40
6.6.1 Configuration 6-40
6.6.2 Results 6-41
6.7 Fissile Material Packages for Air Transport 6-41
6.7.1 Configuration 6-41
6.7.2 Results 6-41
6.8 Benchmark Evaluations 6-41
6.8.1 Applicability of Benchmark Experiments 6-42
6.8.2 Bias Determination 6-48
6.9 Appendices 6-59
6.9.1 References 6-59
6.9.2 TB-1 Containment Vessel Inner Volume 6-62
6.9.3 Applicability of Benchmark Experiments 6-63
6.9.4 Calculation Results 6-76
6.9.5 Sample inputs 6-109
6.9.6 Considerations for Pu/Be Sources 6-116

7. PACKAGE OPERATIONS 7-1
7.1 Package Loading 7-1
7.1.1 Preparation for Loading 7-2
7.1.2 Loading of Contents 7-6

7.1.3 Preparation for Transport 7-21
7.2 Package Unloading 7-23
7.2.1 Receipt of Package from Carrier 7-23
7.2.2 Removal of Contents 7-25
7.3 Preparation of Empty Package for Transport 7-28
7.3.1 Transporting the PAT-1 Package with an Empty T-Ampoule 7-28
7.3.2 Transporting an Empty PAT-1 package without a T-Ampoule 7-29
7.3.3 Storage of an Empty PAT-1 Package with or without the TB-1 and Internal Hardware 7-30
7.4 Other Operations 7-30
7.5 Appendix 7-30
7.5.1 References 7-30

8. ACCEPTANCE TESTS AND MAINTENANCE PROGRAM 8-1
8.1 Acceptance Tests 8-1
8.1.1 Visual Inspections and Measurements 8-2
8.1.2 Weld Examinations 8-2
8.1.3 Structural and Pressure Tests 8-2
8.1.4 Leakage Tests 8-5
8.1.5 Component and Material Tests 8-5
8.1.6 Shielding Tests 8-6
8.1.7 Thermal Tests 8-6
8.1.8 Miscellaneous Tests 8-6
8.2 Maintenance Program 8-6
8.2.1 Structural and Pressure Tests 8-7
8.2.2 Leakage Tests 8-7
8.2.3 Component and Material Tests 8-8
8.2.4 Thermal Tests 8-8
8.2.5 Miscellaneous Tests 8-8
8.3 Appendix 8-8
8.3.1 References 8-8
8.3.2 Leak Testing 8-9

9. QUALITY ASSURANCE 9-1
9.1 Organization 9-1
9.2 Quality Assurance Program 9-3
9.2.1 General 9-3
9.2.2 QA Levels 9-7
9.3 Package Design Control 9-10
9.4 Procurement Document Control 9-11
9.5 Instructions, Procedures, and Drawings 9-12
9.5.1 Operating Procedures for Preparation and Use of Packaging System 9-13
9.5.2 Operating Procedure Changes 9-13
9.6 Document Control 9-13
9.7 Control of Purchased Material, Equipment, and Services 9-14
9.8 Identification and Control of Material, Parts, and Components 9-15

9.9 Control of Special Processes 9-16
9.10 Internal Inspection 9-17
9.10.1 Inspections During Fabrication 9-18
9.10.2 Inspections during Initial Acceptance and during Service Life 9-19
9.11 Test Control 9-19
9.11.1 Acceptance Tests 9-20
9.11.2 Maintenance Tests 9-20
9.11.3 Preshipment Tests 9-20
9.12 Control of Measuring and Test Equipment 9-20
9.13 Handling, Storage, and Shipping Control 9-21
9.14 Inspection, Test, and Operating Status 9-21
9.15 Nonconforming Materials, Parts, or Components 9-22
9.16 Corrective Action 9-24
9.17 Quality Assurance Records 9-24
9.17.1 Subcontractor/Supplier Submittal Requirements Summary 9-25
9.18 Audits 9-26
9.19 Appendix 9-26
9.19.1 References 9-26

LIST OF FIGURES

Figure 1-1. Assembled PAT-1 Showing AQ-1, TB-1, and T-Ampoule 1-2
Figure 1-2. T-Ampoule within the TB-1 1-4
Figure 1-3. Two Sample Containers (SC-2) Nested within T-Ampoule and TB-1 1-6
Figure 1-4. Three Sample Containers (SC-1) Nested within T-Ampoule and TB-1 1-7
Figure 1-5. 831 gram (1.83 lb) Pu Hollow Cylinder within T-Ampoule and TB-1 1-8

Figure 2-1. Locus in Equivalent Plastic Strain–Stress Triaxiality Space Developed from Titanium Impact Test 2-8
Figure 2-2. Center of Gravity for PAT-1. (Note That the Center of Gravity Varies with the Inclusion of the Support Structure and Could Vary Because of the Natural Weight Variation of the Kiln-Dried Redwood.) 2-10
Figure 2-3. Flowchart of PAT-1 Analyses 2-23
Figure 2-4. Strain Locus Developed from Titanium Experiment and Finite Element Model 2-25
Figure 2-5. Summary of Highest Tearing Parameter versus Plastic Strain Elements for HAC and High Velocity Analyses 2-29
Figure 2-6. Summary of B-W Strain Locus Values for the Highest Tearing Parameter Elements. 2-29
Figure 2-7. Finite Element Model of the Complete PAT-1 Package 2-36
Figure 2-8. Details of the High-Velocity Finite Element Validation Model 2-37
Figure 2-9. Redwood Force-Deflection Curve Used in Orthotropic Crush Model 2-38
Figure 2-10. Model Slice Configuration for the Orthotropic Crush Material Model 2-40
Figure 2-11. Deformation from an End-On Impact of 445 ft/sec 2-42
Figure 2-12. PAT-1 Dimensions Following 422-FPS Top End Impact (from SAR Figure 2.18) 2-42

Figure 2-13. Full Model TB-1 Deceleration Curve for End-On Impact Analysis (10 CFR 71.74) 2-43
Figure 2-14. Deformation of the Full Package Model after a Side Impact of 445 ft/sec 2-43
Figure 2-15. PAT-1 Dimensions Following 445 FPS Side Impact (from SAR Figure 2.242)... 2-44
Figure 2-16. Full Model TB-1 Deceleration Curve for Side Impact Analysis (10 CFR 71.74) 2-44
Figure 2-17. Deformation of the Full Package Model after a CGOC Impact of 445 ft/sec 2-45
Figure 2-18. PAT-1 Dimensions Following 443-FPS Bottom Corner Impact (CGOC) (from SAR Figure 2.27 SAR) 2-45
Figure 2-19. Full Model TB-1 Deceleration Curve for CGOC Impact Analysis (10 CFR 71.74) 2-46
Figure 2-20. NCT and HAC Package Model with Lid Flange 2-47
Figure 2-21. Flange Details of NCT Model (Dimensions in Inches) 2-47
Figure 2-22. Experimental Concept 2-49
Figure 2-23. Cross-Section of Impactor Assembly and TB-1/Ampoule Assembly 2-50
Figure 2-24. Complete Test Assembly Prior to the Test 2-51
Figure 2-25. (a) Titanium Ampoule and TB-1 Fixture Attached to Actuator Sled; (b) View of Suspended Impactor 2-51
Figure 2-26. DT-45 Drop Table Shock Machine 2-52
Figure 2-27. Solid model of the Ampoule Test Assemble for Drop Table Tests 2-52
Figure 2-28. Photograph of Ampoule Test Assembly Prior to Testing 2-53
Figure 2-29. Finite Element Model for the Brass Impact Test 2-54
Figure 2-30. Equivalent Plastic Strain in the Ampoule Dish at an Impact Velocity of 175 ft/sec 2-54
Figure 2-31. Deformed Shape of and Plastic Strain in the Brass-Tipped Impactor at an Impact Velocity of 175 ft/sec 2-55
Figure 2-32. Deformed Shape of the Brass Impactor Overlaid on the Test Specimen 2-55
Figure 2-33. Comparison of the Brass-Tipped Impactor Acceleration from the Test and the Finite Element Model 2-56
Figure 2-34. Deformed Mesh of the Titanium Tipped Impactor, at an Impact Velocity of 200 ft/sec 2-57
Figure 2-35. Equivalent Plastic Strain in the Ampoule Dish at an Impact Velocity of 200 ft/sec with a Titanium Tipped Impactor 2-57
Figure 2-36. Deformed Finite Element Mesh of Titanium Impactor with Contours of Equivalent Plastic Strain 2-58
Figure 2-37. Deformed Shape of the Titanium Impactor Overlaid on the Test Specimen 2-58
Figure 2-38. Finite Element Model of the Drop Table Ampoule Test 2-59
Figure 2-39. Drop Table Acceleration 2-60
Figure 2-40. Finite Element Results Showing the Deformed Shape of the Ampoule Test Specimen 2-60
Figure 2-41. Photographs of the Deformed Ampoule Specimen (a) Top View (b) Inner Surface 2-61
Figure 2-42. Maximum Equivalent Plastic Strain in Sample Test Specimen 2-61
Figure 2-43. Nominal Element Radial Strain Compared to Strain Gage Data 2-62
Figure 2-44. Crush Plate Acceleration 2-62
Figure 2-45. Plastic Strain versus Stress Triaxiality from Johnson and Cook 2-64

Figure 2-46. Stress Failure Locus of Al2024-T351 Developed from Bao 2-64
Figure 2-47. General Failure Locus of Ductile Metals Developed by Bao and Wierzbicki. 2-65
Figure 2-48. Equivalent Plastic Strain in the Titanium Tip for an Impact Velocity of 200 ft/sec 2-66
Figure 2-49. Equivalent Plastic Strain in the Titanium Ampoule in the Drop Table Test 2-67
Figure 2-50. Locus in Equivalent Plastic Strain–Stress Triaxiality Space Developed from Titanium Impact Tests 2-67
Figure 2-51. Stress Triaxiality and Equivalent Plastic Strain versus Time for Element 46152 2-68
Figure 2-52. Stress Triaxiality and Average Stress Triaxiality as a Function of Equivalent Plastic Strain for Element 46152 2-69
Figure 2-53. Finite Element Model of Titanium Tensile Test Specimen (a) Original Mesh (b) Deformed Mesh (c) Equivalent Plastic Strain 2-70
Figure 2-54. Stress Triaxiality and Equivalent Plastic Strain versus Displacement for Center Element 2-70
Figure 2-55. Stress Triaxiality and Average Stress Triaxiality as a Function of Plastic Strain for the Highest Stressed Element 2-71
Figure 2-56. Tensile Test Results Showing Peak Value of Failure Parameter TP 2-72
Figure 2-57. Redwood Force Deflection Curve Compared to Test Data from Joseph and Hill 2-76
Figure 2-58. Comparison of Power-Law Curve Fit with Data from Tensile Test 2-84
Figure 2-59. Effect of Temperature on the Tensile Ultimate Strength and Tensile Yield Strength of Annealed Ti-6-Al-4V Alloy (Ref. 2, Taken from MIL-HDBK-5E, Figure 5.4.1.1.1.1) 2-85
Figure 2-60. Effect of Temperature on the Elongation of Annealed Ti-6-Al-4V Alloy (Ref. 2, Taken from MIL-HDBK-5E, Figure 5.4.1.1.5) 2-85
Figure 2-61. Pu Stress-Strain Curves Taken from Hecker and Stevens [Figure 2(a)] 2-87
Figure 2-62. Pu Stress-Strain Curves Taken from Hecker and Stevens (Figure 10[b]). 2-88
Figure 2-63. Comparison of Power-Law Curve Fit with Data from Tensile Test 2-91
Figure 2-64. Comparison of Power-Law Curve Fit with Data from Tensile Test 2-92
Figure 2-65. Common Components of the Model for Top and CGOC Impact Orientation 2-95
Figure 2-66. Common Components of the Model for a Side Impact Orientation 2-95
Figure 2-67. Support Structure with 0° Rotation and Spacers for SC-1 2-96
Figure 2-68. Support Structure with 45° Rotation and Spacer for SC-2 2-96
Figure 2-69. Mesh Refinement in Support Structure with 0° Rotation and Spacer for SC-1 2-97
Figure 2-70. 831-g Cylinder Finite Element Model 2-98
Figure 2-71. 731-g Cylinder Finite Element Model 2-98
Figure 2-72. Finite Element Model of SC-1 with Pu Cylinder Contents 2-99
Figure 2-73. Finite Element Model of SC-2 with Pu Cylinder Contents 2-99
Figure 2-74. NCT SC-2 Side Impact with Support Structure Rotated 45° 2-100
Figure 2-75. NCT SC-1 Side Impact with Support Structure Rotated 0° 2-101
Figure 2-76. NCT SC-1 End Impact with Support Structure Rotated 0° 2-101
Figure 2-77. NCT SC-2 End Impact with Support Structure Rotated 0° 2-102
Figure 2-78. NCT SC-1 End Impact with Support Structure Rotated 0° – Final Displacement 2-103

Figure 2-79. NCT SC-2 End Impact with Support Structure Rotated 0° – Final Displacement....2-103
Figure 2-80. NCT SC-1 End Impact with Support Structure Rotated 0° - Kinetic Energy Time History....2-104
Figure 2-81. NCT SC-2 End Impact with Support Structure Rotated 0° - Kinetic Energy Time History....2-104
Figure 2-82. NCT SC-1 End Impact with Support Structure Rotated 0° - EQPS in Bottom Legs....2-105
Figure 2-83. NCT SC-1 End Impact with Support Structure Rotated 0° - EQPS in Top Legs....2-105
Figure 2-84. NCT SC-1 End Impact with Support Structure Rotated 0° – EQPS in Top Dish....2-106
Figure 2-85. NCT SC-2 End Impact with Support Structure Rotated 0° – EQPS in Bottom Legs....2-106
Figure 2-86. NCT SC-2 End Impact with Support Structure Rotated 0° – EQPS in Top Dish....2-107
Figure 2-87. NCT SC-1 Side Impact with Support Structure Rotated 45°....2-108
Figure 2-88. NCT SC-2 Side Impact with Support Structure Rotated 0°....2-108
Figure 2-89. NCT SC-1 Side Impact with Support Structure Rotated 45° – Final Displacement....2-109
Figure 2-90. NCT SC-1 Side Impact with Support Structure Rotated 0° – Final Displacement....2-109
Figure 2-91. NCT SC-2 Side Impact with Support Structure Rotated 45° – Final Displacement....2-110
Figure 2-92. NCT SC-2 Side Impact with Support Structure Rotated 0° - Final Displacement....2-110
Figure 2-93. NCT SC-1 Side Impact with Support Structure Rotated 45° - Kinetic Energy Time History....2-111
Figure 2-94. NCT SC-2 Side Impact with Support Structure Rotated 45° - Kinetic Energy Time History....2-111
Figure 2-95. NCT SC-1 Side Impact with Support Structure Rotated 0° – Kinetic Energy Time History....2-112
Figure 2-96. NCT SC-2 Side Impact with Support Structure Rotated 0° – Kinetic Energy Time History....2-112
Figure 2-97. NCT SC-1 Side Impact with Support Structure Rotated 45° – EQPS in Bottom Dish....2-113
Figure 2-98. NCT SC-1 Side Impact with Support Structure Rotated 45° – EQPS in Top Legs....2-113
Figure 2-99. NCT SC-1 Side Impact with Support Structure Rotated 45° – EQPS in Top Dish....2-114
Figure 2-100. NCT SC-2 Side Impact with Support Structure Rotated 45° – EQPS in Bottom Dish....2-114
Figure 2-101. NCT SC-2 Side Impact with Support Structure Rotated 45° – EQPS in Top Legs....2-115
Figure 2-102. NCT SC-2 Side Impact with Support Structure Rotated 45° – EQPS in Top Dish....2-115

Figure 2-103. NCT SC-1 Side Impact with Support Structure Rotated 0° – EQPS in Bottom Legs 2-116
Figure 2-104. NCT SC-1 Side Impact with Support Structure Rotated 0° – EQPS in Top Dish 2-116
Figure 2-105. NCT SC-2 Side Impact with Support Structure Rotated 0° – EQPS in Bottom Legs 2-117
Figure 2-106. NCT SC-2 Side Impact with Support Structure Rotated 45° - EQPS in T-Ampoule 2-118
Figure 2-107. NCT SC-2 Side Impact with Support Structure Rotated 45° - EQPS in TB-1 2-118
Figure 2-108. NCT SC-2 Side Impact with Support Structure Rotated 45° - Tresca Stress in TB-1 2-119
Figure 2-109. Finite Element Mesh for the 831-g, Plutonium Metal Hollow Cylinder, Bottom Position, End Impact 2-123
Figure 2-110. Finite Element Mesh for the 831-g, Plutonium Metal Hollow Cylinder, Bottom Position, End Impact – Final Displacement 2-123
Figure 2-111. Kinetic Energy Time History for the 831-g, ER Cylinder, Bottom Position, End Impact 2-124
Figure 2-112. EQPS in the TB-1 for the 831-g, ER Cylinder, Bottom Position, End Impact 2-124
Figure 2-113. EQPS in TB-1 (Range Zoomed in to Show All Elements with non-zero EQPS) for the 831-g, Hollow Cylinder, Bottom Position, End Impact 2-125
Figure 2-114. von Mises Stress in the TB-1 for the 831-g Plutonium Metal Hollow Cylinder, Bottom Position, End Impact (Rotated Forward for Ease of Viewing) 2-125
Figure 2-115. von Mises Stress in the TB-1 for the 831-g, Plutonium Metal Hollow Cylinder, Bottom Position, End Impact (Rotated Backward for Ease of Viewing) 2-126
Figure 2-116. Summed Contact Force on the TB-1 Top for a 831-g, Plutonium Metal Hollow Cylinder, Top Impact 2-126
Figure 2-117. Finite Element Mesh for the 831-g, Angled, ER Cylinder, Bottom Position, End Impact 2-127
Figure 2-118. Finite Element Mesh for the 831-g, Angled, ER, Cylinder, Bottom Position, End Impact – Final Displacement 2-128
Figure 2-119. Kinetic Energy Time History for the 831-g, Angled, Plutonium Metal Hollow Cylinder, Bottom Position, End Impact 2-128
Figure 2-120. Graph of Average Stress Triaxiality versus EQPS of Elements Exceeding the Experimental Strain Locus for the 831-g, Angled, Plutonium Metal Hollow Cylinder, Bottom Position, End Impact 2-129
Figure 2-121. Graph of Average Stress Triaxiality versus EQPS of Elements Exceeding the Experimental Strain Locus (Zoomed In) for the 831-g, Angled, Plutonium Metal Hollow Cylinder, Bottom Position, End Impact 2-129
Figure 2-122. Graph of Tearing Parameter versus EQPS for Elements Exceeding the Experimental Strain Locus for the 831-g, Angled, Plutonium Metal Hollow Cylinder, Bottom Position, End Impact 2-130
Figure 2-123. Plot of Elements Exceeding the Experimental Strain Locus for the 831-g, Angled, Plutonium Metal Hollow Cylinder, Bottom Position, End Impact 2-130
Figure 2-124. Plot of EQPS in the TB-1 for the 831-g Angled, ER, Cylinder, Bottom Position, End Impact 2-131

Figure 2-125. Plot of EQPS in the TB-1 (Range Zoomed in to Show all Elements with Non-Zero EQPS) for the 831-g, Angled, Plutonium Metal Hollow Cylinder, Bottom Position, End Impact 2-131
Figure 2-126. Plot of von Mises Stress in the TB-1 for the 831-g, Angled, Plutonium Metal Hollow Cylinder, Bottom Position, End Impact 2-132
Figure 2-127. Plot of von Mises Stress in the TB-1 for the 831-g, Angled, Plutonium Metal Hollow Cylinder, Bottom Position, End Impact 2-132
Figure 2-128. Plot of Contact Force in the TB-1 for the 831-g, Angled Plutonium Metal Hollow Cylinder, Bottom Position, End Impact 2-133
Figure 2-129. Finite Element Mesh for the 831-g, Angled, ER Cylinder, Bottom Position, CGOC Impact 2-134
Figure 2-130. Finite Element Mesh for the 831-g, Angled, ER Cylinder, Bottom Position, CGOC Impact – Final Displacement 2-135
Figure 2-131. Kinetic Energy Time History for the 831-g, Angled, Plutonium Metal Hollow Cylinder, Bottom Position, CGOC Impact 2-135
Figure 2-132. Graph of Average Stress Triaxiality versus EQPS of Elements Exceeding the Experimental Strain Locus for the 831-g, Angled, Plutonium Metal Hollow Cylinder, Bottom Position, CGOC Impact 2-136
Figure 2-133. Graph of Average Stress Triaxiality versus EQPS of Elements Exceeding the Experimental Strain Locus (Zoomed in) for the 831-g, Angled, Plutonium Metal Hollow Cylinder, Bottom Position, CGOC Impact 2-136
Figure 2-134. Graph of Tearing Parameter versus EQPS of Elements Exceeding the Experimental Strain Locus for the 831-g Angled, Plutonium Metal Hollow Cylinder, Bottom Position, CGOC Impact 2-137
Figure 2-135. Plot of Elements Exceeding the Experimental Strain Locus for the 831-g, Angled, Plutonium Metal Hollow Cylinder, Bottom Position, CGOC Impact 2-137
Figure 2-136. Plot of Elements Exceeding the Experimental Strain Locus for the 831-g, Angled, Plutonium Metal Hollow Cylinder, Bottom Position, CGOC Impact 2-138
Figure 2-137. Plot of Elements Exceeding the Experimental Strain Locus for the 831-g, Angled, Plutonium Metal Hollow Cylinder, Bottom Position, CGOC Impact 2-138
Figure 2-138. Plot of EQPS in the TB-1 for the 831-g, Angled, Plutonium Metal Hollow Cylinder, Bottom Position, CGOC Impact 2-139
Figure 2-139. Plot of EQPS in the TB-1 for the 831-g, Angled, Plutonium Metal Hollow Cylinder, Bottom Position, CGOC Impact 2-139
Figure 2-140. Plot of von Mises Stress in the TB-1 for the 831-g, Angled, Plutonium Metal Hollow Cylinder, Bottom Position, CGOC Impact 2-140
Figure 2-141. Finite Element Mesh for the 831-g, ER, Cylinder, Far Side Position, Side Impact 2-141
Figure 2-142. Finite Element Mesh for the 831-g, Plutonium Metal Hollow Cylinder, Far Side Position, Side Impact – Final Displacement 2-141
Figure 2-143. Kinetic Energy Time History for the 831-g, ER, Cylinder, Far Side Position, Side Impact 2-142
Figure 2-144. Graph of Stress Triaxiality versus EQPS of Elements Exceeding the Experimental Strain Locus for the 831-g, Plutonium Metal Hollow Cylinder, Far Side Position, Side Impact 2-142

Figure 2-145. Graph of Stress Triaxiality versus EQPS of Elements Exceeding the Experimental Strain Locus (Zoomed In) for the 831-g, Plutonium Metal Hollow Cylinder, Far Side Position, Side Impact 2-143
Figure 2-146. Graph of Tearing Parameter versus EQPS of Elements Exceeding the Experimental Strain Locus for the 831-g, Plutonium Metal Hollow Cylinder, Far Side Position, Side Impact 2-143
Figure 2-147. Plot of Elements Exceeding the Experimental Strain Locus for the 831-g, Plutonium Metal Hollow Cylinder, Far Side Position, Side Impact 2-144
Figure 2-148. Plot of Elements Exceeding the Experimental Strain Locus for the 831-g, Plutonium Metal Hollow Cylinder, Far Side Position, Side Impact 2-144
Figure 2-149. Plot of EQPS in the TB-1 for the 831-g, ER, Cylinder, Far Side Position, Side Impact 2-145
Figure 2-150. Plot of EQPS in the TB-1 for the 831-g, ER Cylinder, Far Side Position, Side Impact 2-145
Figure 2-151. Plot of von Mises Stress in the TB-1 for the 831-g, ER Cylinder, Far Side Position, Side Impact 2-146
Figure 2-152. Plot of von Mises Stress in the TB-1 for the 831-g, ER, Cylinder, Far Side Position, Side Impact 2-146
Figure 2-153. Finite Element Mesh for the 831-g, Angled, ER Cylinder, Far Side Position, Side Impact 2-147
Figure 2-154. Finite Element Mesh for the 831-g, Angled, ER Cylinder, Far Side Position, Side Impact – Final Displacement 2-148
Figure 2-155. Kinetic Energy Time History for the 831-g, Angled, Plutonium Metal Hollow Cylinder, Far Side Position, Side Impact 2-148
Figure 2-156. Graph of Average Stress Triaxiality versus EQPS of Elements Exceeding the Experimental Strain Locus for the 831-g, Angled, Plutonium Metal Hollow Cylinder, Far Side Position, Side Impact 2-149
Figure 2-157. Graph of Average Stress Triaxiality versus EQPS of Elements Exceeding the Experimental Strain Locus (Zoomed In) for the 831-g, Angled, Plutonium Metal Hollow Cylinder, Far Side Position, Side Impact 2-149
Figure 2-158. Graph of Tearing Parameter versus EQPS of Elements Exceeding the Experimental Strain Locus for the 831-g, Angled, Plutonium Metal Hollow Cylinder, Far Side Position, Side Impact 2-150
Figure 2-159. Plot of Elements Exceeding the Experimental Strain Locus for the 831-g, Angled, Plutonium Metal Hollow Cylinder, Far Side Position, Side Impact 2-151
Figure 2-160. Plot of EQPS in the TB-1 for the 831-g, Angled, ER Cylinder, Far Side Position, Side Impact 2-152
Figure 2-161. Plot of EQPS in the TB-1 for the 831-g, Angled, ER Cylinder, Far Side Position, Side Impact 2-152
Figure 2-162. Plot of von Mises Stress in the TB-1 for the 831-g, Angled, Plutonium Metal Hollow Cylinder, Far Side Position, Side Impact 2-153
Figure 2-163. Plot of von Mises Stress in the TB-1 for the 831-g, Angled, Plutonium Metal Hollow Cylinder, Far Side Position, Side Impact 2-153
Figure 2-164. Finite Element Mesh for the 731-g, ER, Cylinder, Bottom Position, Top Impact 2-154

Figure 2-165. Finite Element Mesh for the 731-g, ER, Cylinder, Bottom Position, Top Impact – Final Displacement 2-155
Figure 2-166. Kinetic Energy Time History for the 731-g, ER, Cylinder, Bottom Position, Top Impact 2-155
Figure 2-167. EQPS in the TB-1 for the 731-g, Plutonium Metal Hollow Cylinder, Bottom Position, Top Impact 2-156
Figure 2-168. von Mises Stress in the TB-1 for the 731-g, ER, Cylinder, Bottom Position, Top Impact 2-156
Figure 2-169. von Mises Stress in the TB-1 for the 731-g, ER, Cylinder, Bottom Position, Top Impact 2-157
Figure 2-170. Contact Forces in the TB-1 for the 731-g, ER, Cylinder, Bottom Position, Top Impact 2-157
Figure 2-171. Finite Element Mesh for the 731-g, Angled, ER Cylinder, Bottom Position, Top Impact 2-158
Figure 2-172. Finite Element Mesh for the 731-g, Angled, ER Cylinder, Bottom Position, Top Impact – Final Displacement 2-159
Figure 2-173. Kinetic Energy Time History for the 731-g, Angled, Plutonium Metal Hollow Cylinder, Bottom Position, Top Impact 2-159
Figure 2-174. Graph of Average Stress Triaxiality versus EQPS of Elements Exceeding the Experimental Strain Locus for the 731-g, Angled, Plutonium Metal Hollow Cylinder, Bottom Position, Top Impact 2-160
Figure 2-175. Graph of Average Stress Triaxiality versus EQPS of Elements Exceeding the Experimental Strain Locus (Zoomed In) for the 731-g, Angled, Plutonium Metal Hollow Cylinder, Bottom Position, Top Impact 2-160
Figure 2-176. Graph of Tearing Parameter versus EQPS of Elements Exceeding the Experimental Strain Locus for the 731-g, Angled, Plutonium Metal Hollow Cylinder, Bottom Position, Top Impact 2-161
Figure 2-177. Plot of Elements Exceeding the Experimental Strain Locus for the 731-g, Angled, Plutonium Metal Hollow Cylinder, Bottom Position, Top Impact 2-161
Figure 2-178. Plot of EQPS in the TB-1 for the 731-g, Angled, Plutonium Metal Hollow Cylinder, Bottom Position, Top Impact 2-162
Figure 2-179. Plot of von Mises Stress for the 731-g, Angled, Plutonium Metal Hollow Cylinder, Bottom Position, Top Impact 2-162
Figure 2-180. Plot of von Mises Stress for the 731-g, Angled, Plutonium Metal Hollow Cylinder, Bottom Position, Top Impact 2-163
Figure 2-181. Plot of Contact Force for the 731-g, Angled, Plutonium Metal Hollow Cylinder, Bottom Position, Top Impact 2-163
Figure 2-182. Finite Element Mesh for the 731-g, Angled, Plutonium Metal Hollow Cylinder, Bottom Position, CGOC Impact 2-164
Figure 2-183. Finite Element Mesh for the 731-g, Angled, Plutonium Metal Hollow Cylinder, Bottom Position, CGOC Impact – Final Displacement 2-165
Figure 2-184. Kinetic Energy Time History for the 731-g, Angled, Plutonium Metal Hollow Cylinder, Bottom Position, CGOC Impact 2-165
Figure 2-185. Graph of Average Stress Triaxiality versus EQPS of Elements Exceeding the Experimental Strain Locus for the 731-g, Angled, Plutonium Metal Hollow Cylinder, Bottom Position, CGOC Impact 2-166

Figure 2-186. Graph of Average Stress Triaxiality versus EQPS of Elements Exceeding the Experimental Strain Locus (Zoomed In) for the 731-g, Angled, Plutonium Metal Hollow Cylinder, Bottom Position, CGOC Impact 2-166
Figure 2-187. Graph of Tearing Parameter versus EQPS of Elements Exceeding the Experimental Strain Locus for the 731-g, Angled, Plutonium Metal Hollow Cylinder, Bottom Position, CGOC Impact 2-167
Figure 2-188. Plot of Elements Exceeding the Experimental Strain Locus for the 731-g, Angled, Plutonium Metal Hollow Cylinder, Bottom Position, CGOC Impact 2-167
Figure 2-189. Plot of Elements Exceeding the Experimental Strain Locus for the 731-g, Angled, Plutonium Metal Hollow Cylinder, Bottom Position, CGOC Impact 2-168
Figure 2-190. Plot of EQPS in the TB-1 for the 731-g, Angled, Plutonium Metal Hollow Cylinder, Bottom Position, CGOC Impact 2-168
Figure 2-191. Plot of von Mises Stress in the TB-1 for the 731-g, Angled, Plutonium Metal Hollow Cylinder, Bottom Position, CGOC Impact 2-169
Figure 2-192. Finite Element Mesh for the 731-g, ER, Cylinder, Far Side Position, Side Impact 2-170
Figure 2-193. Finite Element Mesh for the 731-g, Plutonium Metal Hollow Cylinder, Far Side Position, Side Impact – Final Displacement 2-170
Figure 2-194. Kinetic Energy Time History for the 731-g, ER, Cylinder, Far Side Position, Side Impact 2-171
Figure 2-195. Graph of Average Stress Triaxiality versus EQPS of Elements Exceeding the Experimental Strain Locus for the 731-g, Plutonium Metal Hollow Cylinder, Far Side Position, Side Impact 2-171
Figure 2-196. Graph of Average Stress Triaxiality versus EQPS of Elements Exceeding the Experimental Strain Locus (Zoomed In) for the 731-g, Plutonium Metal Hollow Cylinder, Far Side Position, Side Impact 2-172
Figure 2-197. Graph of Tearing Parameter versus EQPS of Elements Exceeding the Experimental Strain Locus for the 731-g, Plutonium Metal Hollow Cylinder, Far Side Position, Side Impact 2-172
Figure 2-198. Plot of Elements Exceeding the Experimental Strain Locus for the 731-g, Plutonium Metal Hollow Cylinder, Far Side Position, Side Impact 2-173
Figure 2-199. Plot of EQPS in the TB-1 for the 731-g, ER Cylinder, Far Side Position, Side Impact 2-173
Figure 2-200. Plot of EQPS in the TB-1 for the 731-g, ER Cylinder, Far Side Position, Side Impact 2-174
Figure 2-201. Plot of EQPS in the TB-1 for the 731-g, ER Cylinder, Far Side Position, Side Impact 2-174
Figure 2-202. Plot of EQPS in the TB-1 for the 731-g, Plutonium Metal Hollow Cylinder, Far Side Position, Side Impact (Range Adjusted to Highlight Small Stains in the TB-1 Not Visible in Figure 2-201) 2-175
Figure 2-203. Plot of von Mises Stress in the TB-1 for the 731-g, Plutonium Metal Hollow Cylinder, Far Side Position, Side Impact 2-175
Figure 2-204. Plot of von Mises Stress in the TB-1 for the 731-g, Plutonium Metal Hollow Cylinder, Far Side Position, Side Impact (see Figure 2-203 Rotated to Show Internal Stresses) 2-176

Figure 2-205. Finite Element Mesh for the 731-g, Angled, ER Cylinder, Far Side Position, Side Impact 2-177
Figure 2-206. Finite Element Mesh for the 731-g, Angled, ER Cylinder, Far Side Position, Side Impact – Final Displacement 2-177
Figure 2-207. Kinetic Energy Time History for the 731-g, Angled, Plutonium Metal Hollow Cylinder, Far Side Position, Side Impact 2-178
Figure 2-208. Graph of Average Stress Triaxiality versus EQPS of Elements Exceeding the Experimental Strain Locus for the 731-g, Angled, Plutonium Metal Hollow Cylinder, Far Side Position, Side Impact 2-178
Figure 2-209. Graph of Average Stress Triaxiality versus EQPS of Elements Exceeding the Experimental Strain Locus (Zoomed In) for the 731-g, Angled, Plutonium Metal Hollow Cylinder, Far Side Position, Side Impact 2-179
Figure 2-210. Graph of Tearing Parameter versus EQPS of Elements Exceeding the Experimental Strain Locus for the 731-g, Angled, Plutonium Metal Hollow Cylinder, Far Side Position, Side Impact 2-179
Figure 2-211. Plot of Elements Exceeding the Experimental Strain Locus for the 731-g, Angled, Plutonium Metal Hollow Cylinder, Far Side Position, Side Impact 2-180
Figure 2-212. Plot of EQPS in the TB-1 for the 731-g, Angled, Plutonium Metal Hollow Cylinder, Far Side Position, Side Impact 2-180
Figure 2-213. Plot of EQPS in the TB-1 for the 731-g, Angled, Plutonium Metal Hollow Cylinder, Far Side Position, Side Impact 2-181
Figure 2-214. Plot of von Mises Stress in the TB-1 for the 731-g, Angled, Plutonium Metal Hollow Cylinder, Far Side Position, Side Impact 2-181
Figure 2-215. Plot of von Mises Stress in the TB-1 for the 731-g, Angled, Plutonium Metal Hollow Cylinder, Far Side Position, Side Impact 2-182
Figure 2-216. Finite Element Mesh for the SC-1, Pu Contents, End Impact 2-184
Figure 2-217. Finite Element Mesh for the SC-1, Pu Contents, End Impact – Final Displacement 2-184
Figure 2-218. Kinetic Energy Time History for the SC-1, Pu Contents, End Impact 2-185
Figure 2-219. Plot of EQPS in the TB-1 for the SC-1, Pu Contents, End Impact 2-185
Figure 2-220. Plot of von Mises Stress in the TB-1 for the SC-1, Pu Contents, End Impact 2-186
Figure 2-221. Plot of Contact Force in the TB-1 for the SC-1, Pu Contents, End Impact 2-186
Figure 2-222. Finite Element Mesh for the SC-1, Pu Contents, Side Impact, 0° Support Structure 2-187
Figure 2-223. Finite Element Mesh for the SC-1, Pu Contents, Side Impact, 0° Support Structure – Final Displacement 2-188
Figure 2-224. Kinetic Energy Time History for the SC-1, Pu Contents, Side Impact, 0° Support Structure 2-188
Figure 2-225. Graph of Average Stress Triaxiality versus EQPS of Elements Exceeding the Experimental Strain Locus for the SC-1, Pu Contents, Side Impact, 0° Support Structure 2-189
Figure 2-226. Graph of Tearing Parameter versus EQPS of Elements Exceeding the Experimental Strain Locus for the SC-1, Pu Contents, Side Impact, 0° Support Structure 2-189
Figure 2-227. Plot of Elements Exceeding the Experimental Strain Locus for the SC-1, Pu Contents, Side Impact, 0° Support Structure 2-190

Figure 2-228. Plot of Elements Exceeding the Experimental Strain Locus for the SC-1, Pu Contents, Side Impact, 0° Support Structure 2-190
Figure 2-229. Plot of Elements Exceeding the Experimental Strain Locus for the SC-1, Pu Contents, Side Impact, 0° Support Structure 2-191
Figure 2-230. Plot of EQPS in the TB-1 for the SC-1, Pu Contents, Side Impact, 0° Support Structure 2-191
Figure 2-231. Plot of EQPS in the TB-1 for the SC-1, Pu Contents, Side Impact, 0° Support Structure 2-192
Figure 2-232. Plot of EQPS in the TB-1 for the SC-1, Pu Contents, Side Impact, 0° Support Structure 2-192
Figure 2-233. Plot of EQPS in the TB-1 for the SC-1, Pu Contents, Side Impact, 0° Support Structure 2-193
Figure 2-234. Plot of von Mises Stress in the TB-1 for the SC-1, Pu Contents, Side Impact, 0° Support Structure 2-193
Figure 2-235. Finite Element Mesh for the SC-1, Pu Contents, Side Impact, 45° Support Structure 2-194
Figure 2-236. Finite Element Mesh for the SC-1, Pu Contents, Side Impact, 45° Support Structure – Final Displacement 2-195
Figure 2-237. Kinetic Energy Time History for the SC-1, Pu Contents, Side Impact, 45° Support Structure 2-195
Figure 2-238. Graph of Average Stress Triaxiality versus EQPS of Elements Exceeding the Experimental Strain Locus for the SC-1, Pu Contents, Side Impact, 45° Support Structure 2-196
Figure 2-239. Graph of Tearing Parameter versus EQPS of Elements Exceeding the Experimental Strain Locus for the SC-1, Pu Contents, Side Impact, 45° Support Structure 2-196
Figure 2-240. Plot of Elements Exceeding the Experimental Strain Locus for the SC-1, Pu Contents, Side Impact, 45° Support Structure 2-197
Figure 2-241. Plot of Elements Exceeding the Experimental Strain Locus for the SC-1, Pu Contents, Side Impact, 45° Support Structure 2-197
Figure 2-242. Plot of EQPS in the TB-1 for the SC-1, Pu Contents, Side Impact, 45° Support Structure 2-198
Figure 2-243. Plot of EQPS in the TB-1 for the SC-1, Pu Contents, Side Impact, 45° Support Structure 2-198
Figure 2-244. Plot of EQPS in the TB-1 for the SC-1, Pu Contents, Side Impact, 45° Support Structure 2-199
Figure 2-245. Plot of EQPS in the TB-1 for the SC-1, Pu Contents, Side Impact, 45° Support Structure 2-199
Figure 2-246. Plot of von Mises Stress in the TB-1 for the SC-1, Pu Contents, Side Impact, 45° Support Structure 2-200
Figure 2-247. Finite Element Mesh for the SC-1, Pu Contents, CGOC Impact, 0° Support Structure 2-201
Figure 2-248. Finite Element Mesh for the SC-1, Pu Contents, CGOC Impact, 0° Support Structure – Final Displacement 2-201
Figure 2-249. Kinetic Energy Time History for the SC-1, Pu Contents, CGOC Impact, 0° Support Structure 2-202

Figure 2-250. Plot of EQPS in the TB-1 for the SC-1, Pu Contents, CGOC Impact, 0° Support Structure 2-202
Figure 2-251. Plot of EQPS in the TB-1 for the SC-1, Pu Contents, CGOC Impact, 0° Support Structure 2-203
Figure 2-252. Plot of von Mises Stress in the TB-1 for the SC-1, Pu Contents, CGOC Impact, 0° Support Structure 2-203
Figure 2-253. Plot of Contact Force in the TB-1 for the SC-1, Pu Contents, CGOC Impact, 0° Support Structure 2-204
Figure 2-254. Finite Element Mesh for the SC-1, Pu Contents, CGOC Impact, 45° Support Structure 2-205
Figure 2-255. Finite Element Mesh for the SC-1, Pu Contents, CGOC Impact, 45° Support Structure – Final Displacement 2-205
Figure 2-256. Kinetic Energy Time History for the SC-1, Pu Contents, CGOC Impact, 45° Support Structure 2-206
Figure 2-257. Plot of EQPS in the TB-1 for the SC-1, Pu Contents, CGOC Impact, 45° Support Structure 2-206
Figure 2-258. Plot of EQPS in the TB-1 for the SC-1, Pu Contents, CGOC Impact, 45° Support Structure 2-207
Figure 2-259. Plot of von Mises Stress in the TB-1 for the SC-1, Pu Contents, CGOC Impact, 45° Support Structure 2-207
Figure 2-260. Plot of Contact Forces in the TB-1 for the SC-1, Pu Contents, CGOC Impact, 45° Support Structure 2-208
Figure 2-261. Finite Element Mesh for the SC-2, End Impact, 0° Support Structure 2-209
Figure 2-262. Finite Element Mesh for the SC-2, End Impact, 0° Support Structure – Final Displacement 2-209
Figure 2-263. Kinetic Energy Time History for the SC-2, End Impact, 0° Support Structure 2-210
Figure 2-264. Plot of EQPS in the TB-1 for the SC-2, End Impact, 0° Support Structure 2-210
Figure 2-265. Plot of von Mises Stress in the TB-1 for the SC-2, End Impact, 0° Support Structure 2-211
Figure 2-266. Plot of Contact Forces in the TB-1 for the SC-2, End Impact, 0° Support Structure 2-211
Figure 2-267. Finite Element Mesh for the SC-2, Side Impact, 0° Support Structure 2-212
Figure 2-268. Finite Element Mesh for the SC-2, Side Impact, 0° Support Structure – Final Displacement 2-213
Figure 2-269. Kinetic Energy Time History for the SC-2, Side Impact, 0° Support Structure 2-213
Figure 2-270. Graph of Average Stress Triaxiality versus EQPS of Elements Exceeding the Experimental Strain Locus for the SC-2, Side Impact, 0° Support Structure 2-214
Figure 2-271. Graph of Tearing Parameter versus EQPS of Elements Exceeding the Experimental Strain Locus for the SC-2, Side Impact, 0° Support Structure 2-214
Figure 2-272. Plot of Elements Exceeding the Experimental Strain Locus for the SC-2, Side Impact, 0° Support Structure 2-215
Figure 2-273. Plot of Elements Exceeding the Experimental Strain Locus for the SC-2, Side Impact, 0° Support Structure 2-215
Figure 2-274. Plot of EQPS in the TB-1 for the SC-2, Side Impact, 0° Support Structure 2-216
Figure 2-275. Plot of EQPS in the TB-1 for the SC-2, Side Impact, 0° Support Structure 2-216

Figure 2-276. Plot of von Mises Stress in the TB-1 for |the SC-2, Side Impact, 0° Support Structure 2-217
Figure 2-277. Finite Element Mesh for the SC-2, Side Impact, 45° Support Structure 2-218
Figure 2-278. Finite Element Mesh for the SC-2, Side Impact, 45° Support Structure – Final Displacement 2-218
Figure 2-279. Kinetic Energy Time History for the SC-2, Side Impact, 45° Support Structure 2-219
Figure 2-280. Graph of Average Stress Triaxiality versus EQPS of Elements Exceeding the Experimental Strain Locus for the SC-2, Side Impact, 45° Support Structure 2-219
Figure 2-281. Graph of Tearing Parameter versus EQPS of Elements Exceeding the Experimental Strain Locus for the SC-2, Side Impact, 45° Support Structure 2-220
Figure 2-282. Plot of Elements Exceeding the Experimental Strain Locus for the SC-2, Side Impact, 45° Support Structure 2-221
Figure 2-283. Plot of Elements Exceeding the Experimental Strain Locus for the SC-2, Side Impact, 45° Support Structure 2-222
Figure 2-284. Plot of EQPS in the TB-1 for the SC-2, Side Impact, 45° Support Structure 2-222
Figure 2-285. Plot of EQPS in the TB-1 for the SC-2, Side Impact, 45° Support Structure 2-223
Figure 2-286. Plot of EQPS in the TB-1 for the SC-2, Side Impact, 45° Support Structure 2-223
Figure 2-287. Plot of von Mises Stress in the TB-1 for the SC-2, Side Impact, 45° Support Structure 2-224
Figure 2-288. Finite Element Mesh for the SC-2, CGOC Impact, 0° Support Structure 2-225
Figure 2-289. Finite Element Mesh for the SC-2, CGOC Impact, 0° Support Structure – Final Displacement 2-225
Figure 2-290. Kinetic Energy Time History for the SC-2, CGOC Impact, 0° Support Structure 2-226
Figure 2-291. Plot of EQPS in the TB-1 for the SC-2, CGOC Impact, 0° Support Structure 2-226
Figure 2-292. Plot of von Mises Stress in the TB-1 for the SC-2, CGOC Impact, 0° Support Structure 2-227
Figure 2-293. Plot of Contact Forces in the TB-1 for the SC-2, CGOC Impact, 0° Support Structure 2-227
Figure 2-294. Finite Element Mesh for the SC-2, CGOC Impact, 45° Support Structure 2-228
Figure 2-295. Finite Element Mesh for the SC-2, CGOC Impact, 45° Support Structure – Final Displacement 2-229
Figure 2-296. Kinetic Energy Time History for the SC-2, CGOC Impact, 45° Support Structure 2-229
Figure 2-297. Plot of EQPS in the TB-1 for the SC-2, CGOC Impact, 45° Support Structure 2-230
Figure 2-298. Plot of von Mises Stress in the TB-1 for the SC-2, CGOC Impact, 45° Support Structure 2-230
Figure 2-299. Plot of Contact Forces in the TB-1 for the SC-2, CGOC Impact, 45° Support Structure 2-231
Figure 2-300. Finite Element Mesh for the SC-1, End Impact, 0° Support Structure, Be Contents 2-232
Figure 2-301. Finite Element Mesh for the SC-1, End Impact, 0° Support Structure, Be Contents – Final Displacement 2-232
Figure 2-302. Kinetic Energy Time History for the SC-1, End Impact, 0° Support Structure, Be Contents 2-233

Figure 2-303. Plot of EQPS in the TB-1 for the SC-1, End Impact, 0° Support Structure, Be Contents 2-233
Figure 2-304. Plot of von Mises Stress in the TB-1 for the SC-1, End Impact, 0° Support Structure, Be Contents 2-234
Figure 2-305. Finite Element Mesh for the SC-1, Side Impact, 0° Support Structure, Be Contents 2-235
Figure 2-306. Finite Element Mesh for the SC-1, Side Impact, 0° Support Structure, Be Contents – Final Displacement 2-235
Figure 2-307. Kinetic Energy Time History for the SC-1, Side Impact, 0° Support Structure, Be Contents 2-236
Figure 2-308. Graph of Average Stress Triaxiality versus EQPS of the Elements Exceeding the Experimental Strain Locus for the SC-1, Side Impact, 0° Support Structure, Be Contents 2-236
Figure 2-309. Graph of Average Stress Triaxiality versus EQPS of the Elements Exceeding the Experimental Strain Locus (Zoomed In) for the SC-1, Side Impact, 0° Support Structure, Be Contents 2-237
Figure 2-310. Graph of Tearing Parameter versus EQPS of the Elements Exceeding the Experimental Strain Locus for the SC-1, Side Impact, 0° Support Structure, Be Contents 2-237
Figure 2-311. Plot of the Elements Exceeding the Experimental Strain Locus for the SC-1, Side Impact, 0° Support Structure, Be Contents 2-238
Figure 2-312. Plot of the Elements Exceeding the Experimental Strain Locus for the SC-1, Side Impact, 0° Support Structure, Be Contents 2-238
Figure 2-313. Plot of EQPS in the TB-1 for the SC-1, Side Impact, 0° Support Structure, Be Contents 2-239
Figure 2-314. Plot of von Mises Stress in the TB-1 for the SC-1, Side Impact, 0° Support Structure, Be Contents 2-239
Figure 2-315. Finite Element Mesh for the SC-1, Side Impact, 45° Support Structure, Be Contents 2-240
Figure 2-316. Finite Element Mesh for the SC-1, Side Impact, 45° Support Structure, Be Contents – Final Displacement 2-241
Figure 2-317. Kinetic Energy Time History for the SC-1, Side Impact, 45° Support Structure, Be Contents 2-241
Figure 2-318. Graph of Average Stress Triaxiality versus EQPS of Elements Exceeding the Experimental Strain Locus for the SC-1, Side Impact, 45° Support Structure, Be Contents 2-242
Figure 2-319. Graph of Tearing Parameter versus EQPS of Elements Exceeding the Experimental Strain Locus for the SC-1, Side Impact, 45° Support Structure, Be Contents 2-242
Figure 2-320. Plot of Elements Exceeding the Experimental Strain Locus for the SC-1, Side Impact, 45° Support Structure, Be Contents 2-243
Figure 2-321. Plot of Elements Exceeding the Experimental Strain Locus for the SC-1, Side Impact, 45° Support Structure, Be Contents 2-243
Figure 2-322. Plot of EQPS in the TB-1 for the SC-1, Side Impact, 45° Support Structure, Be Contents 2-244

Figure 2-323. Plot of von Mises Stress in the TB-1 for the SC-1, Side Impact, 45° Support Structure, Be Contents 2-244
Figure 2-324. Finite Element Mesh for the SC-1, CGOC Impact, 0° Support Structure, Be Contents 2-245
Figure 2-325. Finite Element Mesh for the SC-1, CGOC Impact, 0° Support Structure, Be Contents – Final Displacement 2-246
Figure 2-326. Kinetic Energy Time History for the SC-1, CGOC Impact, 0° Support Structure, Be Contents 2-246
Figure 2-327. Plot of EQPS in the TB-1 for the SC-1, CGOC Impact, 0° Support Structure, Be Contents 2-247
Figure 2-328. Plot of von Mises Stress in the TB-1 for the SC-1, CGOC Impact, 0° Support Structure, Be Contents 2-247
Figure 2-329. Finite Element Mesh for the SC-1, CGOC Impact, 45° Support Structure, Be Contents 2-248
Figure 2-330. Finite Element Mesh for the SC-1, CGOC Impact, 45° Support Structure, Be Contents – Final Displacement 2-249
Figure 2-331. Kinetic Energy Time History for the SC-1, CGOC Impact, 45° Support Structure, Be Contents 2-249
Figure 2-332. Plot of EQPS in the TB-1 for the SC-1, CGOC Impact, 45° Support Structure, Be Contents 2-250
Figure 2-333. Plot of EQPS in the TB-1 for the SC-1, CGOC Impact, 45° Support Structure, Be Contents 2-250
Figure 2-334. Plot of von Mises Stress in the TB-1 for the SC-1, CGOC Impact, 45° Support Structure, Be Contents 2-251
Figure 2-335. Finite Element Mesh for the SC-2, Side Impact, 45° Support Structure, Friction 0.4 2-252
Figure 2-336. Finite Element Mesh for the SC-2, Side Impact, 45° Support Structure, Friction 0.4 – Final Displacement 2-253
Figure 2-337. Kinetic Energy Time History for the SC-2, Side Impact, 45° Support Structure, Friction 0.4 2-253
Figure 2-338. Graph of Average Stress Triaxiality versus EQPS of Elements Exceeding the Experimental Strain Locus for the SC-2, Side Impact, 45° Support Structure, Friction 0.4 2-254
Figure 2-339. Graph of Tearing Parameter versus EQPS of Elements Exceeding the Experimental Strain Locus for the SC-2, Side Impact, 45° Support Structure, Friction 0.4 2-254
Figure 2-340. Plot of Elements Exceeding the Experimental Strain Locus for the SC-2, Side Impact, 45° Support Structure, Friction 0.4 2-255
Figure 2-341. Plot of Elements Exceeding the Experimental Strain Locus for the SC-2, Side Impact, 45° Support Structure, Friction 0.4 2-255
Figure 2-342. Plot of Elements Exceeding the Experimental Strain Locus for the SC-2, Side Impact, 45° Support Structure, Friction 0.4 2-256
Figure 2-343. Plot of EQPS in the TB-1 for the SC-2, Side Impact, 45° Support Structure, Friction 0.4 2-256
Figure 2-344. Plot of EQPS in the TB-1 for the SC-2, Side Impact, 45° Support Structure, Friction 0.4 2-257

Figure 2-345. Plot of von Mises Stress in the TB-1 for the SC-2, Side Impact, 45° Support Structure, Friction 0.4 2-257
Figure 2-346. Finite Element Mesh for the SC-2, Side Impact, 45° Support Structure, Friction 0.2 2-259
Figure 2-347. Finite Element Mesh for the SC-2, Side Impact, 45° Support Structure, Friction 0.2 – Final Displacement 2-259
Figure 2-348. Kinetic Energy Time History for the SC-2, Side Impact, 45° Support Structure, Friction 0.2 2-260
Figure 2-349. Graph of Average Stress Triaxiality versus EQPS of Elements Exceeding the Experimental Strain Locus for the SC-2, Side Impact, 45° Support Structure, Friction 0.2 2-260
Figure 2-350. Graph of Tearing Parameter versus EQPS of Elements Exceeding the Experimental Strain Locus for the SC-2, Side Impact, 45° Support Structure, Friction 0.2 2-261
Figure 2-351. Plot of Elements Exceeding the Experimental Strain Locus for the SC-2, Side Impact, 45° Support Structure, Friction 0.2 2-261
Figure 2-352. Plot of Elements Exceeding the Experimental Strain Locus for the SC-2, Side Impact, 45° Support Structure, Friction 0.2 2-262
Figure 2-353. Plot of EQPS in the TB-1 for the SC-2, Side Impact, 45° Support Structure, Friction 0.2 2-262
Figure 2-354. Plot of EQPS in the TB-1 for the SC-2, Side Impact, 45° Support Structure, Friction 0.2 2-263
Figure 2-355. Plot of von Mises Stress in the TB-1 for the SC-2, Side Impact, 45° Support Structure, Friction 0.2 2-263
Figure 2-356. Summary Plot of Lid Retaining Forces and Component Impulse Loads 2-267
Figure 2-357. Summary Plot of Plastic Stress Triaxiality for Selected Runs 2-267
Figure 2-358. Finite Element Mesh for HAC Run 1, SC-2, End Impact 2-270
Figure 2-359. Finite Element Mesh for HAC Run 1, SC-2, End Impact – Final Displacement 2-271
Figure 2-360. Kinetic Energy Time History for HAC Run 1, SC-2, End Impact 2-271
Figure 2-361. Tresca Stress in TB-1 for HAC Run 1, SC-2, End Impact 2-272
Figure 2-362. Tresca Stress of TB-1 for HAC Run 1, SC-2, End Impact 2-272
Figure 2-363. Tresca Stress of TB-1 for HAC Run 1, SC-2, End Impact when Plate Velocity Reaches Zero 2-273
Figure 2-364. Finite Element Mesh for HAC Run 2, SC-2, Side Impact, Support Structure 0° 2-274
Figure 2-365. Finite Element Mesh for HAC Run 2, SC-2, Side Impact, Support Structure 0° - Final Displacement 2-274
Figure 2-366. Kinetic Energy Time History for HAC Run 2, SC-2, Side Impact, Support Structure 0° 2-275
Figure 2-367. Graph of Average Stress Triaxiality versus EQPS for Element Exceeding Experimental Strain Locus for HAC Run 2, SC-2, Side Impact, Support Structure 0° 2-275
Figure 2-368. Graph of Average Stress Triaxiality versus EQPS for Element Exceeding Experimental Strain Locus (Zoomed In) for HAC Run 2, SC-2, Side Impact, Support Structure 0° 2-276

Figure 2-369. Graph of Tearing Parameter versus EQPS for Element Exceeding Experimental Strain Locus for HAC Run 2, SC-2, Side Impact, Support Structure 0° 2-276
Figure 2-370. Plot of Element Exceeding Experimental Strain Locus for HAC Run 2, SC 2, Side Impact, Support Structure 0° 2-277
Figure 2-371. Graph of EQPS in the TB-1 for HAC Run 2, SC-2, Side Impact, Support Structure 0° 2-277
Figure 2-372. Plot of Tresca Stress in the TB-1 for HAC Run 2, SC-2, Side Impact, Support Structure 0° 2-278
Figure 2-373. Plot of Tresca Stress in the TB-1 for HAC Run 2, SC-2, Side Impact, Support Structure 0° when Plate Velocity Reaches Zero 2-278
Figure 2-374. Finite Element Mesh for HAC Run 3, SC-2, Side Impact, Support Structure 45° 2-279
Figure 2-375. Finite Element Mesh for HAC Run 3, SC-2, Side Impact, Support Structure 45° - Final Displacement 2-280
Figure 2-376. Kinetic Energy Time History for HAC Run 3, SC-2, Side Impact, Support Structure 45° 2-280
Figure 2-377. Graph of Average Stress Triaxiality versus EQPS of Element Exceeding Experimental Strain Locus for HAC Run 3, SC-2, Side Impact, Support Structure 45° 2-281
Figure 2-378. Graph of Tearing Parameter versus EQPS of Element Exceeding Experimental Strain Locus (Zoomed In) for HAC Run 3, SC-2, Side Impact, Support Structure 45° 2-281
Figure 2-379. Plot of Element Exceeding Experimental Strain Locus for HAC Run 3, SC 2, Side Impact, Support Structure 45° 2-282
Figure 2-380. Plot of EQPS in the TB-1 for HAC Run 3, SC-2, Side Impact, Support Structure 45° 2-282
Figure 2-381. Plot of Tresca Stress in the TB-1 for HAC Run 3, SC-2, Side Impact, Support Structure 45° 2-283
Figure 2-382. Plot of Tresca Stress in the TB-1 for HAC Run 3, SC-2, Side Impact, Support Structure 45° 2-283
Figure 2-383. Plot of Tresca Stress in the TB-1 for HAC Run 3, SC-2, Side Impact, Support Structure 45° when Plate Velocity Reaches Zero 2-284
Figure 2-384. Finite Element Mesh for HAC Run 4, SC-2, CGOC Impact, Support Structure 0° 2-285
Figure 2-385. Finite Element Mesh for HAC Run 4, SC-2, CGOC Impact, Support Structure 0°, Final Displacement 2-285
Figure 2-386. Kinetic Energy Time History for HAC Run 4, SC-2, CGOC Impact, Support Structure 0° 2-286
Figure 2-387. Plot of EQPS in TB-1 for HAC Run 4, SC-2, CGOC Impact, Support Structure 0° 2-286
Figure 2-388. Plot of Tresca Stress in TB-1 for HAC Run 4, SC-2, CGOC Impact, Support Structure 0° 2-287
Figure 2-389. Plot of Tresca Stress in the TB-1 for HAC Run 4, SC-2, CGOC Impact, Support Structure 0° when Plate Velocity Reaches Zero 2-287

Figure 2-390. Finite Element Mesh for HAC Run 5, SC-2, CGOC Impact, Support Structure 45° 2-288
Figure 2-391. Finite Element Mesh for HAC Run 5, SC-2, CGOC Impact, Support Structure 45° - Final Displacement 2-289
Figure 2-392. Kinetic Energy Time History for HAC Run 5, SC-2, CGOC Impact, Support Structure 45° 2-289
Figure 2-393. Plot of Tresca Stress in the TB-1 for HAC Run 5, SC-2, CGOC Impact, Support Structure 45° when Stress is a Maximum 2-290
Figure 2-394. Finite Element Mesh for HAC Run 6, SC-1, End Impact, Support Structure 0° 2-291
Figure 2-395. Finite Element Mesh for HAC Run 6, SC-1, End Impact, Support Structure 0° - Final Displacement 2-291
Figure 2-396. Kinetic Energy Time History for HAC Run 6, SC-1, End Impact, Support Structure 0° 2-292
Figure 2-397. Plot of Tesca Stress in the TB-1 for HAC Run 6, SC-1, End Impact, Support Structure 0° 2-292
Figure 2-398. Plot of Tresca Stress in the TB-1 for HAC Run 6, SC-1, End Impact, Support Structure 0° when Plate Velocity Reaches Zero 2-293
Figure 2-399. Finite Element Mesh for HAC Run 7, SC-1, Side Impact, Support Structure 0°. 2-294
Figure 2-400. Finite Element Mesh for HAC Run 7, SC-1, Side Impact, Support Structure 0° - Final Displacement 2-294
Figure 2-401. Kinetic Energy Time History for HAC Run 7, SC-1, Side Impact, Support Structure 0° 2-295
Figure 2-402. Plot of EQPS in TB-1 for HAC Run 7, SC-1, Side Impact, Support Structure 0° 2-295
Figure 2-403. Plot of Tresca Stress in the TB-1 for HAC Run 7, SC-1, Side Impact, Support Structure 0° 2-296
Figure 2-404. Plot of Tresca Stress in the TB-1 for HAC Run 7, SC-1, Side Impact, Support Structure 0° when Plate Velocity Reaches Zero 2-296
Figure 2-405. Finite Element Mesh for HAC Run 8, SC-1, Side Impact, Support Structure 45° 2-297
Figure 2-406. Finite Element Mesh for HAC Run 8, SC-1, Side Impact, Support Structure 45° - Final Displacement 2-298
Figure 2-407. Kinetic Energy Time History for HAC Run 8, SC-1, Side Impact, Support Structure 45° 2-298
Figure 2-408. Plot of EQPS in TB-1 for HAC Run 8, SC-1, Side Impact, Support Structure 45° 2-299
Figure 2-409. Plot of Tresca Stress in TB-1 for HAC Run 8, SC-1, Side Impact, Support Structure 45° 2-299
Figure 2-410. Plot of Tresca Stress in TB-1 for HAC Run 8, SC-1, Side Impact, Support Structure 45° 2-300
Figure 2-411. Plot of Tresca Stress in TB-1 for HAC Run 8, SC-1, Side Impact, Support Structure 45° when Plate Velocity Reaches Zero 2-300
Figure 2-412. Finite Element Mesh for HAC Run 9, SC-1, CGOC Impact, Support Structure 0° 2-301

Figure 2-413. Finite Element Mesh for HAC Run 9, SC-1, CGOC Impact, Support Structure 0° - Final Displacement 2-302
Figure 2-414. Kinetic Energy Time History for HAC Run 9, SC-1, CGOC Impact, Support Structure 0° 2-302
Figure 2-415. Tresca Stress for HAC Run 9, SC-1, CGOC Impact, Support Structure 0° 2-303
Figure 2-416. Plot of Tresca Stress in the TB-1 for HAC Run 9, SC-1, CGOC Impact, Support Structure 0° when Plate Velocity Reaches Zero 2-303
Figure 2-417. Finite Element Mesh for HAC Run 10, SC-1, CGOC Impact, Support Structure 45° 2-304
Figure 2-418. Finite Element Mesh for HAC Run 10, SC-1, CGOC Impact, Support Structure 45° - Final Displacement 2-305
Figure 2-419. Kinetic Energy Time History for HAC Run 10, SC-1, CGOC Impact, Support Structure 45° 2-305
Figure 2-420. Plot of Tresca Stress in the TB-1 for HAC Run 10, SC-1, CGOC Impact, Support Structure 45° 2-306
Figure 2-421. Plot of Tresca Stress in the TB-1 for HAC Run 10, SC-1, CGOC Impact, Support Structure 45° when Plate Velocity Reaches Zero 2-306
Figure 2-422. Finite Element Mesh for HAC Run 11, 831 g Plutonium Metal Hollow Cylinder, End Impact 2-307
Figure 2-423. Finite Element Mesh for HAC Run 11, 831 g, Plutonium Metal Hollow Cylinder, End Impact – Final Displacement 2-308
Figure 2-424. Kinetic Energy Time History for HAC Run 11, 831 g, Plutonium Metal Hollow Cylinder, End Impact 2-308
Figure 2-425. Plot of EQPS in the TB-1 for HAC Run 11, 831 g, Plutonium Metal Hollow Cylinder, End Impact 2-309
Figure 2-426. Plot of Tresca Stress in the TB-1 for HAC Run 11, 831 g, Plutonium Metal Hollow Cylinder, End Impact 2-309
Figure 2-427. Plot of Tresca Stress in the TB-1 for HAC Run 11, 831 g Plutonium Metal Hollow Cylinder, End Impact when Plate Velocity Reaches Zero 2-310
Figure 2-428. Finite Element Mesh for HAC Run 12, 831 g, Plutonium Metal Hollow Cylinder, Side Impact 2-311
Figure 2-429. Finite Element Mesh for HAC Run 12, 831 g, Plutonium Metal Hollow Cylinder, Side Impact – Final Displacement 2-311
Figure 2-430. Kinetic Energy Time History for HAC Run 12, 831 g, Plutonium Metal Hollow Cylinder, Side Impact 2-312
Figure 2-431. Plot of EQPS in the TB-1 for HAC Run 12, 831 g, Plutonium Metal Hollow Cylinder, Side Impact 2-312
Figure 2-432. Plot of Tresca Stress in the TB-1 for HAC Run 12, 831 g Plutonium Metal Hollow Cylinder, Side Impact 2-313
Figure 2-433. Plot of Tresca Stress for HAC Run 12, 831 g Plutonium Metal Hollow Cylinder, Side Impact 2-313
Figure 2-434. Plot of Tresca Stress for HAC Run 12, 831 g Plutonium Metal Hollow Cylinder, Side Impact when Plate Velocity Reaches Zero 2-314
Figure 2-435. Finite Element Mesh for HAC Run 13, 831 g, Angled, Plutonium Metal Hollow Cylinder, End Impact 2-315

Figure 2-436. Finite Element Mesh for HAC Run 13, 831 g, Angled, Plutonium Metal Hollow Cylinder, End Impact – Final Displacement....2-315
Figure 2-437. Kinetic Energy Time History for HAC Run 13, 831 g, Angled, Plutonium Metal Hollow Cylinder, End Impact....2-316
Figure 2-438. Plot of EQPS in the TB-1 for HAC Run 13, 831 g, Angled, Plutonium Metal Hollow Cylinder, End Impact....2-316
Figure 2-439. Plot of Tresca Stress in the TB-1 for HAC Run 13, 831 g, Angled, Plutonium Metal Hollow Cylinder, End Impact....2-317
Figure 2-440. Plot of Tresca Stress in the TB-1 for HAC Run 13, 831 g Angled Plutonium Metal Hollow Cylinder, End Impact when Plate Velocity Reaches Zero....2-317
Figure 2-441. Finite Element Mesh for HAC Run 14, 831 g, Angled, Plutonium Metal Hollow Cylinder, Side Impact....2-318
Figure 2-442. Finite Element Mesh for HAC Run 14, 831 g, Angled, Plutonium Metal Hollow Cylinder, Side Impact – Final Displacement....2-319
Figure 2-443. Kinetic Energy Time History for HAC Run 14, 831 g Angled Plutonium Metal Hollow Cylinder, Side Impact....2-319
Figure 2-444. Plot of EQPS in the TB-1 for HAC Run 14, 831 g Angled Plutonium Metal Hollow Cylinder, Side Impact....2-320
Figure 2-445. Plot of Tresca Stress in the TB-1 for HAC Run 14, 831 g, Angled, Plutonium Metal Hollow Cylinder, Side Impact....2-320
Figure 2-446. Plot of Tresca Stress in the TB-1 for HAC Run 14, 831 g Angled Plutonium Metal Hollow Cylinder, Side Impact when Plate Velocity Reaches Zero....2-321
Figure 2-447. Finite Element Mesh for HAC Run 15, 831 g Angled Plutonium Metal Hollow Cylinder, CGOC Impact....2-322
Figure 2-448. Finite Element Mesh for HAC Run 15, 831 g, Angled Plutonium Metal Hollow Cylinder, CGOC Impact – Final Displacement....2-322
Figure 2-449. Kinetic Energy Time History for HAC Run 15, 831 g Angled Plutonium Metal Hollow Cylinder, CGOC Impact....2-323
Figure 2-450. Plot of Tresca Stress in the TB-1 for HAC Run 15, 831 g Angled Plutonium Metal Hollow Cylinder, CGOC Impact....2-323
Figure 2-451. Plot of Tresca Stress in the TB-1 for HAC Run 15, 831 g Angled Plutonium Metal Hollow Cylinder, CGOC Impact when Plate Velocity Reaches Zero....2-324
Figure 2-452. Finite Element Mesh for HAC Run 16, 731 g, Plutonium Metal Hollow Cylinder, End Impact....2-325
Figure 2-453. Finite Element Mesh for HAC Run 16, 731 g, Plutonium Metal Hollow Cylinder, End Impact – Final Displacement....2-325
Figure 2-454. Kinetic Energy Time History for HAC Run 16, 731 g, Plutonium Metal Hollow Cylinder, End Impact....2-326
Figure 2-455. Plot of EQPS in the TB-1 for HAC Run 16, 731 g, Plutonium Metal Hollow Cylinder, End Impact....2-326
Figure 2-456. Plot of EQPS in the TB-1 for HAC Run 16, 731 g, Plutonium Metal Hollow Cylinder, End Impact....2-327
Figure 2-457. Plot of Tresca Stress in the TB-1 for HAC Run 16, 731 g, Plutonium Metal Hollow Cylinder, End Impact....2-327
Figure 2-458. Plot of Tresca Stress in the TB-1 for HAC Run 16, 731 g Plutonium Metal Hollow Cylinder, End Impact when Plate Velocity Reaches Zero....2-328

Figure 2-459. Finite Element Mesh for HAC Run 17, 731 g, Plutonium Metal Hollow Cylinder, Side Impact 2-329
Figure 2-460. Finite Element Mesh for HAC Run 17, 731 g, Plutonium Metal Hollow Cylinder, Side Impact – Final Displacement 2-329
Figure 2-461. Kinetic Energy Time History for HAC Run 17, 731 g, Plutonium Metal Hollow Cylinder, Side Impact 2-330
Figure 2-462. Plot of EQPS in the TB-1 for HAC Run 17, 731 g, Plutonium Metal Hollow Cylinder, Side Impact 2-330
Figure 2-463. Plot of Tresca Stress in the TB-1 for HAC Run 17, 731 g, Plutonium Metal Hollow Cylinder, Side Impact 2-331
Figure 2-464. Plot of Tresca Stress in the TB-1 for HAC Run 17, 731 g, Plutonium Metal Hollow Cylinder, Side Impact 2-331
Figure 2-465. Plot of Tresca Stress in the TB-1 for HAC Run 17, 731 g Plutonium Metal Hollow Cylinder, Side Impact when Plate Velocity Reaches Zero 2-332
Figure 2-466. Finite Element Mesh for HAC Run 18, 731 g, Angled, Plutonium Metal Hollow Cylinder, End Impact 2-333
Figure 2-467. Finite Element Mesh for HAC Run 18, 731 g, Angled, Plutonium Metal Hollow Cylinder, End Impact – Final Displacement 2-333
Figure 2-468. Kinetic Energy Time History for HAC Run 18, 731 g, Angled, Plutonium Metal Hollow Cylinder, End Impact 2-334
Figure 2-469. Plot of EQPS in the TB-1 for HAC Run 18, 731 g, Angled, Plutonium Metal Hollow Cylinder, End Impact 2-334
Figure 2-470. Plot of Tresca Stress in the TB-1 for HAC Run 18, 731 g, Angled, Plutonium Metal Hollow Cylinder, End Impact 2-335
Figure 2-471. Plot of Tresca Stress in the TB-1 for HAC Run 18, 731 g, Angled, Plutonium Metal Hollow Cylinder, End Impact 2-335
Figure 2-472. Plot of Tresca Stress in the TB-1 for HAC Run 18, 731 g Angled Plutonium Metal Hollow Cylinder, End Impact when Plate Velocity Reaches Zero 2-336
Figure 2-473. Finite Element Mesh for HAC Run 19, 731 g, Angled, Plutonium Metal Hollow Cylinder, Side Impact 2-337
Figure 2-474. Finite Element Mesh for HAC Run 19, 731 g, Angled, Plutonium Metal Hollow Cylinder, Side Impact – Final Displacement 2-337
Figure 2-475. Kinetic Energy Time History for HAC Run 19, 731 g, Angled, Plutonium Metal Hollow Cylinder, Side Impact 2-338
Figure 2-476. Graph of Average Stress Triaxiality versus EQPS for Elements Exceeding the Experimental Strain Locus for HAC Run 19, 731 g, Angled, Plutonium Metal Hollow Cylinder, Side Impact 2-338
Figure 2-477. Graph of Average Stress Triaxiality versus EQPS for Elements Exceeding the Experimental Strain Locus (Zoomed In) for HAC Run 19, 731 g, Angled, Plutonium Metal Hollow Cylinder, Side Impact 2-339
Figure 2-478. Graph of Tearing Parameter versus EQPS for Elements Exceeding the Experimental Strain Locus for HAC Run 19, 731 g, Angled, Plutonium Metal Hollow Cylinder, Side Impact 2-339
Figure 2-479. Plot of Elements Exceeding the Experimental Strain Locus for HAC Run 19, 731 g, Angled, Plutonium Metal Hollow Cylinder, Side Impact 2-340

Figure 2-480. Plot of EQPS in the TB-1 for HAC Run 19, 731 g, Angled, Plutonium Metal Hollow Cylinder, Side Impact 2-340
Figure 2-481. Plot of Tresca Stress in the TB-1 for HAC Run 19, 731 g, Angled, Plutonium Metal Hollow Cylinder, Side Impact 2-341
Figure 2-482. Plot of Tresca Stress in the TB-1 for HAC Run 19, 731 g, Angled, Plutonium Metal Hollow Cylinder, Side Impact 2-341
Figure 2-483. Plot of Tresca Stress in the TB-1 for HAC Run 19, 731 g Angled Plutonium Metal Hollow Cylinder, Side Impact when Plate Velocity Reaches Zero 2-342
Figure 2-484. Finite Element Mesh for HAC Run 20, 731 g, Angled, Plutonium Metal Hollow Cylinder, CGOC Impact 2-343
Figure 2-485. Finite Element Mesh for HAC Run 20, 731 g, Angled, Plutonium Metal Hollow Cylinder, CGOC Impact – Final Displacement 2-343
Figure 2-486. Kinetic Energy Time History for HAC Run 20, 731 g, Angled, Plutonium Metal Hollow Cylinder, CGOC Impact 2-344
Figure 2-487. Plot of EQPS in the TB-1 for HAC Run 20, 731 g, Angled, Plutonium Metal Hollow Cylinder, CGOC Impact 2-344
Figure 2-488. Plot of Tresca Stress in the TB-1 for HAC Run 20, 731 g, Angled, Plutonium Metal Hollow Cylinder, CGOC Impact 2-345
Figure 2-489. Plot of Tresca Stress in the TB-1 for HAC Run 20, 731 g Angled Plutonium Metal Hollow Cylinder, CGOC Impact when Plate Velocity Reaches Zero 2-345
Figure 2-490. Finite Element Mesh for 30-ft Drop Run 1 – SC-2 with Support Structure Rotated 45 Degrees and Side Impact 2-346
Figure 2-491. Final Displacement in Finite Element Mesh for 30-ft Drop Run 1 – SC-2 with Support Structure Rotated 45 Degrees and Side Impact 2-347
Figure 2-492. Final Displacement in SAR Test for 30-ft Drop 2-347
Figure 2-493. Kinetic Energy for 30-ft Drop Run 1 – SC-2 with Support Structure Rotated 45 Degrees and Side Impact 2-348
Figure 2-494. EQPS in the T-Amp for 30-ft Drop Run 1 – SC-2 with Support Structure Rotated 45 Degrees and Side Impact 2-348
Figure 2-495. Tresca Stress in the TB-1 for 30-ft Drop Run 1 – SC-2 with Support Structure Rotated 45 Degrees and Side Impact 2-349
Figure 2-496. Finite Element Mesh for 30-ft Drop Run 2 – Angled 831 g Plutonium Metal Hollow Cylinder with End Impact 2-350
Figure 2-497. Final Displacement for 30-ft Drop Run 2 – Angled 831 g Plutonium Metal Hollow Cylinder with End Impact 2-350
Figure 2-498. Kinetic Energy for 30-ft Drop Run 2 – Angled 831 g Plutonium Metal Hollow Cylinder with End Impact 2-351
Figure 2-499. EQPS in TB-1 for 30-ft Drop Run 2 – Angled 831 g Plutonium Metal Hollow Cylinder with End Impact 2-351
Figure 2-500. Tresca Stress in the TB-1 for 30-ft Drop Run 2 – Angled 831 g Plutonium Metal Hollow Cylinder with End Impact 2-352
Figure 2-501. Finite Element Mesh for 30-ft Drop Run 3 – Angled 831 g Plutonium Metal Hollow Cylinder with CGOC Impact 2-353
Figure 2-502. Final Displacement for 30-ft Drop Run 3 – Angled 831 g Plutonium Metal Hollow Cylinder with CGOC Impact 2-353

Figure 2-503. Kinetic Energy for 30-ft Drop Run 3 – Angled 831 g Plutonium Metal Hollow Cylinder with CGOC Impact 2-354
Figure 2-504. Tresca Stress in the TB-1 for 30-ft Drop Run 3 – Angled 831 g Plutonium Metal Hollow Cylinder with CGOC Impact 2-354
Figure 2-505. Contact Forces on the Top Surface of the TB-1 Lid 2-356
Figure 2-506. Contact Forces on the Top Surface of the TB-1 Lid Along with Impulse Loads from Various Contents 2-357

Figure 3-1. Schematic of Assumed Worst-Case Heating-to-the-Seal Scenario 3-3
Figure 3-2. Schematic of Approximated Projected Heating Area [m=0.0254*in.; m2=6.45x10-4*in.2] 3-3
Figure 3-3. Finite Element Mesh of the PAT-1 Half-Symmetry Thermal Model and Enlarged Load Spreader, Copper Cylinder, TB-1, and T-Ampoule 3-9
Figure 3-4. Low-Temperature Thermal Test Simulation Results. (°C=[°F-32]/1.8) 3-11
Figure 3-5. Seven-day Thermal Cycling for Quasi-Steady-State Analysis – Package Mid Height Response (°C=[°F-32]/1.8) 3-12
Figure 3-6. NCT Daily Thermal Cycle (Quasi-Steady-State NCT Solution) – Package Mid Height Response (°C=[°F-32]/1.8) 3-12
Figure 3-7. Temperature Distribution of PAT-1 Just Before Sundown – Most Severe Case of Transient NCT SAR1 Analysis (Plot of ¼ of Package, °C=[°F-32]/1.8) 3-13
Figure 3-8. Temperature Distribution of PAT-1 – Steady-State NCT SAR1 Analysis (Plot of ¼ of Package, °C=[°F-32]/1.8) 3-13
Figure 3-9. NCT Steady-State Temperature Distribution (°C=[°F-32]/1.8) 3-14
Figure 3-10. Steady-State Analysis in the Shade – 10 CFR 71.43(g) (°C=[°F-32]/1.8) 3-15
Figure 3-11. Temperature Distribution of the Verification Model at the End of the 52 Minute Fire — Complete Model (°C=[°F-32]/1.8) 3-19
Figure 3-12. Temperature Distribution of the Verification Model at the End of the 52 Minute Fire — T-Ampoule, TB-1, Heat Transfer Cu Cylinder, and Aluminum Load Spreader (°C=[°F-32]/1.8) 3-19
Figure 3-13. Temperature Distribution of the Verification Model at t=352 Minutes (300 Minutes after the 52 Minute Fire) — Complete Model (°C=[°F-32]/1.8) 3-20
Figure 3-14. Temperature Distribution of the Verification Model at t=352 Minutes (300 Minutes after the 52 Minute Fire) — T-Ampoule, TB-1, Heat Transfer Cu Cylinder, and Aluminum Load Spreader (°C=[°F-32]/1.8) 3-20
Figure 3-15. Temperature History at T-Ampoule Seal Height for the 52-Minute Fire Model Verification Exercise (°C=[°F-32]/1.8). Note: In the schematic above the plot, the reference yellow line crosses the cask at the T-Ampoule-seal height and the white dots are the approximate locations of the temperature history lines in the plot. The "T-Ampoule (Seal)" curve is completely covered by the "TB-1" curve. 3-22
Figure 3-16. Temperature Distribution at the End of the 30 Minute Regulatory Fire — Complete Model (°C=[°F-32]/1.8) 3-23
Figure 3-17. Temperature Distribution at the End of the 30 Minute Regulatory Fire — T-Ampoule, TB-1, Heat Transfer Cu Cylinder, and Aluminum Load Spreader (°C=[°F-32]/1.8) 3-24

Figure 3-18. Temperature Distribution at t=290 Minutes (260 Minutes after the 30 Minute Fire) — Complete Model (°C=[°F-32]/1.8) 3-24
Figure 3-19. Temperature Distribution at t=290 Minutes (260 Minutes after the 30 Minute Fire) — T-Ampoule, TB-1, Heat Transfer Cu Cylinder, and Aluminum Load Spreader (°C=[°F-32]/1.8) 3-25
Figure 3-20. Temperature History at T-Ampoule Seal Height for the 30-Minute Regulatory Fire (°C=[°F-32]/1.8). Note: In the schematic above the plot, the reference yellow line crosses the cask at T-Ampoule-seal height and the white dots are the approximate locations of the temperature history lines in the plot. 3-26

Figure 4-1. TB-1 Containment Vessel and T-Ampoule Contents Container 4-2

Figure 5-1. Cylindrical Shielding Model of PAT-1 Used in This Analysis (see Table 5 6 for Dimensional Information) 5-7
Figure 5-2. Dose Locations Analyzed for the PAT-1 Package 5-11
Figure 5-3. Photon Source per Gram of Each Isotope of Pu Initially Present (Note That Pu-241 Data Includes Buildup of Am-241) 5-16
Figure 5-4. Neutron Source per Gram of Each Isotope of Pu Initially Present (Includes Both Spontaneous Fission and (α,n) Components with an Oxide Matrix; Also Note That Pu-241 Data Includes Buildup of Am-241) 5-17
Figure 5-5. Watts per Gram of Each Isotope of Pu Initially Present (Note That Pu-241 Data Includes Buildup of Am-241) 5-18

Figure 6-1. Detailed Model of a Single Package 6-5
Figure 6-2. Simplified Model of a Single Package 6-6
Figure 6-3. End-Impact Damaged Package Model 6-9
Figure 6-4. Side-Impact Damaged Package Model 6-10
Figure 6-5. HAC Single Package Model for 10 CFR 71.55(f) Analysis 6-11
Figure 6-6. Sensitivity of keff to Steel Density 6-15
Figure 6-7. Single Package Moderation Study 6-19
Figure 6-8. Normal Conditions of Transport – Square-Pitched Array 6-22
Figure 6-9. Normal Conditions of Transport – Square-Pitched Array Results 6-23
Figure 6-10. Normal Conditions of Transport – Hexagonal-Pitched Array 6-24
Figure 6-11. Normal Conditions of Transport – Hexagonal-Pitched Array Results 6-25
Figure 6-12. Damaged Packages – Side-Impact Hexagonal-Pitch Array, Top View 6-27
Figure 6-13. Damaged Packages – Side-Impact Square-Pitch Array, Top View 6-28
Figure 6-14. Damaged Packages – Side-Impact Nested Arrangement No. 1, Top View 6-29
Figure 6-15. Damaged Packages – Side-Impact Nested Arrangement No. 2, Top View 6-30
Figure 6-16. Damaged Packages – End-Impact Array, Repeated Layers, Side View 6-30
Figure 6-17. Damaged Packages – End-Impact Array, Alternating Layers, Side View 6-31
Figure 6-18. Damaged Packages – End-Impact Arrays, Repeated and Alternating Layers, Top View 6-31
Figure 6-19. Damaged Package Array Study 6-32
Figure 6-20. Damaged Package Array Internal (redwood zone) Moderation Study 6-33
Figure 6-21. Damaged Package TB-1 Location Study 6-34
Figure 6-22. Damaged Package External Moderation Study 6-35

Figure 6-23. Damaged Package External Moderation Study (Package Spacing Varied).....6-36
Figure 6-24. Single Package HAC for Air Transport.....6-38
Figure 6-25. Pu Metal Sphere Critical Benchmark Histogram.....6-52
Figure 6-27. Single Unit Solution Critical Benchmark Histogram.....6-55
Figure 6-28. Dry Lattice Critical Benchmark Histogram.....6-56
Figure 6-29. USLSTATS Plot for HEXSDRY Application of ck vs. keff.....6-57
Figure 6-30. USLSTATS Plot for OCTSDRY Application of ck vs. keff.....6-58
Figure 6-31. Spherical Segment Volume Calculations.....6-62

Figure 7-1. Assembled PAT-1 Showing AQ-1, TB-1, and T-Ampoule.....7-2

Figure 9-1 Organization Chart for PAT-1 Recertification.....9-3

LIST OF TABLES

Table 1-1. Payload and Contents Configurations.....1-13

Table 2-1. Weight of Plutonium Metal Contents and T-Ampoule and Packing for Six Loading Configurations.....2-2
Table 2-2. Load Combinations for NCT and HAC.....2-5
Table 2-3. Allowable Stresses for NCT and HAC Based on Regulatory Guide 7.6 (Room Temperature).....2-7
Table 2-4. Allowable Stresses for NCT and HAC Based on Regulatory Guide 7.6, (Elevated Temperatures).....2-7
Table 2-5. Approximate Weights of PAT-1 Package Components.....2-10
Table 2-6. Listing of Material for Each Component in the Finite Element Models.....2-12
Table 2-7. Normal Conditions of Transport (NCT) Impact Analyses (6), Components, and Orientations.....2-35
Table 2-8. Hypothetical Accident Condition (HAC) Dynamic Crush Analyses (20), Components, and Orientations.....2-35
Table 2-9. High Velocity (Aircraft) Impact Analyses (27), Components, and Orientations..2-36
Table 2-10. 30-ft Drop Impact Analyses (3), Components, and Orientations.....2-37
Table 2-11. High Velocity (Aircraft) Impact Analyses Peak Tearing Parameter Values.....2-39
Table 2-12. Redwood Orthotropic Crush Model Parameters.....2-49
Table 2-13. Power-Law Hardening Constitutive Model Parameters.....2-51
Table 2-14. Listing of Material for Each Components in the Finite Element Models.....2-90
Table 2-15. Redwood Orthotropic Crush Model Parameters.....2-91
Table 2-16. Maximum Strains in 4 ft End Drop Models.....2-119
Table 2-17. Maximum Strains in 4 ft Side Drop Models.....2-129
Table 2-18. Aircraft Accident Impact Analyses, Components, and Orientations.....2-132
Table 2-19. High Velocity (Aircraft) Impact Analyses Peak Tearing Parameter Values.....2-277
Table 2-20. Summary of Hypothetical Accident Condition (HAC) Dynamic Crush Analyses (20), Components, and Orientations.....2-281
Table 2-21. 30-ft Drop Impact Analyses (3), Components, and Orientations.....2-358

Table 3-1. Summary of Temperatures Under NCT and HAC.....3-4

Table 3-2. Summary of Maximum Pressures inside the T-Ampoule for NCT and HAC 3-4
Table 3-3. Thermophysical Properties Used to Represent Redwood 3-5
Table 3-4. Thermophysical Properties of the Titanium Ampoule (Ti 6Al-4V) 3-6
Table 3-5. Service Temperatures of Packaging Components and Content Inside the TB-1 ... 3-6
Table 3-6. Boundary Conditions Used for the "Heat" NCT Thermal Evaluation 3-9
Table 3-7. Comparison of Test and Analysis Temperatures – Low Temperature Test 3-11
Table 3-8. Boundary Conditions Used for the Transient Model Verification Exercise 3-16
Table 3-9. Grashof, Reynolds, Nusselt Numbers for Calm Wind, Open-Pool Fire Conditions 3-17
Table 3-10. Boundary Conditions Used for the HAC Thermal Evaluation 3-23
Table 3-11. Summary of Maximum Temperatures and Times for the HAC 3-27

Table 4-1. PAT-1 Package Post-Test Containment 4-3
Table 4-2. Regulatory Leakage Criteria for 1300 g Plutonium (Bounding Case) 4-5
Table 4-3. 831 g (1.83 lb): 3,000 A2 Quantity of ER Plutonium Metal Assuming No Pu-241 Decay to Am-241 4-9
Table 4-4. 707 g (1.56 lb): 3,000 A2 Quantity of ER Plutonium Metal Assuming 100% Pu-241 Decay to Am-241 4-9
Table 4-5. 676 g (1.49 lb): Alloyed Plutonium Metal Assuming 100% Pu-241 Decay to Am-241 4-10
Table 4-6. 676 g (1.49 lb): Alloyed Plutonium Metal Assuming No Pu-241 Decay to Am-241 4-10

Table 5-1. Summary Table of External Radiation Levels (Non-Exclusive Use) 5-2
Table 5-2. Plutonium Isotopics Used for Source Generation 5-3
Table 5-3. Gamma-Ray Source Used in the Shielding Analysis (2197 g Pu) 5-4
Table 5-4. Neutron Source Used in the Shielding Analysis (2197 g Pu) 5-5
Table 5-5. Dimensions of Materials Regions Used in Shielding Analyses 5-8
Table 5-6. Elemental Compositions Used in Shielding Analysis 5-9
Table 5-7. Neutron Flux-to-Dose Conversion Factors Used in Shielding Analysis 5-12
Table 5-8. Gamma Flux-to-Dose Conversion Factors Used in Shielding Analysis 5-13
Table 5-9. Source Geometry Optimization Dose Results (at PAT-1 Side Surface) 5-14
Table 5-10. Pu Isotope Wt % Under Various Depletion Scenarios 5-19
Table 5-11. Bounding Pu Isotope Mass Fraction Used in This Study 5-20
Table 5-12. Estimation of Degree of Overprediction in Bounding Pu Source Used in This Study 5-20
Table 5-13. Pu/Be Source Specification Used in This Study 5-21
Table 5-14. Neutron Source Spectrum Used in the Pu/Be Source Shielding Analysis 5-22
Table 5-15. Dose Results for Pu/Be Source Content 5-24

Table 6-1. Summary Table of Criticality Evaluation Results 6-2
Table 6-2. Material Specifications 6-11
Table 6-3. Stainless Steel PH 13-8 Mo Composition (wt %) 6-14
Table 6-4. Detailed Model, Plutonium Metal Sphere, Modeling Impact Study 6-20
Table 6-5. Detailed Model, Plutonium and Water Solution Cylinder, Modeling Impact Study 6-21

Table 6-6. Summary of Similarity Between Benchmark Configurations and Applications ... 6-46
Table 6-7. USL and Bias Data Summary ... 6-58
Table 6-8. List of Validation Critical Configurations ... 6-63
Table 6-9. Comparison of Tsunami Sensitivities and Direct Perturbation Sensitivities for a Representative Selection of Benchmark Critical Configurations ... 6-67
Table 6-10. Comparison of Direct Perturbation Sensitivities and Tsunami Sensitivities for the 11 Representative Applications ... 6-68
Table 6-11. Comparison of METAL SPHERE Applications to Critical Benchmarks ... 6-68
Table 6-12. Comparison of SOLUTION LATTICE Applications to Critical Benchmarks ... 6-69
Table 6-13. Comparison of SINGLE UNIT SOLUTION Applications to Critical Benchmarks ... 6-71
Table 6-14. Comparison of DRY LATTICE Applications to Critical Benchmarks ... 6-75
Table 6-15. Tabulation of Calculations Supporting the Standard Single Package Analysis for Normal Conditions of Transport and Hypothetical Accident Conditions ... 6-77
Table 6-16. Tabulation of Calculations Supporting the Analysis of Arrays of Undamaged Packages ... 6-87
Table 6-17. Tabulation of Calculations Supporting the Analysis of Arrays of Damaged Packages ... 6-102
Table 6-18. Tabulation of Calculations Supporting the Analysis of a Single Package of Fissile Material Intended for Air Transport ... 6-108
Table 6-19. Scoping Calculation Results for Single Packages ... 6-118
Table 6-20. Scoping Calculation Results for Normal Conditions of Transport Arrays ... 6-119
Table 6-21. Scoping Calculation Results for Hypothetical Accident Condition Arrays ... 6-120
Table 6-22. Scoping Calculation Results for Single Package, Air Transport Accident Provision ... 6-121
Table 6-23. Additional Scoping Calculation Results for Hypothetical Accident Condition Arrays ... 6-122

Table 7-1. Replacement Parts for the PAT-1 Packaging with T-Ampoule Assembly ... 7-6
Table 7-2. Parts List for T-Ampoule Loading ... 7-9
Table 7-3. Parts List for Loading the T-Ampoule into the TB-1 ... 7-15
Table 7-4. Parts List for Loading the TB-1 Containment Vessel into the AQ-1 Overpack ... 7-19

Table 8-1. T-Ampoule Components ... 8-1
Table 8-2. Acceptance Tests for T-Ampoule Components ... 8-3

Table 9-1. Relationship between QA Implementing Documents and Elements of 10 CFR 71, Subpart H ... 9-4
Table 9-2. Project Tasks and Quality Categories for PAT-1 Addendum ... 9-8
Table 9-3. QA Categories for Design and Procurement of T-Ampoule Assembly and Inner Packing ... 9-8
Table 9-4. Level of QA Control Per QA Element ... 9-9

1. GENERAL INFORMATION

1.1 Introduction

The Plutonium Air Transportable Package, Model PAT-1, is certified under Title 10, Code of Federal Regulations Part 71[1] by the U.S. Nuclear Regulatory Commission (NRC) per Certificate of Compliance (CoC) USA/0361B(U)F-96, (currently Revision 9).[2]

The primary components of the currently certified PAT-1 configuration include the PC-1 stainless steel inner container, the TB-1 stainless steel containment vessel (*Containment Vessel*[A] Drawing 1017, designated TB-1), and the AQ-1 protective overpack assembly (*Overpack, AQ*, Drawing 1002, designated AQ-1). The *Safety Analysis Report for the Plutonium Air Transportable Package, Model PAT-1*, NUREG-0361,[3] as supplemented by Issue B of Drawings 1004, 1009, 1013, 1016, 1017, 1019, 1020 and 1022, provides detailed material specifications and drawings of the current PAT-1 packaging components, and demonstrates compliance with 10 CFR 71.[1] Issue B versions of Drawings 1004, 1009, 1013, 1016, 1017, 1019, 1020 and 1022 are listed and provided in Section 1.3.2 of this Safety Analysis Report (SAR) Addendum. For the plutonium metal shipments described in this SAR Addendum, the O-ring in the TB-1 (Item 5 in Drawing 1017 of the SAR) is not used for shipping (See Section 1.3.4 for justification for excluding the O-ring, Section 7 for operating procedures, and Section 8 for procedures for acceptance testing.) The current authorized contents are plutonium oxide (PuO_2) and its daughter products, or a mixture of PuO_2 and uranium oxide (UO_2) and its daughter products, as further described in CoC USA/0361/B(U) F-96 Revision 9, Section 5.[2]

The purpose of this SAR Addendum is to incorporate plutonium (Pu) metal as a new payload for the PAT-1 package. The Pu metal is packed in an inner container (*T-Ampoule Assembly*, Drawing 2A0261, designated the T-Ampoule) that replaces the PC-1 inner container. The T-Ampoule and associated Pu metal contents packing configurations are further described in Section 1.2.1 and Section 1.2.2 of this addendum, respectively.

Based on the proposed maximum content of 831 g (1.83 lb) of plutonium metal, the PAT-1 with T-Ampoule is designated a Category I, Type B fissile material package, and the Criticality Safety Index (CSI) is 0.1. The Transportation Index (TI) is based on the maximum radiation level at a distance of 1 m (39.4 in.) from the external surface of the package and will be established each time a PAT-1 package is loaded with approved content. The actual TI measured at the time of shipment can be no greater than the calculated value of 2.5 (see Table 5-1). All other PAT-1 packaging component designs, currently authorized content mass and form, and 25 watt (85.3 Btu/hr) maximum decay heat remain unchanged from that documented in NUREG-0361.[3]

The documentation and results from analysis contained in this addendum demonstrate that the replacement of the PC-1 and associated packaging material with the T-Ampoule and associated packaging, and the addition of the plutonium metal content, are not significant with respect to the design, operating characteristics, or safe performance of the containment system and prevention of criticality when the package is subjected to the tests specified in 10 CFR 71.71, 71.73 and 71.74.

[A] The drawing titles are in italics and are used interchangeably with the designated names in this addendum. See Section 1.3.2 in this addendum and Chapter 9 in the SAR[3] for drawing number, title, and revision.

The Quality Assurance Program requirements for the PAT-1 package and the T-Ampoule are discussed in Section 9 of this addendum.

1.2 Package Description

1.2.1 Packaging

Details for the PAT-1 packaging components: AQ-1 overpack, TB-1 containment vessel, PC-1 inner container, and associated packing materials (which are unaffected by the packaging component design and content modifications addressed in this addendum), are contained in NUREG-0361 as supplemented by Issue B of Drawings 1004, 1009, 1013, 1016, 1017, 1019, 1020 and 1022. Note that the TB-1 O-ring (Item 5 in Drawing 1017) is not used for the plutonium metal shipments.

The difference between the PAT-1 with T-Ampoule configuration (see Figure 1-1) and the currently certified PAT-1 with PC-1 configuration is the PAT-1 with T-Ampoule configuration (see *PAT-1/TB-1/T-Ampoule Assembly* [Drawing R99794 in this addendum] and *TB-1/ T-Ampoule Shipping Vessel Assembly* [Drawing 2A0263 in this addendum]) consists of (1) a *T-Ampoule* (see Figure 1-2 and Drawing 2A0261 listed in Section 1.3.2) containing plutonium metals in the configurations illustrated in Figures 1-3 through 1-5, and (2) the *Ring, Filler* (Drawing 2A0262, designated Ring Filler). The PAT-1 with PC-1 configuration consists of the PC-1, aluminum honeycomb spacer, 2000 g (4.41 lb) authorized content, and associated packing material. The TB-1 O-ring is not used for the plutonium metal shipments. The weight of the PAT-1 packaging for plutonium oxide is presented in Section 1.2.1 and Section 2.2 of the SAR. The approximate weights from the SAR for the AQ-1 overpack, TB-1 containment vessel, PC-1 Product Can (including aluminum spacer), and contents is 225 kg (496 lb). The PAT-1 with T-Ampoule configuration is limited to the current certified TB-1 gross payload weight of 2100 g (4.7 lbs).

1.2.1.1 Ring Filler

The Ring Filler is used to fill the void space between the top of the T-Ampoule and the TB-1 closure lid. The Ring Filler is 10.72 cm (4.22 in.) in diameter, 1.27 cm (0.5 in.) thick, and is manufactured of titanium (Ti) alloy 6A1-4V (hereafter referred to as Ti-6A1-4V, Grade 5).

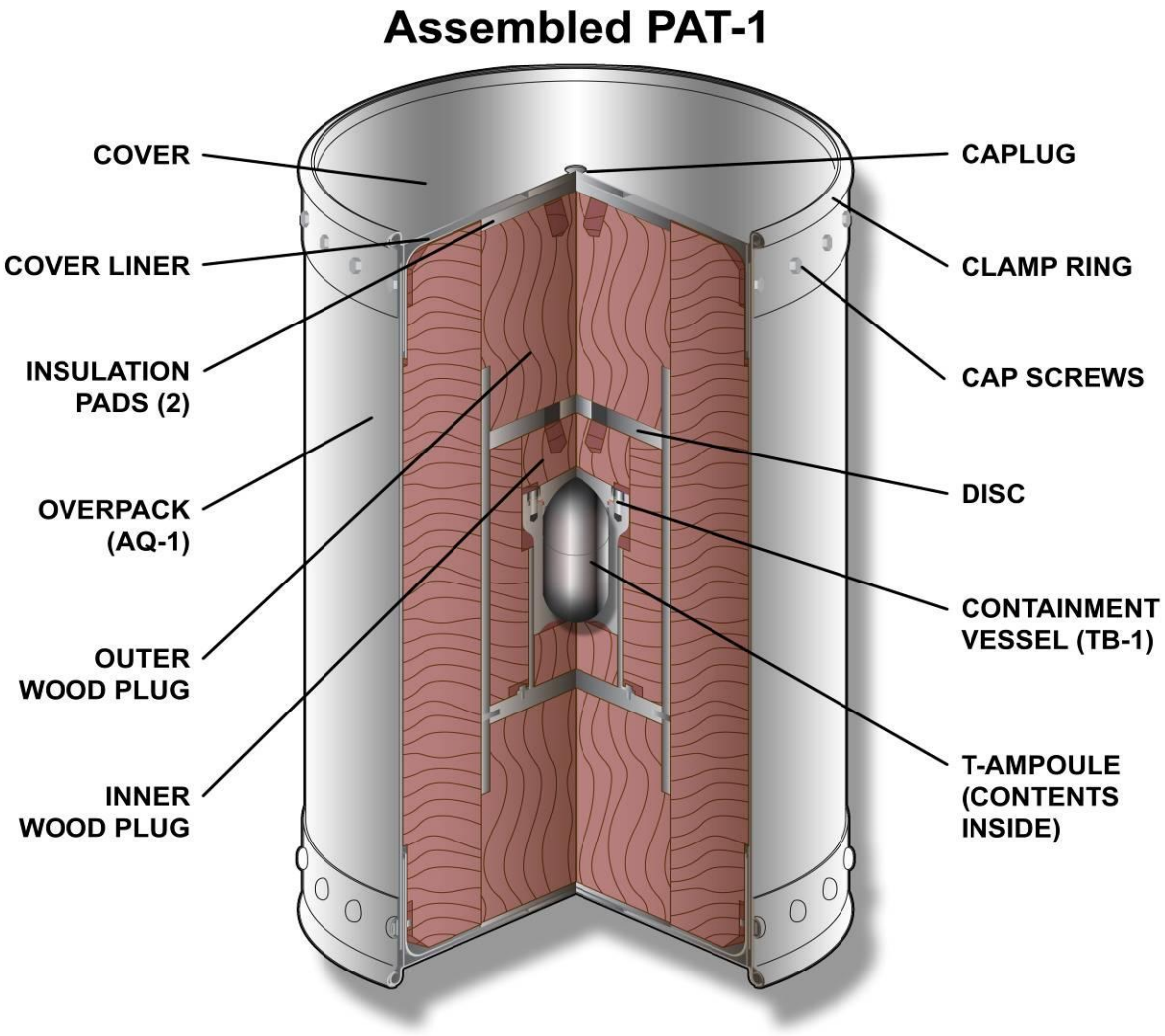

Figure 1-1. Assembled PAT-1 Showing AQ-1, TB-1, and T-Ampoule

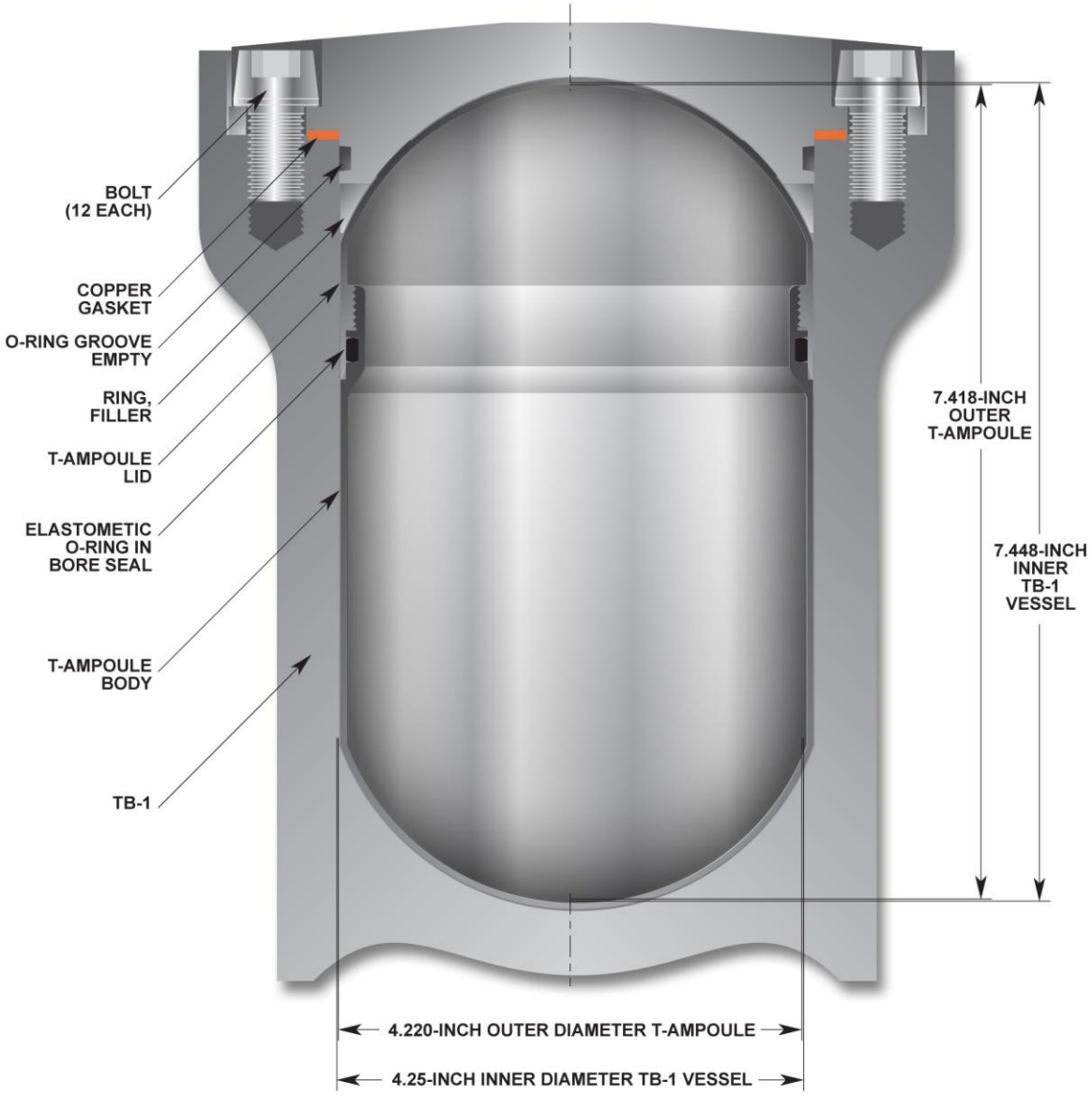

Figure 1-2. T-Ampoule within the TB-1

1.2.1.2 T-Ampoule and Internal Packing

The T-Ampoule's primary components consist of a body (bottom), lid (top), and elastomeric Viton® O-ring. The *Body, T-Ampoule* (Drawing 2A0259, designated T-Ampoule Body), and *Lid, T-Ampoule* (Drawing 2A0260, designated T-Ampoule Lid) are fabricated to a nominal wall thickness of 1.5875±0.0635 mm (0. 0625±0.0025 in.) from solid billets of Ti-6A1-4V, Grade 5. The PAT-1040 *Titanium and O-Ring and Component Fabrication Specification* in Section 1.3.3.1 provides the manufacturing and quality assurance specification for the T-Ampoule, Filler Ring, *Inner Cradle* (Drawing 2A0385, designated Inner Cradle), *Sample Container-1 (SC-1) Assembly* (Drawing 2A0268, designated SC-1), *Sample Container-2 (SC-2) Assembly* (Drawing 2A0265 designated SC-2), and O-rings for the T-Ampoule, SC-1 and SC-2. Ti-6A1-4V, Grade 5 was selected for its high strength, light weight, and high resistance to eutectic reaction with plutonium metal. The T-Ampoule has a smooth finish on the interior and exterior surfaces to facilitate decontamination, and its body and lid sections are joined together and sealed using a screw-thread joint with an elastomeric Viton® O-ring bore seal to maintain content quality.

The T-Ampoule's internal packing consists of:

1. A nested two-sample-container configuration (see Figure 1-3) SC-2, including one spacer) packed and supported by a titanium Inner Cradle, or
2. A nested three-sample-container configuration (see Figure 1-4) SC-1, including two spacers) packed and supported by a titanium Inner Cradle, or
3. A Pu hollow cylinder (Figure 1-5, also designated plutonium metal hollow cylinder) with or without tantalum foil wrapped around the outside of the cylinder (and having the free ends of the foils tucked into the cylinder). The Pu hollow cylinder may or may not be surrounded by crushed/crumpled foil depending on the operational needs.

The plutonium metal contents may be wrapped with tantalum foil or not wrapped based on operational need before they are loaded in SC-1 or SC-2 sample containers. The tantalum foil ranges in thickness from 0.00254 cm (0.001 in.) to 0.0229 cm (0.009 in.), and the minimum purity ranges from 99.75% (3N5), to 99.98% (3N8), or to 99.99% (4N).

For packing the Pu hollow cylinder content, tantalum foil may be used, but is not required. The plutonium metal contents contained in the T-Ampoule and its packing is described in the following section.

1.2.2 Contents

The plutonium metal contents contained within the T-Ampoule in the TB-1 containment vessel of the PAT-1 package are limited by the following requirements:

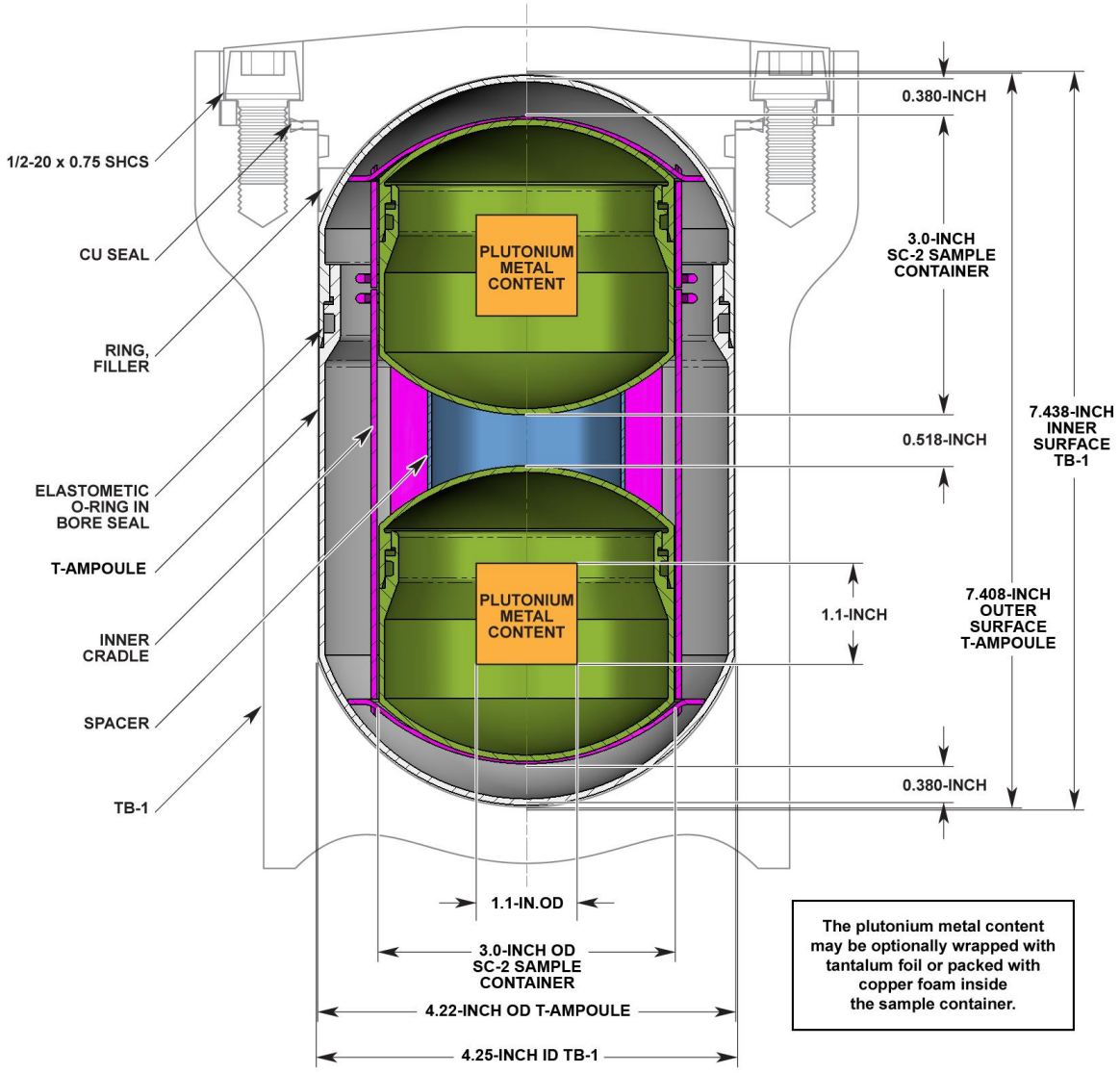

Figure 1-3. Two Sample Containers (SC-2) Nested within T-Ampoule and TB-1

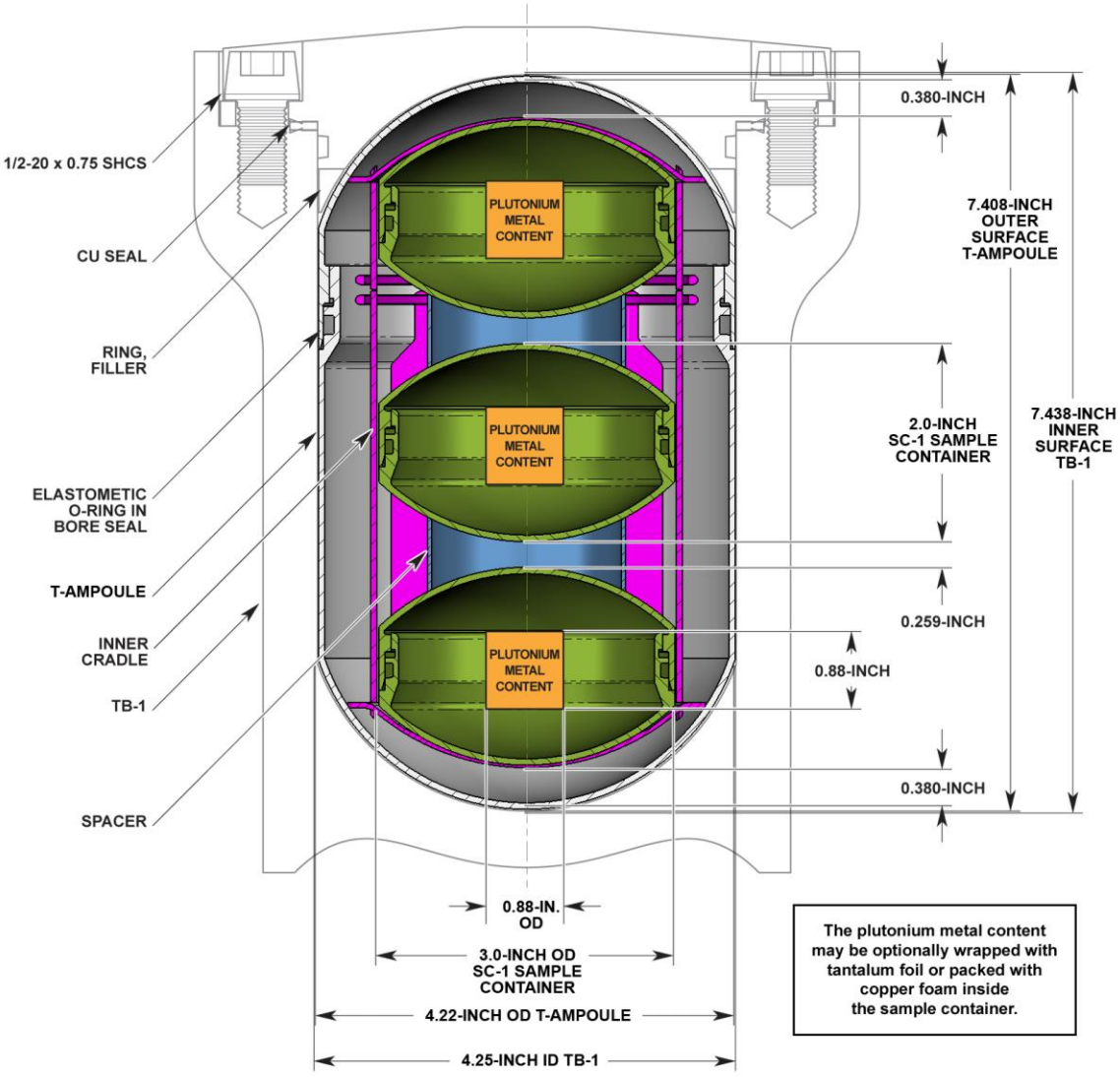

Figure 1-4. Three Sample Containers (SC-1) Nested within T-Ampoule and TB-1

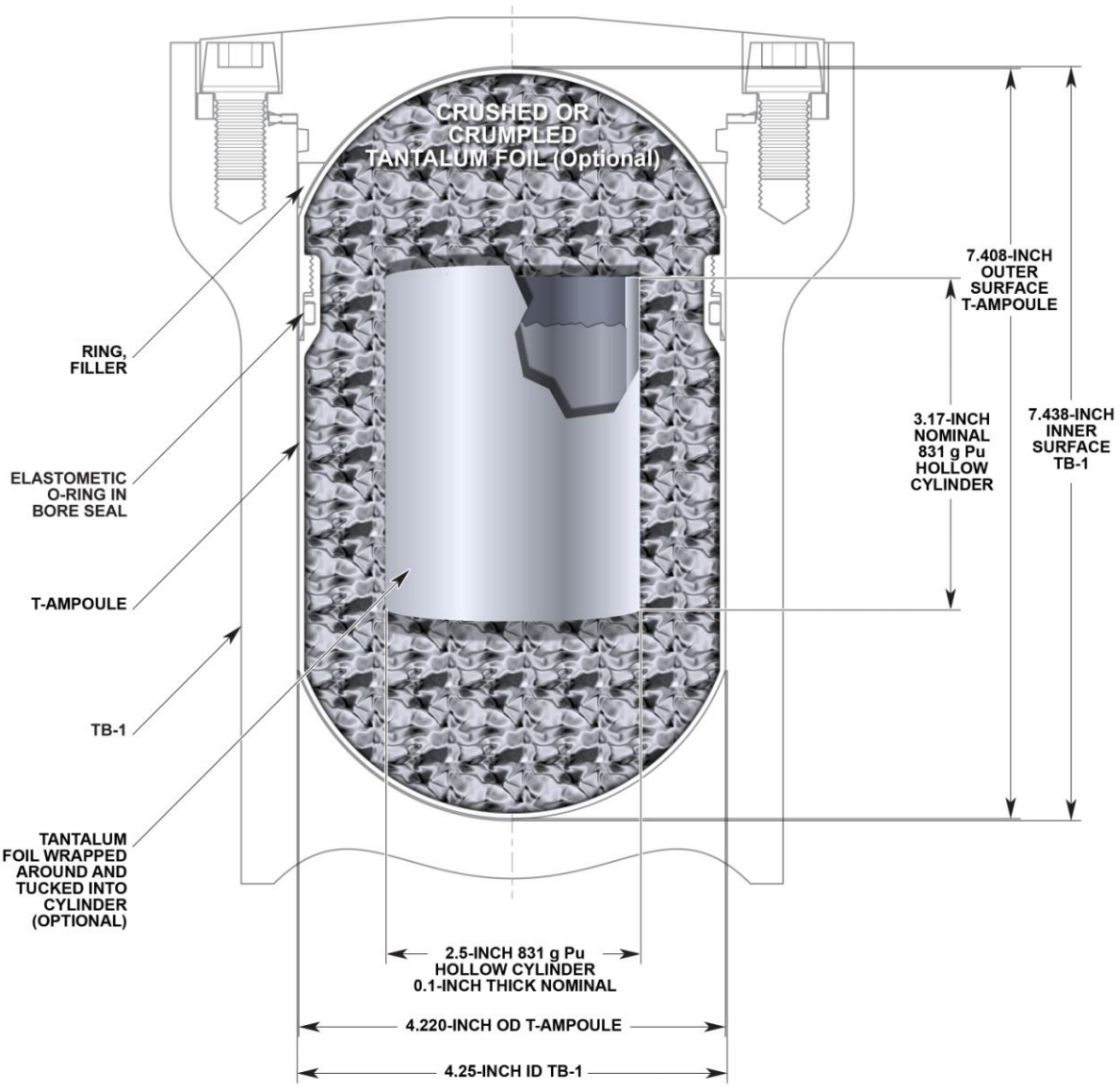

Figure 1-5. 831 gram (1.83 lb) Pu Hollow Cylinder within T-Ampoule and TB-1

a. Material Description

- Material type: The T-Ampoule and its packing will hold plutonium metal in various isotopic compositions and composite (Pu and beryllium [Be] separated by a titanium layer) material.[4] The plutonium metal compositions, decay heat, activity and A_2 are listed below for the largest content of the Pu hollow cylinder, alloyed samples and composite materials:
    - 831 g (1.83 lb) Pu Hollow Cylinder – alpha or delta phase, information for 3000 A_2 quantity of Electro-refined (ER) plutonium metal assuming no Pu-241 decay, 829.67 g (1.83 lb) Pu is shown below. The minimum weight of the Pu hollow cylinder is 731 g (1.61 lb) Pu.

831 grams: 3,000 A_2 quantity of ER Pu metal assuming no Pu241 decay to Am241									
Metal Mass (g) (max)	Mass % (max)	Grams (max)	LANL Specification 55Y-638728	Isotope	Pu Isotopic % (max)	Pu Isotopic mass (g)	Decay Heat (W)	Activity (Ci)	A_2
831.00	Plutonium 99.84%	Plutonium 829.67		Pu238	0.05%	0.41	2.35E-01	7.05E+00	2.61E+02
				Pu239*	92.35%	766.20	1.46E+00	4.75E+01	1.76E+03
				Pu240	6.50%	53.93	3.83E-01	1.24E+01	4.59E+02
				Pu241	1.00%	8.30	1.04E-01	8.30E+02	5.19E+02
				Pu242	0.10%	0.83	8.30E-05	3.24E-03	1.20E-01
				Am241	0.00%	0.00	0.00E+00	0.00E+00	0.00E+00
	Impurities 0.16%	Impurities 1.33		Impurities: N/A					
* stated as % balance						Total:	2.18E+00	8.97E+02	3.00E+03

- 676 g (1.49 lb) Maximum Content in SC-2 Sample Container – Alloyed plutonium metal assuming no Pu-241 decay and 100% Pu-241 decay, 668.16 g (1.47 lb) Pu. Note: the SC-2 sample container configuration has the highest plutonium content within the TB-1 for the sample containers.

676 grams: Alloyed Pu metal assuming no Pu241 decay to Am241									
Metal Mass (g) (max)	Mass % (max)	Grams (max)	LANL Specification 55Y-638728	Isotope	Pu Isotopic % (max)	Pu Isotopic mass (g)	Decay Heat (W)	Activity (Ci)	A_2
676.00	Plutonium 98.84%	Plutonium 668.16		Pu238	0.05%	0.33	1.89E-01	5.68E+00	2.10E+02
				Pu239*	92.35%	617.04	1.17E+00	3.83E+01	1.42E+03
				Pu240	6.50%	43.43	3.08E-01	9.99E+00	3.70E+02
				Pu241	1.00%	6.68	8.35E-02	6.68E+02	4.18E+02
				Pu242	0.10%	0.67	6.68E-05	2.61E-03	9.65E-02
				Am241	0.00%	0.00	0.00E+00	0.00E+00	0.00E+00
	Impurities 0.16%	Impurities 1.08		Impurities: N/A					
	Gallium 1.00%	Gallium 6.76		Gallium: N/A					
* stated as % balance						Total:	1.75E+00	7.22E+02	2.41E+03

676 grams: Alloyed Pu metal assuming 100% Pu241 decay to Am241									
Metal Mass (g) (max)	Mass % (max)	Grams (max)	LANL Specification 55Y-638728	Isotope	Pu Isotopic % (max)	Pu Isotopic mass (g)	Decay Heat (W)	Activity (Ci)	A_2
676.00	Plutonium 98.84%	Plutonium 668.16		Pu238	0.05%	0.33	1.89E-01	5.68E+00	2.10E+02
				Pu239*	92.35%	617.04	1.17E+00	3.83E+01	1.42E+03
				Pu240	6.50%	43.43	3.08E-01	9.99E+00	3.70E+02
				Pu241	0.00%	0.00	0.00E+00	0.00E+00	0.00E+00
				Pu242	0.10%	0.67	6.68E-05	2.61E-03	9.65E-02
				Am241	1.00%	6.68	7.67E-01	2.27E+01	8.41E+02
	Impurities 0.16%	Impurities 1.08		Impurities: N/A					
	Gallium 1.00%	Gallium 6.76		Gallium: N/A					
* stated as % balance						Total:	2.44E+00	7.66E+01	2.84E+03

- 60 g (0.13 lb) per disk – Bonded Pu/Be metal disc assuming 100% Pu-241 decay, 52.2 g (0.115 lb) Pu, 7.80 g (0.172 lb) Be (includes alpha barrier between Pu and Be). Composition, decay heat, activity, and A_2 for other shapes would be similar.

60 grams: Bonded Pu/Be metal disc assuming 100% Pu241 decay to Am241										
Composite %	Metal Mass (g) (max)	Mass % (max)	Grams (max)	LANL Specification 55Y-638728	Isotope	Pu Isotopic % (max)	Pu Isotopic mass (g)	Decay Heat (W)	Activity (Ci)	A_2
Pu metal 87.00%	52.20	MT52 Plutonium 98.84%	MT52 Plutonium 51.59		Pu238	0.05%	0.03	1.46E-02	4.39E-01	1.62E+01
					Pu239*	92.35%	47.65	9.05E-02	2.95E+00	1.09E+02
					Pu240	6.50%	3.35	2.38E-02	7.71E-01	2.86E+01
					Pu241	0.00%	0.00	0.00E+00	0.00E+00	0.00E+00
					Pu242	0.10%	0.05	5.16E-06	2.01E-04	7.45E-03
					Am241	1.00%	0.52	5.92E-02	1.75E+00	6.50E+01
		Impurities 0.16%	Impurities 0.08		Impurities: N/A					
		Gallium 1.00%	Gallium 0.52		Gallium: N/A					
Beryllium 13.00%	7.80	Beryllium 13.00%	Beryllium 7.80		Beryllium: N/A					
Alpha Barrier 0.00%	0.00	Alpha Barrier 0.00%	Alpha Barrier 0.00		Assumes no alpha barrier to yield maximum dose					
100.00%	60.00	◄◄◄ Totals ►►►						1.88E-01	5.92E+00	2.19E+02
*stated as % balance										

- Material form: The plutonium metal must be in solid form (may be pure, alloyed or composite).[5] A small amount of surface oxides is permitted while still maintaining product quality. An estimate of oxides based on 100 ppm oxygen concentration in the inert glove box atmosphere is 1.65 mg. The amount of surface oxides does not affect safety as demonstrated in Section 4.5.5 and 4.5.6 where 100% oxide was assumed in the leakage and release calculations. Material shapes are provided below:
  - Hollow right-circular cylinders of Pu metal as specified in Table 1-1,
  - Various geometric shapes of alloyed Pu metal, including (1) circular discs of varying diameters and thicknesses, (2) rectangular strips of varying lengths, widths, and thicknesses, (3) cylinders in sizes and masses up to those used in the structural analysis, (4) random shapes used for chemistry analysis, and (5) composites as specified in Table 1-1.
- Material quantity: The maximum mass of the plutonium metal (fissile material) contained in the T-Ampoule is 831 g (1.83 lb). The maximum quantity and range for each content and packing configuration is shown in Table 1-1:
  - There are two configurations of Pu hollow cylinders. The maximum cylinder weight has a metal mass of 831 g (1.83 lb) (see Figure 1-5). The minimum hollow cylinder weight has a metal mass of 731 g (1.61 lb). The Pu hollow cylinders may be positioned anywhere within the T-Ampoule.

- Each SC-2 sample container can carry up to 338 g (0.75 lb) of plutonium metal, and each SC-1 sample container can carry up to 174 g (0.38 lb) of plutonium metal. The sample containers are supported within the T-Ampoule by the Inner Cradle as shown in Figures 1-3 and 1-4. The T-Ampoule with its packing and contents is limited to the current certified TB-1 gross payload weight of 2100 g (4.7 lb). The plutonium metal contents may be positioned anywhere in the sample container (SC-1 or SC-2), as applicable.

For the composite Pu/Be samples, each sample container (SC-1 or SC-2) may contain up to 60 g (0.132 lb) each. The total composite mass is 120 grams (0.264 lb) for the two SC-2 configuration and 180 g (0.397 lb) for the three SC-1 configuration.

- Density of Plutonium: Both alpha and delta density plutonium and composite Pu/Be material may be shipped. The densities used for the structural analysis are presented below:
  - Alpha and delta phase: 19.8 g/cc (0.716 lb/in^3)
  - Composite Pu/Be: 15.9 g/cc (0.5745 lb/in^3)

  Page 103 of the Plutonium Handbook[6] published by the American Nuclear Society lists various densities for the different phases of plutonium (see Table 5.1 in the Handbook). These are calculated densities from x-ray diffraction measurements of lattice spacings and represent "theoretical" values for unalloyed plutonium (at temperatures where they are in equilibrium). Several caveats affect the density of "real" Pu. For delta phase at ambient temperature, some alloying elements must be added to stabilize this phase and thus, lowers the theoretical density to below 15.92 g/cc (this value is at a nominal temperature of 320ºC). For alpha phase (unalloyed) at ambient temperature, typical as-cast densities of high-quality temperature phases range from 19.4 to 19.7 g/cc due to three factors: typical impurities, retained higher temperature phases with lower density, and microcracking due to residual stresses. For the structural analysis in Section 2 of this addendum, a value of 19.8 g/cc (0.716 lb/in^3) is used for both the alpha and delta phase plutonium. For the composite Pu/Be material, the density of the delta phase plutonium 15.9 g/cc (0.5745 lb/in^3) is conservatively used in the structural analysis presented in Section 2 of this addendum.
- Chemical form: The chemical form of the plutonium is metal, with possible surface oxides, PuO_2. The metal may be alloyed with gallium.
- Nonfissile materials used as neutron absorbers or moderators: There are no nonfissile materials used as neutron absorbers or moderators.
- Materials subject to chemical, galvanic, or other reactions, including generation of gases: The plutonium metal contents may be subject to oxidation in air (see Section 4.5.2 in this addendum for estimate of oxidation). Eutectic formation between the plutonium metal contents and the iron in the TB-1 is prevented by a eutectic barrier made of titanium. See Section 3.5.2 in this addendum for discussion of eutectics. The O-rings in the T-Ampoule, and SC-1 or SC-2 sample containers are subject to volatilization in a plutonium air transport accident fire, and the pressure generation discussed in Section 4.5.4 of this addendum. The plutonium will decay, forming helium gas. The gas generation is discussed in Sections 2.12.8 and 4.5.3.

- Moisture content: The T-Ampoule, SC-1 or SC-2 sample containers, and radioactive materials will be assembled in a typical glove box and/or laboratory with a standard line atmosphere consisting of nitrogen (N), argon (Ar), or helium (He) inert gas, with an oxygen and water content < 100 ppm. The glove box atmosphere is to maintain product quality of the plutonium metal contents and does not affect safety.
- Internal decay heat: The isotopic composition of all contents must be such that a thermal activity of 25 watts (85.3 Btu/hr) is not exceeded while the contents are in the PAT-1 package.

b. Additional Requirements

- The T-Ampoule must be used for Pu metal shipments.
- Sample containers (SC-1 of SC-2) may be used within the T-Ampoule only if supported by the Inner Cradle as shown in Figures 1-3 and 1-4.
- Sample containers may include tantalum foil as packing material for Pu.
- The Pu or ER hollow cylinder may be wrapped with tantalum foil or not wrapped based on operational need.
- The total weight of the Ring Filler, T-Ampoule, packing materials (tantalum foil), elastomeric O-rings, SC-1 or SC-2 sample containers and Inner Cradle (if used), and Pu metal shall not exceed 2100 g (4.7 lb).
- The Ring Filler must be used with the T-Ampoule.

1.2.2.1 Plutonium Contents and Packing

Plutonium metal contents carried within the T-Ampoule and sample containers include the following configurations:

- Various geometric shapes of alloyed Pu metal, including (1) circular discs of varying diameters and thicknesses, (2) rectangular strips of varying lengths, widths, and thicknesses, (3) cylinders in sizes and masses up to those used in the structural analysis, (4) random shapes used for chemistry analysis, and (5) composites as specified in Table 1-1.
- Hollow right-circular cylinders of alloyed plutonium metal specified in Table 1-1.
- Composite Pu/Be materials of different geometries.

The payload and contents configurations are presented in Table 1-1.

Table 1-1. Payload and Contents Configurations

Payload Configuration	Total Plutonium Content Weight in T-Ampoule (g)	Dimensions of Plutonium Contents
Pu hollow cylinder[a] (Electro-Refined or alloyed) in *T-Ampoule Assembly*	731 to 831[d]	6.350 cm (2.500 in.) OD, 5.801 cm (2.284 in.) ID × 7.087 cm (2.790 in.) length for 731 g payload to 6.350 cm (2.500 in.) OD, 5.801 cm (2.284 in.) ID × 8.054 cm (3.171 in.) length for 831 g payload Unilateral tolerances for the cylinder: -0.000 in./+0.010 in. applied to the outside diameter -0.010 in./+0.000 in. applied to the inside diameter
Sample Container-1 (SC-1) Assembly; up to 174 g alloyed delta phase Pu metal[b] in each container in *T-Ampoule Assembly*	0 to 523	Any configuration of plutonium metal, not to exceed maximum gross Pu weight specified per sample container. (Bounding analysis performed with a 2.23 cm (0.88 in.) OD × 2.23 cm (0.88 in.) long solid cylinder[b]).
Sample Container-2 (SC-2) Assembly up to 338 g alloyed delta phase Pu metal[b] in each container in *T-Ampoule Assembly*	0 to 676	Any configuration of plutonium metal, not to exceed maximum gross Pu weight specified per sample container. (Bounding analysis performed with a 2.79 cm (1.10 in.) OD × 2.79 cm (1.10 in.) long solid cylinder[b]).
Sample Container-1 (SC-1) Assembly, up to 60 g bonded Pu/Be metal content with alpha barrier[c] in each container in *T-Ampoule Assembly*	0 to 180	Composite content not to exceed 60 g[c] per sample container *SC-1*
Sample Container-2 (SC-2) Assembly, up to 60 g bonded Pu/Be metal content with alpha barrier[c] in each container in *T-Ampoule Assembly*	0 to 120	Composite content not to exceed 60 g[c] per sample container *SC-2*

[a] The Pu hollow cylinder may be wrapped in tantalum foil and placed in the T-Ampoule. Additional crushed tantalum foil may be used to pack around the hollow cylinder. For the structural analysis in Section 2, the following bounding conditions are used:

1. For the 731 g cylinder, 6.375 cm (2.510 in.) OD, 5.776 cm (2.274 in.) ID × 6.490 cm (2.555 in.) length.
2. For the 831 g cylinder, 6.375 cm (2.510 in.) OD, 5.776 cm (2.274 in.) ID × 7.374 cm (2.903 in.) length.

[b] A solid cylinder shape in the analysis is assumed for the alloyed delta phase Pu content. The actual shape and number of pieces within the sample convenience container may vary, but cannot exceed the weight limit specified for each container. Tantalum foil may be used to wrap the samples as well as to provide additional packing.

[c] The composite disc may be wrapped in tantalum foil with crushed tantalum foil as packing The alternate configurations for the 60 gram content in an individual sample container include:

1. Multiple small cylinders approximately 5.1 mm (0.2") diameter x 5.1 mm (0.2") height at an individual mass of 1.7 grams and optionally clustered (35 each) for a total of 60 grams per sample container.
2. Multiple disks with varying diameters - (12 mm to 45 mm) and thickness (2.37 to 6 mm) with an individual mass range (10.8 to 59.9 grams) for a total of 60 grams per sample container.
3. A flat plate with varying thickness (up to 6 mm), fixed width (12.5 mm (0.49"), and variable length (30 mm to 50 mm) with an individual mass range (35.8 to 59.6 grams) individually loaded in a sample container.
4. Multiple "long" cylindrical specimens with a diameter range of 7.62 to 8.9 mm (0.3" to 0.35") with varying length (26 mm (1.02") to 60 mm (2.36") with an individual mass range of (18.9 to 59.3 grams) for a total of 60 grams per sample container.

[d] The maximum and minimum weights of the plutonium hollow cylinder are specified because those values were analyzed in the structural analysis (Section 2) for containment and safety. The damage potential (based on relative impact velocity, kinetic energy of the cylinder and buckling resistance) to the T-Ampoule was bounded by the weight of the plutonium hollow cylinder for the 731 to 831 gram range. The hollow cylinders will be fabricated to diameters and thicknesses specified in the table within that mass range (different heights).

The packing requirements are:

- The Inner Cradle must be used to position the SC-1 or SC-2 sample containers within the T-Ampoule.
- The hollow cylinders may be wrapped with tantalum foil for contamination control or not wrapped based on operational need and packed with crushed tantalum foil.
- Plutonium metal contents may be wrapped with tantalum foil for contamination control or not wrapped based on operational need and packed in the sample containers (SC-1 or SC-2).
- Only one type of plastic bagging or tagging material is permitted in the TB-1 per shipment for use external to the sample containers and for labeling of the T-Ampoule. The plastic material is not to be used directly on the Pu contents. The weight limits are specified below.
    - Polyethylene terephthalate (such as Metalized PET, Mylar™) 6.9 gram
    - Polyethylene (such as HDPE, LDPE) 3.5 gram
    - Polyvinyl chloride (PVC) 12.2 gram
    - Polytetrafluoroethylene (PTFE, such as Teflon™) 12.5 gram

  All previous labels must be removed prior to application of new labels.

1.2.3 Special Requirements for Pu

The Pu contents of the PAT-1 package specified in this addendum are of a solid metallic form and will remain in solid form following the testing specified in 10 CFR 71.73.

1.2.4 Operational Features

The operational features of the PAT-1 package (the AQ-1 overpack and the TB-1 containment vessel) require minimal instruction for assembly, disassembly, handling, and transport. The PAT-1 package is transported on its shipping skid and is loaded or unloaded by means of a sling and hoist or forklift with barrel clamp adapter as described in Section 7 of this addendum. Ordinary socket wrenches (3/8 and 5/8 inch) and open-ended adjustable wrenches are used to attach or remove the AQ-1 *Ring, Clamp Modified* (Drawing 1006, designated Clamp Ring). A soft-faced mallet may be used to loosen or install the removable covers if the assembly is tight. No tools are necessary, after this operation, to assemble or disassemble the other AQ-1 removable covers, plugs, load spreaders, and insulation pad, or to insert or remove the TB-1 containment vessel as described in Chapter 7 of the SAR. Only hand tools will be used to assemble or disassemble the TB-1. No use of power or pneumatic tools is authorized.

The physical operating features which assure TB-1 integrity following the 10 CFR 71 NCT, HAC, and accident conditions for air transport of plutonium are the TB-1 *Gasket Copper* (Drawing 1019, designated Copper Gasket) and the TB-1 containment vessel. These features of the TB-1, when assembled to procedures described in Chapter 7 of the SAR and acceptance tested and maintained as described in Chapter 8 of the SAR, assure that the TB-1 will meet the containment acceptance criteria for test requirements in 10 CFR 71.71, 71.73, and 71.74.

The T-Ampoule is sealed with an elastomeric O-ring in a bore seal to maintain content quality. The container is designed to be tightened or loosened by hand or with aids such as strap wrenches, clamp fixtures, etc.

1.3 Appendix

1.3.1 References

1. United States. Nuclear Regulatory Commission. Code of Federal Regulations, 10 CFR 71, "Packaging and Transportation of Radioactive Material." January 1, 2009.

2. United States. Nuclear Regulatory Commission. "Certificate of Compliance for Radioactive Material Packages," Certificate Number 0361, Revision Number 9, Docket Number 71-0361, Package Identification Number USA/0361/B(U)F-96. March 4, 2009.

3. United States. Nuclear Regulatory Commission. NUREG-0361, "Safety Analysis Report for the Plutonium Air Transportable Package, Model PAT-1." Washington, D.C. 1978.

4. United States. Nuclear Regulatory Commission. NUREG-0360, "Qualification Criteria To Certify A Package For Air Transport Of Plutonium." Washington, D.C. 1978.

5. Caviness, M. L., and Rubin, J.B. "Authorized Contents Proposed for the Plutonium Air Transporter (PAT-1) Packaging (U)," LA-UR-08-05154. Los Alamos National Laboratory. Los Alamos, NM: August 7, 2008.

6. Wick, O. J., *Plutonium Handbook, A Guide to the Technology, Volume I*, Pacific Northwest Laboratories, Battelle Memorial Institute, The American Nuclear Society, La Grange Park, Illinois: 1980.

1.3.2 Drawings

Drawing Number	Title	Revision
1004	DRUM	B
1009	CYLINDER, WOOD	B
1013	PLUG, WOOD, REMOVABLE	B
1016	LOAD SPREADER ASSEMBLY	B
1017	CONTAINMENT VESSEL	B
1019	GASKET COPPER	B
1020	LID, TB	B
1022	BODY, TB	B
R99794	PAT-1/TB-1/T-AMPOULE ASSEMBLY (U)	A
2A0263	TB-1/T-AMPOULE SHIPPING VESSEL ASSEMBLY (U)	B
2A0259	BODY T-AMPOULE (U)	A
2A0260	LID T-AMPOULE (U)	A
2A0261	T-AMPOULE ASSEMBLY (U)	B
2A0262	RING, FILLER (U)	A
2A0264	BODY SAMPLE CONTAINER-1 (SC-1) (U)	A
2A0265	SAMPLE CONTAINER-2 (SC-2) ASSEMBLY (U)	B
2A0266	BODY SAMPLE CONTAINER-2 (SC-2) (U)	A
2A0267	LID SAMPLE CONTAINER-1 (SC-1) (U)	A
2A0268	SAMPLE CONTAINER-1 (SC-1) ASSEMBLY (U)	B
2A0269	LID SAMPLE CONTAINER-2 (SC-2) (U)	A
2A0385	INNER CRADLE (U)	A

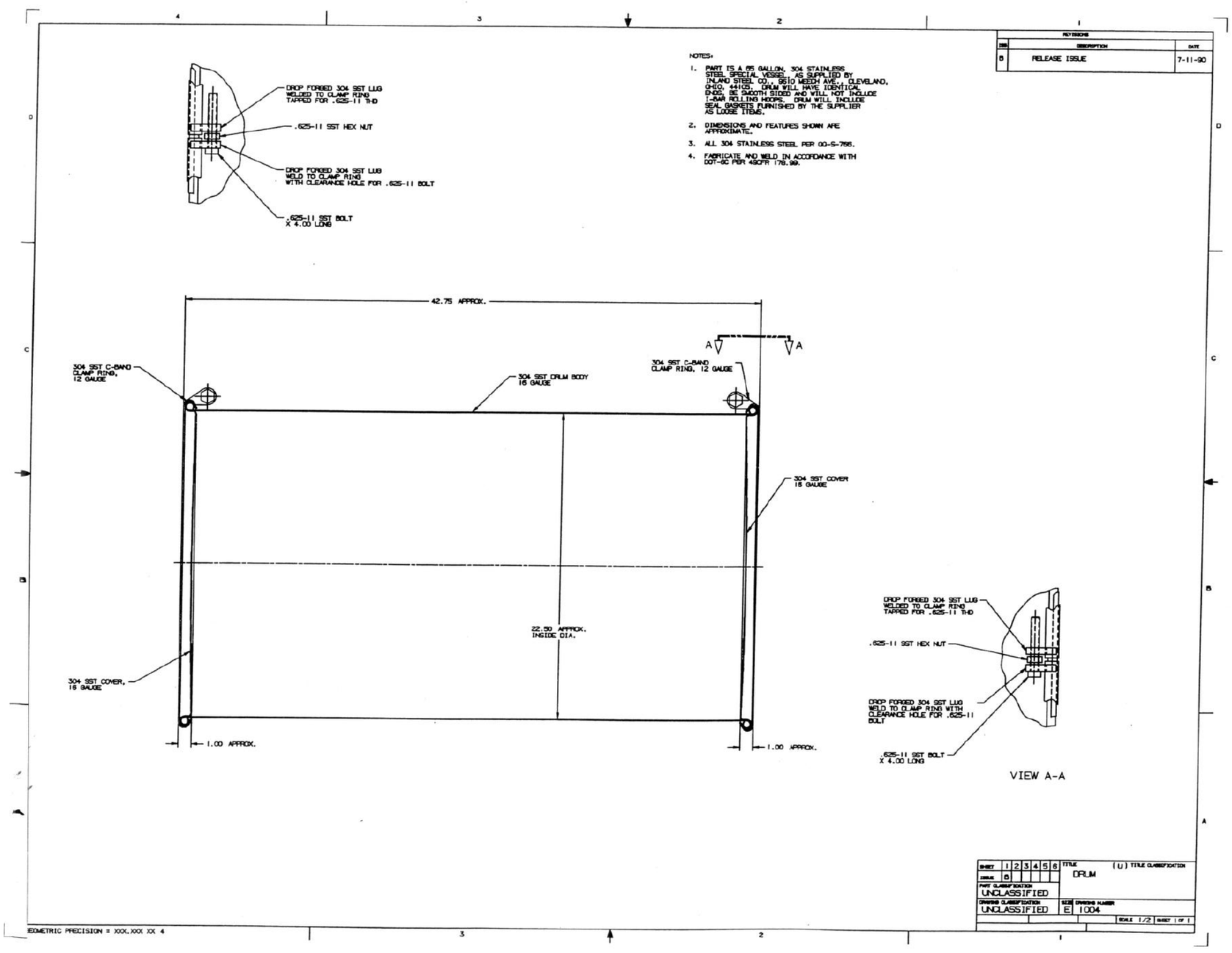
DROP FORGED 304 SST LUG WELDED TO CLAMP RING TAPPED FOR .625-11 THD
.625-11 SST HEX NUT
DROP FORGED 304 SST LUG WELD TO CLAMP RING WITH CLEARANCE HOLE FOR .625-11 BOLT
.625-11 SST BOLT X 4.00 LONG
NOTES:
1. PART IS A 85 GALLON, 304 STAINLESS STEEL SPECIAL VESSEL, AS SUPPLIED BY INLAND STEEL CO., 9610 WEECH AVE., CLEVELAND, OHIO, 44105. DRUM WILL HAVE IDENTICAL ENDS, BE SMOOTH SIDED AND WILL NOT INCLUDE I-BAR ROLLING HOOPS. DRUM WILL INCLUDE SEAL GASKETS FURNISHED BY THE SUPPLIER AS LOOSE ITEMS.
2. DIMENSIONS AND FEATURES SHOWN ARE APPROXIMATE.
3. ALL 304 STAINLESS STEEL PER 00-S-766.
4. FABRICATE AND WELD IN ACCORDANCE WITH DOT-6C PER 49CFR 178.99.
REVISIONS
ZONE DESCRIPTION DATE
B RELEASE ISSUE 7-11-90
42.75 APPROX.
304 SST C-BAND CLAMP RING, 12 GAUGE
304 SST DRUM BODY 16 GAUGE
304 SST C-BAND CLAMP RING, 12 GAUGE
304 SST COVER 16 GAUGE
22.50 APPROX. INSIDE DIA.
304 SST COVER, 16 GAUGE
1.00 APPROX.
1.00 APPROX.
A
A
DROP FORGED 304 SST LUG WELDED TO CLAMP RING TAPPED FOR .625-11 THD
.625-11 SST HEX NUT
DROP FORGED 304 SST LUG WELD TO CLAMP RING WITH CLEARANCE HOLE FOR .625-11 BOLT
.625-11 SST BOLT X 4.00 LONG
VIEW A-A
SHEET 1 2 3 4 5 6
ZONE B
PART CLASSIFICATION UNCLASSIFIED
DRAWING CLASSIFICATION UNCLASSIFIED
TITLE (U) TITLE CLASSIFICATION
DRUM
SIZE E DRAWING NUMBER 1004
SCALE 1/2 SHEET 1 OF 1
EDMETRIC PRECISION = XXX.XXX XX 4

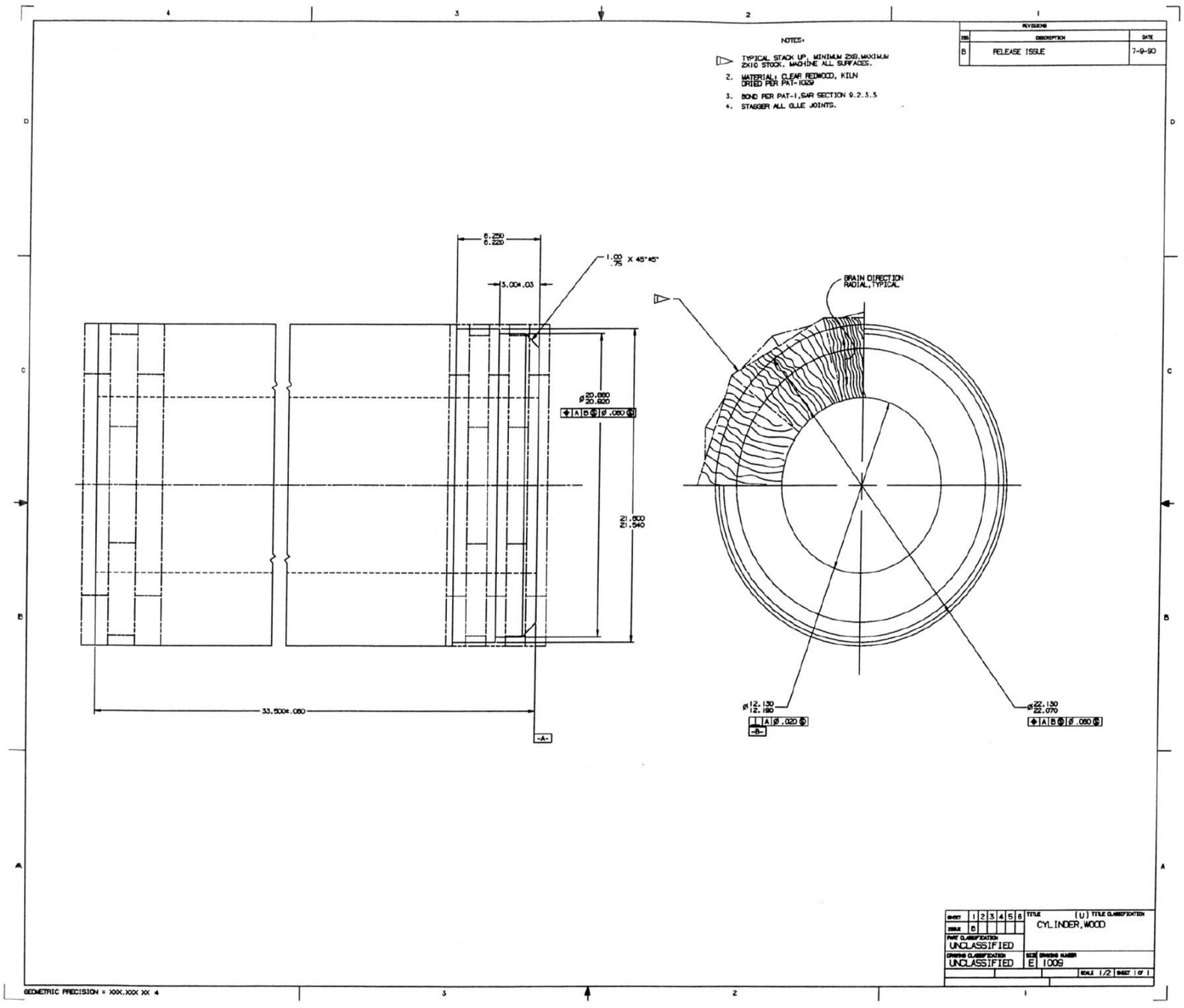
NOTES:
1. TYPICAL STACK UP, MINIMUM 2X8, MAXIMUM 2X10 STOCK. MACHINE ALL SURFACES.
2. MATERIAL: CLEAR REDWOOD, KILN DRIED PER PAT-1029
3. BOND PER PAT-1, SAR SECTION 9.2.3.3
4. STAGGER ALL GLUE JOINTS.
REVISIONS
REV. DESCRIPTION DATE
B RELEASE ISSUE 7-9-90
6.250 6.220
3.00±.03
1.00 .75 X 45°45°
ø20.880 20.820
A B ø .080
21.800 21.540
33.500±.060
-A-
GRAIN DIRECTION RADIAL, TYPICAL
ø12.130 12.180
A ø .020
-B-
ø22.130 22.070
A B ø .060
GEOMETRIC PRECISION = XXX.XXX XX ±
SHEET 1 2 3 4 5 6
SIZE B
PART CLASSIFICATION UNCLASSIFIED
DRAWING CLASSIFICATION UNCLASSIFIED
TITLE (U) TITLE CLASSIFICATION
CYLINDER, WOOD
SIZE DRAWING NUMBER E 1009
SCALE 1/2 SHEET 1 OF 1

REVISIONS		
ISS	DESCRIPTION	DATE
B	RELEASE ISSUE	7-5-90

NOTES:

1. COAT EXPOSED SURFACES, PER PAT-1, SAR SECTION 9.2.3.3.b.
2. MATERIAL: CLEAR REDWOOD, KILN DRIED PER PAT-1025.
3. BOND PER PAT-1, SAR SECTION 9.2.3.3 USING MMM-A-180.
4. STAGGER ALL GLUE JOINTS.
5. TYPICAL STACK UP, MINIMUM 2 X 4 STOCK, MACHINE ALL SURFACES.
6. PART NUMBER MARKING PER PAT-1, SAR SECTION 9.
7. THIS PART IS 11.00"±.06 DUE TO CENTER SECTION SHIFTING UP DURING BONDING. THERE IS A 1/2" THICK BOND JOINT UNDER THE FIXED PLUG.

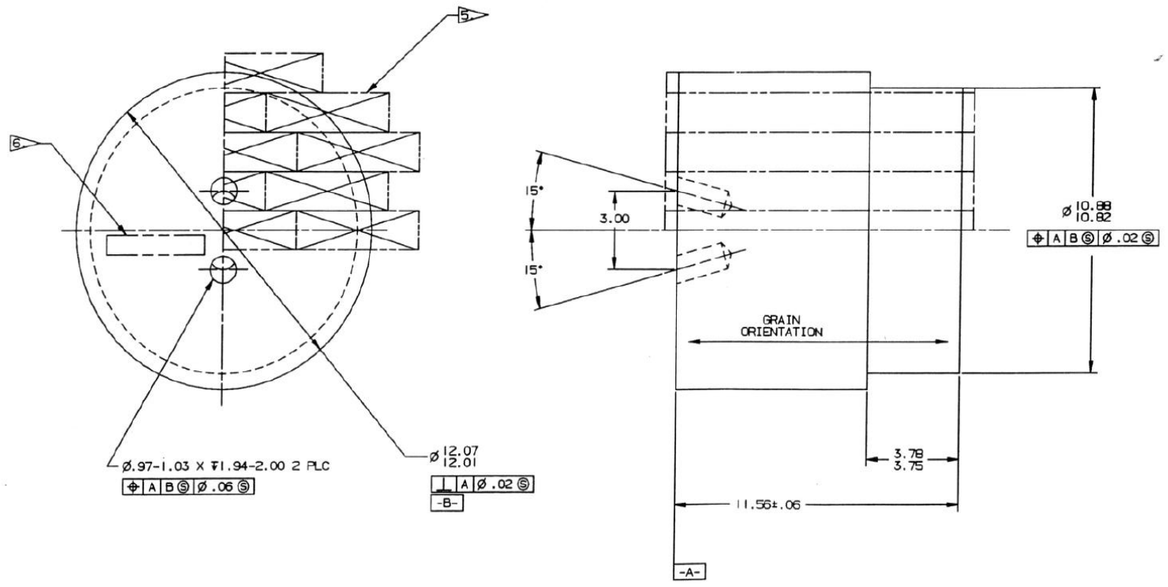

SHEET	1	2	3	4	5	6	TITLE	(U) TITLE CLASSIFICATION
ISSUE	B							PLUG, WOOD, REMOVABLE
PART CLASSIFICATION	UNCLASSIFIED							
DRAWING CLASSIFICATION	UNCLASSIFIED						SIZE	DRAWING NUMBER
							D	1013
							SCALE 1/2	SHEET 1 OF 1

GEOMETRIC PRECISION ± XXX.XXX XX

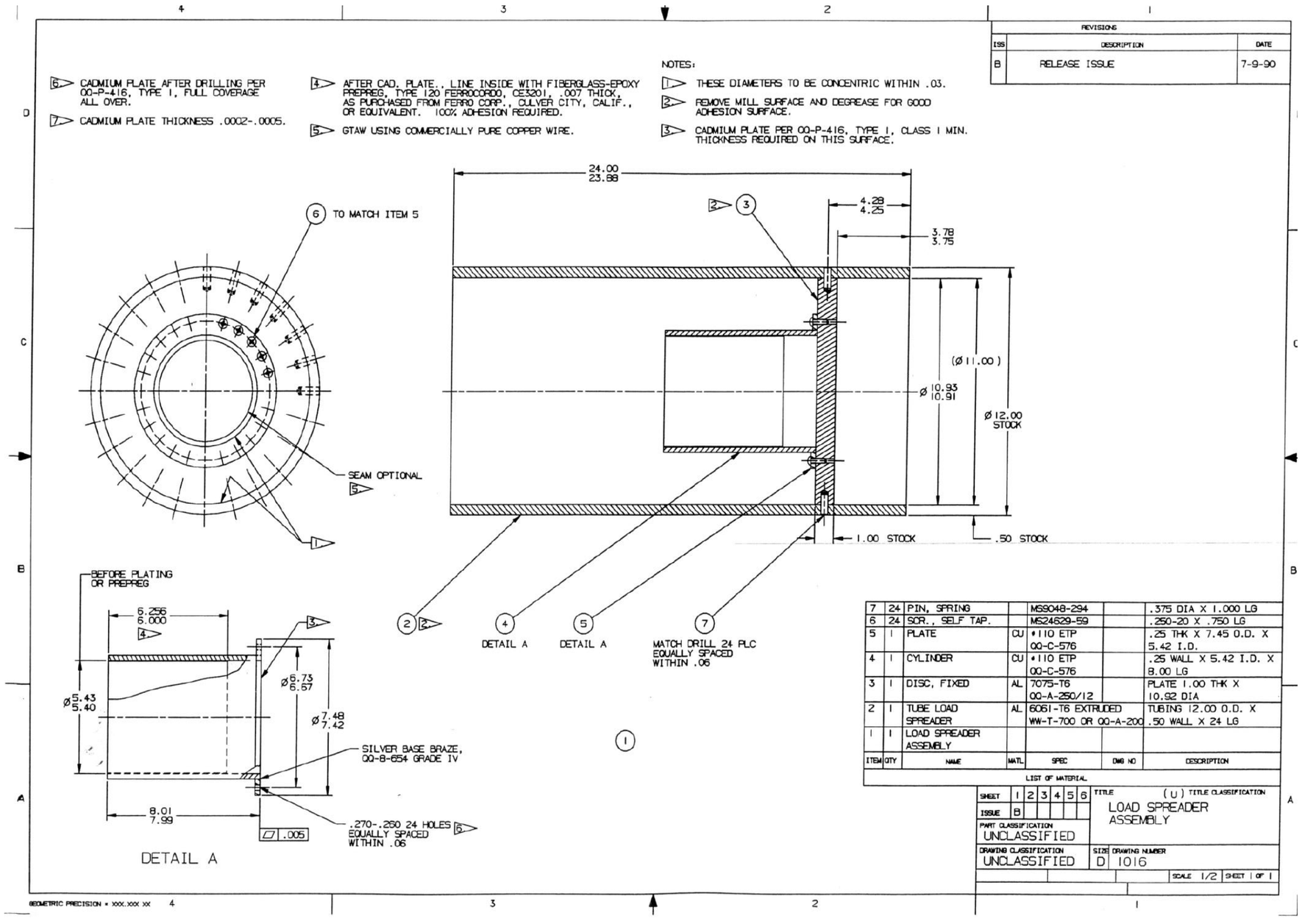
REVISIONS
ISS | DESCRIPTION | DATE
B | RELEASE ISSUE | 7-9-90
NOTES:
6> CADMIUM PLATE AFTER DRILLING PER QQ-P-416, TYPE I, FULL COVERAGE ALL OVER.
7> CADMIUM PLATE THICKNESS .0002-.0005.
4> AFTER CAD. PLATE., LINE INSIDE WITH FIBERGLASS-EPOXY PREPREG, TYPE 120 FERROCORDO, CE3201, .007 THICK, AS PURCHASED FROM FERRO CORP., CULVER CITY, CALIF., OR EQUIVALENT. 100% ADHESION REQUIRED.
5> GTAW USING COMMERCIALLY PURE COPPER WIRE.
1> THESE DIAMETERS TO BE CONCENTRIC WITHIN .03.
2> REMOVE MILL SURFACE AND DEGREASE FOR GOOD ADHESION SURFACE.
3> CADMIUM PLATE PER QQ-P-416, TYPE I, CLASS 1 MIN. THICKNESS REQUIRED ON THIS SURFACE.
6 TO MATCH ITEM 5
SEAM OPTIONAL
24.00
23.88
4.28
4.25
3.78
3.75
(Ø11.00)
Ø10.93
10.91
Ø12.00
STOCK
1.00 STOCK
.50 STOCK
DETAIL A
DETAIL A
MATCH DRILL 24 PLC EQUALLY SPACED WITHIN .06
BEFORE PLATING OR PREPREG
6.256
6.000
Ø5.43
5.40
Ø6.73
6.67
Ø7.48
7.42
SILVER BASE BRAZE, QQ-B-654 GRADE IV
8.01
7.99
.005
.270-.260 24 HOLES EQUALLY SPACED WITHIN .06
DETAIL A
7 24 PIN, SPRING MS9048-294 .375 DIA X 1.000 LG
6 24 SCR., SELF TAP. MS24529-59 .250-20 X .750 LG
5 1 PLATE CU #110 ETP QQ-C-576 .25 THK X 7.45 O.D. X 5.42 I.D.
4 1 CYLINDER CU #110 ETP QQ-C-576 .25 WALL X 5.42 I.D. X 8.00 LG
3 1 DISC, FIXED AL 7075-T6 QQ-A-250/12 PLATE 1.00 THK X 10.92 DIA
2 1 TUBE LOAD SPREADER AL 6061-T6 EXTRUDED WW-T-700 OR QQ-A-200 TUBING 12.00 O.D. X .50 WALL X 24 LG
1 1 LOAD SPREADER ASSEMBLY
ITEM | QTY | NAME | MATL | SPEC | DWG NO | DESCRIPTION
LIST OF MATERIAL
SHEET 1 2 3 4 5 6
ISSUE B
TITLE (U) TITLE CLASSIFICATION
LOAD SPREADER ASSEMBLY
PART CLASSIFICATION UNCLASSIFIED
DRAWING CLASSIFICATION UNCLASSIFIED
SIZE D DRAWING NUMBER 1016
SCALE 1/2 SHEET 1 OF 1
GEOMETRIC PRECISION ± XXX.XXX XX

REVISIONS		
ISS	DESCRIPTION	DATE
B	RELEASE ISSUE	7-19-90

NOTES:

3. PART NUMBER MARKING PER PAT-1, SAR SECTION 9.
4. QUALITY ASSURANCE AND FABRICATION PER PAT-1, SAR SECTION 9.
5. PURCHASE ORDER READS:
   "O" RING VITRON
   V747-75-242

1. SEAR THE EXPOSED ENDS OF NYLON MATERIAL SEARING SHALL NOT LEAVE SHARP EDGES.
2. ALL STRAIGHT STITCHING SHALL CONFORM TO FED-STD-751, USING STITCH CLASS 300, STITCH TYPE 301. USE 7 TO 11 STITCHES PER INCH WITH FF SIZE THREAD. ALL STRAIGHT STITCHING SHALL BE STITCHED A MINIMUM OF 0.500 INCH.

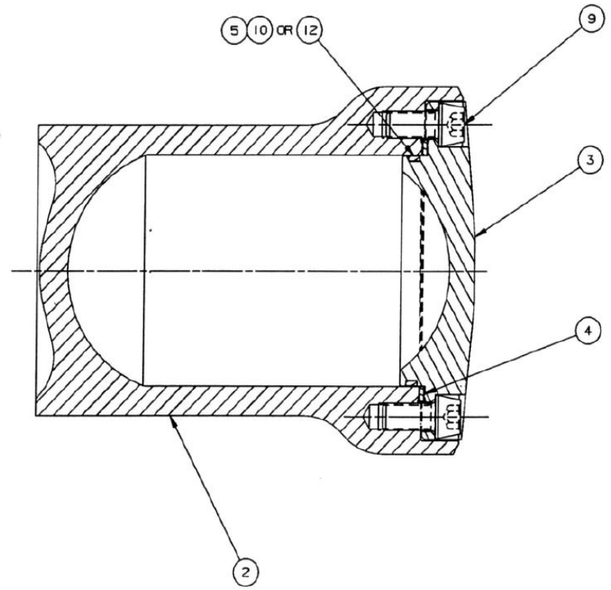

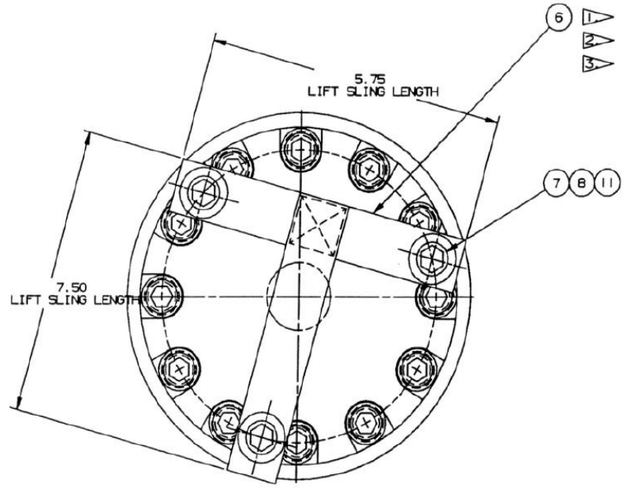

ITEM	QTY	NAME	MATL	SPEC	DWG NO	DESCRIPTION
12	AR	SILICONE GREASE DOW CORNING		DC-4 (MIL-S-8660)		
11	3	GROMMET		MIL-G-16491		METALLIC, TY.3.CL.1, SIZE 3, SPUR
10	AR	SILICONE GREASE GENERAL ELECTRIC		G-624 (MIL-S-8660)		
9	12	BOLT, SOCKET HD			1018	SPECIAL .500-20
8	3	WASHER	STL	MS27183-10		.281 I.D. X .625 X .065
7	3	SCREW, CAP, HEX HD		MS90726-6		.250-28 X .750 LG
6	1	SLING, LIFTING		NYLON		NYLON WEBBING 1" WIDE
5	1	"O" RING, VITON		V747-75-242		
4	1	GASKET, COPPER			1019	
3	1	LID, TB			1020	
2	1	BODY, TB			1022	
1	AR	CONTAINMENT VESSEL				

LIST OF MATERIAL

SHEET	1	2	3	4	5	6
ISSUE	B					

TITLE (U) TITLE CLASSIFICATION: CONTAINMENT VESSEL

PART CLASSIFICATION: UNCLASSIFIED

DRAWING CLASSIFICATION: UNCLASSIFIED

SIZE D | DRAWING NUMBER 1017

SCALE 1/1 | SHEET 1 OF 1

GEOMETRIC PRECISION ± XXX.XXX XX

REVISIONS		
ISS	DESCRIPTION	DATE
B	RELEASE ISSUE	7-10-90

NOTES

1. PART NUMBER MARKING PER PAT-1, SAR SECTION 9.
2. MATERIAL: COPPER, HALF HARD 110 ETP PER QQ-C-576.
3. 63 ALL OVER.
4. PURCHASE ORDER READS: "COPPER; HALF HARD"-110 ETP-QQ-C-576.

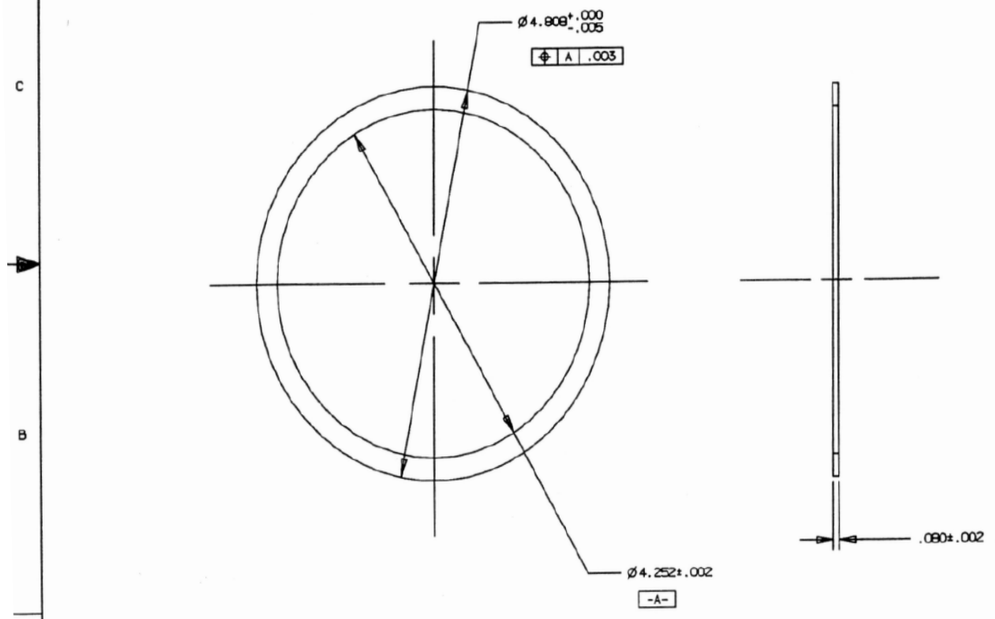

SHEET	1	2	3	4	5	6	TITLE	(U) TITLE CLASSIFICATION
ISSUE	B						GASKET COPPER	
PART CLASSIFICATION: UNCLASSIFIED								
DRAWING CLASSIFICATION: UNCLASSIFIED							SIZE C	DRAWING NUMBER 1019
							SCALE 1/1	SHEET 1 OF 1

GEOMETRIC PRECISION = XXX.XXX XX

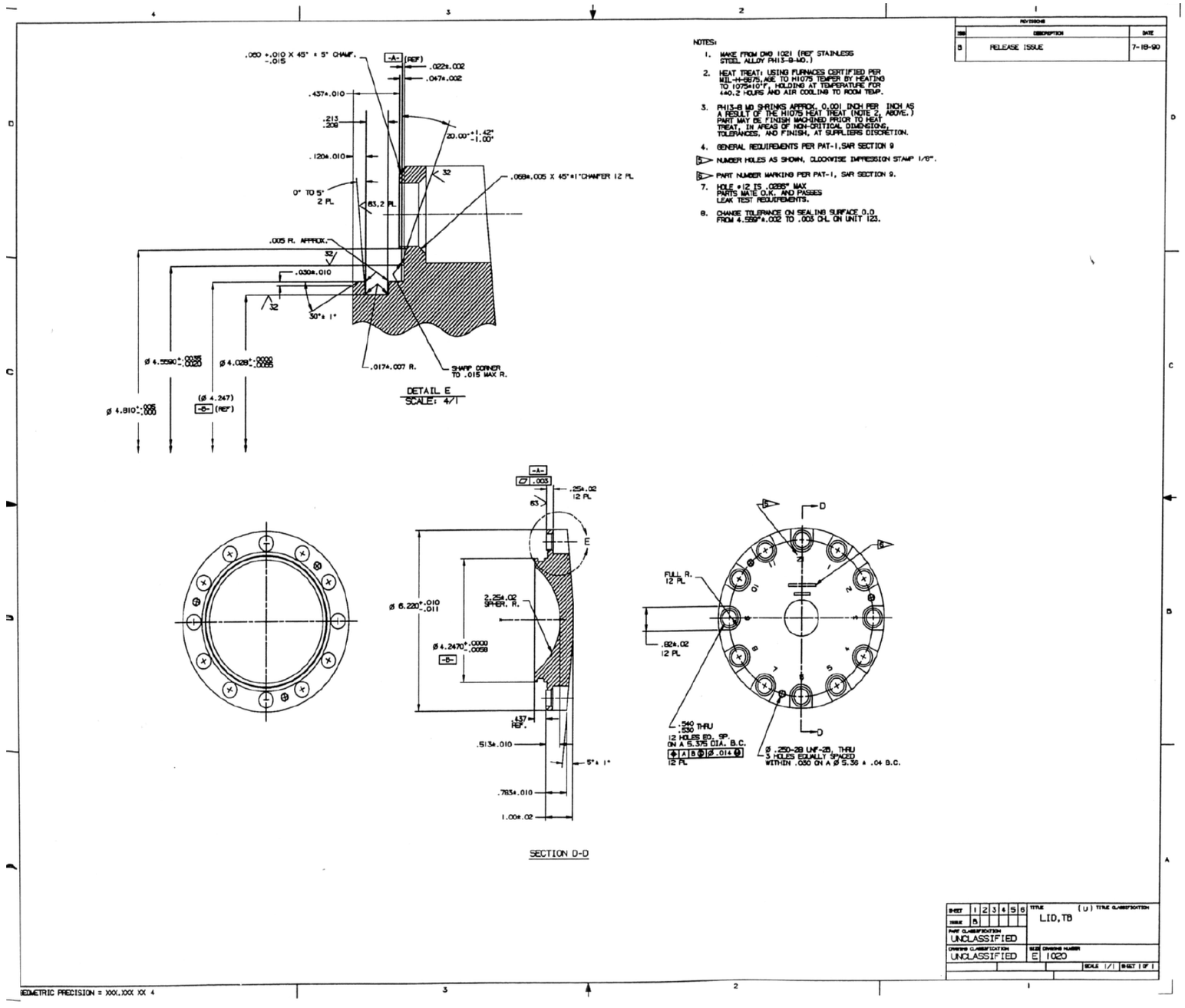
NOTES:
1. MAKE FROM DWG 1021 (REF STAINLESS STEEL ALLOY PH13-8-MO.)
2. HEAT TREAT: USING FURNACES CERTIFIED PER MIL-H-6875, AGE TO H1075 TEMPER BY HEATING TO 1075±10°F, HOLDING AT TEMPERATURE FOR 4±0.2 HOURS AND AIR COOLING TO ROOM TEMP.
3. PH13-8 MO SHRINKS APPROX. 0.001 INCH PER INCH AS A RESULT OF THE H1075 HEAT TREAT (NOTE 2, ABOVE.) PART MAY BE FINISH MACHINED PRIOR TO HEAT TREAT, IN AREAS OF NON-CRITICAL DIMENSIONS, TOLERANCES, AND FINISH, AT SUPPLIERS DISCRETION.
4. GENERAL REQUIREMENTS PER PAT-1, SAR SECTION 9
5. NUMBER HOLES AS SHOWN, CLOCKWISE IMPRESSION STAMP 1/8".
6. PART NUMBER MARKING PER PAT-1, SAR SECTION 9.
7. HOLE ø.12 IS .0285" MAX PARTS MATE O.K. AND PASSES LEAK TEST REQUIREMENTS.
8. CHANGE TOLERANCE ON SEALING SURFACE D.O FROM 4.559"±.002 TO .003 O-L ON UNIT 123.
REVISIONS
DESCRIPTION
DATE
B RELEASE ISSUE 7-18-90
DETAIL E
SCALE: 4/1
SECTION D-D
LID, TB
UNCLASSIFIED
UNCLASSIFIED
E 1020
SCALE 1/1 SHEET 1 OF 1

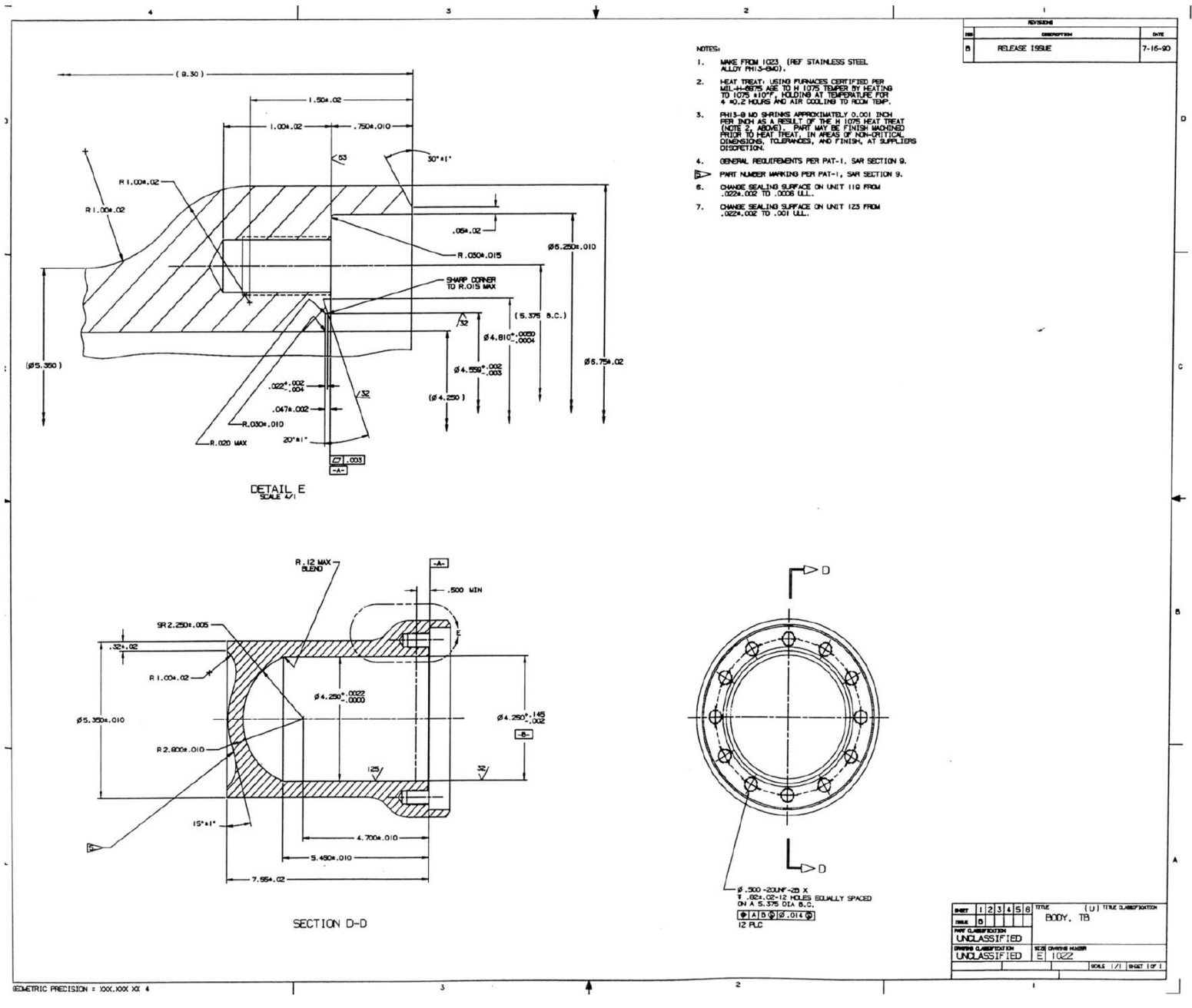
REVISIONS
B RELEASE ISSUE 7-16-90
NOTES:
1. MAKE FROM 1023. (REF STAINLESS STEEL ALLOY PH13-8MO).
2. HEAT TREAT: USING FURNACES CERTIFIED PER MIL-H-6875 ASE TO H 1075 TEMPER BY HEATING TO 1075 ±10°F. HOLDING AT TEMPERATURE FOR 4 ±0.2 HOURS AND AIR COOLING TO ROOM TEMP.
3. PH13-8 MO SHRINKS APPROXIMATELY 0.001 INCH PER INCH AS A RESULT OF THE H 1075 HEAT TREAT (NOTE 2, ABOVE). PART MAY BE FINISH MACHINED PRIOR TO HEAT TREAT, IN AREAS OF NON-CRITICAL DIMENSIONS, TOLERANCES, AND FINISH, AT SUPPLIERS DISCRETION.
4. GENERAL REQUIREMENTS PER PAT-1, SAR SECTION 9.
5. PART NUMBER MARKING PER PAT-1, SAR SECTION 9.
6. CHANGE SEALING SURFACE ON UNIT 119 FROM .022±.002 TO .0008 U.L.
7. CHANGE SEALING SURFACE ON UNIT 123 FROM .022±.002 TO .001 U.L.
DETAIL E
SCALE 4/1
SECTION D-D
.500 MIN
.500-20UNF-2B X .82±.02-12 HOLES EQUALLY SPACED ON A 5.375 DIA B.C.
12 PLC
BODY, TB
UNCLASSIFIED
UNCLASSIFIED
E 1022

DESIGN AGENCY PART NUMBER	REVISIONS						
	ISS	SHEET ZONE	PREPARED BY DESCRIPTION	DATE	CHKR	APVD
R99794-000	A		J. SANCHEZ, 2992/ R. H. YOSHIMURA, 6765	08-13-09		RHY

NOTES:
1. QUALITY ASSURANCE AND FABRICATION PER PAT-1, SAR SECTION 9 AND SAR ADDENDUM SECTION 9.

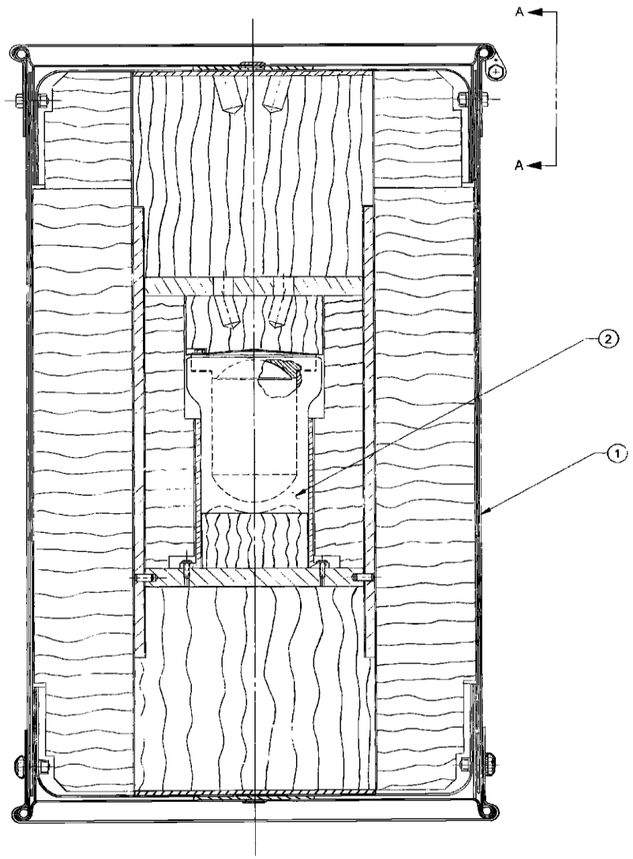

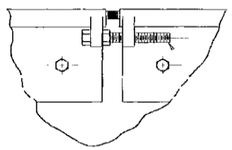

VIEW A-A

- BOLT & NUT PROVIDED WITH DRUM, MUST BE PRESENT

NO. REQD	PART/CONTROL NO.	DESCRIPTION/MATERIAL	NOTE	SHEET ZONE	ITEM
NA	240263	TB-1/T-AMPOULE SHIPPING VESSEL ASSEMBLY (U)			2
NA	1002	OVERPACK, AQ			1

ALT-ALTERNATE AR-AS REQ'D ARS-AS REQ'D PER ASSY EM-EXPENSE MATERIAL NA-DOCUMENT PM-PROCESS MATERIAL

SHEET 1 2 3 4 5 6
ISSUE A
PART CLASSIFICATION UNCLASSIFIED
DRAWING CLASSIFICATION UNCLASSIFIED
TITLE PAT-1/TB-1/T-AMPOULE ASSEMBLY (U)
SIZE E DRAWING NUMBER R99794
CAGEC 14213 SCALE NONE SHEET 1 OF 1
STATUS SA-REL-08/13/09 ORIGIN SA-MST-V8

RASTER FILE NOT TO SCALE

UNCLASSIFIED

NOTES: (UNLESS OTHERWISE SPECIFIED)

1. GENERAL REQUIREMENTS & DRAWING INTERPRETATIONS ARE DEFINED IN 9900000.
2. ABBREVIATIONS IN ACCORDANCE WITH ASME Y14.38-1999.
3. DIMENSIONING AND TOLERANCING IN ACCORDANCE WITH ASME Y14.5M-1994.
4. ALL DIMENSIONS ARE IN INCHES.
5. MARK DESIGN AGENCY PART NUMBER PER 9919100, CLASS H-1-A.
6. PART WEIGHT ITEMS 1, 2, 3, 4, 5 AND 9 = 14.52 LBS.
7. ITEM 6, 7 AND 8 REMOVED FOR CLARITY. (NOT INCLUDED IN PART WEIGHT).
8. MARK MANUFACTURES SERIALIZATION NUMBER ON ALL PARTS PER EACH ASSEMBLY PER 9919100, CLASS H-1-A (LASER). .188" HIGH CHARACTERS, LOCATE APPROX. AS SHOWN.

PART NUMBER	REVISIONS			
	ISS	SHEET ZONE	DESCRIPTION	DATE
2A0263-000	A		ORIGINAL ISSUE	08-13-09
	5		DELETED O-RING UP DATED NOTES 6 AND 7	07-19-10

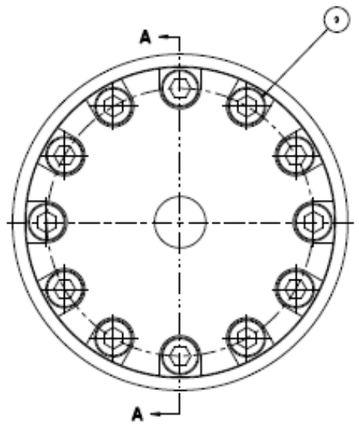

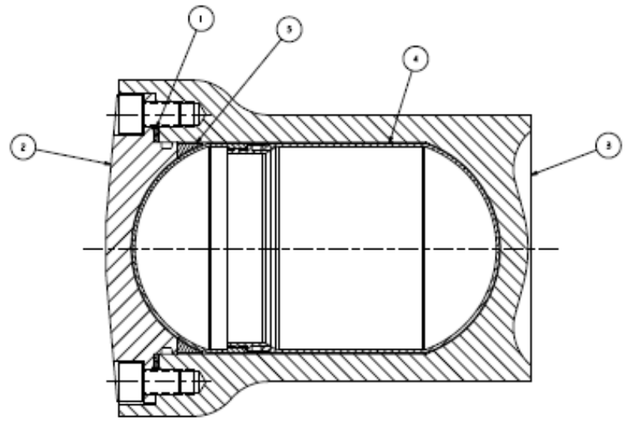

SECTION A-A

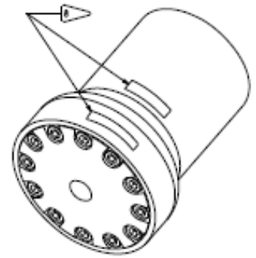

PICTORIAL VIEW
SCALE 1/2

12	12	12	1018	BOLT, SOCKET HEAD SPECIAL .500-20			9
1	1		2A0385-000	INNER CRADLE			8
3			2A0268-000	SAMPLE CONTAINER-1 (SC-1) ASSEMBLY			7
	2		2A0265-000	SAMPLE CONTAINER-2 (SC-2) ASSEMBLY			6
1	1	1	2A0262-000	RING, FILLER			5
1	1	1	2A0261-000	T-AMPOULE ASSEMBLY			4
1	1	1	1022	BODY, TB			3
1	1	1	1020	LID, TB			2
1	1	1	1019	GASKET COPPER			1
NA	NA	NA	9919100	MARKING, GENERAL METHODS			
NA	NA	NA	9900000	GENERAL REQUIREMENTS			
NO HC00	20 HC00	20 HC00	PART/CONTROL NO	DESCRIPTION/MATERIAL	NOTE	SHEET ZONE	ITEM

QUANTITY ABBREVIATIONS: NA = NO QUANTITY FOR DOCUMENTS PM = PROCESS MATERIAL SM = SPECIFIC MATERIAL AR = AS REQUIRED ARS = AS REQUIRED FOR ASSEMBLY

2A0263-200	2A0263-100	2A0263-000
DRAWING: 2A0263-UNC MODEL: 2A0263-000-UNC TYPE: ASSEM		
SANDIA NATIONAL LABORATORIES (NM) ENGLISH		
THIRD ANGLE PROJECTION		

TITLE: TB-1 / T-AMPOULE SHIPPING VESSEL ASSEMBLY (U)

PART CLASSIFICATION: UNCLASSIFIED

DRAWING CLASSIFICATION: UNCLASSIFIED

SIZE: D | DRAWING NUMBER: 2A0263 | ISSUE: B

CAGEC: 4213 | SCALE: 1/1 | SHEET 1 OF 1

ORIGIN: PRO/E-WILDFIRE 4 | STATUS: SA-CHK-07-19-10

NEXT ASSY:	FINAL ASSY:
PROJECT NAME: PAT-1 PACKAGING	DRAWING LEVEL:

UNLESS OTHERWISE SPECIFIED DIMENSIONS ARE IN INCHES. TOLERANCES ARE:
DECIMALS .XX = ± .03, .XXX = ± .005
ANGULAR = ± 1°
MACHINED = 63
FINISH

CURRENT ISSUE APPROVALS		DATE
DRAWN:	F. DI SONA - 2991	07-19-10
CHECKED:	R. YOSHIMURA - 6765	
DESIGNED:	C.W. MORROW - 6774	
APPROVED:	R. YOSHIMURA - 6765	

UNCLASSIFIED

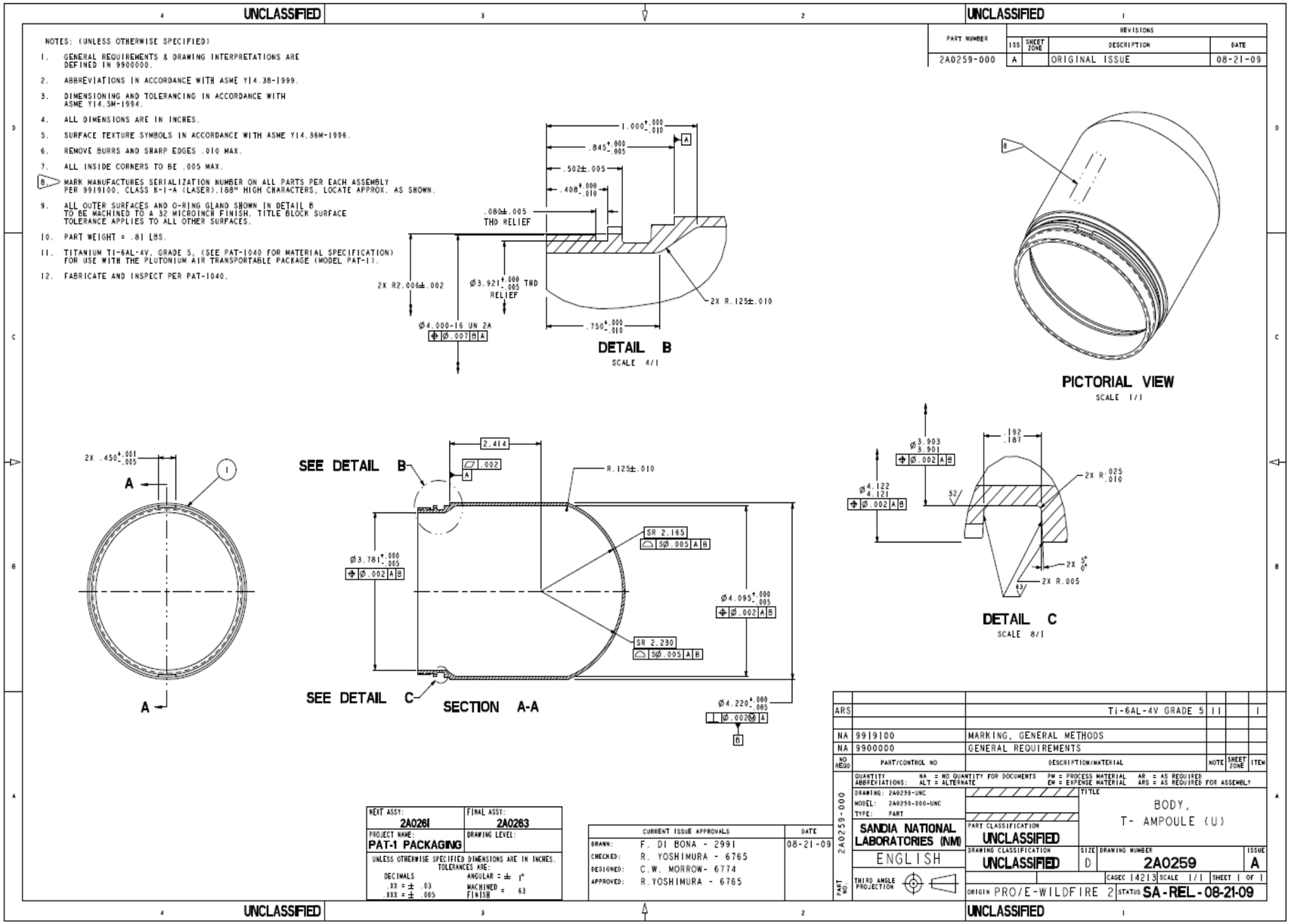
UNCLASSIFIED
UNCLASSIFIED
NOTES: (UNLESS OTHERWISE SPECIFIED)
1. GENERAL REQUIREMENTS & DRAWING INTERPRETATIONS ARE DEFINED IN 9900000.
2. ABBREVIATIONS IN ACCORDANCE WITH ASME Y14.38-1999.
3. DIMENSIONING AND TOLERANCING IN ACCORDANCE WITH ASME Y14.5M-1994.
4. ALL DIMENSIONS ARE IN INCHES.
5. SURFACE TEXTURE SYMBOLS IN ACCORDANCE WITH ASME Y14.36M-1996.
6. REMOVE BURRS AND SHARP EDGES .010 MAX.
7. ALL INSIDE CORNERS TO BE .005 MAX.
8. MARK MANUFACTURES SERIALIZATION NUMBER ON ALL PARTS PER EACH ASSEMBLY PER 9919100, CLASS N-1-A (LASER).188" HIGH CHARACTERS, LOCATE APPROX. AS SHOWN.
9. ALL OUTER SURFACES AND O-RING GLAND SHOWN IN DETAIL B TO BE MACHINED TO A 32 MICROINCH FINISH. TITLE BLOCK SURFACE TOLERANCE APPLIES TO ALL OTHER SURFACES.
10. PART WEIGHT = .81 LBS.
11. TITANIUM TI-6AL-4V, GRADE 5, (SEE PAT-1040 FOR MATERIAL SPECIFICATION) FOR USE WITH THE PLUTONIUM AIR TRANSPORTABLE PACKAGE (MODEL PAT-1).
12. FABRICATE AND INSPECT PER PAT-1040.
PART NUMBER
REVISIONS
ISS SHEET ZONE DESCRIPTION DATE
2A0259-000 A ORIGINAL ISSUE 08-21-09
1.000 +.000 -.010
.845 +.000 -.005
.502±.005
.408 +.000 -.010
.086±.005 THD RELIEF
2X R2.006±.002
Ø3.921 +.000 -.005 THD RELIEF
Ø4.000-16 UN 2A
Ø.007 M A
.750 +.000 -.010
2X R.125±.010
DETAIL B
SCALE 4/1
PICTORIAL VIEW
SCALE 1/1
2X .450 +.001 -.005
A
SEE DETAIL B
2.414
.002 A
R.125±.010
SR 2.165
SØ.005 A B
Ø3.781 +.000 -.005
Ø.002 A B
Ø4.095 +.000 -.005
Ø.002 A B
SR 2.230
SØ.005 A B
SEE DETAIL C
SECTION A-A
Ø4.220 +.000 -.005
Ø.002 B A
B
Ø3.903 3.901
Ø.002 A B
.192 .187
2X R.025 .010
Ø4.122 4.121
Ø.002 A B
32
2X 5°
2X R.005
63
DETAIL C
SCALE 8/1
NEXT ASSY: 2A0261
FINAL ASSY: 2A0263
PROJECT NAME: PAT-1 PACKAGING
DRAWING LEVEL:
UNLESS OTHERWISE SPECIFIED DIMENSIONS ARE IN INCHES. TOLERANCES ARE:
DECIMALS .XX = ± .03 .XXX = ± .005
ANGULAR = ± 1°
MACHINED FINISH = 63
CURRENT ISSUE APPROVALS DATE
DRAWN: F. DI BONA - 2991 08-21-09
CHECKED: R. YOSHIMURA - 6765
DESIGNED: C.W. MORROW- 6774
APPROVED: R.YOSHIMURA - 6765
ARS Ti-6AL-4V GRADE 5 11 1
NA 9919100 MARKING, GENERAL METHODS
NA 9900000 GENERAL REQUIREMENTS
NO REQD PART/CONTROL NO DESCRIPTION/MATERIAL NOTE SHEET ZONE ITEM
QUANTITY NA = NO QUANTITY FOR DOCUMENTS PM = PROCESS MATERIAL AR = AS REQUIRED
ABBREVIATIONS: ALT = ALTERNATE EM = EXPENSE MATERIAL ARS = AS REQUIRED FOR ASSEMBLY
DRAWING: 2A0259-UNC
MODEL: 2A0259-000-UNC
TYPE: PART
SANDIA NATIONAL LABORATORIES (NM)
ENGLISH
THIRD ANGLE PROJECTION
PART NO 2A0259-000
TITLE
BODY, T- AMPOULE (U)
PART CLASSIFICATION UNCLASSIFIED
DRAWING CLASSIFICATION UNCLASSIFIED
SIZE D DRAWING NUMBER 2A0259 ISSUE A
CAGEC 14213 SCALE 1/1 SHEET 1 OF 1
ORIGIN PRO/E-WILDFIRE 2 STATUS SA-REL-08-21-09
UNCLASSIFIED
UNCLASSIFIED

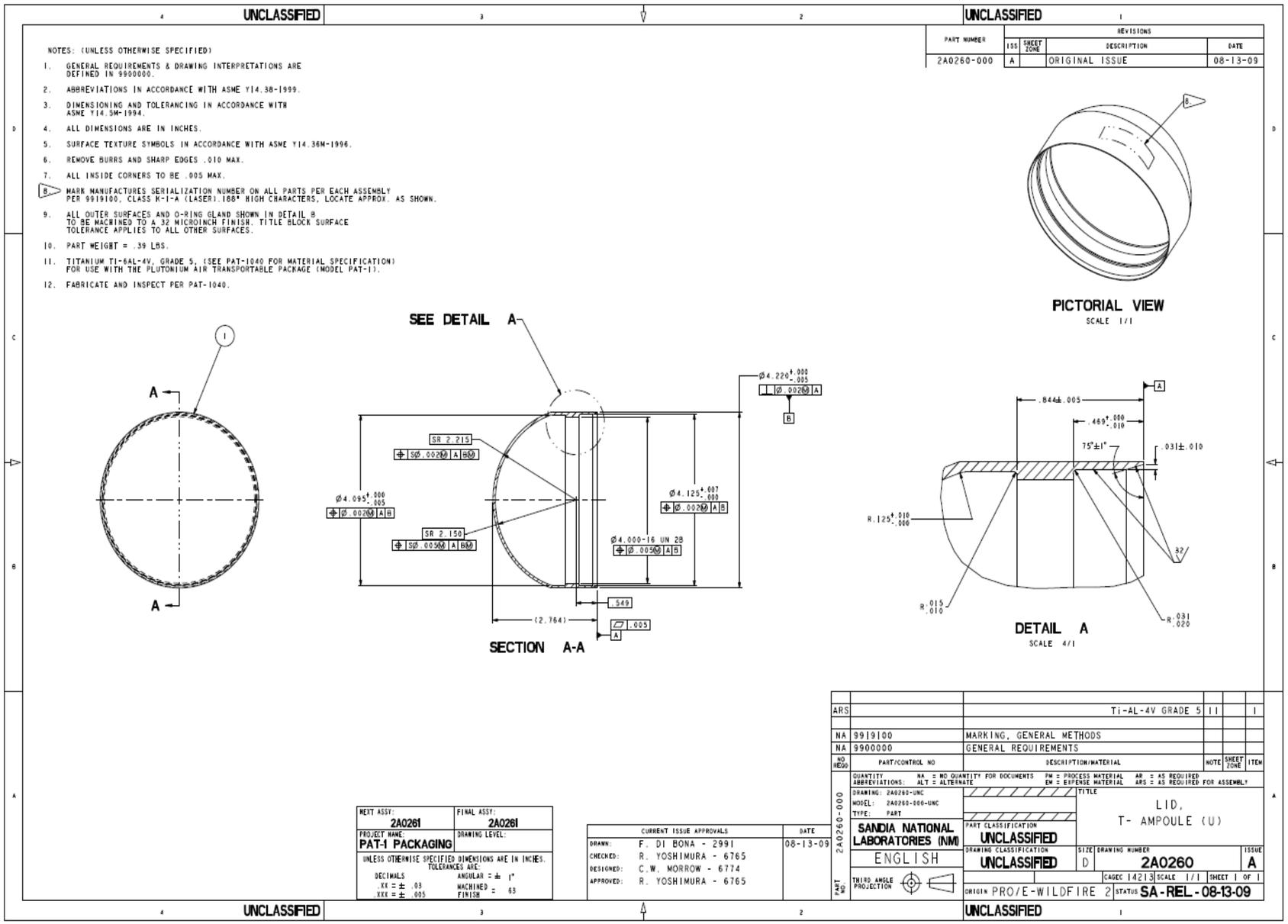
UNCLASSIFIED
UNCLASSIFIED
NOTES: (UNLESS OTHERWISE SPECIFIED)
1. GENERAL REQUIREMENTS & DRAWING INTERPRETATIONS ARE DEFINED IN 9900000.
2. ABBREVIATIONS IN ACCORDANCE WITH ASME Y14.38-1999.
3. DIMENSIONING AND TOLERANCING IN ACCORDANCE WITH ASME Y14.5M-1994.
4. ALL DIMENSIONS ARE IN INCHES.
5. SURFACE TEXTURE SYMBOLS IN ACCORDANCE WITH ASME Y14.36M-1996.
6. REMOVE BURRS AND SHARP EDGES .010 MAX.
7. ALL INSIDE CORNERS TO BE .005 MAX.
8. MARK MANUFACTURES SERIALIZATION NUMBER ON ALL PARTS PER EACH ASSEMBLY PER 9919100, CLASS K-1-A (LASER).188" HIGH CHARACTERS, LOCATE APPROX. AS SHOWN.
9. ALL OUTER SURFACES AND O-RING GLAND SHOWN IN DETAIL B TO BE MACHINED TO A 32 MICROINCH FINISH. TITLE BLOCK SURFACE TOLERANCE APPLIES TO ALL OTHER SURFACES.
10. PART WEIGHT = .39 LBS.
11. TITANIUM TI-6AL-4V, GRADE 5, (SEE PAT-1040 FOR MATERIAL SPECIFICATION) FOR USE WITH THE PLUTONIUM AIR TRANSPORTABLE PACKAGE (MODEL PAT-1).
12. FABRICATE AND INSPECT PER PAT-1040.
PART NUMBER
REVISIONS
ISS
SHEET ZONE
DESCRIPTION
DATE
2A0260-000
A
ORIGINAL ISSUE
08-13-09
PICTORIAL VIEW
SCALE 1/1
SEE DETAIL A
SECTION A-A
DETAIL A
SCALE 4/1
NEXT ASSY: 2A0261
FINAL ASSY: 2A0261
PROJECT NAME: PAT-1 PACKAGING
DRAWING LEVEL:
UNLESS OTHERWISE SPECIFIED DIMENSIONS ARE IN INCHES. TOLERANCES ARE:
DECIMALS
.XX = ± .03
.XXX = ± .005
ANGULAR = ± 1°
MACHINED = 63
FINISH
CURRENT ISSUE APPROVALS
DATE
DRAWN: F. DI BONA - 2991
CHECKED: R. YOSHIMURA - 6765
DESIGNED: C.W. MORROW - 6774
APPROVED: R. YOSHIMURA - 6765
08-13-09
ARS
Ti-AL-4V GRADE 5
NA 9919100 MARKING, GENERAL METHODS
NA 9900000 GENERAL REQUIREMENTS
NO REQD
PART/CONTROL NO
DESCRIPTION/MATERIAL
NOTE
SHEET ZONE
ITEM
QUANTITY ABBREVIATIONS: NA = NO QUANTITY FOR DOCUMENTS ALT = ALTERNATE PM = PROCESS MATERIAL EM = EXPENSE MATERIAL AR = AS REQUIRED ARS = AS REQUIRED FOR ASSEMBLY
DRAWING: 2A0260-UNC
MODEL: 2A0260-000-UNC
TYPE: PART
SANDIA NATIONAL LABORATORIES (NM)
ENGLISH
THIRD ANGLE PROJECTION
TITLE
LID, T- AMPOULE (U)
PART CLASSIFICATION
UNCLASSIFIED
DRAWING CLASSIFICATION
UNCLASSIFIED
SIZE D
DRAWING NUMBER 2A0260
ISSUE A
CAGEC 14213 SCALE 1/1 SHEET 1 OF 1
ORIGIN PRO/E-WILDFIRE 2
STATUS SA-REL-08-13-09
2A0260-000
PART NO
UNCLASSIFIED
UNCLASSIFIED

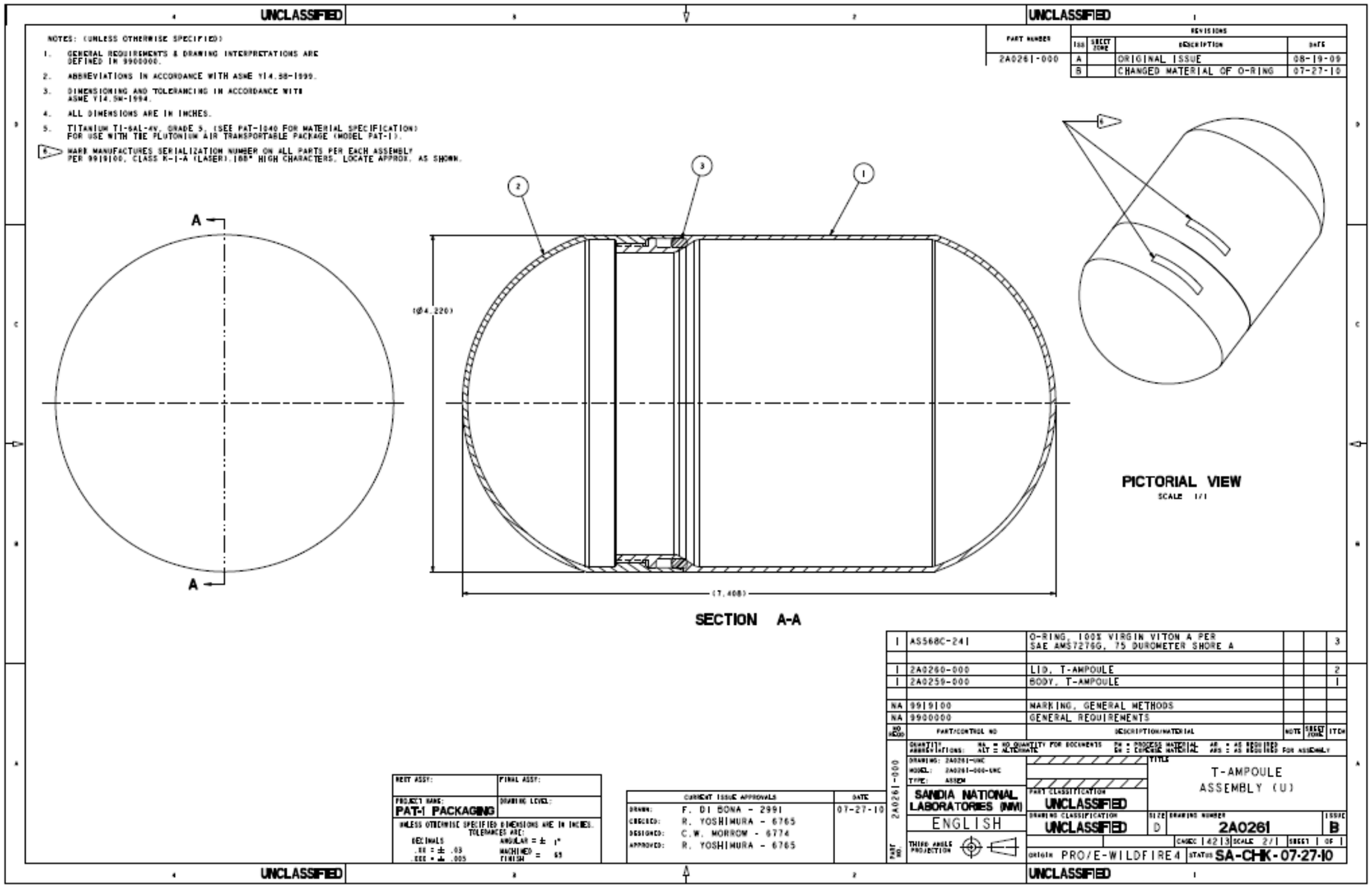
UNCLASSIFIED
UNCLASSIFIED
NOTES: (UNLESS OTHERWISE SPECIFIED)
1. GENERAL REQUIREMENTS & DRAWING INTERPRETATIONS ARE DEFINED IN 9900000.
2. ABBREVIATIONS IN ACCORDANCE WITH ASME Y14.38-1999.
3. DIMENSIONING AND TOLERANCING IN ACCORDANCE WITH ASME Y14.5M-1994.
4. ALL DIMENSIONS ARE IN INCHES.
5. TITANIUM TI-6AL-4V, GRADE 5, (SEE PAT-1040 FOR MATERIAL SPECIFICATION) FOR USE WITH THE PLUTONIUM AIR TRANSPORTABLE PACKAGE (MODEL PAT-1).
6 WARR MANUFACTURES SERIALIZATION NUMBER ON ALL PARTS PER EACH ASSEMBLY PER 9919100, CLASS K-1-A (LASER), .188" HIGH CHARACTERS, LOCATE APPROX. AS SHOWN.
PART NUMBER 2A0261-000
REVISIONS
TSR | SHEET ZONE | DESCRIPTION | DATE
A | ORIGINAL ISSUE | 08-19-09
B | CHANGED MATERIAL OF O-RING | 07-27-10
A
A
(Ø4.220)
(7.408)
1
2
3
6
PICTORIAL VIEW
SCALE 1/1
SECTION A-A
1 AS568C-241 O-RING, 100% VIRGIN VITON A PER SAE AMS7276G, 75 DUROMETER SHORE A 3
1 2A0260-000 LID, T-AMPOULE 2
1 2A0259-000 BODY, T-AMPOULE 1
NA 9919100 MARKING, GENERAL METHODS
NA 9900000 GENERAL REQUIREMENTS
QTY REQD | PART/CONTROL NO | DESCRIPTION/MATERIAL | NOTE | SHEET ZONE | ITEM
QUANTITY ABBREVIATIONS: NA = NO QUANTITY FOR DOCUMENTS ALT = ALTERNATE
PM = PROCESS MATERIAL EM = EXPENDABLE MATERIAL
AR = AS REQUIRED ARS = AS REQUIRED FOR ASSEMBLY
NEXT ASSY:
FINAL ASSY:
PROJECT NAME: PAT-1 PACKAGING
DRAWING LEVEL:
UNLESS OTHERWISE SPECIFIED DIMENSIONS ARE IN INCHES. TOLERANCES ARE:
DECIMALS .XX = ± .03 .XXX = ± .005
ANGULAR = ± 1°
MACHINED =
FINISH =
CURRENT ISSUE APPROVALS
DRAWN: F. DI SONA - 2991
CHECKED: R. YOSHIMURA - 6765
DESIGNED: C.W. MORROW - 6774
APPROVED: R. YOSHIMURA - 6765
DATE 07-27-10
PART NO 2A0261-000
DRAWING: 2A0261-UNC
MODEL: 2A0261-000-UNC
TYPE: ASSEM
SANDIA NATIONAL LABORATORIES (NM)
ENGLISH
THIRD ANGLE PROJECTION
TITLE
T-AMPOULE ASSEMBLY (U)
PART CLASSIFICATION UNCLASSIFIED
DRAWING CLASSIFICATION UNCLASSIFIED
SIZE D
DRAWING NUMBER 2A0261
ISSUE B
CHECK 4213 SCALE 2/1 SHEET 1 OF 1
ORIGIN PRO/E-WILDFIRE 4
STATUS SA-CHK-07-27-10
UNCLASSIFIED
UNCLASSIFIED

UNCLASSIFIED

NOTES: (UNLESS OTHERWISE SPECIFIED)

1. GENERAL REQUIREMENTS & DRAWING INTERPRETATIONS ARE DEFINED IN 9900000.
2. ABBREVIATIONS IN ACCORDANCE WITH ASME Y14.38-1999.
3. DIMENSIONING AND TOLERANCING IN ACCORDANCE WITH ASME Y14.5M-1994.
4. ALL DIMENSIONS ARE IN INCHES.
5. REMOVE BURRS AND SHARP EDGES .010 MAX.
6. ALL INSIDE CORNERS TO BE .005 MAX.
7. MARK DESIGN AGENCY PART NUMBER PER 9919100, CLASS K-1A (LASER) .120 HIGH CHARACTERS, LOCATE APPROXIMATELY AS SHOWN.
8. PART WEIGHT = .14 LBS.
9. TITANIUM TI-6AL-4V, GRADE 5, (SEE PAT-1040 FOR MATERIAL SPECIFICATION) FOR USE WITH THE PLUTONIUM AIR TRANSPORTABLE PACKAGE (MODEL PAT-1).
10. FABRICATE AND INSPECT PER PAT-1040.

PART NUMBER	REVISIONS			
	ISS	SHEET ZONE	DESCRIPTION	DATE
2A0262-000	A		ORIGINAL ISSUE	08-13-09

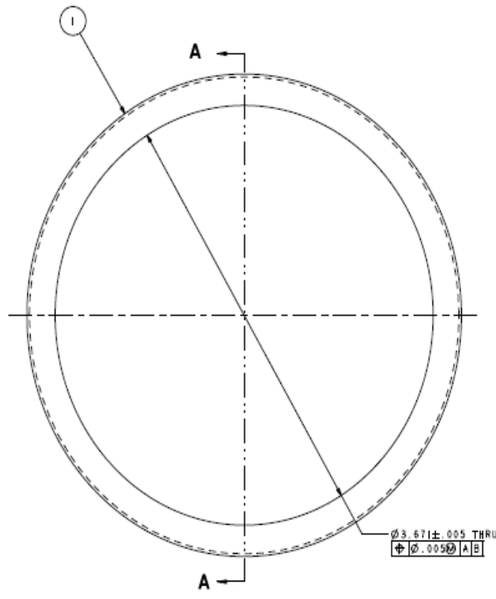

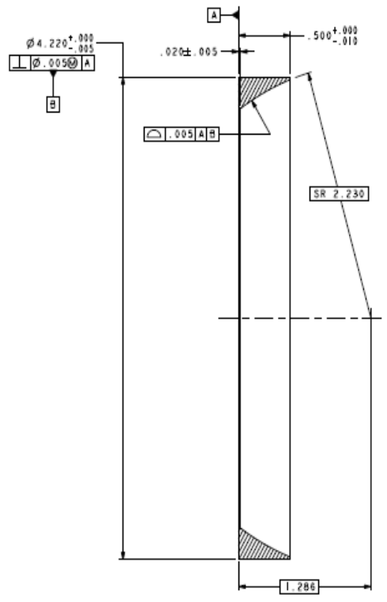

SECTION A-A

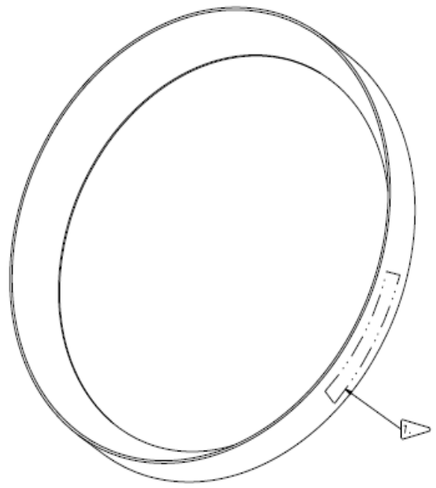

PICTORIAL VIEW
SCALE 2/1

ARS		Ti-6AL-4V GRADE 5	9		1
NA	9919100	MARKING, GENERAL METHODS			
NA	9900000	GENERAL REQUIREMENTS			
NO REQD	PART/CONTROL NO	DESCRIPTION/MATERIAL	NOTE	SHEET ZONE	ITEM

QUANTITY ABBREVIATIONS: NA = NO QUANTITY FOR DOCUMENTS, ALT = ALTERNATE, PM = PROCESS MATERIAL, EM = EXPENSE MATERIAL, AR = AS REQUIRED, ARS = AS REQUIRED FOR ASSEMBLY

NEXT ASSY: 2A0263	FINAL ASSY: 2A0263
PROJECT NAME: PAT-1 PACKAGING	DRAWING LEVEL:

UNLESS OTHERWISE SPECIFIED DIMENSIONS ARE IN INCHES. TOLERANCES ARE:
DECIMALS .XX = ± .03, .XXX = ± .005; ANGULAR = ± 1°; MACHINED = 63; FINISH

CURRENT ISSUE APPROVALS		DATE
DRAWN:	F. DI BONA - 2991	08-13-09
CHECKED:	R. YOSHIMURA - 6765	
DESIGNED:	C.W. MORROW - 6774	
APPROVED:	R. YOSHIMURA - 6765	

PART NO. 2A0262-000

SANDIA NATIONAL LABORATORIES (NM)
ENGLISH
THIRD ANGLE PROJECTION

DRAWING: 2A0262-UNC
MODEL: 2A0262-000-UNC
TYPE: PART

TITLE: RING, FILLER (U)

PART CLASSIFICATION: UNCLASSIFIED
DRAWING CLASSIFICATION: UNCLASSIFIED
SIZE: D | DRAWING NUMBER: 2A0262 | ISSUE: A
CAGEC 14213 | SCALE 2/1 | SHEET 1 OF 1
ORIGIN PRO/E-WILDFIRE 2 | STATUS SA-REL-08-13-09

UNCLASSIFIED

UNCLASSIFIED

NOTES: (UNLESS OTHERWISE SPECIFIED)

1. GENERAL REQUIREMENTS & DRAWING INTERPRETATIONS ARE DEFINED IN 9900000.
2. ABBREVIATIONS IN ACCORDANCE WITH ASME Y14.38-1999.
3. DIMENSIONING AND TOLERANCING IN ACCORDANCE WITH ASME Y14.5M-1994.
4. ALL DIMENSIONS ARE IN INCHES.
5. SURFACE TEXTURE SYMBOLS IN ACCORDANCE WITH ASME Y14.36M-1996.
6. REMOVE BURRS AND SHARP EDGES .010 MAX.
7. ALL INSIDE CORNERS TO BE .005 MAX.
8. MARK MANUFACTURES SERIALIZATION NUMBER ON ALL PARTS PER EACH ASSEMBLY PER 9919100, CLASS K-1-A (LASER) .188" HIGH CHARACTERS, LOCATE APPROX. AS SHOWN.
9. ALL OUTER SURFACES AND O-RING GLAND SHOWN IN DETAIL B TO BE MACHINED TO A 32 MICROINCH FINISH. TITLE BLOCK SURFACE TOLERANCE APPLIES TO ALL OTHER SURFACES.
10. PART WEIGHT = .18 LBS.
11. TITANIUM TI-6AL-4V, GRADE 5, (SEE PAT-1040 FOR MATERIAL SPECIFICATION) FOR USE WITH THE PLUTONIUM AIR TRANSPORTABLE PACKAGE (MODEL PAT-1).
12. FABRICATE AND INSPECT PER PAT-1040.

PART NUMBER	REVISIONS			
	ISS	SHEET ZONE	DESCRIPTION	DATE
2A0264-000	A		ORIGINAL ISSUE	08-13-09

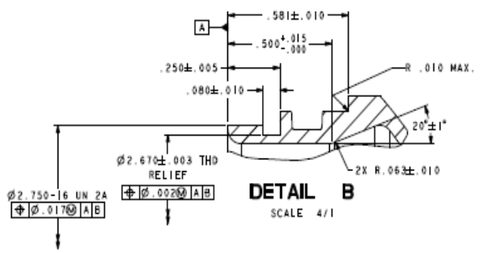

DETAIL B
SCALE 4/1

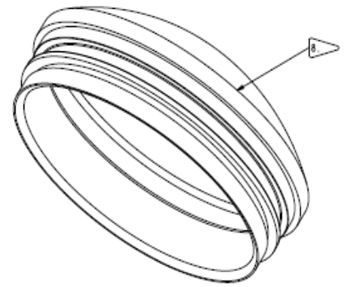

PICTORIAL VIEW
SCALE 2/1

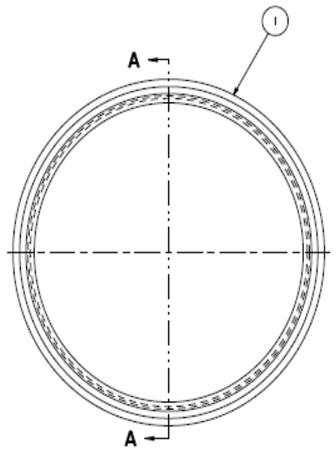

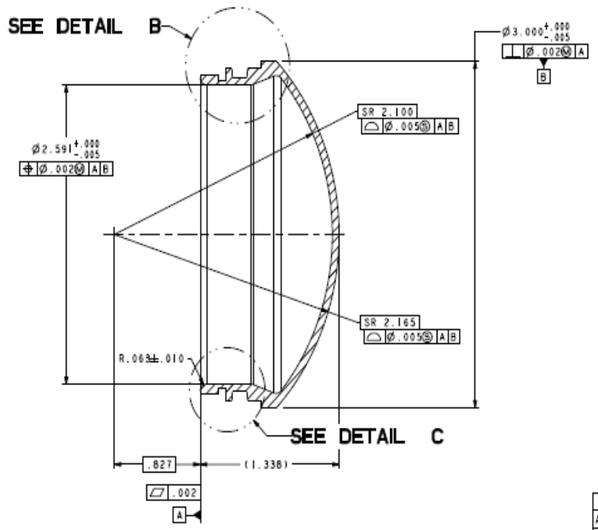

SECTION A-A

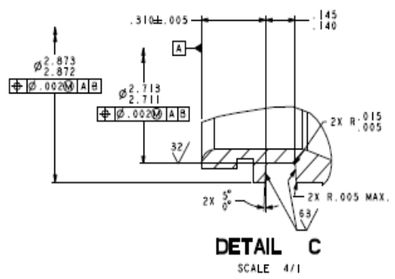

DETAIL C
SCALE 4/1

NEXT ASSY:	FINAL ASSY:
2A0265	2A0261
PROJECT NAME: PAT-1 PACKAGING	DRAWING LEVEL:

UNLESS OTHERWISE SPECIFIED DIMENSIONS ARE IN INCHES. TOLERANCES ARE:
DECIMALS .XX = ± .03 .XXX = ± .005
ANGULAR = ± 1°
MACHINED FINISH = 63

CURRENT ISSUE APPROVALS		DATE
DRAWN:	F. DI BONA - 2991	08-13-09
CHECKED:	R. YOSHIMURA - 2992	
DESIGNED:	C.W. MORROW - 6774	
APPROVED:	R. YOSHIMURA - 2992	

ARS		Ti-6AL-4V GRADE 5	11		1
NA	9919100	MARKING, GENERAL METHODS			
NA	9900000	GENERAL REQUIREMENTS			
NO REQD	PART/CONTROL NO	DESCRIPTION/MATERIAL	NOTE	SHEET ZONE	ITEM

QUANTITY ABBREVIATIONS: NA = NO QUANTITY FOR DOCUMENTS ALT = ALTERNATE PM = PROCESS MATERIAL EM = EXPENSE MATERIAL AR = AS REQUIRED ARS = AS REQUIRED FOR ASSEMBLY

DRAWING: 2A0264-UNC
MODEL: 2A0264-000-UNC
TYPE: PART

SANDIA NATIONAL LABORATORIES (NM)

ENGLISH

THIRD ANGLE PROJECTION

TITLE: BODY, SAMPLE CONTAINER-1 (SC-1) (U)

PART CLASSIFICATION: UNCLASSIFIED

DRAWING CLASSIFICATION: UNCLASSIFIED

SIZE	DRAWING NUMBER	ISSUE
D	2A0264	A

CAGEC 14213 SCALE 2/1 SHEET 1 OF 1

ORIGIN PRO/E-WILDFIRE 2 STATUS SA-REL-08-13-09

PART NO. 2A0264-000

UNCLASSIFIED

UNCLASSIFIED

NOTES: (UNLESS OTHERWISE SPECIFIED)

1. GENERAL REQUIREMENTS & DRAWING INTERPRETATIONS ARE DEFINED IN 9900000.
2. ABBREVIATIONS IN ACCORDANCE WITH ASME Y14.38-1999.
3. DIMENSIONING AND TOLERANCING IN ACCORDANCE WITH ASME Y14.5M-1994.
4. ALL DIMENSIONS ARE IN INCHES.
5. MARK DESIGN AGENCY PART NUMBER PER 9919100, CLASS H-I-A.
6. PART WEIGHT = .43 LBS.
7. TITANIUM TI-6AL-4V, GRADE 5, (SEE PAT-1040 FOR MATERIAL SPECIFICATION) FOR USE WITH THE PLUTONIUM AIR TRANSPORTABLE PACKAGE (MODEL PAT-1).
8. MARK MANUFACTURES SERIALIZATION NUMBER ON ALL PARTS PER EACH ASSEMBLY PER 9919100, CLASS E-I-A (LASER) .188" HIGH CHARACTERS, LOCATE APPROX. AS SHOWN.

PART NUMBER	REVISIONS			
	ISS	SHEET ZONE	DESCRIPTION	DATE
2A0265-000	A		ORIGINAL ISSUE	08-19-09
	B		CHANGED MATERIAL OF O-RING	07-26-10

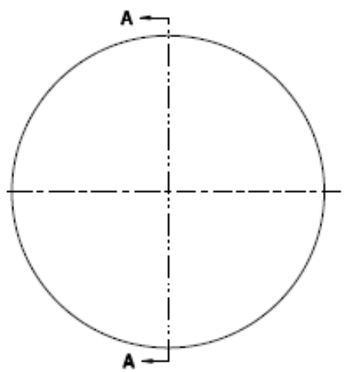

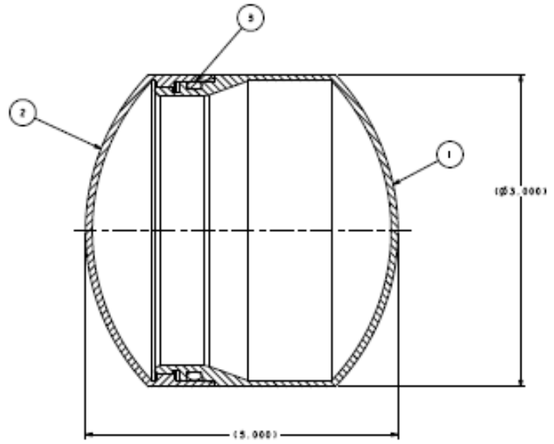

SECTION A-A

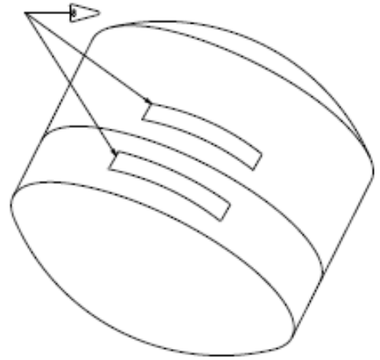

PICTORIAL VIEW
SCALE 2/1

ITEM	PART/CONTROL NO	DESCRIPTION/MATERIAL	NOTE	SHEET ZONE	QTY
1	AS568C-147	O-RING, 100% VIRGIN VITON A PER SAE AMS7276G, 75 DUROMETER SHORE A			3
1	2A0269-000	LID, SAMPLE CONTAINER-2 (SC-2)			2
1	2A0266-000	BODY, SAMPLE CONTAINER-2 (SC-2)			1
NA	9919100	MARKING, GENERAL METHODS			
NA	9900000	GENERAL REQUIREMENTS			

QUANTITY ABBREVIATIONS: NA = NO QUANTITY FOR DOCUMENTS ALT = ALTERNATE
PA = PROCESS MATERIAL EM = EXPOSE MATERIAL AR = AS REQUIRED ARS = AS REQUIRED FOR ASSEMBLY

DRAWING: 2A0265-UNC
MODEL: 2A0265-000-UNC
TYPE: ASSEM

SANDIA NATIONAL LABORATORIES (NM)

ENGLISH

THIRD ANGLE PROJECTION

TITLE: SAMPLE CONTAINER-2 (SC-2) ASSEMBLY (U)

PART CLASSIFICATION: UNCLASSIFIED

DRAWING CLASSIFICATION: UNCLASSIFIED

SIZE: D | DRAWING NUMBER: 2A0265 | ISSUE: B

CAGEC 4213 | SCALE 2/1 | SHEET 1 OF 1

ORIGIN: PRO/E-WILDFIRE4 | STATUS: SA-CHK-07-26-10

NEXT ASSY: | FINAL ASSY:

PROJECT NAME: PAT-1 PACKAGING | DRAWING LEVEL:

UNLESS OTHERWISE SPECIFIED DIMENSIONS ARE IN INCHES. TOLERANCES ARE:
DECIMALS .XX = ± .05 .XXX = ± .005
ANGULAR = ± 1°
MACHINED = 63
FINISH

CURRENT ISSUE APPROVALS		DATE
DRAWN:	F. DI BONA - 2991	07-26-10
CHECKED:	R. YOSHIMURA - 6765	
DESIGNED:	C.W. MORROW - 6774	
APPROVED:	R. YOSHIMURA - 6765	

UNCLASSIFIED

UNCLASSIFIED

NOTES: (UNLESS OTHERWISE SPECIFIED)

1. GENERAL REQUIREMENTS & DRAWING INTERPRETATIONS ARE DEFINED IN 9900000.
2. ABBREVIATIONS IN ACCORDANCE WITH ASME Y14.38-1999.
3. DIMENSIONING AND TOLERANCING IN ACCORDANCE WITH ASME Y14.5M-1994.
4. ALL DIMENSIONS ARE IN INCHES.
5. SURFACE TEXTURE SYMBOLS IN ACCORDANCE WITH ASME Y14.36M-1996.
6. REMOVE BURRS AND SHARP EDGES .010 MAX.
7. ALL INSIDE CORNERS TO BE .005 MAX.
8. MARK MANUFACTURES SERIALIZATION NUMBER ON ALL PARTS PER EACH ASSEMBLY PER 9919100, CLASS K-1-A (LASER), .188" HIGH CHARACTERS, LOCATE APPROX. AS SHOWN.
9. ALL OUTER SURFACES AND O-RING GLAND SHOWN IN DETAIL B TO BE MACHINED TO A 32 MICROINCH FINISH. TITLE BLOCK SURFACE TOLERANCE APPLIES TO ALL OTHER SURFACES.
10. PART WEIGHT = .27 LBS.
11. TITANIUM TI-6AL-4V, GRADE 5, (SEE PAT-1040 FOR MATERIAL SPECIFICATION) FOR USE WITH THE PLUTONIUM AIR TRANSPORTABLE PACKAGE (MODEL PAT-1).
12. FABRICATE AND INSPECT PER PAT-1040.

PART NUMBER	REVISIONS			
	ISS	SHEET ZONE	DESCRIPTION	DATE
2A0266-000	A		ORIGINAL ISSUE	08-13-09

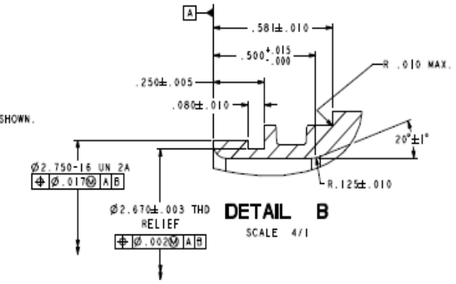

DETAIL B
SCALE 4/1

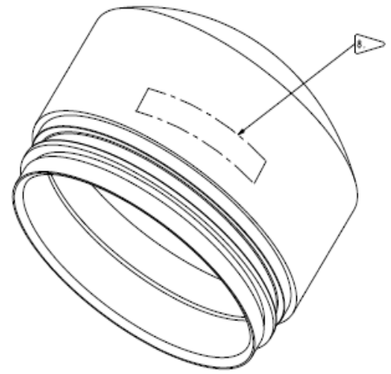

PICTORIAL VIEW
SCALE 2/1

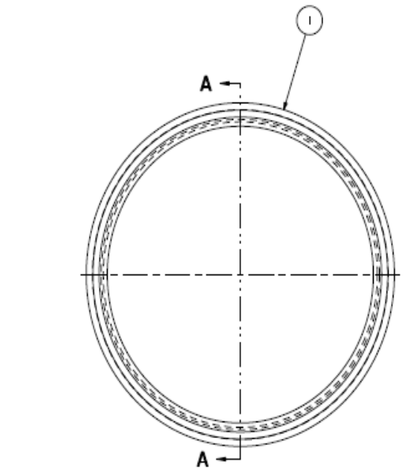

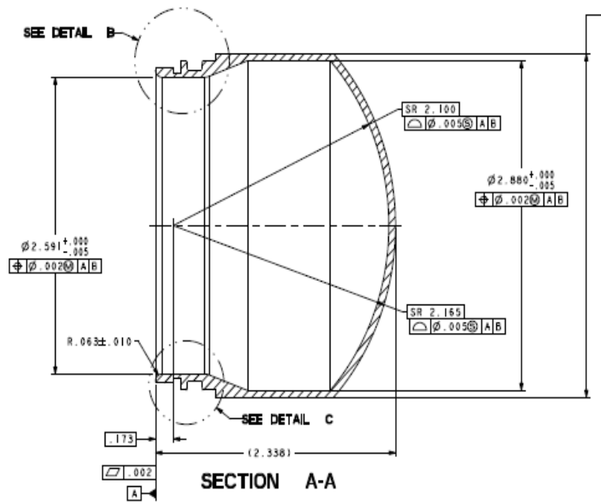

SECTION A-A

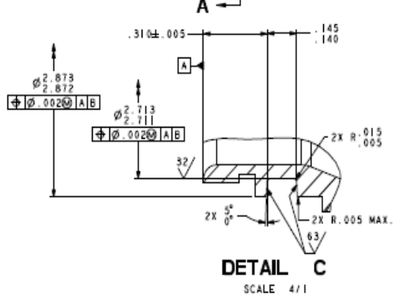

DETAIL C
SCALE 4/1

NEXT ASSY:	FINAL ASSY:
2A0265	2A0261
PROJECT NAME: PAT-1 PACKAGING	DRAWING LEVEL:

UNLESS OTHERWISE SPECIFIED DIMENSIONS ARE IN INCHES. TOLERANCES ARE:
DECIMALS .XX = ± .03 .XXX = ± .005
ANGULAR = ± 1°
MACHINED = 63
FINISH

CURRENT ISSUE APPROVALS		DATE
DRAWN:	F. DI BONA - 2991	08-13-09
CHECKED:	R. YOSHIMURA - 6765	
DESIGNED:	C.W. MORROW - 6774	
APPROVED:	R. YOSHIMURA - 6765	

ARS		Ti-6AL-4V GRADE 5				1
NA	9919100	MARKING, GENERAL METHODS				
NA	9900000	GENERAL REQUIREMENTS				
NO. REQD	PART/CONTROL NO	DESCRIPTION/MATERIAL		NOTE	SHEET ZONE	ITEM

QUANTITY ABBREVIATIONS: NA = NO QUANTITY FOR DOCUMENTS ALT = ALTERNATE PM = PROCESS MATERIAL EM = EXPENSE MATERIAL AR = AS REQUIRED ARS = AS REQUIRED FOR ASSEMBLY

DRAWING: 2A0266-UNC
MODEL: 2A0266-000-UNC
TYPE: PART

SANDIA NATIONAL LABORATORIES (NM)
ENGLISH

THIRD ANGLE PROJECTION

2A0266-000 PART NO.

TITLE: BODY, SAMPLE CONTAINER-2 (SC-2) (U)

PART CLASSIFICATION: UNCLASSIFIED
DRAWING CLASSIFICATION: UNCLASSIFIED

SIZE	DRAWING NUMBER	ISSUE
D	2A0266	A

CAGEC 14213 SCALE 2/1 SHEET 1 OF 1

ORIGIN PRO/E-WILDFIRE 2 STATUS SA-REL-08-13-09

UNCLASSIFIED

UNCLASSIFIED

NOTES: (UNLESS OTHERWISE SPECIFIED)

1. GENERAL REQUIREMENTS & DRAWING INTERPRETATIONS ARE DEFINED IN 9900000.
2. ABBREVIATIONS IN ACCORDANCE WITH ASME Y14.38-1999.
3. DIMENSIONING AND TOLERANCING IN ACCORDANCE WITH ASME Y14.5M-1994.
4. ALL DIMENSIONS ARE IN INCHES.
5. SURFACE TEXTURE SYMBOLS IN ACCORDANCE WITH ASME Y14.36M-1996.
6. REMOVE BURRS AND SHARP EDGES .010 MAX.
7. ALL INSIDE CORNERS TO BE .005 MAX.
8. MARK MANUFACTURES SERIALIZATION NUMBER ON ALL PARTS PER EACH ASSEMBLY PER 9919100, CLASS K-1-A (LASER), .188" HIGH CHARACTERS, LOCATE APPROX. AS SHOWN.
9. ALL OUTER SURFACES AND O-RING GLAND SHOWN IN DETAIL B TO BE MACHINED TO A 32 MICROINCH FINISH. TITLE BLOCK SURFACE TOLERANCE APPLIES TO ALL OTHER SURFACES.
10. PART WEIGHT = .15 LBS.
11. TITANIUM TI-6AL-4V, GRADE 5, (SEE PAT-1040 FOR MATERIAL SPECIFICATION) FOR USE WITH THE PLUTONIUM AIR TRANSPORTABLE PACKAGE (MODEL PAT-1).
12. FABRICATE AND INSPECT PER PAT-1040.

PART NUMBER	REVISIONS			
	ISS	SHEET ZONE	DESCRIPTION	DATE
2A0267-000	A		ORIGINAL ISSUE	08-13-09

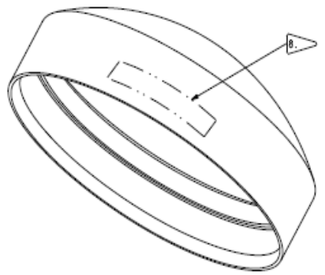

PICTORIAL VIEW
SCALE 2/1

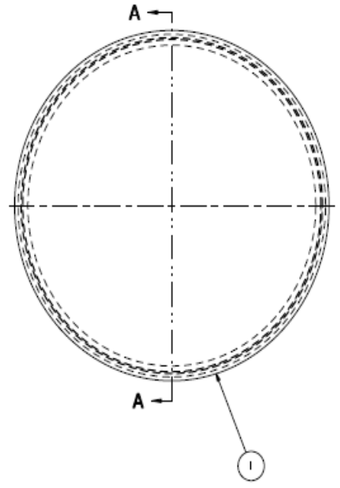

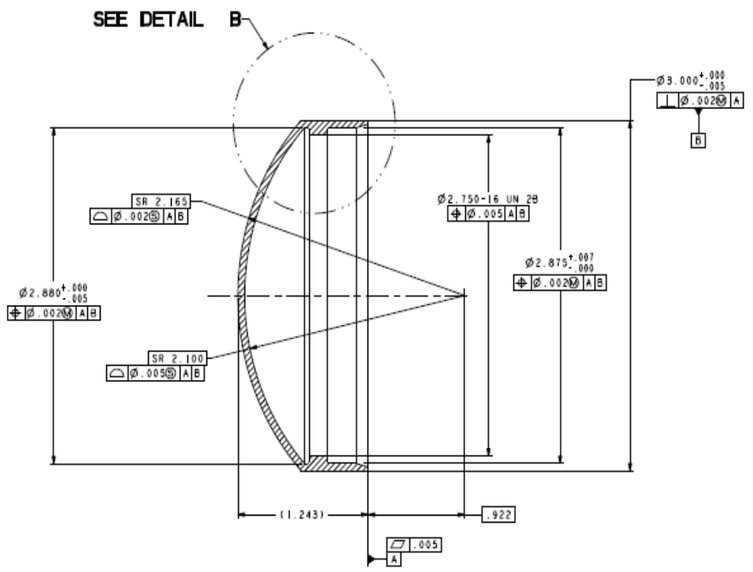

SECTION A-A

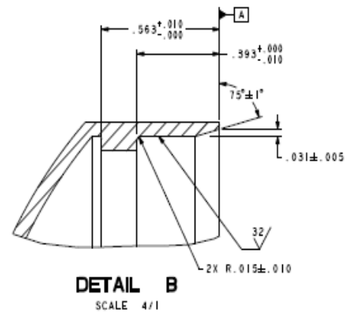

DETAIL B
SCALE 4/1

ARS		Ti-6AL-4V GRADE 5	11		1
NA	9919100	MARKING, GENERAL METHODS			
NA	9900000	GENERAL REQUIREMENTS			
NO REQD	PART/CONTROL NO	DESCRIPTION/MATERIAL	NOTE	SHEET ZONE	ITEM

QUANTITY ABBREVIATIONS: NA = NO QUANTITY FOR DOCUMENTS ALT = ALTERNATE PM = PROCESS MATERIAL EM = EXPENSE MATERIAL AR = AS REQUIRED ARS = AS REQUIRED FOR ASSEMBLY

NEXT ASSY: 2A0268	FINAL ASSY: 2A0263
PROJECT NAME: PAT-1 PACKAGING	DRAWING LEVEL:

UNLESS OTHERWISE SPECIFIED DIMENSIONS ARE IN INCHES. TOLERANCES ARE:
DECIMALS .XX = ± .05 .XXX = ± .005
ANGULAR = ± 1°
MACHINED = 63
FINISH

CURRENT ISSUE APPROVALS		DATE
DRAWN:	F. DI BONA - 2991	08-13-09
CHECKED:	R. YOSHIMURA - 6765	
DESIGNED:	C.W. MORROW - 6774	
APPROVED:	R. YOSHIMURA - 6765	

DRAWING: 2A0267-UNC
MODEL: 2A0267-000-UNC
TYPE: PART

SANDIA NATIONAL LABORATORIES (NM)
ENGLISH
THIRD ANGLE PROJECTION

TITLE: LID, SAMPLE CONTAINER-1 (SC-1) (U)

PART CLASSIFICATION: UNCLASSIFIED
DRAWING CLASSIFICATION: UNCLASSIFIED
SIZE: D
DRAWING NUMBER: 2A0267
ISSUE: A
CAGEC 14213 SCALE 2/1 SHEET 1 OF 1
ORIGIN PRO/E-WILDFIRE STATUS SA-REL-08-13-09

PART NO. 2A0267-000

UNCLASSIFIED

UNCLASSIFIED

NOTES: (UNLESS OTHERWISE SPECIFIED)

1. GENERAL REQUIREMENTS & DRAWING INTERPRETATIONS ARE DEFINED IN 9900000.
2. ABBREVIATIONS IN ACCORDANCE WITH ASME Y14.38-1999.
3. DIMENSIONING AND TOLERANCING IN ACCORDANCE WITH ASME Y14.5M-1994.
4. ALL DIMENSIONS ARE IN INCHES.
5. MARK DESIGN AGENCY PART NUMBER PER 9919100, CLASS B-I-A.
6. PART WEIGHT = .53 LBS.
7. TITANIUM TI-6AL-4V, GRADE 5, (SEE PAT-1040 FOR MATERIAL SPECIFICATION) FOR USE WITH THE PLUTONIUM AIR TRANSPORTABLE PACKAGE (MODEL PAT-1).
8. MARK MANUFACTURES SERIALIZATION NUMBER ON ALL PARTS PER EACH ASSEMBLY PER 9919100, CLASS N-I-A (LASER).188" HIGH CHARACTERS, LOCATE APPROX. AS SHOWN.

PART NUMBER	REVISIONS			
	ltr	SHEET ZONE	DESCRIPTION	DATE
2A0268-000	A		ORIGINAL ISSUE	08-19-09
	B		CHANGED MATERIAL OF O-RING	07-22-10

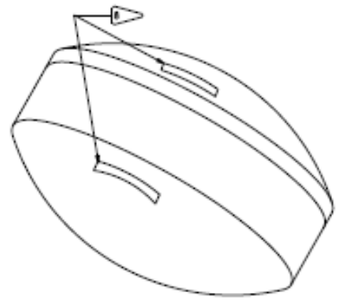

PICTORIAL VIEW
SCALE 2/1

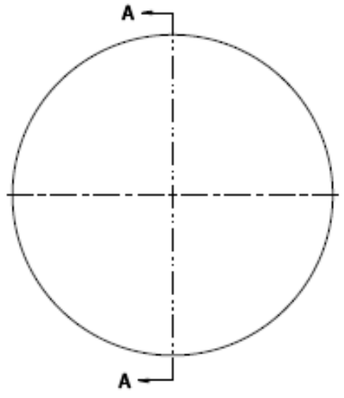

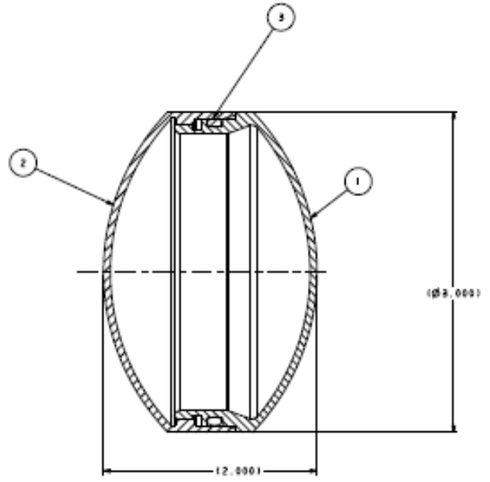

SECTION A-A

ITEM NO	PART/CONTROL NO	DESCRIPTION/MATERIAL	NOTE	SHEET ZONE	QTY
1	AS568C-147	O-RING, 100% VIRGIN VITON A PER SAE AMS7276G, 75 DUROMETER SHORE A			3
1	2A0267-000	LID, SAMPLE CONTAINER-1 (SC-1)			2
1	2A0264-000	BODY, SAMPLE CONTAINER-1 (SC-1)			1
NA	9919100	MARKING, GENERAL METHODS			
NA	9900000	GENERAL REQUIREMENTS			

QUANTITY ABBREVIATIONS: NA = NO QUANTITY FOR DOCUMENTS PM = PROCESS MATERIAL CM = CONCRETE MATERIAL AR = AS REQUIRED ARS = AS REQUIRED FOR ASSEMBLY

DRAWING: 2A0268-UNC
MODEL: 2A0268-000-UNC
TYPE: ASSEM

SANDIA NATIONAL LABORATORIES (NM)

ENGLISH

THIRD ANGLE PROJECTION

TITLE: SAMPLE CONTAINER-1 (SC-1) ASSEMBLY (U)

PART CLASSIFICATION: UNCLASSIFIED

DRAWING CLASSIFICATION: UNCLASSIFIED

SIZE: D | DRAWING NUMBER: 2A0268 | ISSUE: B

CADD: 4213 | SCALE: 2/1 | SHEET 1 OF 1

ORIGIN: PRO/E-WILDFIRE4 | STATUS: SA-CHK-07-22-10

2A0268-000 PART NO

NEXT ASSY:	FINAL ASSY:
PROJECT NAME: PAT-1 PACKAGING	DRAWING LEVEL:

UNLESS OTHERWISE SPECIFIED DIMENSIONS ARE IN INCHES.
TOLERANCES ARE:
DECIMALS: .XX = ± .03, .XXX = ± .005
ANGULAR = ± 1°
MACHINED FINISH = 63

CURRENT ISSUE APPROVALS		DATE
DRAWN:	F. DI BONA - 2991	07-22-10
CHECKED:	R. YOSHIMURA - 6765	
DESIGNED:	C.W. MORROW - 6774	
APPROVED:	R. YOSHIMURA - 6765	

UNCLASSIFIED

UNCLASSIFIED

NOTES: (UNLESS OTHERWISE SPECIFIED)

1. GENERAL REQUIREMENTS & DRAWING INTERPRETATIONS ARE DEFINED IN 9900000.
2. ABBREVIATIONS IN ACCORDANCE WITH ASME Y14.38-1999.
3. DIMENSIONING AND TOLERANCING IN ACCORDANCE WITH ASME Y14.5M-1994.
4. ALL DIMENSIONS ARE IN INCHES.
5. SURFACE TEXTURE SYMBOLS IN ACCORDANCE WITH ASME Y14.36M-1996.
6. REMOVE BURRS AND SHARP EDGES .010 MAX.
7. ALL INSIDE CORNERS TO BE .005 MAX.
8. MARK MANUFACTURES SERIALIZATION NUMBER ON ALL PARTS PER EACH ASSEMBLY PER 9919100, CLASS K-1-A (LASER).188" HIGH CHARACTERS, LOCATE APPROX. AS SHOWN.
9. ALL OUTER SURFACES AND O-RING GLAND SHOWN IN DETAIL B TO BE MACHINED TO A 32 MICROINCH FINISH. TITLE BLOCK SURFACE TOLERANCE APPLIES TO ALL OTHER SURFACES.
10. PART WEIGHT = .15 LBS.
11. TITANIUM TI-6AL-4V, GRADE 5, (SEE PAT-1040 FOR MATERIAL SPECIFICATION) FOR USE WITH THE PLUTONIUM AIR TRANSPORTABLE PACKAGE (MODEL PAT-1).
12. FABRICATE AND INSPECT PER PAT-1040.

PART NUMBER	REVISIONS			
	ISS	SHEET ZONE	DESCRIPTION	DATE
2A0269-000	A		ORIGINAL ISSUE	08-13-09

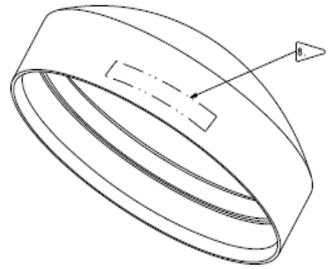

PICTORIAL VIEW
SCALE 2/1

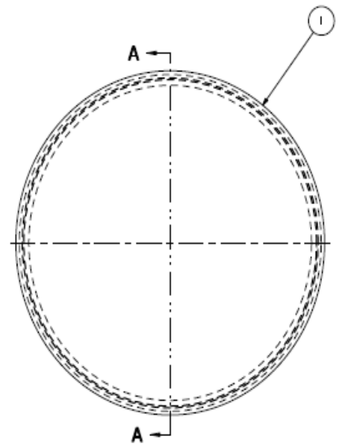

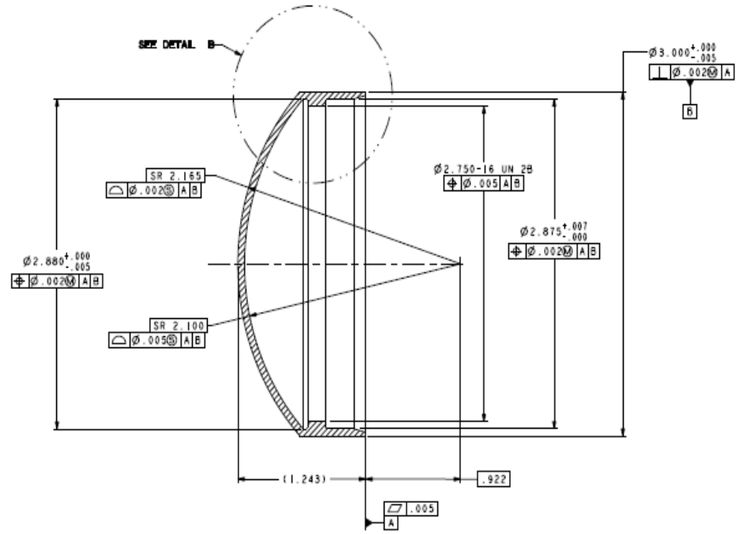

SECTION A-A

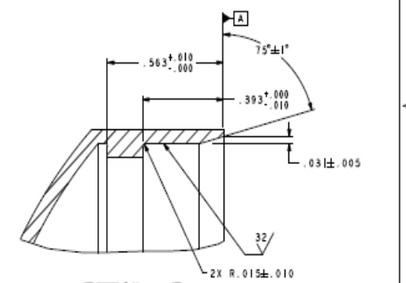

DETAIL B
SCALE 4/1

NEXT ASSY:	FINAL ASSY:
2A0265	2A0261
PROJECT NAME: PAT-1 PACKAGING	DRAWING LEVEL:

UNLESS OTHERWISE SPECIFIED DIMENSIONS ARE IN INCHES. TOLERANCES ARE:
DECIMALS .XX = ± .05 .XXX = ± .005
ANGULAR = ± 1°
MACHINED = 63
FINISH =

CURRENT ISSUE APPROVALS		DATE
DRAWN:	F. DI BONA - 2991	08-13-09
CHECKED:	R. YOSHIMURA - 6765	
DESIGNED:	C.W. MORROW - 6774	
APPROVED:	R. YOSHIMURA - 6765	

ARS		Ti-6AL-4V GRADE 5	11		1
NA	9919100	MARKING, GENERAL METHODS			
NA	9900000	GENERAL REQUIREMENTS			
NO MEGO	PART/CONTROL NO	DESCRIPTION/MATERIAL	NOTE	SHEET ZONE	ITEM

QUANTITY: NA = NO QUANTITY FOR DOCUMENTS PM = PROCESS MATERIAL AR = AS REQUIRED
ABBREVIATIONS: ALT = ALTERNATE EM = EXPENSE MATERIAL ARS = AS REQUIRED FOR ASSEMBLY

DRAWING: 2A0269-UNC
MODEL: 2A0269-000-UNC
TYPE: PART

SANDIA NATIONAL LABORATORIES (NM)
ENGLISH
THIRD ANGLE PROJECTION

TITLE: LID, SAMPLE CONTAINER-2 (SC-2) (U)
PART CLASSIFICATION: UNCLASSIFIED
DRAWING CLASSIFICATION: UNCLASSIFIED
SIZE: D
DRAWING NUMBER: 2A0269
ISSUE: A
CAGEC 14213 SCALE 2/1 SHEET 1 OF 1
ORIGIN PRO/E-WILDFIRE
STATUS SA-REL-08-13-09

2A0269-000 PART NO

UNCLASSIFIED

UNCLASSIFIED

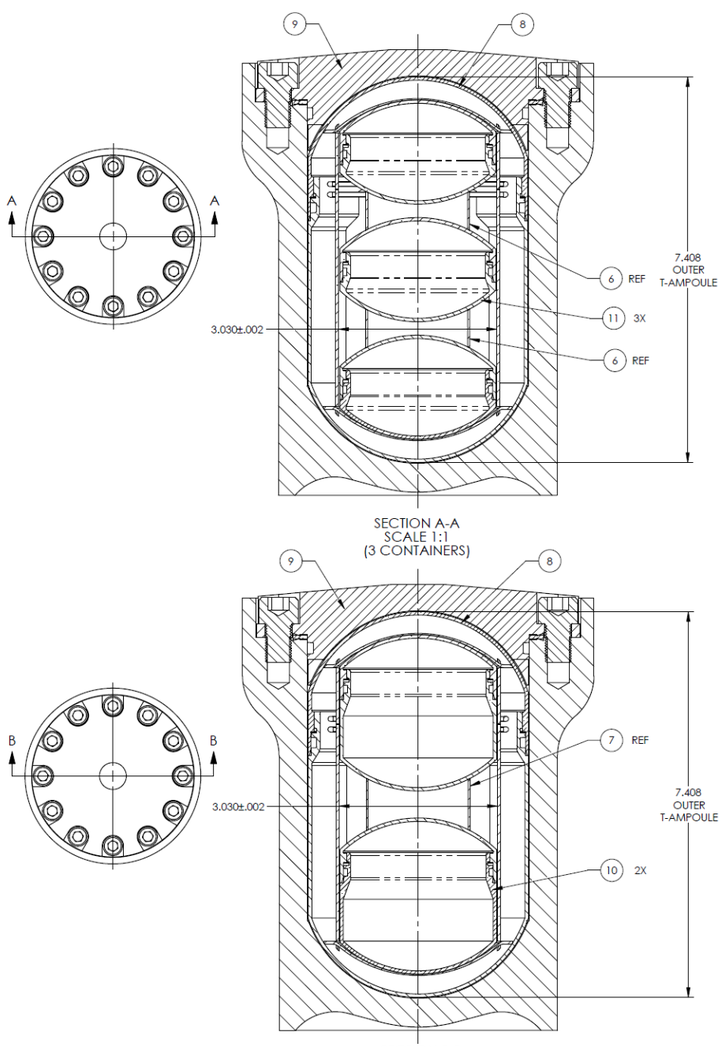

NOTES: (UNLESS OTHERWISE SPECIFIED)

1. GENERAL REQUIREMENTS AND DRAWING INTERPRETATION PER 9900000.
2. ABBREVIATIONS IN ACCORDANCE WITH ASME Y14.38-1999.
3. DIMENSIONING AND TOLERANCING IN ACCORDANCE WITH ASME Y14.5M-1994.
4. ALL DIMENSIONS ARE IN INCHES.
5. REMOVE BURRS AND SHARP EDGES .010 MAX.
6. MARK TEXT PER 9919100, CLASS K-1-A (LASER) .188" HIGH CHARACTERS, LOCATE APPROX. AS SHOWN.
7. TITANIUM TI-6AL-4V, GRADE 5. (SEE PAT-1040 FOR MATERIAL SPECIFICATION) FOR USE WITH THE PLUTONIUM AIR TRANSPORTABLE PACKAGE (MODEL PAT-1).
8. FABRICATE AND INSPECT PER PAT-1040.
9. R2.376 AND CONICAL SURFACE ARE NOT TANGENT.
10. ASSEMBLY WEIGHT FOR (SC-1, 3 CONTAINER CONFIGURATION = 364.16 GRAMS) AND (SC-2, 2 CONTAINER CONFIGURATION = 355.45 GRAMS).
11. MARK MANUFACTURER SERIALIZATION NUMBER ON ALL PARTS PER EACH ASSEMBLY PER 9919100, CLASS K-1-A (LASER) .188" HIGH CHARACTERS, LOCATE APPROX. AS SHOWN.

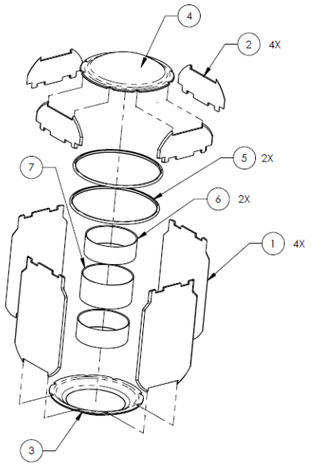

DESIGN AGENCY PART NUMBER	REVISION ISSUE	SHEET ZONE	PREPARED BY DESCRIPTION	DATE	CHKR	APVD
2A0385-000	A		K.D. McBRIDE, 2992/ R.H. YOSHIMURA, 6765/D.T. SCHMALE, 1813	08/18/2009	DTS	RHY

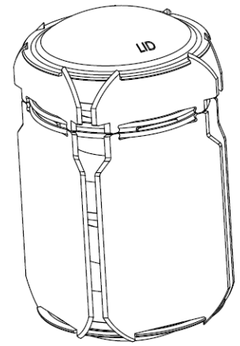

QTY.	PART/CONTROL NO.	DESCRIPTION/MATERIAL	NOTE	ZONE	ITEM
3	2A0268-000	SAMPLE CONTAINER-1 (SC-1) ASSEMBLY			11
2	2A0265-000	SAMPLE CONTAINER-2 (SC-2) ASSEMBLY			10
2	2A0263-000	TB-1/T-AMPOULE SHIPPING VESSEL ASSEMBLY			9
2	2A0261-000	T-AMPOULE ASSEMBLY			8
1	2A0385-045	SPACER, FOR 2 CONTAINERS	7,8,11		7
2	2A0385-040	SPACER, FOR 3 CONTAINERS	7,8,11		6
2	2A0385-030	LOCK RING	7,8		5
1	2A0385-025	DISH IN LID	6-9,11		4
1	2A0385-020	DISH IN BODY	7-9,11		3
4	2A0385-015	UPPER LEG	7,8,11		2
4	2A0385-010	LEG	7,8,11		1
NA	9919100	MARKING, GENERAL METHODS			
NA	9900000	GENERAL REQUIREMENTS			

ALT-ALTERNATE AR-AS REQ'D ARS-AS REQ'D PER ASS'Y EM-EXPENSE MATERIAL NA-DOCUMENT PM-PROCESS MATERIAL

SHEET	1	2	3	4	5	6
ISSUE	A	A	A	A	A	

TITLE: INNER CRADLE (U)

PART CLASSIFICATION: **UNCLASSIFIED**

DRAWING CLASSIFICATION: **UNCLASSIFIED**

SIZE: D DRAWING NUMBER: 2A0385

CAGEC 14213 SCALE 1/2 SHEET 1 OF 5

STATUS SA-REL-08/18/2009 ORIGIN SolidWorks 2008

GEOMETRIC PRECISION = NA

UNCLASSIFIED

DTS415

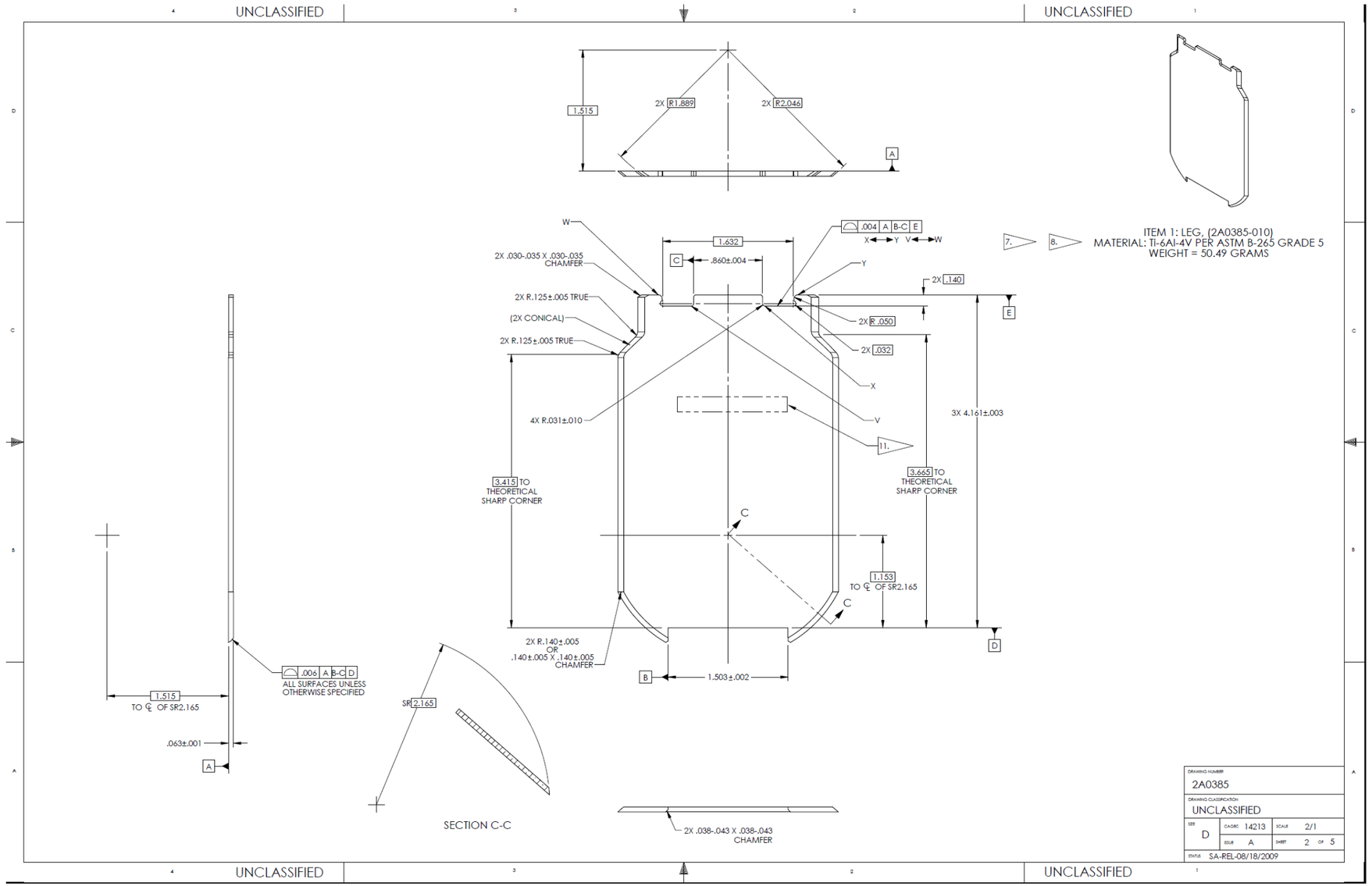
UNCLASSIFIED
UNCLASSIFIED
1.515
2X R1.889
2X R2.046
A
ITEM 1: LEG, (2A0385-010)
MATERIAL: Ti-6Al-4V PER ASTM B-265 GRADE 5
WEIGHT = 50.49 GRAMS
W
2X .030-.035 X .030-.035 CHAMFER
2X R.125±.005 TRUE
(2X CONICAL)
2X R.125±.005 TRUE
1.632
C
.860±.004
.004 A B-C E
X Y V W
Y
2X .140
E
2X R .050
2X .032
X
V
4X R.031±.010
11.
3X 4.161±.003
3.415 TO THEORETICAL SHARP CORNER
3.665 TO THEORETICAL SHARP CORNER
C
1.153 TO ℄ OF SR2.165
C
2X R.140±.005 OR .140±.005 X .140±.005 CHAMFER
D
B
1.503±.002
.006 A B-C D
ALL SURFACES UNLESS OTHERWISE SPECIFIED
1.515 TO ℄ OF SR2.165
.063±.001
A
SR2.165
SECTION C-C
2X .038-.043 X .038-.043 CHAMFER
DRAWING NUMBER 2A0385
DRAWING CLASSIFICATION UNCLASSIFIED
SIZE D
CAGEC 14213
SCALE 2/1
ISSUE A
SHEET 2 OF 5
STATUS SA-REL-08/18/2009
UNCLASSIFIED
UNCLASSIFIED

UNCLASSIFIED

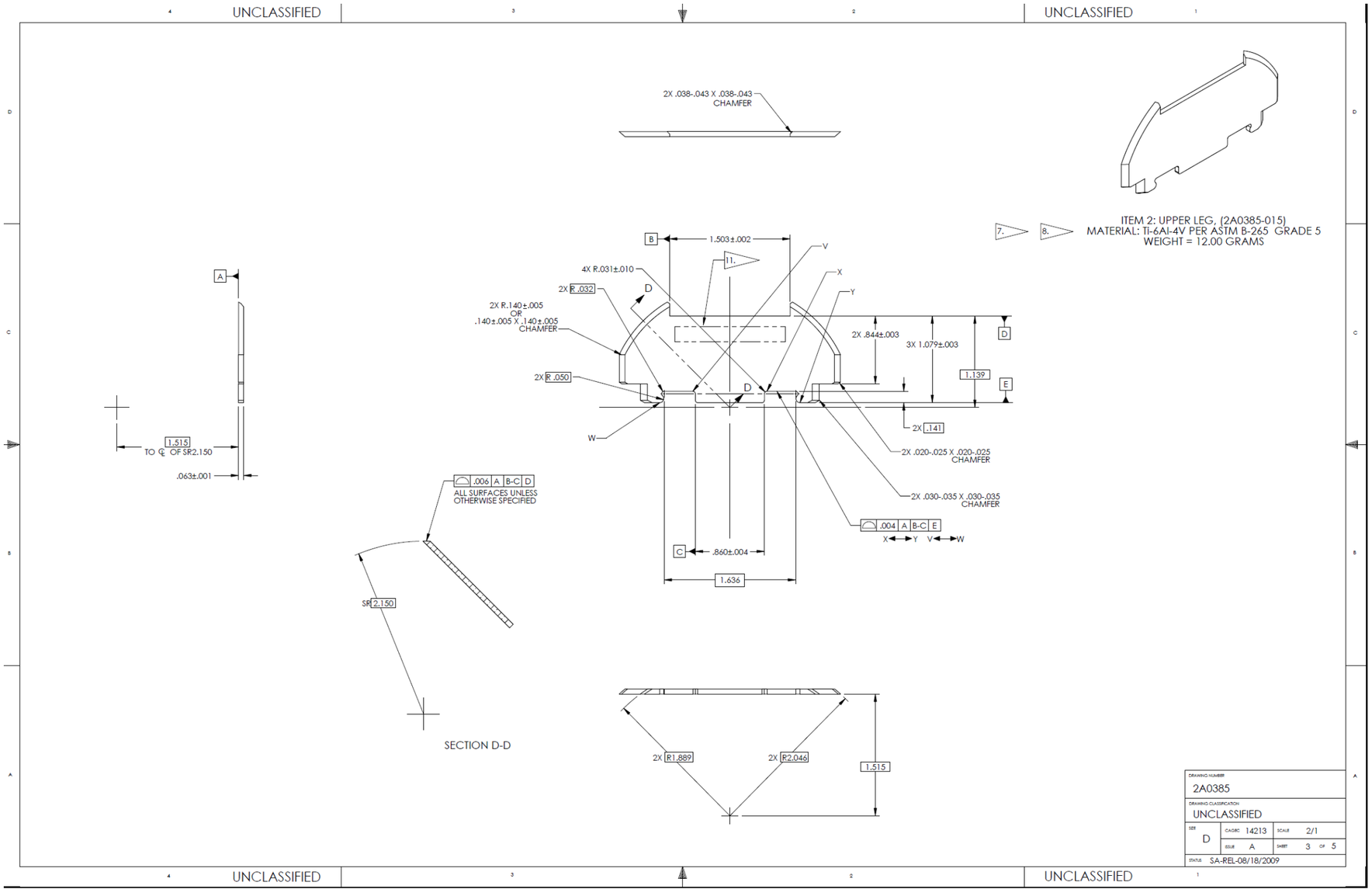

UNCLASSIFIED

UNCLASSIFIED

PART NUMBER	DIM "A"	DIM "B"
2A0385-020	.025±.002	.017±.002
2A0385-025	.039±.002	.025±.002

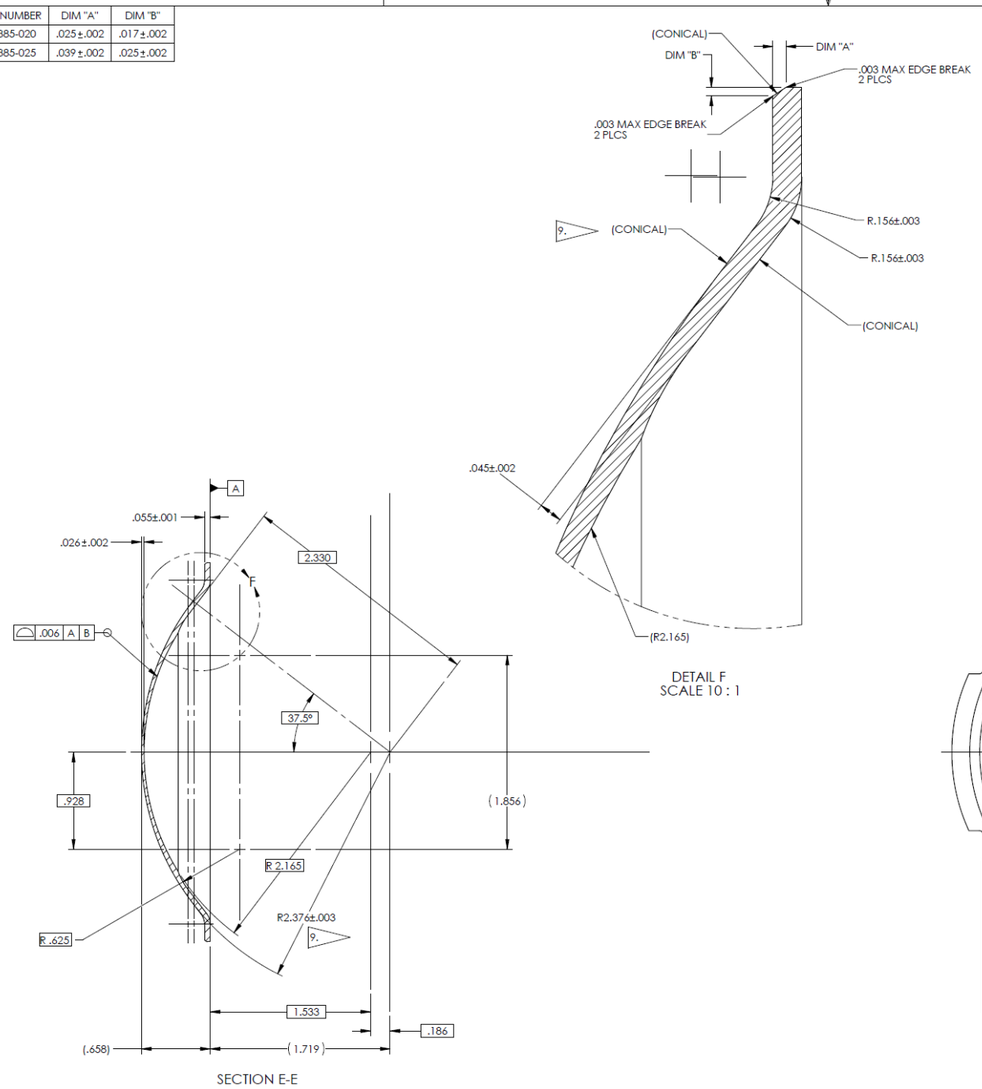

DETAIL F
SCALE 10 : 1

SECTION E-E

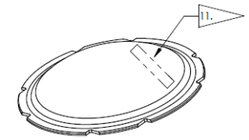

ITEM 3: DISH IN BODY, (2A0385-020)
MATERIAL: TI-6AI-4V PER ASTM B-348 GRADE 5
WEIGHT = 37.16 GRAMS
7. 8. 9.

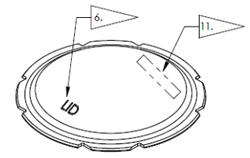

ITEM 4: DISH IN LID, (2A0385-025)
MATERIAL: TI-6AI-4V PER ASTM B-348 GRADE 5
WEIGHT = 37.16 GRAMS
7. 8. 9.

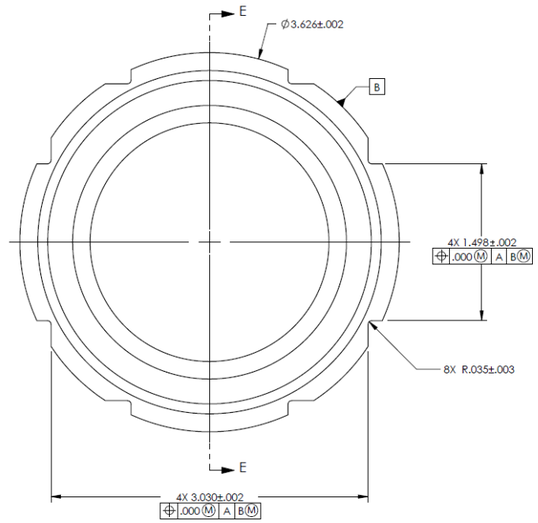

DRAWING NUMBER	2A0385
DRAWING CLASSIFICATION	UNCLASSIFIED
SIZE D	CAGEC 14213 SCALE 2/1
	ISSUE A SHEET 4 OF 5
STATUS	SA-REL-08/18/2009

UNCLASSIFIED

UNCLASSIFIED

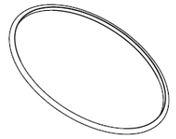

7. 8. ITEM 5: LOCK RING, (2A0385-030)
MATERIAL: TI-6AI-4V PER ASTM B-265 GRADE 5
WEIGHT = 6.42 GRAMS

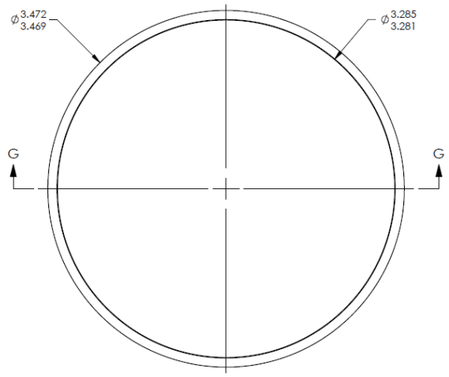

SECTION G-G

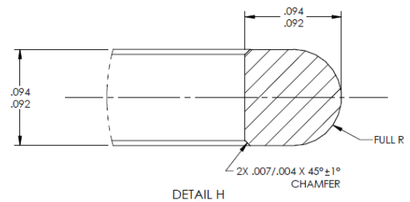

DETAIL H
SCALE 20 : 1

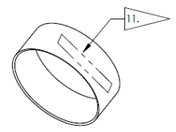

7. 8. ITEM 6: SPACER, FOR 3 CONTAINERS, (2A0385-040)
MATERIAL: TI-6AI-4V PER ASTM B-348 GRADE 5
WEIGHT = 13.52 GRAMS

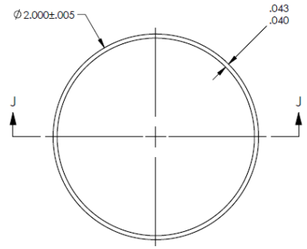

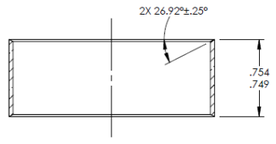

SECTION J-J

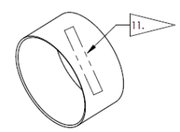

7. 8. ITEM 7: SPACER, FOR 2 CONTAINERS, (2A0385-045)
MATERIAL: TI-6AI-4V PER ASTM B-348 GRADE 5
WEIGHT = 18.33 GRAMS

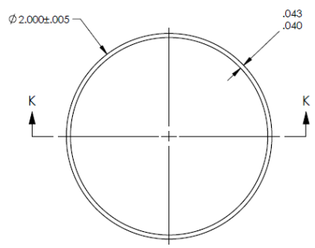

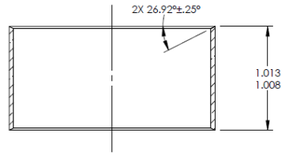

SECTION K-K

DRAWING NUMBER 2A0385
DRAWING CLASSIFICATION UNCLASSIFIED
SIZE D | CAGE 14213 | SCALE 2/1 | ISSUE A | SHEET 5 OF 5
STATUS SA-REL-08/18/2009

UNCLASSIFIED

This page intentionally left blank

1.3.3 Specifications

The following subsection includes the specifications for procuring titanium and O-ring materials.

1.3.3.1 PAT-1040 Titanium and O-Ring Materials and Component Fabrication Specification

See stand-alone document in Section 1.3.5.

1.3.4 Justification for Exclusion of the TB-1 Elastomer O-ring for Plutonium Metal Shipments

The copper gasket within the TB-1 containment vessel is the containment boundary seal and is supplemented by the elastomer O-ring for the plutonium oxide contents except in the case of the accident conditions for air transport of plutonium one hour fire where the elastomer seal decomposed. For the plutonium metal contents covered by this Addendum, the copper seal is the containment boundary seal and the elastomer O-ring is not used. The following arguments demonstrate that the copper gasket is the containment boundary seal for NCT, HAC, and accident conditions for air transport of plutonium.

A comparison is made for the copper gasket and elastomeric seal leakage rates. The copper gasket provided the low leakage rates observed in the NCT and HAC (Appendix A and B, resp., of 10 CFR 71 for the 1978 period) as cited in Table 4-1 of the PAT-1 SAR which shows the post test results of helium leak rate of less than 1×10^{-10} atm-cc/sec for NCT and 1×10^{-10} atm-cc/sec for HAC. Note that 10^{-7} atm-cc/sec is the leak test criteria for the TB-1 for the acceptance and maintenance tests. The 1×10^{-10} atm-cc/sec leakage rate demonstrated that the copper gasket with knife edge sealing surfaces was the containment boundary seal because this very low leak rate can only be achieved with a copper gasket and not with an elastomer seal due to helium permeation. The elastomer seal would have been saturated with helium and would have produced a permeation leak rate of about 10^{-6} std cc/sec. From page 691 of the "Nondestructive Testing Handbook," Table 2, Air permeabilities of elastomers,[1] the permeability for Viton A is $(0.88 \times 10^{-7}$ std $cm^3/s)/(cm^2/cm)$. The air permeability multiplied by the length of the O-ring (πD or $\pi \times 4.22$) $\times 0.88 \times 10^{-7} = 1.17 \times 10^{-6}$ std cm^3/s in the permeation leakage rate.

Since the measured leak rate was less than 1×10^{-10} atm-cc/sec for the TB-1 for both NCT and HAC, clearly it was the copper seal that provided the very low leak rate since O-ring would have been saturated after more than a day of being exposed to the helium fill tracer gas within the TB-1 in preparation for and during testing. The helium leak test measurement device would have produced a higher leak rate measurement if the copper seal had not functioned properly.

For accident conditions of air transport of plutonium (10 CFR 71.74), the copper gasket clearly provided the containment boundary seal since the elastomer decomposed under the 582°C (1080°F) environment experienced by the TB-1 in the post test fire environment.

No leakage or seal area (or any other visible) deformation occurred during the original PAT-1 certification tests, and based upon the structural analysis performed in Section 2 of the Addendum, none would occur with the new metal contents except for minimal localized denting of the TB-1. Thus for NCT, HAC, and accident conditions for air transport of plutonium, the

area around the copper seal remained elastic. Because the strength of the elastomer is negligible relative to the strength of the PH13-8Mo stainless steel of the TB-1, the structural performance of the TB-1 containment vessel without the elastomeric O-ring will not be affected.

Reference:

1. Nondestructive Testing Handbook, Second Edition, Volume One, Leak Testing, ASNT and ASM, 1982, page 691, Table 2.

1.3.5 PAT-1040 Titanium and O-Ring Materials and Component Fabrication Specification

The stand-alone document below includes the specifications for procuring titanium and O-ring materials.

PAT-1040 Titanium and O-Ring Materials and Component Fabrication Specification

Sandia National Laboratories

August 23, 2010

Prepared by: Richard H. Yoshimura, PAT-1 Project — Date: August 17, 2010

Reviewed by: Robert R. Richards, QA Coordinator — Date: Aug. 16, 2010

Approved by: David R. Miller, Manager — Date: Aug 19, 2010

Revision Log

Revision No.	Date	Description of Change
0	August 3, 2009	Original Release
1	August 23, 2010	Changed material for T-Ampoule, SC-1 and SC-2 O-ring seals to DuPont Viton® A and revised requirements documents accordingly

1 General

1.1 Summary

This fabrication specification establishes the quality, workmanship requirements and defines how quality is measured for the titanium components and procured parts within the Plutonium Air Transportable Package (PAT-1). The titanium components serve as a eutectic barrier, plutonium metal packaging containers, and support cradle for sample containers. This specification defines the titanium 6Al-4V (Ti-6Al-4V) Grade 5 material specification for the fabrication of the *T-Ampoule; Ring, Filler; Sample Container-1 (SC-1) Assembly; Sample Container-2 (SC-2) Assembly; Inner Cradle* and the procurement requirement for the *O-rings.* ASTM material specifications for the Ti-6Al-4V Grade 5 bar or sheet stock include minimum requirements specified in Section 3.1 of this document.

1.2 Definitions

Terms and Definitions

Certified Material Test Report - A document attesting that the material is in accordance with specified requirements, including actual results of all required chemical analyses, mechanical tests, and examinations. In addition to technical data, the document shall contain the SNL purchase order number, manufacturer or testing agency name and address and shall be signed by an authorized company representative.

Certificate of Conformance - A document signed and otherwise authenticated by an authorized company representative certifying the items meet all specified requirements.

Nonconformance - A deficiency in characteristic or documentation that renders the quality of an item unacceptable or indeterminate.

1.3 Abbreviations/Acronyms

Term	Description
ASNT	American Society for Nondestructive Testing
ASTM	American Society for Testing and Materials
CMTR	Certified Material Test Report
COC	Certificate of Conformance
SNL	Sandia National Laboratories
SAE	Society of Automotive Engineers
QAP	Quality Assurance Program

1.4 Requirements Documents

Unless otherwise approved, the following codes and standards (latest issue at the time of work) shall apply to establish the applicable minimum requirements for the titanium components and elastomeric O-rings. Reference test methods, specifications, and recommended practices are to be used to verify material properties and identify acceptable practices applicable to titanium and

O-ring components. Failure to identify applicable codes and standards does not imply elimination of required knowledge and compliance to perform work.

Document Number	Document Title
ASME Y14.5M	Dimensioning and Tolerancing
ASME BPVC	American Society of Mechanical Engineers (ASME); Boiler and Pressure Vessel Code, Section VIII Division 1, Rules for Construction of Pressure Vessels, 2007
ASME BPVC	American Society of Mechanical Engineers (ASME); Boiler and Pressure Vessel Code, Section II Materials Part D Properties (Customary), 2007
ASNT TC-1A	Recommended Practice for Personnel Qualification and Certification of Nondestructive Testing
ASTM B 348 (latest version)	Standard Specification for Titanium and Titanium Alloy Bars and Billets
ASTM B 265 (latest version)	Standard Specification for Titanium and Titanium Alloy Strip, Sheet and Plate
MIL-HDBK-5J*	Department of Defense Handbook, Metallic Materials and Elements for Aerospace Vehicle Structures," 31 January 2003
SAE AMS 7276G	Rings, Sealing, Fluorocarbon (FKM) Rubber High-Temperature-Fluid Resistant Low Compression Set 70 to 80
SAE AS568C	Aerospace Size Standard for O-rings
SAE AMS 2801B	Heat Treatment of Titanium Alloy Parts

1.5 Reference Documents

Document Number	Document Title
Ring, Filler	2A0262
T-Ampoule Assembly	2A0261
Sample Container-1 (SC-1) Assembly	2A0268
Sample Container-2 (SC-2) Assembly	2A0265
Inner Cradle	2A0385
O-ring, Viton® A, for T-*Ampoule Assembly*	2A0261, Item 3
O-ring, Viton® A, for *SC-1* and *SC-2*	2A0268, Item 3; 2A0265, Item 3

* This document is still available and used by industry.

1.6 Technical Submittals

All required submittals stated in this specification shall be submitted to SNL for review and documented approval in accordance with Section 4.6 Documentation, which present a summary of Subcontractor/Supplier submittal requirements. Submittals that do not meet the project requirements shall be rejected. Rejected submittals shall be corrected and resubmitted in a timely manner to avoid delays.

2 Quality Assurance Requirements

The quality assurance requirements are set forth in Section 9 of the PAT-1 Addendum and shall be incorporated in the procurement.

2.1 Quality Assurance Program

The vendor's QAP shall describe systems for planning, performing, and assessing work, which ensure materials, systems, results, and personnel meet stated quality objectives. The vendor shall qualify and approve any material suppliers and subcontractors utilized during the performance of the contract to the vendor's QAP. The vendor shall pass down all applicable QA requirements to any subcontractors. The vendor's QAP shall be submitted to SNL for review and written approval prior to the start of any work. Other quality requirements (audits and assessments, access to vendor facilities, on-site inspection and witnessing, qualification of vendor inspectors, nonconformance reporting, receiving and inspection, CMTRs, and COCs) apply per the contract documentation.

2.2 Evaluation and Approval

The supplier shall be evaluated and approved to furnish precision machining, metal fabrication, and assembly of components by SNL prior to contract award.

2.3 Audits and Assessments

SNL reserves the right to audit and assess the Supplier and Supplier's subcontractors and suppliers to verify conformance to the quality assurance program prior to the award of the contract, and at any time during performance of the contract.

Access to Supplier Facilities

SNL reserves the right to have its own qualified inspectors and personnel present during fabrication and inspection activities. At least five working days notice is required prior to inspection and testing activities planned by the Supplier so SNL can arrange for its staff's participation. Hold points may be identified in the schedule for coordination of inspection activities.

2.4 Qualification of the Supplier's Inspectors

Inspectors shall be suitably experienced and qualified. Inspectors independent of the operation shall carry out acceptance inspections.

2.5 Nonconformance Reporting

Nonconforming items are to be reported as outlined in the Supplier's approved QAP, with immediate written notification to SNL. Nonconformance Reports (NCR) shall be compiled to document the details of the nonconformance. Any nonconforming components shall be clearly identified and segregated. NCRs shall be traceable to actual components(s) affected. SNL shall disposition "Use-As-Is", "Repair", or "Reject" nonconforming items in writing prior to the Supplier proceeding with the next activity or step in the fabrication process. A copy of the completed NCR shall be submitted to SNL by the Supplier as part of the manufacturing documentation for "Use-As-Is" or "Repair" dispositions.

2.6 Receiving and Inspection

Upon delivery to SNL, the parts will be dimensionally and visually inspected by SNL authorized receipt inspectors as follows:

- Visually inspect components and assemblies for damage
- Verify purchase order number is marked on the parts, packaging, or accompanying documentation
- Verify CMTR contains manufacturer or testing agency name and address, and is signed by an authorized company representative
- Verify COC provided for each individual or lot of components
- Verify COC contains SNL purchase order, Supplier name and address and is signed by an authorized company representative

3.0 Materials

3.1 Titanium Components

3.1.1 Specific Material Requirements - ASTM requirements for the Ti-6Al-4V Grade 5 material are specified except minimums are specified for yield strength, ultimate tensile strength, elongation at tensile failure, reduction of area at failure. In some cases, heat treating may be required to meet the requirement of the solution treated and aged (STA) condition. The following presents specific material requirements for the titanium materials required for the following components:

Component	Specification
• T-Ampoule Assembly, 2A0261	Procure Ti-6Al-4V material meeting requirements of ASTM B-348 Grade 5 (use latest version for all documents), rough machine to drawing dimensions, leaving 0.05"+/-0.01" machining allowance on all surfaces. The titanium parts shall be protected from iron contamination before and during heat treatment. Heat treat to MIL-HDBK-5J strength requirements [see note *a* below] for STA condition per requirements and procedures of SAE AMS 2801B. Finish machine to drawing dimensions.
• Ring, Filler, 2A0262 • Sample Container-1 (SC-1) Assembly, 2A0268 • Sample Container-2 (SC-2) Assembly, 2A0265 • Inner Cradle, 2A0385: (Components) o 2A0385-025 Dish in Lid o 2A0385-020 Dish in Body o 2A0385-010 Leg (4 each) o 2A0385-015 Upper Leg (4 each) o 2A0385-030 Lock Ring (2 each)	Procure Ti-6Al-4V material meeting requirements of ASTM B-265 Grade 5, except with minimum values as follows: 0.2% yield strength: 140 ksi; ultimate tensile strength: 150 ksi; elongation at tensile failure: 10%; reduction of area at failure 20% [See note *b* below].
• Inner Cradle, 2A0385: (Components) o 2A0385-045 Spacer (2 each for SC-2) o 2A0385-040 Spacer (3 each for SC-1).	Procure Ti-6Al-4V material meeting requirements of ASTM B-348 Grade 5, except with minimum room temperature values as follows: 0.2% yield strength: 140 ksi; ultimate tensile strength: 150 ksi; elongation at tensile failure: 10%; reduction of area at failure 20% [see note *b* below].

a If material purchased already meets the requirements for the STA condition, the rough machine and heat treatment parts of the procedure stated above are not necessary.

b Procure Ti-6Al-4V material meeting requirements of ASTM B-348 or B-265 Grade 5 (use latest version for all documents), rough machine to drawing dimensions, leaving 0.05"+/-0.01" machining allowance on all surfaces. The titanium parts shall be protected from iron contamination before and during heat treatment. Heat treat to MIL-HDBK-5J strength requirements for STA condition per requirements and procedures of SAE AMS 2801B.

If material purchased already meets the requirements for the STA condition, the rough machine and heat treatment parts of the procedure stated above are not necessary. Finish machine to drawing dimensions.

3.1.2 The CMTR for the titanium material used to fabricate the titanium components shall be submitted for SNL approval prior to the start of fabrication activities.

3.2 Elastomeric O-Ring Seals

3.2.1 The elastomeric compound material used to manufacture all O-ring seals for the *T-Ampoule* and *SC-1* and *SC-2* sample containers shall be 100% virgin DuPont Viton® A conforming to SAE AMS 7276G Rings, Sealing, Fluorocarbon (FKM) Rubber High-Temperature-Fluid Resistant Low Compression Set 70 to 80. The hardness based on Shore A is 75.

3.2.2 The manufacturing tolerances for furnished O-ring seals shall conform to SAE AS 568C, *Aerospace Size Standard for O-rings*.

3.2.3 O-ring vendor shall provide a COC verifying that O-ring seals conform to the specifications above with the construction report. SAE AS568C provides standards on O-ring dimensions.

4.0 Fabrication Requirements

4.1 Equipment

The machine shop performing this fabrication shall supply all tooling, fixtures, and machines necessary to meet the fabrication requirements.

4.2.1 Inspection and Examination Requirements

Qualified and certified inspectors meeting the requirements of ASNT TC-1A shall perform all inspections.

4.2.2 A full dimensional inspection of the hardware shall be performed and documented to assure adherence to the dimensions and associated tolerances in the engineering drawings. ASME Y14.5M, *Dimensioning and Tolerancing*, shall serve as the basic standard for the dimensional inspection.

4.3 Product Marking

Vendor shall mark the product, packaging and accompanying documentation with the Item's part number. Laser marking is required on all metal part areas identified in the engineering drawing set (2A0259, 2A0260, 2A0261, 2A0262, 2A0264, 2A0265, 2A0266, 2A0267, 2A0268, 2A0269, 2A0385).

4.4 Surface Finish

All titanium surfaces shall be cleaned to remove grease, oil, salt, chemicals, etc. prior to packaging. The cleaning operation shall not use abrasives, and all machined surfaces shall be protected from damage.

O-ring seal areas will meet specific surface finish requirements as set out on the fabrication drawings.

4.5 Packaging and Shipping Requirements

Items fabricated to this technical specification shall be packaged to prevent damage during shipping or transport to SNL.

4.6 Documentation

The Supplier shall submit a formal construction report to SNL for review and written approval prior to shipment. The construction report shall contain the minimum documentation listed below and a minimum of three copies of the required document submittals.

The construction report shall contain the following documentation at a minimum:

- Vendor's Quality Assurance Program Manual

- CMTRs for procured raw materials including stress strain curves, heat treatment
- Certificates of Conformances for procured components
- Certificated of Conformance for fabricated T-Ampoule; Ring, Filler; Sample Container-1; Sample Container-2; Inner Cradle and O-rings.
- Product Travelers
- Qualifications and Certifications of Personnel Performing Inspection Activities
- Inspection Records
- Engineering Change Notices, Design Deviation Requests or similar documents
- Non-Conformance Reports
- Construction Report

5.0 Requirements Specific to the T-Ampoule Titanium Components Fabrication and Inspection

With the exception of the elastomeric (O-ring) seal, the T-Ampoule (Drawing 2A0261) was designed, will be fabricated and will be inspected to meet the requirements of the ASME Boiler and Pressure Vessel Code (Section VIII) with the following exceptions or explanations:

1. The T-Ampoule meets the requirements of Section VIII as modified by this document.
    a. The size requirements of section *U-1(c)(2)(i)* of Section VIII do not apply.
    b. The marking requirements of parts UG 115-119 do not apply. T-Ampoules will be marked with part and serial numbers.
2. Given the dry inert gaseous initial atmosphere and the general non-reactivity of titanium with vessel contents, design calls for no corrosion allowance.
3. T-Ampoule MAWP will be established by calculations as set forth in this document. Allowable pressure calculations will be performed based on the following paragraphs of Section VIII:
    a. Torispherical Head allowable pressure is calculated based on the requirements of Section VIII's Mandatory Appendix 1, Supplementary Design Formulas, paragraph 1-4(d).
    b. Allowable pressure, based on membrane stress in the hemispherical head, is estimated based on the criteria set forth in paragraph UG-32.
    c. Allowable pressures in both the longitudinal and circumferential direction of the shell and lid are estimated based on the criteria set forth in paragraph UG-27.

d. T-Ampoule is exempt from the requirements of paragraph UG 32, *Thickness of Shells and Tubes Under External Pressure*. As the T-Ampoule will be subject to impact loading a separate impact analysis will be conducted as described in Section 2 of the document PAT-1 Safety Analysis Report Addendum Docket No. 71-0361, Rev. 0, August 2009.

e. Since no welded joints exist on the T-Ampoule, joint efficiency, E, in all Section VIII equations were taken as 1.0.

4. The requirements of paragraph UG-125 regarding pressure relief devices do not apply. Overpressure response will be discussed in detail in the body of this paper.

5. T-Ampoule will be fabricated of Ti-6Al-4V titanium alloy produced to the specifications in Section 3.1 of this specification except as modified below.

    a. Temperature-dependent allowable stress criteria will be determined using the procedures outlined in the ASME Boiler and Pressure Vessel Code, Section II Part D, *Mandatory Appendix 1 Basis for Establishing Stress Values in Tables 1A and 1B.*

    b. In either case, titanium maintains ductility at low temperatures and is therefore exempt from the requirements of Sections UCS 66 through 68 pertaining to derating allowable stress for low-temperature operation.

6. In the case of analysis of the torispherical heads, and in accordance with Section UG-32(e), allowable stress will be limited to 20,000 psi for temperatures below 77ºF, and will be reduced proportional to the curves developed in 2.b above for temperatures above 77ºF.

7. In addition to the quality requirements of Section 2 of this specification, the T-Ampoule quality program will meet the requirements of Section VIII with the following exceptions:

    a. The standard hydrostatic test of paragraph UG-99 or the pneumatic test of paragraph UG-100 are not required.

    b. The requirements of paragraph UF-55 regarding ultrasonic examination do not apply. Inspection will consist of visual inspection and physical measurement of specified dimensions.

    c. As the T-Ampoule components are machined without welding, the requirements of part UW and part UB do not apply.

    d. In lieu of the requirements of paragraph UG-91, the inspector will meet the requirements listed below:

        i. Inspector will demonstrate experience with spinning and fabrication processes.

        ii. Inspector will demonstrate experience with Section VIII.

2. STRUCTURAL EVALUATION

The structural evaluation in this addendum examines the incorporation of plutonium metal as a new payload for the PAT-1 package. The Pu metal is packed in an inner container (*T-Ampoule Assembly,*[A] Drawing 2A0261, designated the T-Ampoule) that replaces the inner container (*Can Assembly*, Drawing 1024, designated PC-1) that is carried within the TB-1 *Containment Vessel* (Drawing 1017, designed TB-1). The T-Ampoule and associated Pu metal contents packing configurations are described in Section 1.2.1, and the Pu metal contents are discussed in Section 1.2.2 of this addendum.

2.1 Description of Structural Design

This section describes the structural evaluation of the T-Ampoule and its contents and packing. The T-Ampoule and its loading configurations replace the PC-1 and its contents described in the SAR.[1] In the case of the PAT-1, (1) the aluminum honeycomb (*Spacer, Top,* Drawing 1015, designated Top Spacer) and the PC-1 stainless steel inner container is being replaced by the titanium T-Ampoule, and (2) the PuO_2 content is being replaced by plutonium metals or sample containers containing plutonium metal and composite materials. The primary purpose of this addendum is to demonstrate that the modifications to the TB-1 of replacing the PC-1 and its contents and packing with the T-Ampoule and its contents and packing do not significantly change the design, operating characteristics, or safe performance of the package so that the requirements of 10 CFR 71.19(d) are met.

The T-Ampoule is not a containment boundary; it is similar to the PC-1 in the SAR.[1] Its function is to provide a eutectic prevention barrier between the plutonium metal contents and the stainless steel (*TB-1 Containment Vessel,* Drawing 1017, designated TB-1) throughout normal and accident conditions. The PAT-1 (*Overpack, AQ,* Drawing 1002, designated AQ-1 and TB-1) with the Ti-6Al-4V Grade 5 T-Ampoule is designed to transport bulk plutonium metal in the form of hollow cylinders, as well as various shaped plutonium metal contents packed in sample containers. The plutonium metal may be in alloyed or pure form.

A. The Pu hollow cylinders (Electro-Refined [ER] material is analyzed, see Section 1.2.2) are cast in two weights – 831 g (6.350 cm [2.500 in.] OD, 5.801 cm [2.284 in.] ID × 8.054 cm [3.171 in.] length) and 731 g (6.350 cm [2.500 in.] OD, 5.801 cm [2.284 in.] ID × 7.087 cm [2.790 in.] length).[B] Two sizes of Ti-6Al-4V Grade 5 sample containers (SC-1 or SC-2) provide for two- and three-sample-container stacked configurations nested within a Ti-6Al-4V Grade 5 Inner Cradle, which is installed inside of the T-Ampoule. Pure and alloyed plutonium metal sample contents in the form of disks, cylinders, and assorted shapes can be carried, weighing a maximum of 174 g in each SC-1 or 338 g in each SC-2. For the bounding analysis of the Pu contents in SC-1 and SC-2, solid Pu cylinders of 2.23 cm (0.88 in. dia.) × 2.23 cm (0.88 in.) height and 2.79 cm (1.1 in.) dia. × 2.79 cm (1.1 in.) height were analyzed respectively. Pu/Be composite samples in the form of disks, cylinders and assorted shapes can be carried, weighing a

[A] The drawing titles are in italics and are used interchangeably with the designated names in this addendum. See Section 1.3.2 in this addendum and Chapter 9 in the SAR[1] for drawing number, title, and revision.

[B] These are the general dimensions provided without tolerances.

maximum of 60 g in SC-1 or SC-2. For the bounding analysis of the Pu/Be contents in the SC-1 and SC-2, solid Pu cylinders of 0.663 in. dia. × 0.663 in. height (60 g in each SC) were analyzed.

Optional Packing material in the form of tantalum foil is used within the sample containers to pack the Pu contents. The Pu hollow metal cylinders are wrapped with tantalum foil to prevent contamination and for packing.

See Table 2-1 for the mass limits of the Pu contents for four loading configurations, the weights of the various components within the TB-1, and the weight allowances for the packing material, assuming loading of the maximum Pu content weight for each configuration. Detailed descriptions of the T-Ampoule and sample containers are presented in Section 1 of this addendum. The AQ-1 and TB-1 are described in Chapter 1 of the PAT-1 Safety Analysis Report (SAR).[1] The maximum bounding activity of the contents is 897 Ci (3000 A_2), as discussed in Section 1.2.2 for 831 g of plutonium metal hollow cylinders (excluding Pu-241 decay).

As described in the following sections, the analysis and testing documented herein demonstrates that the T-Ampoule maintains its integrity as a eutectics prevention barrier under plutonium air transport accident conditions, thus demonstrating that the TB-1 maintains its integrity and provides containment of its contents under normal conditions of transport (NCT), hypothetical accident conditions (HAC), and plutonium air transport accident conditions.

Table 2-1. Weight of Plutonium Metal Contents and T-Ampoule and Packing for Six Loading Configurations.

Component	831 g Pu Hollow Cylinder[a] (g)	731 g Pu Hollow Cylinder[b] (g)	Three Stack SC-1, Solid Pu Cylinders (Bounding) (g)	Two Stack SC-2, Solid Pu Cylinders (Bounding) (g)	Three Stack SC-1, Composite Contents (Bounding) (g)	Two Stack SC-2, Composite Contents (Bounding) (g)
Total Weight Allowance Inside TB-1	2100	2100	2100	2100	2100	2100
Titanium Filler Ring[k]	65	65	65	65	65	65
Titanium Ampoule[k]	571	571	571	571	571	571
Sample Containers (Total Weight) [k]	NA	NA	454[c]	391[d]	454[c]	391[d]
Inner Cradle[g]	NA[h]	NA	364	356	364	356
Plutonium Contents	831	731	523[e]	676[f]	180[i]	120[j]
Maximum Weight Allowance for	633	733	123	41	466	597

Component	831 g Pu Hollow Cylinder[a] (g)	731 g Pu Hollow Cylinder[b] (g)	Three Stack SC-1, Solid Pu Cylinders (Bounding) (g)	Two Stack SC-2, Solid Pu Cylinders (Bounding) (g)	Three Stack SC-1, Composite Contents (Bounding) (g)	Two Stack SC-2, Composite Contents (Bounding) (g)
Tantalum Foil Packing and Ancillary Plastics[l]						

[a] Dimensions of the 831 g. Pu hollow cylinder: 6.350 cm (2.500 in.) OD, 5.801 cm (2.284 in.) ID × 8.054 cm (3.171 in.) length. The bounding dimensions for the structural analysis are 6.375 cm (2.510 in.) OD × 5.801 cm (2.274 in.) ID×7.374 cm (2.903) in. length.

[b] Dimensions of the 731 g Pu hollow cylinder: 6.350 cm (2.500 in.) OD, 5.801 cm (2.284 in.) ID × 7.087 cm (2.790 in.) length. The bounding dimensions for the structural analysis are 6.375 cm (2.510 in.) OD×5.776 cm (2.274 in.) ID×6.490 cm (2.555 in.) length bounding dimensions.

[c] 3 SC-1 Sample Containers, 151 g each.

[d] 2 SC-2 Sample Containers, 196 g each.

[e] 174 g Pu content per container. A Pu metal cylinder of 2.23 cm (0.88 in). dia. × 2.23 cm (0.88 in.) height is used as the bounding configuration for the structural analysis. See Section 1 for other forms.

[f] 338 g Pu content per container. A Pu metal cylinder of 2.79 cm (1.1 in. dia.) × 2.79 cm (1.1 in.) height is used as the bounding configuration for the structural analysis. See Section 1 for other forms.

[g] Inner cradle part weights: Leg, Body, each 50.49 g; Leg, Lid, each 12.00 g; Dish, each 37.16 g; Ring, each 6.42 g, Spacer, SC-1, each 13.52 g; Spacer, SC-2, each 18.33 g. Calculated weight from SolidWorks. (http://www.solidworks.com/)

[h] Not Applicable.

[I] 60 g composite sample per container.

[j] 60 g composite sample per container.

[k] Calculated weight from ProENGINEER (http://www.ptc.com/products/proengineer/).

[l] See Sections 1.2.2.1 and 7.1.2.1 for ancillary plastic amount permitted.

2.1.1 Discussion

Several tests on the PAT-1 package are prescribed in 10 CFR 71, Subpart F (from 1978); the results of these tests are described in the SAR.[1] The PAT-1 package meets the containment criteria for NCT, HAC, and plutonium air transport accident conditions. Conditions for meeting these criteria are described in the following sections:

- Section 2.6 of the SAR[1] describes the response of the PAT-1 package design to the NCT performance tests specified in 10 CFR 71.71.
- Section 2.7 of the SAR[1] describes the response of the PAT-1 package design to the HAC performance tests prescribed in 10 CFR 71.73.
- Section 2.8 of the SAR[1] describes the response of five specimen PAT-1 packages to the sequential tests prescribed in 10 CFR 71.74(a), as well as the response of a TB-1 containment vessel to the 600 psi immersion test prescribed in 10 CFR 71.74(c).

Structural calculations described in Section 2.12.2 were performed to model and benchmark the response of the PAT-1 package to end-on, side-on, and center-of-gravity-over-corner (CGOC) high-speed impact tests. These analyses were used to determine the response of the TB-1

containment vessel and T-Ampoule eutectic barrier for NCT, HAC, and plutonium air transport accident conditions.

The TB-1 was also analyzed under the HAC dynamic crush condition since it was not considered during the performance tests conducted for the SAR.[1] In addition, the differences in the contents from the original package lead to different internal pressures and are therefore analyzed in this addendum. These analyses were used to verify that the TB-1 is within design limits (see Sections 2.6 and 2.7).

2.1.2 Design Criteria

A general description of the PAT-1 package was provided in Chapter 1 of the SAR.[1] Additional structural design descriptions of the AQ-1 and TB-1 are provided in Chapter 2 of the SAR.[1] This section of the addendum focuses on the structural design criteria for the TB-1 in areas not addressed in the SAR[1] or affected by changes in the package. The addendum also includes structural analyses of the T-Ampoule during the air transport accident conditions to ensure that a eutectic barrier is maintained.

The design criteria for the TB-1 containment vessel for NCT and HAC are described in Section 2.1.2.1 below. The design criteria for the TB-1 for the aircraft accident conditions are that the average through-wall stresses remain elastic and the forces on the closure joint do not exceed the aggregate bolt preload force.

The design criterion for the T-Ampoule eutectic prevention barrier under NCT is that it remains fully elastic. The design criteria for the T-Ampoule eutectic prevention barrier under HAC are described in Section 2.1.2.1 below. The design criteria for the T-Ampoule eutectic prevention barrier under aircraft accident conditions are described in Section 2.1.2.2 of this addendum.

2.1.2.1 NCT and HAC

The design criterion for the T-Ampoule under HAC environments is that the eutectic prevention barrier maintains structural integrity, i.e., avoiding even the initiation of a ductile tear. This is proven by analytically demonstrating that all 580,000 finite elements representing the T-Ampoule remain within a tested stress-triaxiality-versus-equivalent-plastic-strain locus, and below an empirically-based failure criterion that would indicate initiation of ductile tearing if exceeded.

For the assessment of the stainless steel TB-1 containment vessel under the NCT and HAC, Regulatory Guides 7.6[2] and 7.8[3] and 10 CFR 71.71 and 71.73 were used to determine the appropriate allowable stress values and load combinations. Acceptance criteria for the PAT-1 package are defined in 10 CFR 71.73 for Type-B dynamic crush hypothetical accident conditions as the containment boundary remaining essentially elastic (through-thickness stresses below ASME allowables), as well as maintaining containment to a release of less than 1 A_2 in a week.

Table 2-2 summarizes the load combinations for the NCT and HAC as given in Regulatory Guide 7.8. The "Crush" condition for the HAC was added to the table based on 10 CFR 71.73. The TB-1 containment vessel was heat treated to the H1075 condition after forging, thus minimizing fabrication stresses which were not examined in the analyses. In addition, the majority of load combinations in Table 2-2 were analyzed during the testing performed for the SAR.[1]

Replacement of the PC-1 with the T-Ampoule and the associated contents require additional NCT and HAC analysis of the load combinations that affect the TB-1. Checks for NCT are performed on the TB-1 to determine if the change in contents causes any internal pressure effects or differential thermal expansion/contraction interaction with the T-Ampoule (Hot Environment and Cold Environment). For the HAC, the dynamic crush analysis is included as well as a discussion on the potential effects from thermal fire. All other load combinations for the NCT and HAC are bounded by the testing and analysis performed in support of the SAR[1] and the results of the air transport accident analyses described in Sections 2.1.2.2, 2.8, 2.12.2, and 2.12.5. Specifically, the original tests did not show any effect on the TB-1 from the 4-foot or 30-foot drops for the NCT or HAC. Since there are now different contents within the TB-1, the results of the air transport accident analyses performed for this addendum are used for comparison. In these analyses, the T-Ampoule remains intact and the TB-1 remains essentially elastic, excepting minimal localized denting from the solid metal contents. Since the impact velocity for the air transport accident of 422 ft/s is substantially greater that the 44 ft/s for the HAC and the 16 ft/s for the NCT, the HAC and NCT free-drops will not threaten the integrity of the TB-1.

Table 2-2. Load Combinations for NCT and HAC

	Applicable Initial Condition								
	Ambient Temperature[1]		**Insolation**		**Decay Heat**		**Internal Pressure[2]**		**Fabrication Stresses[3]**
	100˚F	**-20˚F**	**Max[1]**	**Zero**	**Max**	**Zero**	**Max**	**Min**	
NORMAL CONDITIONS (Analyze Separately)									
Hot environment: 100˚F ambient temp.			X		X		X		X
Cold environment: -40˚F ambient temp.				X		X		X	X
Increased external pressure: 20 psia		X		X		X		X	X
Minimum external pressure: 3.5 psia	X		X		X		X		X
Vibration and shock[4] (normally incident to the mode of transport)	X		X		X		X		X
		X		X		X		X	X
Free-drop: 4-foot drop	X		X		X		X		X
		X		X		X		X	X
ACCIDENT CONDITIONS (Apply sequentially)									
Free drop: 30-foot drop	X		X		X		X		X
		X		X		X		X	X
Crush:[6] 1100 lb drop from 30 ft	X		X		X		X		X
		X		X		X		X	X

Applicable Initial Condition									
	Ambient Temperature[1]		Insolation		Decay Heat		Internal Pressure[2]		Fabrication Stresses[3]
	100˚F	-20˚F	Max[1]	Zero	Max	Zero	Max	Min	
Puncture: Drop onto bar	X		X		X		X		X
		X		X		X		X	X
Thermal[5]: Fire accident	X		X		X		X		X

This table is from Regulatory Guide 7.8[3]

X designates the initial conditions included for a given load combination.

1 See Regulatory Position 1.1. For this addendum, Section 2.8.5.1 Cold Ambient Temperature Tests and Section 2.8.5.2 High Ambient Temperature Tests in the SAR[1] indicate that the PAT-1 that testing at -40ºF and 130ºF ambient temperature (higher than the current regulation of 100ºF) would have no significant adverse effect on the PAT-1 package. The NCT, HAC, and accident conditions for air transport of plutonium were evaluated at room temperature.

2 See Regulatory Positions 1.3 and 1.4. The MNOP gage pressure calculated in Section 2.6.1.1 of this addendum of 4.2 psig is negligible when one considers that the TB-1 withstands a pressure of 1110 psia during the accident conditions for air transport of plutonium fire test evaluated in Section 3.6.4 in the SAR[1]. Internal pressure was not included in the structural calculations of NCT, HAC, and accident conditions for air transport of plutonium in this addendum.

3 See Regulatory Position 1.5. The T-Ampoule is machined from a block of solid titanium stock procured to PAT-1040 in this addendum. Since the T-Ampoule is machined and heat treated, there are no fabrication stresses.

4 See Regulatory Position 2.5. The shock and vibration loads encompassing road, rail, and air transportation are negligible compared to the impact loads associated with the NCT drop test [ref: NUREG/CR-0030[133]], for which a detailed analysis showed elastic response for both the T-Ampoule and TB-1 (see Section 2.12.5.3.2 of this addendum).

5 Evaluations should be made 30 minutes after start of fire and at postfire steady-state conditions.

6 Sequential application of crush test described in 10 CFR 71.73(c)(2) and 10 CFR 71.55(f)(1)(ii).

Regulatory Guide 7.6 states that Section III of the ASME Boiler and Pressure Vessel (B&PV) Code[5] should be used to compute the allowable stress intensity, S_m. The TB-1 was constructed in the 1970s from PH13-8Mo stainless steel with a H1075 heat treat. This material is chemically identical to SA-705, XM-13 as specified in ASME Section II, Part A. Section II, Part A of the B&PV Code defines the yield stress (S_y) as 150 ksi (averaged between H1050 and H1100), and the ultimate or tensile stress (S_u or S_T) as 162 ksi. Note that these values are the same as specified in the Military Handbook.[6] However, in Section II, Part D, the PH13-8Mo material is not listed among materials whose allowable stress intensity is provided. Therefore, Appendix 2 of Section II, Part D was mandatory and used to establish the allowable stress intensity. Based on Appendix 2, S_m is equal to the smaller of 1/3 S_T or 2/3 S_y, establishing the allowable stress intensity, S_m, at 54 ksi.

Table 2-3 lists the primary membrane stress and the primary membrane plus bending stress for both NCT and HAC, and the primary plus secondary stress for the NCT, based on Regulatory Guide 7.6 at room temperature.

Table 2-3. Allowable Stresses for NCT and HAC Based on Regulatory Guide 7.6 (Room Temperature)

	NCT		HAC	
Primary membrane stress	S_m	54 ksi	smaller of 2.4 S_m or 0.7 S_u	113.4 ksi
Primary membrane plus bending stress	1.5 S_m	81 ksi	smaller of 3.6 S_m or S_u	162 ksi
Primary stress plus secondary stress	3 S_m	162 ksi		

The NCT and HAC conditions are not at room temperature. At an increased temperature of 114°C (238°F) (see TB-1 maximum NCT temperatures in Table 3-1 of Section 3) for the NCT, the yield and tensile strength of PH 13-8Mo is determined to be 141 and 152.3 ksi, respectively (Figure 2.6.5.1.1 of the Military Handbook, 94% of room temperature strength[6]). Based on Mandatory Appendix 2 of Section II, Part D, the allowable stress intensity is the smaller of 2/3 S_y and 1/3 S_T, or 50.8 ksi. For the HAC impact analyses at 114°C (238°F), prior to the fire, Mandatory Appendix 2 of Section II, Part D, gives the same allowable stress intensity as for NCT, 50.8 ksi. At an increased temperature of 147°C (296°F) (see TB-1 maximum HAC temperatures in Table 3-1 of Section 3) for the HAC during the fire, the yield and tensile strength of PH 13-8Mo is determined to be 137 and 147 ksi, respectively.[5] Based on Mandatory Appendix 2 of Section II, Part D, the allowable stress intensity is the smaller of 2/3 S_y and 1/3 S_T, or 49 ksi.

Table 2-4 lists the primary membrane stress and the primary membrane plus bending stress for both NCT and HAC (at both 114°C (238°F) and 147°C (296°F), and the primary plus secondary stress for the NCT, based on Mandatory Appendix 2 of Section II, Part D. These stresses will be used to assess the NCT and HAC load conditions.

Table 2-4. Allowable Stresses for NCT and HAC Based on Regulatory Guide 7.6, (Elevated Temperatures)

	NCT (114 °C)		HAC (at 114 °C, 147 °C)	
Primary membrane stress	S_m	50.8 ksi	smaller of 2.4 S_m or 0.7 S_u	106.6 ksi, 102.9 ksi
Primary membrane plus bending stress	1.5 S_m	76.2 ksi	smaller of 3.6 S_m or S_u	152.3 ksi, 147 ksi
Primary stress plus secondary stress	3 S_m	152.4 ksi		

2.1.2.2 Accident Conditions for Air Transport of Pu

The TB-1 was shown in the SAR[1] aircraft impact tests to remain elastic and to maintain containment to a release of less than 1 A_2 in a week. With similar mass contents, similar TB-1 response would be expected, excepting the possibility of minor localized denting due to more dense contents (solid Pu vs. oxide powder). Since there are no stress limits required for the containment vessel during 10 CFR 71.74 air transport accidents (only < A_2/week release rate), demonstrating the avoidance of yielding was conservatively set as the primary goal. Von Mises

stress (distortion-energy theory) predicts yielding with the greatest accuracy for all stress states, and thus this stress was conservatively compared against the stress intensity limits for surface transport (10 CFR-71.73) shown in Table 2-4. An acceptance criterion of "below through-thickness yielding" was used to demonstrate similar TB-1 behavior as in the original regulatory testing. This also means zero plasticity in the seal area of the TB-1, ensuring similar containment requirements of < A_2/week release rate performance of the containment vessel.

For the evaluation of the T-Ampoule eutectic prevention barrier in the PAT-1 package subjected to the requirements of 10 CFR 71.74 (Accident conditions for air transport of plutonium), two strain-based criteria are used to ensure that its structural integrity is maintained. The first is a locus in stress triaxiality–equivalent strain space developed from impact tests conducted using the Sandia National Laboratories (SNL) 18" horizontal actuator, along with a finite element model of these tests. The impact tests are described in Section 2.1.1, along with the detailed development of the strain locus for the titanium material. The second is an empirically-based failure criterion in the form of an evolution integral in plastic strain modified by the stress state called, Tearing Parameter, which is described in Sections 2.1.1.1 and 2.12.3.8.

Although the tested strain locus encompasses most of the stress triaxiality—equivalent plastic strain space needed for the SAR Addendum analyses, velocity limits at the test facility required the use of a second, complimentary criterion to demonstrate that the T-Ampoule integrity would be maintained throughout all regulatory accident environments. Tearing Parameter is a true analytical failure criterion, which is based on material tensile tests to failure, and is valid over the entire range of stress triaxialities. The two strain-based integrity criteria are complimentary in that the two combined provide additional confidence that even the initiation of a ductile tear will be avoided, and thus T-Ampoule structural integrity will be maintained.

A plot of the strain locus is shown in Figure 2-1. It should be noted that this is not a failure locus, since no cracks were formed in the test. However, it does represent regions in strain space where failure does not occur; therefore, the container is safe. In this sense, the data from the component analyses (see Section 2.12.5) can be compared with the locus in Figure 2-1, and a safety margin based on the strain generated in the test can be calculated. For elements exceeding the tested strain locus, Tearing Parameter is integrated over the plastic strain, and is compared to the critical Tearing Parameter value for the Ti-6Al-4V to determine a safety margin.

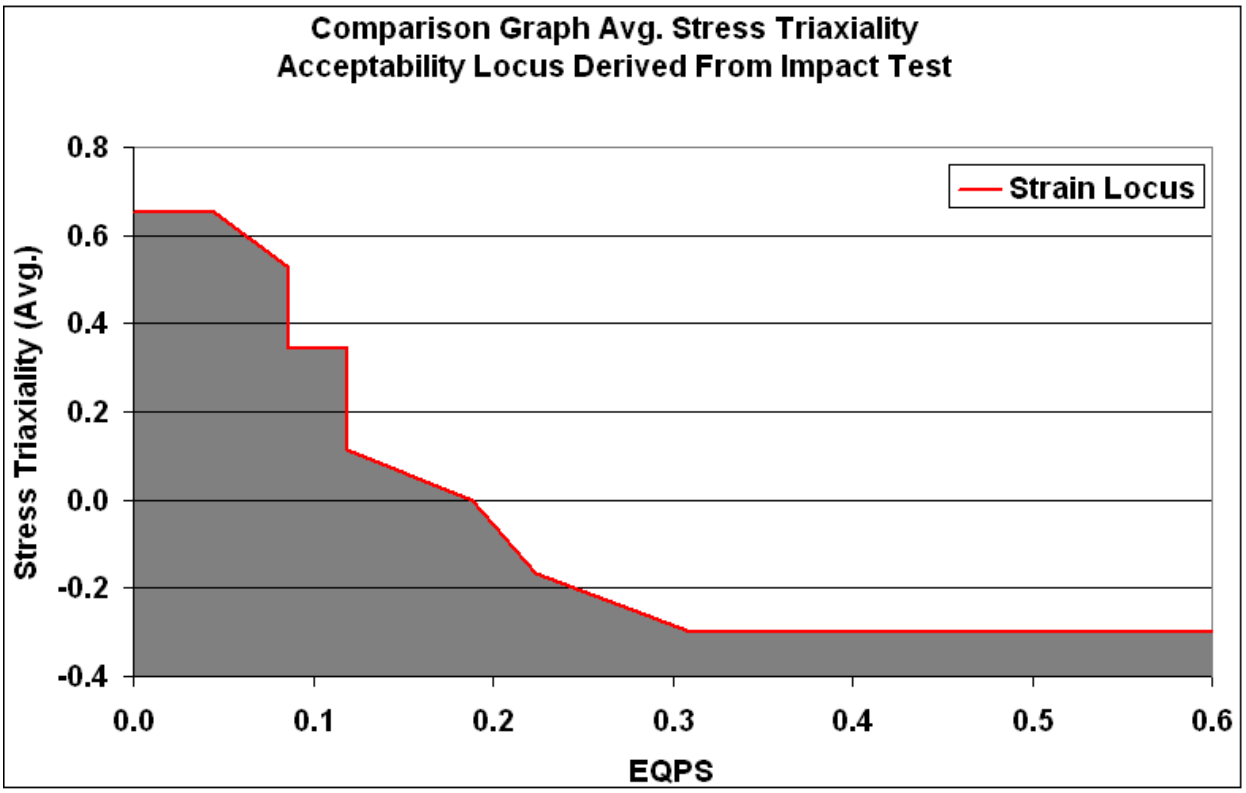

Figure 2-1. Locus in Equivalent Plastic Strain–Stress Triaxiality Space Developed from Titanium Impact Test

2.1.3 Weights and Centers of Gravity

The approximate weights of the three basic components of the PAT-1 package for this addendum are shown in Table 2-5.

Table 2-5. Approximate Weights of PAT-1 Package Components

Component	Weight (kg)	Weight (lb)
AQ-1 Overpack	206[a]	454[a]
TB-1 Containment Vessel[c]	16.8	37
T-Ampoule and its Packing[b]	See Table 2-1	See Table 2-1
Pu Metal Contents[b]	See Table 2-1	See Table 2-1
Total	225	496

[a] The weight of the AQ-1 can vary due to the natural weight variation of kiln-dried redwood as stated in Section 2.2 of the SAR.[1]

[b] The weights of the T-Ampoule and its packing are calculated using ProENGINEER (http://www.ptc.com/products/proengineer/) and SolidWorks (http://www.solidworks.com/) commercial drafting programs. The T-Ampoule and its contents within the TB-1 do not exceed the 2.1 kg weight of the PC-1 and its contents as shown in Section 2.2 of the SAR.[1]

[c] The weight of the TB-1 is from Section 2.2 of the SAR.[1]

The center of gravity (CG) of the PAT-1 package is located along its longitudinal centerline, approximately 20.2 inches from the bottom end (see Figure 2-2). The variation in the CG for the plutonium metal contents within the T-Ampoule and its packing for the Pu hollow cylinder to the sample containers with Pu contents and Inner Cradle is less than ±1/4 inch.

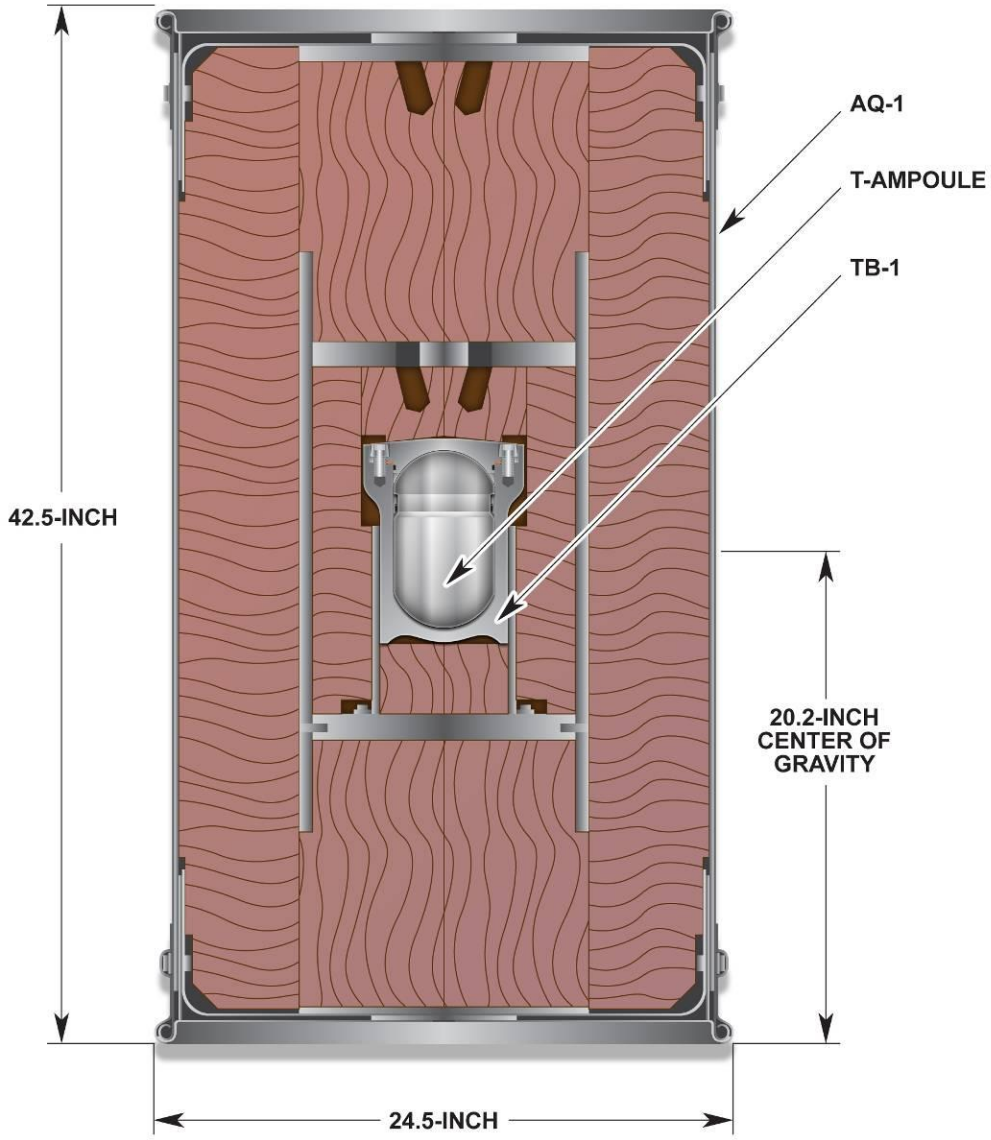

Figure 2-2. Center of Gravity for PAT-1. (Note That the Center of Gravity Varies with the Inclusion of the Support Structure and Could Vary Because of the Natural Weight Variation of the Kiln-Dried Redwood.)

2.1.4 Identification of Codes and Standards for the Package Design

The codes and standards used for design and fabrication of the AQ-1 overpack, TB-1, and PC-1 are the same as those described in the SAR.[1] The TB-1 uses design values derived from ASME B&PV Code for both NCT and HAC. For evaluation of the T-Ampoule eutectic barrier in air transport accident conditions, a strain-based criterion is used based on testing at SNL and on Bao and Wierzbicki[7,12], as well as a stress-state modified strain-based failure criterion called Tearing Parameter[13,14]. The T-Ampoule design was evaluated using ASME B&PV Code Section VIII Division I (See Section 2.12.8) and uses fabrication and acceptance criteria from the code as defined in PAT-1040. The titanium components within the TB-1 are procured using ASTM material standards with increased minimums for yield and ultimate strength, elongation at tensile

failure, and reduction in area at failure. For the TB-1 and AQ-1, the codes and standards are provided in Section 9 of the SAR.[1]

2.2 Materials

2.2.1 Material Properties and Specifications

A list of materials used in the finite element models for the structural evaluation of the PAT-1 package is presented in Table 2-6. The table lists the model, the component, and the component material, along with the appendix where the material's reference information, material properties, and constitutive model parameters are listed.

Table 2-6. Listing of Material for Each Component in the Finite Element Models

Model	Component	Material	Appendix
Full Models			
	Redwood Impact Material	Redwood	2.1.1.1
	Load Spreader Cylinder	Aluminum 6061	2.12.4.3
	Load Spreader Top Plate	Aluminum 7075	2.12.4.5
	Load Spreader Lower Plate	Aluminum 7075	2.12.4.5
	Copper Cylinder	Copper	2.12.4.7
	TB-1 Container	Stainless PH13-8-Mo	2.12.4.9
	TB-1 Contents	Elastic Plastic Soft	2.12.4.11
	Can Shell and Flange	Stainless 304	2.12.4.12
	T-Ampoule	Titanium 6Al-4V	2.12.4.14
	Sample Container	Titanium 6Al-4V	2.12.4.14
	Sample Container Cylinder	Plutonium (delta)	2.12.4.18
	ER Cylinders	Plutonium (alpha)	2.12.4.16
	Be Composite Cylinder	Beryllium	2.12.4.24
Impact Test Model			
	Tungsten Ballast	Tungsten	2.12.4.20
	Impact Specimen Brass	Brass UNS C36000	2.12.4.22
	Impact Specimen Titanium	Titanium 6Al-4V	2.12.4.14
	Ampoule Specimen	Titanium 6Al-4V	2.12.4.14
	Hemisphere Fixture	Stainless PH13-8-Mo	2.12.4.9

2.2.2 Chemical, Galvanic, or Other Reactions

The chemical and galvanic reaction evaluations of the AQ-1 and TB-1 are documented in Section 2.4.1 of the SAR.[1] The evaluation concluded that there was no significant potential for chemical or galvanic reactions to occur.

There is no potential for significant chemical or galvanic reactions to occur with the T-Ampoule or materials contained therein under 10 CFR 71.71, 71.73, and 71.74 conditions because containment is maintained by the TB-1 in those environments as demonstrated in Sections 2, 3, and 4 of this addendum. Within the T-Ampoule, contact is made between the plutonium metal surrounded by tantalum foil (optional packing) and the inside surfaces of the titanium T-Ampoule or sample container (SC-1 or SC-2). These surfaces have no significant potential for corrosion since the atmosphere within the T-Ampoule and sample container(s) (if used) is the same as the glove box atmosphere in which the plutonium metal contents are handled. The standard glove box line atmosphere consists of nitrogen/argon/helium, with an oxygen and a moisture content less than 100 ppm.

If water in flooding is assumed as in the criticality analysis, there is a galvanic potential (assume flowing sea water for the galvanic analysis) between the plutonium metal content and the materials within the T-Ampoule which include beryllium (as part of the content), titanium, tantalum and PH13-8Mo stainless steel material of the TB-1. There is virtually no chance for water in flooding to occur based upon the accident conditions for air transport of plutonium tests in Section 2.8 and Section 3.6 of the SAR,[1] the accident conditions for air transport of plutonium analyses in Section 2.8 of this addendum, and the hypothetical accident conditions for fissile material packages for air transport analyses in Section 3.4.5 of this addendum.

There is possible gas generation from alpha decay of plutonium which yields helium gas. The helium gas is non-reactive with the materials within the TB-1.Evaluation of the potential for a Pu/Fe eutectic reaction is documented in Section 3.5.2 of the SAR Addendum. The eutectics evaluation of the plutonium metal contents; the titanium materials used for the T-Ampoule, Sample Container-1, Sample Container-2, and Inner Cradle; and the optional tantalum foil packing in Section 3.5.2 concluded, by analysis of phase diagrams for all possible binary systems, that no liquid phases are expected in this system at 582ºC (1080ºF). Furthermore, it is anticipated that the lowest melting point phase that may form within this system is 595ºC (1103ºF) – the plutonium/beryllium eutectic temperature. This is 13ºC (23ºF) greater than the highest temperature excursion that occurs in the system. This is not a large margin but the 595ºC (1103ºF) value is a conservative estimate, thus the system in a transient reaching 582ºC (1080ºF) is still considered safe. Review of ternary phase diagrams in the literature involving components of this system supports the conclusions drawn from the binary systems, however, the ternary systems are limited and this is a much more complex system than reviewed in binary or ternary systems available in the literature.

2.2.3 Effects of Radiation on Materials

This section reviews the effects of radiation on materials from the plutonium content. Section 2.2.3.1 provides contact dose estimates based upon the shielding analyses in Section 5 for evaluation of the Viton® seals. Section 2.2.3.2 discusses the effect on the physical properties of the elastomer seal material. Section 2.2.3.3 examines the potential for HF gas generation due to radiation exposure.

2.2.3.1 Dose Estimates

A calculation of contact dose for an elastomer seal using surface dose rates based on a bounding source mass model (a cylinder with a hemisphere on the bottom as described in Section 5 of the

SAR Addendum) was performed. The mass was distributed to minimize the self-shielding due to the source material. Note that previous sensitivity analyses have shown that the dose rates were insensitive to the source geometry. Based on this model, a conservative estimate of the contact gamma dose with the elastomer is 8.3×10^5 rad/year and contact neutron dose is 1.7×10^5 rem/year using the source terms in Table 5.3 and 5.4 of the SAR Addendum. Further review of Table 5-12, Estimation of Degree of Overprediction in Bounding Pu Source Used in This Study, indicated that the gamma source could be overpredicted by 36.3 times and the neutron source by 6.0 times. These source strengths were based on 1300 grams of plutonium with an isotopic distribution corresponding to source scenario "N_Reactor 2 GWd/t." The shielding analyst recommended the following for realistic doses (taking partial credit using reduction factors of 30 for gamma and 5 for neutron) for the elastomer dose calculation:

Realistic surface gamma dose = $8.3\times10^5/30 = 2.8\times10^4$ rad/year
Realistic neutron dose = $1.7\times10^5/5 = 3.4\times10^4$ rem/year

The results for neutrons are expressed in rem rather than rad because the neutron results have been multiplied by a quality factor to account for the greater damage caused by neutrons than gamma rays. The quality factor makes the doses from different radiation sources approximately additive. Quality factor for neutrons of unknown energy is given as 10 in Table 1004(b).1-Quality Factors and Absorbed Dose Equivalences in 10 CFR 20.1004.

2.2.3.2 Effect on Physical Properties and Operating Time

The combined gamma and neutron doses in Section 2.2.3.1 are not high enough to affect mechanical properties of the PH13-8Mo, Ti-6Al-4V, and tantalum material in the TB-1.

The compound for the T-Ampoule and sample container SC-1 and SC-1 O-rings is Viton® A, which is a fluorocarbon elastomer trademarked by DuPont. The "Viton® fluoroelastomer from DuPont Performance Elastomers" on the Radiation Resistance of Viton® states that "Vulcanizates of Viton® fluoroelastomer, irrespective of the type or filler, can withstand 10^5 – 10^6 rad (10^3 – 10^4 J/kg) with little or no effect on physical properties and 10^6 - 10^7 rad (10^4 – 10^5 J/kg) with moderate effect (50% loss of elongation at break, 50% increase in modulus); 10^8 rad (10^6 J/kg) produces a severe effect (final elongation at break <50%). The technical brochure further states "Concerning elastomer serviceability, a gamma radiation dose less than 5×10^6 rad (5×10^4 J/kg) is considered low. Up to 10^8 rad (10^6 J/kg) is considered intermediate and 10^8-10^9 rad (10^6-10^7 J/kg) is high."

The combined predicted doses for gamma (2.8×10^4 rad/year) and neutron (3.4×10^4 rem/year) based on a realistic source are less than the 10^5 rad cited for no effect in the DuPont technical bulletin and are only marginally above 10^4 rad[25] treating neutrons and gammas equally and exposing for a full year. Note that Bouquet Reference 25 only cites "fluorocarbons" and does not provide further details regarding manufacturers' data. In a 1985 article by Bouquet (Reference 26), the author shows in *Figure 4 Summary of Radiation Data for Elastomers. Property: Tensile Strength. Above Average Response Level* that the lowest threshold damage for Viton® A starts at about 6×10^6 rads, and the 25% change dose is at about 6×10^7 rads. In *Figure 6 Summary of Radiation Data for Elastomers. Property: Elongation. Average Response Level for*

Viton® A of the same article, the lowest threshold dose starts at about 10^7 rads and the 25% change dose is slightly above 10^7 rads.

The combined realistic dose estimates (gamma, 2.8×10^4 rad/year and neutron, 3.4×10^4 rem/year) from the shielding analyses place the seals in the "little or no effect" dose range according to DuPont for Viton® seals with a full year of contact (also conservative since most shipments should be completed within a month) and (from Reference 26) at least an order of magnitude below the threshold damage level data for tensile strength and elongation. Furthermore, the amount of time the seals would typically be in close proximity to the contents would make these estimates even closer to a 1×10^4 rad cumulative dose for one year operating time.

Based upon the DuPont data and Bouquet 1985 report,[26] the operating time of the package up to one year is acceptable since the Viton® elastomer seals would experience little or no effect, if any, in mechanical properties from radiation from the plutonium metal during NCT. The Viton® elastomer seals in the *T-Ampoule* and *SC-1* and *SC-2* sample containers are to maintain product quality and are not containment boundary components and thus do not provide a safety function.

2.2.3.3 Radiation Induced Gas Generation and Materials Compatibility

There is a possibility that high radiation doses could cause the O-rings to degrade by forming gaseous products. No data was found in a literature survey of regarding the onset of outgassing of HF due to gamma radiation. The likelihood of HF outgassing is very low for the realistic radiation doses calculated for NCT (2.8×10^4 rad/year gamma and 3.4×10^4 rem/year neutron) considering the data in the DuPont literature because mechanical properties are minimally affected at radiation doses of 10^5 rad.

An evaluation of O-ring materials such as Viton®, Kel-F®, FKM, Fluorel™ and Kalrez® was performed examining the compatibility of fluorocarbon O-ring decomposition products and containment materials in the TB-1. The structural materials considered are Ti-6Al-4V in the T-Ampoule and sample containers, the PH13-8Mo material in the TB-1, and the tantalum foil as packing material. The concern is that degradation of fluorine bearing elastomers, by decomposition and outgassing, could result in the release of corrosive fluorine compounds during normal conditions of transport. It is assumed that "corrosive fluorine compounds" refers to the formation of hydrogen fluorine (HF). In the presence of water, HF (gas) reacts to form aqueous HF, or hydrofluoric acid, which is a corrosive, according to the reaction below:

$$HF + H_20 \rightarrow H_30^+ + F^-$$

Considering the availability of water within the T-Ampoule, which is closely surrounded by the TB-1, the atmosphere within the T-Ampoule, which is sealed by an O-ring, is filled with a standard glove box atmosphere consisting of a gaseous mixture of N/Ar/He with an oxygen and moisture content not exceeding 100 ppm. In this case, the water content is not a concern, because the dew point corresponding to 100 ppm (by volume), assuming all water, is -40°C (-40°F). In addition to the negligible moisture content, the sample container is at a temperature of 103.3°C (218°F) at NCT. Therefore, for NCT, there is insufficient water content within the TB-1 to react with any available outgassed HF species. Even in an air environment, which is

considered the worst case scenario, any available water would likely be evaporated due to heating (103.3°C (218°F)) from the plutonium content.

For the corrosion resistance of the materials within the TB-1, the Ti-6Al-4V T-Ampoule is susceptible to corrosive attack when exposed to 1wt% hydrofluoric acid solutions. As noted above, free water is not available in the glove box atmosphere that fills the T-Ampoule (< 100 ppm oxygen or moisture concentration) and is certainly unavailable at NCT temperature and pressure [103.3°C (218°F), 29 kPa (4.2 psig)].

Per a literature search, no information on the resistance of PH13-8Mo stainless steel to corrosive attack by fluorine compounds was found. The corrosion resistance of this material (which nominally contains 13wt% Cr) is considered to be similar to that of type 302 stainless steel, and is susceptible to pitting attack in the presence of halide species (Cl^-, F^-, etc.). During NCT, the scenario in which this material would come into contact with an aqueous halide species is not considered likely.

For the tantalum packing foil, tantalum is nonresistant to both aqueous and anhydrous hydrofluoric acid. Tantalum is a packing material and does not provide any structural strength.

For NCT, there is insufficient water content within the TB-1 to react with any available outgassed HF species. Even in an air environment, which is considered the worst case scenario, any available water would likely be evaporated due to heating (218°F) from the plutonium content.[28]

Based on calculated doses of $< 10^5$ rad/year for the T-Ampoule and sample container O-rings, there is little possibility that degradation of the material due to radiation would cause release of HF to form corrosive fluorine compounds under NCT for a period of one year.

2.2.3.4 Radiation Resistance of Viton®: Technical Information Brochure

See stand-alone document below.

Technical Information

Viton® fluoroelastomer

From DuPont Performance Elastomers

Radiation Resistance of Viton®

Introduction

Vulcanizates of Viton® fluoroelastomer, irrespective of type or filler, can withstand 10^5–10^6 rad (10^3–10^4 J/kg) with little or no effect on physical properties and 10^6–10^7 rad (10^4–10^5 J/kg) with moderate effect (50% loss of elongation at break, 50% increase in modulus); 10^8 rad (10^6 J/kg) produces a severe effect (final elongation at break <50%).

Handling Precautions

Using recommended handling procedures, Viton® fluoroelastomer polymers and products based on them, in themselves, present no health hazards of which DuPont Performance Elastomers is aware. However, certain hazards may arise during the compounding and processing of the raw polymers into finished products. For example, toxic vapors, which may include hydrogen fluoride,* may be liberated from products based on Viton® during cure, post-cure, or service at temperatures above 200°C (393°F). Adequate ventilation should be provided in work areas where compounds or parts of Viton® are being processed or are likely to be exposed to temperatures in this range. Avoid breathing vapors or dusts from such operations. If vapors or dusts are inhaled move to fresh air. By following these precautions, there should be no problem in staying within the limits set by OSHA. Before handling or processing Viton®, be sure to read and be guided by suggestions in DuPont Performance Elastomers technical bulletin H-71129-02, "Handling Precautions for Viton® and Related Chemicals."

Compounding ingredients that are used with Viton® to prepare finished products may present hazards in handling and use. Before proceeding with any compounding or processing work, consult and follow label directions and handling precautions from suppliers of all ingredients.

Radiation Resistance of Viton®

The radiation resistance of Viton® fluoroelastomer is summarized in the following tables. Before discussing the results, the following guidelines and definitions will be useful:

- Radiation can be defined as the transmission of high-energy waves or particles through space or through a material medium. Energy absorption by the material may produce a variety of effects such as crosslinking and degradation. Excessive energy absorption usually results in failure of the substance, either by embrittlement due to overcrosslinking or by reversion (degradation) due to chain cleavage.
- *Gamma* radiation may be considered typical of the type to which elastomers would be subjected and is used in many laboratory radiation studies. However, due to equipment availability, test results reported in this technical bulletin are from exposure to *beta* radiation. Based on these and other tests, evidence indicates that equivalent damage is incurred by equivalent dosages of *beta* and *gamma*

*Hydrogen fluoride is regulated as an air contaminant in the United States under the Occupational Safety and Health Act (refer to CFR Title 29 1910.1000). This sets the 8-hr time-weighted average in any 8-hr work shift of a 40-hr work week at 3 ppm.

radiation under identical environmental conditions.

- Radiation dose is expressed as rad. One rad is the dose that produces an energy absorption of 100 erg per gram in 1 cm^3 of air at standard temperature and pressure. 10^6 rad = 1 megarad; also 1 rad = 0.01 J/kg.
- In general, radiation doses are additive. A material can be assumed to have a perfect memory with regard to radiation exposures. Thus, ten exposures of 10^4 rad (10^2 J/kg) are equivalent to one exposure of 10^5 rad (10^3 J/kg).
- Concerning elastomer serviceability, a *gamma* radiation dose less than 5×10^5 rad (5×10^4 J/kg) is considered low. Up to 10^8 rad (10^6 J/kg) is considered intermediate and 10^8–10^9 rad (10^6–10^7 J/kg) is high.

Data in *Table 1* indicate that the type of Viton® polymer has little or no effect on radiation resistance. Viton® A-HV and Viton® B are identical to Viton® A at equal exposures. *Table 2* demonstrates that the use of Viton® E-60C, with a variety of fillers, does not improve resistance.

In summary, exposure of vulcanizates of Viton® to more than 10^6–10^7 rad (10^4–10^5 J/kg) produces moderate to severe effects on physical properties.

Table 1
Comparative Radiation* Resistance of Viton® Fluoroelastomer

Compound	1A	1B	1C
Viton® A	100	—	—
Viton® B	—	100	—
Viton® A-HV	—	—	100
MT Carbon Black	20	20	20
Low Activity MgO	15	15	15
Diak™ No. 1	1	1	1
Vulcanizate Properties			
Press Cure: 30 min at 149°C (300°F)			
Oven Post-Cure: step plus 24 hr at 204°C (400°F)			
Stress/Strain and Hardness—at 24°C (75°F)			
Original			
100% Modulus, MPa (psi)	2.6 (375)	2.6 (375)	3.2 (475)
Tensile Strength, MPa (psi)	15.2 (2,200)	15.2 (2,200)	16.8 (2,425)
Elongation at Break, %	320	380	290
Hardness, Durometer A, points	68	69	69
After 5 x 10^6 Rad (5 x 10^4 J/kg) Radiation			
100% Modulus, MPa (psi)	4.4 (650)	4.4 (650)	4.8 (700)
Tensile Strength, MPa (psi)	15.4 (2,225)	15.2 (2,200)	15.0 (2,175)
Elongation at Break, %	230	230	220
Hardness, Durometer A, points	71	71	71
After 10^7 Rad (10^5 J/kg) Radiation			
100% Modulus, MPa (psi)	6.0 (875)	5.8 (850)	5.8 (850)
Tensile Strength, MPa (psi)	13.8 (2,000)	13.2 (1,925)	13.2 (1,925)
Elongation at Break, %	170	160	170
Hardness, Durometer A, points	70	72	71
After 2.5 x 10^7 Rad (2.5 x 10^5 J/kg) Radiation			
100% Modulus, MPa (psi)	10.4 (1,500)	11.0 (1,600)	9.6 (1,400)
Tensile Strength, MPa (psi)	11.8 (1,700)	12.6 (1,825)	11.2 (1,625)
Elongation at Break, %	110	120	110
Hardness, Durometer A, points	73	78	74
After 5 x 10^7 Rad (5 x 10^5 J/kg) Radiation			
Tensile Strength, MPa (psi)	8.6 (1,250)	9.2 (1,325)	9.2 (1,325)
Elongation at Break, %	50	55	60
Hardness, Durometer A, points	78	79	78
After 10^8 Rad (10^6 J/kg) Radiation			
Tensile Strength, MPa (psi)	7.6 (1,100)	7.8 (1,125)	7.4 (1,075)
Elongation at Break, %	10	10	10
Hardness, Durometer A, points	87	87	86

*Beta radiation at room temperature in air in a Van de Graaf generator

Table 2
Test Compounds of Viton® E-60C for Radiation* Experiments

Compound	2A	2B	2C	2D	2E
Viton® E-60C	100	100	100	100	100
High Activity MgO	3	3	3	3	3
Calcium Hydroxide	6	6	6	6	6
Fine Ground Calcium Carbonate	—	—	—	30	—
Blanc Fixe	—	—	—	—	70
MT Black	—	30	20	—	—
Vulcanizate Properties					
Press Cure: 15 min at 177°C (350°F)					
Oven Post-Cure: 24 hr at 232°C (450°F)					
Stress/Strain and Hardness—at 24°C (75°F)					
Original					
100% Modulus, MPa (psi)	2.0 (300)	6.2 (900)	4.8 (700)	6.6 (950)	6.4 (925)
Tensile Strength, MPa (psi)	7.4 (1,075)	13.0 (1,900)	11.8 (1,700)	15.6 (2,250)	11.2 (1,625)
Elongation at Break, %	200	180	180	190	180
Hardness, Durometer A, points	53	72	66	68	73
After 5 x 10^7 Rad (5 x 10^5 J/kg) Radiation					
Tensile Strength, MPa (psi)	5.4 (775)	9.3 (1,350)	9.3 (1,350)	9.3 (1,350)	—
Elongation at Break, %	65	45	60	45	—
Hardness, Durometer A, points	71	85	80	85	—
After 10^8 Rad (10^6 J/kg) Radiation					
Tensile Strength, MPa (psi)	6.2 (900)	9.6 (1,400)	7.6 (1,100)	8.8 (1,275)	—
Elongation at Break, %	45	40	25	20	—
Hardness, Durometer A, points	82	90	88	88	—
After 2.5 x 10^8 Rad (2.5 x 10^6 J/kg) Radiation					
Tensile Strength, MPa (psi)	10.8 (1,575)	—	—	6.9 (1,000)	11.9 (1,725)
Elongation at Break, %	15	—	—	<20	<20
Hardness, Durometer D, points	64	77	70	75	76
After 5 x 10^8 Rad (5 x 10^6 J/kg) Radiation					
Tensile Strength, MPa (psi)	—	—	—	—	—
Elongation at Break, %	—	—	—	—	—
Hardness, Durometer D, points	80	81	80	85	80

*Beta radiation from a G.E. electron resonant transformer

Test Procedures

Property Measured	Test Procedure
Compression Set	ASTM D395-85, Method B (25% deflection)
Compression Set — Low Temperature	ASTM D1229-87, Method B (25% deflection)
Compression Set, O-rings	ASTM D1414-78 (87)
Hardness	ASTM D2240-87, Durometer A
Mooney Scorch	ASTM D1646-87, using the small rotor Minimum viscosity and time to a 1-, 5- or a 10-unit rise are reported.
Mooney Viscosity	ASTM D1646-87, ten pass 100°C (212°F), 121°C (250°F)
ODR (Vulcanization characteristics measured with an oscillating disk cure meter)	ASTM D2084
Property Change After Oven Heat-Aging	ASTM D573-88
Stress/Strain Properties 100% Modulus Tensile Strength Elongation at Break	ASTM D412-87, pulled at 8.5 mm/s (20 in/min)
Stiffness, Torsional, Clash-Berg	ASTM D1043-87
Temperature Retraction	ASTM D1329-88
Volume Change in Fluids	ASTM D471-79

Note: Test temperature is 24°C (75°F) except where specified otherwise

For further information please contact one of the offices below, or visit our website at www.dupontelastomers.com/viton

Global Headquarters – Wilmington, DE USA
Tel. +1-800-853-5515
+1-302-792-4000
Fax +1-302-792-4450

European Headquarters - Geneva
Tel. +41-22-717-4000
Fax +41-22-717-4001

South & Central America Headquarters - Brazil
Tel. +55-11-4166-8978
Fax +55-11-4166-8989

Asia Pacific Headquarters - Singapore
Tel. +65-6275-9383
Fax +65-6275-9395

Japan Headquarters – Tokyo
Tel. +81-3-6402-6300
Fax. +81-3-6402-6301

The information set forth herein is furnished free of charge and is based on technical data that DuPont Performance Elastomers believes to be reliable. It is intended for use by persons having technical skill, at their own discretion and risk. Handling precaution information is given with the understanding that those using it will satisfy themselves that their particular conditions of use present no health or safety hazards. Since conditions of product use and disposal are outside our control, we make no warranties, express or implied, and assume no liability in connection with any use of this information. As with any material, evaluation of any compound under end-use conditions prior to specification is essential. Nothing herein is to be taken as a license to operate or a recommendation to infringe on patents. While the information presented here is accurate at the time of publication, specifications can change. Check www.dupontelastomers.com for the most up-to-date information.

Caution: Do not use in medical applications involving permanent implantation in the human body. For other medical applications, discuss with your DuPont Performance Elastomers customer service representative and read Medical Caution Statement H-69237.

DuPont™ is a trademark of DuPont and its affiliates.

Viton® is a registered trademark of DuPont Performance Elastomers.

Copyright © 2006 DuPont Performance Elastomers. All Rights Reserved.

(12/98) Printed in U.S.A.
Reorder no: VTE-H73594-00-A1298

DuPont Performance Elastomers

2.3 Fabrication and Examination

PAT-1040 "Titanium and O-ring Materials and Component Fabrication Specification" (see Section 1.3.3 in this addendum) provides for the procurement, fabrication, and examination of the T-Ampoule, Sample Container-1, Sample Container-2, Inner Cradle, and O-rings. Areas described include:

- ASTM materials specifications, minimums are specified for yield strength, ultimate tensile strength, elongation at tensile failure, reduction in area at failure
- SAE AMS O-ring specifications for material and tolerances
- Fabrication – includes requirements for quality assurance, fabrication, inspection and examination, product marking, surface finish, packaging and shipping, and documentation

2.3.1 Fabrication

The fabrication specification for the T-Ampoule and other components is provided in Section 1.3.3, "PAT-1040 Titanium and O-ring Materials and Component Fabrication Specification." Since the T-Ampoule is considered as an "Other Safety Component" of a Category I package (see NUREG/CR-3854[20]), the selected standard for the T-Ampoule is ASME Boiler and Pressure Vessel Code (Section VIII, Division 1[21]). As defined in Section 5.0 within the PAT-1040 specification, the T-Ampoule was designed (see Section 2.12.8) and will be fabricated and inspected to meet the requirements of ASME Boiler and Pressure Vessel Code (Section VIII, Division 1). ASTM standards are used for the procurement of the materials used for fabrication.

2.3.2 Examination

The examination requirements for the T-Ampoule and other components are provided in Section 1.3.3, "PAT-1040 Titanium and O-ring Materials and Component Fabrication Specification." As defined in Section 5.0 in the PAT-1040 specification, the T-Ampoule will be inspected to meet the requirements of ASME Boiler and Pressure Vessel Code (Section VIII, Division 1).

2.4 General Requirements for All Packages

2.4.1 Minimum Package Size

The PAT-1 package measures 62 cm (24 ½ in.) outside diameter (OD) by 108 cm (42 ½ in.) long.

2.4.2 Tamper-Indicating Device

A wire tamper seal is wired to the bolted connection on the lid clamping ring (*Ring, Clamp, Modified* (1006))* on the AQ-1 drum closure.

* The drawing title names are shown in italics. See Section 1.3.2 for engineering drawings of the components.

2.4.3 Positive Closure

No change for the PAT-1. Positive closure of the PAT-1 is described in Section 2.4.2 of the SAR.[1]

2.5 Lifting and Tie-Down Standards for All Packages

2.5.1 Lifting Devices

No change. This analysis for the PAT-1 package is covered in Section 2.4.3 of the SAR.[1]

2.5.2 Tie-Down Devices

No change. This analysis for the PAT-1 package is covered in Section 2.4.3 of the SAR.[1]

2.6 Normal Conditions of Transport

This section evaluates the replacement of the PC-1 and its contents and associated packing with the T-Ampoule and its contents and associated packing. The T-Ampoule replacement has no effect on the NCT structural performance of the TB-1 and AQ-1 overpack as demonstrated in this section. The temperature invariance of titanium alloy, T-Ampoule material properties, is shown in Section 2.12.4.14, vibration is addressed in Section 2.6.5, and free drops from the NCT (see Section 2.12.5.3), HAC (see Section 2.1.1.1) Dynamic Crush, and 30 ft Drop (see Section 2.1.1.1).

The wall structure in the T-Ampoule did not rupture and the TB-1 remains nearly elastic (excepting minimal localized internal "denting" from contents impacts) during the 10 CFR 71.74 air transport accident impact evaluations described in Section 2.8 and Section 2.12.5.4. Since the loads imposed by the T-Ampoule contents in the 10 CFR 71.71 NCT impact test are considerably smaller, they will not threaten the integrity of the T-Ampoule or TB-1. In addition, the original NCT testing performed for the SAR[1] showed no effect on the TB-1. This was verified in Section 2.12.5.3.2 analytically for the NCT side drop, which showed no plasticity in either the T-Ampoule or the TB-1, and TB-1 through-thickness stress intensities below ASME limits in Table 2-4. The only condition examined is the potential for different thermal effects due to the change in contents (e.g., T-Ampoule). Possible deformation of the sample container Inner Cradle was investigated analytically, as well, in order to verify that the initial position of the sample containers was not changed for the HAC and air transport accident environments.

The following sections on the NCT provide a discussion of the NCT tests required by 10 CFR 71.71 and demonstrate that the package meets the acceptance criteria.

2.6.1 Heat

The following section summarizes the stresses induced in the TB-1 under the thermal conditions of NCT.

2.6.1.1 Summary of Pressures and Temperatures

The average internal surface temperature of the T-Ampoule during NCT has been found in Section 3 to be 103.3ºC (218ºF). This produces a maximum internal pressure in the TB-1 of 18.8 psia due to the temperature difference, with a total internal pressure of 18.9 psia if helium generation (0.067 psia, computed in Section 4) is included. Ignoring any containment by the

T-Ampoule and regardless of specific contents, this pressure (18.9 psia, 130.3 kPa; 4.2 psig, 29 kPa absolute) defines the maximum normal operating pressure (MNOP) for the TB-1.

2.6.1.2 Differential Thermal Expansion

Since the original testing did not observe any effect of differential thermal expansion on the TB-1, only the potential for the T-Ampoule expanding into contact with the TB-1 will be examined. Differential thermal expansion is evaluated for the NCT temperature of 103ºC (218ºF), which produces the highest differential thermal expansion between room temperature and the lowest (-40ºC (-40ºF) and the highest 103ºC (218ºF) NCT temperature for the TB-1. The Military Handbook[6] reports a coefficient of thermal expansion (α) for the Ti-6Al-4V used for the T-Ampoule of 5.1×10^{-6} in./in./°F in the range of temperatures from 70ºF to 312ºF (see also Section 2.12.4.14 in this addendum).

A conservative estimate of the maximum expansion of the T-Ampoule can be calculated by assuming the T-Ampoule is a 7.418-in.-long cylinder (the actual T-Ampoule is capped) with an outer diameter of 4.22 in. The T-Ampoule reaches a maximum temperature of 250ºF (121ºC) as stated in Section 3, Table 3-1. Assuming a temperature increase of 180ºF (250ºF – 70ºF), the expansion produced equals $\alpha \Delta TL$, or 0.0068 in. in the longitudinal direction and 0.0122 in. in circumference (or 0.0039 in. in diameter). Since the gap between the T-Ampoule and the TB-1 is 0.015 in. around the entire perimeter, the expansion is conservatively estimated to be about 13% to 23% of the total gap because the TB-1 would also expand outward, allowing for more expansion of the T-Ampoule. Therefore, no stresses are induced by differential thermal expansion for NCT conditions.

2.6.1.3 Stress Calculations

Since the testing for the SAR[1] documents the adequacy of the TB-1 under pressures exceeding 34.3 psia, the Maximum Normal Operating Pressure (MNOP) for this addendum of 18.9 psia pressure possible for the NCT decay heat and helium generation will also be in compliance. A simple check of the stresses in a cylinder under 18.9 psia pressure, using the outer diameter of the cylindrical section of the TB-1 (5.35 in.) and a thickness of 0.55 in., yields pr/t = 20.4 psi (4.2 psig × 2.675 in./0.55 in.). Since this stress is considerably below the allowable stress, and because of the test results from the SAR,[1] no detailed stress calculation was performed due to thermal effects.

Although the T-Ampoule is only a eutectic barrier, it is useful to show that the stresses due to NCT decay heat and helium generation are low. Using the T-Ampoule outer diameter of 4.220 in. and a minimum thickness of 0.060 in. yields pr/t = 147.7 psi (4.2 psig × 2.11 in./0.060 in.). Since this stress is considerably low (<1 ksi), as well as being considerably below localized contact stresses from impacting contents in accident conditions (shown in subsequent sections), it can be neglected in those detailed structural analyses.

2.6.1.4 Comparison with Allowable Stresses

The first load combination listed under NCT in Table 2-2 consists of a hot environment of 100°F with maximum insolation, maximum decay heat, and maximum internal pressure. In Section 3, the average internal surface temperature obtained from the decay heat in the T-Ampoule was 103.3°C (218°F) for the analysis starting at 38ºC (100°F) with maximum insolation as specified

in 10 CFR 71.71. These temperatures were used to compute the MNOP at 4.2 psig (18.9 psia), which is extended out to the TB-1 by ignoring any containment by the T-Ampoule. Since the decay heat does not cause the gap between the T-Ampoule and the TB-1 to close, no stresses are induced as a result of thermal expansion due to the change in the package. A simple pr/t estimate of the stress due to the 4.2 psig internal pressure produces a stress of 20.4 psi. This is considerably below the 50,800 psi allowable stress in the TB-1 at 114°C (238°F).

2.6.2 Cold

The second load combination listed under NCT in Table 2-2 consists of a cold environment of -40°F, with no insolation, decay heat, or internal pressure. The assumption of no insolation and no decay heat is conservative since the lowest temperature would produce the large differential temperature. The MNOP gage pressure calculated in Section 2.6.1.1 of this addendum of 4.2 psig is negligible when any expansion of the T-Ampoule or TB-1 due to internal pressure is considered. During the testing for the SAR,[1] the package was cold soaked for 48 hours at –40°F. Only the thermal contraction of the TB-1 vessel into contact with the newly added T-Ampoule could impose different stresses on the TB-1 than those that occurred in the original test. As shown in Section 2.12.4.9, the coefficient of thermal expansion of the stainless steel PH13-8Mo used for the TB-1 is approximately 5.9E-6 in/in/°F. A temperature decrease from 70°F to –40°F produces a 110°F temperature reduction. Assuming the TB-1 to be a cylinder of length 8.68 in. with a 5.35 in. diameter (outer diameter of main TB-1 body) gives a reduction of length equal to $\alpha \Delta TL$, or 0.0056 in. and a decrease in circumference of approximately 0.011 in. (a decrease of 0.0035 in. in diameter). Since the gap between the T-Ampoule and the TB-1 is 0.015 in. around the entire perimeter, the contraction is conservatively estimated to be between 12 and 19% of the total gap. This does not account for the reduction in size of the T-Ampoule. Therefore, there is no potential for stress induced in the TB-1 due to differential thermal expansion/contraction with the T-Ampoule.

2.6.3 Reduced External Pressure

The PAT-1 package was subjected to and shown capable of withstanding a reduced external pressure of less than 0.5 atmospheres (<7.35 psia) during the SAR[1] testing to show compliance with 10 CFR 71.71. The changes in this addendum will have no effect on these results.

2.6.4 Increased External Pressure

The PAT-1 package was subjected to and shown capable of withstanding an external pressure of 600 psi during the SAR[1] testing. It will therefore, be capable of withstanding the 20 psi absolute pressure required by 10 CFR 71.71. The changes in this addendum will have no effect on these results.

2.6.5 Vibration

Vibration was examined during the testing for the SAR[1] and showed no effect on the package. The shock and vibration loads encompassing road, rail, and air transportation are negligible compared to the impact loads associated with the NCT drop test,[15] for which a detailed analysis showed elastic response for both the T-Ampoule and TB-1 (see Section 2.12.5.3). The changes in this addendum will have no effect on these results.

2.6.6 Water Spray

The water spray test was conducted during the SAR[1] testing and showed no effect.

2.6.7 Free Drop

A series of free drops were conducted during the testing for the SAR.[1] The effects were determined to be "inconsequential" and the package met the acceptance standards specified in 10 CFR 71.71. However, this addendum proposes a change in contents within the TB-1. The air transport accident analyses performed with the new contents (see Section 2.8) show that the TB-1 remains essentially elastic for each of the cases examined. Since the air transport accident will be considerably more severe than the NCT 4-foot drops, the TB-1 will remain elastic for the NCT free drops supported by analyses in Section 2.12.5.3.

2.6.8 Corner Drop

Since the PAT-1 package exceeds 220 lbs, it is not required to be subjected to the corner drop.

2.6.9 Compression

This analysis is covered in Section 2.6.10 of the SAR.[1] The package was unaffected by the compression test. The changes in this addendum will have no effect on these results.

2.6.10 Penetration

This analysis is covered in Section 2.6.9 of the SAR.[1] The TB-1 was unaffected by the penetration test. The changes in this addendum will have no effect on these results.

2.7 Hypothetical Accident Conditions

This section evaluates the replacement of the PC-1 and its contents and associated packing with the T-Ampoule and its contents and associated packing. The T-Ampoule replacement has no effect on the HAC structural performance of the TB-1 and AQ-1 overpack as documented in this section.

The wall structure in the T-Ampoule does not rupture and the TB-1 remains essentially elastic during the 10 CFR 71.74 air transport accident impact evaluations described in Section 2.8 and Section 2.12.5. Since the loads imposed by the T-Ampoule contents in the 10 CFR 71.73 HAC impact test are considerably smaller, they will not threaten the integrity of the T-Ampoule or TB-1. In addition, the original HAC testing performed for the SAR[1] showed no effect on the TB-1. A 30-ft drop analysis in each of the end, side, and corner impact orientations was performed in Section 2.1.1.1 to demonstrate these assumptions and verify acceptable T-Ampoule and TB-1 response. Other conditions examined in this addendum are the potential for different thermal effects due to the change in contents (e.g., T-Ampoule) and the dynamic crush event, which was not examined in the SAR[1] testing.

The dynamic crush event was evaluated using an undamaged package, although a small quantity of overpack crush would have occurred in the 30-ft drop. This assumption is justified because less than 2% of the available redwood in each of the three linear dimensions (for end, side, and CGOC) is crushed in the 30-ft drop. For example, in the CGOC 0.684 inches of lineal diagonal redwood is crushed out of the 36 inches of diagonally available redwood on both sides of the

TB-1 (even lower percentages for side and end impacts); thus at least 98% of the lineal redwood is still available for crush in the dynamic crush event. Since the overpack is thick enough and designed to absorb the energy of a 422 ft/sec impact (not just a 44 ft/sec impact, which is only 1% of the kinetic energy), it still has sufficient crush capacity to absorb the subsequent dynamic crush event after a 30 ft drop, and no additional loading would occur to the TB-1 since it remains fully elastic in both cases. Only minimal localized plasticity (0.26%) occurred in the T-Ampoule during the 30-ft side impact (none seen in the other 30 ft drops), so assuming an essentially undamaged package for the subsequent dynamic crush is justified.

The following HAC sections provide a discussion of the HAC tests required by 10 CFR 71.73 and demonstrates that the package meets the acceptance criteria.

2.7.1 Free Drop

Based on the series of analyses performed for the high-speed aircraft impact which showed that the TB-1 remains essentially elastic under that more severe condition, and that the testing for the SAR[1] showed no damage to the TB-1, only three 30-ft drop analyses were performed for this addendum: a side, end, and CG-over-corner drop. The contents for each case were chosen to have the likely highest stresses and/or strains based on extensive aircraft impact analyses.

2.7.1.1 End Drop

One end drop analysis is examined: a lid-end impact with an angled 831 g plutonium metal hollow cylinder.

2.7.1.2 Side Drop

One side drop analyses is examined: a two-sample-container 45-degree-rotated side impact.

2.7.1.3 Corner Drop

One corner drop analyses is examined: a CG-over-corner impact with a straight 831 g plutonium metal hollow cylinder.

2.7.1.4 Oblique Drops

No oblique drop analyses are examined.

2.7.1.5 Summary of Results

In order to verify package response with the different contents from the original SAR,[1] one end, side, and corner drop analysis was performed. As shown in Section 2.1.1.1, TB-1 through-thickness stress intensities remained below allowables in Table 2-4 and the containment vessel response was elastic (excepting small localized outer surface points where contact modeling artifacts exist). The seal and closure area of the TB-1 also remained fully elastic (like the test results from the SAR[1]), so the vessel maintained containment to a release of less than 1 A_2 in a week. The T-Ampoule had only the smallest of plasticity at points where the plutonium metal hollow cylinder impacted it, and thus its seal and structural integrity as a eutectic barrier were maintained.

2.7.2 Crush

The dynamic crush load combination was examined because the PAT-1 overall density fell below 62.4 lb/ft^3 at approximately 50.8 lb/ft^3, and the overall mass of approximately 500 lb fell below 1100 lb (10 CFR 71.73). Therefore, the full model of the PAT-1 (see Figure 2-7 of Section 2.12.2) was subjected to the drop of an 1100 lb steel plate from a height of 30 ft. The PAT-1 was placed in the side position and resting on an unyielding surface. The side position has the least quantity of redwood between the TB-1 and the steel impacting plate, however end and CG-over-corner cases were also analyzed. The 40 in. × 40 in. × 2.4 in. steel plate was oriented in a flat position when dropped, impacting the PAT-1 at 528 in./s. The 831 g and 731 g plutonium metal hollow cylinders (straight and angled), as well as 2 and 3 sample container contents analysis cases were examined in the dynamic crush environment. These analyses are summarized in Section 2.12.5, Subsections 2.1.1.1. The contents models were constructed by conservatively ignoring the optional tantalum foil packing and placing the cylinder and sample containers at the bottom of the T-Ampoule (when placed in a side orientation). For the plutonium metal hollow cylinders contents, as well as the sample containers contents dynamic crush analyses, the maximum observed through-thickness stress intensity was less than 23.5 ksi at any time during the event, which is far below the allowable through-thickness primary membrane stress of 106.6 ksi at 238°F (114°C).

The analyses were performed on an undamaged package although the free drop is required to precede the crush. This is justified due to only minor denting of the outer drum observed during the 30-foot free drop testing for the SAR.[1] In addition, the high-speed aircraft accident analyses described in Section 2.12.5 show that the TB-1 remains elastic except for localized deformations in much more severe impacts. Therefore, no damage will occur to the TB-1 during the free drop, which further demonstrates the acceptability of analyzing the crush with an undamaged package. This is supported by the free drop analyses summarized in Section 2.1.1.1.

2.7.3 Puncture

The original test produced only a minor imprint on the outer drum of the AQ-1; there was no effect on the TB-1.

2.7.4 Thermal

The following section summarizes the stresses induced in the TB-1 under the thermal conditions of HAC.

2.7.4.1 Summary of Pressures and Temperatures

The average internal surface temperature of the T-Ampoule during HAC was found to be 136°C (276°F) as documented in Section 3. As calculated in Section 4, the combination of temperature increase and helium generation produces a maximum internal pressure in the TB-1 for HAC of 20.5 psia.

2.7.4.2 Differential Thermal Expansion

Since the original testing did not observe any effect of differential thermal expansion on the TB-1, only the potential for the T-Ampoule expanding into contact with the TB-1 will be examined. The Military Handbook[6] reports a coefficient of thermal expansion (α) for the Ti-6Al-4V used for the T-Ampoule of 5.1×10^{-6} in./in./°F in the range of temperatures for the HAC.

A conservative estimate of the maximum expansion of the T-Ampoule can be calculated by assuming the T-Ampoule is a 7.418-in.-long cylinder (the actual T-Ampoule is capped) with a diameter of 4.22 in. The T-Ampoule reaches a maximum temperature of 308ºF (153ºC) as stated in Section 3. Assuming a temperature increase of 238ºF (308ºF – 70ºF), the expansion produced equals $\alpha\Delta TL$, or 0.0090 in. in the longitudinal direction and 0.0161 in. in circumference (or 0.0051 in. in diameter). Since the gap between the T-Ampoule and the TB-1 is 0.015 in. around the entire perimeter, the expansion is conservatively estimated to be about 17% to 30% of the total gap because the TB-1 would also expand outward, allowing for more expansion of the T-Ampoule. Therefore, no stresses are induced by differential thermal expansion for HAC conditions.

2.7.4.3 Stress Calculations

Since the testing for the SAR[1] showed the adequacy of the TB-1 under pressures exceeding 34.3 psia, the 20.5 psia pressure possible for the HAC thermal event will also be in compliance. A simple check of the stresses in a cylinder under 20.5 psia pressure, using the outer diameter or the cylindrical section of the TB-1 (5.35 in.) and a thickness of 0.55 in., yields pr/t = 28.2 psi (5.8 psig × 2.675 in./0.55 in.). Since this stress is considerably below the allowable stress, and because of the test results from the SAR,[1] no detailed stress calculation was performed.

2.7.4.4 Comparison with Allowable Stresses

The thermal fire load combination listed under HAC in Table 2-2 consists of the fire conditions examined in Section 3 with maximum insolation, maximum decay heat, and maximum internal pressure. In Section 3, the average internal surface temperature obtained in the T-Ampoule was 136 °C (277 °F) for the analysis. The internal pressure in the TB-1 increased from the MNOP value of 18.9 psia to 20.5 psia during the fire (ignoring containment by the T-Ampoule). The maximum internal pressure during the fire therefore induces a primary membrane stress of 28.2 psi. Since the decay heat and fire do not cause the gap between the T-Ampoule and the TB-1 to cause compression in the T-Ampoule, no stresses are induced as the result of thermal expansion. Therefore, the total primary membrane stresses induced by the fire load combination for the HAC is 28.2 psi, far below the allowable membrane stress of 102,900 psi at 147ºC (296ºF).

2.7.5 Immersion – Fissile Material

The TB-1 remained sealed during the immersion test (see Section 2.7.5 of the SAR[1]).

2.7.6 Immersion – All Packages

The TB-1 remained sealed during the immersion test (see Section 2.8.3 of the SAR[1]).

2.7.7 Deep Water Immersion Test (for Type B Packages Containing More than 10^5 A_2)

This test does not apply for Type B packages containing less than 10^5 A_2.

2.7.8 Summary of Damage

Since no damage was observed in the TB-1 during the original 30-foot free drop conducted for the SAR[1] and since the high-speed aircraft accident examined in Section 2.8 shows the TB-1

remaining essentially elastic (excepting minimal localized denting from solid metal contents) under those conditions, only a few free drop analyses were conducted to verify the fully-elastic condition of the TB-1, and to assess overpack deformation before dynamic crush. The dynamic crush event was not examined during the SAR[1] testing and was therefore examined here, in Sections 2.8.4 and 2.1.1.1. The numerous cases examined included side, end, and CG-over-corner impacts with two sizes and orientations of plutonium metal hollow cylinders, as well as 2 and 3 sample container sets of contents. The maximum dynamic crush stresses observed in the TB-1 were those resulting from local impacts of the contents on the T-Ampoule and then to the TB-1. These stresses are not primary membrane stresses, but are conservatively compared with those allowables. Although some localized high stresses exist on the outer TB-1 surface due to minor contact modeling artifacts, neither peak internal denting stresses from impacts of the contents nor peak through-thickness stresses in the containment vessel (all less than 40 ksi) do not approach the allowable 106.6 ksi from Table 2-4.

For the dynamic crush plutonium metal hollow cylinder contents, as well as the sample container contents analyses, the maximum observed through-thickness stress intensity was less than 23.5 ksi at any time during the event which is far below the allowable through-thickness primary membrane stress of 106.6 ksi at 238°F (114°C). The peak TB-1 stress magnitudes (localized, not through-thickness) were higher, but were either due to localized contents impacts or due to small contact issues at the outer corners of the TB-1, and in no way threaten the integrity of the containment boundary.

No examination of the puncture was performed because no damage was observed during the original test. For the fire test, the average temperature of the TB-1 during HAC was found to be 136°C (276°F) as determined in Section 3.4.3. This produces a maximum internal pressure in the TB-1 of 5.8 psig as computed in Section 4.3, ignoring any containment by the T-Ampoule. Using a simple *pr/t* estimate of the stresses in the TB-1, the internal pressure due to the fire induces a primary membrane stress of 28.2 psi. This is far below the allowable membrane stress of 102,900 psi at 153°C (308°F). It was also demonstrated that no stresses will be induced in the TB-1 as the result of differential thermal expansion with the T-Ampoule. Finally, the SAR[1] demonstrated that the TB-1 will not be susceptible to the immersion tests required for HAC. Overall, no damage will be experienced by the TB-1 during the HAC conditions outlined in 10 CFR 71.73. The TB-1 maintained containment during the original testing and will continue to do so here.

2.8 Accident Conditions for Air Transport of Plutonium

2.8.1 Discussion

This section discusses the analyses conducted on the PAT-1 package subjected to the requirements of 10 CFR 71.74 (Accident conditions for air transport of plutonium[4]). The analyses were performed using the SNL-developed, nonlinear finite element code, PRONTO-3D.[8] PRONTO-3D is a structural mechanics code developed specifically for impact analysis. It uses an explicit time-integration algorithm for solving equations of motion and accurately calculating highly nonlinear deformations, including automatically determining buckling response. PRONTO has been used successfully at Sandia National Laboratories for many years to accurately model impact and large-deformation solid mechanics problems.[11, 12, 15, 16, 17, 18]

The primary purpose of these analyses is to show that the inner container, the T-Ampoule, does not rupture during the air transport accident condition. The complete analyses consist of six separate sets of analyses, as shown in the flowchart in Figure 2-3. The first sets of analyses are of the full package assembly (see Section 2.12.2, Full Model Validation Analysis, in this addendum). These consist of a full package model, high-speed impact analysis to simulate the requirements of 10 CFR 71.74, as well as a full package analysis of the low-velocity NCT free drop for determining the positioning of the internals.

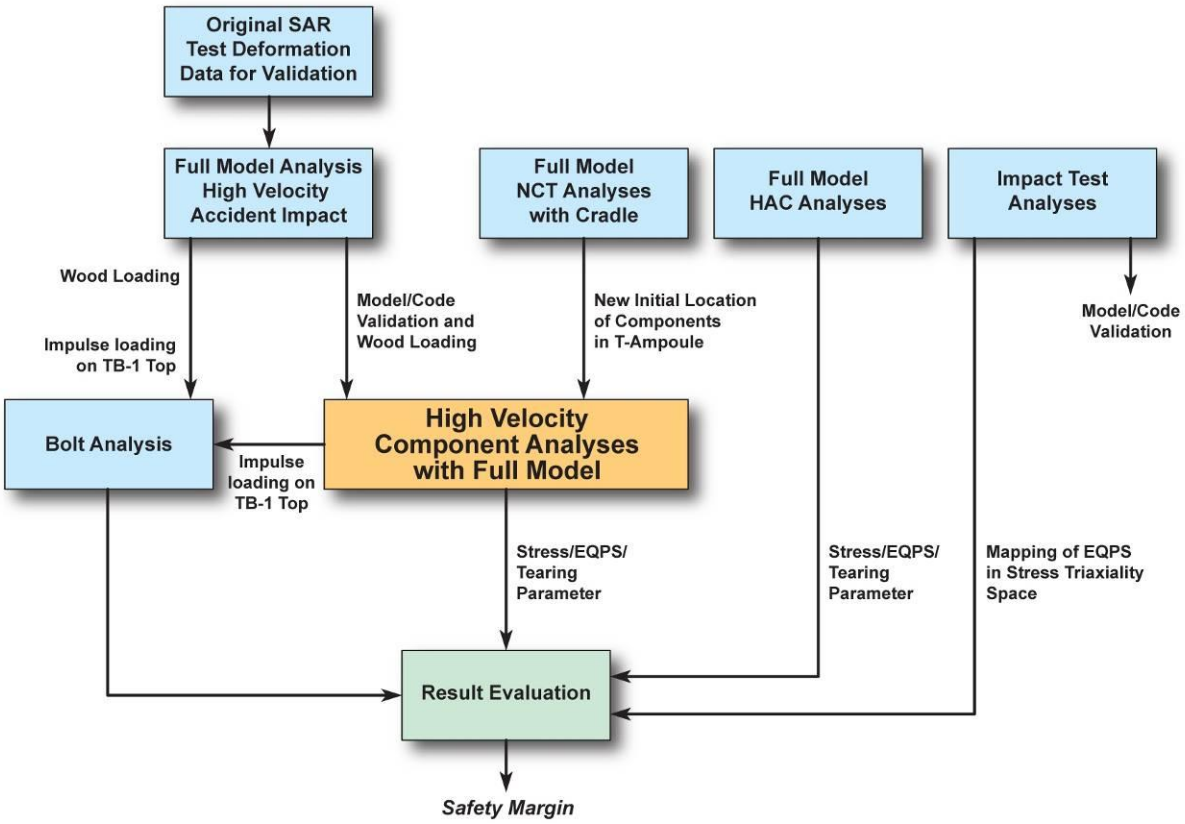

Figure 2-3. Flowchart of PAT-1 Analyses

The original package certification was performed by testing the PAT-1 package assembly. During these tests, neither accelerometers nor strain gages were placed on the package. Therefore, elastic strains and deceleration impulses of the test package are not known. Redwood overpack gross deformations were measured and photographed, and this deformation data from the original certification tests was used to validate the high-speed impact model. This overpack performance evaluation was done with a simplified model of the original PuO_2 powder and at the higher impact velocity of the actual test (445 ft/sec) (see Section 2.12.2.3, Original Certification Test Analysis with the Validation Model, in this addendum).

A "most detailed" model of the package and its various solid metal contents (including the rolled 304 SS outer skin lids on each end, the T-Ampoule, cradle, and sample containers) was used in

NCT 4-ft. drop impacts to verify that the Inner Cradle remains essentially elastic, so that position of the sample containers can be verified for subsequent HAC and high speed (air transport) impact analyses (see Section 2.12.2.7, Full Model NCT and HAC, in this addendum). This "most detailed" finite element model was also used for HAC dynamic crush impact analyses, since the outer skin lid deformation provides significant energy absorption in this relatively low-energy event. A slightly less detailed model (no rolled lids on each end of the 304 SS overpack skin) was used for the high-velocity impact analyses where virtually all of the energy absorption occurs in the redwood overpack. The primary outputs from the high-velocity impact analyses are stresses and plastic strains in the T-Ampoule wall and the TB-1. These outputs will be used to evaluate the integrity of the T-Ampoule and the TB-1. TB-1 wall stress outputs in the HAC dynamic crush cases are used to compare to through-thickness ASME stress allowables, verifying the primary containment boundary's integrity in 10 CFR 71.73 environments.

A series of impact tests (see Section 2.1.1, Impact Test and Material Failure Criterion, in the addendum) were also conducted on the TB-1 component materials.[9] Analysis of these tests served two purposes: (1) to provide additional benchmarking and validation for the analyses and for the finite element code, and (2) to provide data for developing a strain-based locus in stress triaxiality and equivalent strain space. These data, along with the results from the high-velocity impact analyses, are used in the result evaluation step to determine a safety margin on the strength of the T-Ampoule wall. Although the impact tests and full package impact analyses were conducted using room-temperature materials, this is deemed a reasonable approximation because of the constant value of the elongation of titanium shown in Figure 2-60 and the small change in yield strength shown in Figure 2-59 over a temperature range of −20°F to 200°F.

The final analysis (see Section 2.8.5, Bolt Analysis, Section 2.12.6 Bolt Analysis, and Figure 2-506 is a bolt analysis performed on the TB-1 closure bolts. Using the impulse loading determined in the high-velocity TB-1 end impact analyses, along with the loading from the original full model (validation) analyses, an analytical calculation is performed to determine the margin of safety in the TB-1 lid bolts.

2.8.2 Full Package Validation Model

Analyses of the original PAT-1 package certification tests were performed to validate the redwood overpack constitutive model during the high-speed aircraft accident test condition (10 CFR 71.74). A full description of the model and results are presented in Section 2.12.2, Full Model Validation Analyses, in this addendum. The same overpack model is then combined with more detailed models of the new solid metal contents and used in NCT, HAC, and high velocity impact analyses to determine the effect of the internal components on the integrity of the titanium T-Ampoule, which acts as a eutectic barrier between the contents and the stainless-steel TB-1 vessel.

2.8.3 Impact Test and Material Failure

In support of the PAT-1 SAR[1] analysis, a series of impact tests were conducted using the SNL 18" horizontal actuator[9] and the DT-45 drop table.[19] These tests had two main purposes: (1) to provide data for validating the finite element model, and (2) to provide data for developing a strain-based failure locus. A brief summary of the impact tests is given in Section 2.1.1, Impact

Test and Material Failure Criterion, in this addendum, along with details of the finite element model used for code validation.

Using the finite element model and the data from the titanium impact tests, a strain locus in stress-triaxiality–equivalent strain space was developed for the titanium material. The resulting locus is shown in Figure 2-4; the development of these curves is presented in Section 2.12.3.3. The curves were developed with data from the titanium impact or and the titanium cup (simulated T-Ampoule). The curves represent highly strained regions of the test specimens, showing their loading path and stress states. It should be noted that this is not a failure locus, since no cracks were formed in the test. The only curve that was taken to failure is the tensile test specimen, which had a failure strain of 62%. In this sense, the highly strained regions of the T-Ampoule in the high velocity impact analyses (see Section 2.12.5) can be compared with the locus in Figure 2-4, and a safety margin based on comparing the strains generated in the test specimen to the strains generated in the submodel finite element analysis can be calculated based on its location in the locus. For elements exceeding the tested strain locus, a Tearing Parameter is integrated over the plastic strain, and is compared to the critical Tearing Parameter value for the Ti-6Al-4V to determine a safety margin.

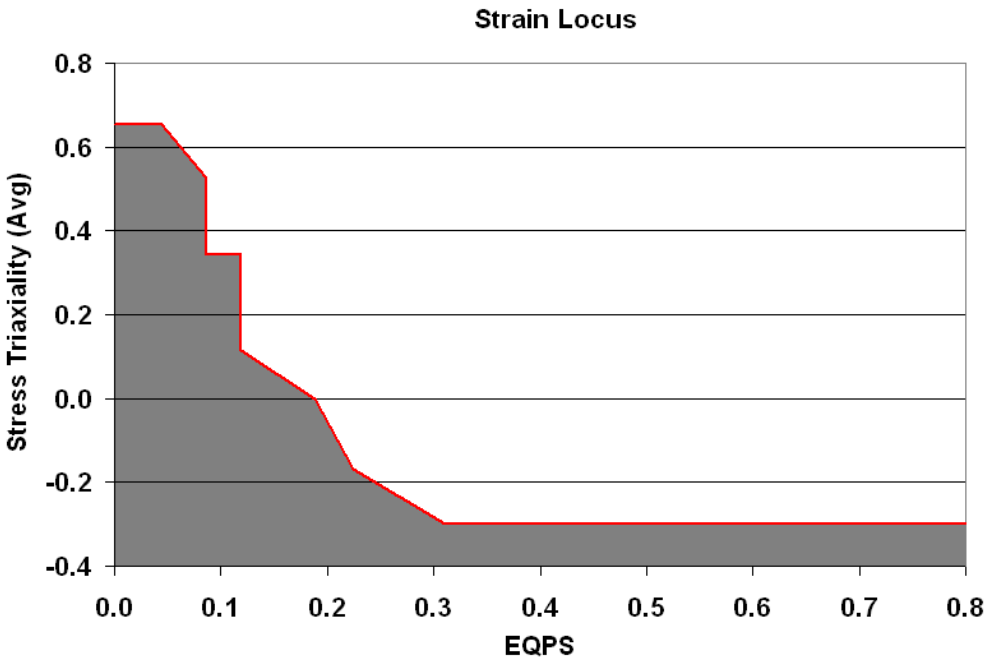

Figure 2-4. Strain Locus Developed from Titanium Experiment and Finite Element Model

2.8.4 NCT, HAC, and High Velocity Impact Analyses

Detailed impact analyses of the PAT-1 package and its components were conducted to determine the response of the TB-1 and T-Ampoule to internal impacts from the contents, as well as external compressive and bending loads from the redwood overpack. As discussed in Section 2.1, the components within the titanium T-Ampoule consist of either cast plutonium metal hollow cylinders with a mass of 831 g or 731 g, or titanium sample containers containing

plutonium material (or a Pu/Be composite). A full description of the detailed package models and results are presented in Section 2.12.5, Component Analyses Using Complete Model, in this addendum. Numerous impact cases were analyzed: end, side, CG-over-corner impacts for plutonium metal hollow cylinders, solid delta-phase Pu cylinders inside sample containers, and smaller Pu/Be composite cylinders inside sample containers.

Table 2-7, Table 2-8, Table 2-9, and Table 2-10 list the various NCT, HAC, and High Velocity impact analyses that were conducted for evaluating package performance with the solid metal contents.

Table 2-7. Normal Conditions of Transport (NCT)
Impact Analyses (6), Components, and Orientations

Run No.	Component	Submodel Orientation
1	2 SC-2 Sample Containers, delta Pu	Lid end impact
4	3 SC-1 Sample Containers, delta Pu	Lid end impact
2	2 SC-2 Sample Containers, delta Pu	Side impact
3	2 SC-2 Sample Containers, delta Pu	Side impact, 45-degree-rotated
5	3 SC-1 Sample Containers, delta Pu	Side impact
6	3 SC-1 Sample Containers, delta Pu	Side impact, 45-degree-rotated

Table 2-8. Hypothetical Accident Condition (HAC) Dynamic Crush Analyses (20), Components, and Orientations

Run No.	Component	Submodel Orientation
1	2 SC-2 Sample Containers, delta Pu	Lid end impact
2	2 SC-2 Sample Containers, delta Pu	Side impact
3	2 SC-2 Sample Containers, delta Pu	Side impact, 45-degree-rotated
4	2 SC-2 Sample Containers, delta Pu	CGOC impact
5	2 SC-2 Sample Containers, delta Pu	CGOC impact, 45-degree-rotated
6	3 SC-1 Sample Containers, delta Pu	Lid end impact
7	3 SC-1 Sample Containers, delta Pu	Side impact
8	3 SC-1 Sample Containers, delta Pu	Side impact, 45-degree-rotated
9	3 SC-1 Sample Containers, delta Pu	CGOC impact
10	3 SC-1 Sample Containers, delta Pu	CGOC impact, 45-degree-rotated
11	831 g Plutonium Metal Hollow Cylinder, alpha Pu	Lid end impact
12	831 g Plutonium Metal Hollow Cylinder, alpha Pu	Side impact
13	831 g Plutonium Metal Hollow Cylinder, alpha	Lid end impact, angled cylinder

Run No.	Component	Submodel Orientation
	Pu	
14	831 g Plutonium Metal Hollow Cylinder, alpha Pu	Side impact, angled cylinder
15	831 g Plutonium Metal Hollow Cylinder, alpha Pu	CGOC impact, angled cylinder
16	731 g Plutonium Metal Hollow Cylinder, alpha Pu	Lid end impact
17	731 g Plutonium Metal Hollow Cylinder, alpha Pu	Side impact
18	731 g Plutonium Metal Hollow Cylinder, alpha Pu	Lid end impact, angled cylinder
19	731 g Plutonium Metal Hollow Cylinder, alpha Pu	Side impact, angled cylinder
20	731 g Plutonium Metal Hollow Cylinder, alpha Pu	CGOC impact, angled cylinder

Table 2-9. High Velocity (Aircraft) Impact Analyses (27), Components, and Orientations

Run No.	Component	Submodel Orientation
1	831 g Plutonium Metal Hollow Cylinder, alpha Pu	Bottom position, top impact
2	831 g Plutonium Metal Hollow Cylinder, alpha Pu	Bottom position (angled), top impact
3	831 g Plutonium Metal Hollow Cylinder, alpha Pu	Bottom position (angled), CGOC impact
4	831 g Plutonium Metal Hollow Cylinder, alpha Pu	Far side position, side impact
5	831 g Plutonium Metal Hollow Cylinder, alpha Pu	Far side position (angled), side impact
6	731 g Plutonium Metal Hollow Cylinder, alpha Pu	Bottom position, top impact
7	731 g Plutonium Metal Hollow Cylinder, alpha Pu	Bottom position (angled), top impact
8	731 g Plutonium Metal Hollow Cylinder, alpha Pu	Bottom position (angled), CGOC impact
9	731 g Plutonium Metal Hollow Cylinder, alpha Pu	Far side position, side impact
10	731 g Plutonium Metal Hollow Cylinder, alpha Pu	Far side position (angled), side impact
11	SC-1 – Pu	Bottom position, support structure 0°, top impact
12	SC-1 – Pu	Far side position, support structure 0°,side impact

Run No.	Component	Submodel Orientation
13	SC-1 – Pu	Far side position, support structure 45°, side impact
14	SC-1 – Pu	Bottom position, support structure 0°, CGOC impact
15	SC-1 – Pu	Bottom position, support structure 45°, CGOC impact
16	SC-2 – Pu	Bottom position, support structure 0°, top impact
17	SC-2 – Pu	Far side position, support structure 0°,side impact
18	SC-2 – Pu	Far side position, support structure 45°, side impact
19	SC-2 – Pu	Bottom position, support structure 0°, CGOC impact
20	SC-2 – Pu	Bottom position, support structure 45°, CGOC impact
21	SC-1 - Be	Bottom position, angled Be, support structure 0°, top impact
22	SC-1 – Be	Far side position, angled Be, support structure 0°, side impact
23	SC-1 – Be	Far side position, angled Be, support structure 45°, side impact
24	SC-1 – Be	Bottom position, angled Be, support structure 0°, CGOC impact
25	SC-1 – Be	Bottom position, angled Be, support structure 45°, CGOC impact
26	SC-2 – Pu	Far side position, support structure 45°, side impact, friction 0.4
27	SC-2 – Pu	Far side position, support structure 45°, side impact, friction 0.2

Table 2-10. 30-ft Drop Impact Analyses (3), Components, and Orientations

Run No.	Component	Submodel Orientation
1	SC-2 - Pu	Far side position, support structure 45°, side impact
2	831 g Plutonium Metal Hollow Cylinder, alpha Pu	Bottom position (angled), top impact
3	831 g Plutonium Metal Hollow Cylinder, alpha Pu	Bottom position (angled), CGOC impact

Figure 2-5 is a summary plot of the Tearing Parameter versus equivalent plastic strain for the highest-value elements in the T-Ampoule body from 19 of the HAC and High Velocity impact analyses, or at least those that have any elements extending beyond the Bao-Wierzbicki (B-W) strain locus. The purpose of the plot is to assess the margin that exists in the T-Ampoule wall for sites that may initiate ductile tearing. The lowest factor of safety shown in this plot is 1.63 (critical Tearing Parameter is 1.012, divided by peak Tearing Parameter value of 0.62, equals 1.63). It is important to note that some of the element locations within the T-Ampoule body are along the internal closure lip, which would not threaten T-Ampoule integrity even if tear initiation were ever to occur. As detailed in Section 2.12.5, the maximum number of elements exceeding the B-W strain locus in any one impact analysis is 126 (out of 580,000 elements in the T-Ampoule model).

Figure 2-6 is a summary plot of the B-W strain locus for the highest-TP value element in Figure 2-5, for comparison. Note that although all of these elements extend beyond the B-W dashed

line locus from test data, they only exceed the tested locus by a relatively small quantity (less than 0.3, and stress triaxiality can theoretically be infinitely positive or negative as perfect hydrostatic tension or compression is approached). A factor of safety cannot be quantified from this B-W strain locus, since points outside the locus do not necessarily indicate failure (they are only outside the tested stress triaxiality—plastic strain region of non-failure). This should give additional confidence that even the elements with the lowest factor of safety (based on Tearing Parameter) are nearly within the tested range of stress-triaxiality versus EQPS that did not fail.

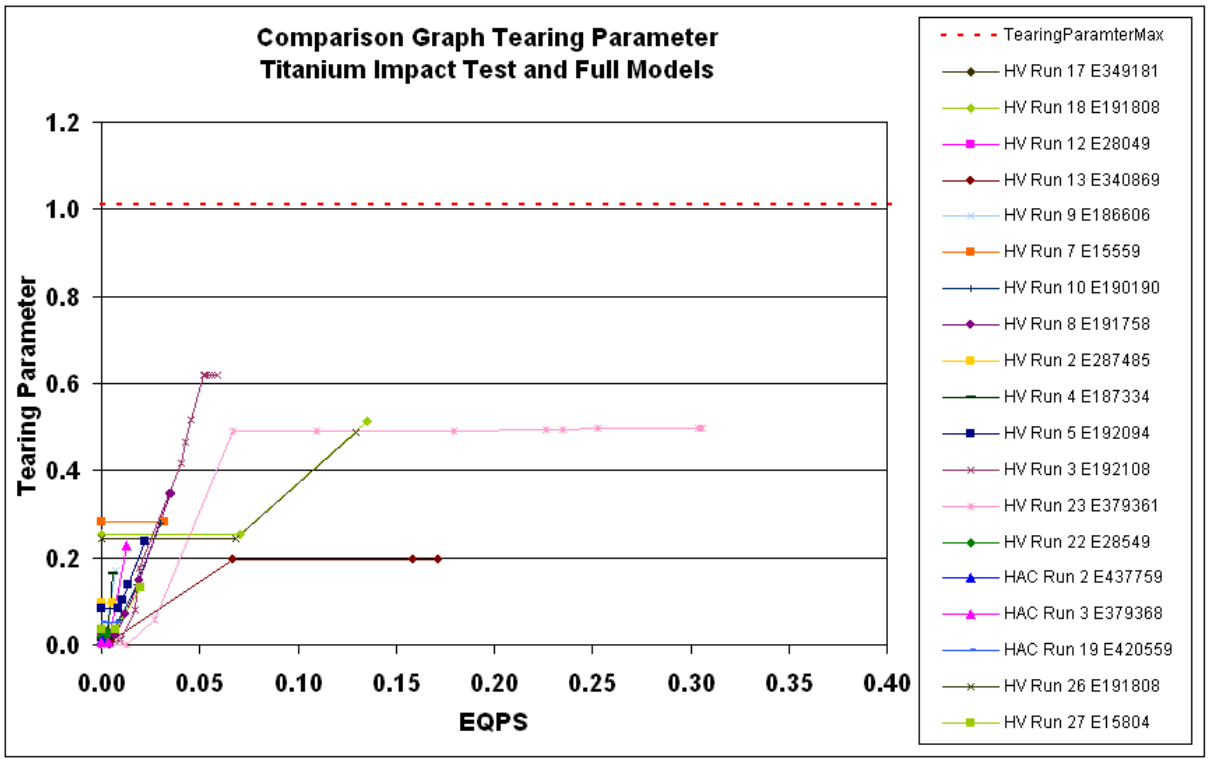

Figure 2-5. Summary of Highest Tearing Parameter versus Plastic Strain Elements for HAC and High Velocity Analyses

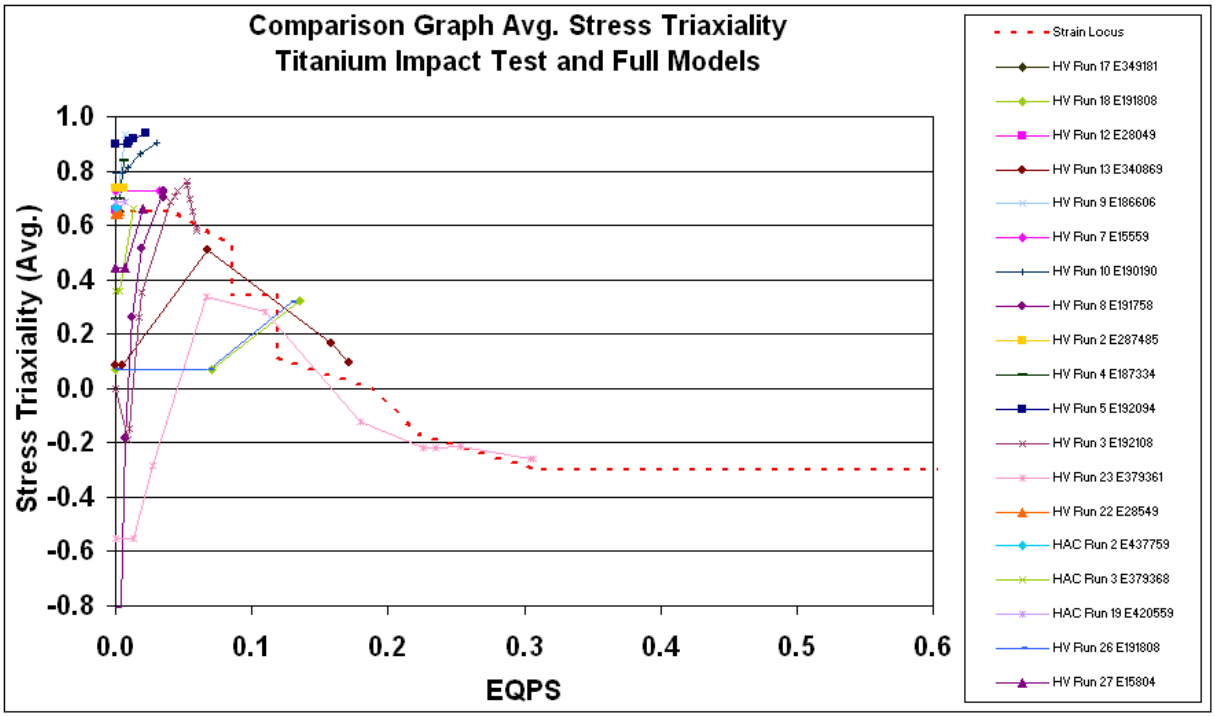

Figure 2-6. Summary of B-W Strain Locus Values for the Highest Tearing Parameter Elements.

As discussed in detail in Section 2.12.5.5.3, these curves all terminate below the critical Tearing Parameter of 1.012. Therefore, they do not to pose a threat to the integrity of the T-Ampoule body. From Figure 2-5 and Table 2-11 (which shows the peak Tearing Parameter value for all high speed impact analyses), the smallest margin of safety based on Tearing Parameter is 1.63 from the 831 g angled plutonium metal hollow cylinder high-speed CG-over-corner impact analysis case. Two important points must be noted when using this as a safety margin. First, this is not based on through-thickness failure of the T-Ampoule, but it is based on the stress-modified integrated strain limit for any element that might merely *initiate* a ductile tear. Second, there are many additional conservatisms inherent in the finite element analyses, which calculated the maximum plastic strains in the T-Ampoule wall. In addition to the plastic strains in the T-Ampoule wall, stresses in the TB-1 remain essentially elastic (except localized denting) and do not threaten the structural integrity of this vessel.

Table 2-11. High Velocity (Aircraft) Impact Analyses Peak Tearing Parameter Values

Run No.	Component	Model Orientation	Maximum Tearing Parameter (T-Ampoule)
1	831 g Plutonium Metal Hollow Cylinder, alpha Pu	Bottom position, top impact	0.0528
2	831 g Plutonium Metal Hollow Cylinder, alpha Pu	Bottom position (angled), top impact	0.2115

Run No.	Component	Model Orientation	Maximum Tearing Parameter (T-Ampoule)
3	831 g Plutonium Metal Hollow Cylinder, alpha Pu	Bottom position (angled), CGOC impact	0.6177
4	831 g Plutonium Metal Hollow Cylinder, alpha Pu	Far side position, side impact	0.2896
5	831 g Plutonium Metal Hollow Cylinder, alpha Pu	Far side position (angled), side impact	0.2389
6	731 g Plutonium Metal Hollow Cylinder, alpha Pu	Bottom position, top impact	0.1507
7	731 g Plutonium Metal Hollow Cylinder, alpha Pu	Bottom position (angled), top impact	0.2831
8	731 g Plutonium Metal Hollow Cylinder, alpha Pu	Bottom position (angled), CGOC impact	0.3967
9	731 g Plutonium Metal Hollow Cylinder, alpha Pu	Far side position, side impact	0.4896
10	731 g Plutonium Metal Hollow Cylinder, alpha Pu	Far side position (angled), side impact	0.2842
11	SC-1 – Pu	Bottom position, support structure 0°, top impact	0.0319
12	SC-1 – Pu	Far side position, support structure 0°,side impact	0.2417
13	SC-1 – Pu	Far side position, support structure 45°, side impact	0.1958
14	SC-1 – Pu	Bottom position, support structure 0°, CGOC impact	0.0935
15	SC-1 – Pu	Bottom position, support structure 45°, CGOC impact	0.3061
16	SC-2 – Pu	Bottom position, support structure 0°, top impact	0.0132
17	SC-2 – Pu	Far side position, support structure 0°,side impact	0.4788
18	SC-2 – Pu	Far side position, support structure 45°, side impact	0.5137
19	SC-2 – Pu	Bottom position, support structure 0°, CGOC impact	0.0953
20	SC-2 – Pu	Bottom position, support structure 45°, CGOC impact	0.0540
21	SC-1 – Be	Bottom position, angled Be, support structure 0°, top impact	0.0155
22	SC-1 – Be	Far side position, angled Be, support structure 0°, side impact	0.2075

Run No.	Component	Model Orientation	Maximum Tearing Parameter (T-Ampoule)
23	SC-1 – Be	Far side position, angled Be, support structure 45°, side impact	0.4970
24	SC-1 – Be	Bottom position, angled Be, support structure 0°, CGOC impact	0.0597
25	SC-1 – Be	Bottom position, angled Be, support structure 45°, CGOC impact	0.1197
26	SC-2 – Pu	Far side position, support structure 45°, side impact, friction 0.4	0.4888
27	SC-2 – Pu	Far side position, support structure 45°, side impact, friction 0.2	0.4673

Numerous conservative assumptions were made in the modeling and assessment of the TB-1 and especially the T-Ampoule integrity. Other conservatisms include: neglecting the tantalum foil packing material which would perform some small load spreading and energy absorbing function, neglecting the rolled lid of the outer package skin in aircraft impacts, always assuming the content location and orientation most damaging to the T-Ampoule, e.g., "strongest" plutonium metal hollow cylinder dimensions to resist buckling; most dense, compact, and sharp shape for the delta Pu and Be composite cylinders; delta Pu contents have higher density of alpha Pu; sharpest orientation for the strong Be cylinders, etc. Also, the material properties for these contents are conservatively assumed to have infinite plasticity, when in fact the alpha Pu is very brittle and the Be has rather limited ductility. These conservative assumptions maximize the loading and damage potential to the T-Ampoule, yet it retains structural integrity as a eutectic barrier.

2.8.5 Bolt Analysis

Although the bolts in the PAT-1 package were already shown to remain elastic and the lid maintained containment during the original certification testing, a simplified analysis was performed on the bolts securing the TB-1 lid when subjected to the high-speed aircraft accident test condition (10 CFR 71.74). The bolts are not explicitly modeled in the TB-1, but the net balance of compression from the redwood in an end impact along with the bolt preload versus the internal impact loading from various impacting contents can be determined. The impulse loads, which are applied to the underside of the lid, are obtained from the high velocity impact analyses (see Section 2.12.5). The forces holding the lid in place are the bolt preload and the redwood contact force. These forces are plotted in Figure 2-506 and the analysis is described in Section 2.12.6, Bolt Analysis, in this addendum. As shown in the figure, the forces from the components are only a fraction of the bolt preload. The peak impulse load is a factor of 2.0 less than the bolt preload, and is a factor of 6 less than the total of the sum of the wood retaining force and the bolt preload. Therefore, the lid of the TB-1 will remain properly torqued during the aircraft impact accident.

Other factors, besides impact loads, can contribute to the loss of bolt preloads and proper seal compression.[14] Protecting the closure lid from direct impact, using a lid design that minimizes

prying loads on bolts, recessing bolts within the lid, lubricating bolts to reduce necessary torque to achieve desired preload, using a large enough preload to minimize fatigue and loosening of bolts by vibration, and finally using similar thermal expansion coefficient materials for the bolt, lid, and cask body have all been done for the PAT-1. The TB-1 is a "protected lid and bolt head" closure design,[14] which is most resistant to potential shear and bending bolt loads. Bolt bending and prying forces are minimized by the design of the TB-1 closure, which has inner and outer bore surfaces (the inner with an O-ring bore seal, the TB-1 O-ring is not used for plutonium metal shipments) with a flange surface in between (with the primary copper metal gasket flange seal). The body of the TB-1 containment vessel is also significantly thickened in the bolted closure region to accommodate these multiple bore surfaces and resist bending loads in side and CGOC impacts. It is important to highlight that the TB-1's bolted closure met all containment requirements in SAR[1] aircraft accident condition testing with same-mass contents, and the effective bolt load calculations provided in Section 2.12.6 confirm that the solid metal contents do not adversely affect containment.

2.8.6 Summary

A series of analyses were performed on the PAT-1 package and its contents to determine the integrity of the TB-1 and T-Ampoule when subjected to the requirements of 10 CFR 71.71 (Normal conditions of transport), 10 CFR 71.73 (Hypothetical accident conditions) and 10 CFR 71.74 (Accident conditions for air transport of plutonium). Six sets of analyses were conducted, leading up to detailed impact analyses of the PAT-1 package, including its TB-1 containment vessel and the T-Ampoule eutectic barrier. Using a strain-based failure criterion, it was shown that the T-Ampoule would not rupture and would continue to function as a eutectic barrier between the stainless steel TB-1 vessel and the solid metal plutonium contents. In addition, an analysis of the bolts securing the TB-1 lid showed that the lid will remain intact and tight.

No fire simulations required for the air transport accident were conducted; however, a simple check of the potential for differential thermal expansion was performed, similar to the checks for the NCT and HAC conditions. Since the T-Ampoule is the only change being made from the original package Hypothetical accident conditions, the only concern would be the expansion of the T-Ampoule resulting in contact with the TB-1.

The Military Handbook[6] reports a coefficient of thermal expansion (α) for Ti-6Al-4V used for the T-Ampoule of 5.1×10^{-6} in./in./°F in the range of temperatures of concern. A conservative estimate of the maximum expansion of the T-Ampoule can be calculated by assuming the T-Ampoule is a 7.418-in.-long cylinder (the actual T-Ampoule is capped) with a diameter of 4.22 in. The T-Ampoule is assumed to reach the maximum temperature of the TB-1 in the original fire test which was estimated at 1080ºF (582ºC). Assuming a temperature increase of 1010ºF (1080ºF – 70ºF), the expansion produced equals $\alpha \Delta TL$, or 0.038 in. in the longitudinal direction, and 0.0683 in. in circumference (or 0.0217 in. in diameter). Since the gap between the T-Ampoule and the TB-1 is 0.015 in. around the entire perimeter, the expansion in the longitudinal direction is slightly more than the total gap (0.038 in. > 0.30 in.). However, the TB-1 would also expand outward, allowing for the expansion of the T-Ampoule. As shown in Section 2.12.4.9, the coefficient of thermal expansion of the Stainless PH13-8Mo used for the TB-1 is approximately 5.9E-6 in/in/°F. The same temperature change from 70^{o}F to 1080^{o}F produces a 1010^{o} F temperature increase. Assuming that the TB-1 is a cylinder of length 8.68 in.

with a 5.35 in. diameter (outer diameter of main TB-1 body) increases the length equal to $\alpha \Delta TL$, or 0.0517 in. in the longitudinal direction, and a increases the circumference by approximately 0.100 in. (0.0319 in. in diameter). The TB-1 expands outward more than the T-Ampoule, therefore, no stresses will be induced by differential thermal expansion for the air transport accident. In Section 2.12.8, the pressure generated within the TB-1, which included temperature, helium gas generation from alpha decay, and decomposition of O-rings and ancillary plastics, from the accident conditions for air transport of plutonium fire environment was set equal for ancillary plastic weight determination to a pressure of 1110 psia which is the same as that reported in the SAR[1] of 1110 psia.

2.9 Accident Conditions for Fissile Material Packages for Air Transport

For 10 CFR 71.55(f), the requirements for accident conditions for air transport of plutonium evaluated in this addendum cover this section.

2.10 Special Form

No change. This addendum covers transport of normal form material for PAT-1.

2.11 Fuel Rods

No change. This addendum does not consider transport of fuel rods for PAT-1.

2.12 Appendix

2.12.1 References

1. United States. Nuclear Regulatory Commission. NUREG-0361. "Safety Analysis Report for the Plutonium Air Transportable Package, Model PAT-1." Washington, D.C. 1978.

2. United States. Nuclear Regulatory Commission. Regulatory Guide 7.6. "Design Criteria for the Structural Analysis of Shipping Cask Containment Vessels," Revision 1. Washington, D.C.: March 1978.

3. United States. Nuclear Regulatory Commission. Regulatory Guide 7.8. "Load Combinations for the Structural Analysis of Shipping Casks for Radioactive Material," Revision 1. Washington, D.C.: March 1989.

4. United States. Nuclear Regulatory Commission. Code of Federal Regulations. 10 CFR 71.73. "Hypothetical Accident Conditions for the Packaging and Transport of Radioactive Materials."

5. American Society of Mechanical Engineers (ASME). "Boiler & Pressure Vessel Code." 2007.

6. Department of Defense. *Military Standardization Handbook: Metallic Materials and Elements for Aerospace Vehicle Structures.* MIL-HDBK-5E: May 1988.

7. Bao, Y., and T. Wierzbicki. "On the Cut-Off Value of Negative Triaxiality for Fracture." Engineering Fracture Mechanics, 72, pp. 1049-1069, 2005.

8. Taylor, L.M. and D.P. Flanagan. "PRONTO3D: A Three-Dimensional Transient Solid Dynamics Program," SAND87-1912. Sandia National Laboratories. Albuquerque, NM. March 1989.

9. Davie, N., et al. "Test Report PAT-1/TB-1 Impact Test Series." Sandia National Laboratories. August 30, 2007.

10. Bao, Y. "Prediction of Ductile Crack Formation in Uncracked Bodies," Report 100, 2003. Impact & Crash Worthiness Laboratory. Massachusetts Institute of Technology. Cambridge, MS.

11. Wellman, G.W., Diegert, K.V., and Saizbrenner, R. "Two-Dimensional Quasistatic Modeling of Exclusion Region Barriers in Support of Design Guide Development." SAND93-0905. Sandia National Laboratories. Albuquerque, NM. 1993.

12. Dawson, D.B., Antoun, B.R., and Mosher, D.A. "MAVEN Progress Report for FY98 Second Half (Fracture of Weapons Materials)." Sandia National Laboratories Memo Report to Distribution, October 5, 1998.

13. Andersen, J.A., Duffey, T.A., Dupree, S.A., and Nilson, R.H., "PARC (Plutonium Accident Resistant Container) Program Research, Design, and Development, SAND76-0587, NUREG/CR-0030. Sandia National Laboratories. Albuquerque, NM. July 1978.

14. Mok, G.C., Fischer, L.E., and Hsu, S.T., "Stress Analysis of Closure Bolts for Shipping Casks," NUREG/CR-6007, UCRL-ID-110637, Prepared for the US NRC, April 1992.

15. Bessette, G.C., et al. "Methodology Assessment and Recommendations for the Mars Science Laboratory Launch Safety Analysis," SAND2006-4563. Sandia National Laboratories. Albuquerque, NM. September 2006.

16. Ammerman, D.J., and Hoffman, E.L., "Dynamic Pulse Buckling of Cylindrical Shells Under Axial Impact: A Comparison of 2D and 3D Finite Element Calculations With Experimental Data," SAND93-0350. Sandia National Laboratories. Albuquerque, NM. 1993.

17. United States. Nuclear Regulatory Commission. NUREG/CR-6672. Sprung, J.L., Ammerman, D.J., Breivik, N.L., Dukart, R.J., Kanipe, F.L., Koski, J.A., Mills, G.S., Neuhauser, K.S., Radloff, H.D., Weiner, R.F., and Yoshimura, H.R. "Re-examination of Spent Fuel Shipment Risk Estimates." SAND2000-0234. Sandia National Laboratories. Albuquerque, NM. March 2000.

18. United States. Nuclear Regulatory Commission. NUREG-1768. "Package Performance Study Test Protocols." February 2003.

19. VanGoethem, D. et al. "Test memo report for PAT-1/T-Ampoule drop table shock tests." Sandia National Laboratories. Albuquerque, NM. December 12, 2008.

20. Fischer, L. E., W. Lai, "Fabrication Criteria for Shipping Containers," NUREG/CR-3854, Lawrence Livermore National Laboratory, April 1984.

21. American Society of Mechanical Engineers (ASME). "Boiler and Pressure Vessel Code," Section VIII, Division 1, Rules for Construction of Pressure Vessels. July 1, 2009 Addenda.

22. Holmes-Siedle, A. and L. Adams. Handbook of Radiation Effects, Section Edition. pp. 568. UK: Oxford University Press, 2002.

23. Chao, A. W. C and M Tigner. Handbook of Accelerator Physics and Engineering. Singapore: World Scientific Publishing Co. Pte. Ltd., 2002.

24. American Society for Testing and Materials. Younger, C. L. and Haley, F. A. "Irradiation Effects at Cyrogenic Temperature on Tensile Properties of Titanium and Titanium-Base Alloys." Irradiation Effects on Structural Alloys for Nuclear Reactor Applications, STP 484, (1970), pp. 537-563.

25. Bouquet, F., *Radiation Damage in Materials*, 3rd Edition, Systems Company, 1990.

26. Bouquet, F., *Radiation Thresholds for Synthetic Elastomers*, IEEE Transactions on Nuclear Science, Vol. NS-32, No. 6, December 1985.

27. DuPont Performance Elastomers, "Radiation Resistance of Viton," Technical Information, Wilmington, DE, December 1998.

28. Serna, Lysle, private communication, Sandia National Laboratories, Albuquerque, NM, March 10, 2010.

2.12.2 Full Model Validation Analyses

2.12.2.1 Discussion

This section describes the side, end, and CG-over-corner high velocity impact analyses of the original PAT-1 package certification tests. There are two general overpack models, one to model the high-speed aircraft accident test condition (10 CFR 71.74[2]), and the other to model the NCT (10 CFR 71.71[2]) and HAC test conditions (10 CFR 71.73[2]). The original certification of the PAT-1 was performed through testing with only minimal instrumentation, so the overpack deformations were used for comparison to those analyzed in the validation model (with simplified PuO_2 contents and the certification test impact velocity of 445 ft/sec). Subsequently, similar overpack models with the detailed solid metal contents (and T-Ampoule) will be used to evaluate the position of the contents in NCT 4 ft impacts, and to determine the effect of the solid internal components on the integrity of the titanium T-Ampoule, which acts as a eutectic prevention barrier between the contents and the stainless-steel TB-1 vessel.

2.12.2.2 Model Description

The finite element model used in the high-velocity validation analyses is shown in Figure 2-7. This is a half-symmetry model, with the plane of symmetry running along the center axis. The

principal components of the model are the redwood impact-limiting material, the load spreader assembly, the copper cylinder, the TB-1 containment vessel, and the plutonium oxide mass. The PAT-1 package is encased in a stainless drum approximately 41.5 in. in length. This includes an approximate 1–in. flange on each end for the outer drum lid and seal. To simplify the finite element model, the details of the outer drum lid are not included. This area consists mostly of thin sheet metal components, and the energy absorbed in their deformation is conservatively ignored. Therefore, the height of the finite element model is only 39.75 in., which is the length of the redwood impact-limiting material.

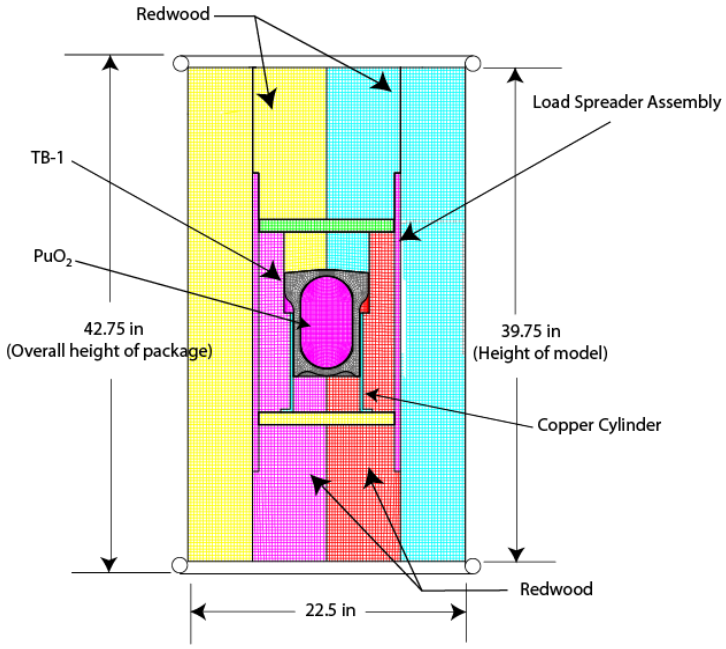

Figure 2-7. Finite Element Model of the Complete PAT-1 Package

In the full package validation model, the TB-1 is modeled as a solid, one-piece object. The bolted connection for the lid is not modeled; instead the net loading on the lid from contents impacts and overpack compression is shown to be significantly less than the bolt pre-load, and thus detailed modeling of the closure is not necessary. This bolted joint was also shown in the SAR[1] aircraft impact tests to meet containment requirements of < A_2/week release rate with same-mass contents. In addition, the plutonium oxide mass inside the TB-1 is modeled as a very soft elastic plastic material with the correct density. These simplifications are acceptable, since the primary purpose of the analysis is to validate the model's redwood overpack crush in the three certification high velocity impact tests.

The finite element validation model contains 378,439 elements: 366,258 hexahedral elements and 12,181 quadratic shell elements. All components with hexahedral elements have at least 3 elements through the thickness to accurately capture potential bending and shear responses, and aspect ratios of approximately 1.0, following common large-deformation explicit analysis practice for accurate FEA model response. As shown in Figure 2-8(a), the outside of the redwood material is wrapped in a 0.0625 in., stainless steel shell layer. The shells are attached to the hexahedral elements using coincident nodes to simulate the gluing of these components in the actual PAT-1 assembly. Their primary purpose is to provide confinement of the redwood

material. Figure 2-8(b) shows the density of the mesh in the load spreader assembly region; three elements are used across the load spreader pipe to capture any potential bending.

The top removable plug, the removable disk, the TB-1, the PuO_2, and the lower removable plug are modeled as individual components; they are not attached to other components in the model. The remaining pieces are attached using coincident nodes in order to simulate the gluing together of these components in the actual assembly.

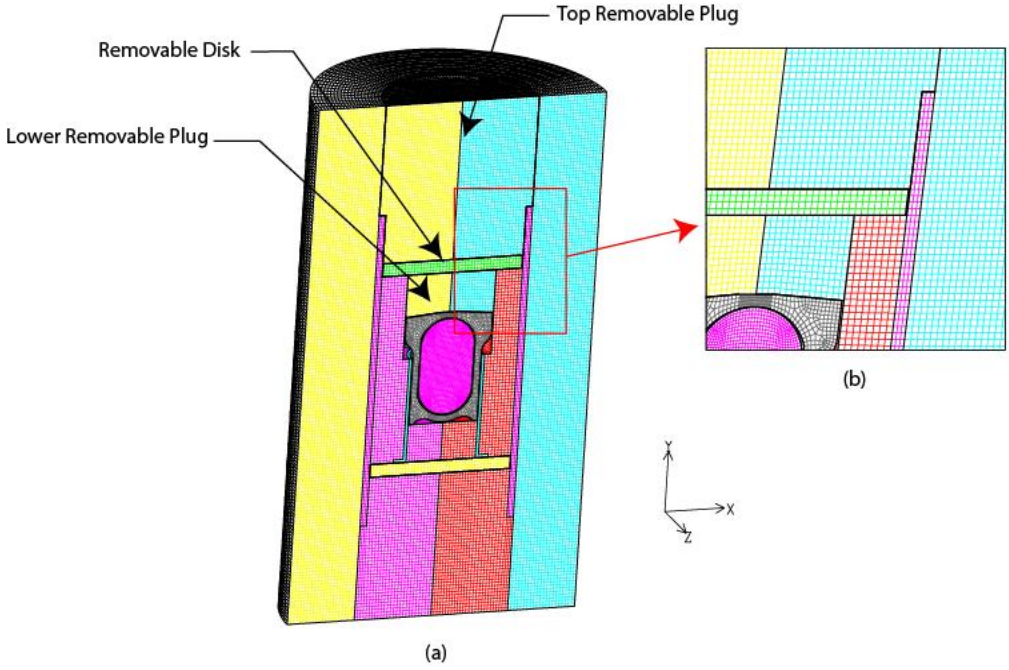

Figure 2-8. Details of the High-Velocity Finite Element Validation Model

The redwood material is modeled using the orthotropic crush model in PRONTO-3D.[3] The orthotropic crush model is an empirically based constitutive relation used to model materials like metallic honeycomb and wood. The force deflection curve used to simulate the compression of the redwood material is presented in Figure 2-9 along with data from Joseph and Hill.[4] These values, along with the other modeling parameters, are presented in Table 2-12, and details of the material properties are presented in Section 2.12.4. The redwood material model (as well as simulating the grain orientation with sections of stronger and weaker redwood) was previously validated against regulatory aircraft impact test data associated with the slightly smaller PAT-2 package.[6]

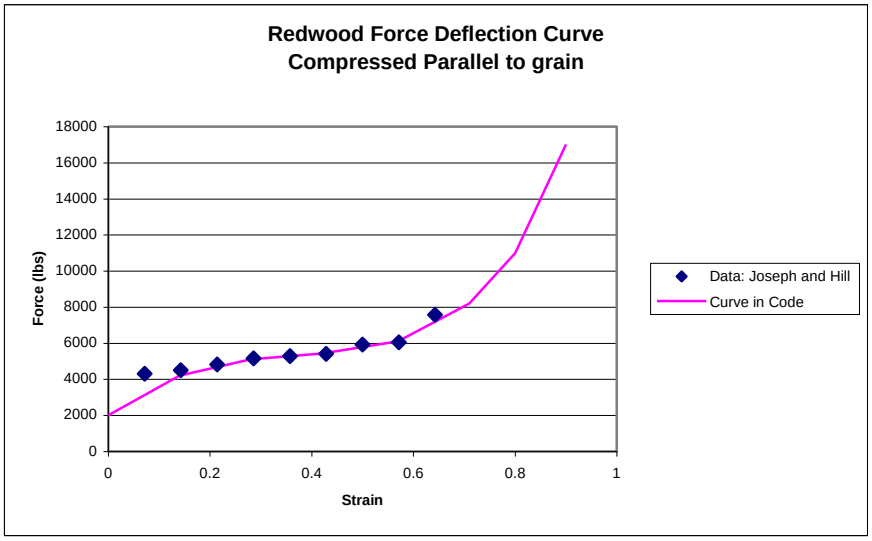

Figure 2-9. Redwood Force-Deflection Curve Used in Orthotropic Crush Model

The metal components were modeled using a power-law hardening constitutive model:

$$\sigma = \sigma_y + A\left(\varepsilon_p\right)^n \tag{2-1}$$

where σ_y is the yield stress, A is a hardening constant, and n is a hardening exponent. Values for the material parameters for each material are given in Table 2-13. The PuO_2 powder is also modeled as a very soft material using the power-law hardening model. This is deemed reasonable, since the mass of the material and its loading on the TB-1 and the redwood is the primary factor; modeling the detailed response of the oxide is not important.

The circumferential orientation of the pie-shaped redwood around the PAT-1 package ranges from 8 to 10 segments. This is an attempt to keep the grain of the wood parallel to the direction of the load, and the strong axis of the grain can thus be misaligned with the impact orientation by, at most, 22.5 degrees. However, the orthotropic crush model in PRONTO-3D[3] is oriented relative to the three orthogonal global axes of the model; a local coordinate system is not available in this model. Modeling many small segments around the circumference is not necessary since strength variation due to grain orientation can be more easily accomplished by assigning different crush behavior to a smaller number of segments. Thus, the model material blocks were constructed in 90º segments rotated 45º to the model's global axes; this is shown in Figure 2-10. This is an attempt to maximize the strength of the material in the radial direction during side impacts within the constraints imposed by the constitutive model. Modeling the redwood blocks in this fashion ensures that the strong axis of the grain is oriented with the impact axis, just as would occur (or very nearly so) in any randomly oriented impact test.

Table 2-12. Redwood Orthotropic Crush Model Parameters

Parameter	Value	
Compacted YOUNGS MODULUS (psi)	1.5E6	
Compacted POISSONS RATIO	0.3	
Compacted YIELD STRESS (psi)	20000	
Full Compaction	0.9	
Modulus x (psi)	1.5E6	
Modulus y (psi)	0.3E6	
Modulus z (psi)	0.3E6	
Modulus xy (psi)	0.2E6	
Modulus yz (psi)	0.25E6	
Modulus zx (psi)	0.2E6	
Function 1 $ T-Direction	**Strain**	**Pressure (psi)**
	0.	2000
	0.14	4200
	0.28	5100
	0.42	5430
	0.57	6100
	0.71	10100
	0.80	15000
	0.90	20000
Function 2 $ L-Direction		
	0	400
	0.14	986
	0.28	1200
	0.42	1275
	0.57	1432
	0.71	2371
	0.80	3521
Function 4 $ sigxy or sigxz vs. volume		
	0.0	1000
	0.6	1000
	0.7	10000
	0.9	10000
Function 5 $ sigyz vs. volume		

Parameter	Value	
	0	1000
	0.6	1000
	0.7	10000
	0.9	10000

2.12.2.3 Original Certification Test Analyses with the Validation Model

The validation model was analyzed for the three basic impact directions, end-on, side-on, and center-of-gravity-over-corner (CGOC). The primary purpose of these analyses is to compare overpack deformations with the previous impact tests. Subsequent analyses with the same overpack model, but more detailed solid metal contents models (including the T-Ampoule) will be performed to verify structural integrity of the TB-1 and T-Ampoule in HAC dynamic crush, as well as high velocity impact conditions (see Section 2.12.5).

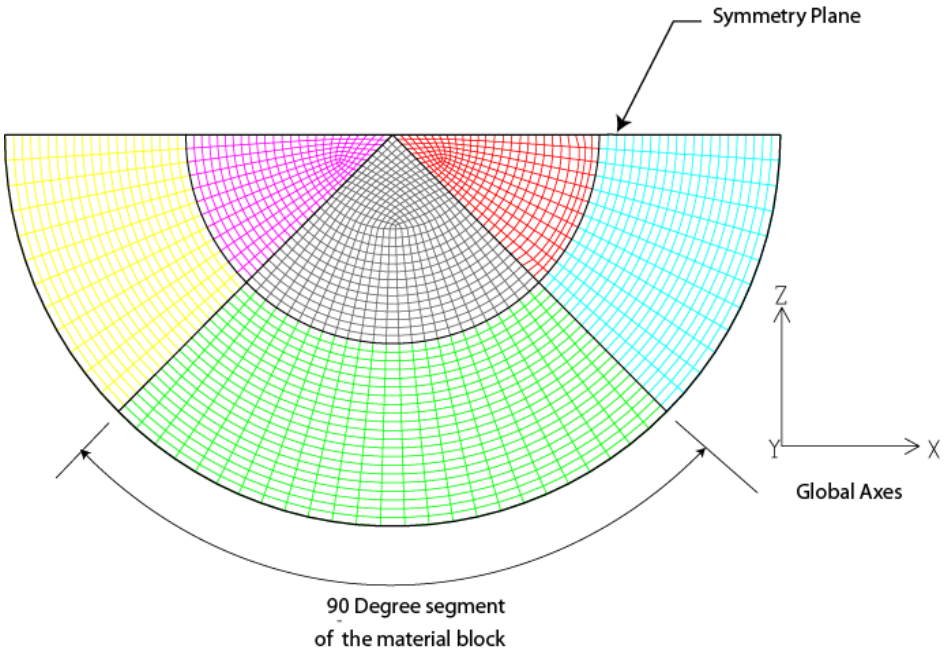

Figure 2-10. Model Slice Configuration for the Orthotropic Crush Material Model

Table 2-13. Power-Law Hardening Constitutive Model Parameters

Material	E (ksi)	ν	σ_y (ksi)	*A* (ksi)	n	Reference (from addendum)
Aluminum 6060-T6	9,900	0.3	45	37.8	0.55	2.12.4.3
Aluminum 7075-T6	10,400	0.33	73	37.8	0.55	2.12.4.5
Copper	17,200	0.33	45	38.0	0.55	2.12.4.7
Stainless Steel	28,000	0.27	40	192.7	0.748	2.12.4.12
Pu Oxide	1000	0.3	2	100	1.0	2.12.4.11
PH13-8MO	30,000	0.3	141.0[A]	30	1.0	2.12.4.9

[A] In the full model analyses to determine the deceleration of the whole package, a yield strength of 200 ksi was inadvertently used for the Ph138Mo TB-1 material. This represents the material in forged condition and does not reflect the subsequent heat treatment. However, since this model was used only to generate the rigid body deceleration of the package and not to determine the inelastic response of the TB-1 vessel, the change in the yield stress is immaterial. The table above reflects what is in the final model.

2.12.2.4 End Impact

The results from an end-on impact of the complete PAT-1 package for an initial velocity of 445 ft/sec are presented in Figure 2-11. This was the velocity used in the test, which is slightly higher than the 422 ft/sec specified in 10 CFR 71.74.[2] The overall length of the deformed model is 32.75 in., which is slightly longer that the 31.5 in. produced in the test as shown in Figure 2-12 (from Figure 2.18, Reference 1). This 4% difference in overpack crush is likely well within the variability of the redwood crush properties purely due to moisture content and age.[5] Note that the overpack skin buckling pattern observed in the test cannot be reproduced in the FEA model since the stainless steel skin is "tied" to the redwood (the nodes are equivalenced) and no slipping between the surfaces is allowed.

Since the crush distance of the finite element model is shorter than the crush distance observed in the same velocity end impact certification test, the TB-1 and contents loading applied using the shorter (and higher) finite element model acceleration will be more severe than the impulse applied in the certification test (i.e., the redwood properties are conservatively modeled as being slightly too stiff). The deceleration curve for the end impact analysis is shown in Figure 2-13.

2.12.2.5 Side Impact

The deformed shape of the full package model for side-on impact at a velocity of 445 ft/sec is shown in Figure 2-14. The resulting width of the package ranges from 15.5 in. to 16.5 in. This compares well to the deformed packages shown in Figure 2-15 (from Figure 2.24 of the SAR[1]), which gives deformed thicknesses of 15 to 15.5 in. The results of the finite element model are conservatively stiffer than the actual package. The deceleration curve for the side impact analysis is shown in Figure 2-16.

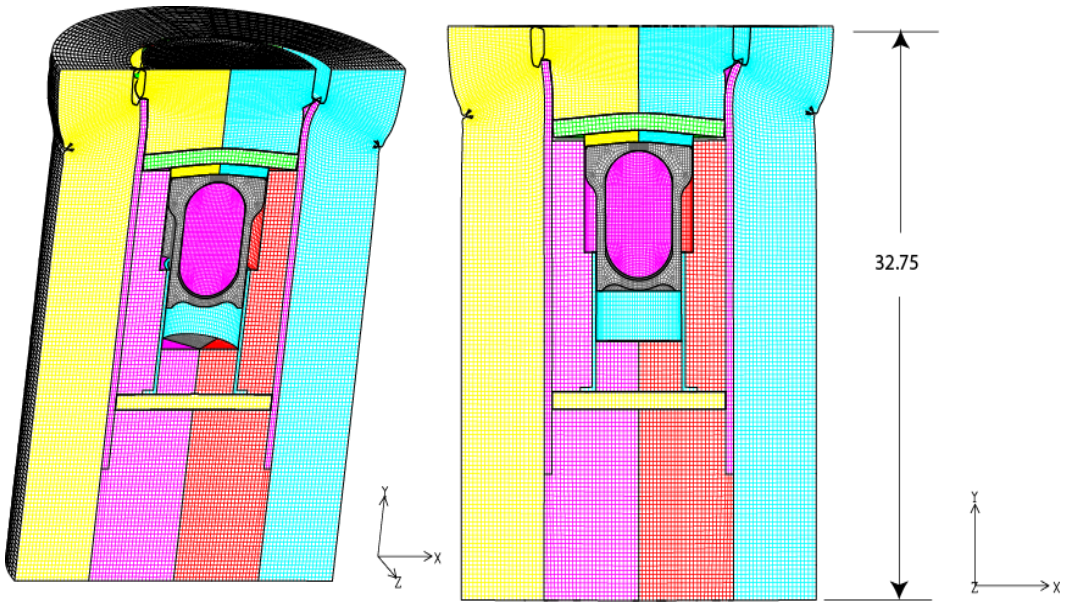

Figure 2-11. Deformation from an End-On Impact of 445 ft/sec

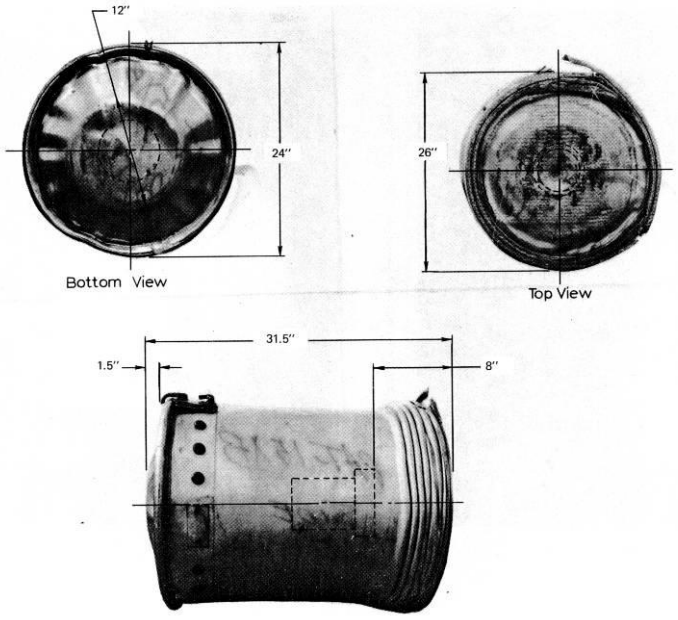

Figure 2-12. PAT-1 Dimensions Following 422-FPS Top End Impact (from SAR Figure 2.18[1])

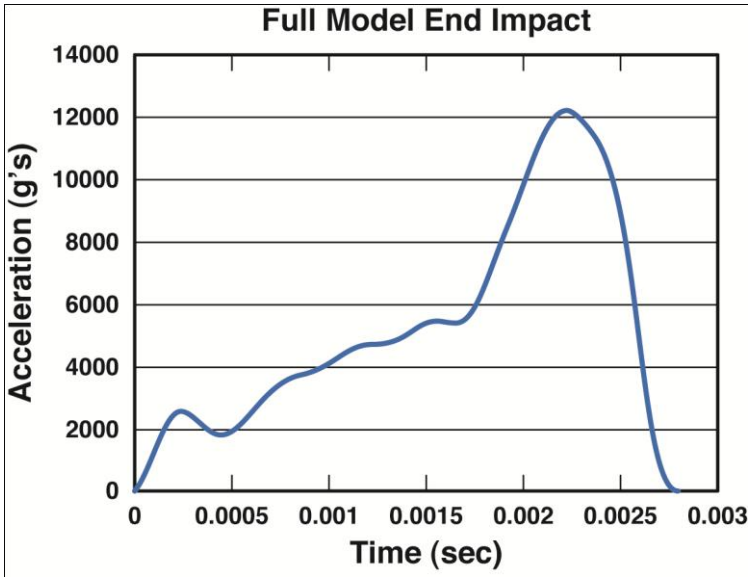

Figure 2-13. Full Model TB-1 Deceleration Curve for End-On Impact Analysis (10 CFR 71.74)

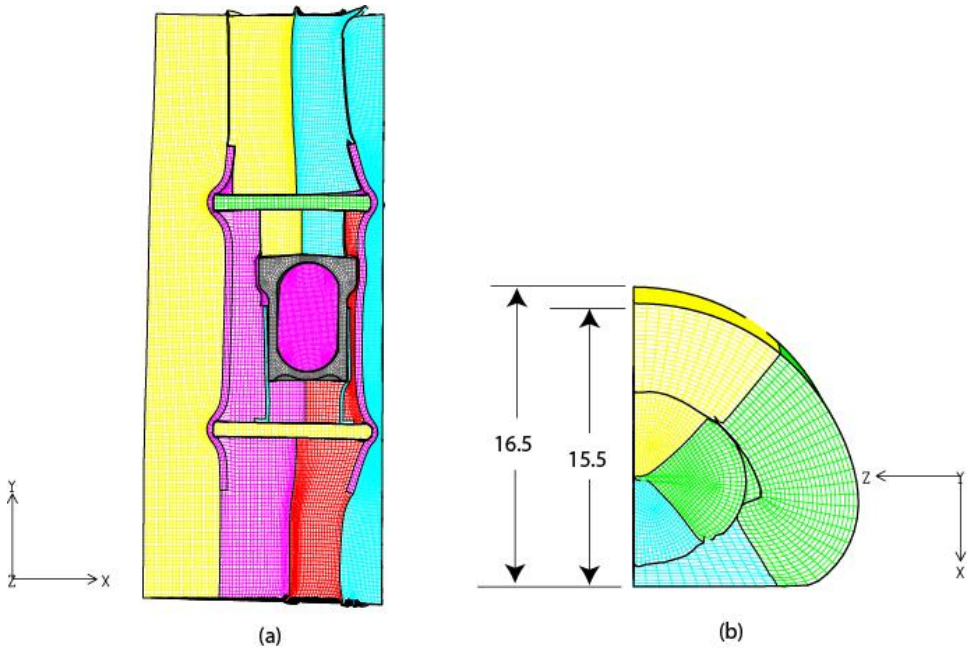

Figure 2-14. Deformation of the Full Package Model after a Side Impact of 445 ft/sec

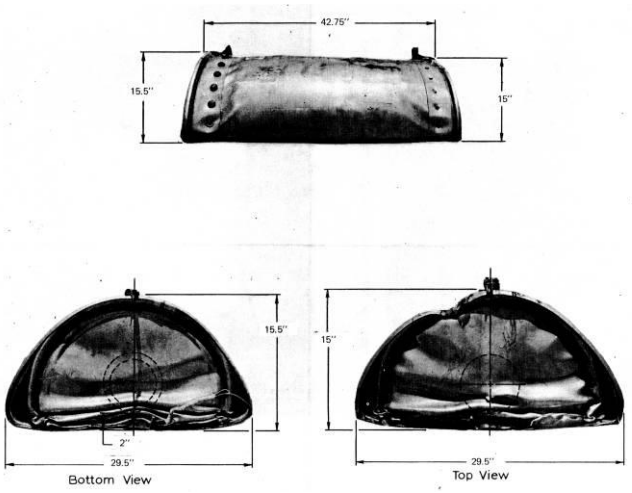

Figure 2-15. PAT-1 Dimensions Following 445 FPS Side Impact (from SAR Figure 2.24[1])

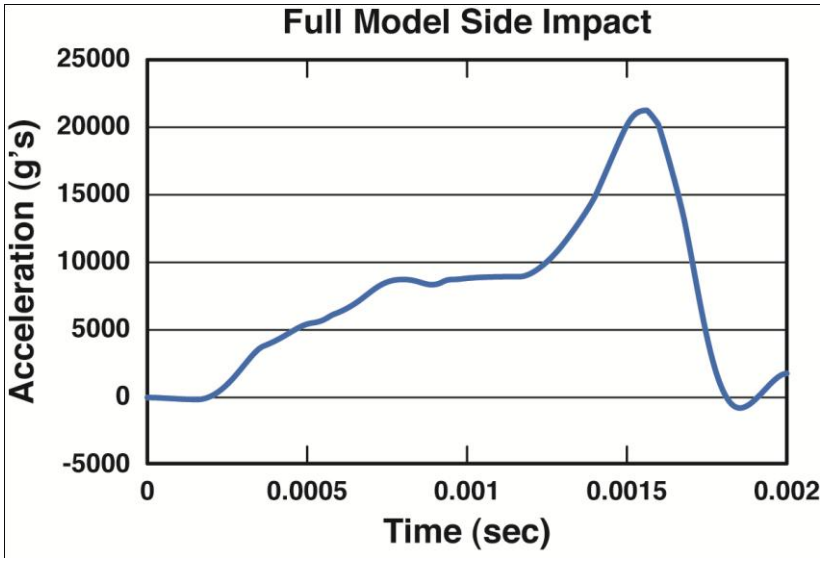

Figure 2-16. Full Model TB-1 Deceleration Curve for Side Impact Analysis (10 CFR 71.74)

2.12.2.6 CGOC Impact

The resulting deformation for the CGOC impact is shown in Figure 2-17. The finite element model has an unreformed side length of 23 in., which is longer than the 19 in. shown in Figure 2-18 (from Figure 2.27 of the SAR[1]). However, there is some rounding of the corner during the test, which is not seen in the model (probably due to the outer overpack skin shell elements being equivalenced to the redwood), and this makes measurement of the tested specimen less precise. This corner rounding would change this dimension without absorbing significant quantities of energy. The SAR figure also gives a nominal dimension of 25 in. to the edge of the TB-1 top. This agrees closely with the model results. Again, excepting the outer skin buckling pattern, the overpack deformation observed in the FEA validation model compares very well with the test results documented in the SAR.[1] The deceleration curve for the CGOC analysis is shown in Figure 2-19.

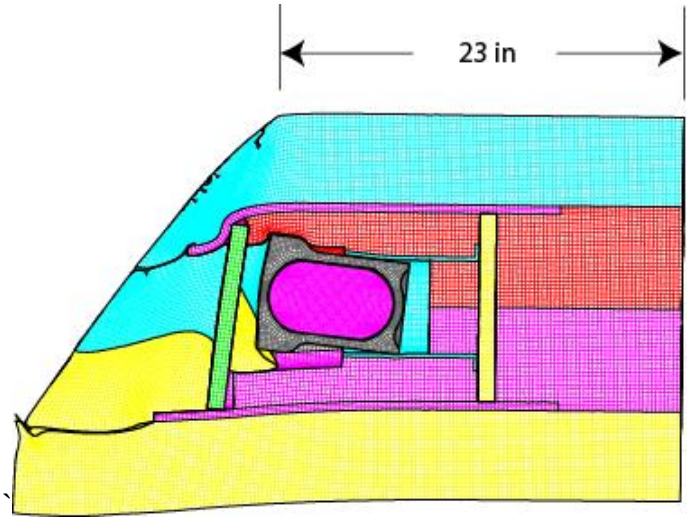

Figure 2-17. Deformation of the Full Package Model after a CGOC Impact of 445 ft/sec

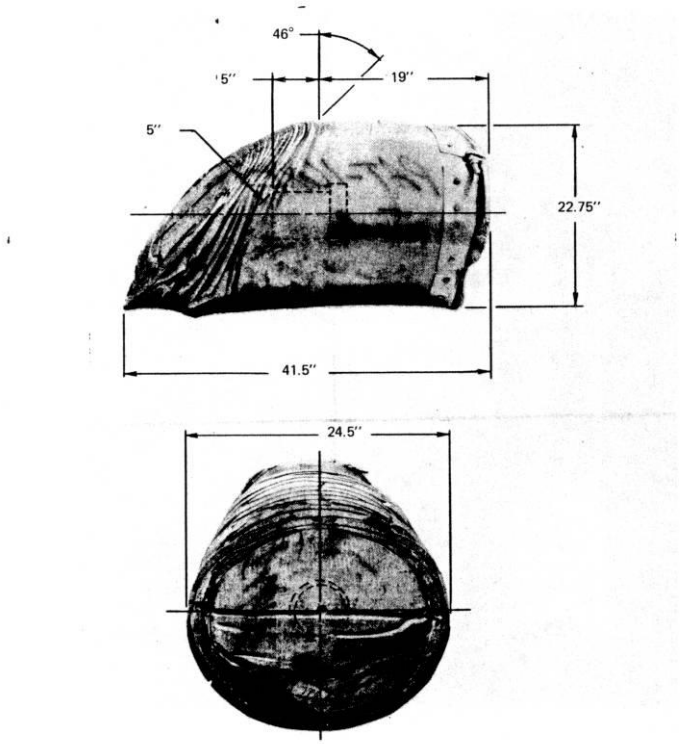

Figure 2-18. PAT-1 Dimensions Following 443-FPS Bottom Corner Impact (CGOC) (from SAR Figure 2.27 SAR[1])

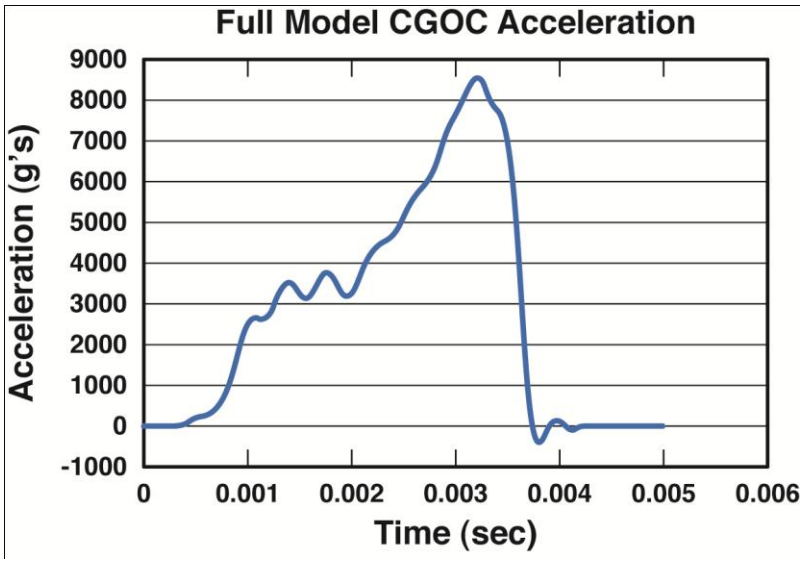

Figure 2-19. Full Model TB-1 Deceleration Curve for CGOC Impact Analysis (10 CFR 71.74)

2.12.2.7 Full Model NCT and HAC

The full package model (with detailed solid metal contents and T-Ampoule) will be analyzed for the NCT (10 CFR 71.71[2]) and HAC (10 CFR 71.73[2]) test conditions to verify contents positioning (NCT) for subsequent 10 CFR 71.74[2] analyses and to verify structural integrity of the TB-1 and T-Ampoule (HAC dynamic crush).

The orientation of the package for the full model NCT analyses will be of the side-on (0 and 45-degree-rotated) and lid end-on orientations, since these analyses generated the largest accelerations in the TB-1 containment vessel.

In addition, end, side, and CG-over-corner dynamic crush events were examined for the HAC to compare TB-1 through-thickness wall stresses with ASME allowables, and to verify T-Ampoule structural integrity. The same model used for the NCT positioning analyses was used for the HAC dynamic crush analysis. Some validation of this model is shown in Section 2.12.5.7.1, where the FEA side impact model overpack deformation matches the SAR[1] impact test results (see Figure 2-490 through Figure 2-495).

2.12.2.8 Model Description

As shown in Figure 2-20, the NCT full package model is very similar to the high-speed aircraft accident model. The only difference is the addition of the lid cover and ring clamp. While these components absorb very little of the kinetic energy during the high-speed impact, and were therefore ignored in that model, they are very important in the low-speed NCT accident condition. In the low-speed NCT condition, they are the primary energy absorber. Details of the lid area are presented in Figure 2-21. The lid and clamp ring consist of three separate pieces that are bolted to the package side and secured with a circumferential ring. The assembly is simplified and modeled in the finite element model as a group of shell elements joined by coincident nodes. The thickness of the shells is varied to account for the overlapping of the different components. To reduce the size of the end-on model, the flange elements were removed from the non-impacting end in the NCT runs. Analysis results are detailed in Section 2.12.5.

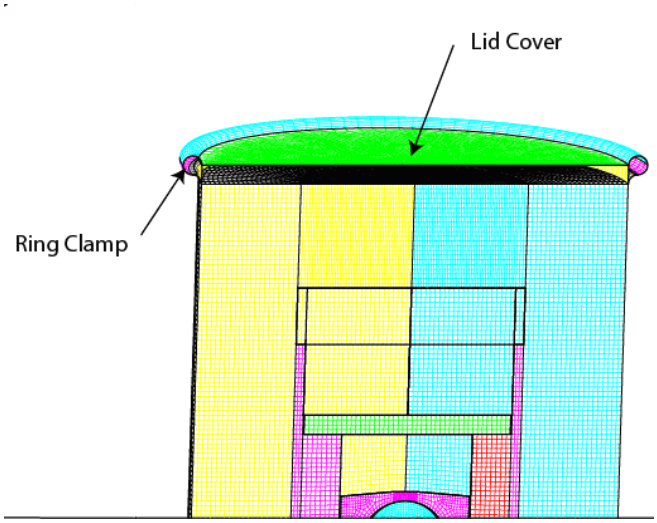

Figure 2-20. NCT and HAC Package Model with Lid Flange

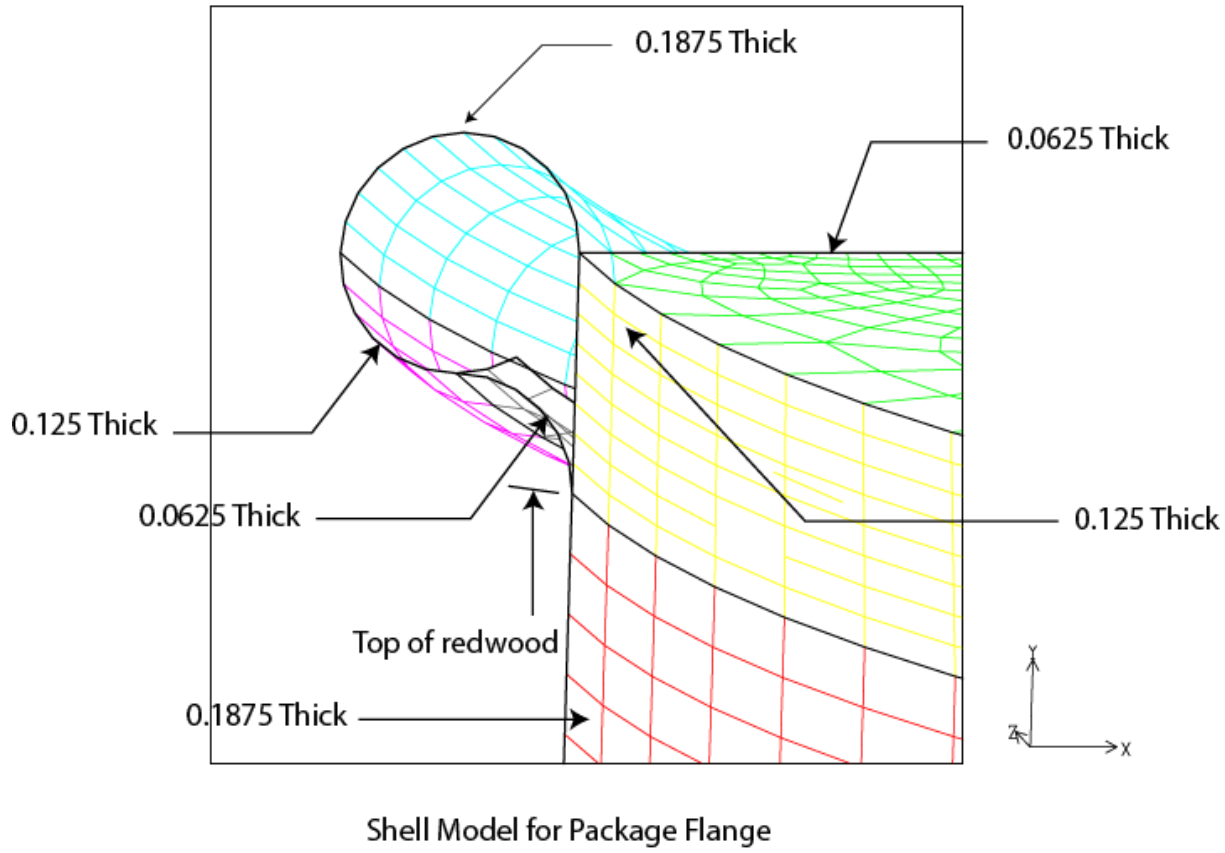

Figure 2-21. Flange Details of NCT Model (Dimensions in Inches)

2.12.2.9 References

1. United States. Nuclear Regulatory Commission. NUREG-0361. "Safety Analysis Report for the Plutonium Air Transportable Package, Model PAT-1." Washington, D.C. 1978

2. United States. Nuclear Regulatory Commission. Code of Federal Regulations, 10 CFR 71. "Packaging and Transportation of Radioactive Material." January 1, 2009.

3. Taylor, L.M. and D.P. Flanagan. "PRONTO3D: a Three-Dimensional Transient Solid Dynamics Program," SAND87-1912. Sandia National Laboratories. Albuquerque, NM. March 1989.

4. Joseph, Walter W. and Thomas K. Hill. "Energy-Absorbing Characteristics of California Redwood Subjected to High Strain." SAND76-0087. Sandia National Laboratories. Albuquerque, NM. 1976.

5. Cramer, S.M, Hermanson, J.C., and McMurtry, W.M. "Characterizing the Large Strain Crush Response of Redwood." SAND96-2966, Sandia National Laboratories. Albuquerque, NM. 1996.

6. Attaway, S.W., "A Local Isotropic Global Orthotropic Finite Element Technique for Modeling the Crush of Wood," SAND88-1449, Sandia National Laboratories, Albuquerque, NM. 1988.

2.12.3 Impact Test and Material Failure Criterion

2.12.3.1 Impact Test Description

In support of the PAT-1 SAR[1] analysis, a series of impact tests were conducted using the Sandia National Laboratories (SNL) 18" horizontal actuator and the DT-45 drop table. These tests had two main purposes: (1) to provide data for validating the finite element model, and (2) to provide data for estimating the margin in support of the strain-based failure criteria. Both test series were required to provide a sufficient range of data in stress space for the strain-based locus. A brief summary of the impact tests is given in this section (full details of the test can be found in "*Test Report PAT-1/TB-1 Impact Test Series*"[1] and "*Test Report PAT-1 T-Ampoule Drop Table Shock Machine Tests*"[2]). In addition, details of the finite element models used for code and model validation, along with the finite element models used to support the strain-based failure criterion, are also presented.

A schematic drawing of the impact test using the 18" horizontal actuator is presented in Figure 2-22. This is a reverse ballistic test in which the sled containing a cup, which represents the T-Ampoule and the TB-1 container, is propelled into a suspended impactor assembly containing a brass or titanium tip. The object of the test was to simulate the impact of the T-Ampoule contents on the T-Ampoule wall, and the T-Ampoule and its contents on the TB-1 inner surface, during a plutonium air transport accident. A brass tip was used to simulate a fine grain alpha-plutonium material impacting the T-Ampoule, and a titanium tip was used in an attempt to generate plastic strain in the T-Ampoule wall. Although the actuator assembly has a limited velocity of 200 ft/sec, which is less than the 422 ft/sec specified for the aircraft accident (10 CFR 71.74), this is not a problem, since the impact between the TB-1 wall and the contents will not be at the maximum velocity. The impact between the contents and the TB-1 occurs while the TB-1 is decelerating but is still moving. Therefore, the relative velocity between the TB-1 and the contents is only a fraction of the initial package velocity.

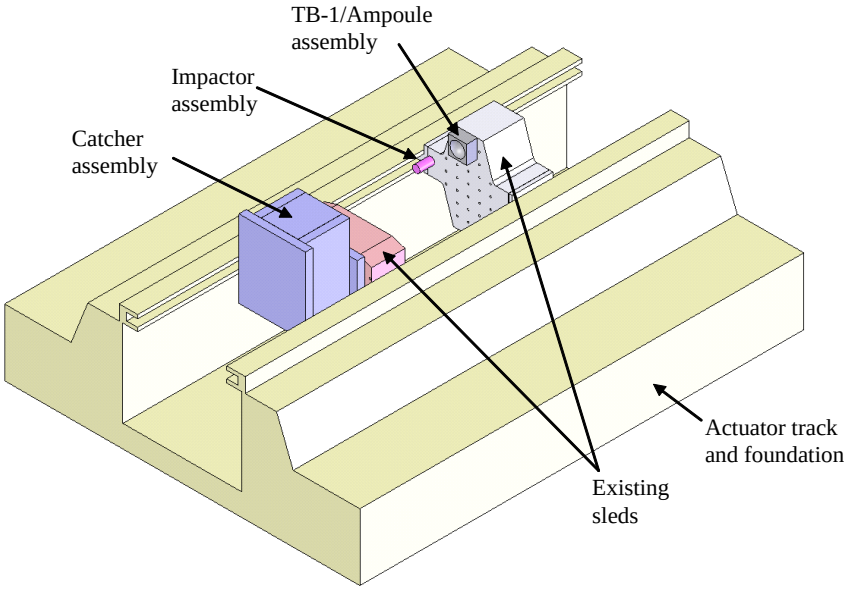

Figure 2-22. Experimental Concept[1]

Figure 2-23 is a schematic of the impactor and T-Ampoule assemblies for the 18" horizontal actuator test. A spherical titanium ampoule specimen is used to represent the top dome of the T-Ampoule in the TB-1. The TB-1 fixture is constructed with the same high-strength 13-8 Mo stainless steel, and an aluminum adaptor is used to secure the TB-1 fixture to the actuator sled. The body of the impactor is constructed from tungsten in order to provide sufficient mass and strength. An aluminum adapter is connected to the back end of the tungsten body to attach the accelerometers. The tip of the impactor, which has a spherical shape (not shown in the figure), is constructed from free cutting brass UNS C36000 (as drawn) or Titanium 6Al-4V (mill-annealed condition). The brass is a surrogate for a fine-grain alpha-plutonium material. The titanium tip is used to provide a material strong enough to produce plastic strain in the T-Ampoule specimen, and to provide additional data for the strain locus in the strain-based failure criteria.

Photos of the actual test setup are shown in Figures 2-24 and 2-25. Figure 2-24 shows the complete test assembly prior to the test. The impactor, suspended over the actuator track using Kevlar string has been meticulously aligned so that it impacts the center of the titanium cup. Figure 2-25(a) shows a close-up view of the titanium cup and TB-1 fixture bolted to the actuator sled, and Figure 2-25(b) shows a close-up view of the suspended impactor.

Additional impact tests were performed using the Drop Table Shock Machine, DT-45, located in Building 860 in Area I. A schematic view of the drop table is presented in Figure 2-26. The DT-45 is capable of a velocity change of 150 ft/s and a peak acceleration of 20,000 g. The pulse durations range from 0.2 to 150 ms. In this test, the test item is attached to the carriage assembly, which is raised above the reaction mass. Upon release, the carriage and the test item are accelerated by gravity and a series of bungee cords. The accelerated items strike a stack of programming material (typically wool felt) which is placed on top of the reaction mass to produce the desired shock pulse.

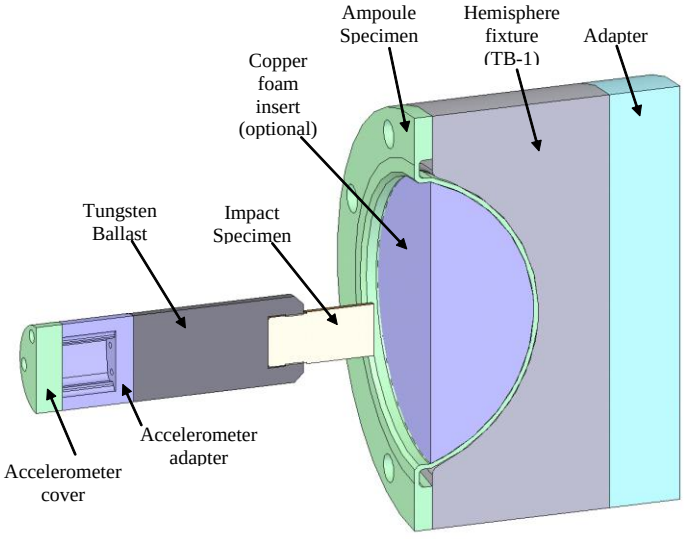

Figure 2-23. Cross-Section of Impactor Assembly and TB-1/Ampoule Assembly[1]

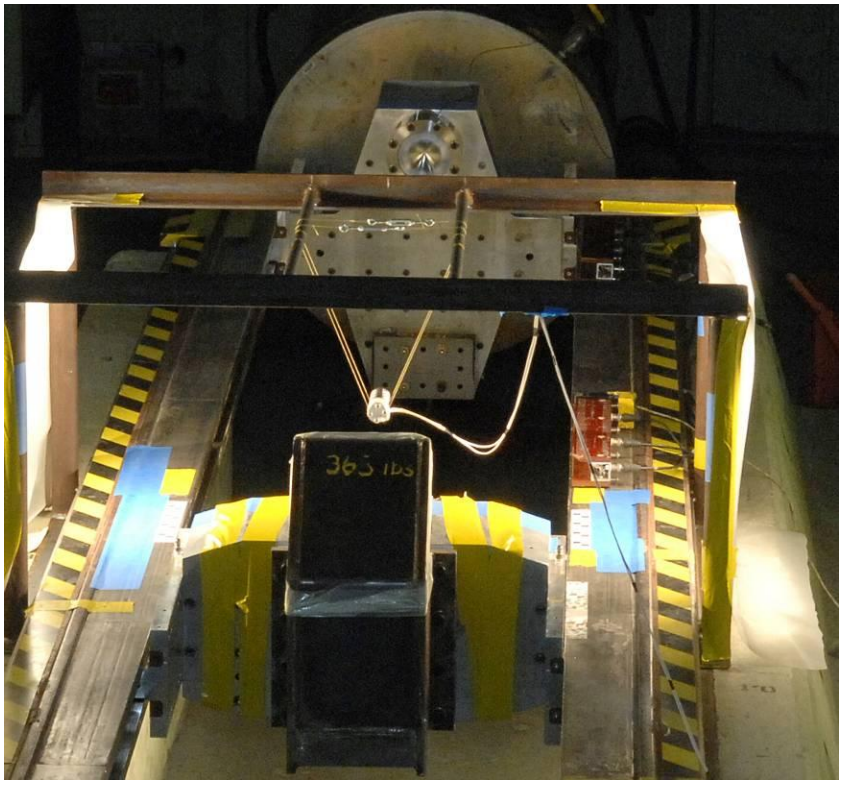

Figure 2-24. Complete Test Assembly Prior to the Test

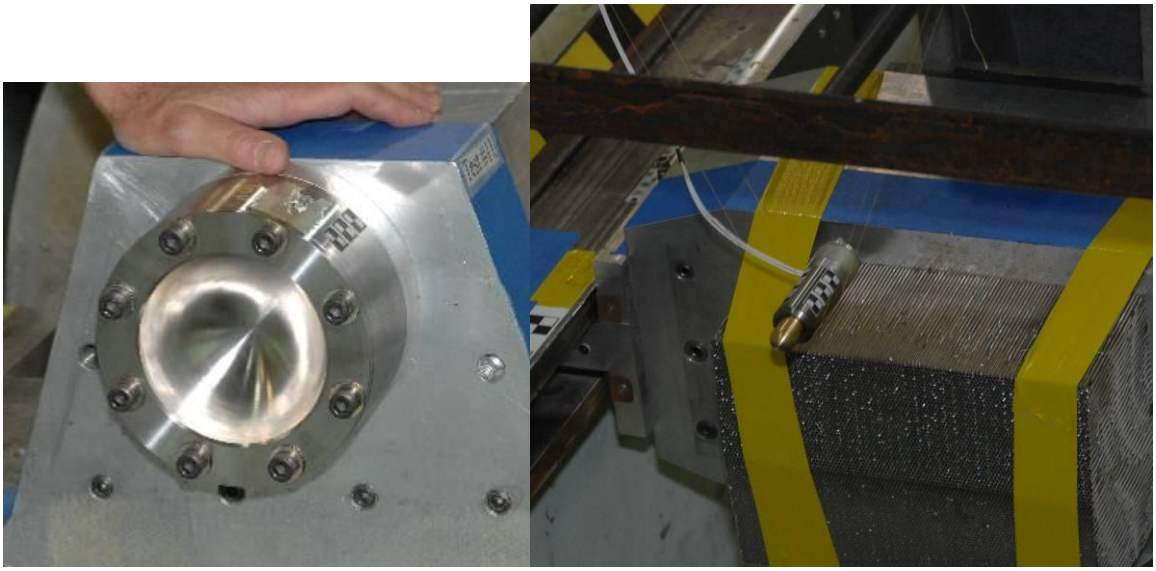

Figure 2-25. (a) Titanium Ampoule and TB-1 Fixture Attached to Actuator Sled; (b) View of Suspended Impactor

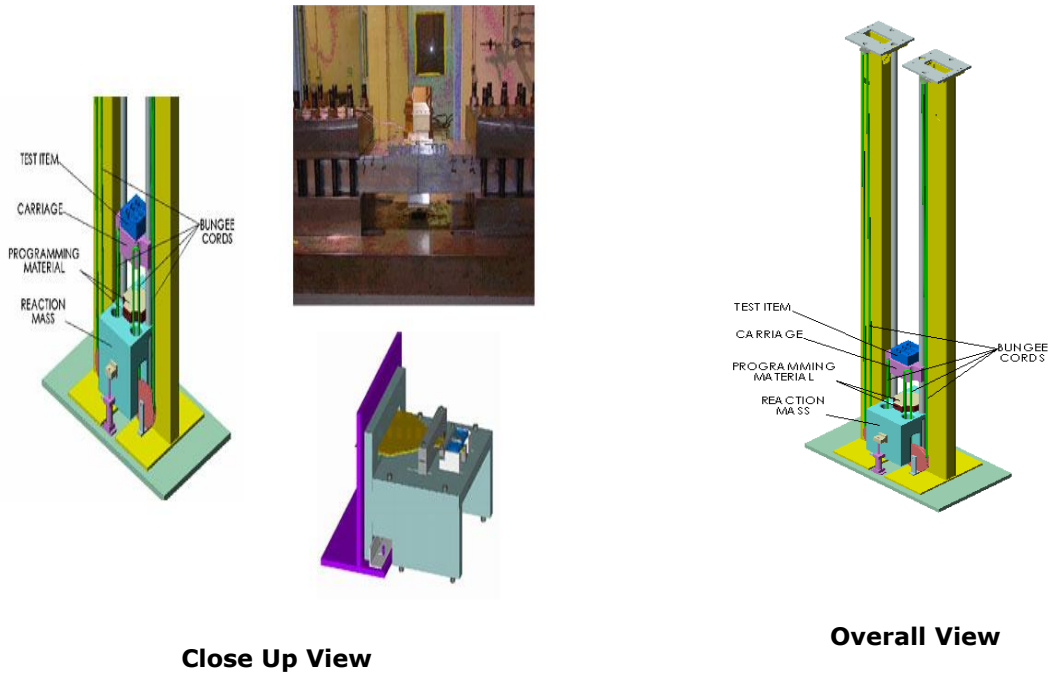

Figure 2-26. DT-45 Drop Table Shock Machine

A solid model of the ampoule test assembly for the drop table test is shown in Figure 2-27. The same type T-Ampoule specimen from the actuator tests is used in this test. The sample specimen is bolted to an adaptor plate, which is attached to the carriage. A 20 lb. crush plate is placed on top of the ampoule. During the deceleration of the carriage, the crush plate will compress and buckle the ampoule test specimen before it strikes the stop blocks. A photograph of the test assembly, prior to testing, is presented in Figure 2-28.

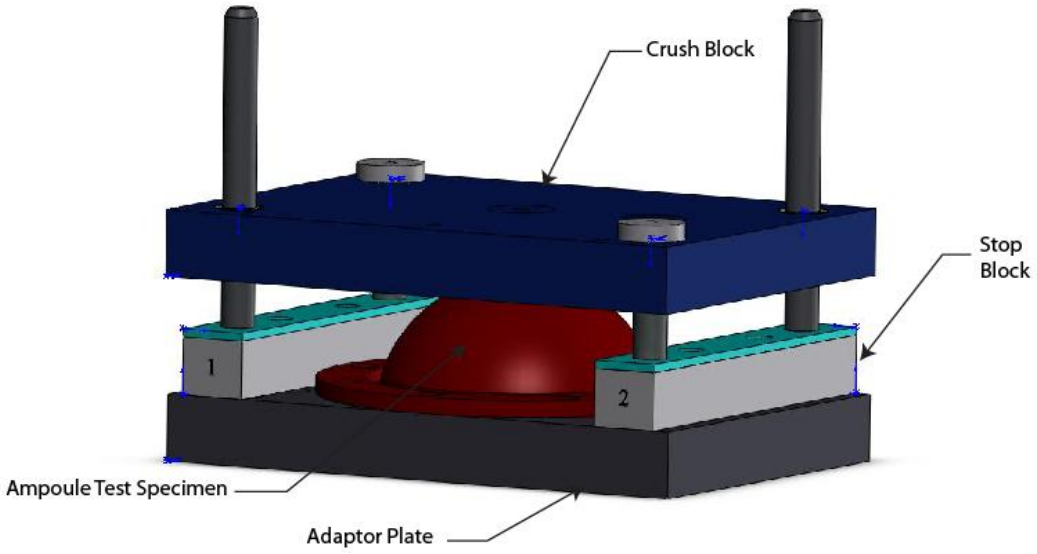

Figure 2-27. Solid model of the Ampoule Test Assemble for Drop Table Tests

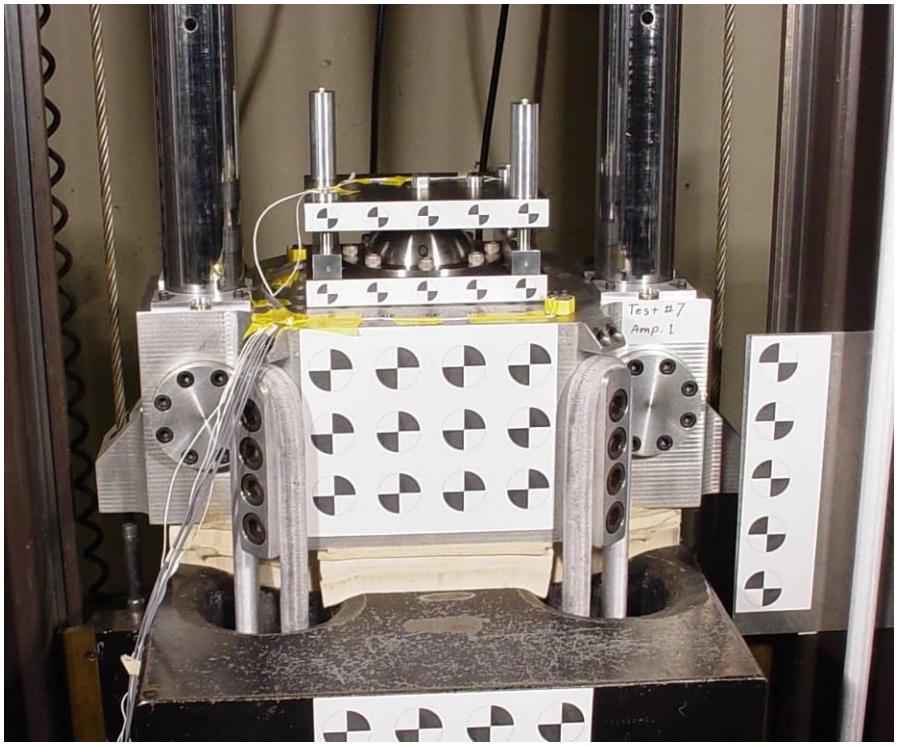

Figure 2-28. Photograph of Ampoule Test Assembly Prior to Testing

2.12.3.1.1 Brass Actuator Test Finite Element Model

The brass actuator test, finite element model provides additional validation of the PRONTO3D finite element code. The finite element model of the brass-tipped impactor and test fixture, shown in Figure 2-29(a) is a three-dimensional model composed of hexahedral elements. There is a plane of symmetry through the center of the model (Z=0), which contains 395,000 elements. The constitutive model of the brass material is given in Section 2.12.4.

The deformed mesh for an impact velocity of 175 ft/sec is shown in Figure 2-29(b). The maximum plastic strain in the ampoule is shown in Figure 2-30. A maximum value of 1% is calculated directly under the point of impact. The change in thickness of the ampoule at the point of impact is 0.00035 in. This is very close to the 0.0002-0.0005 in. measured in the impact tests.[1]

Figure 2-31(a) and (b) present a close-up view of the impactor mesh and the final deformed shape, along with the equivalent plastic strain in the impactor tip. As shown in the figure, very large strains of over 80% are produced in the center of the brass tip. Figure 2-32 shows the deformed tip overlaid on the deformed experimental specimen. The two deformed shapes match extremely well. Finally, a comparison of the acceleration measured in the experiment with the acceleration determined from the analysis is presented in Figure 2-33. The acceleration data from the analysis is determined by taking the nodal velocity of a node in the brass tip, differentiating it, and then filtering it, at the same frequency as the original acceleration data from the impact test. As shown in the figure, the two sets of data match very well.

(a)

(b)

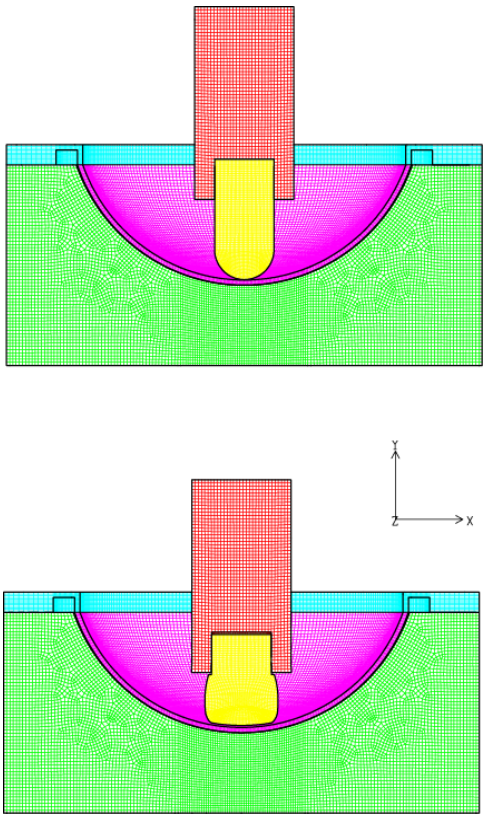

Figure 2-29. Finite Element Model for the Brass Impact Test

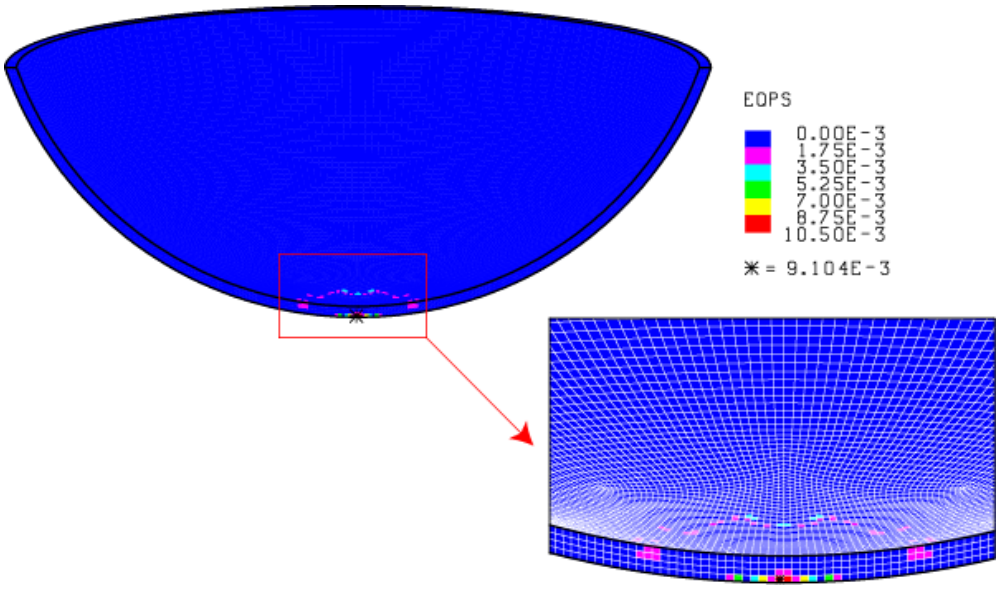

Figure 2-30. Equivalent Plastic Strain in the Ampoule Dish at an Impact Velocity of 175 ft/sec

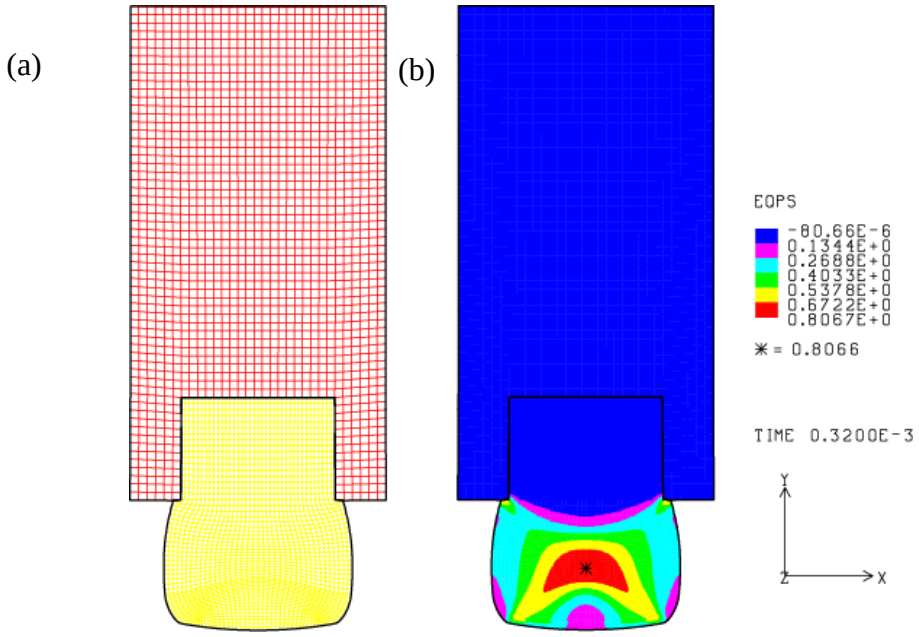

Figure 2-31. Deformed Shape of and Plastic Strain in the Brass-Tipped Impactor at an Impact Velocity of 175 ft/sec

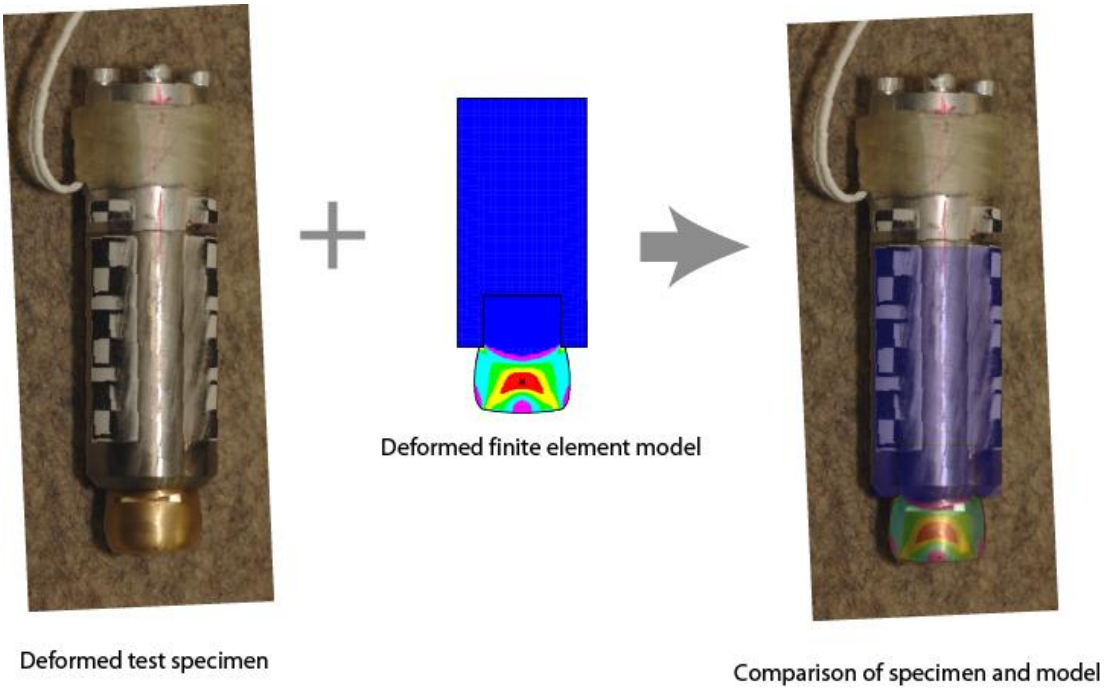

Figure 2-32. Deformed Shape of the Brass Impactor Overlaid on the Test Specimen

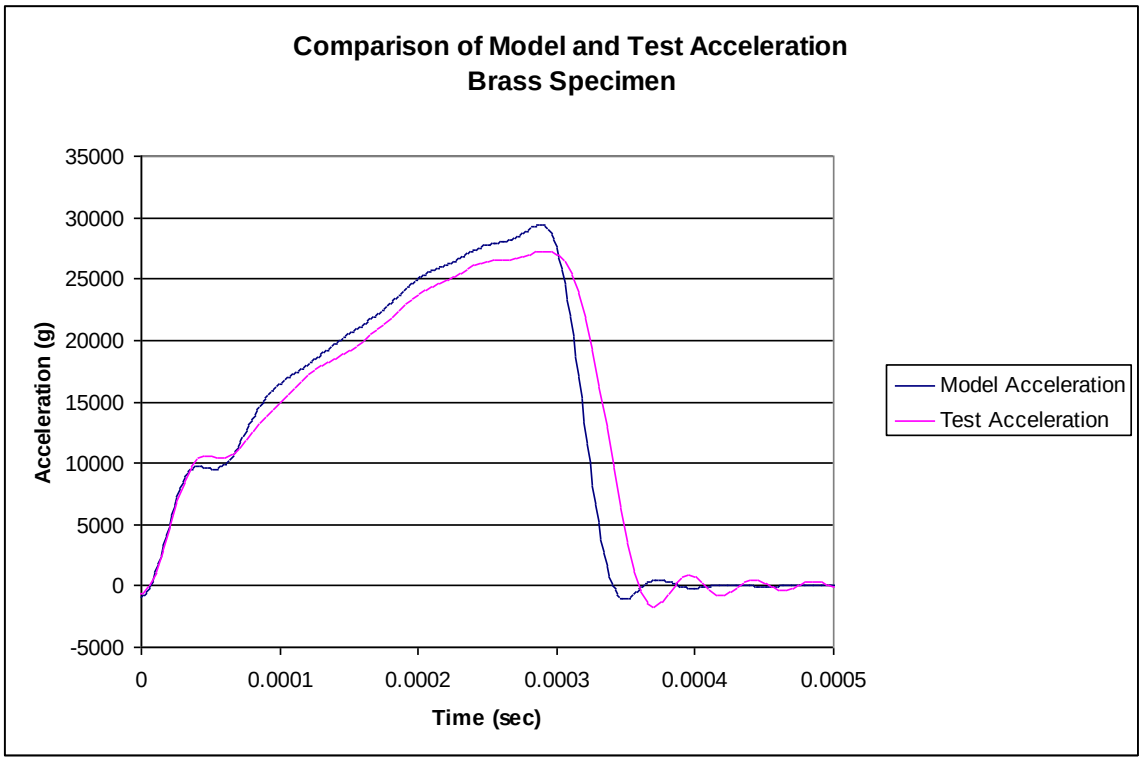

Figure 2-33. Comparison of the Brass-Tipped Impactor Acceleration from the Test and the Finite Element Model

2.12.3.1.2 Titanium Actuator Test Model

The purpose of the titanium-tipped impact model is to provide data for the strain locus used in the strain-based acceptability criterion. This data is obtained from both the T-Ampoule specimen and the tip of the impactor. The finite element model for the actuator titanium test is the same as those used in the brass, except for the constitutive model of the tip material. The constitutive model for the titanium tip is given in Section 2.12.4.

The deformed mesh of the titanium-tipped impactor for an impact velocity of 200 ft/sec is given in Figure 2-34. The maximum equivalent plastic strain and deformation in the ampoule specimen is presented in Figure 2-35. The maximum deformation of the ampoule under the tip of the impactor is 0.010 in., which is in good agreement with the 0.006 – 0.009 in. of deformation measured in the test specimens.[1] The maximum calculated plastic strain in the titanium cup is 17%. Figure 2-36 presents a close-up view of the deformed impactor along with the equivalent plastic strain in the impactor tip. As shown in the figure, very large strains of greater than 50% are produced in the center of the titanium tip. Figure 2-37 shows the deformed shape of the titanium impactor overlaid on the deformed experimental specimen. There is very good agreement between the experiment and the analysis.

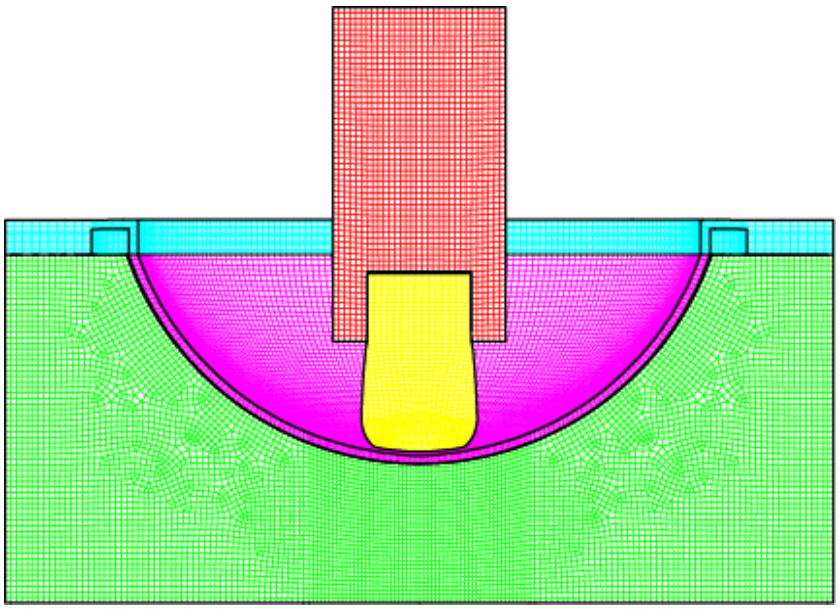

Figure 2-34. Deformed Mesh of the Titanium Tipped Impactor, at an Impact Velocity of 200 ft/sec

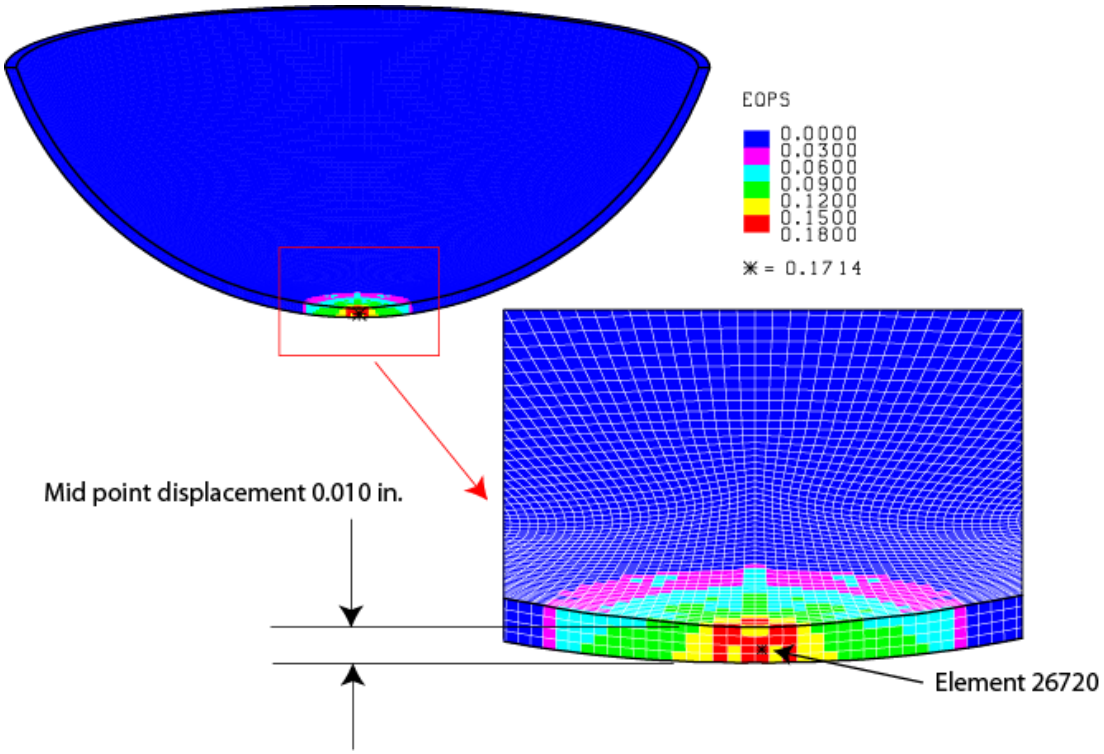

Figure 2-35. Equivalent Plastic Strain in the Ampoule Dish at an Impact Velocity of 200 ft/sec with a Titanium Tipped Impactor

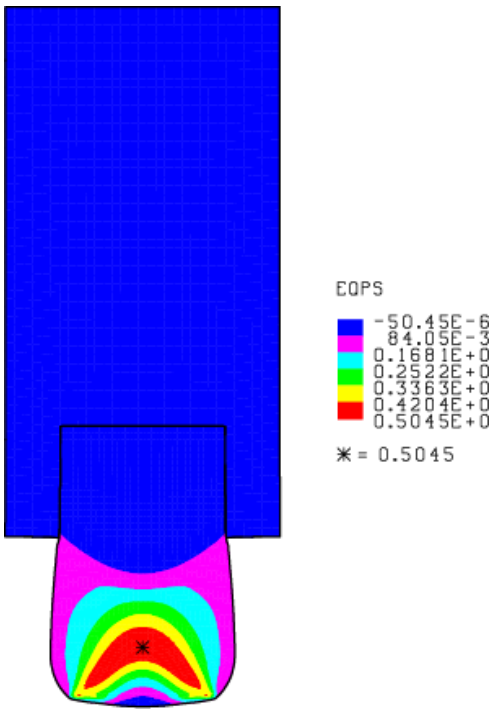

Figure 2-36. Deformed Finite Element Mesh of Titanium Impactor with Contours of Equivalent Plastic Strain

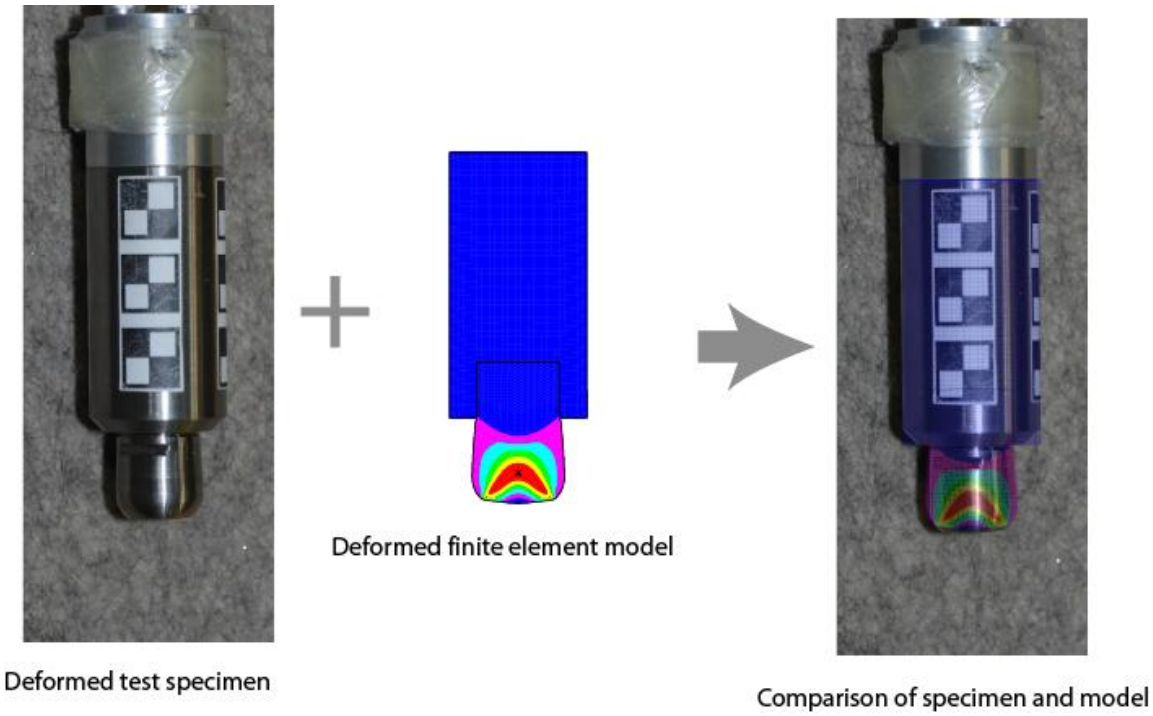

Figure 2-37. Deformed Shape of the Titanium Impactor Overlaid on the Test Specimen

2.12.3.1.3 Drop Table Test Finite Element Model

The purpose of the titanium ampoule drop table test is to provide additional data for the strain locus used in the strain-based failure criterion. This data is obtained as the result of the strain induced by buckling of the T-Ampoule specimen. The finite element model for the drop table test is shown in Figure 2-38. This is a three-dimensional model composed of hexahedral elements. There is a plane of symmetry through the center of the model (Z=0), and the model contains 297,000 elements. The constitutive model of the titanium material is given in Section 2.12.4. The crush plate and the adaptor plate are modeled as an elastic carbon steel material.

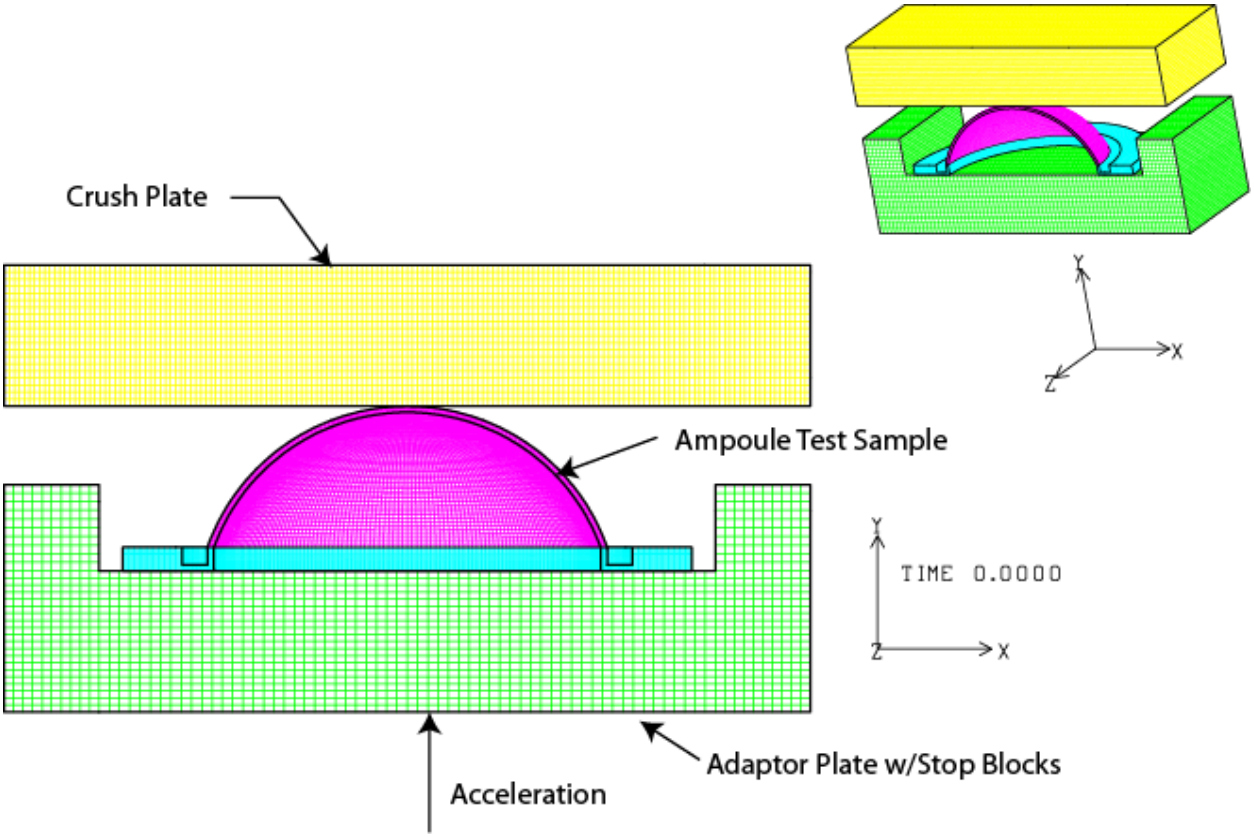

Figure 2-38. Finite Element Model of the Drop Table Ampoule Test

Figure 2-39 documents the drop table carriage acceleration recorded during the pretest calibration of the drop table. This acceleration was applied to the adaptor plate in the finite element model. The resulting deformation from the analysis is presented in Figure 2-40. The crush plate compresses the ampoule test specimen and contacts the stop blocks. There is a small quantity of elastic deflection of the crush plate, which increases the total crush of the ampoules. Post-test photographs of the ampoule test specimen are shown in Figure 2-41.

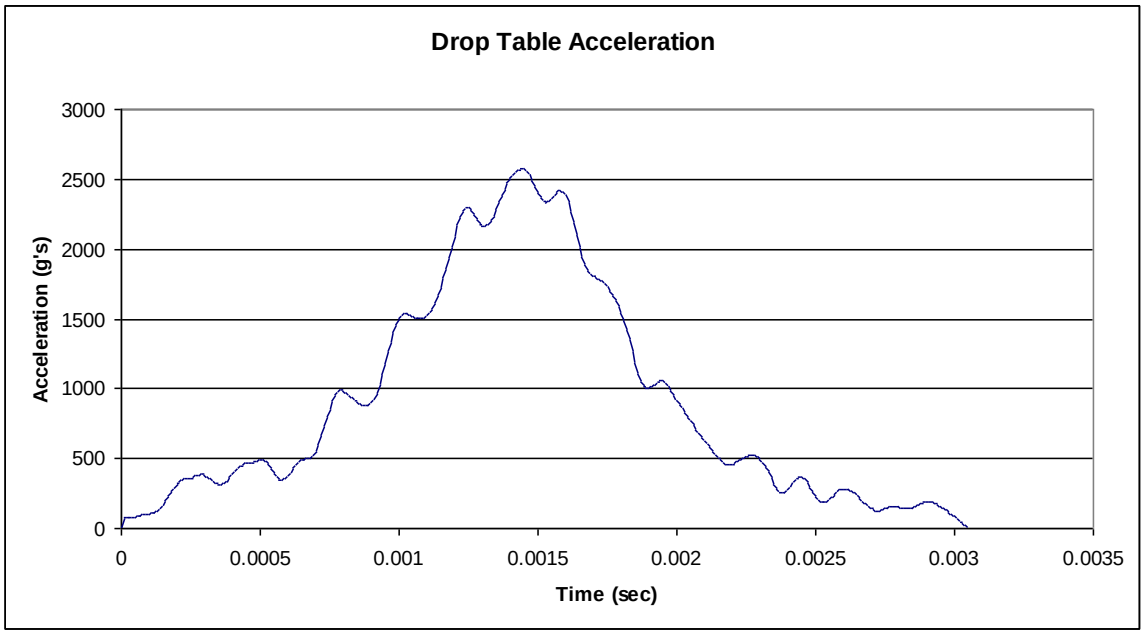

Figure 2-39. Drop Table Acceleration

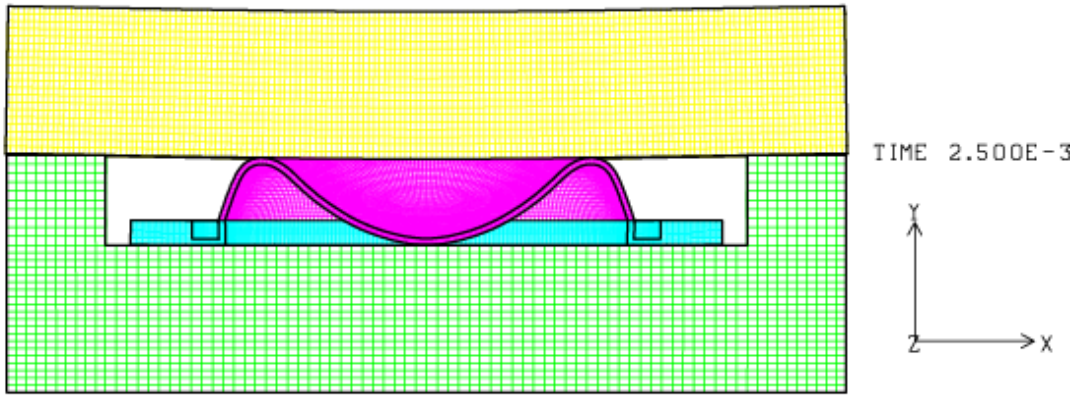

Figure 2-40. Finite Element Results Showing the Deformed Shape of the Ampoule Test Specimen

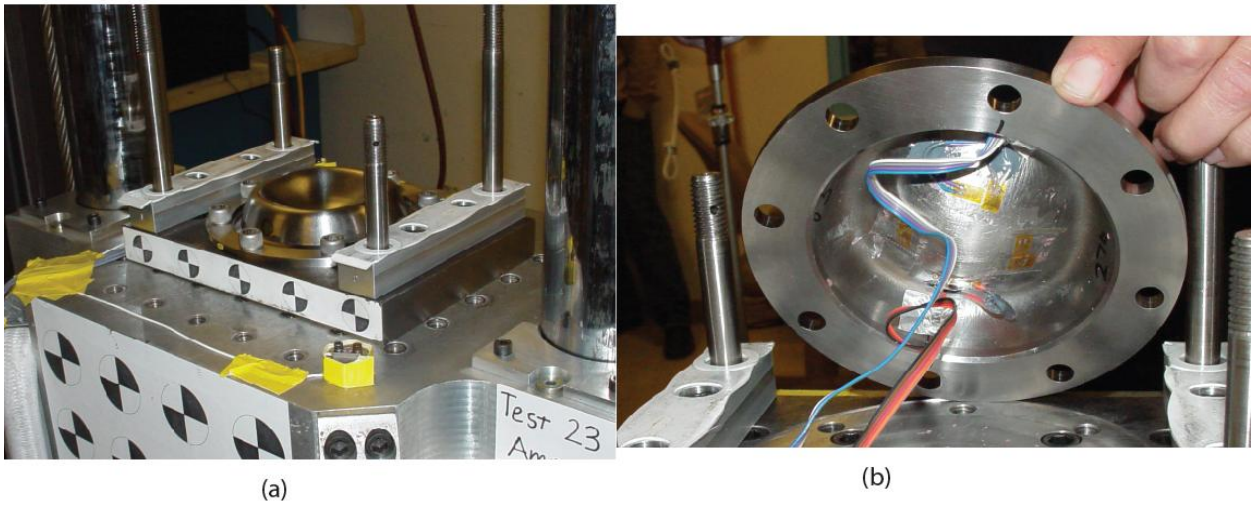

Figure 2-41. Photographs of the Deformed Ampoule Specimen (a) Top View (b) Inner Surface

The maximum calculated equivalent plastic strain is shown in Figure 2-42. A maximum value of 19.4% is found on the inside surface of the ampoule test specimen. Strain gauges were placed on the inside of the ampoule test specimen at a radius of 0.8 in. Figure 2-43 shows the nominal radial strain in an element at this location along with the data from the strain gauges. Due to the reversal in strain along the inside surface of the ampoule, the strain gauges detached halfway through the test. However, comparison of the nominal radial strain in the element to the strain measured by the gauges prior to failure shows good agreement.

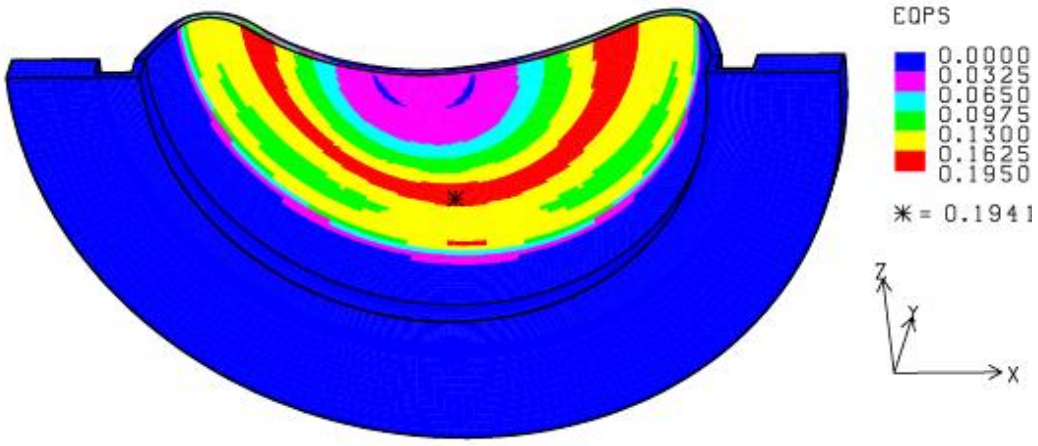

Figure 2-42. Maximum Equivalent Plastic Strain in Sample Test Specimen

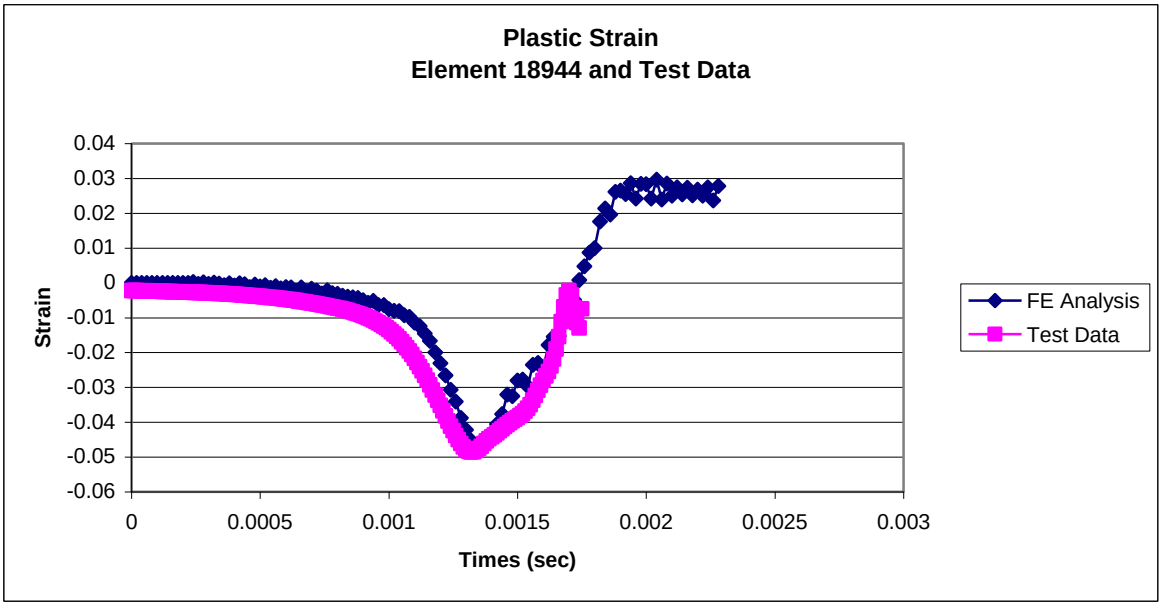

Figure 2-43. Nominal Element Radial Strain Compared to Strain Gage Data

Figure 2-44 shows the deceleration of the crush plate during the test and the deceleration calculated in the analysis. The impact of the crush plate with the stop blocks produced resonance in the accelerometers, which corrupted the data beyond this point. However, the two curves show good agreement during the crushing of the test ampoule specimen.

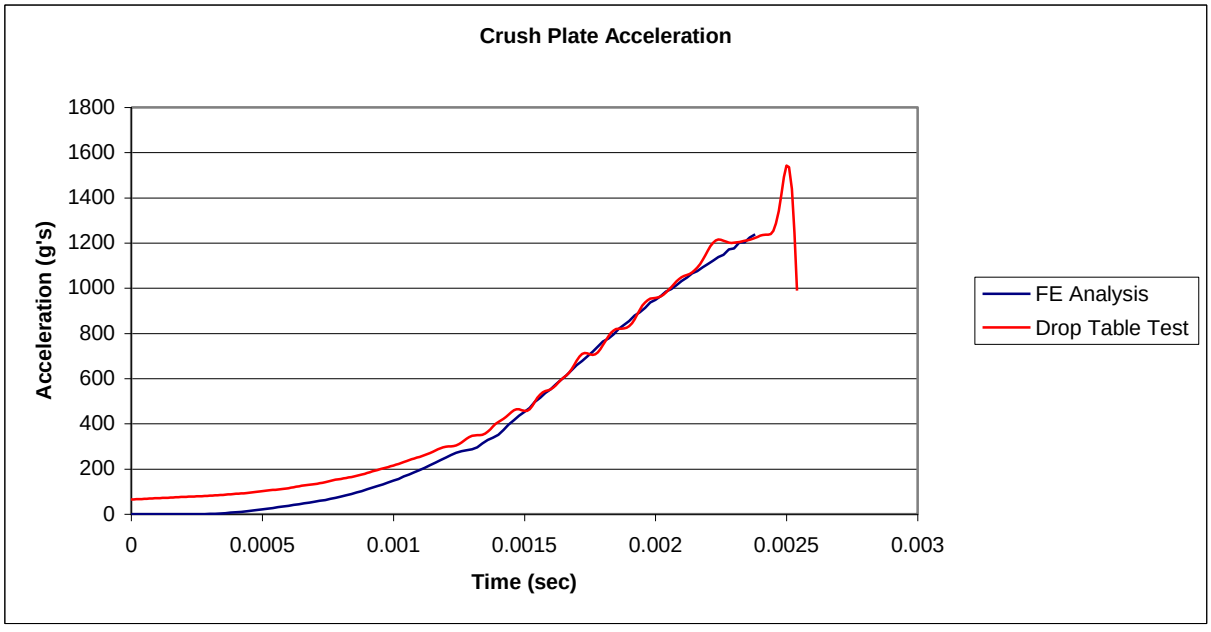

Figure 2-44. Crush Plate Acceleration

2.12.3.2 Stress-Informed Strain-Based Failure

2.12.3.2.1 Discussion

Bridgman performed the seminal work on the effect of hydrostatic pressure on ductile rupture in the 1940s and 1950s.[3] He conducted over 350 tensile tests, on 20 different types of steel, of different heat treatments. These experiments showed that the strain to fracture is an increasing function of the superposed hydrostatic pressure. Brozzo, et al., simulated failure for the sheet metal forming industry and also noted that ductility diminishes with the hydrostatic stress.[4] Their experience with simulating testing to failure led to the following failure index:

$$I = \int_0^{\bar{\varepsilon}_{pf}} \frac{2\sigma_1}{3(\sigma_1 - \sigma_m)} d\bar{\varepsilon}_p \qquad (2\text{-}6)$$

where σ_1 is the maximum principal stress, σ_m is the average of the three principal or normal stresses, $\bar{\varepsilon}_p$ is the equivalent plastic strain, and $\bar{\varepsilon}_{pf}$ is the equivalent plastic strain at failure.

This work was further developed by Johnson and Cook,[5] who developed fracture models for OFHC copper, Armco iron, and 4340 steel using notched tensile specimens. Their model contained three primary terms: one with a dimensionless strain rate; one for dimensionless temperature; and one with a dimensionless pressure-stress ratio $\sigma^* = \frac{\sigma_m}{\bar{\sigma}}$, where σ_m is the average of the three normal stresses and $\bar{\sigma}$ is the von Mises equivalent stress. The pressure-stress ratio is commonly referred to as the stress triaxiality. In their work, Johnson and Cook[5] noted:

> "It would appear that the pressure-stress ratio is of primary importance. As the hydrostatic tension is increased, the strain to fracture decreases rapidly. The strain rate and temperature effect appear to be less important."

Figure 2-45 shows a plot of the data developed by Johnson and Cook and the corresponding curves developed in their failure models.

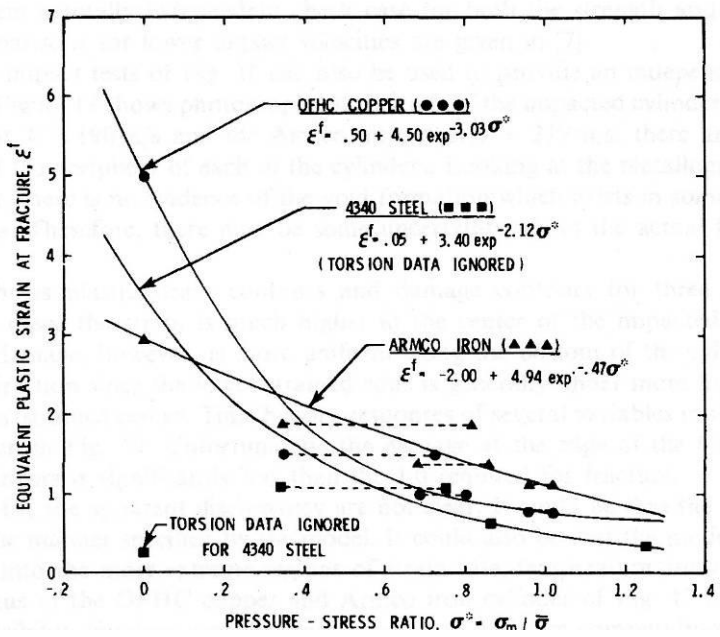

Figure 2-45. Plastic Strain versus Stress Triaxiality from Johnson and Cook[5]

A fairly recent (2007) journal article[19] reviewed numerous ductile fracture prediction models, including those of Brozzo, et al. and Johnson & Cook, mentioned above. This review stated that it is generally accepted that ductile damage criteria should take into account the following:

- The deformation path, because the current stress/strain state is not enough to characterize the damage state.
- The hydrostatic or mean stress, σ_m, because ductility grows rapidly as σ_m decreases.
- An adequate ratio of stresses, namely the triaxiality stress ratio, σ_m / σ_{eq}, in which σ_{eq} is the equivalent or Mises stress, so that the general state of plasticity and fracture may be better described.

Recently, Bao[7] developed a new criterion for ductile crack formation. This work is based on extensive testing of 2024-T351 aluminum. He developed the failure locus in stress triaxiality–equivalent plastic strain space shown in Figure 2-46, based on calculating the average stress triaxiality as:

$$\left(\frac{\sigma_m}{\bar{\sigma}}\right)_{av} = \frac{1}{\varepsilon_f}\int_0^{\bar{\varepsilon}_f} \frac{\sigma_m(\bar{\varepsilon})}{\bar{\sigma}(\bar{\varepsilon})} d\varepsilon \qquad (2\text{-}7)$$

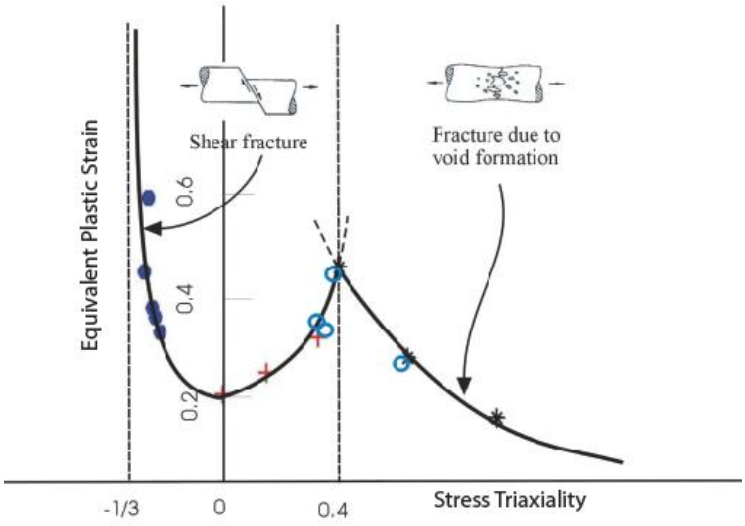

Figure 2-46. Stress Failure Locus of Al2024-T351 Developed from Bao[7]

In addition, using this formulation along with the data from Bridgman,[3] Bao and Wierzbicki[8] were able to show the existence of a limit in the negative average stress triaxiality space of -1/3, below which failure of the specimens never occurred. This limit is shown in Figure 2-46, as well as in Figure 2-47, which Bao and Wierzbicki showed to be true for numerous tested ductile metals. This figure also shows the different failure modes common to shear versus biaxial tension regions of stress triaxiality.

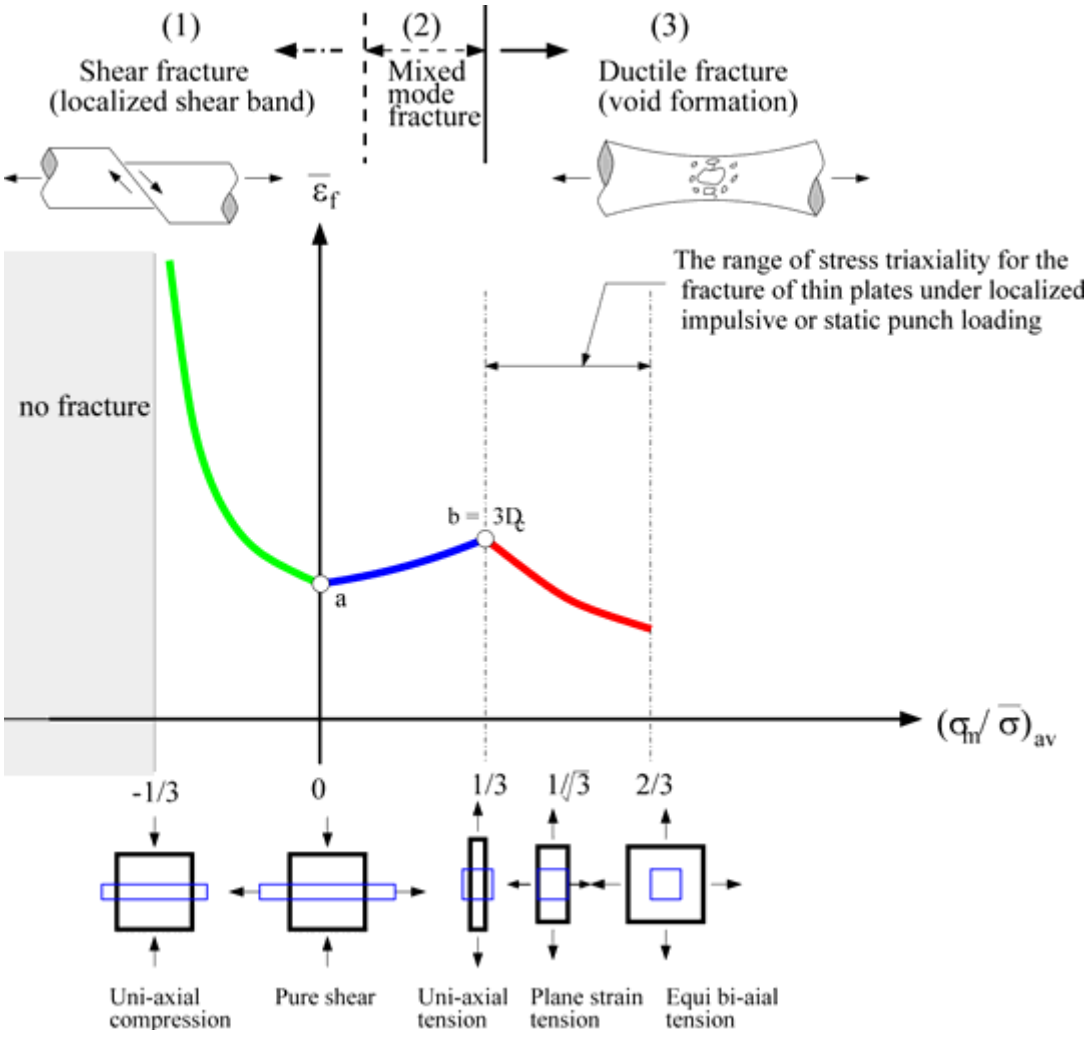

Figure 2-47. General Failure Locus of Ductile Metals Developed by Bao and Wierzbicki.[8]

2.12.3.3 Strain Locus for Titanium

Using Equation 2-7 and data from the titanium impact tests, a strain locus in stress triaxiality–equivalent plastic strain space is developed for titanium. This strain locus is used along with the finite element analyses of the PAT-1 components (see Section 2.12.5) to determine a margin on fracture, based on equivalent plastic strain, for the T-Ampoule.

Figure 2-48 shows a close-up view of the equivalent plastic strain in the titanium tip from the actuator tests for an impact velocity of 200 ft/sec, and Figure 2-49 presents the equivalent plastic strain in the ampoule from the drop table test. The strains in the tip of the impactor reach a

maximum value of 50% at the center of the specimen, with smaller strains developing along the side. A maximum strain of over 19% is reached in the ampoule during the drop table test. Using the stress and equivalent plastic strain data from the finite element models along with Equation 2-7, the strain locus shown in Figure 2-50 was developed for the elements indicated in Figure 2-48 and Figure 2-49, as well as all the other elements in these models. The friction coefficients between the Ti-6Al-4V impactor and the Ti-6Al-4V simulated T-Ampoule were 0.30 for static friction and 0.36 for dynamic friction.[6] The figure also contains a curve from a finite element model of the tension test, as well as the limit line developed by Bao and Wierzbicki.[8] It should be noted that this is not a failure locus, since no cracks were formed in the tests. However, it does represent regions in strain space where failure does not occur; therefore, the part is safe. In this sense, the data from the PAT-1 package impact analyses (see Section 2.12.5) can be compared with the locus in Figure 2-50, and a safety margin based on the strain generated in the test can be calculated.

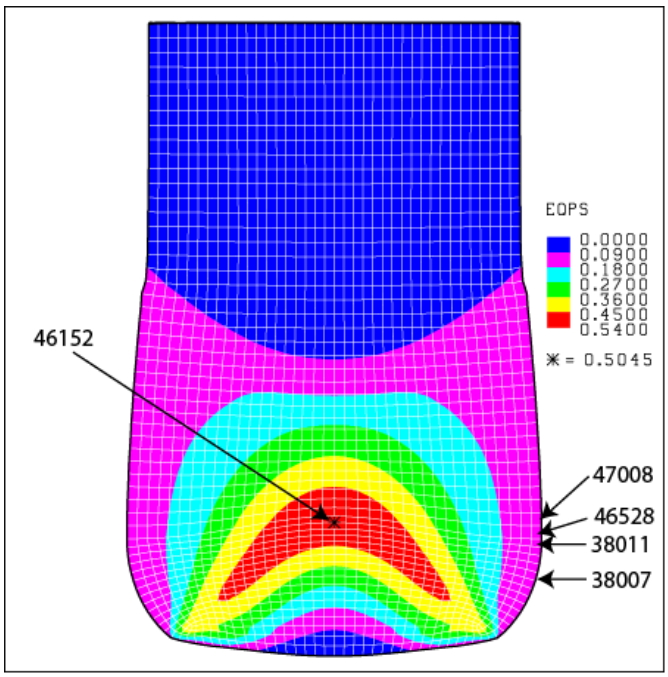

Figure 2-48. Equivalent Plastic Strain in the Titanium Tip for an Impact Velocity of 200 ft/sec

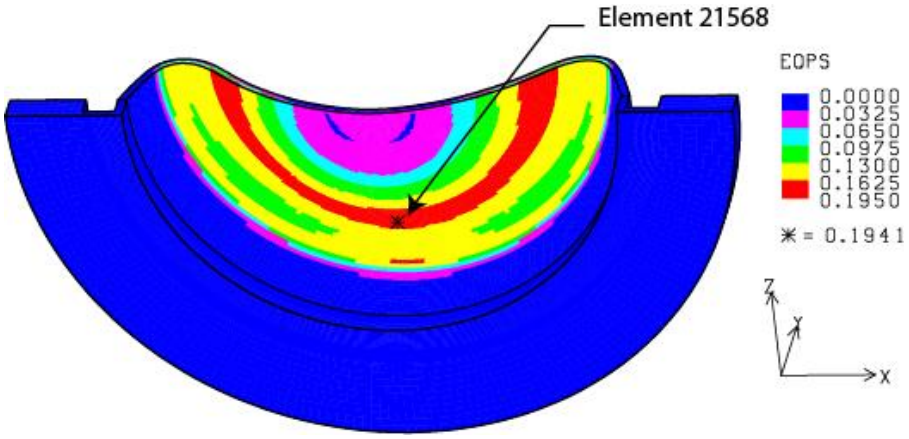

Figure 2-49. Equivalent Plastic Strain in the Titanium Ampoule in the Drop Table Test

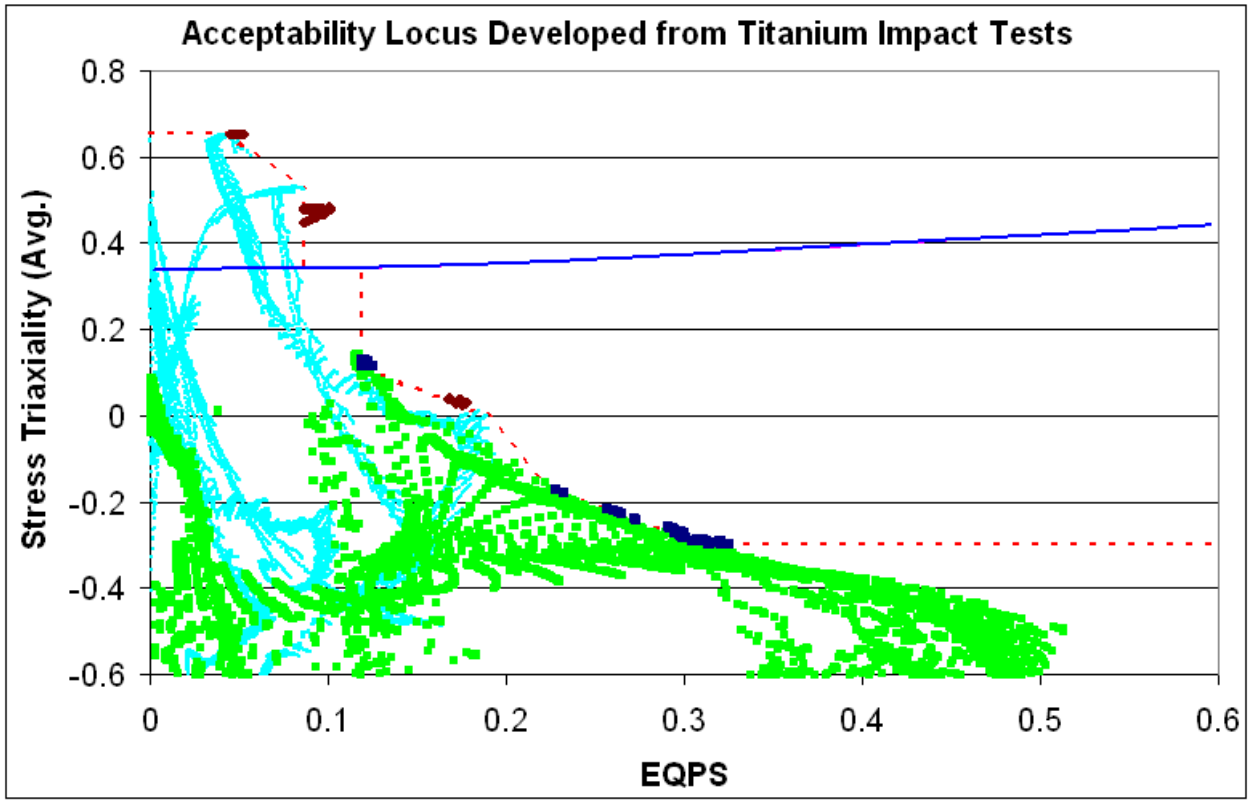

Figure 2-50. Locus in Equivalent Plastic Strain–Stress Triaxiality Space Developed from Titanium Impact Tests

2.12.3.4 Bounding Examples

To illustrate the construction of the locus in Figure 2-50, the development of the two bounding curves (maximum tension and maximum compression) will be presented in the following section. The maximum compression curve is derived using data for Element 46152 and data generated in the titanium impact test. The tension test curve is derived from a separate tension

test and a finite element model of the test, which was originally conducted to gather material data for the constitutive model.

2.12.3.5 Curves for Element 46152

The development of the average stress triaxiality function for the strain locus was done as a post-processing operation. First, the stress triaxiality, as defined in Equation 2-8, is calculated as a function of time using the element integration point stress

$$\frac{\sigma_m}{\bar{\sigma}} \tag{2-8}$$

Where σ_m is the average of the three normal stresses and $\bar{\sigma}$ is the von Mises equivalent stress. A plot of this function for Element 46152 is shown in Figure 2-51, along with the equivalent plastic strain. Next, the stress triaxiality is plotted as a function of equivalent plastic strain as shown in Figure 2-51. Then, using Equation 2-9, the average value of the stress triaxiality function over the interval of plastic strain is determined. The average stress triaxiality for Element 46152 as a function of plastic strain is also plotted in Figure 2-52.

$$\frac{1}{b-a}\int_a^b f(x)\,dx \quad \text{on the interval} \quad a \le x \le b \tag{2-9}$$

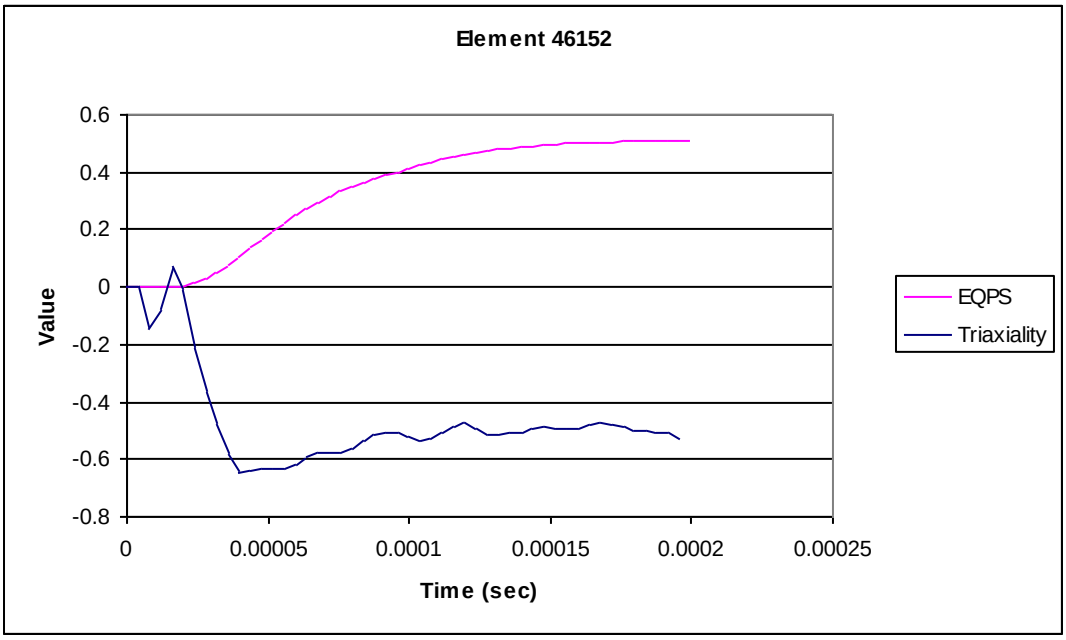

Figure 2-51. Stress Triaxiality and Equivalent Plastic Strain versus Time for Element 46152

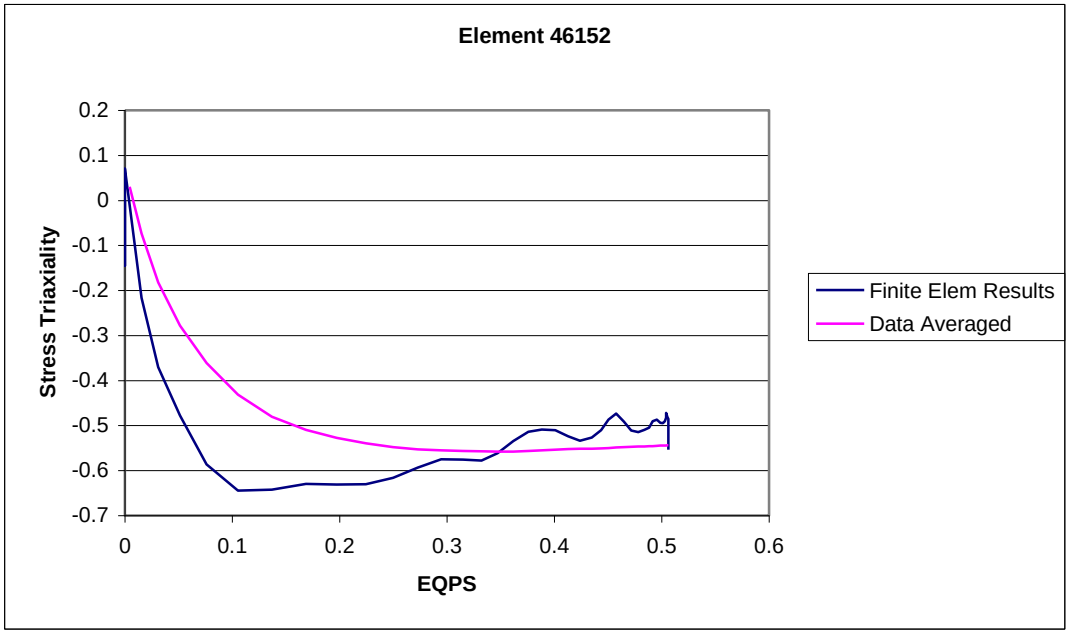

Figure 2-52. Stress Triaxiality and Average Stress Triaxiality as a Function of Equivalent Plastic Strain for Element 46152

2.12.3.6 Titanium Tension Test

A finite element analysis was conducted of the titanium test specimen. This tensile test was performed to failure while recording stresses and strains, including reduction in area. An analysis of this test was performed using the SNL-developed finite element code JAS3D. JAS3D is a nonlinear quasi-static code that uses a conjugate gradient solver to solve the equation of equilibrium. The finite element model is shown in Figure 2-53(a). The model is an axi-symmetric, quarter-symmetry model with two planes of symmetry. The model is loaded by displacing the upper end at a constant rate. The mesh contains 1804 elements and is refined heavily along the center symmetry plane.

Figure 2-53(b) shows the deformed mesh at a point where the cross-sectional area at the centerline matched the reduction in area at failure during the tensile test. The power-law hardening parameters of the Ti-6Al-4V material constitutive model were chosen so that the analytical behavior of the specimen matched the actual tensile test specimen. Figure 2-53(c) gives the distribution of plastic strain for this same configuration. The maximum plastic strain occurs in the center of the specimen and has a magnitude of 63%.

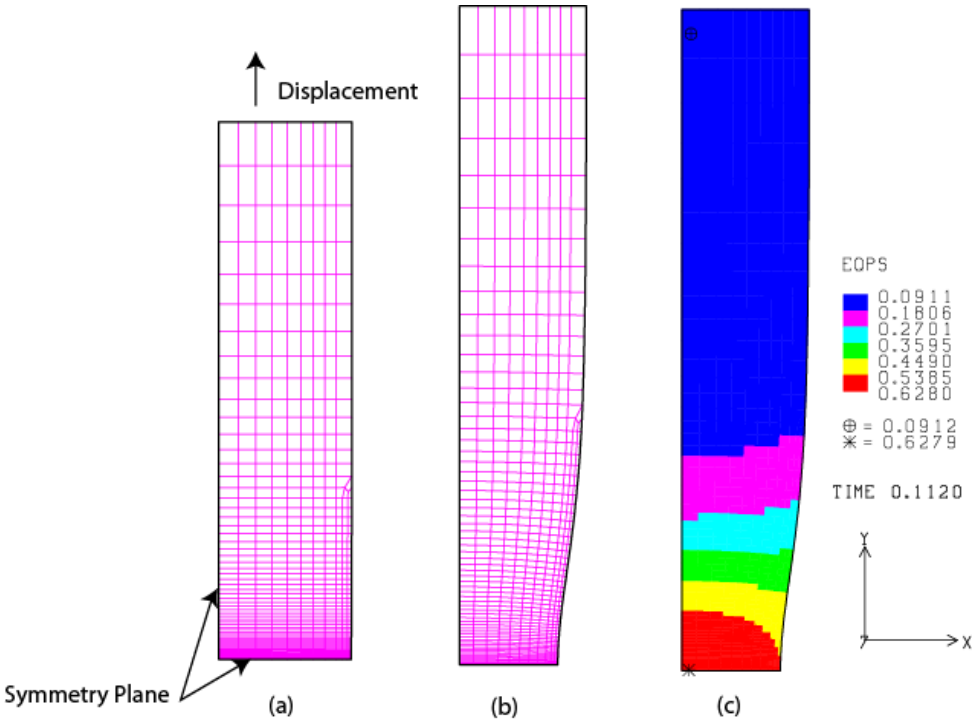

Figure 2-53. Finite Element Model of Titanium Tensile Test Specimen (a) Original Mesh (b) Deformed Mesh (c) Equivalent Plastic Strain

The plastic strain in the highest stressed element as a function of the specimen displacement is shown in Figure 2-54 along with the stress triaxiality. A plot of the stress triaxiality versus plastic strain for this element is presented in Figure 2-55, along with the averaged stress triaxiality.

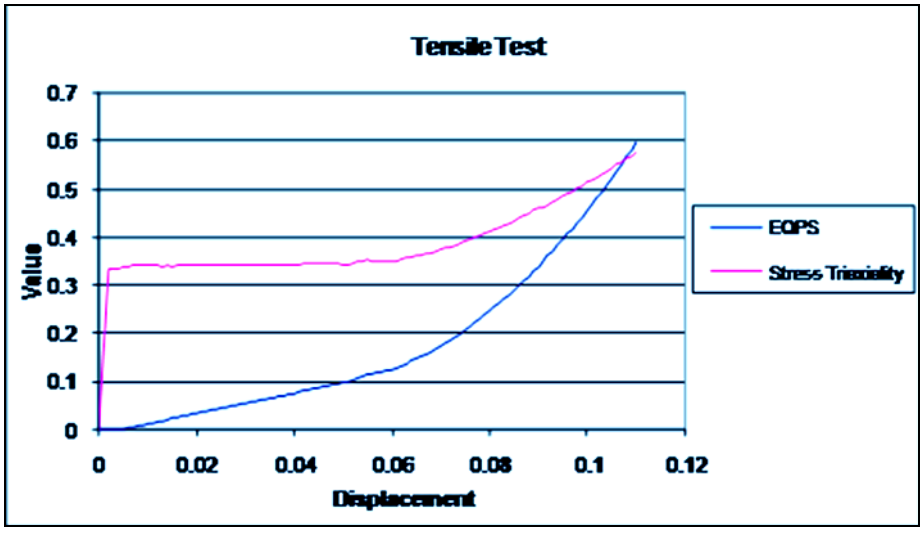

Figure 2-54. Stress Triaxiality and Equivalent Plastic Strain versus Displacement for Center Element

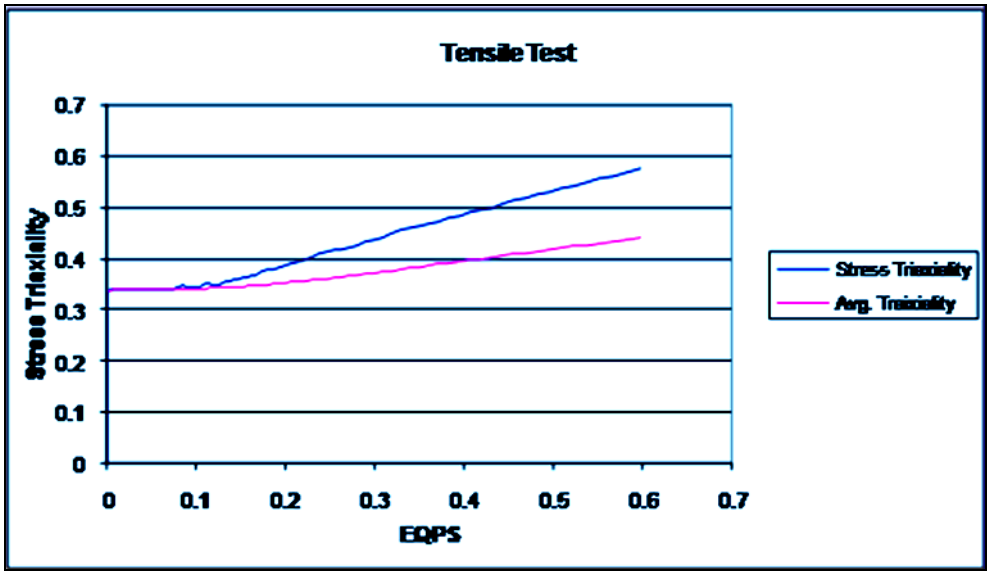

Figure 2-55. Stress Triaxiality and Average Stress Triaxiality as a Function of Plastic Strain for the Highest Stressed Element

2.12.3.7 Strain Rate Dependencies

Some materials have high strain rate dependencies, but Ti-6Al-4V was chosen for the T-Ampoule eutectic barrier material due to not only its high strength, light weight, good ductility, and excellent corrosion resistance, but also because of its low strain rate sensitivity. For example, the material is commonly used in the aerospace industry for jet engine fan blades, in part because of its resistance to failure during bird strikes. At lower strain rates (0 to 1 inverse seconds), the yield and ultimate stresses harden slightly, but ductility is unaffected.[20] Los Alamos National Laboratories compiled historical data on higher strain rate testing of Ti-6Al-4V[21] and it shows only relatively modest increases in strength and slight decreases in ductility up to 1340 /sec strain rates.

Although Sandia did test lower strain rate deformations of the T-Ampoule material (using softer impactor materials such as brass), SNL believed it was more important to use strain rates similar to the regulatory high-speed impact tests. The net impact velocity between solid contents and the T-Ampoule (and indirectly TB-1 wall) during regulatory high-speed impacts was less than the regulatory impact velocity since the wall is still slowing down when contents/T-Ampoule contact occurs. Analyses of the 200 ft/sec horizontal actuator tests of a Ti-6Al-4V slug impacting a hemispherical T-Ampoule and TB-1 combination show peak strain rates at individual elements of -1.18E5 to +1.19E5 1/sec in the T-Ampoule and -4.11E4 to +5.40E4 1/sec in the Ti slug (as shown in Table 2-13a below, which also lists the peak strain rate in any element within individual "high speed" or "HSRun" analyses). Since Ti-6Al-4V has a high yield strength of about 141 ksi, these are quite high strain rates (titanium impactor plug on thin titanium T-Ampoule, backed by 140 ksi PH13-8Mo SS TB-1, which was held rigidly). It is important to note that these horizontal actuator tests were used to generate a locus of stress triaxiality versus equivalent plastic strain that did not induce any ductile tearing (no failure).

Table 2-13a. Peak Strain Rates from Analyses of Component Tests and High Speed Impact Tests

Run	Max Strain Rate	Min Strain Rate
Impact Test (dish)	1.19E+05	-1.18E+05
Impact Test (plug)	5.40E+04	-4.11E+04
Drop Table	1.78E+03	-2.73E+03
HSRun2	7.42E+04	-6.30E+04
HSRun3	1.71E+04	-2.99E+04
HSRun4	4.72E+04	-9.04E+04
HSRun5	1.21E+04	-1.70E+04
HSRun7	5.92E+04	-8.07E+04
HSRun8	2.20E+04	-2.47E+04
HSRun9	4.26E+04	-9.18E+04
HSRun10	4.14E+04	-5.15E+04
HSRun12	3.66E+04	-2.05E+04
HSRun13	4.98E+04	-4.06E+04
HSRun17	3.92E+04	-3.63E+04
HSRun18	8.94E+04	-1.08E+05
HSRun22	3.15E+04	-2.75E+04
HSRun23	1.84E+04	-2.14E+04
HSRun26	9.75E+04	-7.59E+04
HSRun27	4.06E+04	-5.30E+04

Although the 422 ft/sec impact analyses with various contents (ER cylinders, SC-1s and SC-2s) had a higher overall initial velocity, the relative velocities between the Pu contents and the T-Ampoule were in the 186-405 ft/sec range due to overpack crush still occurring upon contents impact with the T-Ampoule. Higher relative impact velocities are typically associated with smaller contents located initially farther away from the T-Ampoule wall. More importantly than these relative impact velocities, though, is the peak strain rates in the T-Ampoule, which were always lower than any peaks during the horizontal actuator tests, and ranged from -9.18E4 to +9.75E4 1/sec. This slightly lower strain rate is due largely to the lower yield strengths of the Pu (36 ksi for alpha and 9.2 ksi for delta) impacting the T-Ampoule in the regulatory high-speed impact analyses versus the "harder" Ti-on-Ti with rigid backing for the actuator tests.

Thus, any small strain rate sensitivity of the Ti-6Al-4V T-Ampoule (which is not a containment boundary; only a eutectic barrier) material would have been observed in the horizontal actuator tests. No failure occurred in these component tests at even higher strain rates (and virtually identical stress-tri/EQPS states), thus none would be anticipated due to small rate sensitivities during regulatory high-speed impacts.

2.12.3.8 Alternate Failure Criteria Used to Model Failure in Sample Containers and T-Ampoule

Prior to the work of Bao and Wierzbicki,[8,9] Wellman et al.[10] and Dawson et al.[11] developed a failure criterion, which also uses an evolution equation based on the plastic strain. This model has been implemented in the PRONTO3D finite code under the material model Ductile Tearing. This is a power-law-hardening model with a ductile failure criterion. The ductile failure criterion is based on an evolution equation in which the plastic strain increment, scaled by the stress ratio, is accumulated until a critical value is reached, at which point the initiation of the ductile tearing is predicted. The evolution equation calculates the Tearing Parameter (TP) as follows:

$$TP = \int_0^{\bar{\varepsilon}_{pf}} \left\langle \frac{2\sigma_1}{3(\sigma_1 - \sigma_m)} \right\rangle^4 d\bar{\varepsilon}_p \qquad (2\text{-}10)$$

where $\bar{\varepsilon}_p$ is the plastic strain at failure in a tensile test, σ_1 is the maximum principal stress, and σ_m is the mean (hydrostatic) stress. Note that Tearing Parameter is identical to the failure indicator Brozzo, et al. developed in the 1970's, with the exception of the 4th power and the Heaviside brackets. This was added in the late 1990's at Sandia National Laboratories to not only fit uniaxial tensile test data, but also notched tensile specimens with higher stress triaxiality.[11]

The integral accumulates plastic strain only when the maximum principal stress is positive, as indicated by the Heavyside function brackets, $\langle\ \rangle$. Thus, plastic strain with a negative maximum principal stress causes no change in the values of TP. Due to restriction of the Heavyside function, regions of positive stress triaxiality cause the integral to accumulate value quickly (the denominator becomes small), which fits well with experimental data showing low plastic strains to failure in bi- and tri-axial tension for ductile materials. In addition, it is easy to implement, since the critical value of TP for a particular material is established by performing an analysis of a tensile test specimen. The TP for the specimen is then calculated using the computed stress

state from the finite element model and substituting the plastic strain-to-failure, $\bar{\varepsilon}_f$, as the upper integration limit. This provides a critical value of TP, which can be used to predict failure in other analyses. The strain-to-failure is computed from the reduction in area of the tensile specimen in the actual tensile test. This ductile Tearing Parameter has been used successfully at Sandia National Laboratories for many years to simulate ductile failure.[11,12,13,14,15,16,17,18]

In the component analyses presented in Section 2.12.5, large plastic strains are developed in the outer shell of the sample containers. To prevent the sample containers from absorbing unrealistic quantities of energy through unrealistic quantities of plastic deformation, a failure criterion was needed to allow the shell to rupture during theses analyses. Since the Ductile Tearing model has already been incorporated in PRONTO3D, and since it performs well in the high stress triaxiality region, it was used in the element death criteria of the sample container models to allow the shells of the sample containers to fracture.

To determine the required failure parameter needed for the Ductile Tearing model, the same tensile test finite element model discussed above was used. Determination of the Critical Tearing Parameter requires performing a tensile test to failure, then modeling it using a constitutive model to match the test data, and iteratively arriving at a Critical Tearing Parameter value which matches the initiation of failure in the tested tensile specimen. The output data was post-processed using Equation 2-10 (and the constitutive model in Figure 2-59, Section 2.12.4.14), and the results of this analysis are presented in Figure 2-56. A value of 1.012 was used in the material model to initiate failure of the sample container shells and this same value is used for comparison with calculated Tearing Parameter values in the eutectic barrier T-Ampoule.

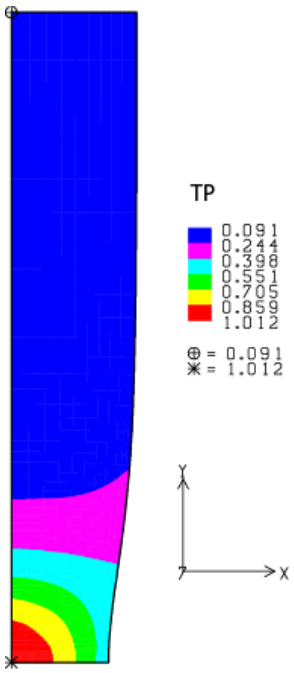

Figure 2-56. Tensile Test Results Showing Peak Value of Failure Parameter TP

2.12.3.9 References

1. Sandia National Laboratories. "Test Report PAT-1/TB-1 Impact Test Series." Albuquerque, NM. August 30, 2007.

2. VanGoethem, D. "PAT-1 Ampoule Drop Table Shock," MECH-678, Sandia National Laboratories. Albuquerque, NM. November 25, 2008.

3. Bridgman, P.W. "Studies in Large Plastic Flow and Fracture" Harvard University Press. Cambridge, MS. 1964.

4. Brozzo, P., Deluca, B., Redina, R.A. "A New Method for the Prediction of the Formability Limits of Metal Sheets," Proceedings of the 7th Biennial Conference of the International Deep Drawing Research Group. 1972.

5. Johnson, G.R., and Cook, W.H., "Fracture Characteristics of Three Metals Subjected to Various Strains, Strain Rates, Temperature and Pressures." *Engineering Fracture Mechanics* 21 (1985):31-48.

6. Sliding and Static Friction Coefficients for Various Materials: http://www.roymech.co.uk/Useful_Tables/Tribology/co_of_frict.htm

7. Bao, Y. "Prediction of Ductile Crack Formation in Uncracked Bodies," Report 100. Impact & Crash Worthiness Laboratory. Massachusetts Institute of Technology, Cambridge, MA. 2003.

8. Bao, Y., and Wierzbicki, T. "On the Cut-Off Value of Negative Triaxiality for Fracture." *Engineering Fracture Mechanics*, 72 (2005): 1049-1069.

9. Wierzbicki, T., Bao, Y., and Teng, X. "High Velocity Impact Fracture." Seminar Presented to Sandia National Laboratories. January 2004.

10. Wellman, G.W., Diegert, K.V., and Salzbrenner, R. "Two-Dimensional Quasistatic Modeling of Exclusion Region Barriers in Support of Design Guide Development." SAND93-0905. Sandia National Laboratories. Albuquerque, NM. 1993.

11. Dawson, D.B., Antoun, B.R., and Mosher, D.A. "MAVEN Progress Report for FY98 Second Half (Fracture of Weapons Materials)." Sandia National Laboratories Memo Report to Distribution. October 5, 1998.

12. Wellman, G.W, and Boyce, B.L. "Exclusion Region Barrier Crush Specimens Made from 304L Stainless Steel." Sandia National Laboratories Memo Report to R.D. Pedersen. August 26, 2004.

13. Wellman, G.W, and Boyce, B.L. "Materials Properties and Modeling Techniques used in the Analysis of Exclusion Region Barrier Test Specimens." Sandia National Laboratories Memo Report to R.D. Pedersen. December 13, 2005.

14. Wellman, G.W. 4th MIT Workshop on Fracture. November 1, 2007.

15. Metzinger, K. E. "Structural Analysis of a Frangible Nut Used on the NASA Space Shuttle." SAND93-1720. Sandia National Laboratories. Albuquerque, NM. 1993.

16. Gwinn, K.W. and Metzinger, K.E. "Analyses of Foam Impact Onto the Columbia Shuttle Wing Leading Edge Panels Using PRONTO3D/SPH." SAND2003-3853C. Sandia National Laboratories. Albuquerque, NM. 2003.

17. Hinnerichs, T. "Constitutive Model Report for the B61 Radar Nose Assembly Crush Model." Sandia National Laboratories Memo Report to Distribution. August 2, 2000.

18. Duong, H., Hinnerichs, T., Pott, J., Gwinn, K., Lo, D. "Independent Technical Review of Intermediate Angle Impact Analysis for B61 Common Radar Nose." September 11, 2001.

19. Zheng, C., Cesar de Sa, J. M. A., Andrade Pires, F. M., "A Comparison of Models for Ductile Fracture Prediction in Forging Processes," Computer Methods in Computer Science, Vol. 7, 2007, No. 4.

20. Department of Defense, Mechanical Properties Data Center, "Aerospace Structural Metals Handbook," Code 3707, Page 12, March 1965.

21. Strain Rate Sensitivity Data Used in LANL's Ti-6Al-4V MTS Strength Model, e-mail from George T. Gray (Los Alamos National Labs) to David C. Harding (Sandia National Laboratories), February 19, 2010.

2.12.4 Material Data

This section discusses the material data used in the finite element analyses. Material test data and references are provided along with the appropriate power-law hardening curves. Table 2-14 lists the model component, the material of the component, and the section in Section 2.12.4 containing the material data and constitutive model.

Table 2-14. Listing of Material for Each Components in the Finite Element Models

Model	Component	Material	Section
Full PAT-1Models			
	Redwood Impact Material	Redwood	2.1.1.1
	Load Spreader Cylinder	Aluminum 6061	2.12.4.3
	Load Spreader Top Plate	Aluminum 7075	2.12.4.5
	Load Spreader Lower Plate	Aluminum 7075	2.12.4.5
	Copper Cylinder	Copper	2.12.4.7
	TB-1 Container	Stainless PH13-8-Mo	2.12.4.9
	TB-1 Contents	Elastic Plastic Soft	2.12.4.11
	Can Shell and Flange	Stainless 304	2.12.4.12
	T-Ampoule	Titanium 6Al-4V	2.12.4.14
	Sample Container	Titanium 6Al-4V	2.12.4.14
	Sample Container Cylinder	Plutonium (delta)	2.12.4.18
	ER Cylinders	Plutonium (alpha)	2.12.4.16
	Be Composite Cylinder	Beryllium	2.12.4.24
Impact Test Model			
	Tungsten Ballast	Tungsten	2.12.4.20
	Impact Specimen Brass	Brass UNS 36000	2.12.4.22
	Impact Specimen Titanium	Titanium 6Al-4V	2.12.4.14
	Ampoule Specimen	Titanium 6Al-4V	2.12.4.14
	Hemisphere Fixture	Stainless PH13-8-Mo	2.12.4.9

2.12.4.1 Redwood

The redwood material is modeled using the Orthotropic Crush model in PRONTO-3D. The Orthotropic Crush model is an empirically based constitutive relation used to model material like metallic honeycomb and wood. The force deflection curve used to simulate the compression of the redwood material is presented in Figure 2-57 along with data from Joseph and Hill. These values along with the other modeling parameters for the Orthotropic Crush model are presented in Table 2-15.

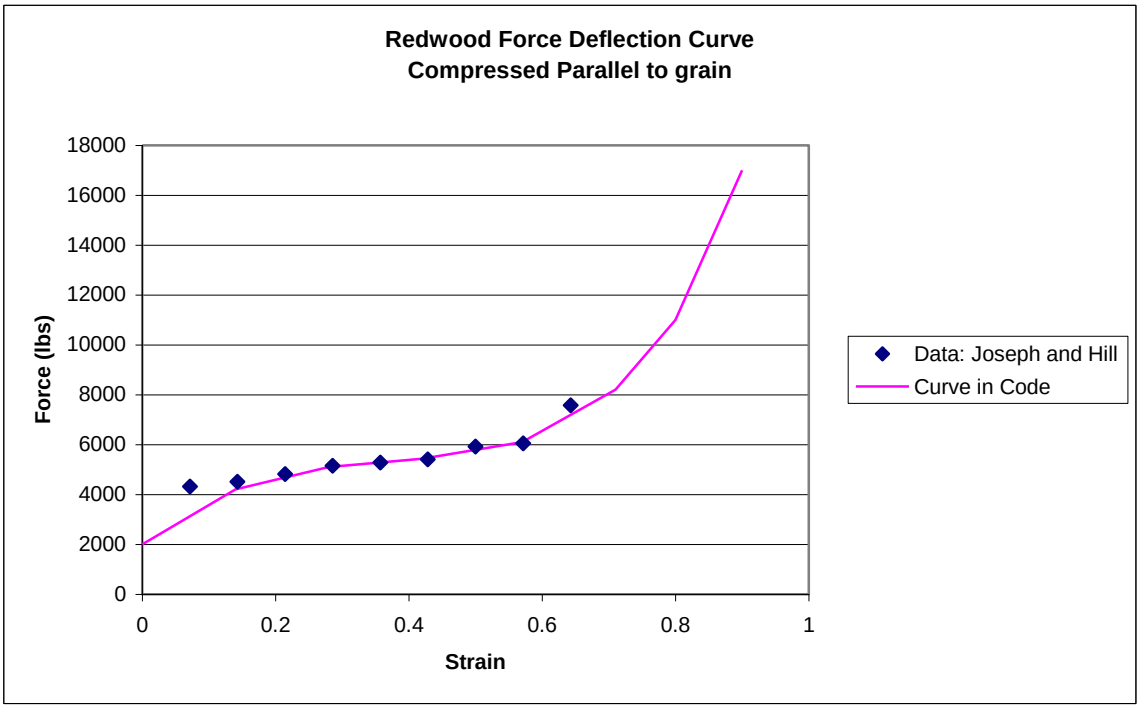

Figure 2-57. Redwood Force Deflection Curve Compared to Test Data from Joseph and Hill

Table 2-15. Redwood Orthotropic Crush Model Parameters

Parameter	Value
Compacted YOUNGS MODULUS (psi)	1.5E6
Compacted POISSONS RATIO	0.3
Compacted YIELD STRESS (psi)	20000
Full Compaction	0.9
Modulus x (psi)	1.5E6
Modulus y (psi)	0.3E6
Modulus z (psi)	0.3E6
Modulus xy (psi)	0.2E6
Modulus yz (psi)	0.25E6
Modulus zx (psi)	0.2E6

Table 2-15. Redwood Orthotropic Crush Model Parameters (Continued)

Parameter	Value	
	Strain	Pressure (psi)
Function 1 $ T-Direction	0	2000
	0.14	4200
	0.28	5100
	0.42	5430
	0.57	6100
	0.71	10100
	0.80	15000
	0.90	20000
Function 2 $ L-Direction		
	0	400
	0.14	986
	0.28	1200
	0.42	1275
	0.57	1432
	0.71	2371
	0.80	3521
Function 4 $ sigxy or sigxz vs volume		
	0.0	1000
	0.6	1000
	0.7	10000
	0.9	10000
Function 5 $ sigyz vs volume		
	0	1000
	0.6	1000
	0.7	10000
	0.9	10000

2.12.4.2 Reference

1. Joseph, Walter W., Thomas K. Hill. “Energy-Absorbing Characteristics of California Redwood Subjected to High Strain.” SAND76-0087. Sandia National Laboratories. Albuquerque, NM. 1976.

2. Cramer, S.M, Hermanson, J.C., and McMurtry, W.M. “Characterizing the Large Strain Crush Response of Redwood.” SAND96-2966, Sandia National Laboratories. Albuquerque, NM. 1996.

3. Attaway, S.W., "A Local Isotropic Global Orthotropic Finite Element Technique for Modeling the Crush of Wood," SAND88-1449, Sandia National Laboratories, Albuquerque, NM. 1988.

2.12.4.3 Aluminum 6061

Property		Reference
Density	0.098 lb/in^3	
Young's Modulus	9.9E06 psi	1, 2
Poisson's Ratio	0.3	1, 2
Yield Stress	45000 psi	1
Hardening Constant	37852 psi	
Hardening Exponent	0.55	
Reduction in Area	0.503-0.520	1

The aluminum 6061 components were modeled using a power-law hardening constitutive model:

$$\sigma = \sigma_y + A(\varepsilon_p)^n$$

where σ_y is the yield stress, A is a hardening constant, and n is a hardening exponent.

2.12.4.4 Reference

1. Wellman, J. "Sandia National Laboratories, Personal communication regarding Organization 1800 Laboratory Tests on Aluminum. (April 19, 1991)." 2007.

2. Rice, R. C., Jackson, J. L., Bakuckas, J., and Thompson, S. "Metallic Materials Properties Development and Standardization (MMPDS) DOT/FAA/AR-MMPDS-01." January 2003.

2.12.4.5 Aluminum 7075

Property		Reference
Density	0.098 lb/in^3	1
Young's Modulus	10.4E6 psi	1
Poisson's Ratio	0.3	
Yield Stress	73.0E3 psi	1
Hardening constant,	37852 psi	
Hardening exponent	0.55	

The aluminum 7075 components were modeled using a power-law hardening constitutive model:

$$\sigma = \sigma_y + A\left(\varepsilon_p\right)^n$$

where σ_y is the yield stress, A is a hardening constant, and n is a hardening exponent.

2.12.4.6 Reference

1. Department of Defense. *Military Standardization Handbook: Metallic Materials and Elements for Aerospace Vehicle Structures.* MIL-HDBK-5E pp. 3-337, Figure 3.7.4.1.6(n): May 1986.

2.12.4.7 Copper Cylinder

Property		Reference
Density	0.322 lb/in^3	1
Young's Modulus,	17.2E06 psi	1
Poisson's Ratio,	0.33	1
Yield Stress,	45.0E03 psi	1
Hardening Constant,	38000 psi	
Hardening exponent	0.55	

The copper cylinder was modeled using a power-law hardening constitutive model:

$$\sigma = \sigma_y + A\left(\varepsilon_p\right)^n$$

where σ_y is the yield stress, A is a hardening constant, and n is a hardening exponent.

2.12.4.8 Reference

1. ASTM B152/B152M. "Standard Specification for Copper Sheet, Strip, Plate and Rolled Bar." ASTM International. West Conshochocken, PA.

2.12.4.9 Stainless PH13-8-Mo

Property		Reference
Density	0.286 lb/in^3	1, 2, 3
Young's Modulus	30.E06 psi	2, 3
Poisson's Ratio	0.30	2, 3
Yield Stress,	141.0E03 psi	4
Hardening Constant	30.0E4 psi	
Hardening exponent	1.0	
Thermal Expansion Coefficient (from 70ºF to 203ºF and from 70ºF to 401ºF, respectively)	5.9E-6 to 6.0E-6 in./in./ºF	5 (Figure 2.6.5.1.1)

The TB-1 was modeled using a power-law hardening constitutive model:

$$\sigma = \sigma_y + A\left(\varepsilon_p\right)^n$$

where σ_y is the yield stress, A is a hardening constant, and n is a hardening exponent.

2.12.4.10 Reference

1. Shigley, J.E. *Mechanical Engineering Design*. McGraw-Hill: 1977.

2. Harvey, P.D., ed. *Engineering Properties of Steels*. American Society for Metals: Metals. Park, OH: 1982.

3. Boyer, H.E., and Gall, T.L. ed. *Metals Handbook.* American Society for Metals: Materials. Park, OH: 1985.

4. American Society of Mechanical Engineers (ASME), "Boiler and Pressure Vessel Code," Section II, Part A, Table 3: Mechanical Test Requirements After Age Hardening Heat Treatment. pp. 1287. 2007.

5. Department of Defense. *Military Standardization Handbook: Metallic Materials and Elements for Aerospace Vehicle Structures."* (Effect of temperature on tensile ultimate and yield strength, Figure 2.6.5.1.1, pp. 2-148). MIL-HNDBK-5E: June 1, 1987.

2.12.4.11 TB-1 Contents

Property		Reference
Density	0.051 lb/in^3	See below
Young's Modulus	1.0E06 psi	See below
Poisson's Ratio	0.30	See below
Yield Stress	2000 psi	See below
Hardening Constant	100000 psi	
Hardening Exponent	1.0	

The material was modeled as Elastic-Plastic with a density to match the oxide powder. The material properties were based on approximating the behavior of oxide power. The material is used inside the TB-1 in the full model analyses. Those analyses are used only to determine rigid body motion of the TB-1, and the yield stress and hardness behavior will not affect the rigid body motion of the TB-1.

2.12.4.12 Stainless 304

Property		Reference
Density	0.286 lb/in^3	1
Young's Modulus	28.0E06 psi	1
Poisson's Ratio	0.33	1
Yield Stress	40000 psi	1
Hardening Constant	192746 psi	
Hardening Exponent	0.74819	

The stainless steel components were modeled using a power-law hardening constitutive model:

$$\sigma = \sigma_y + A\left(\varepsilon_p\right)^n$$

where σ_y is the yield stress, A is a hardening constant, and n is a hardening exponent.

2.12.4.13 Reference

1. United States. Nuclear Regulatory Commission. NUREG-1768. "Package Performance Study Test Protocols." 2003.

2.12.4.14 Titanium 6Al-4V

Property		Reference
Density	0.160 lb/in^3	2
Young's Modulus	15.5E06 psi	2
Poisson's Ratio	0.3	2
Yield Stress	141700 psi	1, 3
Hardening Constant	12.6E4 psi	
Hardening Exponent	0.6554	
Failure Value (TP)	1.012	

Thermal Expansion Coefficient 4.9E-6 to 5.1E-6 in./in./°F (from 70°F to 100°F and from 70°F to 312°F, respectively) 2 (Figure 5.4.1.0

The titanium components were modeled using a power-law hardening constitutive model:

$$\sigma = \sigma_y + A(\varepsilon_p)^n$$

where σ_y is the yield stress, A is a hardening constant, and n is a hardening exponent.

The Ductile Tearing model was used for the sample containers to allow the material to fracture under tensile strains. Figure 2-58 shows the power-law curve fit and data taken from a tensile test. Figure 2-59 and Figure 2-60 show the relative temperature insensitivity of Ti-6-4 alloy, justify the use of nominal (ambient) material properties in the analyses, and negate any brittle fracture concern at NCT cold temperatures.

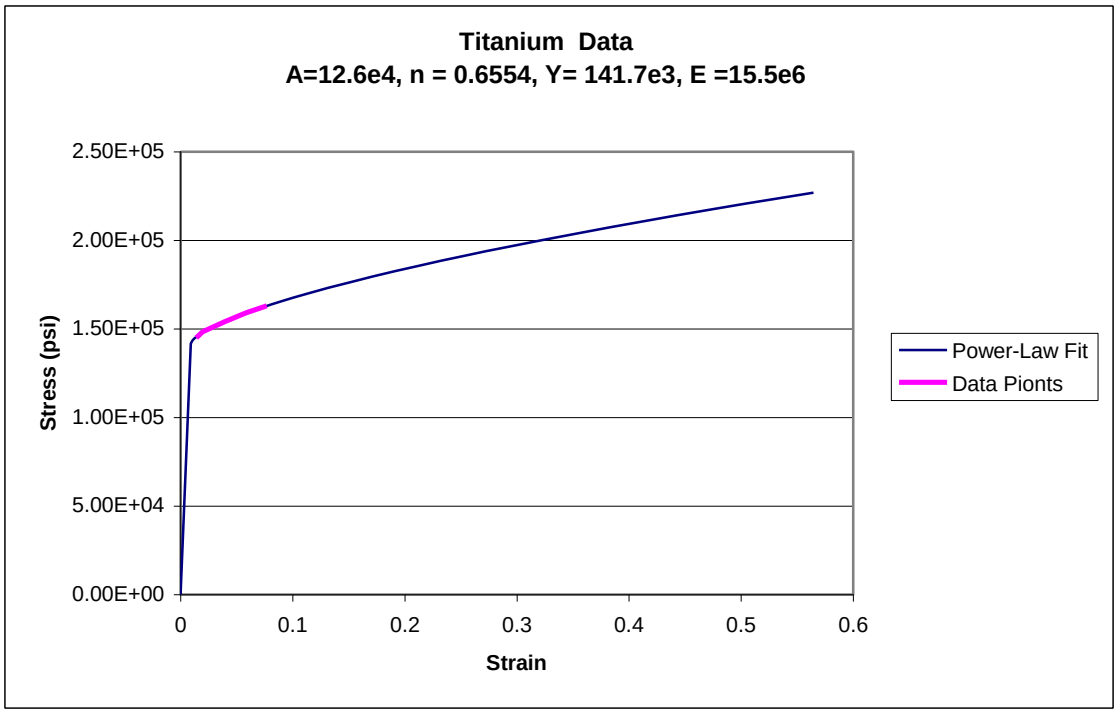

Figure 2-58. Comparison of Power-Law Curve Fit with Data from Tensile Test

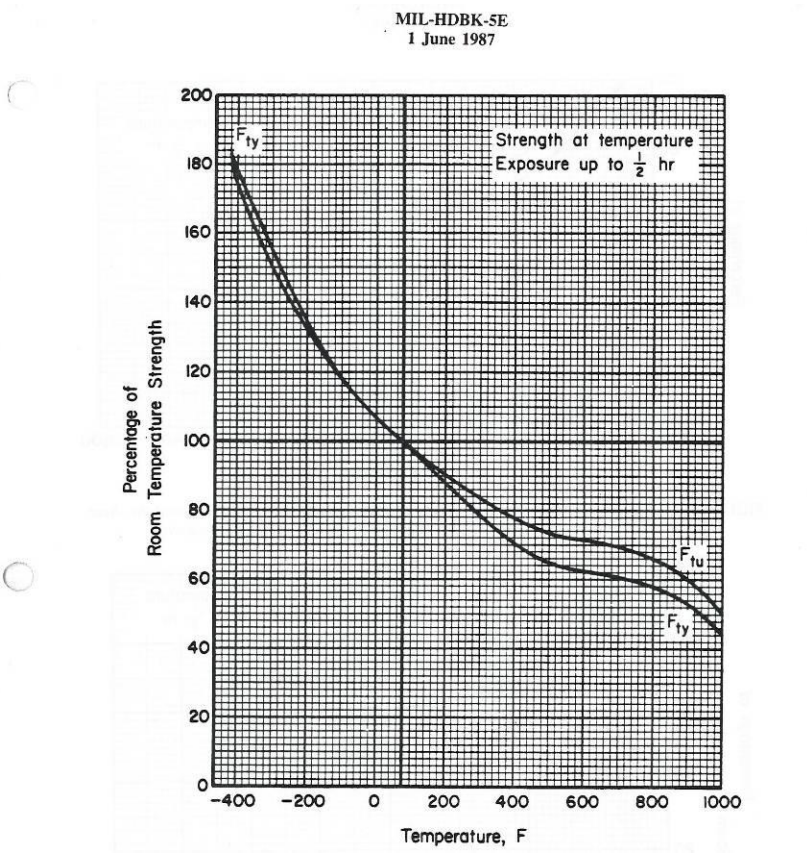

Figure 2-59. Effect of Temperature on the Tensile Ultimate Strength and Tensile Yield Strength of Annealed Ti-6-Al-4V Alloy (Ref. 2, Taken from MIL-HDBK-5E, Figure 5.4.1.1.1.1)

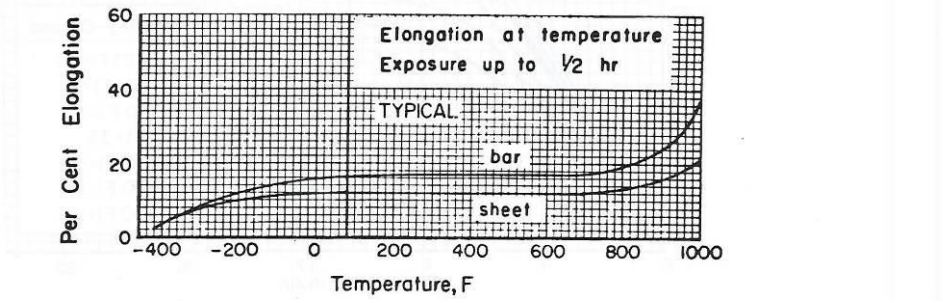

Figure 2-60. Effect of Temperature on the Elongation of Annealed Ti-6-Al-4V Alloy (Ref. 2, Taken from MIL-HDBK-5E, Figure 5.4.1.1.5)

2.12.4.15 Reference

1. Westmoreland Mechanical Testing and Research Inc. "WMT&R Report No. 7-38060." Youngstown, PA. 2007.

2. Department of Defense. *Military Standardization Handbook: Metallic Materials and Elements for Aerospace Vehicle Structures.* MIL-HDBK-5E: May 1988.

3. PAT-1040, Titanium and O-Ring Materials and Component Fabrication Specification, August 23, 2010. (Provided in Section 1.3.3.1 of this addendum.)

2.12.4.16 Plutonium (alpha phase)

Property		Reference
Density	0.716 lb/in^3	1
Young's Modulus	14.1E06 psi	1
Poisson's Ratio	0.3	1
Yield Stress	36000 psi	
Hardening Constant	85000 psi	
Hardening Exponent	0.4	

The alpha-plutonium components were modeled using a power-law hardening constitutive model:

$$\sigma = \sigma_y + A\left(\varepsilon_p\right)^n$$

where σ_y is the yield stress, A is a hardening constant, and n is a hardening exponent. As shown in Figures 2-61 and 2-62, alpha-plutonium is a brittle material. The alpha-plutonium material in Figure 2-62 has a finer grain structure than the alpha-plutonium material in Figure 2-61 and it is therefore more ductile. The material parameters were fit to the curve in Figure 2-62. To conservatively maximize the load induced by the impacting Pu material, it was modeled as a continuously hardening material that does not fracture (and is thus, "infinitely ductile," with hardening), matching the finer grain structure stress-strain curve of Figure 2-62.

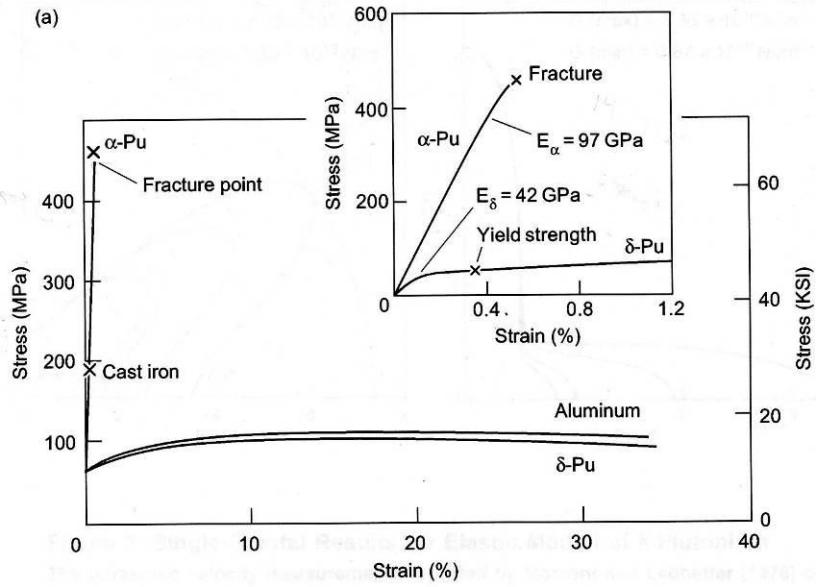

Figure 2-61. Pu Stress-Strain Curves Taken from Hecker and Stevens [Figure 2(a)]

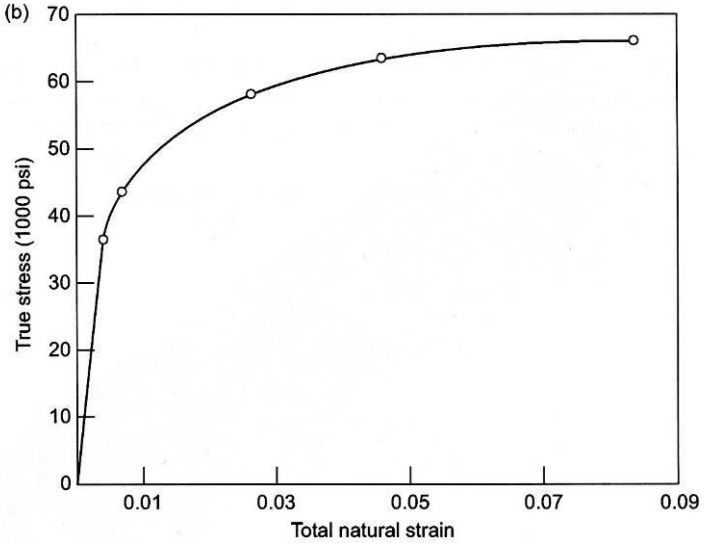

Figure 2-62. Pu Stress-Strain Curves Taken from Hecker and Stevens (Figure 10[b]).

2.12.4.17 Reference

1. Hecker, Siegfried S. and Michael F. Stevens. "Mechanical Behavior of Plutonium and Its Alloys." *Los Alamos Science* Number 26 (2000).

2.12.4.18 Plutonium (delta phase)

Property		Reference
Density	0.716 lb/in^3	1
Young's Modulus	6.1E06 psi	1
Poisson's Ratio	0.3	1
Yield Stress	9200 psi	
Hardening Constant	9000 psi	
Hardening Exponent	0.4	

The delta-plutonium components were modeled using a power-law hardening constitutive model. As shown in Figure 2-61 this is a fairly soft and ductile material. The material parameters were fit to the delta-phase curve in Figure 2-61. To maximize the load induced by the impacting Pu material, it was modeled as a continuously hardening material that does not fracture. The density of alpha phase plutonium was conservatively used as the density for the delta phase plutonium in the modeling.

2.12.4.19 Reference

1. Hecker, Siegfried S. and Michael F. Stevens. "Mechanical Behavior of Plutonium and Its Alloys." *Los Alamos Science* Number 26 (2000).

2.12.4.20 Tungsten

Property		Reference
Density	0.680 lb/in^3	1
Young's Modulus	58.3E06 psi	1
Poisson's Ratio	0.3	1
Yield Stress	80000 psi	
Hardening Constant	78000 psi	
Hardening Exponent	0.4	

The tungsten holder was modeled using a power-law hardening constitutive model with nominal hardening values. The actual component remained elastic.

2.12.4.21 Reference

1. Lassner, Erik and Wolf-Dieter, Schubert. "Tungsten: Properties, Chemistry, Technology of the Element, Alloys, and Chemical Compounds." Academic/Plenum Publishers (1999).

2.12.4.22 Brass (UNS C36000)

Property		Reference
Density	0.309 lb/in^3	2
Young's Modulus	13.1E06 psi	2
Poisson's Ratio	0.3	2
Yield Stress	43300 psi	1
Hardening Constant	79400 psi	
Hardening Exponent	0.6248	

The brass components were modeled using a power-law hardening constitutive model:

$$\sigma = \sigma_y + A(\varepsilon_p)^n$$

where σ_y is the yield stress, A is a hardening constant, and n is a hardening exponent. Figure 2-63 shows the power-law curve fit and data taken from the tensile test.

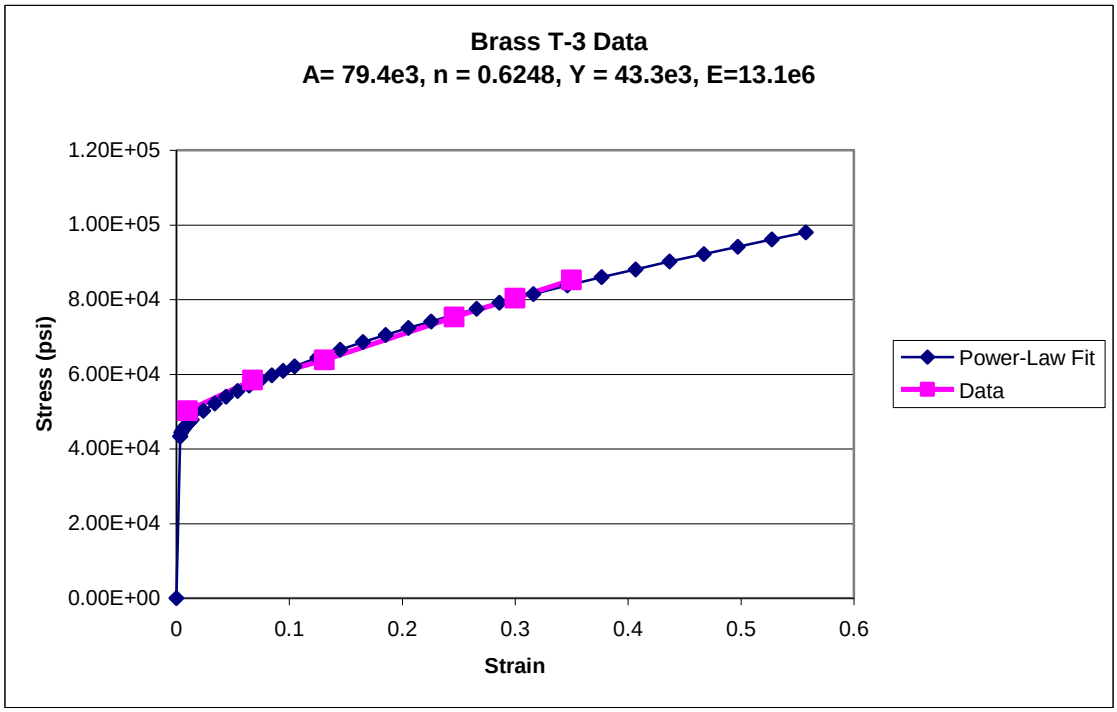

Figure 2-63. Comparison of Power-Law Curve Fit with Data from Tensile Test

2.12.4.23 Reference

1. Westmoreland Mechanical Testing and Research Inc. "WMT&R Report No. 7-38060." Youngstown, PA. 2007.

2. ASTM B16 CDA 360, Free Cutting Brass, Copper Alloy No C36000.

2.12.4.24 Beryllium

Property		Reference
Density	0.5745 lb/in^3 (conservatively assumed density of delta Pu)	
Young's Modulus	1.7092E7 psi	1
Poisson's Ratio	0.3	1
Yield Stress	23929 psi	1
Hardening Constant	38350 psi	
Hardening Exponent	0.461407	

The Be composite cylinder was modeled using a power-law hardening constitutive model:

$$\sigma = \sigma_y + A(\varepsilon_p)^n$$

where σ_y is the yield stress, A is a hardening constant, and n is a hardening exponent. Figure 2-64 shows the power-law curve fit and data taken from the tensile test.

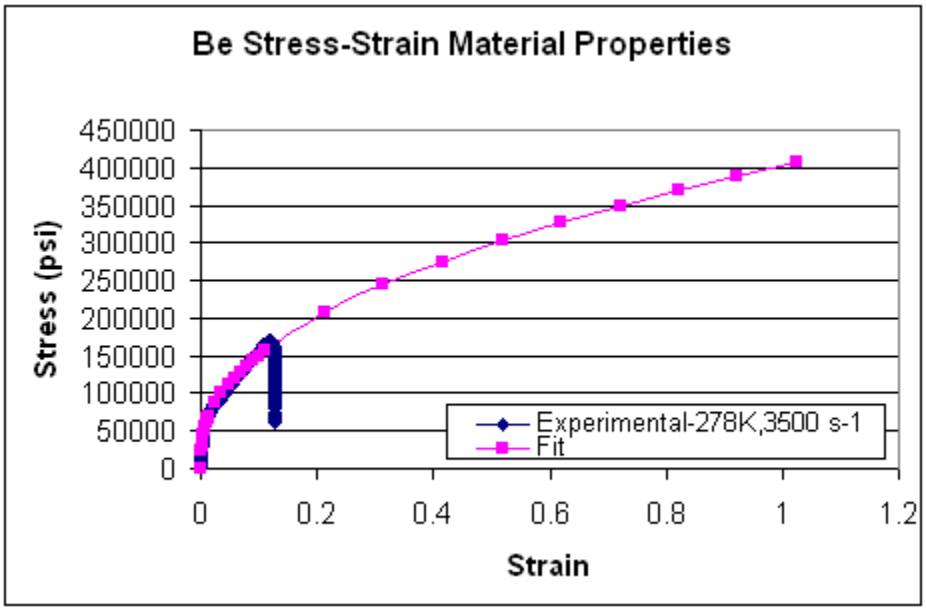

Figure 2-64. Comparison of Power-Law Curve Fit with Data from Tensile Test

2.12.4.25 References

1. Wick, O.J., ed. *Plutonium Handbook: A Guide to the Technology, Volume 1*. American Nuclear Society, 1980.

2. Lindholm, U.S., and Yeakley, L.M. "Effect of Strain rate, Temperature, and Multiaxial Stress on the Strength and Ductility of S200E Beryllium and 6Al-4V Titanium." Air Force Materials Laboratory Report. AFML-TR-71-37. Wright-Patterson Air Force Base. OH. 1971.

2.12.5 Component Analyses Using Complete Model

The following section describes the full model analyses of the TB-1 containment vessel and its detailed components. As discussed in Section 1, the components within the titanium T-Ampoule consist of either cast plutonium (Pu) cylinders with a mass of 831 g or 731 g, small sample containers (SC-1), or medium sample containers (SC-2) containing Pu material or a Be composite material. Each component will be analyzed for three orientations, the end-on impact, the side-on impact, and the CGOC impact for the high-speed aircraft impact. For the hypothetical accident conditions (HAC) dynamic crush analyses, the same sets of analyses were performed. In the NCT 4-ft-drop scenario, only the side and end impact for the SC-1 and SC-2 cases were analyzed to assure the positioning of the sample containers did not require adjustment for the HAC and high-speed aircraft impact analyses.

2.12.5.1 Finite Element Model

2.12.5.1.1 Common Model Components

The common components of the models are presented in Figures 2-65 and 2-66. The T-Ampoule is designed to fit snugly inside the TB-1 and to be loaded primarily in compression during impact. The finite element models of the T-Ampoule and TB-1 have a plane of symmetry along the center axis of the TB-1 (Z=0). Figure 2-65 shows the T-Ampoule and the TB-1 model for the top impact orientation. A hexagonal mesh with .015-in. elements is used to model the top of the T-Ampoule. This results in four elements through the thickness of the T-Ampoule shell. Since the primary strains are compressive, this allows for a time step which keeps the problem tractable, while providing adequate resolution of the T-Ampoule strain field. The mesh of the TB-1 is refined in the upper region with a hexagonal element size of 0.040 in. to adequately model the contact between the T-Ampoule top and the TB-1. The titanium Ring Filler, which fills the small void between the T-Ampoule and the TB-1 near the bottom of the TB-1 lid, is installed during preparations for shipment to provide uniform support to the ellipsoid T-Ampoule. As shown in Figure 2-66, the Ring Filler is not modeled explicitly, but is modeled as an integral part of the TB-1 body, with PH13-8-Mo material properties. Although the elastic moduli do differ, the yield strengths of the 13-8 (141 ksi) vs. Ti-6-4 (141.7 ksi) materials do not differ significantly, and this small gap-filling component was simplified to be continuous with the TB-1 since it provides no additional strength and only provides a smoothed inner surface for contact with the T-Ampoule and its contents. The stresses in this region are monitored to ensure that they do not threaten the integrity of the Ring Filler. For end impacts, the lower region of the TB-1 is modeled with a coarser mesh; for side impacts, the non-impact side has the coarser mesh. The TB-1 halves are tied together using the tied contact algorithm.

In the TB-1 finite element model, the lid and the body are modeled as one unit. The bolted connection is not modeled. There is a separate analytical bolt analysis in Section 2.12.6. This analysis uses the peak impulse force from the component finite element models to determine the bolt loading.

The model developed for the side-on impact analyses is presented in Figure 2-66. The model is similar to the top impact model except that the mesh for the TB-1 is refined on the sides of the component. The mesh discretization of the T-Ampoule top and T-Ampoule bottom is the same

0.015-in. hexagonal element size as that used in the end-on impact analysis. The thread region, where the top and bottom of the T-Ampoule are joined, is modeled using coincident nodes.

The SC-1 and SC-2 are fit inside a support structure within the T-Ampoule. This structure, shown in Figures 2-67 and 2-68, is constructed from Titanium 6Al-4V (see Section 2.12.4.14). The support structure consists of two dishes placed on each end of the T-Ampoule for vertical positioning (with a thickness that varies from 0.055 in. at the edge to 0.025 in. at the center), 4 upper and lower legs which centrally position the containers within the T-Ampoule (with a thickness of 0.063 in.), two rings which hold the legs in place (0.094 in. diameter), and either one or two spacers for the SC-1 and SC-2, respectively to separate the containers (with a thickness of 0.043 in. and a height of 0.749 in. and 1.008 in., respectively). The legs and rings were meshed to have 4 elements through the thickness, while the dishes have 5 elements through the thickness (see Figure 2-69 for mesh refinement). Figure 2-67 shows the support structure as used for the 0° rotated models while Figure 2-68 shows the structure used for the 45° rotated models. These two orientations were used to ensure worst cases analyses were performed in terms of loads on the support structure and loads on the T-Ampoule.

As detailed in Section 2.12.4.9, the high-strength PH13-8Mo stainless steel TB-1 is modeled using an elastic-plastic, power-law constitutive model to assure accurate capture of denting internally within the TB-1. The Ti-6Al-4V T-Ampoule and support structure are modeled using an elastic-plastic, power-law constitutive model.

The PRONTO3D code used in this analysis uses the Flanagan-Belytschko hexahedral element with one center integration point. The results are presented with contour plots showing element integration point values; they are not smoothed contours of extrapolated nodal values. Although the plots will look rough, the integration point strains are the primary variable of concern, since these values will be used in the strain locus plots. Therefore, integration point contours will be used throughout the analysis.

Included in the high speed aircraft analysis results and the HAC results are plots of kinetic energy versus time. These were included to demonstrate that the peak loads were captured in the analyses. The models were all run without built-in units, thus the kinetic energy plots presented for the high speed aircraft analyses and HAC analyses do not have labels. The x-axis of these plots, time, is in units of seconds. The y-axis of these plots, kinetic energy, is in units of pounds inches.

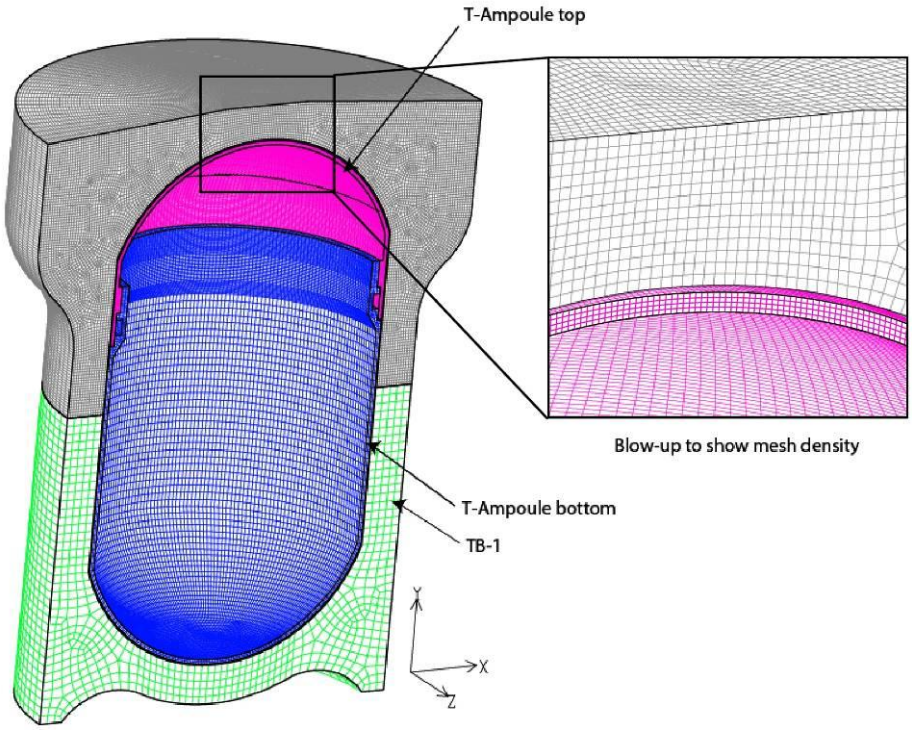

Figure 2-65. Common Components of the Model for Top and CGOC Impact Orientation

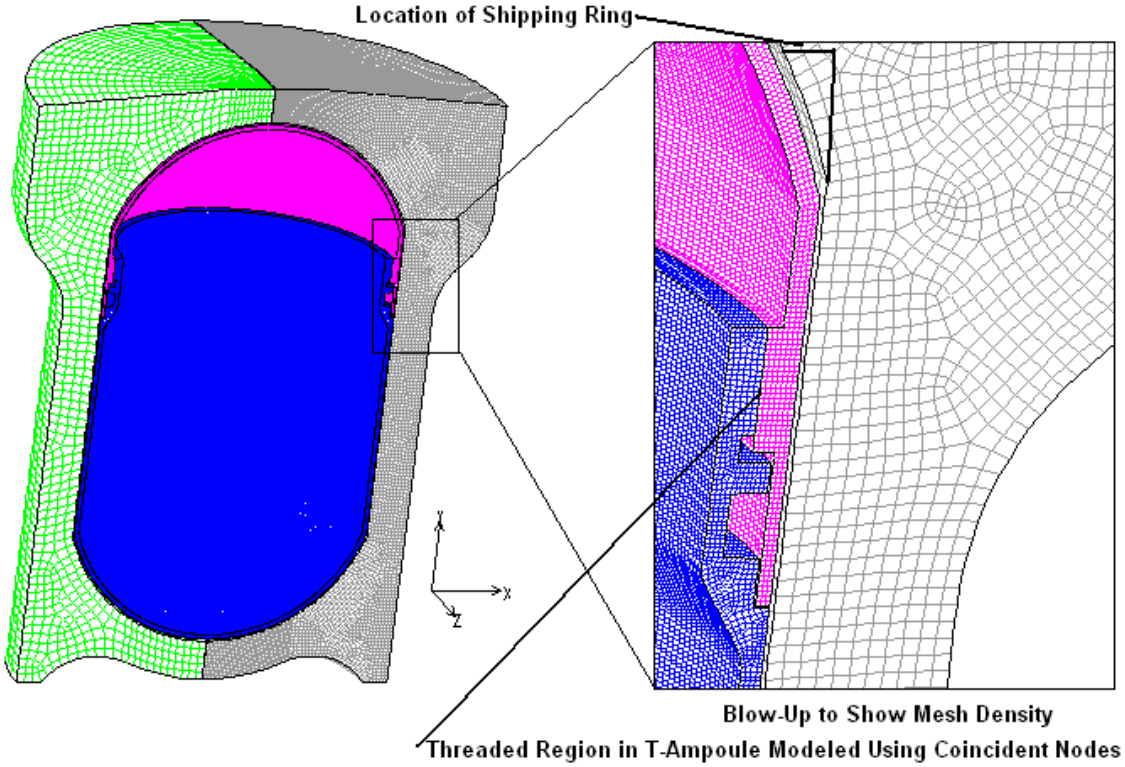

Figure 2-66. Common Components of the Model for a Side Impact Orientation

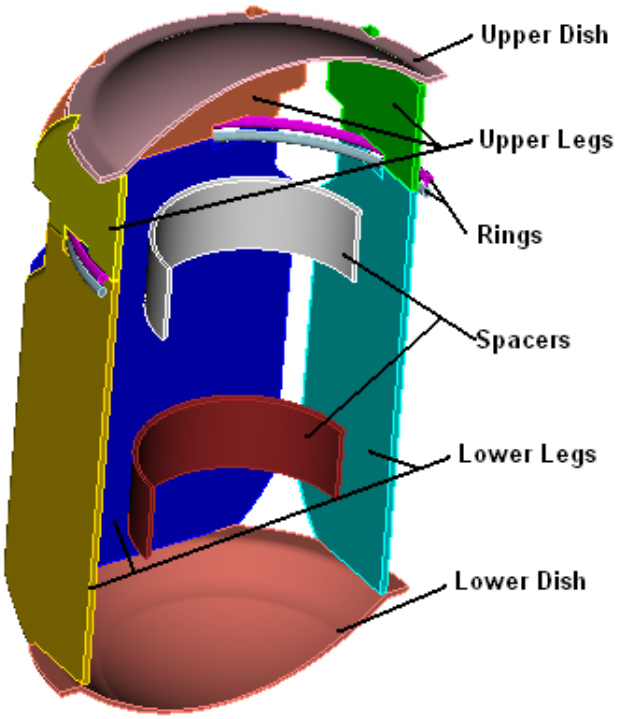

Figure 2-67. Support Structure with 0° Rotation and Spacers for SC-1

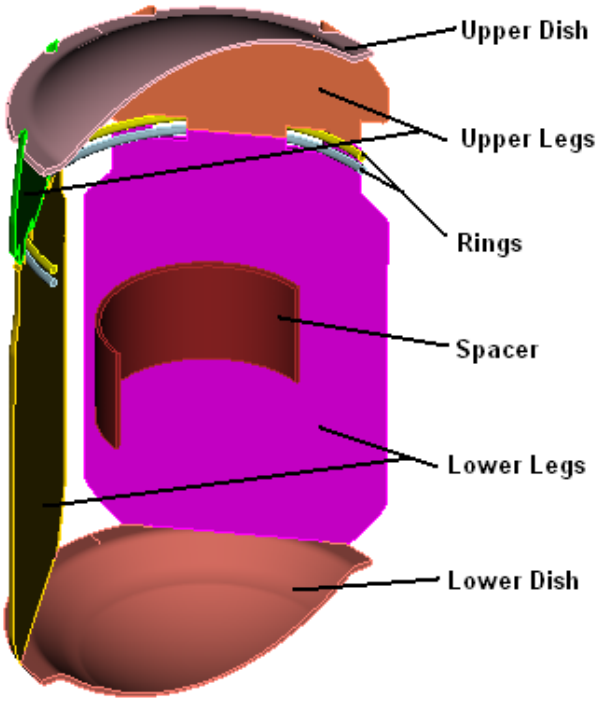

Figure 2-68. Support Structure with 45° Rotation and Spacer for SC-2

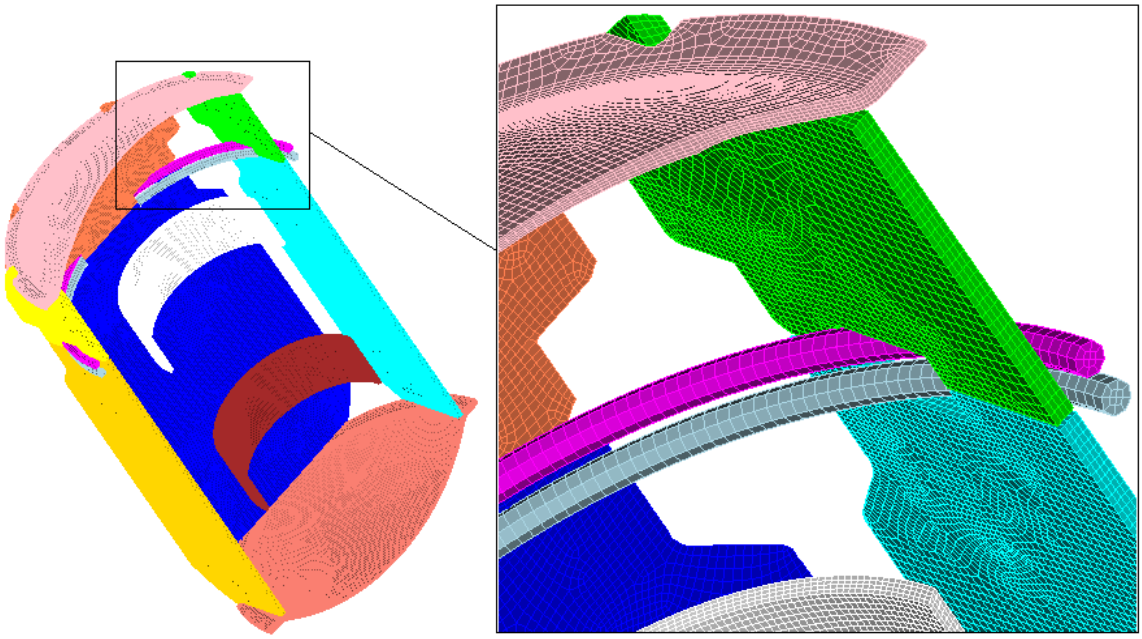

Figure 2-69. Mesh Refinement in Support Structure with 0° Rotation and Spacer for SC-1

2.12.5.2 Component Models

Models of the content components consist of an 831-g plutonium metal hollow cylinder, a 731-g plutonium metal hollow cylinder, a small sample container (SC-1) and a medium sample container (SC-2). The sample containers will be used to transport Pu and a Pu/Be composite. These components are presented in Figures 2-70 through 2-73. The 831-g plutonium metal hollow cylinder shown in Figure 2-70 has a 2.51-in. diameter and a 2.903-in. length. The wall thickness is 0.118 in. It is modeled using 0.018 in. hexahedral elements, which results in 6 elements through the thickness. The material of the cylinder is modeled as alpha-plutonium as described in Section 2.12.4.16. The 731-g plutonium metal hollow cylinder model is very similar to the 831-g model, except that the length is reduced to account for the reduced material weight. It is also modeled as an alpha-plutonium material.

The finite element models for the sample containers are also similar to each other. The SC-1 model shown in Figure 2-72 is 3 in. in diameter and 2 in. high. The shell thickness is 0.065 in. The container is meshed with 0.020-in. hexagonal elements, which results in 3 elements through the shell thickness. The model is shown with the 0.88-in. diameter X 0.88-in. long right circular cylinder, which is modeled as delta-plutonium and has a mass of 174 g. Note that the Pu cylinder is located in the bottom of the sample container, which is farthest away from the T-Ampoule for a top-end impact (producing the highest net velocity difference between the two upon impact, and thus the highest load to the T-Ampoule). For a right side impact case, the Pu cylinder would be located on the far left side of the sample container, for the same reason. The contents of the sample containers are packed in the T-Ampoule with the support structure shown in Figures 2-67 and 2-68. The SC-2, shown in Figure 2-73, has the same basic geometry and mesh as the SC-1. The length of the sidewall has been lengthened by 1 in., and the mass of the

contents has been increased. The contents of the SC-2 are modeled using a 1.1 in. diameter X 1.1-in. long right circular cylinder, which has a mass of 338 g.

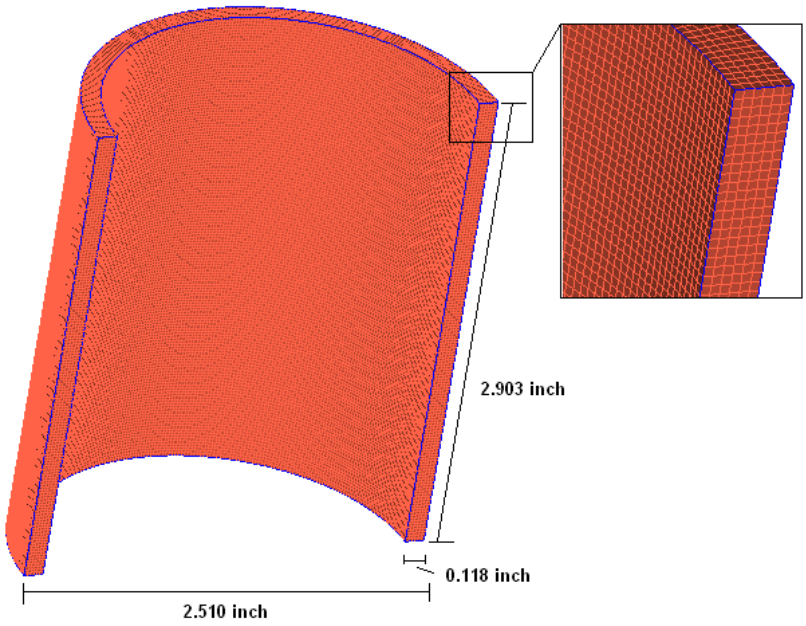

Figure 2-70. 831-g Cylinder Finite Element Model

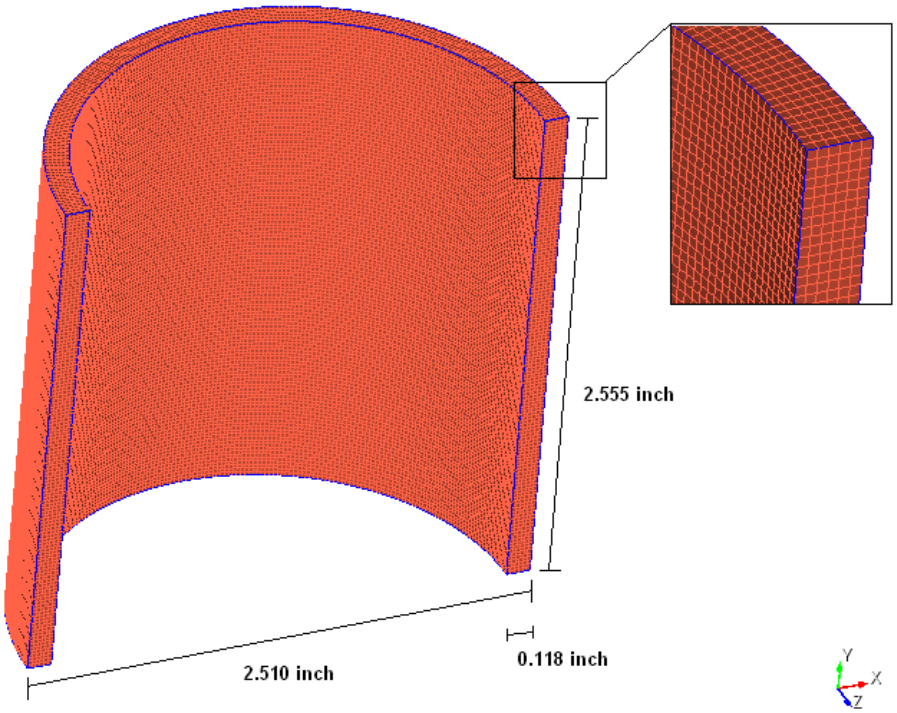

Figure 2-71. 731-g Cylinder Finite Element Model

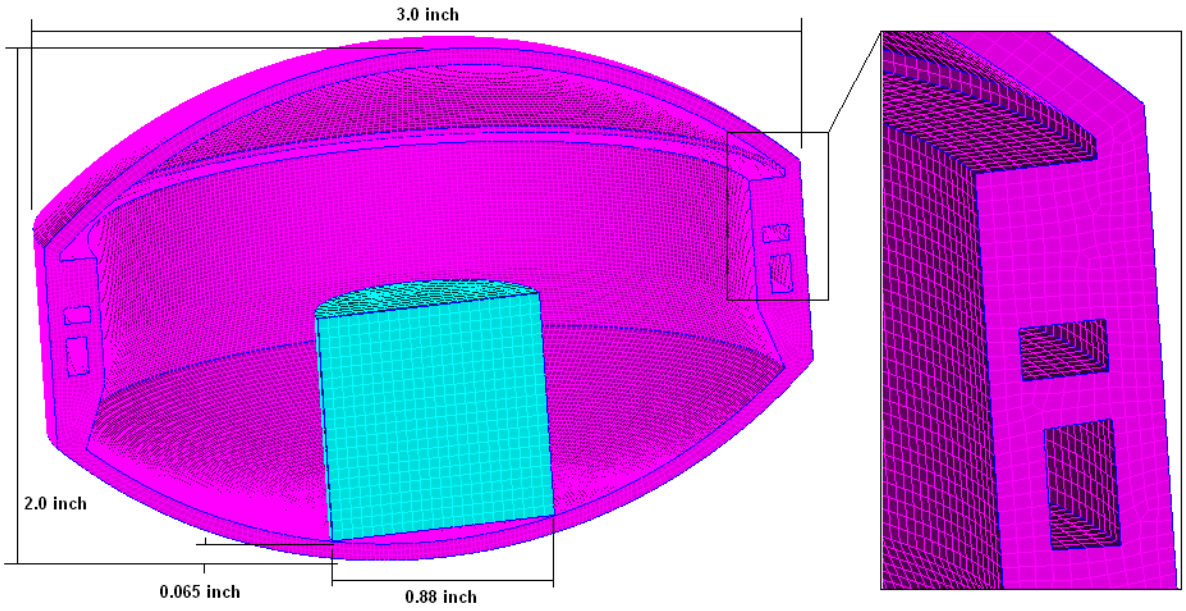

Figure 2-72. Finite Element Model of SC-1 with Pu Cylinder Contents

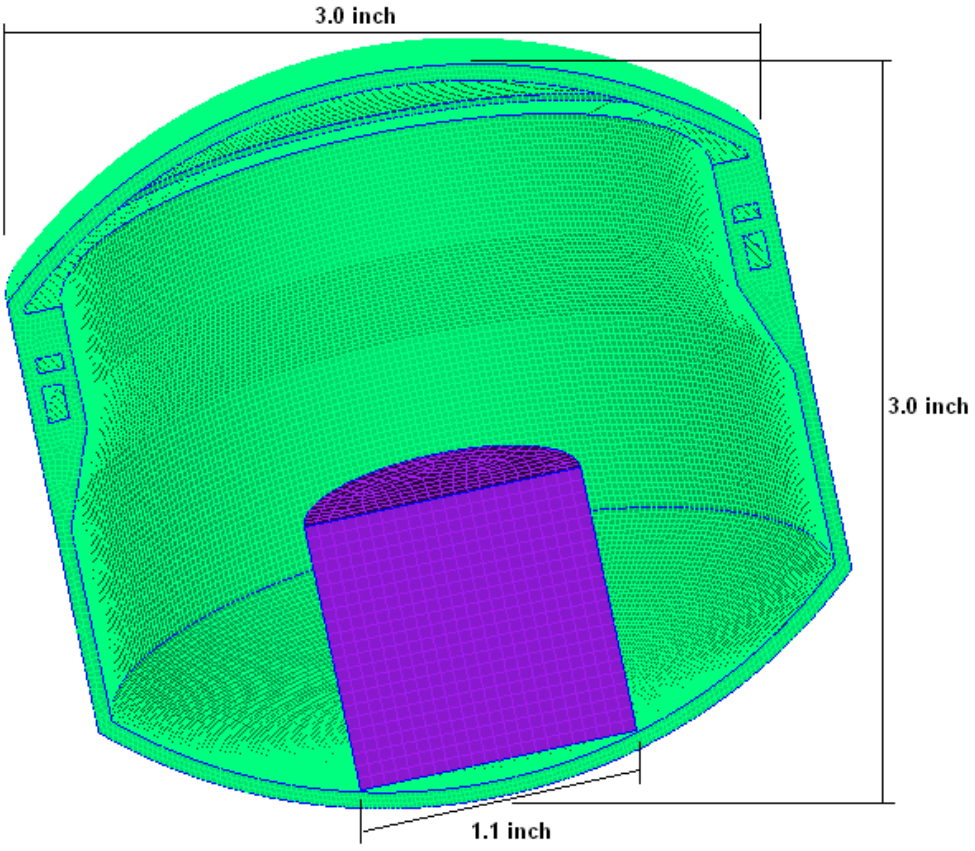

Figure 2-73. Finite Element Model of SC-2 with Pu Cylinder Contents

2.12.5.3 Normal Conditions of Transport Displacement Analyses

The plutonium contents in the sample containers will be packaged in the T-Ampoule using the support structure shown in Figures 2-67 and 2-68. Under the NCT free drop, the support structure integrity must be assessed to assure the positioning of the sample containers for HAC and high-speed crash need not be adjusted. Therefore, the SC-1 and SC-2 were evaluated for 4-ft-drop end and side impacts. Under side impact, the model was oriented with the support structure at 0 and 45 degrees.

These analyses were completed for only the sample container components. The design of the support structure is meant to prevent the sample containers from shifting during normal operating conditions. If the Pu and Pu/Be-composite cylinders did shift to the outer edge of the T-Ampoule, and subsequently traveled across its entire width during an HAC or high speed impact, this would increase loads on the T-Ampoule and TB-1 vessel. Due to the thin walls and open shape of the hollow cylinder components which are extremely soft, the positioning of the plutonium metal hollow cylinders did not need restriction, and no support structure was designed to cradle the cylinders. The Ta foil packing material for the plutonium metal hollow cylinders and the sample container contents was conservatively neglected to allow for bounding higher net impact velocities between contents and T-Ampoule wall, and to conservatively omit any energy absorbing or load spreading from the packing material. In the high-speed impact analyses, the cylinders were positioned to allow for the maximum displacement (most conservative with the largest velocity difference between the cylinder and T-Ampoule at time of contact). The NCT analyses were performed to assure the positioning of the sample containers does not change after the 4-ft-drop. This was done by confirming the support structure does not undergo large plastic deformation throughout its thickness.

Three examples of the models created to determine the behavior of the support structure and sample containers when subjected to the NCT (10 CFR 71.71) performance tests are shown in Figures 2-74 through 2-76. Not shown are the SC-1 side impact at 45 degrees, the SC-2 side impact at 0 degrees, and the SC-2 end impact at 0 degrees, due to their similarity to the models shown. The support structure, sample containers, and plutonium are given an initial velocity of 192 in/sec, corresponding to the NCT regulatory condition. The models are half symmetry models, with the plane of symmetry passing through the center of the TB-1.

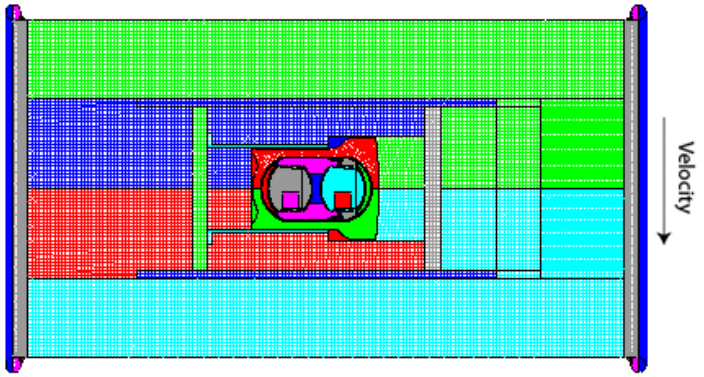

Figure 2-74. NCT SC-2 Side Impact with Support Structure Rotated 45°

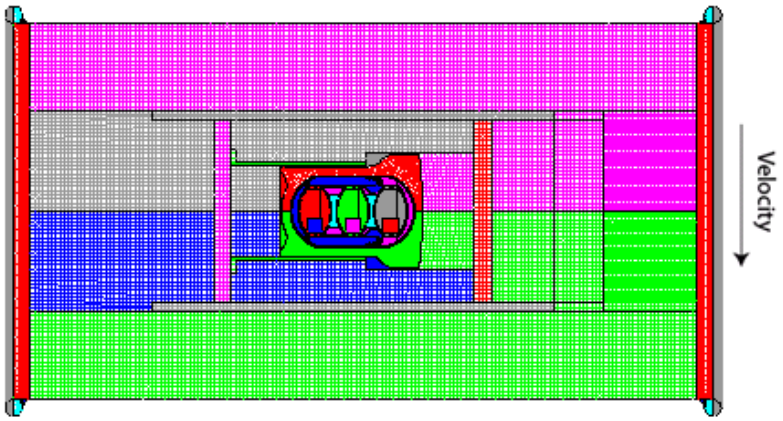

Figure 2-75. NCT SC-1 Side Impact with Support Structure Rotated 0°

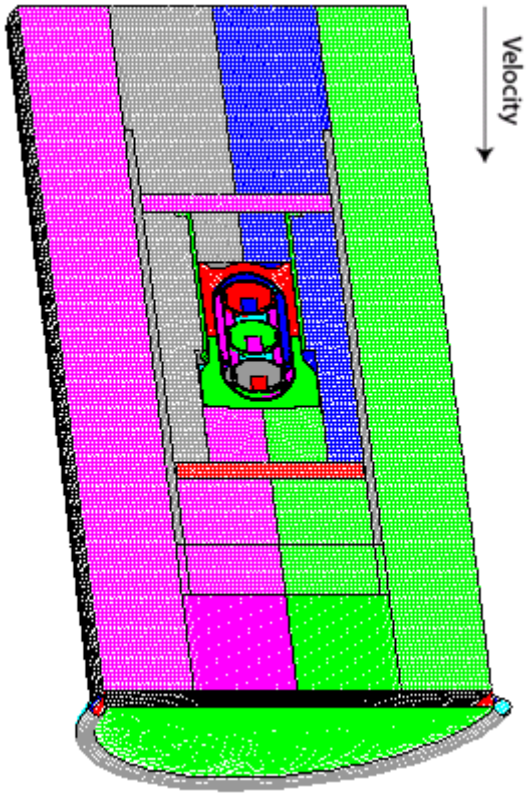

Figure 2-76. NCT SC-1 End Impact with Support Structure Rotated 0°

2.12.5.3.1 NCT End Drop Analysis

The models created for the 4-ft-drop end impact for the SC-1 and SC-2 at time 0 are shown in Figures 2-76 and 2-77, respectively. The post-4-ft-drop models are shown in Figures 2-78 and 2-79, although almost no discernable difference can be seen since the package overpack lid ring is only slightly dented. The kinetic energy histories for these two impacts are shown in Figures 2-80 and 2-81, indicating that sufficient analysis time transpired to capture the entire impact event, and the PAT-1 package actually bounced after impact. As shown in Figures 2-82 through 2-86 and Table 2-16, the minimal plasticity (less than 4%, and only in small localized areas of internal or external corners) observed in the titanium support structure, or cradle, verifies that the overall structure remained essentially elastic and the original position of the sample containers would remain unchanged.

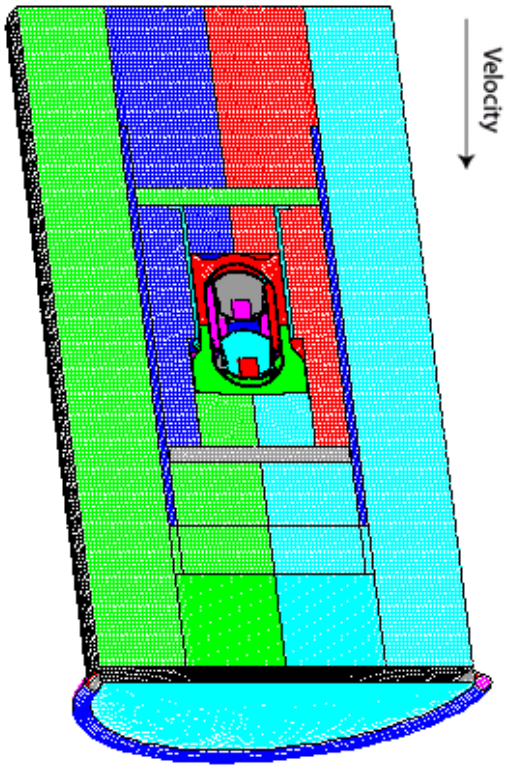

Figure 2-77. NCT SC-2 End Impact with Support Structure Rotated 0°

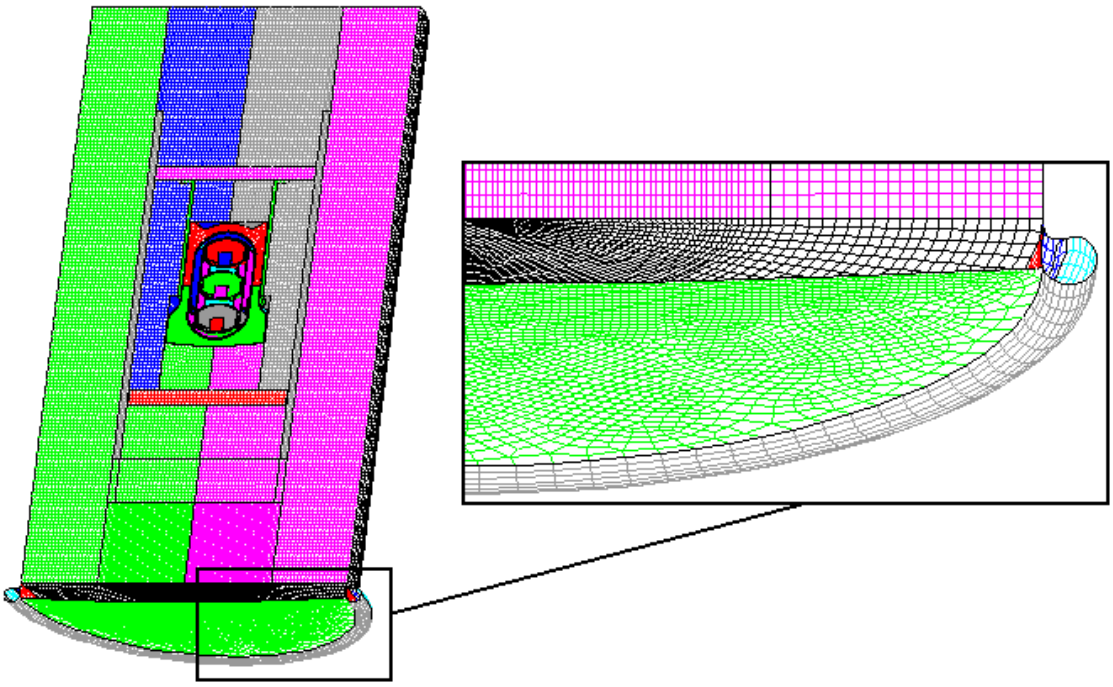

Figure 2-78. NCT SC-1 End Impact with Support Structure Rotated 0° – Final Displacement

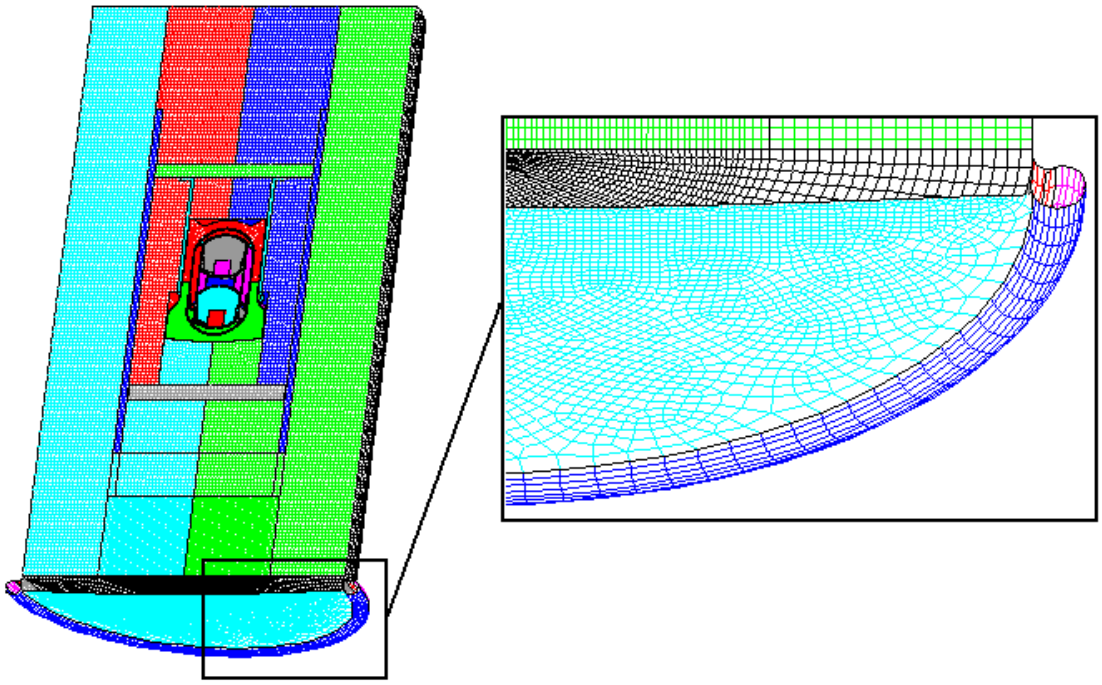

Figure 2-79. NCT SC-2 End Impact with Support Structure Rotated 0° – Final Displacement

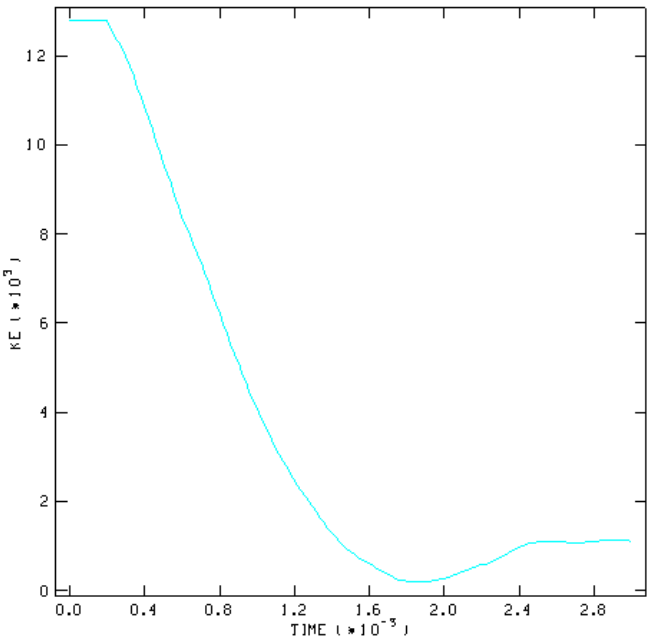

Figure 2-80. NCT SC-1 End Impact with Support Structure Rotated 0° - Kinetic Energy Time History

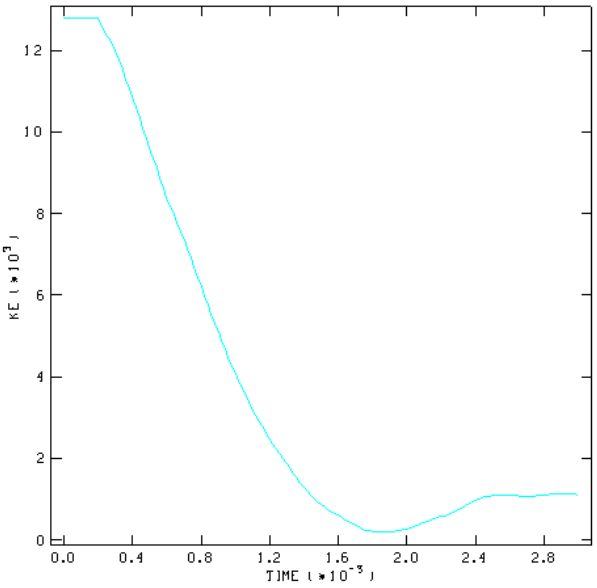

Figure 2-81. NCT SC-2 End Impact with Support Structure Rotated 0° - Kinetic Energy Time History

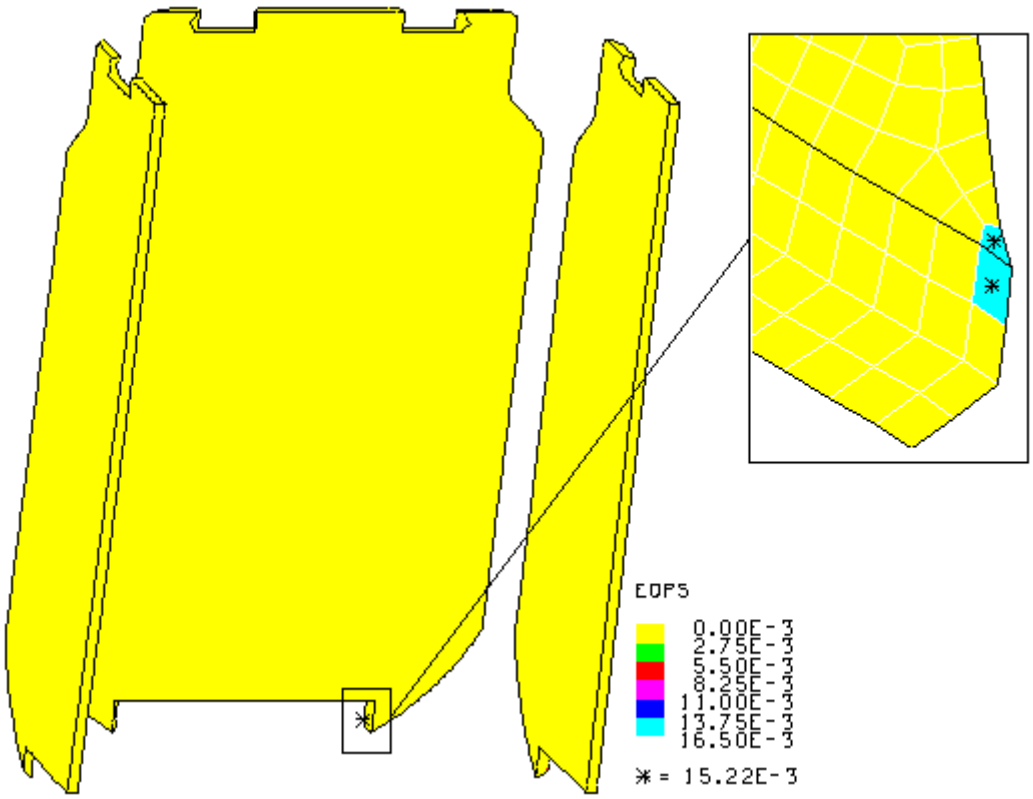

Figure 2-82. NCT SC-1 End Impact with Support Structure Rotated 0° - EQPS in Bottom Legs

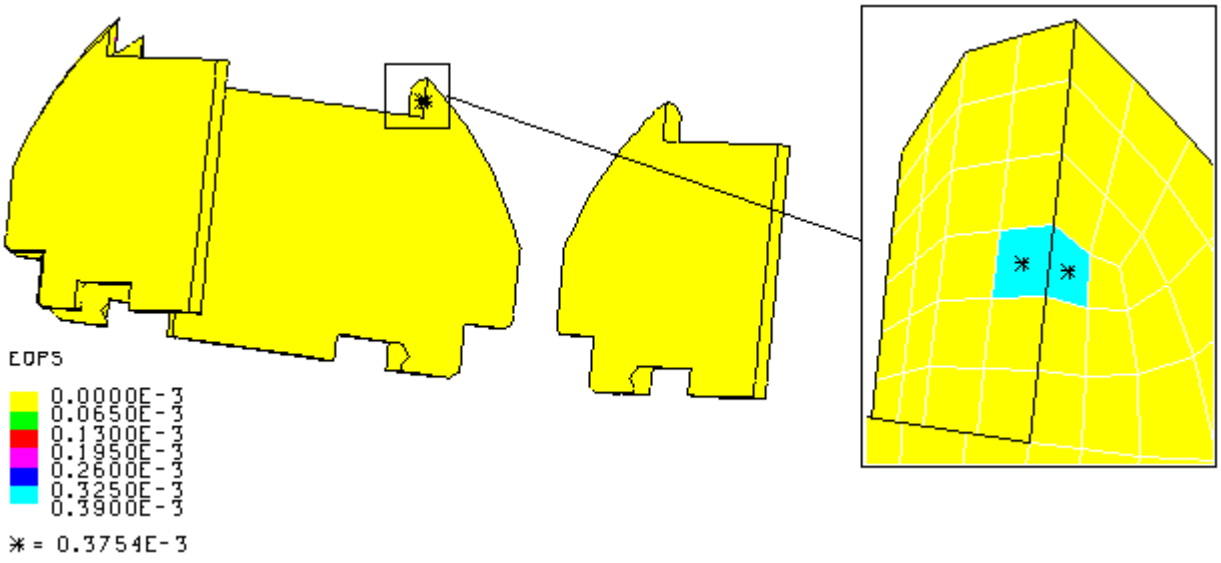

Figure 2-83. NCT SC-1 End Impact with Support Structure Rotated 0° - EQPS in Top Legs

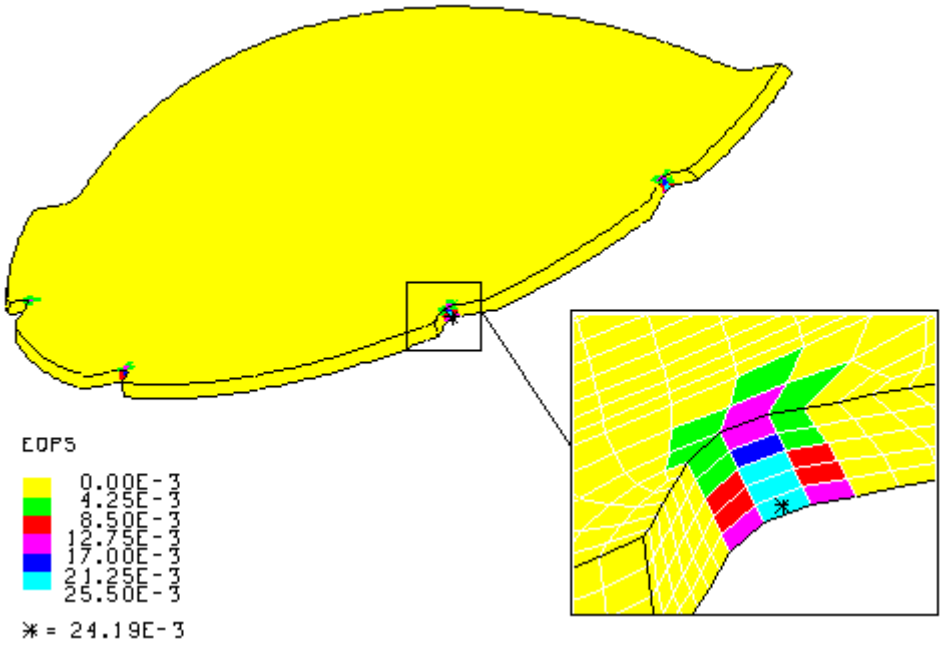

Figure 2-84. NCT SC-1 End Impact with Support Structure Rotated 0° – EQPS in Top Dish

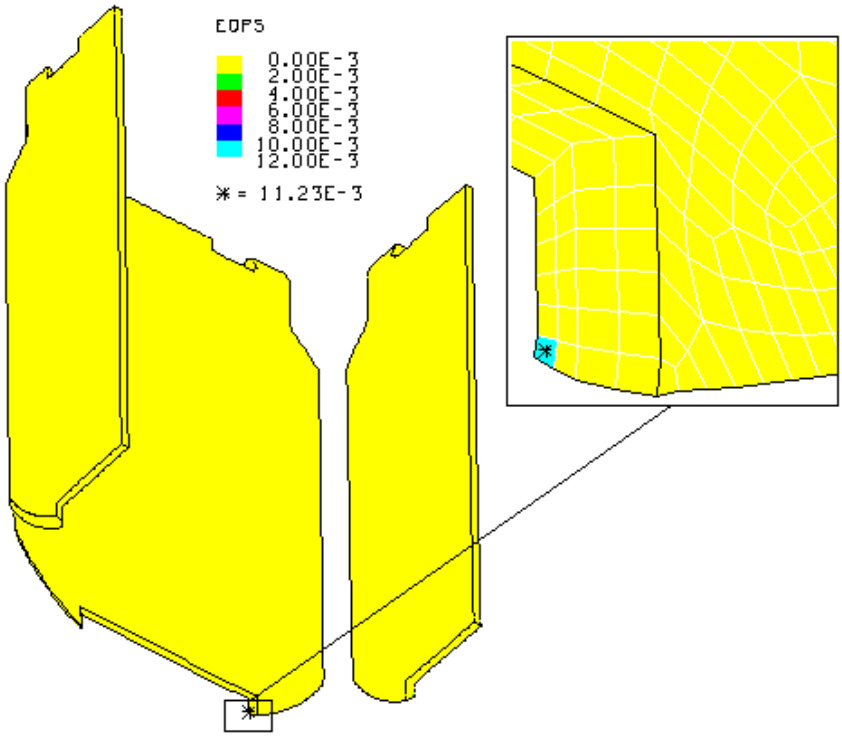

Figure 2-85. NCT SC-2 End Impact with Support Structure Rotated 0° – EQPS in Bottom Legs

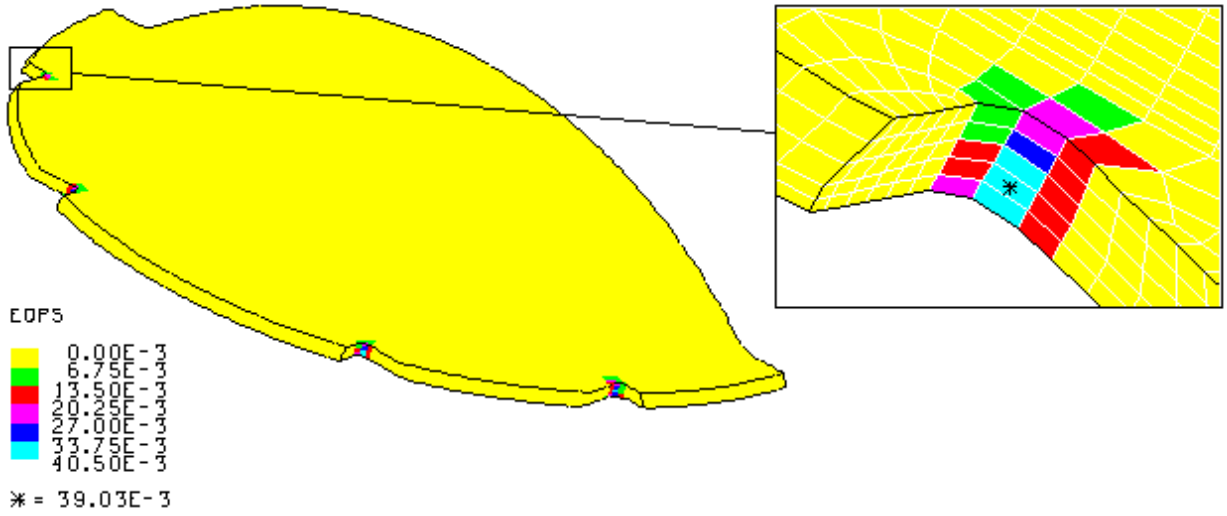

Figure 2-86. NCT SC-2 End Impact with Support Structure Rotated 0° – EQPS in Top Dish

Table 2-16. Maximum Strains in 4 ft End Drop Models

Model/Part	EQPS
SC-1 End Impact	
Bottom Legs	1.52e-2
Upper Legs	3.75e-4
Upper Dish	2.42e-2
SC-2 End Impact	
Bottom Legs	1.12e-2
Upper Dish	3.90e-2

2.12.5.3.2 NCT Side Drop Analysis

The models created for the 4-ft-drop side impact for the SC-1 AND SC-2 (0 and 45 degree rotated) at time 0 are shown in Figure 2-87 and Figure 2-88. The post-4-ft-drop models are shown in Figure 2-89 through Figure 2-92, and for these side impact cases more localized denting of the overpack lid rings is visible than for the end impact cases. The kinetic energy histories for these four impacts are shown in Figure 2-93 through Figure 2-96, indicating that sufficient analysis time transpired to capture the entire impact event, and the PAT-1 package actually bounced after impact. As shown in Figure 2-97 through Figure 2-105 and Table 2-17, the minimal plasticity (less than 7% and only in small localized areas of internal or external corners) observed in the titanium support structure, or inner cradle, verifies that the overall structure remained essentially elastic and the original position of the sample containers would remain unchanged. The zero plasticity post-drop condition of the T-Ampoule is shown in Figure 2-106, as well as zero plasticity in the TB-1 in Figure 2-107 and extremely low through-thickness stress intensities in Figure 2-108, below ASME limits shown in Table 2-4.

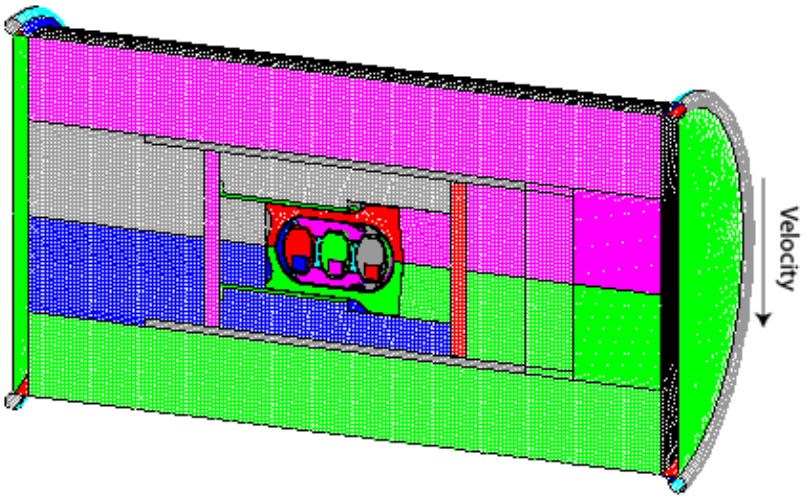

Figure 2-87. NCT SC-1 Side Impact with Support Structure Rotated 45°

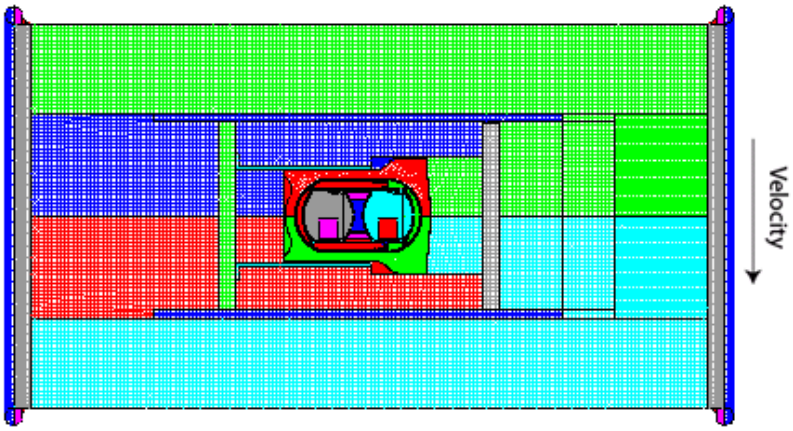

Figure 2-88. NCT SC-2 Side Impact with Support Structure Rotated 0°

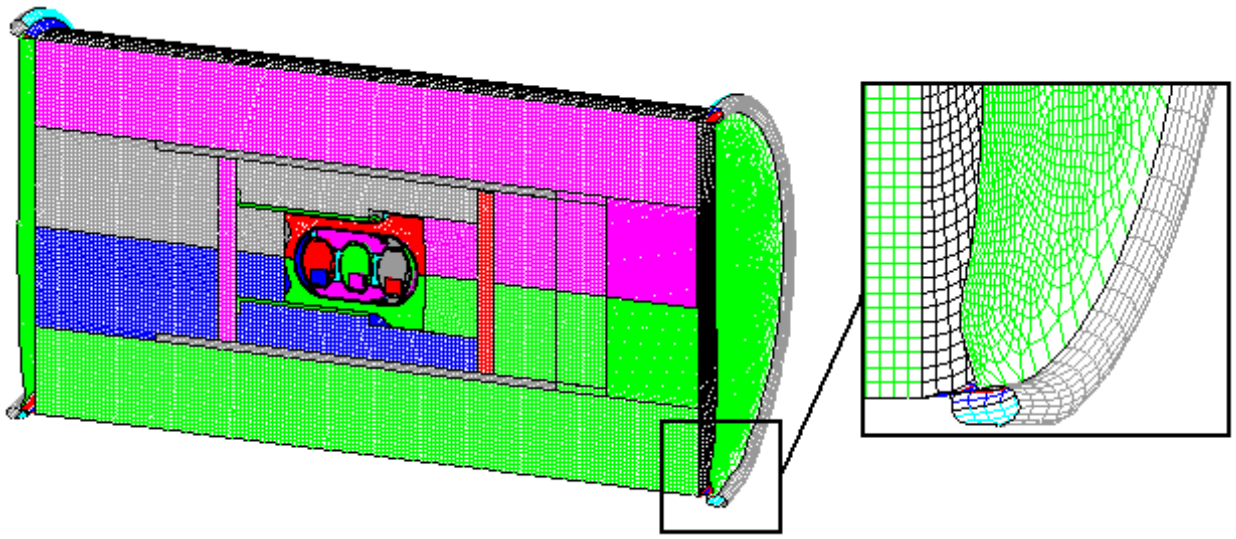

Figure 2-89. NCT SC-1 Side Impact with Support Structure Rotated 45° – Final Displacement

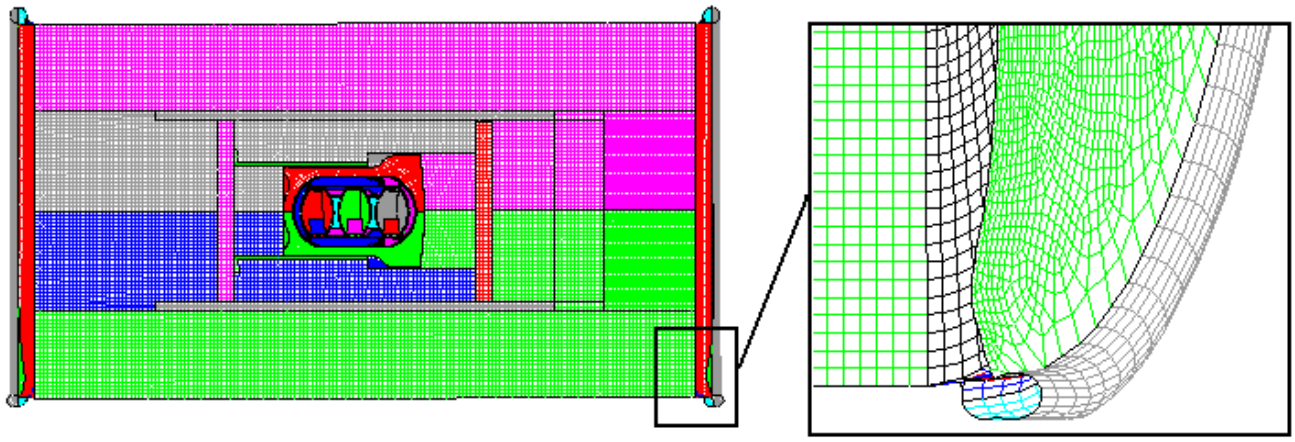

Figure 2-90. NCT SC-1 Side Impact with Support Structure Rotated 0° – Final Displacement

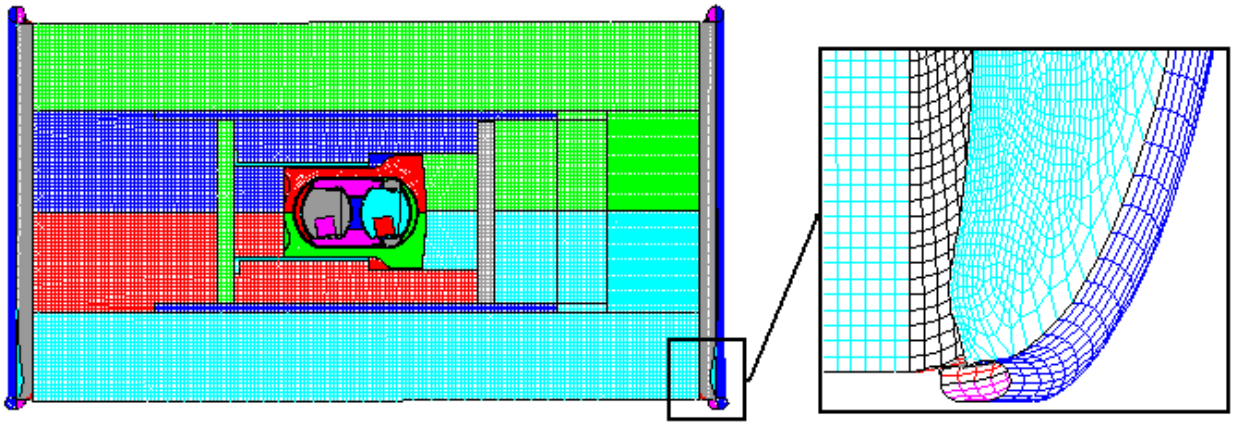

Figure 2-91. NCT SC-2 Side Impact with Support Structure Rotated 45° – Final Displacement

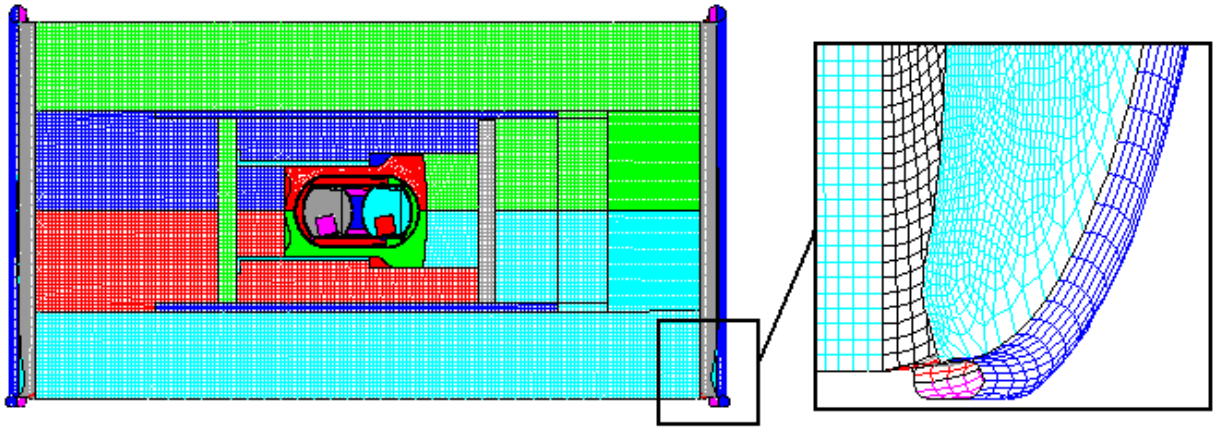

Figure 2-92. NCT SC-2 Side Impact with Support Structure Rotated 0° - Final Displacement

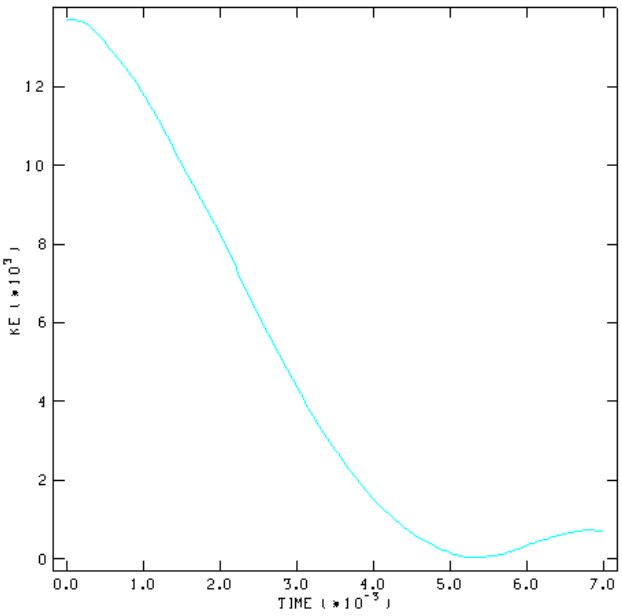

Figure 2-93. NCT SC-1 Side Impact with Support Structure Rotated 45° - Kinetic Energy Time History

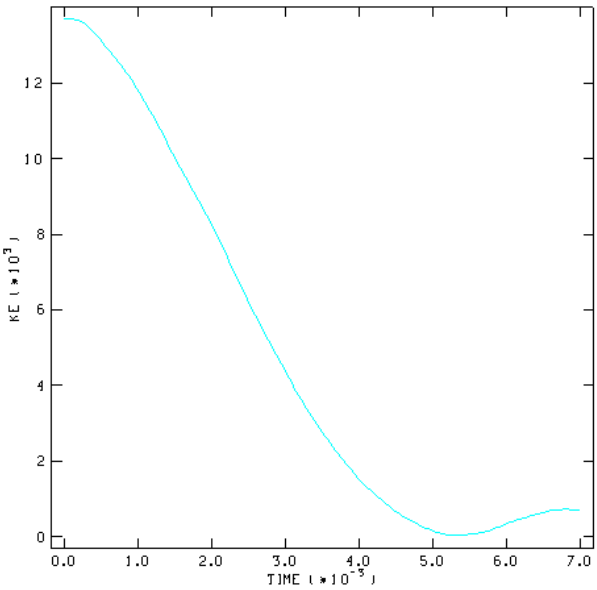

Figure 2-94. NCT SC-2 Side Impact with Support Structure Rotated 45° - Kinetic Energy Time History

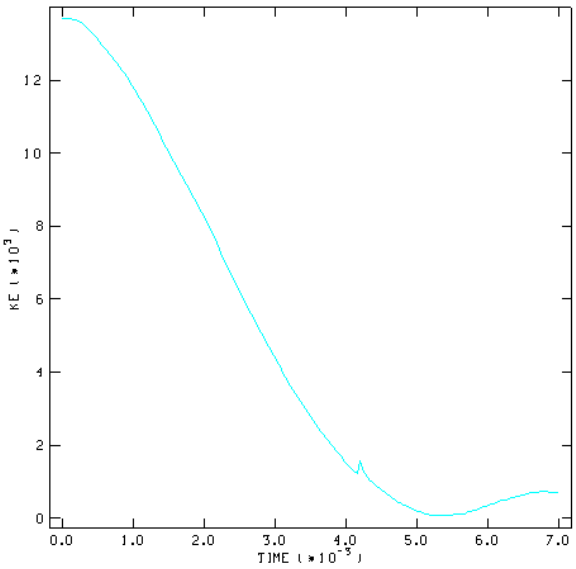

Figure 2-95. NCT SC-1 Side Impact with Support Structure Rotated 0° – Kinetic Energy Time History

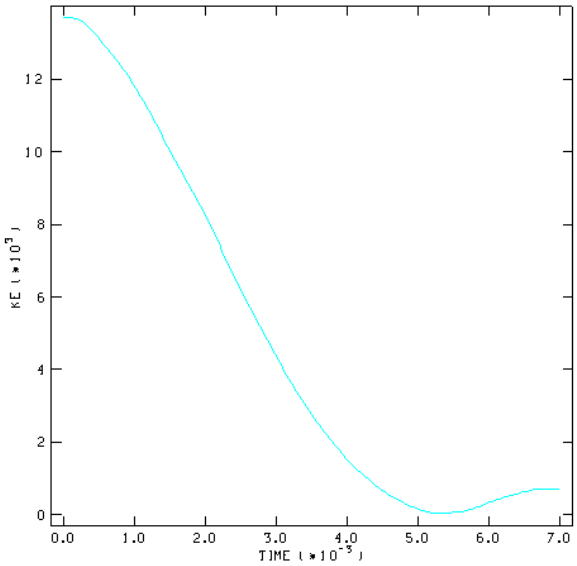

Figure 2-96. NCT SC-2 Side Impact with Support Structure Rotated 0° – Kinetic Energy Time History

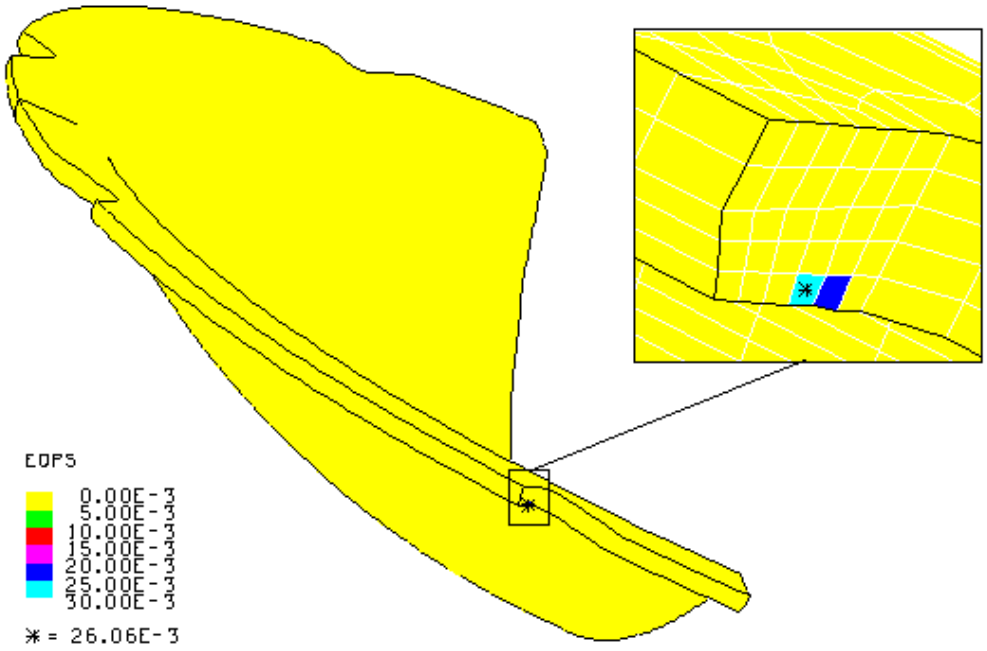

Figure 2-97. NCT SC-1 Side Impact with Support Structure Rotated 45° – EQPS in Bottom Dish

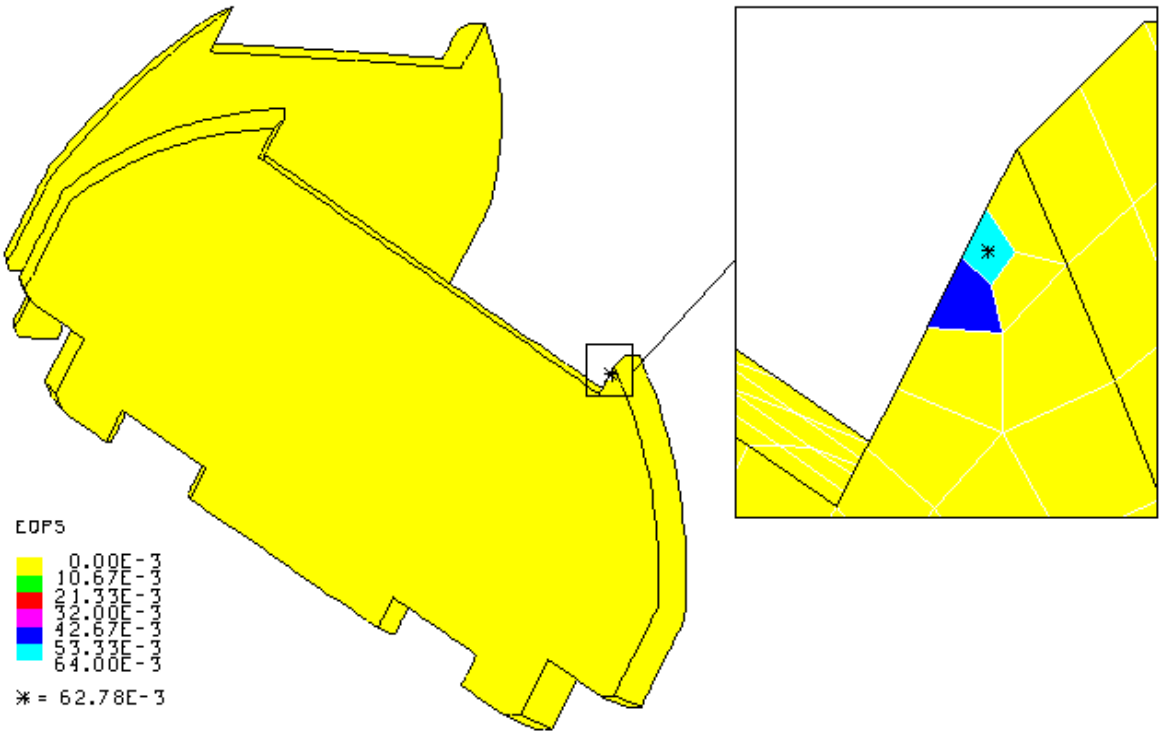

Figure 2-98. NCT SC-1 Side Impact with Support Structure Rotated 45° – EQPS in Top Legs

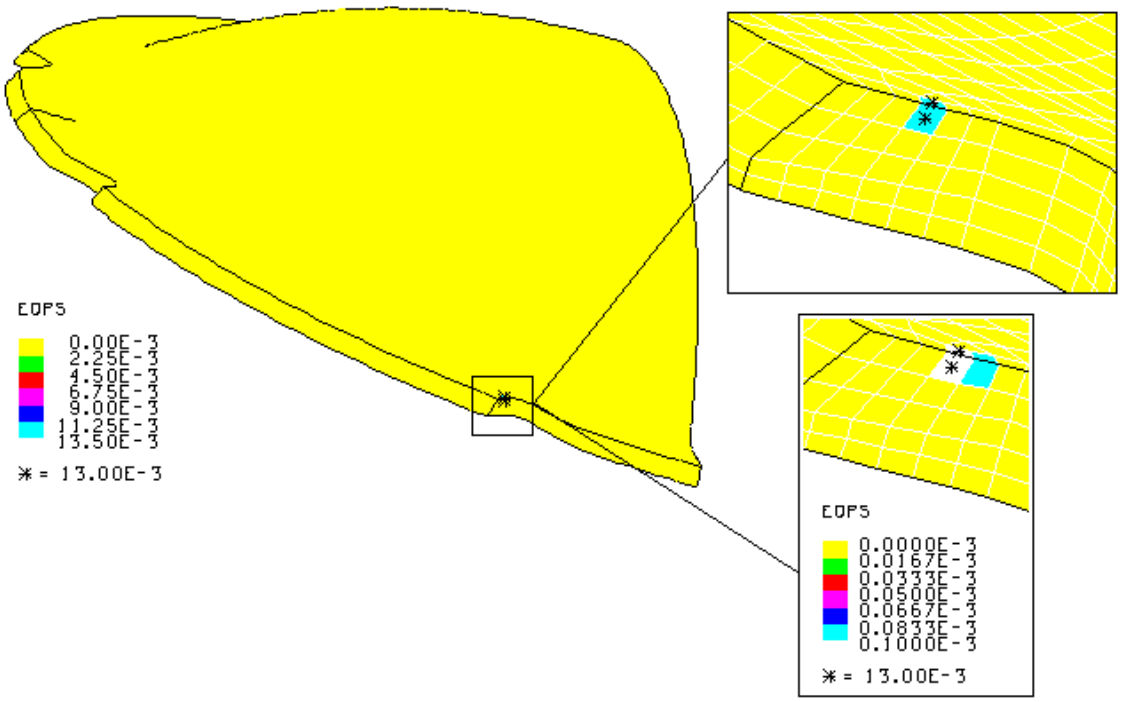

Figure 2-99. NCT SC-1 Side Impact with Support Structure Rotated 45° – EQPS in Top Dish

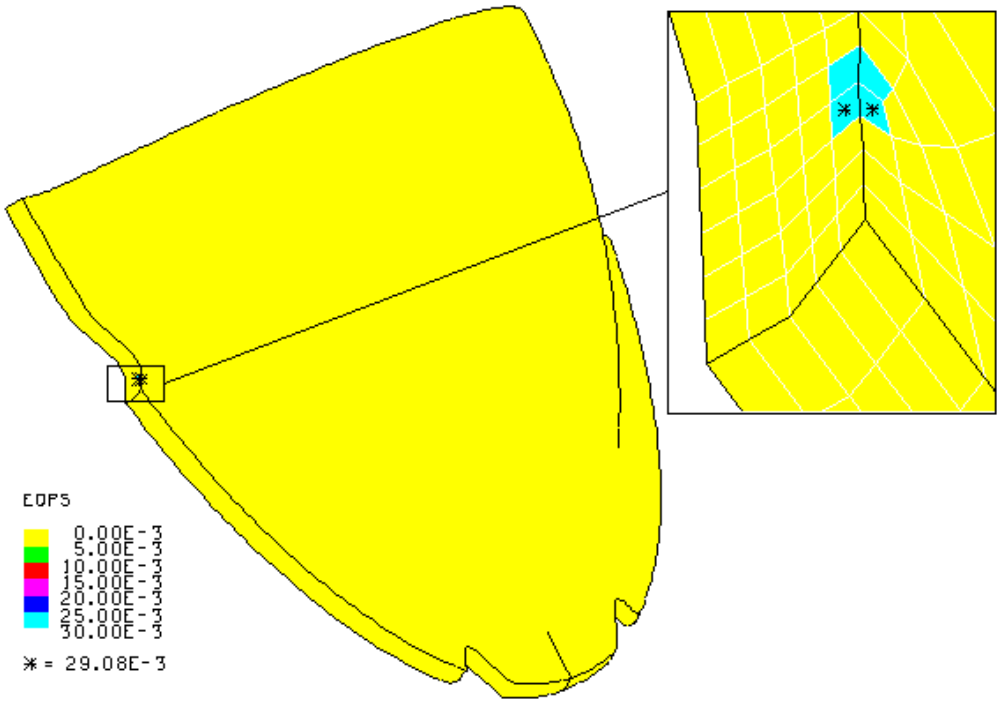

Figure 2-100. NCT SC-2 Side Impact with Support Structure Rotated 45° – EQPS in Bottom Dish

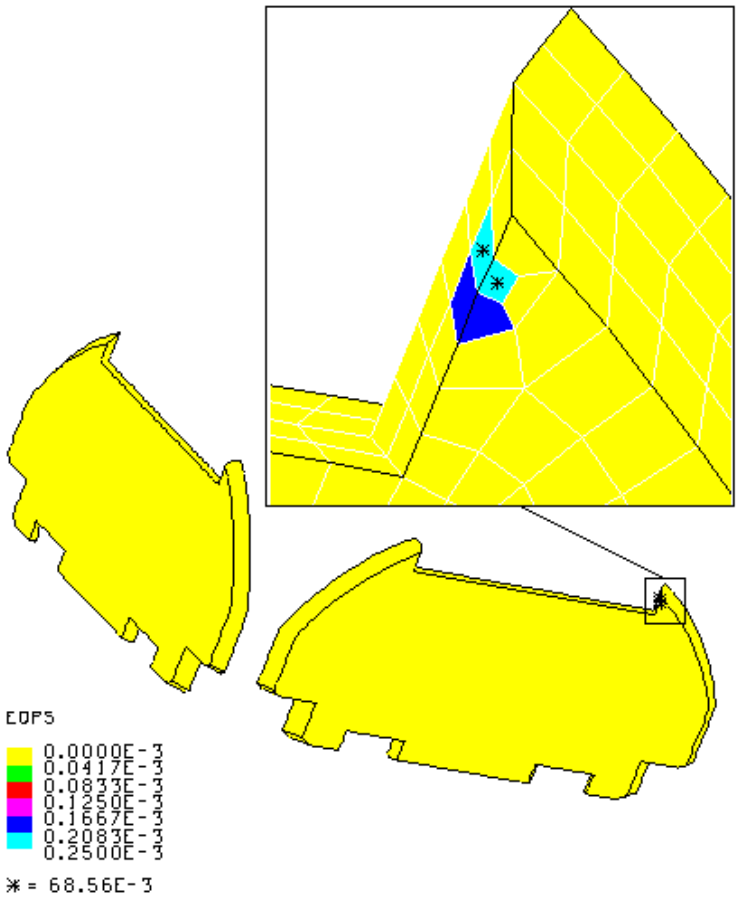

Figure 2-101. NCT SC-2 Side Impact with Support Structure Rotated 45° – EQPS in Top Legs

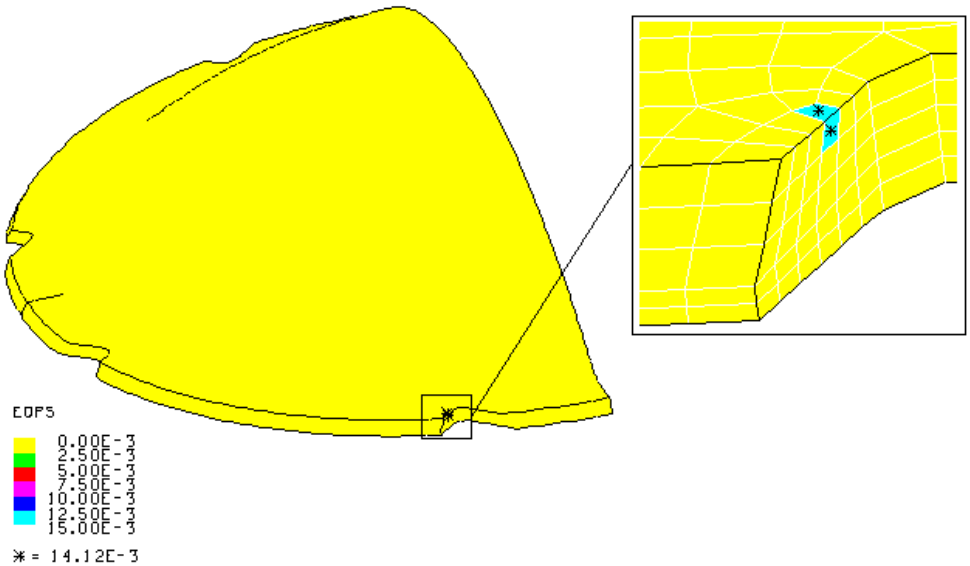

Figure 2-102. NCT SC-2 Side Impact with Support Structure Rotated 45° – EQPS in Top Dish

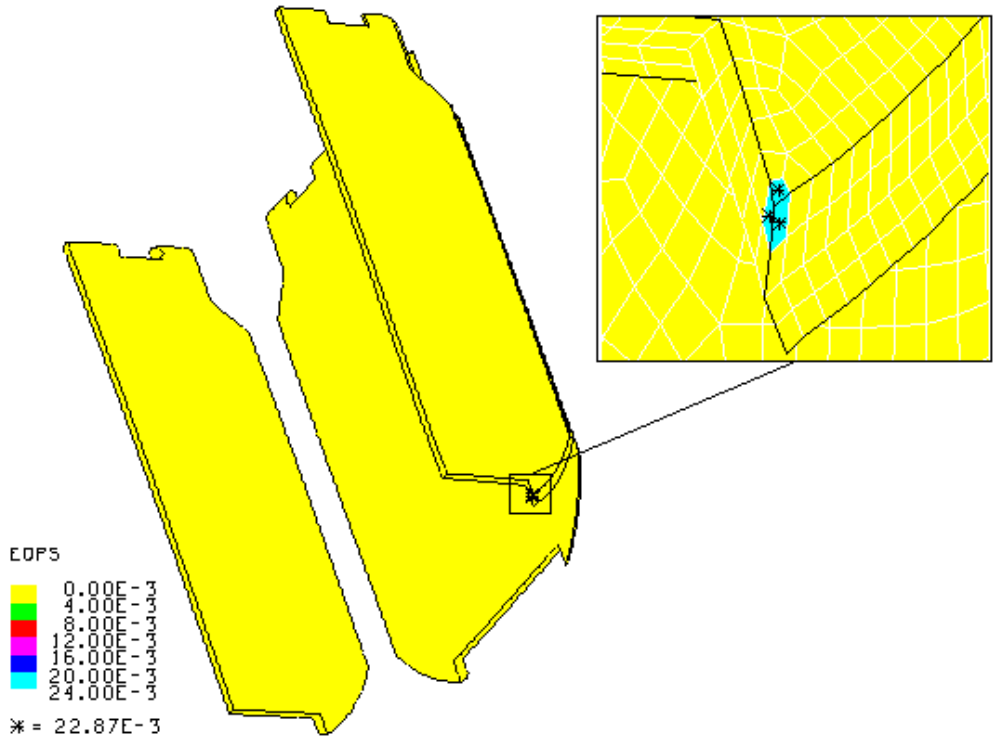

Figure 2-103. NCT SC-1 Side Impact with Support Structure Rotated 0° – EQPS in Bottom Legs

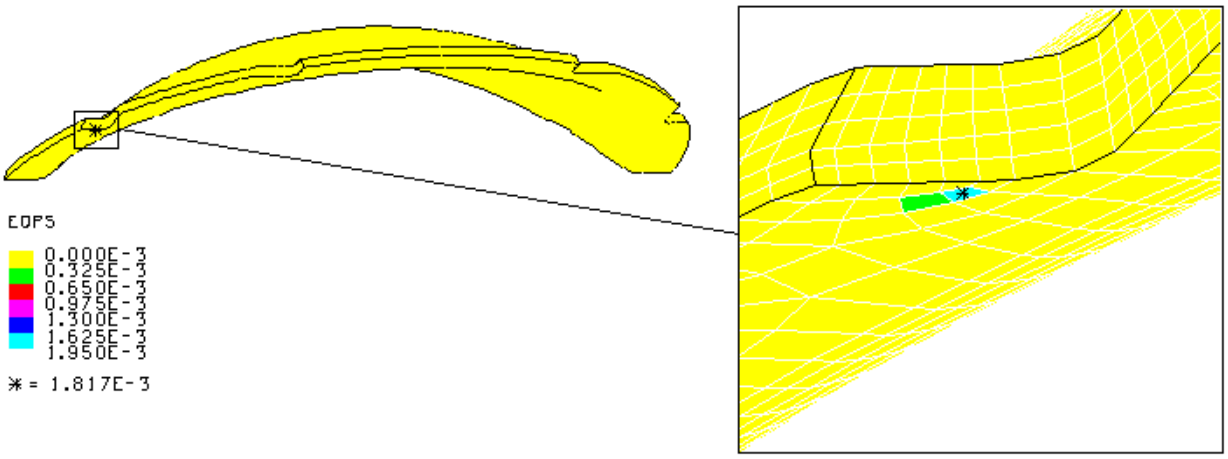

Figure 2-104. NCT SC-1 Side Impact with Support Structure Rotated 0° – EQPS in Top Dish

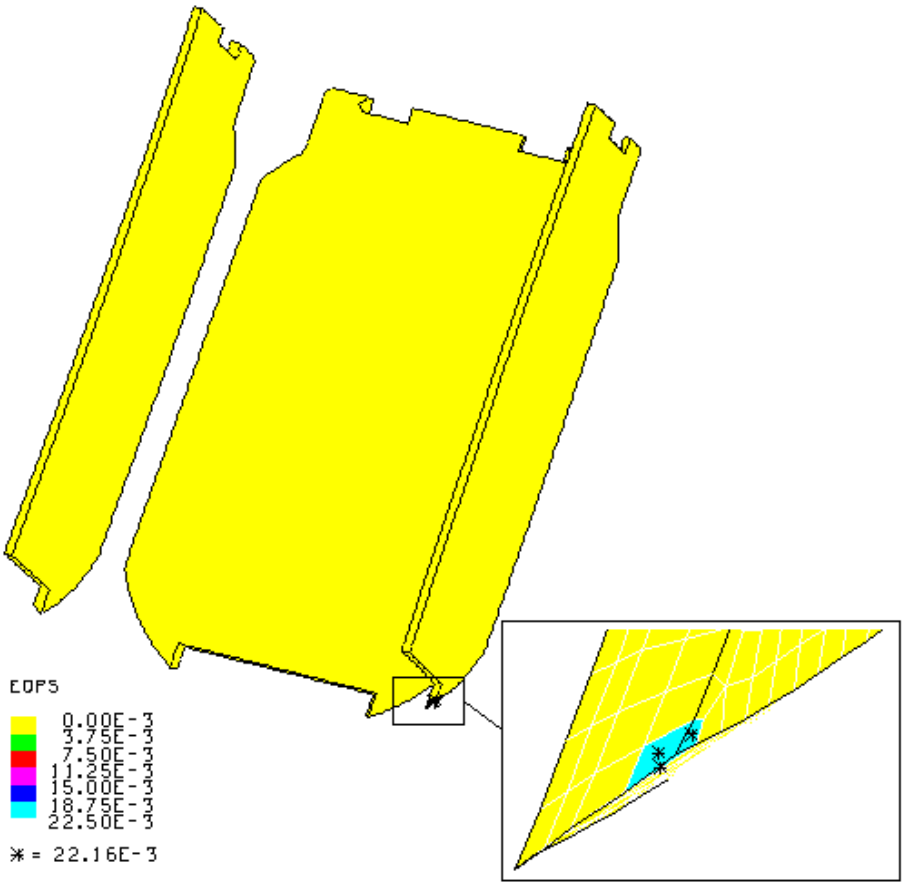

Figure 2-105. NCT SC-2 Side Impact with Support Structure Rotated 0° – EQPS in Bottom Legs

Table 2-17. Maximum Strains in 4 ft Side Drop Models

Model/Part	EQPS
SC-1 45° Side Impact	
Bottom Dish	2.61e-2
Upper Legs	6.28e-2
Upper Dish	1.30e-2
SC-2 45° Side Impact	
Bottom Dish	2.91e-2
Upper Legs	6.86e-2
Upper Dish	1.41e-2
SC-1 0° Side Impact	
Bottom Legs	2.29e-2
Upper Dish	1.82e-3
SC-2 0° Side Impact	
Bottom Legs	2.22e-2

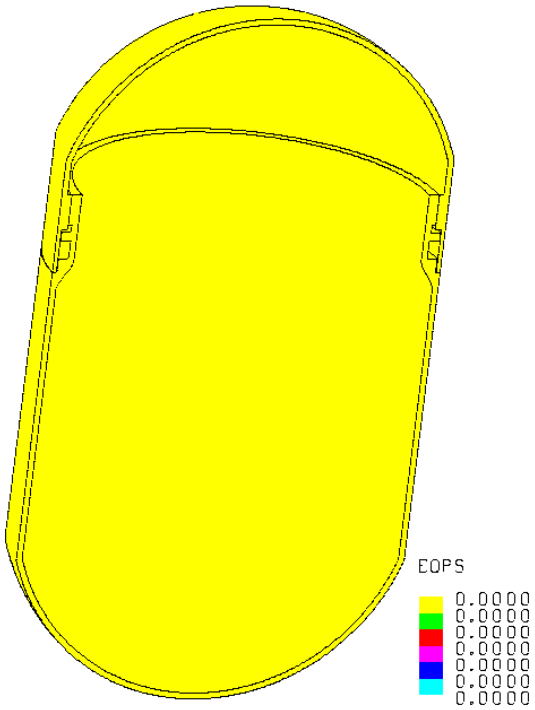

Figure 2-106. NCT SC-2 Side Impact with Support Structure Rotated 45° - EQPS in T-Ampoule

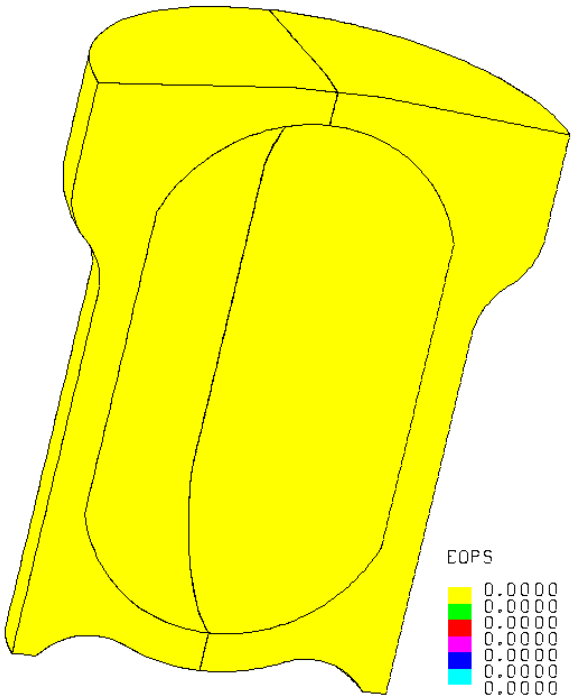

Figure 2-107. NCT SC-2 Side Impact with Support Structure Rotated 45° - EQPS in TB-1

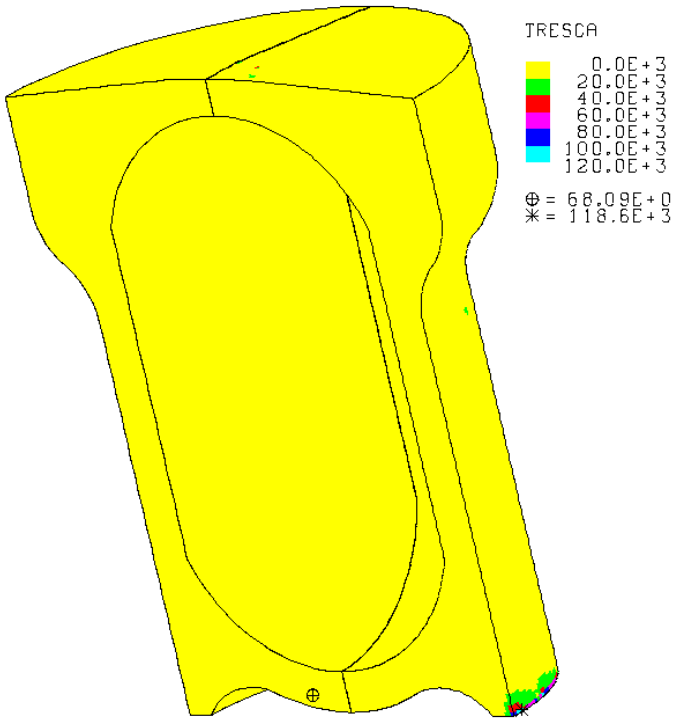

Figure 2-108. NCT SC-2 Side Impact with Support Structure Rotated 45° - Tresca Stress in TB-1

2.12.5.3.1 NCT End and Side Drop Analysis Summary

The two previous sections highlight the fact that the position of the contents within their sample containers and support cradle is essentially unchanged after 4-ft NCT drops. The titanium Inner Cradle remains essentially undeformed and the contents' positions no farther from the T-Ampoule than pre-drop, as well as no plasticity in the TB-1 and the T-Ampoule, all means that HAC and aircraft impact analyses are justified in assuming an undamaged PAT-1 package and contents before those events.

2.12.5.4 Aircraft Accident Impact Analyses

Detailed PAT-1 package models identical to those shown in the previous NCT section, except for neglecting the rolled ring lid ends, were analyzed to determine the response of the T-Ampoule and TB-1 when subjected to the loading of 10 CFR 71.74 (accident conditions for air transport of plutonium). Each combination of package orientation (lid end, side, and CG-over-corner) and contents was analyzed at an initial velocity of 422 ft/sec and each package impacts onto an analytically unyielding target.

The TB-1 was shown in the SAR[1] aircraft impact tests to remain elastic and maintain containment. With similar mass contents, similar TB-1 response would be expected, excepting the possibility of minor localized denting due to more dense contents (solid Pu vs. oxide powder). Effective or von Mises stresses (which capture three-dimensional stress states well and is more conservative than Tresca stress to show avoidance of yielding) were calculated and an acceptance criterion of "below through-thickness yielding" used to demonstrate similar TB-1

behavior as in the original regulatory testing. This also means zero plasticity in the seal area of the TB-1, ensuring similar containment requirements performance of the containment vessel.

A total of twenty-seven high speed impact analyses were conducted for the five potential contents in various orientations; the analyses are listed below in Table 2-18. In the hollow-cylinder (ER cylinder) component models, as well as the sample container models, no credit is taken for the positioning of the cylinders with the tantalum packing foil. Each form contents are assumed to be unconstrained and are placed in the worst orientation and most severe location for each impact. The delta-plutonium in the sample containers is relatively soft and has a greater degree of plasticity, so although its location will affect T-Ampoule loading, its local orientation would not. However, the beryllium composite cylinders are much harder and stronger, so their orientation is always rotated such that they present a sharp corner (CGOC, actually) towards the normal surface of the T-Ampoule, parallel with the impact direction.

Table 2-18. Aircraft Accident Impact Analyses, Components, and Orientations

Run No.	Component	Submodel Orientation
1	831 g Plutonium Metal Hollow Cylinder, alpha Pu	Bottom position, top impact
2	831 g Plutonium Metal Hollow Cylinder, alpha Pu	Bottom position (angled), top impact
3	831 g Plutonium Metal Hollow Cylinder, alpha Pu	Bottom position (angled), CGOC impact
4	831 g Plutonium Metal Hollow Cylinder, alpha Pu	Far side position, side impact
5	831 g Plutonium Metal Hollow Cylinder, alpha Pu	Far side position (angled), side impact
6	731 g Plutonium Metal Hollow Cylinder, alpha Pu	Bottom position, top impact
7	731 g Plutonium Metal Hollow Cylinder, alpha Pu	Bottom position (angled), top impact
8	731 g Plutonium Metal Hollow Cylinder, alpha Pu	Bottom position (angled), CGOC impact
9	731 g Plutonium Metal Hollow Cylinder, alpha Pu	Far side position, side impact
10	731 g Plutonium Metal Hollow Cylinder, alpha Pu	Far side position (angled), side impact
11	SC-1 – Pu	Bottom position, support structure 0°, top impact
12	SC-1 – Pu	Far side position, support structure 0°,side impact
13	SC-1 – Pu	Far side position, support structure 45°, side impact
14	SC-1 – Pu	Bottom position, support structure 0°, CGOC impact
15	SC-1 – Pu	Bottom position, support structure 45°, CGOC impact

Table 2-18. Aircraft Accident Impact Analyses, Components, and Orientations (Continued)

Run No.	Component	Submodel Orientation
16	SC-2 – Pu	Bottom position, support structure 0°, top impact
17	SC-2 – Pu	Far side position, support structure 0°,side impact
18	SC-2 – Pu	Far side position, support structure 45°, side impact
19	SC-2 – Pu	Bottom position, support structure 0°, CGOC impact
20	SC-2 – Pu	Bottom position, support structure 45°, CGOC impact
21	SC-1 – Be	Bottom position, angled Be, support structure 0°, top impact
22	SC-1 – Be	Far side position, angled Be, support structure 0°, side impact
23	SC-1 – Be	Far side position, angled Be, support structure 45°, side impact
24	SC-1 – Be	Bottom position, angled Be, support structure 0°, CGOC impact
25	SC-1 – Be	Bottom position, angled Be, support structure 45°, CGOC impact
26	SC-2 – Pu	Far side position, support structure 45°, side impact, friction 0.4
27	SC-2 – Pu	Far side position, support structure 45°, side impact, friction 0.2

2.12.5.4.1 ER Cylinder Analyses

Ten separate plutonium metal hollow cylinder, high-speed impact analyses were conducted. There are several inherent conservatisms in this model:

1. The tantalum foil used to package the plutonium metal hollow cylinders inside the T-Ampoule is not modeled. The small quantity of energy it would absorb, and load spreading it would provide, is conservatively ignored. In addition, any initial positioning that would be provided by the foil is also ignored. Each analysis is run with the plutonium metal hollow cylinder in a location farthest from the impact surface.

2. The Pu material is modeled using a power-law hardening constitutive model without fracture. Hecker and Stevens[3] present two curves for alpha-plutonium; one curve depicts a very brittle material, and the other represents a finer-grain material with more ductility. To maximize the energy and impulse load applied to the T-Ampoule wall, the plutonium metal was modeled as a continuously hardening material that does not fracture, which is extremely conservative in terms of the reaction loading of the T-Ampoule. This conservatism (stronger alpha material, continuously hardening) allows for the possibility that the cylinder could also consist of delta Pu, if transport of that material were desired instead.

3. The dimensions of the plutonium metal hollow cylinders are conservatively assumed to be the "strongest" possible. Within the bounds of LANL-defined tolerances of machining these cylinders, they are the most resistant to buckling (shortest, thickest wall,

maximum OD and minimum ID, see Figures 2-70and 2-71), which allows for the greatest loading of the T-Ampoule.

2.12.5.4.2 Run 1 - 831-g Plutonium Metal Hollow Cylinder with Bottom Initial Location and a Top Impact

The top end impact model for the plutonium metal hollow cylinder, oriented axially (with the impact direction, as opposed to angled) is shown in Figure 2-109. Note that the cylinder is located at the bottom of the T-Ampoule so that its net impact velocity with the top of the T-Ampoule is maximized. The post-impact deformation is shown in Figure 2-110 and its kinetic energy history in Figure 2-111. Note the similar degree of overpack crush up as compared to the certification test end impact analysis in Figure 2-12, despite the slightly reduced impact velocity of 422 ft/sec versus the tested 445 ft/sec. The plutonium metal hollow cylinder exhibits significant buckling, despite its conservatively "strongest shape" definition.

Equivalent Plastic Strain (EQPS) in the TB-1 vessel is shown in Figures 2-112 and 2-113 to be less than 2.3%, and only in some localized outer contact regions with the redwood overpack. This localized ring of plasticity in the top outer surface of the TB-1 lid is due to a minor contact over closure between the TB-1 and the redwood; it is only a minor modeling artifact. This minor modeling artifact is not a concern because even though it produces elevated localized stresses and even miniscule plasticity, it does not increase through-thickness stresses or in any way negatively affect the integrity of the containment vessel. The von Mises stresses (see Figures 2-114 and 2-115) peak at 147.5 ksi, just above the elevated-temperature minimum yield strength for the TB-1 of 141 ksi, but more importantly, through-thickness TB-1 stress values are in the less-than-50 ksi range, below yield. The time at which the peak value of the von Mises stress occurs coincides with the peak value of the contact force (summed over the lid area). A plot of this force as a function of time is shown in Figure 2-116. A maximum contact load of 66,000 lbs is applied to the inner surface of the TB-1 lid during the impact, which is below the 108,000 lb preload in the bolts. No T-Ampoule elements exceeded the tested B-W strain locus, and the peak Tearing Parameter value (see Table 2-11, High Velocity (Aircraft) Impact Analyses Peak Tearing Parameter Values, run #1) of 0.0528 was below the critical Tearing Parameter value of 1.012 for Ti-6Al-4V.

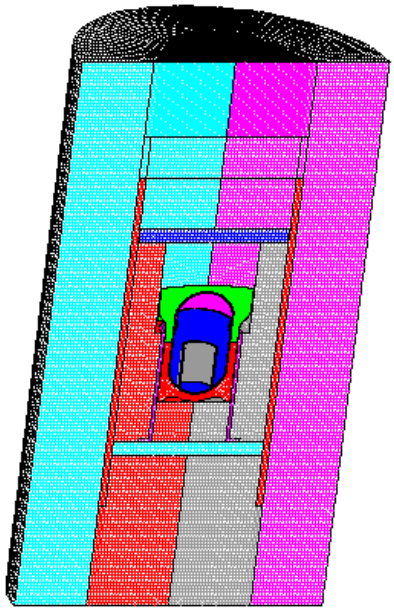

Figure 2-109. Finite Element Mesh for the 831-g, Plutonium Metal Hollow Cylinder, Bottom Position, End Impact

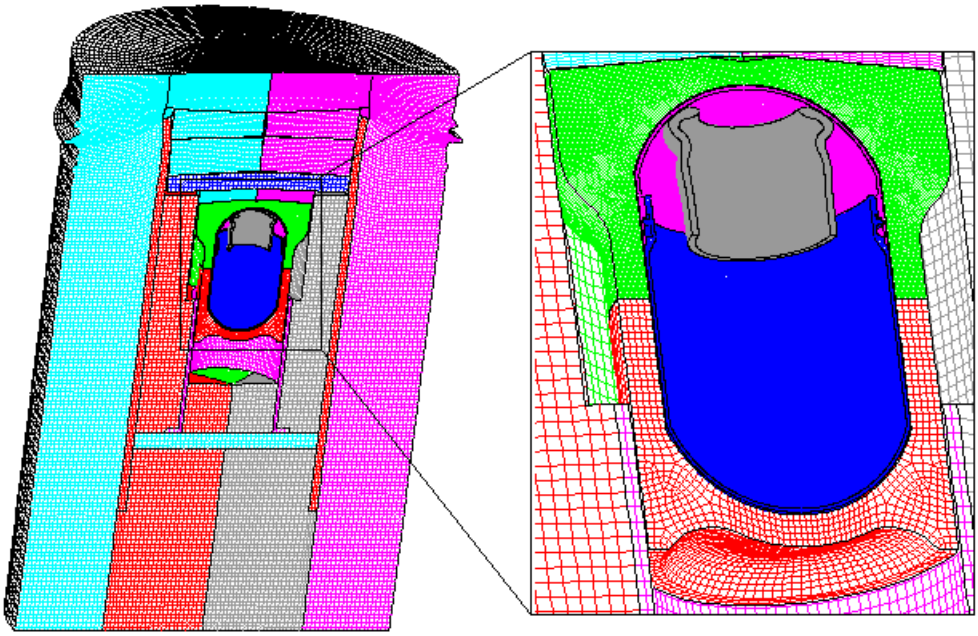

Figure 2-110. Finite Element Mesh for the 831-g, Plutonium Metal Hollow Cylinder, Bottom Position, End Impact – Final Displacement

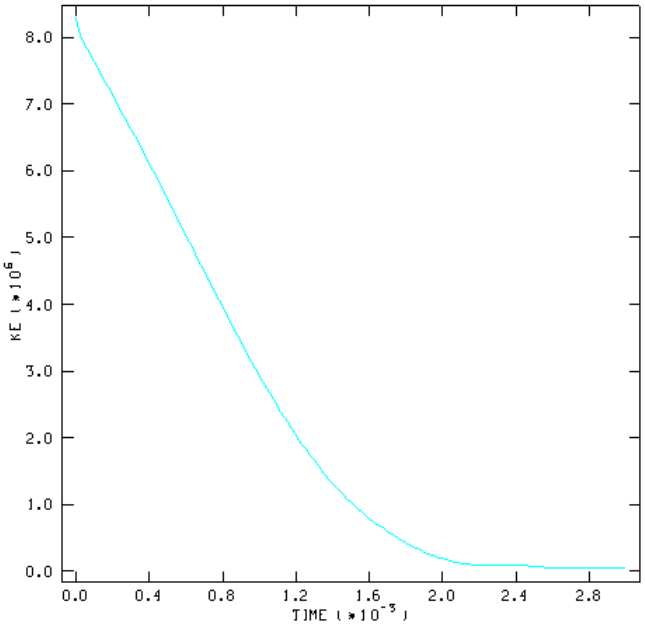

Figure 2-111. Kinetic Energy Time History for the 831-g, ER Cylinder, Bottom Position, End Impact

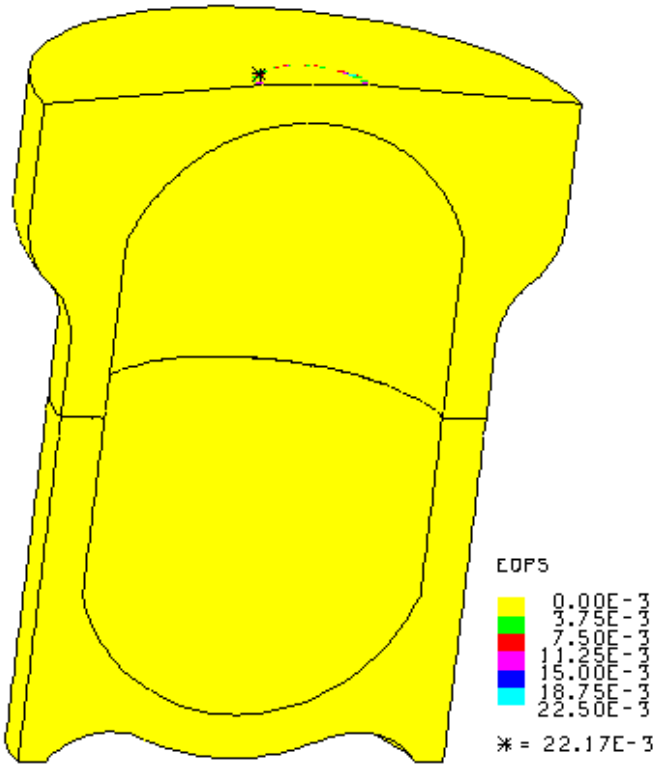

Figure 2-112. EQPS in the TB-1 for the 831-g, ER Cylinder, Bottom Position, End Impact

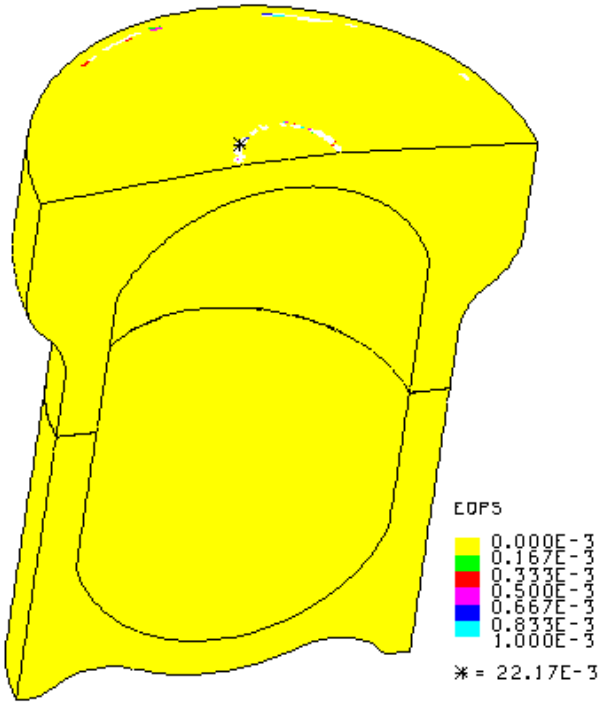

Figure 2-113. EQPS in TB-1 (Range Zoomed in to Show All Elements with non-zero EQPS) for the 831-g, Hollow Cylinder, Bottom Position, End Impact

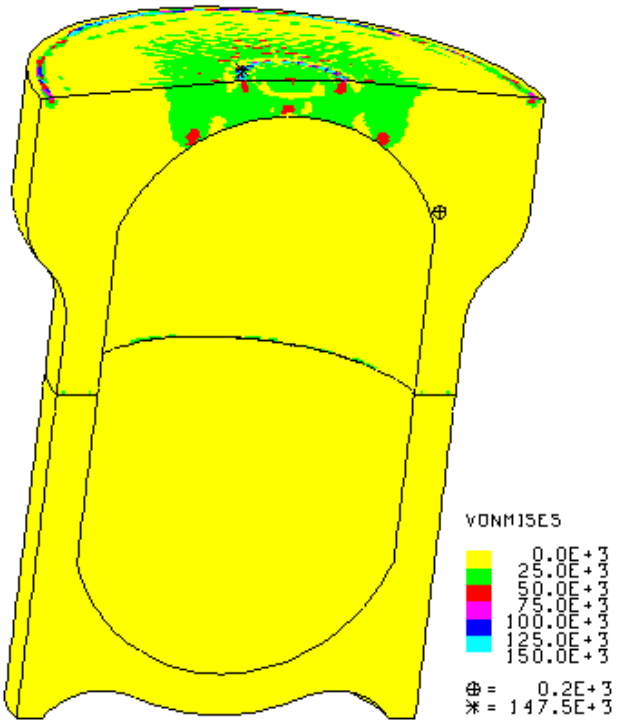

Figure 2-114. von Mises Stress in the TB-1 for the 831-g Plutonium Metal Hollow Cylinder, Bottom Position, End Impact (Rotated Forward for Ease of Viewing)

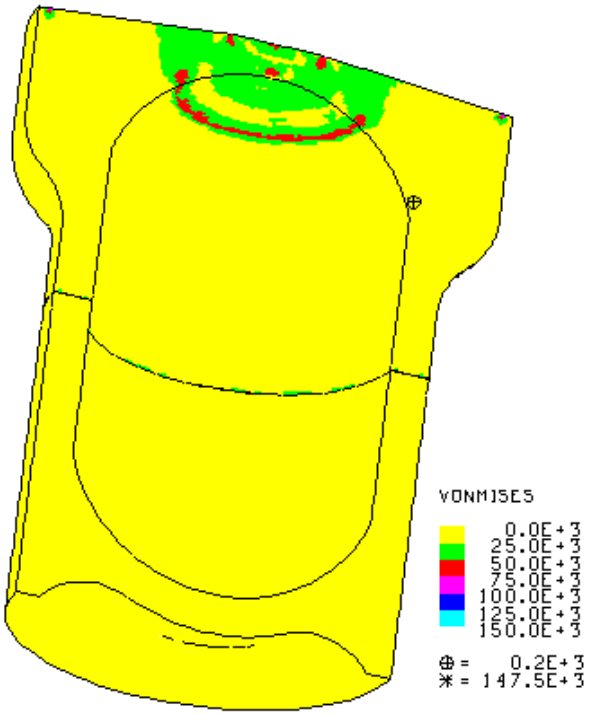

Figure 2-115. von Mises Stress in the TB-1 for the 831-g, Plutonium Metal Hollow Cylinder, Bottom Position, End Impact (Rotated Backward for Ease of Viewing)

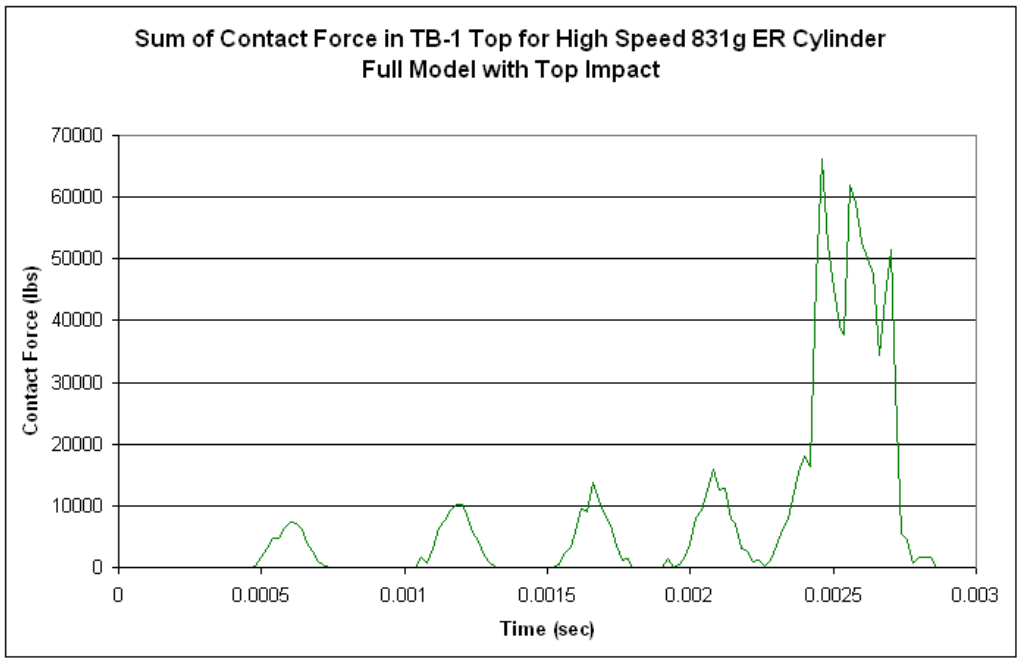

Figure 2-116. Summed Contact Force on the TB-1 Top for a 831-g, Plutonium Metal Hollow Cylinder, Top Impact

2.12.5.4.3 Run 2 - 831-g Angled Cylinder with Bottom Initial Location and a Top Impact

The top end impact model for the plutonium metal hollow cylinder with angled orientation is shown in Figure 2-117. The cylinder is located at the bottom of the T-Ampoule so that its net impact velocity with the top of the T-Ampoule is maximized. The post-impact deformation is shown in Figure 2-118 and its kinetic energy history in Figure 2-119. The plutonium metal hollow cylinder deforms but maintains much of its original shape because of its conservatively assumed "infinitely ductile," with hardening material constitutive model definition (despite its alpha Pu being a relatively brittle material in reality). If the plutonium metal hollow cylinder were modeled as a brittle material with very low ductility, it would effectively shatter and present a much less concentrated load on the T-Ampoule and TB-1.

Average stress-triaxiality versus EQPS is shown in Figures 2-120 and 2-121 for the 19 elements extending beyond the tested Bao-Wierzbicki strain locus. All of these elements are at high stress triaxiality and low EQPS. The Tearing Parameter values for these same 19 elements are shown in Figure 2-122, and all are below the critical Tearing Parameter value of 1.012 for Ti-6Al-4V. These elements are highlighted in red Figure 2-123, but note that these elements are still below even the initiation of a ductile tear.

Peak EQPS in the TB-1 vessel is shown in Figures 2-124 and 2-125 to be about 2.4%, and only in some localized outer contact regions with the redwood overpack (contact modeling artifact). The von Mises stresses (see Figures 2-126 and 2-127) peak at 148.2 ksi, just above the elevated-temperature minimum yield strength for the TB-1 of 141 ksi, but more importantly, through-thickness TB-1 stress values are less than 50 ksi, below yield. The time at which the peak value of the von Mises stress occurs coincides with the peak value of the contact force (summed over the lid area). A plot of this force as a function of time is shown in Figure 2-128. A maximum contact load of 54,509 lbs is applied to the inner surface of the TB-1 lid during the impact.

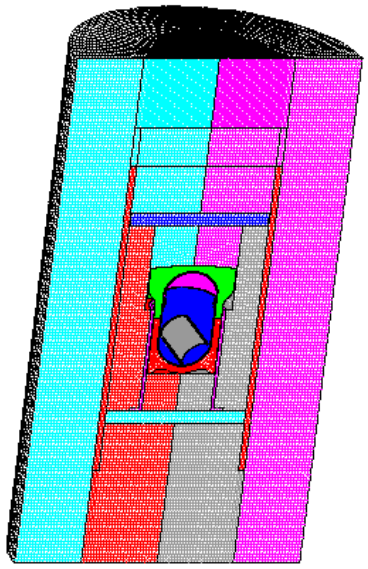

Figure 2-117. Finite Element Mesh for the 831-g, Angled, ER Cylinder, Bottom Position, End Impact

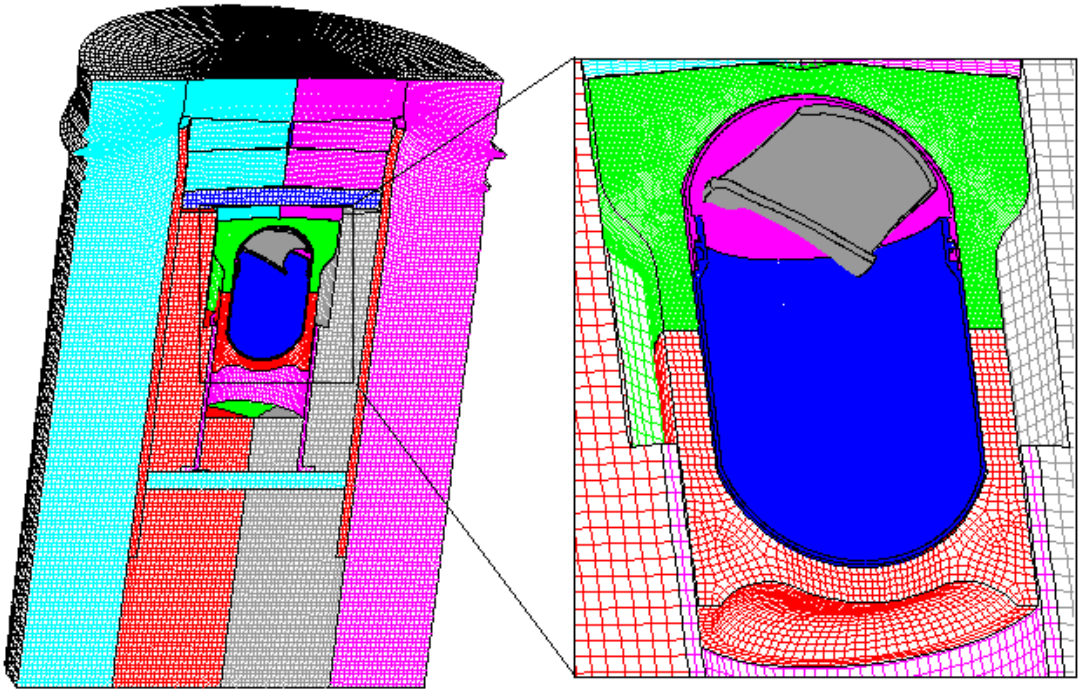

Figure 2-118. Finite Element Mesh for the 831-g, Angled, ER, Cylinder, Bottom Position, End Impact – Final Displacement

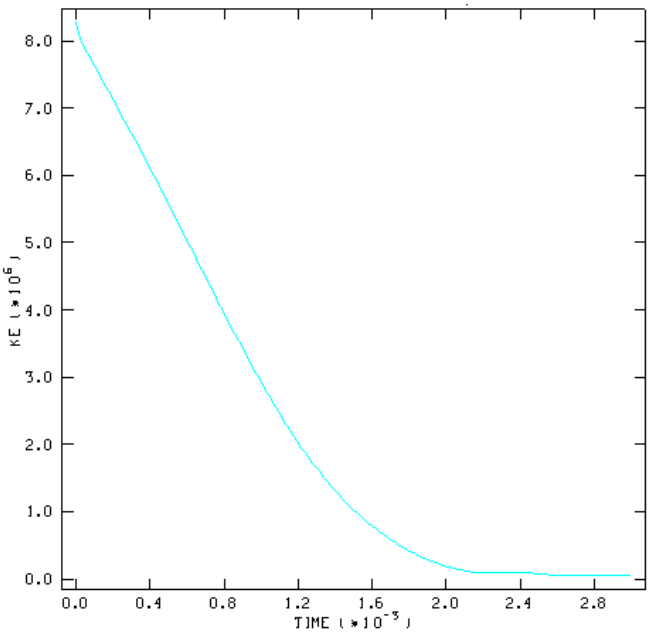

Figure 2-119. Kinetic Energy Time History for the 831-g, Angled, Plutonium Metal Hollow Cylinder, Bottom Position, End Impact

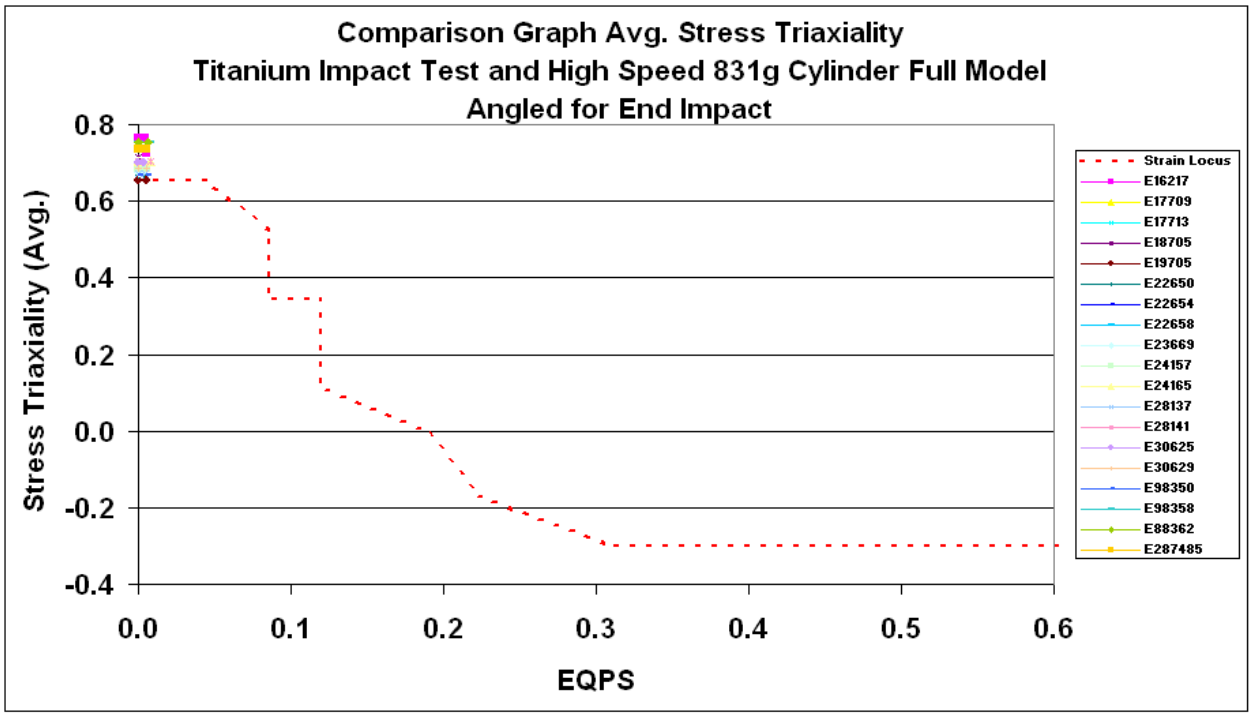

Figure 2-120. Graph of Average Stress Triaxiality versus EQPS of Elements Exceeding the Experimental Strain Locus for the 831-g, Angled, Plutonium Metal Hollow Cylinder, Bottom Position, End Impact

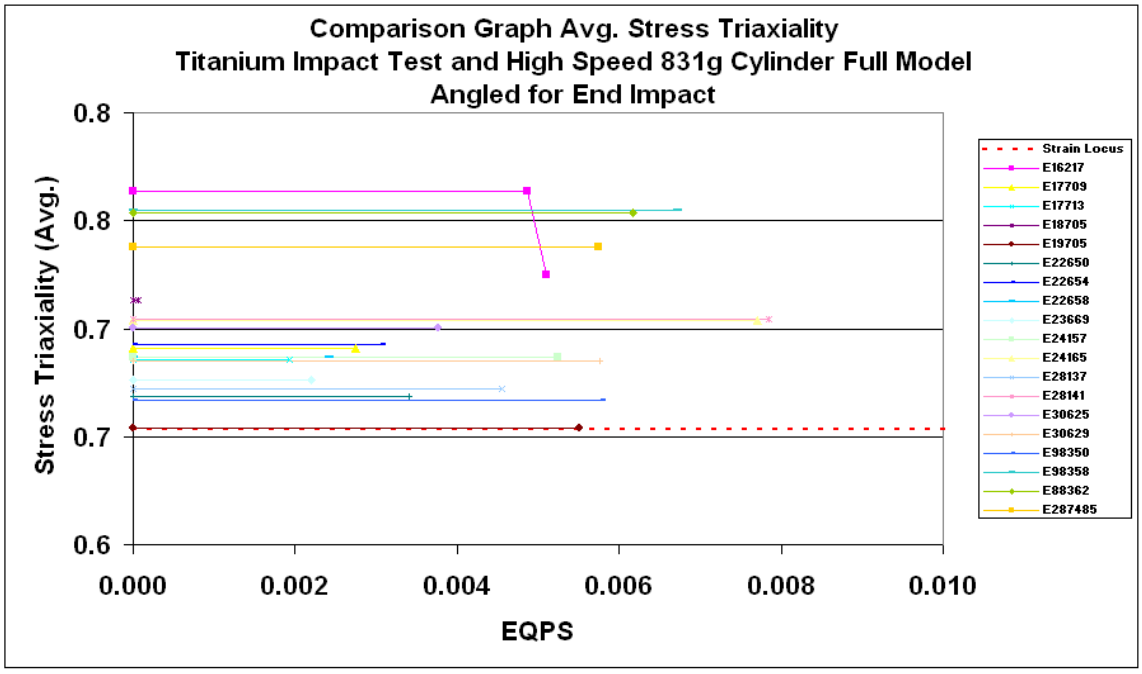

Figure 2-121. Graph of Average Stress Triaxiality versus EQPS of Elements Exceeding the Experimental Strain Locus (Zoomed In) for the 831-g, Angled, Plutonium Metal Hollow Cylinder, Bottom Position, End Impact

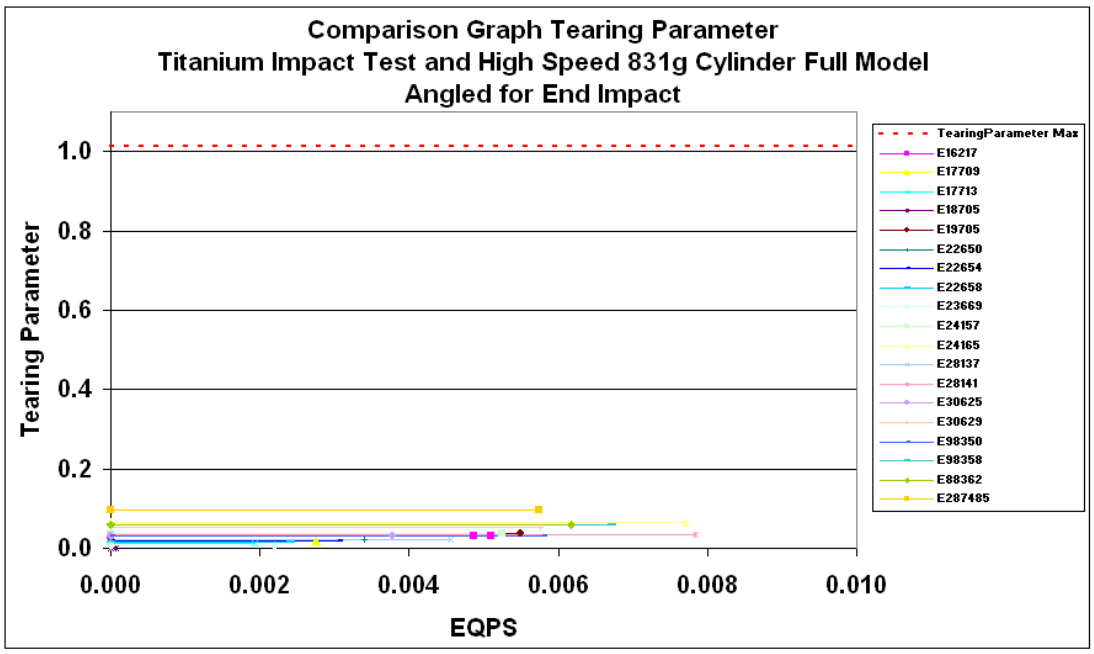

Figure 2-122. Graph of Tearing Parameter versus EQPS for Elements Exceeding the Experimental Strain Locus for the 831-g, Angled, Plutonium Metal Hollow Cylinder, Bottom Position, End Impact

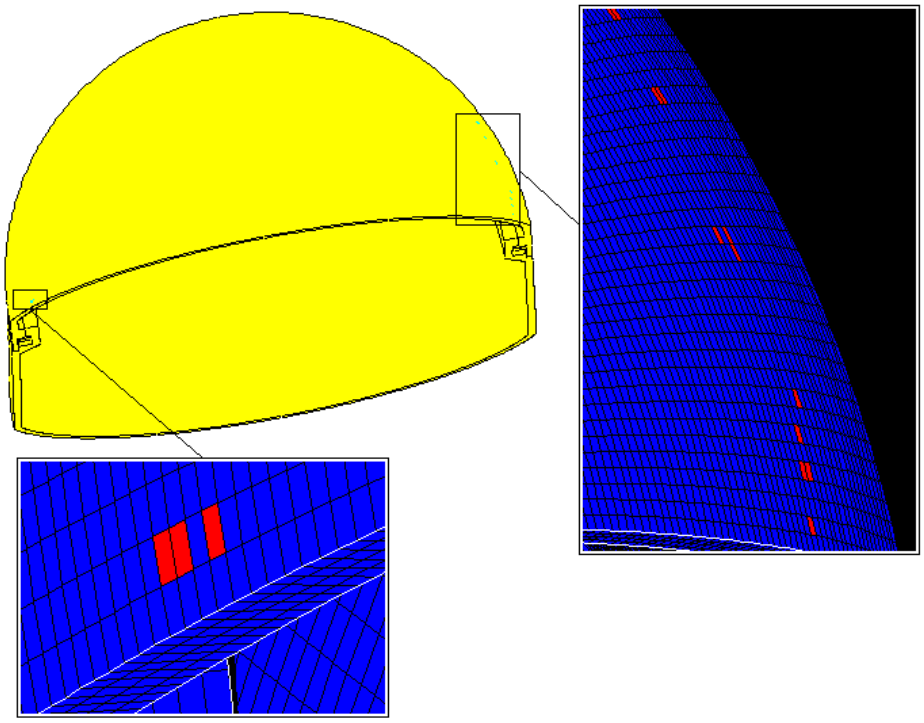

Figure 2-123. Plot of Elements Exceeding the Experimental Strain Locus for the 831-g, Angled, Plutonium Metal Hollow Cylinder, Bottom Position, End Impact

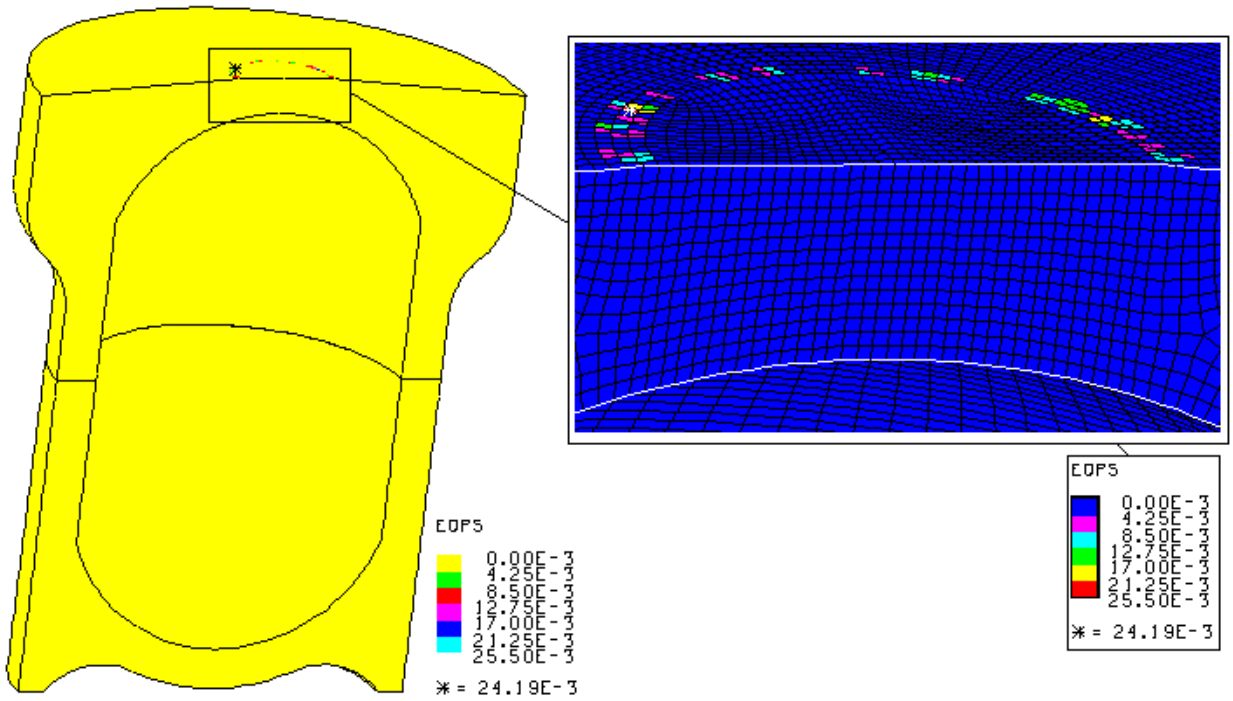

Figure 2-124. Plot of EQPS in the TB-1 for the 831-g Angled, ER, Cylinder, Bottom Position, End Impact

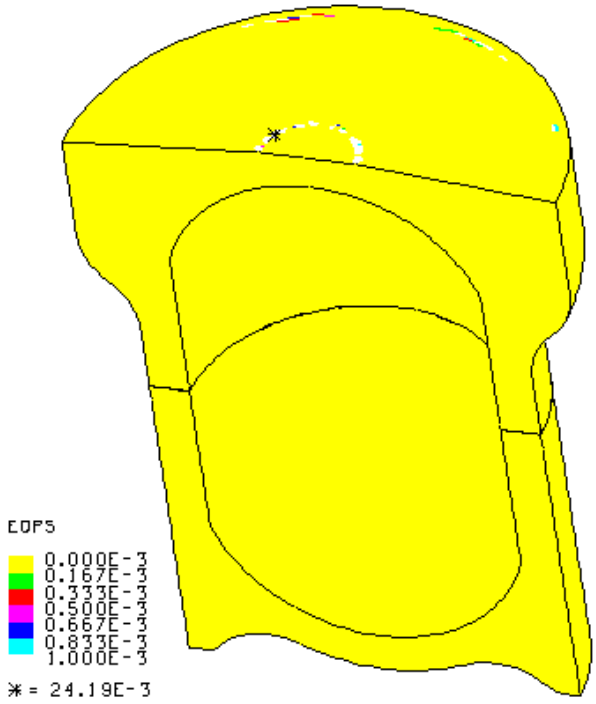

Figure 2-125. Plot of EQPS in the TB-1 (Range Zoomed in to Show all Elements with Non-Zero EQPS) for the 831-g, Angled, Plutonium Metal Hollow Cylinder, Bottom Position, End Impact

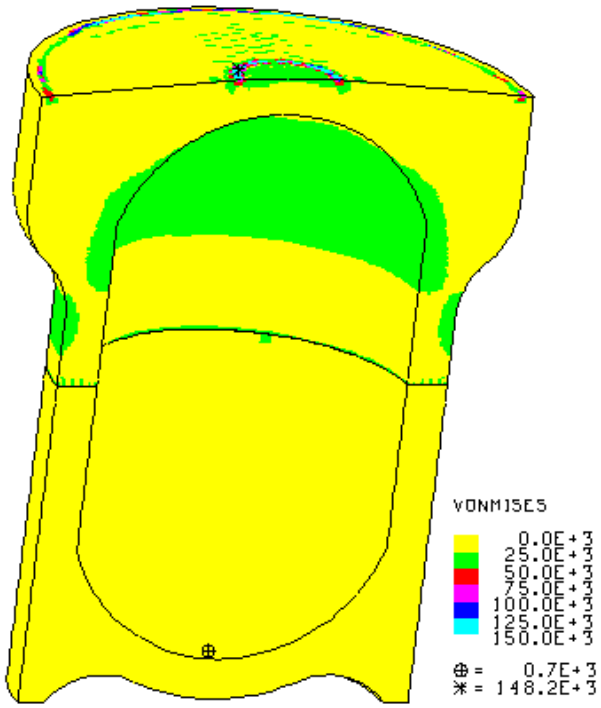

Figure 2-126. Plot of von Mises Stress in the TB-1 for the 831-g, Angled, Plutonium Metal Hollow Cylinder, Bottom Position, End Impact

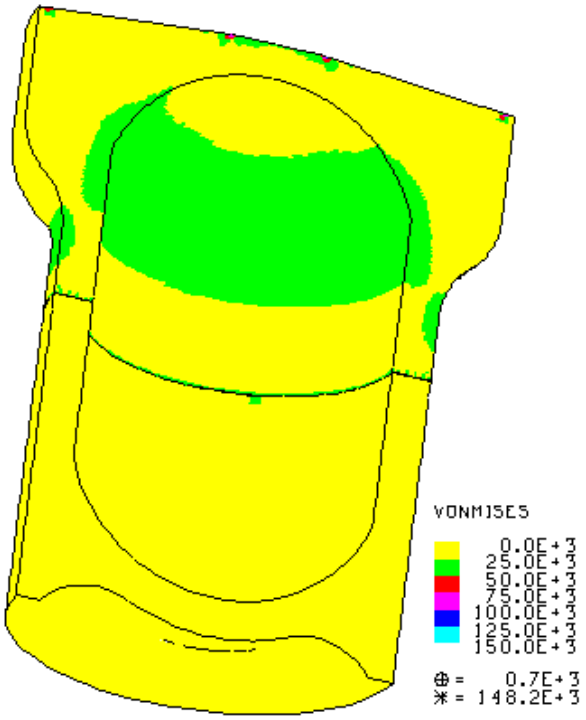

Figure 2-127. Plot of von Mises Stress in the TB-1 for the 831-g, Angled, Plutonium Metal Hollow Cylinder, Bottom Position, End Impact

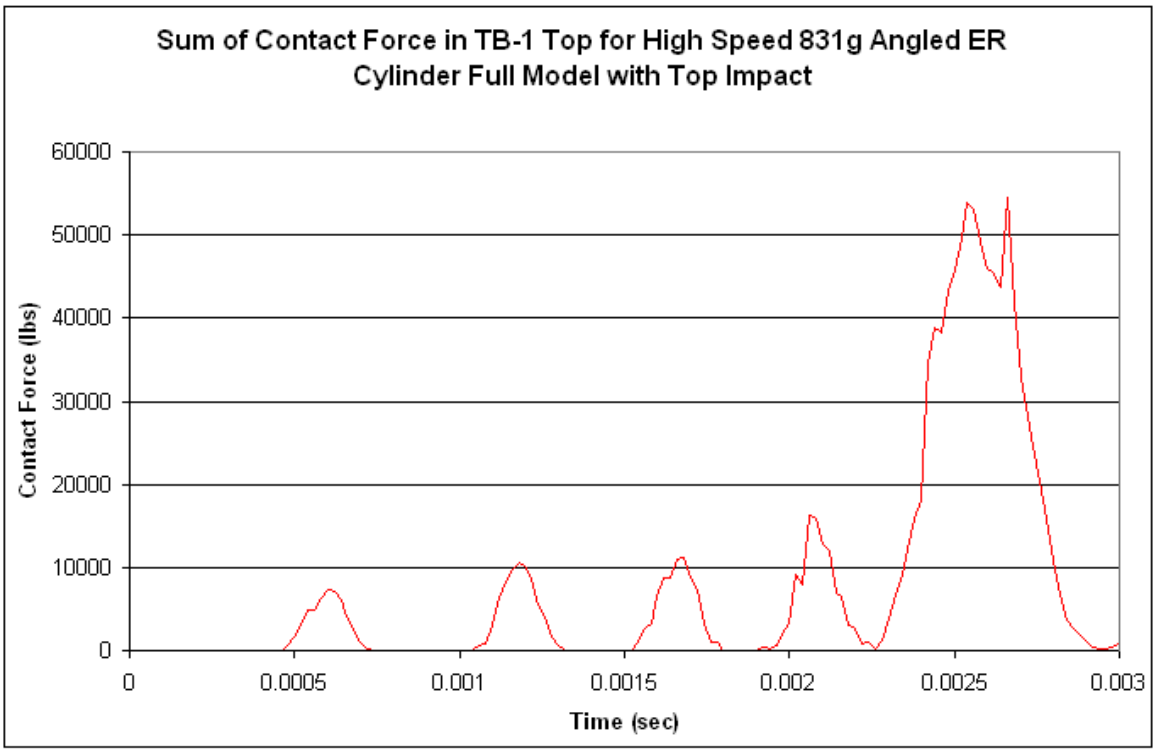

Figure 2-128. Plot of Contact Force in the TB-1 for the 831-g, Angled Plutonium Metal Hollow Cylinder, Bottom Position, End Impact

2.12.5.4.4 Run 3 – 831-g Angled Plutonium Metal Hollow Cylinder with Bottom Initial Location and a CGOC Impact

The lid end CG-over-corner impact model for the plutonium metal hollow cylinder is shown in Figure 2-129. The cylinder is located at the bottom of the T-Ampoule so that its net impact velocity with the top of the T-Ampoule is maximized. The post-impact deformation is shown in Figure 2-130 and its kinetic energy history in Figure 2-131. The plutonium metal hollow cylinder deforms slightly more than the previous case because of the slightly more side-impact-like orientation but maintains much of its original shape because of its conservatively "infinitely ductile" material constitutive model definition. If the plutonium metal hollow cylinder were modeled as a brittle material with very low ductility, it would effectively shatter and present a much less concentrated load on the T-Ampoule and TB-1.

Average stress-triaxiality versus EQPS is shown in Figures 2-132 and 2-133 for the 126 elements extending beyond the tested Bao-Wierzbicki strain locus. All of these elements are at relatively high stress triaxiality and low EQPS. The Tearing Parameter values for these same 126 elements are shown in Figure 2-134 and all are still safely below the critical Tearing Parameter value of 1.012 for Ti-6Al-4V. These elements are highlighted in red in Figures 2-135 through 2-137, but these elements are still below the critical value. Note that this impact analysis case produced the highest value of Tearing Parameter, 0.6177, which still yields a minimum factor of safety of 1.012 divided by 0.6177 equals 1.64 against even the initiation of a ductile tear. With all the analysis conservatisms in the model, the factor of safety is greater, and the T-Ampoule eutectic barrier integrity is maintained.

Peak EQPS in the TB-1 containment vessel is shown in Figures 2-138 and 2-139 to be about 18.5%, although this peak is only in a highly, localized, outer corner region where there is a slight contact over closure issue with the redwood overpack. This is a minor modeling artifact that produces localized plasticity that otherwise would not exist. It occurs when the redwood compresses well into its "lock-up" phase and becomes analytically stiffer than it would realistically be, due to limitations in the orthotropic crush constitutive model of the redwood. Nonetheless, through-thickness plasticity is non-existent and the TB-1 integrity is maintained. The von Mises stresses (see Figure 2-140) peak is 196 ksi (due to the localized redwood contact), above the elevated-temperature minimum yield strength for the TB-1 of 141 ksi, but more importantly, through-thickness TB-1 stress values are less than 35 ksi, below yield.

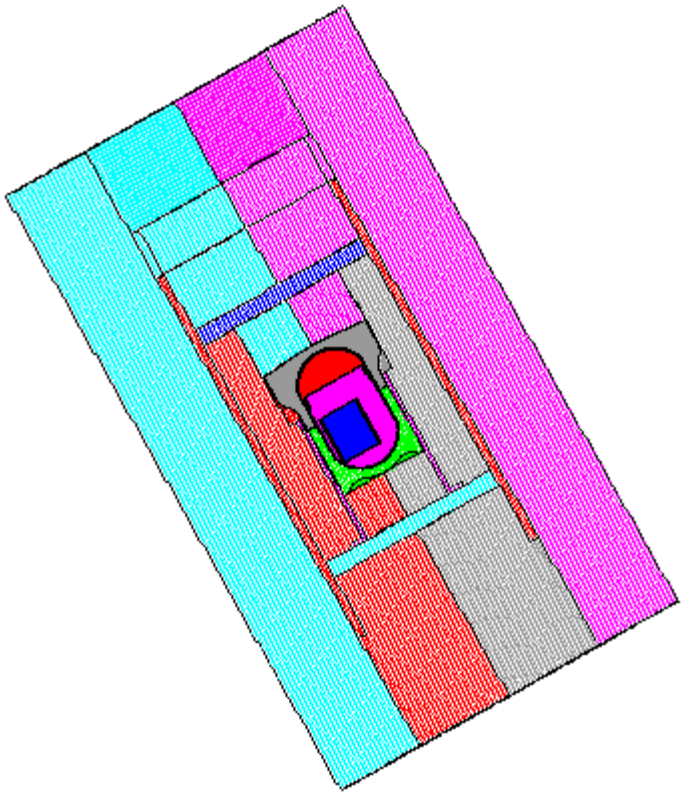

Figure 2-129. Finite Element Mesh for the 831-g, Angled, ER Cylinder, Bottom Position, CGOC Impact

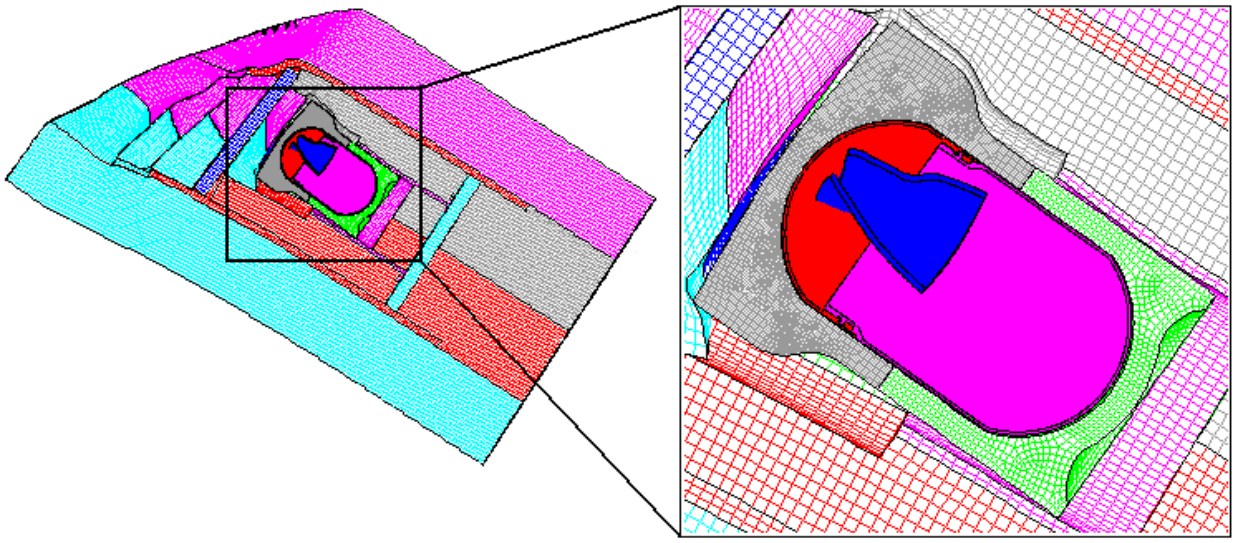

Figure 2-130. Finite Element Mesh for the 831-g, Angled, ER Cylinder, Bottom Position, CGOC Impact – Final Displacement

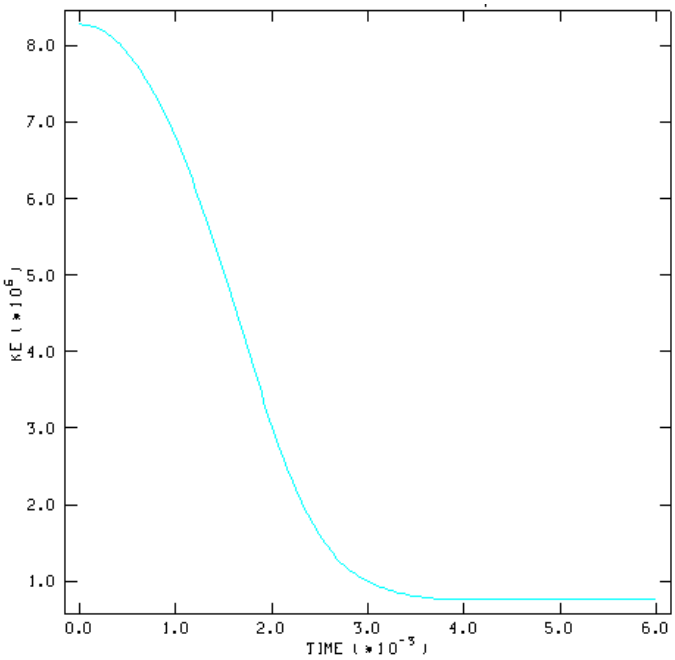

Figure 2-131. Kinetic Energy Time History for the 831-g, Angled, Plutonium Metal Hollow Cylinder, Bottom Position, CGOC Impact

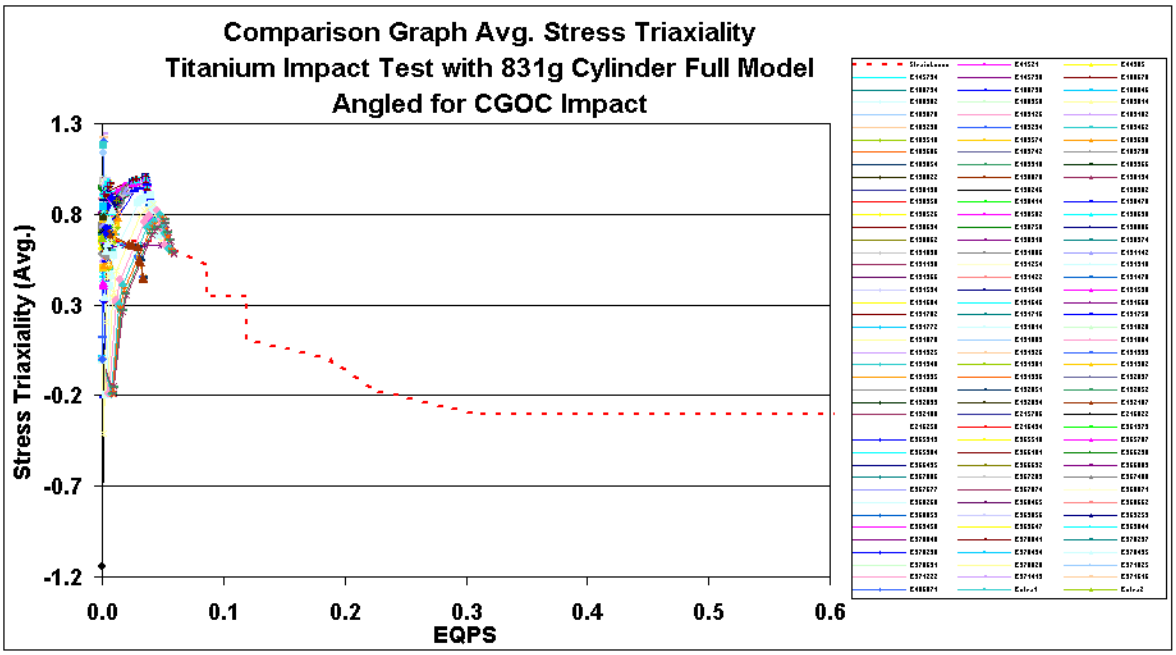

Figure 2-132. Graph of Average Stress Triaxiality versus EQPS of Elements Exceeding the Experimental Strain Locus for the 831-g, Angled, Plutonium Metal Hollow Cylinder, Bottom Position, CGOC Impact

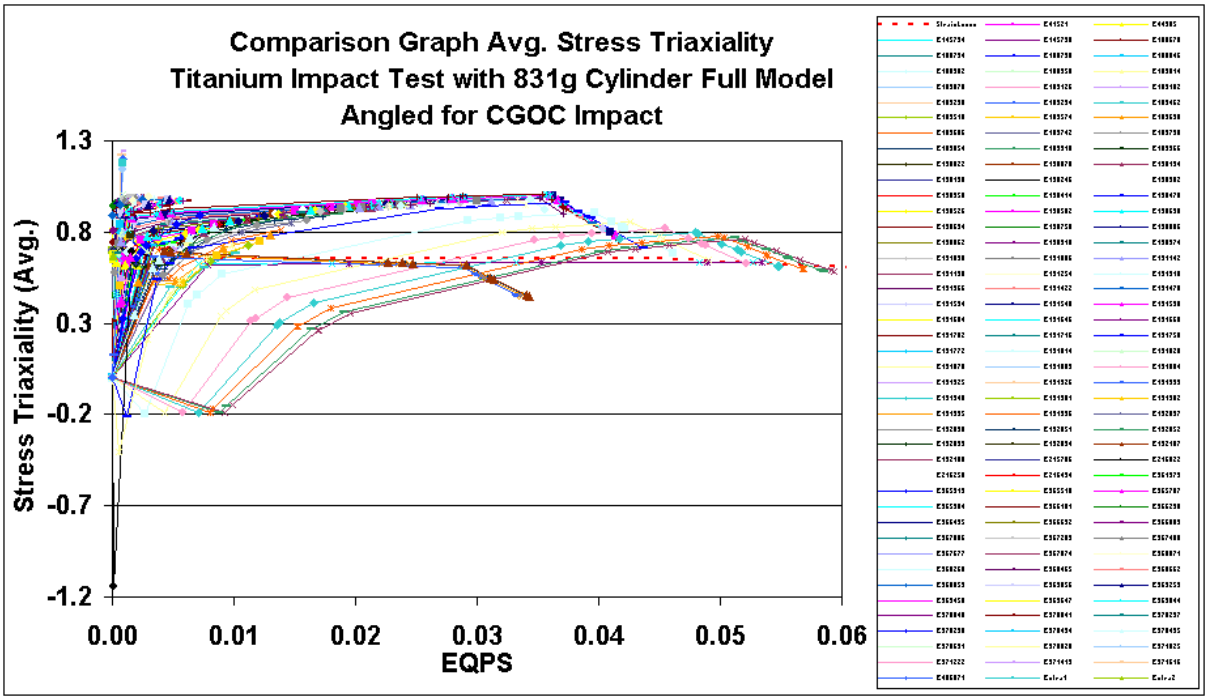

Figure 2-133. Graph of Average Stress Triaxiality versus EQPS of Elements Exceeding the Experimental Strain Locus (Zoomed in) for the 831-g, Angled, Plutonium Metal Hollow Cylinder, Bottom Position, CGOC Impact

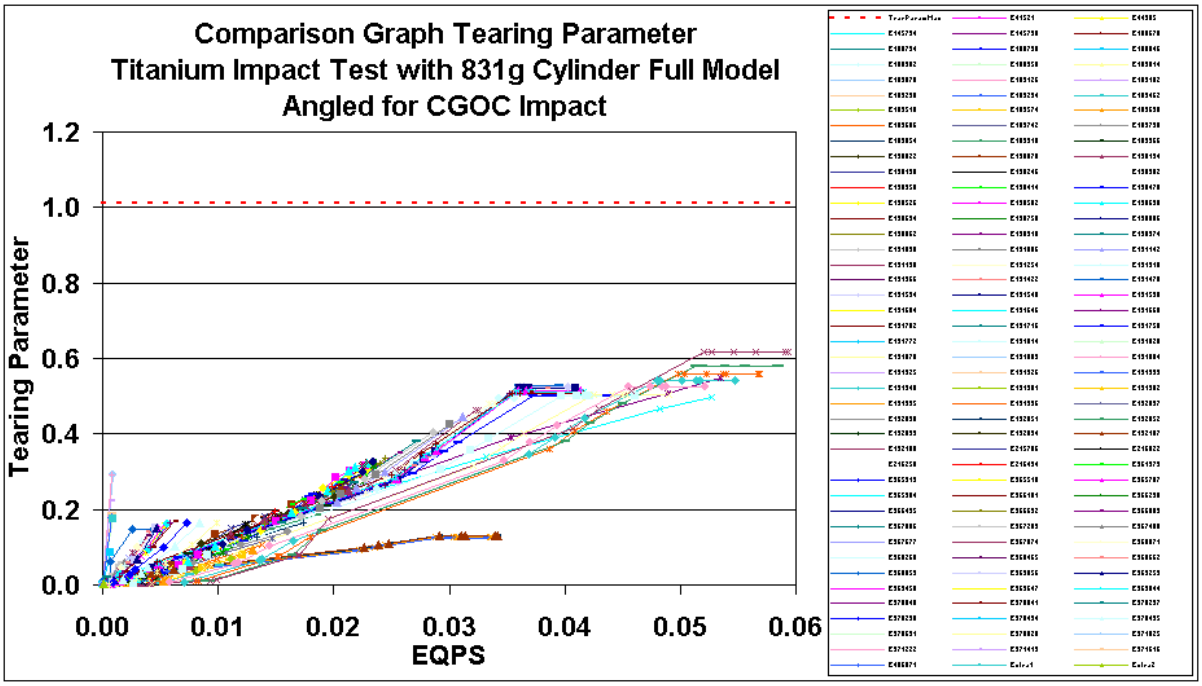

Figure 2-134. Graph of Tearing Parameter versus EQPS of Elements Exceeding the Experimental Strain Locus for the 831-g Angled, Plutonium Metal Hollow Cylinder, Bottom Position, CGOC Impact

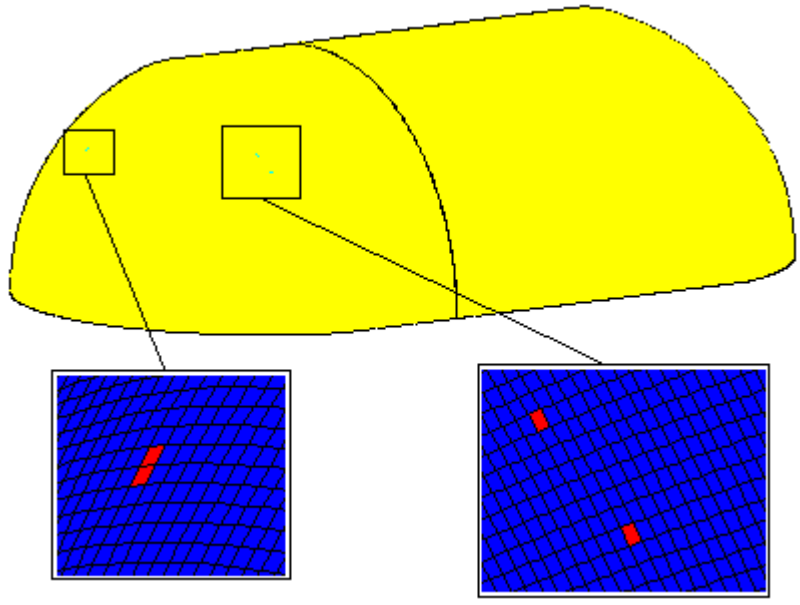

Figure 2-135. Plot of Elements Exceeding the Experimental Strain Locus for the 831-g, Angled, Plutonium Metal Hollow Cylinder, Bottom Position, CGOC Impact

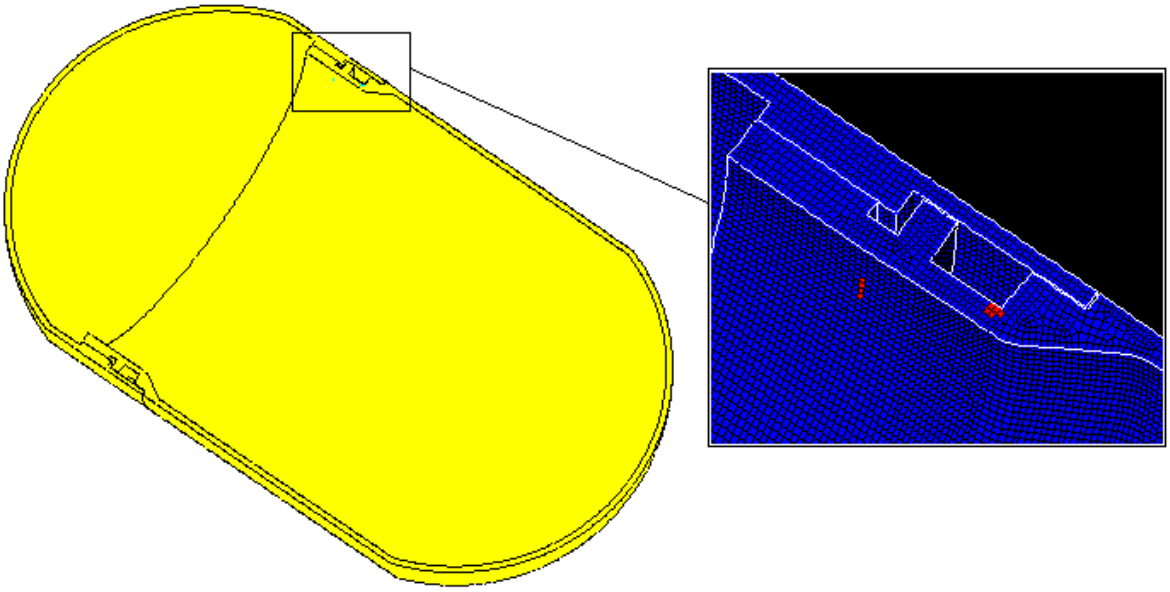

Figure 2-136. Plot of Elements Exceeding the Experimental Strain Locus for the 831-g, Angled, Plutonium Metal Hollow Cylinder, Bottom Position, CGOC Impact

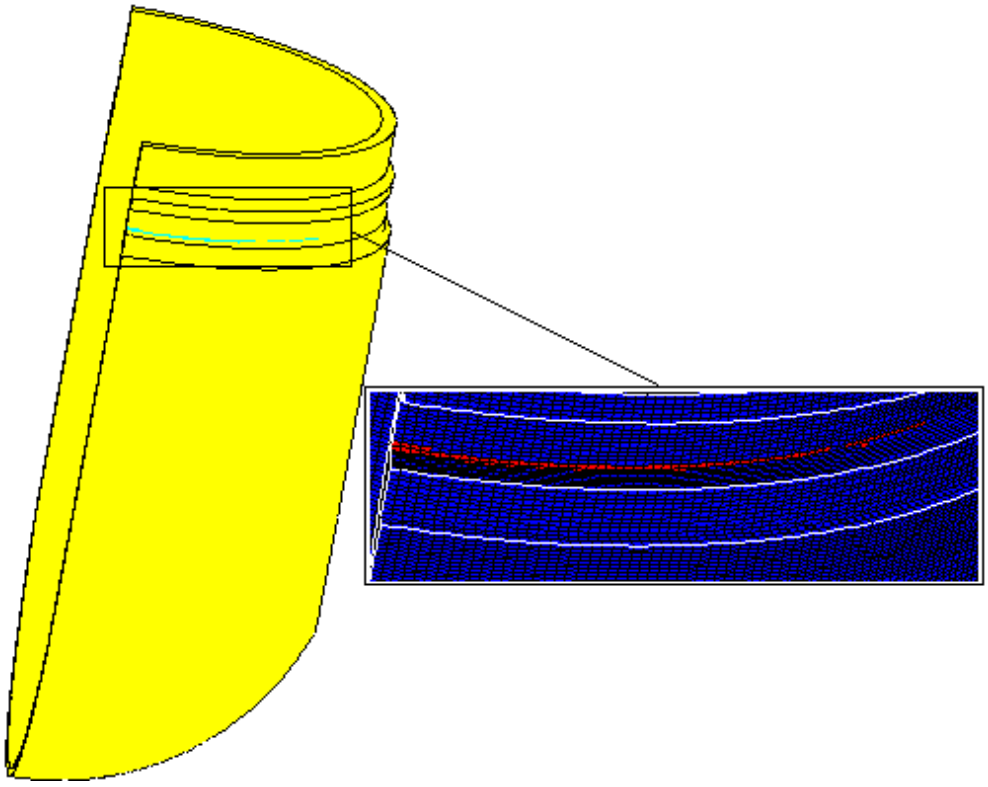

Figure 2-137. Plot of Elements Exceeding the Experimental Strain Locus for the 831-g, Angled, Plutonium Metal Hollow Cylinder, Bottom Position, CGOC Impact

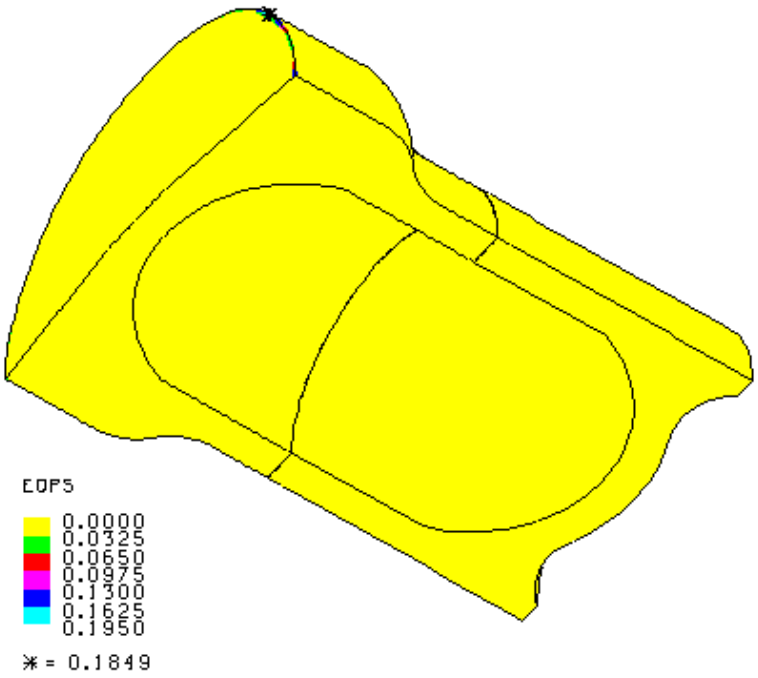

Figure 2-138. Plot of EQPS in the TB-1 for the 831-g, Angled, Plutonium Metal Hollow Cylinder, Bottom Position, CGOC Impact

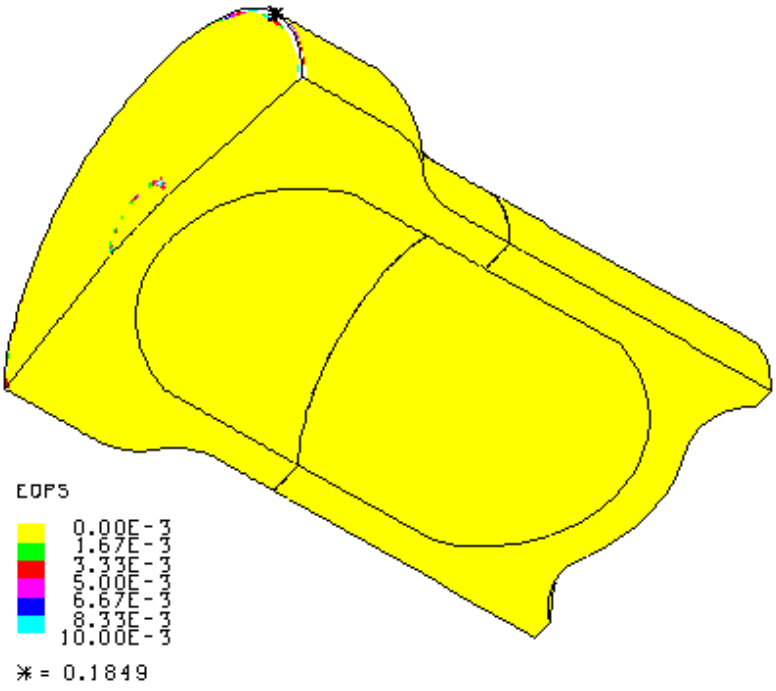

Figure 2-139. Plot of EQPS in the TB-1 for the 831-g, Angled, Plutonium Metal Hollow Cylinder, Bottom Position, CGOC Impact

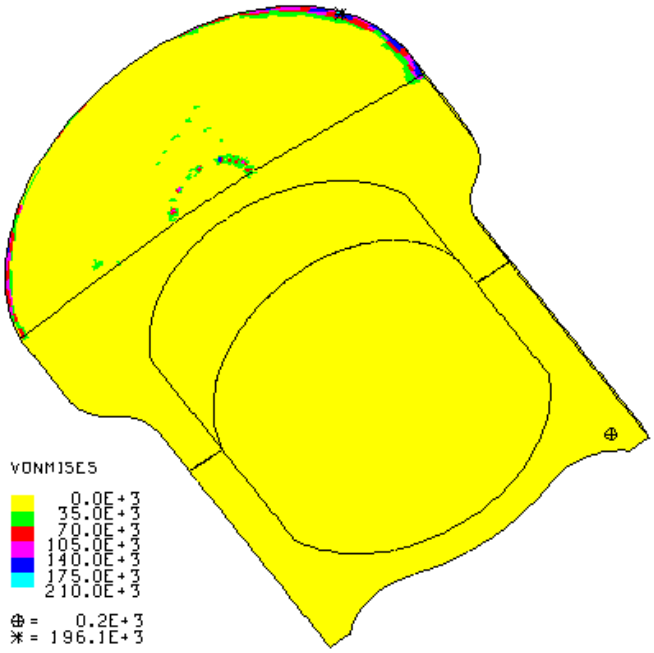

Figure 2-140. Plot of von Mises Stress in the TB-1 for the 831-g, Angled, Plutonium Metal Hollow Cylinder, Bottom Position, CGOC Impact

2.12.5.4.5 Run 4 – 831-g Plutonium Metal Hollow Cylinder Side Impact

The side impact model for the hollow plutonium metal hollow cylinder is shown in Figure 2-141. The cylinder is located at the far side of the T-Ampoule so that its net impact velocity with the side of the T-Ampoule is maximized. The post-impact deformation is shown in Figure 2-142 and its kinetic energy history in Figure 2-143. The plutonium metal hollow cylinder deforms much more than the previous case because of its weaker side-impact orientation.

Average stress-triaxiality versus EQPS is shown in Figures 2-144 and 2-145 for the 67 elements extending beyond the tested Bao-Wierzbicki strain locus. All of these elements are at relatively high stress triaxiality and low EQPS. The Tearing Parameter values for these same 67 elements are shown in Figure 2-146 and all are still below the critical Tearing Parameter value of 1.012 for Ti-6Al-4V. These elements are highlighted in red in Figures 2-147 and 2-148, but these elements are still below the critical value and do not indicate failure; T-Ampoule integrity is maintained.

Peak EQPS in the TB-1 containment vessel is shown in Figures 2-149 and 2-150 to be about 27.4%, although this peak is only in a highly localized outer corner region where there is a slight contact overclosure issue with the redwood overpack. A slight (<1% EQPS) dent is visible in Figure 2-150 from the internal impact of the plutonium metal hollow cylinder with the TB-1 wall (via the T-Ampoule). Through-thickness plasticity is non-existent and the TB-1 integrity is maintained. The von Mises stresses (see Figures 2-151 and 2-152) peak at 222 ksi (due to the localized redwood contact), which is above the elevated-temperature minimum yield strength for the TB-1 of 141 ksi, but more importantly, through-thickness TB-1 stress values are less than 37.5 ksi, below yield.

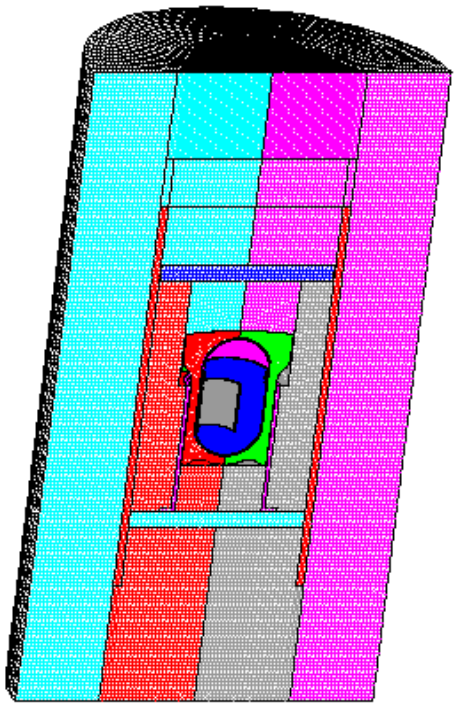

Figure 2-141. Finite Element Mesh for the 831-g, ER, Cylinder, Far Side Position, Side Impact

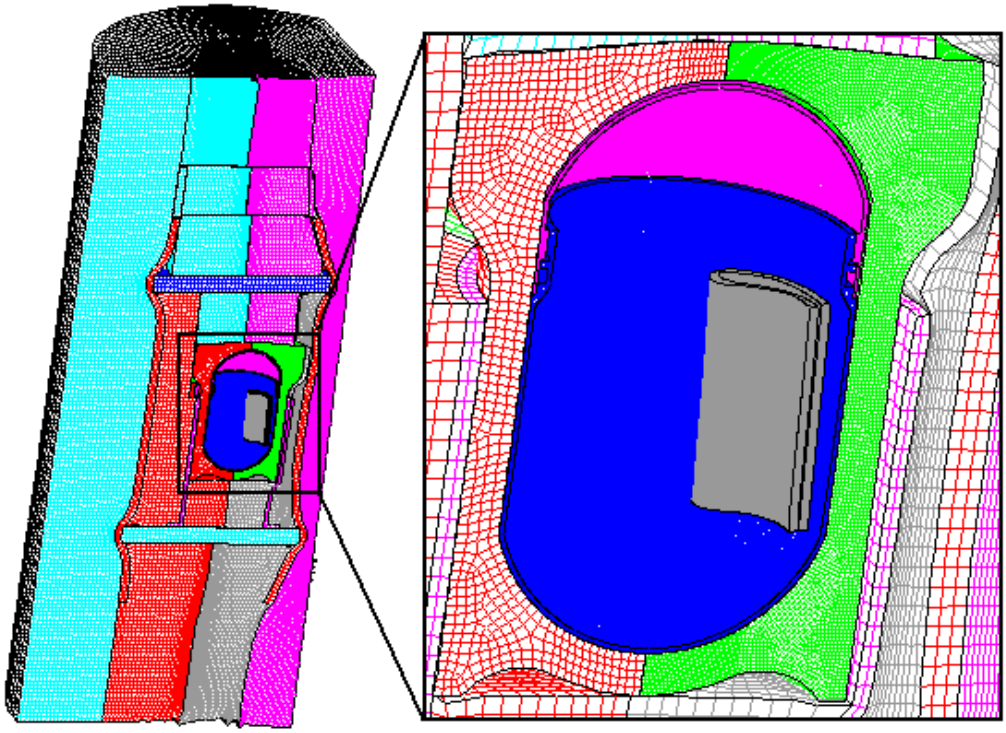

Figure 2-142. Finite Element Mesh for the 831-g, Plutonium Metal Hollow Cylinder, Far Side Position, Side Impact – Final Displacement

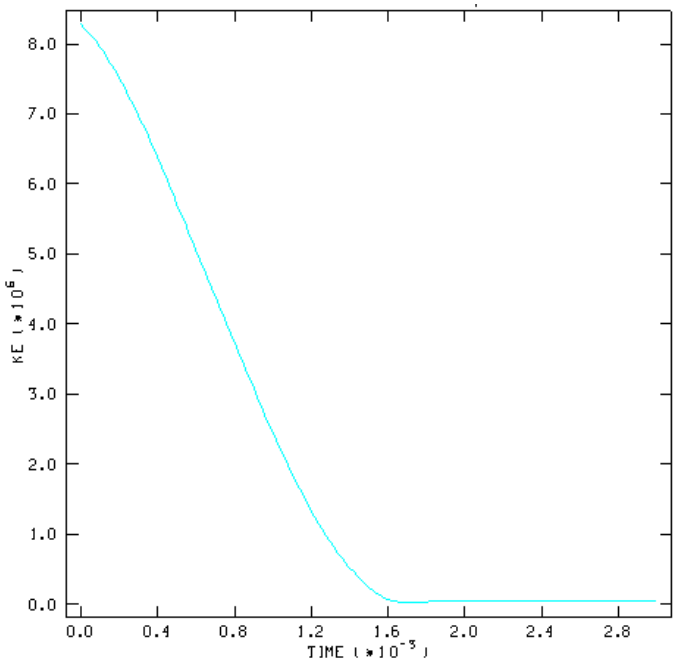

Figure 2-143. Kinetic Energy Time History for the 831-g, ER, Cylinder, Far Side Position, Side Impact

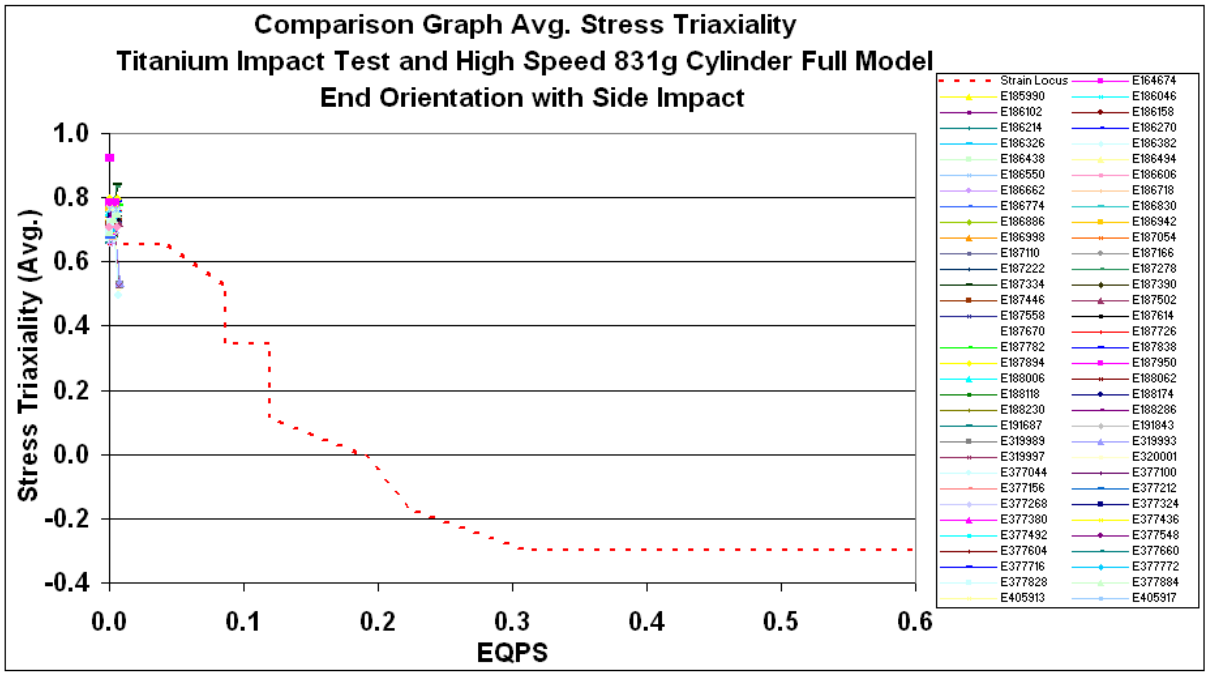

Figure 2-144. Graph of Stress Triaxiality versus EQPS of Elements Exceeding the Experimental Strain Locus for the 831-g, Plutonium Metal Hollow Cylinder, Far Side Position, Side Impact

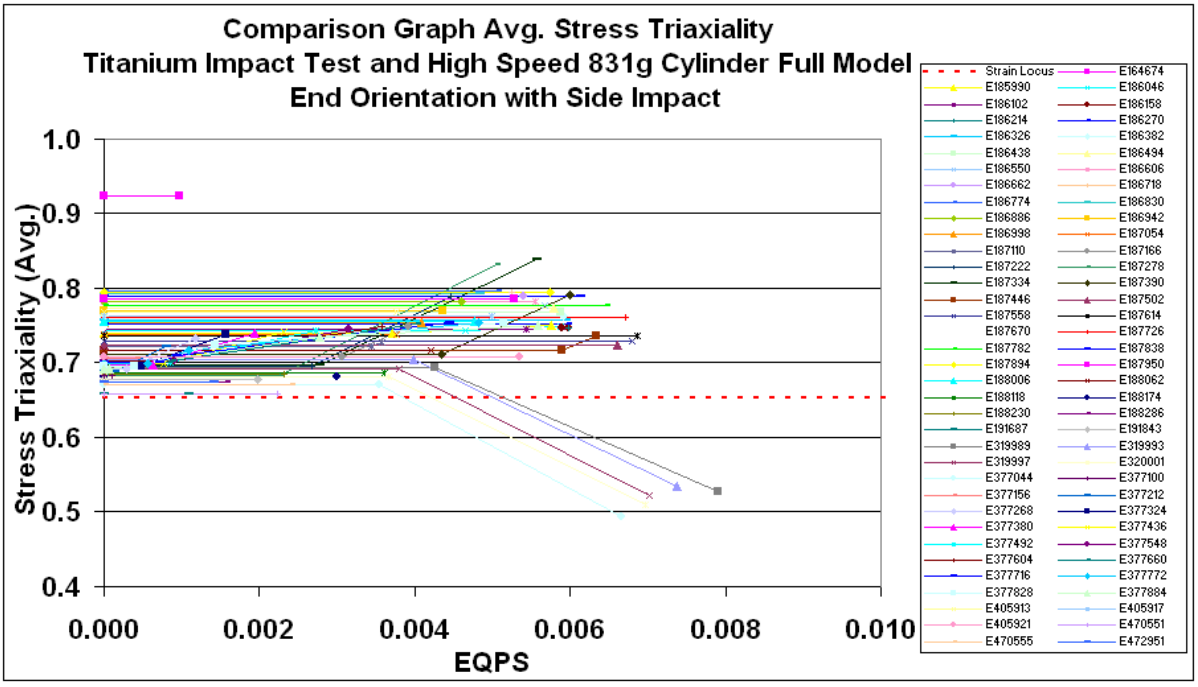

Figure 2-145. Graph of Stress Triaxiality versus EQPS of Elements Exceeding the Experimental Strain Locus (Zoomed In) for the 831-g, Plutonium Metal Hollow Cylinder, Far Side Position, Side Impact

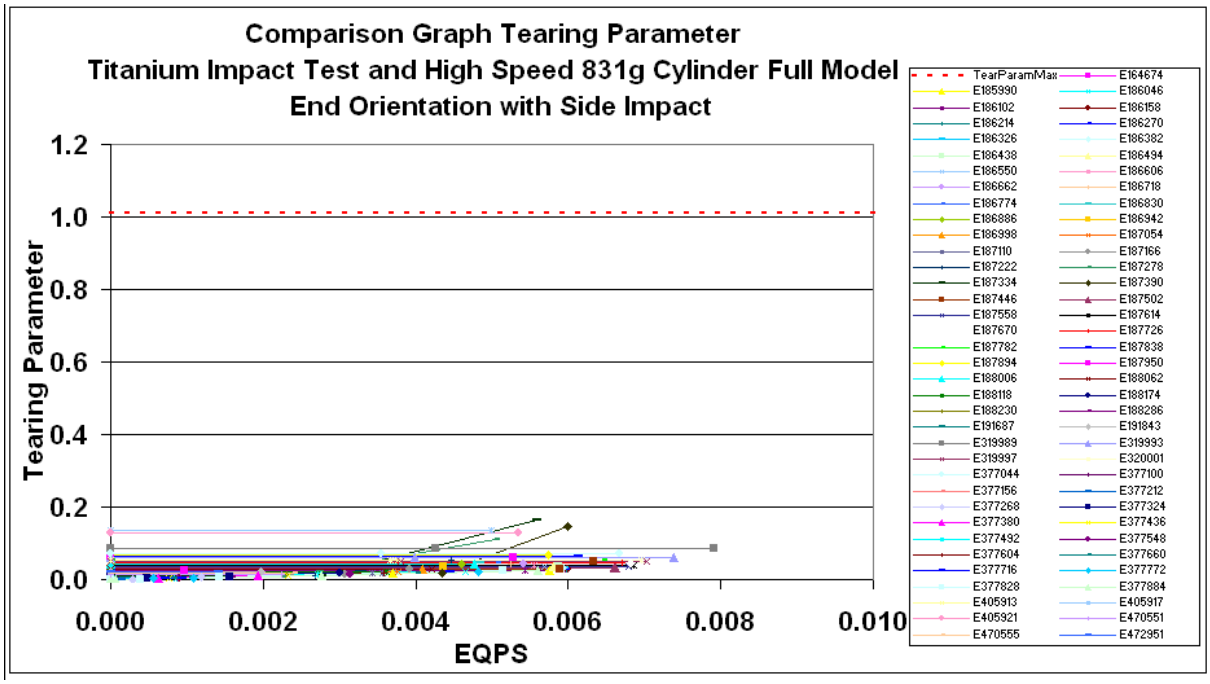

Figure 2-146. Graph of Tearing Parameter versus EQPS of Elements Exceeding the Experimental Strain Locus for the 831-g, Plutonium Metal Hollow Cylinder, Far Side Position, Side Impact

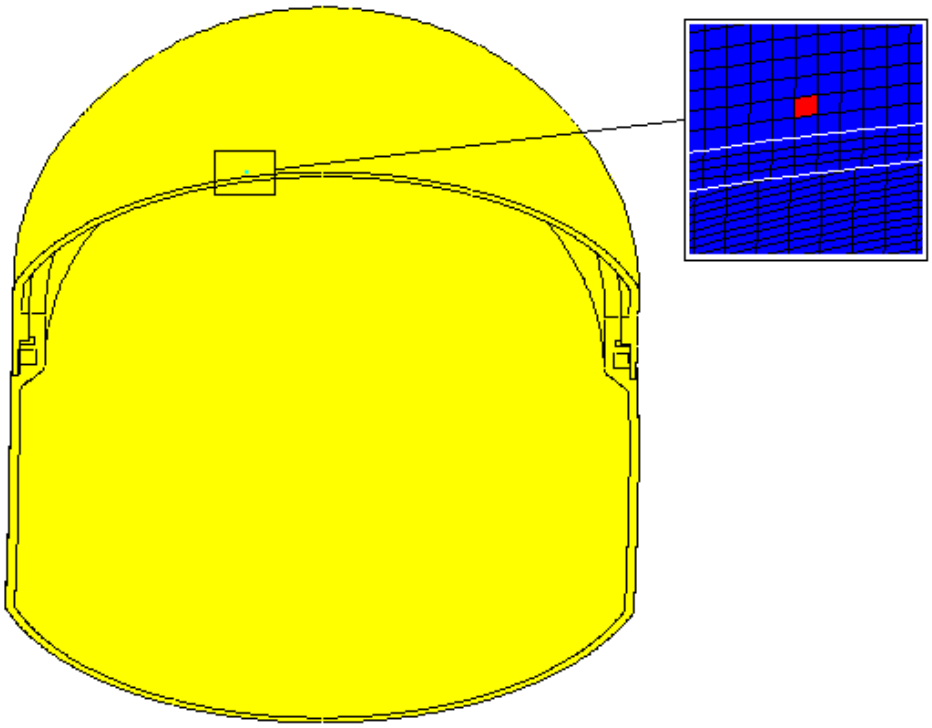

Figure 2-147. Plot of Elements Exceeding the Experimental Strain Locus for the 831-g, Plutonium Metal Hollow Cylinder, Far Side Position, Side Impact

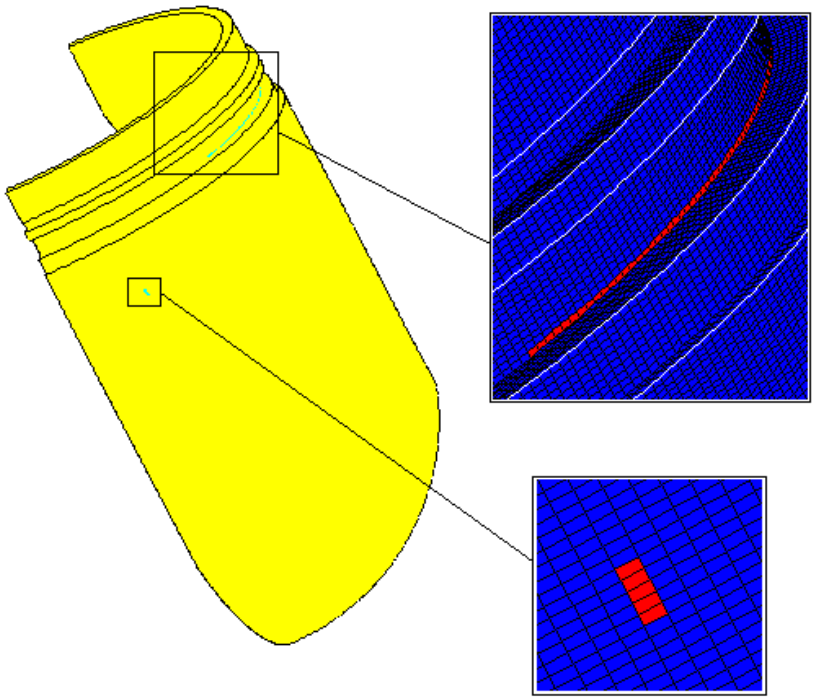

Figure 2-148. Plot of Elements Exceeding the Experimental Strain Locus for the 831-g, Plutonium Metal Hollow Cylinder, Far Side Position, Side Impact

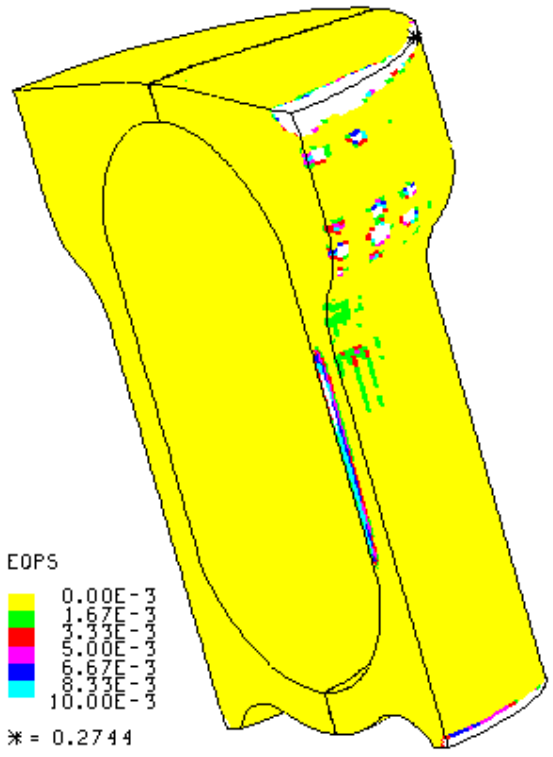

Figure 2-149. Plot of EQPS in the TB-1 for the 831-g, ER, Cylinder, Far Side Position, Side Impact

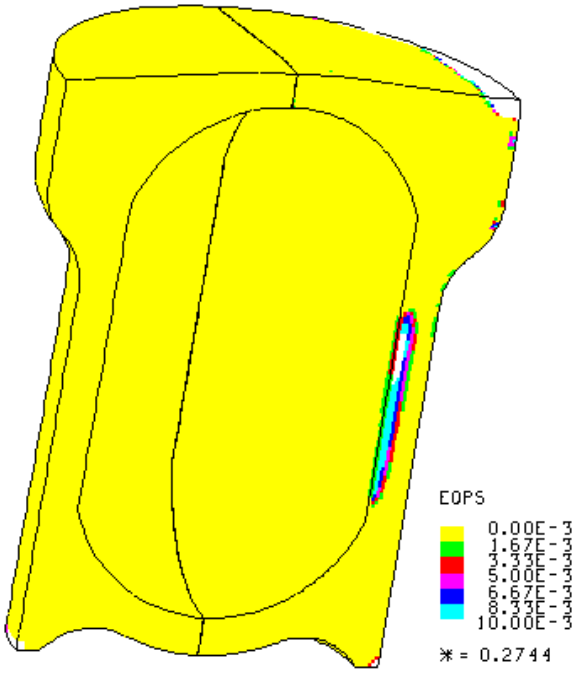

Figure 2-150. Plot of EQPS in the TB-1 for the 831-g, ER Cylinder, Far Side Position, Side Impact

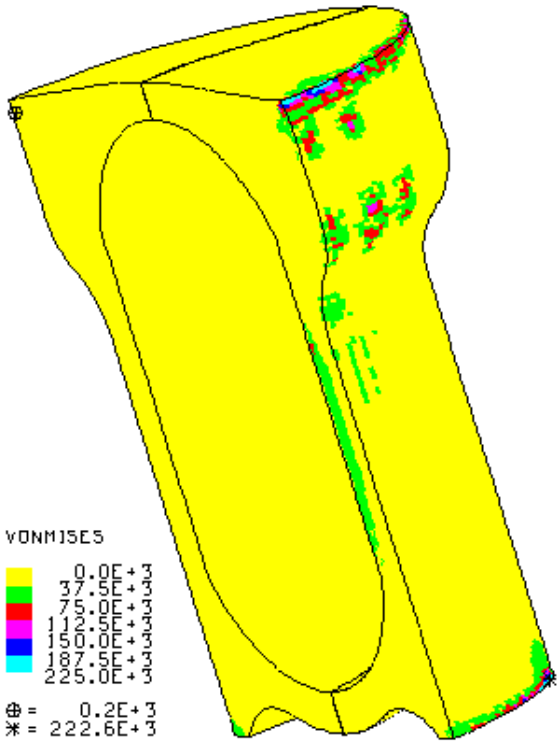

Figure 2-151. Plot of von Mises Stress in the TB-1 for the 831-g, ER Cylinder, Far Side Position, Side Impact

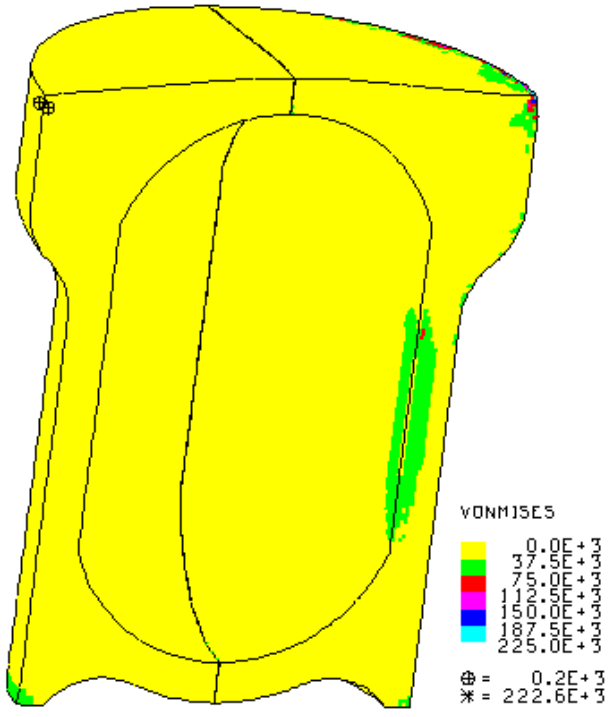

Figure 2-152. Plot of von Mises Stress in the TB-1 for the 831-g, ER, Cylinder, Far Side Position, Side Impact

2.12.5.4.6 Run 5 - 831-g Angled Plutonium Metal Hollow Cylinder Side Impact

The side impact model for the plutonium metal hollow cylinder, angled orientation, is shown in Figure 2-153. The cylinder is located at the far side of the T-Ampoule so that its net impact velocity with the side of the T-Ampoule is maximized, but also angled to present a sharp corner impact with the T-Ampoule surface. The post-impact deformation is shown in Figure 2-154 and its kinetic energy history in Figure 2-155. The plutonium metal hollow cylinder deforms moderately but maintains much of its original shape because of its conservatively "infinitely ductile" material constitutive model definition.

Average stress-triaxiality versus EQPS is shown in Figures 2-156 and 2-157 for the 91 elements extending beyond the tested Bao-Wierzbicki strain locus. All of these elements are at relatively high stress triaxiality and low EQPS. The Tearing Parameter values for these same 91 elements are shown in Figure 2-158, and all are still below the critical Tearing Parameter value of 1.012 for Ti-6Al-4V. These elements are highlighted in red Figure 2-159, but these elements are still below the critical value and do not indicate failure; T-Ampoule integrity is maintained.

Peak EQPS in the TB-1 vessel is shown in Figures 2-160 and 2-161 to be about 26.7%, although this peak is only in a highly localized outer corner region where there is a slight contact overclosure issue with the redwood overpack. Through-thickness plasticity is non-existent and the TB-1 integrity is maintained. The von Mises stresses (see Figures 2-162 and 2-163) peak at 221 ksi (due to the localized redwood contact), which is above the elevated-temperature minimum yield strength for the TB-1 of 141 ksi, but more importantly, through-thickness TB-1 stress values are less than 112.5 ksi, below yield.

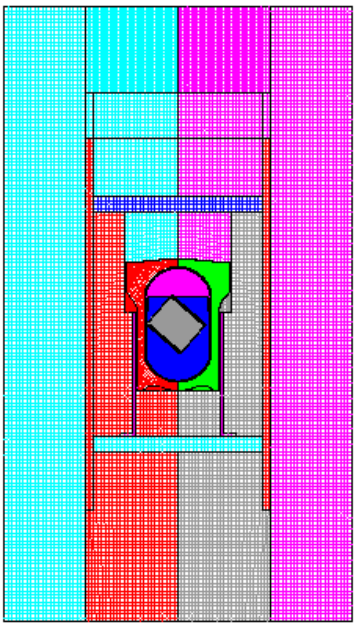

Figure 2-153. Finite Element Mesh for the 831-g, Angled, ER Cylinder, Far Side Position, Side Impact

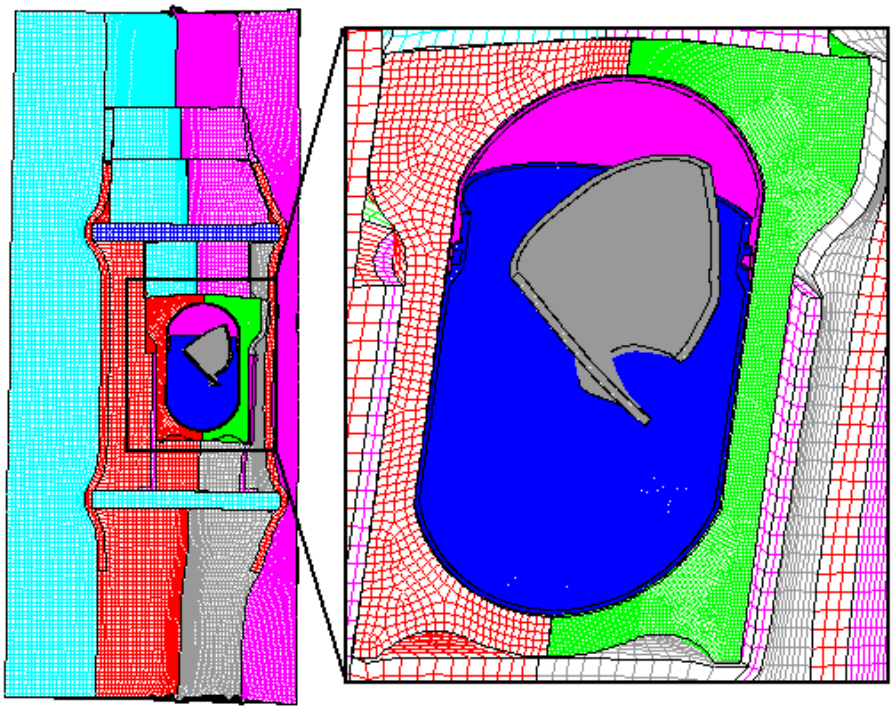

Figure 2-154. Finite Element Mesh for the 831-g, Angled, ER Cylinder, Far Side Position, Side Impact – Final Displacement

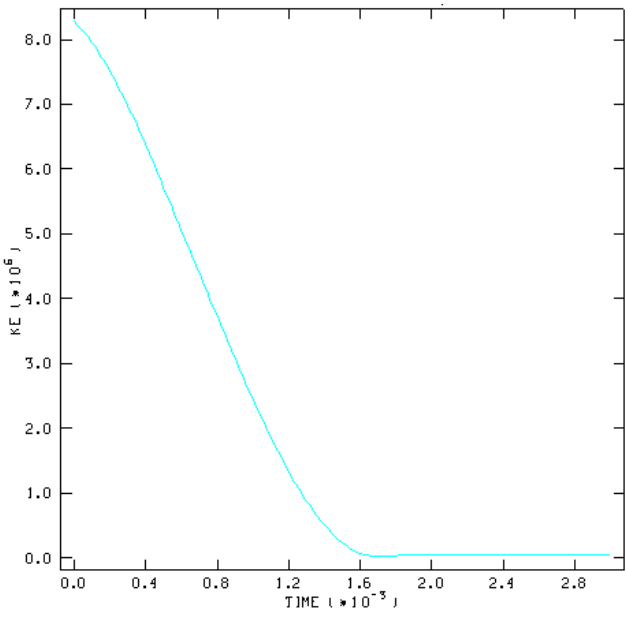

Figure 2-155. Kinetic Energy Time History for the 831-g, Angled, Plutonium Metal Hollow Cylinder, Far Side Position, Side Impact

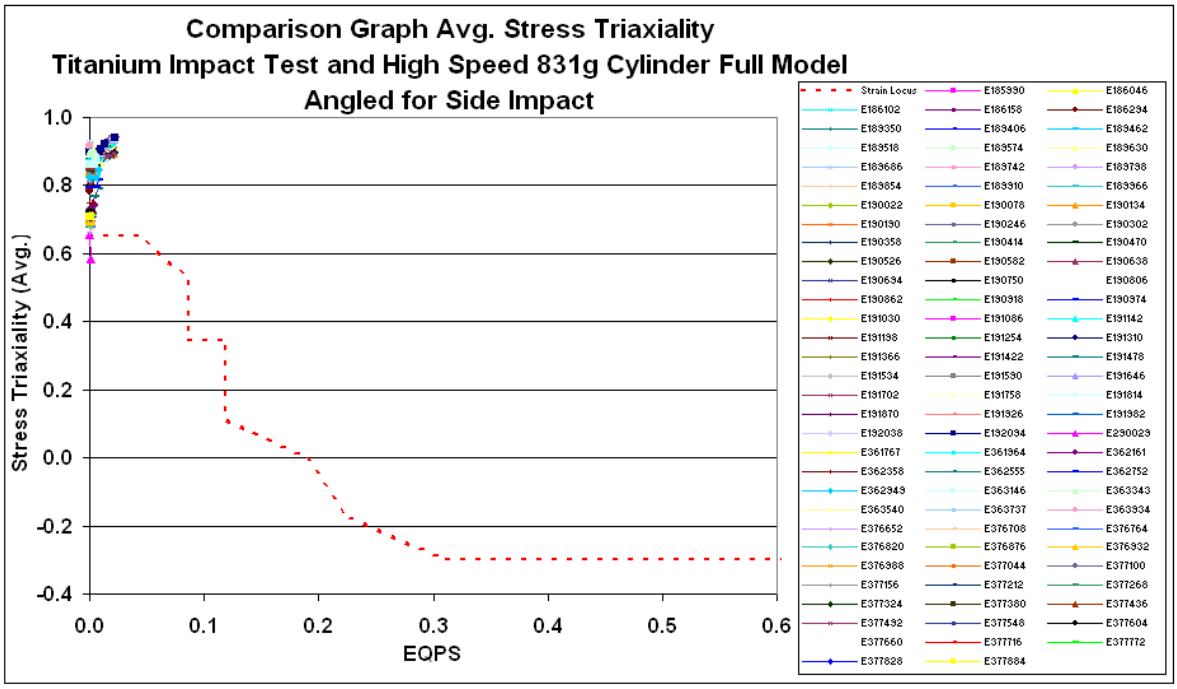

Figure 2-156. Graph of Average Stress Triaxiality versus EQPS of Elements Exceeding the Experimental Strain Locus for the 831-g, Angled, Plutonium Metal Hollow Cylinder, Far Side Position, Side Impact

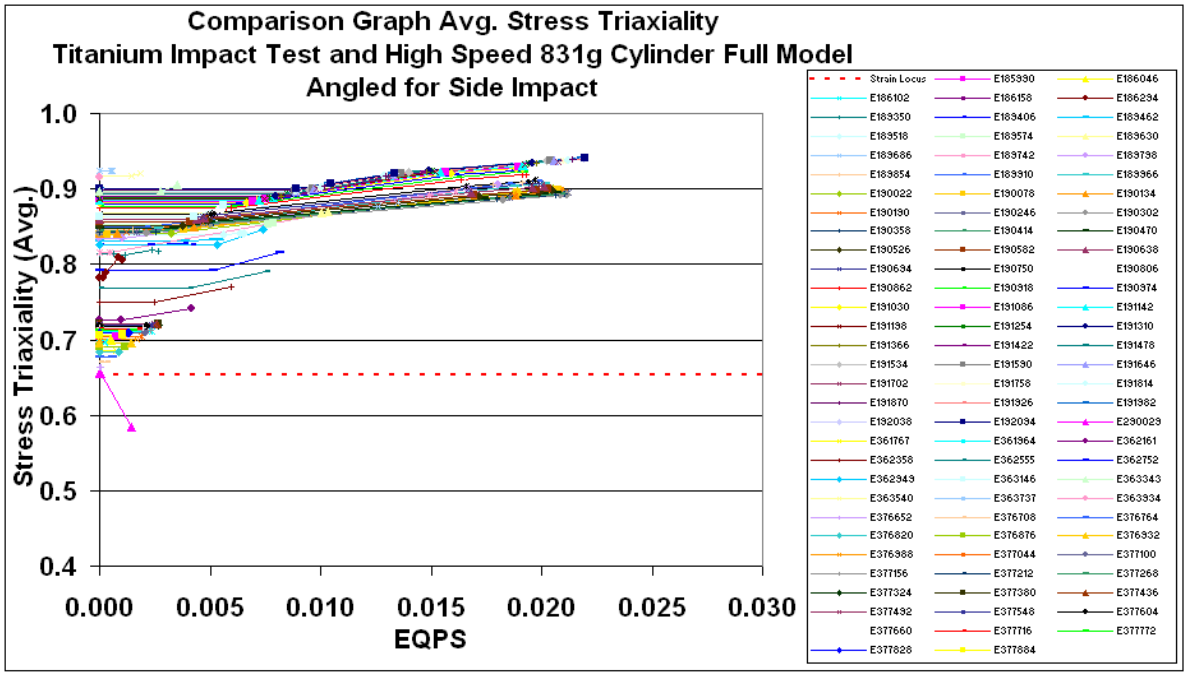

Figure 2-157. Graph of Average Stress Triaxiality versus EQPS of Elements Exceeding the Experimental Strain Locus (Zoomed In) for the 831-g, Angled, Plutonium Metal Hollow Cylinder, Far Side Position, Side Impact

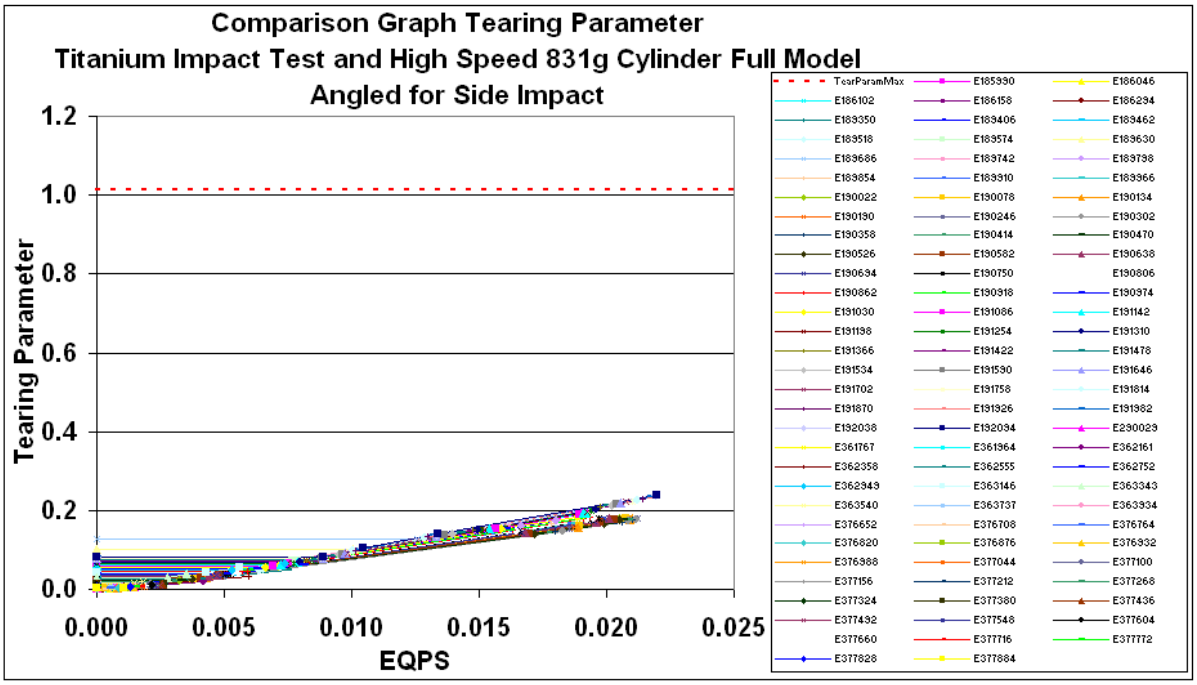

Figure 2-158. Graph of Tearing Parameter versus EQPS of Elements Exceeding the Experimental Strain Locus for the 831-g, Angled, Plutonium Metal Hollow Cylinder, Far Side Position, Side Impact

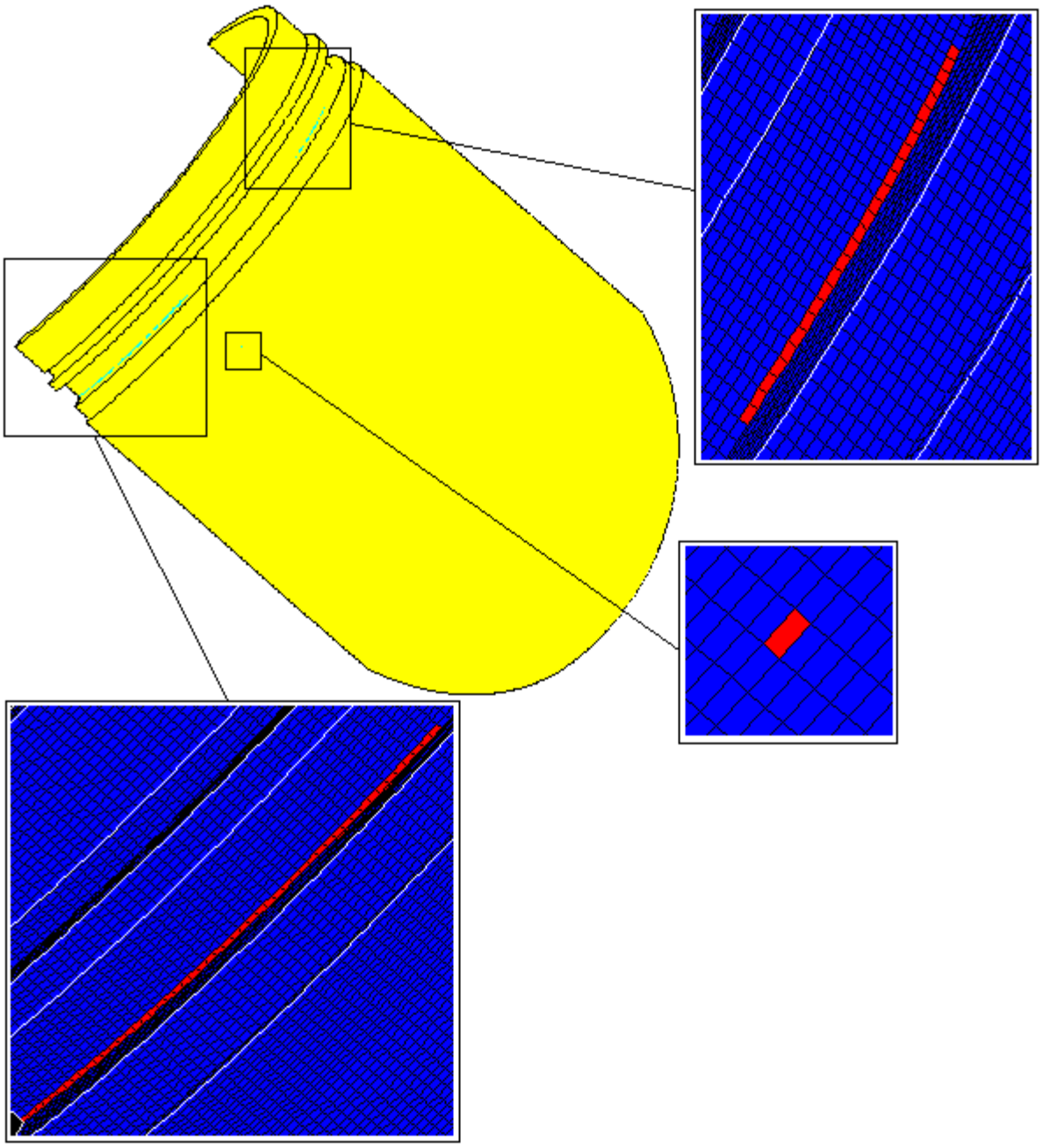

Figure 2-159. Plot of Elements Exceeding the Experimental Strain Locus for the 831-g, Angled, Plutonium Metal Hollow Cylinder, Far Side Position, Side Impact

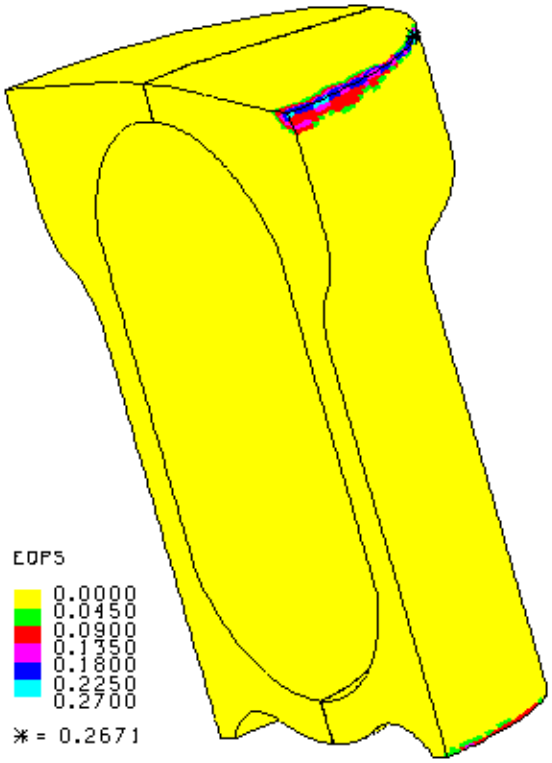

Figure 2-160. Plot of EQPS in the TB-1 for the 831-g, Angled, ER Cylinder, Far Side Position, Side Impact

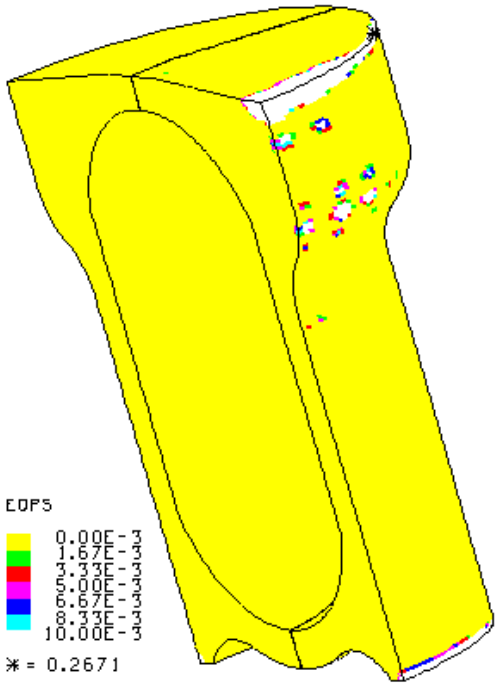

Figure 2-161. Plot of EQPS in the TB-1 for the 831-g, Angled, ER Cylinder, Far Side Position, Side Impact

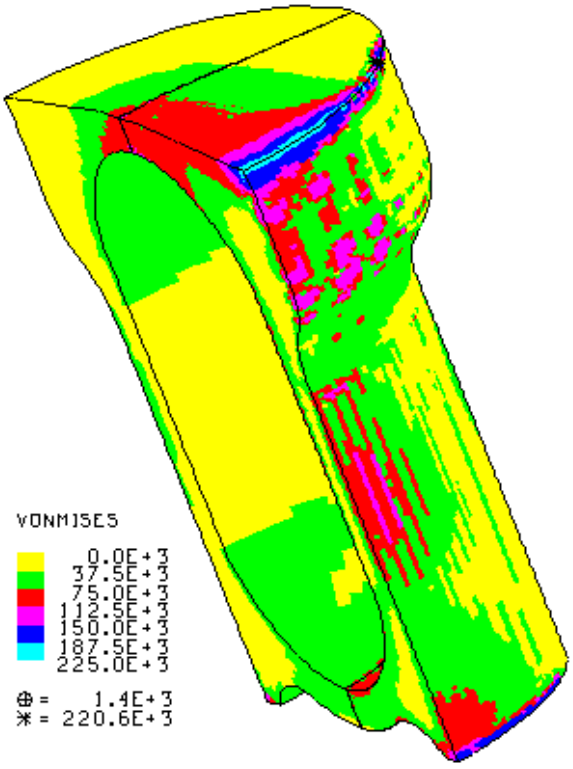

Figure 2-162. Plot of von Mises Stress in the TB-1 for the 831-g, Angled, Plutonium Metal Hollow Cylinder, Far Side Position, Side Impact

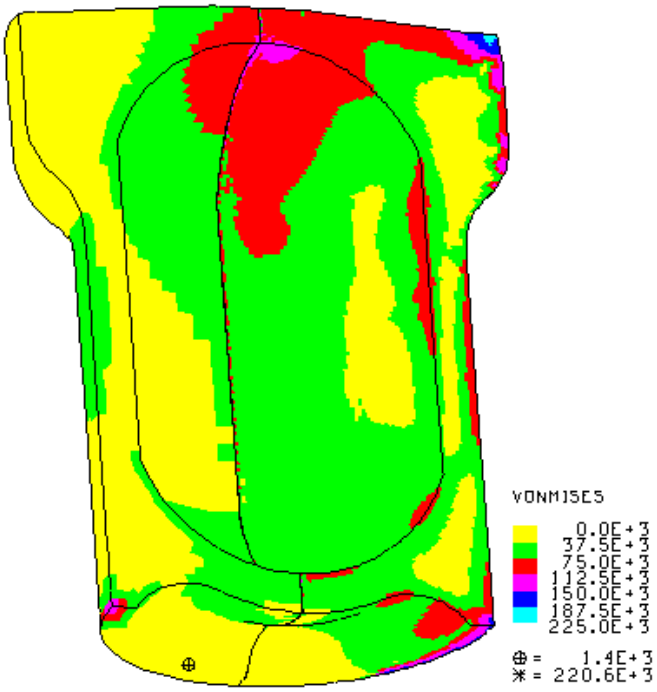

Figure 2-163. Plot of von Mises Stress in the TB-1 for the 831-g, Angled, Plutonium Metal Hollow Cylinder, Far Side Position, Side Impact

2.12.5.4.7 Run 6 - 731-g Plutonium Metal Hollow Cylinder Top Impact

The top end impact model for the slightly smaller (731 g) plutonium metal hollow cylinder, oriented axially (with the impact direction, as opposed to angled) is shown in Figure 2-164. Note that the cylinder is located at the bottom of the T-Ampoule so that its net impact velocity with the top of the T-Ampoule is maximized. The post-impact deformation is shown in Figure 2-165 and its kinetic energy history in Figure 2-166. This slightly shorter plutonium metal hollow cylinder still exhibits buckling, despite its conservatively "strongest shape" definition.

Equivalent Plastic Strain (EQPS) in the TB-1 vessel is shown in Figure 2-167 to be less than 2.7%, and only in some localized outer contact regions with the redwood overpack. The von Mises stresses (see Figures 2-168 and 2-169) peak at 148.5 ksi, is just above the elevated-temperature minimum yield strength for the TB-1 of 141 ksi, but more importantly, through-thickness TB-1 stress values are in the less-than-25 ksi range, below yield. The time at which the peak value of the von Mises stress occurs coincides with the peak value of the contact force (summed over the lid area). A plot of this force as a function of time is shown in Figure 2-170. A maximum contact load of 66,273 lbs is applied to the inner surface of the TB-1 lid during the impact. No T-Ampoule elements exceeded the tested B-W strain locus, and the peak Tearing Parameter value (see Table 2-11, run #6) of 0.1507 was below the critical Tearing Parameter value of 1.012 for Ti-6Al-4V. Note that the peak Tearing Parameter value for the T-Ampoule in this 731 g, plutonium metal hollow cylinder impact case is slightly larger than that of the 831 g cylinder impact, because the shorter plutonium metal hollow cylinder has a slightly higher net impact velocity with the T-Ampoule.

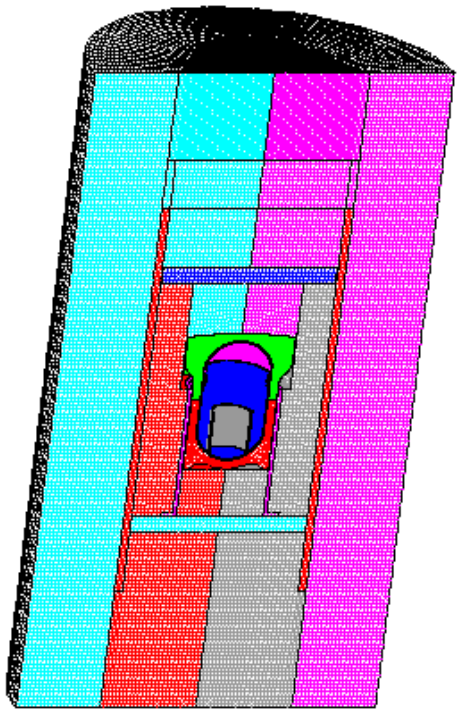

Figure 2-164. Finite Element Mesh for the 731-g, ER, Cylinder, Bottom Position, Top Impact

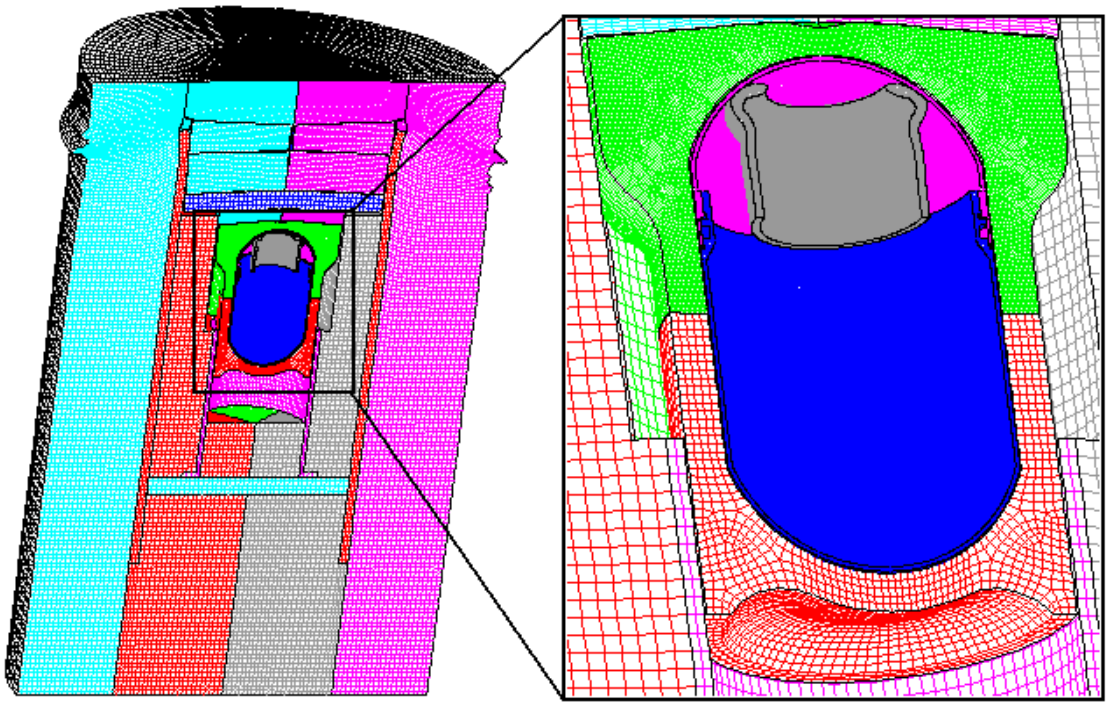

Figure 2-165. Finite Element Mesh for the 731-g, ER, Cylinder, Bottom Position, Top Impact – Final Displacement

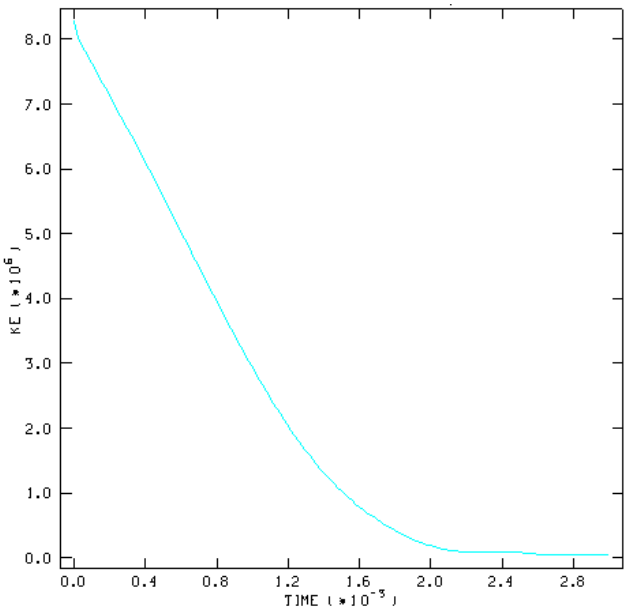

Figure 2-166. Kinetic Energy Time History for the 731-g, ER, Cylinder, Bottom Position, Top Impact

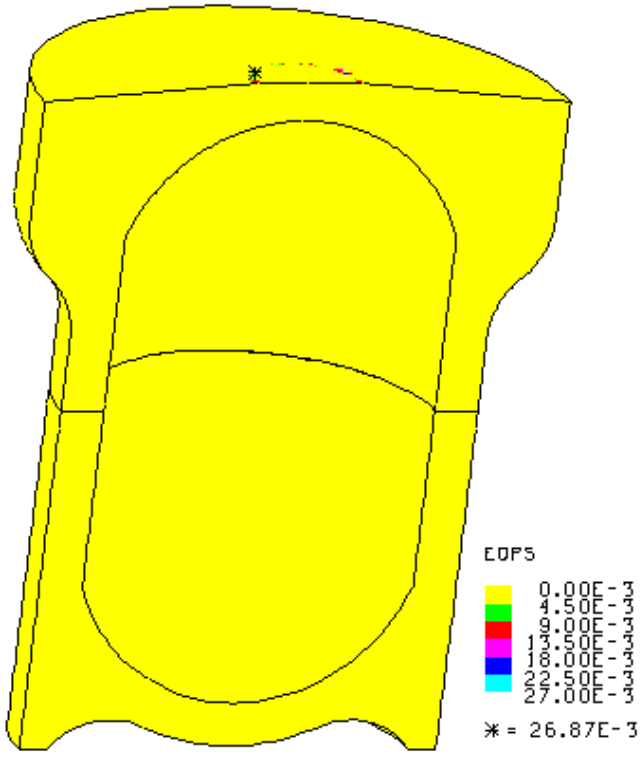

Figure 2-167. EQPS in the TB-1 for the 731-g, Plutonium Metal Hollow Cylinder, Bottom Position, Top Impact

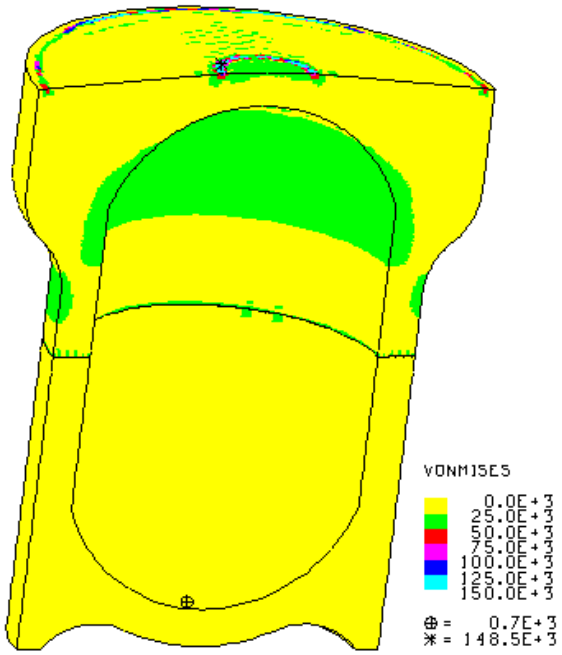

Figure 2-168. von Mises Stress in the TB-1 for the 731-g, ER, Cylinder, Bottom Position, Top Impact

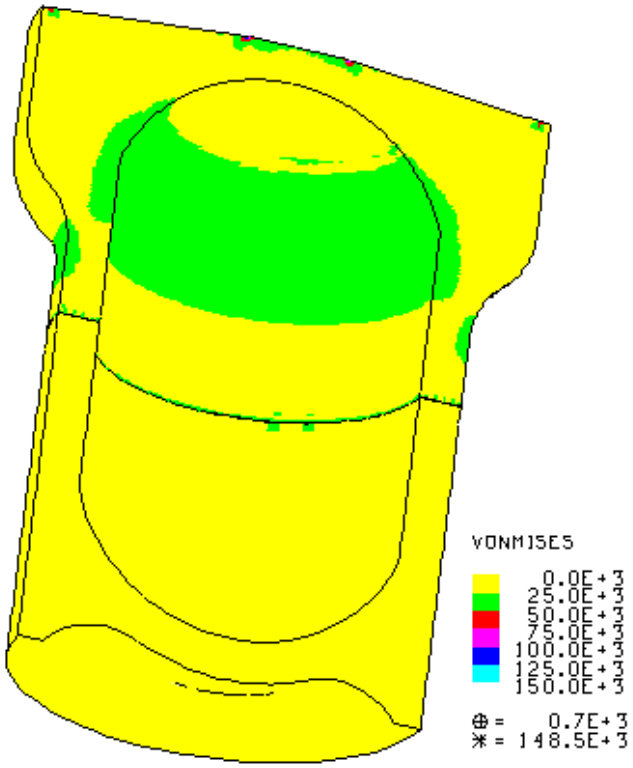

Figure 2-169. von Mises Stress in the TB-1 for the 731-g, ER, Cylinder, Bottom Position, Top Impact

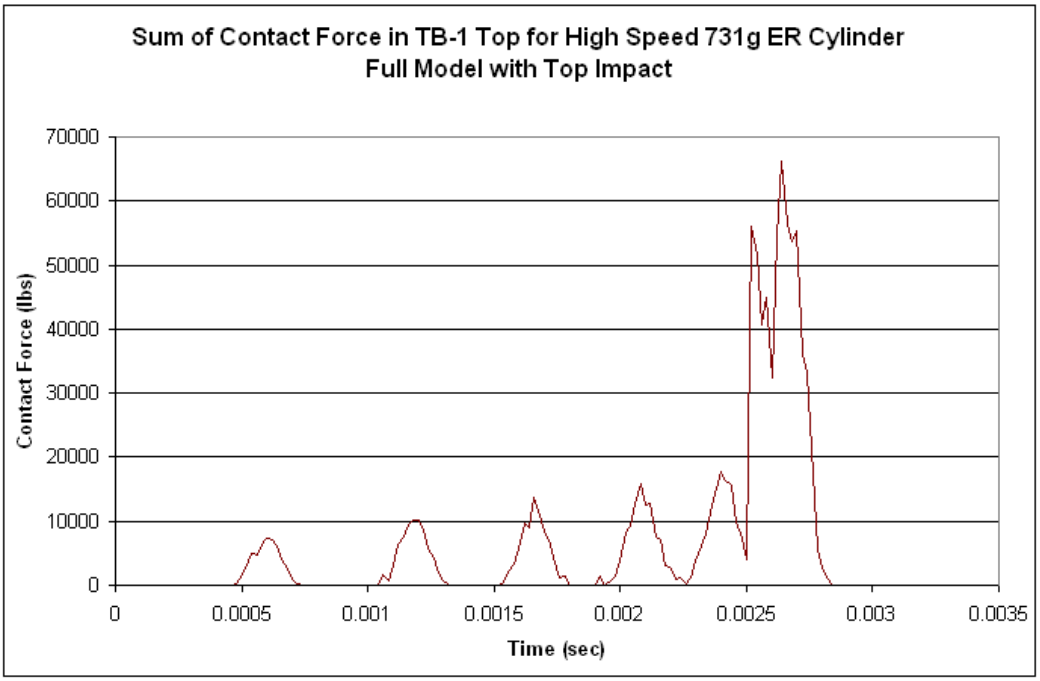

Figure 2-170. Contact Forces in the TB-1 for the 731-g, ER, Cylinder, Bottom Position, Top Impact

2.12.5.4.8 Run 7 - 731-g, Angled, Plutonium Metal Hollow Cylinder Top Impact

The top end impact model for the shorter 731 g plutonium metal hollow cylinder, oriented angled, is shown in Figure 2-171. The cylinder is located at the bottom of the T-Ampoule so that its net impact velocity with the top of the T-Ampoule is maximized. The post-impact deformation is shown in Figure 2-172 and its kinetic energy history in Figure 2-173. The plutonium metal hollow cylinder deforms but maintains much of its original shape because of its conservatively "infinitely ductile" material constitutive model definition (despite its alpha Pu being a relatively brittle material in reality).

Average stress-triaxiality versus EQPS is shown in Figures 2-174 and 2-175 for the 21 elements extending beyond the tested Bao-Wierzbicki strain locus. All of these elements are at high stress triaxiality and low EQPS. The Tearing Parameter values for these same 21 elements are shown in Figure 2-176, and all are below the critical Tearing Parameter value of 1.012 for Ti-6Al-4V. These elements are highlighted in red Figure 2-177, but note that these elements are still below the initiation of a ductile tear, thus T-Ampoule integrity is maintained.

Peak EQPS in the TB-1 vessel, shown in Figure 2-178, is about 2.4% and is only in some localized outer contact regions with the redwood overpack. The von Mises stresses (see Figures 2-179 and 2-180) peak at 148.5 ksi, is just above the elevated-temperature minimum yield strength for the TB-1 of 141 ksi, but more importantly, through-thickness TB-1 stress values are less than 25 ksi, below yield. The time at which the peak value of the von Mises stress occurs coincides with the peak value of the contact force (summed over the lid area). A plot of this force as a function of time is shown in Figure 2-181. A maximum contact load of 58,873 lbs is applied to the inner surface of the TB-1 during the impact.

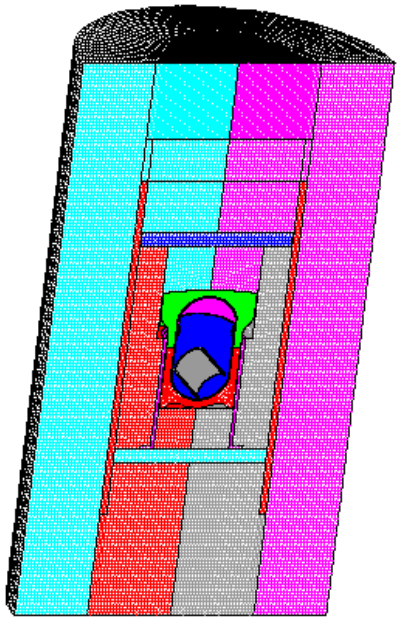

Figure 2-171. Finite Element Mesh for the 731-g, Angled, ER Cylinder, Bottom Position, Top Impact

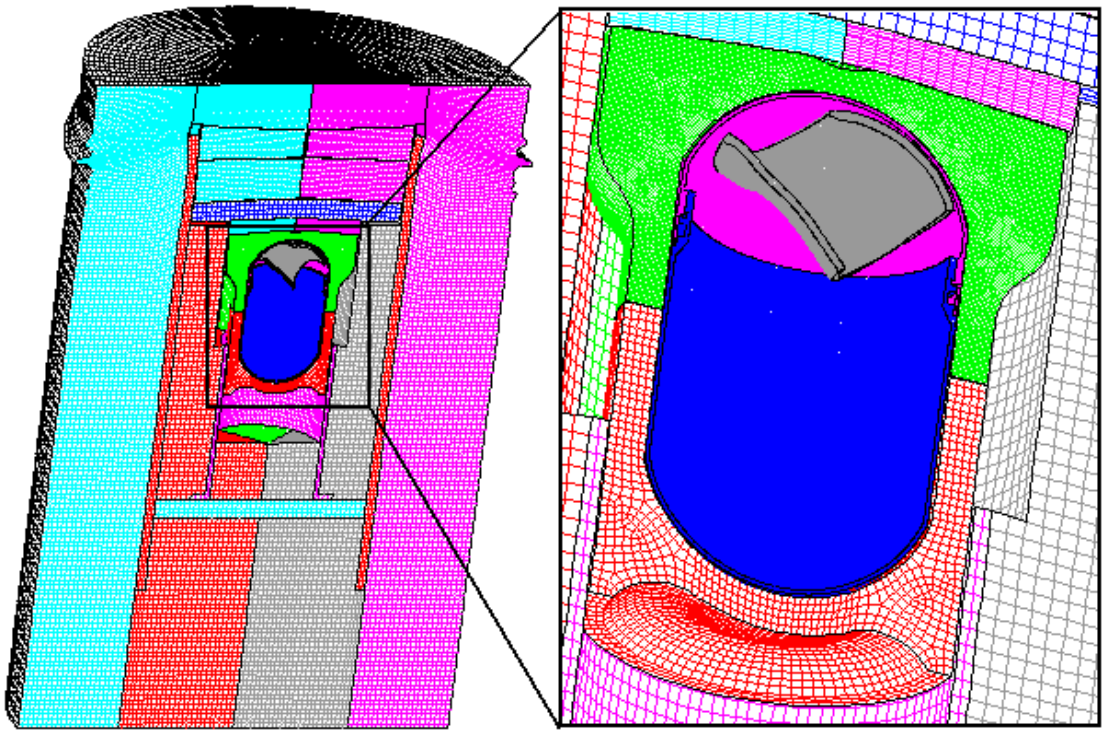

Figure 2-172. Finite Element Mesh for the 731-g, Angled, ER Cylinder, Bottom Position, Top Impact – Final Displacement

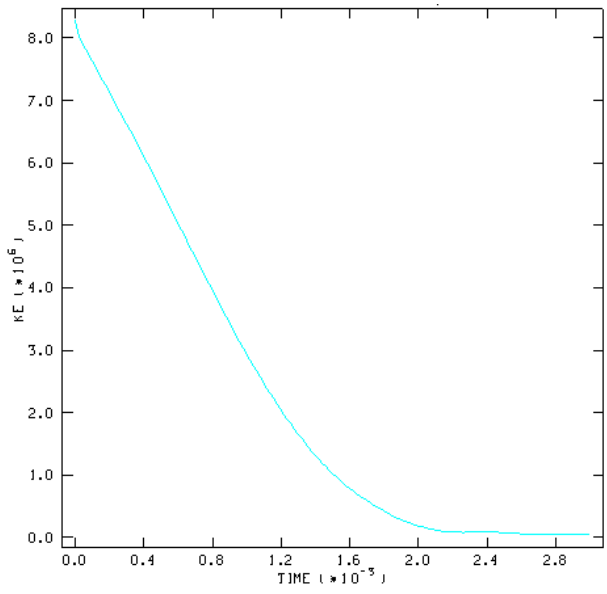

Figure 2-173. Kinetic Energy Time History for the 731-g, Angled, Plutonium Metal Hollow Cylinder, Bottom Position, Top Impact

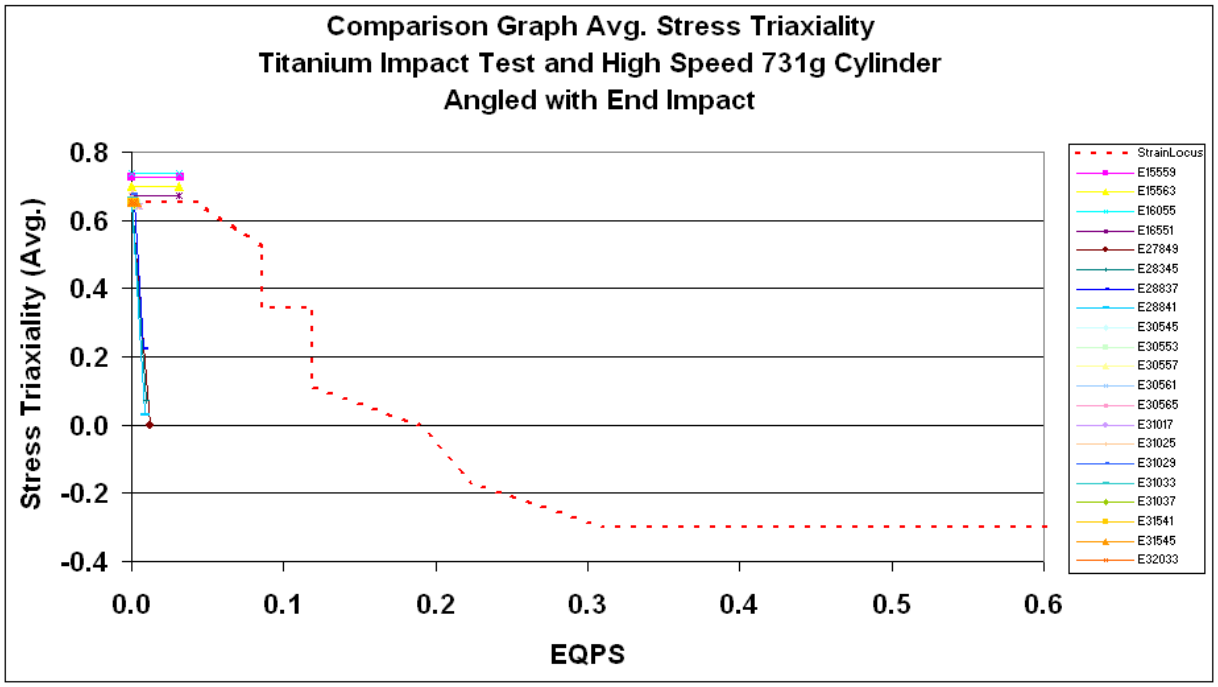

Figure 2-174. Graph of Average Stress Triaxiality versus EQPS of Elements Exceeding the Experimental Strain Locus for the 731-g, Angled, Plutonium Metal Hollow Cylinder, Bottom Position, Top Impact

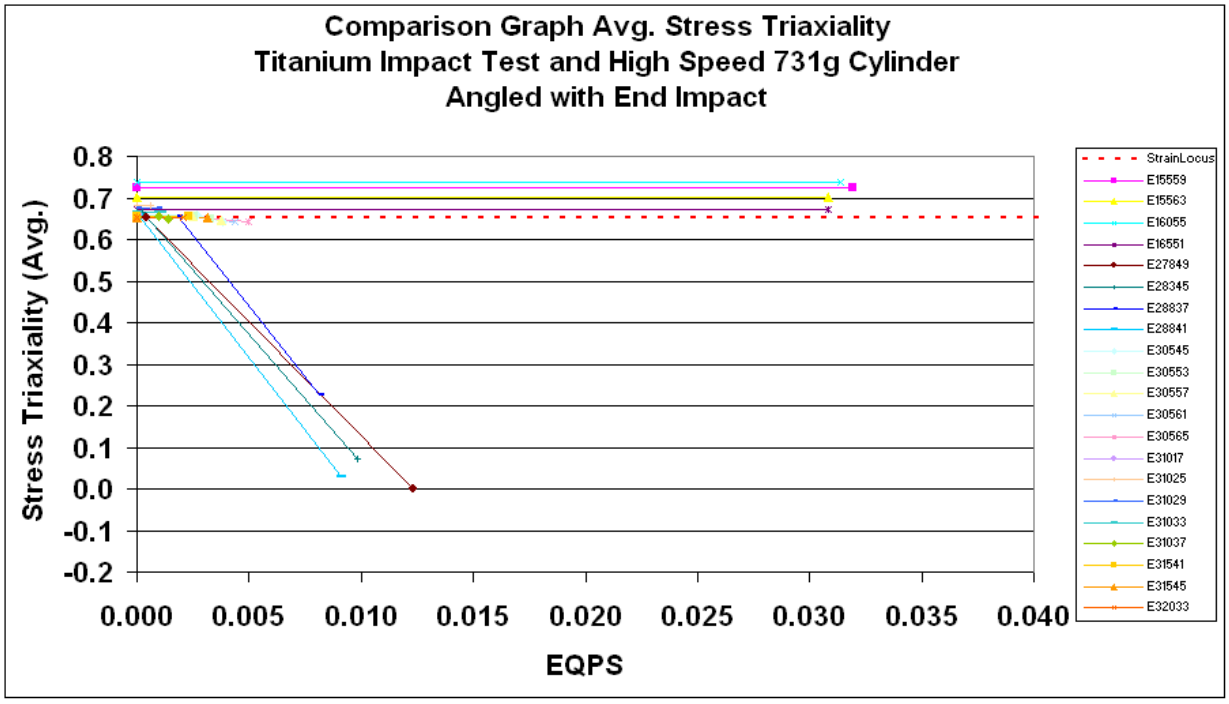

Figure 2-175. Graph of Average Stress Triaxiality versus EQPS of Elements Exceeding the Experimental Strain Locus (Zoomed In) for the 731-g, Angled, Plutonium Metal Hollow Cylinder, Bottom Position, Top Impact

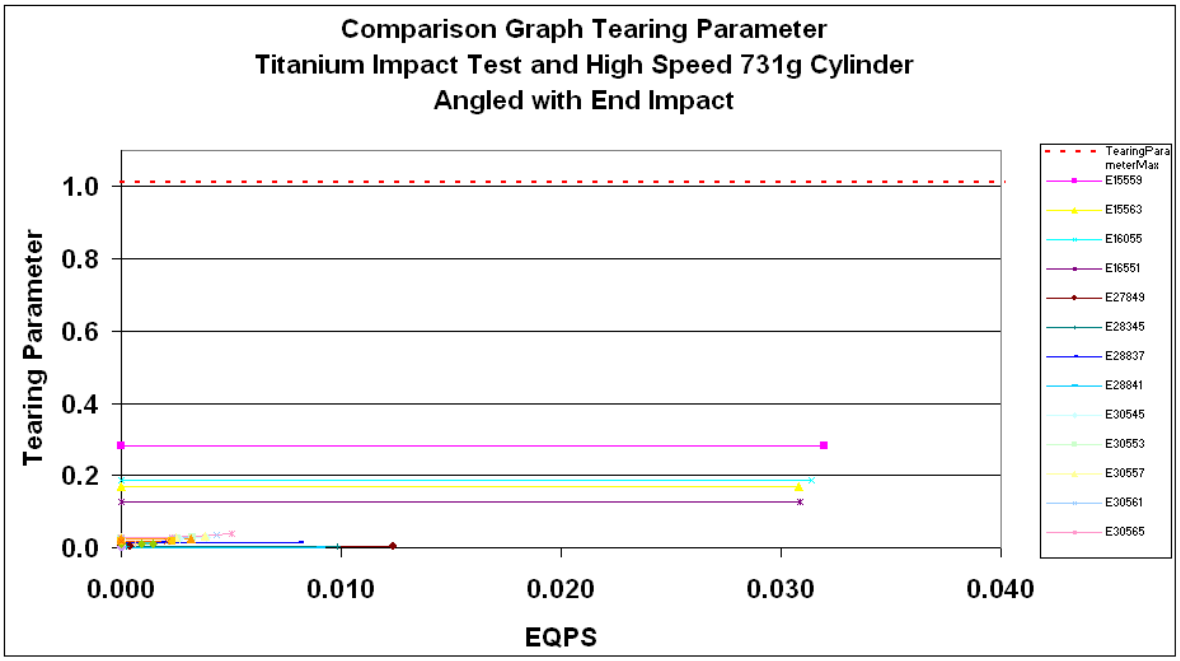

Figure 2-176. Graph of Tearing Parameter versus EQPS of Elements Exceeding the Experimental Strain Locus for the 731-g, Angled, Plutonium Metal Hollow Cylinder, Bottom Position, Top Impact

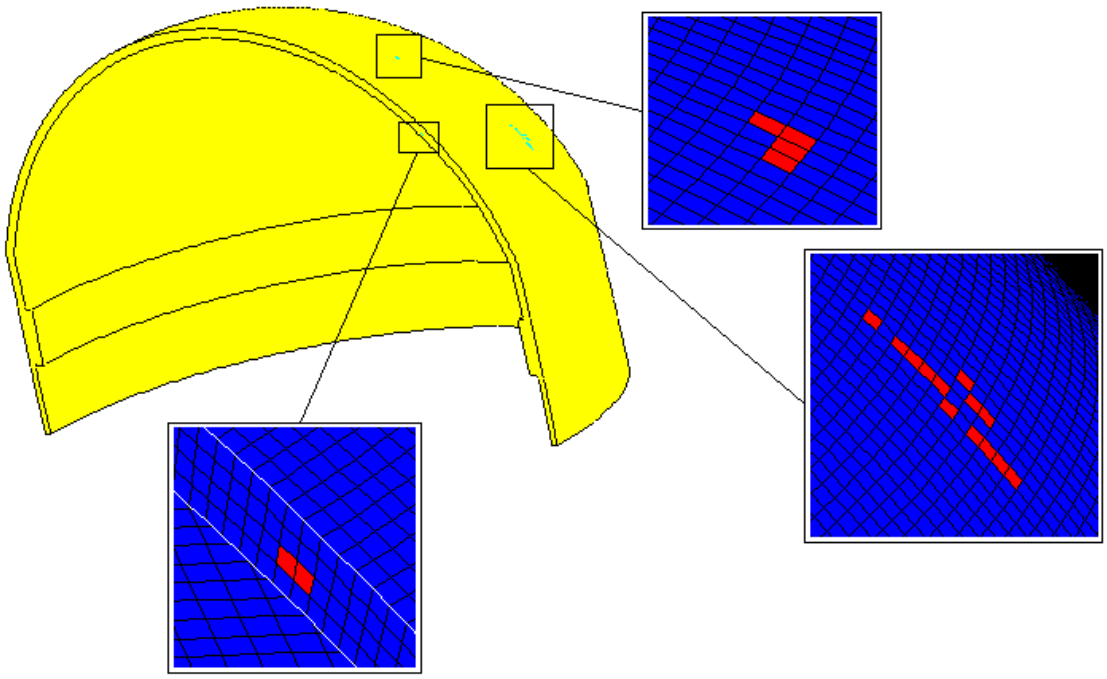

Figure 2-177. Plot of Elements Exceeding the Experimental Strain Locus for the 731-g, Angled, Plutonium Metal Hollow Cylinder, Bottom Position, Top Impact

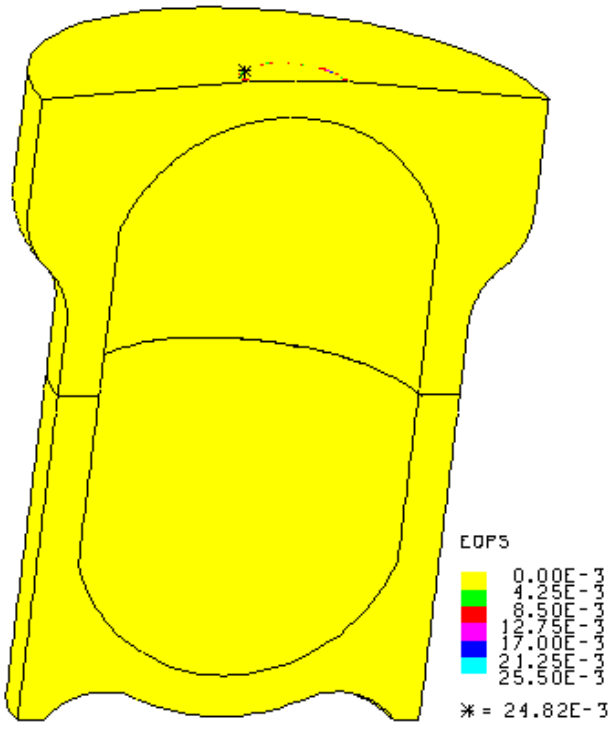

Figure 2-178. Plot of EQPS in the TB-1 for the 731-g, Angled, Plutonium Metal Hollow Cylinder, Bottom Position, Top Impact

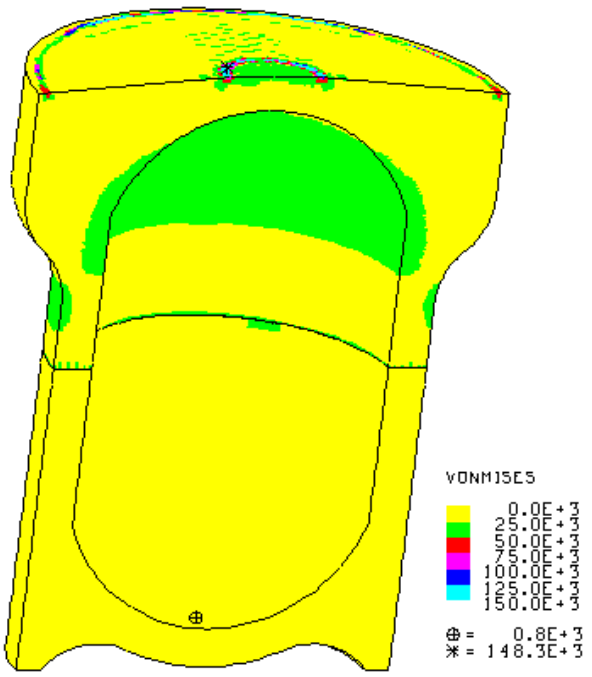

Figure 2-179. Plot of von Mises Stress for the 731-g, Angled, Plutonium Metal Hollow Cylinder, Bottom Position, Top Impact

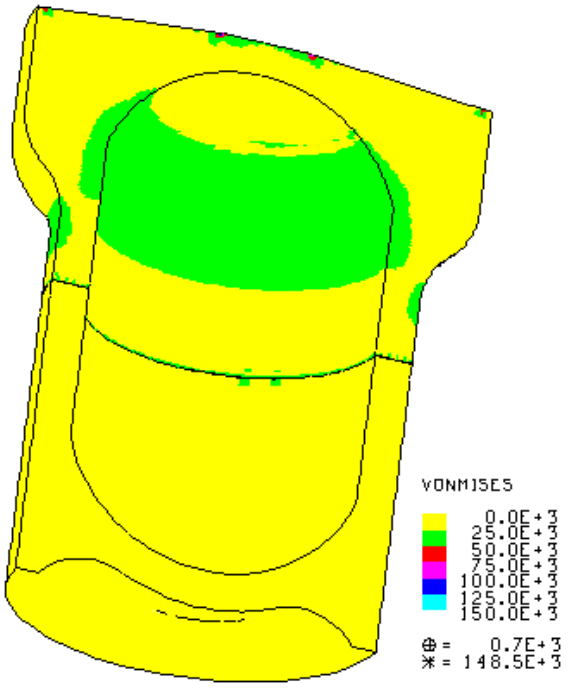

Figure 2-180. Plot of von Mises Stress for the 731-g, Angled, Plutonium Metal Hollow Cylinder, Bottom Position, Top Impact

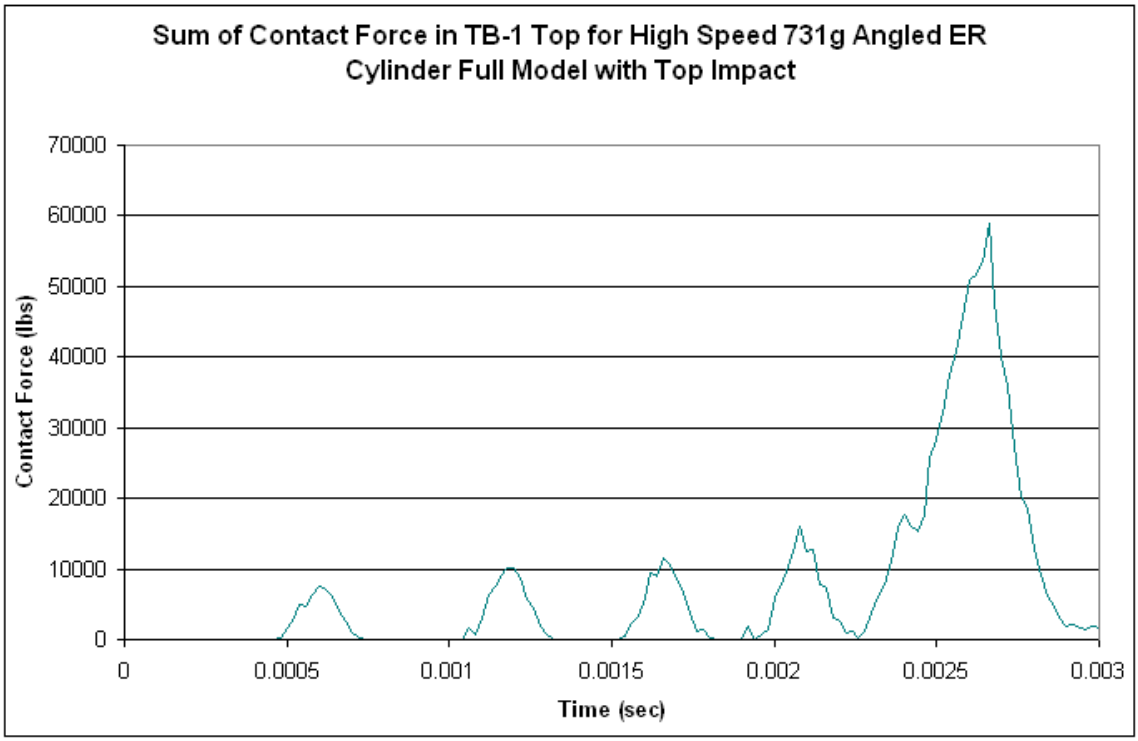

Figure 2-181. Plot of Contact Force for the 731-g, Angled, Plutonium Metal Hollow Cylinder, Bottom Position, Top Impact

2.12.5.4.9 Run 8 - 731-g Angled Plutonium Metal Hollow Cylinder CGOC Impact

The lid end CG-over-corner impact model for the shorter 731 g plutonium metal hollow cylinder is shown in Figure 2-182. The cylinder is located at the bottom of the T-Ampoule so that its net impact velocity with the top of the T-Ampoule is maximized. The post-impact deformation is shown in Figure 2-183 and its kinetic energy history in Figure 2-184. The plutonium metal hollow cylinder deforms slightly more than the previous case because of the slightly more side-impact-like orientation but maintains much of its original shape because of its conservatively "infinitely ductile" material constitutive model definition.

Average stress-triaxiality versus EQPS is shown in Figures 2-185 and 2-186 for the 84 elements extending beyond the tested Bao-Wierzbicki strain locus. All of these elements are at relatively high stress triaxiality and low EQPS. The Tearing Parameter values for these same 84 elements are shown in Figure 2-187 and all are still safely below the critical Tearing Parameter value of 1.012 for Ti-6Al-4V. These elements are highlighted in red in Figures 2-188 and 2-189 but these elements are still below the critical value, thus the T-Ampoule eutectic barrier integrity is maintained.

Peak EQPS in the TB-1 vessel is shown in Figure 2-190 to be about 28.5%, although this peak is only in a highly localized outer corner region where there is a slight contact over closure issue with the redwood overpack. Through-thickness plasticity is non-existent and the TB-1 integrity is maintained. The von Mises stress (see Figure 2-191) peak at 225 ksi (due to the localized redwood contact) is above the elevated-temperature minimum yield strength for the TB-1 of 141 ksi, but more importantly, through-thickness TB-1 stress values are less than 37.5 ksi, below yield.

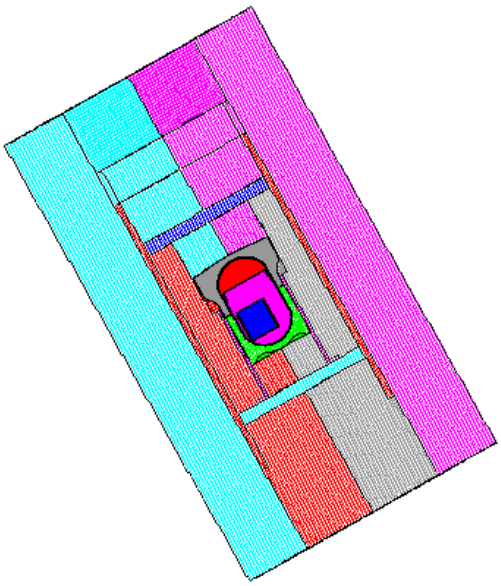

Figure 2-182. Finite Element Mesh for the 731-g, Angled, Plutonium Metal Hollow Cylinder, Bottom Position, CGOC Impact

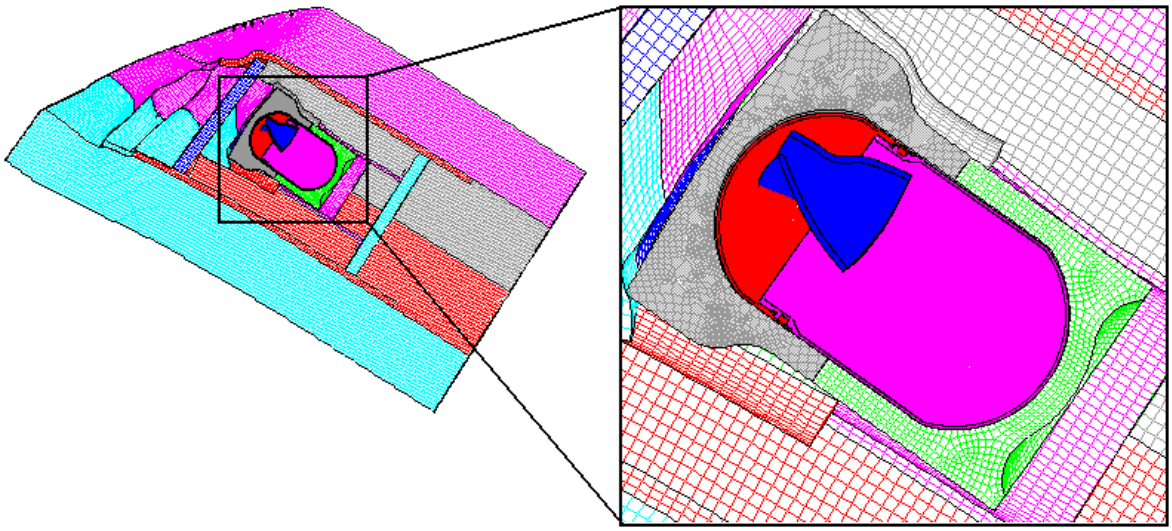

Figure 2-183. Finite Element Mesh for the 731-g, Angled, Plutonium Metal Hollow Cylinder, Bottom Position, CGOC Impact – Final Displacement

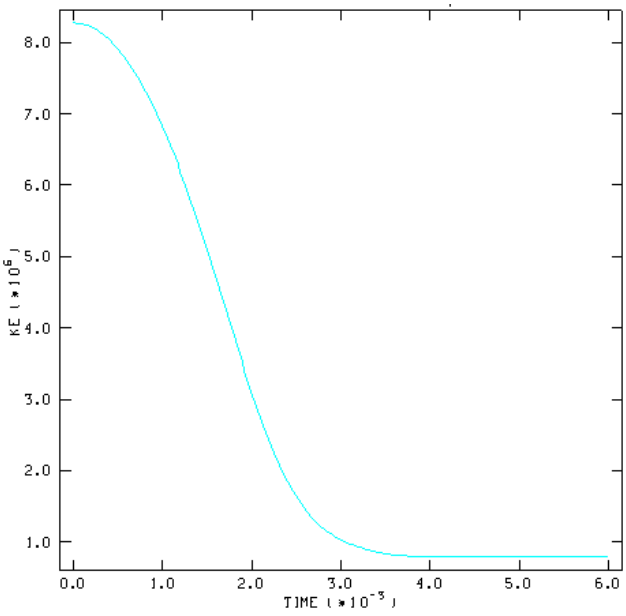

Figure 2-184. Kinetic Energy Time History for the 731-g, Angled, Plutonium Metal Hollow Cylinder, Bottom Position, CGOC Impact

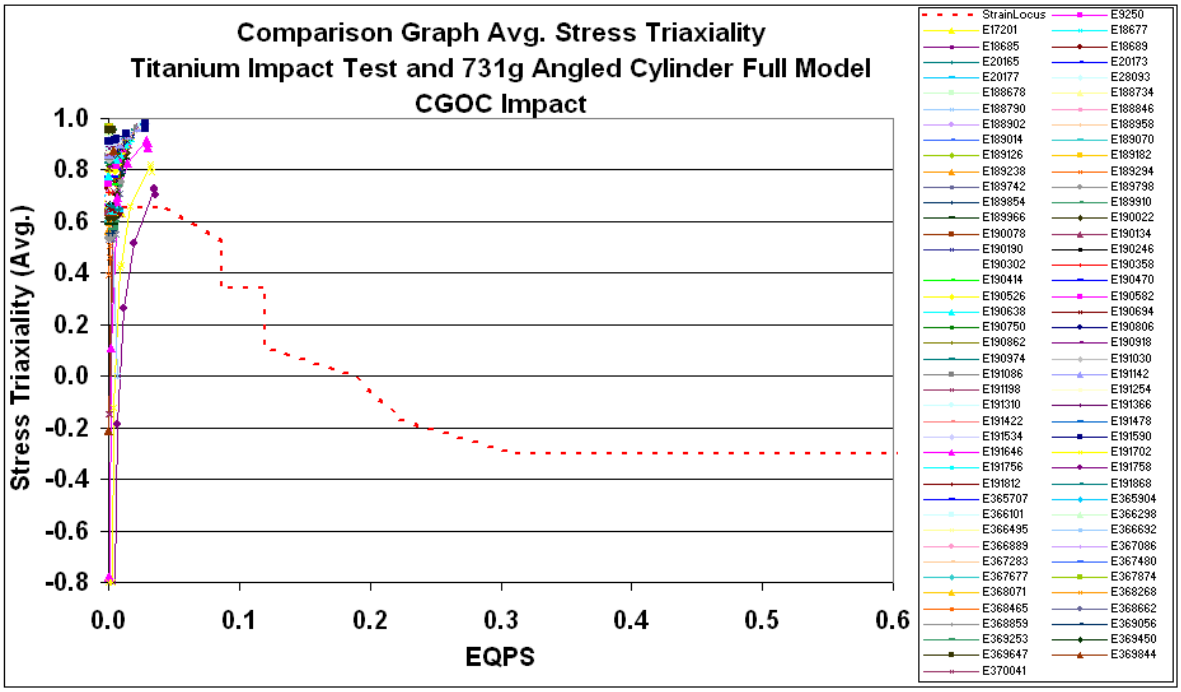

Figure 2-185. Graph of Average Stress Triaxiality versus EQPS of Elements Exceeding the Experimental Strain Locus for the 731-g, Angled, Plutonium Metal Hollow Cylinder, Bottom Position, CGOC Impact

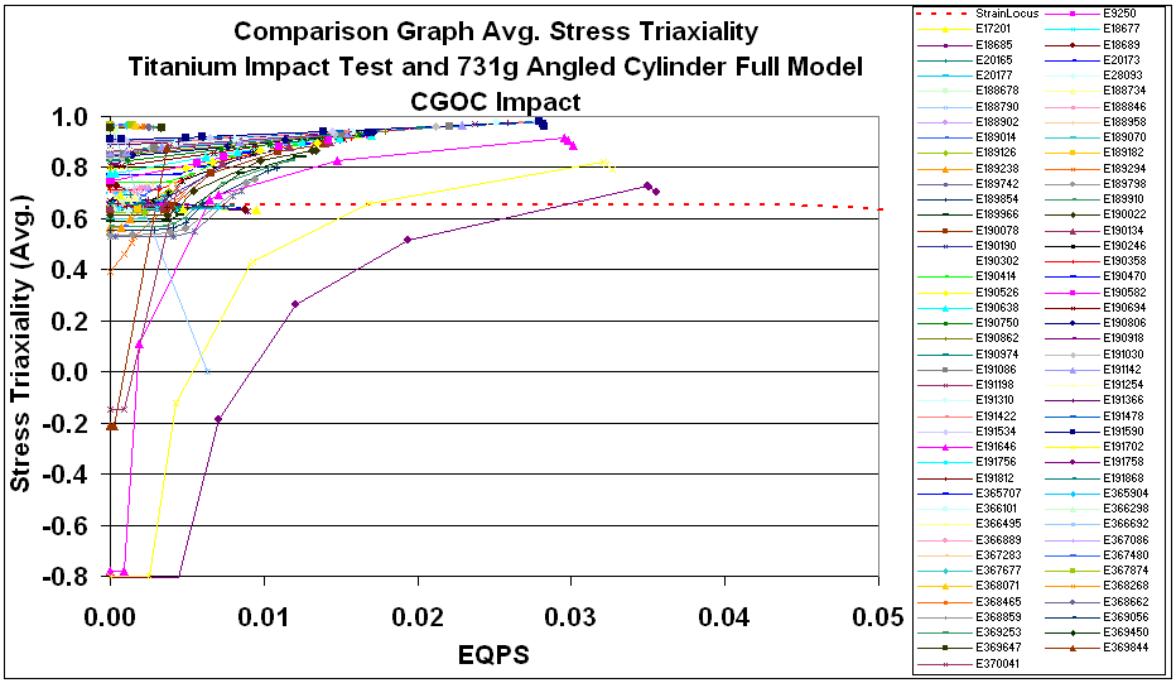

Figure 2-186. Graph of Average Stress Triaxiality versus EQPS of Elements Exceeding the Experimental Strain Locus (Zoomed In) for the 731-g, Angled, Plutonium Metal Hollow Cylinder, Bottom Position, CGOC Impact

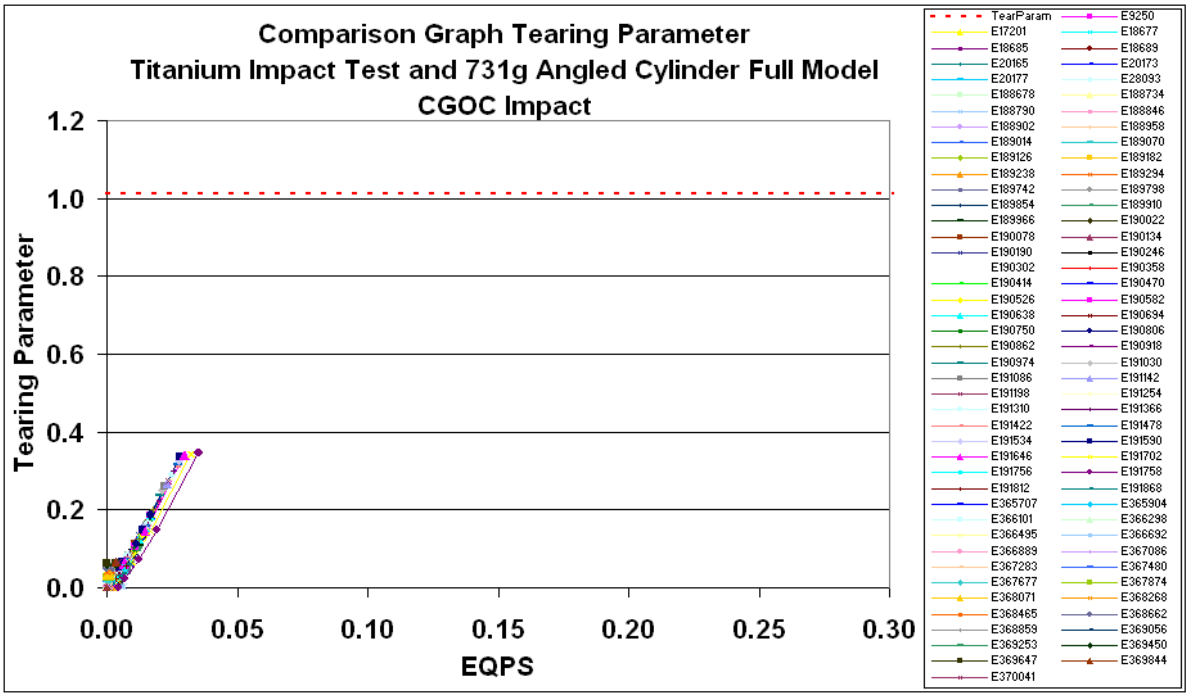

Figure 2-187. Graph of Tearing Parameter versus EQPS of Elements Exceeding the Experimental Strain Locus for the 731-g, Angled, Plutonium Metal Hollow Cylinder, Bottom Position, CGOC Impact

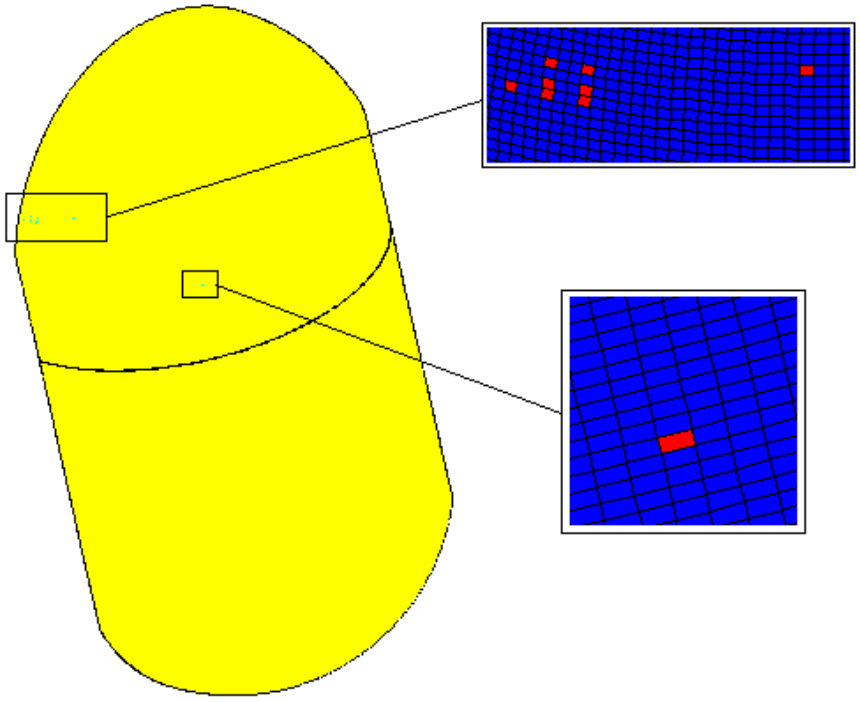

Figure 2-188. Plot of Elements Exceeding the Experimental Strain Locus for the 731-g, Angled, Plutonium Metal Hollow Cylinder, Bottom Position, CGOC Impact

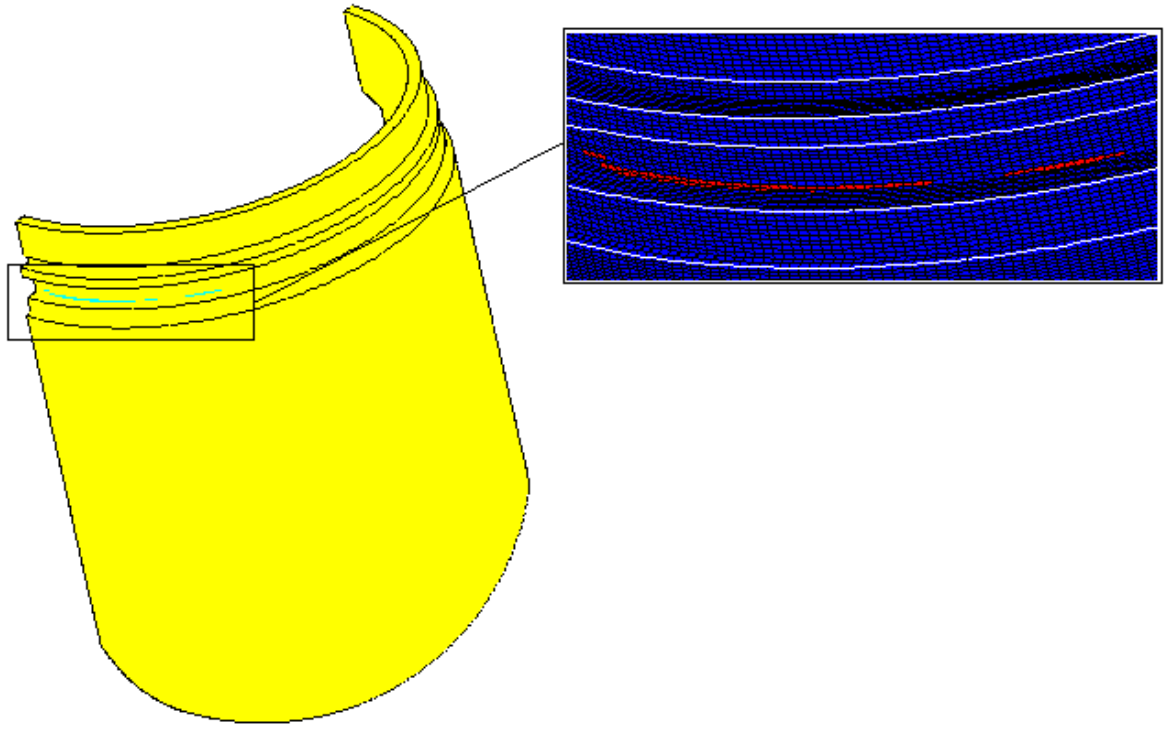

Figure 2-189. Plot of Elements Exceeding the Experimental Strain Locus for the 731-g, Angled, Plutonium Metal Hollow Cylinder, Bottom Position, CGOC Impact

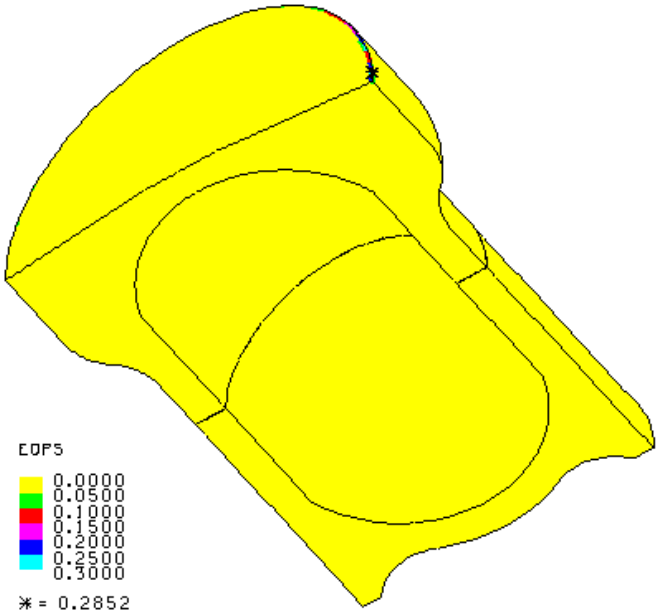

Figure 2-190. Plot of EQPS in the TB-1 for the 731-g, Angled, Plutonium Metal Hollow Cylinder, Bottom Position, CGOC Impact

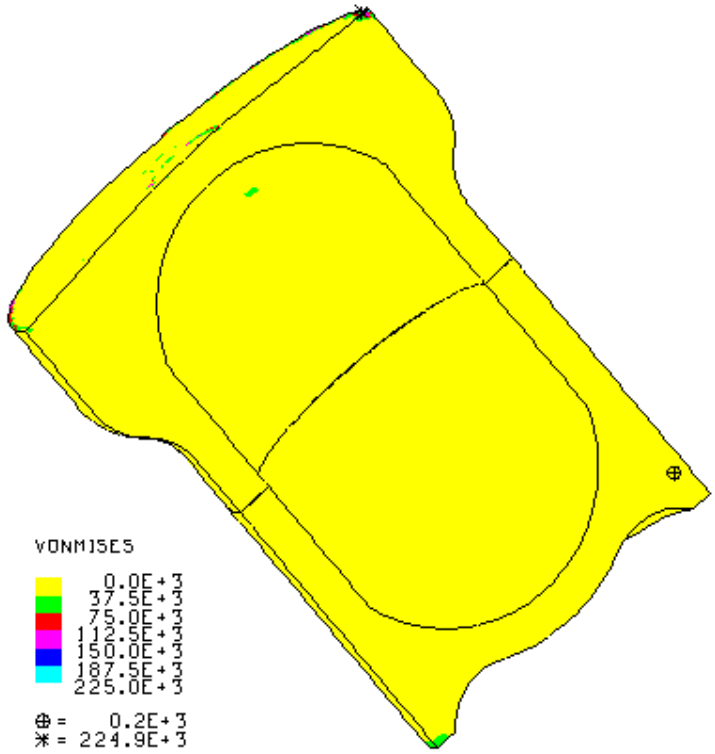

Figure 2-191. Plot of von Mises Stress in the TB-1 for the 731-g, Angled, Plutonium Metal Hollow Cylinder, Bottom Position, CGOC Impact

2.12.5.4.10 Run 9 - 731-g Plutonium Metal Hollow Cylinder Side Impact

The side impact model for the shorter and lighter 731 g plutonium metal hollow cylinder is shown in Figure 2-192. The cylinder is located at the far side of the T-Ampoule so that its net impact velocity with the side of the T-Ampoule is maximized. The post-impact deformation is shown in Figure 2-193 and its kinetic energy history in Figure 2-194. The plutonium metal hollow cylinder deforms much more than the previous case because of its weaker side-impact-like orientation.

Average stress-triaxiality versus EQPS is shown in Figures 2-195 and 2-196 for the 63 elements extending beyond the tested Bao-Wierzbicki strain locus. All of these elements are at relatively high stress triaxiality and low EQPS. The Tearing Parameter values for these same 63 elements are shown in Figure 2-197 and all are still below the critical Tearing Parameter value of 1.012 for Ti-6Al-4V. These elements are highlighted in red Figure 2-198 but these elements are still below the critical value and do not indicate failure; T-Ampoule integrity is maintained.

Peak EQPS in the TB-1 vessel is shown in Figures 2-199 through 2-202 and is about 30%, although this peak is only in a highly localized outer corner region where there is a slight contact overclosure issue with the redwood overpack. A slight (<1% EQPS) dent is visible in Figure 2-202 from the internal impact of the plutonium metal hollow cylinder into the TB-1 wall (via the T-Ampoule). Through-thickness plasticity is non-existent and the TB-1 integrity is maintained. The von Mises stresses (see Figures 2-203 and 2-204) peak at 225 ksi (due to the localized redwood contact), above the elevated-temperature minimum yield strength for the TB-1

of 141 ksi, but more importantly, through-thickness TB-1 stress values are less than 80 ksi, below yield.

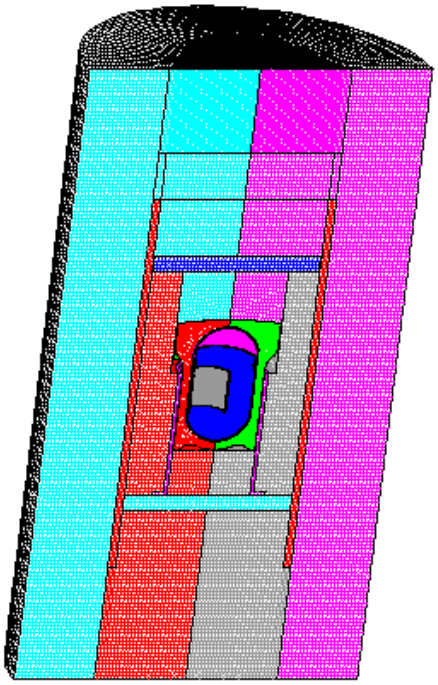

Figure 2-192. Finite Element Mesh for the 731-g, ER, Cylinder, Far Side Position, Side Impact

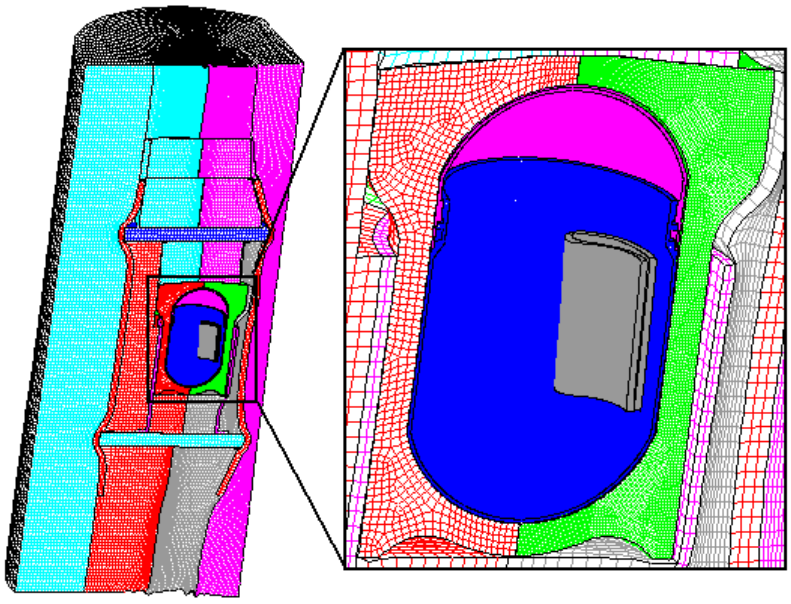

Figure 2-193. Finite Element Mesh for the 731-g, Plutonium Metal Hollow Cylinder, Far Side Position, Side Impact – Final Displacement

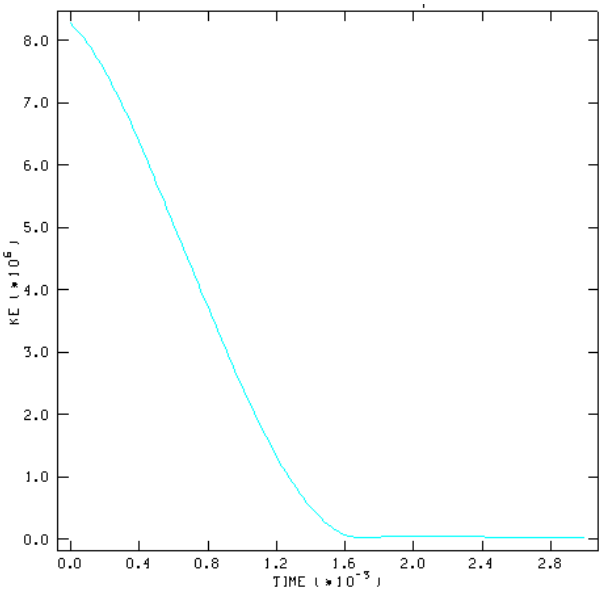

Figure 2-194. Kinetic Energy Time History for the 731-g, ER, Cylinder, Far Side Position, Side Impact

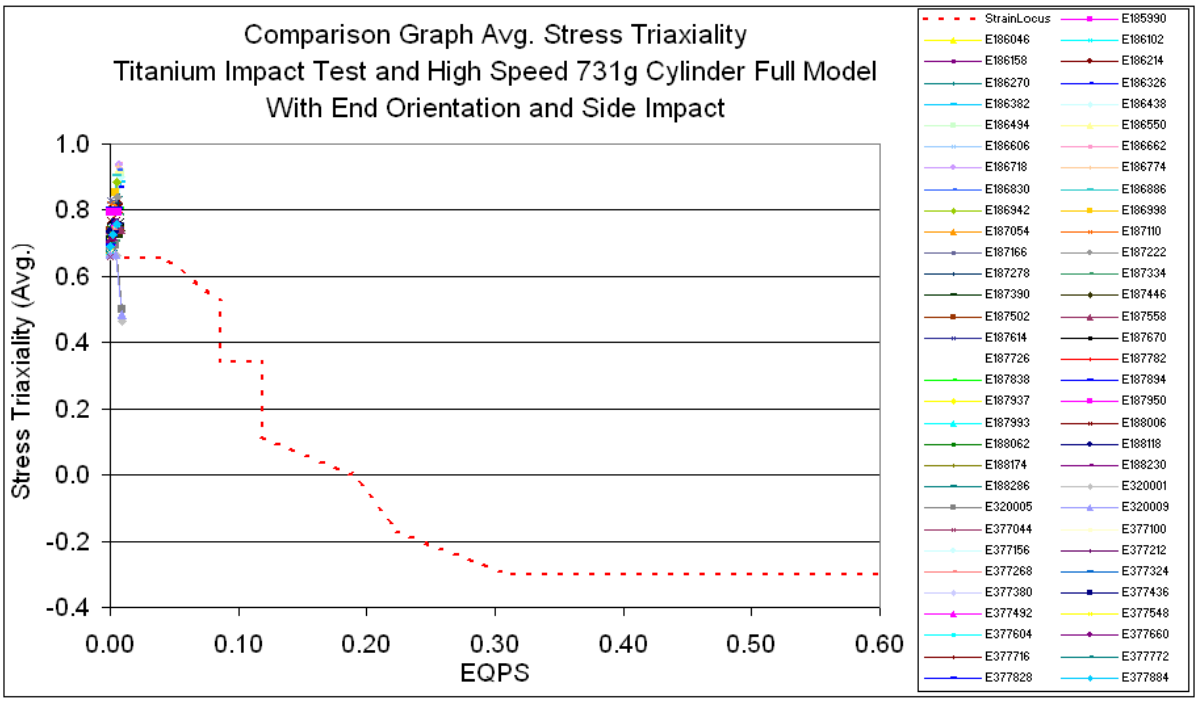

Figure 2-195. Graph of Average Stress Triaxiality versus EQPS of Elements Exceeding the Experimental Strain Locus for the 731-g, Plutonium Metal Hollow Cylinder, Far Side Position, Side Impact

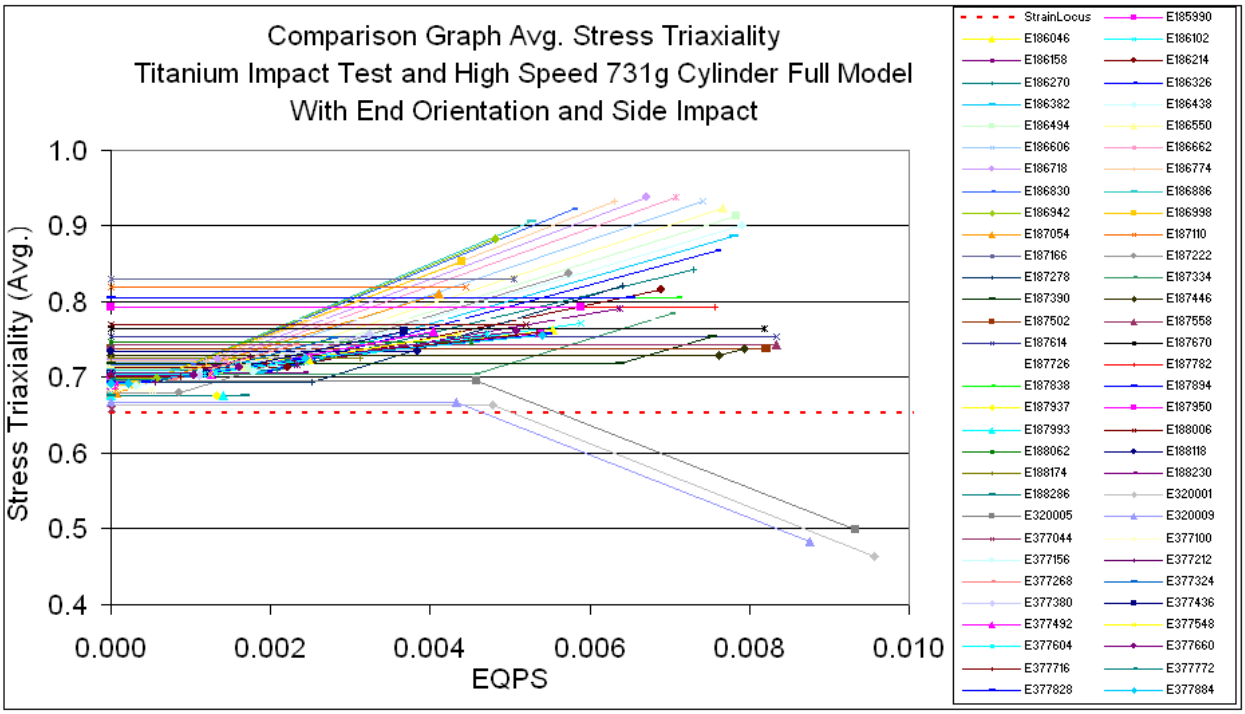

Figure 2-196. Graph of Average Stress Triaxiality versus EQPS of Elements Exceeding the Experimental Strain Locus (Zoomed In) for the 731-g, Plutonium Metal Hollow Cylinder, Far Side Position, Side Impact

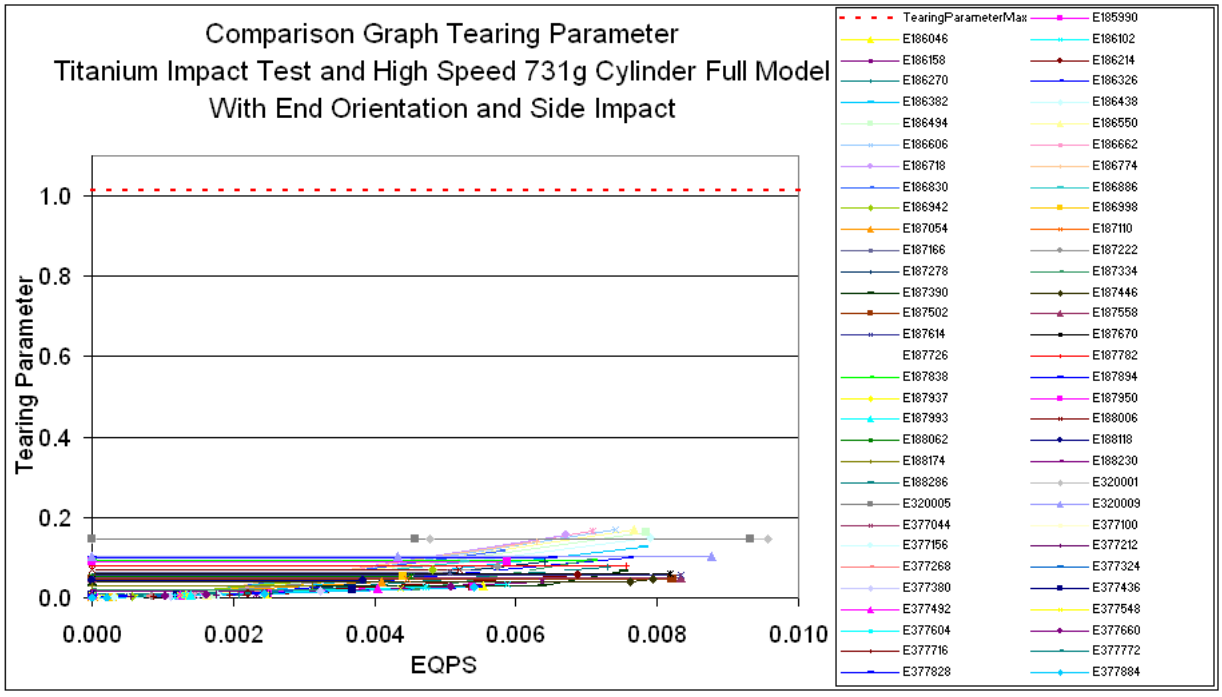

Figure 2-197. Graph of Tearing Parameter versus EQPS of Elements Exceeding the Experimental Strain Locus for the 731-g, Plutonium Metal Hollow Cylinder, Far Side Position, Side Impact

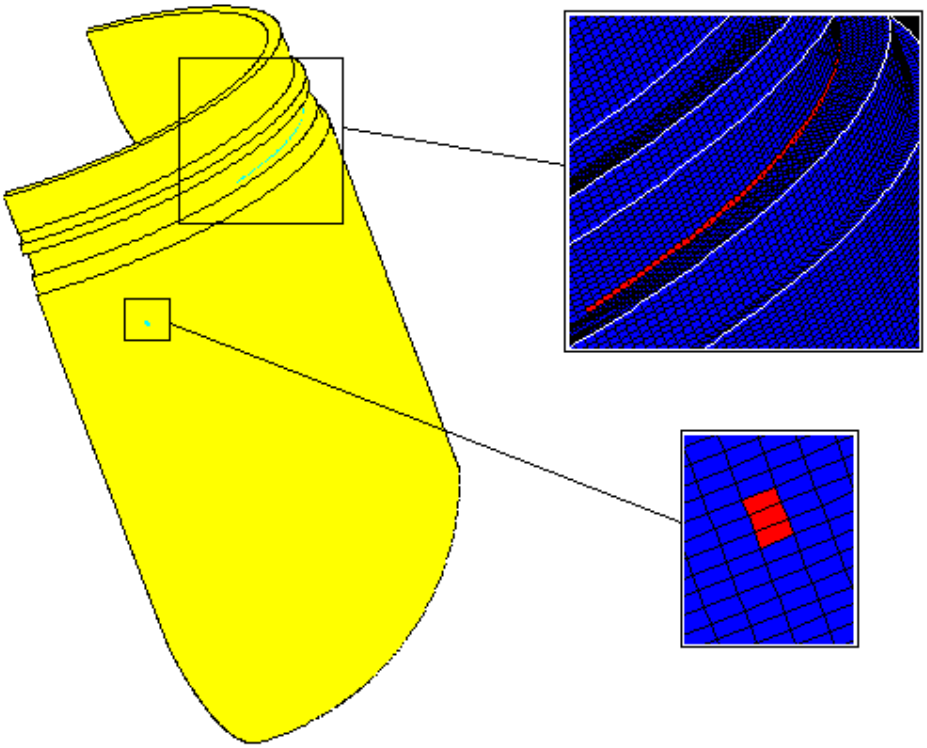

Figure 2-198. Plot of Elements Exceeding the Experimental Strain Locus for the 731-g, Plutonium Metal Hollow Cylinder, Far Side Position, Side Impact

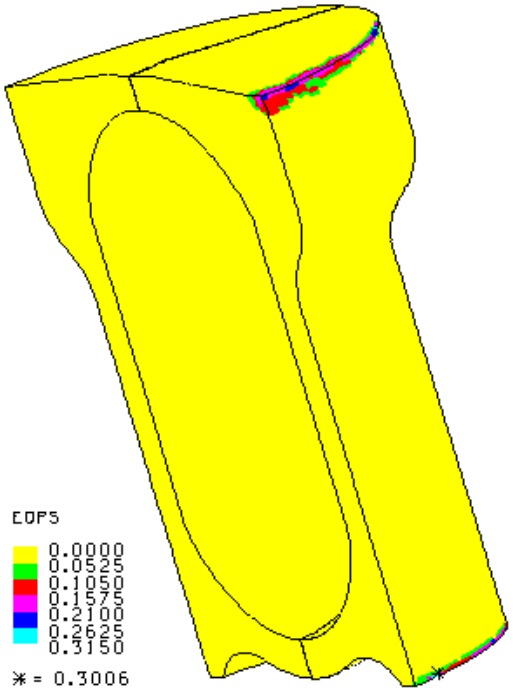

Figure 2-199. Plot of EQPS in the TB-1 for the 731-g, ER Cylinder, Far Side Position, Side Impact

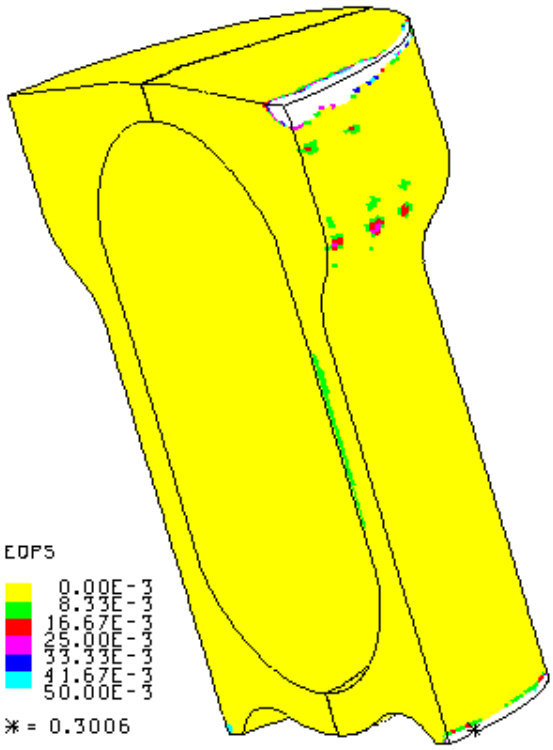

Figure 2-200. Plot of EQPS in the TB-1 for the 731-g, ER Cylinder, Far Side Position, Side Impact

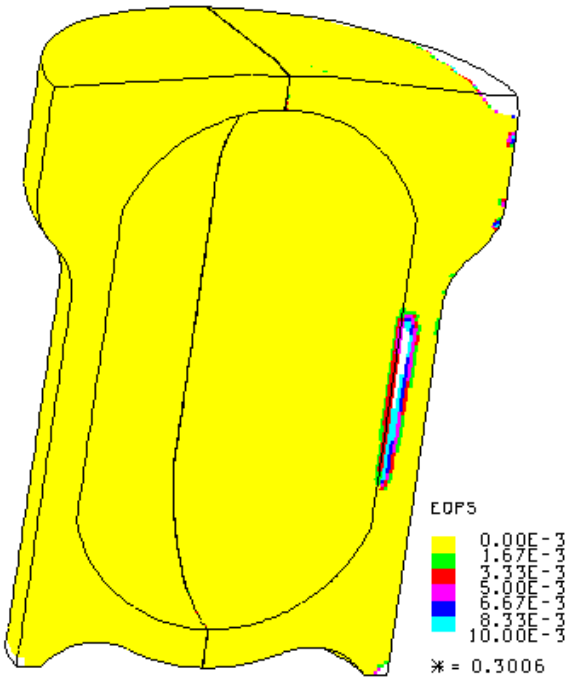

Figure 2-201. Plot of EQPS in the TB-1 for the 731-g, ER Cylinder, Far Side Position, Side Impact

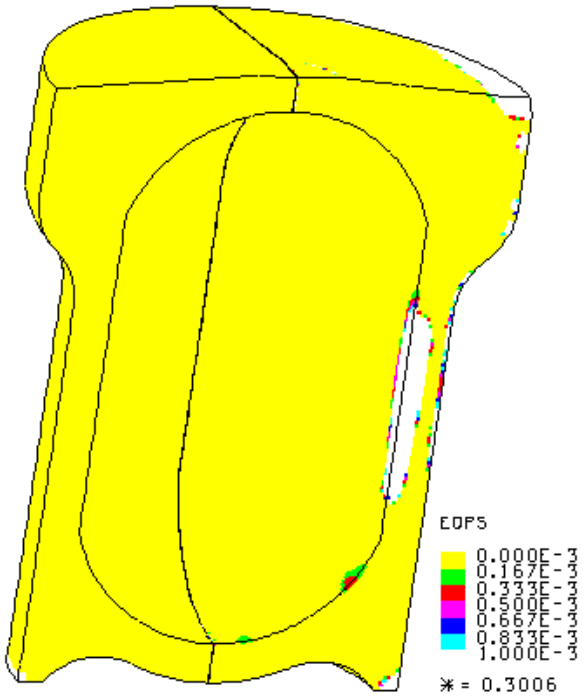

Figure 2-202. Plot of EQPS in the TB-1 for the 731-g, Plutonium Metal Hollow Cylinder, Far Side Position, Side Impact (Range Adjusted to Highlight Small Stains in the TB-1 Not Visible in Figure 2-201)

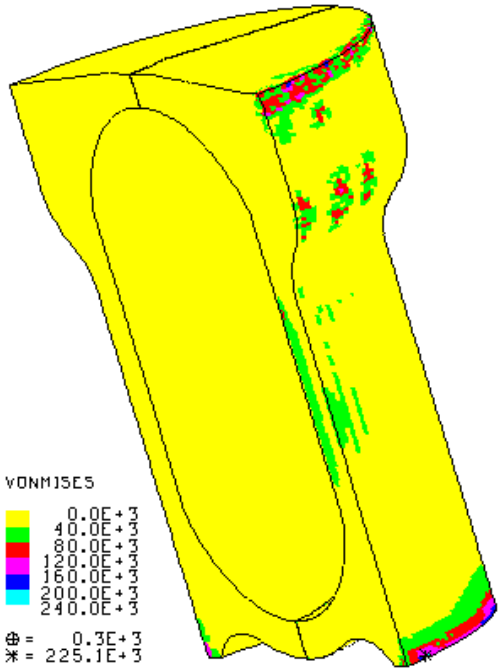

Figure 2-203. Plot of von Mises Stress in the TB-1 for the 731-g, Plutonium Metal Hollow Cylinder, Far Side Position, Side Impact

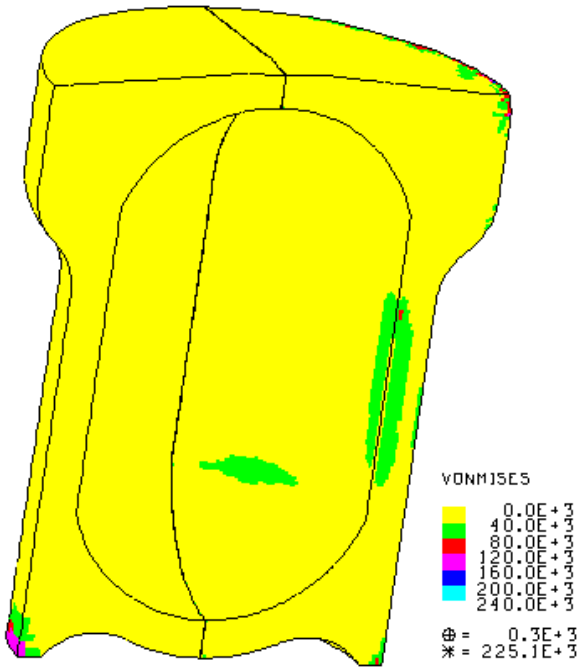

Figure 2-204. Plot of von Mises Stress in the TB-1 for the 731-g, Plutonium Metal Hollow Cylinder, Far Side Position, Side Impact (see Figure 2-203 Rotated to Show Internal Stresses)

2.12.5.4.11 Run 10 - 731-g Angled Plutonium Metal Hollow Cylinder Side Impact

The side impact model for the lighter, 731 g plutonium metal hollow cylinder, angled orientation, is shown in Figure 2-205. The cylinder is located at the far side of the T-Ampoule so that its net impact velocity with the side of the T-Ampoule is maximized, but also angled to present a sharp corner impact with the T-Ampoule surface. The post-impact deformation is shown in Figure 2-206 and its kinetic energy history in Figure 2-207. The plutonium metal hollow cylinder deforms moderately but maintains much of its original shape because of its conservatively "infinitely ductile" material constitutive model definition.

Average stress-triaxiality versus EQPS is shown in Figures 2-208 and 2-209 for the 94 elements extending beyond the tested Bao-Wierzbicki strain locus. All of these elements are at relatively high stress triaxiality and low EQPS. The Tearing Parameter values for these same 94 elements are shown in Figure 2-210 and all are still below the critical Tearing Parameter value of 1.012 for Ti-6Al-4V. These elements are highlighted in red Figure 2-211 but these elements are still below the critical value and do not indicate failure; T-Ampoule integrity is maintained.

Peak EQPS in the TB-1 vessel is shown in Figures 2-212 and 2-213 and is about 27.6%, although this peak is only in a highly localized outer corner region where there is a slight contact over closure issue with the redwood overpack. Through-thickness plasticity is non-existent and the TB-1 integrity is maintained. The von Mises stresses (see Figures 2-214 and 2-215) peak at 224 ksi (due to the localized redwood contact), above the elevated-temperature minimum yield strength for the TB-1 of 141 ksi, but more importantly, through-thickness TB-1 stress values are less than 112.5 ksi, below yield.

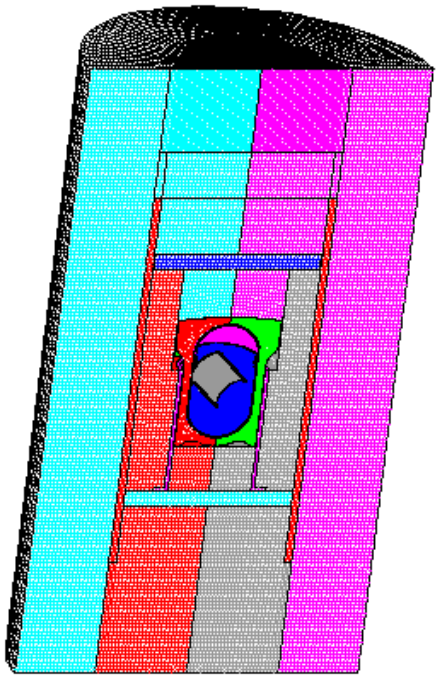

Figure 2-205. Finite Element Mesh for the 731-g, Angled, ER Cylinder, Far Side Position, Side Impact

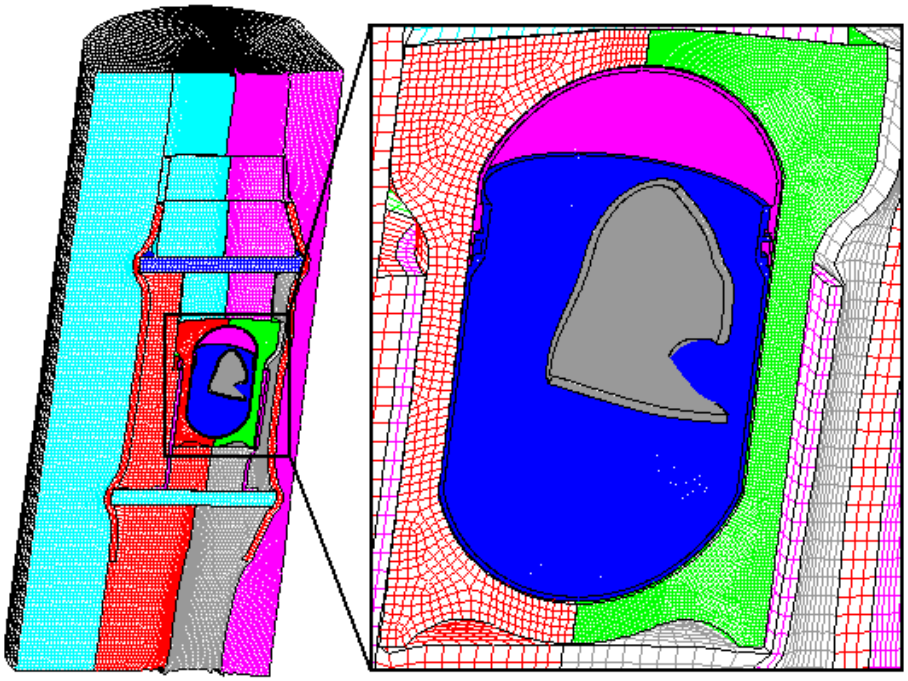

Figure 2-206. Finite Element Mesh for the 731-g, Angled, ER Cylinder, Far Side Position, Side Impact – Final Displacement

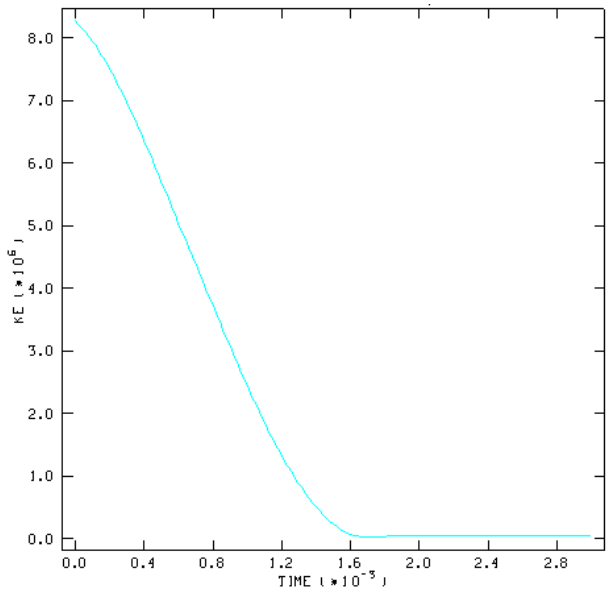

Figure 2-207. Kinetic Energy Time History for the 731-g, Angled, Plutonium Metal Hollow Cylinder, Far Side Position, Side Impact

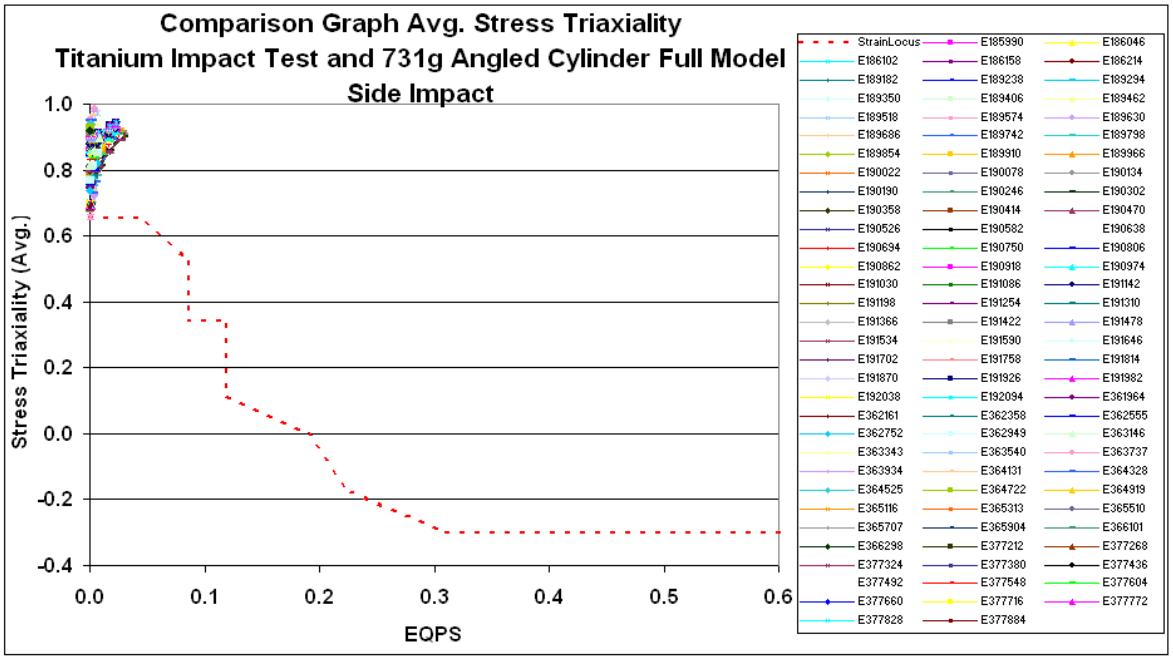

Figure 2-208. Graph of Average Stress Triaxiality versus EQPS of Elements Exceeding the Experimental Strain Locus for the 731-g, Angled, Plutonium Metal Hollow Cylinder, Far Side Position, Side Impact

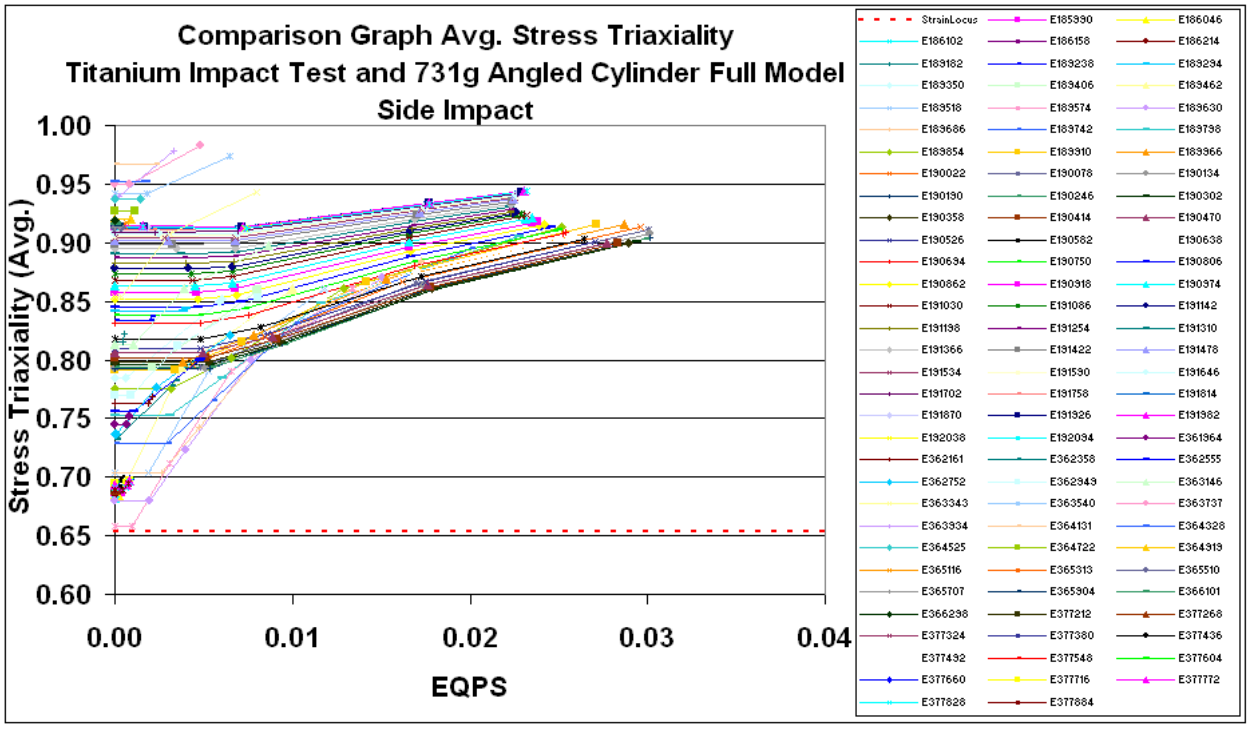

Figure 2-209. Graph of Average Stress Triaxiality versus EQPS of Elements Exceeding the Experimental Strain Locus (Zoomed In) for the 731-g, Angled, Plutonium Metal Hollow Cylinder, Far Side Position, Side Impact

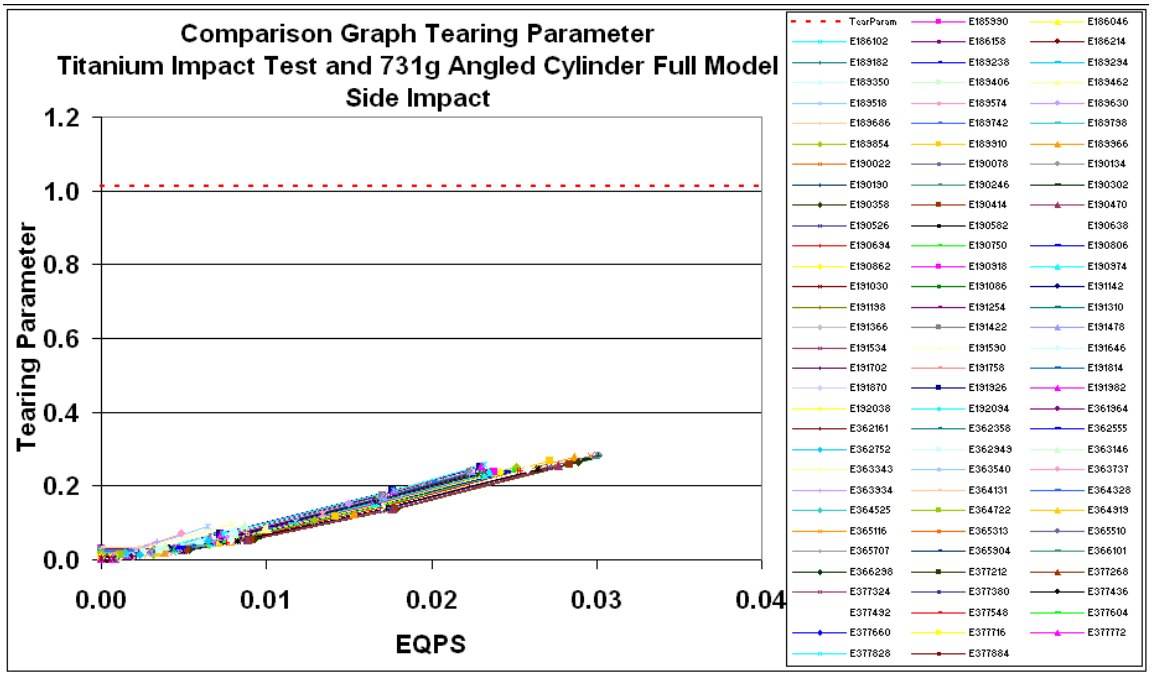

Figure 2-210. Graph of Tearing Parameter versus EQPS of Elements Exceeding the Experimental Strain Locus for the 731-g, Angled, Plutonium Metal Hollow Cylinder, Far Side Position, Side Impact

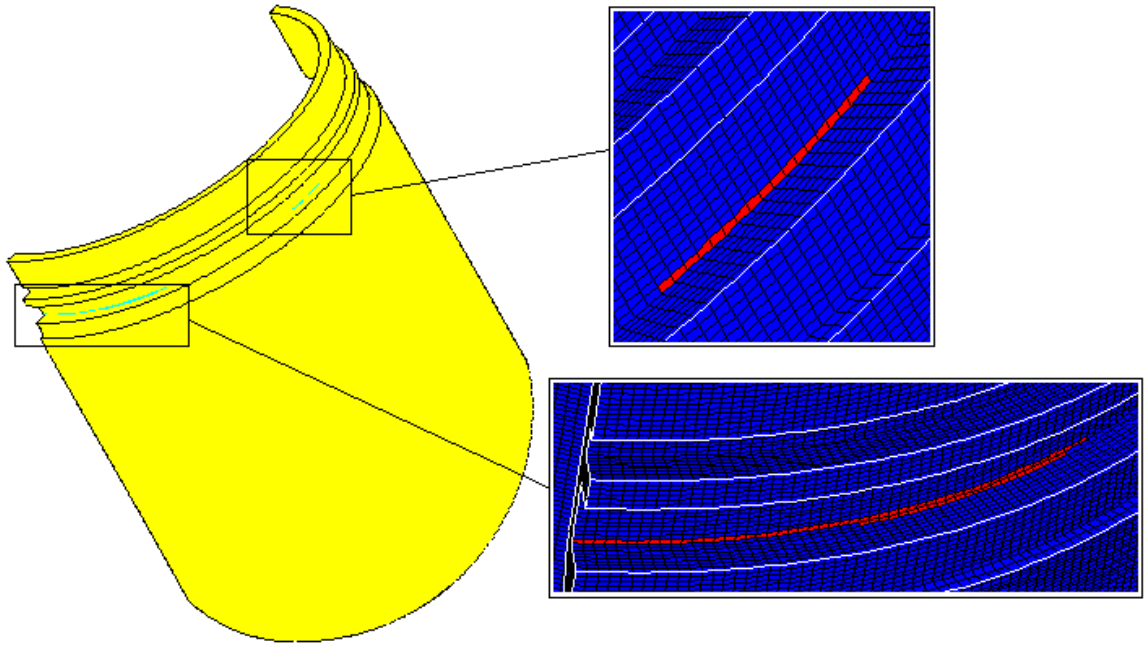

Figure 2-211. Plot of Elements Exceeding the Experimental Strain Locus for the 731-g, Angled, Plutonium Metal Hollow Cylinder, Far Side Position, Side Impact

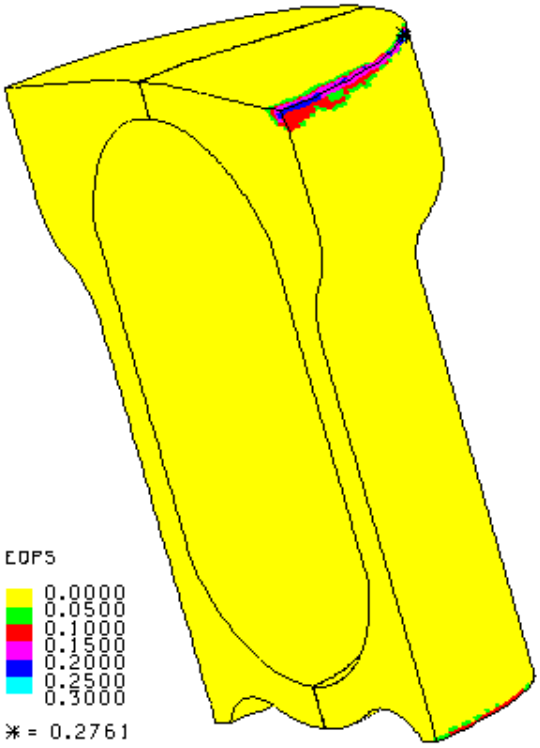

Figure 2-212. Plot of EQPS in the TB-1 for the 731-g, Angled, Plutonium Metal Hollow Cylinder, Far Side Position, Side Impact

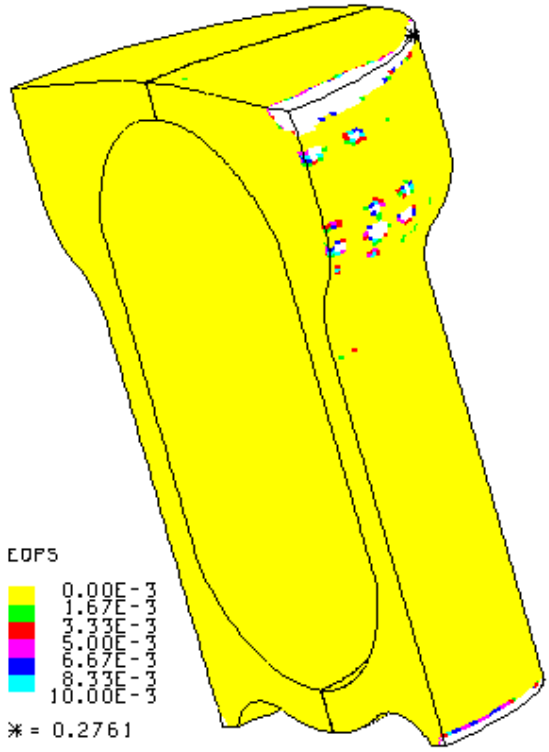

Figure 2-213. Plot of EQPS in the TB-1 for the 731-g, Angled, Plutonium Metal Hollow Cylinder, Far Side Position, Side Impact

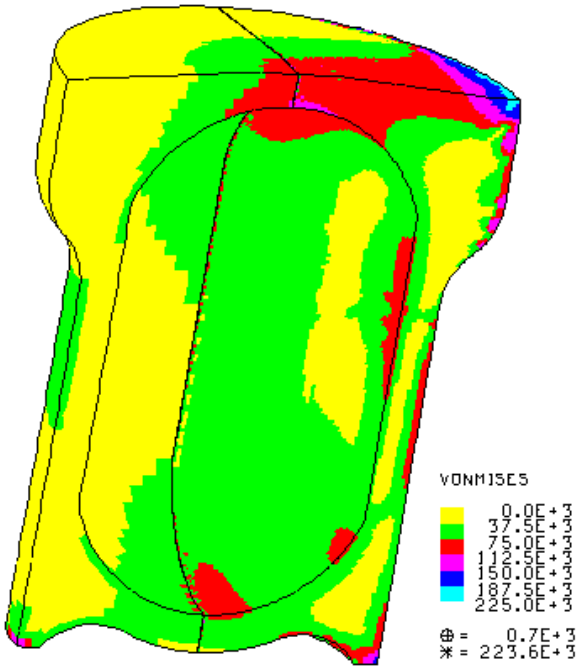

Figure 2-214. Plot of von Mises Stress in the TB-1 for the 731-g, Angled, Plutonium Metal Hollow Cylinder, Far Side Position, Side Impact

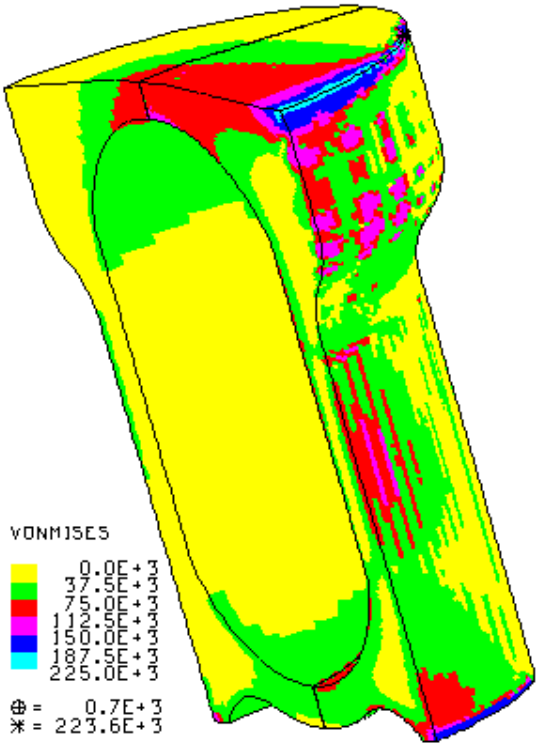

Figure 2-215. Plot of von Mises Stress in the TB-1 for the 731-g, Angled, Plutonium Metal Hollow Cylinder, Far Side Position, Side Impact

2.12.5.5 Sample Container Analyses

Seventeen separate sample container high speed impact analyses were conducted. The SC-1 (3 per cradle) sample containers can each contain 174 g solid cylinders of delta Pu or 60 g solid cylinders of Pu/Be composite. The larger SC-2 sample containers (2 per cradle) can contain 338 g solid cylinders of delta Pu each. Pu/Be composite payload is maximized using 3 SC-1 sample containers, so that case was analyzed as the bounding condition. There are several inherent conservatisms in the models:

1. In the sample containers, the tantalum foil used to package the cylinders inside the T-Ampoule is not modeled. The small quantity of energy it would absorb, and load spreading it would provide, is conservatively ignored. The sample container body is initially positioned with the Ti-6Al-4V support structure (inner cradle) and was shown in the NCT analyses to be unaltered after 4 ft. drops.

2. Although the plutonium contents are positioned using tantalum foil, no credit is taken for positioning the cylinder inside the sample container. Each analysis is run with the cylinder inside the ampoule positioned in a location farthest from the impact surface.

3. The Pu material is modeled using a power-law hardening constitutive model without fracture. The plutonium content of the sample containers is modeled as delta-plutonium, with material properties derived from Hecker and Stevens.[3] This material is very ductile; in order to maximize the energy and impulse load applied to the T-Ampoule wall, the

cylinder is modeled as a continuously hardened material model that does not fracture. Heavier alpha Pu density was assumed for the delta Pu to further decrease the cylinder size and increase its net impact velocity (for higher loads).

4. The beryllium composite material is modeled using a power-law hardening constitutive model without fracture. The Be composite content of the sample containers is conservatively modeled as delta-plutonium density (heavier and more compact than Be), yet higher material strength properties of Be. This material is very ductile; in order to maximize the energy and impulse load applied to the T-Ampoule wall, the cylinder is modeled as a continuously hardened material model that does not fracture. Heavier delta Pu density was assumed for the Be composite to further decrease the cylinder size and increase its net impact velocity (for higher loads).

5. The Be composite solid cylinders are always analyzed with their local orientation in a CG-over-corner fashion, so that their sharpest corner is presented to the SC wall and the T-Ampoule wall. This is not necessary for the much softer delta Pu cylinders.

6. The Pu and Be composite solid cylinders were dimensioned to represent the bounding configuration in terms of weight and size. They were sized to represent the worst-case for both impacting mass (maximizing the kinetic energy that needs to be absorbed by the T-Ampoule) and differential impact velocity between the cylinders and T-Ampoule.

7. The deformation of the sample container body does absorb a significant quantity of energy. To prevent the sample container body from absorbing an unrealistic quantity of energy, the Tearing Parameter failure criterion was implemented to limit the plastic deformation of the sample container and allow it to fracture. The fracture criterion, based on the work of Wellman,[4] was chosen for several reasons. First, the criterion works well for material in the high stress triaxiality region, which is the region where large bending stresses in the ampoule shell will lie. Second, the failure model has been implemented in the PRONTO-3D finite element code. Finally, the failure parameter can be determined from a tensile test model. Details of this model are presented in Section 2.12.3.8.

2.12.5.5.1 Run 11 - SC-1, Top Impact, Pu Contents

The top end impact model for each SC-1 with delta Pu contents is shown in Figure 2-216. Note that each Pu cylinder is located at the bottom of each SC-1 so that its net impact velocity with the top of the T-Ampoule is maximized. The post-impact deformation is shown in Figure 2-217 and its kinetic energy history in Figure 2-218. Note the similar degree of overpack crush up as compared to the certification test end impact in Figure 2-12, despite the slightly reduced impact velocity of 422 ft/sec versus the tested 445 ft/sec. The top SC-1 is crushed from the subsequent impacts of lower SC-1's, and its Pu contents nearly penetrate its upper wall, which directly impacts the T-Ampoule.

Equivalent Plastic Strain (EQPS) in the TB-1 containment vessel is shown, in Figure 2-219, to be less than 7.5% and exists only in some localized outer contact regions with the redwood overpack. The von Mises stresses (see Figure 2-220) peak at 147.1 ksi is just above the elevated-temperature minimum yield strength for the TB-1 of 141 ksi but more importantly, through-thickness TB-1 stress values are in the less-than-27.5 ksi range, below yield. The time at which

the peak value of the von Mises stress occurs coincides with the peak value of the contact force (summed over the lid area). A plot of this force as a function of time is shown in Figure 2-221. A maximum contact load of 27,874 lbs is applied to the inner surface of the TB-1 lid during the impact. No T-Ampoule elements exceeded the tested B-W strain locus and the peak Tearing Parameter value (see Table 2-11, run #11) of 0.0319 was below the critical Tearing Parameter value of 1.012 for Ti-6Al-4V.

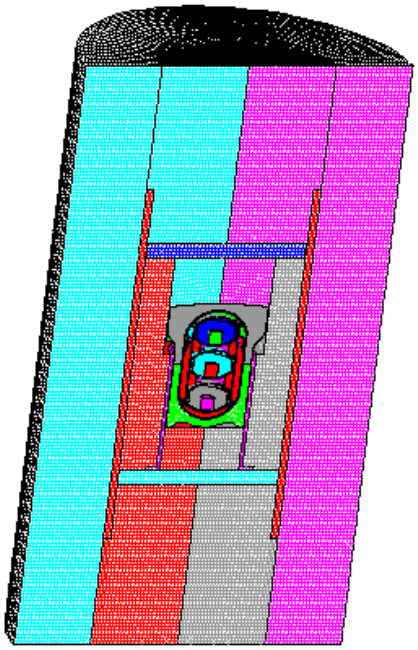

Figure 2-216. Finite Element Mesh for the SC-1, Pu Contents, End Impact

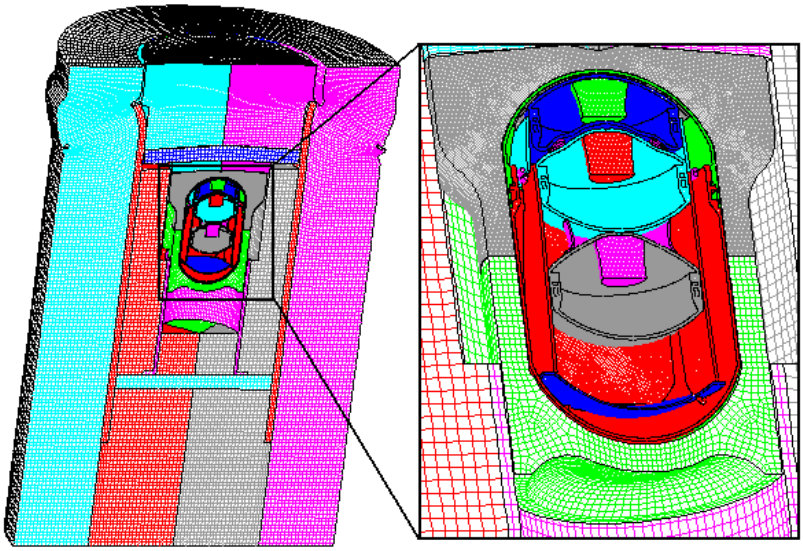

Figure 2-217. Finite Element Mesh for the SC-1, Pu Contents, End Impact – Final Displacement

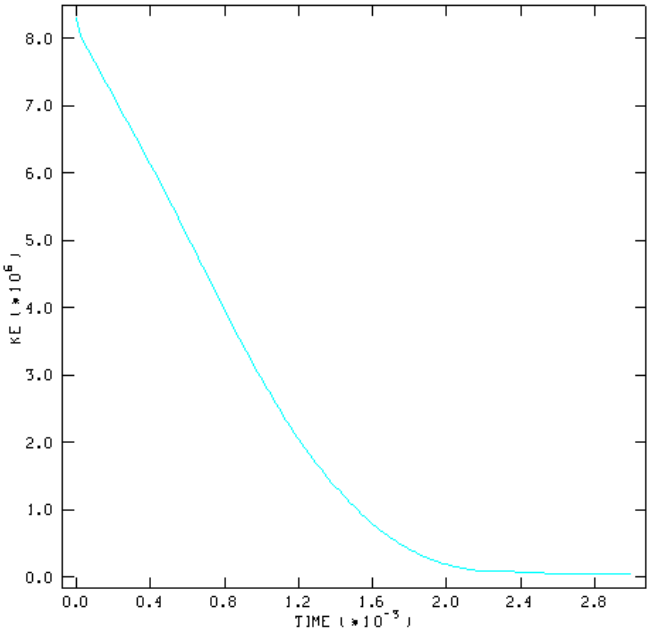

Figure 2-218. Kinetic Energy Time History for the SC-1, Pu Contents, End Impact

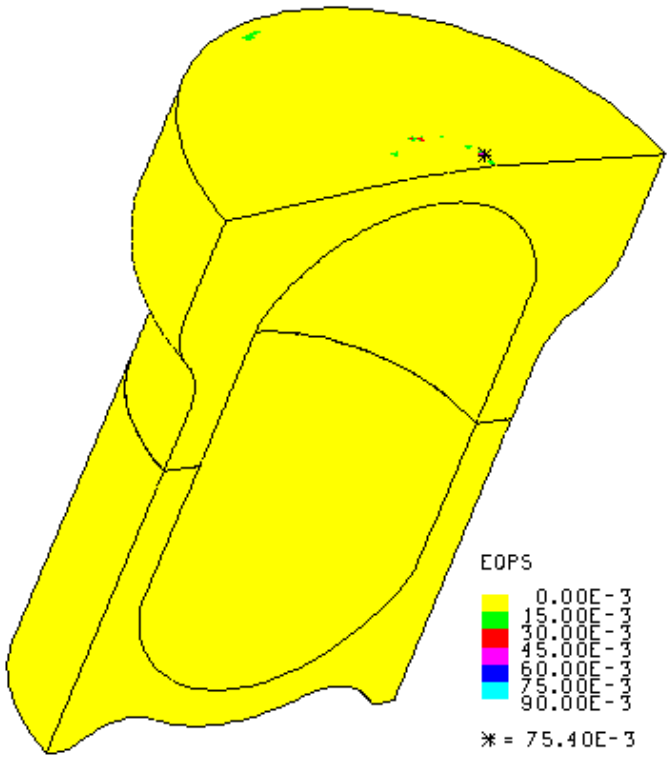

Figure 2-219. Plot of EQPS in the TB-1 for the SC-1, Pu Contents, End Impact

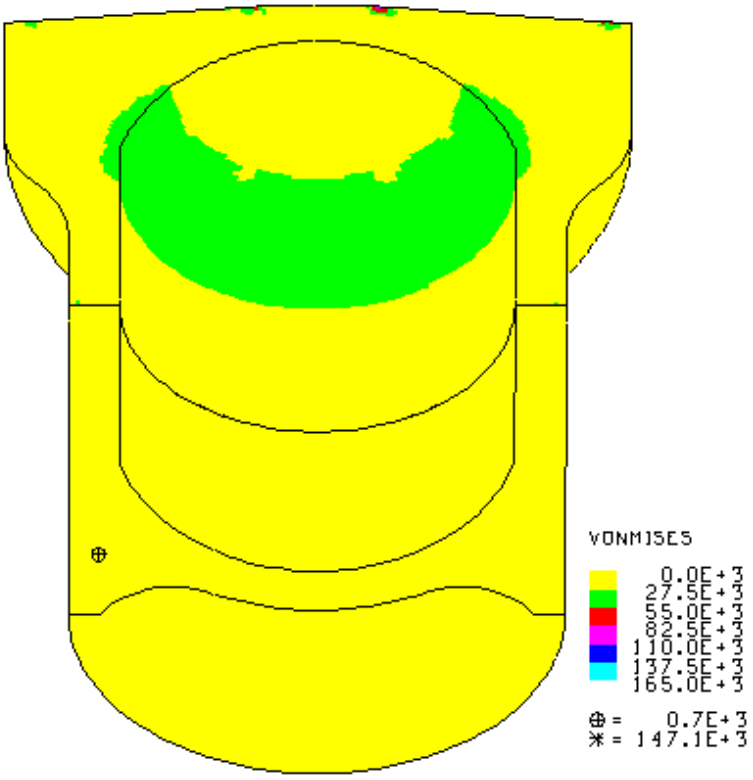

Figure 2-220. Plot of von Mises Stress in the TB-1 for the SC-1, Pu Contents, End Impact

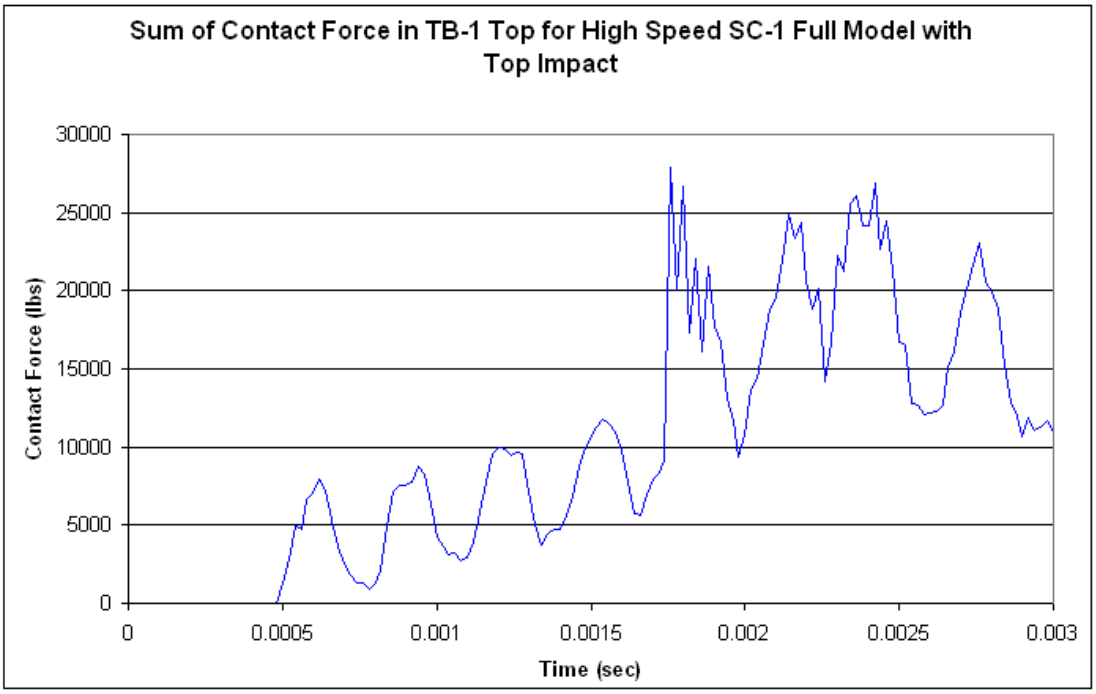

Figure 2-221. Plot of Contact Force in the TB-1 for the SC-1, Pu Contents, End Impact

2.12.5.5.2 Run 12 - SC-1 Sample Container, Side Impact, Support Structure 0°, Pu Contents

The side impact model for each SC-1 with delta Pu contents (cradle rotated 0 degrees) is shown in Figure 2-222. Note that each Pu cylinder is located at the far left side of each SC-1 so that its net impact velocity with the right side of the T-Ampoule is maximized. The post-impact deformation is shown in Figure 2-223 and its kinetic energy history in Figure 2-224. Note the similar degree of overpack crush up as compared to the certification test side impact in Figure 2-15, despite the slightly reduced impact velocity of 422 ft/sec versus the tested 445 ft/sec. The Pu contents penetrate each of the SC-1 side walls and directly impact the T-Ampoule.

Average stress-triaxiality versus EQPS is shown in Figure 2-225 for the 52 elements extending beyond the tested Bao-Wierzbicki strain locus. All of these elements are outside the B-W locus, for a variety of stress triaxialities, although most of the 580,000 T-Ampoule elements are inside the B-W locus. The Tearing Parameter values for these same 52 elements are shown in Figure 2-226 and all are below the critical Tearing Parameter value of 1.012 for Ti-6Al-4V. These elements are highlighted in red in Figures 2-227, 2-228, and 2-229, but note that these elements are still below the initiation of a ductile tear and thus T-Ampoule integrity is maintained.

Equivalent Plastic Strain (EQPS) in the TB-1 vessel is shown in Figures 2-230, 2-231, 2-232, and 2-233 to be less than 45% but only in some localized outer contact regions with the redwood overpack (contact modeling artifact). The EQPS due to internal denting of the upper SC-1 is shown in Figure 2-232 to be less than 0.01%, which is essentially elastic. The von Mises stresses (see Figure 2-234) peak at 273.5 ksi, above the elevated-temperature minimum yield strength for the TB-1 of 141 ksi but more importantly, through-thickness TB-1 stress values are in the less-than-47.5 ksi range, below yield.

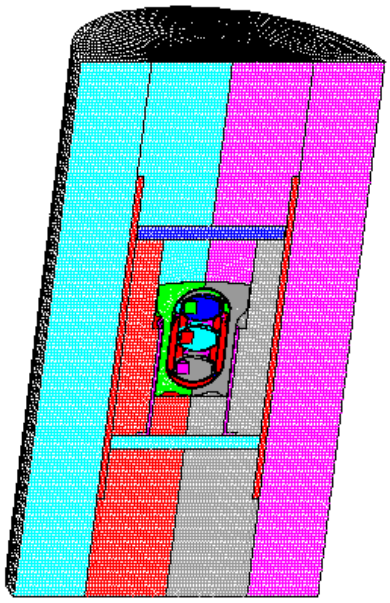

Figure 2-222. Finite Element Mesh for the SC-1, Pu Contents, Side Impact, 0° Support Structure

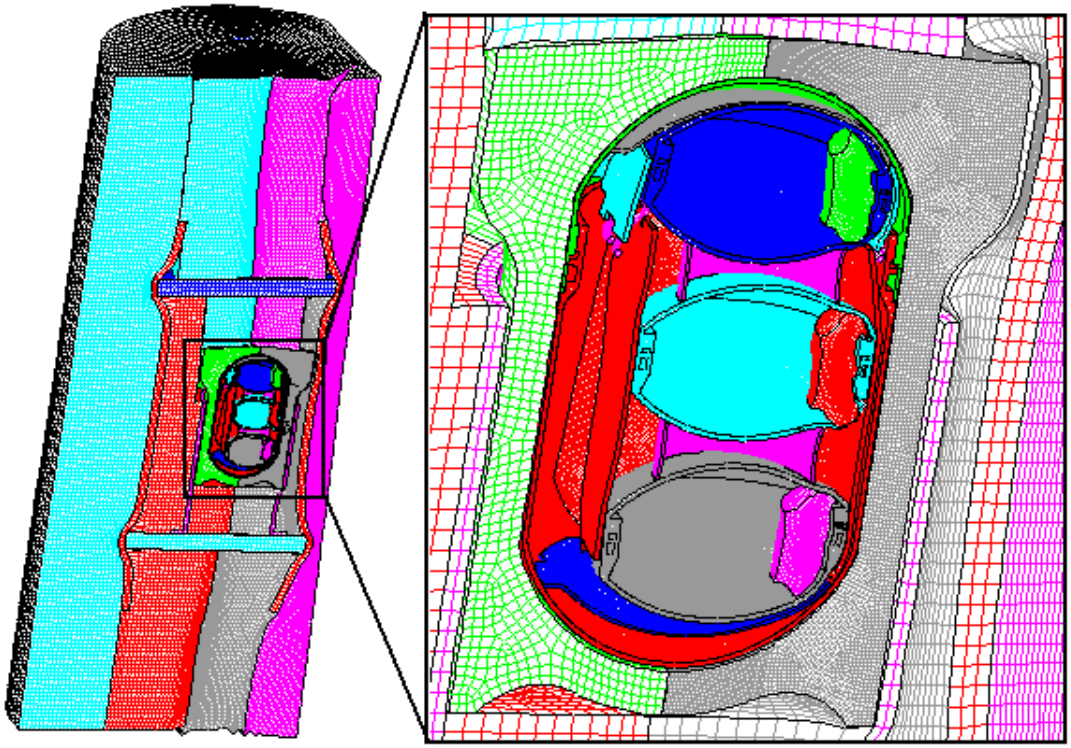

Figure 2-223. Finite Element Mesh for the SC-1, Pu Contents, Side Impact, 0° Support Structure – Final Displacement

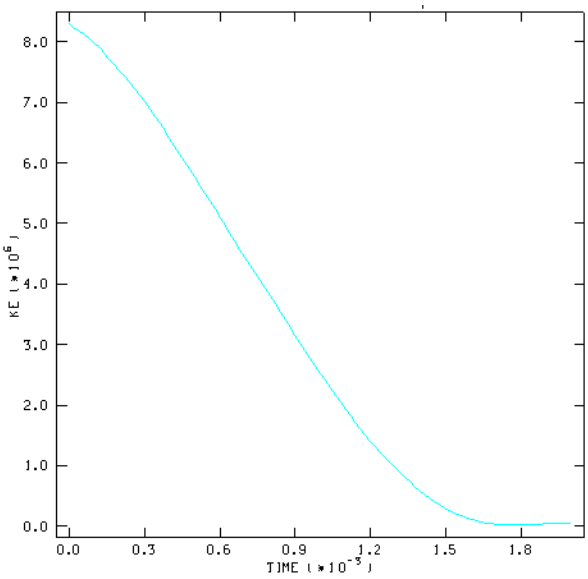

Figure 2-224. Kinetic Energy Time History for the SC-1, Pu Contents, Side Impact, 0° Support Structure

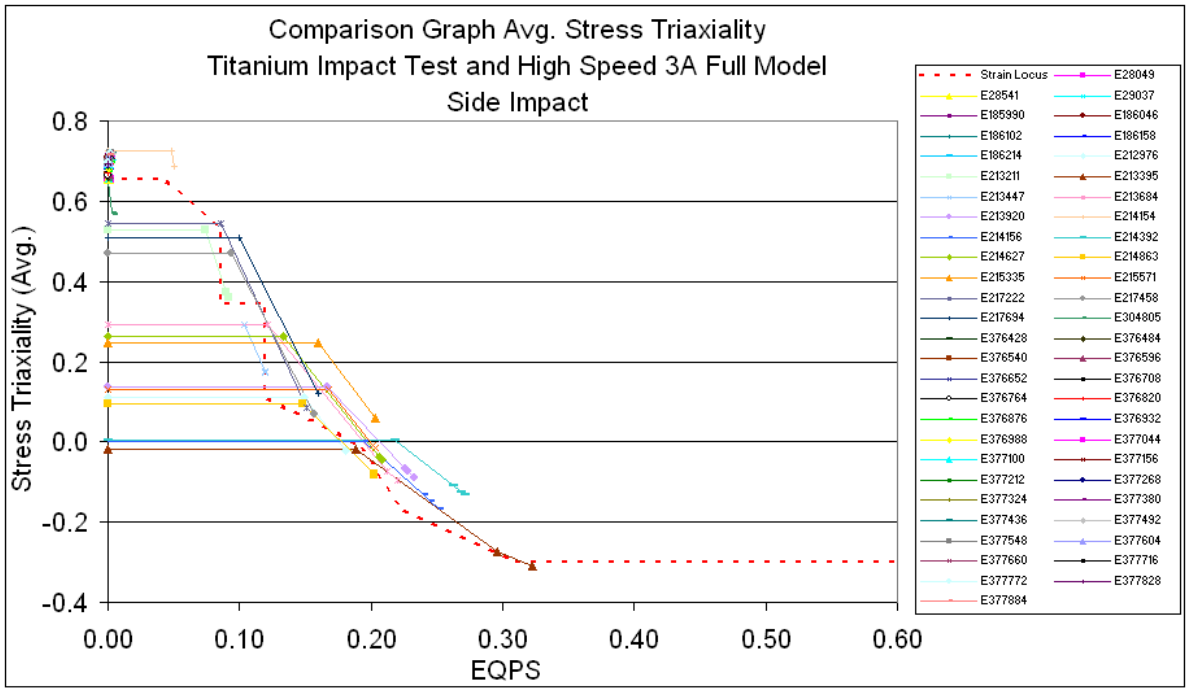

Figure 2-225. Graph of Average Stress Triaxiality versus EQPS of Elements Exceeding the Experimental Strain Locus for the SC-1, Pu Contents, Side Impact, 0° Support Structure

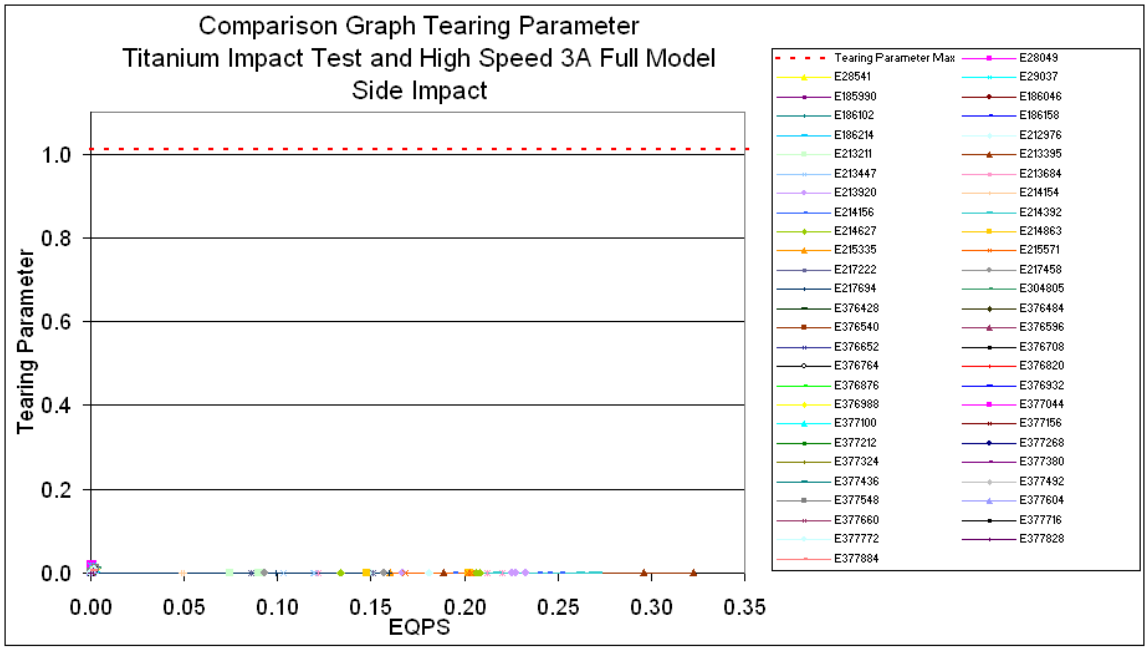

Figure 2-226. Graph of Tearing Parameter versus EQPS of Elements Exceeding the Experimental Strain Locus for the SC-1, Pu Contents, Side Impact, 0° Support Structure

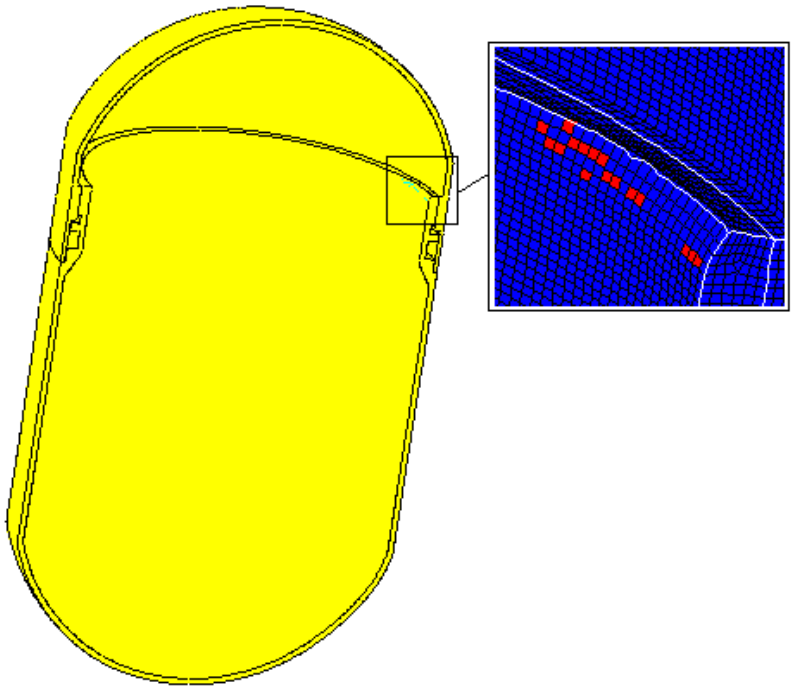

Figure 2-227. Plot of Elements Exceeding the Experimental Strain Locus for the SC-1, Pu Contents, Side Impact, 0° Support Structure

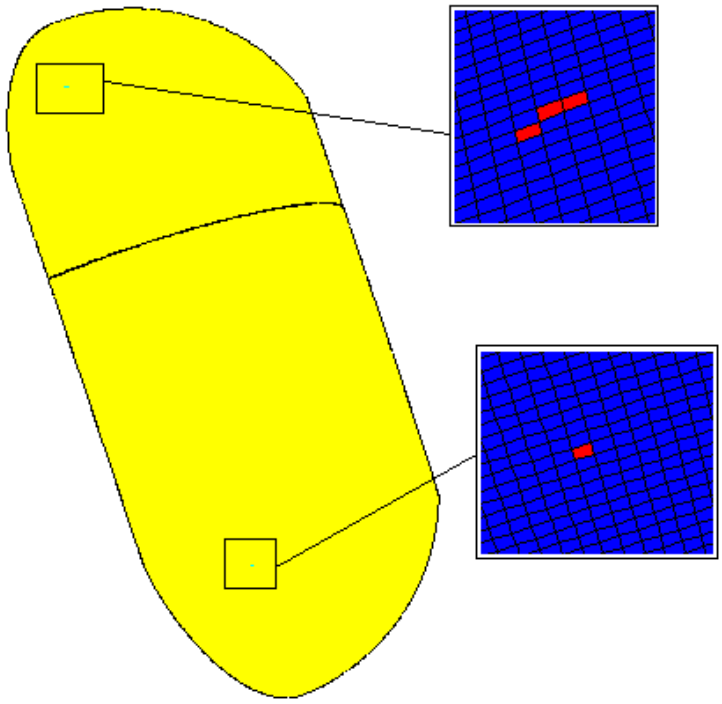

Figure 2-228. Plot of Elements Exceeding the Experimental Strain Locus for the SC-1, Pu Contents, Side Impact, 0° Support Structure

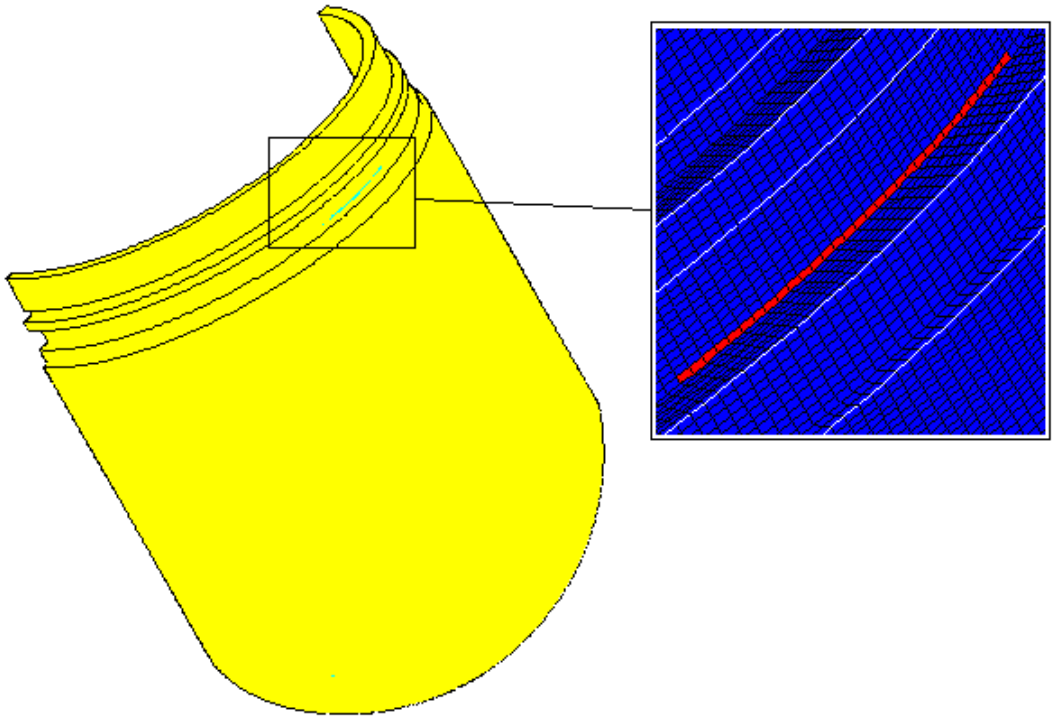

Figure 2-229. Plot of Elements Exceeding the Experimental Strain Locus for the SC-1, Pu Contents, Side Impact, 0° Support Structure

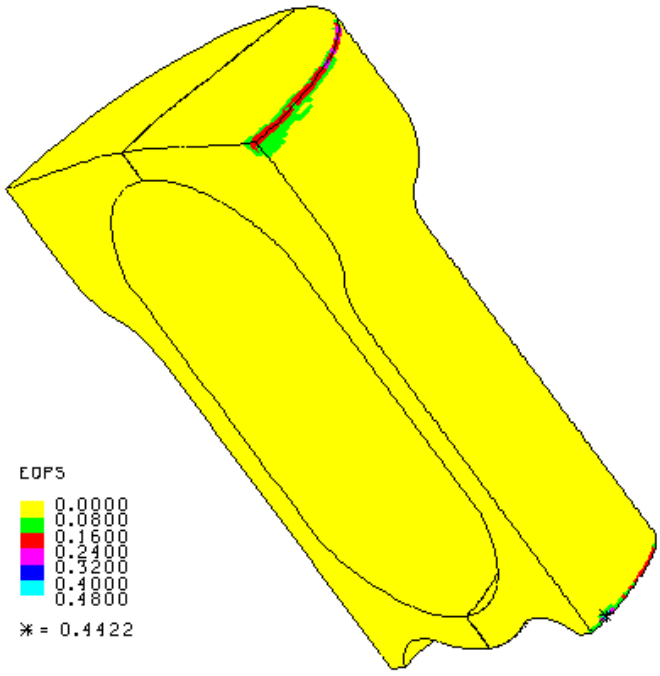

Figure 2-230. Plot of EQPS in the TB-1 for the SC-1, Pu Contents, Side Impact, 0° Support Structure

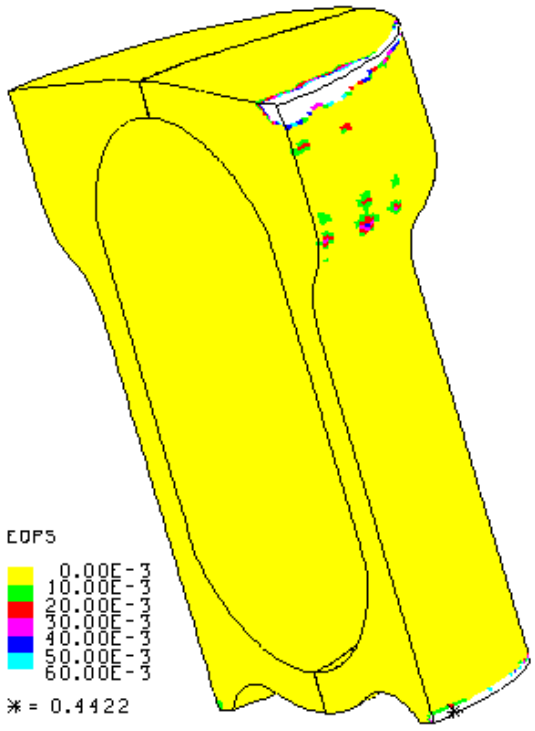

Figure 2-231. Plot of EQPS in the TB-1 for the SC-1, Pu Contents, Side Impact, 0° Support Structure

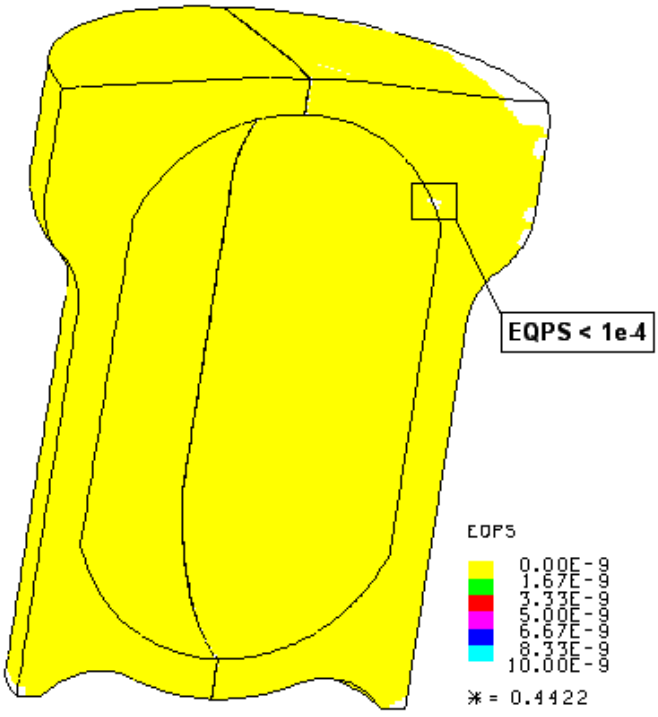

Figure 2-232. Plot of EQPS in the TB-1 for the SC-1, Pu Contents, Side Impact, 0° Support Structure

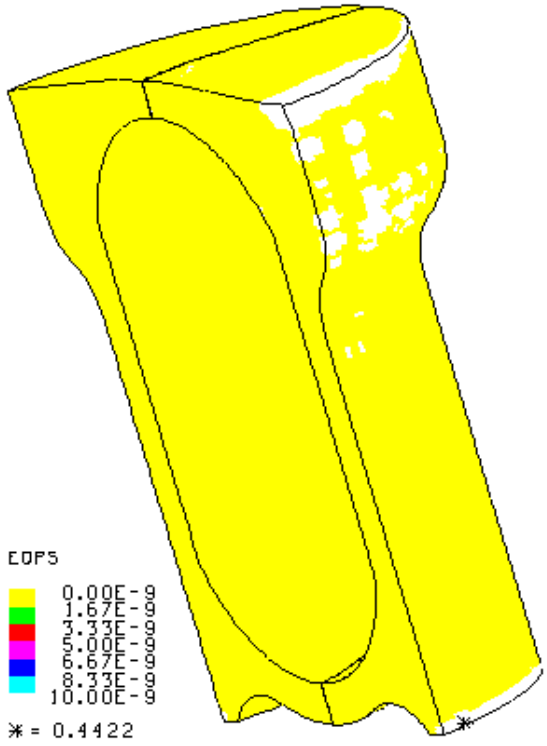

Figure 2-233. Plot of EQPS in the TB-1 for the SC-1, Pu Contents, Side Impact, 0° Support Structure

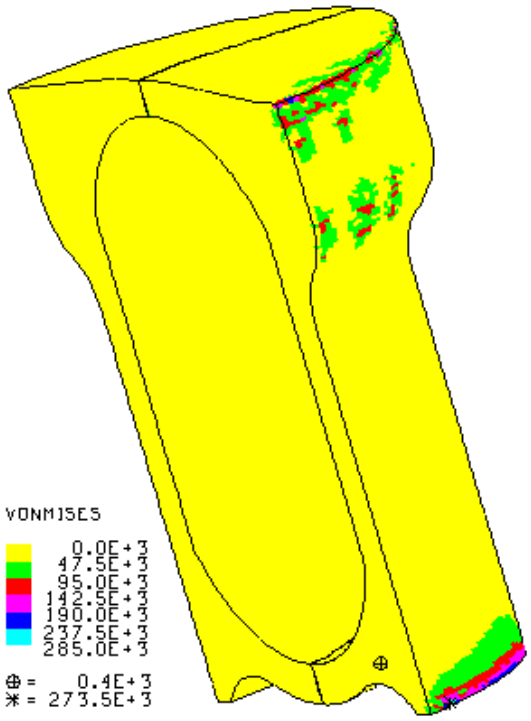

Figure 2-234. Plot of von Mises Stress in the TB-1 for the SC-1, Pu Contents, Side Impact, 0° Support Structure

2.12.5.5.3 Run 13 – SC-1, Side Impact, Support Structure 45°, Pu Contents

The side impact model for each SC-1 with delta Pu contents (cradle rotated 45 degrees to evaluate effect of sharp edges being pinched) is shown in Figure 2-235. Each Pu cylinder is located at the far left side of each SC-1 so that its net impact velocity with the right side of the T-Ampoule is maximized. The post-impact deformation is shown in Figure 2-236 and its kinetic energy history in Figure 2-237 indicating the container has begun to bounce and thus, peak loading has already occurred. In side impacts, the Pu contents penetrate each of the SC-1 side walls and directly impact the T-Ampoule.

Average stress-triaxiality versus EQPS is shown in Figure 2-238 for the 7 elements extending beyond the tested Bao-Wierzbicki strain locus. All of these elements are outside the B-W locus, for a variety of stress triaxialities, although most of the 580,000 T-Ampoule elements are inside the B-W locus. The Tearing Parameter values for these same 7 elements are shown in Figure 2-239, and all are below the critical Tearing Parameter value of 1.012 for Ti-6Al-4V. These elements are highlighted in red in Figures 2-240 and 2-241. Some localized crease-like deformations in Figure 2-240 are indicative of a slight contact issue, but these red elements (and all ~580,000 T-Ampoule elements) are still below the initiation of a ductile tear and thus, T-Ampoule integrity is maintained.

Equivalent Plastic Strain (EQPS) in the TB-1 vessel is shown in Figures 2-242 through 2-245 to be less than 31% but only in some localized outer contact regions with the redwood overpack. The EQPS due to internal denting of the upper SC-1 is shown in Figure 2-243 to be less than 0.017%, which is essentially elastic. The von Mises stresses (see Figure 2-246) peak at 230 ksi is above the elevated-temperature minimum yield strength for the TB-1 of 141 ksi but more importantly, through-thickness TB-1 stress values are in the less-than-120 ksi range, which is below yielding.

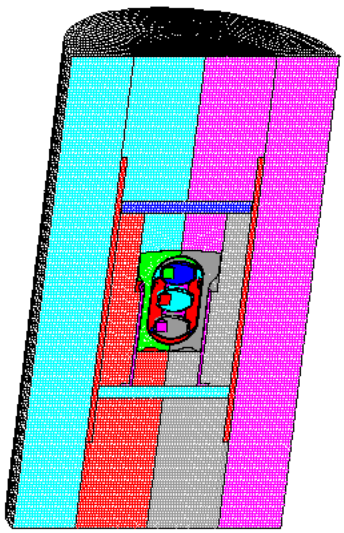

Figure 2-235. Finite Element Mesh for the SC-1, Pu Contents, Side Impact, 45° Support Structure

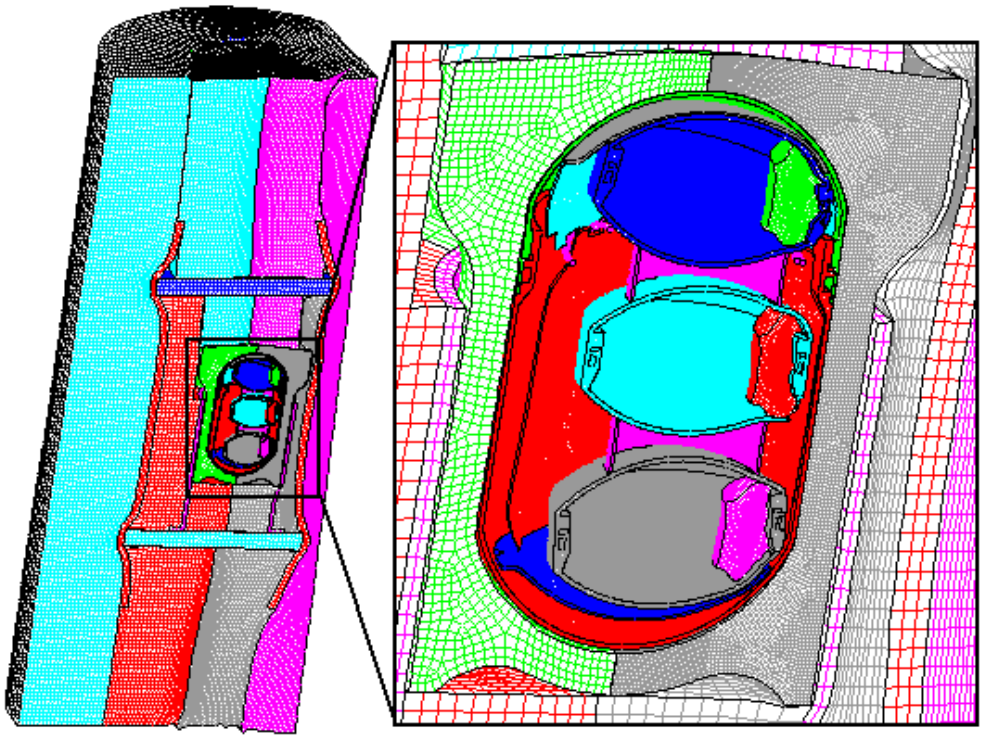

Figure 2-236. Finite Element Mesh for the SC-1, Pu Contents, Side Impact, 45° Support Structure – Final Displacement

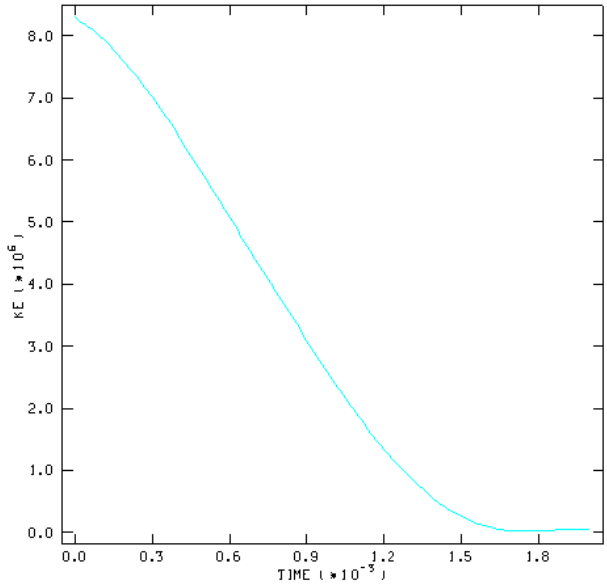

Figure 2-237. Kinetic Energy Time History for the SC-1, Pu Contents, Side Impact, 45° Support Structure

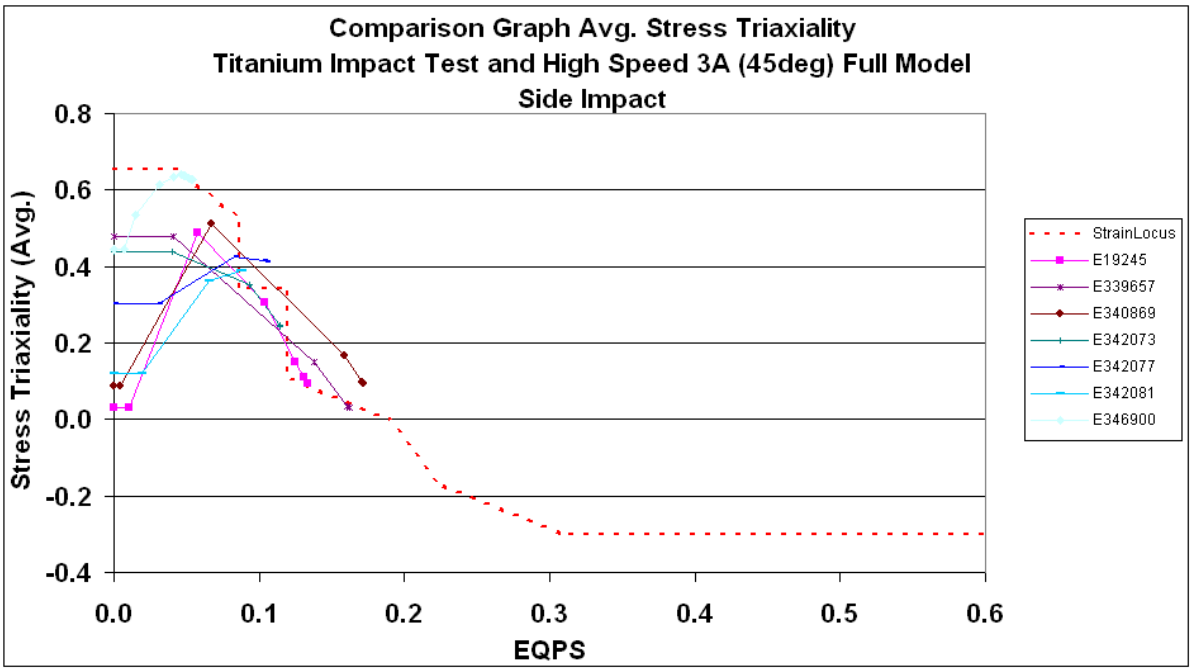

Figure 2-238. Graph of Average Stress Triaxiality versus EQPS of Elements Exceeding the Experimental Strain Locus for the SC-1, Pu Contents, Side Impact, 45° Support Structure

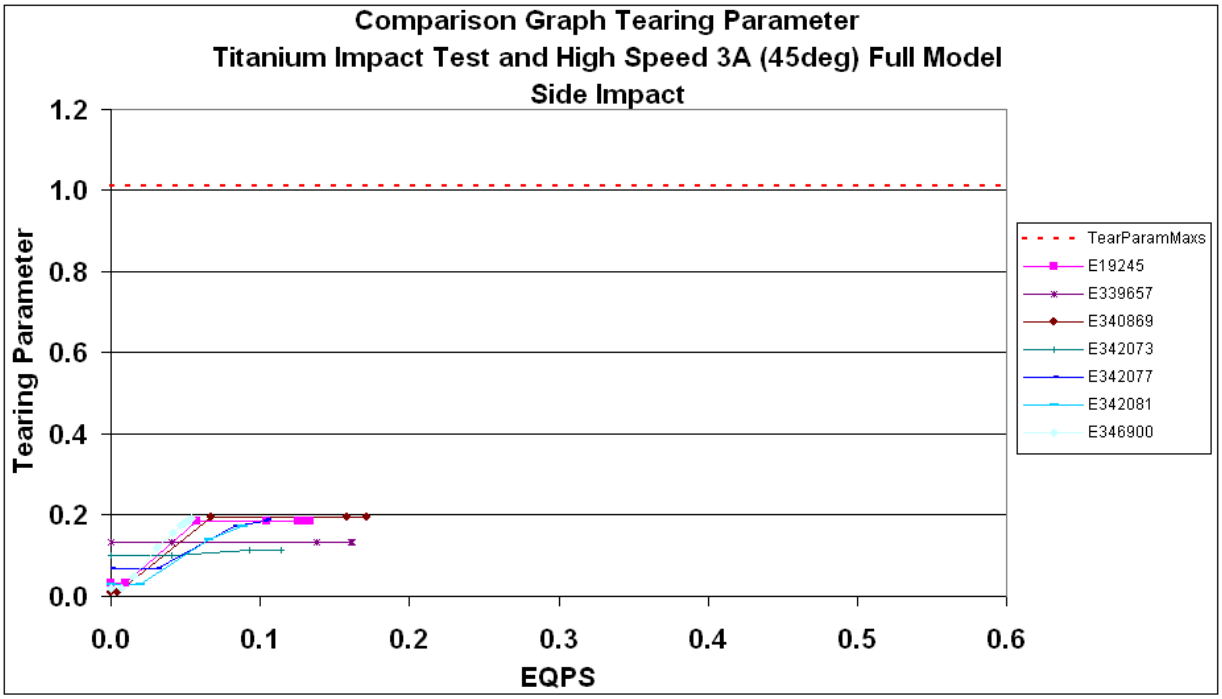

Figure 2-239. Graph of Tearing Parameter versus EQPS of Elements Exceeding the Experimental Strain Locus for the SC-1, Pu Contents, Side Impact, 45° Support Structure

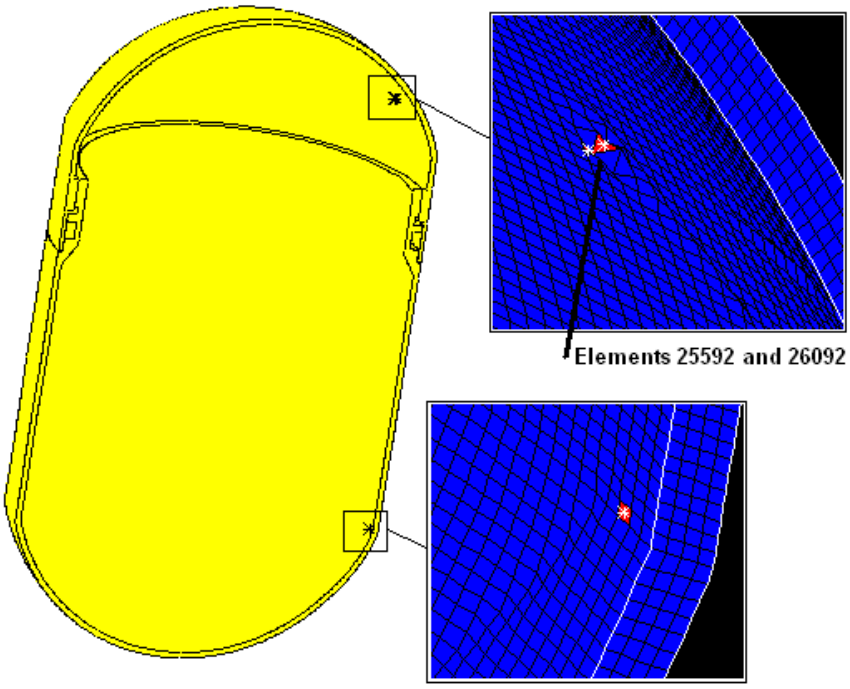

Figure 2-240. Plot of Elements Exceeding the Experimental Strain Locus for the SC-1, Pu Contents, Side Impact, 45° Support Structure

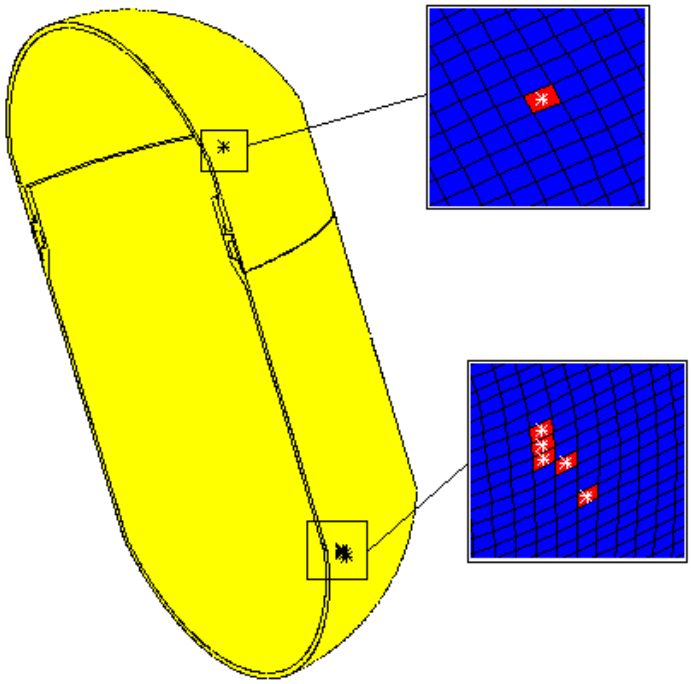

Figure 2-241. Plot of Elements Exceeding the Experimental Strain Locus for the SC-1, Pu Contents, Side Impact, 45° Support Structure

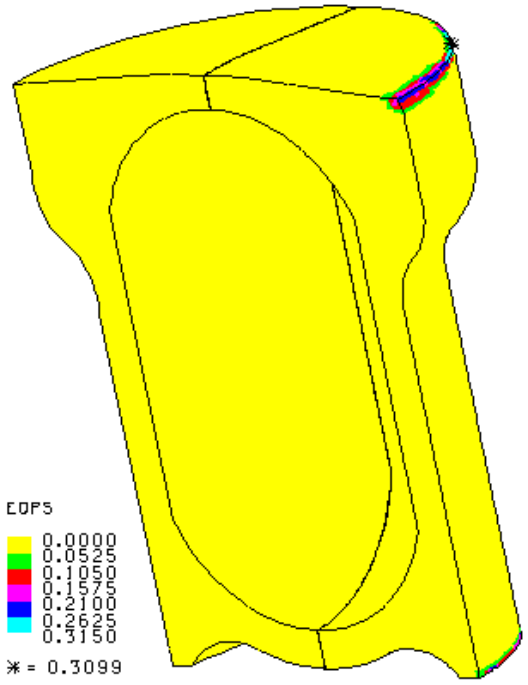

Figure 2-242. Plot of EQPS in the TB-1 for the SC-1, Pu Contents, Side Impact, 45° Support Structure

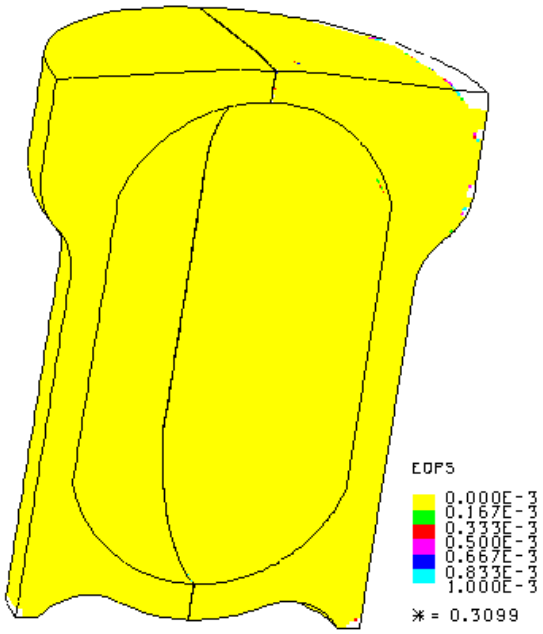

Figure 2-243. Plot of EQPS in the TB-1 for the SC-1, Pu Contents, Side Impact, 45° Support Structure

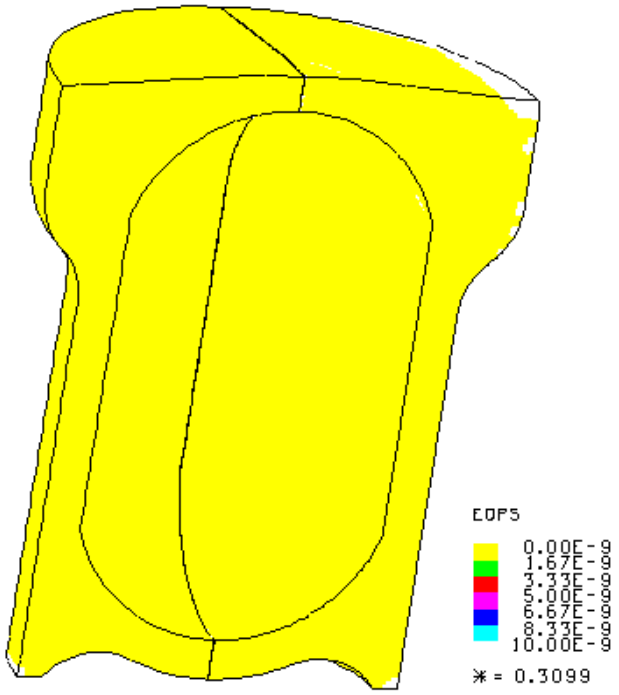

Figure 2-244. Plot of EQPS in the TB-1 for the SC-1, Pu Contents, Side Impact, 45° Support Structure

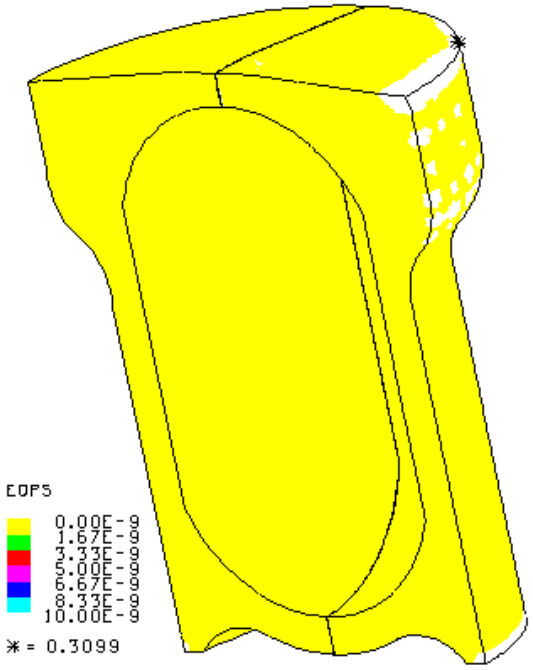

Figure 2-245. Plot of EQPS in the TB-1 for the SC-1, Pu Contents, Side Impact, 45° Support Structure

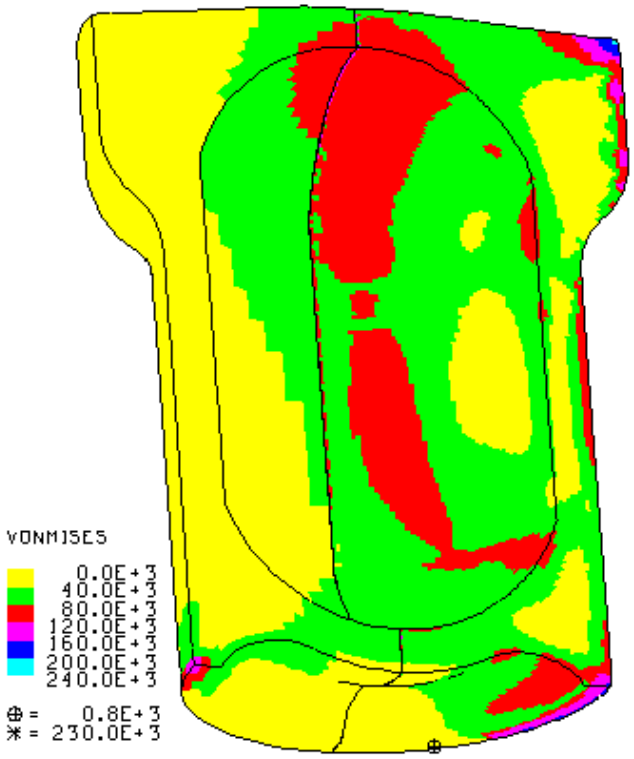

Figure 2-246. Plot of von Mises Stress in the TB-1 for the SC-1, Pu Contents, Side Impact, 45° Support Structure

2.12.5.5.4 Run 14 – SC-1, CGOC Impact, Pu Contents, Support Structure 0°

The lid end CG-over-corner impact model for each SC-1 with delta Pu contents (cradle rotated 0 degrees) is shown in Figure 2-247. Each Pu cylinder is located at the rotated bottom of each SC-1 so that its net impact velocity with the top of the T-Ampoule is maximized. The post-impact deformation is shown in Figure 2-248 and its kinetic energy history in Figure 2-249. Note the similar degree of overpack crush up as compared to the certification test corner impact in Figure 2-18, despite the slightly reduced impact velocity of 422 ft/sec versus the tested 445 ft/sec. The Pu cylinder contents remain largely confined within each SC-1, although significant localized deformation of the SC-1 has occurred.

Equivalent Plastic Strain (EQPS) in the TB-1 vessel is shown in Figures 2-250 and 2-251 to peak at about 27% but only in some localized outer contact regions with the redwood overpack. The von Mises stresses (see Figure 2-252) peak at 163.1 ksi is just above the elevated-temperature minimum yield strength for the TB-1 of 141 ksi but more importantly, through-thickness TB-1 stress values are in the less-than-25 ksi range, below yield. The time at which the peak value of the von Mises stress occurs coincides with the peak value of the contact force (summed over the lid area). A plot of this force as a function of time is shown in Figure 2-253. A maximum contact load of 14,225 lbs is applied to the inner surface of the TB-1 lid during the impact. No T-Ampoule elements exceeded the tested B-W strain locus and the peak Tearing Parameter value (see Table 2-11, run #14) of 0.0935 was below the critical Tearing Parameter value of 1.012 for Ti-6Al-4V.

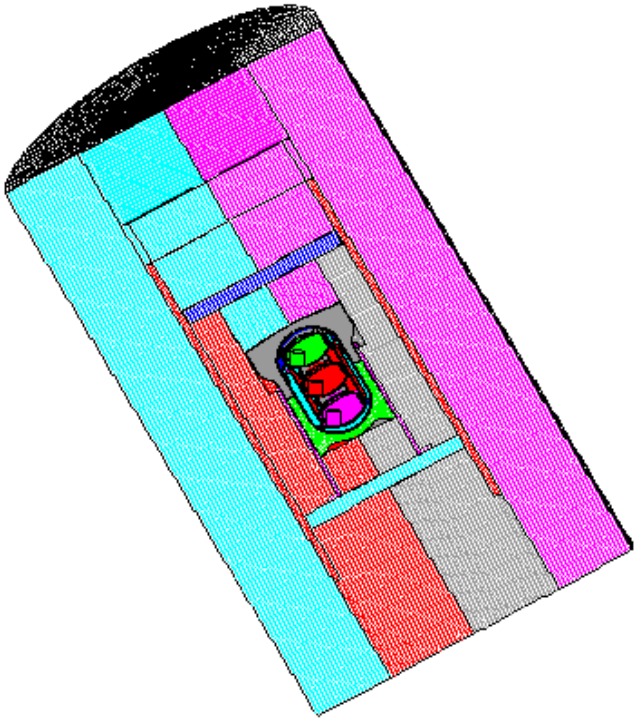

Figure 2-247. Finite Element Mesh for the SC-1, Pu Contents, CGOC Impact, 0° Support Structure

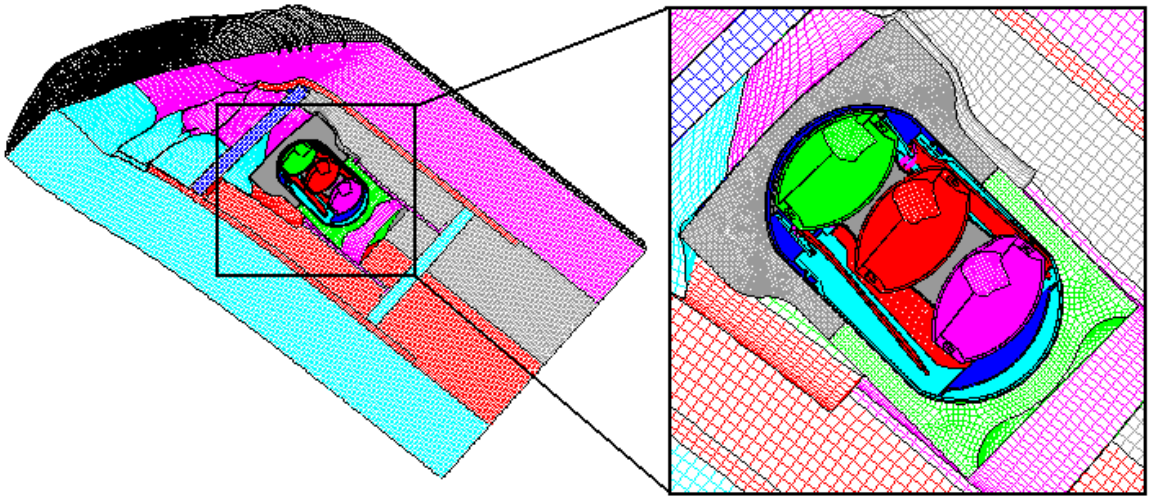

Figure 2-248. Finite Element Mesh for the SC-1, Pu Contents, CGOC Impact, 0° Support Structure – Final Displacement

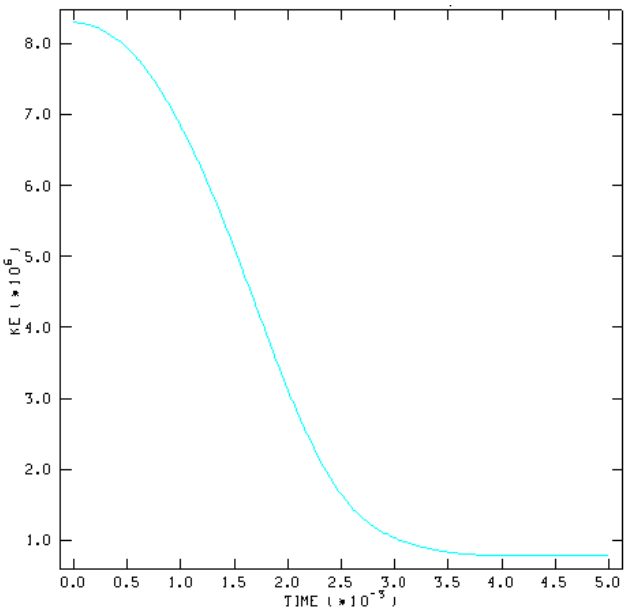

Figure 2-249. Kinetic Energy Time History for the SC-1, Pu Contents, CGOC Impact, 0° Support Structure

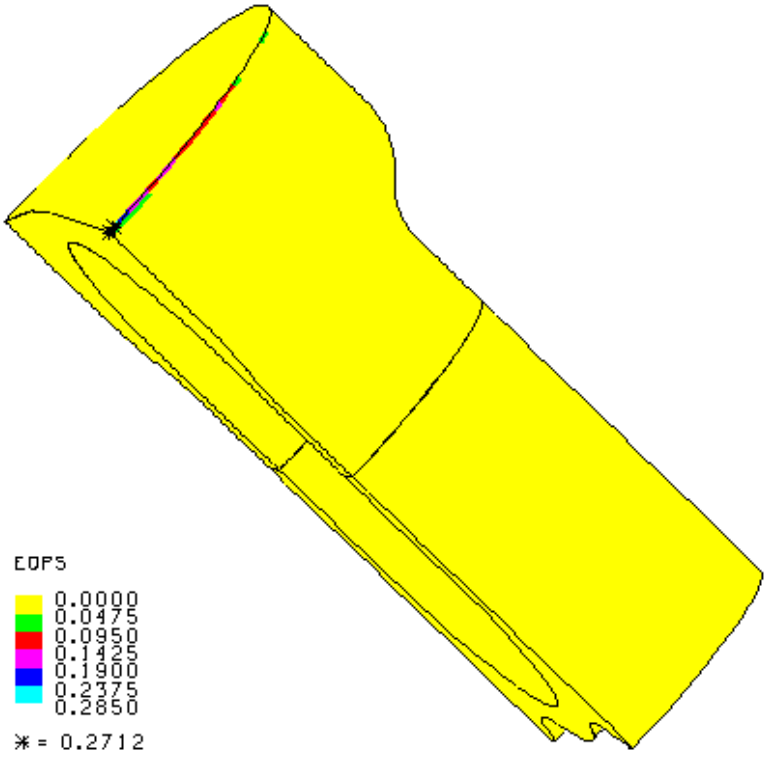

Figure 2-250. Plot of EQPS in the TB-1 for the SC-1, Pu Contents, CGOC Impact, 0° Support Structure

Figure 2-251. Plot of EQPS in the TB-1 for the SC-1, Pu Contents, CGOC Impact, 0° Support Structure

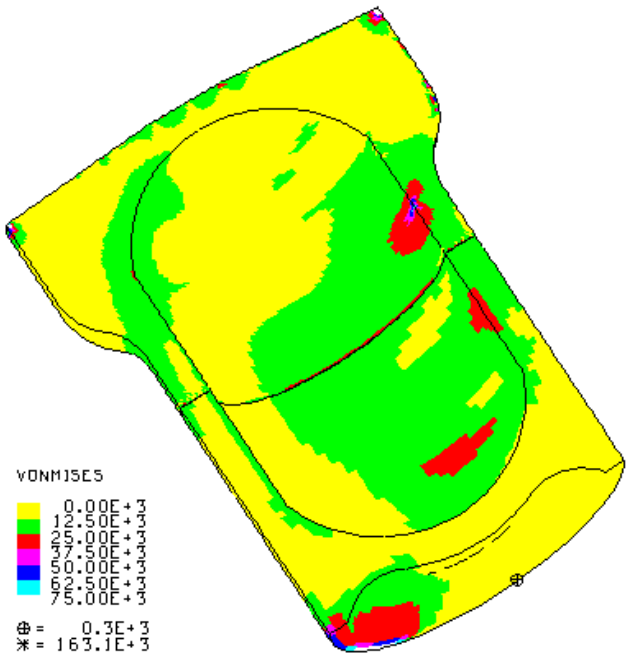

Figure 2-252. Plot of von Mises Stress in the TB-1 for the SC-1, Pu Contents, CGOC Impact, 0° Support Structure

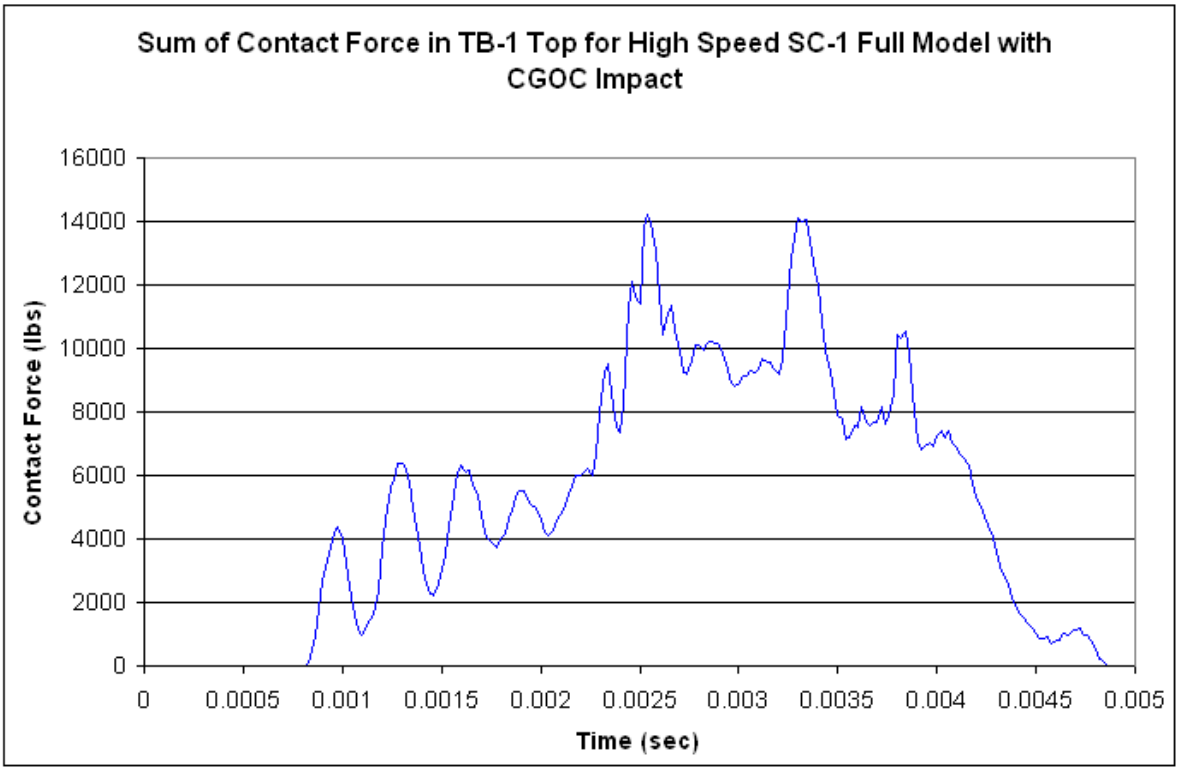

Figure 2-253. Plot of Contact Force in the TB-1 for the SC-1, Pu Contents, CGOC Impact, 0° Support Structure

2.12.5.5.5 Run 15 – SC-1, CGOC Impact, Pu Contents, Support Structure 45°

The lid end CG-over-corner impact model for each SC-1 with delta Pu contents (cradle rotated 45 degrees) is shown in Figure 2-254. Each Pu cylinder is located at the rotated bottom of each SC-1 so that its net impact velocity with the top of the T-Ampoule is maximized. The post-impact deformation is shown in Figure 2-255 and its kinetic energy history in Figure 2-256. The Pu cylinder contents remain largely confined within each SC-1, although significant localized deformation of the SC-1 has occurred.

Equivalent Plastic Strain (EQPS) in the TB-1 vessel is shown in Figures 2-257 and 2-258 to peak at about 21% but only in some localized outer contact regions with the redwood overpack. The von Mises stresses (see Figure 2-259) peak locally due to redwood contacts at 230 ksi, above the elevated-temperature minimum yield strength for the TB-1 of 141 ksi but more importantly, through-thickness TB-1 stress values are in the 80 ksi range, which is below yield. The time at which the peak value of the von Mises stress occurs coincides with the peak value of the contact force (summed over the lid area). A plot of this force as a function of time is shown in Figure 2-260. A maximum contact load of less than 15,613 lbs is applied to the inner surface of the TB-1 lid during the impact. No T-Ampoule elements exceeded the tested B-W strain locus, and the peak Tearing Parameter value (see Table 2-11, run #15) of 0.3061 was below the critical Tearing Parameter value of 1.012 for Ti-6Al-4V; thus T-Ampoule integrity was maintained.

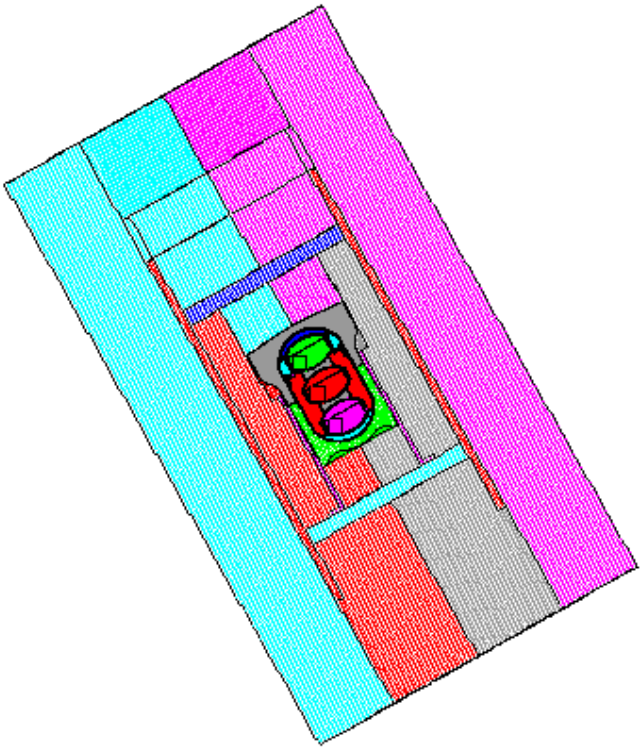

Figure 2-254. Finite Element Mesh for the SC-1, Pu Contents, CGOC Impact, 45° Support Structure

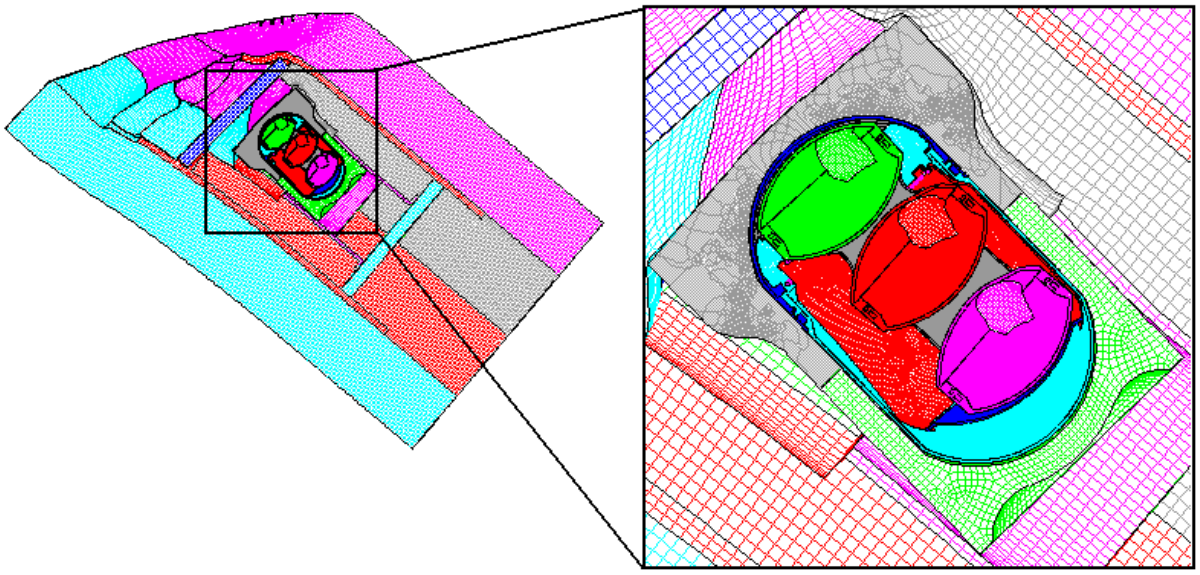

Figure 2-255. Finite Element Mesh for the SC-1, Pu Contents, CGOC Impact, 45° Support Structure – Final Displacement

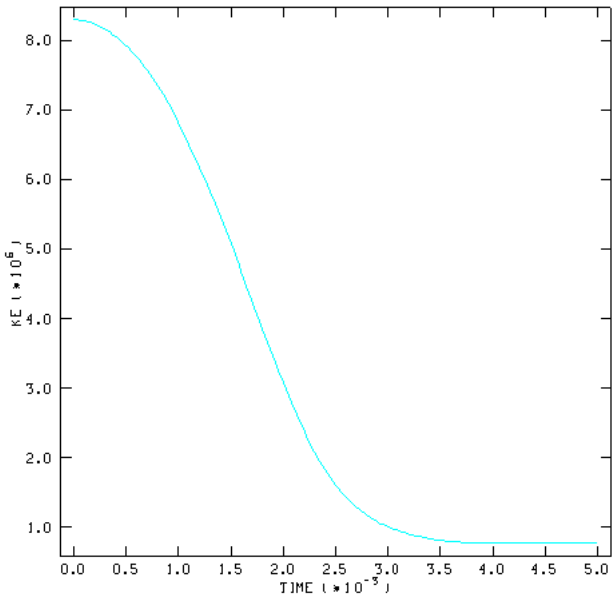

Figure 2-256. Kinetic Energy Time History for the SC-1, Pu Contents, CGOC Impact, 45° Support Structure

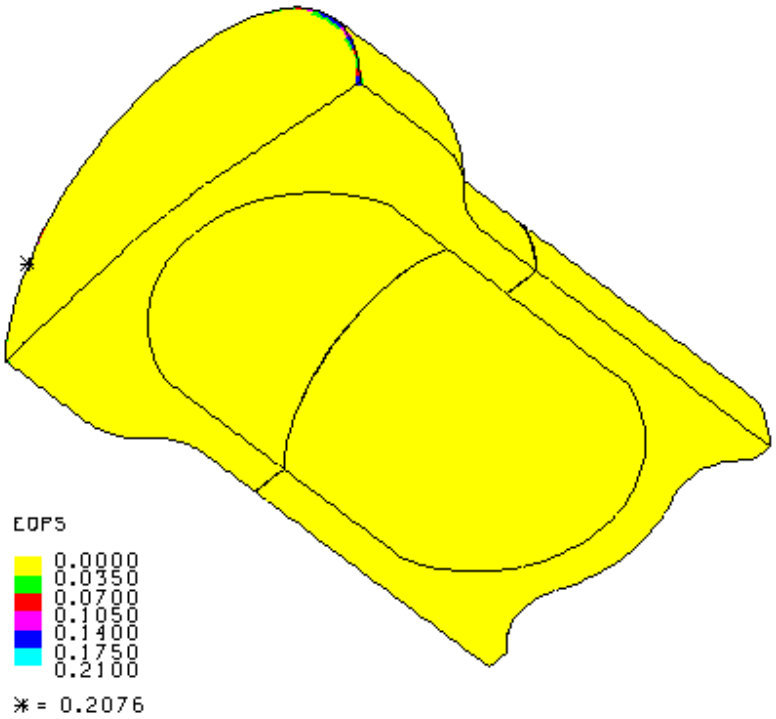

Figure 2-257. Plot of EQPS in the TB-1 for the SC-1, Pu Contents, CGOC Impact, 45° Support Structure

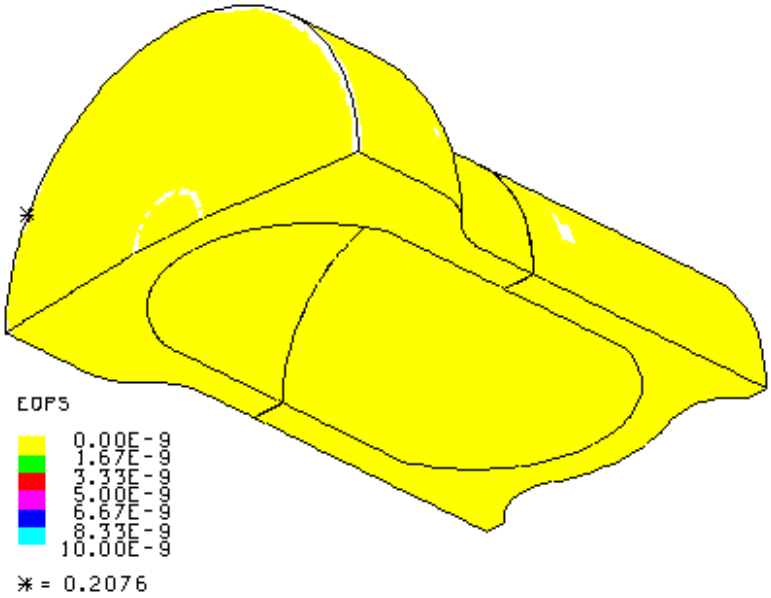

Figure 2-258. Plot of EQPS in the TB-1 for the SC-1, Pu Contents, CGOC Impact, 45° Support Structure

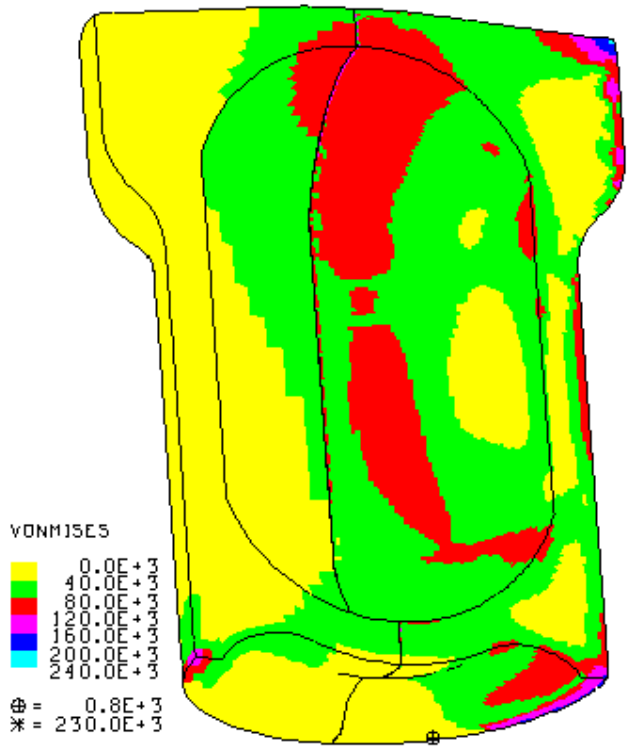

Figure 2-259. Plot of von Mises Stress in the TB-1 for the SC-1, Pu Contents, CGOC Impact, 45° Support Structure

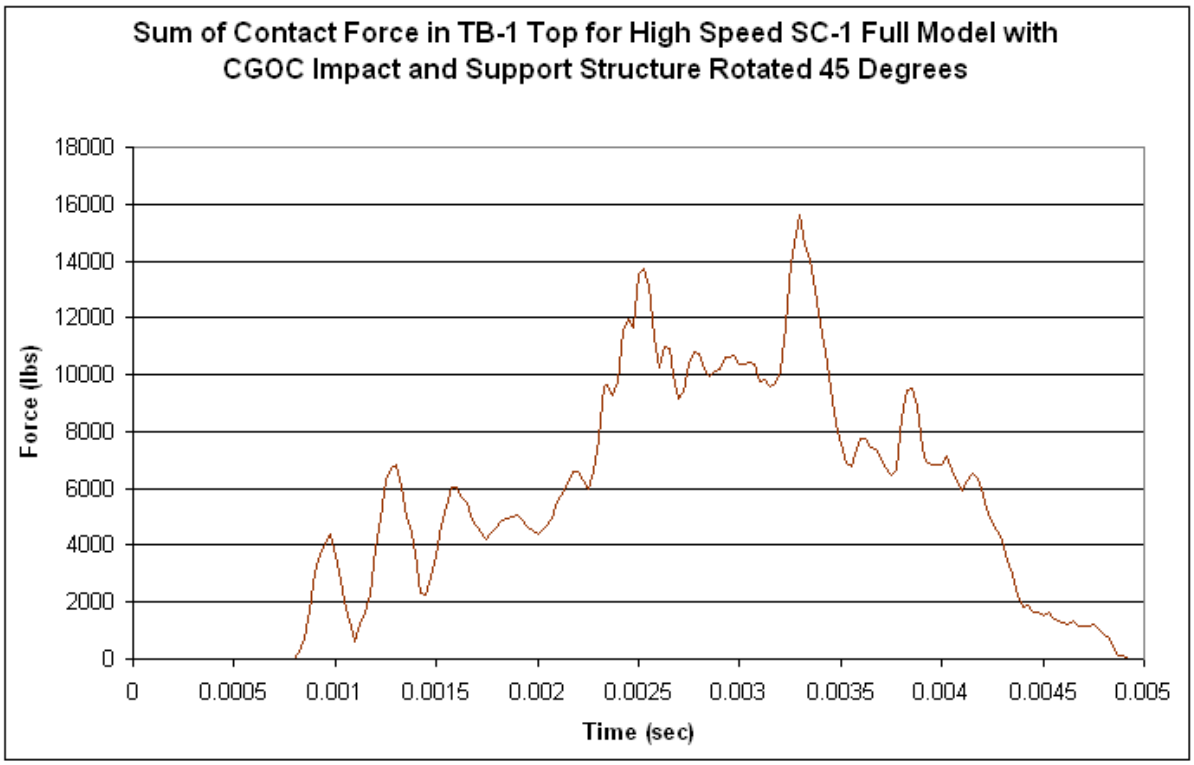

Figure 2-260. Plot of Contact Forces in the TB-1 for the SC-1, Pu Contents, CGOC Impact, 45° Support Structure

2.12.5.5.6 Run 16 - SC-2, Top Impact, Support Structure 0°

The top end impact model for the larger SC-2, each with 338 g of delta Pu contents is shown in Figure 2-261. Note that each Pu cylinder is located at the bottom of each SC-2 so that its net impact velocity with the top of the T-Ampoule is maximized. The post-impact deformation is shown in Figure 2-262 and its kinetic energy history in Figure 2-263. The top SC-2 is crushed from the subsequent impacts of the lower SC-2, and its Pu contents nearly penetrate its upper wall, which directly impacts the T-Ampoule. The lower SC-2 Pu contents nearly penetrate into the upper SC-2.

Equivalent Plastic Strain (EQPS) in the TB-1 vessel is shown in Figure 2-264 to be less than 3.7%, and only in some localized outer contact regions with the redwood overpack. The von Mises stresses (see Figure 2-265) peak at 147.3 ksi is just above the elevated-temperature minimum yield strength for the TB-1 of 141 ksi but more importantly, through-thickness TB-1 stress values are in the 37 ksi range, below yield. The time at which the peak value of the von Mises stress occurs coincides with the peak value of the contact force (summed over the lid area). A plot of this force as a function of time is shown in Figure 2-266. A maximum contact load of about 49,090 lbs is applied to the inner surface of the TB-1 lid during the impact. No T-Ampoule elements exceeded the tested B-W strain locus and the peak Tearing Parameter value (see Table 2-11, run #16) of 0.0132 was below the critical Tearing Parameter value of 1.012 for Ti-6Al-4V.

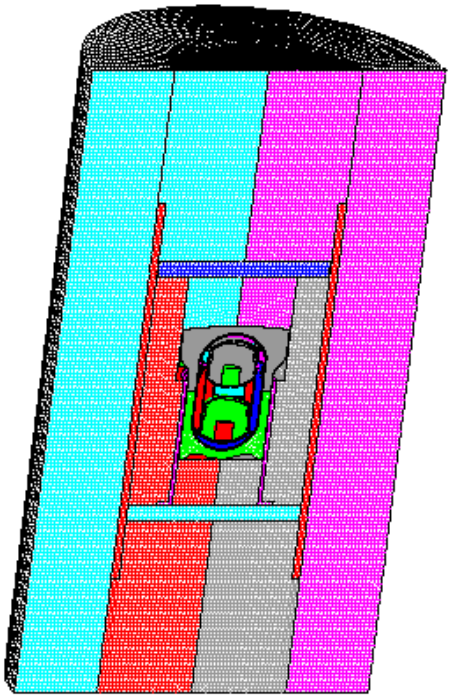

Figure 2-261. Finite Element Mesh for the SC-2, End Impact, 0° Support Structure

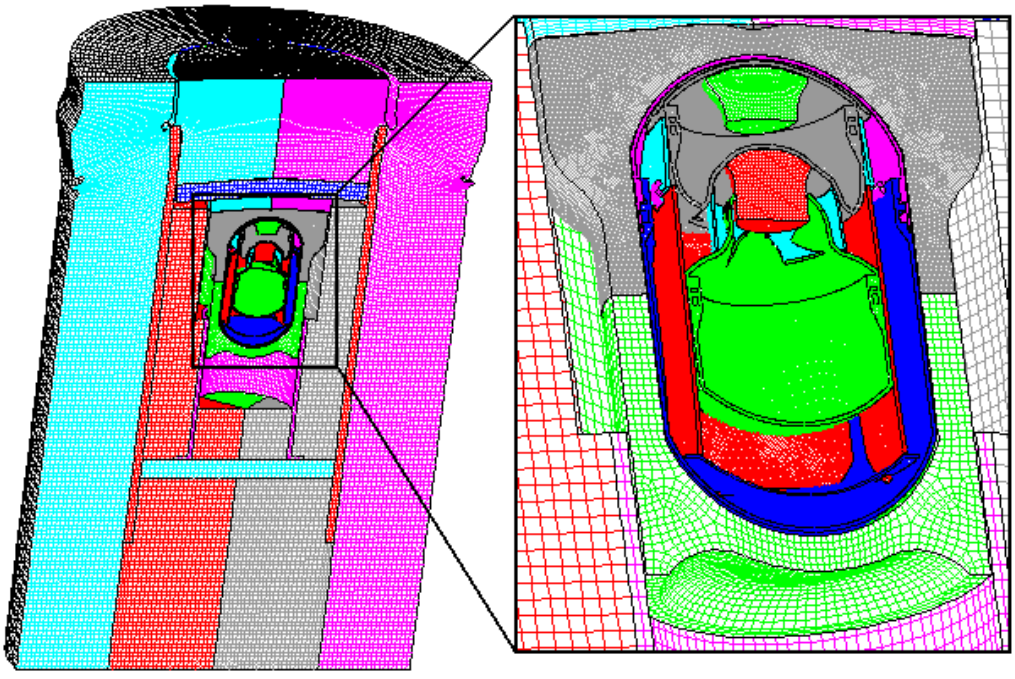

Figure 2-262. Finite Element Mesh for the SC-2, End Impact, 0° Support Structure – Final Displacement

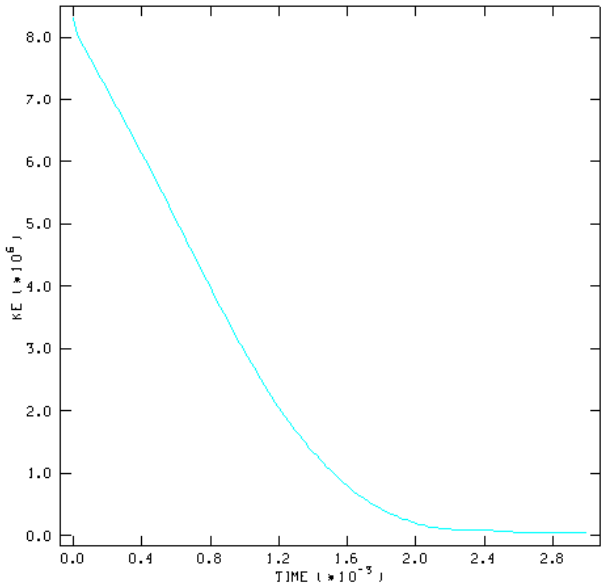

Figure 2-263. Kinetic Energy Time History for the SC-2, End Impact, 0° Support Structure

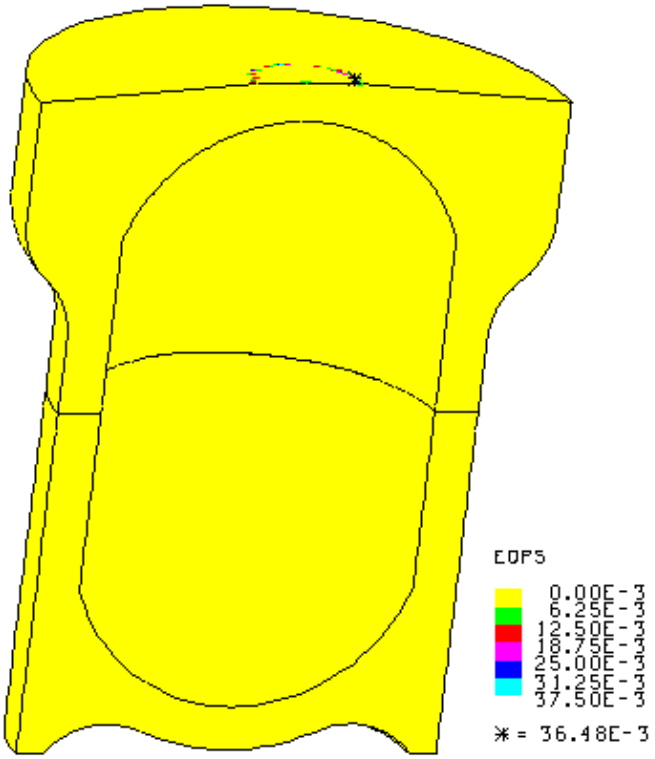

Figure 2-264. Plot of EQPS in the TB-1 for the SC-2, End Impact, 0° Support Structure

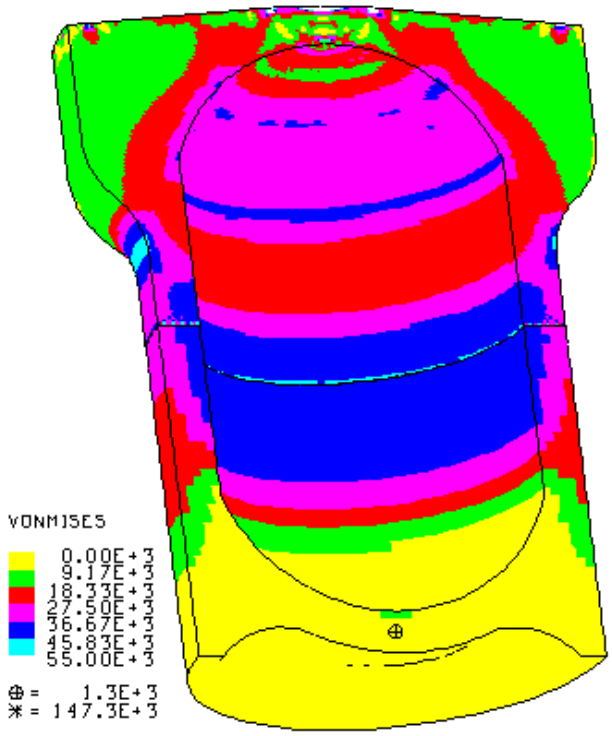

Figure 2-265. Plot of von Mises Stress in the TB-1 for the SC-2, End Impact, 0° Support Structure

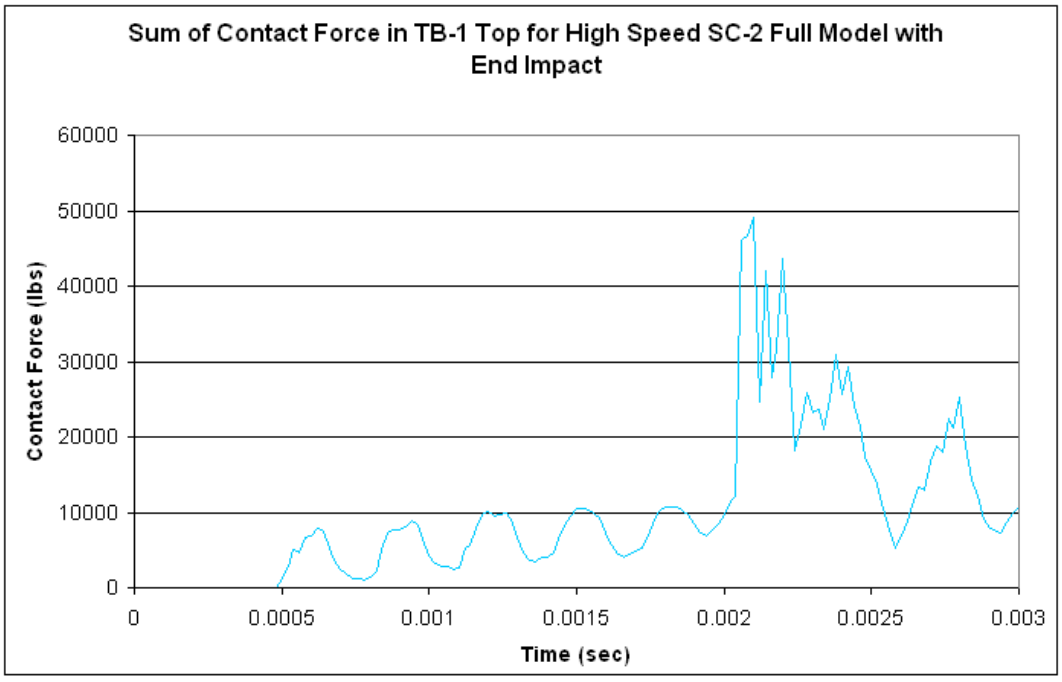

Figure 2-266. Plot of Contact Forces in the TB-1 for the SC-2, End Impact, 0° Support Structure

2.12.5.5.7 Run 17 - SC-2 Sample Container, Side Impact, Support Structure 0°

The side impact model for the larger SC-2 each with 338 g of delta Pu contents (inner cradle rotated 0 degrees) is shown in Figure 2-267. Note that each Pu cylinder is located at the far left side of each SC-2 so that its net impact velocity with the right side of the T-Ampoule is maximized. The post-impact deformation is shown in Figure 2-268 and its kinetic energy history in Figure 2-269. The Pu contents penetrate each of the SC-2 side walls and directly impact the T-Ampoule.

Average stress-triaxiality versus EQPS is shown in Figure 2-270 for the 55 elements extending beyond the tested Bao-Wierzbicki strain locus. All of these elements are outside the B-W locus, for a variety of stress triaxialities, although most of the 580,000 T-Ampoule elements are inside the B-W locus. The Tearing Parameter values for these same 55 elements are shown in Figure 2-271 and all are below the critical Tearing Parameter value of 1.012 for Ti-6Al-4V. These elements are highlighted in red in Figures 2-272 and 2-273, but note that these elements are still below the initiation of a ductile tear and thus, T-Ampoule integrity is maintained.

Equivalent Plastic Strain (EQPS) in the TB-1 vessel is shown in Figures 2-274 and 2-275 to be less than 39% but only in some localized outer contact regions with the redwood overpack. The EQPS due to internal denting of the upper TB-1 is shown in Figure 2-275 to be less than 0.07%, which is essentially elastic. The von Mises stresses (see Figure 2-276) peak at 225 ksi, is above the elevated-temperature minimum yield strength for the TB-1 of 141 ksi but more importantly, through-thickness TB-1 stress values are in the less-than-135 ksi range, which is below yield.

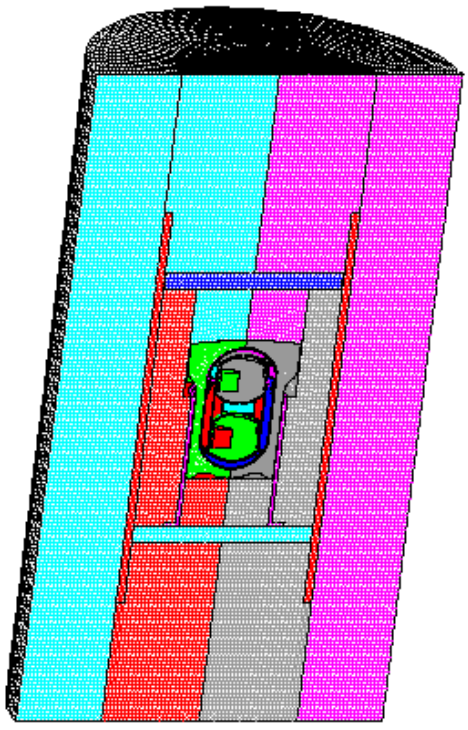

Figure 2-267. Finite Element Mesh for the SC-2, Side Impact, 0° Support Structure

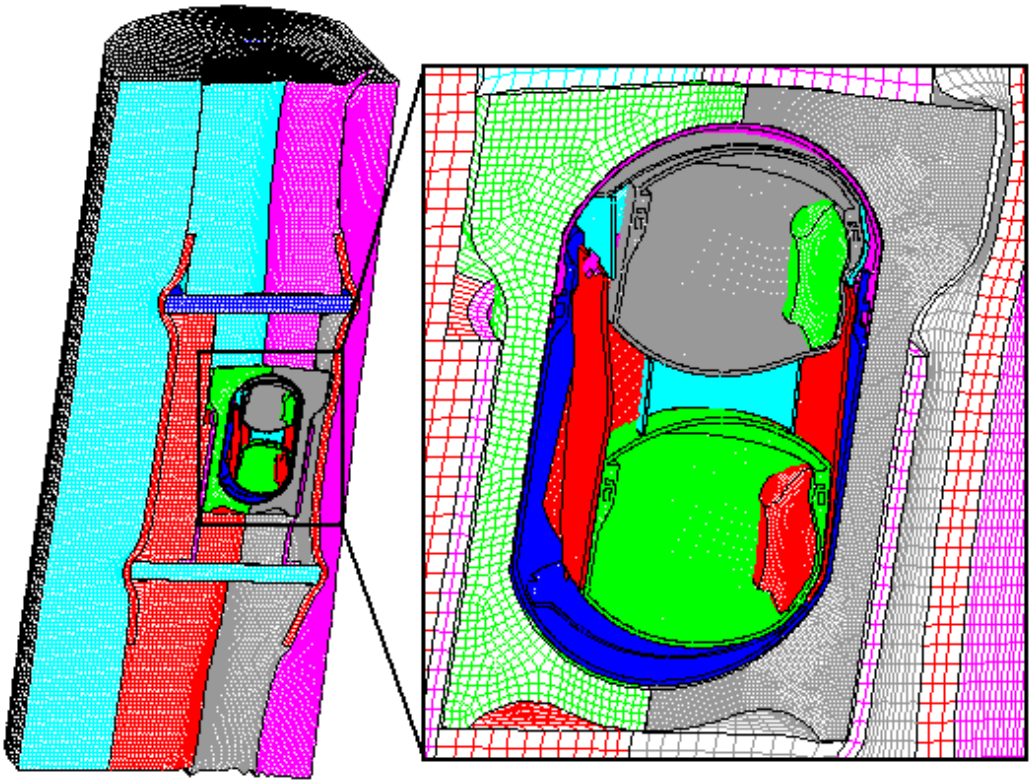

Figure 2-268. Finite Element Mesh for the SC-2, Side Impact, 0° Support Structure – Final Displacement

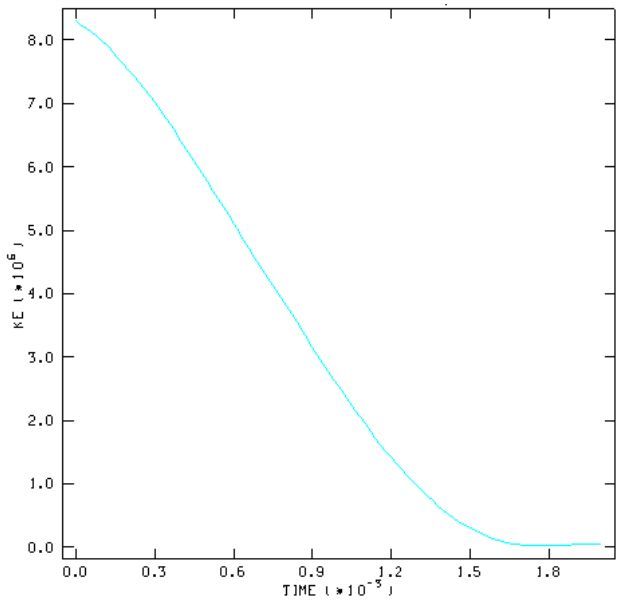

Figure 2-269. Kinetic Energy Time History for the SC-2, Side Impact, 0° Support Structure

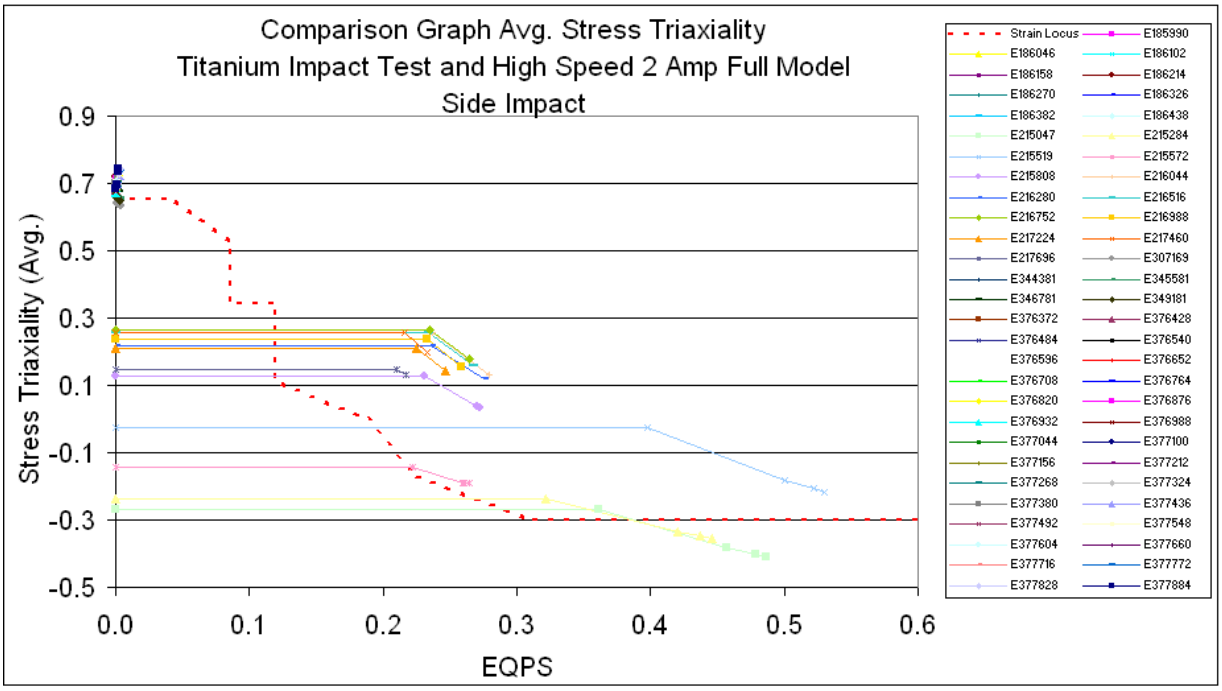

Figure 2-270. Graph of Average Stress Triaxiality versus EQPS of Elements Exceeding the Experimental Strain Locus for the SC-2, Side Impact, 0° Support Structure

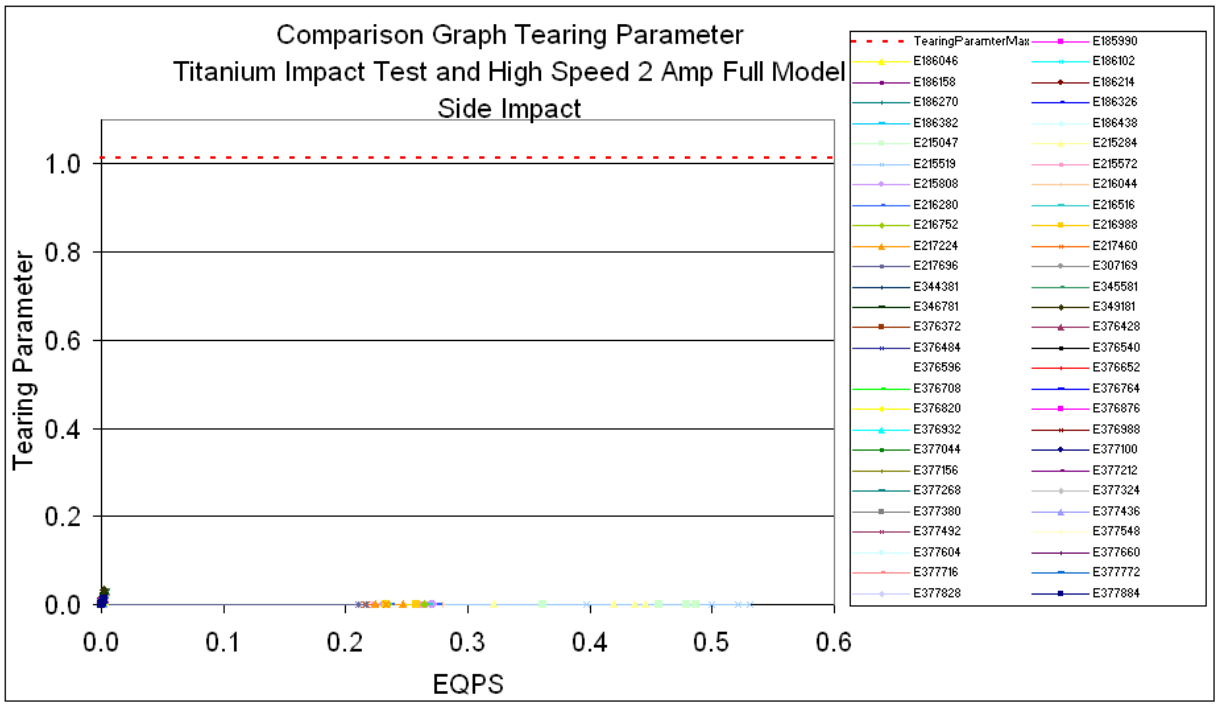

Figure 2-271. Graph of Tearing Parameter versus EQPS of Elements Exceeding the Experimental Strain Locus for the SC-2, Side Impact, 0° Support Structure

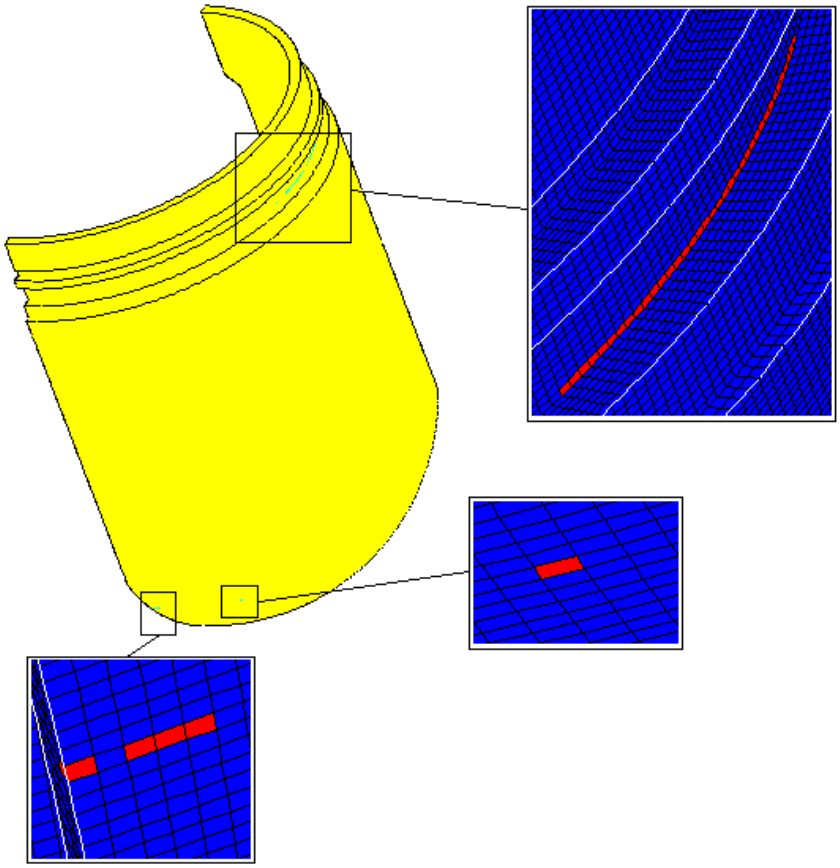

Figure 2-272. Plot of Elements Exceeding the Experimental Strain Locus for the SC-2, Side Impact, 0° Support Structure

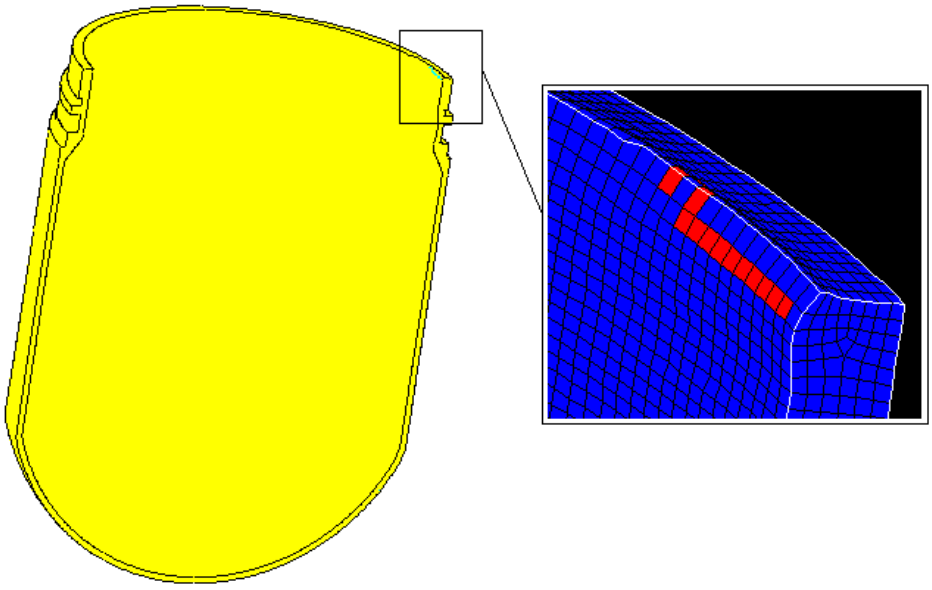

Figure 2-273. Plot of Elements Exceeding the Experimental Strain Locus for the SC-2, Side Impact, 0° Support Structure

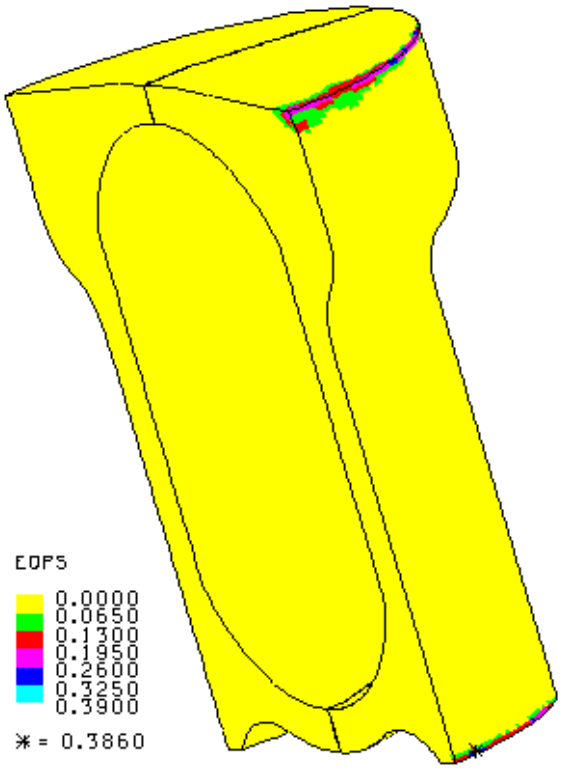

Figure 2-274. Plot of EQPS in the TB-1 for the SC-2, Side Impact, 0° Support Structure

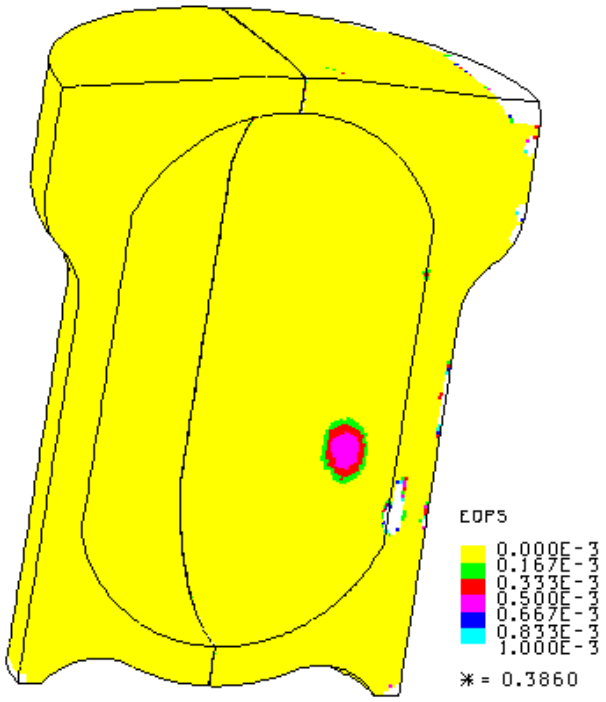

Figure 2-275. Plot of EQPS in the TB-1 for the SC-2, Side Impact, 0° Support Structure

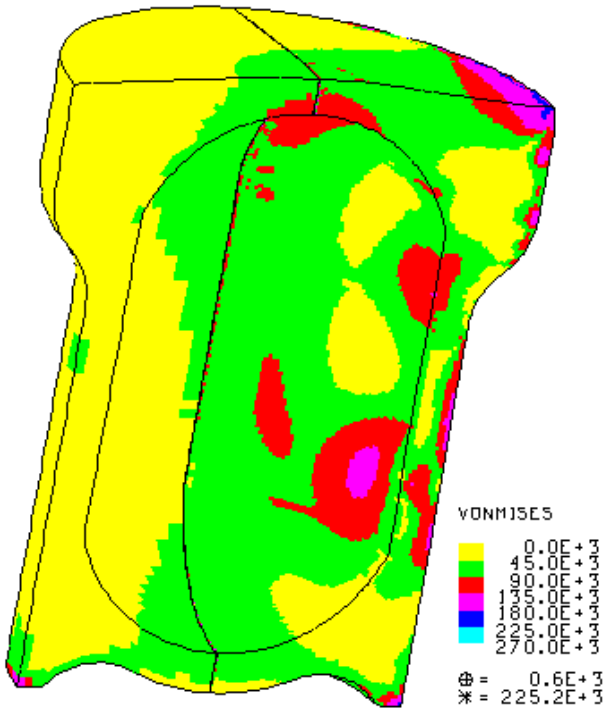

Figure 2-276. Plot of von Mises Stress in the TB-1 for |the SC-2, Side Impact, 0° Support Structure

2.12.5.5.8 Run 18 - SC-2 Sample Container, Side Impact, Support Structure 45°

The side impact model for each of the larger SC-2 sample containers with 338 g of delta Pu contents (inner cradle rotated 45 degrees for SC impingement onto sharp cradle edge) is shown in Figure 2-277. Note that each Pu cylinder is located at the far left side of each SC-2 so that its net impact velocity with the right side of the T-Ampoule is maximized. The post-impact deformation is shown in Figure 2-278 and its kinetic energy history in Figure 2-279. The Pu contents penetrate each of the SC-2 side walls and directly impact the T-Ampoule.

Average stress-triaxiality versus EQPS is shown in Figure 2-280 for the 82 elements extending beyond the tested Bao-Wierzbicki strain locus. All of these elements are outside the B-W locus, for a variety of stress triaxialities, although most of the 580,000 T-Ampoule elements are inside the B-W locus. The Tearing Parameter values for these same 82 elements are shown in Figure 2-281 and all are below the critical Tearing Parameter value of 1.012 for Ti-6Al-4V. These elements are highlighted in red in Figures 2-282 and 2-283, but note that these elements are still below the initiation of a ductile tear and thus T-Ampoule integrity is maintained.

Equivalent Plastic Strain (EQPS) in the TB-1 vessel is shown in Figures 2-284, 2-285, and 2-286 to be less than 29%, but only in some localized outer contact regions with the redwood overpack. The EQPS due to internal denting of the upper TB-1 is shown in Figure 2-286 to be less than 0.083%, which is essentially elastic. The von Mises stresses (see Figure 2-287) peak at 227 ksi, above the elevated-temperature minimum yield strength for the TB-1 of 141 ksi but more importantly, through-thickness TB-1 stress values are in the less-than-120 ksi range, which is below yield.

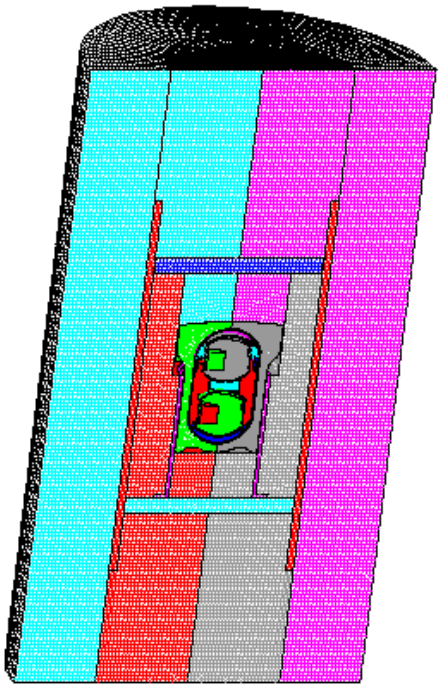

Figure 2-277. Finite Element Mesh for the SC-2, Side Impact, 45° Support Structure

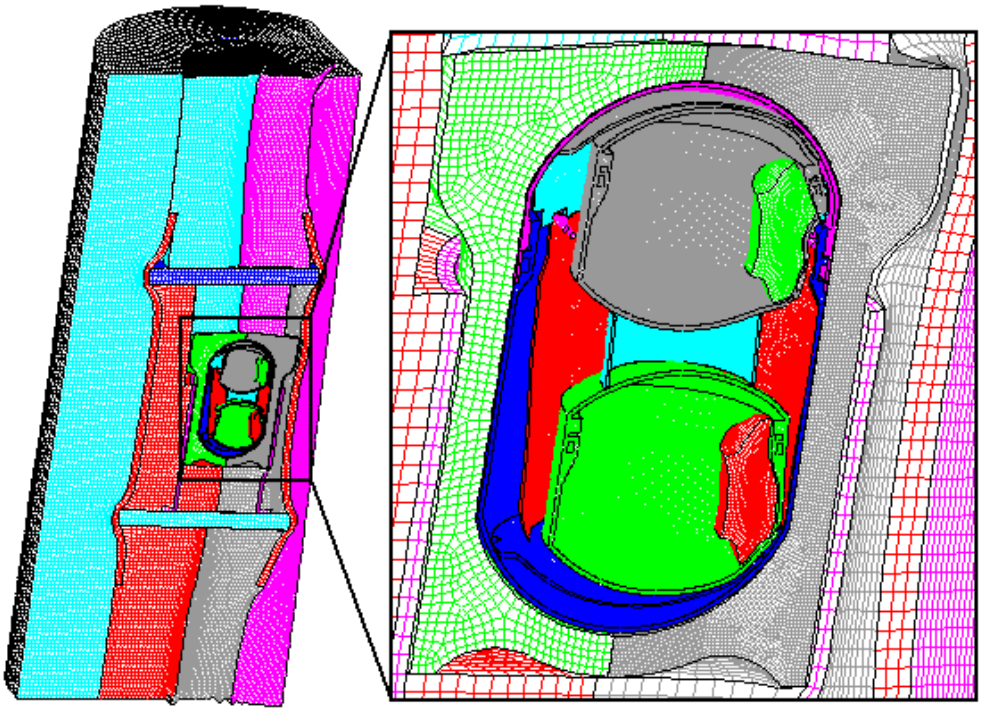

Figure 2-278. Finite Element Mesh for the SC-2, Side Impact, 45° Support Structure – Final Displacement

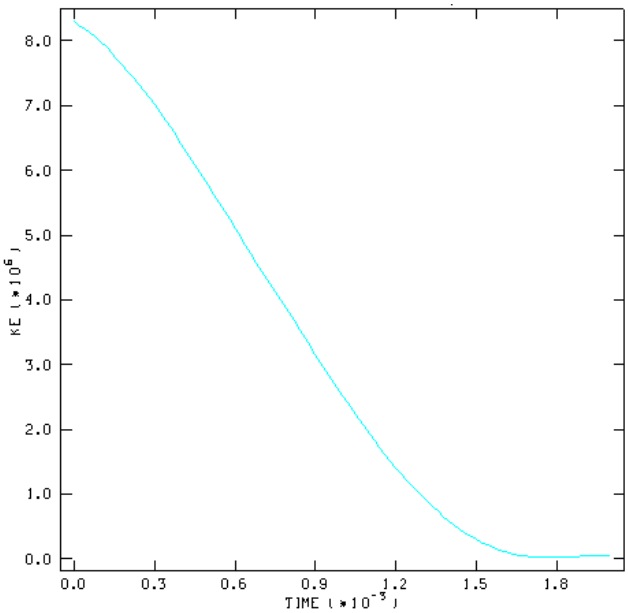

Figure 2-279. Kinetic Energy Time History for the SC-2, Side Impact, 45° Support Structure

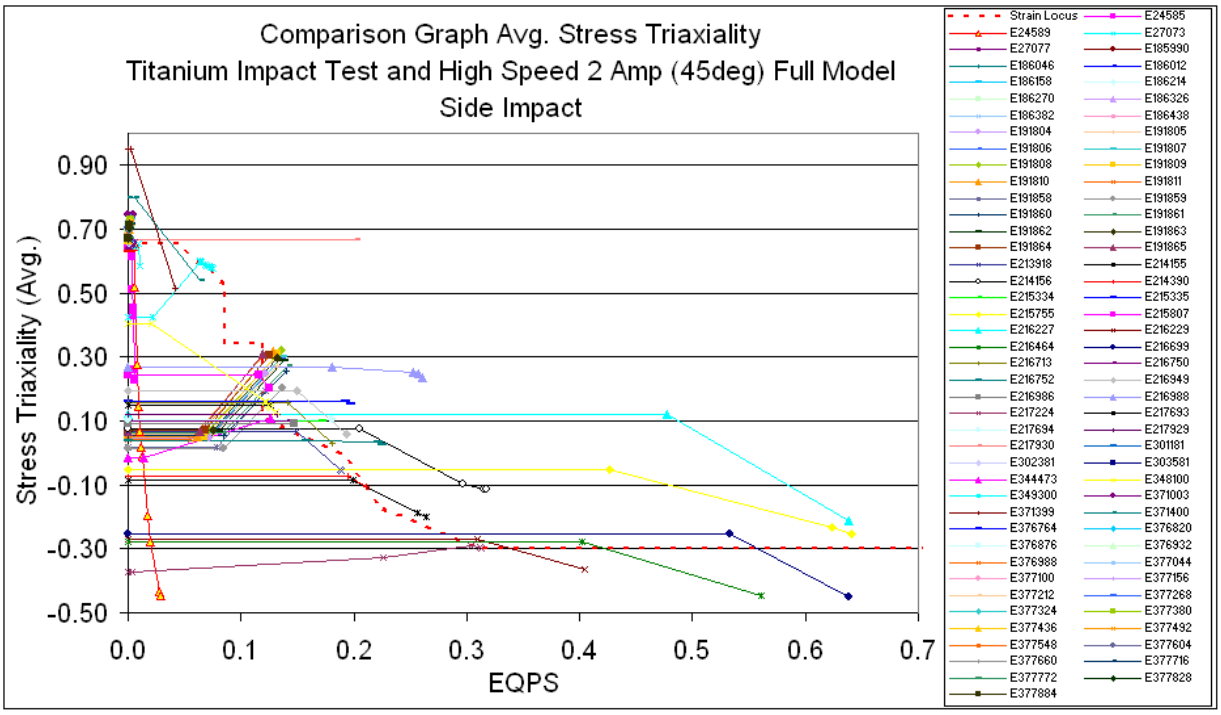

Figure 2-280. Graph of Average Stress Triaxiality versus EQPS of Elements Exceeding the Experimental Strain Locus for the SC-2, Side Impact, 45° Support Structure

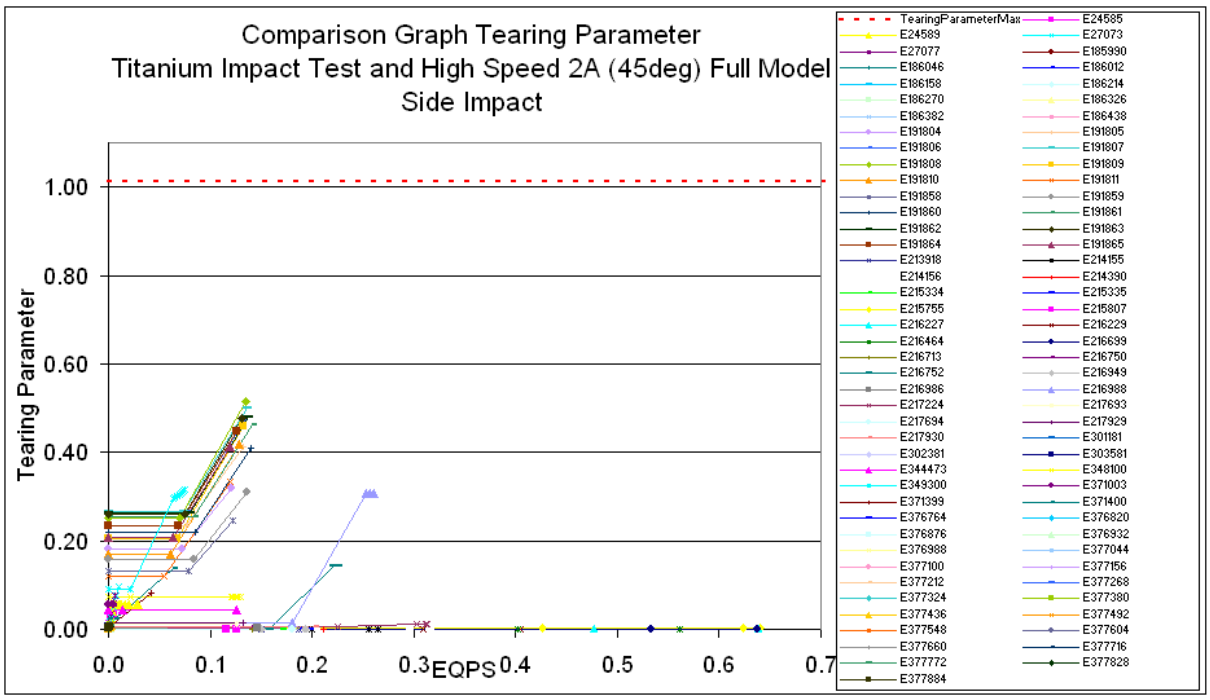

Figure 2-281. Graph of Tearing Parameter versus EQPS of Elements Exceeding the Experimental Strain Locus for the SC-2, Side Impact, 45° Support Structure

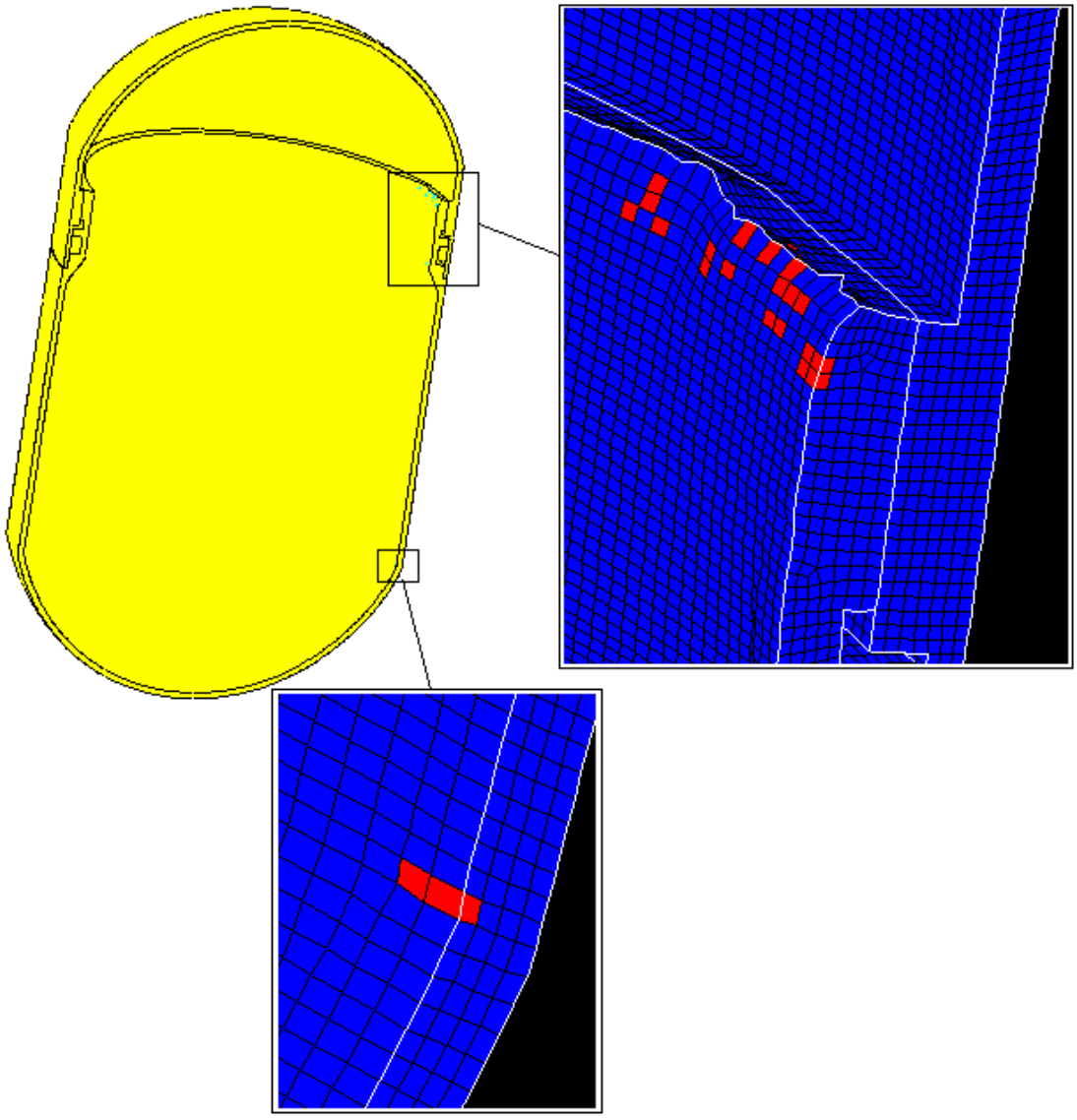

Figure 2-282. Plot of Elements Exceeding the Experimental Strain Locus for the SC-2, Side Impact, 45° Support Structure

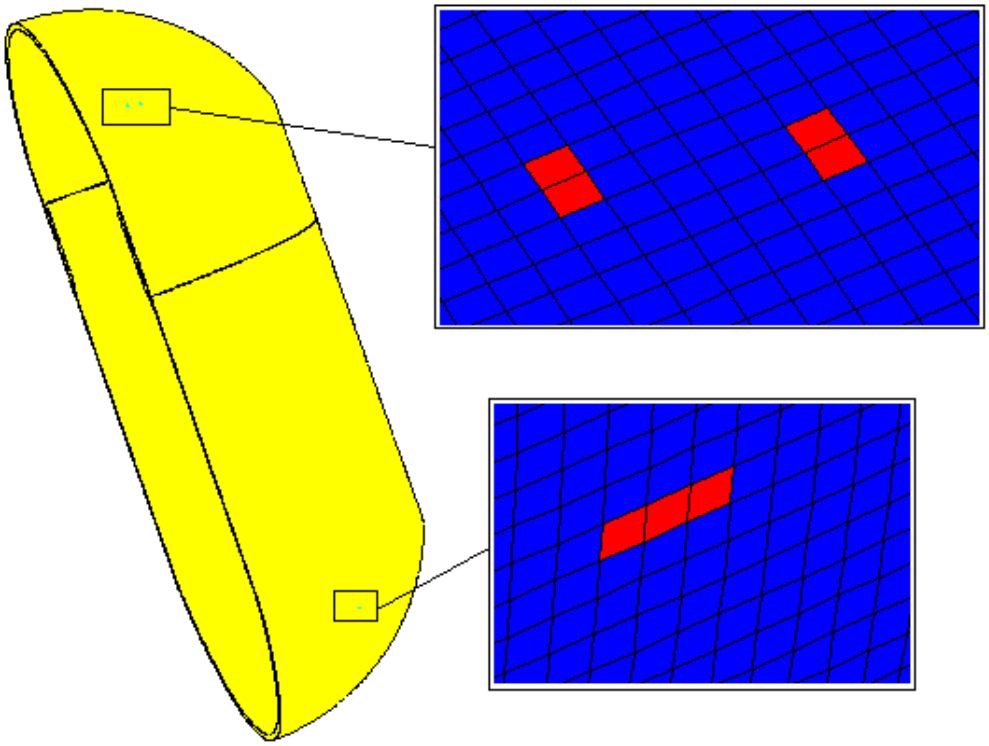

Figure 2-283. Plot of Elements Exceeding the Experimental Strain Locus for the SC-2, Side Impact, 45° Support Structure

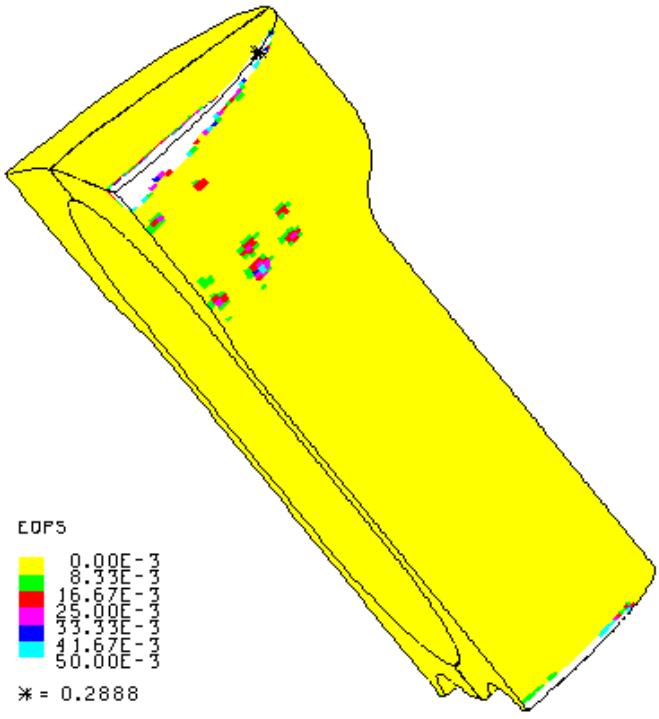

Figure 2-284. Plot of EQPS in the TB-1 for the SC-2, Side Impact, 45° Support Structure

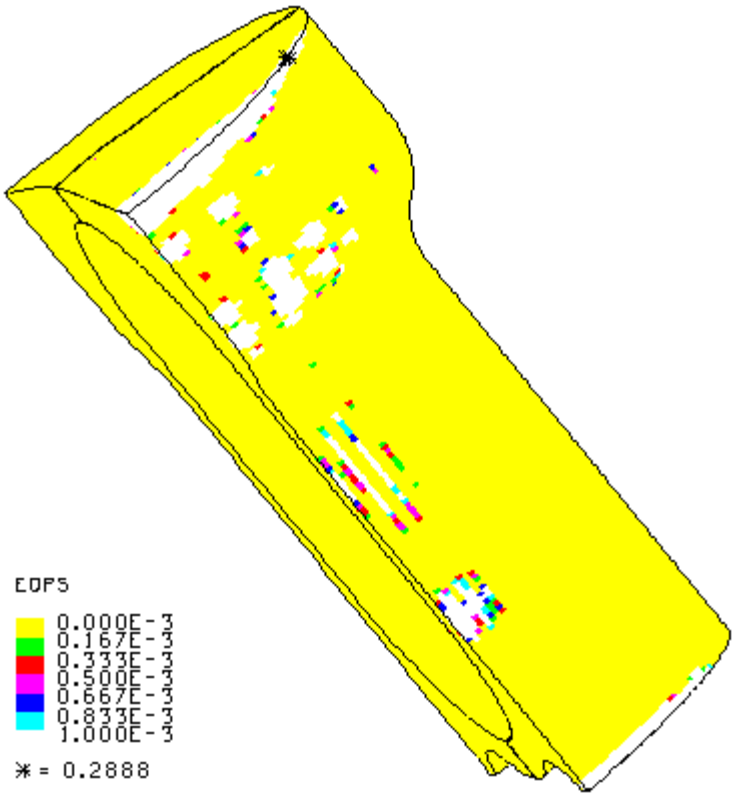

Figure 2-285. Plot of EQPS in the TB-1 for the SC-2, Side Impact, 45° Support Structure

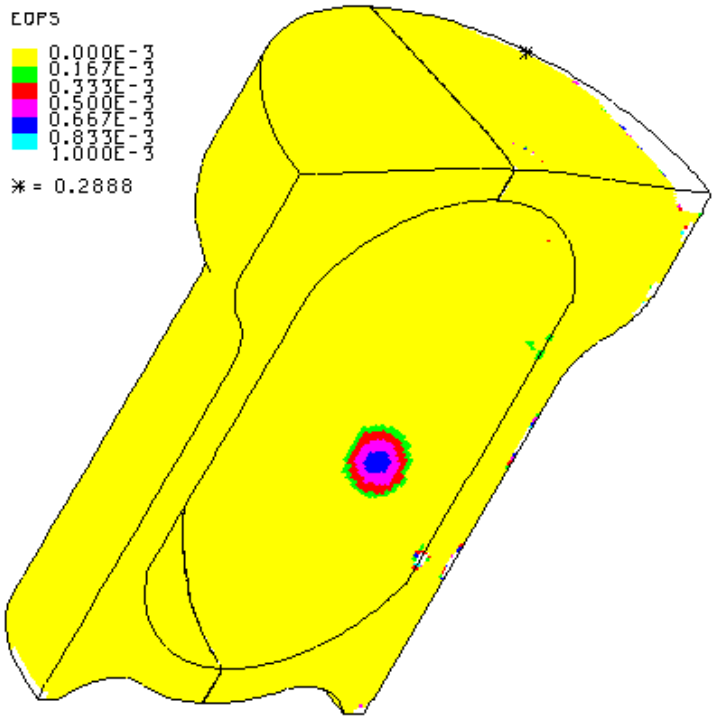

Figure 2-286. Plot of EQPS in the TB-1 for the SC-2, Side Impact, 45° Support Structure

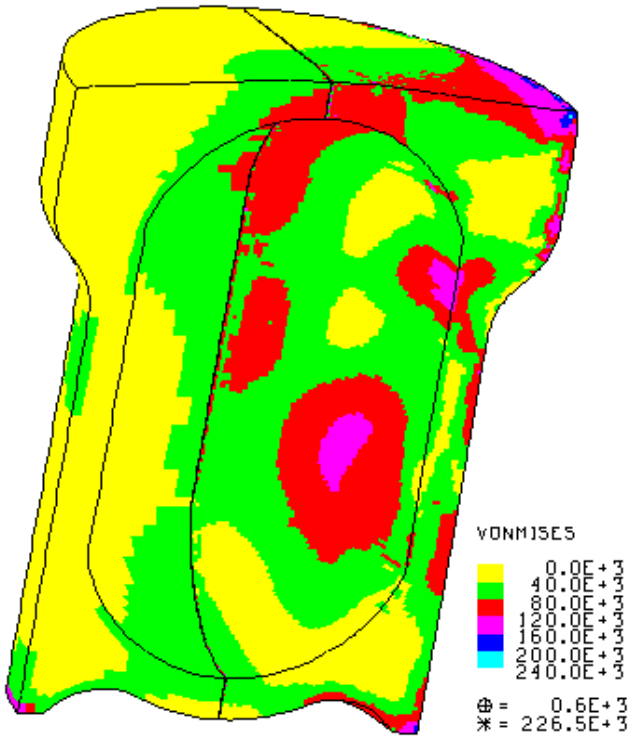

Figure 2-287. Plot of von Mises Stress in the TB-1 for the SC-2, Side Impact, 45° Support Structure

2.12.5.5.9 Run 19 - SC-2 Sample Container, CGOC Impact, Support Structure 0°

The lid end CG-over-corner impact model for each large SC-2 with delta Pu contents (inner cradle rotated 0 degrees) is shown in Figure 2-288. Each Pu cylinder is located at the rotated bottom of each SC-2 so that its net impact velocity with the top of the T-Ampoule is maximized. The post-impact deformation is shown in Figure 2-289 and its kinetic energy history in Figure 2-290. The Pu cylinder contents remain largely confined within the SC-2's, although significant localized deformation of the SC-2's has occurred.

Equivalent Plastic Strain (EQPS) in the TB-1 vessel is shown in Figure 2-291 to peak at about 18.5%, but only in some localized outer contact regions with the redwood overpack. The von Mises stresses (see Figure 2-292) peak at 145 ksi, just above the elevated-temperature minimum yield strength for the TB-1 of 141 ksi but more importantly, through-thickness TB-1 stress values are in the 47 ksi range, below yield. The time at which the peak value of the von Mises stress occurs coincides with the peak value of the contact force (summed over the lid area). A plot of this force as a function of time is shown in Figure 2-293. A maximum contact load of 34,253 lbs is applied to the inner surface of the TB-1 lid during the impact. No T-Ampoule elements exceeded the tested B-W strain locus, and the peak Tearing Parameter value (see Table 2-11, run #19) of 0.0953 was below the critical Tearing Parameter value of 1.012 for Ti-6Al-4V.

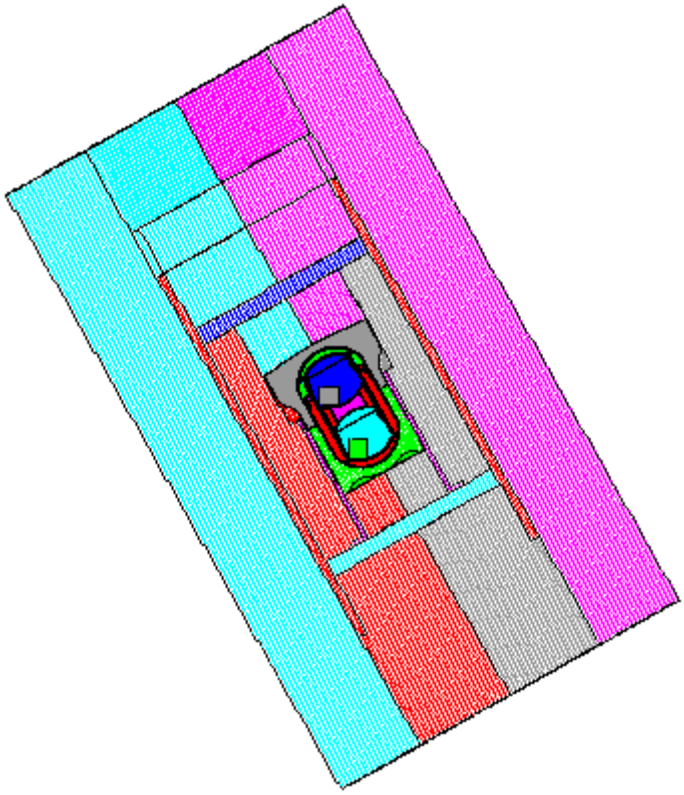

Figure 2-288. Finite Element Mesh for the SC-2, CGOC Impact, 0° Support Structure

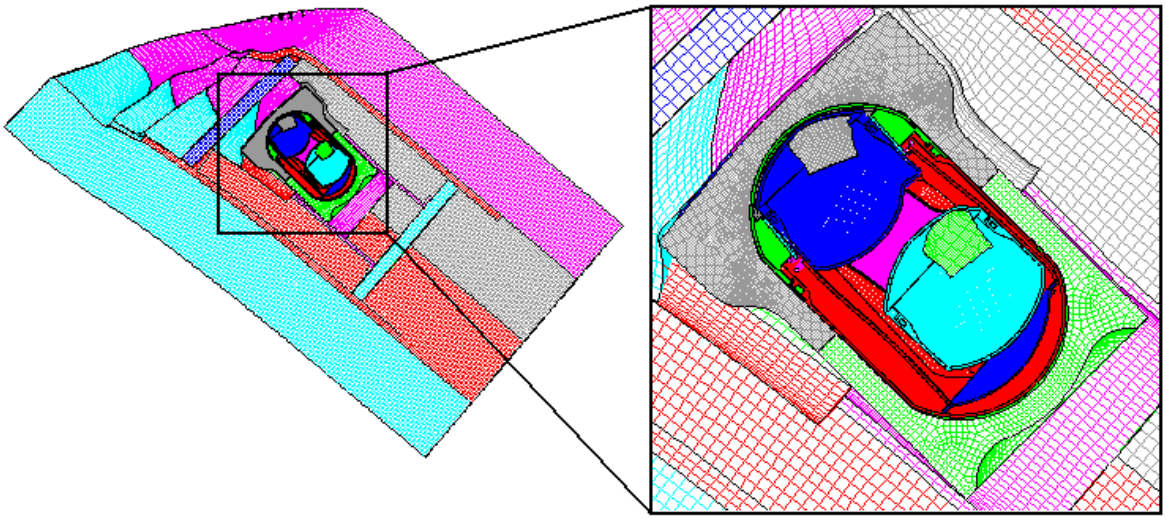

Figure 2-289. Finite Element Mesh for the SC-2, CGOC Impact, 0° Support Structure – Final Displacement

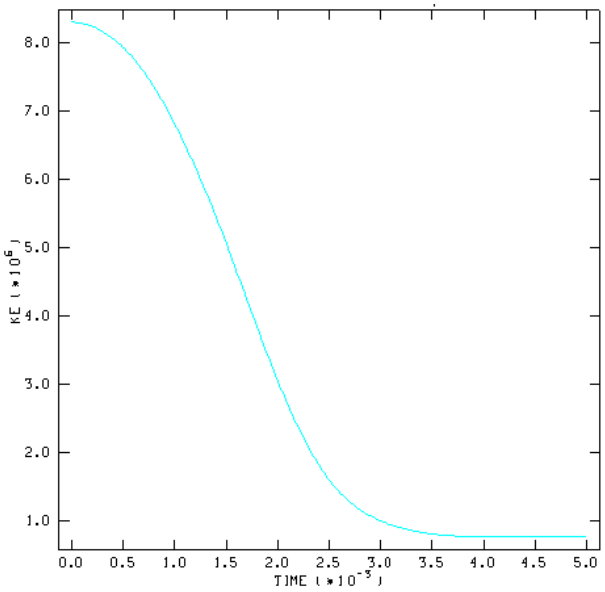

Figure 2-290. Kinetic Energy Time History for the SC-2, CGOC Impact, 0° Support Structure

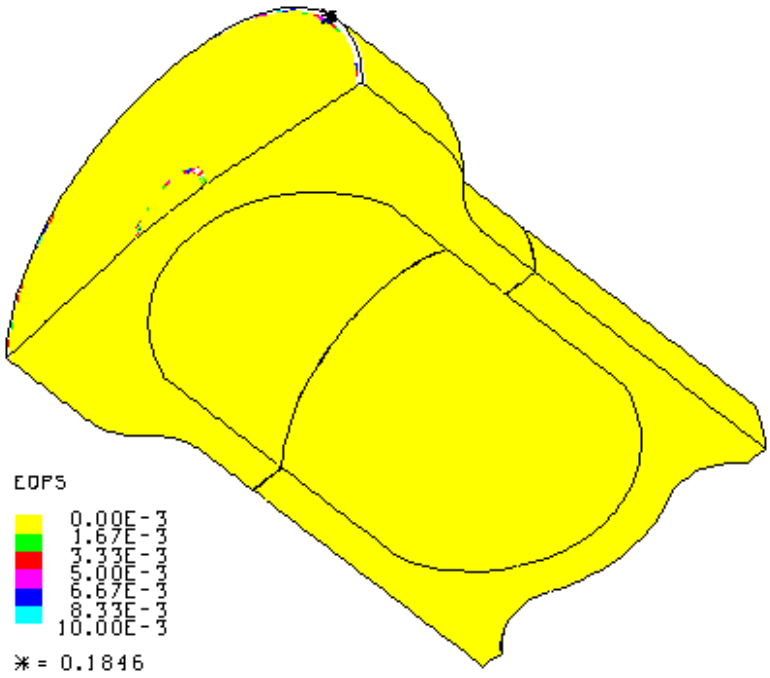

Figure 2-291. Plot of EQPS in the TB-1 for the SC-2, CGOC Impact, 0° Support Structure

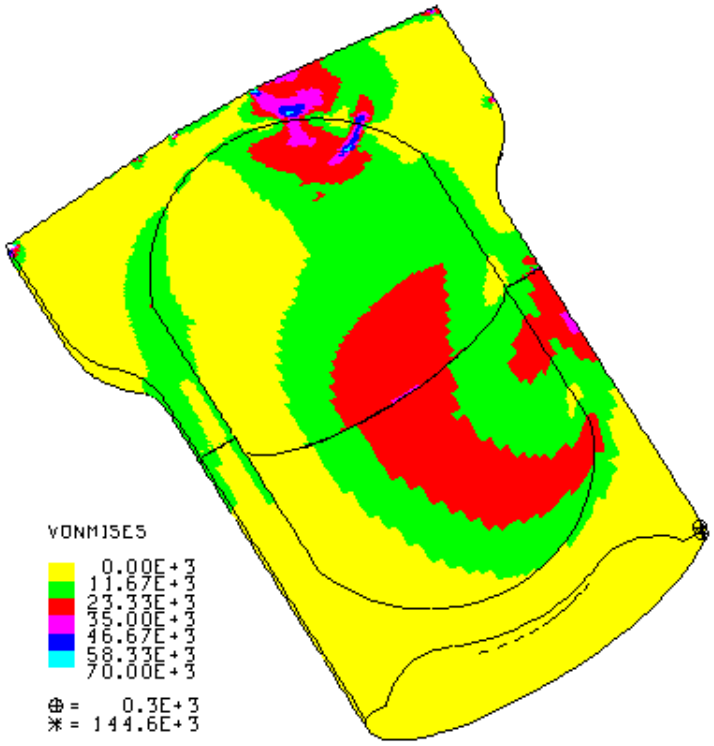

Figure 2-292. Plot of von Mises Stress in the TB-1 for the SC-2, CGOC Impact, 0° Support Structure

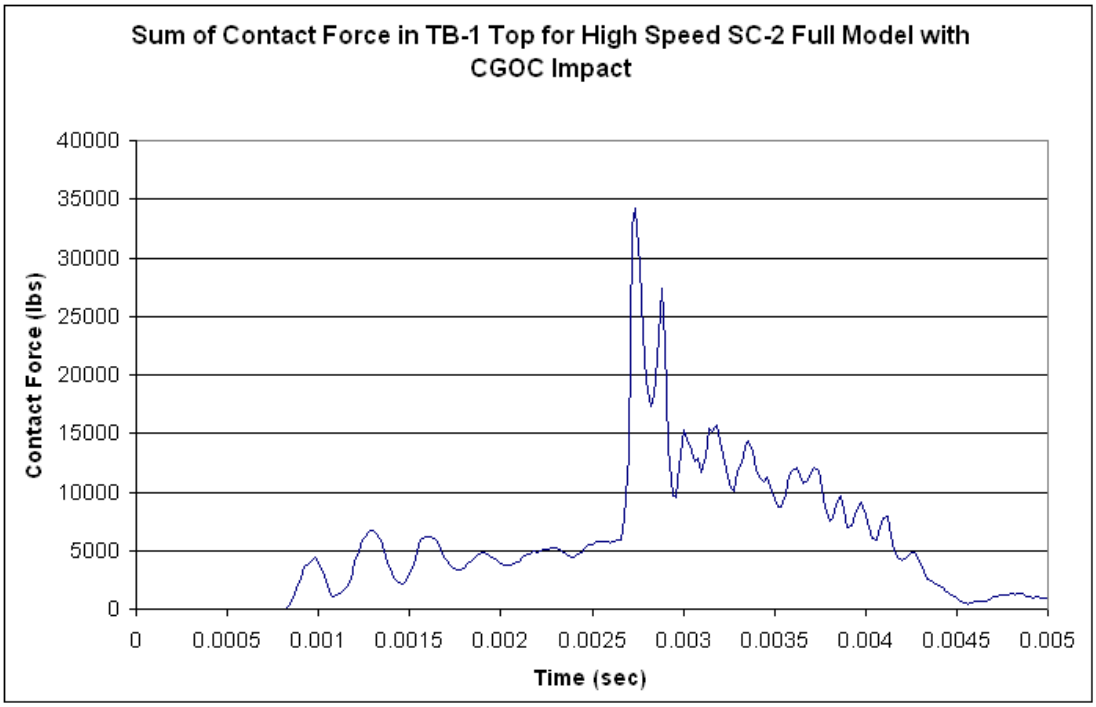

Figure 2-293. Plot of Contact Forces in the TB-1 for the SC-2, CGOC Impact, 0° Support Structure

2.12.5.5.10 Run 20 - SC-2 Sample Container, CGOC Impact, Support Structure 45°

The lid end CG-over-corner impact model for each large SC-2 with delta Pu contents (inner cradle rotated 45 degrees) is shown in Figure 2-294. Each Pu cylinder is located at the rotated bottom of each SC-2 so that its net impact velocity with the top of the T-Ampoule is maximized. The post-impact deformation is shown in Figure 2-295 and its kinetic energy history in Figure 2-296. The Pu cylinder contents remain largely confined within each SC-2, although localized deformation of the SC-2 has occurred.

Equivalent Plastic Strain (EQPS) in the TB-1 vessel is shown in Figure 2-297 to peak at about 20%, but only in some localized outer contact regions with the redwood overpack. The von Mises stresses (see Figure 2-298) peak at 143 ksi, just above the elevated-temperature minimum yield strength for the TB-1 of 141 ksi but more importantly, through-thickness TB-1 stress values are in the 37.5 ksi range, below yield. The time at which the peak value of the von Mises stress occurs coincides with the peak value of the contact force (summed over the lid area). A plot of this force as a function of time is shown in Figure 2-299. A maximum contact load of 31,307 lbs is applied to the inner surface of theTB-1 lid during the impact. No T-Ampoule elements exceeded the tested B-W strain locus, and the peak Tearing Parameter value (see Table 2-11, run #20) of 0.054 was below the critical Tearing Parameter value of 1.012 for Ti-6Al-4V.

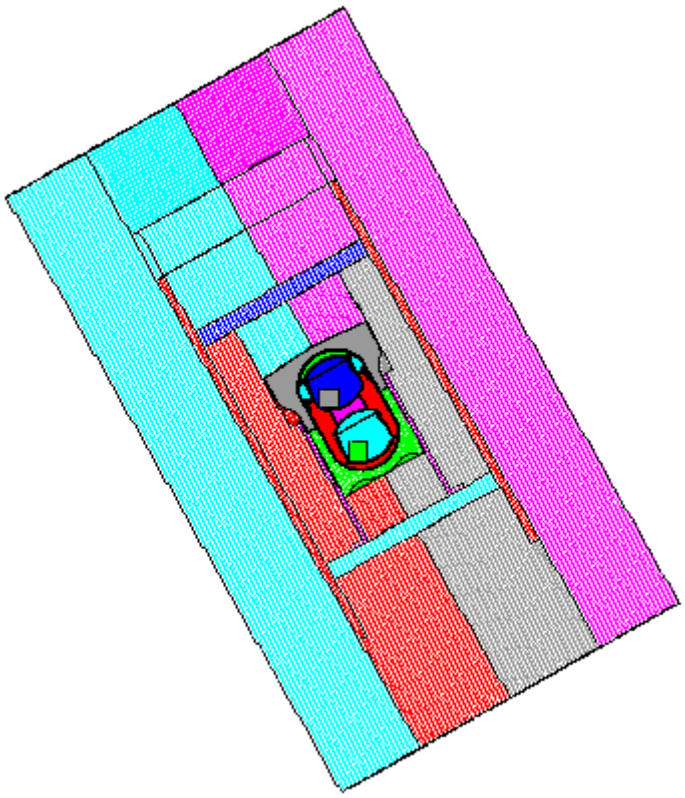

Figure 2-294. Finite Element Mesh for the SC-2, CGOC Impact, 45° Support Structure

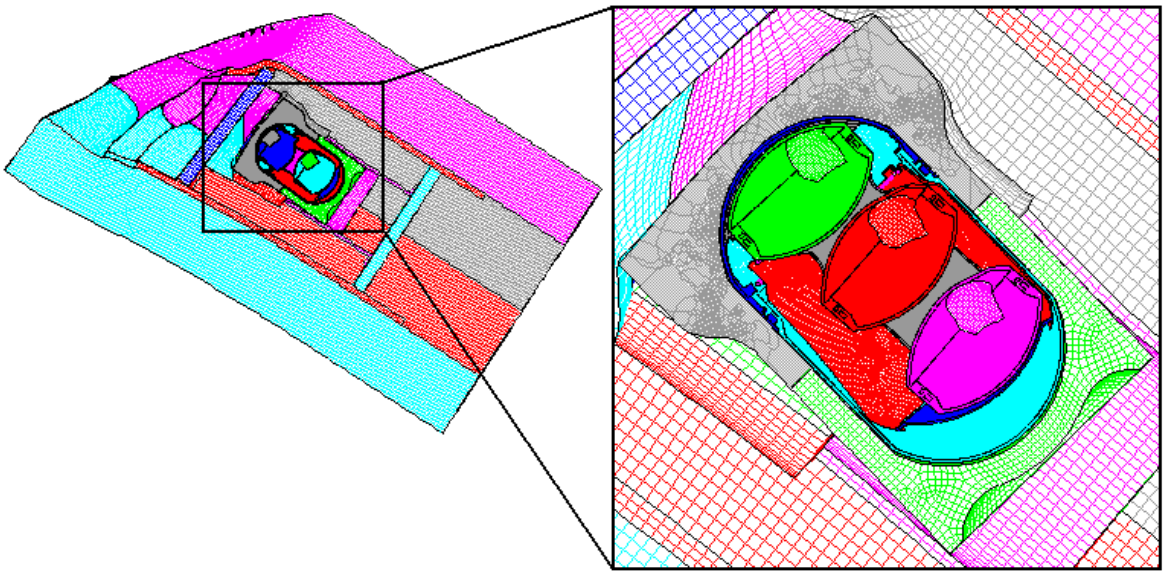

Figure 2-295. Finite Element Mesh for the SC-2, CGOC Impact, 45° Support Structure – Final Displacement

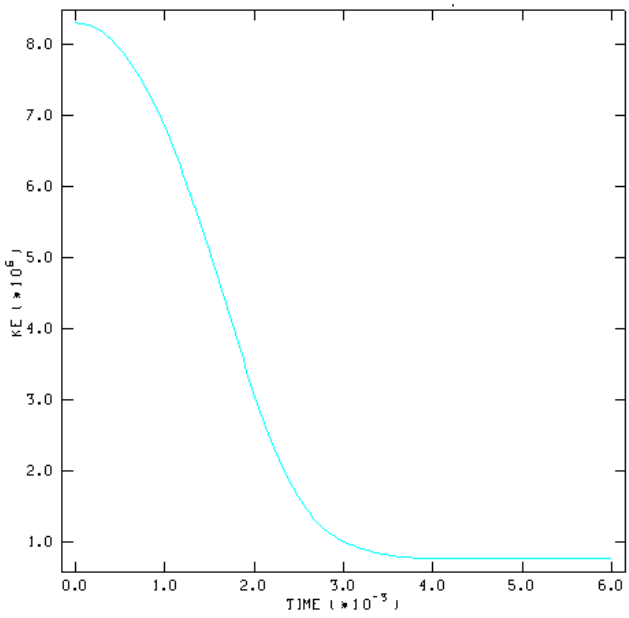

Figure 2-296. Kinetic Energy Time History for the SC-2, CGOC Impact, 45° Support Structure

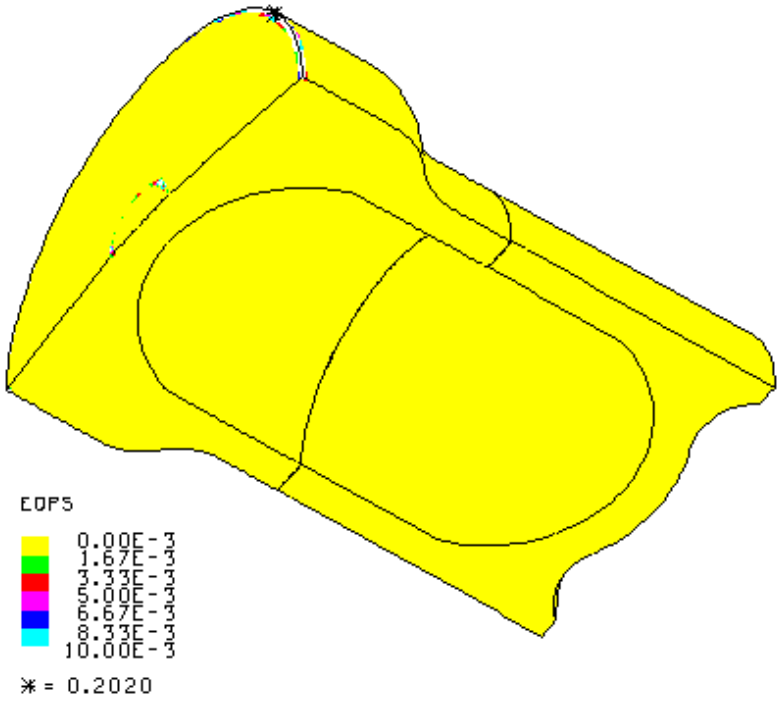

Figure 2-297. Plot of EQPS in the TB-1 for the SC-2, CGOC Impact, 45° Support Structure

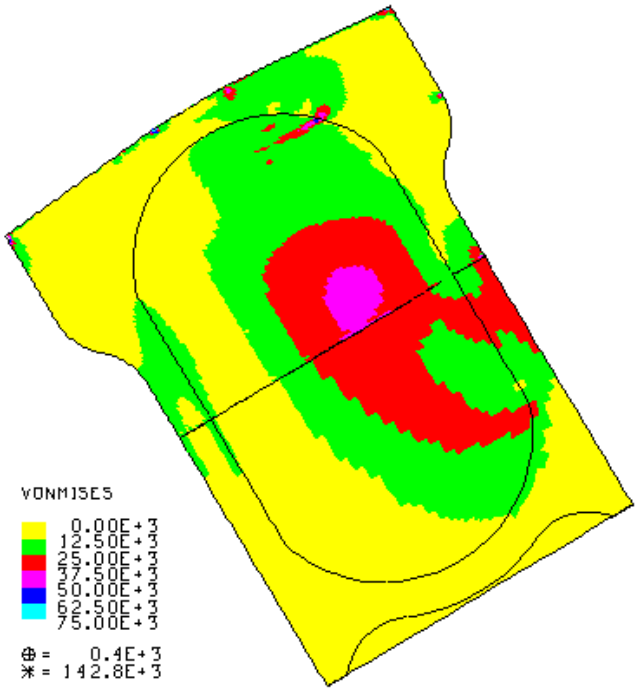

Figure 2-298. Plot of von Mises Stress in the TB-1 for the SC-2, CGOC Impact, 45° Support Structure

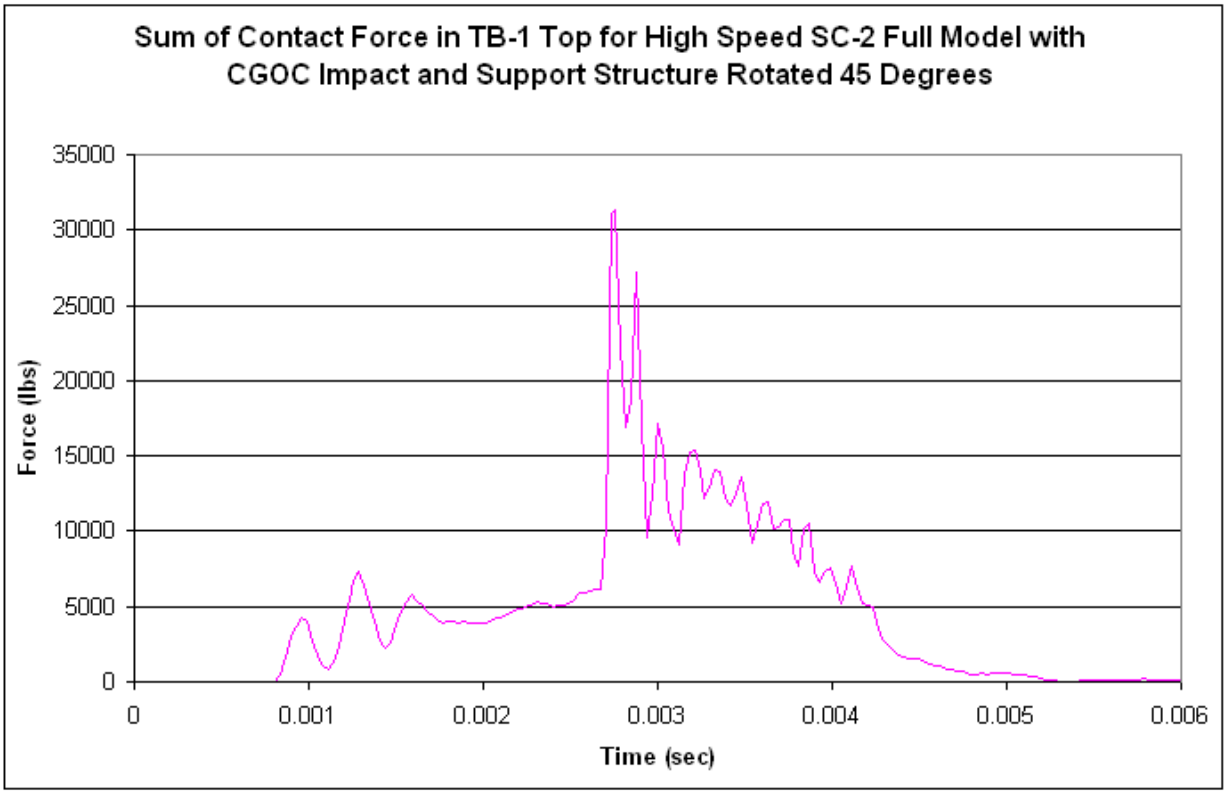

Figure 2-299. Plot of Contact Forces in the TB-1 for the SC-2, CGOC Impact, 45° Support Structure

2.12.5.5.11 Run 21 – SC-1 Sample Container, End Impact, Support Structure 0°, Be Contents

The top end impact model for each SC-1 with a smaller solid cylinder Be composite contents is shown in Figure 2-300. Note that each Be cylinder is located at the bottom of each SC-1 so that its net impact velocity with the top of the T-Ampoule is maximized. Also note that the orientation of each Be cylinder is CG-over-corner so its sharp corner is first to impact the SC-1 and the T-Ampoule. The post-impact deformation is shown in Figure 2-301 and its kinetic energy history in Figure 2-302. The top SC-1 is crushed from the subsequent impacts from the lower SC-1, and its Be contents do not quite locally penetrate its upper wall, which directly impacts the T-Ampoule. Note the relatively smaller deformation of the Be cylinders versus the previous (softer) Pu cylinders.

Equivalent Plastic Strain (EQPS) in the TB-1 vessel is shown in Figure 2-303 to be less than 3%, and only in some localized outer contact regions with the redwood overpack. A very small area of localized internal denting occurs, with plasticity less than 0.05%. The von Mises stresses (see Figure 2-304) peak at 143 ksi, just above the elevated-temperature minimum yield strength for the TB-1 of 141 ksi, but more importantly, through-thickness TB-1 stress values are in the less-than-75 ksi range, below yield. No T-Ampoule elements exceeded the tested B-W strain locus, and the peak Tearing Parameter value (see, Table 2-11 run #21) of 0.0155 was below the critical Tearing Parameter value of 1.012 for Ti-6Al-4V.

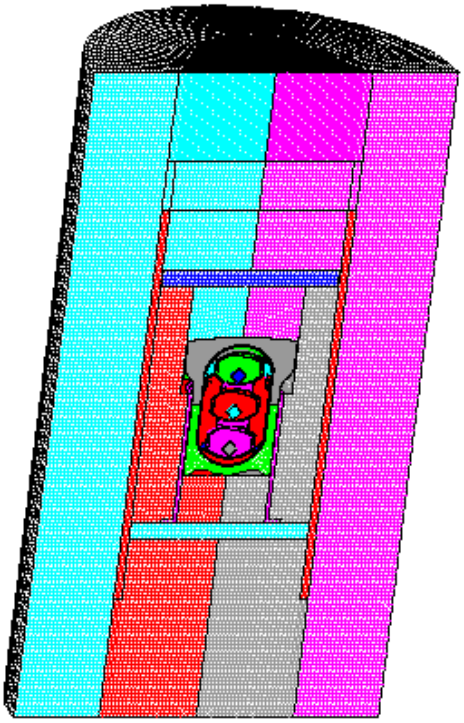

Figure 2-300. Finite Element Mesh for the SC-1, End Impact, 0° Support Structure, Be Contents

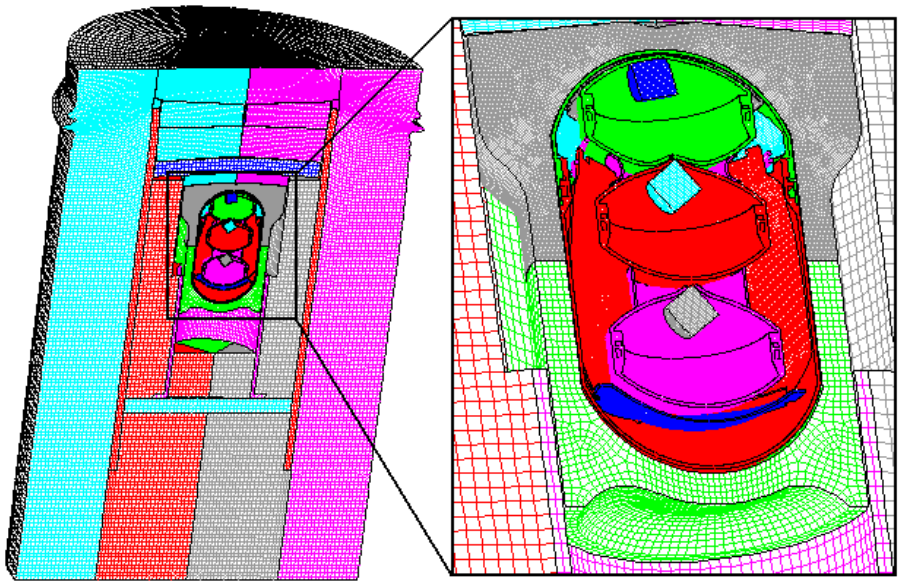

Figure 2-301. Finite Element Mesh for the SC-1, End Impact, 0° Support Structure, Be Contents – Final Displacement

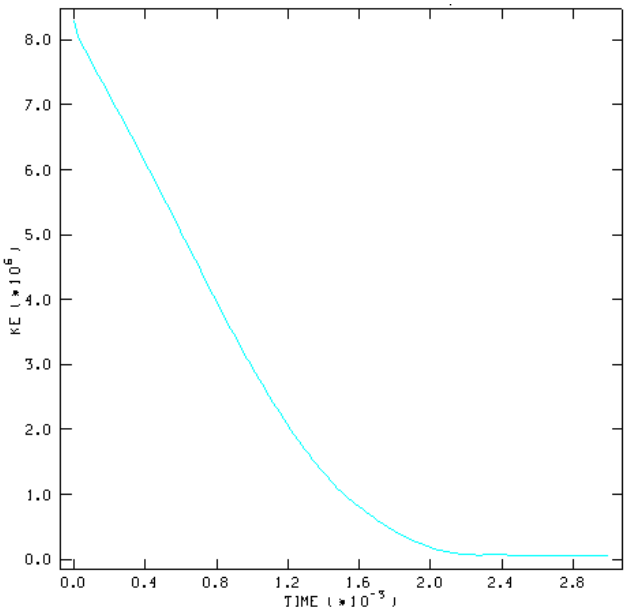

Figure 2-302. Kinetic Energy Time History for the SC-1, End Impact, 0° Support Structure, Be Contents

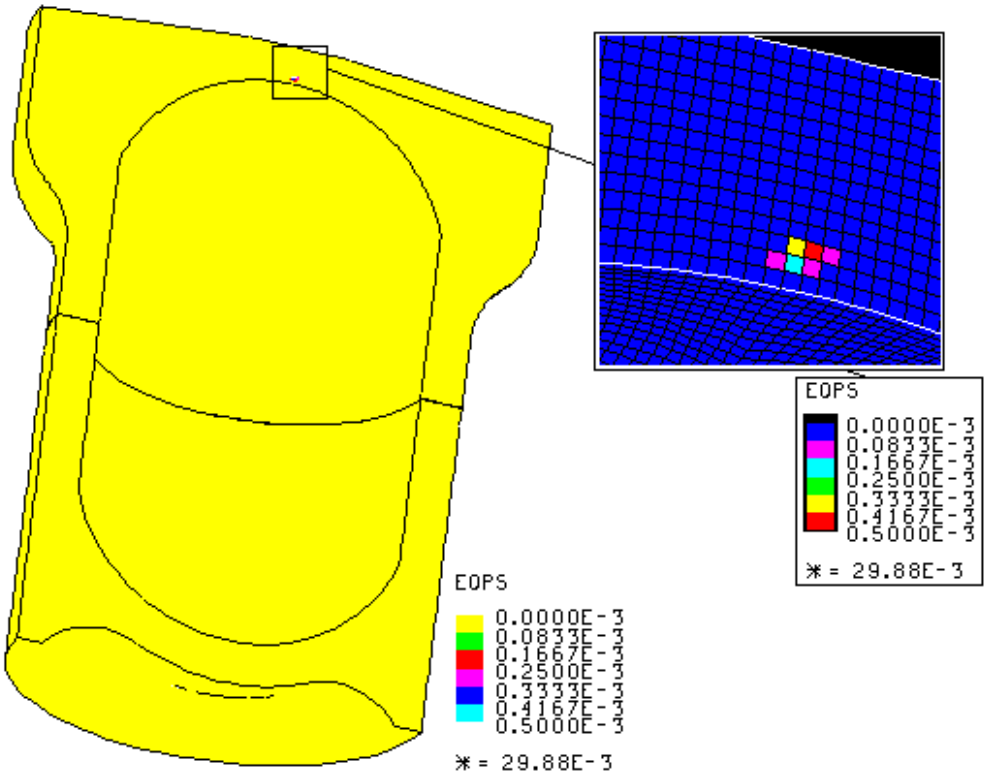

Figure 2-303. Plot of EQPS in the TB-1 for the SC-1, End Impact, 0° Support Structure, Be Contents

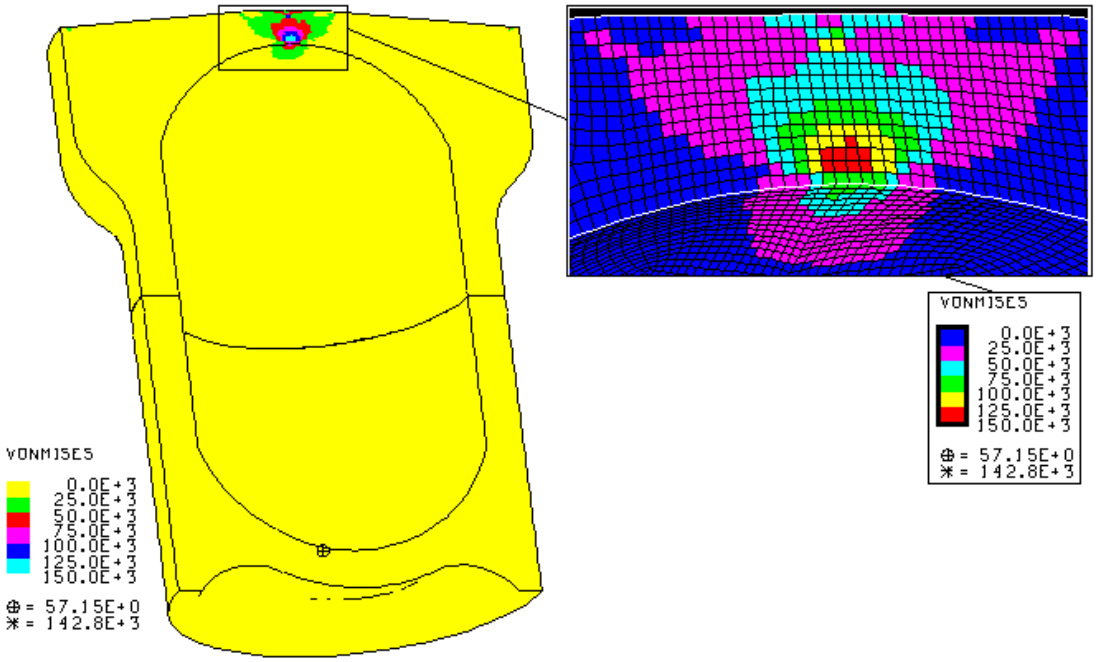

Figure 2-304. Plot of von Mises Stress in the TB-1 for the SC-1, End Impact, 0° Support Structure, Be Contents

2.12.5.5.12 Run 22 – SC-1 Sample Container, Side Impact, Support Structure 0°, Be Contents

The side impact model for each SC-1 with a smaller Be composite cylinder contents (inner cradle rotated 0 degrees) is shown in Figure 2-305. Note that each Be cylinder is located at the far left side of each SC-1 so that its net impact velocity with the right side of the T-Ampoule is maximized. Also note that the orientation of each Be cylinder is CG-over-corner so it sharp corner is first to impact the SC-1 and the T-Ampoule. The post-impact deformation is shown in Figure 2-306 and its kinetic energy history in Figure 2-307. Unlike the heavier Pu cylinders, the lighter Be contents do not penetrate the SC-1 side walls and directly impact the T-Ampoule.

Average stress-triaxiality versus EQPS is shown in Figures 2-308 and 2-309 (zoomed in view) for the 14 elements extending beyond the tested Bao-Wierzbicki strain locus. All of these elements are outside the B-W locus, in a region of high stress triaxiality. The Tearing Parameter values for these same 14 elements are shown in Figure 2-310, and all are below the critical Tearing Parameter value of 1.012 for Ti-6Al-4V. These elements are highlighted in red in Figures 2-311 and 2-312, but note that these elements are still below the initiation of a ductile tear and thus T-Ampoule integrity is maintained.

Equivalent Plastic Strain (EQPS) in the TB-1 vessel is shown in Figure 2-313 to be less than 37%, but only in some localized outer contact regions with the redwood overpack. The EQPS due to internal denting of the upper TB-1 is less than 0.07%, which is nearly elastic. The von Mises stresses (see Figure 2-314) peak at 205 ksi, above the elevated-temperature minimum yield strength for the TB-1 of 141 ksi, but more importantly, through-thickness TB-1 stress values are in the 85 ksi range, below yield.

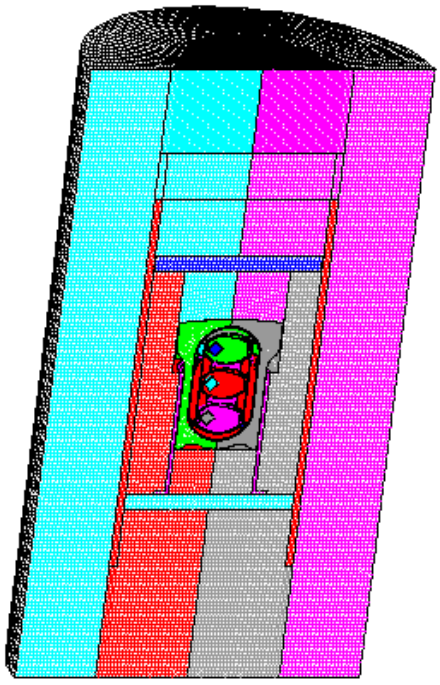

Figure 2-305. Finite Element Mesh for the SC-1, Side Impact, 0° Support Structure, Be Contents

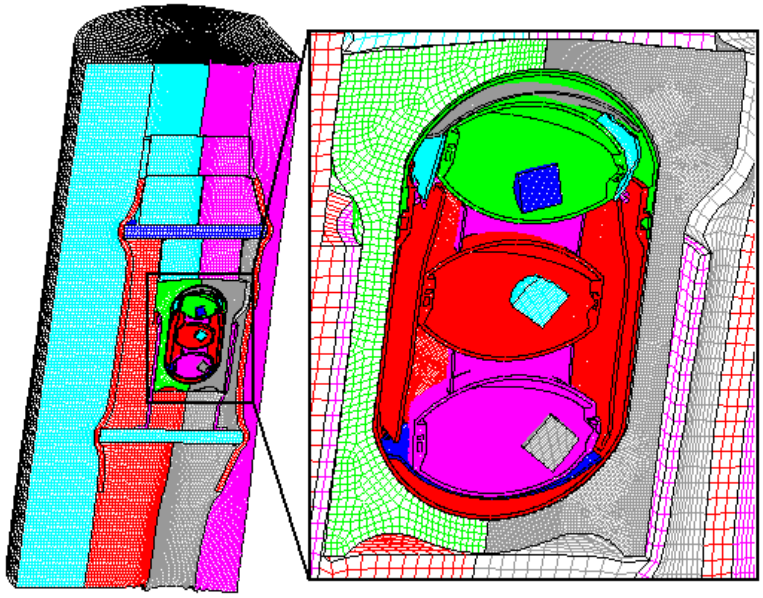

Figure 2-306. Finite Element Mesh for the SC-1, Side Impact, 0° Support Structure, Be Contents – Final Displacement

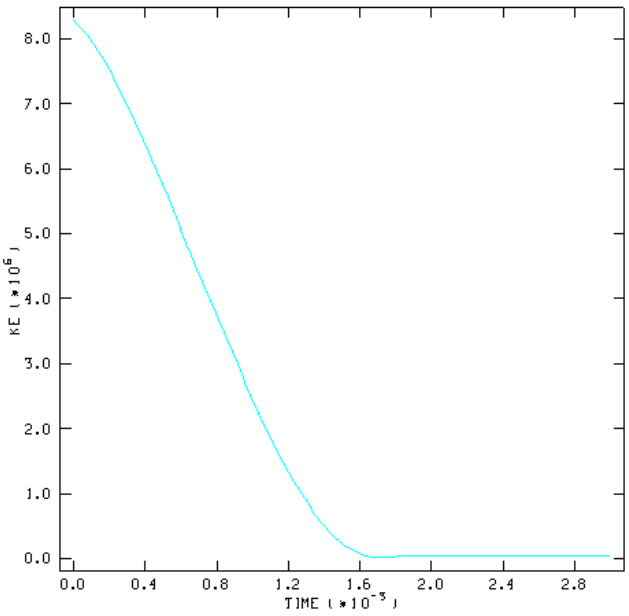

Figure 2-307. Kinetic Energy Time History for the SC-1, Side Impact, 0° Support Structure, Be Contents

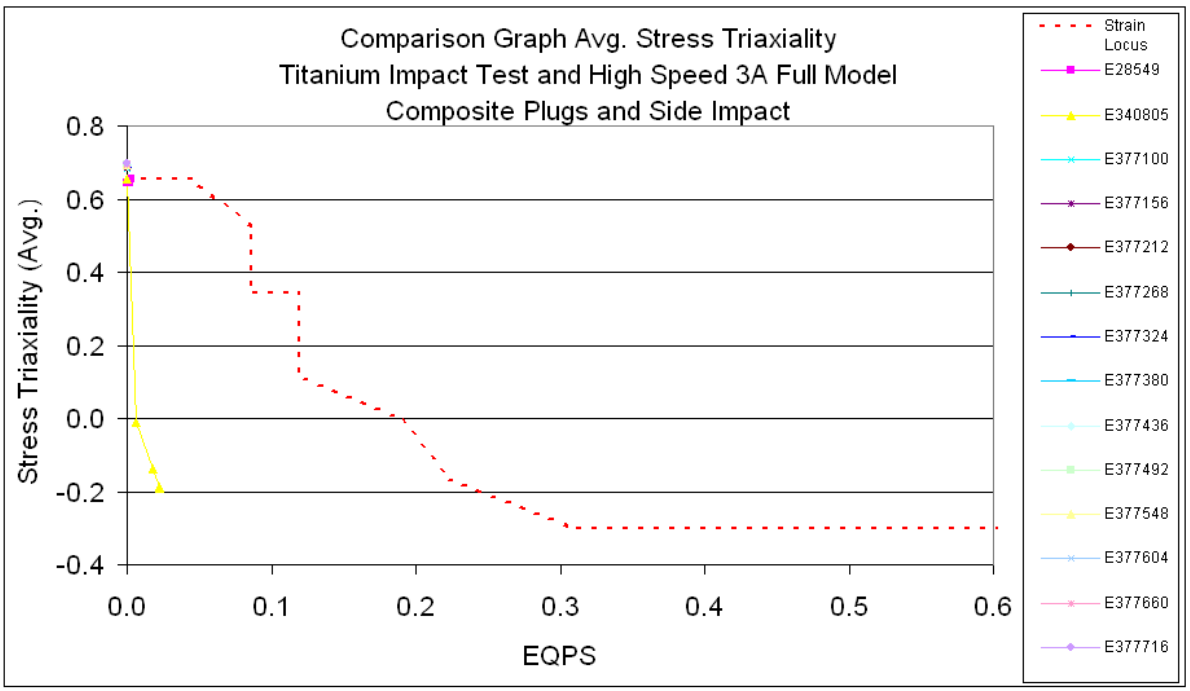

Figure 2-308. Graph of Average Stress Triaxiality versus EQPS of the Elements Exceeding the Experimental Strain Locus for the SC-1, Side Impact, 0° Support Structure, Be Contents

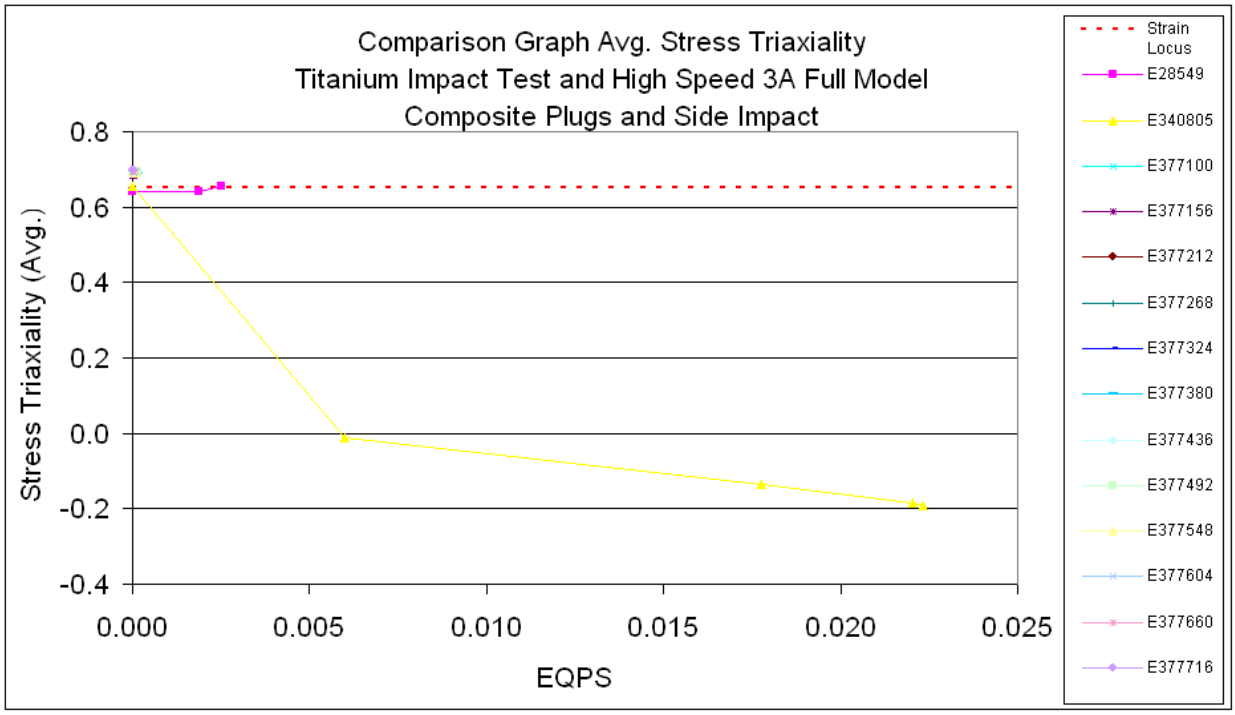

Figure 2-309. Graph of Average Stress Triaxiality versus EQPS of the Elements Exceeding the Experimental Strain Locus (Zoomed In) for the SC-1, Side Impact, 0° Support Structure, Be Contents

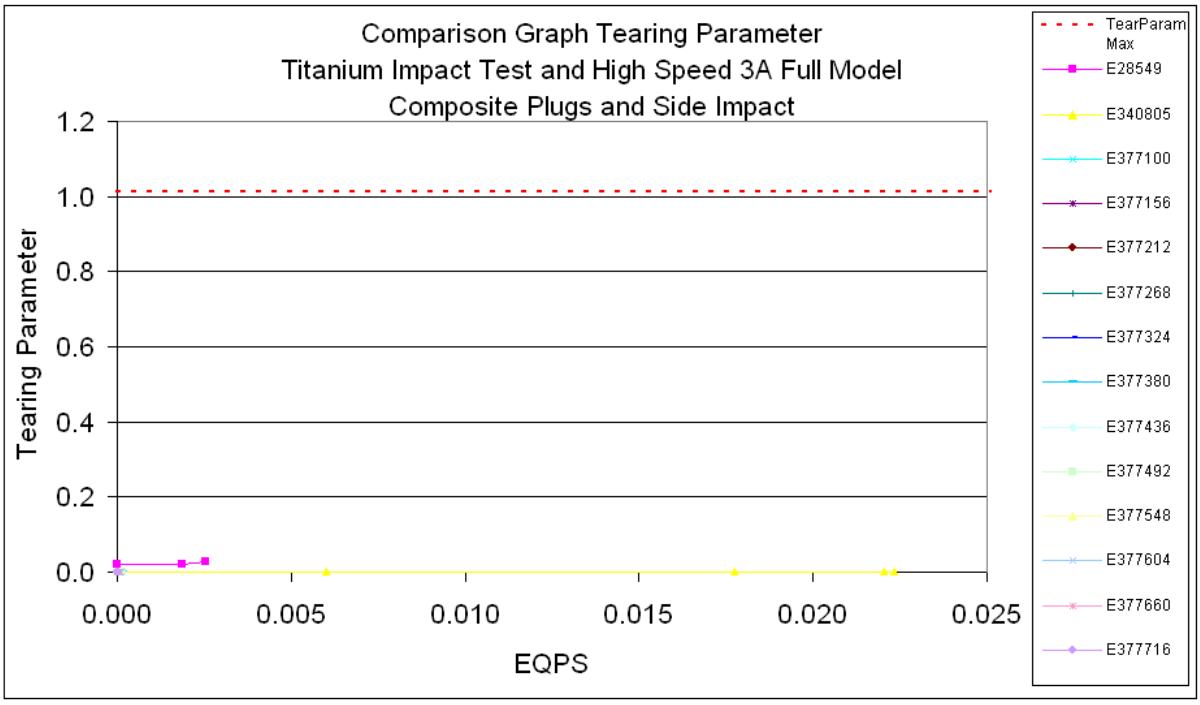

Figure 2-310. Graph of Tearing Parameter versus EQPS of the Elements Exceeding the Experimental Strain Locus for the SC-1, Side Impact, 0° Support Structure, Be Contents

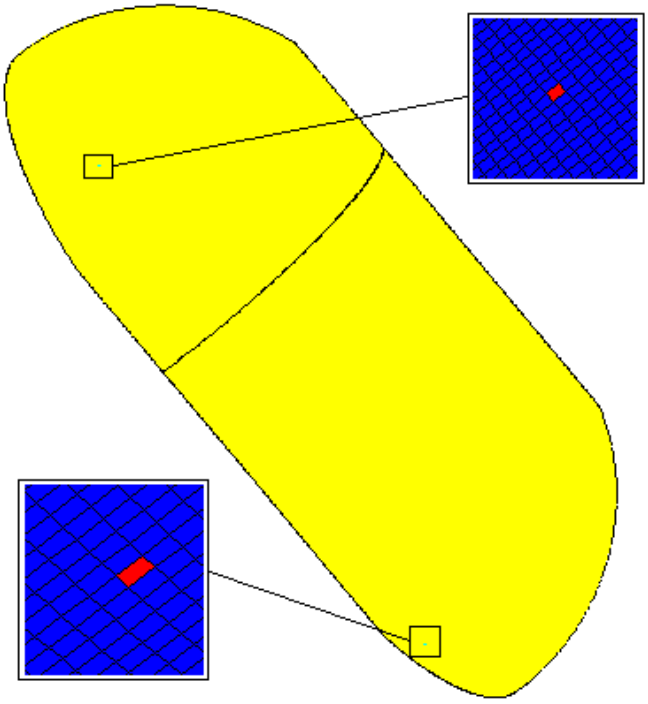

Figure 2-311. Plot of the Elements Exceeding the Experimental Strain Locus for the SC-1, Side Impact, 0° Support Structure, Be Contents

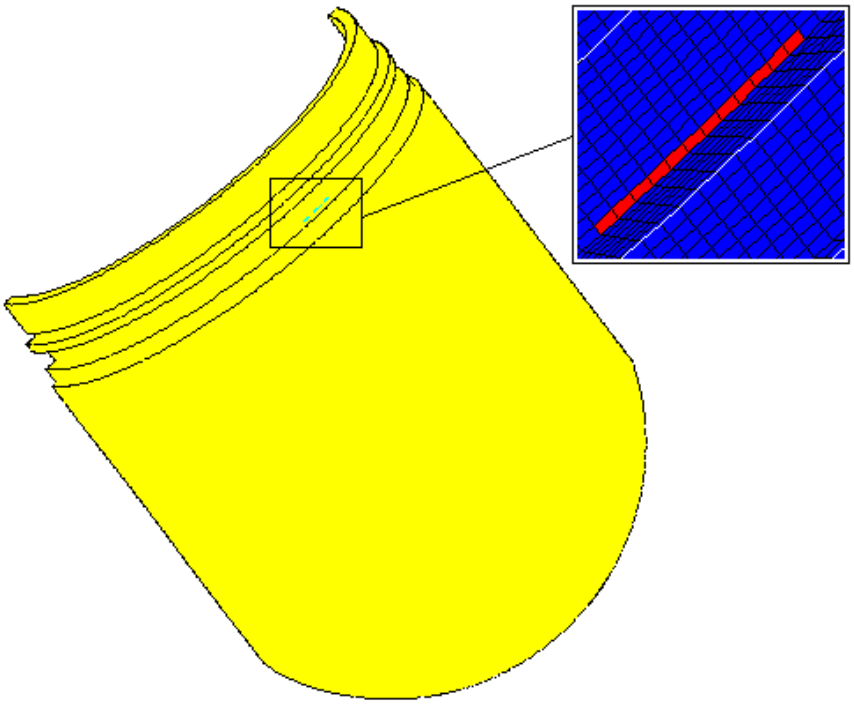

Figure 2-312. Plot of the Elements Exceeding the Experimental Strain Locus for the SC-1, Side Impact, 0° Support Structure, Be Contents

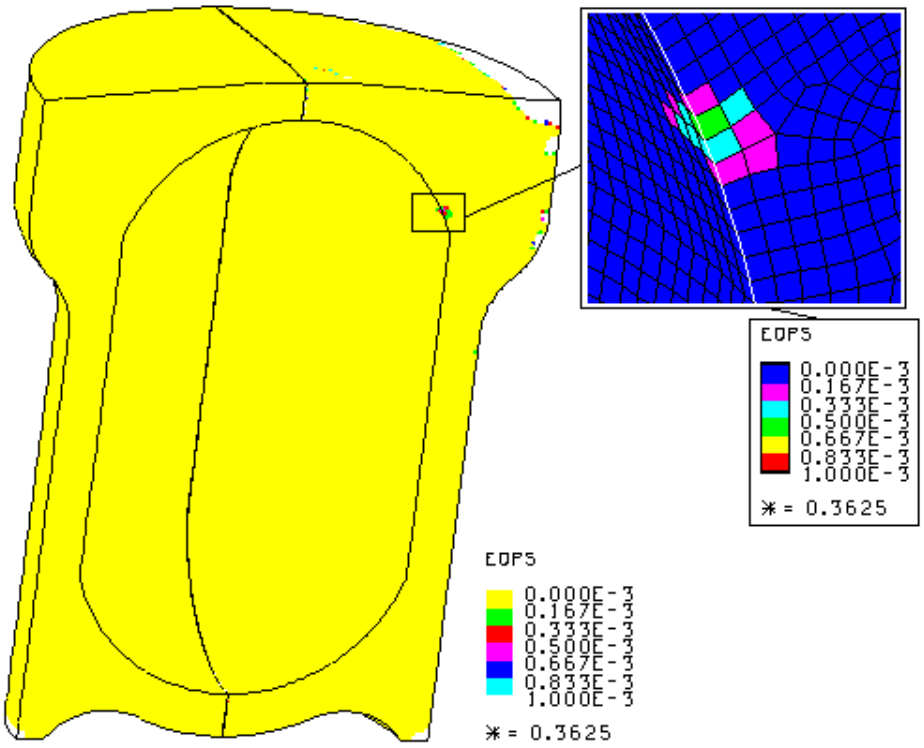

Figure 2-313. Plot of EQPS in the TB-1 for the SC-1, Side Impact, 0° Support Structure, Be Contents

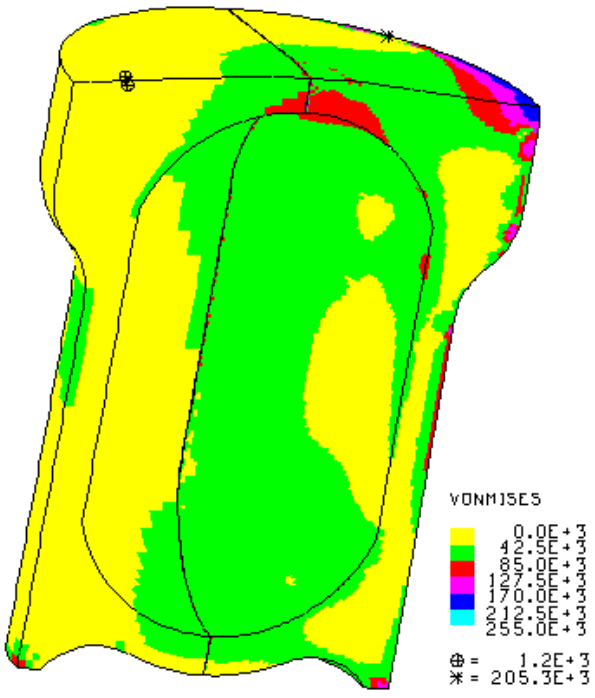

Figure 2-314. Plot of von Mises Stress in the TB-1 for the SC-1, Side Impact, 0° Support Structure, Be Contents

2.12.5.5.13 Run 23 – SC-1 Sample Container, Side Impact, Support Structure 45°, Be Contents

The side impact model for each SC-1 with a smaller Be composite cylinder contents (inner cradle rotated 45 degrees) is shown in Figure 2-315. Note that each Be cylinder is located at the far left side of each SC-1 so that its net impact velocity with the right side of the T-Ampoule is maximized. Also note that the orientation of each Be cylinder is CG-over-corner so it sharp corner is first to impact the SC-1 and the T-Ampoule. The post-impact deformation is shown in Figure 2-316 and its kinetic energy history in Figure 2-317. The lighter Be contents do not penetrate the SC-1 side walls and directly impact the T-Ampoule.

Average stress-triaxiality versus EQPS is shown in Figure 2-318 for the 13 elements extending beyond the tested Bao-Wierzbicki strain locus. All of these elements are outside the B-W locus, in a region of high stress triaxiality. The Tearing Parameter values for these same 13 elements are shown in Figure 2-319, and all are below the critical Tearing Parameter value of 1.012 for Ti-6Al-4V. These elements are highlighted in red in Figures 2-320 and 2-321, but note that these elements are still below the initiation of a ductile tear and thus T-Ampoule integrity is maintained.

Equivalent Plastic Strain (EQPS) in the TB-1 vessel is shown in Figure 2-322 to be less than 28%, but only in some localized outer contact regions with the redwood overpack. The EQPS due to internal denting of the upper TB-1 is less than 0.083%, which is nearly elastic. The von Mises stresses (see Figure 2-323) peak at 206 ksi, above the elevated-temperature minimum yield strength for the TB-1 of 141 ksi, but more importantly, through-thickness TB-1 stress values are in the 75 ksi range, below yield.

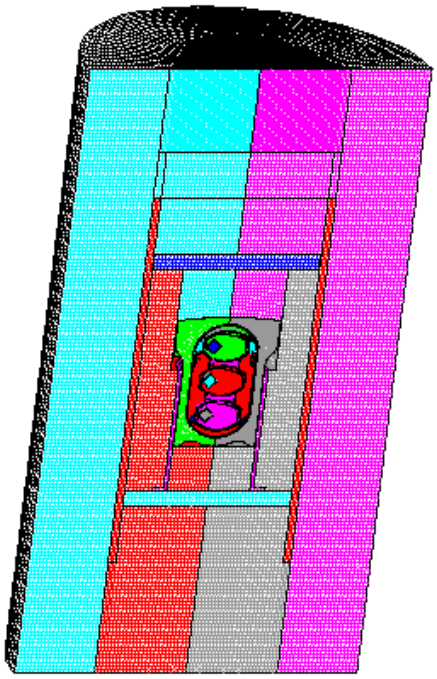

Figure 2-315. Finite Element Mesh for the SC-1, Side Impact, 45° Support Structure, Be Contents

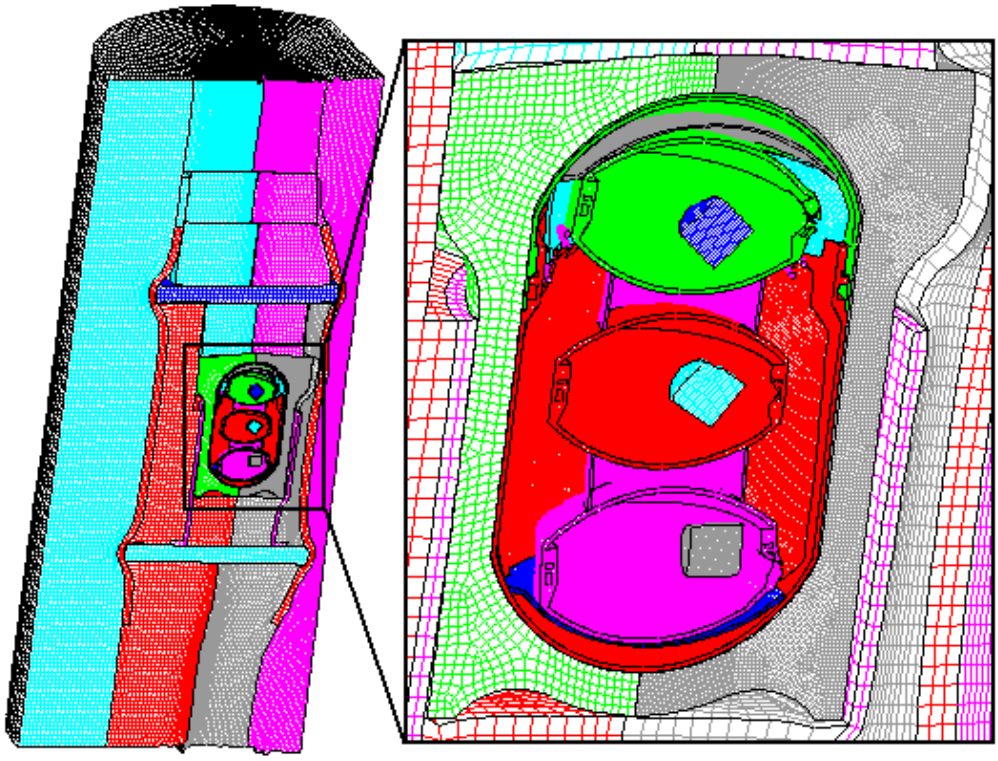

Figure 2-316. Finite Element Mesh for the SC-1, Side Impact, 45° Support Structure, Be Contents – Final Displacement

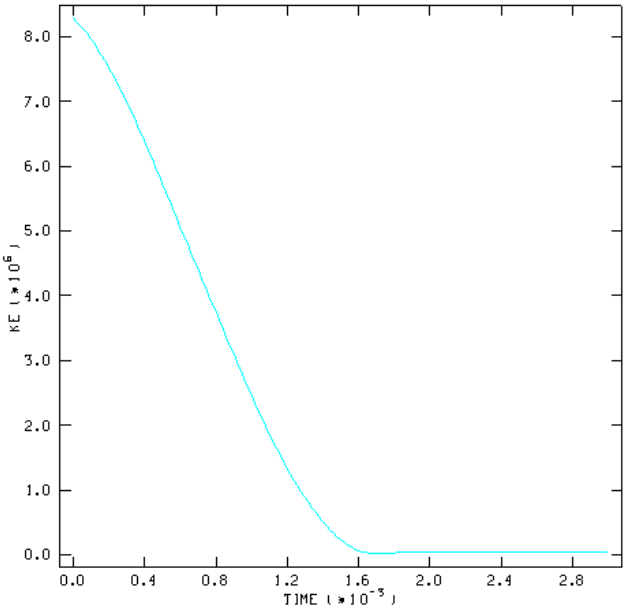

Figure 2-317. Kinetic Energy Time History for the SC-1, Side Impact, 45° Support Structure, Be Contents

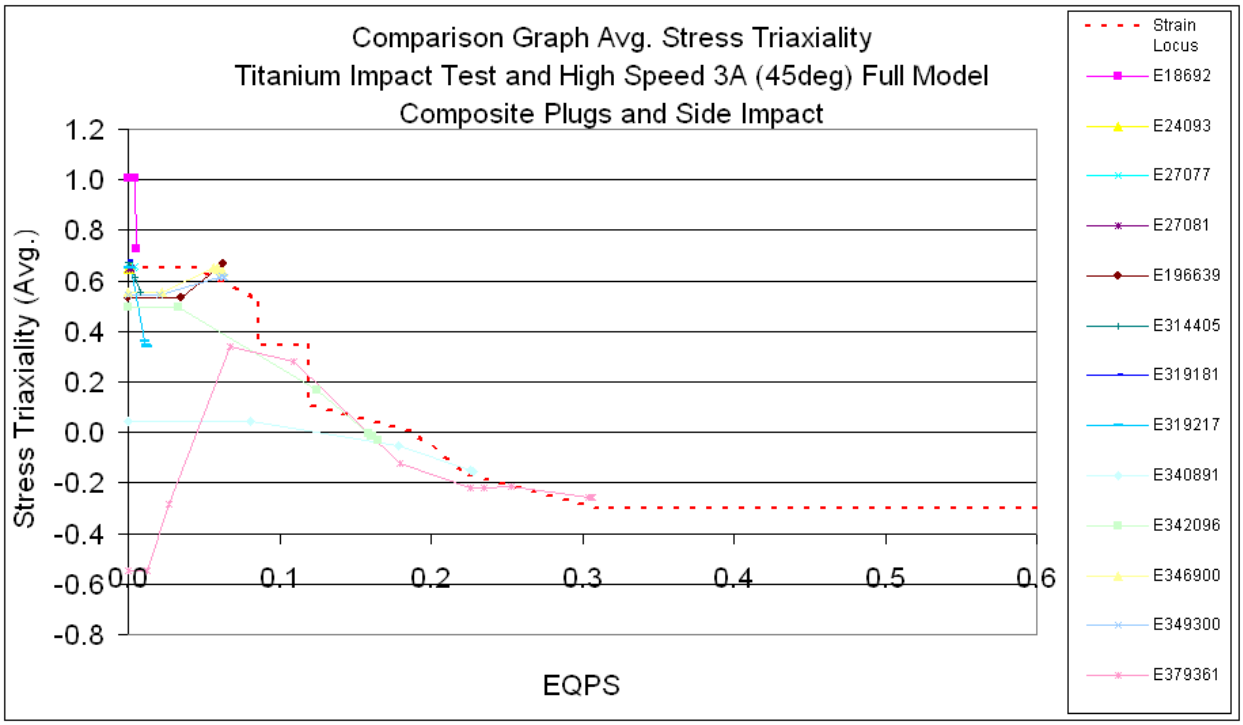

Figure 2-318. Graph of Average Stress Triaxiality versus EQPS of Elements Exceeding the Experimental Strain Locus for the SC-1, Side Impact, 45° Support Structure, Be Contents

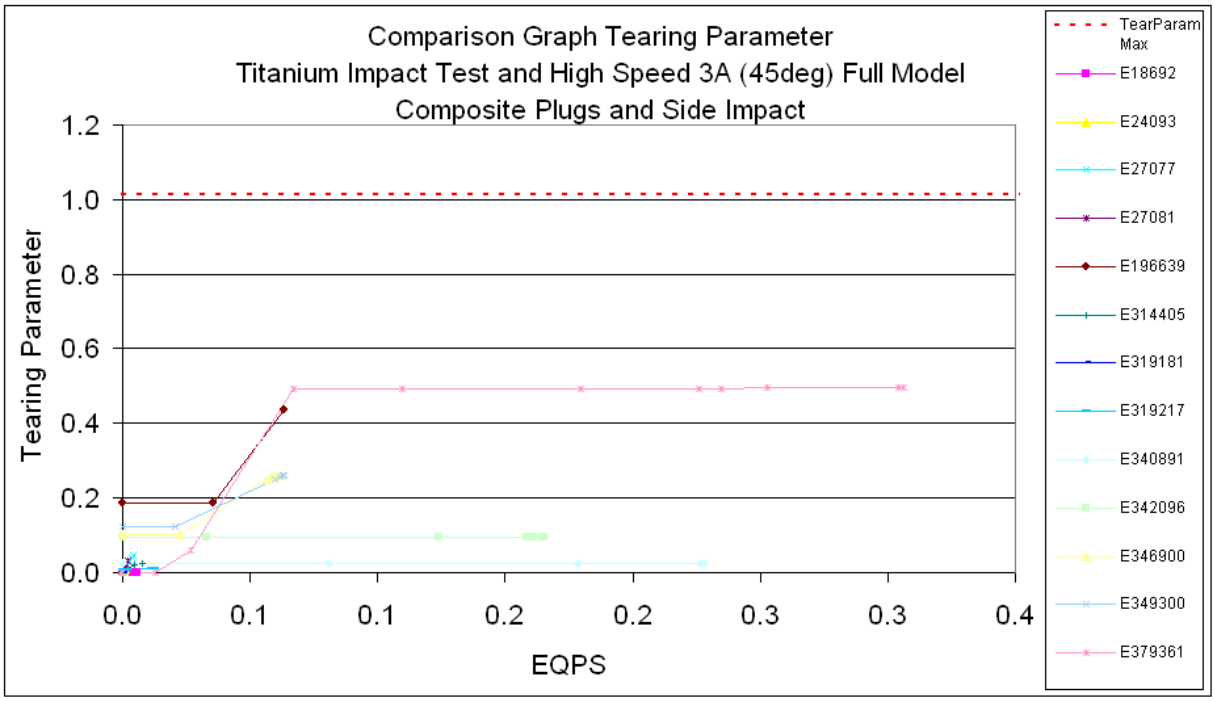

Figure 2-319. Graph of Tearing Parameter versus EQPS of Elements Exceeding the Experimental Strain Locus for the SC-1, Side Impact, 45° Support Structure, Be Contents

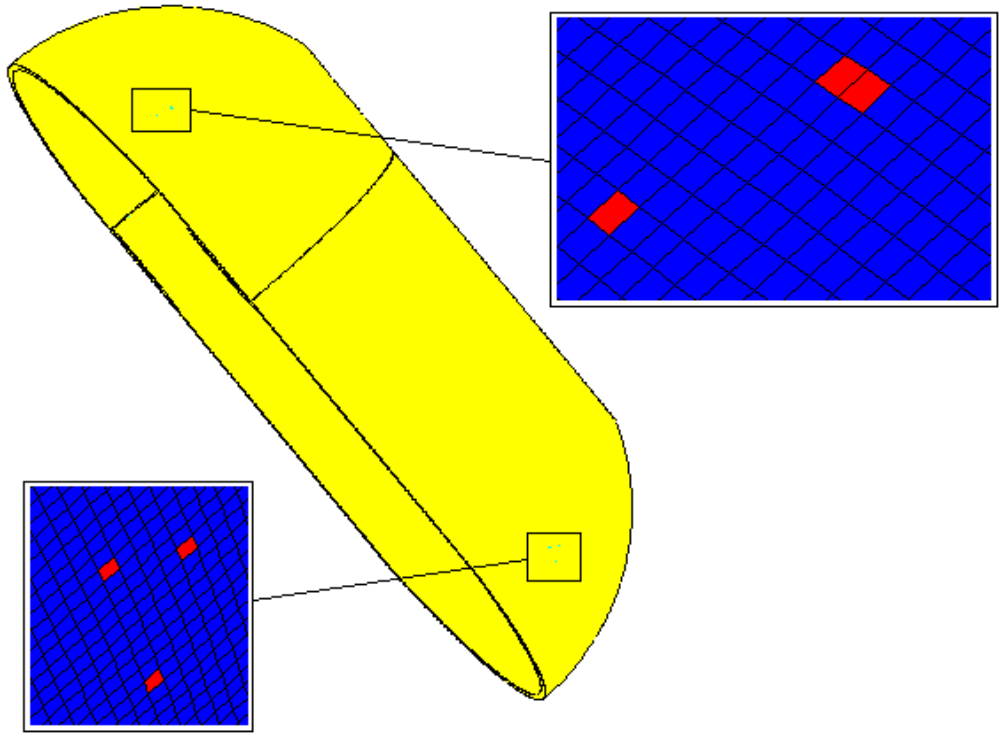

Figure 2-320. Plot of Elements Exceeding the Experimental Strain Locus for the SC-1, Side Impact, 45° Support Structure, Be Contents

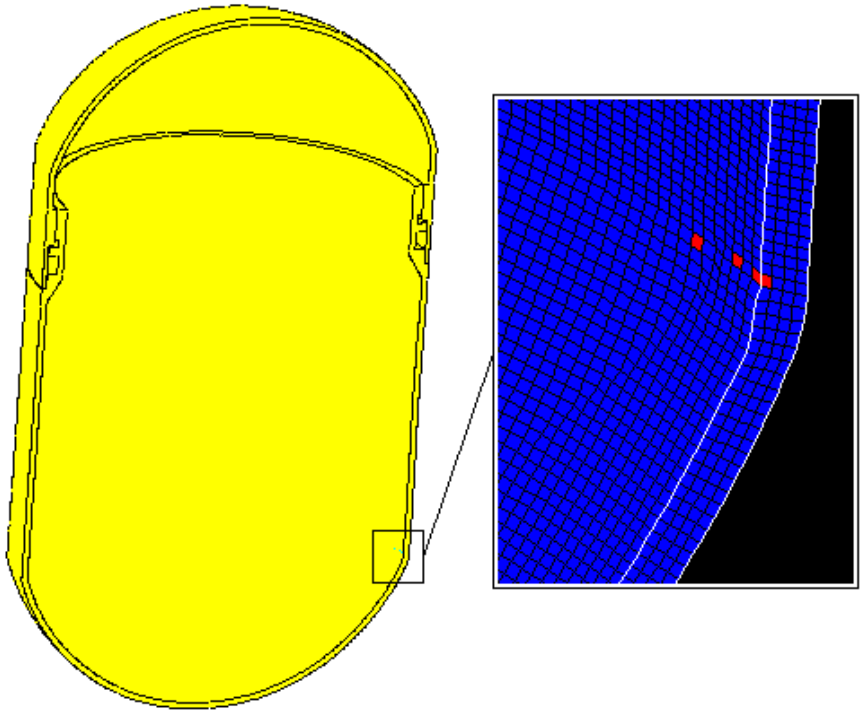

Figure 2-321. Plot of Elements Exceeding the Experimental Strain Locus for the SC-1, Side Impact, 45° Support Structure, Be Contents

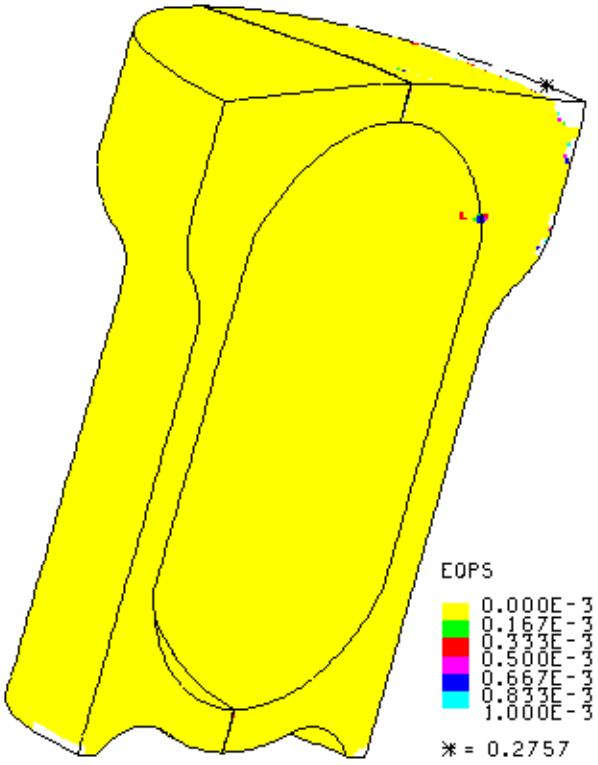

Figure 2-322. Plot of EQPS in the TB-1 for the SC-1, Side Impact, 45° Support Structure, Be Contents

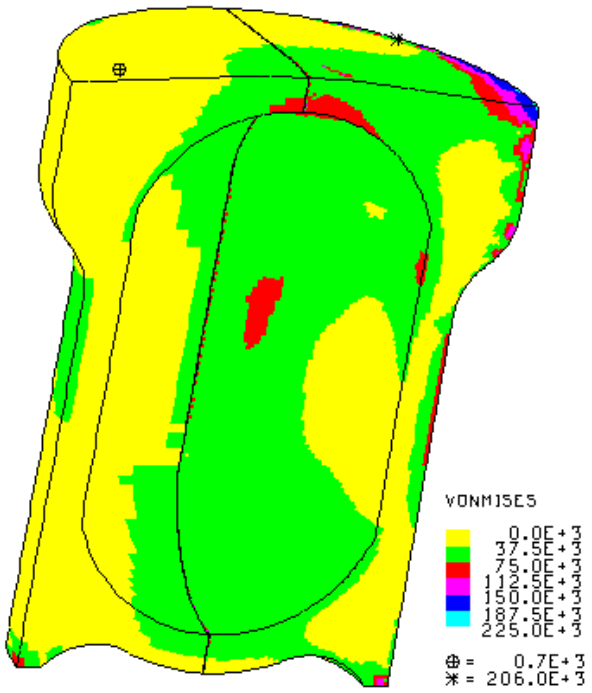

Figure 2-323. Plot of von Mises Stress in the TB-1 for the SC-1, Side Impact, 45° Support Structure, Be Contents

2.12.5.5.14 Run 24 – SC-1 Sample Container, CGOC Impact, Support Structure 0°, Be Contents

The lid end CG-over-corner impact model for each SC-1 with Be composite contents (inner cradle rotated 0 degrees) is shown in Figure 2-324. Each Be cylinder is located at the rotated bottom of each SC-1 so that its net impact velocity with the top of the T-Ampoule is maximized. The post-impact deformation is shown in Figure 2-325 and its kinetic energy history in Figure 2-326. The Be cylinder contents remain largely confined within the SC-1's, although localized deformation of the SC-1's has occurred.

Equivalent Plastic Strain (EQPS) in the TB-1 vessel is shown in Figure 2-327 to peak at about 19%, but only in some localized outer contact regions with the redwood overpack. The von Mises stresses (see Figure 2-328) peak at 181 ksi, just above the elevated-temperature minimum yield strength for the TB-1 of 141 ksi, but more importantly, through-thickness TB-1 stress values are in the 23 ksi range, below yield. No T-Ampoule elements exceeded the tested B-W strain locus, and the peak Tearing Parameter value (see Table 2-11, run #24) of 0.0597 was below the critical Tearing Parameter value of 1.012 for Ti-6Al-4V.

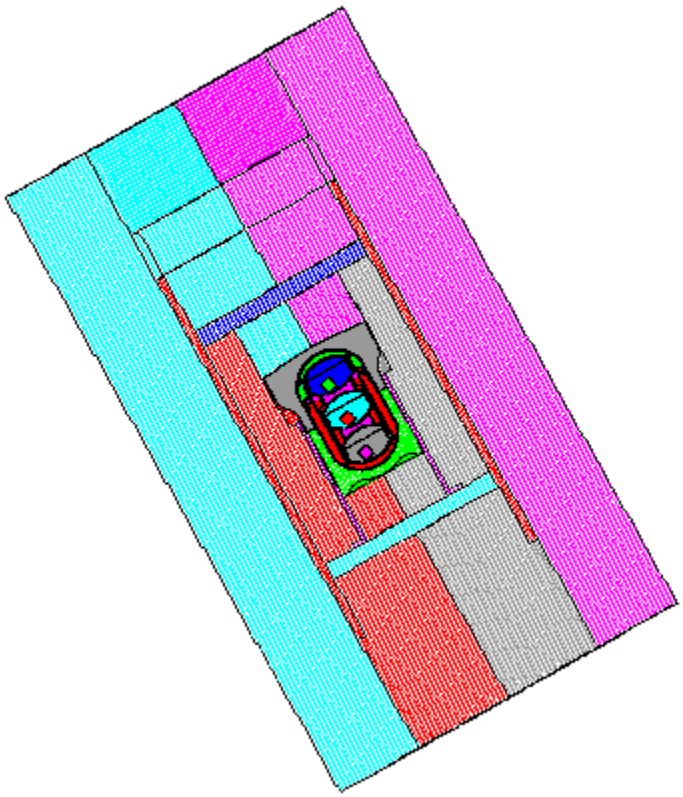

Figure 2-324. Finite Element Mesh for the SC-1, CGOC Impact, 0° Support Structure, Be Contents

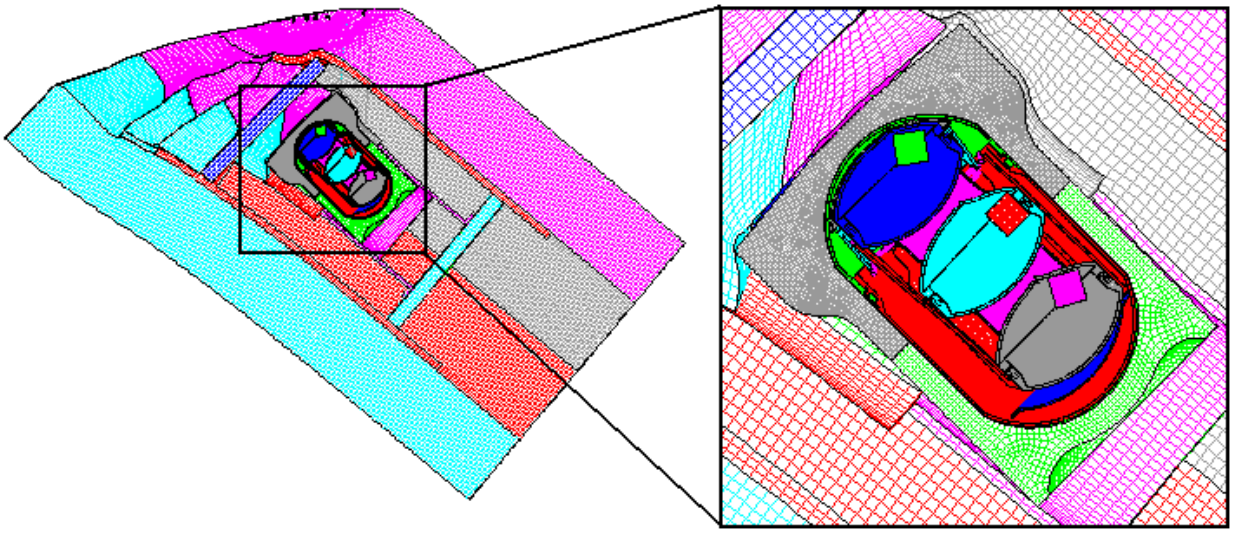

Figure 2-325. Finite Element Mesh for the SC-1, CGOC Impact, 0° Support Structure, Be Contents – Final Displacement

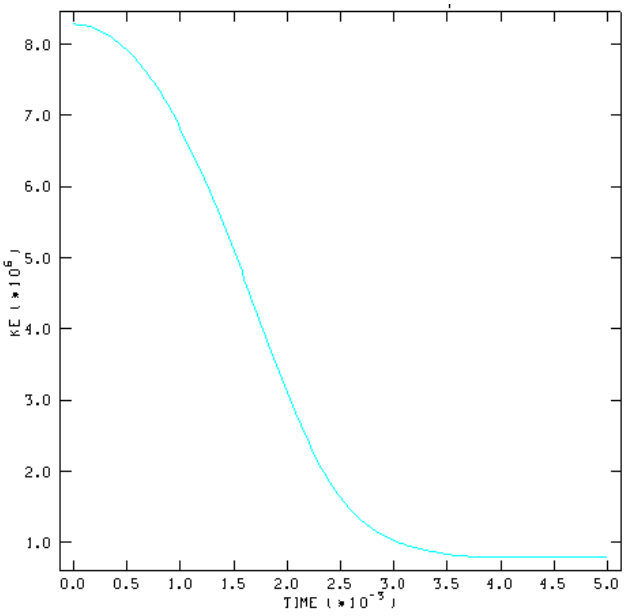

Figure 2-326. Kinetic Energy Time History for the SC-1, CGOC Impact, 0° Support Structure, Be Contents

Figure 2-327. Plot of EQPS in the TB-1 for the SC-1, CGOC Impact, 0° Support Structure, Be Contents

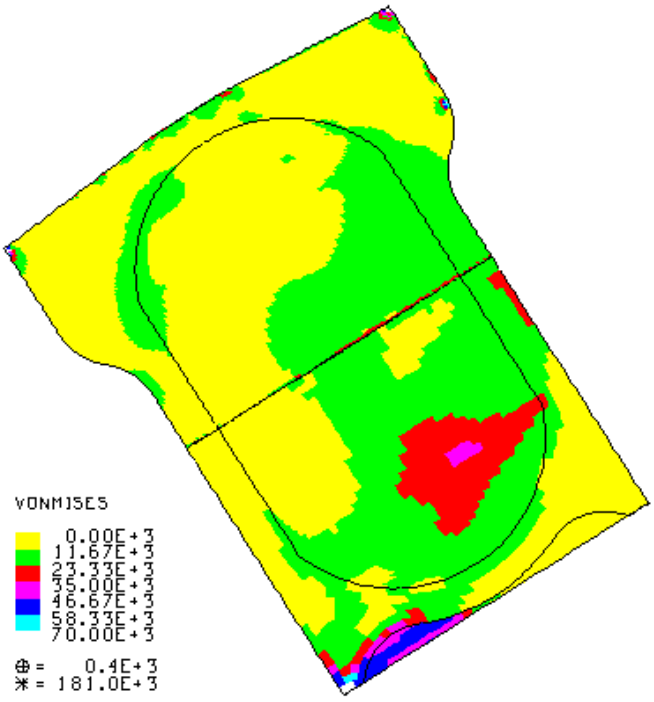

Figure 2-328. Plot of von Mises Stress in the TB-1 for the SC-1, CGOC Impact, 0° Support Structure, Be Contents

2.12.5.5.15 Run 25 – SC-1 Sample Container, CGOC Impact, Support Structure 45°, Be Contents

The lid end CG-over-corner impact model for each SC-1 with Be composite contents (inner cradle rotated 45 degrees) is shown in Figure 2-329. Each Be cylinder is located at the rotated bottom of each SC-1 so that its net impact velocity with the top of the T-Ampoule is maximized. The post-impact deformation is shown in Figure 2-330 and its kinetic energy history in Figure 2-331. The Be cylinder contents remain largely confined within the SC-1's, although localized deformation of the SC-1's has occurred.

Equivalent Plastic Strain (EQPS) in the TB-1 vessel is shown in Figures 2-332 and 2-333 to peak at about 21.3%, but only in some localized outer contact regions with the redwood overpack. The von Mises stresses (see Figure 2-334) peak at 143.3 ksi, just above the elevated-temperature minimum yield strength for the TB-1 of 141 ksi, but more importantly, through-thickness TB-1 stress values are in the 23.3 ksi range, below yield. No T-Ampoule elements exceeded the tested B-W strain locus, and the peak Tearing Parameter value (see Table 2-11, run #25) of 0.1197 was below the critical Tearing Parameter value of 1.012 for Ti-6Al-4V.

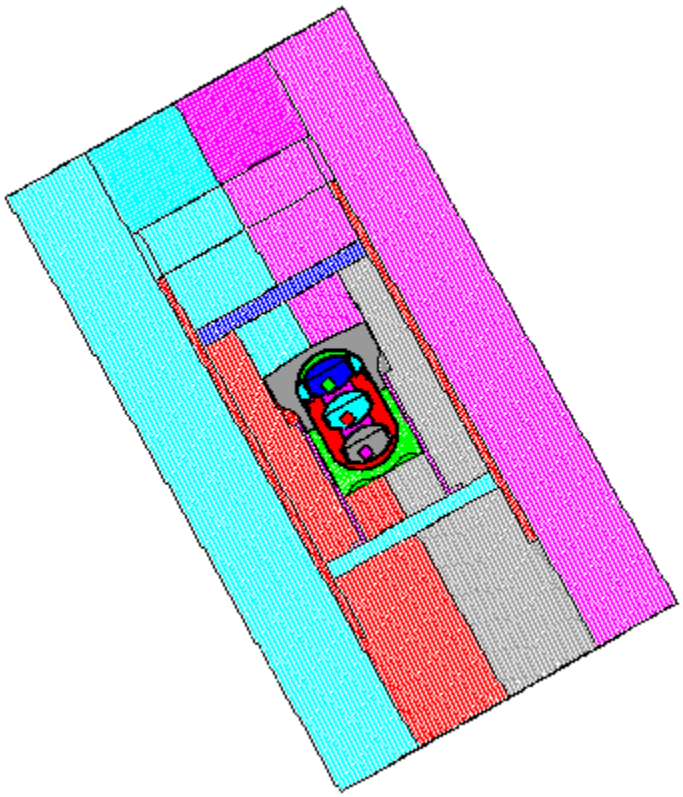

Figure 2-329. Finite Element Mesh for the SC-1, CGOC Impact, 45° Support Structure, Be Contents

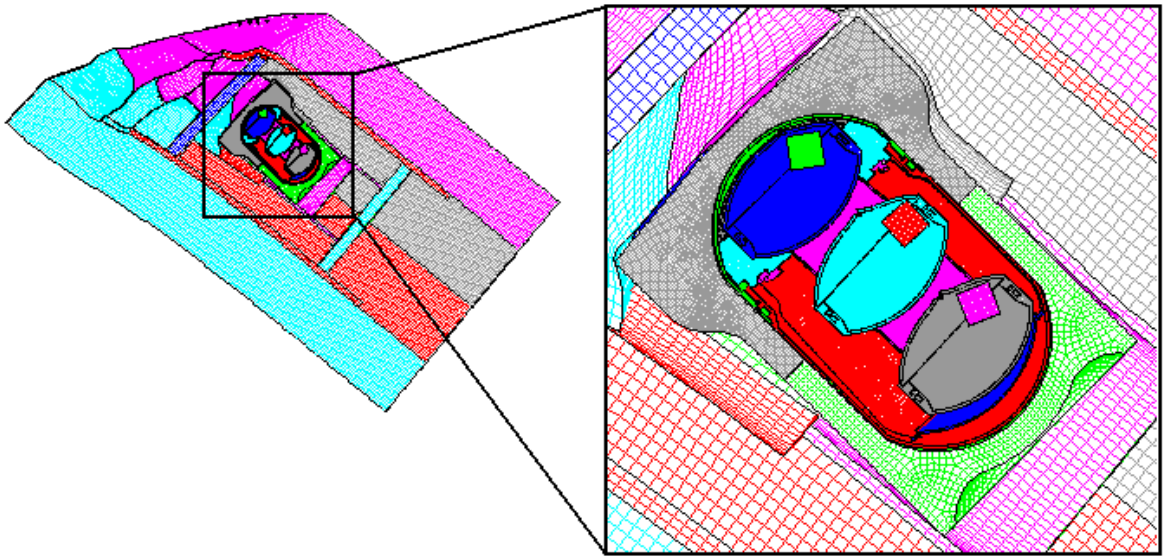

Figure 2-330. Finite Element Mesh for the SC-1, CGOC Impact, 45° Support Structure, Be Contents – Final Displacement

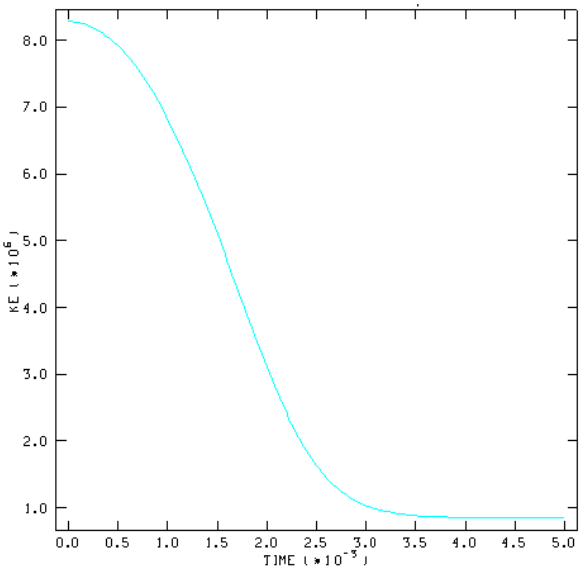

Figure 2-331. Kinetic Energy Time History for the SC-1, CGOC Impact, 45° Support Structure, Be Contents

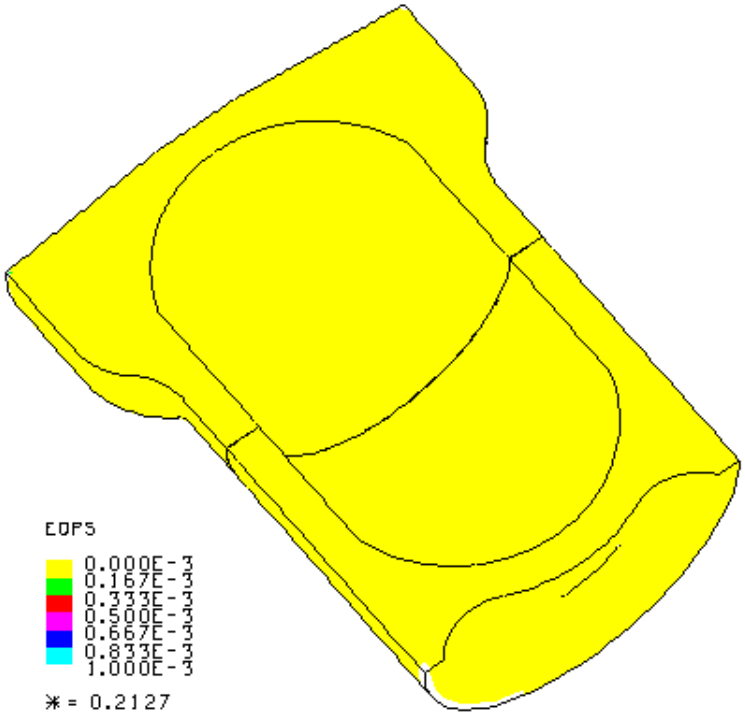

Figure 2-332. Plot of EQPS in the TB-1 for the SC-1, CGOC Impact, 45° Support Structure, Be Contents

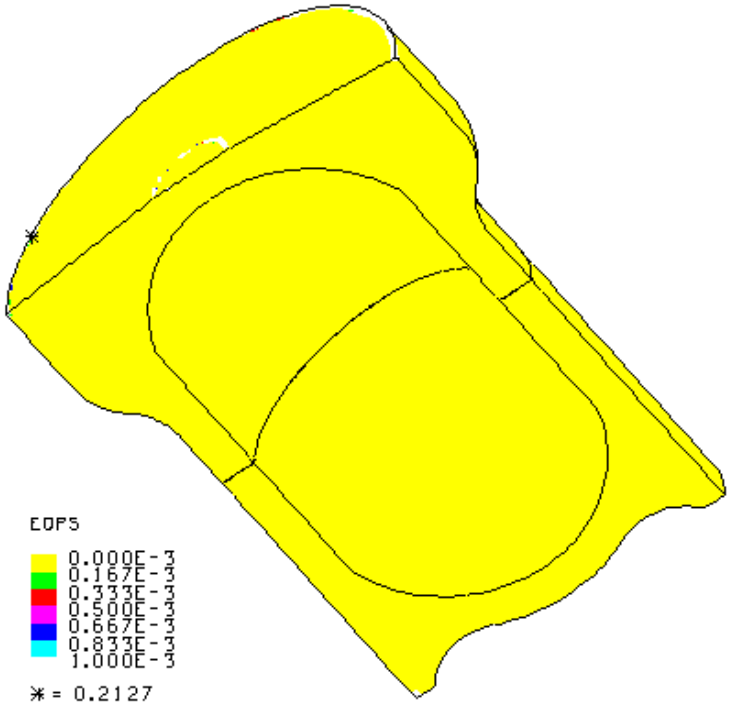

Figure 2-333. Plot of EQPS in the TB-1 for the SC-1, CGOC Impact, 45° Support Structure, Be Contents

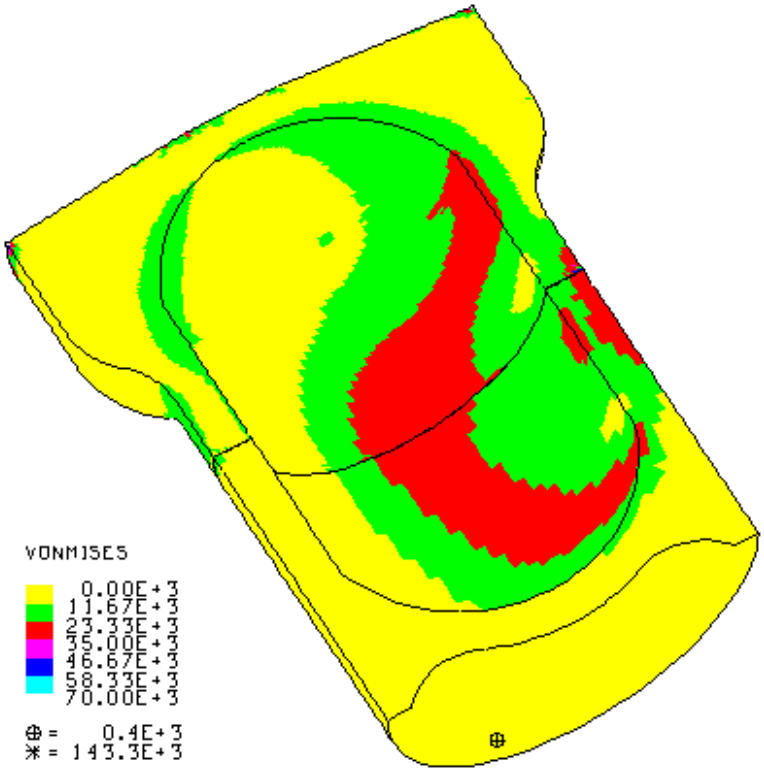

Figure 2-334. Plot of von Mises Stress in the TB-1 for the SC-1, CGOC Impact, 45° Support Structure, Be Contents

2.12.5.5.16 Run 26 – SC-2 Sample Container, Side Impact, Support Structure 45°, Friction 0.4

Two additional analyses were performed to determine the effect of variation in dynamic friction coefficient. The baseline values for all the analyses are 0.30 for dynamic friction and 0.36 for static between each SC and the T-Ampoule, as well as between the Pu cylinders and the T-Ampoule (since they penetrate the SC-2). This analysis was performed increasing the baseline dynamic friction coefficient by 33% to 0.40 (static is the same value). The side impact model for each larger SC-2 with 338 g of delta Pu contents (inner cradle rotated 45 degrees for SC impingement onto sharp cradle edge) was chosen for this parameter study since it produced some element with a relatively high Tearing Parameter value using baseline friction coefficients.

The side impact model with higher friction is shown in Figure 2-335. Note that each Pu cylinder is located at the far left side of each SC-2 so that its net impact velocity with the right side of the T-Ampoule is maximized. The post-impact deformation is shown in Figure 2-336 and its kinetic energy history in Figure 2-337. The Pu contents penetrate each of the SC-2 side walls and directly impact the T-Ampoule.

Average stress-triaxiality versus EQPS is shown in Figure 2-338 for the 73 elements extending beyond the tested Bao-Wierzbicki strain locus (similar to the 82 elements for the 0.3 friction case). All of these elements are outside the B-W locus, for a variety of stress triaxialities, although most of the 580,000 T-Ampoule elements are inside the B-W l locus. The Tearing

Parameter values for these same 73 elements are shown in Figure 2-339, and all are below the critical Tearing Parameter value of 1.012 for Ti-6Al-4V. These elements are highlighted in red in Figures 2-340, 2-341, and 2-342, but note that these elements are still below the initiation of a ductile tear and thus T-Ampoule integrity is maintained. The higher friction coefficients produced only slightly fewer elements exceeding the B-W strain locus, and essentially the same peak Tearing Parameter values (~0.5), indicating lower T-Ampoule "deformation" dependence on the friction coefficient at higher friction values.

Equivalent Plastic Strain (EQPS) in the TB-1 vessel is shown in Figures 2-343 and 2-344 to be less than 29%, but only in some localized outer contact regions with the redwood overpack. The EQPS due to internal denting of the upper SC-1 is shown in Figure 2-344 to be less than 0.067%, which is essentially elastic. The von Mises stresses (see Figure 2-345) peak at 226 ksi, above the elevated-temperature minimum yield strength for the TB-1 of 141 ksi, but more importantly, through-thickness TB-1 stress values are in the less-than-120 ksi range, which is below yield. Stresses and strains in the TB-1 for the higher-friction case appear to be similar to the baseline case.

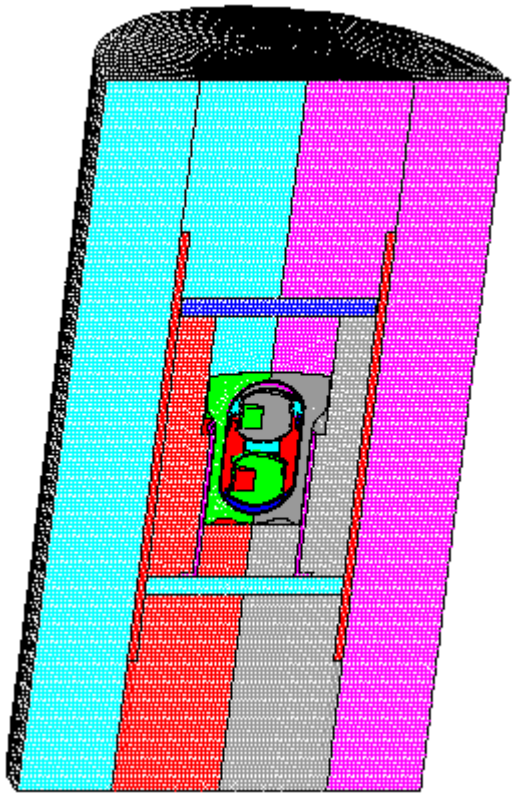

Figure 2-335. Finite Element Mesh for the SC-2, Side Impact, 45° Support Structure, Friction 0.4

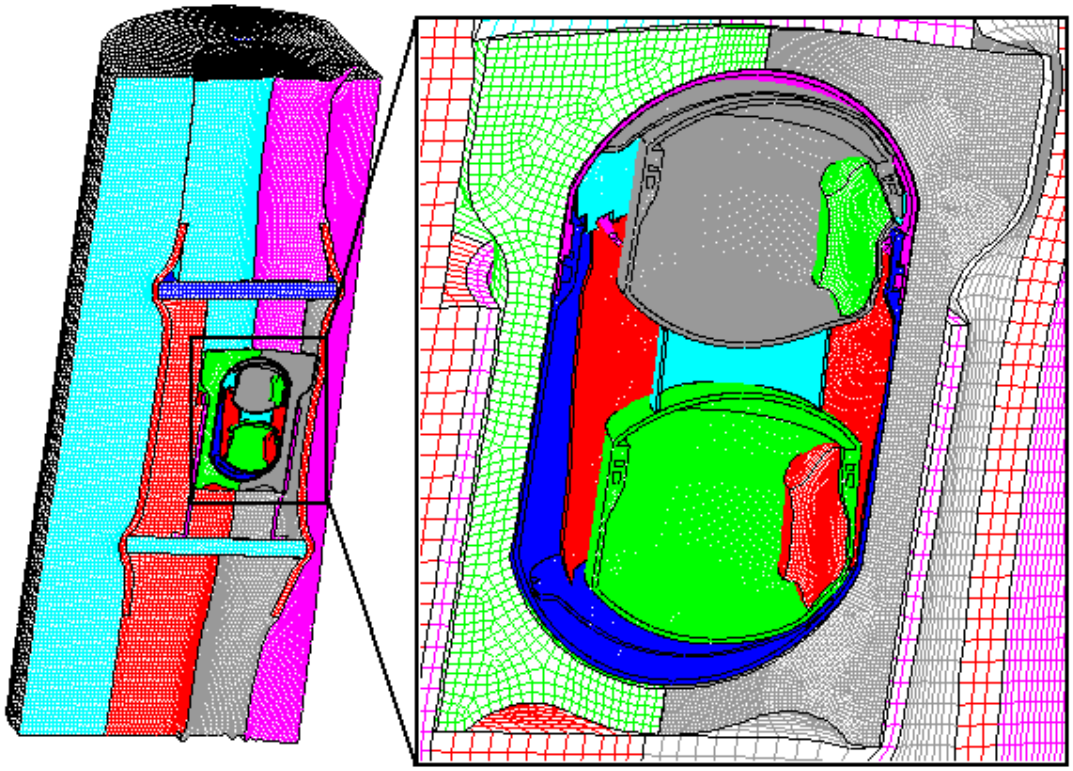

Figure 2-336. Finite Element Mesh for the SC-2, Side Impact, 45° Support Structure, Friction 0.4 – Final Displacement

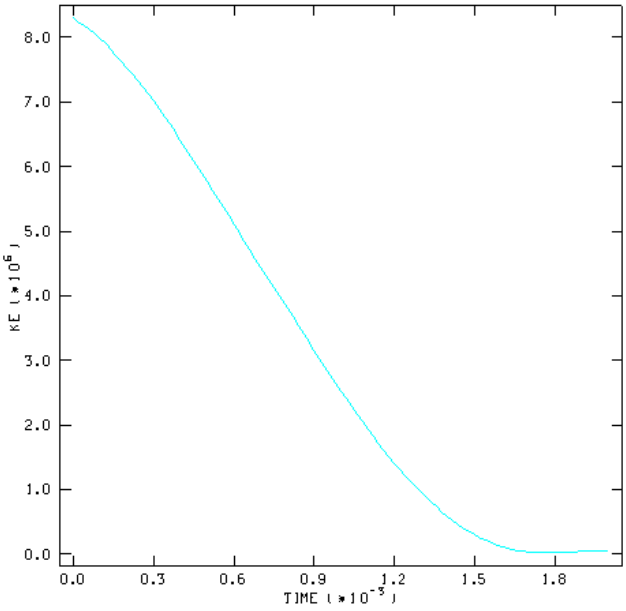

Figure 2-337. Kinetic Energy Time History for the SC-2, Side Impact, 45° Support Structure, Friction 0.4

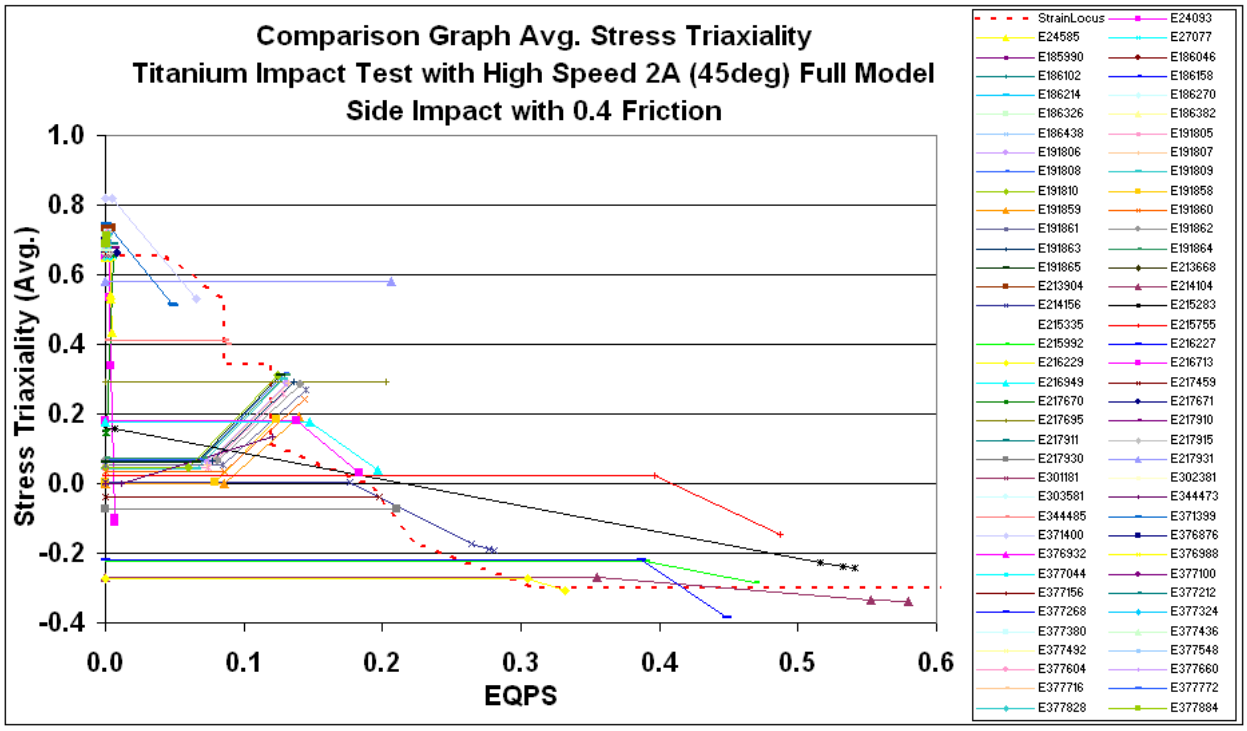

Figure 2-338. Graph of Average Stress Triaxiality versus EQPS of Elements Exceeding the Experimental Strain Locus for the SC-2, Side Impact, 45° Support Structure, Friction 0.4

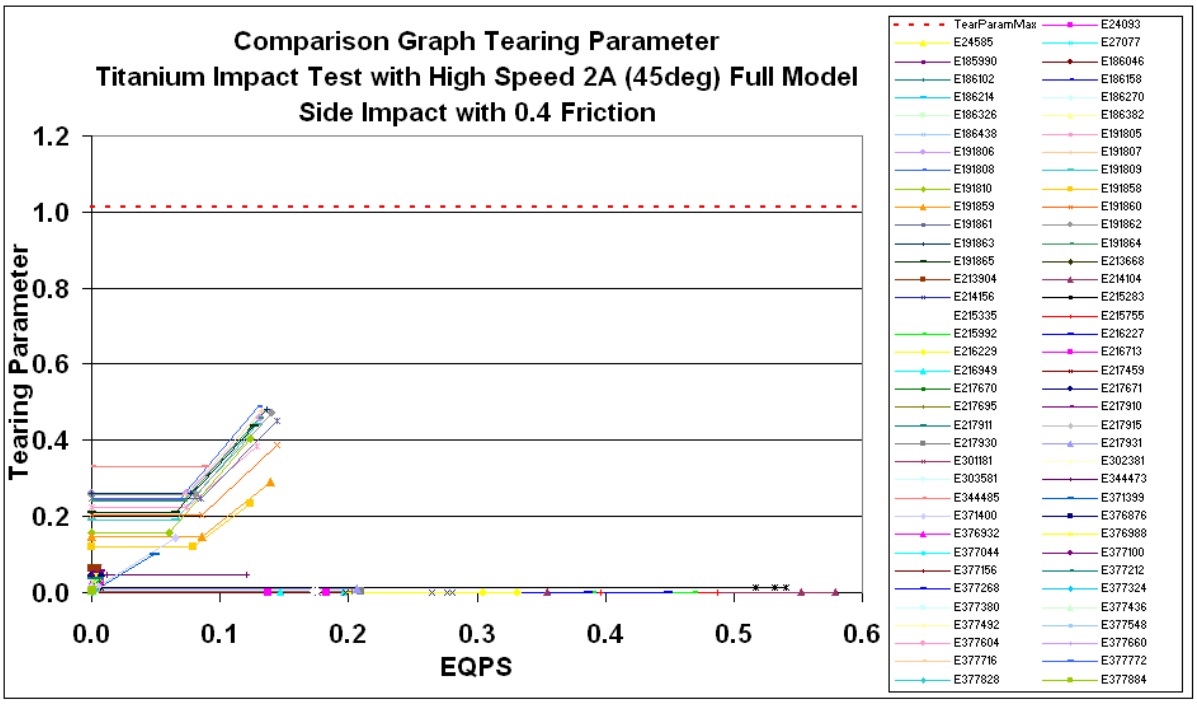

Figure 2-339. Graph of Tearing Parameter versus EQPS of Elements Exceeding the Experimental Strain Locus for the SC-2, Side Impact, 45° Support Structure, Friction 0.4

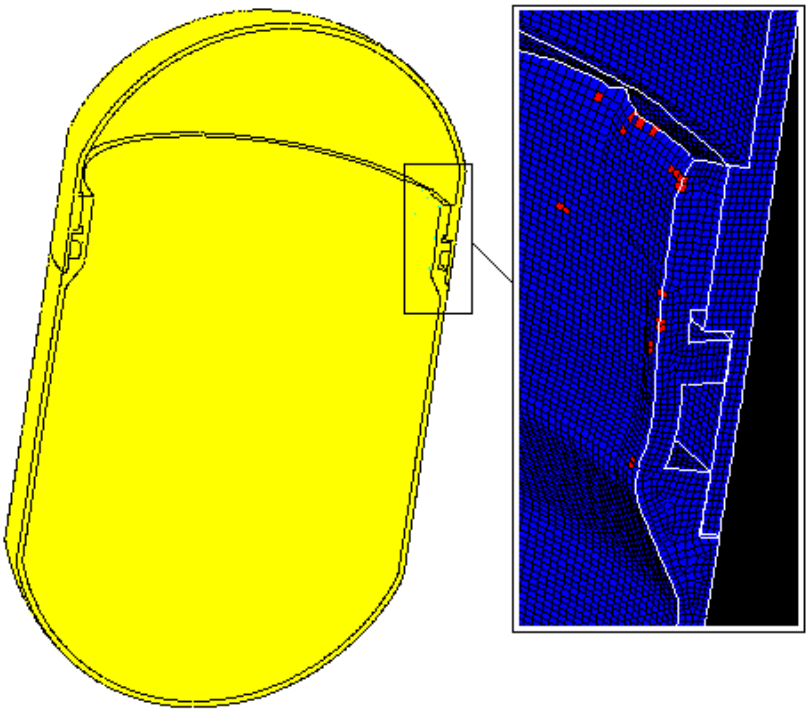

Figure 2-340. Plot of Elements Exceeding the Experimental Strain Locus for the SC-2, Side Impact, 45° Support Structure, Friction 0.4

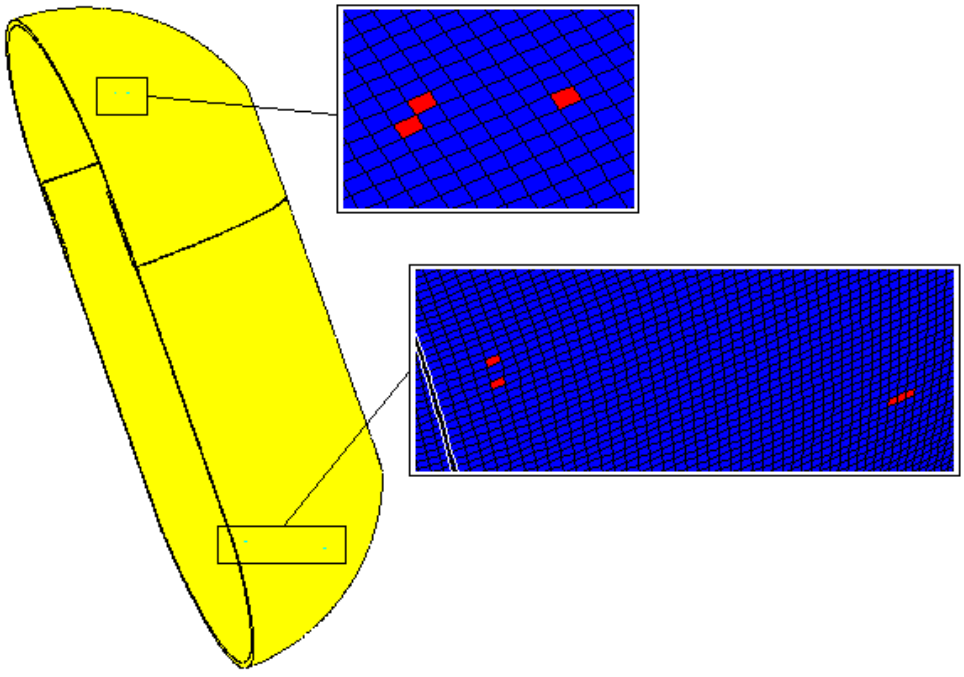

Figure 2-341. Plot of Elements Exceeding the Experimental Strain Locus for the SC-2, Side Impact, 45° Support Structure, Friction 0.4

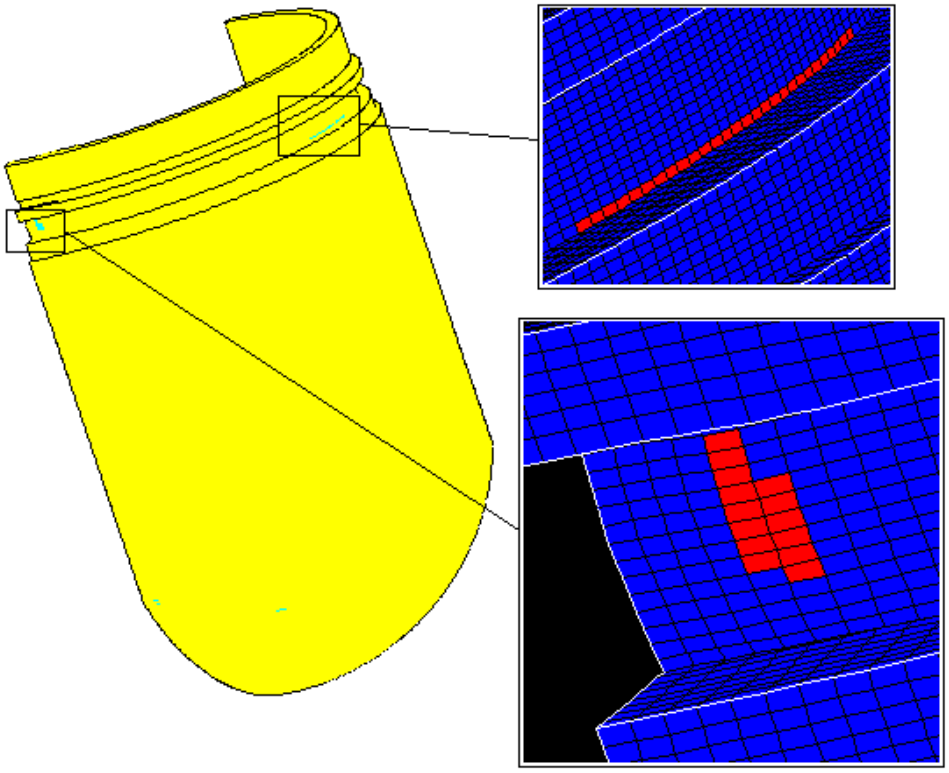

Figure 2-342. Plot of Elements Exceeding the Experimental Strain Locus for the SC-2, Side Impact, 45° Support Structure, Friction 0.4

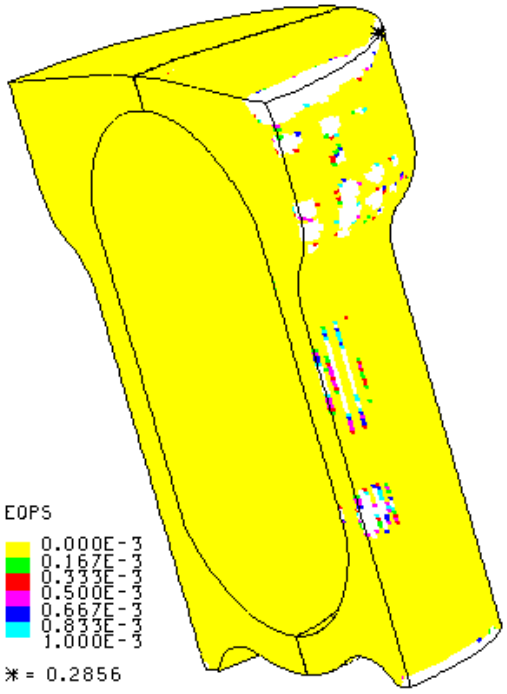

Figure 2-343. Plot of EQPS in the TB-1 for the SC-2, Side Impact, 45° Support Structure, Friction 0.4

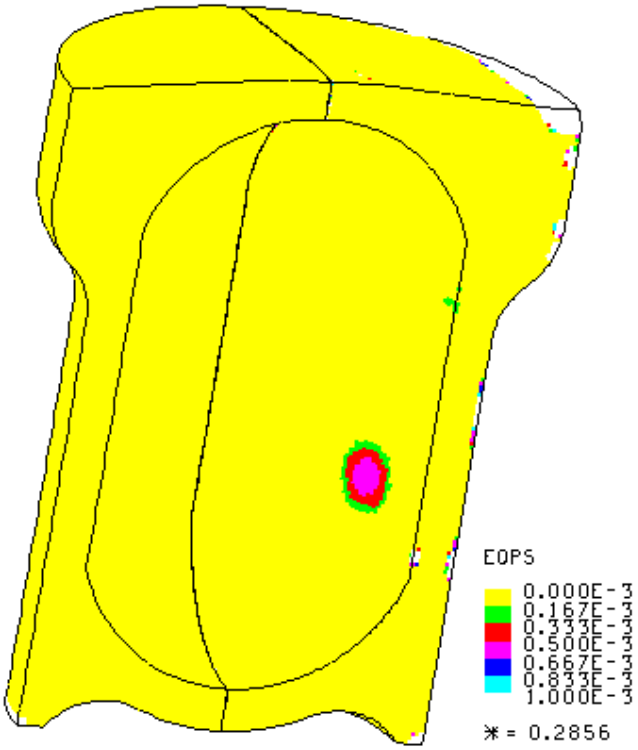

Figure 2-344. Plot of EQPS in the TB-1 for the SC-2, Side Impact, 45° Support Structure, Friction 0.4

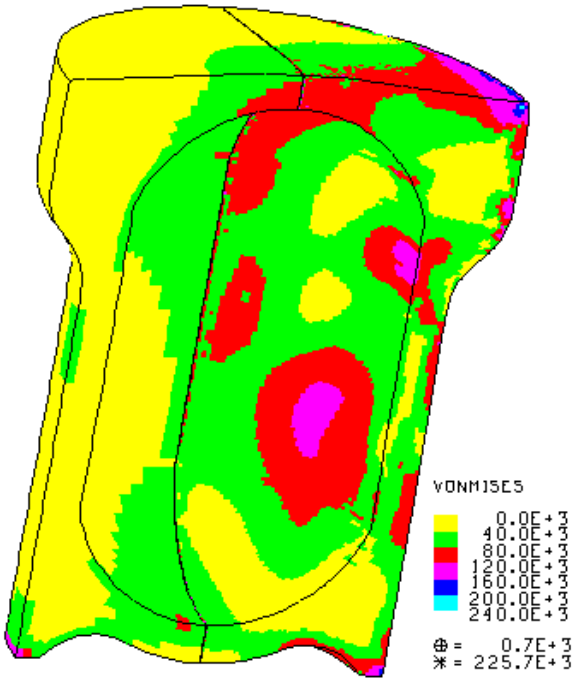

Figure 2-345. Plot of von Mises Stress in the TB-1 for the SC-2, Side Impact, 45° Support Structure, Friction 0.4

2.12.5.5.17 Run 27 – SC-2 Sample Container, Side Impact, Support Structure 45°, Friction 0.2

The second of two additional analyses was also performed to determine the effect of variation in dynamic friction coefficient. The baseline values for all the analyses are 0.30 for dynamic friction and 0.36 for static between each SC and the T-Ampoule, as well as between the Pu cylinders and the T-Ampoule (since they penetrate the SC-2). This analysis was performed decreasing the baseline dynamic friction coefficient by 33% to 0.20 (static is the same value). The side impact model for the larger SC-2's each with 338 g of delta Pu contents (inner cradle rotated 45 degrees for SC impingement onto sharp cradle edge) was chosen for this parameter study since it produced some elements with a relatively high Tearing Parameter value using baseline friction coefficients.

The side impact model with lower friction is shown in Figure 2-346. Note that each Pu cylinder is located at the far left side of each SC-2 so that its net impact velocity with the right side of the T-Ampoule is maximized. The post-impact deformation is shown in Figure 2-347 and its kinetic energy history in Figure 2-348. The Pu contents penetrate each of the SC-2 side walls and directly impact the T-Ampoule.

Average stress-triaxiality versus EQPS is shown in Figure 2-349 for the 49 elements extending beyond the tested Bao-Wierzbicki strain locus (almost half of that for the 0.3 friction case). All of these elements are outside the B-W locus, for a variety of stress triaxialities, although most of the 580,000 T-Ampoule elements are inside the B-W locus. The Tearing Parameter values for these same 49 elements are shown in Figure 2-350, and all are below the critical Tearing Parameter value of 1.012 for Ti-6Al-4V. These elements are highlighted in red in Figures 2-351 and 2-352, but note that these elements are still below the initiation of a ductile tear and thus T-Ampoule integrity is maintained. Fewer T-Ampoule elements extended beyond the B-W locus with lower friction, and the Tearing Parameter values were significantly lower (~0.1 vs. ~0.5, peak), so reducing friction generally decreases the traction loading and deformation in the T-Ampoule. Although the zero-friction case was not included here because it is not realistic, there were zero T-Ampoule elements exceeding the tested strain locus, indicating a high T-Ampoule "deformation" dependence on the friction coefficient at lower friction values.

Equivalent Plastic Strain (EQPS) in the TB-1 vessel is shown in Figures 2-353 and 2-354 to be less than 20.2%, but only in some localized outer contact regions with the redwood overpack. The EQPS due to internal denting of the upper SC-1 is shown in Figure 2-354 to be less than 0.0833%, which is nearly elastic. The von Mises stresses (see Figure 2-355) peak at 225 ksi, above the elevated-temperature minimum yield strength for the TB-1 of 141 ksi, but more importantly, through-thickness TB-1 stress values are in the less-than-120 ksi range, which is below yield. Stresses and strains in the TB-1 appear relatively similar to the baseline and higher-friction analyses. From this lower-friction analysis and the higher-friction analysis, there does not appear to be a strong TB-1 stress or T-Ampoule deformation dependency on friction, at least in the nominal plus/minus 33% range.

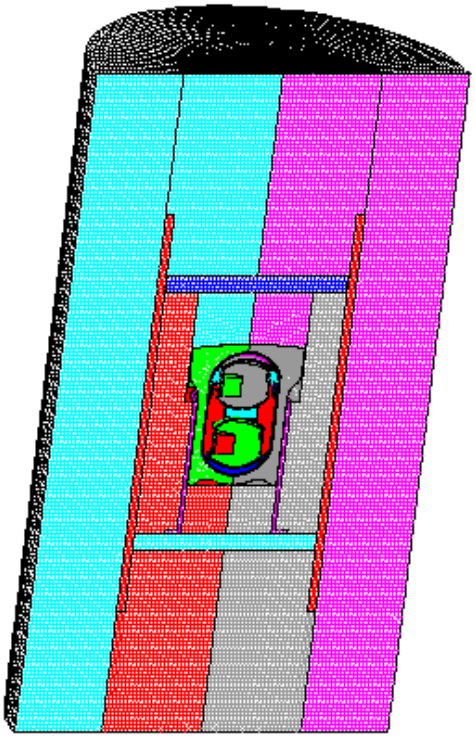

Figure 2-346. Finite Element Mesh for the SC-2, Side Impact, 45° Support Structure, Friction 0.2

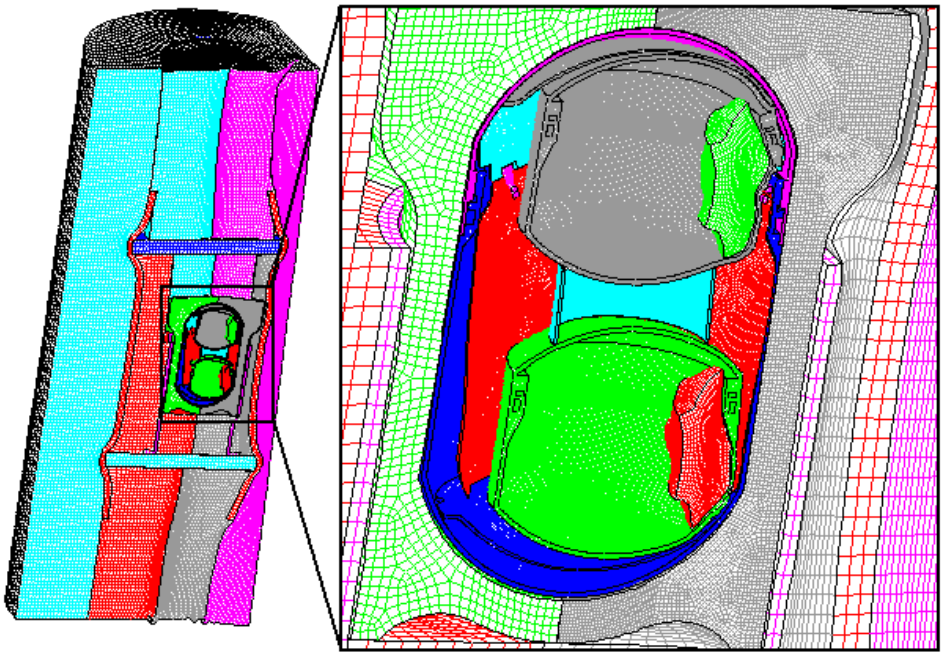

Figure 2-347. Finite Element Mesh for the SC-2, Side Impact, 45° Support Structure, Friction 0.2 – Final Displacement

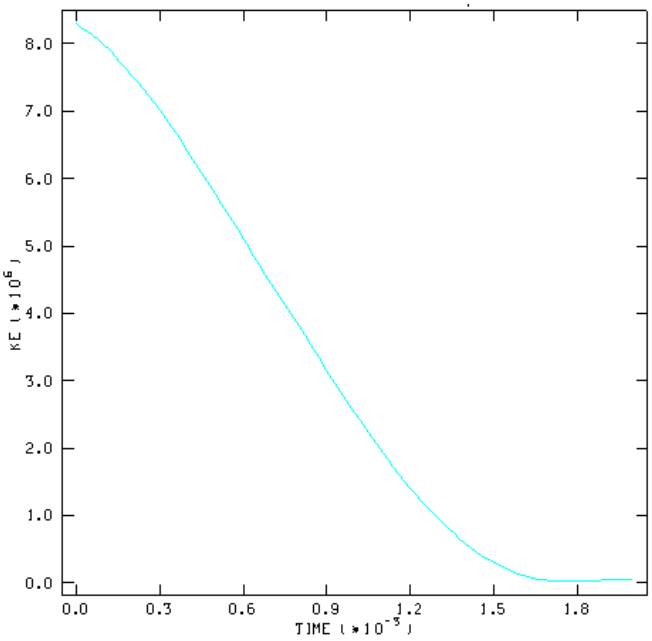

Figure 2-348. Kinetic Energy Time History for the SC-2, Side Impact, 45° Support Structure, Friction 0.2

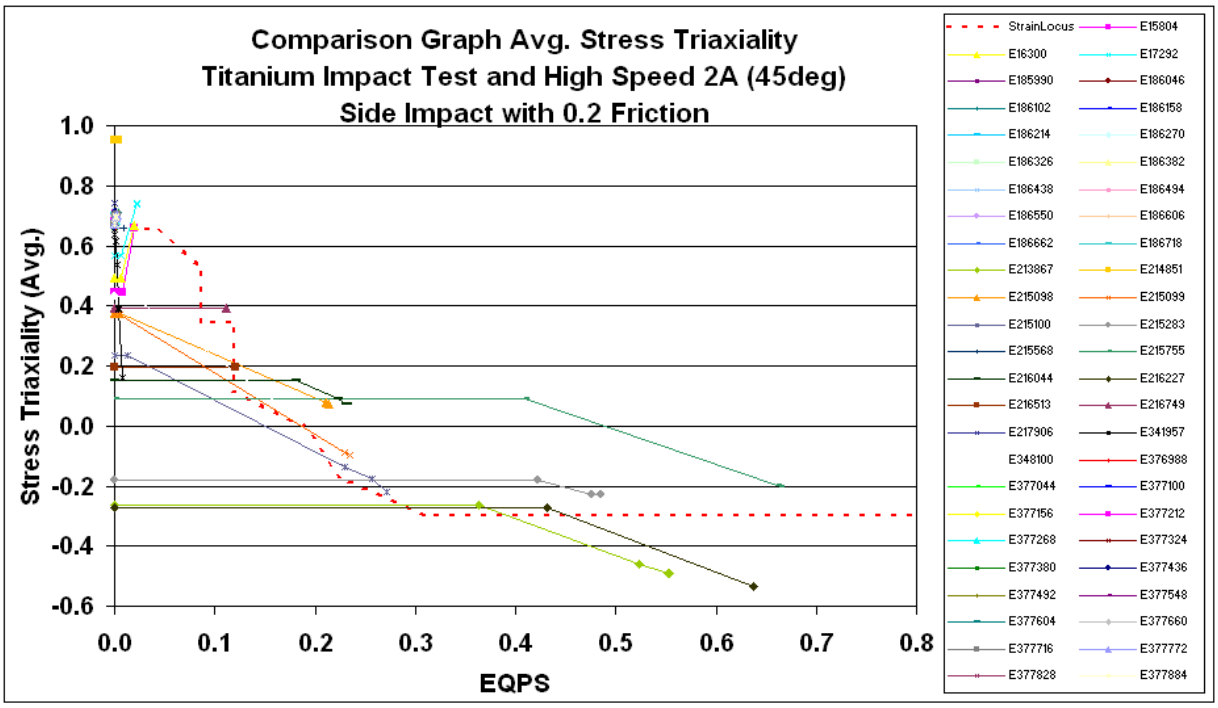

Figure 2-349. Graph of Average Stress Triaxiality versus EQPS of Elements Exceeding the Experimental Strain Locus for the SC-2, Side Impact, 45° Support Structure, Friction 0.2

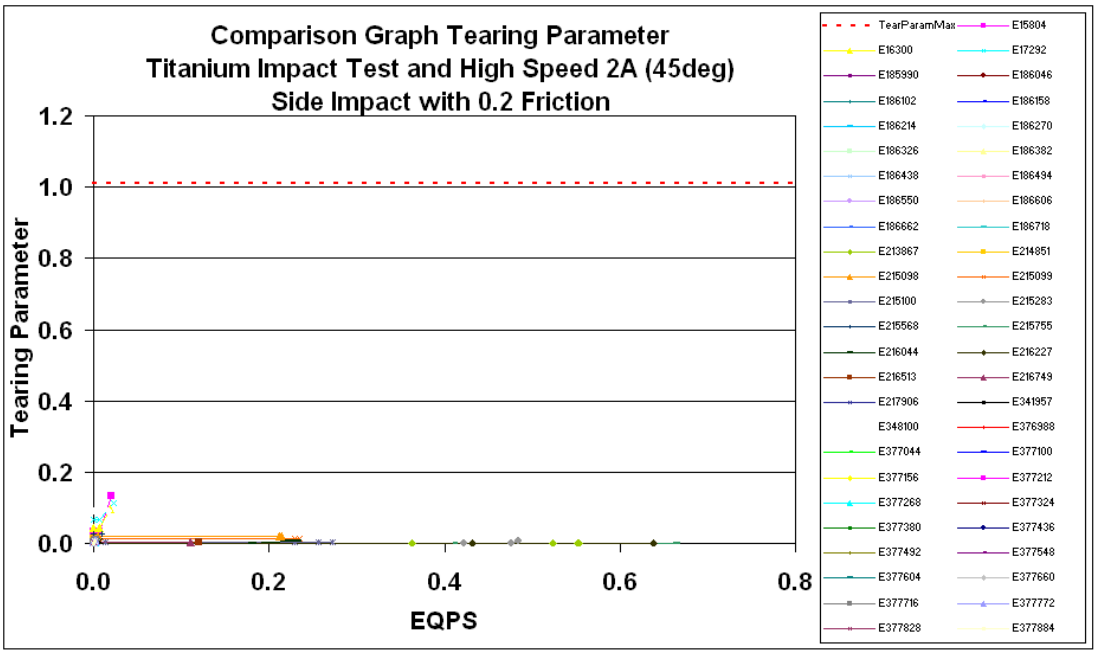

Figure 2-350. Graph of Tearing Parameter versus EQPS of Elements Exceeding the Experimental Strain Locus for the SC-2, Side Impact, 45° Support Structure, Friction 0.2

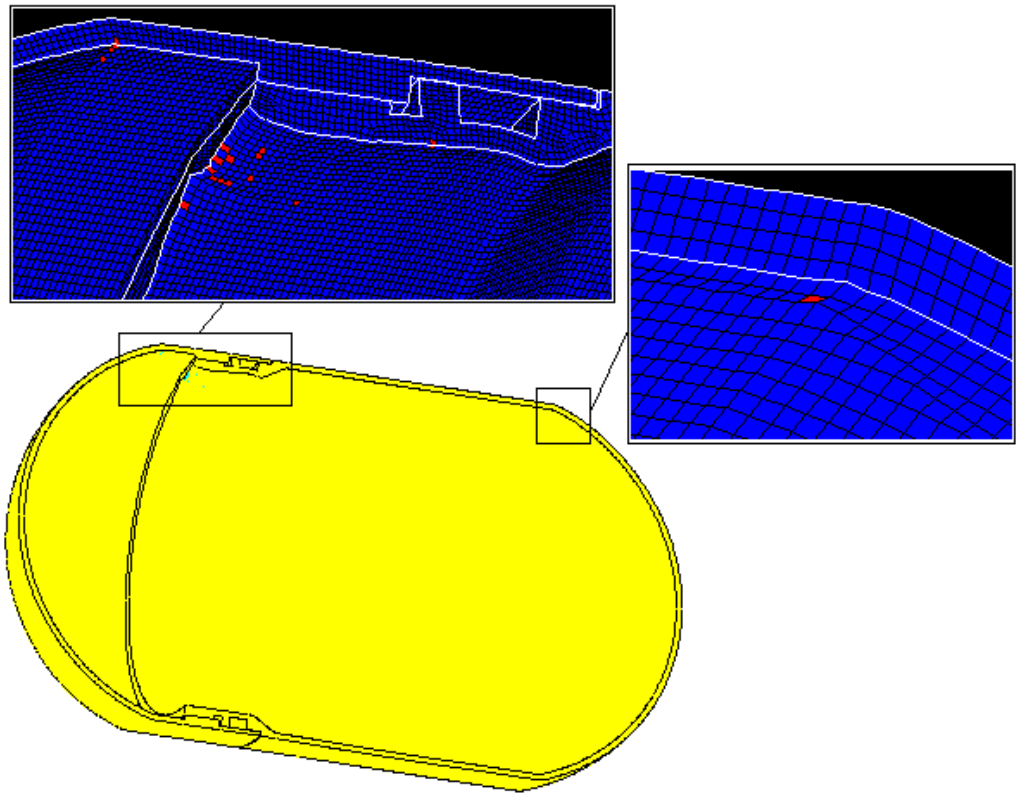

Figure 2-351. Plot of Elements Exceeding the Experimental Strain Locus for the SC-2, Side Impact, 45° Support Structure, Friction 0.2

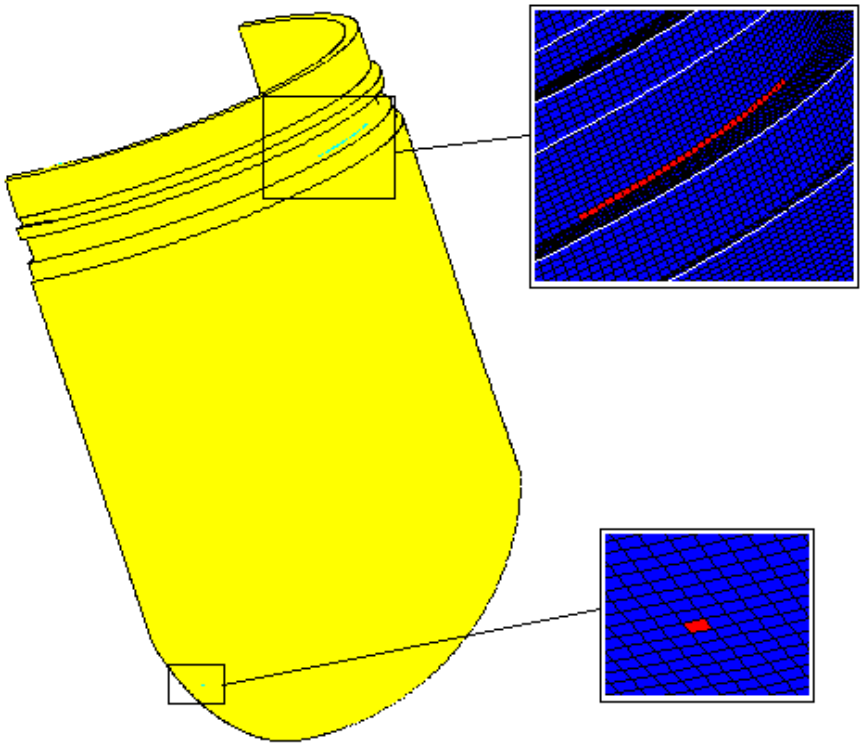

Figure 2-352. Plot of Elements Exceeding the Experimental Strain Locus for the SC-2, Side Impact, 45° Support Structure, Friction 0.2

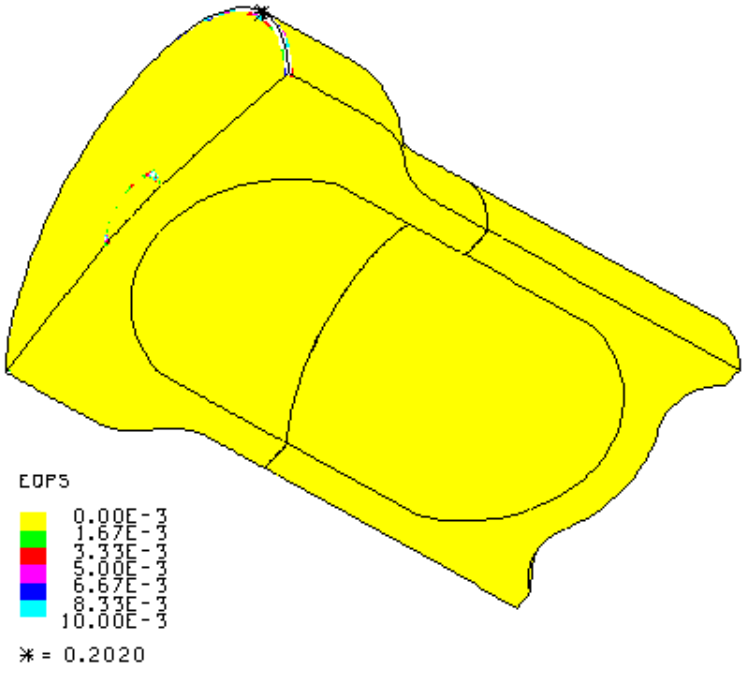

Figure 2-353. Plot of EQPS in the TB-1 for the SC-2, Side Impact, 45° Support Structure, Friction 0.2

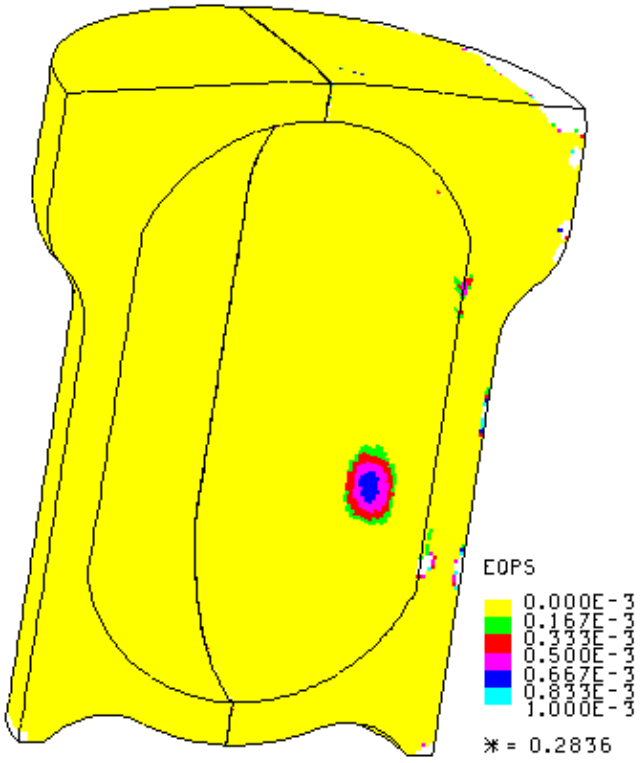

Figure 2-354. Plot of EQPS in the TB-1 for the SC-2, Side Impact, 45° Support Structure, Friction 0.2

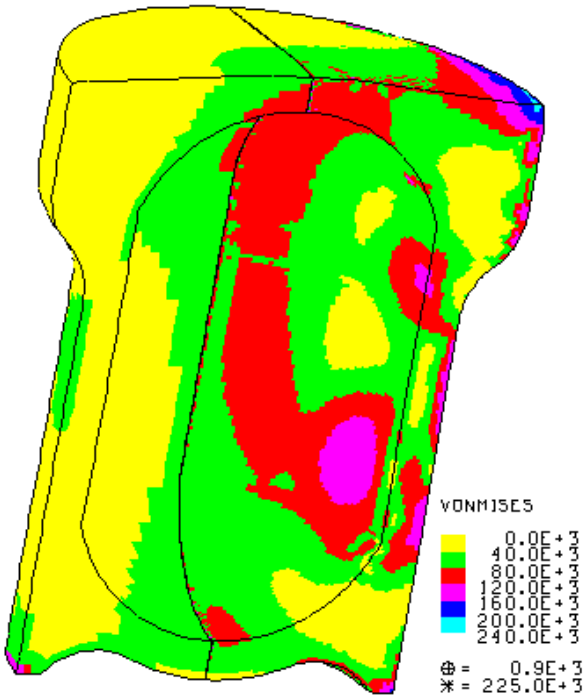

Figure 2-355. Plot of von Mises Stress in the TB-1 for the SC-2, Side Impact, 45° Support Structure, Friction 0.2

2.12.5.5.18 Summary and Conclusion (for High Velocity Impact Analyses)

Although plastic deformation is produced in the T-Ampoule body during the high-speed aircraft accident condition (10 CFR 71.74), using the strain based fracture model developed by Bao and Wierzbicki[5] along with data derived from experimental impact tests, these strains were found not to pose a threat to the integrity of the T-Ampoule body. In addition, stresses in the TB-1 remain virtually elastic and do not threaten the structural integrity of this vessel.

Analyses presented in the high velocity impact section have demonstrated that the PAT-1 package maintains its structural integrity under regulatory 422 ft/sec impacts. Bolt loads, as shown in Figure 2-356 comparing the sum of redwood compression and bolt preload against the under-lid forces from impacting solid metal contents, are minimal and thus lid closure is maintained. Through-thickness stresses in the primary containment vessel, the TB-1, are shown to be below yield values for the S13800 high strength stainless steel material (see Section 2.12.4.9). Only localized minor "denting" occurs in the TB-1, and it would be invisible to the naked eye. And deformations in the T-Ampoule eutectic barrier are shown to be below levels that could initiate a ductile tear, and are largely within the tested locus of stress-triaxiality and plastic strain that precludes failure. Many of the elements with the highest Tearing Parameter values are plotted in stress-triaxiality versus EQPS space in Figure 2-357, demonstrating how close they are to the tested locus, which is not a failure boundary: it is a tested locus of non-failure.

All 27 of the high velocity impact analysis are summarized in Table 2-19, which lists the T-Ampoule contents, overall model and contents orientations, as well as the maximum Tearing Parameter value for all T-Ampoule elements in that particular run or analysis number. The lowest factor of safety against merely *initiating* a ductile tear occurs for a single element in run number 3 with a maximum Tearing Parameter value of 0.6177 (compared to a critical Tearing Parameter value of 1.012 for Ti-6Al-4V, so Factor of Safety = 1.012/0.6177 = 1.64). This factor of safety pertains to the integrity of the eutectic barrier T-Ampoule, NOT the TB-1 containment boundary, which is has been shown in previous certification tests and the current analyses to fully maintain its integrity (through-thickness stresses below yield), as well.

The numerous additional conservatisms associated with all of these impact analyses should provide additional confidence that containment (and eutectic barrier integrity) would be maintained, even under severe aircraft accident conditions. Additional conservatisms include: neglecting the tantalum foil packing material which would perform some small load spreading and energy absorbing function; neglecting the rolled lid of the outer package skin in aircraft impacts; always assuming the content location and orientation most damaging to the T-Ampoule, e.g., "strongest" plutonium metal hollow cylinder dimensions to resist buckling; most dense, compact, and sharp shape for the delta Pu and Be composite cylinders; delta Pu contents have higher density of alpha Pu; sharpest orientation for the strong Be cylinders, etc. Also, the material properties for these contents are conservatively assumed to have infinite plasticity, when in fact the alpha Pu is very brittle and the Be has rather limited ductility. The Be cylinders were conservatively assumed to have delta Pu density, thus maximizing their impact velocity (due to smaller size). These conservative assumptions maximize the loading and damage potential to the T-Ampoule (as well as TB-1), yet it retains structural integrity as a eutectic barrier.

Table 2-19. High Velocity (Aircraft) Impact Analyses Peak Tearing Parameter Values

Run No.	Component	Model Orientation	Maximum Tearing Parameter (T-Ampoule)
1	831 g Plutonium Metal Hollow Cylinder	Bottom position, top impact	0.0528
2	831 g Plutonium Metal Hollow Cylinder	Bottom position (angled), top impact	0.2115
3	831 g Plutonium Metal Hollow Cylinder	Bottom position (angled), CGOC impact	0.6177
4	831 g Plutonium Metal Hollow Cylinder	Far side position, side impact	0.2896
5	831 g Plutonium Metal Hollow Cylinder	Far side position (angled), side impact	0.2389
6	731 g Plutonium Metal Hollow Cylinder	Bottom position, top impact	0.1507
7	731 g Plutonium Metal Hollow Cylinder	Bottom position (angled), top impact	0.2831
8	731 g Plutonium Metal Hollow Cylinder	Bottom position (angled), CGOC impact	0.3967
9	731 g Plutonium Metal Hollow Cylinder	Far side position, side impact	0.4896
10	731 g Plutonium Metal Hollow Cylinder	Far side position (angled), side impact	0.2842
11	SC-1 – Pu	Bottom position, support structure 0°, top impact	0.0319
12	SC-1 – Pu	Far side position, support structure 0°,side impact	0.2417
13	SC-1 – Pu	Far side position, support structure 45°, side impact	0.1958
14	SC-1 – Pu	Bottom position, support structure 0°, CGOC impact	0.0935
15	SC-1 – Pu	Bottom position, support structure 45°, CGOC impact	0.3061

Table 2-19. High Velocity (Aircraft) Impact Analyses Peak Tearing Parameter Values (Continued)

Run No.	Component	Model Orientation	Maximum Tearing Parameter (T-Ampoule)
16	SC-2 – Pu	Bottom position, support structure 0°, top impact	0.0132
17	SC-2 – Pu	Far side position, support structure 0°,side impact	0.4788
18	SC-2 – Pu	Far side position, support structure 45°, side impact	0.5137
19	SC-2 – Pu	Bottom position, support structure 0°, CGOC impact	0.0953
20	SC-2 – Pu	Bottom position, support structure 45°, CGOC impact	0.0540
21	SC-1 - Be	Bottom position, angled Be, support structure 0°, top impact	0.0155
22	SC-1 – Be	Far side position, angled Be, support structure 0°, side impact	0.2075
23	SC-1 – Be	Far side position, angled Be, support structure 45°, side impact	0.4970
24	SC-1 – Be	Bottom position, angled Be, support structure 0°, CGOC impact	0.0597
25	SC-1 – Be	Bottom position, angled Be, support structure 45°, CGOC impact	0.1197
26	SC-2 – Pu	Far side position, support structure 45°, side impact, friction 0.4	0.4888
27	SC-2 – Pu	Far side position, support structure 45°, side impact, friction 0.2	0.4673

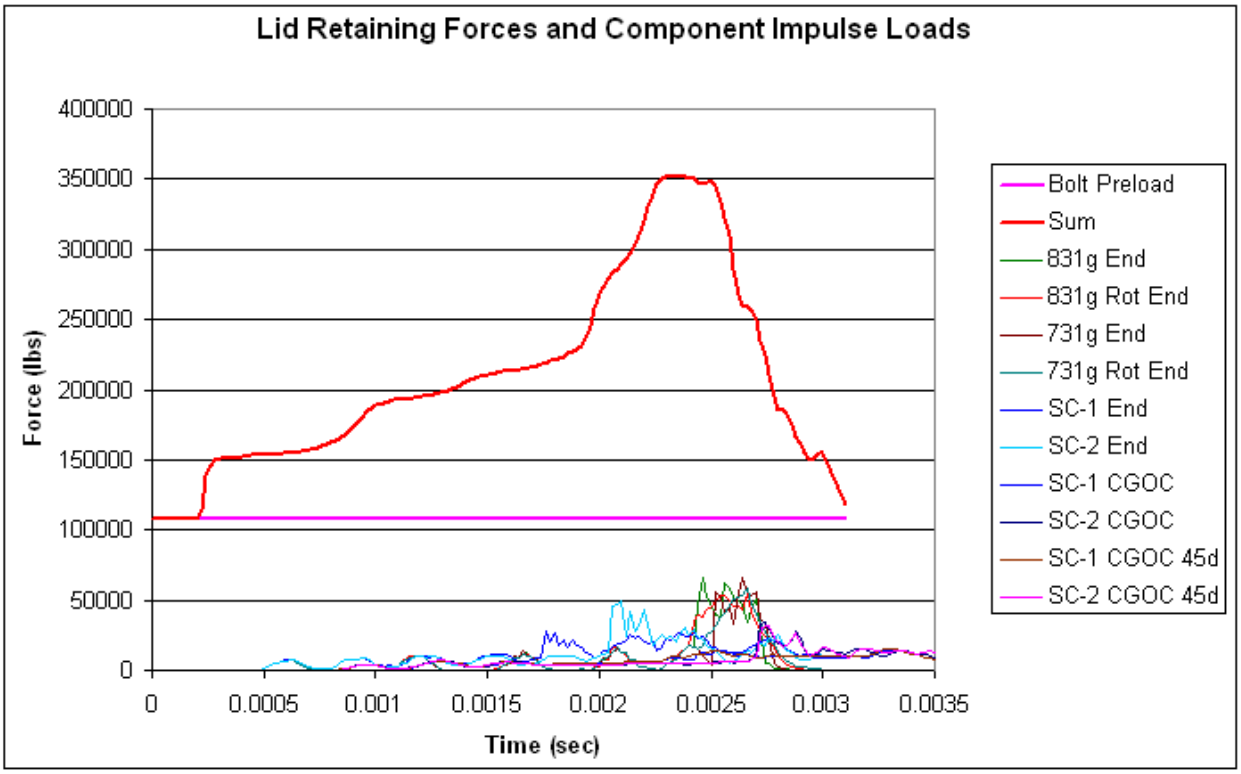

Figure 2-356. Summary Plot of Lid Retaining Forces and Component Impulse Loads

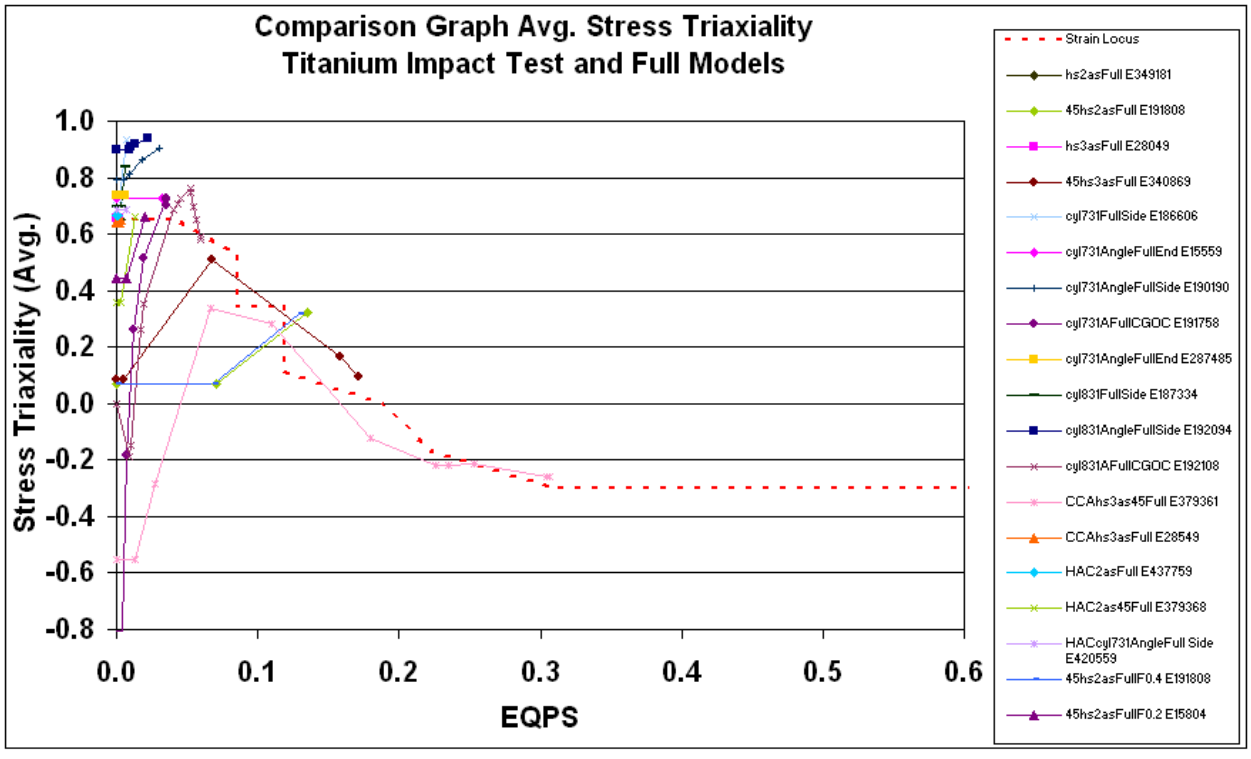

Figure 2-357. Summary Plot of Plastic Stress Triaxiality for Selected Runs

2.12.5.6 HAC – Dynamic Crush Analysis Results

In addition to the high-speed aircraft accident analyses, twenty analyses were performed to explore the HAC dynamic crush event described in 10 CFR 71.73. A description of these analyses is provided in Table 2-20. In all of these models, the 1100-lb plate was given an initial velocity of 528 in/s (which corresponds to a 30 ft drop), and was positioned within 0.12 in (3 mm) of the overpack. The overpack and contents had an initial velocity of 0, and gravity was included to ensure proper contact between the contents and the T-Ampoule. The material properties used for each analysis are the same as for the high-speed aircraft impacts and are provided in Section 2.12.4.

The performance of the T-Ampoule for each run was assessed using the same criteria as in the aircraft impact analyses. The maximum Tearing Parameter results for each run are listed in Table 2-20. None of the runs resulted in Tearing Parameters exceeding the maximum allowable Tearing Parameter, termed critical Tearing Parameter (TP_{crit} = 1.012 for Ti-6Al-4V, based on tensile tests to failure). The relatively large 0.44 and 0.22 Tearing Parameter values in run numbers 2 and 3 came from single elements in each analysis associated with a minor localized contact issue, and would otherwise be much smaller or zero (similar to the other analyses listed).

In addition, the stresses in the TB-1 were compared against HAC Reg. Guide 7.6 and ASME B&PV Code stress allowables. None of the runs resulted in through-thickness containment vessel stresses exceeding the ASME limit of 106.6 ksi, shown in Table 2-4. More conservatively, even using the NCT stress intensity limit of 50.8 ksi (see Table 2-4) or 50.0 from Section II, Part D of the ASME Boiler and Pressure Vessel Code for the S13800 material, none of the runs resulted in through-thickness TB-1 stresses exceeding these values in the dynamic crush environment.[8] Nonmandatory Appendix F of the ASME BPVC[9] lists stress intensity limits for inelastic analysis as the greater of $0.7S_u$ =106.6 ksi or $S_y + 0.33(S_u-S_y)$ =144.8 ksi for the general primary membrane stress intensity, not to exceed $0.9S_u$=137.1 ksi at any location. Conservatively, this limits the peak stress in the dynamic crush events to 137.1 ksi, which is never even approached in any of the HAC analyses, except at the irrelevant regions (due to minor contact modeling artifacts) on some very localized outer surfaces of the TB-1. For example, in Run 3, Section 2.12.5.6.3 for the SC-2 side impact (45-degree rotated) dynamic crush analysis, the through-thickness stress intensity (Tresca stress) is less than 23.5 ksi (Figure 2-382), and the peak stress intensity (excepting the highly localized 226.2 ksi peak due to a contact modeling artifact) was 70.5 ksi where the TB-1 closure diameter necks down to the main body smaller diameter. This 70.5 ksi peak stress intensity is below the Nonmandatory Appendix F peak stress limit of 137.1 ksi.

Table 2-20. Summary of Hypothetical Accident Condition (HAC) Dynamic Crush Analyses (20), Components, and Orientations

Run No.	Component	Submodel Orientation	Maximum Tearing Parameter
1	2 SC-2 Sample Containers, delta Pu	Lid end impact	0
2	2 SC-2 Sample Containers, delta Pu	Side impact	0.4464
3	2 SC-2 Sample Containers, delta Pu	Side impact, 45-degree-rotated	0.2288
4	2 SC-2 Sample Containers, delta Pu	CGOC impact	2.78e-3
5	2 SC-2 Sample Containers, delta Pu	CGOC impact, 45-degree-rotated	0
6	3 SC-1 Sample Containers, delta Pu	Lid end impact	0
7	3 SC-1 Sample Containers, delta Pu	Side impact	3.03e-5
8	3 SC-1 Sample Containers, delta Pu	Side impact, 45-degree-rotated	1.6e-2
9	3 SC-1 Sample Containers, delta Pu	CGOC impact	0
10	3 SC-1 Sample Containers, delta Pu	CGOC impact, 45-degree-rotated	0
11	831 g Plutonium Metal Hollow Cylinder, alpha Pu	Lid end impact	0
12	831 g Plutonium Metal Hollow Cylinder, alpha Pu	Side impact	2.94e-6
13	831 g Plutonium Metal Hollow Cylinder, alpha Pu	Lid end impact, angled cylinder	0
14	831 g Plutonium Metal Hollow Cylinder, alpha Pu	Side impact, angled cylinder	2.01e-2
15	831 g Plutonium Metal Hollow Cylinder, alpha Pu	CGOC impact, angled cylinder	0
16	731 g Plutonium Metal Hollow Cylinder, alpha Pu	Lid end impact	0
17	731 g Plutonium Metal Hollow Cylinder, alpha Pu	Side impact	0
18	731 g Plutonium Metal Hollow Cylinder, alpha Pu	Lid end impact, angled cylinder	0
19	731 g Plutonium Metal Hollow Cylinder, alpha Pu	Side impact, angled cylinder	5.09e-2
20	731 g Plutonium Metal Hollow Cylinder, alpha Pu	CGOC impact, angled cylinder	0

2.12.5.6.1 HAC – Run 1, SC-2, End Impact

The dynamic crush end impact HAC analysis for the 2 SC-2 sample container run uses the same model as that used for the 4-ft-drop, but the flange is added to both ends so that it available to deform where impacted by the plate and the rigid surface upon which it is resting. The finite element mesh and initial position of the model is shown in Figure 2-358. The Pu contents and support structure within the T-Ampoule are positioned at the bottom of the model because it was considered to be at rest.

The post-impact deformation is shown in Figure 2-359 and its kinetic energy history in Figure 2-360. The flanges on the overpack deform, and the contents bounce due to the impact of the plate, but there is no plastic deformation in the T-Ampoule or the TB-1.

Figures 2-361 and 2-362 are plots of the Tresca stresses within the TB-1. The maximum Tresca stress (stress intensity) in the TB-1 is 137.9 ksi due again to a contact modeling artifact), but there are no through thickness stresses exceeding the limit of 106.6 ksi, which can be seen clearly in Figure 2-362. Figure 2-363 is a plot of the Tresca stresses at the time when all of the kinetic energy of the plate has been transferred to the package, just as the plate begins to rebound. The maximum through thickness stress at this time is below 16.7 ksi, below the allowable through thickness stress of 106.6 ksi, as seen in the figure.

As in the high velocity impact analyses, there is a minor modeling artifact occurring due to slight contact over closure between the redwood and the ring of TB-1 top surface elements which is causing this very slight non-realistic localized plasticity.

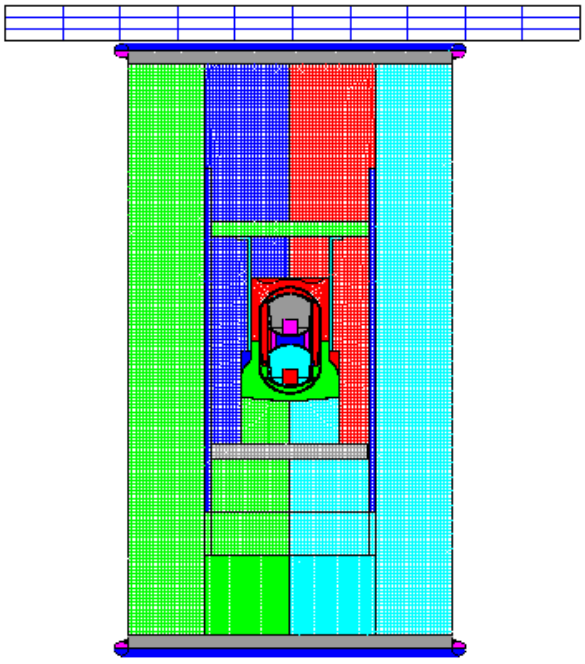

Figure 2-358. Finite Element Mesh for HAC Run 1, SC-2, End Impact

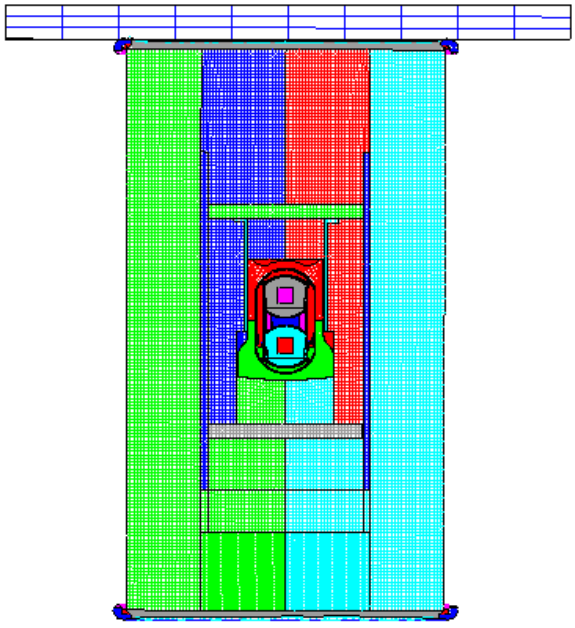

Figure 2-359. Finite Element Mesh for HAC Run 1, SC-2, End Impact – Final Displacement

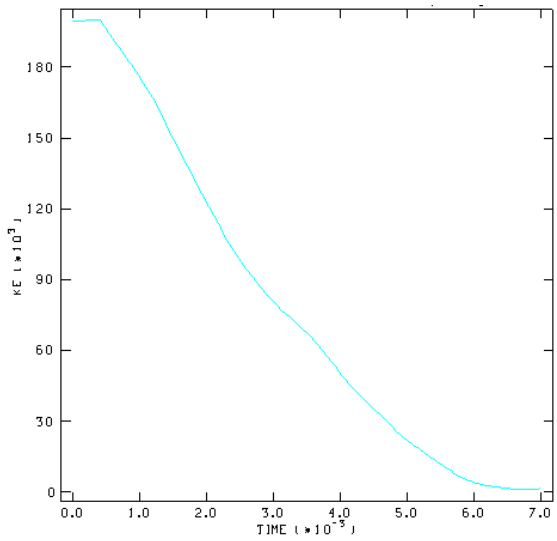

Figure 2-360. Kinetic Energy Time History for HAC Run 1, SC-2, End Impact

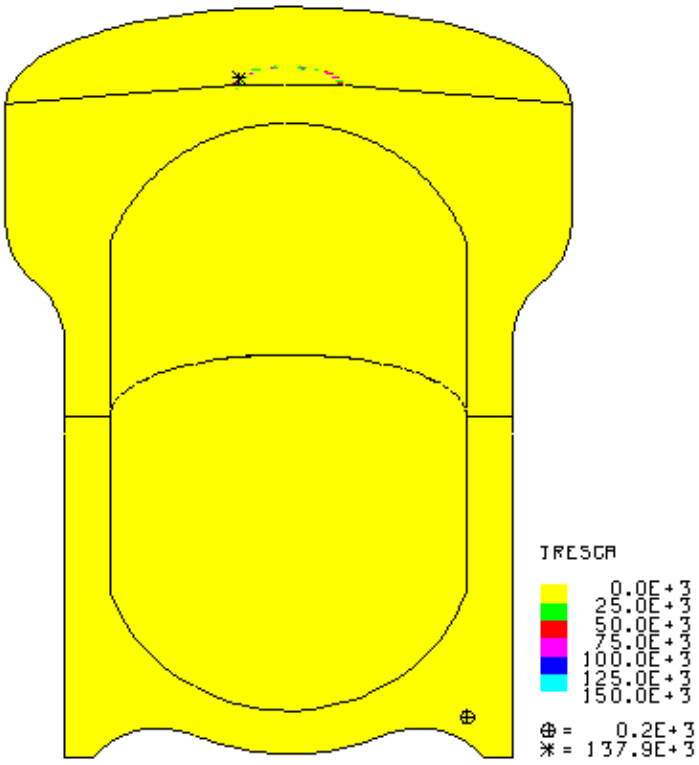

Figure 2-361. Tresca Stress in TB-1 for HAC Run 1, SC-2, End Impact

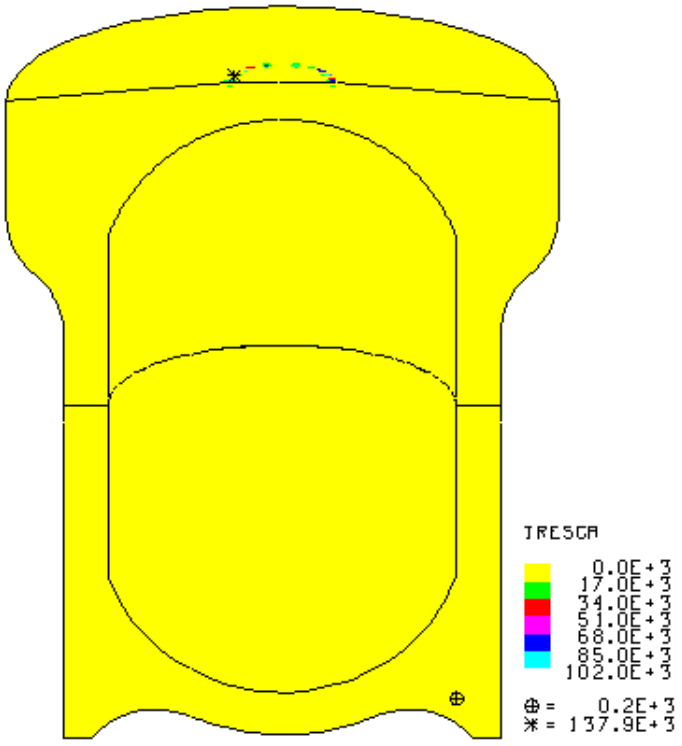

Figure 2-362. Tresca Stress of TB-1 for HAC Run 1, SC-2, End Impact

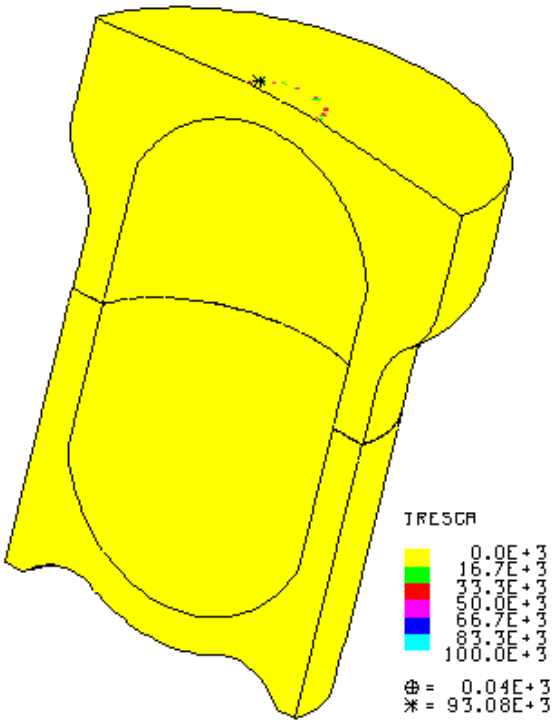

Figure 2-363. Tresca Stress of TB-1 for HAC Run 1, SC-2, End Impact when Plate Velocity Reaches Zero

2.12.5.6.2 HAC- Run 2, SC-2, Side Impact, Support Structure 0°

The dynamic crush end impact HAC analysis for the 2 SC-2 sample container runs uses the same model as that used for the 4-ft-drop, but the flange is added to both ends so that it available to deform where impacted by the plate and the rigid surface upon which it is resting. The finite element mesh and initial position of the model are shown in Figure 2-364. The Pu contents and support structure within the T-Ampoule are positioned at the bottom of the model because it was considered to be at rest. The plate was positioned between the flanges to be most damaging to the TB-1 and contents by preventing the flanges from absorbing energy and slowing down the plate before it hits the overpack.

The post-impact deformation is shown in Figure 2-365 and its kinetic energy history in Figure 2-366. The flanges on the overpack deform, and the contents bounce due to the impact of the plate. Average stress-triaxiality versus EQPS is shown in Figures 2-367 and 2-368 for the one element extending beyond the tested Bao-Wierzbicki strain locus. This element is at high stress triaxiality and low EQPS. The Tearing Parameter values for this same element are shown in Figure 2-369, and are below the critical Tearing Parameter value of 1.012 for Ti-6Al-4V. This element is highlighted in red Figure 2-370, but note that this element is below the initiation of a ductile tear, thus T-Ampoule integrity is maintained.

Peak EQPS in the TB-1 vessel is shown in Figure 2-371 to be 28.31e-3, and is localized in the outer contact regions with the redwood overpack. Figure 2-372 is a plot of the Tresca stresses within the TB-1. The maximum Tresca stress in the TB-1 is 172.3 ksi, but there are no through thickness stresses exceeding the limit of 106.6 ksi, which can be seen clearly in the figure.

Figure 2-373 is a plot of the Tresca stresses at the time when all of the kinetic energy of the plate has been transferred to the package, just as the plate begins to rebound. The maximum through thickness stress at this time is below 26.7 ksi, below the allowable through thickness stress of 106.6 ksi, as seen in the figure.

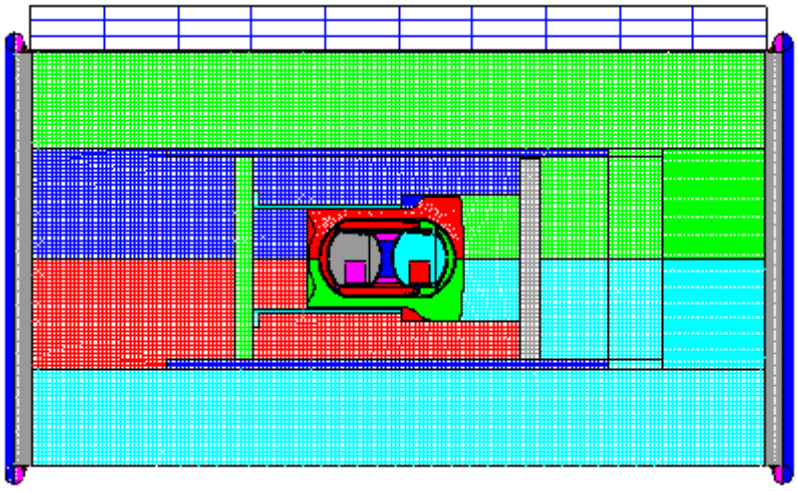

Figure 2-364. Finite Element Mesh for HAC Run 2, SC-2, Side Impact, Support Structure 0°

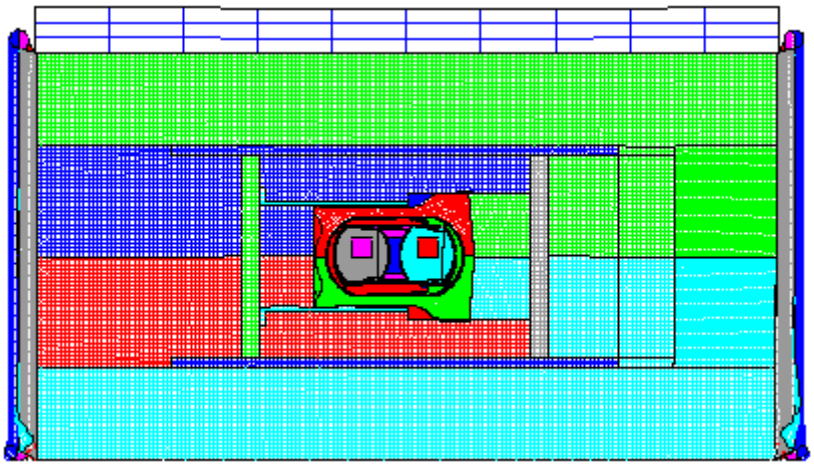

Figure 2-365. Finite Element Mesh for HAC Run 2, SC-2, Side Impact, Support Structure 0° - Final Displacement

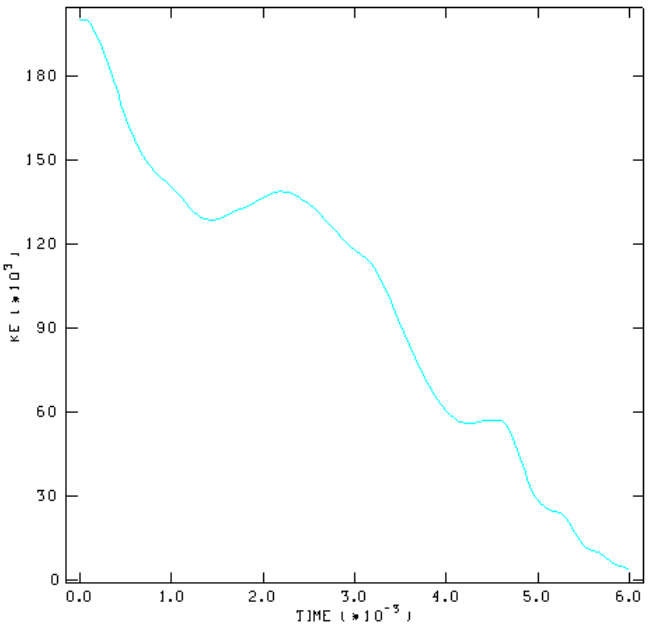

Figure 2-366. Kinetic Energy Time History for HAC Run 2, SC-2, Side Impact, Support Structure 0°

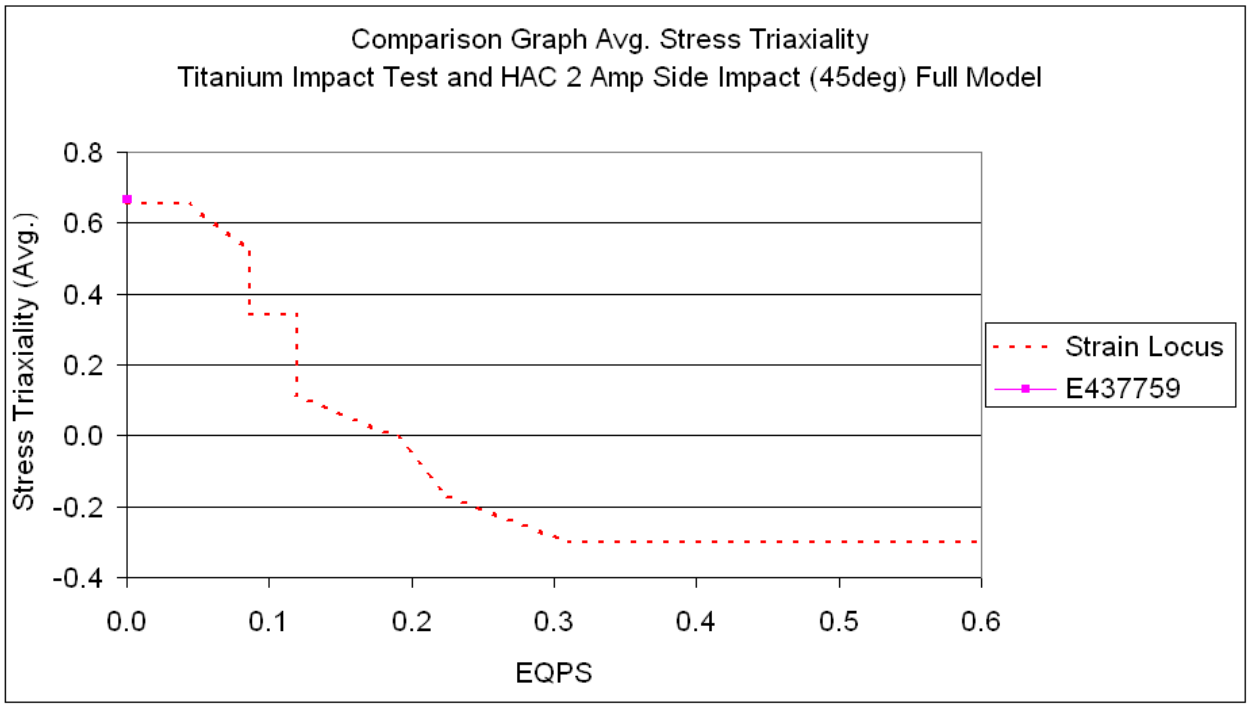

Figure 2-367. Graph of Average Stress Triaxiality versus EQPS for Element Exceeding Experimental Strain Locus for HAC Run 2, SC-2, Side Impact, Support Structure 0°

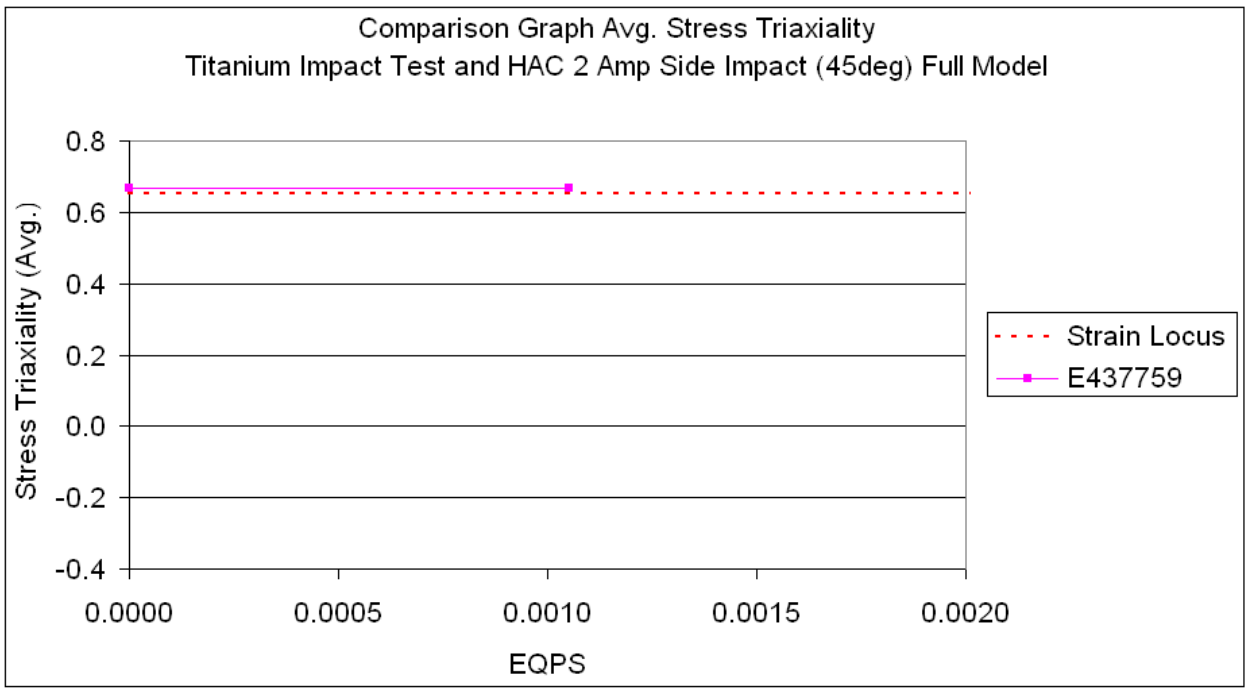

Figure 2-368. Graph of Average Stress Triaxiality versus EQPS for Element Exceeding Experimental Strain Locus (Zoomed In) for HAC Run 2, SC-2, Side Impact, Support Structure 0°

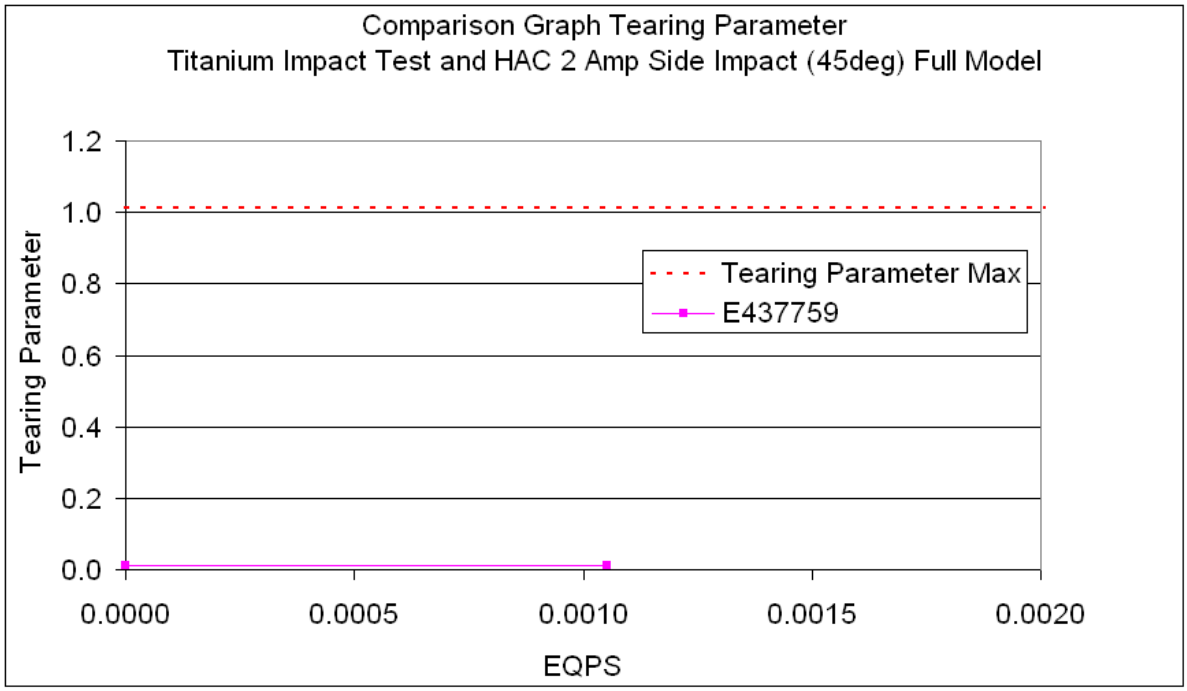

Figure 2-369. Graph of Tearing Parameter versus EQPS for Element Exceeding Experimental Strain Locus for HAC Run 2, SC-2, Side Impact, Support Structure 0°

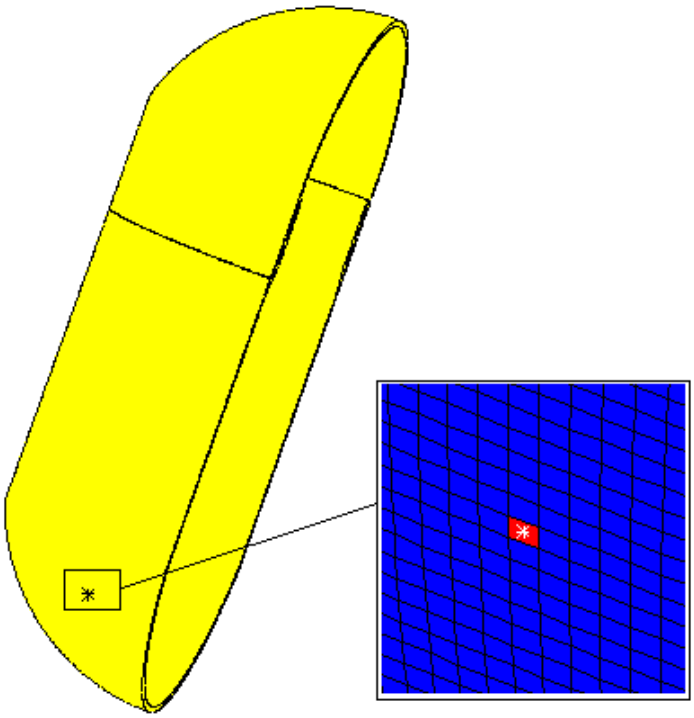

Figure 2-370. Plot of Element Exceeding Experimental Strain Locus for HAC Run 2, SC-2, Side Impact, Support Structure 0°

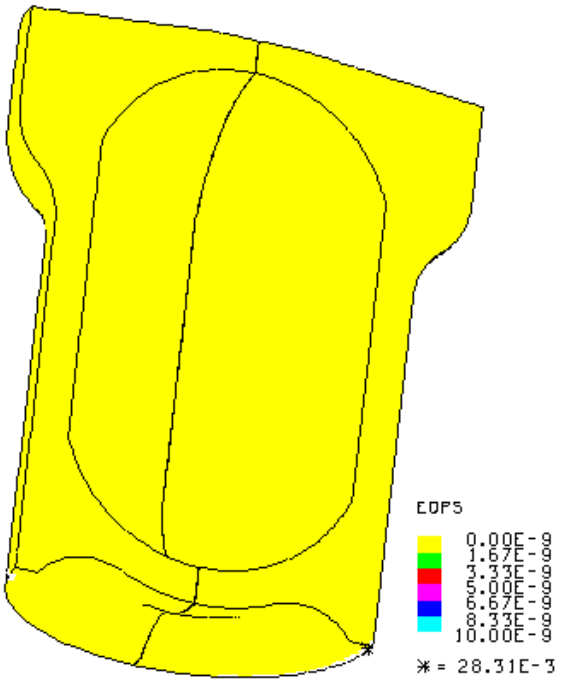

Figure 2-371. Graph of EQPS in the TB-1 for HAC Run 2, SC-2, Side Impact, Support Structure 0°

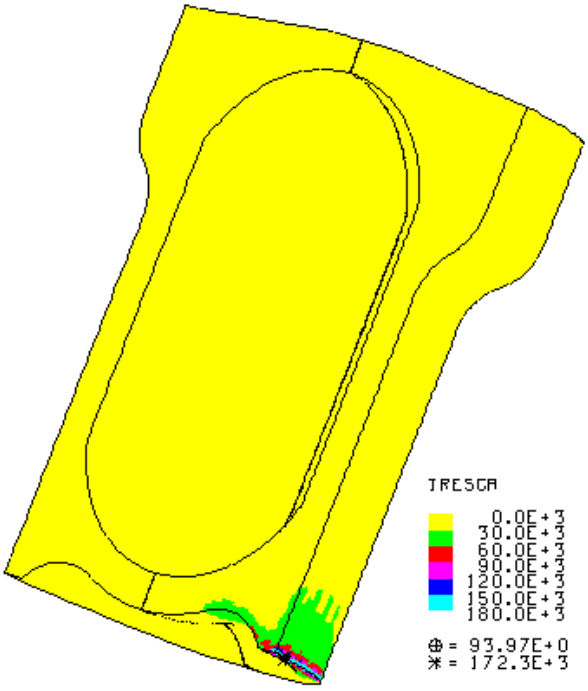

Figure 2-372. Plot of Tresca Stress in the TB-1 for HAC Run 2, SC-2, Side Impact, Support Structure 0°

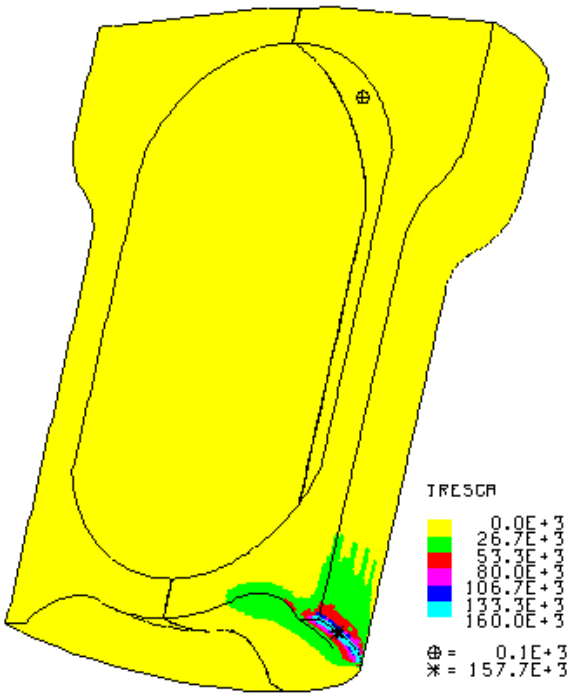

Figure 2-373. Plot of Tresca Stress in the TB-1 for HAC Run 2, SC-2, Side Impact, Support Structure 0° when Plate Velocity Reaches Zero

2.12.5.6.3 HAC- Run 3, SC-2, Side Impact, Support Structure 45°

The dynamic crush side impact HAC analysis run for the 2 SC-2 sample container with its support structure rotated 45° uses the same model as that used for the 4-ft-drop, but the flange is added to both ends so that it available to deform where impacted by the plate and the rigid surface upon which it is resting. The finite element mesh and initial position of the model are shown in Figure 2-374. The Pu contents and support structure within the T-Ampoule are positioned at the bottom of the model because it was considered to be at rest at the time of impact. The plate was positioned between the flanges to be most damaging to the TB-1 and contents by preventing the flanges from absorbing energy and slowing down the plate before it hits the overpack.

The post-impact deformation is shown in Figure 2-375 and its kinetic energy history in Figure 2-376. The flanges on the overpack deform, and the contents bounce due to the impact of the plate. Average stress-triaxiality versus EQPS is shown in Figure 2-377 for the one element extending beyond the tested Bao-Wierzbicki strain locus. This element is at high stress triaxiality and low EQPS. The Tearing Parameter value for this same element is shown in Figure 2-378 and is below the critical Tearing Parameter value of 1.012 for Ti-6Al-4V. This element is highlighted in red Figure 2-379, but note that this element is below the initiation of a ductile tear, thus T-Ampoule integrity is maintained.

Peak EQPS in the TB-1 vessel is shown in Figure 2-380 to be 0.21, and is localized in the outer contact regions with the redwood overpack. Figures 2-381 and 2-382 are plots of the Tresca stresses within the TB-1. The maximum Tresca stress in the TB-1 is 226.7 ksi, but there are no through thickness stresses exceeding the limit of 106.6 ksi, which can be seen clearly in the figures. Figure 2-383 is a plot of the Tresca stresses at the time when all of the kinetic energy of the plate has been transferred to the package, just as the plate begins to rebound. The maximum through thickness stress at this time is below 16.7 ksi, below the allowable through thickness stress of 106.6 ksi, as seen in the figure.

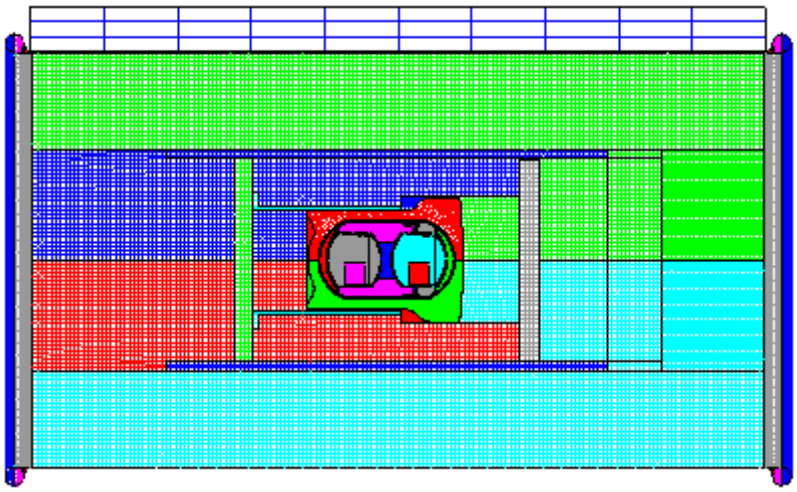

Figure 2-374. Finite Element Mesh for HAC Run 3, SC-2, Side Impact, Support Structure 45°

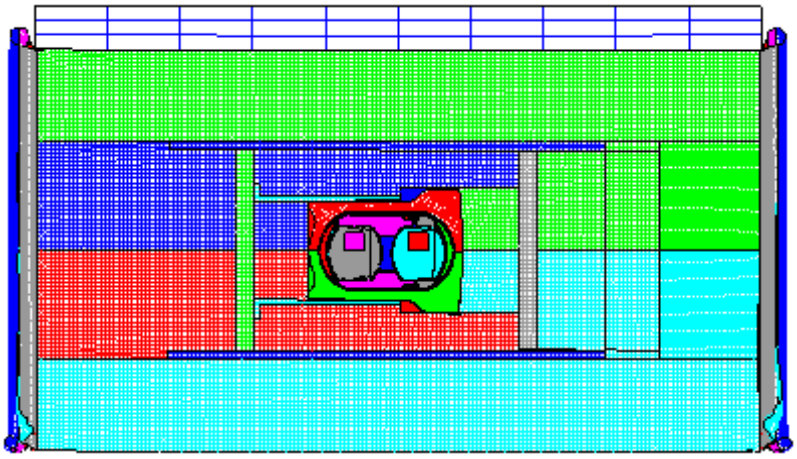

Figure 2-375. Finite Element Mesh for HAC Run 3, SC-2, Side Impact, Support Structure 45° - Final Displacement

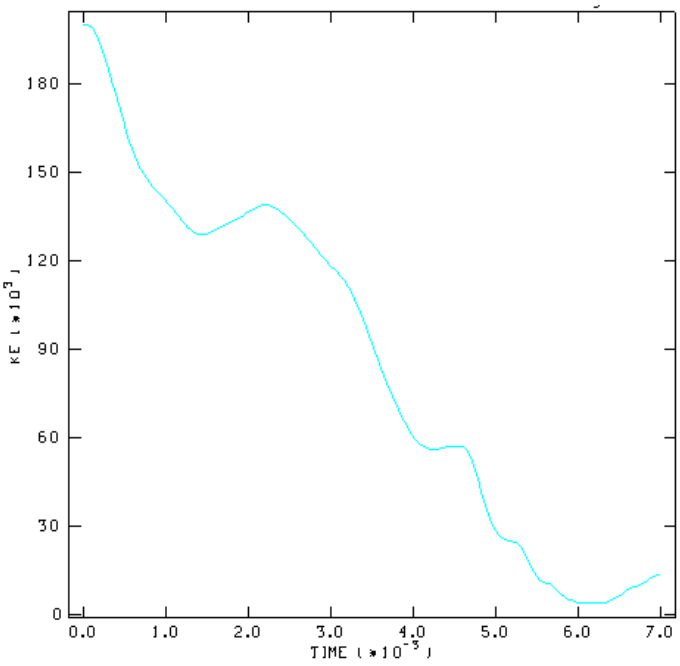

Figure 2-376. Kinetic Energy Time History for HAC Run 3, SC-2, Side Impact, Support Structure 45°

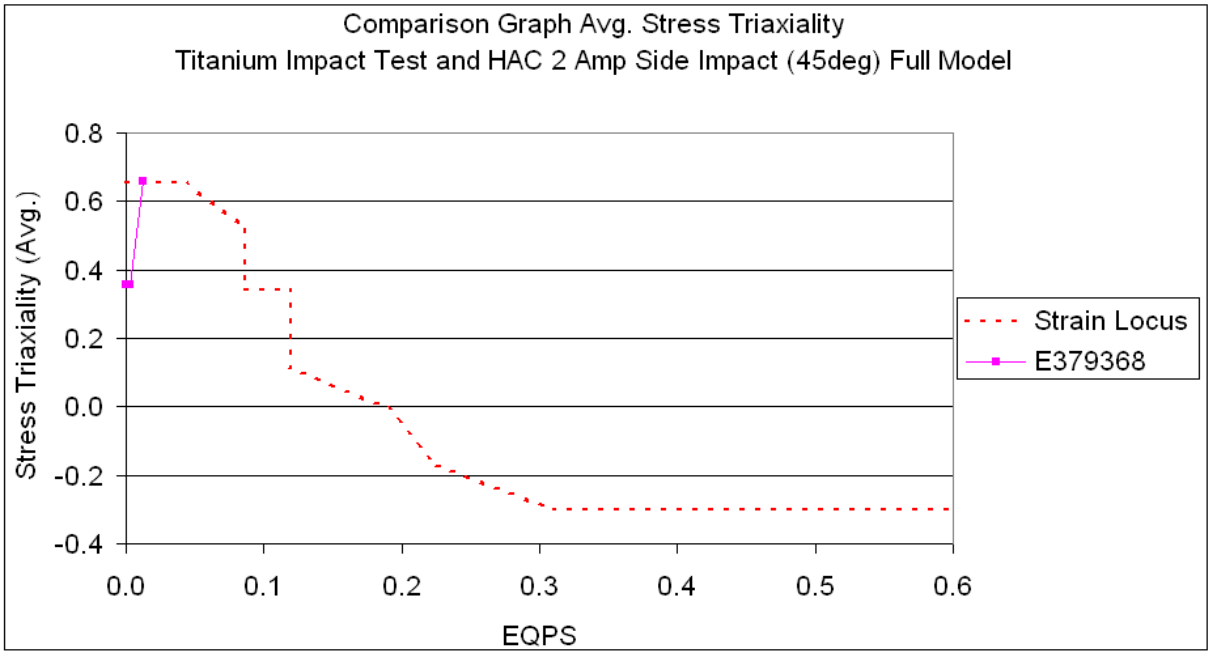

Figure 2-377. Graph of Average Stress Triaxiality versus EQPS of Element Exceeding Experimental Strain Locus for HAC Run 3, SC-2, Side Impact, Support Structure 45°

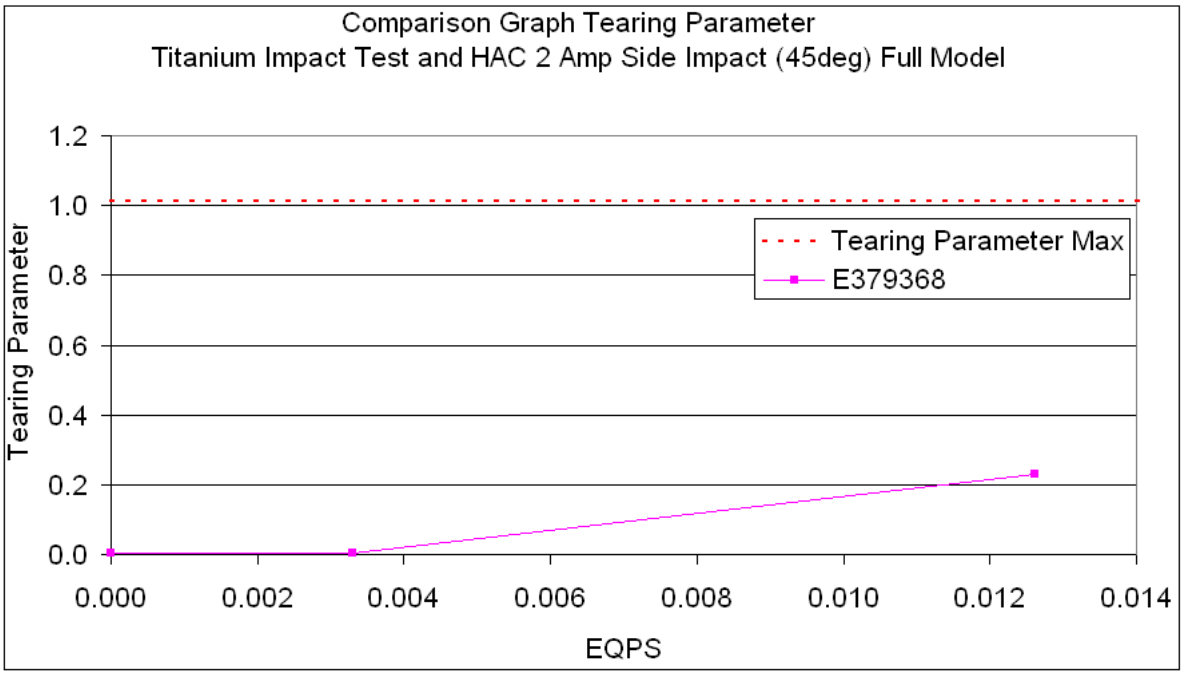

Figure 2-378. Graph of Tearing Parameter versus EQPS of Element Exceeding Experimental Strain Locus (Zoomed In) for HAC Run 3, SC-2, Side Impact, Support Structure 45°

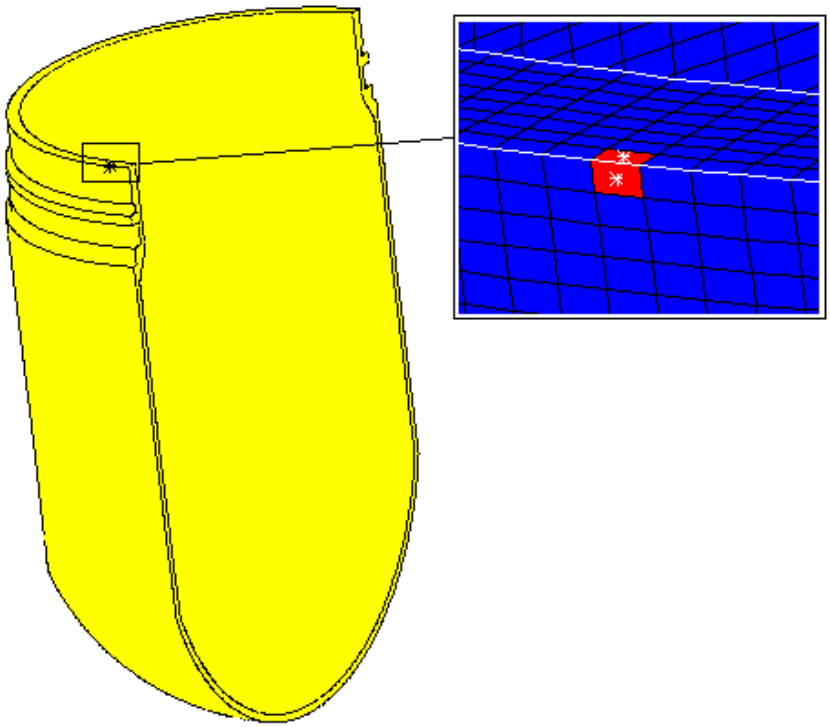

Figure 2-379. Plot of Element Exceeding Experimental Strain Locus for HAC Run 3, SC-2, Side Impact, Support Structure 45°

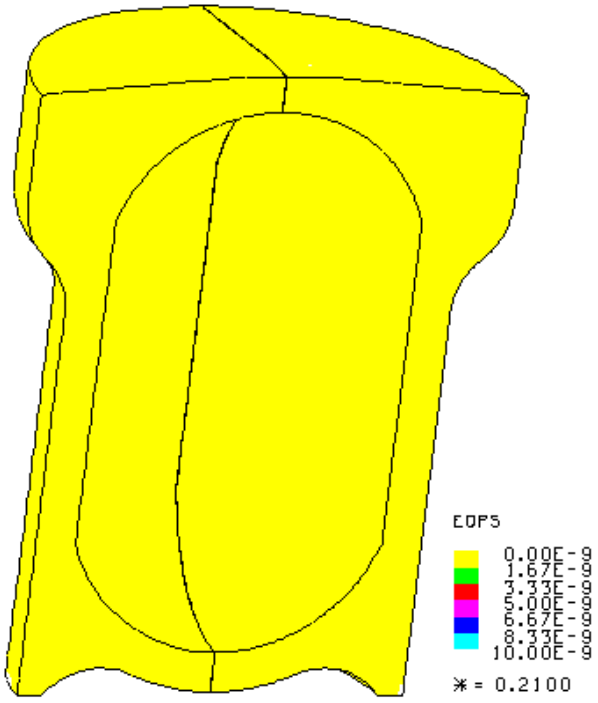

Figure 2-380. Plot of EQPS in the TB-1 for HAC Run 3, SC-2, Side Impact, Support Structure 45°

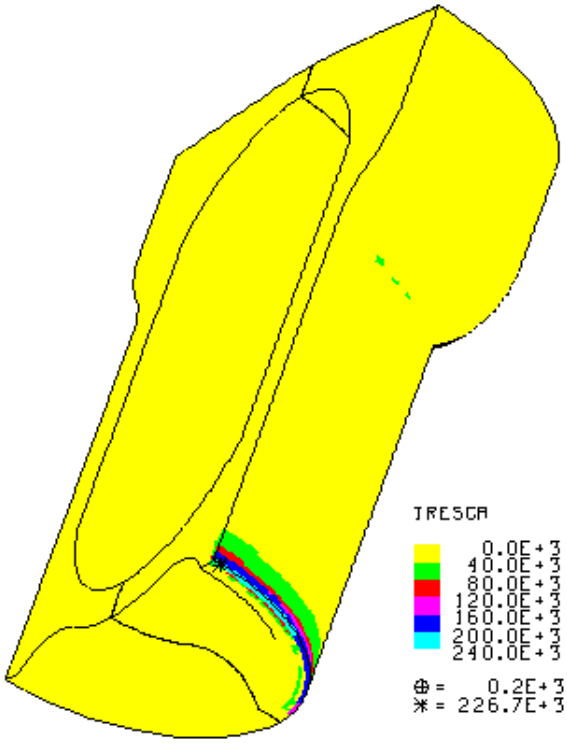

Figure 2-381. Plot of Tresca Stress in the TB-1 for HAC Run 3, SC-2, Side Impact, Support Structure 45°

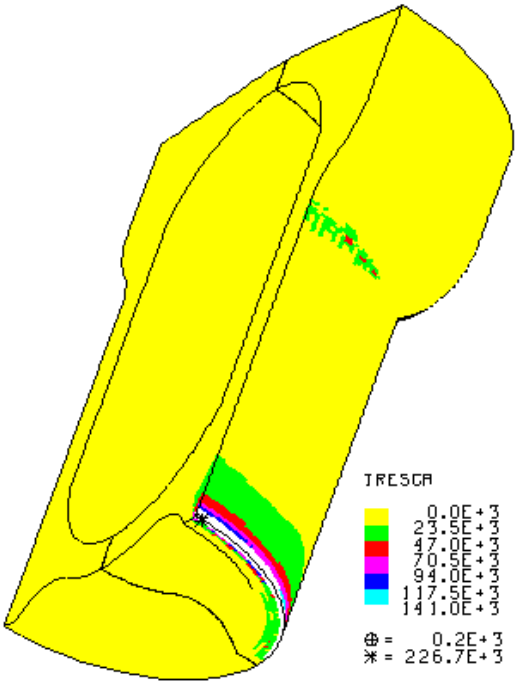

Figure 2-382. Plot of Tresca Stress in the TB-1 for HAC Run 3, SC-2, Side Impact, Support Structure 45°

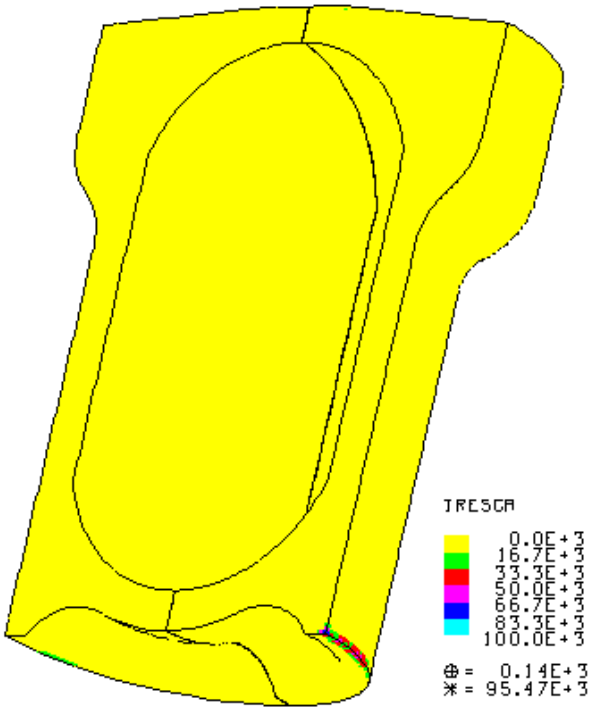

Figure 2-383. Plot of Tresca Stress in the TB-1 for HAC Run 3, SC-2, Side Impact, Support Structure 45° when Plate Velocity Reaches Zero

2.12.5.6.4 HAC- Run 4, SC-2, CGOC Impact, Support Structure 0°

The dynamic crush CGOC impact HAC analysis for the 2 SC-2 sample container run uses the same overpack model as those used in HAC runs 1 through 3. The finite element mesh and initial position of the model are shown in Figure 2-384. The Pu contents and support structure within the T-Ampoule are positioned at the bottom of the model because it was considered to be at rest.

The post-impact deformation is shown in Figure 2-385 and the resulting kinetic energy history is shown in Figure 2-386. The kinetic energy does not drop completely to zero because the plate is still vibrating and internal contents are still in motion. The plutonium cylinders have bounced off of the top and bottom surface of the sample containers, and the plate is now rebounding slowly with the package, ensuring that the highest containment vessel and contents loadings have occurred.

There were no elements that extended beyond the tested Bao-Wierzbicki strain locus. The maximum Tearing Parameter value for this analysis was 2.78e-3, which is below the critical Tearing Parameter value of 1.012 for Ti-6Al-4V, thus T-Ampoule integrity is maintained.

Peak EQPS in the TB-1 vessel is shown in Figure 2-387 to be 1.548e-3, and is localized in the outer contact regions with the redwood overpack. Figures 2-388 and 2-389 are plots of the Tresca stresses within the TB-1. The maximum Tresca stress in the TB-1 is 159.1 ksi, but there are no through thickness stresses exceeding the limit of 106.6 ksi, which can be seen clearly in the figures. Figure 2-389 is a plot of the Tresca stresses at the time when all of the kinetic energy of the plate has been transferred to the package, just as the plate begins to rebound. The

maximum through thickness stress at this time is below 8.33 ksi, below the allowable through thickness stress of 106.6 ksi, as seen in the figure.

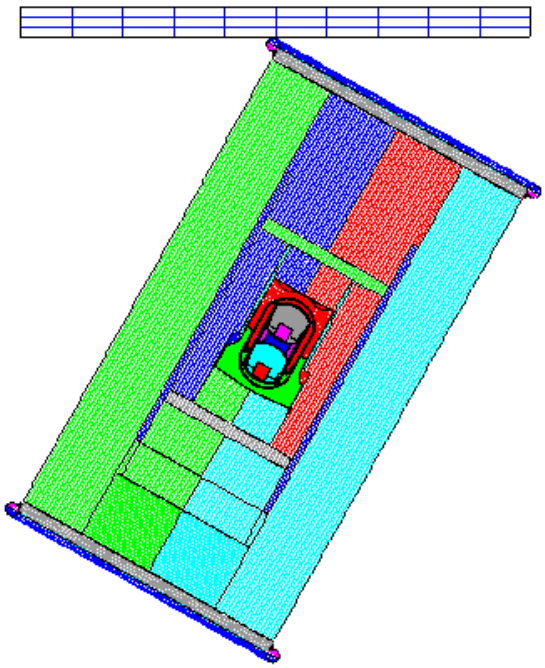

Figure 2-384. Finite Element Mesh for HAC Run 4, SC-2, CGOC Impact, Support Structure 0°

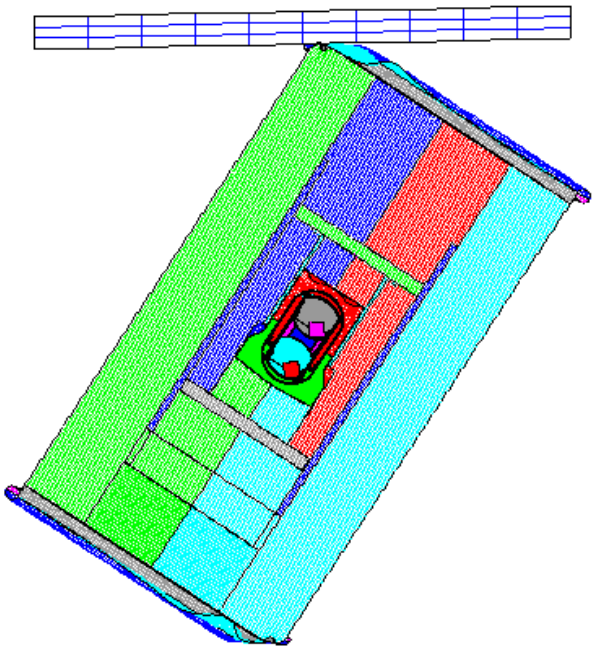

Figure 2-385. Finite Element Mesh for HAC Run 4, SC-2, CGOC Impact, Support Structure 0°, Final Displacement

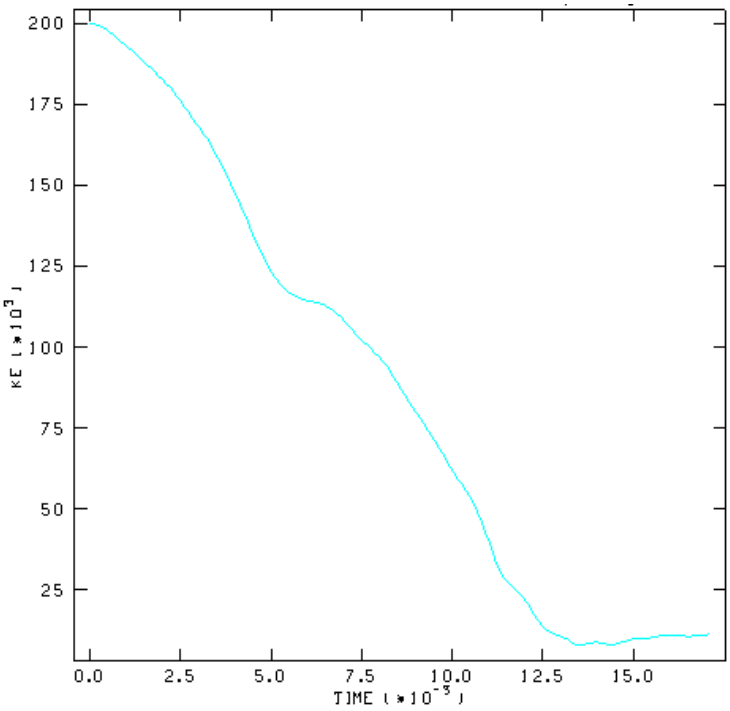

Figure 2-386. Kinetic Energy Time History for HAC Run 4, SC-2, CGOC Impact, Support Structure 0°

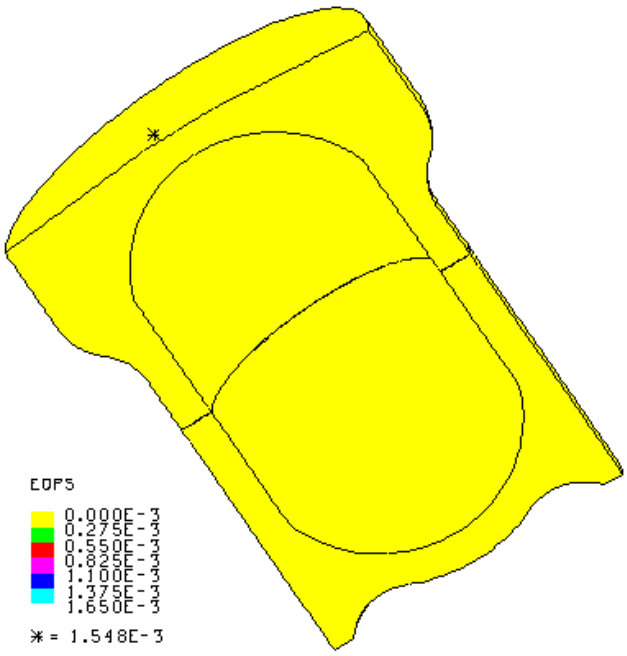

Figure 2-387. Plot of EQPS in TB-1 for HAC Run 4, SC-2, CGOC Impact, Support Structure 0°

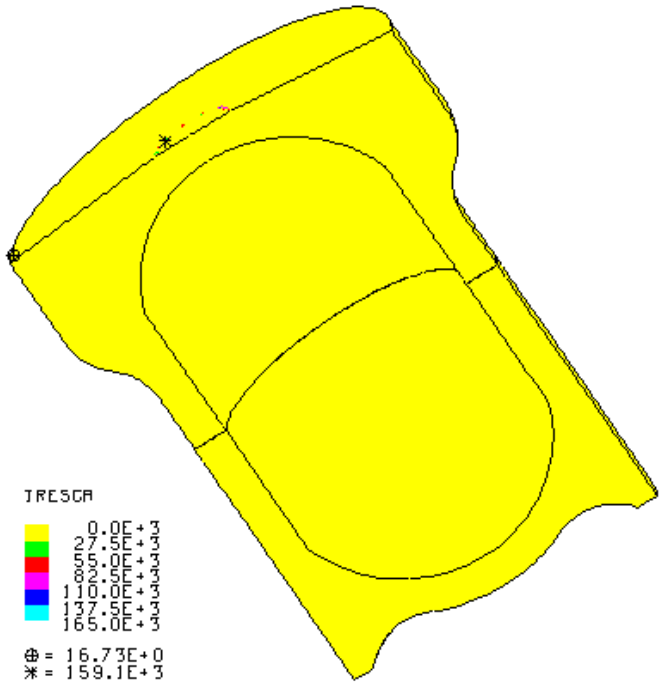

Figure 2-388. Plot of Tresca Stress in TB-1 for HAC Run 4, SC-2, CGOC Impact, Support Structure 0°

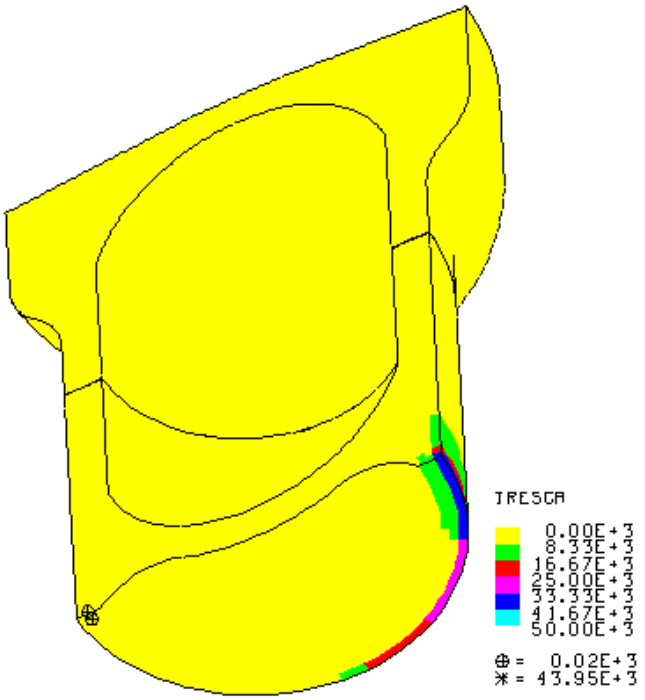

Figure 2-389. Plot of Tresca Stress in the TB-1 for HAC Run 4, SC-2, CGOC Impact, Support Structure 0° when Plate Velocity Reaches Zero

2.12.5.6.5 HAC- Run 5, SC-2, CGOC Impact, Support Structure 45°

The dynamic crush CGOC impact HAC analysis for the 2 SC-2 sample container run uses the same overpack model as those used in HAC runs 1 through 4. The finite element mesh and initial position of the model are shown in Figure 2-390. The Pu contents and support structure within the T-Ampoule are positioned at the bottom of the model because it was considered to be at rest.

The post-impact deformation is shown in Figure 2-391 and its kinetic energy history in Figure 2-392. The flanges on the overpack deform, and the contents bounce due to the impact of the plate. The kinetic energy does not drop completely to zero because the plate is still vibrating and internal contents are still in motion. The plutonium cylinders have bounced off of the top and bottom surface of the sample containers, and the plate is now rebounding slowly with the package, ensuring that the highest containment vessel and contents loadings have occurred.

There was zero EQPS in the T-Ampoule and the TB-1, and the maximum Tearing Parameter was 0. Figure 2-393 is a plot of the Tresca stresses within the TB-1. The maximum Tresca stress in the TB-1 is 157.0 ksi, but there are no through thickness stresses exceeding the limit of 106.6 ksi, which can be seen clearly in the figure. Figure 2-393 is a plot of the Tresca stresses at the time when all of the kinetic energy of the plate has been transferred to the package, just as the plate begins to rebound. The maximum through thickness stress at this time is below 16.7 ksi, below the allowable through thickness stress of 106.6 ksi, as seen in the figure.

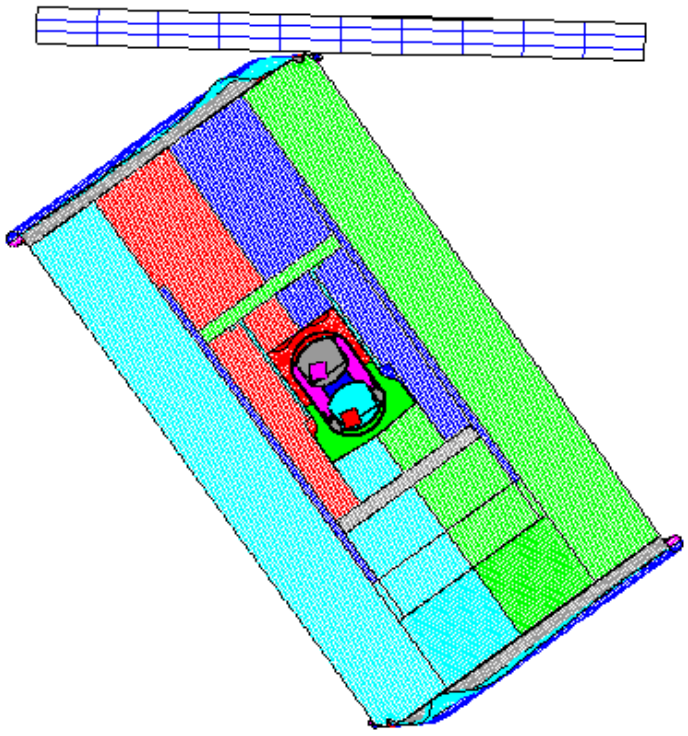

Figure 2-390. Finite Element Mesh for HAC Run 5, SC-2, CGOC Impact, Support Structure 45°

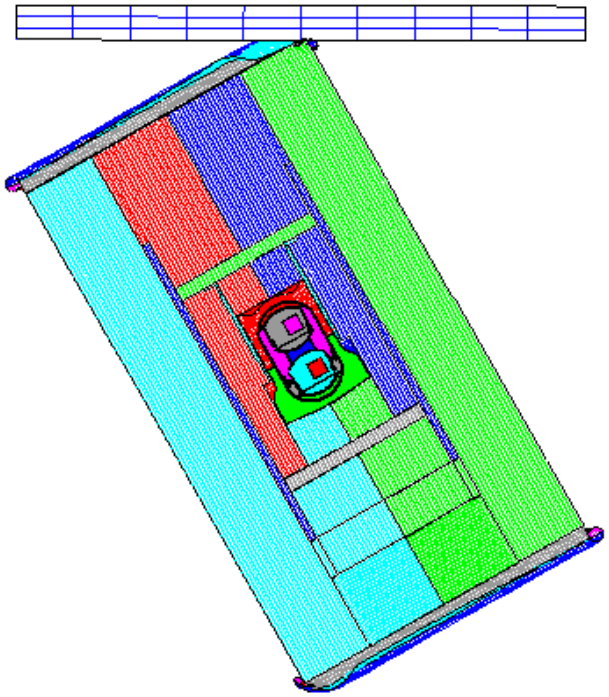

Figure 2-391. Finite Element Mesh for HAC Run 5, SC-2, CGOC Impact, Support Structure 45° - Final Displacement

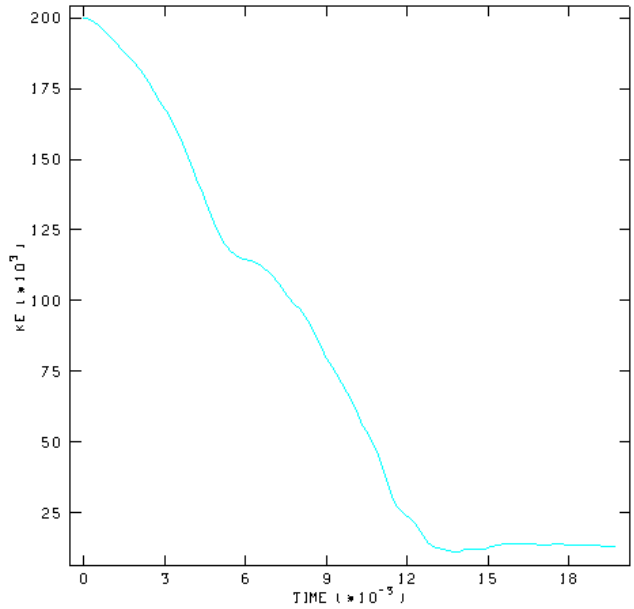

Figure 2-392. Kinetic Energy Time History for HAC Run 5, SC-2, CGOC Impact, Support Structure 45°

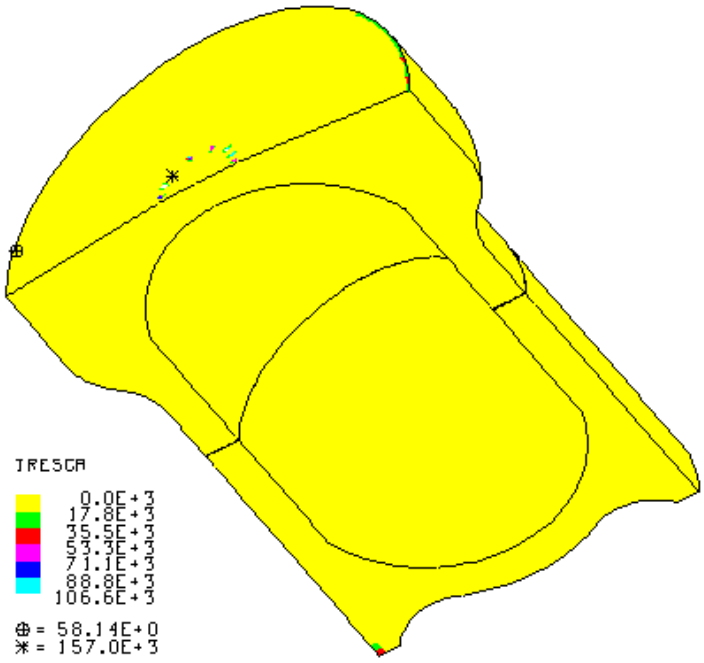

Figure 2-393. Plot of Tresca Stress in the TB-1 for HAC Run 5, SC-2, CGOC Impact, Support Structure 45° when Stress is a Maximum

2.12.5.6.6 HAC- Run 6, SC-1, End Impact

The dynamic crush end impact HAC analysis run for the SC-1 sample container with its support structure rotated 0° uses the same model as that used for the 4-ft-drop, but the flange is added to both ends so that it available to deform where impacted by the plate and the rigid surface upon which it is resting. The finite element mesh and initial position of the model are shown in Figure 2-394. The Pu contents and support structure within the T-Ampoule are positioned at the bottom of the model because it was considered to be at rest at the time of impact.

The post-impact deformation is shown in Figure 2-395 and its kinetic energy history in Figure 2-396. The flanges on the overpack deform, and the contents bounce due to the impact of the plate. There was zero EQPS in the TB-1, and zero elements extended beyond the tested Bao-Wierzbicki strain locus. The maximum Tearing Parameter was 3.03e-5 in the T-Ampoule, and is below the critical Tearing Parameter value of 1.012 for Ti-6Al-4V, thus T-Ampoule integrity is maintained. Figure 2-397 is a plot of the Tresca stresses within the TB-1. The maximum Tresca stress in the TB-1 is 127.1 ksi, but there are no through thickness stresses exceeding the limit of 106.6 ksi, which can be seen clearly in the figures. Figure 2-398 is a plot of the Tresca stresses at the time when all of the kinetic energy of the plate has been transferred to the package, just as the plate begins to rebound. The maximum through thickness stress at this time is below 8.33 ksi, below the allowable through thickness stress of 106.6 ksi, as seen in the figure.

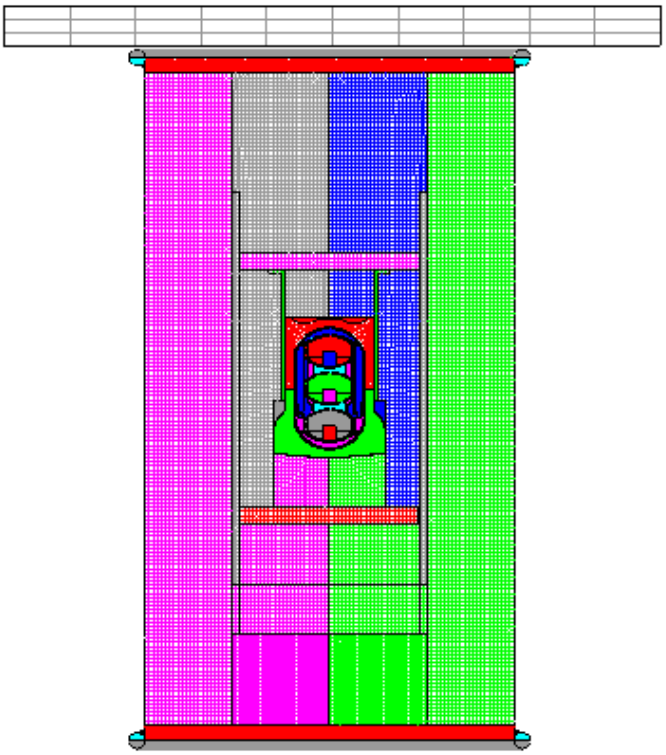

Figure 2-394. Finite Element Mesh for HAC Run 6, SC-1, End Impact, Support Structure 0°

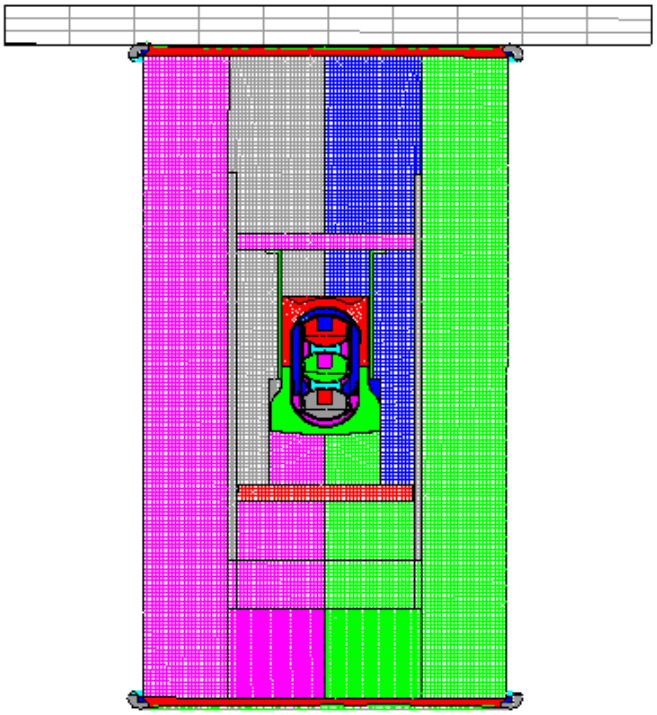

Figure 2-395. Finite Element Mesh for HAC Run 6, SC-1, End Impact, Support Structure 0° - Final Displacement

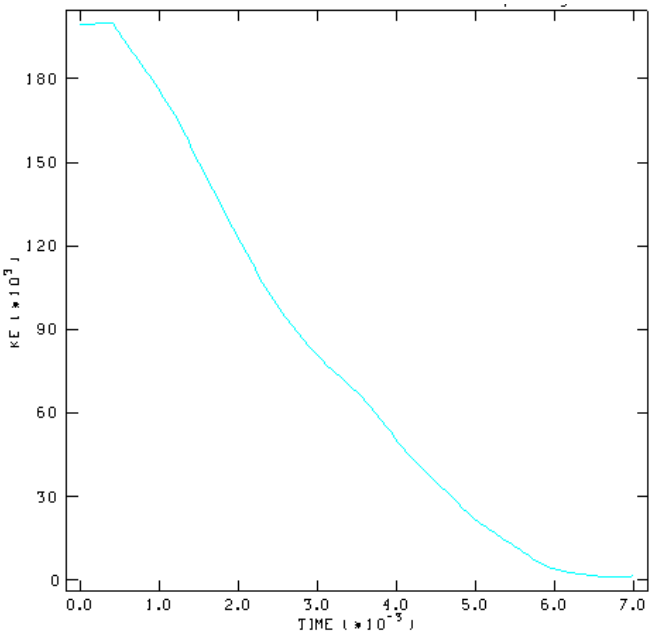

Figure 2-396. Kinetic Energy Time History for HAC Run 6, SC-1, End Impact, Support Structure 0°

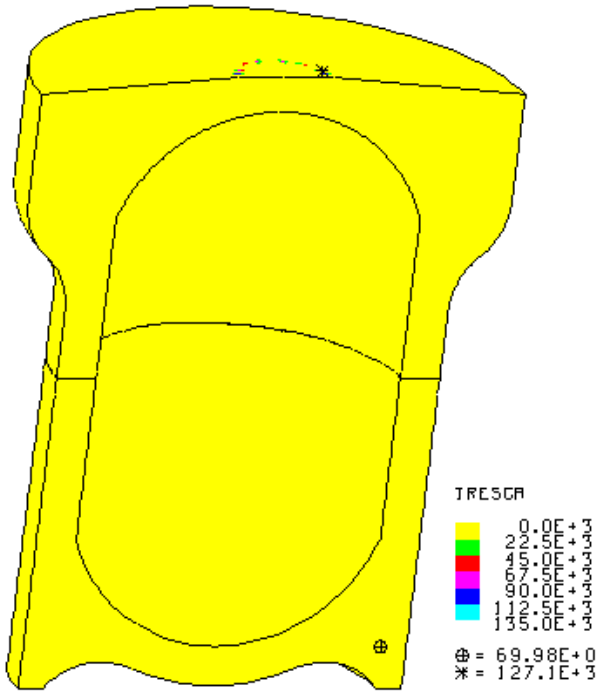

Figure 2-397. Plot of Tresca Stress in the TB-1 for HAC Run 6, SC-1, End Impact, Support Structure 0°

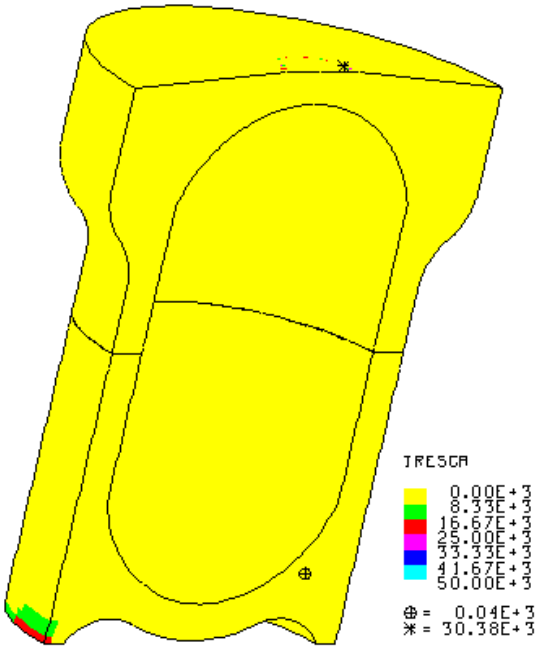

Figure 2-398. Plot of Tresca Stress in the TB-1 for HAC Run 6, SC-1, End Impact, Support Structure 0° when Plate Velocity Reaches Zero

2.12.5.6.7 HAC- Run 7, SC-1, Side Impact, Support Structure 0°

The dynamic crush side impact HAC analysis run for the SC-1 sample containers with its support structure rotated 45° uses the same model as that used for the 4-ft-drop, but the flange is added to both ends so that it available to deform where impacted by the plate and the rigid surface upon which it is resting. The finite element mesh and initial position of the model are shown in Figure 2-399. The Pu contents and support structure within the T-Ampoule are positioned at the bottom of the model because it was considered to be at rest at the time of impact. The plate was positioned between the flanges to be most damaging to the TB-1 and contents by preventing the flanges from absorbing energy and slowing down the plate before it hits the overpack.

The post-impact deformation is shown in Figure 2-400 and its kinetic energy history in Figure 2-401. The flanges on the overpack deform, and the contents bounce due to the impact of the plate. Zero elements extended beyond the tested Bao-Wierzbicki strain locus. The maximum Tearing Parameter value for this analysis was 3.03e-5, and is below the critical Tearing Parameter value of 1.012 for Ti-6Al-4V, thus T-Ampoule integrity is maintained.

Peak EQPS in the TB-1 vessel is shown in Figure 2-402 to be 27.67e-3, and is localized in the outer contact regions with the redwood overpack. Figure 2-403 is a plot of the Tresca stresses within the TB-1. The maximum Tresca stress in the TB-1 is 172.3 ksi, but there are no through thickness stresses exceeding the limit of 106.6 ksi, which can be seen clearly in the figure. Figure 2-404 is a plot of the Tresca stresses at the time when all of the kinetic energy of the plate has been transferred to the package, just as the plate begins to rebound. The maximum through thickness stress at this time is below 25.0 ksi, below the allowable through thickness stress of 106.6 ksi, as seen in the figure.

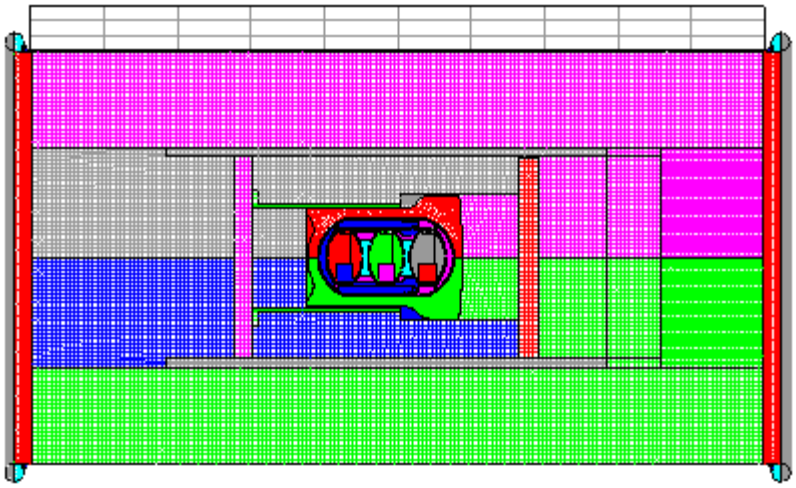

Figure 2-399. Finite Element Mesh for HAC Run 7, SC-1, Side Impact, Support Structure 0°

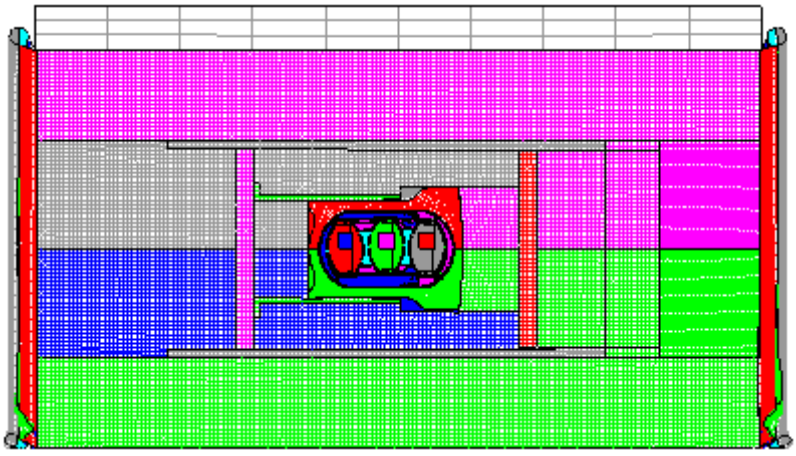

Figure 2-400. Finite Element Mesh for HAC Run 7, SC-1, Side Impact, Support Structure 0° - Final Displacement

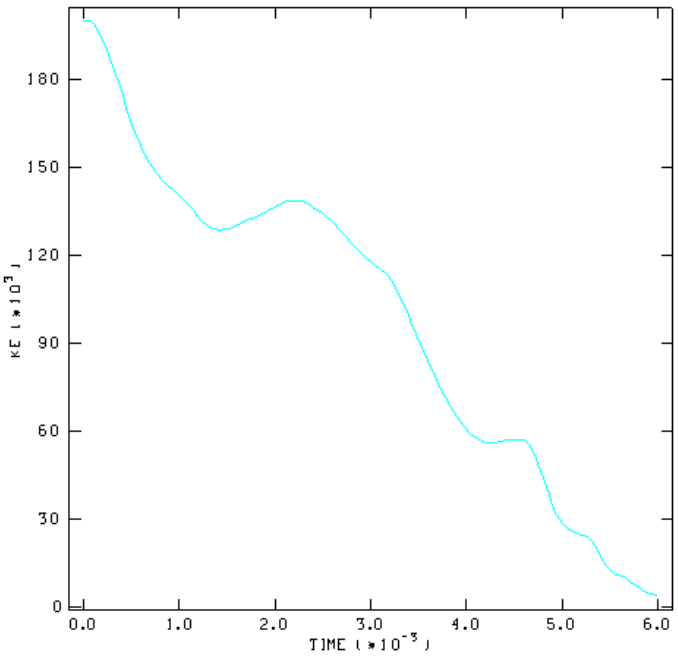

Figure 2-401. Kinetic Energy Time History for HAC Run 7, SC-1, Side Impact, Support Structure 0°

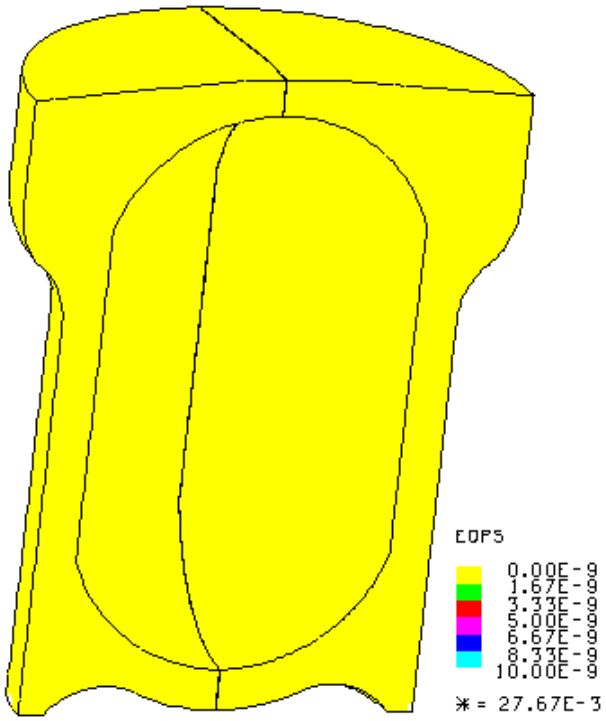

Figure 2-402. Plot of EQPS in TB-1 for HAC Run 7, SC-1, Side Impact, Support Structure 0°

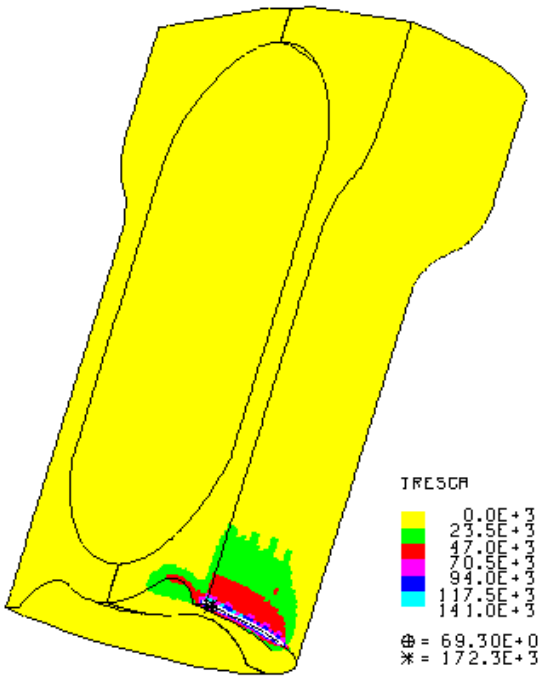

Figure 2-403. Plot of Tresca Stress in the TB-1 for HAC Run 7, SC-1, Side Impact, Support Structure 0°

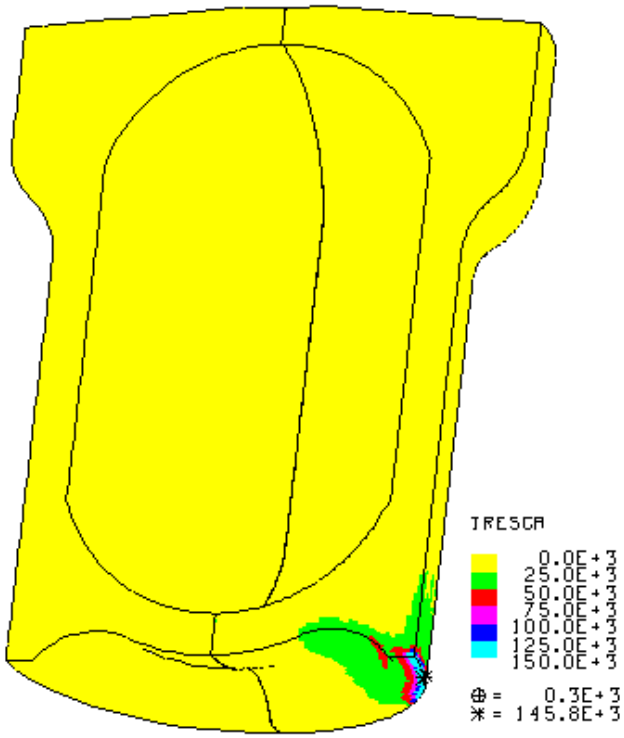

Figure 2-404. Plot of Tresca Stress in the TB-1 for HAC Run 7, SC-1, Side Impact, Support Structure 0° when Plate Velocity Reaches Zero

2.12.5.6.8 HAC- Run 8, SC-1, Side Impact, Support Structure 45°

The dynamic crush side impact HAC analysis run for the SC-1 sample container with its support structure rotated 45° uses the same model as that used for the 4-ft-drop, but the flange is added to both ends so that it available to deform where impacted by the plate and the rigid surface upon which it is resting. The finite element mesh and initial position of the model are shown in Figure 2-405. The Pu contents and support structure within the T-Ampoule are positioned at the bottom of the model because it was considered to be at rest at the time of impact. The plate was positioned between the flanges to be most damaging to the TB-1 and contents by preventing the flanges from absorbing energy and slowing down the plate before it hits the overpack.

The post-impact deformation is shown in Figure 2-406 and its kinetic energy history in Figure 2-407. The flanges on the overpack deform, and the contents bounce due to the impact of the plate. Zero elements extended beyond the tested Bao-Wierzbicki strain locus. The maximum Tearing Parameter value for this analysis was 1.6e-2, and is below the critical Tearing Parameter value of 1.012 for Ti-6Al-4V, thus T-Ampoule integrity is maintained.

Peak EQPS in the TB-1 vessel is shown in Figure 2-408 to be 0.1829, and is localized in the outer contact regions with the redwood overpack. Figures 2-409 and 2-410 are plots of the Tresca stresses within the TB-1. The maximum Tresca stress in the TB-1 is 225.9 ksi (contact modeling artifact), but there are no through thickness stresses exceeding the limit of 106.6 ksi, which can be seen clearly in the figures. Figure 2-411 is a plot of the Tresca stresses at the time when all of the kinetic energy of the plate has been transferred to the package, just as the plate begins to rebound. The maximum through thickness stress at this time is below 33.3 ksi, below the allowable through thickness stress of 106.6 ksi, as seen in the figure.

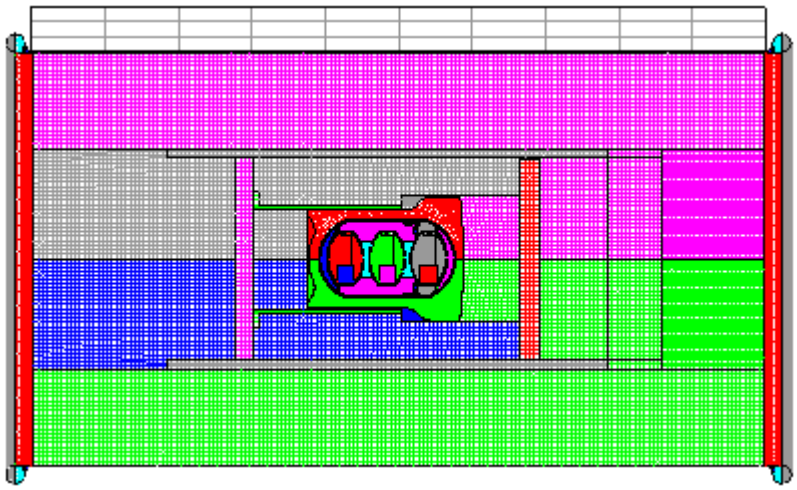

Figure 2-405. Finite Element Mesh for HAC Run 8, SC-1, Side Impact, Support Structure 45°

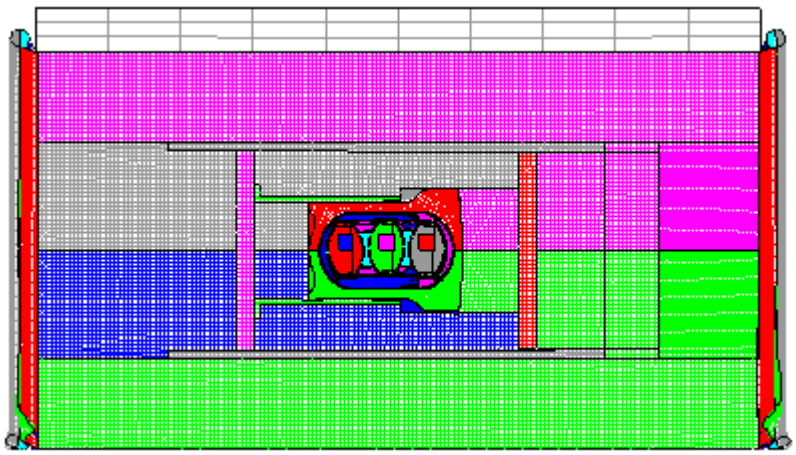

Figure 2-406. Finite Element Mesh for HAC Run 8, SC-1, Side Impact, Support Structure 45° - Final Displacement

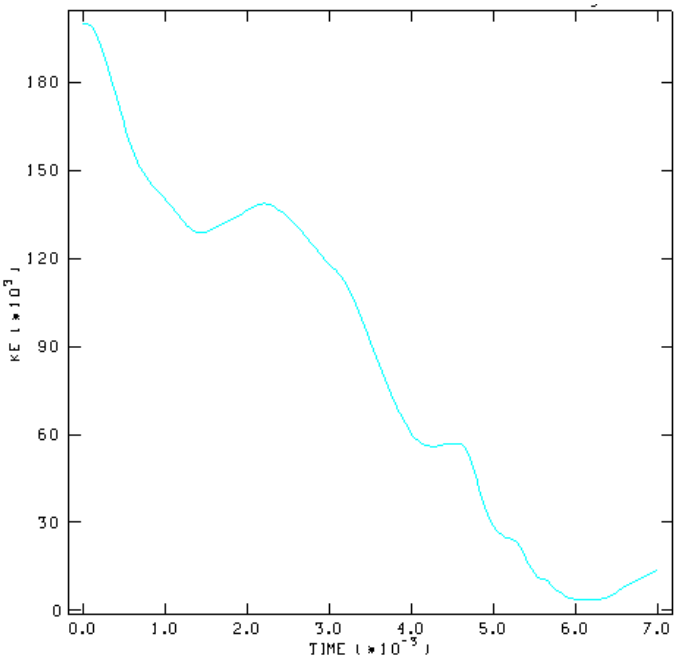

Figure 2-407. Kinetic Energy Time History for HAC Run 8, SC-1, Side Impact, Support Structure 45°

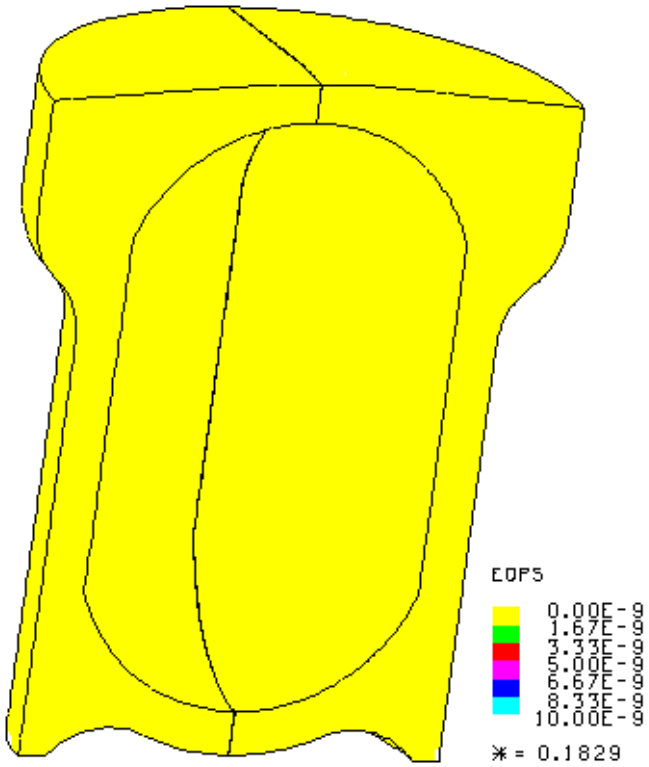

Figure 2-408. Plot of EQPS in TB-1 for HAC Run 8, SC-1, Side Impact, Support Structure 45°

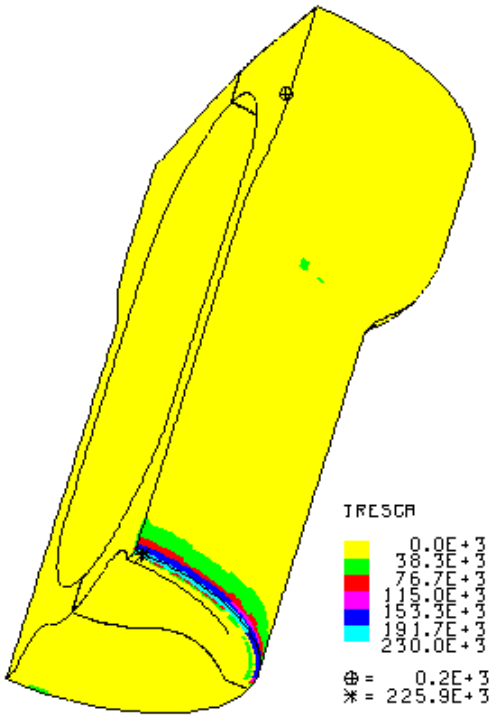

Figure 2-409. Plot of Tresca Stress in TB-1 for HAC Run 8, SC-1, Side Impact, Support Structure 45°

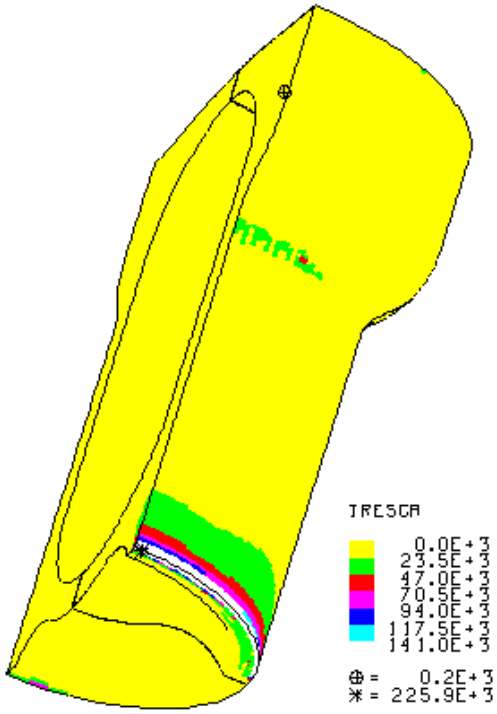

Figure 2-410. Plot of Tresca Stress in TB-1 for HAC Run 8, SC-1, Side Impact, Support Structure 45°

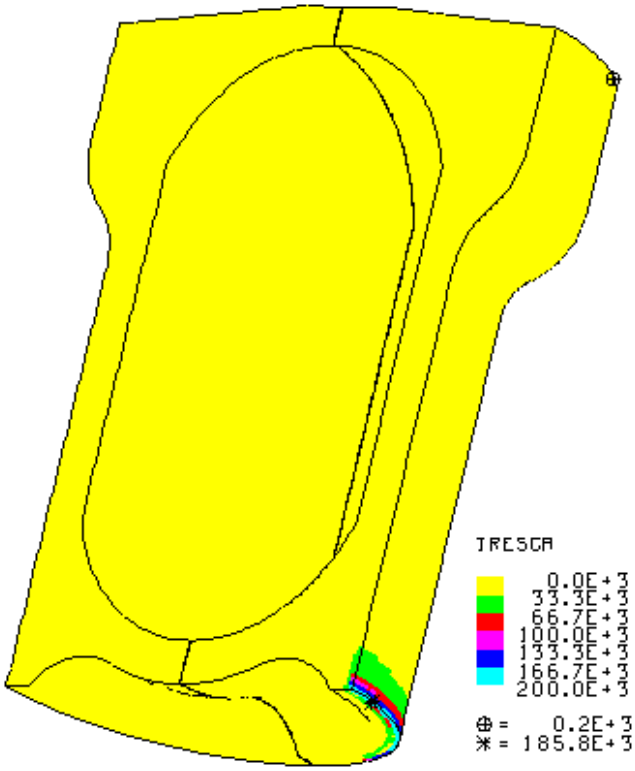

Figure 2-411. Plot of Tresca Stress in TB-1 for HAC Run 8, SC-1, Side Impact, Support Structure 45° when Plate Velocity Reaches Zero

2.12.5.6.9 HAC- Run 9, SC-1, CGOC Impact, Support Structure 0°

The dynamic crush CGOC impact HAC analysis for the SC-1 sample container run uses the same overpack model as those used in HAC runs 1 through 8. The finite element mesh and initial position of the model are shown in Figure 2-412. The Pu contents and support structure within the T-Ampoule are positioned at the bottom of the model because it was considered to be at rest.

The post-impact deformation is shown in Figure 2-413 and its kinetic energy history in Figure 2-414. The flanges on the overpack deform, and the contents bounce due to the impact of the plate. The kinetic energy does not drop completely to zero because the plate is still vibrating and internal contents are still in motion. The plutonium cylinders have bounced off of the top and bottom surface of the sample containers, and the plate is now rebounding slowly with the package, ensuring that the highest containment vessel and contents loadings have occurred.

There was zero EQPS in the T-Ampoule and the TB-1, and the maximum Tearing Parameter was 0. Figure 2-415 is a plot of the Tresca stresses within the TB-1. The maximum Tresca stress in the TB-1 is 146.5 Ksi, but there are no through thickness stresses exceeding the limit of 106.6 ksi, which can be seen clearly in the figure. Figure 2-416 is a plot of the Tresca stresses at the time when all of the kinetic energy of the plate has been transferred to the package, just as the plate begins to rebound. The maximum through thickness stress at this time is below 8.33 ksi, below the allowable through thickness stress of 106.6 ksi, as seen in the figure.

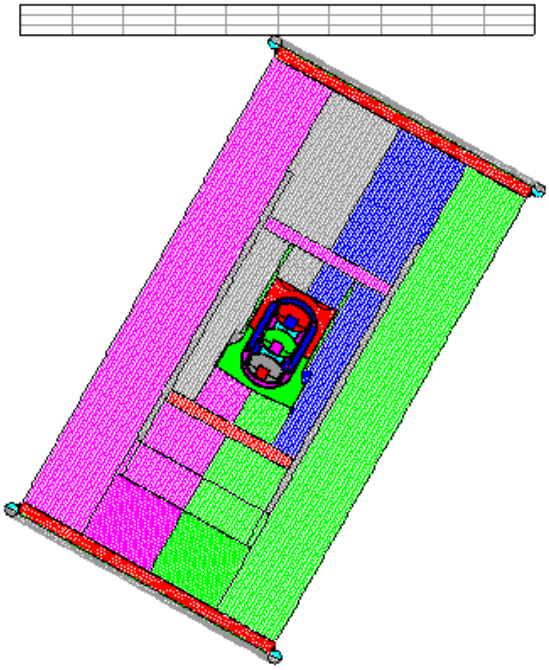

Figure 2-412. Finite Element Mesh for HAC Run 9, SC-1, CGOC Impact, Support Structure 0°

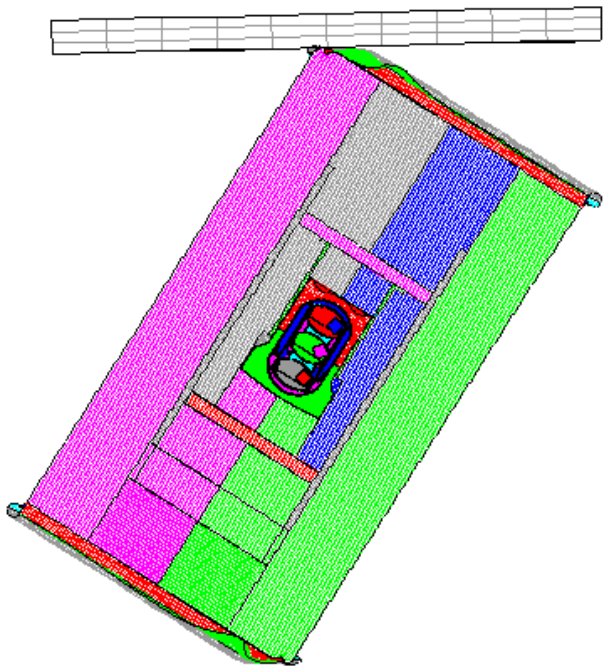

Figure 2-413. Finite Element Mesh for HAC Run 9, SC-1, CGOC Impact, Support Structure 0° - Final Displacement

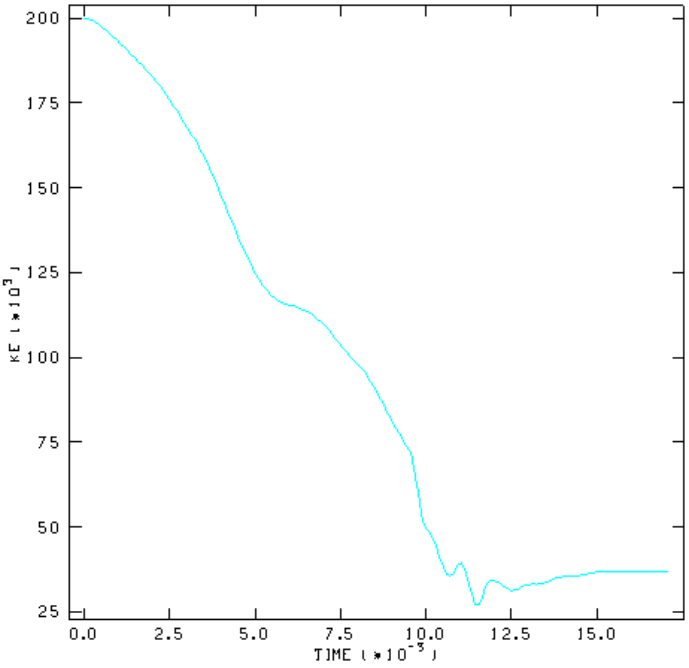

Figure 2-414. Kinetic Energy Time History for HAC Run 9, SC-1, CGOC Impact, Support Structure 0°

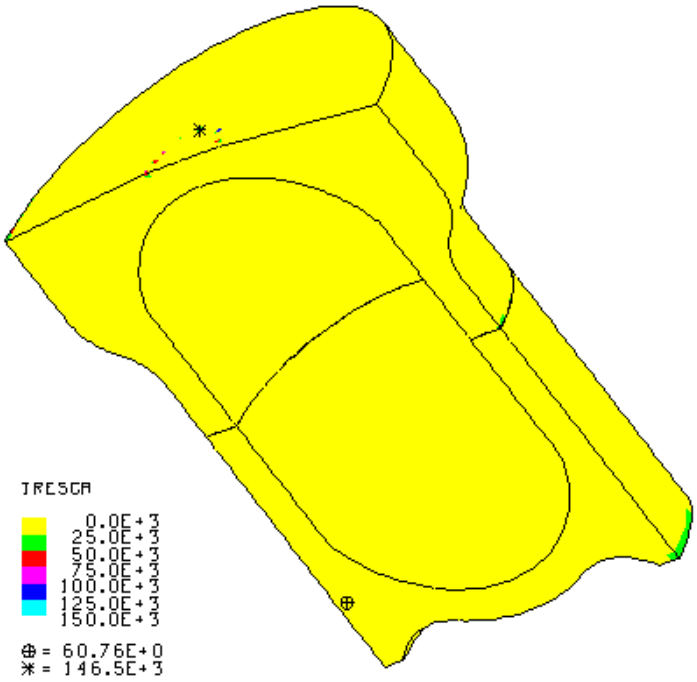

Figure 2-415. Tresca Stress for HAC Run 9, SC-1, CGOC Impact, Support Structure 0°

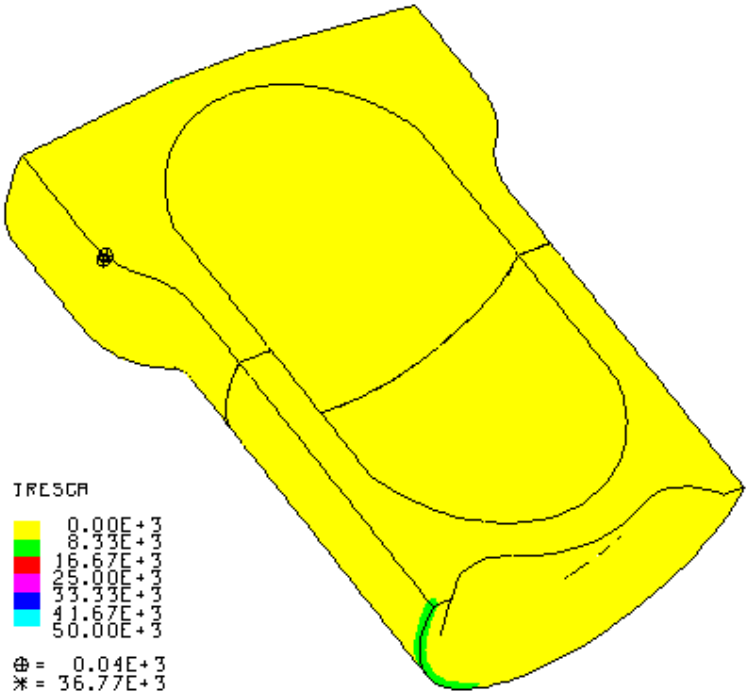

Figure 2-416. Plot of Tresca Stress in the TB-1 for HAC Run 9, SC-1, CGOC Impact, Support Structure 0° when Plate Velocity Reaches Zero

2.12.5.6.10 HAC- Run 10, SC-1, CGOC Impact, Support Structure 45°

The dynamic crush CGOC impact HAC analysis for the SC-1 sample container run uses the same overpack model as those used in HAC runs 1 through 9. The finite element mesh and initial position of the model are shown in Figure 2-417. The Pu contents and support structure within the T-Ampoule are positioned at the bottom of the model because it was considered to be at rest.

The post-impact deformation is shown in Figure 2-418 and its kinetic energy history in Figure 2-419. The flanges on the overpack deform, and the contents bounce due to the impact of the plate. The kinetic energy does not drop completely to zero because the plate is still vibrating and internal contents are still in motion. The plutonium cylinders have bounced off of the top and bottom surface of the sample containers, and the plate is now rebounding slowly with the package, ensuring that the highest containment vessel and contents loadings have occurred.

There was zero EQPS in the T-Ampoule and the TB-1, and the maximum Tearing Parameter was 0. Figure 2-420 is a plot of the Tresca stresses within the TB-1. The maximum Tresca stress in the TB-1 is 158.8 ksi, but there are no through thickness stresses exceeding the limit of 106.6 ksi, which can be seen clearly in the figure. Figure 2-421 is a plot of the Tresca stresses at the time when all of the kinetic energy of the plate has been transferred to the package, just as the plate begins to rebound. The maximum through thickness stress at this time is below 16.7 ksi, below the allowable through thickness stress of 106.6 ksi, as seen in the figure.

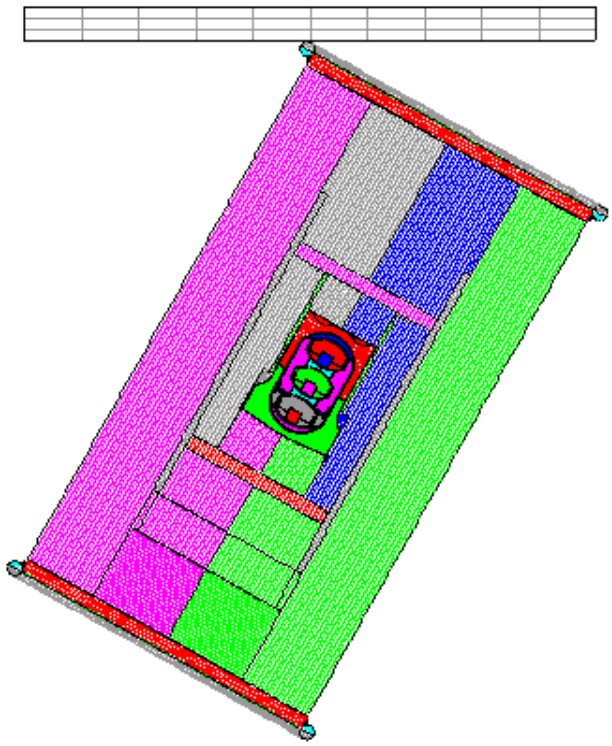

Figure 2-417. Finite Element Mesh for HAC Run 10, SC-1, CGOC Impact, Support Structure 45°

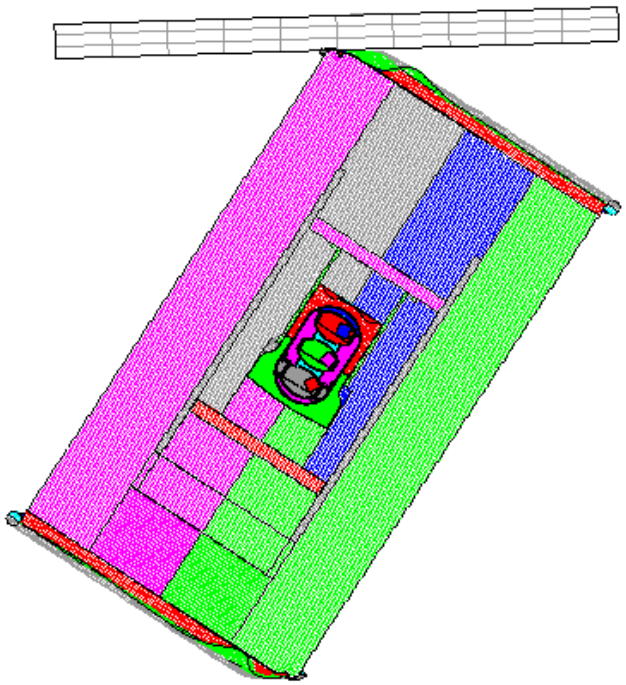

Figure 2-418. Finite Element Mesh for HAC Run 10, SC-1, CGOC Impact, Support Structure 45° - Final Displacement

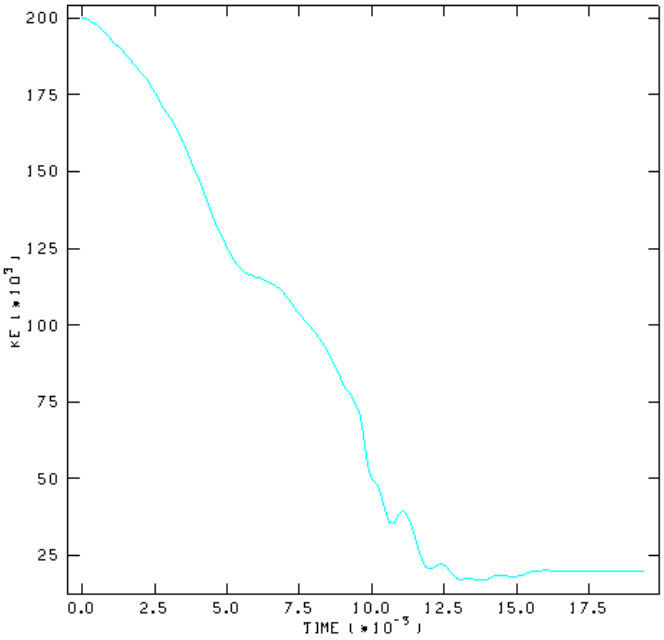

Figure 2-419. Kinetic Energy Time History for HAC Run 10, SC-1, CGOC Impact, Support Structure 45°

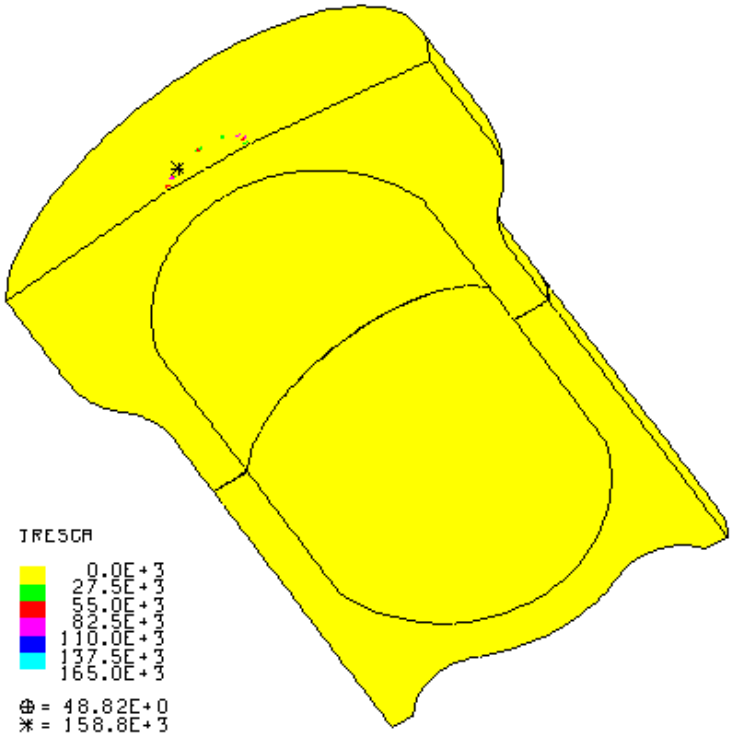

Figure 2-420. Plot of Tresca Stress in the TB-1 for HAC Run 10, SC-1, CGOC Impact, Support Structure 45°

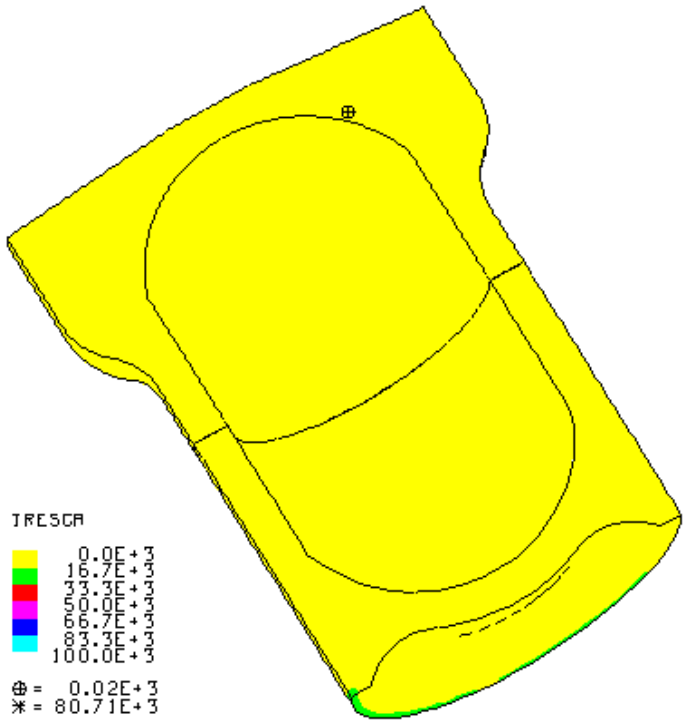

Figure 2-421. Plot of Tresca Stress in the TB-1 for HAC Run 10, SC-1, CGOC Impact, Support Structure 45° when Plate Velocity Reaches Zero

2.12.5.6.11 HAC- Run 11, 831 g Plutonium Metal Hollow Cylinder, End Impact

The dynamic crush end impact HAC analysis run for the 831 g plutonium metal hollow cylinder uses the same model for the overpack as the one used in the previous 10 runs. The TB-1, T-Ampoule, and plutonium metal hollow cylinder are the same model as that used in the aircraft analysis. The finite element mesh and initial position of the model are shown in Figure 2-422. The plutonium metal hollow cylinder within the T-Ampoule is positioned at the bottom of the model because it was considered to be at rest at the time of impact.

The post-impact deformation is shown in Figure 2-423 and its kinetic energy history in Figure 2-424. The flanges on the overpack deform, and the cylinder bounces due to the impact of the plate. Zero elements extended beyond the tested Bao-Wierzbicki strain locus. The maximum Tearing Parameter value for this analysis was 0.

Peak EQPS in the TB-1 vessel is shown in Figure 2-425 to be 2.68e-3, and is localized in the outer contact regions with the redwood overpack. Figure 2-426 plots the Tresca stresses within the TB-1. The maximum Tresca stress in the TB-1 is 156.7 ksi, but there are no through thickness stresses exceeding the limit of 106.6 ksi, which can be seen clearly in the figure. Figure 2-427 is a plot of the Tresca stresses at the time when all of the kinetic energy of the plate has been transferred to the package, just as the plate begins to rebound. The maximum through thickness stress at this time is below 25.0 ksi, below the allowable through thickness stress of 106.6 ksi, as seen in the figure.

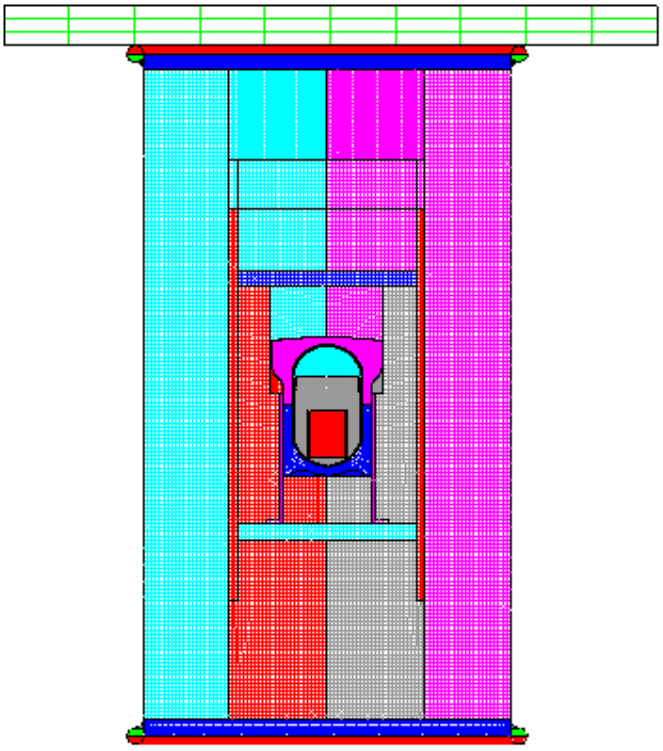

Figure 2-422. Finite Element Mesh for HAC Run 11, 831 g Plutonium Metal Hollow Cylinder, End Impact

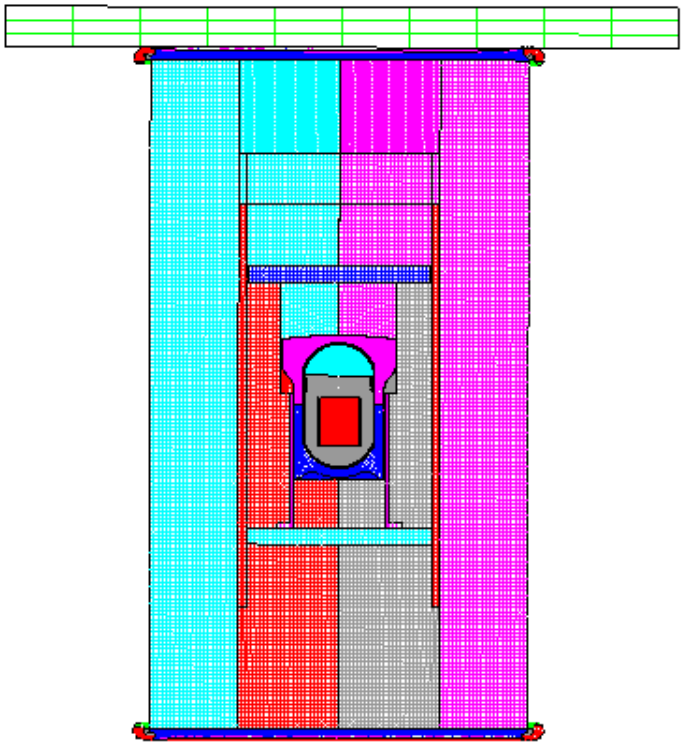

Figure 2-423. Finite Element Mesh for HAC Run 11, 831 g, Plutonium Metal Hollow Cylinder, End Impact – Final Displacement

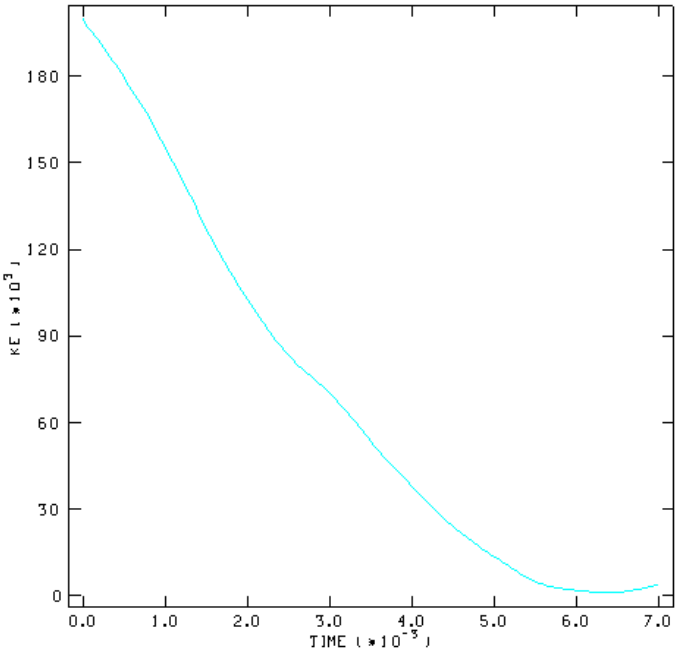

Figure 2-424. Kinetic Energy Time History for HAC Run 11, 831 g, Plutonium Metal Hollow Cylinder, End Impact

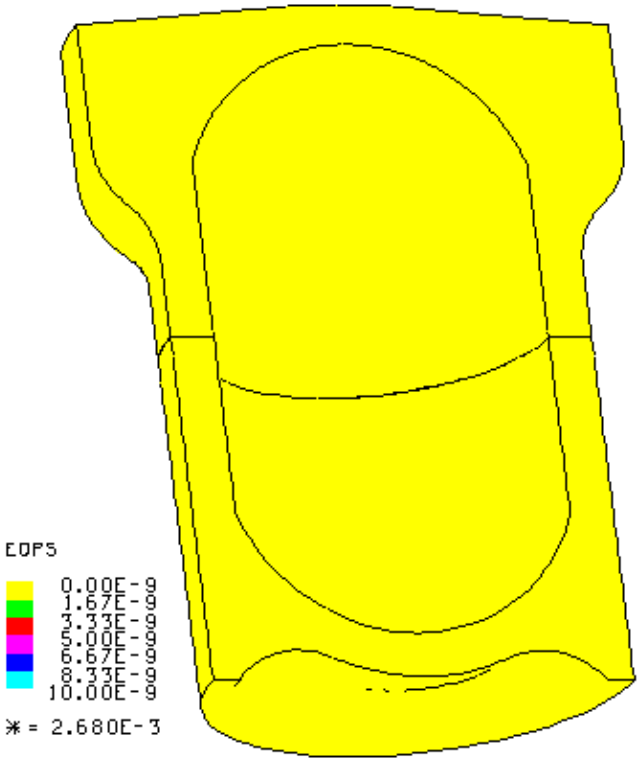

Figure 2-425. Plot of EQPS in the TB-1 for HAC Run 11, 831 g, Plutonium Metal Hollow Cylinder, End Impact

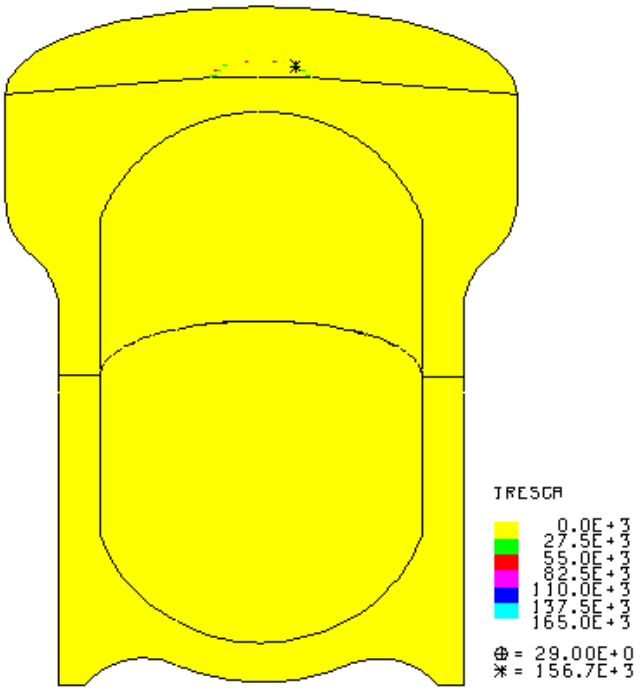

Figure 2-426. Plot of Tresca Stress in the TB-1 for HAC Run 11, 831 g, Plutonium Metal Hollow Cylinder, End Impact

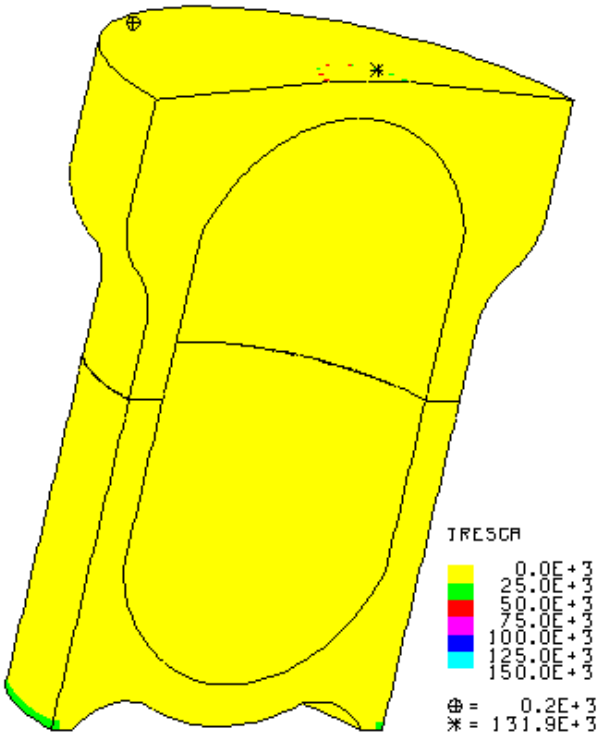

Figure 2-427. Plot of Tresca Stress in the TB-1 for HAC Run 11, 831 g Plutonium Metal Hollow Cylinder, End Impact when Plate Velocity Reaches Zero

2.12.5.6.12 HAC- Run 12, 831 g Plutonium Metal Hollow Cylinder, Side Impact

The dynamic crush side impact HAC analysis run for the 831 g plutonium metal hollow cylinder uses the same model for the overpack as the one used in the previous 11 runs. The TB-1, T-Ampoule, and plutonium metal hollow cylinder are the same model as that used in the aircraft analysis. The finite element mesh and initial position of the model are shown in Figure 2-428. The plutonium metal hollow cylinder within the T-Ampoule is positioned at the bottom of the model because it was considered to be at rest at the time of impact. The plate was positioned between the flanges to be most damaging to the TB-1 and contents by preventing the flanges from absorbing energy and slowing down the plate before it hits the overpack.

The post-impact deformation is shown in Figure 2-429 and its kinetic energy history in Figure 2-430. The flanges on the overpack deform, and the cylinder bounces due to the impact of the plate. Zero elements extended beyond the tested Bao-Wierzbicki strain locus. The maximum Tearing Parameter value for this analysis was 2.94e-6, and is below the critical Tearing Parameter value of 1.012 for Ti-6Al-4V, thus T-Ampoule integrity is maintained.

Peak EQPS in the TB-1 vessel is shown in Figure 2-431 to be 32.78e-3, and is localized in the outer contact regions with the redwood overpack. Figures 2-432 and 2-433 plot the Tresca stresses within the TB-1. The maximum Tresca stress in the TB-1 is 173.8 ksi, but there are no through thickness stresses exceeding the limit of 106.6 ksi, which can be seen clearly in the figure. Figure 2-434 is a plot of the Tresca stresses at the time when all of the kinetic energy of the plate has been transferred to the package, just as the plate begins to rebound. The maximum

through thickness stress at this time is below 20.8 ksi, below the allowable through thickness stress of 106.6 ksi, as seen in the figure.

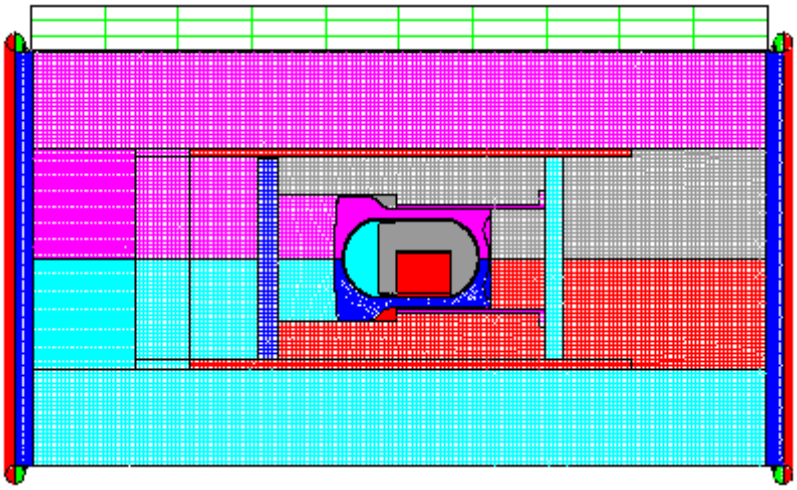

Figure 2-428. Finite Element Mesh for HAC Run 12, 831 g, Plutonium Metal Hollow Cylinder, Side Impact

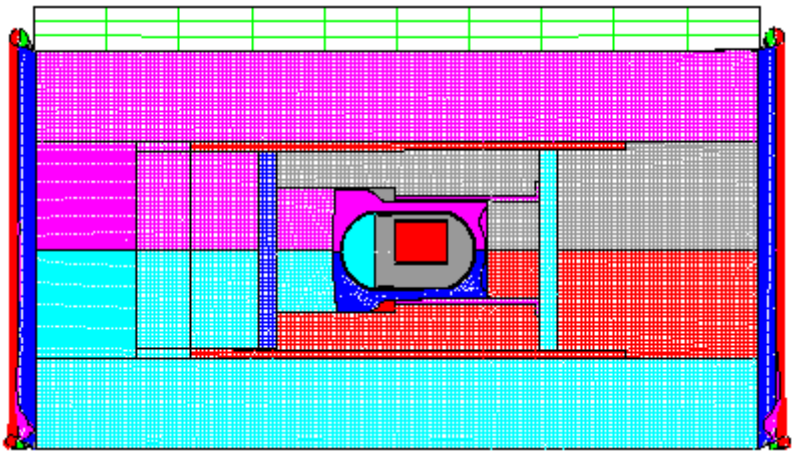

Figure 2-429. Finite Element Mesh for HAC Run 12, 831 g, Plutonium Metal Hollow Cylinder, Side Impact – Final Displacement

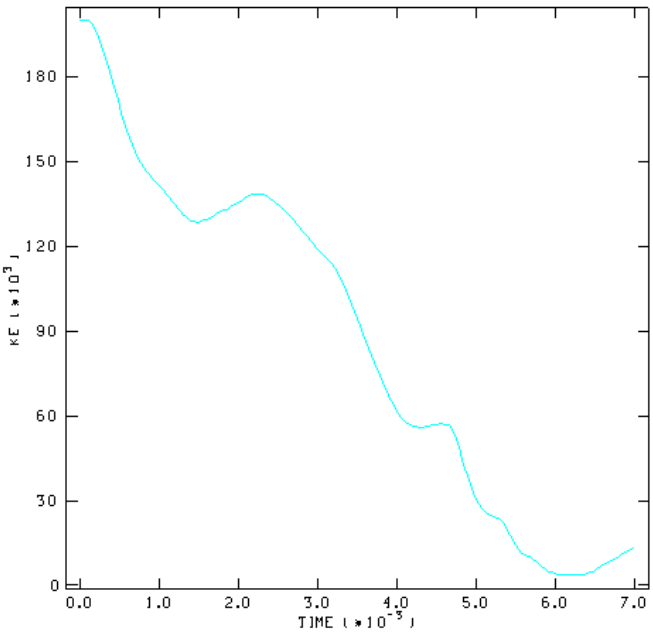

Figure 2-430. Kinetic Energy Time History for HAC Run 12, 831 g, Plutonium Metal Hollow Cylinder, Side Impact

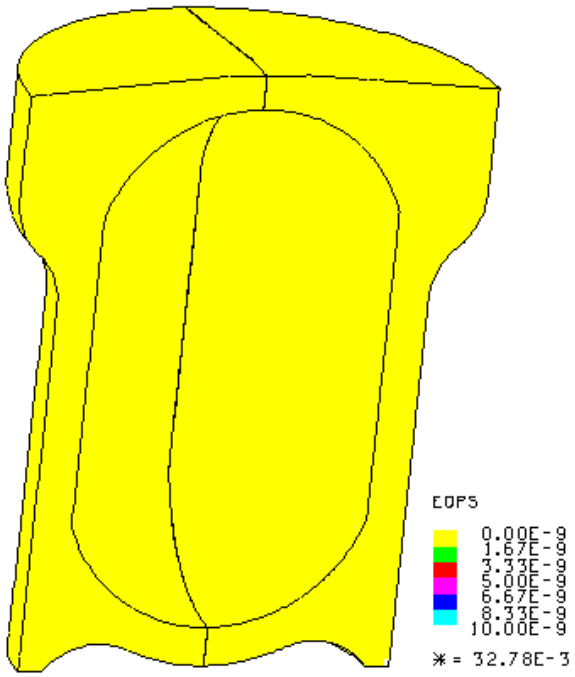

Figure 2-431. Plot of EQPS in the TB-1 for HAC Run 12, 831 g, Plutonium Metal Hollow Cylinder, Side Impact

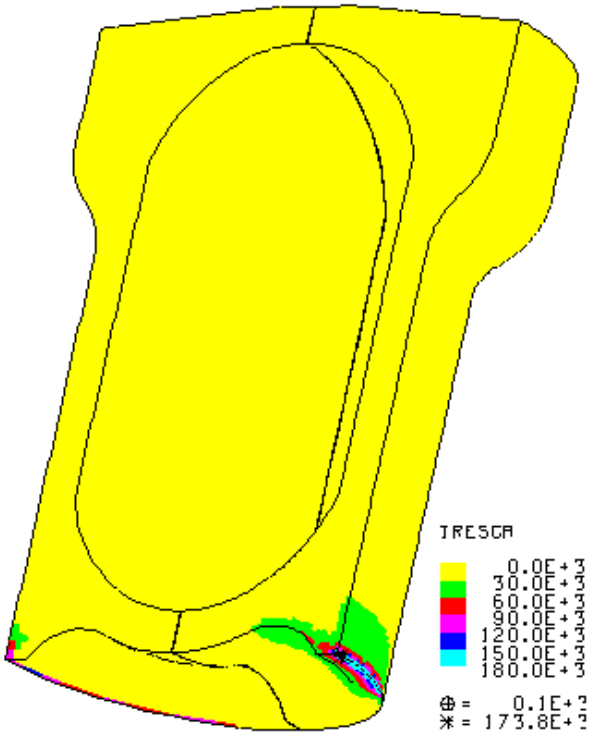

Figure 2-432. Plot of Tresca Stress in the TB-1 for HAC Run 12, 831 g Plutonium Metal Hollow Cylinder, Side Impact

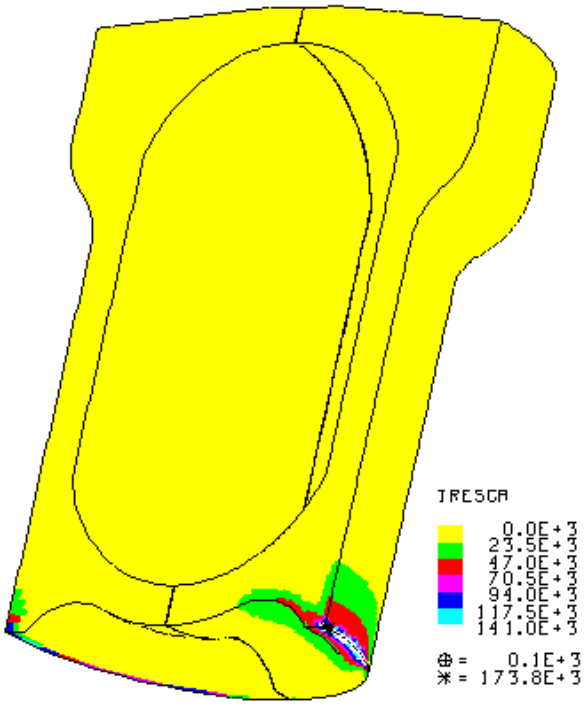

Figure 2-433. Plot of Tresca Stress for HAC Run 12, 831 g Plutonium Metal Hollow Cylinder, Side Impact

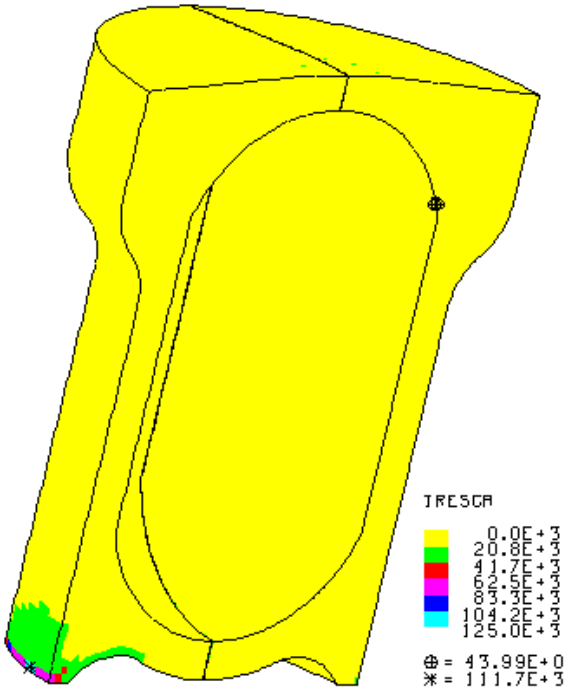

Figure 2-434. Plot of Tresca Stress for HAC Run 12, 831 g Plutonium Metal Hollow Cylinder, Side Impact when Plate Velocity Reaches Zero

2.12.5.6.13 HAC- Run 13, 831 g Angled Plutonium Metal Hollow Cylinder, End Impact

The dynamic crush end impact HAC analysis run for the 831 g angled plutonium metal hollow cylinder uses the same model for the overpack as the one used in the previous 12 runs. The TB-1, T-Ampoule, and plutonium metal hollow cylinder are the same model as that used in the aircraft analysis. The finite element mesh and initial position of the model are shown in Figure 2-435. The plutonium metal hollow cylinder within the T-Ampoule is positioned at the bottom of the model because it was considered to be at rest at the time of impact.

The post-impact deformation is shown in Figure 2-436 and its kinetic energy history in Figure 2-437. The flanges on the overpack deform, and the contents bounce due to the impact of the plate. Zero elements extended beyond the tested Bao-Wierzbicki strain locus. The maximum Tearing Parameter value for this analysis was 0.

Peak EQPS in the TB-1 vessel is shown in Figure 2-438 to be 2.389e-3, and is localized in the outer contact regions with the redwood overpack. Figure 2-439 plots the Tresca stresses within the TB-1. The maximum Tresca stress in the TB-1 is 155.6 ksi, but there are no through thickness stresses exceeding the limit of 106.6 ksi, which can be seen clearly in the figure. Figure 2-440 is a plot of the Tresca stresses at the time when all of the kinetic energy of the plate has been transferred to the package, just as the plate begins to rebound. The maximum through thickness stress at this time is below 25.0 ksi, below the allowable through thickness stress of 106.6 ksi, as seen in the figure.

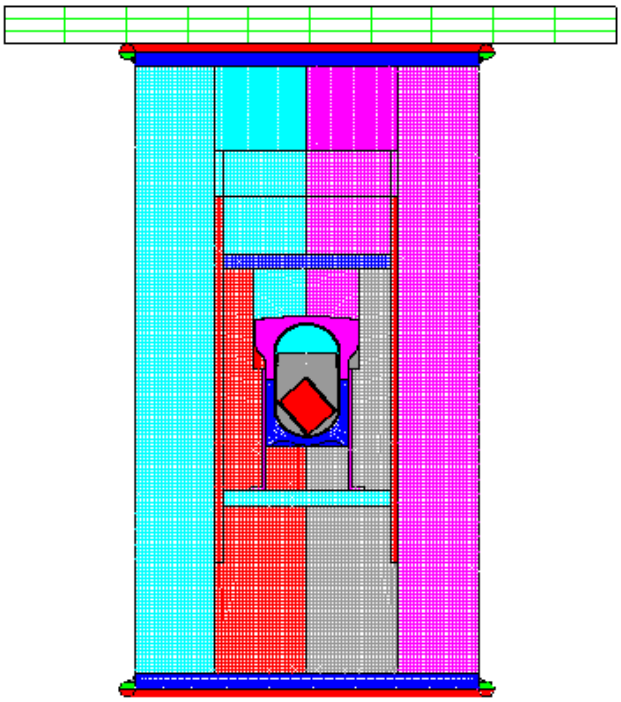

Figure 2-435. Finite Element Mesh for HAC Run 13, 831 g, Angled, Plutonium Metal Hollow Cylinder, End Impact

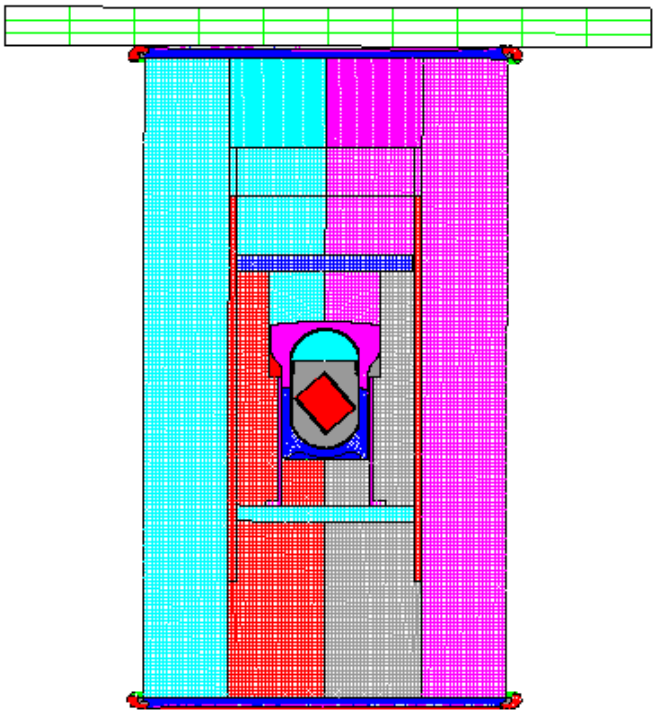

Figure 2-436. Finite Element Mesh for HAC Run 13, 831 g, Angled, Plutonium Metal Hollow Cylinder, End Impact – Final Displacement

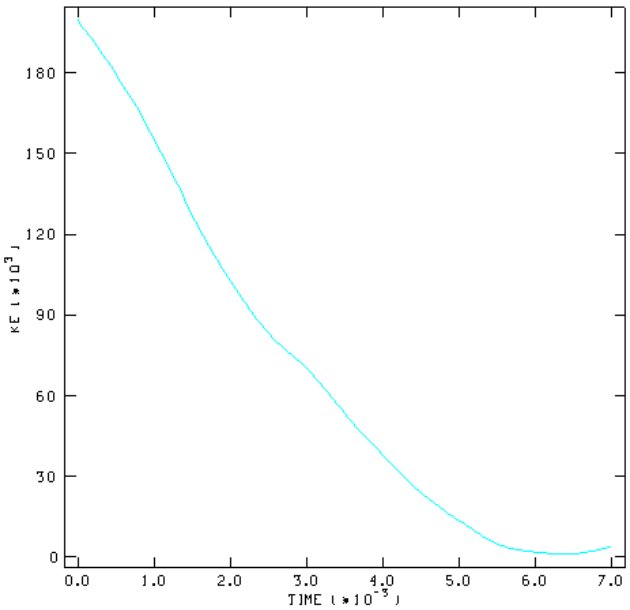

Figure 2-437. Kinetic Energy Time History for HAC Run 13, 831 g, Angled, Plutonium Metal Hollow Cylinder, End Impact

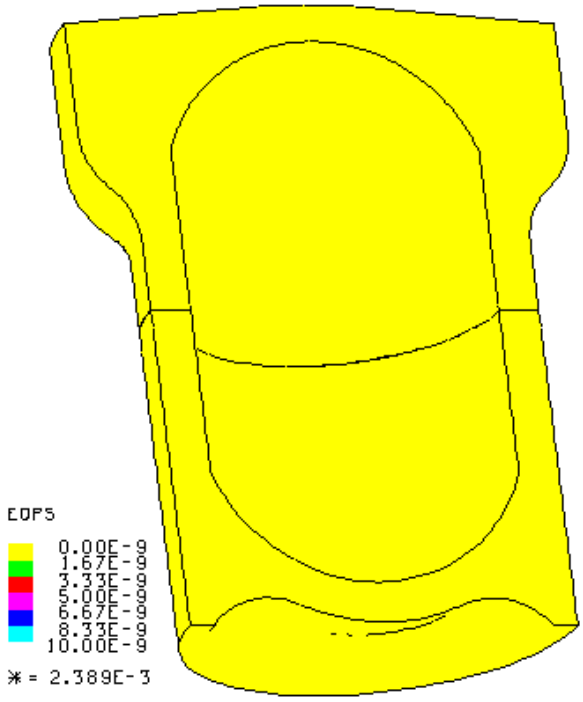

Figure 2-438. Plot of EQPS in the TB-1 for HAC Run 13, 831 g, Angled, Plutonium Metal Hollow Cylinder, End Impact

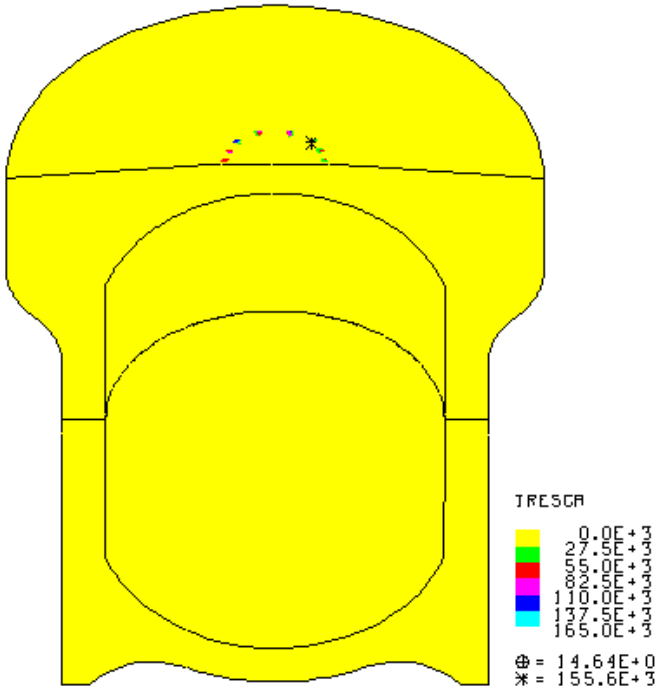

Figure 2-439. Plot of Tresca Stress in the TB-1 for HAC Run 13, 831 g, Angled, Plutonium Metal Hollow Cylinder, End Impact

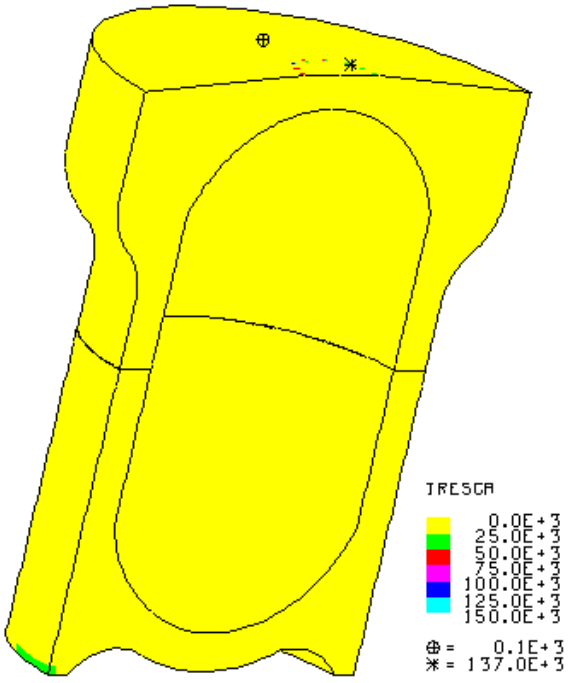

Figure 2-440. Plot of Tresca Stress in the TB-1 for HAC Run 13, 831 g Angled Plutonium Metal Hollow Cylinder, End Impact when Plate Velocity Reaches Zero

2.12.5.6.14 HAC- Run 14, 831 g Angled Plutonium Metal Hollow Cylinder, Side Impact

The dynamic crush side impact HAC analysis run for the 831 g angled plutonium metal hollow cylinder uses the same model for the overpack as the one used in the previous 13 runs. The TB-1, T-Ampoule, and plutonium metal hollow cylinder are the same model as that used in the aircraft analysis. The finite element mesh and initial position of the model are shown in Figure 2-441. The plutonium metal hollow cylinder within the T-Ampoule is positioned at the bottom of the model because it was considered to be at rest at the time of impact. The plate was positioned between the flanges to be most damaging to the TB-1 and contents by preventing the flanges from absorbing energy and slowing down the plate before it hits the overpack.

The post-impact deformation is shown in Figure 2-442 and its kinetic energy history in Figure 2-443. The flanges on the overpack deform, and the cylinder bounces due to the impact of the plate. Zero elements extended beyond the tested Bao-Wierzbicki strain locus. The maximum Tearing Parameter value for this analysis was 2.01e-2, and is below the critical Tearing Parameter value of 1.012 for Ti-6Al-4V, thus T-Ampoule integrity is maintained.

Peak EQPS in the TB-1 vessel is shown in Figure 2-444 to be 31.46e-3, and is localized in the outer contact regions with the redwood overpack. Figure 2-445 plots the Tresca stresses within the TB-1. The maximum Tresca stress in the TB-1 is 172.5 ksi, but there are no through thickness stresses exceeding the limit of 106.6 ksi, which can be seen clearly in the figure. Figure 2-446 is a plot of the Tresca stresses at the time when all of the kinetic energy of the plate has been transferred to the package, just as the plate begins to rebound. The maximum through thickness stress at this time is below 25.0 ksi, below the allowable through thickness stress of 106.6 ksi, as seen in the figure.

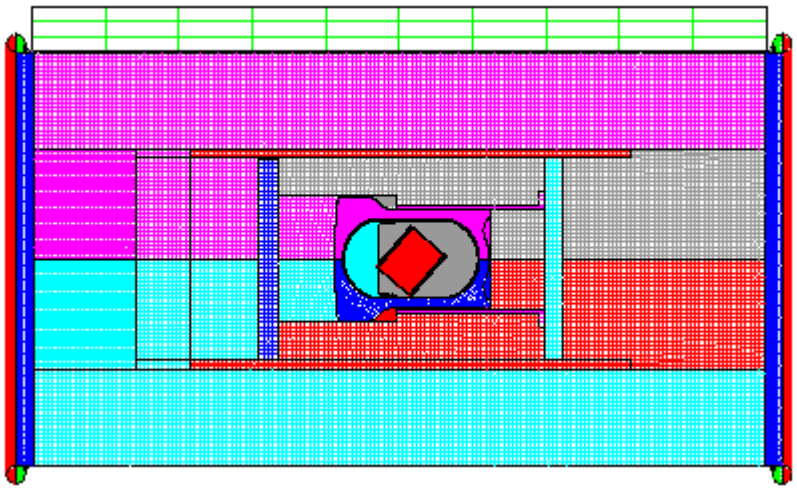

Figure 2-441. Finite Element Mesh for HAC Run 14, 831 g Angled Plutonium Metal Hollow Cylinder, Side Impact

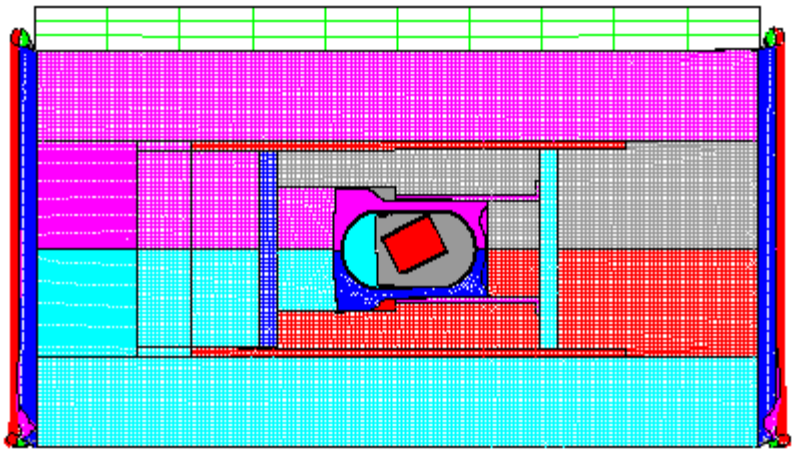

Figure 2-442. Finite Element Mesh for HAC Run 14, 831 g Angled Plutonium Metal Hollow Cylinder, Side Impact – Final Displacement

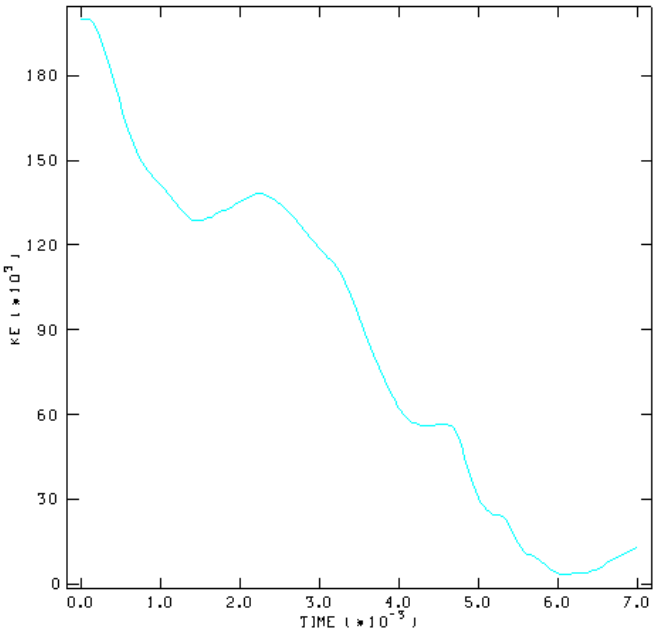

Figure 2-443. Kinetic Energy Time History for HAC Run 14, 831 g Angled Plutonium Metal Hollow Cylinder, Side Impact

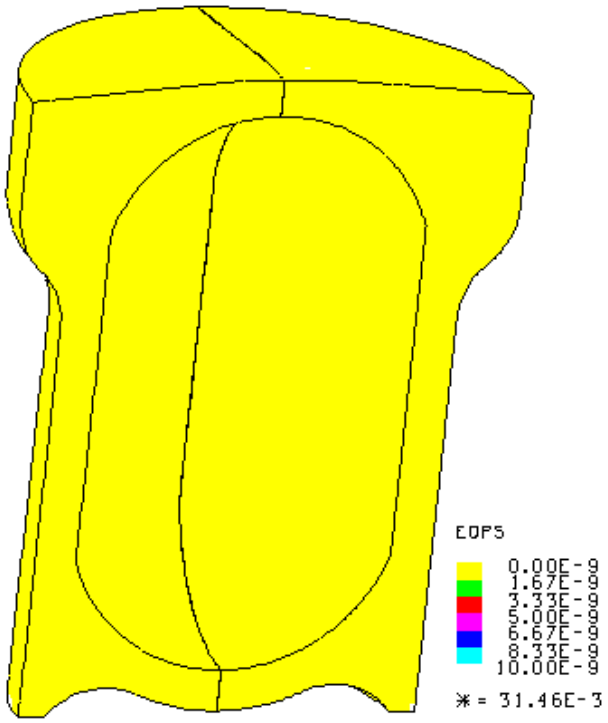

Figure 2-444. Plot of EQPS in the TB-1 for HAC Run 14, 831 g Angled Plutonium Metal Hollow Cylinder, Side Impact

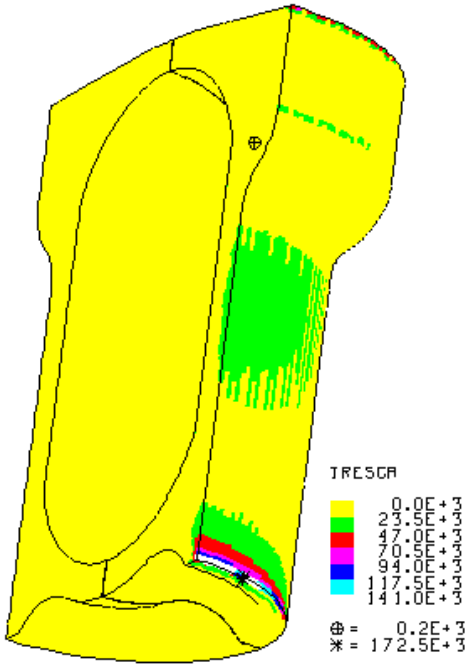

Figure 2-445. Plot of Tresca Stress in the TB-1 for HAC Run 14, 831 g Angled, Plutonium Metal Hollow Cylinder, Side Impact

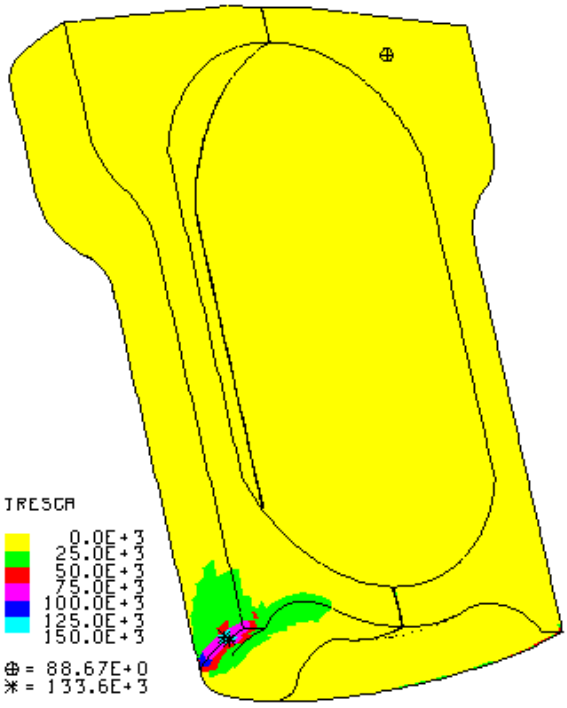

Figure 2-446. Plot of Tresca Stress in the TB-1 for HAC Run 14, 831 g Angled Plutonium Metal Hollow Cylinder, Side Impact when Plate Velocity Reaches Zero

2.12.5.6.15 HAC- Run 15, 831 g Angled Plutonium Metal Hollow Cylinder, CGOC Impact

The dynamic crush CGOC impact HAC analysis run for the 831 g angled plutonium metal hollow cylinder uses the same overpack model as those used in HAC runs 1 through 14. The finite element mesh and initial position of the model are shown in Figure 2-447. The plutonium metal hollow cylinder within the T-Ampoule is positioned at the bottom of the model because it was considered to be at rest.

The post-impact deformation is shown in Figure 2-448 and its kinetic energy history in Figure 2-449. The flanges on the overpack deform, and the cylinder bounces due to the impact of the plate. The kinetic energy does not drop completely to zero because the plate is still vibrating and internal contents are still in motion. The plutonium metal hollow cylinder has bounced off of the top and bottom surface of the T-Ampoule, and the plate is now rebounding slowly with the package, ensuring that the highest containment vessel and contents loadings have occurred.

There was zero EQPS in the T-Ampoule and the TB-1, and the maximum Tearing Parameter was 0. Figure 2-450 is a plot of the Tresca stresses within the TB-1. The maximum Tresca stress in the TB-1 is 147.1 ksi, but there are no through thickness stresses exceeding the limit of 106.6 ksi, which can be seen clearly in the figure. Figure 2-451 is a plot of the Tresca stresses at the time when all of the kinetic energy of the plate has been transferred to the package, just as the plate begins to rebound. The maximum through thickness stress at this time is below 16.7 ksi, below the allowable through thickness stress of 106.6 ksi, as seen in the figure.

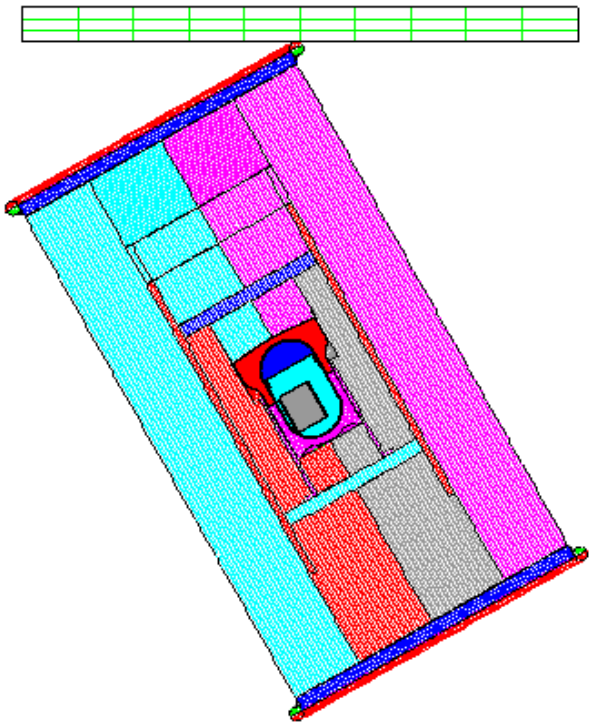

Figure 2-447. Finite Element Mesh for HAC Run 15, 831 g Angled Plutonium Metal Hollow Cylinder, CGOC Impact

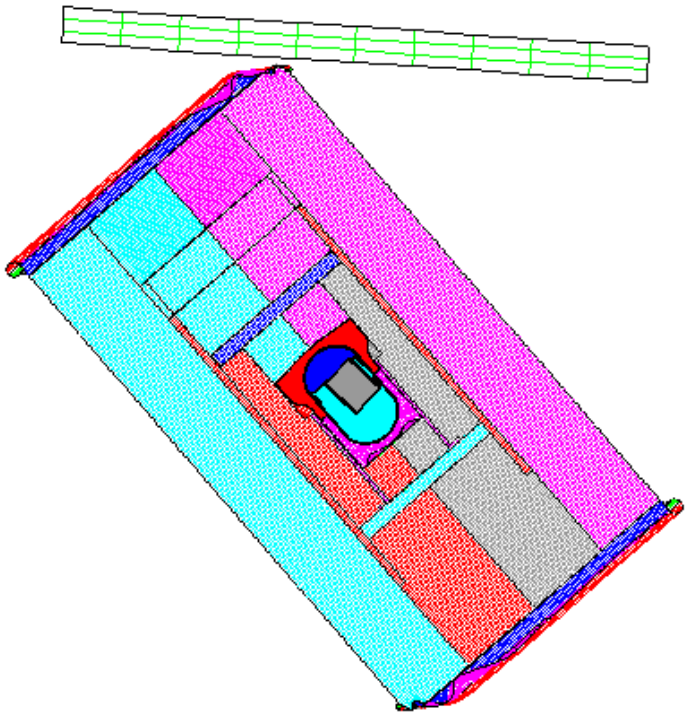

Figure 2-448. Finite Element Mesh for HAC Run 15, 831 g Angled Plutonium Metal Hollow Cylinder, CGOC Impact – Final Displacement

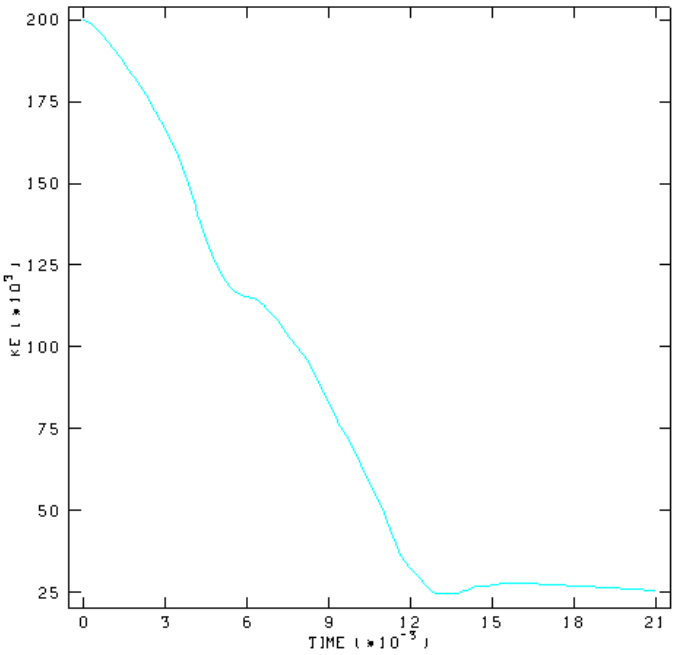

Figure 2-449. Kinetic Energy Time History for HAC Run 15, 831 g Angled Plutonium Metal Hollow Cylinder, CGOC Impact

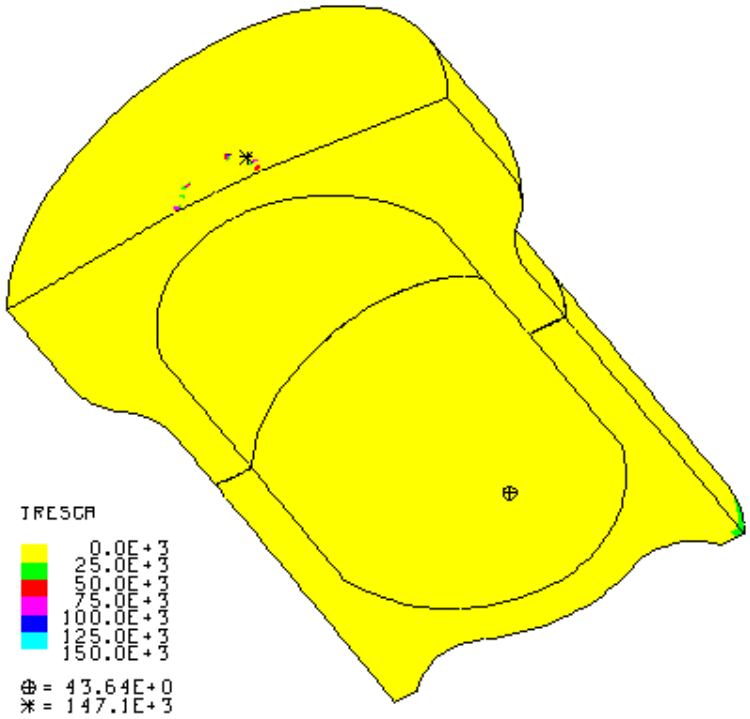

Figure 2-450. Plot of Tresca Stress in the TB-1 for HAC Run 15, 831 g Angled Plutonium Metal Hollow Cylinder, CGOC Impact

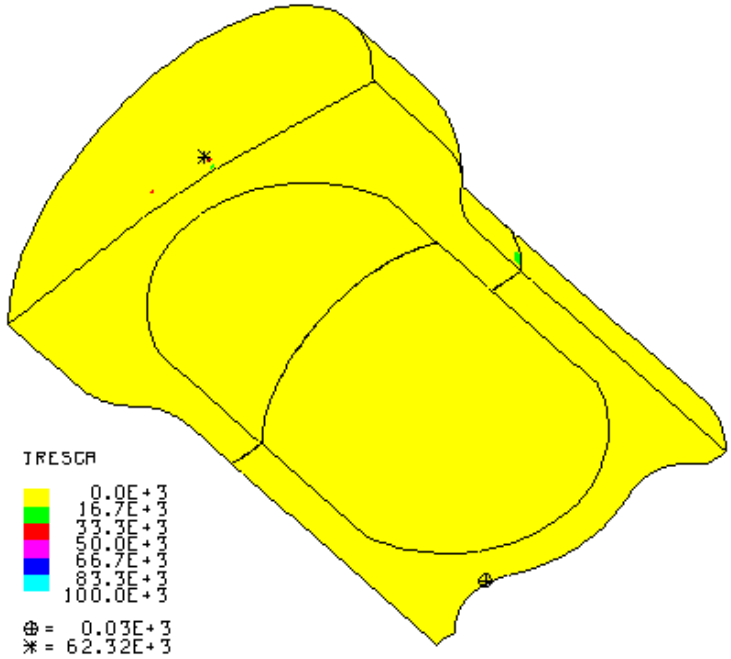

Figure 2-451. Plot of Tresca Stress in the TB-1 for HAC Run 15, 831 g Angled Plutonium Metal Hollow Cylinder, CGOC Impact when Plate Velocity Reaches Zero

2.12.5.6.16 HAC- Run 16, 731 g Plutonium Metal Hollow Cylinder, End Impact

The dynamic crush end impact HAC analysis run for the 731 g angled plutonium metal hollow cylinder uses the same model for the overpack as the one used in the previous 15 runs. The TB-1, T-Ampoule, and plutonium metal hollow cylinder are the same model as that used in the aircraft analysis. The finite element mesh and initial position of the model are shown in Figure 2-452. The plutonium metal hollow cylinder within the T-Ampoule is positioned at the bottom of the model because it was considered to be at rest at the time of impact.

The post-impact deformation is shown in Figure 2-453 and its kinetic energy history in Figure 2-454. The flanges on the overpack deform, and the cylinder bounces due to the impact of the plate. Zero elements extended beyond the tested Bao-Wierzbicki strain locus. The maximum Tearing Parameter value for this analysis was 0.

Peak EQPS in the TB-1 vessel is shown in Figures 2-455 and 2-456 to be 2.237e-3, and is localized in the outer contact regions with the redwood overpack. Figure 2-457 plots the Tresca stresses within the TB-1. The maximum Tresca stress in the TB-1 is 157.2 ksi, but there are no through thickness stresses exceeding the limit of 106.6 ksi, which can be seen clearly in the figure. Figure 2-458 is a plot of the Tresca stresses at the time when all of the kinetic energy of the plate has been transferred to the package, just as the plate begins to rebound. The maximum through thickness stress at this time is below 25.0 ksi, below the allowable through thickness stress of 106.6 ksi, as seen in the figure.

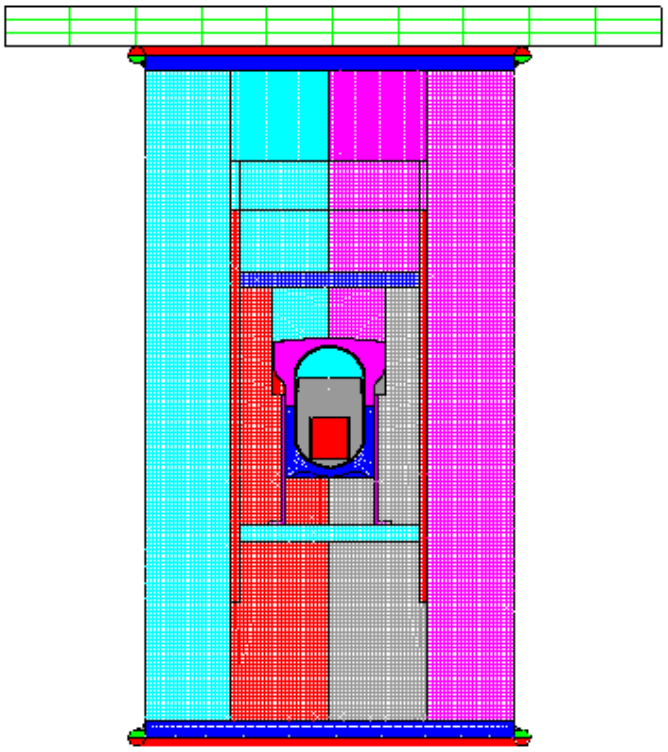

Figure 2-452. Finite Element Mesh for HAC Run 16, 731 g Plutonium Metal Hollow Cylinder, End Impact

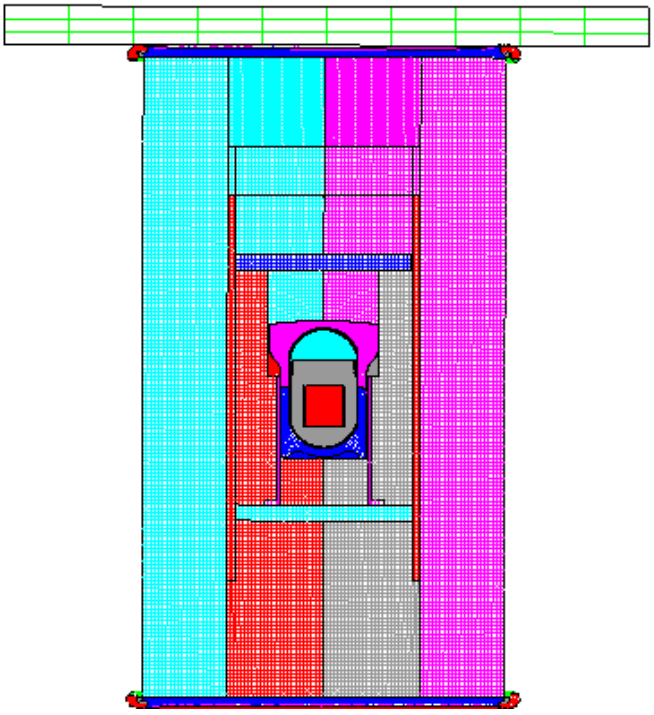

Figure 2-453. Finite Element Mesh for HAC Run 16, 731 g Plutonium Metal Hollow Cylinder, End Impact – Final Displacement

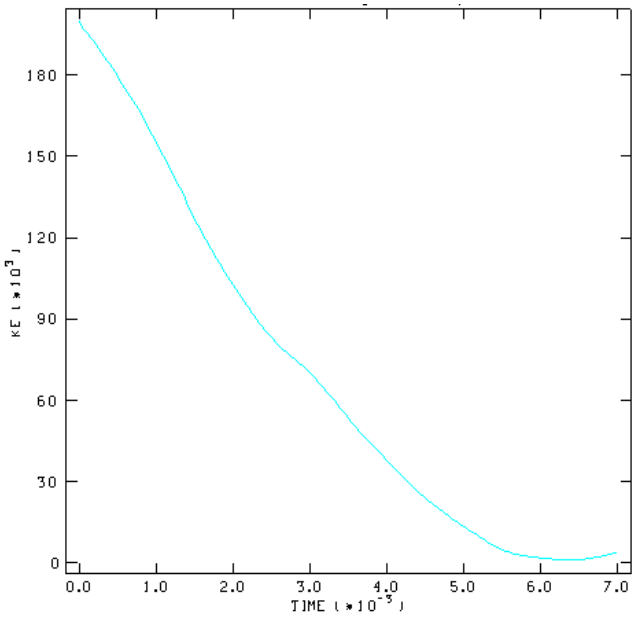

Figure 2-454. Kinetic Energy Time History for HAC Run 16, 731 g Plutonium Metal Hollow Cylinder, End Impact

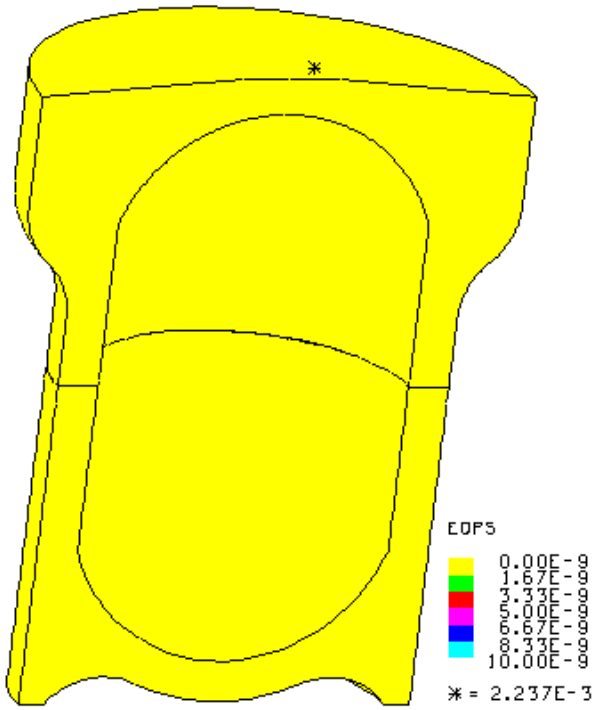

Figure 2-455. Plot of EQPS in the TB-1 for HAC Run 16, 731 g Plutonium Metal Hollow Cylinder, End Impact

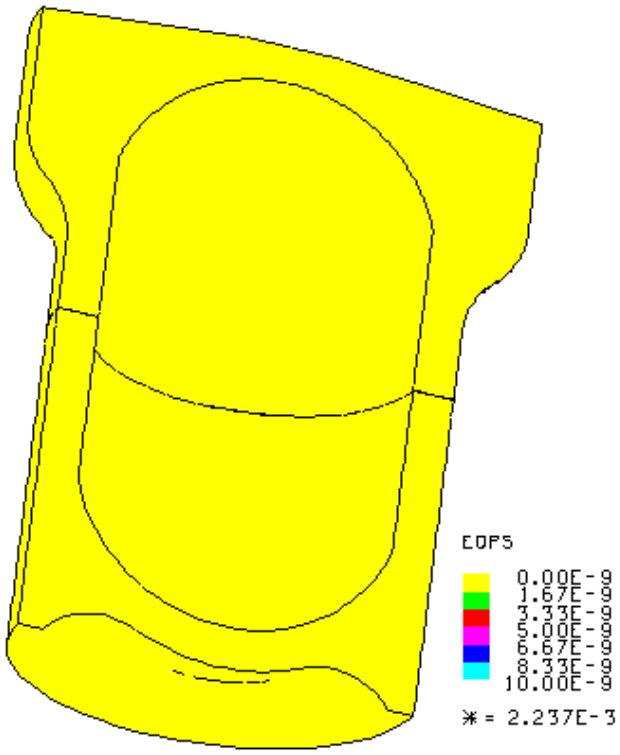

Figure 2-456. Plot of EQPS in the TB-1 for HAC Run 16, 731 g Plutonium Metal Hollow Cylinder, End Impact

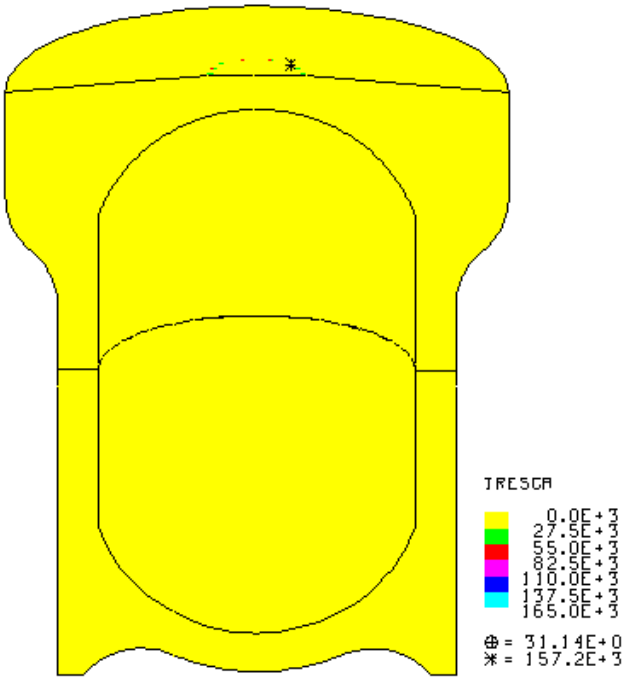

Figure 2-457. Plot of Tresca Stress in the TB-1 for HAC Run 16, 731 g Plutonium Metal Hollow Cylinder, End Impact

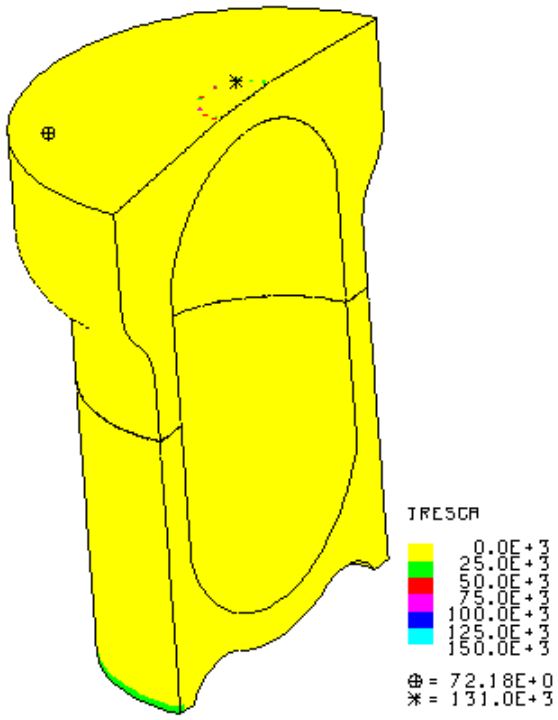

Figure 2-458. Plot of Tresca Stress in the TB-1 for HAC Run 16, 731 g Plutonium Metal Hollow Cylinder, End Impact when Plate Velocity Reaches Zero

2.12.5.6.17 HAC- Run 17, 731 g Plutonium Metal Hollow Cylinder, Side Impact

The dynamic crush side impact HAC analysis run for the 731 g angled plutonium metal hollow cylinder uses the same model for the overpack as the one used in the previous 16 runs. The TB-1, T-Ampoule, and plutonium metal hollow cylinder are the same model as that used in the aircraft analysis. The finite element mesh and initial position of the model are shown in Figure 2-459. The plutonium metal hollow cylinder within the T-Ampoule is positioned at the bottom of the model because it was considered to be at rest at the time of impact. The plate was positioned between the flanges to be most damaging to the TB-1 and contents by preventing the flanges from absorbing energy and slowing down the plate before it hits the overpack.

The post-impact deformation is shown in Figure 2-460 and its kinetic energy history in Figure 2-461. The flanges on the overpack deform, and the cylinder bounces due to the impact of the plate. Zero elements extended beyond the tested Bao-Wierzbicki strain locus. The maximum Tearing Parameter value for this analysis was 0.

Peak EQPS in the TB-1 vessel is shown in Figure 2-462 to be 45.76-3, and is localized in the outer contact regions with the redwood overpack. Figures 2-463 and 2-464 plot the Tresca stresses within the TB-1. The maximum Tresca stress in the TB-1 is 177.9 ksi, but there are no through thickness stresses exceeding the limit of 106.6 ksi, which can be seen clearly in the figure. Figure 2-465 is a plot of the Tresca stresses at the time when all of the kinetic energy of the plate has been transferred to the package, just as the plate begins to rebound. The maximum through thickness stress at this time is below 20.8 ksi, below the allowable through thickness stress of 106.6 ksi, as seen in the figure.

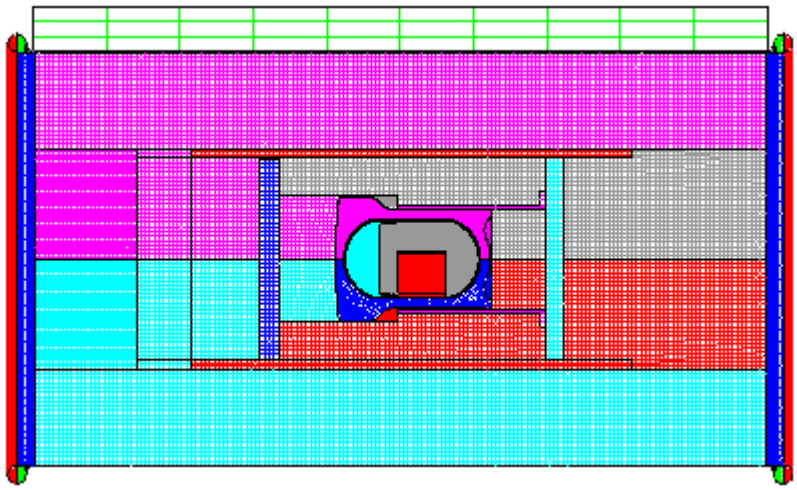

Figure 2-459. Finite Element Mesh for HAC Run 17, 731 g Plutonium Metal Hollow Cylinder, Side Impact

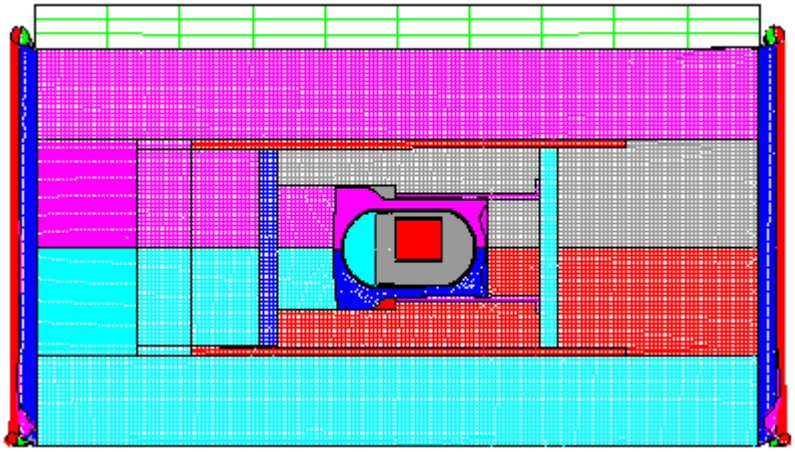

Figure 2-460. Finite Element Mesh for HAC Run 17, 731 g Plutonium Metal Hollow Cylinder, Side Impact – Final Displacement

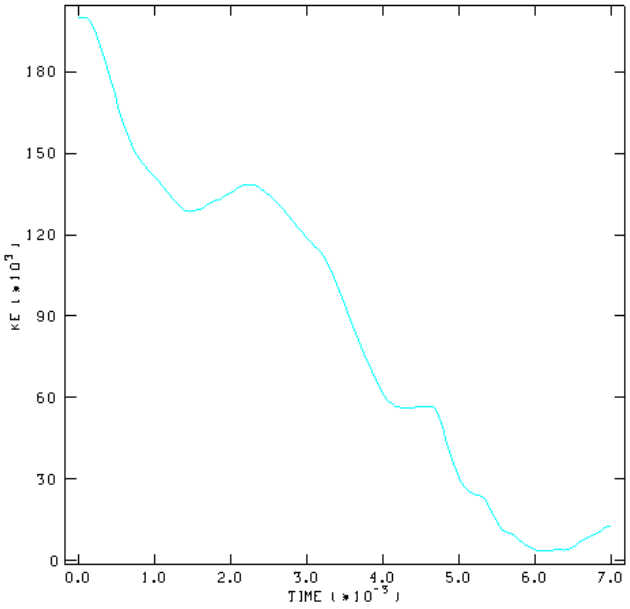

Figure 2-461. Kinetic Energy Time History for HAC Run 17, 731 g Plutonium Metal Hollow Cylinder, Side Impact

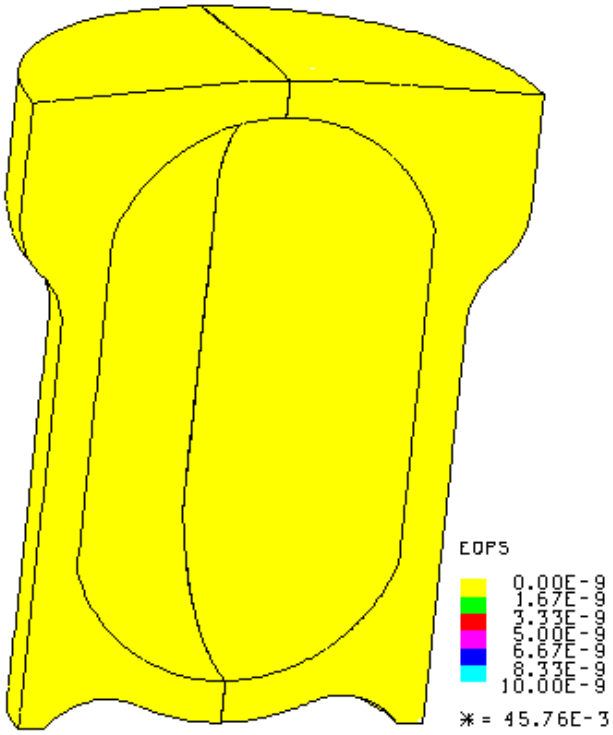

Figure 2-462. Plot of EQPS in the TB-1 for HAC Run 17, 731 g Plutonium Metal Hollow Cylinder, Side Impact

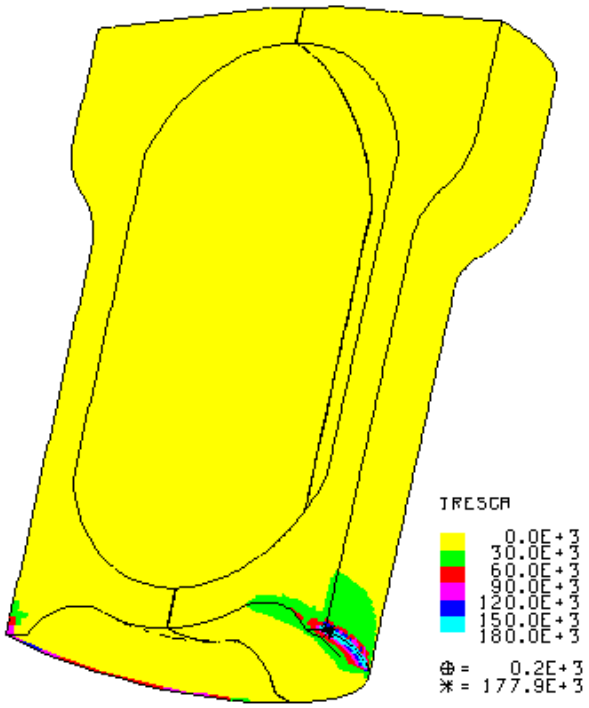

Figure 2-463. Plot of Tresca Stress in the TB-1 for HAC Run 17, 731 g Plutonium Metal Hollow Cylinder, Side Impact

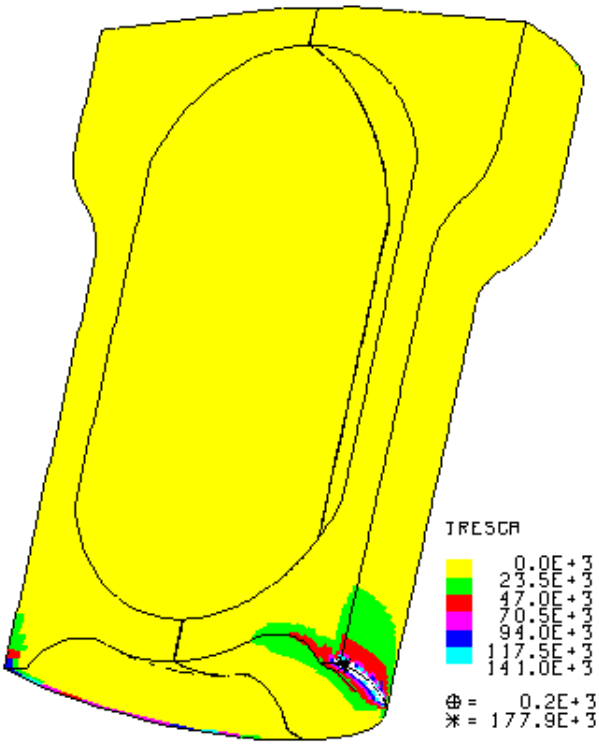

Figure 2-464. Plot of Tresca Stress in the TB-1 for HAC Run 17, 731 g Plutonium Metal Hollow Cylinder, Side Impact

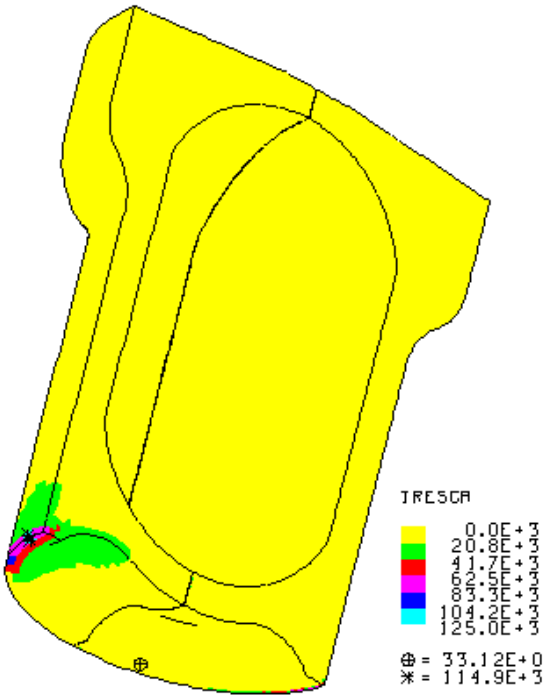

Figure 2-465. Plot of Tresca Stress in the TB-1 for HAC Run 17, 731 g Plutonium Metal Hollow Cylinder, Side Impact when Plate Velocity Reaches Zero

2.12.5.6.18 HAC- Run 18, 731 g Angled Plutonium Metal Hollow Cylinder, End Impact

The dynamic crush end impact HAC analysis run for the 731 g angled plutonium metal hollow cylinder uses the same model for the overpack as the one used in the previous 17 runs. The TB-1, T-Ampoule, and plutonium metal hollow cylinder are the same model as that used in the aircraft analysis. The finite element mesh and initial position of the model are shown in Figure 2-466. The plutonium metal hollow cylinder within the T-Ampoule is positioned at the bottom of the model because it was considered to be at rest at the time of impact.

The post-impact deformation is shown in Figure 2-467 and its kinetic energy history in Figure 2-468. The flanges on the overpack deform, and the cylinder bounces due to the impact of the plate. Zero elements extended beyond the tested Bao-Wierzbicki strain locus. The maximum Tearing Parameter value for this analysis was 0.

Peak EQPS in the TB-1 vessel is shown in Figure 2-469 to be 0.2813e-3, and is localized in the outer contact regions with the redwood overpack. Figures 2-470 and 2-471 plot the Tresca stresses within the TB-1. The maximum Tresca stress in the TB-1 is 157.3 ksi, but there are no through thickness stresses exceeding the limit of 106.6 ksi, which can be seen clearly in the figure. Figure 2-472 is a plot of the Tresca stresses at the time when all of the kinetic energy of the plate has been transferred to the package, just as the plate begins to rebound. The maximum through thickness stress at this time is below 20.8 ksi, below the allowable through thickness stress of 106.6 ksi, as seen in the figure.

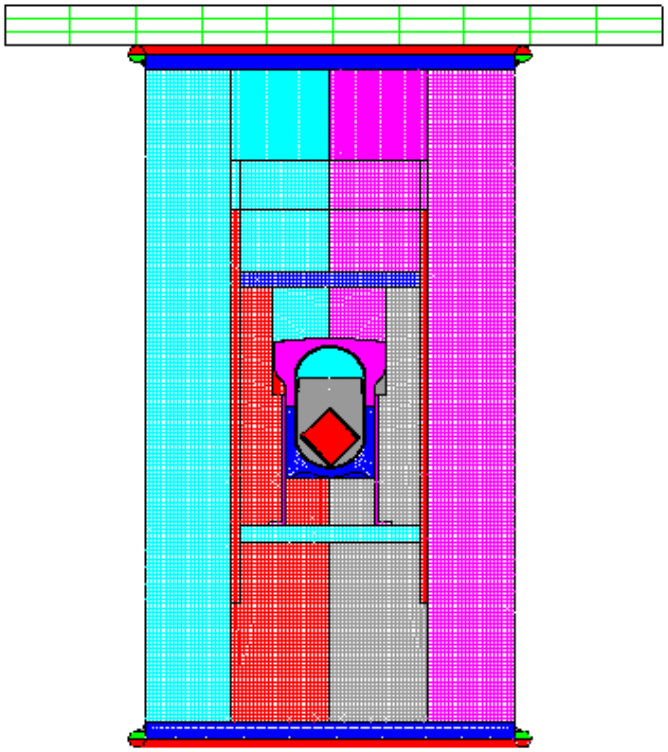

Figure 2-466. Finite Element Mesh for HAC Run 18, 731 g Angled Plutonium Metal Hollow Cylinder, End Impact

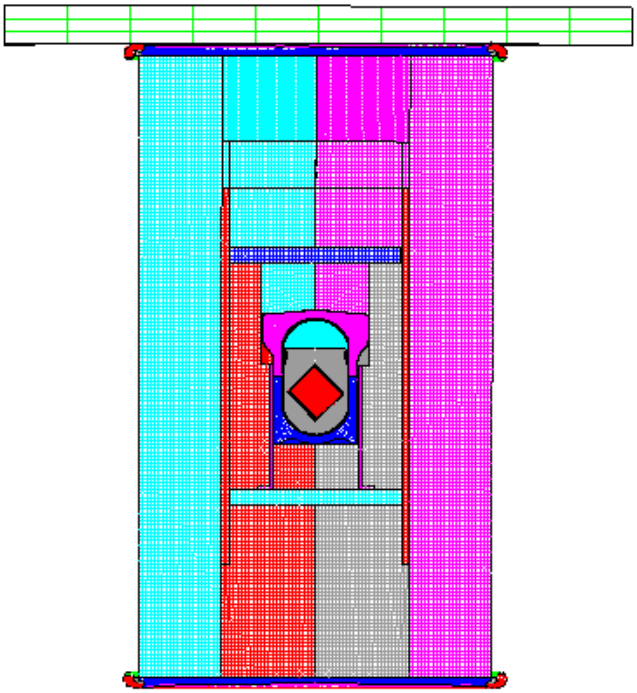

Figure 2-467. Finite Element Mesh for HAC Run 18, 731 g Angled Plutonium Metal Hollow Cylinder, End Impact – Final Displacement

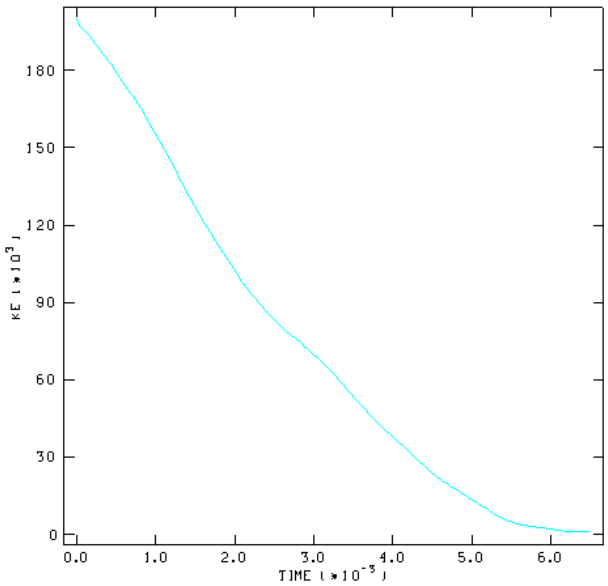

Figure 2-468. Kinetic Energy Time History for HAC Run 18, 731 g Angled Plutonium Metal Hollow Cylinder, End Impact

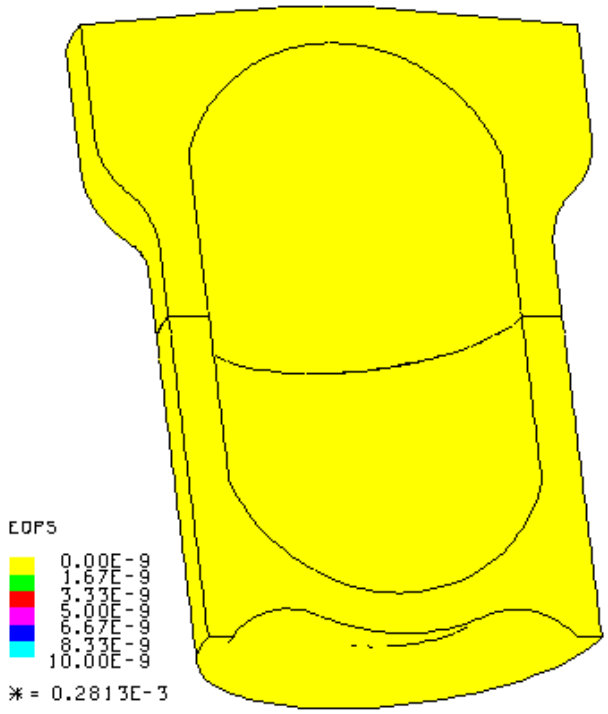

Figure 2-469. Plot of EQPS in the TB-1 for HAC Run 18, 731 g Angled Plutonium Metal Hollow Cylinder, End Impact

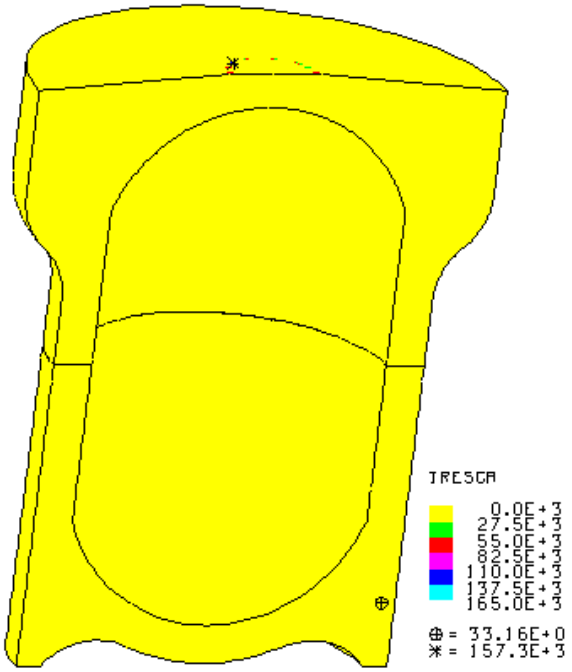

Figure 2-470. Plot of Tresca Stress in the TB-1 for HAC Run 18, 731 g Angled Plutonium Metal Hollow Cylinder, End Impact

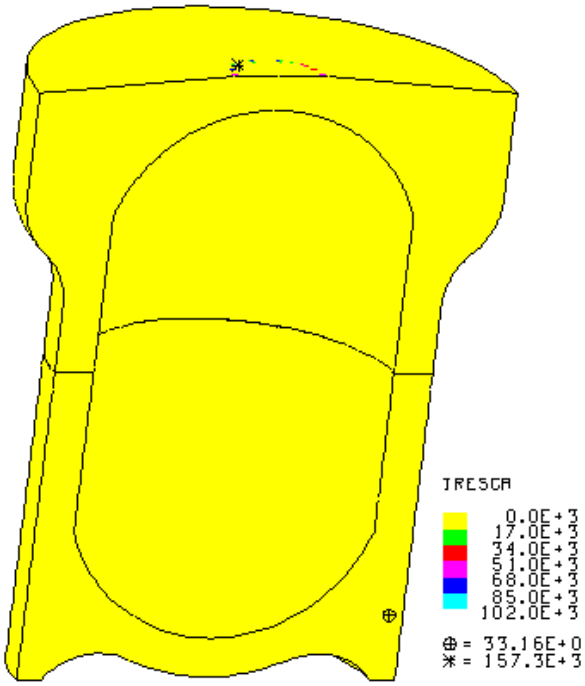

Figure 2-471. Plot of Tresca Stress in the TB-1 for HAC Run 18, 731 g Angled Plutonium Metal Hollow Cylinder, End Impact

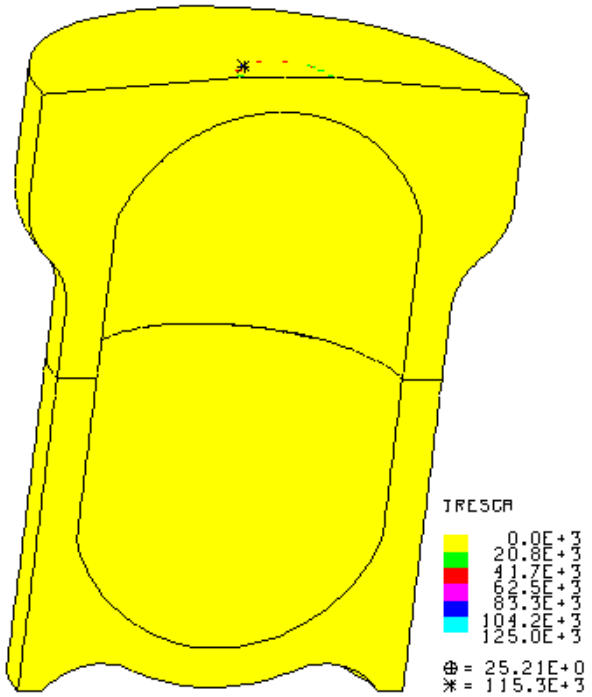

Figure 2-472. Plot of Tresca Stress in the TB-1 for HAC Run 18, 731 g Angled Plutonium Metal Hollow Cylinder, End Impact when Plate Velocity Reaches Zero

2.12.5.6.19 HAC- Run 19, 731 g Angled Plutonium Metal Hollow Cylinder, Side Impact

The dynamic crush side impact HAC analysis run for the 731 g angled plutonium metal hollow cylinder uses the same model for the overpack as the one used in the previous 18 runs. The TB-1, T-Ampoule, and plutonium metal hollow cylinder are the same model as that used in the aircraft analysis. The finite element mesh and initial position of the model are shown in Figure 2-473. The plutonium metal hollow cylinder within the T-Ampoule is positioned at the bottom of the model because it was considered to be at rest at the time of impact. The plate was positioned between the flanges to be most damaging to the TB-1 and contents by preventing the flanges from absorbing energy and slowing down the plate before it hits the overpack.

The post-impact deformation is shown in Figure 2-474 and its kinetic energy history in Figure 2-475. The flanges on the overpack deform, and the cylinder bounces due to the impact of the plate. Average stress-triaxiality versus EQPS is shown in Figures 2-476 and 2-477 for the elements extending beyond the tested Bao-Wierzbicki strain locus. These elements are at high stress triaxiality and low EQPS. The graph of Tearing Parameter versus EQPS for those elements extending beyond the strain locus is shown in Figure 2-478. The elements that exceeded the strain locus are highlighted in red Figure 2-479. The maximum Tearing Parameter value for this analysis was 5.092e-2, and is below the critical Tearing Parameter value of 1.012 for Ti-6Al-4V, thus T-Ampoule integrity is maintained.

Peak EQPS in the TB-1 vessel is shown in Figure 2-480 to be 0.1124, and is localized in the outer contact regions with the redwood overpack. Figures 2-481 and 2-482 plot the Tresca stresses within the TB-1. The maximum Tresca stress in the TB-1 is 201.7 ksi, but there are no through thickness stresses exceeding the limit of 106.6 ksi, which can be seen clearly in the

figures. Figure 2-483 is a plot of the Tresca stresses at the time when all of the kinetic energy of the plate has been transferred to the package, just as the plate begins to rebound. The maximum through thickness stress at this time is below 33.3 ksi, below the allowable through thickness stress of 106.6 ksi, as seen in the figure.

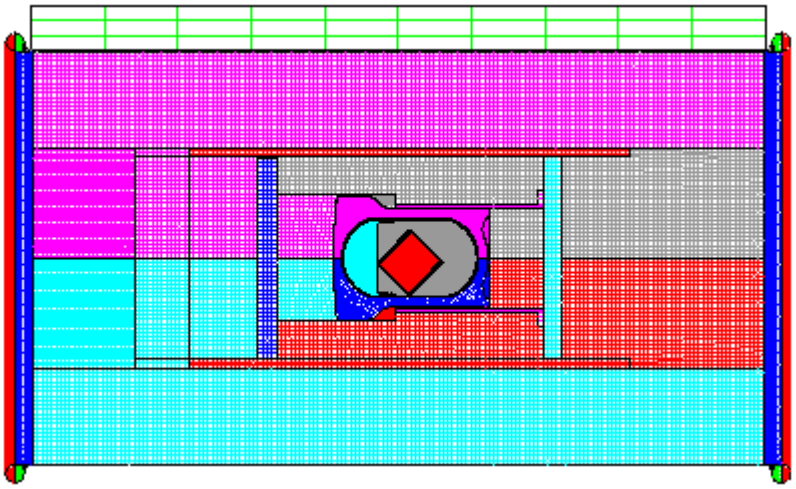

Figure 2-473. Finite Element Mesh for HAC Run 19, 731 g Angled Plutonium Metal Hollow Cylinder, Side Impact

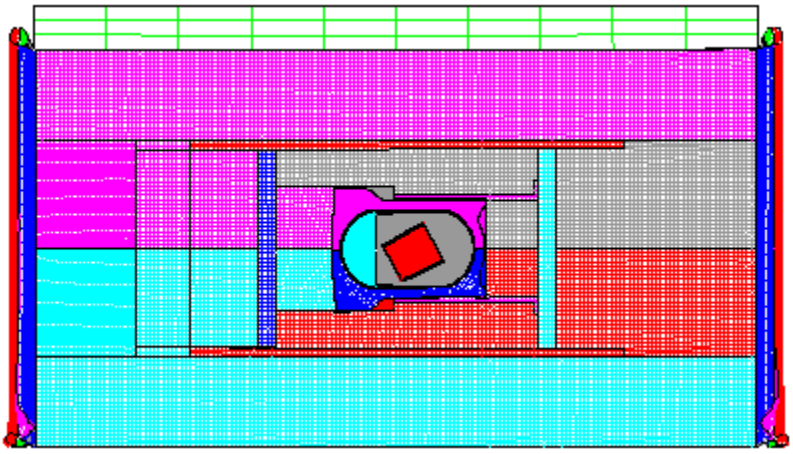

Figure 2-474. Finite Element Mesh for HAC Run 19, 731 g Angled Plutonium Metal Hollow Cylinder, Side Impact – Final Displacement

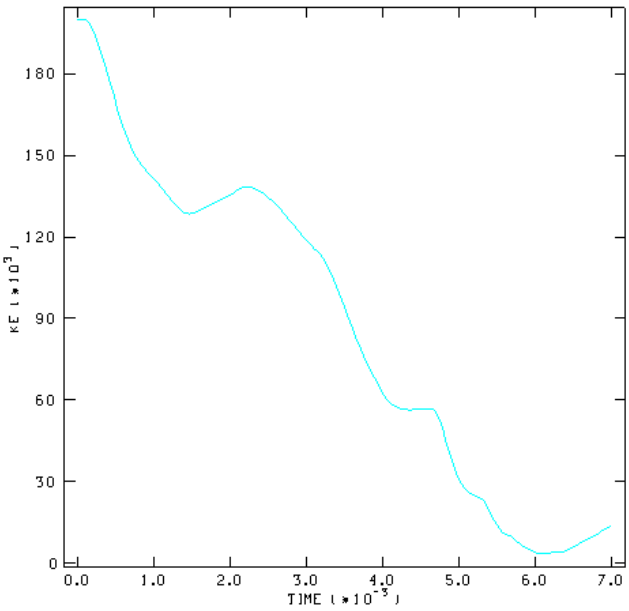

Figure 2-475. Kinetic Energy Time History for HAC Run 19, 731 g Angled Plutonium Metal Hollow Cylinder, Side Impact

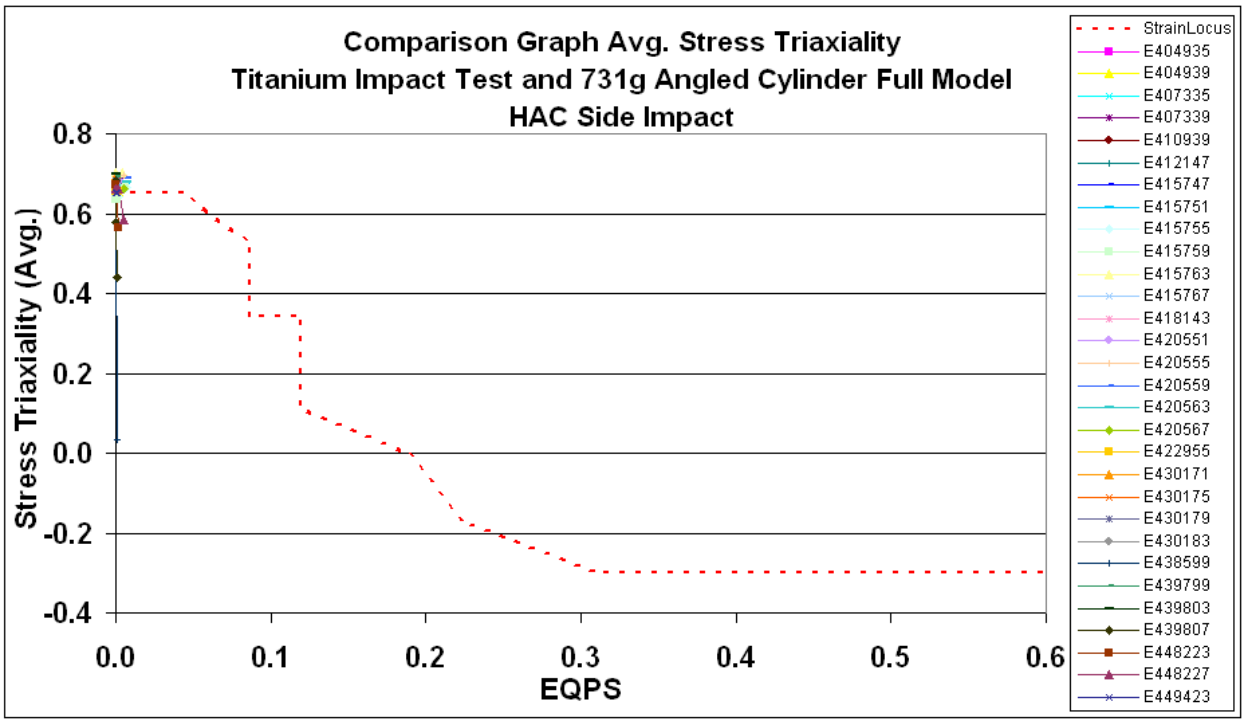

Figure 2-476. Graph of Average Stress Triaxiality versus EQPS for Elements Exceeding the Experimental Strain Locus for HAC Run 19, 731 g Angled Plutonium Metal Hollow Cylinder, Side Impact

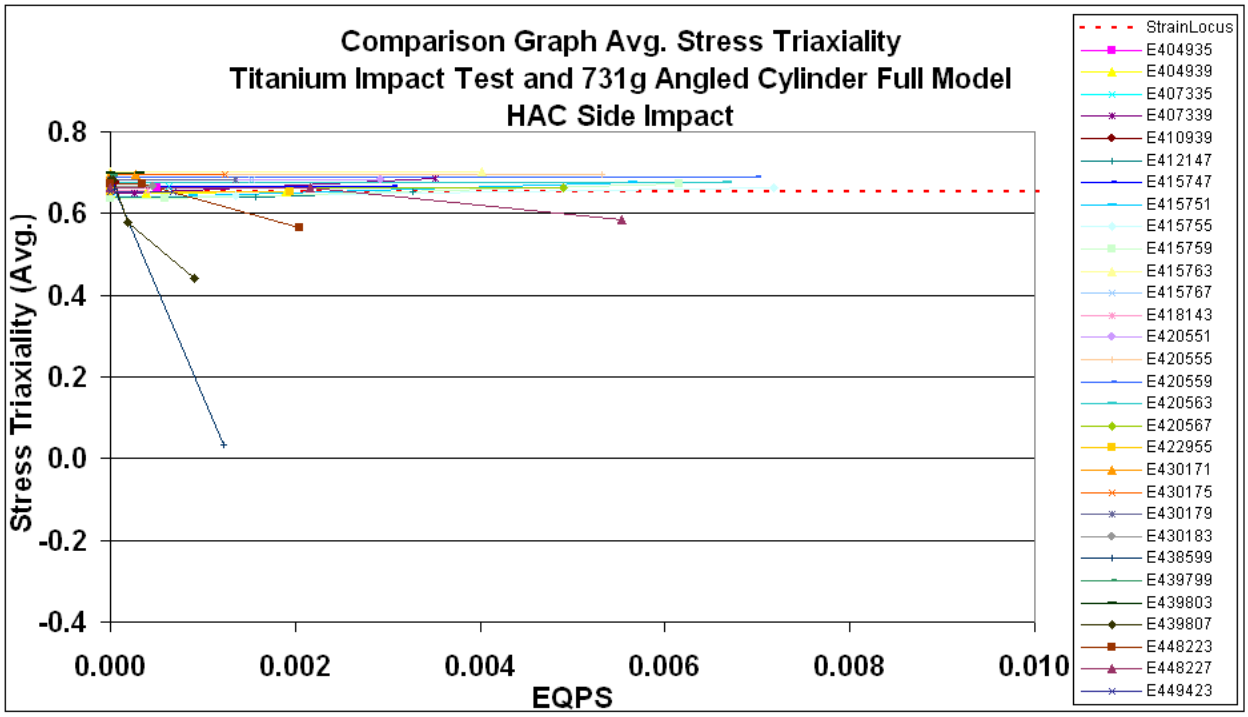

Figure 2-477. Graph of Average Stress Triaxiality versus EQPS for Elements Exceeding the Experimental Strain Locus (Zoomed In) for HAC Run 19, 731 g Angled Plutonium Metal Hollow Cylinder, Side Impact

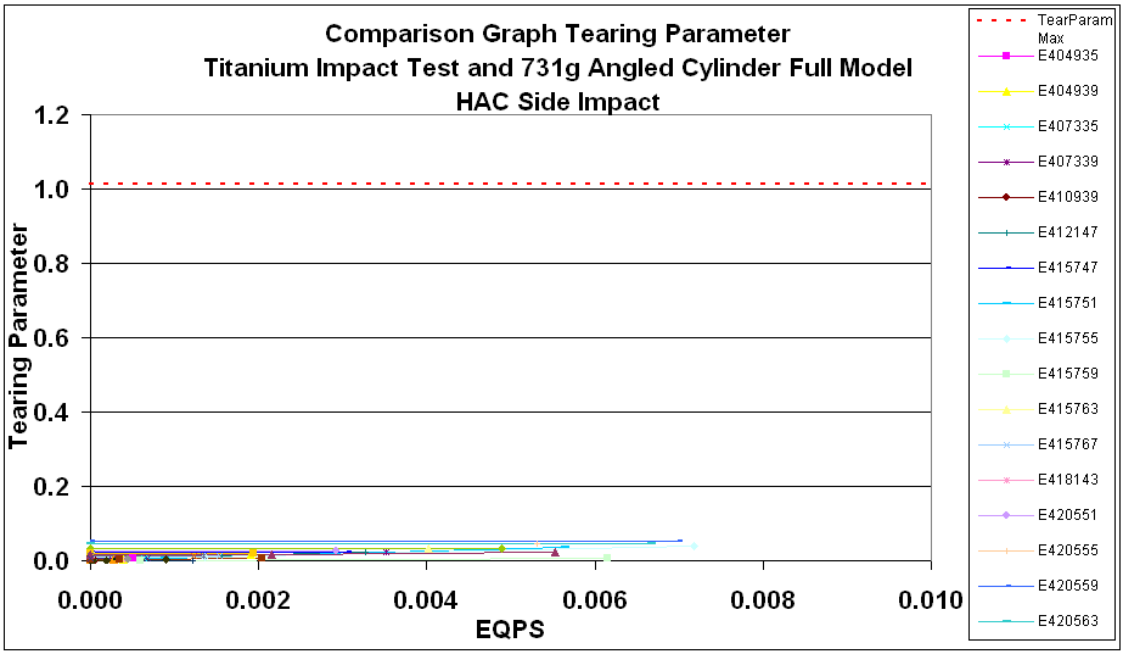

Figure 2-478. Graph of Tearing Parameter versus EQPS for Elements Exceeding the Experimental Strain Locus for HAC Run 19, 731 g Angled Plutonium Metal Hollow Cylinder, Side Impact

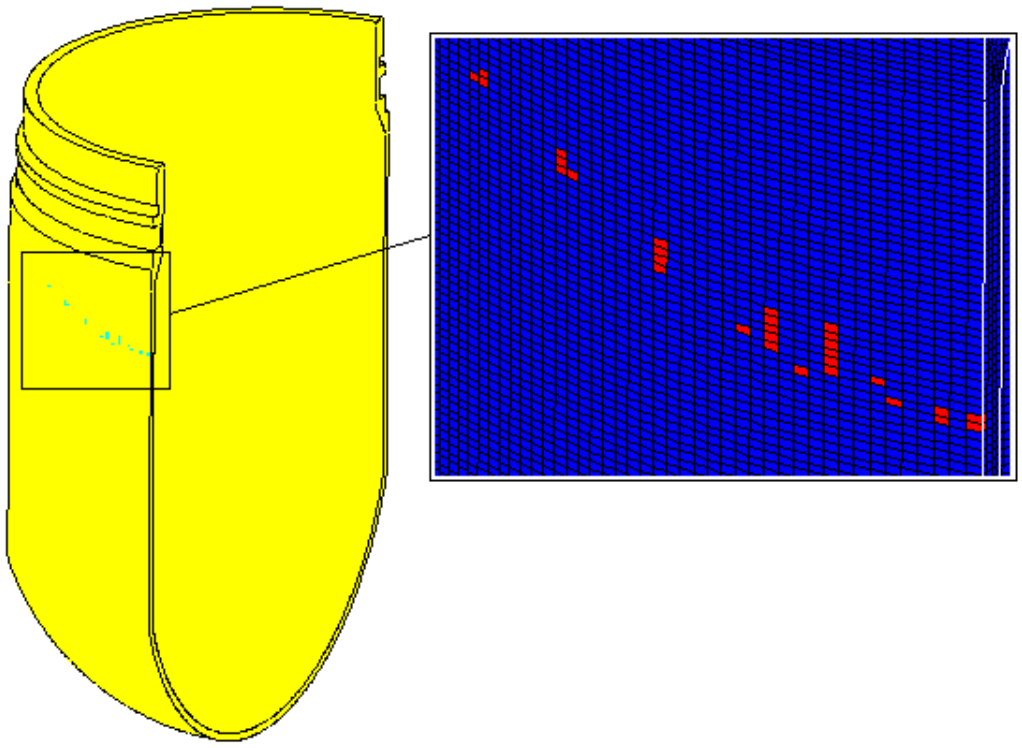

Figure 2-479. Plot of Elements Exceeding the Experimental Strain Locus for HAC Run 19, 731 g Angled Plutonium Metal Hollow Cylinder, Side Impact

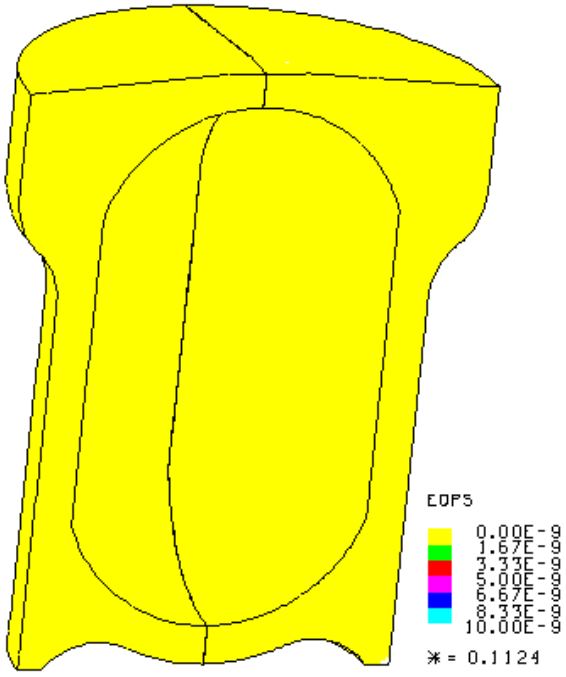

Figure 2-480. Plot of EQPS in the TB-1 for HAC Run 19, 731 g Angled Plutonium Metal Hollow Cylinder, Side Impact

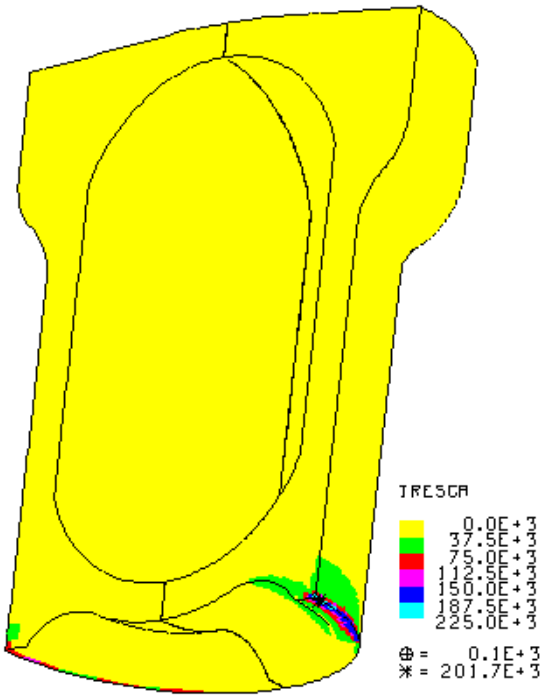

Figure 2-481. Plot of Tresca Stress in the TB-1 for HAC Run 19, 731 g Angled Plutonium Metal Hollow Cylinder, Side Impact

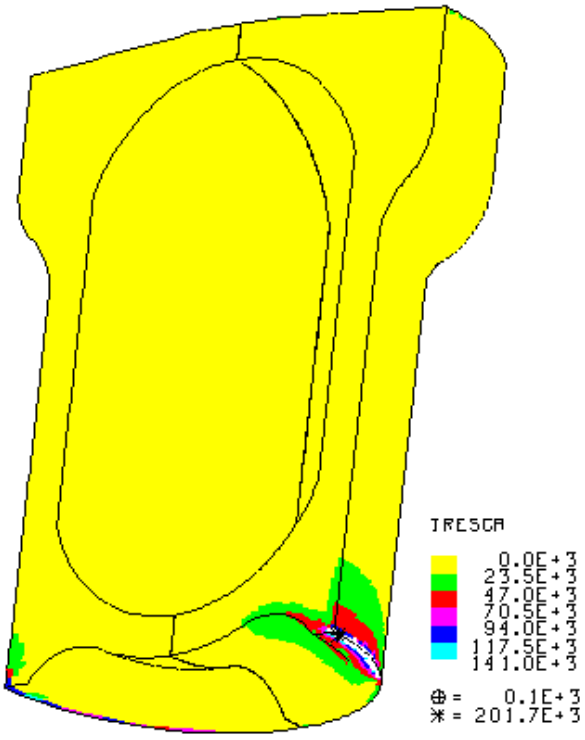

Figure 2-482. Plot of Tresca Stress in the TB-1 for HAC Run 19, 731 g Angled Plutonium Metal Hollow Cylinder, Side Impact

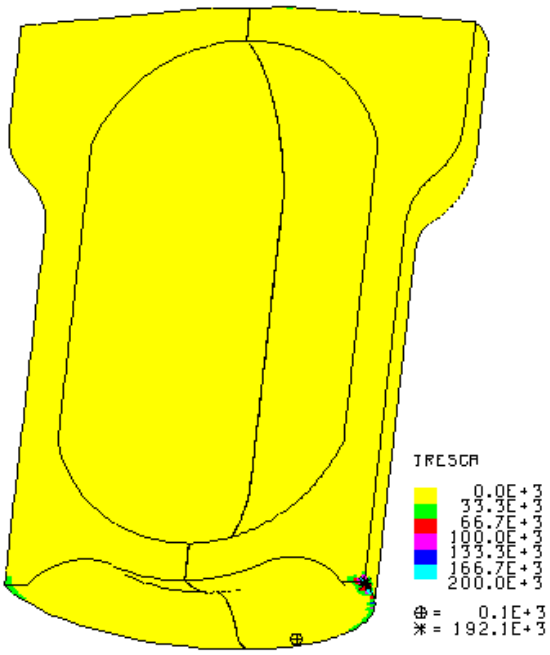

Figure 2-483. Plot of Tresca Stress in the TB-1 for HAC Run 19, 731 g Angled Plutonium Metal Hollow Cylinder, Side Impact when Plate Velocity Reaches Zero

2.12.5.6.20 HAC- Run 20, 731 g Angled Plutonium Metal Hollow Cylinder, CGOC Impact

The dynamic crush CGOC impact HAC analysis run for the 731 g angled plutonium metal hollow cylinder uses the same overpack model as those used in HAC runs 1 through 19. The finite element mesh and initial position of the model are shown in Figure 2-484. The plutonium metal hollow cylinder within the T-Ampoule is positioned at the bottom of the model because it was considered to be at rest.

The post-impact deformation is shown in Figure 2-485 and its kinetic energy history in Figure 2-486. The flanges on the overpack deform, and the cylinder bounces due to the impact of the plate. The kinetic energy does not drop completely to zero because the plate is still vibrating and internal contents are still in motion. The plutonium metal hollow cylinder has bounced off of the top and bottom surface of the T-Ampoule, and the plate is now rebounding slowly with the package, ensuring that the highest containment vessel and contents loadings have occurred.

There was zero EQPS in the T-Ampoule and nearly zero in the TB-1 (see Figure 2-487), and the maximum Tearing Parameter was 0. Figure 2-488 is a plot of the Tresca stresses within the TB-1. The maximum Tresca stress in the TB-1 is 70.57 ksi, which is below the maximum through thickness allowable stress of 106.6 ksi. Figure 2-489 is a plot of the Tresca stresses at the time when all of the kinetic energy of the plate has been transferred to the package, just as the plate begins to rebound. The maximum through thickness stress at this time is below 16.7 ksi, below the allowable through thickness stress of 106.6 ksi, as seen in the figure.

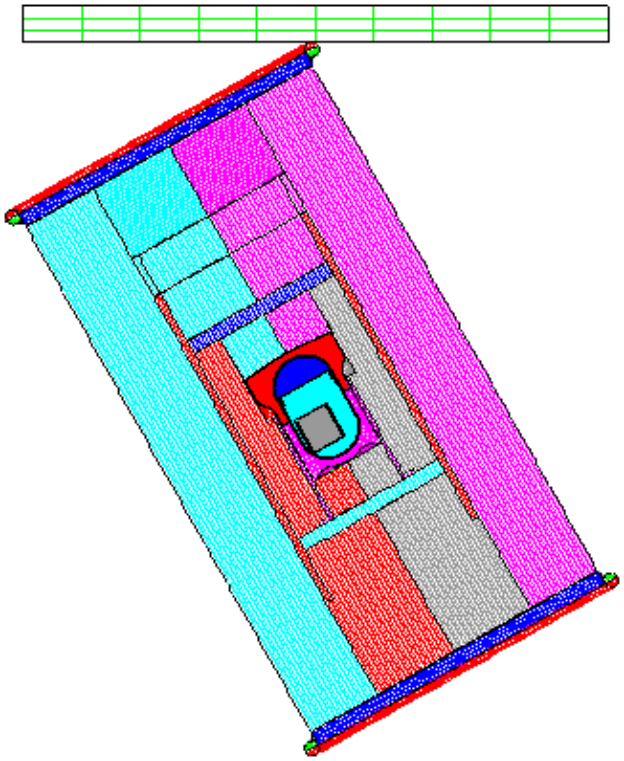

Figure 2-484. Finite Element Mesh for HAC Run 20, 731 g Angled Plutonium Metal Hollow Cylinder, CGOC Impact

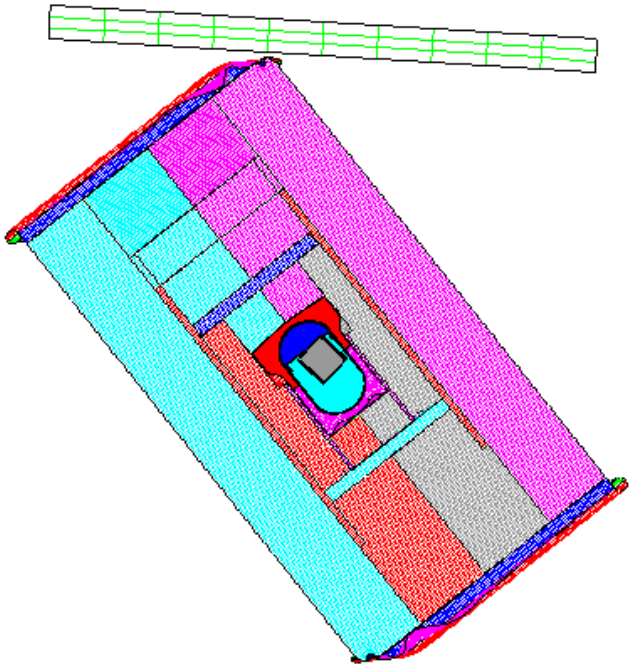

Figure 2-485. Finite Element Mesh for HAC Run 20, 731 g Angled Plutonium Metal Hollow Cylinder, CGOC Impact – Final Displacement

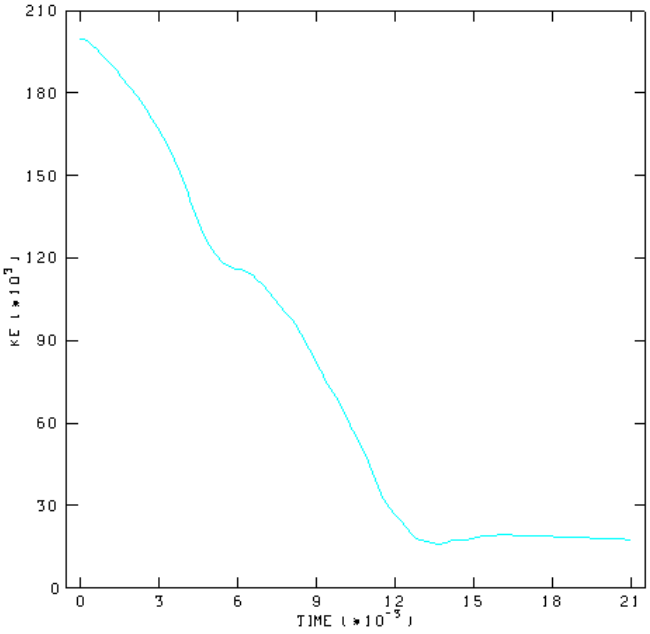

Figure 2-486. Kinetic Energy Time History for HAC Run 20, 731 g Angled Plutonium Metal Hollow Cylinder, CGOC Impact

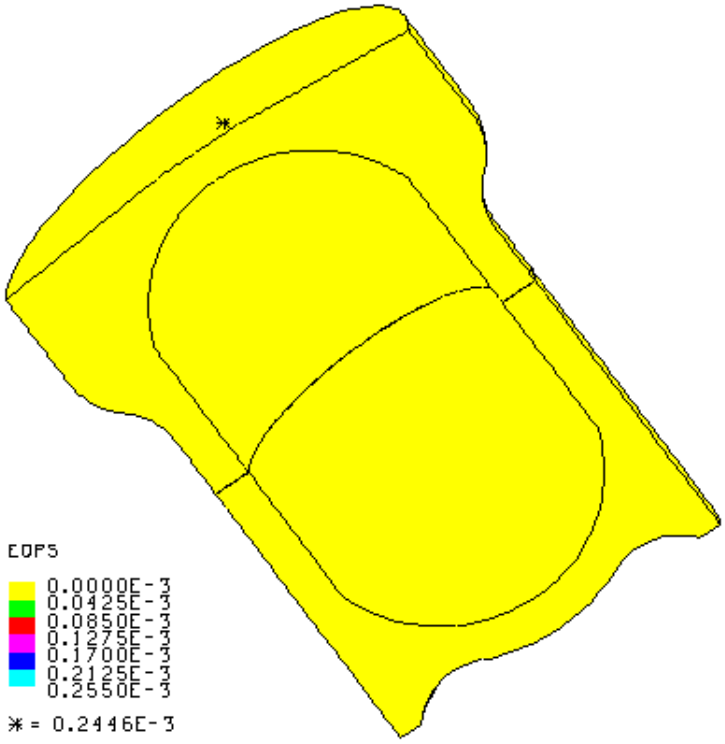

Figure 2-487. Plot of EQPS in the TB-1 for HAC Run 20, 731 g Angled Plutonium Metal Hollow Cylinder, CGOC Impact

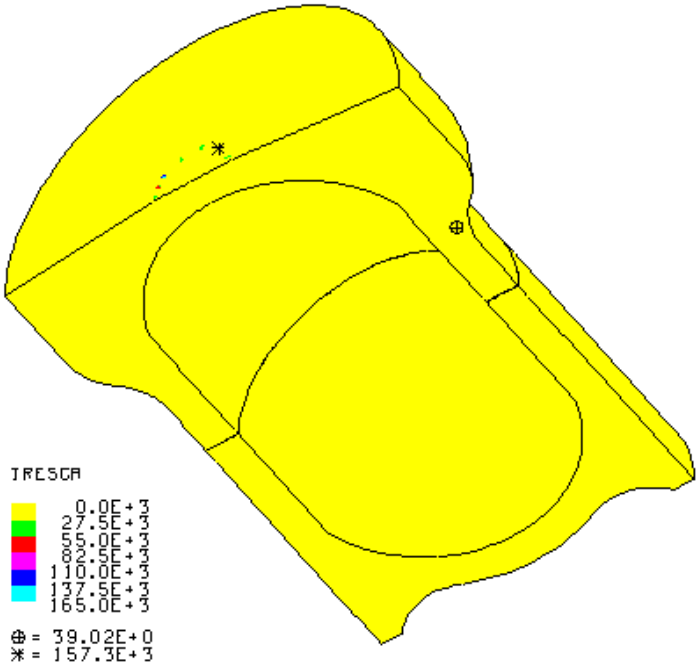

Figure 2-488. Plot of Tresca Stress in the TB-1 for HAC Run 20, 731 g Angled Plutonium Metal Hollow Cylinder, CGOC Impact

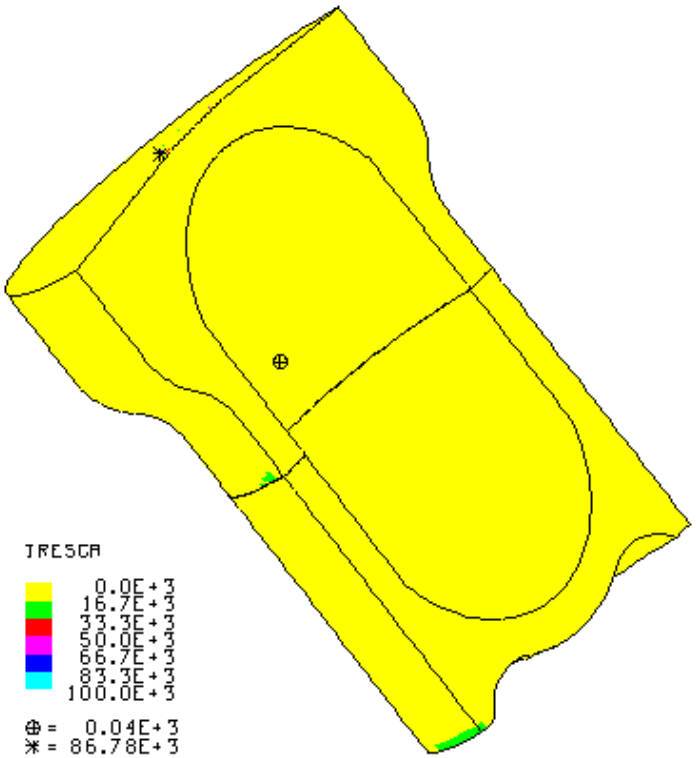

Figure 2-489. Plot of Tresca Stress in the TB-1 for HAC Run 20, 731 g Angled Plutonium Metal Hollow Cylinder, CGOC Impact when Plate Velocity Reaches Zero

2.12.5.7 30-foot Drop Analyses

Table 2-21 describes the three runs for the 30-foot drop analyses.

Table 2-21. 30-ft Drop Impact Analyses (3), Components, and Orientations

Run No.	Component	Submodel Orientation
1	SC-2 - Pu	Far side position, support structure 45°, side impact
2	831 g Plutonium Metal Hollow Cylinder, alpha Pu	Bottom position (angled), top impact
3	831 g Plutonium Metal Hollow Cylinder, alpha Pu	Bottom position (angled), CGOC impact

2.12.5.7.1 SC-2 45 Degree Rotated Support Structure with Side Impact

The two-sample-container 45-degree rotated support structure contents was used for the 30-ft drop with side impact since this case produced the most severe loading of the aircraft side impacts. Pre-impact model geometry shown in Figure 2-490, and the final displacement shown in Figure 2-491. Note that the overall overpack deformation (rolled outer skin end closures, and slight denting of redwood) resulting from the 30-ft side impact analysis (half-symmetric model) compares well with the test result documented in the SAR,[1] shown in Figure 2-492. The kinetic energy history is shown in Figure 2-493 to verify that the analysis ran through the time of rebound. The negligible 0.26% equivalent plastic strain in the T-Ampoule eutectic boundary is shown in Figure 2-494. There were no T-Ampoule elements exceeding the experimental strain locus. Tresca stress in the TB-1 is shown in Figure 2-495, with through-thickness values below even the NCT allowables from Table 2-4.

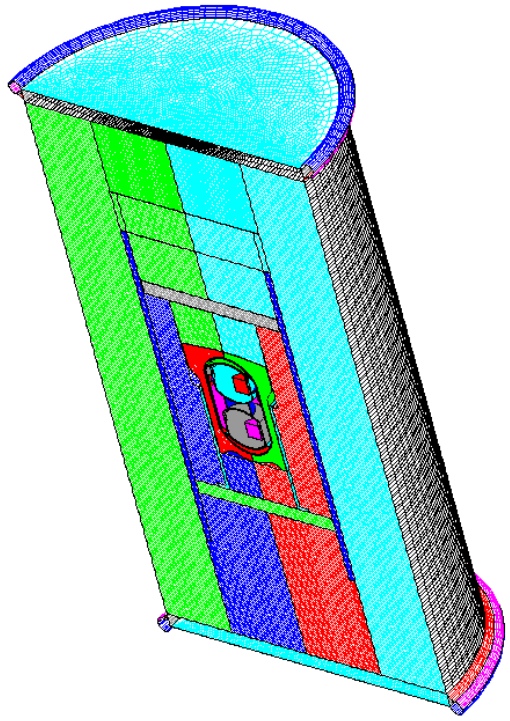

Figure 2-490. Finite Element Mesh for 30-ft Drop Run 1 – SC-2 with Support Structure Rotated 45 Degrees and Side Impact

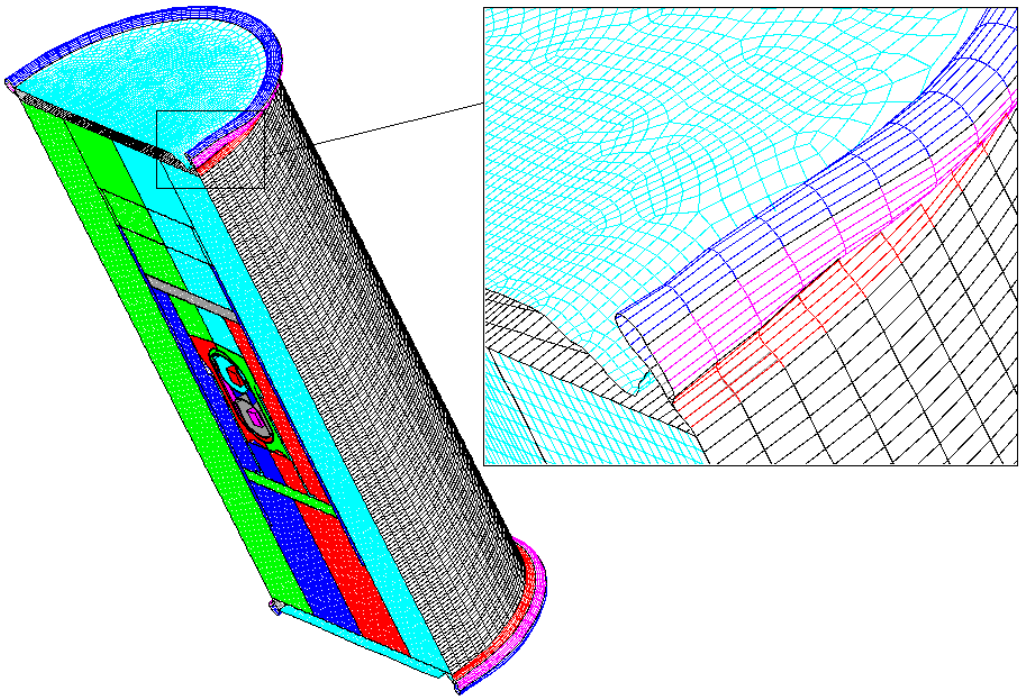

Figure 2-491. Final Displacement in Finite Element Mesh for 30-ft Drop Run 1 – SC-2 with Support Structure Rotated 45 Degrees and Side Impact

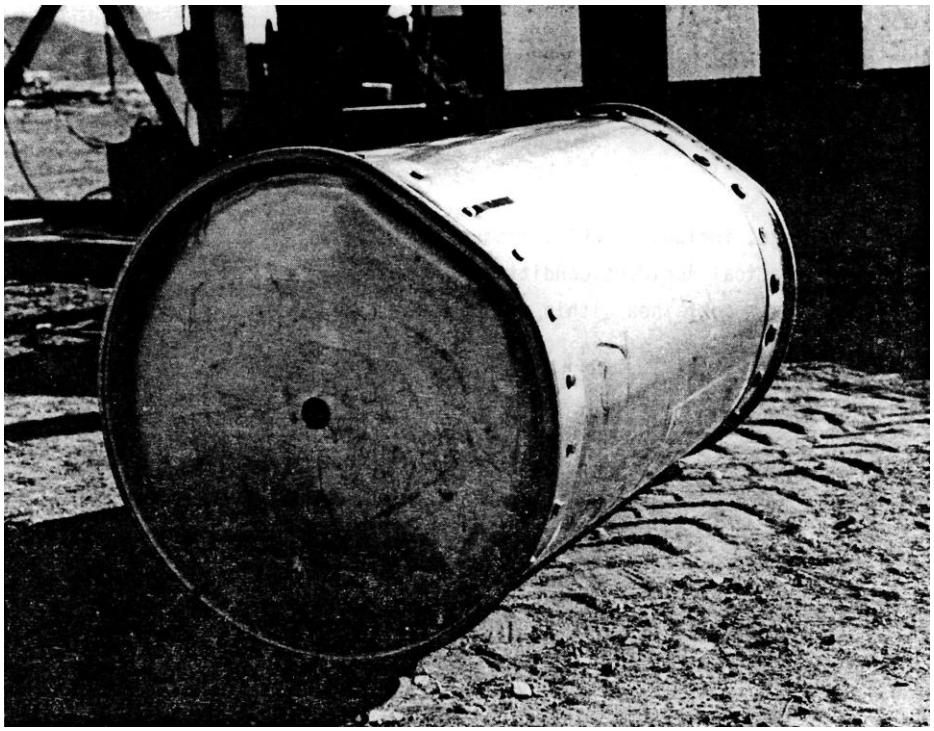

Figure 2-492. Final Displacement in SAR[1] Test for 30-ft Drop

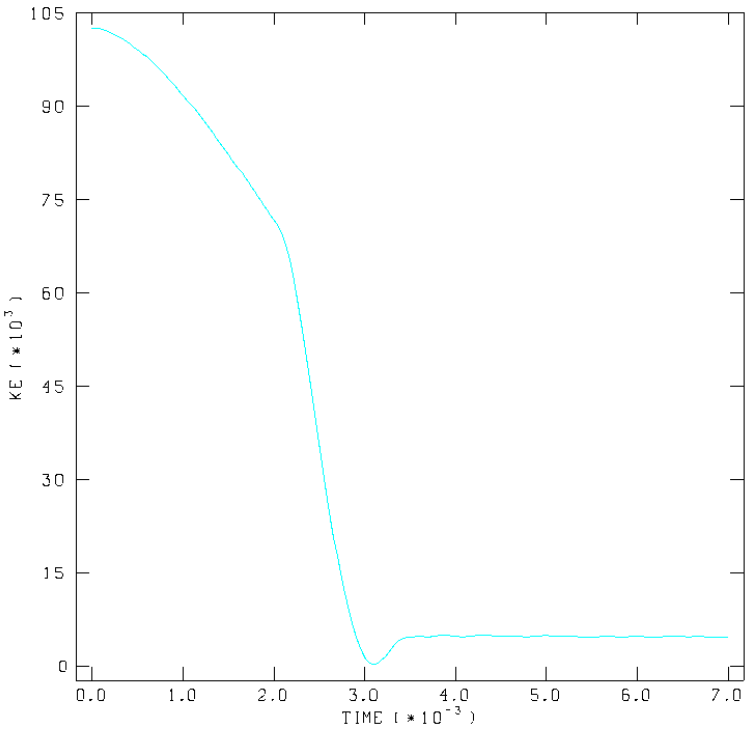

Figure 2-493. Kinetic Energy for 30-ft Drop Run 1 – SC-2 with Support Structure Rotated 45 Degrees and Side Impact

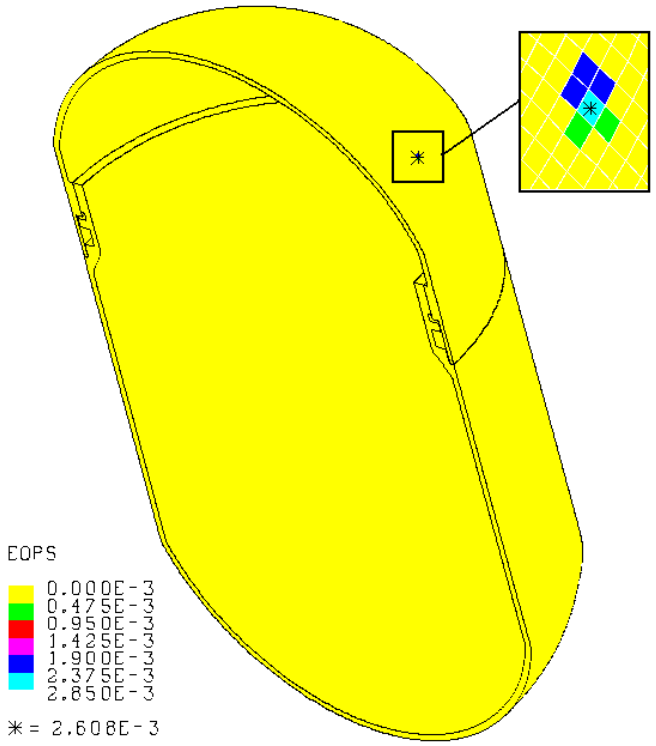

Figure 2-494. EQPS in the T-Amp for 30-ft Drop Run 1 – SC-2 with Support Structure Rotated 45 Degrees and Side Impact

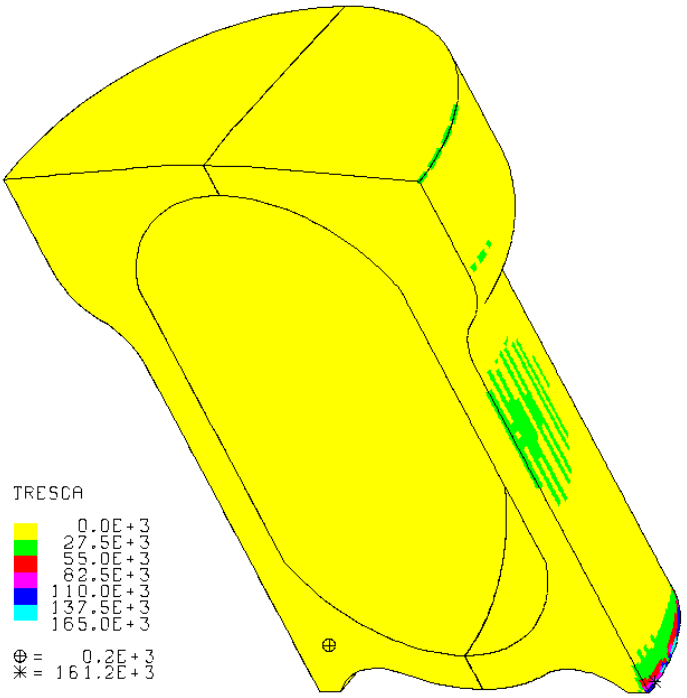

Figure 2-495. Tresca Stress in the TB-1 for 30-ft Drop Run 1 – SC-2 with Support Structure Rotated 45 Degrees and Side Impact

2.12.5.7.2 831g Plutonium Metal Hollow Cylinder Angled with End Impact

The 831g plutonium metal hollow cylinder contents was used for the 30-ft drop with end impact since this case produced one of the most severe loadings of the aircraft end impacts. Pre-impact model geometry shown in Figure 2-496, and the final displacement shown in Figure 2-497. The kinetic energy history is shown in Figure 2-498 to verify that the analysis ran through the time of rebound. The T-Ampoule equivalent plastic strain was zero, and there were no T-Ampoule elements exceeding the experimental strain locus. The negligible 0.255% equivalent plastic strain in the localized outer surface of the TB-1 (due to a minor contact modeling artifact) is shown in Figure 2-499. Tresca stress in the TB-1 is shown in Figure 2-500, with through-thickness values below even the NCT allowables from Table 2-4.

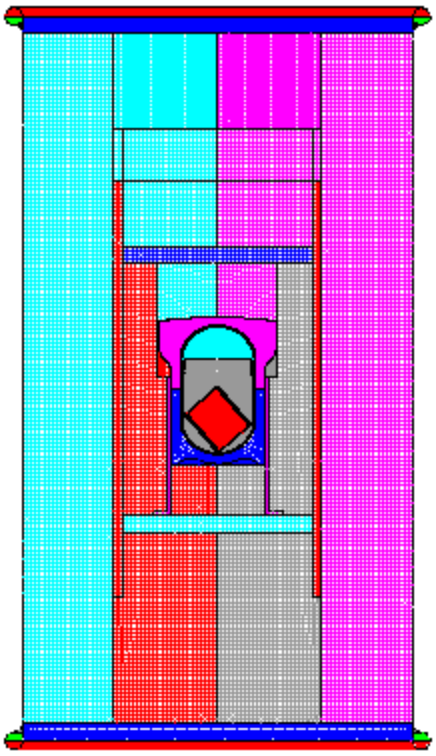

Figure 2-496. Finite Element Mesh for 30-ft Drop Run 2 – Angled 831 g Plutonium Metal Hollow Cylinder with End Impact

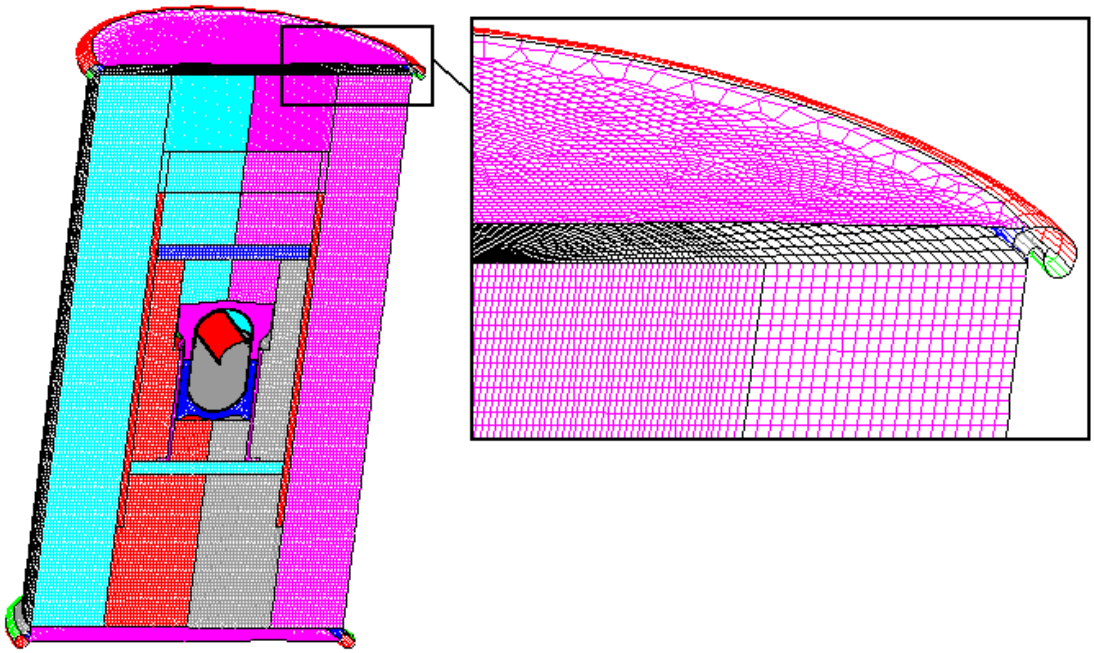

Figure 2-497. Final Displacement for 30-ft Drop Run 2 – Angled 831 g Plutonium Metal Hollow Cylinder with End Impact

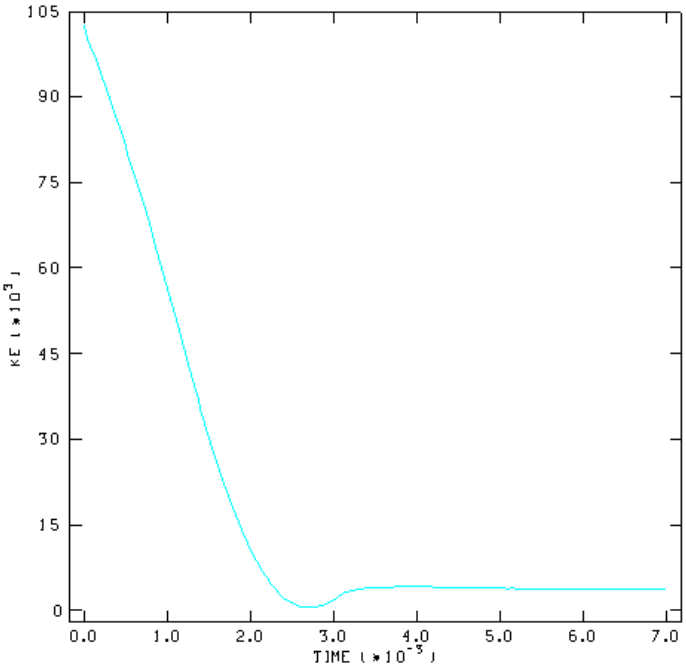

Figure 2-498. Kinetic Energy for 30-ft Drop Run 2 – Angled 831 g Plutonium Metal Hollow Cylinder with End Impact

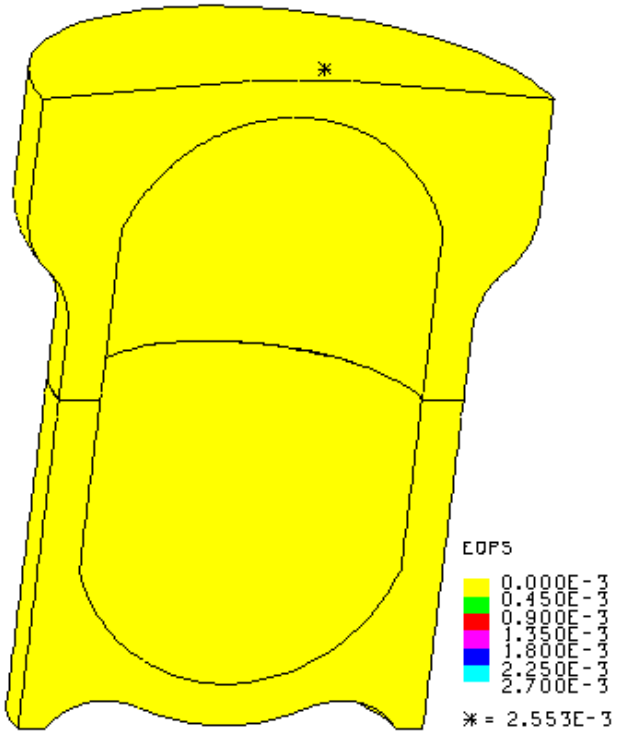

Figure 2-499. EQPS in TB-1 for 30-ft Drop Run 2 – Angled 831 g Plutonium Metal Hollow Cylinder with End Impact

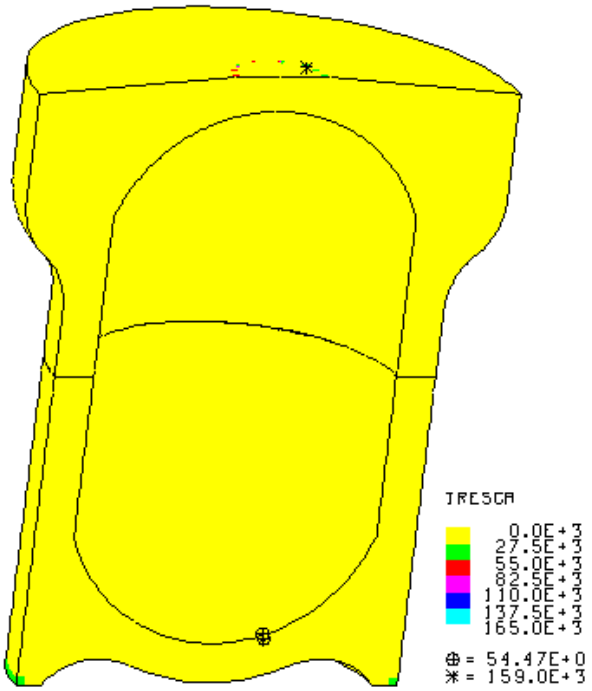

Figure 2-500. Tresca Stress in the TB-1 for 30-ft Drop Run 2 – Angled 831 g Plutonium Metal Hollow Cylinder with End Impact

2.12.5.7.3 831g Plutonium Metal Hollow Cylinder Angled with CGOC Impact

The angled 831g plutonium metal hollow cylinder contents was used for the 30-ft drop with corner impact since this case produced one of the most severe loadings of the aircraft CGOC impacts. Pre-impact model geometry is shown in Figure 2-501, and the final displacement shown in Figure 2-502. The kinetic energy history is shown in Figure 2-503 to verify that the analysis ran through the time of rebound. The T-Ampoule equivalent plastic strain was zero, and there were no T-Ampoule elements exceeding the experimental strain locus. There was zero equivalent plastic strain in the TB-1. Tresca stress in the TB-1 is shown in Figure 2-504, with through-thickness values below even the NCT allowables from Table 2-4.

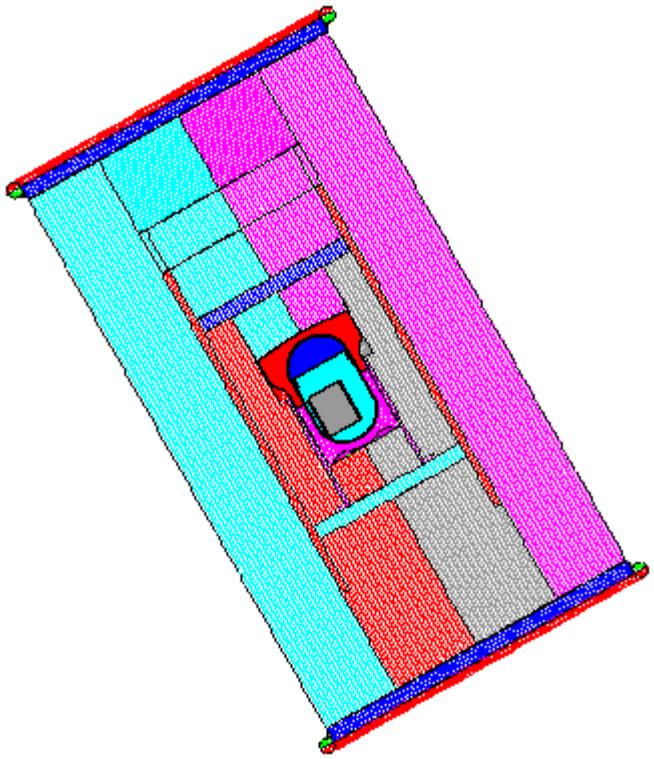

Figure 2-501. Finite Element Mesh for 30-ft Drop Run 3 – Angled 831 g Plutonium Metal Hollow Cylinder with CGOC Impact

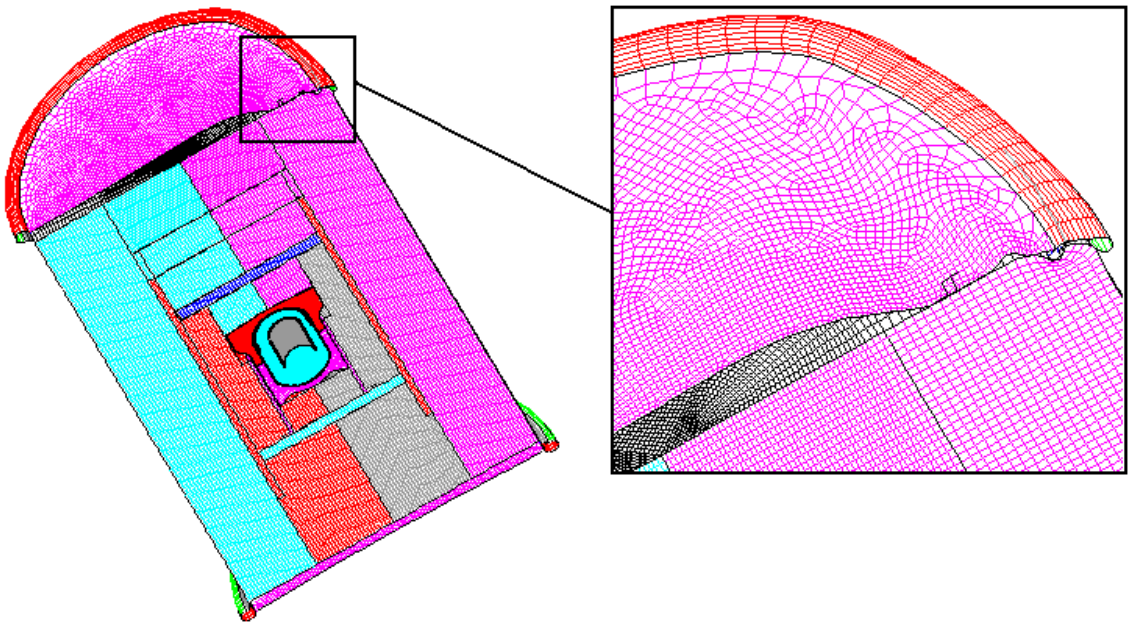

Figure 2-502. Final Displacement for 30-ft Drop Run 3 – Angled 831 g Plutonium Metal Hollow Cylinder with CGOC Impact

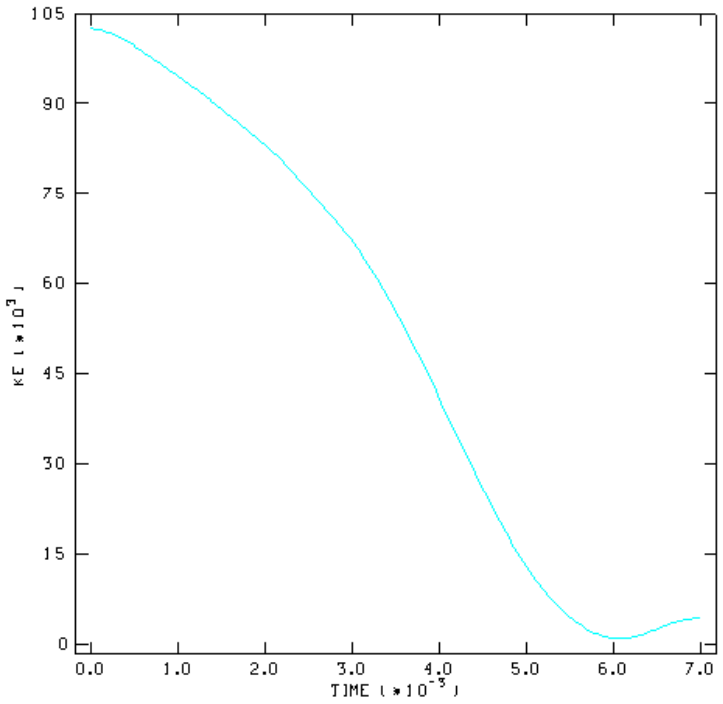

Figure 2-503. Kinetic Energy for 30-ft Drop Run 3 – Angled 831 g Plutonium Metal Hollow Cylinder with CGOC Impact

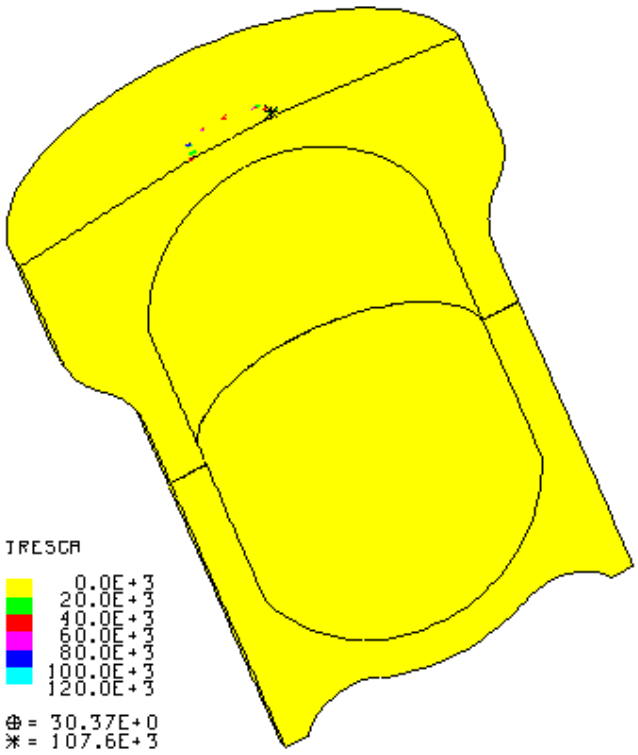

Figure 2-504. Tresca Stress in the TB-1 for 30-ft Drop Run 3 – Angled 831 g Plutonium Metal Hollow Cylinder with CGOC Impact

2.12.5.8 References

1. USNRC, NUREG-0361. Safety Analysis Report for the Plutonium Air Transportable Package, Model PAT-1. Washington, D.C. 1978.

2. Reference deleted.

3. Hecker, Siegfried S. and Michael F. Stevens. "Mechanical Behavior of Plutonium and Its Alloys." *Los Alamos Science* Number 26 (2000).

4. Wellman, G.W., Diegert, K.V., and Saizbrenner, R. "Two-Dimensional Quasistatic Modeling of Exclusion Region Barriers in Support of Design Guide Development." SAND93-0905. Sandia National Laboratories. Albuquerque, NM. 1993.

5. Bao, Y., and T. Wierzbicki. "On the Cut-Off Value of Negative Triaxiality for Fracture." Engineering Fracture Mechanics, 72, pp. 1049-1069, 2005..

6. Johnson, G.R., and Cook, W.H., "Fracture Characteristics of Three Metals Subjected to Various Strains, Strain Rates, Temperature and Pressures." *Engineering Fracture Mechanics* 2**1** (1985):31-48.

7. Bao, Y. "Prediction of Ductile Crack Formation in Uncracked Bodies," Report 100. Impact & Crash Worthiness Laboratory, Massachusetts Institute of Technology. Cambridge, MA. 2003.

8. Amer*ican Society of Mechanical Eng*ineers (ASME). "Boiler and Pressure Vessel Code," 2008a, Section II, Part D, Table 2A: Design Stress Intensity Values S_m for Ferrous Materials. pp. 298. 2008.

9. American Society of Mechanical Engineers (ASME). "Boiler and Pressure Vessel Code," Section III, Division 1--Appendices, Nonmandatory Appendix F: Article F-1000, Rules for Evaluation of Service Loadings with Level D Service Limits. pp. 232. 2007.

2.12.6 Bolt Analysis

The following section is an analysis of the bolts that secure the TB-1 lid when subjected to the loads applied during the high-speed aircraft accident test condition (10 CFR 71.74). The impulse loads are obtained from the component analyses (see Section 2.12.5).

The TB-1 lid is secured by (12) ½ -20 UNJF-3A bolts. The following calculation shows that the total bolt preload is approximately 108,000 lbs.

$$\text{Bolt torque}: T = 75\ \text{ft-lbs}$$

$$\text{Nominal bolt diameter}\ \ d = 0.5\,\text{in}$$

$$\text{Friction coefficien t}: K = 0.2$$

$$\text{Shigley}^{1}\ \text{Bolt force}: F_i = \frac{T}{Kd}$$

$$Fi = \frac{900}{(0.2)(0.5)} = 9000\,\text{lbf}$$

$$(12\ \text{bolts}) \times 9000 = 108{,}000\,\text{lbf}$$

The contact force of the redwood pushing on the top of the TB-1 to decelerate it is shown as the dashed curve in Figure 2-505. The bolt preload is also shown along with the sum of the contact force and the total bolt preload. These are the forces holding the lid in place during the end impact event.

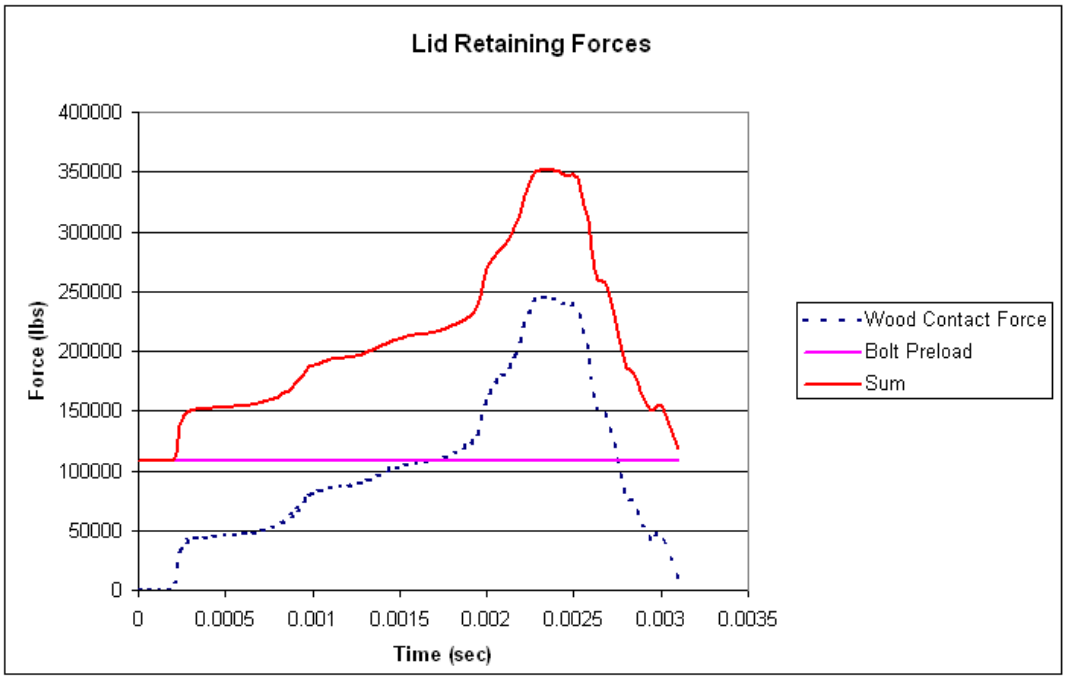

Figure 2-505. Contact Forces on the Top Surface of the TB-1 Lid

The force generated by the impacting components calculated in Section 2.12.5 along with the redwood contact force and bolt preload are shown in Figure 2-506. As shown in the figure, the forces from the components are only a fraction of the bolt preload. The peak impulse load is a factor of 2.1 less than the bolt preload and a factor of 6 less than the total of the sum of the wood retaining force and the bolt preload. Therefore, the lid of the TB-1 will remain tight and torqued during the aircraft impact accident.

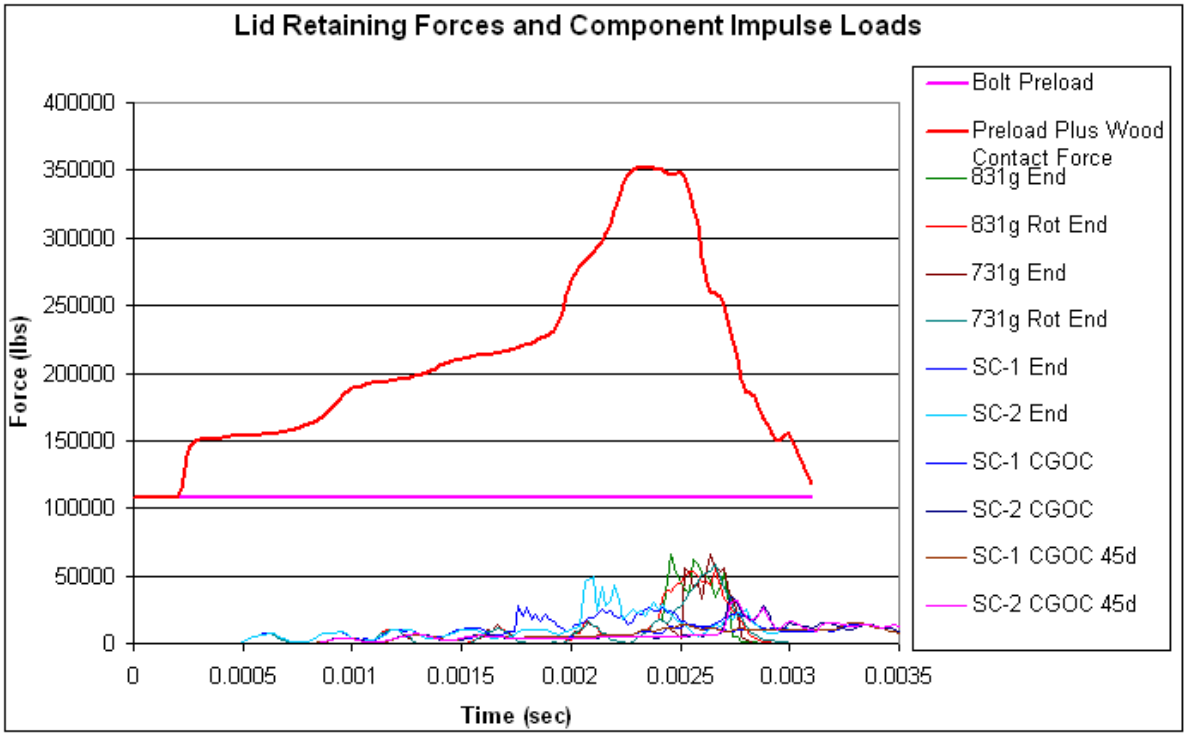

Figure 2-506. Contact Forces on the Top Surface of the TB-1 Lid Along with Impulse Loads from Various Contents

2.12.6.1 References

1. Shigley, J. E. *Mechanical Engineering Design*. McGraw-Hill, 1977.

2.12.7 Sample Input

The PRONTO3D input file for Run 3 of the high speed aircraft impact analysis (831 gram angled cylinder with CGOC impact) which resulted in the highest tearing parameter in the T-Ampoule is included below. Dollar signs designate comment lines.

```
TITLE
Full Overpack with TB1 with 831g cylinder top rot CGOC impact
$
TERM TIME,0.006
PLOT TIME,0.00003
PLOT NODAL,DISPLACEMENT, VELOCITY, ACCELERATION,reactions,force
PLOT ELEMENT, STRESS, VONMISES,DOPT, EPS
PLOT STATE, EQPS
SUM NODAL_MOMENTUMY MATERIAL 5
```

```
SUM CONTACT_FORCEY NODESET 500
SUM CONTACT_FORCEX NODESET 500
SUM CONTACT_FORCEZ NODESET 500
write restart .0005
$
$ symmetry boundary condition
$
$  no displ, y, 100
$  no displ, x, 100
  no displ, z, 100
  no displ, z, 101
$
$ hourglass control
$
$   assumed strain hourglass
    hourglass stiffening .08 .09
$
$ set up initial velocity
$
  initial velocity material 1   0.0  5064.0  0.0    $ cantop
  initial velocity material 2   0.0  5064.0  0.0    $ canbot
  initial velocity material 4   0.0  5064.0  0.0    $ TB-1 top
  initial velocity material 5   0.0  5064.0  0.0    $ PU cylinder (1)
  initial velocity material 6   0.0  5064.0  0.0    $ TB-1 bot
  initial velocity material 20  0.0  5064.0  0.0    $ spreader
  initial velocity material 21  0.0  5064.0  0.0    $ copper
  initial velocity material 22  0.0  5064.0  0.0    $ top plate 7075
  initial velocity material 23  0.0  5064.0  0.0    $ lower plate 7075
  initial velocity material 10  0.0  5064.0  0.0    $ shell
  initial velocity material 24  0.0  5064.0  0.0    $ wood 1 X
  initial velocity material 25  0.0  5064.0  0.0    $ wood 1 Z
  initial velocity material 26  0.0  5064.0  0.0    $ wood 1 X
  initial velocity material 27  0.0  5064.0  0.0    $ wood 2 X
  initial velocity material 28  0.0  5064.0  0.0    $ wood 2 Z
  initial velocity material 29  0.0  5064.0  0.0    $ wood 2 X
  initial velocity material 30  0.0  5064.0  0.0    $ wood 3 X
  initial velocity material 31  0.0  5064.0  0.0    $ wood 3 Z
  initial velocity material 32  0.0  5064.0  0.0    $ wood 3 X
  initial velocity material 33  0.0  5064.0  0.0    $ wood 4 X
  initial velocity material 34  0.0  5064.0  0.0    $ wood 4 Z
  initial velocity material 35  0.0  5064.0  0.0    $ wood 4 X
  initial velocity material 36  0.0  5064.0  0.0    $ wood 5 X
  initial velocity material 37  0.0  5064.0  0.0    $ wood 5 Z
  initial velocity material 38  0.0  5064.0  0.0    $ wood 5 X
  initial velocity material 39  0.0  5064.0  0.0    $ wood 6 X
  initial velocity material 40  0.0  5064.0  0.0    $ wood 6 Z
  initial velocity material 41  0.0  5064.0  0.0    $ wood 6 X
$
$ Death
$
$
$ set up contact by region for  model
$
  contact material 1
  contact material 2
  contact material 4
  contact material 5
```

```
  contact material 6
  contact material 20
  contact material 21
  contact material 22
  contact material 23
  contact material 24
  contact material 25
  contact material 26
  contact material 27
  contact material 28
  contact material 29
  contact material 30
  contact material 31
  contact material 32
  contact material 33
  contact material 34
  contact material 35
  contact material 36
  contact material 37
  contact material 38
  contact material 39
  contact material 40
  contact material 41
$ contact surfaces
  contact surface 30  $ mid tb1
  contact surface 31  $ mid tb1
  contact surface 800  $ top wood by pipe
  contact surface 801  $ top of pipe
$
$ define surface pairs
$
  contact data surface 800 surface 801 $
  kinematic partition 1.0
  friction static -1.0
  capture tolerance 0.005
  end
  contact data surface 30 surface 31 $
  kinematic partition 0.5
  friction static -1.0
  capture tolerance 0.005
  end
$
$ define friction
$
$ Top of Tamp and Cylinder
  contact data material 1 material 5
   kinematic partition 0.1
   friction static 0.36
   friction dynamic 0.3
  end
$ Bottom of Tamp and Cylinder
  contact data material 2 material 5
   kinematic partition 0.1
   friction static 0.36
   friction dynamic 0.3
  end
$
```

```
$ Rigid surface
$
 rigid surface 700 0.0 23.45 0.0 0.0 -1.0 0.0  $ top impact
$
$ define the shell thickness
$
  scale shell thickness 10 0.0625  $ can shell
$
$
$
$ define material properties
$
$
 MATERIAL, 1, ep power hardening, 0.000414, $  titanium
   YOUNGS MODULUS,       15.5E06
   POISSONS RATIO,        0.3
   YIELD STRESS,         141.7E03
   HARDENING constant,    12.6E04
   hardening exponent    0.6554
   luders strain         0.0
  END
 MATERIAL, 2, ep power hardening, 0.000414, $  titanium
   YOUNGS MODULUS,       15.5E06
   POISSONS RATIO,        0.3
   YIELD STRESS,         141.7E03
   HARDENING constant,    12.6E04
   hardening exponent    0.6554
   luders strain         0.0
  END
 Material, 4, ep power hardening, 0.00074, $  TB1 Top
   YOUNGS MODULUS,       30.E06
   POISSONS RATIO,        0.30
   YIELD STRESS,         141E03
   HARDENING constant,    30e4
   hardening exponent    1
   luders strain         0.0
  END
 MATERIAL, 5, ep power hardening, 0.001853, $  PU alpha phase 1
   YOUNGS MODULUS,       14.1E06
   POISSONS RATIO,        0.3
   YIELD STRESS,         36.0E03
   HARDENING constant,    85000
   hardening exponent    0.4
   luders strain         0.0
  END
 Material, 6, ep power hardening, 0.00074, $  TB1 Left
   YOUNGS MODULUS,       30.E06
   POISSONS RATIO,        0.30
   YIELD STRESS,         141E03
   HARDENING constant,    30e4
   hardening exponent    1
   luders strain         0.0
  END
 MATERIAL, 10, ep power hardening, 0.00074, $  304 stainless shell
   YOUNGS MODULUS,       28.E6
   POISSONS RATIO,        0.27
   YIELD STRESS,         40.E3
```

```
   HARDENING constant,    192746.
   hardening exponent    0.748190
   luders strain         0.0
  END
 MATERIAL, 20, ep power hardening, 0.0002536, $  6061
   YOUNGS MODULUS,       9.9E06
   POISSONS RATIO,        0.3
   YIELD STRESS,         45.0E03
   HARDENING constant,    37852
   hardening exponent    0.55
   luders strain         0.0
  END
 MATERIAL, 21, ep power hardening, 0.000414, $  copper
   YOUNGS MODULUS,       17.2E06
   POISSONS RATIO,        0.33
   YIELD STRESS,         45.0E03
   HARDENING constant,    38000
   hardening exponent    0.55
   luders strain         0.0
  END
 MATERIAL, 22, ep power hardening, 0.000264, $  7075
   YOUNGS MODULUS,       10.4E06
   POISSONS RATIO,        0.33
   YIELD STRESS,         73.0E03
   HARDENING constant,    37852
   hardening exponent    0.55
   luders strain         0.0
  END
 MATERIAL, 23, ep power hardening, 0.000264, $  7075
   YOUNGS MODULUS,       10.4E06
   POISSONS RATIO,        0.33
   YIELD STRESS,         73.0E03
   HARDENING constant,    37852
   hardening exponent    0.55
   luders strain         0.0
  END
MATERIAL 24 = ORTHOTROPIC CRUSH, 5.682e-5
        Compacted YOUNGS MODULUS = 1.5e6
        Compacted POISSONS RATIO = 0.3
        Compacted YIELD STRESS  = 20000.
        X ID = 1   Y ID = 1
        Z ID = 2   XY ID = 4
        YZ ID = 5   ZX ID = 4
        Full Compaction = 0.9 $ 0 = no compaction, 1 = very flat
        Modulus x = 1.5e6
        Modulus y = 0.3e6
        Modulus z = 0.3e6
        Modulus xy = 0.2e6
        Modulus yz = 0.25e6
        Modulus zx = 0.2e6
End
Function 1  $ x-direction ( T-Direction)
        0.       2000.
        0.14     4200.
        0.28     5100.
        0.42     5430.
        0.57     6100.
```

```
        0.71     10100.
        0.80     15000.
        0.90     20000.
End
Function 2    $  y-direction (L-Direction) z-direction approx the same
        0.       400.
        0.14     986.
        0.28     1200.
        0.42     1275.
        0.57     1432.
        0.71     2371.
        0.80     3521.
        0.90     4690.
End
Function 4   $ sigxy or sigxz vs volume
        0.0     1000.
        0.60    1000.
        0.70    10000.
        0.90    10000.
End
Function 5   $ sigyz vs volume
        0.0     1000.
        0.60    1000.
        0.70    10000.
        0.90    10000.
End
MATERIAL 25 = ORTHOTROPIC CRUSH, 5.682e-5
        Compacted YOUNGS MODULUS = 1.5e6
        Compacted POISSONS RATIO = 0.3
        Compacted YIELD STRESS  = 20000.
        X ID = 2   Y ID = 1
        Z ID = 1   XY ID = 4
        YZ ID = 5   ZX ID = 4
        Full Compaction = 0.9 $ 0 = no compaction, 1 = very flat
        Modulus x = 1.5e6
        Modulus y = 0.3e6
        Modulus z = 0.3e6
        Modulus xy = 0.2e6
        Modulus yz = 0.25e6
        Modulus zx = 0.2e6
End
Function 1  $ x-direction ( T-Direction)
        0.       2000.
        0.14     4200.
        0.28     5100.
        0.42     5430.
        0.57     6100.
        0.71     10100.
        0.80     15000.
        0.90     20000.
End
Function 2    $  y-direction (L-Direction) z-direction approx the same
        0.       400.
        0.14     986.
        0.28     1200.
        0.42     1275.
        0.57     1432.
```

```
        0.71     2371.
        0.80     3521.
        0.90     4690.
End
Function 4   $ sigxy or sigxz vs volume
        0.0     1000.
        0.60    1000.
        0.70    10000.
        0.90    10000.
End
Function 5   $ sigyz vs volume
        0.0     1000.
        0.60    1000.
        0.70    10000.
        0.90    10000.
End
MATERIAL 26 = ORTHOTROPIC CRUSH, 5.682e-5
        Compacted YOUNGS MODULUS = 1.5e6
        Compacted POISSONS RATIO = 0.3
        Compacted YIELD STRESS  = 20000.
        X ID = 1   Y ID = 1
        Z ID = 2   XY ID = 4
        YZ ID = 5   ZX ID = 4
        Full Compaction = 0.9 $ 0 = no compaction, 1 = very flat
        Modulus x = 1.5e6
        Modulus y = 0.3e6
        Modulus z = 0.3e6
        Modulus xy = 0.2e6
        Modulus yz = 0.25e6
        Modulus zx = 0.2e6
End
Function 1  $ x-direction ( T-Direction)
        0.       2000.
        0.14     4200.
        0.28     5100.
        0.42     5430.
        0.57     6100.
        0.71     10100.
        0.80     15000.
        0.90     20000.
End
Function 2    $  y-direction (L-Direction) z-direction approx the same
        0.       400.
        0.14     986.
        0.28     1200.
        0.42     1275.
        0.57     1432.
        0.71     2371.
        0.80     3521.
        0.90     4690.
End
Function 4   $ sigxy or sigxz vs volume
        0.0     1000.
        0.60    1000.
        0.70    10000.
        0.90    10000.
End
```

```
Function 5   $ sigyz vs volume
        0.0     1000.
        0.60    1000.
        0.70    10000.
        0.90    10000.
End
MATERIAL 27 = ORTHOTROPIC CRUSH, 5.682e-5
        Compacted YOUNGS MODULUS = 1.5e6
        Compacted POISSONS RATIO = 0.3
        Compacted YIELD STRESS  = 20000.
        X ID = 1   Y ID = 1
        Z ID = 2   XY ID = 4
        YZ ID = 5   ZX ID = 4
        Full Compaction = 0.9 $ 0 = no compaction, 1 = very flat
        Modulus x = 1.5e6
        Modulus y = 0.3e6
        Modulus z = 0.3e6
        Modulus xy = 0.2e6
        Modulus yz = 0.25e6
        Modulus zx = 0.2e6
End
Function 1  $ x-direction ( T-Direction)
        0.       2000.
        0.14     4200.
        0.28     5100.
        0.42     5430.
        0.57     6100.
        0.71     10100.
        0.80     15000.
        0.90     20000.
End
Function 2    $  y-direction (L-Direction) z-direction approx the same
        0.       400.
        0.14     986.
        0.28     1200.
        0.42     1275.
        0.57     1432.
        0.71     2371.
        0.80     3521.
        0.90     4690.
End
Function 4   $ sigxy or sigxz vs volume
        0.0     1000.
        0.60    1000.
        0.70    10000.
        0.90    10000.
End
Function 5   $ sigyz vs volume
        0.0     1000.
        0.60    1000.
        0.70    10000.
        0.90    10000.
End
MATERIAL 28 = ORTHOTROPIC CRUSH, 5.682e-5
        Compacted YOUNGS MODULUS = 1.5e6
        Compacted POISSONS RATIO = 0.3
        Compacted YIELD STRESS  = 20000.
```

```
        X ID = 2   Y ID = 1
        Z ID = 1   XY ID = 4
        YZ ID = 5   ZX ID = 4
        Full Compaction = 0.9 $ 0 = no compaction, 1 = very flat
        Modulus x = 1.5e6
        Modulus y = 0.3e6
        Modulus z = 0.3e6
        Modulus xy = 0.2e6
        Modulus yz = 0.25e6
        Modulus zx = 0.2e6
End
Function 1  $ x-direction ( T-Direction)
        0.       2000.
        0.14     4200.
        0.28     5100.
        0.42     5430.
        0.57     6100.
        0.71     10100.
        0.80     15000.
        0.90     20000.
End
Function 2    $  y-direction (L-Direction) z-direction approx the same
        0.       400.
        0.14     986.
        0.28     1200.
        0.42     1275.
        0.57     1432.
        0.71     2371.
        0.80     3521.
        0.90     4690.
End
Function 4   $ sigxy or sigxz vs volume
        0.0     1000.
        0.60    1000.
        0.70    10000.
        0.90    10000.
End
Function 5   $ sigyz vs volume
        0.0     1000.
        0.60    1000.
        0.70    10000.
        0.90    10000.
End
MATERIAL 29 = ORTHOTROPIC CRUSH, 5.682e-5
        Compacted YOUNGS MODULUS = 1.5e6
        Compacted POISSONS RATIO = 0.3
        Compacted YIELD STRESS  = 20000.
        X ID = 1   Y ID = 1
        Z ID = 2   XY ID = 4
        YZ ID = 5   ZX ID = 4
        Full Compaction = 0.9 $ 0 = no compaction, 1 = very flat
        Modulus x = 1.5e6
        Modulus y = 0.3e6
        Modulus z = 0.3e6
        Modulus xy = 0.2e6
        Modulus yz = 0.25e6
        Modulus zx = 0.2e6
```

```
End
Function 1  $ x-direction ( T-Direction)
        0.       2000.
        0.14     4200.
        0.28     5100.
        0.42     5430.
        0.57     6100.
        0.71     10100.
        0.80     15000.
        0.90     20000.
End
Function 2    $  y-direction (L-Direction) z-direction approx the same
        0.       400.
        0.14     986.
        0.28     1200.
        0.42     1275.
        0.57     1432.
        0.71     2371.
        0.80     3521.
        0.90     4690.
End
Function 4   $ sigxy or sigxz vs volume
        0.0     1000.
        0.60    1000.
        0.70    10000.
        0.90    10000.
End
Function 5   $ sigyz vs volume
        0.0     1000.
        0.60    1000.
        0.70    10000.
        0.90    10000.
End
MATERIAL 30 = ORTHOTROPIC CRUSH, 5.682e-5
        Compacted YOUNGS MODULUS = 1.5e6
        Compacted POISSONS RATIO = 0.3
        Compacted YIELD STRESS  = 20000.
        X ID = 1   Y ID = 1
        Z ID = 2   XY ID = 4
        YZ ID = 5   ZX ID = 4
        Full Compaction = 0.9 $ 0 = no compaction, 1 = very flat
        Modulus x = 1.5e6
        Modulus y = 0.3e6
        Modulus z = 0.3e6
        Modulus xy = 0.2e6
        Modulus yz = 0.25e6
        Modulus zx = 0.2e6
End
Function 1  $ x-direction ( T-Direction)
        0.       2000.
        0.14     4200.
        0.28     5100.
        0.42     5430.
        0.57     6100.
        0.71     10100.
        0.80     15000.
        0.90     20000.
```

```
End
Function 2    $  y-direction (L-Direction) z-direction approx the same
        0.       400.
        0.14     986.
        0.28     1200.
        0.42     1275.
        0.57     1432.
        0.71     2371.
        0.80     3521.
        0.90     4690.
End
Function 4   $ sigxy or sigxz vs volume
        0.0     1000.
        0.60    1000.
        0.70    10000.
        0.90    10000.
End
Function 5   $ sigyz vs volume
        0.0     1000.
        0.60    1000.
        0.70    10000.
        0.90    10000.
End
MATERIAL 31 = ORTHOTROPIC CRUSH, 5.682e-5
        Compacted YOUNGS MODULUS = 1.5e6
        Compacted POISSONS RATIO = 0.3
        Compacted YIELD STRESS  = 20000.
        X ID = 2   Y ID = 1
        Z ID = 1   XY ID = 4
        YZ ID = 5   ZX ID = 4
        Full Compaction = 0.9 $ 0 = no compaction, 1 = very flat
        Modulus x = 1.5e6
        Modulus y = 0.3e6
        Modulus z = 0.3e6
        Modulus xy = 0.2e6
        Modulus yz = 0.25e6
        Modulus zx = 0.2e6
End
Function 1  $ x-direction ( T-Direction)
        0.       2000.
        0.14     4200.
        0.28     5100.
        0.42     5430.
        0.57     6100.
        0.71     10100.
        0.80     15000.
        0.90     20000.
End
Function 2    $  y-direction (L-Direction) z-direction approx the same
        0.       400.
        0.14     986.
        0.28     1200.
        0.42     1275.
        0.57     1432.
        0.71     2371.
        0.80     3521.
        0.90     4690.
```

```
End
Function 4   $ sigxy or sigxz vs volume
        0.0     1000.
        0.60    1000.
        0.70    10000.
        0.90    10000.
End
Function 5   $ sigyz vs volume
        0.0     1000.
        0.60    1000.
        0.70    10000.
        0.90    10000.
End
MATERIAL 32 = ORTHOTROPIC CRUSH, 5.682e-5
        Compacted YOUNGS MODULUS = 1.5e6
        Compacted POISSONS RATIO = 0.3
        Compacted YIELD STRESS  = 20000.
        X ID = 1   Y ID = 1
        Z ID = 2   XY ID = 4
        YZ ID = 5   ZX ID = 4
        Full Compaction = 0.9 $ 0 = no compaction, 1 = very flat
        Modulus x = 1.5e6
        Modulus y = 0.3e6
        Modulus z = 0.3e6
        Modulus xy = 0.2e6
        Modulus yz = 0.25e6
        Modulus zx = 0.2e6
End
Function 1  $ x-direction ( T-Direction)
        0.       2000.
        0.14     4200.
        0.28     5100.
        0.42     5430.
        0.57     6100.
        0.71     10100.
        0.80     15000.
        0.90     20000.
End
Function 2    $  y-direction (L-Direction) z-direction approx the same
        0.       400.
        0.14     986.
        0.28     1200.
        0.42     1275.
        0.57     1432.
        0.71     2371.
        0.80     3521.
        0.90     4690.
End
Function 4   $ sigxy or sigxz vs volume
        0.0     1000.
        0.60    1000.
        0.70    10000.
        0.90    10000.
End
Function 5   $ sigyz vs volume
        0.0     1000.
        0.60    1000.
```

```
        0.70    10000.
        0.90    10000.
End
MATERIAL 33 = ORTHOTROPIC CRUSH, 5.682e-5
        Compacted YOUNGS MODULUS = 1.5e6
        Compacted POISSONS RATIO = 0.3
        Compacted YIELD STRESS  = 20000.
        X ID = 1   Y ID = 1
        Z ID = 2   XY ID = 4
        YZ ID = 5   ZX ID = 4
        Full Compaction = 0.9 $ 0 = no compaction, 1 = very flat
        Modulus x = 1.5e6
        Modulus y = 0.3e6
        Modulus z = 0.3e6
        Modulus xy = 0.2e6
        Modulus yz = 0.25e6
        Modulus zx = 0.2e6
End
Function 1  $ x-direction ( T-Direction)
        0.       2000.
        0.14     4200.
        0.28     5100.
        0.42     5430.
        0.57     6100.
        0.71     10100.
        0.80     15000.
        0.90     20000.
End
Function 2    $  y-direction (L-Direction) z-direction approx the same
        0.       400.
        0.14     986.
        0.28     1200.
        0.42     1275.
        0.57     1432.
        0.71     2371.
        0.80     3521.
        0.90     4690.
End
Function 4   $ sigxy or sigxz vs volume
        0.0     1000.
        0.60    1000.
        0.70    10000.
        0.90    10000.
End
Function 5   $ sigyz vs volume
        0.0     1000.
        0.60    1000.
        0.70    10000.
        0.90    10000.
End
MATERIAL 34 = ORTHOTROPIC CRUSH, 5.682e-5
        Compacted YOUNGS MODULUS = 1.5e6
        Compacted POISSONS RATIO = 0.3
        Compacted YIELD STRESS  = 20000.
        X ID = 2   Y ID = 1
        Z ID = 1   XY ID = 4
        YZ ID = 5   ZX ID = 4
```

```
        Full Compaction = 0.9 $ 0 = no compaction, 1 = very flat
        Modulus x = 1.5e6
        Modulus y = 0.3e6
        Modulus z = 0.3e6
        Modulus xy = 0.2e6
        Modulus yz = 0.25e6
        Modulus zx = 0.2e6
End
Function 1  $ x-direction ( T-Direction)
        0.       2000.
        0.14     4200.
        0.28     5100.
        0.42     5430.
        0.57     6100.
        0.71     10100.
        0.80     15000.
        0.90     20000.
End
Function 2    $  y-direction (L-Direction) z-direction approx the same
        0.       400.
        0.14     986.
        0.28     1200.
        0.42     1275.
        0.57     1432.
        0.71     2371.
        0.80     3521.
        0.90     4690.
End
Function 4   $ sigxy or sigxz vs volume
        0.0     1000.
        0.60    1000.
        0.70    10000.
        0.90    10000.
End
Function 5   $ sigyz vs volume
        0.0     1000.
        0.60    1000.
        0.70    10000.
        0.90    10000.
End
MATERIAL 35 = ORTHOTROPIC CRUSH, 5.682e-5
        Compacted YOUNGS MODULUS = 1.5e6
        Compacted POISSONS RATIO = 0.3
        Compacted YIELD STRESS  = 20000.
        X ID = 1   Y ID = 1
        Z ID = 2   XY ID = 4
        YZ ID = 5   ZX ID = 4
        Full Compaction = 0.9 $ 0 = no compaction, 1 = very flat
        Modulus x = 1.5e6
        Modulus y = 0.3e6
        Modulus z = 0.3e6
        Modulus xy = 0.2e6
        Modulus yz = 0.25e6
        Modulus zx = 0.2e6
End
Function 1  $ x-direction ( T-Direction)
        0.       2000.
```

```
        0.14     4200.
        0.28     5100.
        0.42     5430.
        0.57     6100.
        0.71     10100.
        0.80     15000.
        0.90     20000.
End
Function 2    $  y-direction (L-Direction) z-direction approx the same
        0.       400.
        0.14     986.
        0.28     1200.
        0.42     1275.
        0.57     1432.
        0.71     2371.
        0.80     3521.
        0.90     4690.
End
Function 4   $ sigxy or sigxz vs volume
        0.0     1000.
        0.60    1000.
        0.70    10000.
        0.90    10000.
End
Function 5   $ sigyz vs volume
        0.0     1000.
        0.60    1000.
        0.70    10000.
        0.90    10000.
End
MATERIAL 36 = ORTHOTROPIC CRUSH, 5.682e-5
        Compacted YOUNGS MODULUS = 1.5e6
        Compacted POISSONS RATIO = 0.3
        Compacted YIELD STRESS  = 20000.
        X ID = 1   Y ID = 1
        Z ID = 2   XY ID = 4
        YZ ID = 5   ZX ID = 4
        Full Compaction = 0.9 $ 0 = no compaction, 1 = very flat
        Modulus x = 1.5e6
        Modulus y = 0.3e6
        Modulus z = 0.3e6
        Modulus xy = 0.2e6
        Modulus yz = 0.25e6
        Modulus zx = 0.2e6
End
Function 1  $ x-direction ( T-Direction)
        0.       2000.
        0.14     4200.
        0.28     5100.
        0.42     5430.
        0.57     6100.
        0.71     10100.
        0.80     15000.
        0.90     20000.
End
Function 2    $  y-direction (L-Direction) z-direction approx the same
        0.       400.
```

```
        0.14     986.
        0.28     1200.
        0.42     1275.
        0.57     1432.
        0.71     2371.
        0.80     3521.
        0.90     4690.
End
Function 4   $ sigxy or sigxz vs volume
        0.0     1000.
        0.60    1000.
        0.70    10000.
        0.90    10000.
End
Function 5   $ sigyz vs volume
        0.0     1000.
        0.60    1000.
        0.70    10000.
        0.90    10000.
End
MATERIAL 37 = ORTHOTROPIC CRUSH, 5.682e-5
        Compacted YOUNGS MODULUS = 1.5e6
        Compacted POISSONS RATIO = 0.3
        Compacted YIELD STRESS  = 20000.
        X ID = 2   Y ID = 1
        Z ID = 1   XY ID = 4
        YZ ID = 5   ZX ID = 4
        Full Compaction = 0.9 $ 0 = no compaction, 1 = very flat
        Modulus x = 1.5e6
        Modulus y = 0.3e6
        Modulus z = 0.3e6
        Modulus xy = 0.2e6
        Modulus yz = 0.25e6
        Modulus zx = 0.2e6
End
Function 1  $ x-direction ( T-Direction)
        0.       2000.
        0.14     4200.
        0.28     5100.
        0.42     5430.
        0.57     6100.
        0.71     10100.
        0.80     15000.
        0.90     20000.
End
Function 2    $  y-direction (L-Direction) z-direction approx the same
        0.       400.
        0.14     986.
        0.28     1200.
        0.42     1275.
        0.57     1432.
        0.71     2371.
        0.80     3521.
        0.90     4690.
End
Function 4   $ sigxy or sigxz vs volume
        0.0     1000.
```

```
        0.60    1000.
        0.70    10000.
        0.90    10000.
End
Function 5   $ sigyz vs volume
        0.0     1000.
        0.60    1000.
        0.70    10000.
        0.90    10000.
End
MATERIAL 38 = ORTHOTROPIC CRUSH, 5.682e-5
        Compacted YOUNGS MODULUS = 1.5e6
        Compacted POISSONS RATIO = 0.3
        Compacted YIELD STRESS  = 20000.
        X ID = 1   Y ID = 1
        Z ID = 2   XY ID = 4
        YZ ID = 5   ZX ID = 4
        Full Compaction = 0.9 $ 0 = no compaction, 1 = very flat
        Modulus x = 1.5e6
        Modulus y = 0.3e6
        Modulus z = 0.3e6
        Modulus xy = 0.2e6
        Modulus yz = 0.25e6
        Modulus zx = 0.2e6
End
Function 1  $ x-direction ( T-Direction)
        0.       2000.
        0.14     4200.
        0.28     5100.
        0.42     5430.
        0.57     6100.
        0.71     10100.
        0.80     15000.
        0.90     20000.
End
Function 2    $  y-direction (L-Direction) z-direction approx the same
        0.       400.
        0.14     986.
        0.28     1200.
        0.42     1275.
        0.57     1432.
        0.71     2371.
        0.80     3521.
        0.90     4690.
End
Function 4   $ sigxy or sigxz vs volume
        0.0     1000.
        0.60    1000.
        0.70    10000.
        0.90    10000.
End
Function 5   $ sigyz vs volume
        0.0     1000.
        0.60    1000.
        0.70    10000.
        0.90    10000.
End
```

```
MATERIAL 39 = ORTHOTROPIC CRUSH, 5.682e-5
        Compacted YOUNGS MODULUS = 1.5e6
        Compacted POISSONS RATIO = 0.3
        Compacted YIELD STRESS  = 20000.
        X ID = 1   Y ID = 1
        Z ID = 2   XY ID = 4
        YZ ID = 5   ZX ID = 4
        Full Compaction = 0.9 $ 0 = no compaction, 1 = very flat
        Modulus x = 1.5e6
        Modulus y = 0.3e6
        Modulus z = 0.3e6
        Modulus xy = 0.2e6
        Modulus yz = 0.25e6
        Modulus zx = 0.2e6
End
Function 1  $ x-direction ( T-Direction)
        0.       2000.
        0.14     4200.
        0.28     5100.
        0.42     5430.
        0.57     6100.
        0.71     10100.
        0.80     15000.
        0.90     20000.
End
Function 2    $  y-direction (L-Direction) z-direction approx the same
        0.       400.
        0.14     986.
        0.28     1200.
        0.42     1275.
        0.57     1432.
        0.71     2371.
        0.80     3521.
        0.90     4690.
End
Function 4   $ sigxy or sigxz vs volume
        0.0     1000.
        0.60    1000.
        0.70    10000.
        0.90    10000.
End
Function 5   $ sigyz vs volume
        0.0     1000.
        0.60    1000.
        0.70    10000.
        0.90    10000.
End
MATERIAL 40 = ORTHOTROPIC CRUSH, 5.682e-5
        Compacted YOUNGS MODULUS = 1.5e6
        Compacted POISSONS RATIO = 0.3
        Compacted YIELD STRESS  = 20000.
        X ID = 2   Y ID = 1
        Z ID = 1   XY ID = 4
        YZ ID = 5   ZX ID = 4
        Full Compaction = 0.9 $ 0 = no compaction, 1 = very flat
        Modulus x = 1.5e6
        Modulus y = 0.3e6
```

```
        Modulus z = 0.3e6
        Modulus xy = 0.2e6
        Modulus yz = 0.25e6
        Modulus zx = 0.2e6
End
Function 1  $ x-direction ( T-Direction)
        0.       2000.
        0.14     4200.
        0.28     5100.
        0.42     5430.
        0.57     6100.
        0.71     10100.
        0.80     15000.
        0.90     20000.
End
Function 2    $  y-direction (L-Direction) z-direction approx the same
        0.       400.
        0.14     986.
        0.28     1200.
        0.42     1275.
        0.57     1432.
        0.71     2371.
        0.80     3521.
        0.90     4690.
End
Function 4   $ sigxy or sigxz vs volume
        0.0     1000.
        0.60    1000.
        0.70    10000.
        0.90    10000.
End
Function 5   $ sigyz vs volume
        0.0     1000.
        0.60    1000.
        0.70    10000.
        0.90    10000.
End
MATERIAL 41 = ORTHOTROPIC CRUSH, 5.682e-5
        Compacted YOUNGS MODULUS = 1.5e6
        Compacted POISSONS RATIO = 0.3
        Compacted YIELD STRESS  = 20000.
        X ID = 1   Y ID = 1
        Z ID = 2   XY ID = 4
        YZ ID = 5   ZX ID = 4
        Full Compaction = 0.9 $ 0 = no compaction, 1 = very flat
        Modulus x = 1.5e6
        Modulus y = 0.3e6
        Modulus z = 0.3e6
        Modulus xy = 0.2e6
        Modulus yz = 0.25e6
        Modulus zx = 0.2e6
End
Function 1  $ x-direction ( T-Direction)
        0.       2000.
        0.14     4200.
        0.28     5100.
        0.42     5430.
```

```
        0.57     6100.
        0.71     10100.
        0.80     15000.
        0.90     20000.
End
Function 2    $  y-direction (L-Direction) z-direction approx the same
        0.       400.
        0.14     986.
        0.28     1200.
        0.42     1275.
        0.57     1432.
        0.71     2371.
        0.80     3521.
        0.90     4690.
End
Function 4   $ sigxy or sigxz vs volume
        0.0     1000.
        0.60    1000.
        0.70    10000.
        0.90    10000.
End
Function 5   $ sigyz vs volume
        0.0     1000.
        0.60    1000.
        0.70    10000.
        0.90    10000.
End
 exit
```

2.12.8 Design Pressure Calculations for the T-Ampoule (in Accordance with Section VIII Division 1 of the ASME Boiler and Pressure Vessel Code

See stand-alone document that follows.

This page intentionally left blank

Design Pressure Calculations for the T-Ampoule in Accordance with Section VIII Division 1 of the ASME Boiler and Pressure Vessel Code

The objective of the T-Ampoule (Drawing 2A0261) is to provide a eutectic prevention barrier between the plutonium it contains and the PH13-8Mo stainless steel of the TB-1 containment vessel. The barrier will minimize any formation of a Pu/Fe eutectic under the elevated temperature of 1080ºF during a fire accident. In forming the barrier, the T-Ampoule becomes a pressure vessel requiring analysis.

Section 1 describes the preparation of the pressure-temperature map which is necessary for a full pressure vessel analysis. This includes not only the interaction between the TB-1 pressure vessel and the T-Ampoule, but also the impact of pyrolysis of both O-ring material and of any ancillary plastic used for tagging and bagging within the T-Ampoule.

Section 2 presents an analysis performed to validate the maximum pressure specification of TB-1 taken from the original Safety Analysis Report (SAR).

The third section, Section 3, describes the actual pressure analysis for the T-Ampoule. The criteria selected for the analysis of T-Ampoule pressure containing capability is the ASME Boiler and Pressure Vessel Code (BPVC), Section VIII, Division 1.[1][2] The T-Ampoule's unusual design has some aspects, e.g., its small size or the use of O-ring seals, that require

exceptions to Section VIII. This section enumerates these exceptions. It also identifies specific paragraphs of the ASME Code that do apply to the T-Ampoule design.

Section 4 addresses the O-ring seal, a device not covered by Section VIII.

Throughout this report, individual sections identify and discuss instances of conservatism and uncertainty in the analyses. Chapter 5 accumulates all of these discussions into a single location to help the reader grasp the total level of conservatism and the risk associated with uncertainty involved in the analysis.

Finally, Section 6 recaps the whole paper into a single discussion of the results.

1 Pressure Temperature Map

A previous analysis described in LA-UR-10-05846, [3] addresses increased pressure inside the TB-1 pressure vessel in an aircraft accident scenario. This report treats the TB-1 interior as a single volume subjected to a uniform temperature of 1080ºF. A uniform internal pressure is determined by analysis. This is in fact a good description of the final state of the package. However, the assembly starts out as two pressure envelopes. The T-Ampoule is a pressure vessel itself. Subdividing the TB-1 into two zones, the T-Ampoule forms the first zone; the second zone consists of the extremely small annulus between the T-Ampoule and the TB-1 wall, referred to herein as the Annulus. These two zones exist as separate pressure envelopes until the O-rings inside the vessels decompose and/or the O-ring seal in the T-Ampoule fails and pressures equilibrate. Before equilibration these two zones respond differently to temperature changes. After equilibration, the whole assembly acts as the single pressure containing device described by LA-UR-10-05846.

This analysis uses LA-UR-10-05846's conclusion that packing configuration #3, shown in Figure 1, is the worst case. It also adopts LA-UR-10-05846's assumption that sufficient oxygen somehow enters the vessels to oxidize all char and heavy hydrocarbons resulting from pyrolysis. It is, however, possible to provide a more realistic estimate of the pyrolysis impact. This less conservative calculation is included to provide a measure of the degree of conservatism in this analysis.

1.1 Package Volumes

Consider the assembly drawing in Figure 1: TB-1 Assembly for Packing Configuration #3. Three sample plutonium containers reside within the T-Ampoule. These three containers are designed to carry plutonium and are not pressure vessels. The T-Ampoule with the three containers fits snuggly within the TB-1 containment vessel. This leaves a small annulus volume between the TB-1 wall and the external surface of the T-Ampoule. More detailed inspection of Figure 1 illustrates just how small the annulus volume is. The TB-1 vessel's inner diameter is 4.250 inches. The T-Ampoule's outer diameter is 4.220 inches. Both numbers are average values. Assuming they are somehow perfectly centered, these dimensions leave a 0.015 inch radial gap between the two vessels. This gap integrated around the whole surface of the T-Ampoule creates an annulus volume of just 37.7 cubic centimeters (2.30 cubic inches). This analysis uses SI units to maintain consistency with the LA-UR-10-05846 report.

The T-Ampoule uses an O-ring seal to contain pressure. The three SC-1 containers also use O-rings. However, they are not considered pressure vessels. The T-Ampoule may also contain some PVC labels or polyethylene bags (referred to as ancillary plastic). As temperature increases during a design fire accident, the O-rings and ancillary plastic will decompose, or pyrolyze, increasing the mass of vapor in each pressure envelope. The amount of new vapor

differs between the T-Ampoule and the annulus. These differences plus the volumetric differences cause different pressure responses to temperature increase.

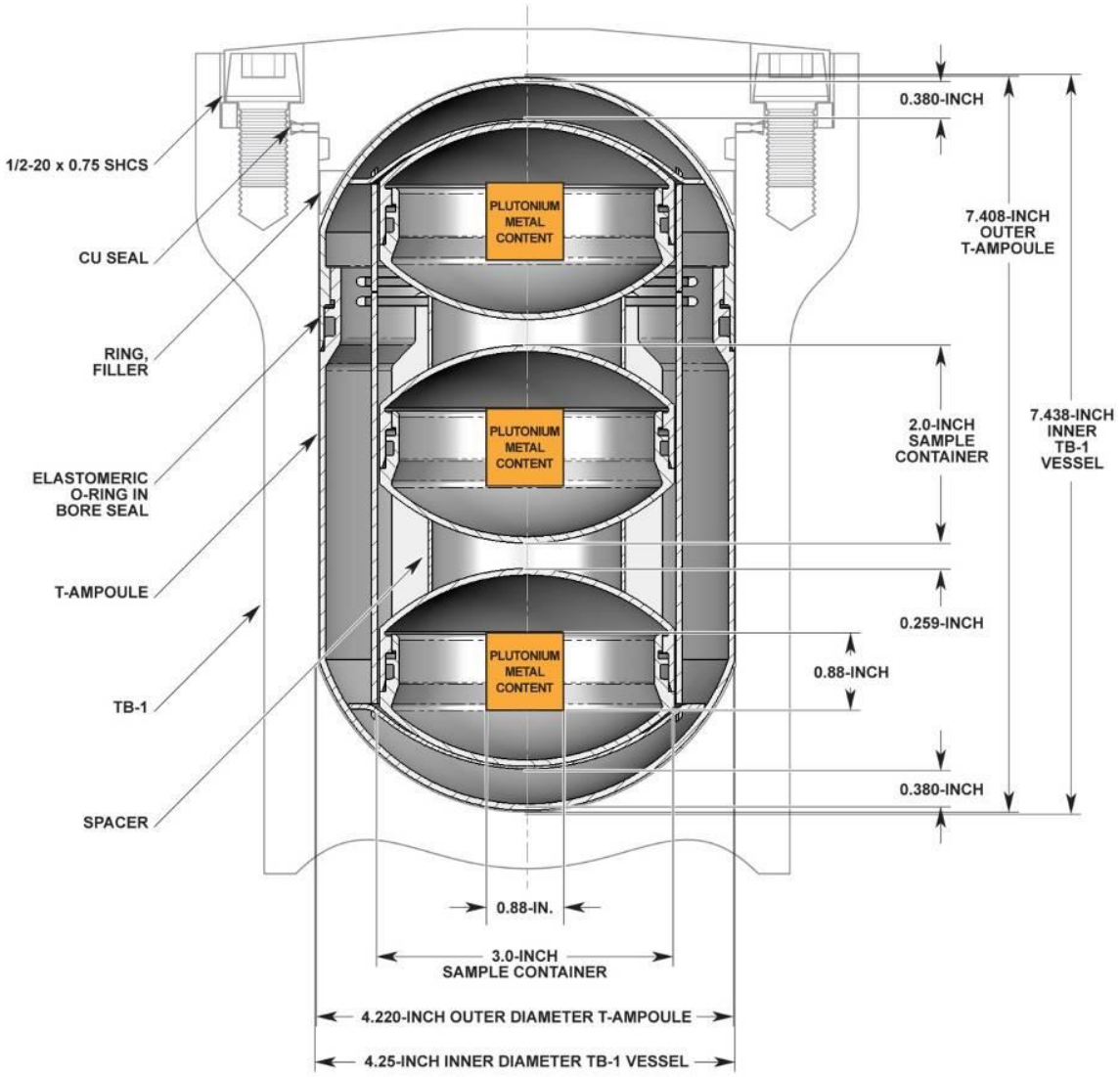

Figure 1: TB-1 Assembly for Packing Configuration #3

The following analysis tracks the response of three individual pressure envelopes:

- The annulus zone is the space between the TB-1 containment vessel and the T-Ampoule.
- The T-Ampoule zone consists of the volume within the T-Ampoule less the volume of solids contained there.
- The third zone is TB-1 volume. It is the sum of the first two volumes.

As will be discussed in detail below, the TB-1 becomes meaningful only after the T-Ampoule's seal fails and pressure equilibrates between the first two zones.

The volumes for each zone are listed in Table 1. They were taken from the LA-UR-10-05846 paper. In addition, the empty internal T-Ampoule volume of 1280 cm^3 was estimated specifically for this analysis. The vapor volume of the TB-1 container remains 1103 cm^3. The T-Ampoule, designed to nestle within the TB-1 container, is only slightly smaller with an internal volume of 1065 cm^3. The difference between these two volumes is the volume of the annulus at 37.7 cm^3.

Table 1: Summary of Pressure Envelope Volumes

Description	TB-1	T-Ampoule	Annulus	Units
Empty Volume	1460	1280		cm^3
Metal Volume		128		cm^3
Occupied Volume		1410		cm^3
Filler Ring	14.75			cm^3
T-Amp Contents Volume		214		cm^3
Vapor Volume (cm^3)	1103	1065	37.7	cm^3
Vapor Volume (m^3)	0.001103	0.001065	0.000038	m^3

The TB-1 device is fabricated from PH13-8Mo, equivalent to 13Cr-8Ni-2Mo, stainless steel while the T-Ampoule is fabricated of Ti-6Al-4V titanium alloy. These two materials have different thermal expansion coefficients with the stainless steel expanding slightly faster with temperature. The relative volume change with temperature between the two materials would be proportional to the cube of the thermal expansion coefficients integrated over the temperature range. These cubes of the thermal expansion coefficients are plotted in Figure 2. The values for thermal expansion coefficients for the two metals were taken from the BPVC, Section II Part D [2]. The volumes are expected to equilibrate pressures at approximately 800°F when O-ring seals fail. At that temperature, the value for the cube of thermal expansion factor for stainless steel is 1.015 in^3/in^3. For the titanium alloy of the T-Ampoule, the value at the same temperature was 1.011 in^3/in^3. Roughly estimated, the annulus volume would grow by the difference between these two values or by about 0.4% when the assembly is heated from 70°F to 800°F. Since the stainless always expands more than the titanium, the annulus volume change with temperature is always positive.

Subsequent analyses assume zero thermal growth. The above discussion demonstrates that the relative volume change with temperature is small but positive. Trying to quantify this volume change further would require significant analysis given the complex shapes involved. Further, since the annulus volume change with temperature is always positive, pressures calculated ignoring this change will slightly exceed actual pressures. Hence the assumption of no growth is conservative.

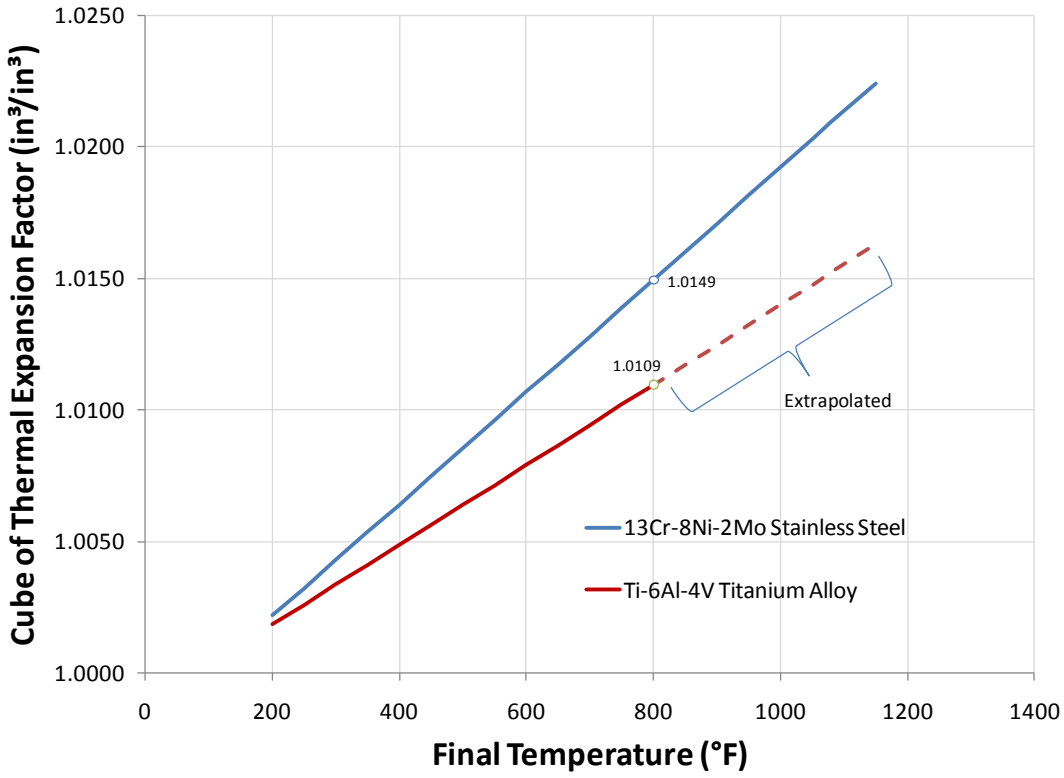

Figure 2: Plot of the Cube of the Thermal Expansion for Selected Materials as a Function of Temperature

1.2 O-ring Decomposition

Table 2 provides a summary of O-ring volumes and masses with the initial volumes extracted from LA-UR-10-05846. The T-Ampoule contains three O-rings, one for each sample container seal. In addition, this analysis allocates one half of the O-ring volume used to seal the T-Ampoule to the T-Ampoule zone's volume. The remaining one half of the T-Ampoule O-ring seal is allocated to the annulus zone volume. The TB-1 column in Table 2 contains the sum of the T-Ampoule and the annulus columns. The masses listed on the last line of Table 2 are based on an O−ring density of 1.8 g/cm^3.

Table 2: O-ring Volumes and Weights

Description	Annulus	TB-1	T-Ampoule	Units
T-Ampoule Seal	1.56	3.12	1.56	cm^2
SC-1 Seals (3 times)	0.00	3.58	3.58	cm^3
Total Volume	1.56	6.70	5.14	cm^3
Total O-ring mass	2.81	12. 1	9.24	g

According to LA-UR-10-05846, a fluoro-elastomeric O-ring decomposes per equation 1

$$0.147CF_2CH_2(s)+0.0178C_3F_6(s)\rightarrow 0.320C(s)+.294HF(g)+.0265CF_4(g) \qquad 1$$

This equation differs slightly from LA-UR-10-05846 in the coefficients of the products. This difference is due to rounding. LA-UR-10-05846 asserts, based on references, that the O-ring initially contains 78% by mass CF_2HC_2 and 22% by mass C_3F_6. The report also assumes complete O-ring decomposition by 1080ºF. For the purposes of the pressure temperature map, this report assumes pyrolysis based on a simplified version Figure 3 that assumes complete pyrolysis by 1080°F.

In fact, fluorocarbon decomposition, or pyrolysis, is a function of temperature as shown in Figure 3. This figure was constructed from data for Viton® A also known as poly (vinylidene fluoride-co-hexafluoro-propylene) CAS # 9011-17-0. The first steep loss of mass on this curve between 700 and 900ºF marks the transition of O-ring material to hydrogen fluoride (*HF*). The remaining slow decline traces the conversion of the remaining material to CF_4. At 1080ºF, approximately 78% of the O-ring material has pyrolized. The above notwithstanding, subsequent analyses assume the O-ring pyrolizes completely at the first step (800ºF). The figure was included to illustrate the degree of conservatism involved.[4]

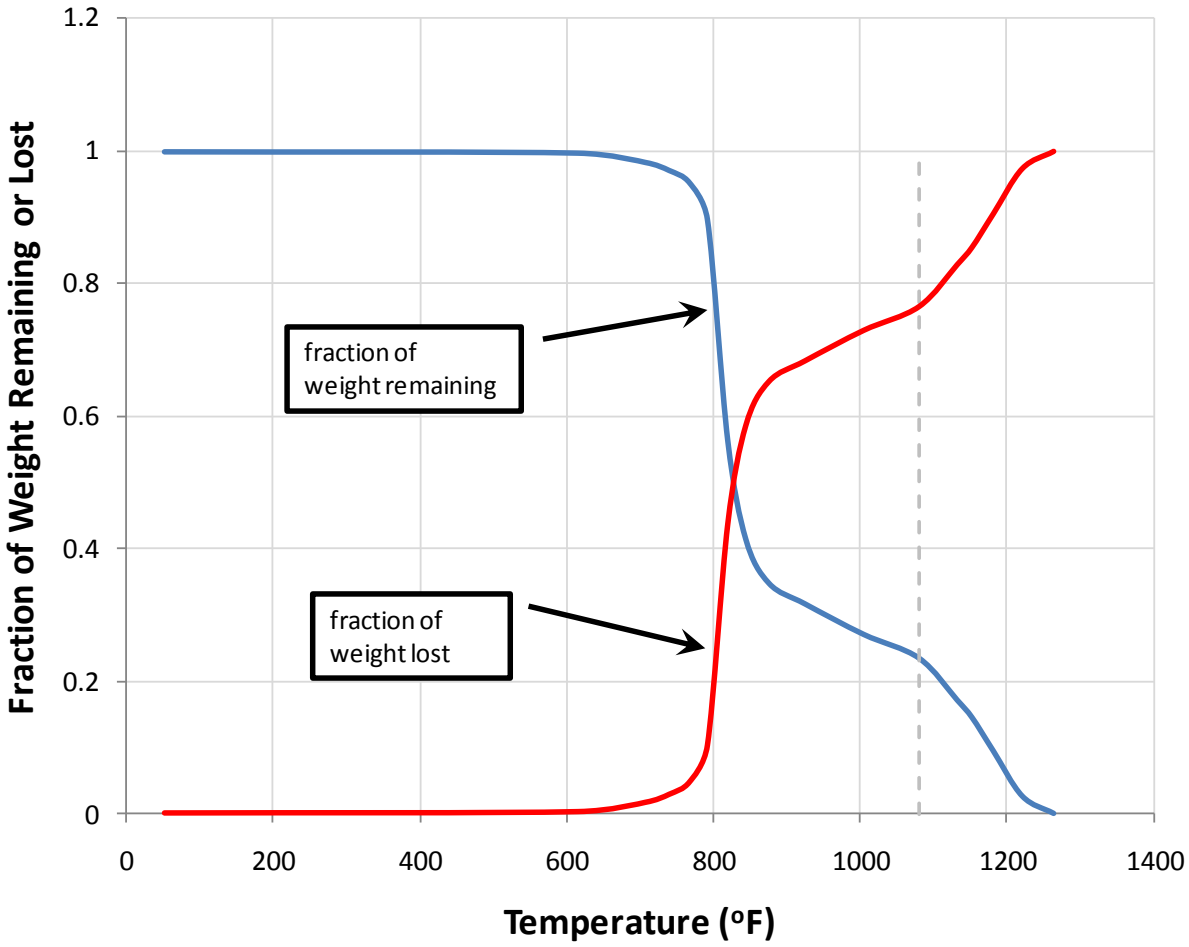

Figure 3: Pyrolysis of vinylidene fluoride-co-hexafluoro-propylene with Temperature [4, Figure 6.3.11]

An additional conservative assumption involves the sequence assumed for pressure release. This analysis assumes that the O-ring contains all pressure until the device reaches full design temperature of 1080°F. Only then does the pressure barrier fail. In fact, failure of the O-ring as a pressure containing device would occur gradually between 700°F when pyrolysis starts and the final temperature of 1300°F.

The LA-UR-10-05846 analysis assumes only two materials evolve during pyrolysis, carbon tetrafluoride (MW = 88 g/mol) and hydrofluoric acid (MW = 20 g/mol). These materials combine for an average molecular mass ratio on the order of 25 to 30 g/mol. On the other hand, Moldoveanu suggests that these reactions are more complex but fails to adequately quantify this assertion. His analysis did, however, say that the resulting products of pyrolysis would have higher molecular mass ratios than were used by LA-UR-10-05846. Compounds with molecular mass ratios exceeding 154 g/mol were seen but were not identified.[4] Higher molecular mass ratios would result in fewer moles released per gram of material generating lower pressures. Use of the LA-UR-10-05846 analysis is therefore conservative.

This analysis assumes, as does LA-UR-10-05846, that the solid carbon, or char, generated in equation 1 is subsequently oxidized into carbon dioxide.

$$0.320C(s) + 0.320O_2(g) \rightarrow 0.320CO_2(g) \qquad 2$$

While LA-UR-10-05846 assumes carbon converts to carbon monoxide, at temperatures less than 3000ºF (1920 K) the carbon monoxide/carbon dioxide equilibrium strongly favors carbon dioxide. In either case the reaction forms the same number of moles of vapor. No attempt is made to identify the source of the oxygen.

The moles of reactants in Equation 1 are based on the calculation summarized in Table 3. The first line, total O-ring mass for the three cases under consideration is a repetition of the last line of Table 2. For the purposes of this table, the molar mass ratio of CF_2CH_2 is 64.0 g/mol and the molar mass ratio of C_3F_6 is 150.0 g/mol.

Table 3: O-ring Decomposition Results -- Reactants

Description	T-Ampoule	Annulus	TB-1	Units
Total O-ring mass	9.25	2.81	12. 06	g
Mass of CF_2CH_2	7.21	2.19	9.41	g
Mass of C_3F_6	2.04	0.62	2.65	g
Moles of CF_2CH_2	0.113	0.0342	0.147	mol
Moles of C_3F_6	0.0136	0.00412	0.0177	mol

Note that LA-UR-10-05846 has adjusted the coefficients in Equation 1 to match the moles of reactants for the TB-1 column. This means the moles products for TB-1 will also match the coefficients of the products in Equation 2 also. The moles of reactants and products for the T-Ampoule and the Annulus will vary as the ratio of the O-ring mass for that volume to the O-ring mass for TB-1. The O-ring mass reported in the TB-1 column is the total of the masses from other two volumes. This results only after equilibration. This carries through to the products also, as shown in Table 4.

Table 4: O-ring Complete Oxidation -- Products

Description	T-Ampoule	Annulus	TB-1	Units
Moles of *HF*	0.225	0.0685	0.294	mol
Moles of CF_4	0.0203	0.00618	0.02650	mol
Moles of CO_2	0.246	0.0747	0.320	mol
Total Moles from O-rings	**0.491**	**0.149**	**0.640**	mol

These molar quantities are constant and contribute a specific amount to the pressure calculation of Section 1.5.

1.3 Ancillary Plastic Pyrolysis/Oxidation

T-Ampoule assembly procedures allow the inclusion of labels and bags inside the T-Ampoule. Labels are typically metalized Poly(Ethylene Terephthalate) or metalized PET. Mylar™ is an example of this material. No specification exists regarding the exact composition and quantity of this packaging material. Nonetheless, this plastic will degrade with temperature in a manner similar to the O-ring pyrolysis discussed in the previous section. The four most likely candidates for inclusion in a PAT-1 package are:

1. Metalized PET, Poly(Ethylene terephthalate), of which only the polyester (Polyethylene terephthalate) is active.
2. Poly(Ethylene) (all densities)
3. PVC, Poly(Vinyl Chloride)
4. PTFE, Poly(TetraFluoroEthylene). An example of PTFE is Teflon™.

For any plastic composed of hydrocarbons and other chemicals, the products of a complete oxidation to carbon dioxide reaction depends on the chemical composition of the plastic's monomer. Each plastic consists of chains built by repeating the same monomer. What happens to that monomer happens to the whole chain. The complete oxidation reaction equations for the four plastics monomers listed above are listed in Table 5.

Table 5: Monomer Complete Oxidation Reactions

Plastic	Monomer	Reaction
PET	Ethylene Terephthalate	$C_{10}H_8O_4 + 10O_2 \rightarrow 10CO_2 + 4H_2O$
PE	Ethylene	$CH_2 + 1.5O_2 \rightarrow CO_2 + H_2O$
PVC	Vinyl Chloride	$C_2H_3Cl + 2.75O_2 \rightarrow 2CO_2 + 1.5H_2O + .5Cl_2$
PTFE	TetraFluoro Ethylene	$C_2F_4 + 2O_2 \rightarrow 2CO_2 + 2F_2$

Table 6 extends the information in Table 5 to include some statistics of the reactions including the number of moles of vapor formed per mole of monomer, the number of moles of oxygen consumed per mole of monomer consumed and the molecular mass ratio of the monomer.

Table 6: Complete Oxidation Reaction Statistics

Plastic	Monomer Molecular Mass (g/mol)	Moles of Vapor per Mole of Monomer	Mols O_2 per mol monomer
PET	192	14	10
PE	14.0	2	1.5
PVC	98.0	4	2.75
PTFE	100	4	2

This information will be used in pressure calculations in Section 1.5. The total number of moles of vapor from ancillary plastic will be adjusted to achieve the final maximum allowable pressure. The number of moles will be the same for any plastic. However, the mass in grams of ancillary plastic allowed depends on the plastic.

1.4 Helium Generation from Alpha Decay

Based on the discussion in Section 4.5.3 of this addendum, alpha decay of plutonium generates an insignificant molar quantity, n_{he}, of helium equal to a rate, r_{he}, of 1.42E-07 mol of helium per gram of plutonium per year. Design mass of plutonium is 821 grams. The value used here is 1300 grams of ^{241}Pu, a bounding condition for the analysis. For the purposes of this study, it was assumed that the T-Ampoule was assembled one year prior to the accident and that no helium leaked from the container via molecular diffusion. With this assumption, the total of helium generated is 4.62E-05 moles. This quantity is assumed constant for this report. It contributes a specific amount to the pressure calculation of Section 1.5.

1.5 Pressure Calculation

Table 7 contains a summary of the pressure calculation to be completed for this report. The first calculation estimates the molar mass of argon initially trapped in the PAT-1 package during loading in the glove box. The second calculation uses the specified final temperature and pressure to estimate the limiting amount of ancillary plastic allowed in the package. This information then contributes to the final calculation of the pressures in the two initial volumes, annulus and T-Ampoule, prior to and after equilibration.

Table 7: Pressure Cases

Description	Pressure (*psia*)	Temperature (°*F*)	Mass Involved (*mol*)	Zones Involved
Initial	14.7	75	to be calculated	Annulus, T-Ampoule
Just before equilibration	to be calculated	800	Initial, Ancillary Plastic, O-Rings, He from alpha decay	Annulus, T-Ampoule
Final	1110	1080	to be calculated	TB-1

Pressure in a pressure envelope is driven by the quantity and properties of the vapor phase constituents in that volume. There will be no liquids in the package; and solids' impact on pressure is so small that its impact is lost in rounding. For a vapor, the relationship between mass, temperature and pressure is

$$P = z\left(\frac{n}{V}\right)R_u T \qquad 3$$

In SI units, the universal gas constant R_u is 8.314 N-m/mol-K, temperature, T, is in Kelvin, volume, V, is in cubic meters and vapor mass, n, is in mols. This analysis will assumes ideal conditions (z = 1) in order to maintain consistency with LA-UR-10-05846 analysis.

As Figure 4 illustrates, ideal gas is a reasonable assumption. This figure contains a standard corresponding states plot over which estimated compressibility factors for the gases involved are plotted for the three cases listed in Table 7. Most points cluster around the z = 1 line. The two outliers are Cl_2 and F_2, which only show up in rare choices of ancillary plastic.

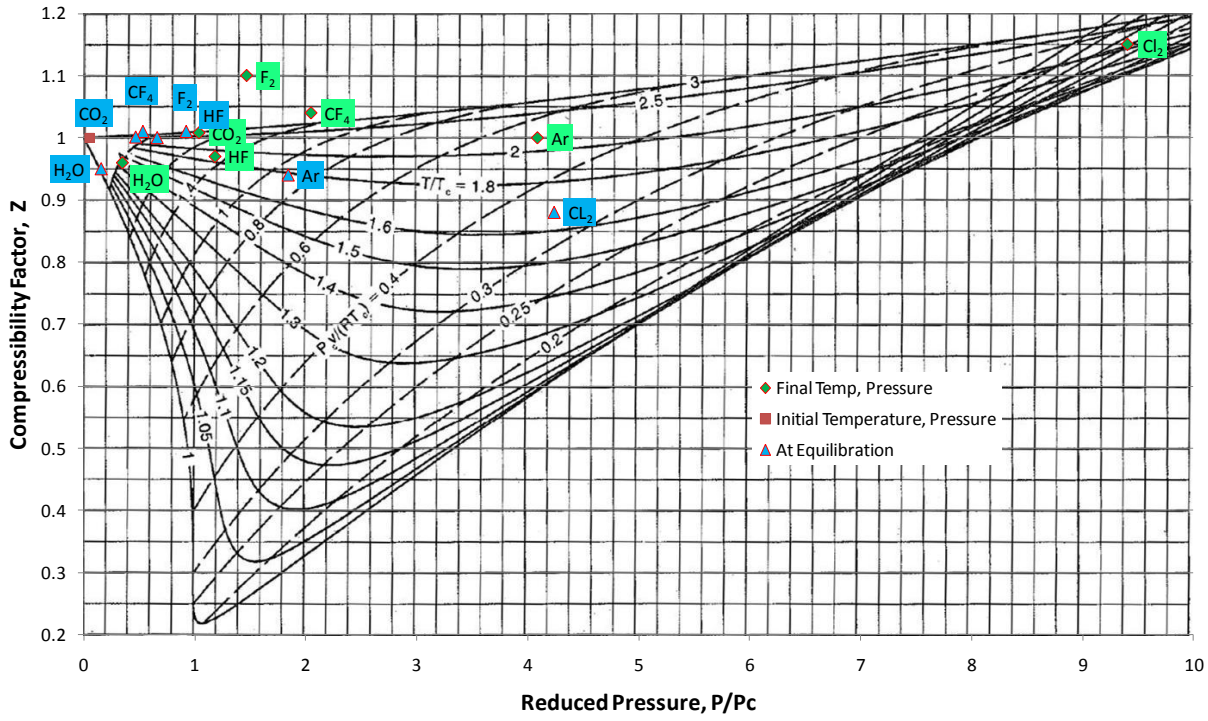

Figure 4: Compressibility Factors for TB-1 Molecules at 1110 psia and 1080 °F[4]

1.5.1 Initial Charge of Argon

The PAT-1 package will be assembled in a glove box. It is assumed here that the glove box contains argon. Since pressure depends only on the moles of vapor present any other inert gas would require the same mass. This report also assumes that the glove box assembly occurs at 14.7 psia (1 atmosphere) and 75 °F. The amount of argon can be estimated via a manipulation of equation 3.

$$n = \frac{PV}{R_u T} \qquad 4$$

Note the omission of the compressibility factor (assumed = 1.0). Table 8: displays the results.

Table 8: Initial Molar Contents

Parameter	T-Ampoule	Annulus	TB-1	Units
Temperature, T	297.	297.	297.	K
Pressure P	101,325	101,325	101,325	N/m^2
Gas Constant, R_u	8.314	8.314	8.314	$N\text{-}m/mol\text{-}K$
Volume, V	0.001065	3.77E-05	0.00110	m^3
moles, n	0.0437	0.00155	0.0453	mol

These moles of initial argon are constant and contribute a specific amount to the pressure calculation.

1.5.2 Final State – Estimate of Ancillary Plastic Content

As Table 7 indicates, the final pressure and temperature are known. The only unknown is the mass of ancillary plastic that can be allowed. With known pressure, temperature and volume, the total moles can be calculated from Equation 3 after minor algebraic manipulation. The calculation returns a total molar mass equaling 1.19 mol. The breakdown by source is shown in Table 9. The molar quantities from argon, helium generated from alpha decay of plutonium, O-ring decomposition, and char oxidation are known. The molar quantity from oxidation of ancillary plastic is back-calculated by subtracting the sum of the above sources from the total moles calculated using equation 3.

Table 9: Final Conditions Molar Estimate

Source	Contribution (mol)	Mol Fraction	Pressure Contribution (psia)
Argon (Original Atmosphere)	0.0453	0.0381	42.3
He (from Alpha Decay)	0.000185	0.00016	0.173
HF (from O-Ring decomposition)	0.294	0.248	275
CF_4 (from O-Ring decomposition)	0.027	0.0227	25.2
CO_2 (from oxidation of char)	0.32	0.27	299
Ancillary Plastic Oxidation	0.501	0.422	468
Total mols Vapor	**1.19**	**1.00**	**1110**

Table 9 provides the allowable contribution to pressure (468 psi) from ancillary plastics based on an allowable amount (0.501 mol). The question to be answered is how much initial plastic in grams should be allowed. Table 10 answers that question.

The first five lines of Table 10 (excluding the titles) contain information repeated from Table 5 and Table 6. Below these lines, the allowable quantity of vapor from plastic (0.501 moles) comes from Table 9. The quantity of moles of monomer derives from the number of moles of vapor per mole of monomer, 14 in the case of metalized PET. The allowable mass is calculated by multiplying the allowable moles of monomer by the molecular mass of the monomer, 6.87 grams of plastic in the case of metalized PET. Note that this is only plastic. Metalized PET will have some additional mass from the metal layered with the plastic.

For the purposes of discussion only, this mass was equated to an equivalent square sheet of 0.001 inch thick material assuming an average density for plastics of 1.4 g/cm³. For metalized PET, for example, 6.87 grams of plastic can be rolled out to a sheet 0.001in. thick and 17.3 in. x 17.3 in.

on each side. For reference, a typical kitchen sandwich bag is 0.001 in. thick and a plastic tarp is 0.005 in. thick.

Table 10: Conversion of Vapor Mass to Grams of Ancillary Plastic

Common Name	Metalized PET	Poly ethylene	PVC	PTFE	Units
Chemical name of monomer	ethylene terephthalate	ethylene	vinyl chloride	tetrafluoro ethylene	
Monomer formula	$C_{10}H_8O_4$	CH_2	C_2H_4Cl	C_2F_4	
Monomer mol/mass ratio	192	14	98	100	g/mol
mol vapor/ mol monomer	14	2	4	4	
mol O_2/mol monomer	10	1.5	2.75	2	
Allowable mols from plastic vapor	0.501	0.501	0.501	0.501	mol
Allowable mols monomer	0.0358	0.251	0.125	0.125	mol
Allowable mass (plastic only)	**6.87**	**3.51**	**12.2**	**12.5**	g
Size of 0.001 in thick square (for illustration only)	17.3	12.4	23.2	23.3	in

As Table 5 demonstrates, the products of oxidation of ancillary plastic differ with monomer. Table 11 lists the pressure contribution of these different products.

Table 11: Pressure Results Showing All Components

Common Name	Metalized PET		Polyethylene		PVC		PTFE	
	mol	psia	mol	psia	mol	psia	mol	psia
Original Atmosphere	0.0452	42.3	0.0452	42.3	0.0452	42.3	0.0452	42.3
Helium generated from alpha decay	0.0002	0.173	0.0002	0.173	0.0002	0.173	0.0002	0.173
O-ring Thermal Decomposition								
HF	0.2940	275	0.2940	275	0.2940	275	0.2940	275
CF_4	0.0270	25.2	0.0270	25.2	0.0270	25.2	0.0270	25.2
CO_2 from char oxidation	0.3200	299	0.3200	299	0.3200	299	0.3200	299
Subtotal of all above sources	**0.6864**	**642**	**0.6864**	**642**	**0.6864**	**642**	**0.6864**	**642**
Ancillary Plastic -- thermal pyrolysis with oxidation								
CO_2	0.3577	334	0.2504	234.1	0.2504	234.1	0.2504	234.1
H_2O	0.1431	134	0.2504	234.1	0.1878	175.6		
Cl_2					0.0626	58.53		
F_2							0.2504	234.1
Total Pressure	**1.1872**	**1110**	**1.1872**	**1110**	**1.1872**	**1110**	**1.1872**	**1110**

It is important to remember that these quantities are mutually exclusive. It is allowable to include 6.88 g of metalized PET or 3.51 grams of grams polyethylene or 12.3 grams of PVC or 12.5 grams of PTFE.

All that remains is to estimate the amount of oxygen required to support all the reactions discussed above. Table 12 provides that answer.

Table 12: Oxygen Required for Oxidation

Description	Metalized PET	Poly ethylene	PVC	PTFE	Units
Moles to oxidize O-ring char	0.320	0.320	0.320	0.320	mol
Moles to oxidize Ancillary Plastic	0.358	0.377	0.344	0.250	mol
Total moles of oxygen (O_2) required	0.678	0.697	0.664	0.570	mol
Equivalent Pressure at 75 °F	220	226	216	185	psia

The moles of O_2 required to oxidize O-ring char is constant because O-ring char mass is constant. The moles of O_2 required to oxidize ancillary plastic varies with the plastic. The calculated amount is the product of line 6 (mol O_2/mol monomer) and line 8 (Allowable moles monomer) of Table 10. The last line of Table 12 contains the result of a simple calculation using equation 3 for the full volume of the TB-1 vessel. In order to enable all of the oxidation assumed in this section, a package assembly containing 12.3 grams PVC (the allowable limit from Table 10) must contain O_2 at 216 psi over and above its original charge of argon. This is impossible and its assumption represents an extreme degree of conservatism. To illustrate the degree of conservatism, Section 1.7 presents an alternative but still conservative calculation of allowable ancillary plastic.

1.6 Pressure before and after Equilibration

Figure 5 contains a plot of the pressure/temperature map for the package. The upper (green) line represents pressure in the small annular space between the TB-1 wall and the T-Ampoule. The solid line denotes pressure before equilibration. The dashed line is what the pressure would be without equilibration. The bottom (red) line represents pressure in the large volume of the T-Ampoule. Again, the dotted line extends the pressure curve to what could be without equilibration. The solid (blue) line denotes the pressure in the combined volumes, called the TB-1 volume in previous sections.

Pressures prior to about 600°F are equal in both the annulus and the T-Ampoule. At these low temperatures, mass and volume are both constant. After 600°F, the O-rings and plastic begin

pyrolysis. The changing mass affects the pressure in the low volume Annulus more severely than it affects the T-Ampoule pressure.

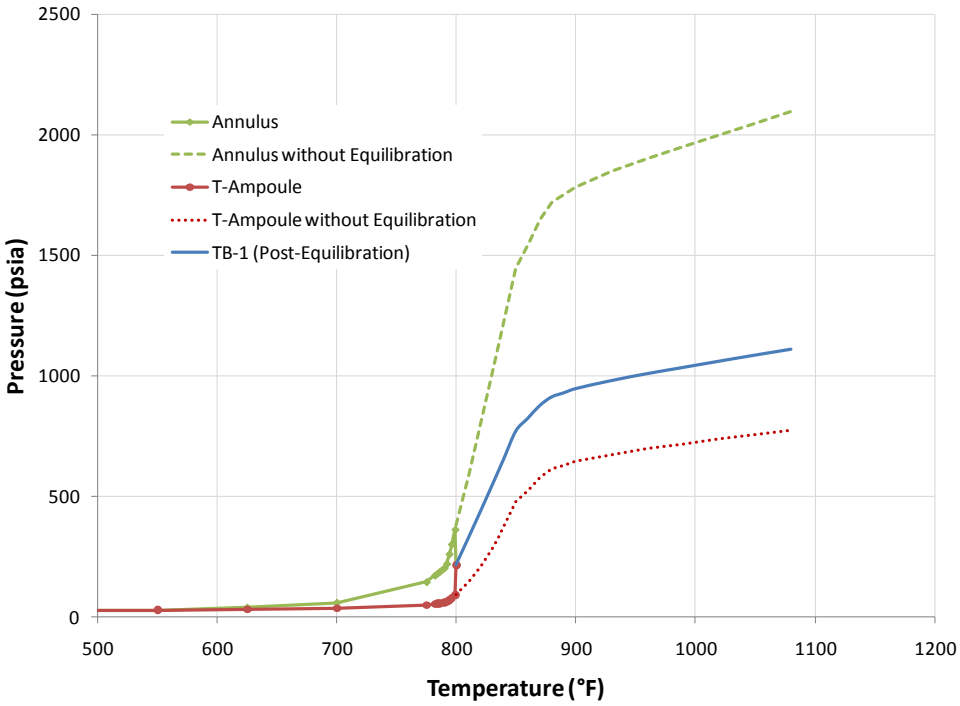

Figure 5: Pressure Temperature Map for Package

At approximately 800°F, the pressure difference between the two pressure envelopes has reached a point such that the O-ring seal fails by design (See Chapter 4). Pressure in the Annulus is higher than is pressure in the T-Ampoule. At this point, the pressure in the two volumes equilibrates and the two pressure envelopes merge into the single TB-1 pressure. The Annulus pressure drops and the T-Ampoule pressure rises. Pressure continues to rise with increasing temperature in the single volume until it reaches 1110 psia at 1080°F.

An issue arises in Chapter 4 regarding the repeatability of the O-ring failure point. This section is intended to provide information for the discussion there. Assume the O-ring seal does not fail. The Annulus pressure will continue to rise, as will the T-Ampoule pressure, as temperature continues to go up. What happens to the differential pressure? It goes up following the rapidly rising Annulus pressure. Figure 6 contains a plot of the annulus pressure as a function of pressure differential.

The O-ring seal is intended to fail when pressure differential reaches 160 psi. At that point, Annulus pressure will be 368 psia, well below the maximum allowable pressure (MAP) for the TB-1 pressure vessel. Pressure against the TB-1 wall stays below the MAP of 1110 psia until the differential pressure reaches 515 psi.

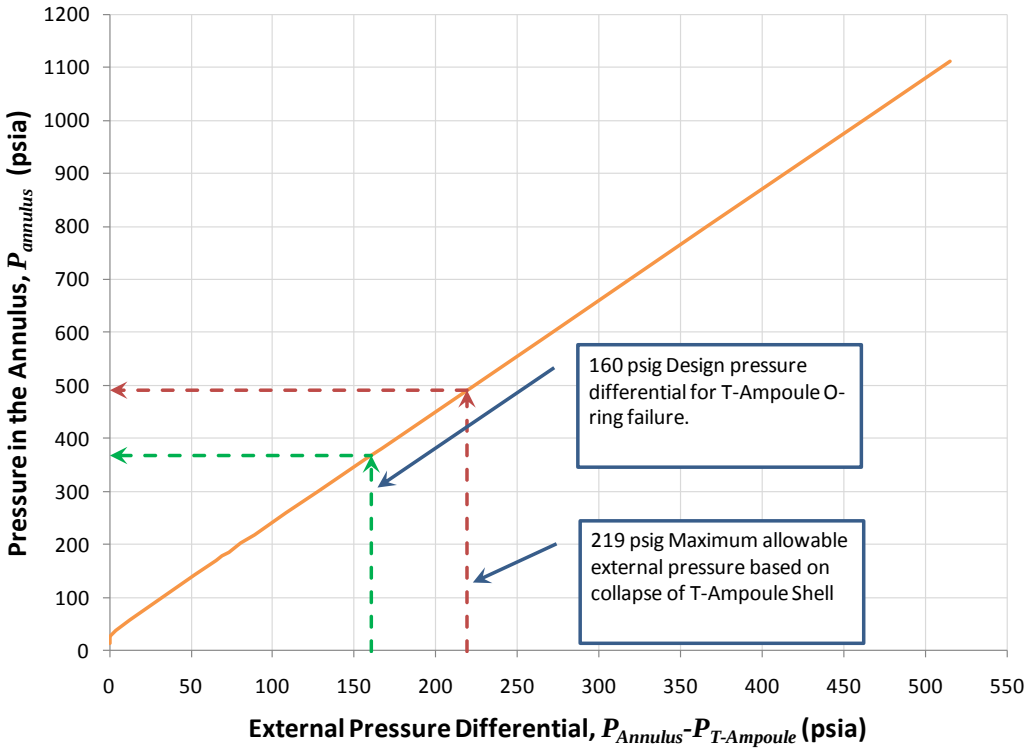

Figure 6: Relationship Between Annulus Pressure and Pressure Difference

In other words, the O-ring seal failure point can be high by a factor of safety of 3.2 (515/160) before its failure to equilibrate affects pressure on the TB-1 vessel wall.

Contingency against buckling failure of the T-Ampoule shell due to excessive external pressure is tighter. The nominal maximum external pressure difference is 219 psi. This is a factor of 1.33 above the nominal failure point of the O-ring.

1.7 Alternative Ancillary Plastic Calculation

As discussed in Section 1.6, the allowable ancillary plastic limit is based on an assumption that oxygen is always available for reaction with the products of pyrolysis. Analysis there assumes the oxygen appears without speculating as to its source. Table 12 demonstrates that the one feasible source, accidental inclusion during assembly is in fact impossible. The initial assembly would have to include between 150 and 350 psi of pure oxygen depending on the monomer involved. Since assembly is in a glove box these levels of pressure are impossible.

A more feasible, but still conservative, scenario assumes package assembly on an open workbench at 75°F and one atmosphere of air. While more feasible, it is still highly unlikely. Both engineering and administrative controls exist to ensure an inert glove box atmosphere during assembly. Nonetheless, this section stipulates that this scenario exists. The package

would be assembled at 14.7 psia and it would contain 79% nitrogen (N_2) and 21% oxygen (O_2) as its initial charge. Only 0.00950 mol of oxygen as O_2, 0.21 x 0.0453 (see Table 8), is available to burn char. Limited O_2 limits CO_2 formation to only 0.00950 moles. The resulting final vapor phase mixture is summarized in Table 13. Compare this to Table 9. Original argon is now original N_2 and is 21% lower. CO_2 has dropped from 0.320 mol contributing 299 psi to final pressure to 0.00950 mol contributing only 8.89 psi to final pressure. Most important, ancillary plastic oxidation has changed to ancillary plastic pyrolysis and has gone numerically from 0.501 mol contributing 468 psi to 0.821 mol contributing 767 psi to the final pressure.

Table 13: Less Conservative Calculation of Ancillary Plastic Contribution

Source	Contribution (mol)	Mol Fraction	Pressure
Original N_2	0.0357	0.0301	33.4
He (from Alpha Decay)	0.00019	0.00016	0.173
HF O-Ring decay	0.294	0.248	275
CF_4 O-Ring decay	0.027	0.0227	25.2
CO_2	0.0095	0.008	8.89
Ancillary Plastic Pyrolysis	0.821	0.691	767
Total mols Vapor	1.19	1.00	1110

How does this increased molar mass impact allowable plastic? Using PET as an example, Figure 7 shows the results of pyrolysis in an inert atmosphere for PET. The analysis was done at 1112°F, sufficiently close to the final PAT-1 temperature of 1080 °F. The figure shows selected mol-mass ratios to illustrate the distribution. In fact the mol fraction weighted average for all 31 compounds is 108 g/mol. Similar analyses were done for all four plastics. The results are tabulated on the third line of Table 14. The table also lists the calculated allowable mass. For PET, allowable ancillary plastic has gone up from 6.87 g (Table 10) to 89.0 g (Table 14) an increase of an order of magnitude. For the purposes of illustration only, and assuming an average plastic density of 1.4 g/cm³, the PET plastic, if rolled out to a 0.001 in. thickness, has gone from a square 17.3 in. on edge to square 62.3 in. on edge.

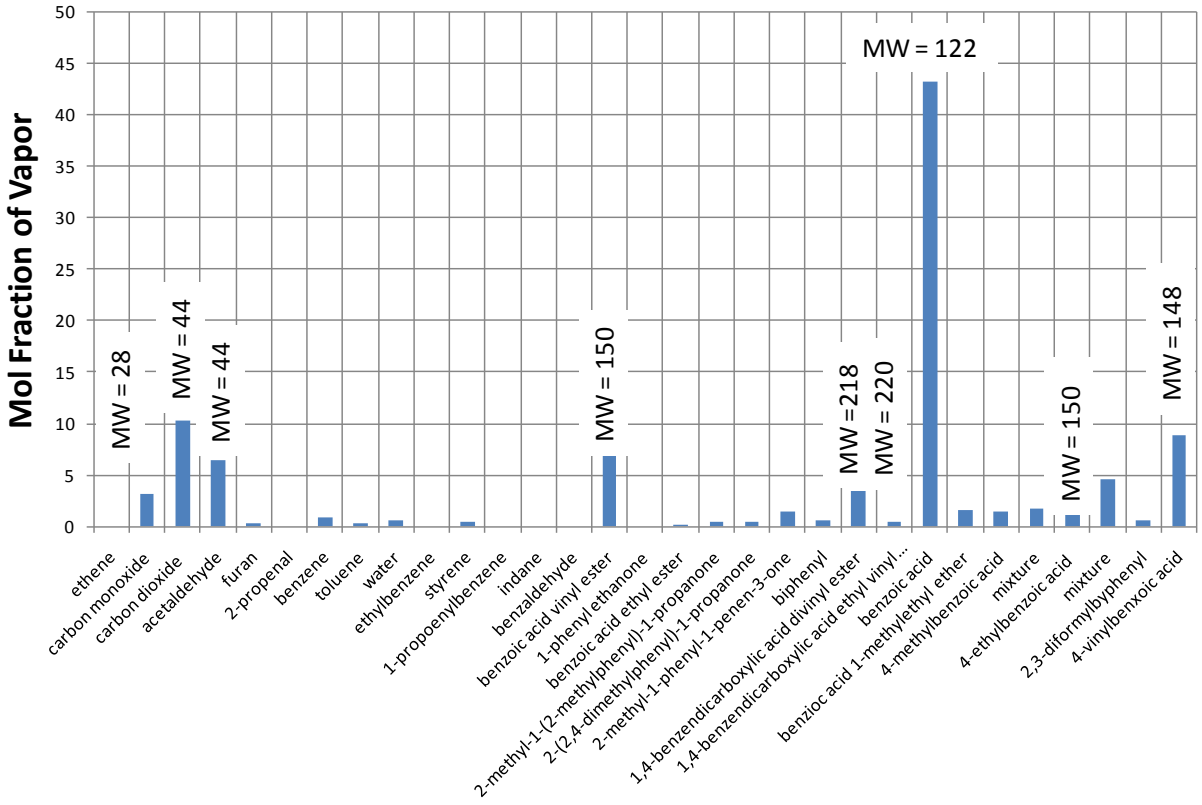

Figure 7: Pyrolysis of PET at 600 °C (1112 °F)[4]

Other plastics have similar increases. Polyethylene increases from 3.52 to 200 g. PVC jumps from 12.2 to 71 g. PTFE goes from 8.35 to 82.4 grams. In conclusion, the more conservative scenario used in this report reduces allowable ancillary plastic mass by as much as an order of magnitude.

Table 14: Pyrolysis Example

Common Name	Metalized PET	Polyethylene	PVC	PTFE	Units
Chemical name of monomer	ethylene terephthalate	ethylene	vinyl chloride	tetrafluoro-ethylene	
Pyrolized Vapor Mole Mass Ratio	108	243	86.1	100	g/mol
Allowable Total mols Vapor	1.19	1.19	1.19	1.19	mol
Moles from all other sources	0.366	0.366	0.366	0.366	mol
Allowable mols monomer	0.824	0.824	0.824	0.824	mol
Allowable mass (plastic only)	89	200	70.9	82.4	g
Size of 0.001 in thick square (for illustration only)	62.3	93.4	55.6	59.9	in

2 Verification of TB-1 Maximum Allowable Pressure

The calculations in this chapter verify the use of 1110 psia (1095.7 psig) as maximum allowable pressure (MAP) at a temperature of 1080 °F. This value for MAP was taken from the original Safety Analysis Report (SAR) for the PAT-1 package.[8]

It is important emphasize that the SAR's MAP will remain the specified maximum pressure for the TB-1. The value of this analysis is in the demonstration of the safety inherent in using the SAR value.

2.1 Results

The analysis of this section demonstrates that the MAP specified by the SAR is safe. Its value of 1110 psia at 1080°F is used elsewhere in this report where a maximum allowable pressure is needed.

Based on an ASME Boiler and Pressure Vessel Code (BPVC) Section VIII, Division 1 analysis, the maximum allowable operating pressure (MAOP) at 1080°F for the TB-1 pressure vessel is 2200 psia. This MAOP exceeds the SAR MAP (1110 psia @ 1080°F) with a factor of safety of 1.98. [1]

The allowable pressure based on vessel wall strength is 5386 psig (5400 psia). The allowable pressure based on closure is 2185 psig (2200 psia). The minimum of the two, 2200 psia, is the MAOP for the TB-1 vessel based on the analysis documented below.

2.2 Method

The following analysis looks first at the vessel wall's strength and then at the ability of its closure to contain pressure. It calculates first the maximum pressure allowed by the shell. It then calculates the maximum pressure allowed by the closure. The MAOP is the minimum of the two. This number is then compared to the SAR's MAP.

The TB-1 vessel is sufficiently thick-walled with sufficient structural reinforcement that a concern arose that a standard BPVC analysis based on a thin-wall model would not provide reasonable or conservative results.[1] Consequently, a simplified Finite Element Method (FEM) model was run first. These results were then compared with a more traditional BPVC type analysis. This comparison will demonstrate that a thin wall assumption is valid. This conclusion clears the way for an allowable pressure calculation using the thin wall model dictated by the BPVC.

The closure analysis concentrates on bolting. The FEM analysis will demonstrate that the stresses in the head are sufficiently low to be accepted without further analysis. The bolting analysis follows standard BPVC methods. It calculates the loading on the bolts needed to offset the pressure on the head and to ensure pressure containment of the gasket material. Pressure is adjusted until this load, converted to a stress per bolt, equals the allowable stress for the given bolting material. This pressure is the allowable pressure based on closure.

The minimum of the two allowable pressures calculated above is the MAOP for the system.

2.3 Allowable Pressure based on Vessel Wall

2.3.1 Numerical Analysis

The FEM model used the same grid generated for impact analysis in Section 2 of the Addendum to the SAR. This grid was imported into the Abaqus FEM program for analysis. This analysis used the MAP (1110 psia) as a boundary condition to the numerical model. This numerical model was simplified in that it ignored the gasket seal. The model was run as a steady state calculation at 1080°F.

Figure 8 shows the calculated hoop stress in the vessel wall. Based on the FEM analysis, maximum hoop stress is 4367 psi (tension). As would be expected in a pressure vessel hoop stress reaches a maximum on the shell wall away from reinforced ends. Again as expected maximum hoop stress occurs on the inner surface of the vessel. In a thin wall analysis, this hoop stress is assumed constant across the vessel. Figure 8 also demonstrates that the variation of stress through the wall is small.

2.3.2 Thin Wall Vessel Analysis

The BPVC uses the following formula from paragraph UG-26 to estimate the maximum allowable pressure, *P*, in a thin-walled shell as a function of hoop stress, *S*.

$$P = \frac{SE_J t}{R_i + 0.6t} \qquad 5$$

Refer to Table 15 for a description of variables, their value and their units. Manipulation of the above allows the estimation of hoop stress as a function of internal pressure:

$$S = \frac{P\left(R_i + 0.6t\right)}{E_J t} \qquad 6$$

Table 15: Summary of Parameters Used in Equation 6

Parameter	Description	Value	Units
P	Internal Pressure	1095.3	psig
R_i	Radius to inside surface of vessel	2.125	in
t	Wall thickness	0.55	in
E_J	Longitudinal Joint Efficiency	1.00	

The longitudinal joint efficiency, E_J, equals 1.0 because the TB-1 vessel is machined from a solid material and has no longitudinal joint.

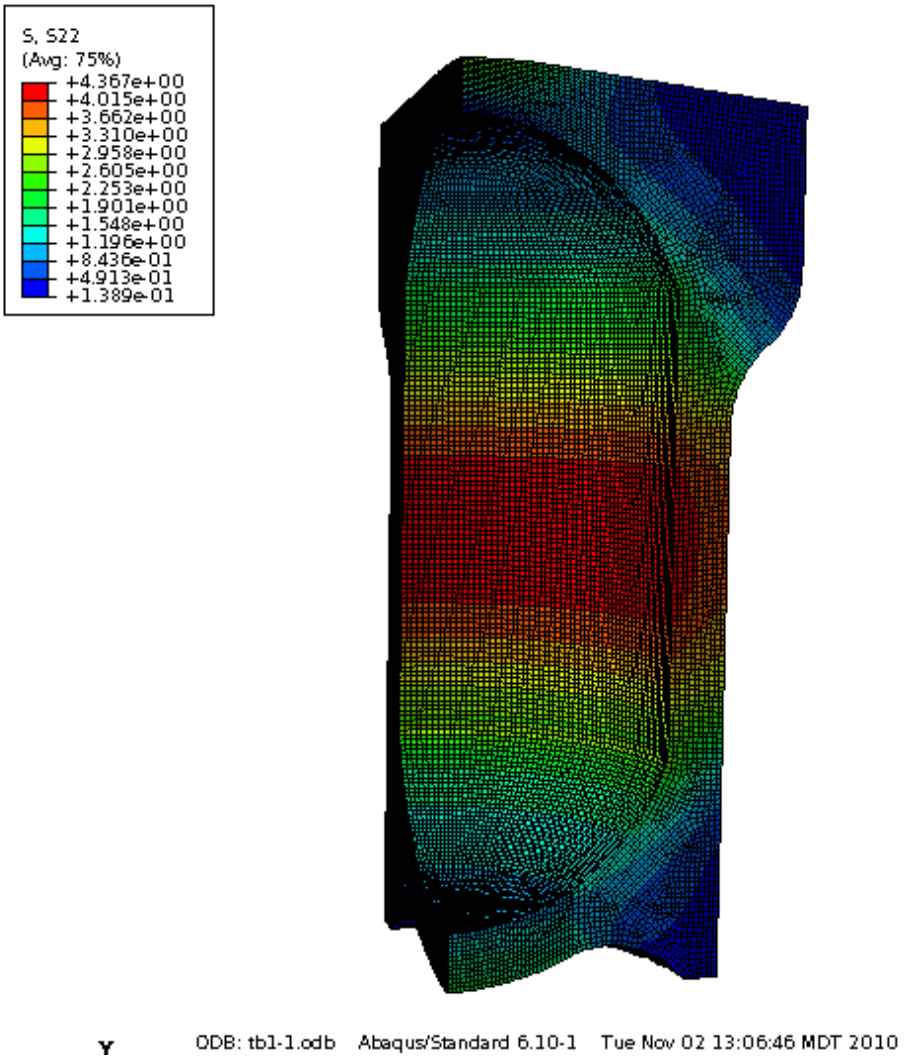

Figure 8: Hoop Stress Experienced by TB-1 with 1110 psia Internal Pressure

Using the values listed in Table 15, equation 6 returns a thin wall hoop stress of 4890 psi. This number compares well with the FEM result of 4367 psi, demonstrating the validity of the BPVC style of thin wall vessel analysis. Since it generates the higher and therefore more conservative stress, the thin wall result will be used for ongoing discussion.

2.3.3 TB-1 Material Strength Criteria

There still remains the issue of comparing this stress to a strength parameter for the material. The BPVC compares hoop stress directly to a strength value called the allowable stress, S_A, which is in turn related to the ultimate tensile strength of the material. This ultimate tensile strength used must be at operating temperature. In this case, operating temperature would be 1080°F.

Per the SAR Addendum, material for the TB-1 is stainless steel with a UNS number 13800 with heat treatment at 1075°F (H1075). This UNS number is equivalent to the designation PH13-8Mo used in the handbook MIL-HDBK-5J from which TB-1 material properties were extracted. Figure 9 contains a curve from that source showing the impact of temperature on tensile ultimate and the tensile yield strength of this material.[7]

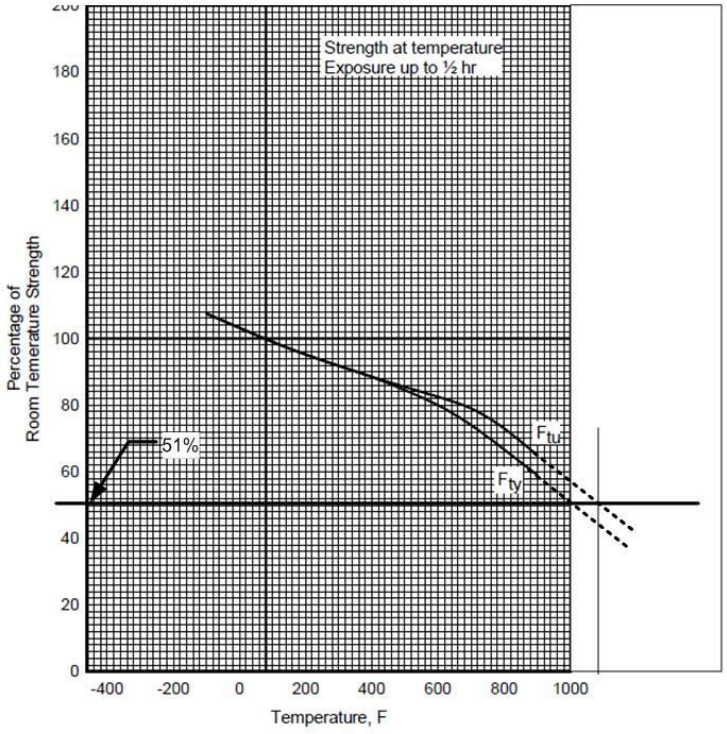

Figure 9: Figure 2.6.6.1.1. Effect of temperature on the tensile ultimate strength (F_{tu}) and the tensile yield strength (F_{ty}) of PH13-8Mo (H950 and H1000) stainless steel bar [7]

For the purposes of the BPVC analysis, ultimate tensile strength is the important parameter. Hence the curve labeled F_{tu} will be used. The curve stops at 900°F making a 180°F extrapolation necessary. Based on this extrapolation, ultimate tensile strength at operating temperature will be 51% of room temperature ultimate tensile strength, S_T. Note that S_T is the same thing as F_{tu} at room temperature.

The same reference provides room temperature tensile strength for two bracketing heat treatment temperatures, 1050°F (175,000 psi) and 1100°F (150,000 psi). The lower of these two values will be used. Thus S_T = 150,000 psi.

Within the BPVC, Section VIII references Section II part D (Section II) for allowable stress values. However, Section II does not tabulate allowable stress properties for this material. In the event allowable stresses are not published in Tables 1A or 1B of that document, Section II refers the user to an internal appendix, *Mandatory Appendix 1 Basis for Establishing Stress Values in Tables 1A and 1B*. The following criteria were extracted from TABLE 1-100 of that appendix:[2]

$$S_A = \begin{cases} \dfrac{S_T}{3.5} & temperature \le 77\,°F \\ \dfrac{1.1 S_T R_T}{3.5} & temperature > 77\,°F \end{cases} \qquad 7$$

In this case, the value for parameter R_T would be 0.51 based on Figure 9. As a result, the allowable stress, S_A, for this high temperature scenario would be 24,000 psi.

2.3.4 Vessel Wall Results

Based on a FEM analysis of the TB-1 vessel, a thin-wall pressure vessel analysis will be valid. Using a thin wall model as outlined in the BPVC with an allowable stress, S_A, of 24,000 and the values for system geometry contained in Table 15, the maximum allowable operating pressure, P calculated using equation 6 would be 5390 psig.

2.4 Allowable Pressure based on Vessel Closure

Based on Figure 8, the stress in the material at the top of the vessel, in the vicinity of the closure, would be on the order of 1,000 psi. This is low enough to assure that material stress will not limit operating pressure. However, bolting needs further review.

The analysis uses the process set forward in BPVC Section VIII Mandatory Appendix 2 Rules for Bolted Flange Connections with Ring Type Gaskets for calculating the load on a set of bolts.

2.4.1 BPVC Closure Analysis

Bolts on a closure generally perform two functions. They contain the pressure in the vessel and they impose sufficient load on the closure gasket to ensure no leakage. In terms of forces on the closure, they can be characterized as follows:

$$W_{m1} = H + H_p \begin{cases} H = Total\ hydrostatic\ end\ \ force, lb_f & \dfrac{\pi G^2}{4} P \\ H_p = Total\ gasket\ compression\ load, lb_v & 2\pi bGmP \end{cases} \qquad 8$$

The first force, *H*, is the force the bolts must exert to counteract the force the internal pressure exerts on the closure. It is equivalent to the pressure, *P*, times the area over which the pressure exerts itself. In this case the area is a circle with diameter, *G*, to the midpoint of the gasket.

The second force, H_p, is the force the bolts must exert to effect a seal on the gasket. The sealing pressure is modeled as a constant factor, *m*, times the external pressure. For soft smooth copper, *m* = 4.75. [1 Table 2-5.1,2]. From the same reference the effective sealing width, *b*, is half the width, *N*, of the gasket. With the geometry of the TB-1 copper gasket (Figure 10) the above equation reduces to.

$$W_{m1} = \left(\frac{\pi G^2}{4} + 2\pi bGm \right) P \qquad 9$$

The TB-1 design actually assumes a single knife edge cutting into the gasket. Hence using smooth copper *m* factor is conservative.

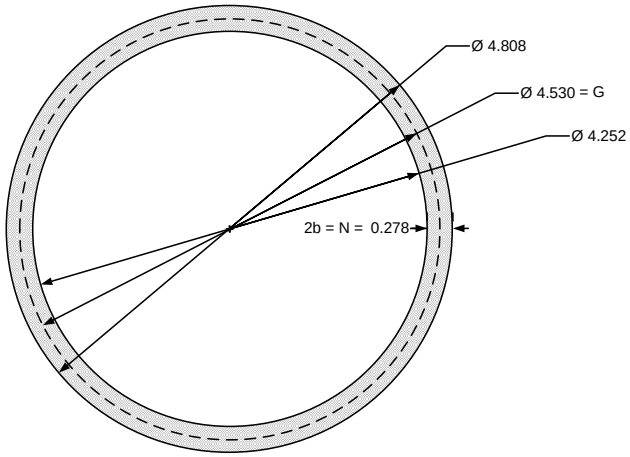

Figure 10: Geometry of TB-1 Gasket

The force, W_{m2}, necessary to initially seat the gasket is the seating stress, y, (13000 psi for soft copper) times the area of the gasket

$$W_{m2} = \pi b G y \tag{10}$$

This equation assumes the TB-1 is assembled with equal pressure internal and external, which is reasonable for this package. The bolts must exert the maximum of either W_{m1} or W_{m2}. The value for W_{m2} is 25,700 lb_f/bolt. Subsequent discussion will demonstrate that W_{m1} is much larger than this. For 12 bolts of diameter, D_b, equal to 0.5 in, the stress, S, in each of the bolts will be

$$S = \frac{\frac{\pi G^2}{4} + 2\pi b G m}{12\pi\left(\frac{D_b}{2}\right)^2} P \tag{11}$$

Using this equation, the maximum allowable operating pressure (MAOP) to be allowed in the vessel can be given in terms of the bolt material's allowable stress:

$$MAOP = \frac{12\pi\left(\frac{D_b}{2}\right)^2}{\frac{\pi G^2}{4} + 2\pi b G m} S_a = 0.0675 S_a \tag{12}$$

2.4.2 Vessel Closure Material Strength

Bolt allowable stress, S_a, is set per BPVC Section VIII, Paragraph UG-23.[1] The bolts are to be fabricated of A-286 stainless steel heat treated per AMS 5731 (Solution treated at 1800°F). Figure 11 contains a curve showing the response to this material to temperature. The vertical axis returns the R_T factor used in equation 7, which applies here in the form:

$$S_a = \begin{cases} \frac{S_T}{3.5} & temperature \le 77\,°F \\ \frac{1.1 S_T R_T}{3.5} & temperature > 77\,°F \end{cases} \tag{13}$$

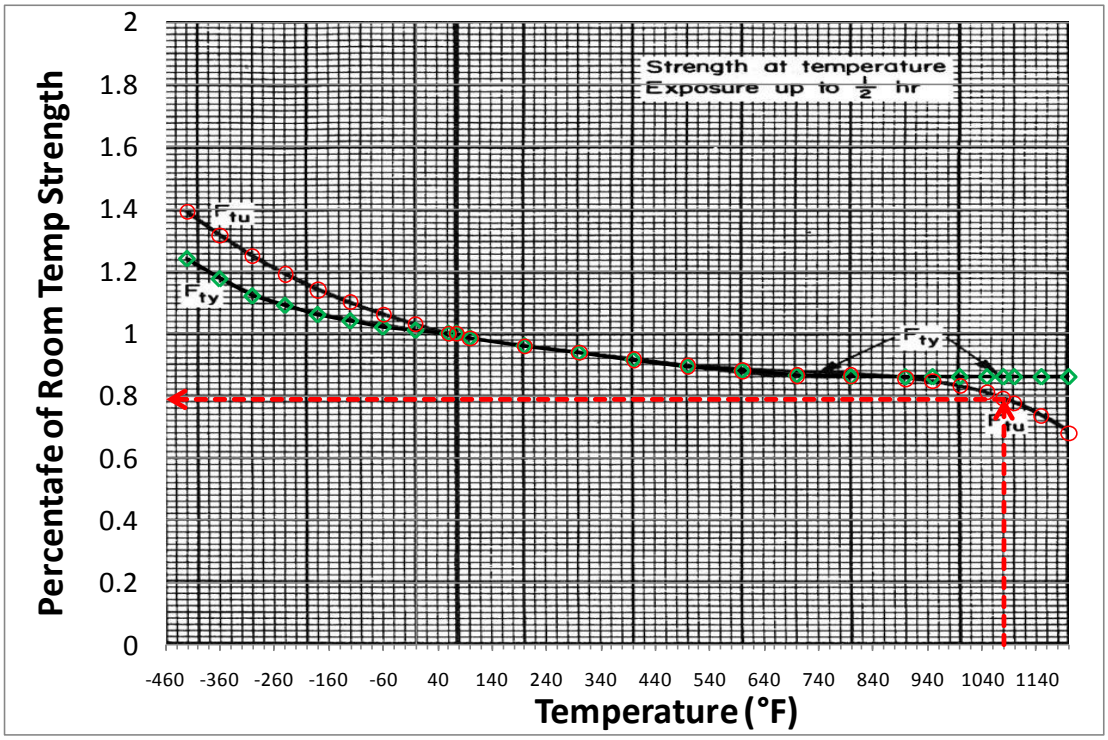

Figure 11: Figure 6.2.1.1.1. Effect of temperature on the tensile yield strength (F_{ty}) and tensile ultimate strength (F_{tu}) of A-286 alloy (1800°F solution treatment temperature).[7]

The ultimate tensile strength at room temperature, S_T, for this material per the reference is 130,000 psi. Note that drawings for these bolts specify a minimum tensile strength of 180,000 psi. The lower value will be used here.

Using equation 13, the allowable stress, S_a, in the bolts is 32,300 psi at 1080 °F. The stress ratio, R_T, is 0.79 from Figure 11. The ultimate tensile strength at room temperature is 130,000 psi.

2.4.3 Vessel Closure Results

Using the bolt allowable stress, S_a, of 32,300 equation 12 returns a maximum pressure safely containable by the closure of 2181 psig (2196 psia). This is a factor of safety of 1.98 over the MAP of 1110 psia specified by the SAR.

At this pressure, the load per bolt, W_{m2}, is 76,100 lb_f, significantly greater than the value for W_{m2} of 25,700 lbf. As initially assumed, W_{m1} dominates the calculation.

3 Application of the Boiler and Pressure Vessel Code (Section VIII)

3.1 Exceptions to the ASME Boiler and Pressure Vessel Code

With the exception of the elastomeric (O-ring) seal, the T-Ampoule (Drawing 2A0261) was designed, and will be fabricated and inspected to meet the requirements of the ASME Boiler and Pressure Vessel Code (Section VIII) [1]. However, the following exceptions or explanations apply:

1) The T-Ampoule was designed to Section VIII as modified by this document:
   a) The size requirements in section *U-1(c)(2)(i)* of Section VIII, do not apply.
   b) The marking requirements of parts UG 115-119 do not apply. T-Ampoules will be marked with part and serial numbers as specified in fabrication specification PAT-1040 [7].
2) Given the dry inert gaseous initial atmosphere and the general non-reactivity of titanium with the vessel contents, the design requires a no corrosion allowance.
3) T-Ampoule MAWP will be established with calculations as set forth in this document. Allowable pressure calculations will be performed based on the following paragraphs of Section VIII:
   a) Torispherical Head allowable pressure was calculated based on the requirements of Section VIII's Mandatory Appendix 1, Supplementary Design Formulas, paragraph 1-4(d).
   b) Allowable pressure, based on membrane stress in the hemispherical head, was estimated based on the criteria set forth in paragraph UG-32.
   c) Allowable pressures in the both the longitudinal and circumferential direction of the shell and lid are estimated based on the criteria set forth in paragraph UG-27 of Section VIII.
   d) T-Ampoule is exempt from the requirements of paragraph UG-32, *Thickness of Shells and Tubes Under External Pressure*. As the T-Ampoule will be subject to impact loading and a separate impact analysis will be conducted as described in Chapter 2 of the PAT-1 Safety Analysis Report Addendum Docket No. 71-0361, Rev. 0, August 2009.
4) T-Ampoule design specifies no welded joints. Consequently joint efficiency, E, in all subsequent Section VIII equations will be applied as 1.0.
5) The requirements of paragraph UG-125 regarding pressure relief devices do not apply. Over pressure response will be discussed in detail in the body of this paper
6) T-Ampoule will be fabricated from Ti-6Al-4V titanium alloy produced to material specification ASTM 348 except, as modified below:
   a) Titanium alloy will have procurement specified values of 150,000 psi ultimate strength and 140,000 psi yield strength, both at 77°F (room temperature).
   b) Temperature dependant allowable stress criteria will be determined using the procedures outlined in the ASME Boiler and Pressure Vessel Code, Section IID, Mandatory Appendix 1 Basis for Establishing Stress Values in Tables 1A and 1B.

c) In either case, titanium maintains ductility at low temperatures and is therefore, exempt from the requirements of Sections UCS 66 through 68 pertaining to derating allowable stress for low temperature operation.

7) In the case of analysis of the torispherical heads, and in accordance with Section UG-32(e), allowable stress will be limited to 20,000 psi for temperatures below 77°F, and will be reduced proportional to the curves developed in 2.b above for temperatures above 77°F.
8) The T-Ampoule quality program will meet the requirements of Section VIII with the following exceptions:
   a) The standard hydrostatic test of paragraph UG-99 or the pneumatic test from paragraph UG-100, are not required.
   b) The requirements of paragraph UF-55 regarding ultrasonic examination do not apply. Inspection will consist of visual inspection and physical measurement of specified dimensions.
   c) As the T-Ampoule components are either formed or spun without welding, the requirements of part UW and part UB do not apply.
9) In lieu of the requirements of paragraph UG-91, the inspector will meet the requirements listed below:
   a) Inspector will demonstrate experience with spinning and fabrication processes, and
   b) Inspector will demonstrate experience with Section VIII.

The elastomeric (O-ring) seal and the associated threaded joint were analyzed using accepted engineering practices and manufacturers' recommendations.

3.2 Pressure Envelope Analysis

Within this section:

- Sections 3.2.1 and 3.2.2 summarize the results used for subsequent analyses. Section 3.2.1 provides a summary of results for internal pressure while Section 3.2.2 does the same for external pressure calculations.
- Section 3.2.3 describes calculations done to provide metal properties for subsequent calculations. The T-Ampoule will be built using an alloy of titanium not addressed, in detail within Section II.
- Sections 3.2.4 through 3.2.7 summarize individual analyses for areas 1 through 4 identified in Figure 12.

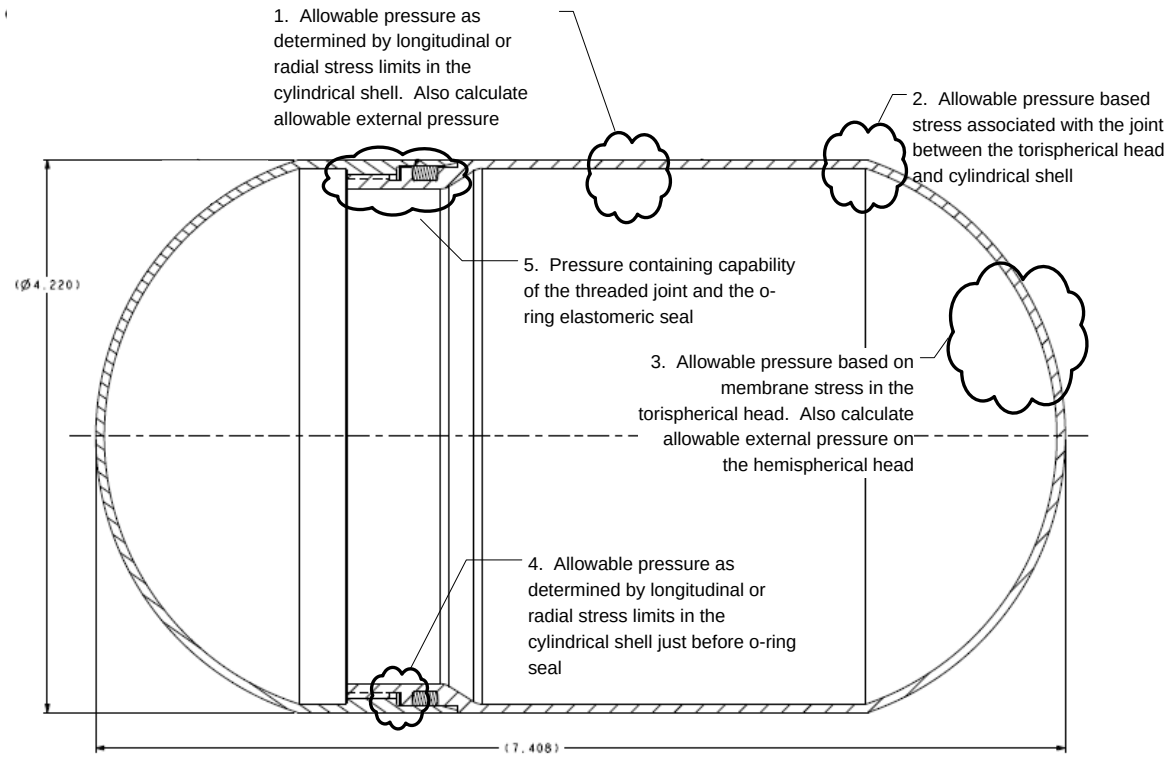

Figure 12: Five Analyses Performed for MAWP Determination

The O-ring seal identified as Area 5 in the figure will be addressed in Chapter 4.

3.2.1 Maximum Allowable Working Pressure (Internal Pressure Limits)

Figure 13 contains a plot of maximum allowable working pressure (MAWP) as a function of temperature for the T-Ampoule. The MAWP declines with temperature from 617 psig at room temperature (77°F) to 263 psig at 1080°F. At temperatures exceeding 1080°F, the T-Ampoule's O-ring seal has failed and pressure has equilibrated with the external environment resulting in zero pressure stress on the T-Ampoule.

It is important to later recall that MAWP is presented as gauge pressure, the difference between external and internal pressures.

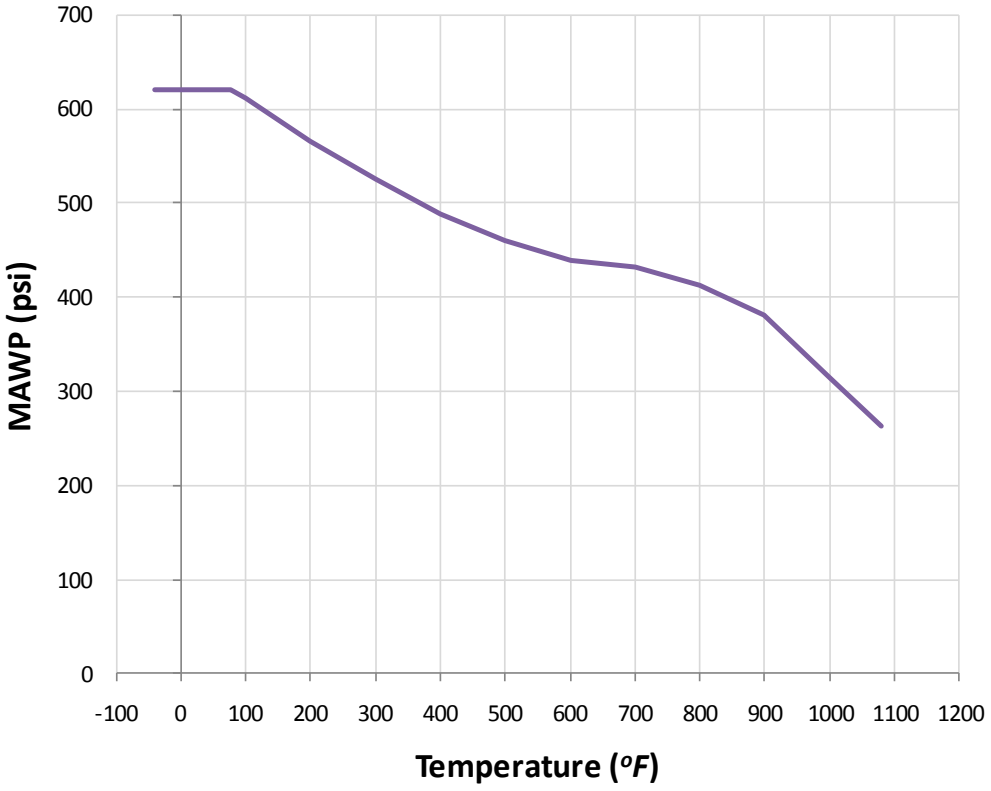

Figure 13: Maximum Allowable Working Pressure (MAWP) for T-Ampoule

Table 16 contains a summary of the results.

Table 16: Summary of Allowable Internal Pressure by Analysis Area

Analysis Area	Description	Allowable Pressure (psig) @ 77°F	Allowable Pressure (psig) @ 1080°F
1	Cylindrical Shell Longitudinal Stress	2790	1180
1	Cylindrical Shell Circumferential Stress	1360	576
2	**Joint, Torispherical Head to Shell**	**624**	**263**
3	Torispherical head, membrane stress	2600	1100
4	Seal Area Longitudinal Stress	1910	809
4	Seal Area Circumferential Stress	935	396
5	O-Ring Seal	900	n/a

The MAWP is set to the lowest allowable pressure for the analysis areas. For this design, the joint between the torispherical head and the cylindrical shell, determined MAWP. The five analyses are summarized below, preceded by a review of the methodology used to determine temperature dependant allowable stresses.

3.2.2 External Pressure Limits

Figure 14 contains a plot of maximum allowable, external pressure as a function of temperature for the cylindrical shell and the hemispherical head. Allowable pressure for the cylindrical head is the lower of the two and would provide the limiting criteria for the T-Ampoule as a pressure vessel. As is discussed in the applicable sections, this is a conservative calculation.

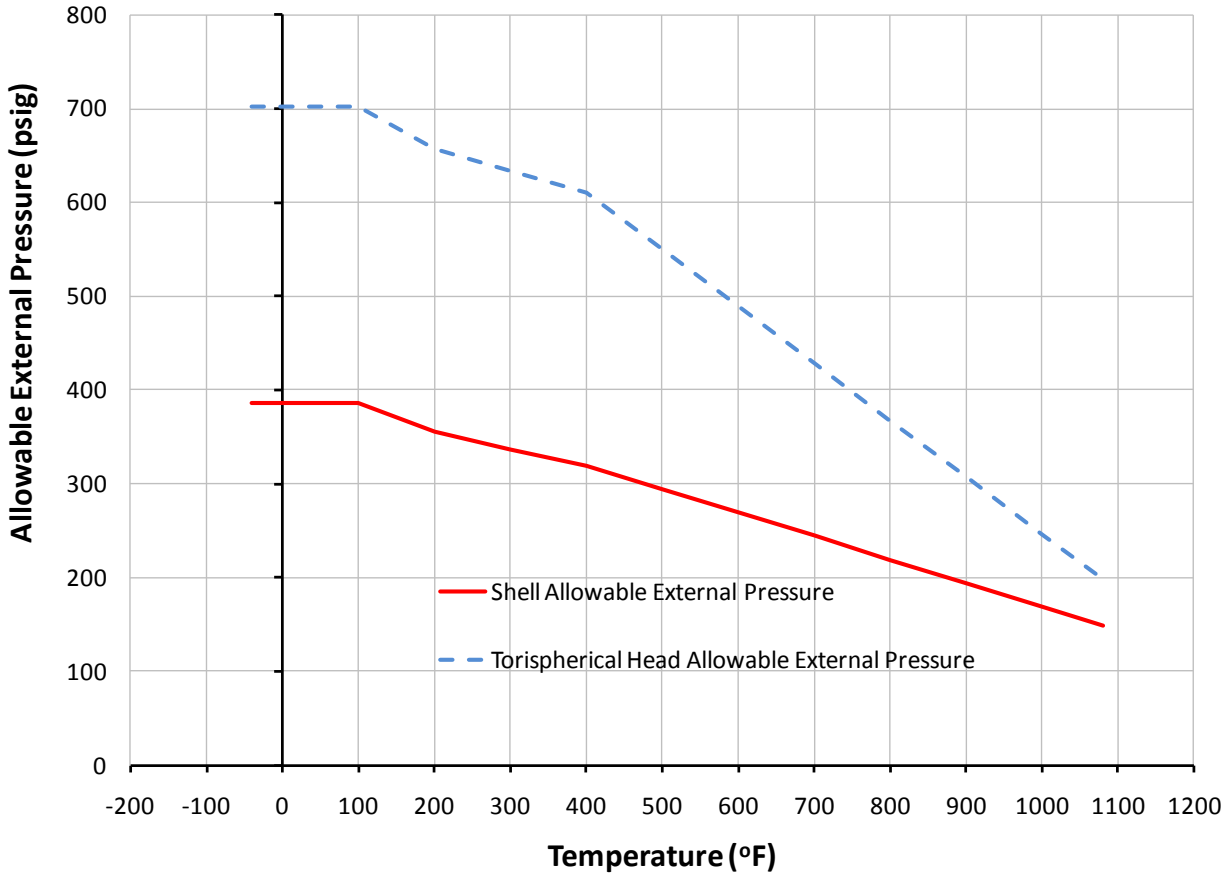

Figure 14: Allowable External Pressure

Table 17 contains a summary of allowable external pressures. This table lists values for room temperature (71°F) and for 700°F, the temperature at which the T-Ampoule's O-ring seal is expected to fail.

Table 17: Summary of Allowable External Pressure by Analysis Area

Analysis Area	Description	Allowable Pressure (psig) @ 71°F	Allowable Pressure (psig) @ 800°F
1	Cylindrical Shell	386	219
3	Torispherical head	687	368
5	O-ring Seal	180	160

3.2.3 Titanium Properties

The document controlling design and fabrication of the T-Ampoule [Reference 6, paragraph 3.1.1] specifies that the titanium alloy Ti-6Al-4V will be procured with a minimum tensile (ultimate) strength, S_T, of 150,000 psi and minimum yield strength, S_Y, of 140,000 psi at room temperature (77°F). The analyses below require allowable stress, S_A, values at temperatures, both below and well above room temperature. Allowable stress values should be for a wrought non-ferrous metal.

Section VIII references Section II part D (Section II) for allowable stress values. However, Section II does not tabulate properties for this material. In the event allowable stresses are not published in Tables 1A or 1B of that document, Section II refers the user to an internal appendix, *Mandatory Appendix 1 Basis for Establishing Stress Values in Tables 1A and 1B*. The following criteria were extracted from TABLE 1-100 of that appendix:

$$S_A = \begin{cases} \dfrac{S_T}{3.5} & temperature \le 77\,°F \\ \dfrac{1.1 S_T R_T}{3.5} & temperature > 77\,°F \end{cases} \qquad 14$$

The Parameter R_T is defined as the ratio of the average temperature dependent, trend curve value of tensile strength to the room temperature tensile strength, the value of which was extracted from the curve F_{tu} in Figure 11.

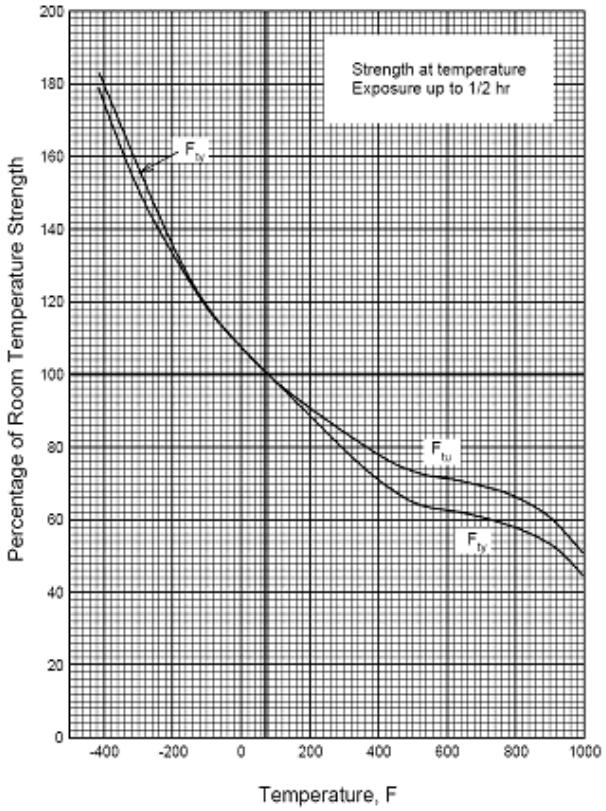

Figure 15: The Effect of Temperature on the Tensile Ultimate Strength of Annealed Ti-6Al-4V Alloy [7, Figure 5.4.1.1.1]

For Titanium, the useful temperature range is from -320 to 750°F [Reference 7, p 5-51]. Unlike ferritic steels, titanium maintains ductility throughout its operating range, as shown in Figure 16. For these reasons, allowable stresses for temperatures below room temperature were extended down to -40°F.

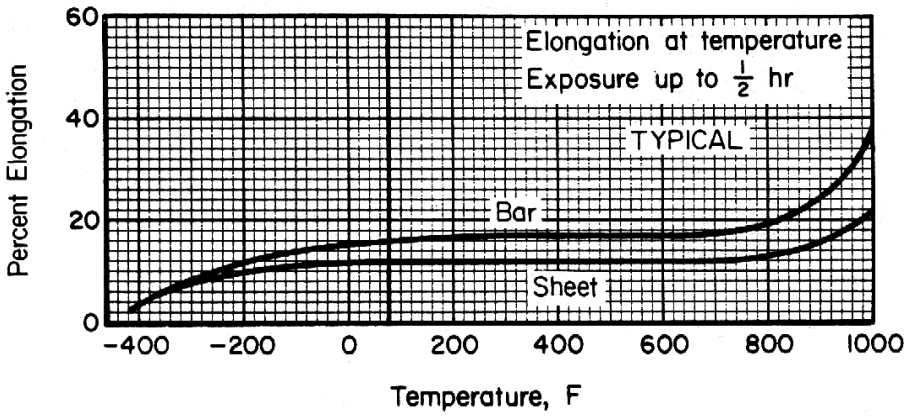

Figure 16: The Effect of Temperature on the Elongation of Annealed Ti-6Al-4V [7, Figure Fig 5.4.1.1.5]

The temperature factor for this analysis was extrapolated to 1080°F, 80°F beyond the data presented in Figure 15 and Figure 16 in order to estimate the response of the T-Ampoule at the theoretical accident temperature (1080°F).

The torispherical head analysis, per Section VIII, paragraph UG-32(e), mandates lower allowable stresses. In this single case, the following applies:

Torispherical Head $$S_A = \begin{cases} 20,000 & temperature \le 77\,°F \\ 20,000 R_T & temperature > 77\,°F \end{cases}$$ 15

Figure 11 contains plots of the allowable stress values that result from the above equations.

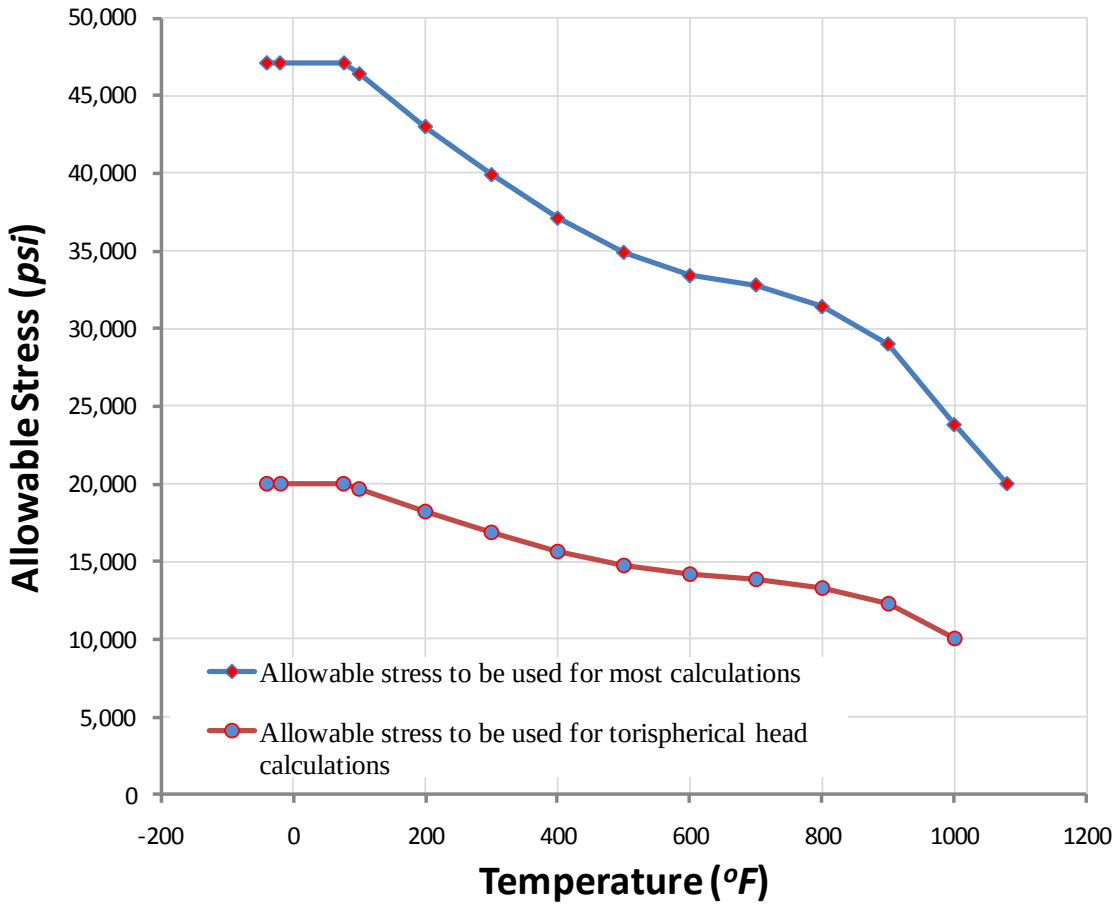

Figure 17: Allowable Stress Values for Ti-6Al-4

Section VIII references Section II part D for computation of yield stress values. In the event yield stresses are not published in Tables 1A or 1B of that document, Section II refers the user to an internal appendix, *Mandatory Appendix 1 Basis for Establishing Stress Values in Tables 1A and 1B.* The following criteria were extracted from TABLE 1-100 of that appendix:

$$Y = \begin{cases} \frac{2}{3} S_Y & temperature \le 77\,°F \\ \frac{2}{3} S_Y R_Y & temperature > 77\,°F \end{cases} \qquad 16$$

The Parameter R_Y is defined as the ratio of the average temperature dependent value of yield strength to the room temperature yield strength, the value of which was extracted from the curve F_{ty} in Figure 15. The results of equation 16 are plotted in Figure 18.

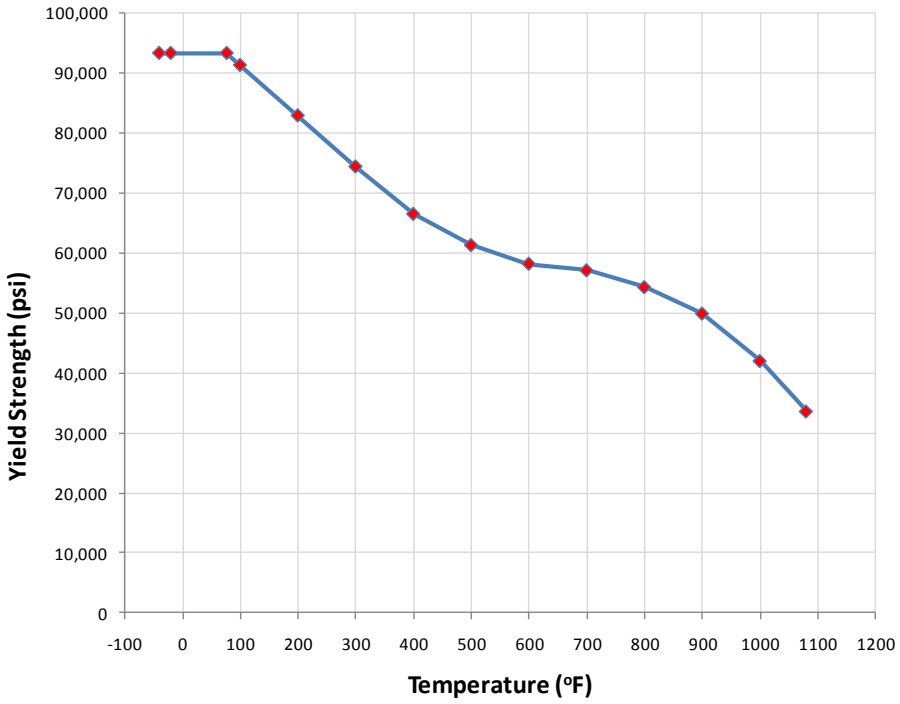

Figure 18: Yield Strength for Ti-6Al-4V

As with tensile strength, the curve is extended to -40°F based on low temperature ductility arguments.

External pressure calculations incorporate the modulus of elasticity at temperature. Figure 19 contains a plot for the T-Ampoule's material based data from a metals handbook published by the U.S. Department of Transportation [7].

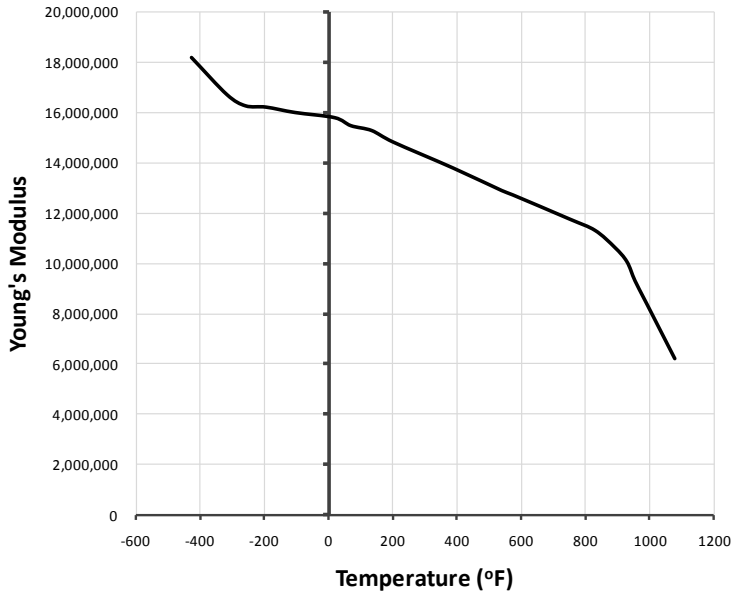

Figure 19: Effect of Temperature on the Young's Modulus of AnnealedTi-6Al-4V [Ref. 7, Figure 5.4.1.1.4]

Figure 20 contains the chart extracted from Section II, from which Factor B was extracted for external pressure calculations. This chart is in fact for an alloy of titanium with similar elastic moduli, but of yield strength half that of Ti-6Al-4V.

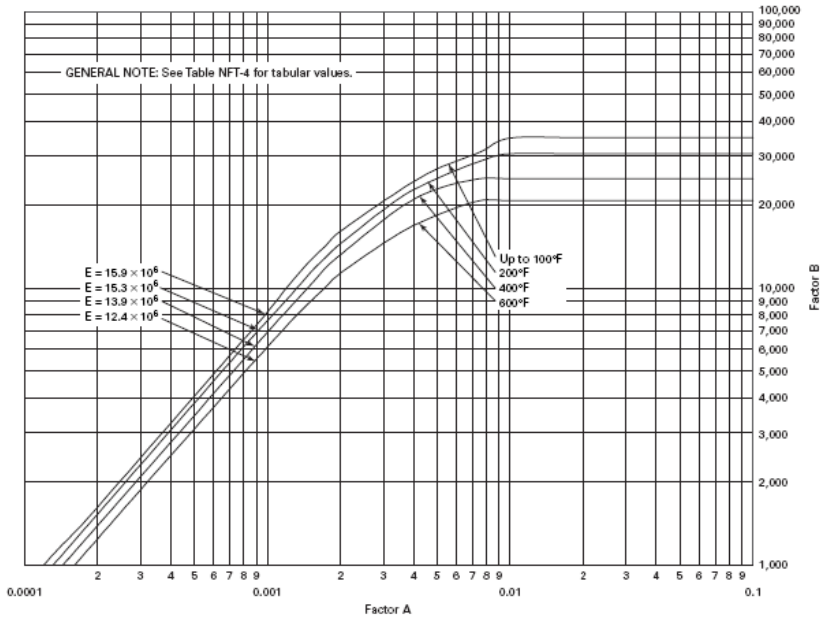

Figure 20: Fig. NFT-4 Chart for Determining Shell Thickness of Components Under External Pressure Developed For Titanium Grade 9 Alloy (Uns R56320) [2]

3.2.4 Analysis 1, Cylindrical Shell

Internal Pressure – This section summarizes the analysis performed on the cylindrical shell, the area designated as analysis area 1 in Figure 12. Allowable pressures in the both the longitudinal and circumferential direction of the shell are based on the criteria set forth in Section UG-27 of Section VIII.

Longitudinal Limit, shell $$P_L = \frac{2S_A Et}{R_i - 0.4t} \quad (17)$$

Circumferential Limit, shell $$P_\phi = \frac{S_A Et}{R_i + 0.6t} \quad (18)$$

The analyst should use data from the upper curve of Figure 17 for allowable stress, S_A because the device in question has a formed joint efficiency, E, of 1.0. The internal radius, R_i, is based on dimensions taken from Figure 21, and uses specified minimum/maximum values that result in the smallest radius value. Wall thickness, t, is derived from the same dimensions. It is based on the difference between outer and inner diameters using tolerances to obtain the largest value.

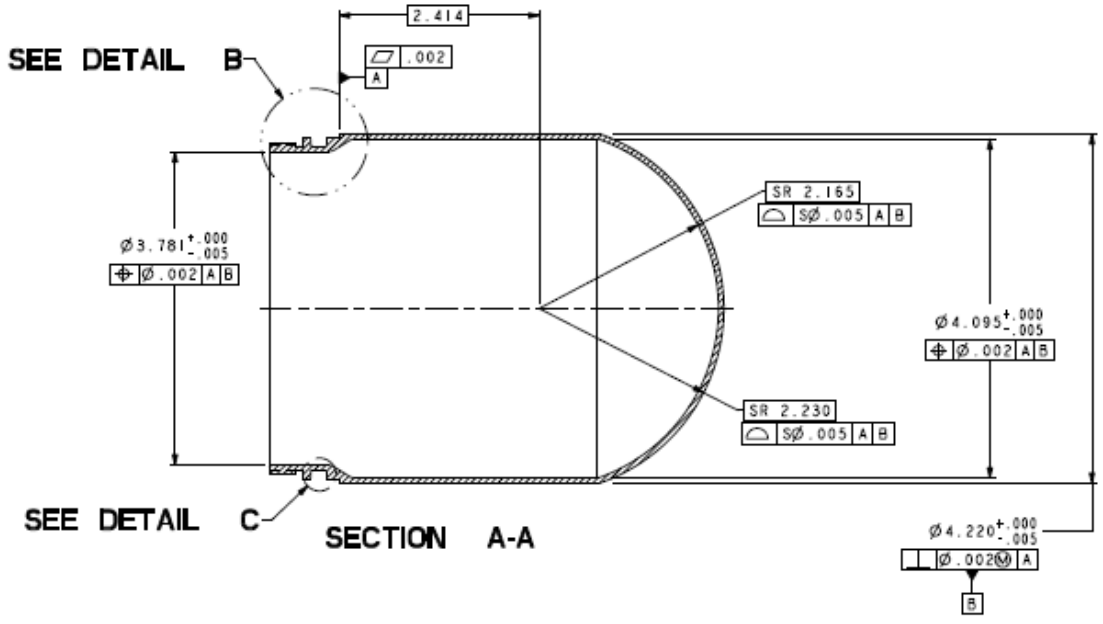

Figure 21: Dimensional Sketch of T-Ampoule Body

Table 18 contains both the input parameters to equations 17 and 18 as well as the final results. The allowable pressure for this analysis area is the pressure determined based on allowable circumferential stress with a value of 1356 psig at room temperature.

Table 18: Parameters and Calculated Values Analysis Area 1

Parameter	Value	Units
d_i	4.095	in
d_o	4.215	in
R_i	2.0475	in
R_o	2.1075	in
t	0.06	in
E	1	n/a
S_A	47100	psi
P_L	**2790**	**psi**
P_ϕ	**1360**	**psi**

Values for allowable stress and therefore, pressure are at room temperature.

External Pressure - This external pressure calculation is conservative. Given the snug fit between the T-Ampoule and the TB-1 containment vessel, it is unlikely that the T-Ampoule will be allowed to flex enough to buckle elastically. The Section VIII external pressure analysis ignores this type of external support and the analysis assumes no support exists. In addition, B factor charts for the Ti-6Al-4V material used for the T-Ampoule do not exist. The curve for a titanium alloy with UNS designation R56320 will be assumed instead. This substitute alloy has a room temperature yield strength of 70,000, a factor of 2 lower than the alloy actually in use. These two assumptions combine to under-predict allowable external pressure. Since the predicted pressures are still sufficiently high that failure is not predicted, no attempt was made to refine the analysis.

Rules for calculating allowable external pressure are presented in Section VIII, paragraph UG-33(d). The methodology is graphic oriented. The first important parameter, A, is obtained from the graph in Section II, Figure G, which correlates A to geometric parameters derived from external diameter, D_o, shell length, SL, and wall thickness, t. Using this value, one can determine the allowable stress, B, from Figure 20. This value of B for room temperature is 18,800 psi.

A B-factor feeds into the following equation:

$$P_{ex} = \frac{4B}{3\left(\frac{L_o}{t}\right)} \qquad 19$$

Table 19 summarizes the results of the above calculations. Allowable external pressure is 481 psig. At 700°F when the T-Ampoule equilibrates with the annulus pressure, the allowable

external pressure difference will be 244 psig, providing a reasonable margin above the estimated equilibration threshold of 150 psig difference.

Table 19: Allowable External Pressure of Hemispherical Head

Parameter	Value	Units
D_o	4.22	In.
t	0.06	In.
SL	4.426	length
SL/D_o	2.098	
D_o/t	64.9	
A	0.00250	
B	18,800	psi
P_{ex}	386	psi

3.2.5 Analysis Area 2, Torispherical Head Joint

Criteria for analysis area 2 are based on paragraph UG-32 *Formed Heads, and Sections, Pressure on the Concave Side* of Section VIII. This paragraph refers in turn to Section VIII's Mandatory Appendix 1, Supplementary Design Formulas, paragraph 1-4(d) which applies the following criteria:

Torispherical Head Joint

$$P_T = \frac{2S_A E t_s}{LM + 0.2t_s} \qquad 20$$

Where

$$M = \frac{1}{4}\left(3 + \sqrt{\frac{L}{r}}\right) \qquad 21$$

In this case the analyst should employ the lower curve of Figure 17 for allowable stress. Dimensions were obtained from Figure 21. The crown radius, L, or the radius of the head, must be the minimum value possible when considering tolerances. The head wall thickness, t_s, should also be the minimum possible value. The parameter M is based on the ratio of crown radius, L, to knuckle radius, r. Knuckle radius is the radius of curvature of the titanium at the joint between the head and the cylindrical shell. This value is specified to be 0.125 inch. As above, the joint efficiency, E, is 1.0 since no joint exists.

In addition to the above, the following criteria apply:

$$\frac{t_s}{L} \geq 0.002,$$
$$L \leq d_o \qquad 22$$

Table 20 contains input parameters and results for the torispherical head joint. The value for t_s is based on the difference between outer and inner crown radii with tolerances chosen to minimize thickness. The allowable stress at room temperature is limited to a maximum of 20,000 psi at room temperature. The two criteria of equation 19 are met. The ratio of head thickness to crown radius is 0.0277, an order of magnitude above the criterion. The crown radius itself, at 2.225 inches is less than the outer diameter of the shell which equals 4.095 inches. All of this results in an allowable pressure of 624 psig. This is, in fact, the lowest allowable pressure of all calculated for the five analysis areas, and as such provides the criteria for MAWP.

Table 20: Parameters and Calculated Values Analysis Area 2

Parameter	Value	Units
d_i	4.095	in
d_o	4.215	in
R_i	2.0475	in
R_o	2.1075	in
L	2.225	in
t_s	0.06	in
E	1	n/a
t_s/L	**0.0277**	nd
S_A	**20,000**	psi
M	**1.790**	nd
P_T	**624**	psi

3.2.6 Analysis Area 3, Head Membrane

Internal Pressure - Stress in the hemispherical head away from the joint is uniform in all directions normal to the radius and is governed by the criteria of paragraph UG-32 of Section VIII, Formed Heads and Sections.

Hemispherical Head Membrane $$P_H = \frac{2S_A E t_s}{L + 0.2t_s} \qquad 23$$

The following additional constraints apply:

$$\frac{t_s}{L} < 0.356$$
$$\frac{P_H}{SE} < 0.665 \qquad 24$$

Values and definitions are as defined in the previous section.

Table 21 contains input parameters and results for the hemispherical head membrane. The two supplemental criteria of equation 24 are satisfied. The calculated value for allowable pressure of 2600 psig is well above the previously calculated allowable pressure for the torispherical joint.

Table 21: Parameters and Calculated Values Analysis Area 3

Parameter	Value	Units
d_i	4.095	*in*
d_o	4.215	*in*
R_i	2.048	*in*
R_o	2.108	*in*
L	2.225	*in*
t_s	0.060	*in*
E	1	*n/a*
S_A	47100	*psi*
t_s/L	0.0277	*nd*
P_H/SE	0.0551	*nd*
P_H	2600	*psi*

External Pressure - This external pressure calculation is conservative. Given the snug fit between the T-Ampoule and the TB-1 containment vessel, it is unlikely that the T-Ampoule will be allowed to flex enough to buckle elastically. The Section VIII external pressure analysis ignores this type of external support and the analysis assumes no support exists. In addition, B factor charts for the Ti-6Al-4V material used for the T-Ampoule do not exist. The curve for a titanium alloy with UNS designation R56320 will be assumed instead. This substitute alloy has a room temperature yield strength of 70,000, a factor of 2 lower than the alloy actually in use. These two assumptions combine to under-predict allowable external pressure. Since the predicted pressures are still sufficiently high that failure is not predicted, no attempt was made to refine the analysis.

Rules for calculating allowable external pressure are presented in Section VIII, paragraph UG-33(e). Methods are graphic oriented. First important parameter, A, is calculated as:

$$A = 0.125\left(\frac{t}{L_o}\right) \qquad 25$$

Note: This equation uses the external crown radius, L_o. Using this value, allowable stress, B from Figure 20 can be determined. This value at room temperature is 23,400 psi. The B factor feeds into the following equation:

$$P_{ex} = \frac{B}{\left(\frac{L_o}{t}\right)} \qquad 26$$

Table 22 summarizes the results of the above calculations. Allowable external pressure is 687 psig. At 700ºF when the T-Ampoule equilibrates with the annulus pressure, the allowable external pressure difference will be 419 psig, providing a reasonable margin above the estimated equilibration threshold of 150 psig, difference between the annulus and the T-Ampoule.

Table 22: Allowable External Pressure of Hemispherical Head

Parameter	Value	Units
L_o	2.22	In.
t	0.065	In.
L	4.43	
L_o/t	34.1	
A	0.00367	psi
B	23,400	psi
P_{ext}	687	

3.2.7 Analysis Area 4, Seal Area

This section summarizes the analysis performed on the cylindrical shell in the area designated as area 5. Figure 22 shows the area in extreme close-up. The thin cap section just after the threads, but before the O-ring is of concern. This section still experiences internal pressure and yet, is substantially thinner than the T-Ampoule body. This analysis ignores possible rib reinforcement from the threaded area.

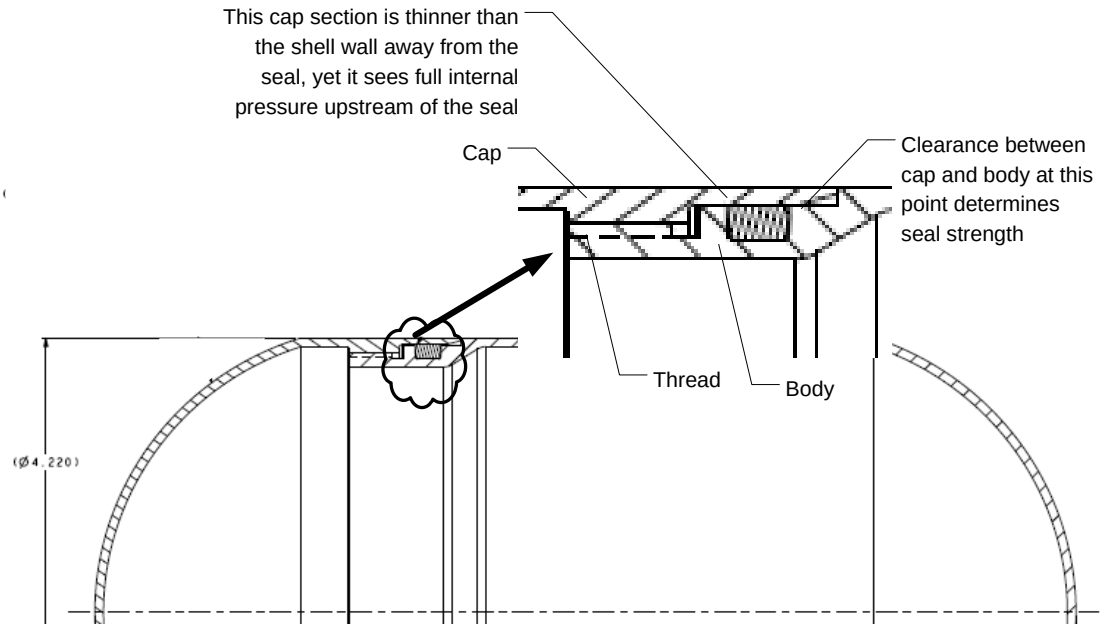

Figure 22: Blowup of Seal Area

The analysis is similar to that already completed for analysis area 1 with the dimensions, however, as specified in Figure 17. Allowable pressures in both the longitudinal and circumferential direction of the shell are based on the criteria set forth in Section UG-27 of Section VIII, and are summarized in equations 17 and 18.

The analyst should use data from the upper curve of Figure 17 for allowable stress, SA. Since the device in question is formed, joint efficiency, E, is 1.0.

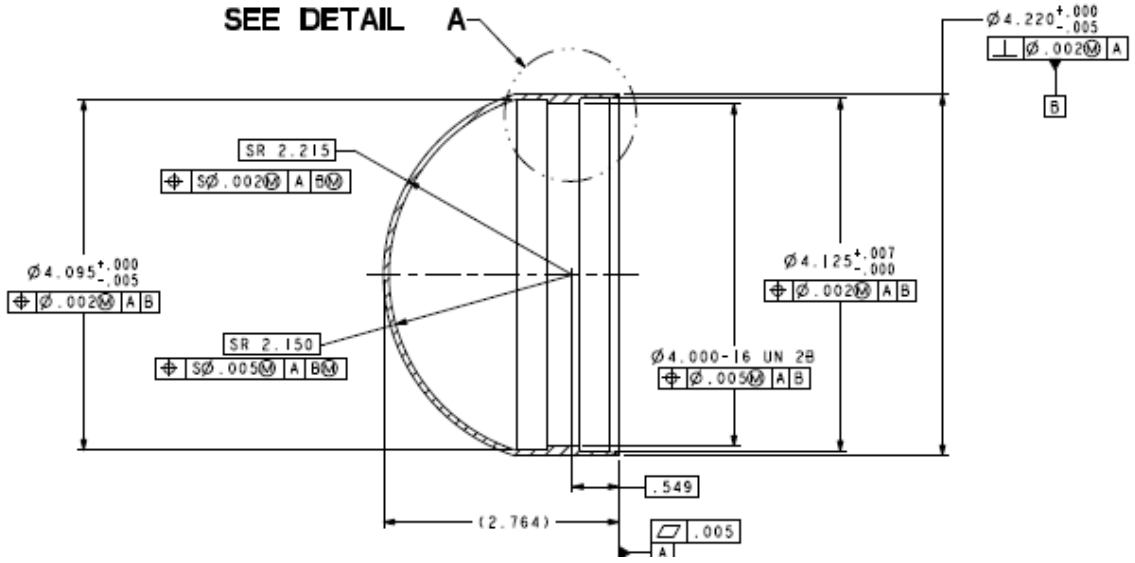

Figure 17: Dimensioned Sketch of T-Ampoule Lid

Table 23 contains both the input parameters to equations 14 and 15, as well as the final results. The allowable pressure for this analysis area is the pressure determined based on allowable circumferential stress with a value of 935 psig at room temperature.

Table 23: Parameters and Calculated Values Analysis Area 4

Parameter	Value	Units
d_i	4.132	in
d_o	4.22	in
R_i	2.066	in
R_o	2.11	in
t	0.0415	in
E	1	n/a
S_A	47100	psi
P_L	1910	psi
$P\phi$	935	psi

4 O-ring Seal Design

While O-ring static seals are ubiquitous in industry and are well respected, their analysis is not part of the Boiler and Pressure Vessel Code. Neither does their analysis possess the rigor found in the Boiler and Pressure Vessel Code. This analysis that follows relies, instead on the vendor's recommendations and good engineering practice.

A static O-ring seal designed to the dimensional specifications of SAE standard AS5857 will hold pressure to 1500 psig [11]. The T-Ampoule design follows this standard with two exceptions. Per the standard, the specified radial clearance in both directions, between the body and the cap should be 0.0015 to 0.003 inches. T-Ampoule clearances for both directions are relaxed for different reasons. Referring to Figure 18, the downstream clearance has been relaxed slightly to facilitate assembly in a glove box. The upstream clearance has relaxed even further to guard against excessive, external pressure. Sustainable pressures therefore require some adjustment.

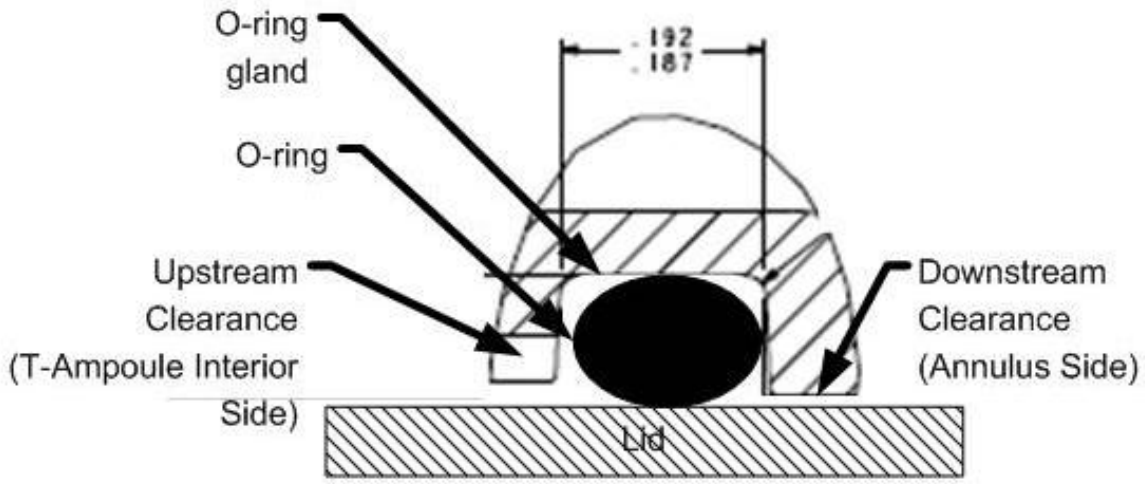

Figure 18: Pressure Containment for O-Ring Seals-[10, 11]

O-rings seal when pressure forces the relatively flexible elastomeric O-ring against the clearance between the cap and the body of the T-Ampoule. The downstream clearance supports the O-ring against internal pressure. The upstream O-ring supports the O-ring against external pressure.

Seal failure occurs when the O-ring extrudes into the clearance. As this clearance becomes tighter (smaller), the seal can sustain more pressure. Loosening (opening) the clearance causes

the seal to hold less pressure. In addition, a seal's ability to withstand pressure depends on O-ring hardness, typically measured on the "Shore A" scale. Figure 19 contains a plot of information taken from an O-ring design manual illustrating the relationship of an O-ring meeting the T-Ampoule seal's hardness specification.

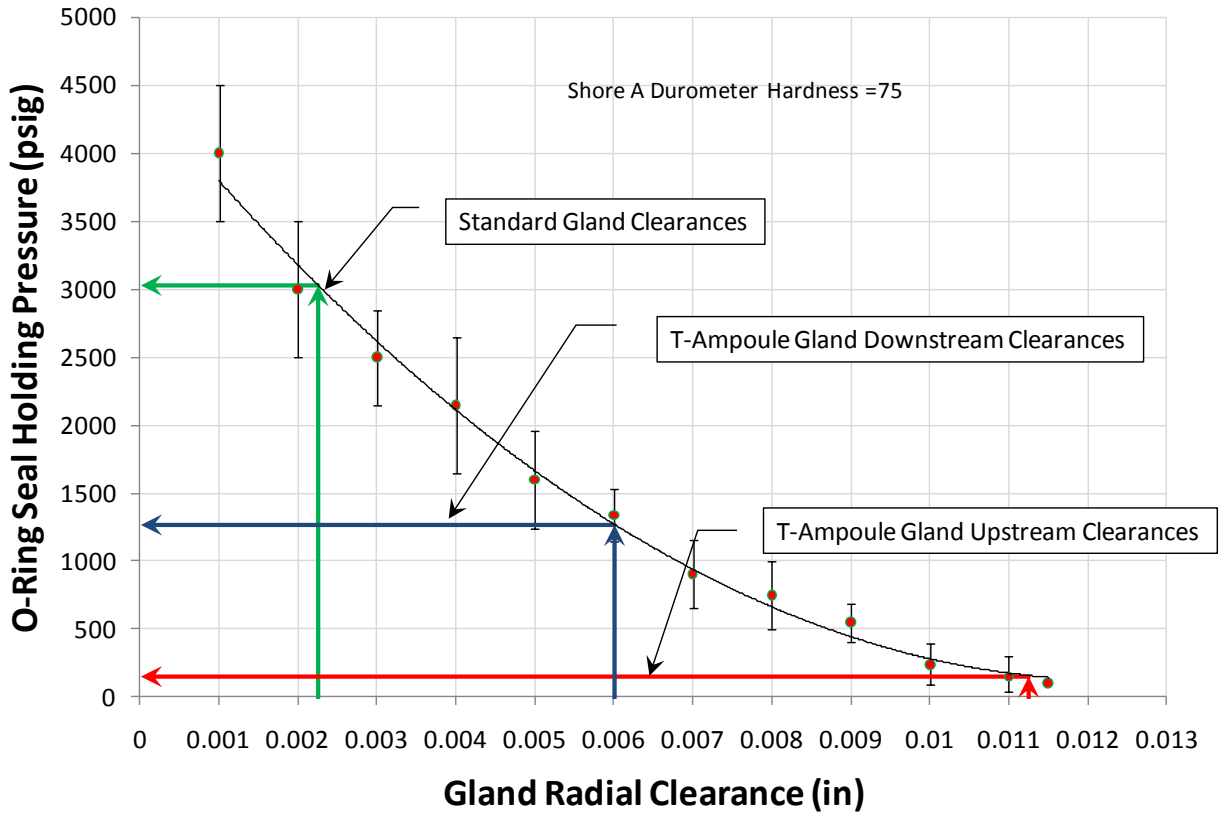

Figure 19: **Internal Pressure Containment for O-Ring Seals [source:10]**

T-Ampoule design specifies an O-ring with a Shore A hardness of 75 over its useful temperature range (-15°F to 400°F). A standard O-ring gland specification would call for a radial clearance between 0.0015 and 0.003 inches. From Figure 19, sustainable pressure is 3000 psig. The difference between this value and the value of 1500 psig quoted by the manufacturer represents factor of safety of 2.0 for a standard gland design.

The downstream clearance (radial) has been increased to 0.006. From the figure, this level of clearance can sustain a pressure of 1270 psig. With the same factor of safety, the seal should be rated for internal pressure at 635 psig.

The upstream clearance (radial) has been relaxed at selected locations to an average radial value of 0.01125 inches. From Figure 19, the seal can sustain a pressure of 160 psig. With the same factor of safety used above, the seal will be rated for a backpressure of 80 psig.

5 Conservatism and Uncertainty

This analysis is conservative. This section is intended to document this conservatism on a section by section basis.

Section 1.1. Analysis ignores the impact of thermal expansion on the annulus volume. Since stainless steel expands faster than titanium, the volume will grow slightly with temperature. As a consequence, real pressures will be slightly lower than predicted by this analysis.

Section 1.2. O-ring decomposition analysis assumes O-rings decompose to relatively low molecular mass ratio materials. This results in a relatively large the molecular population of the vapor. In fact molecules generated could be more than 5 times as large, reducing the contribution of O-ring pyrolysis to final pressure by as much as 80% of predicted.

Section 1.2. The analysis assumes that O-rings decompose completely. As documented, other sources indicate that only 76% of O-rings will decompose at 1080°F. Hence, predicted pressures could be as much as 33% higher than real values.

Section 1.2. The analysis assumes that O-ring failure due to pyrolysis occurs at 1080°F, and after all material has already vaporized. In reality, O-rings will decompose starting as early as 700°F. This earlier decomposition could shift pressure rise to earlier temperatures with vessel strength is greater, thus improving safety margin.

Section 1.3 Analysis assumes sufficient oxygen exists inside TB-1 to completely oxidize ancillary plastic to a vapor. This reduces the allowable ancillary plastic by an order of magnitude.

Section 1.4 Helium generation model assumes helium accumulates without diffusion for one year. The length of time the T-Ampoule exists as an assembly seems excessive. The assumption that no molecular diffusion of helium occurs during that period is conservative.

Section 1.5 O-ring seal is set to relieve with back pressure a factor of 1.33 below allowable back pressure.

Section 2. The ASME BPVC Section VIII, D1 MAOP method is inherently conservative in order to accommodate the wide range of boundary and initial conditions covered by the code. The code's criteria call for a vessel to last for an unspecified long time under extreme conditions in close proximity to humans.

Section 2 The ASME BPVC Section II material properties are inherently conservative. For example, allowable stresses include a safety factor of 3.5 on tensile strength. These tensile strengths are the minimum predicted by the alloy chemistry allowed within a material's specification.

Section 2.1 The MAP has a safety factor of 1.98 when compared to the MAOP calculated using ASME BPVC.

Section 2.3 Thin wall analysis is the most conservative of the two methods used.

Section 2.3 Allowable stress is based on a heat treatment (H1050) lower than that actually specified (H1075). This results in a lower ultimate tensile strength for the material.

Section 2.4 Bolt material strength is conservatively low. SAR specification calls for an ultimate strength of 180,000 psi. Value used in analysis was 130,000 psi because this is the strength defined by the material reference.

Section 3.2 Failure case for the T-Ampoule is via buckling collapse under external pressure. Estimated resistance to buckling pressure is understated. Like all buckling, collapse occurs at the eigenmodes composed of sinusoids with progressively increasing frequencies. Per ASME BPVC Section VIII D1, collapse occurs at the first eigenmode of pressure. Such a collapse requires that the vessel distort to look like a figure eight -- the sides of the vessel displace outwards. Since the TB-1 vessel constrains the T-Ampoule against such flexure, collapse at the first eigenvalue cannot happen. In reality, collapse will occur at a higher pressure where the displacement associated with the eigenmode is small enough to accommodate the physical constraints of the containing vessel.

Section 3.2.3 The theoretical cylinder external collapse critical pressure is based on a material with tensile strength at room temperature of 70,000 psi. The titanium actually used has a tensile strength at room temperature exceeding 100,000. This strength will translate to increased strength at design temperature and increased resistance to buckling.

Uncertainties:

Section 1.2 Analysis assumes one half of the products of O-ring pyrolysis enters the annulus and one half enters T-Ampoule. While both paths are symmetric, nothing exists to force this even distribution. As such, it is conceivable in the extreme that the split could be 10% into one side and 90% into the other. Should this occur, the

only consequence is that the T-Ampoule O-ring seal fails and relieves pressure sooner.

Section 1.2 Uncertainty exists regarding the relationship between the degree of O-ring decomposition and O-ring sealing ability. This analysis assumes the O-ring holds pressure completely until the last of its material has vaporized. In reality, the pressure will equalize much sooner.

Section 1.4 Actual gauge pressure at which the T-Ampoule's O-ring seal fails could be as high as 360 psig (double the design failure point) rather than the 180 psig design pressure. As above, the TB-1 maximum pressure is significantly lower than the design point. Increasing maximum pressure from 600 to 780 still leaves a significant margin for error. Consider this margin for error in the context of the extremely conservative ASME Boiler and Pressure Vessel Code and potential for failure becomes vanishingly small.

6 Conclusions

The objective of the T-Ampoule is to provide a eutectic prevention barrier between the plutonium it contains and the PH13-8Mo stainless steel of the TB-1 containment vessel The barrier will minimize any formation of a Pu/Fe eutectic under the elevated temperature of 1080ºF during a fire accident. In forming the barrier, the T-Ampoule becomes a pressure vessel requiring analysis. A pressure vessel analysis demonstrates that the design is sound and will withstand the environment predicted for it. The analysis is conservative. These conservatisms were included to address a list of uncertainties, all of which are addressed in the analysis.

The TB-1/T-Ampoule system can generate a more complex than normal pressure environment. The assembly involves a titanium T-Ampoule designed to fit snugly inside the stainless steel TB-1 vessel. Both are pressure containing devices. They combine to create a very small annular volume between the inside diameter of the TB-1 and the outside diameter of the T-Ampoule. This arrangement results in a complex pressure/temperature environment. At the high temperatures, the small annular space between the two vessels fills with products of O-ring decomposition and can develop pressures there significantly greater than the interior pressure. This negative pressure difference creates forces potentially capable of buckling the T-Ampoule. At lower temperatures, the T-Ampoule's greater internal pressure creates tensile stresses in the shell, threatening failure via bursting. This analysis demonstrates that the T-Ampoule design is sufficiently robust that neither of these possibilities poses a threat.

Analysis included both the creation of the complex pressure/temperature map for the T-Ampoule vessel. This map is reflected in the graph contained in Figure 5. This map serves as input to a pressure vessel analysis based on the ASME Boiler and Pressure Vessel Code, Section VIII, Division 1 (BPVC). The pressure analysis provided temperature dependent limits for both internal (burst) pressure loading at low temperatures and external (collapse) pressure loading at high temperatures. The parameters of the pressure/temperature map were adjusted to ensure the predicted pressure stayed within these parameters.

The parameter adjustment resulted in two important constraints on T-Ampoule design. First, any ancillary plastic (bags, labels, tape, etc.) is limited to the values listed in Table 10 for four plastics. Second, the O-ring seal must be designed to ensure it will fail inward under high external pressure difference. Thus at a specific point in the accident scenario the TB-1/annulus volume equilibrates with the T-Ampoule interior. These constraints also combine to ensure the maximum TB-1 pressure, either before equilibration or after, never exceeds the 1110 psia (1095 psig) limit imposed by its design.

The special nature of the T-Ampoule design mandated some exceptions to a standard BPVC analysis, which are identified in this report.

7 References

1. American Society of Mechanical Engineers (ASME); Boiler and Pressure Vessel Code, Section VIII Division 1, Rules for Construction of Pressure Vessels. 2007.
2. American Society of Mechanical Engineers (ASME); Boiler and Pressure Vessel Code, Section II Part D, Properties (Customary) Materials; 2007.
3. Rubin, J.B. "Thermal Decomposition of Viton® O-rings for the PAT-1 Packaging Accident Scenario." LA-UR-10-05846. Los Alamos National Laboratory. Los Alamos, NM.
4. Serban Moldoveanu: Analytical Pyrolysis of Synthetic Organic Polymers, Volume 25 (Techniques and Instrumentation in Analytical Chemistry) (Elsevier Science, 2005).
5. W.C. Reynolds; Thermodynamic Properties in SI; Stanford Department of Mechanical Engineering; 1979; ISBN 0-917606-05-1.
6. PAT-1040. Titanium and O-Ring Materials and Component Fabrication Specification.
7. DOT/FAA/AR-MMPDS-01 Metallic Materials Properties Development and Standardization: January 2003.
8. United States. Nuclear Regulatory Commission. NUREG-0361. "Safety Analysis Report for the Plutonium Air Transportable Package, Model PAT-1." Washington, D.C. 1978.
9. Society of Automotive Engineers; Standard AS5857; Gland Design, O-Ring and Other Elastomeric Seals, Static Applications; March 2005.
10. Parker Hannifin Corp document. "Parker O-Ring Handbook." ORD 5700.
11. Minnesota Rubber/Quadion Corporation, Elastomers and Thermoplastics Engineering Design Guide: copyright 2007.

This page intentionally left blank

3. THERMAL EVALUATION

The thermal evaluation in this addendum examines the incorporation of plutonium metal as a new payload for the PAT-1 package. The Pu metal is packed in an inner container (*T-Ampoule Assembly,*[A] Drawing 2A0261, designated the T-Ampoule) that replaces the PC-1 inner container. The T-Ampoule and associated Pu metal contents packing configurations are described in Section 1.2.1 and Section 1.2.2 of this addendum, respectively.

The thermal evaluations documented in Chapter 3 of the Safety Analysis Report (SAR)[1] for the Plutonium Air Transportation Package, Model PAT-1, NUREG-0361[1] (SAR[1]) apply to this PAT-1 Safety Analysis Report Addendum for the T-Ampoule and its contents. The thermal evaluation of the T-Ampoule contents addressed in this addendum assumes a bounding internal heating scenario where three plutonium metal samples (25 watts total) from a three-nested *Sample Container-1 (SC-1) Assembly* configuration, (Drawing 2A0268, designated SC-1) are collocated along the seal area of the T-Ampoule to present a concentrated heat source. The other configurations described in Section 1 of this addendum, which are the 831 g (1.83 lbm) Pu hollow cylinder, wrapped in tantalum foil or not wrapped based on operational determination, supported with crushed tantalum foil, and the two-nested sample container configuration (*Sample Container-2 [SC-2] Assembly*, Drawing 2A0265, designed SC-2) supported by a titanium *Inner Cradle* (Drawing 2A0385, designated Inner Cradle) present a less concentrated heat source against the seal area. Although the quantity of plutonium metal assumed for the bounding case has a lower decay heat energy (see Section 4 of this addendum) than the 25 watts (85.3 Btu/hr) the PAT-1 package is certified for, the 25-watt decay heat limit is conservatively used for this analysis. The heat absorbed by the components within the T-Ampoule is neglected also for conservatism. Results from thermal analyses presented in this section demonstrate that the thermal performance of the PAT-1 with the proposed metal payload will be acceptable under normal conditions of transport (NCT) as defined in 10 CFR 71.71,[2] under hypothetical accident conditions (HAC) as defined in 10 CFR 71.73,[2] and under the accident conditions for air transport of plutonium as defined in 10 CFR 71.74.[2] The results also demonstrate that the T-Ampoule will provide a eutectic barrier for the proposed metal payload under the accident conditions for air transport of plutonium, as defined in 10 CFR 71.74.[2] The components of the PAT–1 packaging not modified by this addendum perform as documented in the SAR.[1]

3.1 Description of Thermal Design

The thermal design description provided in the SAR[1] remains valid for this addendum, as there are no alterations to the AQ-1 protective overpack (*Overpack AQ*, Drawing 1002, designated AQ-1) or the TB-1 stainless steel containment vessel (*Containment Vessel*, Drawing 1017, designated TB-1). The thermal effects of replacing the PC-1 inner container and aluminum spacer with the T-Ampoule inner container inside the TB-1, with the same 25 watts (85.3 Btu/hr) maximum heat generation, were conservatively bounded in the computer analyses, as explained in the next sections. Changing the content form inside the TB-1 has no negative effects on the thermal performance of the AQ-1 overpack thermal design features or the TB-1 containment vessel. The thermal performance of the PAT-1 package is adequate and will safely contain its

[A] The drawing titles are in italics and are used interchangeably with the designated names in this addendum. See Section 1.3.2 in this addendum and Chapter 9 in the SAR[1] for drawing number, title, and revision.

contents as described in this Addendum under the test conditions specified in 10 CFR 71.71, 71.73, and 71.74.[2]

3.1.1 Design Features

The design features of the PAT-1, TB-1 stainless steel containment vessel, and the AQ-1 protective overpack assembly are unchanged and are described in Chapter 3 of the SAR[1]. The *Ring, Filler* (Drawing 2A0262, designated Ring Filler) and the T-Ampoule inner container in the configurations depicted in Figures 1-3 through 1-5 of this addendum replace the PC–1 inner container and aluminum spacer documented in the SAR.[1] The effect of this change was captured in the thermal computer models described later in this section.

There are three basic configurations for plutonium metal contents within the T-Ampoule. One configuration consists of two titanium SC-2 sample containers supported and held in position inside the T-Ampoule by a titanium Inner Cradle (see Figure 1-3 in Section 1 of this addendum). The plutonium metal content within the SC-2 is a solid plutonium (Pu) cylinder of a diameter and length of 1.1 inches (0.0279 m). A second configuration consists of three SC-1 sample containers supported and held in position inside the T-Ampoule by a titanium Inner Cradle (see Figure 1-4). This configuration is similar to the two SC-2 configuration except it consists of three SC-1s and the plutonium metal sample packed in an SC-1 is a solid cylinder 0.88 inches (0.0224 m) in diameter and length. A third configuration consists of a single Pu hollow cylinder weighing from 731 to 831 grams (1.61 to 1.83 lbm) supported by crushed tantalum foil surrounding the cylinder (see Figure 1-5). The T-Ampoule, Ring Filler, SC-1, SC-2, Inner Cradle, and plutonium metal content all have melting temperatures above the 582°C (1080°F) temperature observed in the TB-1 during the plutonium air transport fire test described in SAR,[1] Section 3.6.1.2. Since the maximum total heat generation allowed in the TB-1 is limited to 25 watts (85.3 Btu/hr), a very conservative and bounding case for the application of the internal heating was used in the evaluation discussed in this section.

3.1.2 Decay Heat of the Contents

The PAT-1 package was assessed for a total decay heat load of its radioactive contents of 25 watts (85.3 Btu/hr). Sections 3.3 and 3.4 of this addendum demonstrate that with the 25 watt (85.3 Btu/hr) decay heat, the overall thermal performance of the PAT-1 package with the T-Ampoule and its plutonium metal payload is essentially the same as demonstrated in the SAR.[1] For the purpose of the analysis of the PAT–1 with the T-Ampoule and its plutonium metal content configurations addressed in this evaluation, the decay heat is conservatively assumed to be 25 watts. A bounding internal heating scenario was assumed in the analyses presented in this addendum. All 25 watts (85.3 Btu/hr) were assumed to be concentrated in a small region directly applying heat to the T-Ampoule elastomeric O-ring, as if all the solid plutonium metal cylinders were to group and transfer all their thermal energy to a small seal region. From the three basic configurations of plutonium metal contents discussed in Section 3.1.1 of this addendum, the hypothetical configuration that yields the smallest projected area for heat to flow through and therefore, provides maximum heat flux into the seal region is one where three plutonium metal cylinders are close together and aligned along the seal region as illustrated in Figure 3-1. Assuming the total 25 watts (85.3 Btu/hr) from these three plutonium cylinders are transferred to the seal region through the small projected area illustrated in Figure 3-2, the total concentrated heat flux q'' is:

$$q'' = \frac{25W}{(2.64'')(0.88'')} = \frac{25W}{(0.067056m)(0.022352m)} \cong 16{,}680\frac{W}{m^2} \quad \underline{or} \quad 5{,}288\frac{Btu}{hr - ft^2}. \qquad (3\text{-}1)$$

Note that this scenario is extremely unlikely because the Pu cylinders will not come out of the sample containers during NCT or HAC, as documented in Section 2 of this addendum. In addition, if the three Pu cylinders were to align as described, a portion of the assumed 25 watts (85.3 Btu/hr) will be transferred by convection and radiation to other regions (and components) inside the T-Ampoule, and thereby reduce the actual quantity of energy available to be transferred by conduction through the hypothetical localized heating region described herein. Since this highly concentrated heat flux is understood to bound all plutonium metal loading configurations discussed in Section 3.1.1 of this addendum, only this heat flux was used to very conservatively represent the decay heat inside the T-Ampoule during the NCT and HAC evaluations.

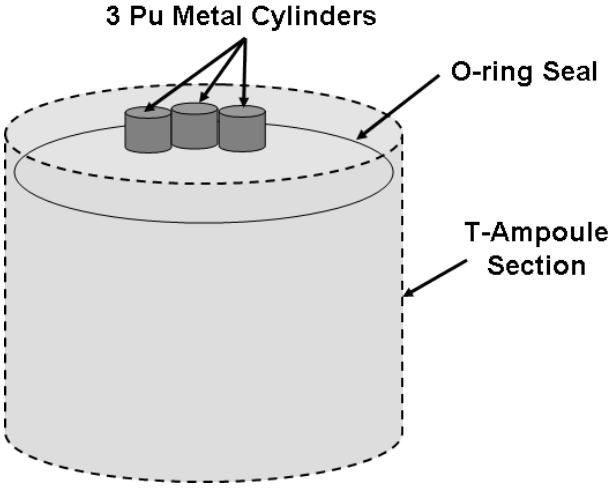

Figure 3-1. Schematic of Assumed Worst-Case Heating-to-the-Seal Scenario

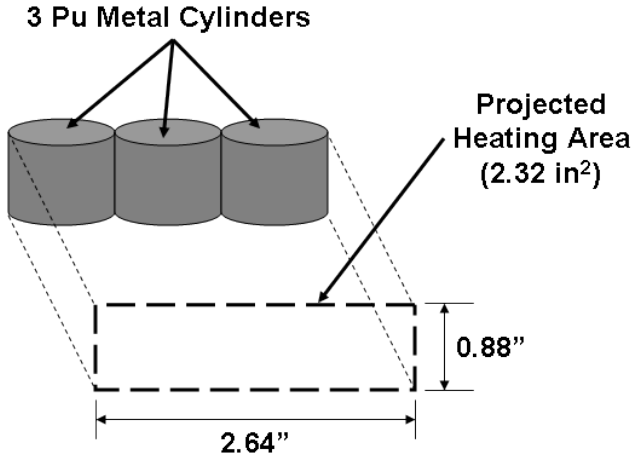

Figure 3-2. Schematic of Approximated Projected Heating Area [m=0.0254*in.; m^2=6.45x10^{-4}*$in.^2$]

3.1.3 Summary Tables of Temperatures

The SAR[1] describes how design features in the PAT-1 adequately contain the material inside the TB-1 even after the PAT–1 is exposed to the regulatory conditions specified in 10 CFR 71.71, 71.73, and 71.74.[2] The results from the thermal evaluation of the AQ-1, TB-1, and the T-Ampoule assuming the bounding concentrated internal heat described in Section 3.1.2 of this addendum are summarized in Table 3-1 of this addendum. These results show that the PAT-1 also protects the new components inside the TB-1 described in this addendum and adequately contains the material inside the TB-1, as the T-Ampoule seal temperatures are within the manufacturer's specifications and the T-Ampoule can withstand the pressure buildup during and after the regulatory specified heating.

Table 3-1. Summary of Temperatures Under NCT and HAC

Component	NCT		HAC
	Maximum	Minimum	Maximum
T-Ampoule (Seal)	122°C (251°F)	-40°C (-40°F)	153°C (308°F) @ 260 minutes after the fire
TB-1 (and TB-1 seal)*	114°C (238°F)	-40°C (-40°F)	147°C (296°F) @ 260 minutes after the 30-minute fire
Center of Redwood Between TB-1 and Load Spreader	99°C (211°F)	-40°C (-40°F)	132°C (270°F) @ 240 minutes after the 30-minute fire
Aluminum Load Spreader	98°C (208°F)	-40°C (-40°F)	131°C (267°F) @ 190 minutes after the 30-minute fire
Center of Redwood Between Load Spreader and Outer Skin	95°C (203°F)	-40°C (-40°F)	164°C (328°F) @ 30 minutes after the 30-minute fire
Stainless Steel Outer Drum	93°C (200°F)	-40°C (-40°F)	1003°C (1837°F) @ end of fire

*Maximum seal temperature was conservatively taken as the TB-1 maximum temperature.

3.1.4 Summary Table of Maximum Pressures

Table 3-2 of this addendum summarizes the maximum pressures inside the T-Ampoule for the NCT, HAC and plutonium air transport accident conditions specified in 10 CFR 71.71,[2] 71.73,[2] and 71.74,[2] respectively. As demonstrated in Sections 2, 3.3.2, 3.4.3, 3.4.5, and 4 of this addendum, the pressures that arise in the container during NCT, HAC, and plutonium air transport accident conditions do not result in a loss of containment.

Table 3-2. Summary of Maximum Pressures inside the T-Ampoule for NCT and HAC

Regulatory Condition	Maximum Pressure
NCT (or MNOP)	29 kPa (4.2 psig)
HAC	40 kPa (5.8 psig)
Plutonium Air Transport	7.55 MPa (1095 psig)

3.2 Material Properties and Component Specifications

3.2.1 Material Properties

A summary of the thermophysical properties of the materials used in PAT-1 is provided in the SAR,[1] Section 3.2, Table 3.2. To be consistent with the SAR[1] the same material properties for aluminum, ETC copper, stainless steel, and redwood (up to a certain temperature as described below) were used for the analyses presented in this addendum.

The following was considered for modeling the thermal response of redwood. Slow degradation (slow pyrolysis) of wood occurs in the temperature range of 200°C to 280°C (392°F to 536°F), until active pyrolysis begins in the 280°C to 500°C (536°F to 932°F) range. A temperature of 288°C (550°F) is used to locate the base of the char layer. Reference 3 (*Application of CMA Program to Wood Charring*) and the references cited therein contain additional information about temperature-dependent wood properties and wood charring. The thermal conductivity and specific heat provided in the SAR[1] are given in expressions that are a function of temperature. While these expressions are valid for the temperature range used for their determination, which was approximately 93°C (200°F) (see Section 3.2 and Appendix 3-A of the SAR[1]), the same equations were used to determine properties up to the temperature at which wood starts to decompose (i.e., 200°C [392°F]). Given that the properties of redwood provided in the SAR[1] do not take degradation of wood into account, property values and mathematical expressions from Reference 3 were used at temperatures greater than 200°C (392°F). For thermal conductivity at temperatures above pyrolysis, a fixed value within the range in Reference 3 for charcoal was used. Therefore, the temperature-dependent thermal properties presented in Table 3-3 of this addendum were specified in the P/Thermal model to adequately represent the state and response of the redwood. In cases were wood reached pyrolysis temperatures, it was assumed that the properties would remain those of charred wood throughout the cool-down process. To corroborate the validity of these modeling assumptions, thermal models discussed in Sections 3.3 and 3.4 of this addendum were completed and results compared with tests of the PAT-1 under transient NCT and HAC documented in the SAR.[1] These comparisons showed acceptable agreement as demonstrated by the data presented in those sections. Thus, a computer model that was calibrated with the test and analysis data presented in the SAR[1] was developed and used.

Table 3-3. Thermophysical Properties Used to Represent Redwood

Wood State	Temperature °C [°F]	Density kg/m^3 [lb/ft^3]	Specific Heat J/kg-K [Btu/lb-F]	Thermal Conductivity W/m-K [Btu/hr-ft-°F]	
				Parallel to Grain	Perpendicular to Grain
Before Pyrolysis	16 [60]	352 [22]	1273 [0.30]	0.330 [0.19]	0.117 [0.07]
	38 [100]	352 [22]	1591 [0.38]	0.390 [0.22]	0.136 [0.08]
	93 [200]	352 [22]	2386 [0.57]	0.533 [0.31]	0.190 [0.11]
	199 [390]	352 [22]	3898 [0.93]	0.810 [0.47]	0.290 [0.17]
During Slow and Active Pyrolysis	200 [392]	214 [13]	1151 [0.28]	0.073 [0.04]	0.026 [0.02]
	280 [536]	214 [13]	1314 [0.34]	0.073 [0.04]	0.026 [0.02]
	500 [932]	214 [13]	1657 [0.44]	0.073 [0.04]	0.026 [0.02]
	800 [1472]	214 [13]	1876 [0.45]	0.073 [0.04]	0.026 [0.02]
	1000 [1832]	214 [13]	1861 [0.45]	0.073 [0.04]	0.026 [0.02]

In addition to the material properties listed in the SAR[1] and in Table 3-3 of this addendum, the thermal properties for Ti-6Al-4V used in the computer analysis are presented in Table 3-4 of this addendum. These values were obtained from the MSC PATRAN Thermal (P/Thermal) computer code materials database,[4] which lists References 5, 6, and 7 as the source. Reference 8 supports the temperature-dependent trend of the data presented in Table 3-4. Materials inside the T-Ampoule were conservatively neglected for the thermal analysis (no credit was taken for heat absorbed by components inside the T-Ampoule); therefore, the thermal properties of those materials are not presented in this section.

Table 3-4. Thermophysical Properties of the Titanium Ampoule (Ti 6Al-4V)

Temperature °C [°F]	Thermal Conductivity W/m-K [Btu/hr-ft-°F]	Specific Heat J/kg-K [Btu/lbm-°F]	Density Kg/m^3 [lbm/ft^3]
-50 [-58]	–	502 [0.120]	4450 [277.8]
0 [32]	6.9 [3.99]	–	
100 [212]	–	561 [0.134]	
200 [392]	9.0 [5.20]	–	
300 [572]	–	615 [0.147]	
400 [752]	11.9 [6.89]	-	

3.2.2 Component Specifications

The service temperature range for package components inside the TB-1 are presented in Table 3-5 of this addendum.

Table 3-5. Service Temperatures of Packaging Components and Content inside the TB-1

Component	Service Temperature Range °C [°F]	Reference
T-Ampoule O-ring	-17°C to 204°C [1.4ºF to 400ºF]	Appendix 3.5.2[i]
TB-1 Copper Gasket	-40°C to >582°C [-40ºF to >1080ºF]	PAT-1 SAR[ii]
T-Ampoule (as eutectic barrier)[iii]	-40°C to 625°C [-40ºF to 1157ºF]	[9]
Titanium Inner Cradle[iii]	-40°C to 625°C [-40ºF to 1157ºF]	[9]
Ring, Filler[iv]	-40°C to >593°C [-40ºF to >1100ºF]	[10]
Pu/Be Content[vi]	-40°C to 595°C [-40ºF to 1103ºF]	[9]
Tantalum Foil[vii]	-40°C to 640°C [-40ºF to 1184ºF]	[9]

[i] Appendix 3.5.2 of this addendum provides the manufacturer's specifications for the O-ring material used in the T-Ampoule and in the SC-1 and SC-2 sample containers.

[ii] Based on thermal tests performed and documented in the PAT-1 SAR,[1] the TB-1 maintained containment after experiencing temperatures as high as 582°C (1080°F). Therefore, the copper gasket in the TB-1 can maintain seal at temperatures above these observed maximums.

[iii] The melting point of the eutectic that may form when titanium is in contact with gallium is 625°C (1157°F).

[iv] Ti-6A1-4V has a yield strength of about 331 MPa (48 ksi) at 593°C (1100°F), which is approximately 40% of the nominal room temperature value of 827 MPa (120 ksi)[9] and there are no forces other than gravitational acting on these components during and after the fire accident condition.

[v] Copper-Plutonium eutectic melting point.

[vi] The plutonium/beryllium eutectic represents the lowest melting point eutectic at 595ºC (1103ºF) in the system. The Pu/Be is a content, not a component within the TB-1.

[vii] Upper temperature assumed to be the Plutonium-Tantalum eutectic melting point. From page 11 of Reference 9, there is insufficient gallium in the entire mass of plutonium metal for Tantalum-Gallium eutectic formation and melting to have a negative effect on the system.

3.3 Thermal Evaluation under NCT

The commercially available MSC Patran Thermal (P/Thermal) finite element (FE) computer code[4] was used for the thermal evaluation of the PAT-1 package under NCT. P/Thermal is a well-respected FE code widely used to analyze a variety of thermal issues, including those related to nuclear transport packages. P/Thermal can solve one-, two-, and three-dimensional conduction, convection, and radiation heat transfer issues.

A three-dimensional model of the PAT-1 package was built using P/Thermal to demonstrate that containment is maintained by the TB-1 and that the temperature of the O-ring in the T-Ampoule does not exceed the manufacturer's recommended temperature range. The computational mesh of the PAT-1 model built using P/Thermal is shown in Figure 3-3. The model consists of 31,180 hexahedral finite elements and 34,697 nodes. Package features such as the different wood grain orientations and the respective anisotropic thermal properties of the redwood, the aluminum Load Spreader, the copper heat transfer tube, the stainless steel TB-1, and the titanium T-Ampoule where included in the model. The thin-walled outer drum was conservatively neglected. As mentioned in Section 3.1.2 of this addendum, the presence of components inside the T-Ampoule such as the sample containers (SC-1 and SC-2) and the titanium Inner Cradle were also conservatively neglected, and no other mass was assumed to absorb heat inside the T-Ampoule. Additionally, the 25-watt (85.3 Btu/hr) power from the Pu was conservatively applied to a small region on the inner surface of the T-Ampoule to maximize the thermal affect to the T-Ampoule seal, as explained in Section 3.1.2 of this addendum. The regions of the T-Ampoule, internal wall that did not receive this localized heat were conservatively assumed to be perfectly insulated (i.e., no heat transfer was allowed within the T-Ampoule, preventing the localized heated region from losing heat through convection or radiation to cooler T-Ampoule surface regions). Therefore, the small heated region was only allowed to transfer heat to the unheated (solid) regions through conduction.

The simplified temperature- and diameter-dependent correlation for a horizontal cylinder with laminar flow as employed in the TOPAZ heat transfer code 10 was used for the determination of the natural convection coefficient during NCT. That is:

$$h_{natural} = 1.32*[(T_{surface} - T_{ambient})/Diameter_{cylinder}]^{0.25}\ W/m^2\text{-}K \qquad (3\text{-}2)$$

Assuming

$T_{surface}$ = 176°F (80°C) (value obtained from NCT solution in the SAR[1])
$T_{ambient}$ = 100°F (38°C) (ambient temperature in 10 CFR 71.71[2])
$Diameter_{cylinder}$ = 20 in. (0.5588 m) (PAT-1 approximate external diameter)

$$h_{natural} = 1.32*[(80°C - 38°C)/0.5588\ m]^{0.25}\ W/m^2\text{-}K \quad (3\text{-}3)$$

$$h_{natural} = 3.9\ W/m^2\text{-}K \text{ or } 0.69\ Btu/hr\text{-}ft^2\text{-}°F \quad (3\text{-}4)$$

This value of $h_{natural}$ is on the low end of typical natural convection heat transfer coefficients for gases[11]. Ultimately, a more conservative value of **$h_{natural}$ = 3.5 W/m^2-K (0.62 Btu/hr-ft^2-°F)** was used for the NCT calculation in this addendum.

The PAT-1 package model was subjected to the thermal conditions specified in 10 CFR 71.71[2] to evaluate if the TB-1 can maintain containment during NCT. It was assumed that the package will be transported horizontally as specified in Section 1 of this addendum. The boundary conditions used in the model to simulate the "heat" conditions specified in 10 CFR 71.71(c)(1)[2] are summarized in Table 3-6 of this addendum. Note that the temperature of the environment was increased to 54.4 °C (130°F) as in the SAR.[1] Also note that the insolation data presented in this table represents a 24-hour average of the values as specified in 10 CFR 71.71,[2] as is typically assumed when a steady-state simulation is used to evaluate packages under the prescribed environment. For example, for curved surfaces, 10 CFR 71[2] specifies a 12-hour–period, total insolation energy of 400 g-cal/cm^2 (16,747 kJ/m^2 or 1,475 Btu/ft^2). In order to more adequately model the NCT in a computer code running in steady-state mode, the total energy per unit area is spread over 24 hours:

$$Insolation_{Curved_Srurfaces} = \frac{400\ \text{g-cal/cm}^2}{(24hr)(3600\,\text{sec}/hr)} \cong 4.63E^{-3}\frac{g-cal}{cm^2-s} \cong 193.8\frac{W}{m^2}\ \ \underline{or}\ \ 61.4\frac{Btu}{hr-ft^2} \quad (3\text{-}5)$$

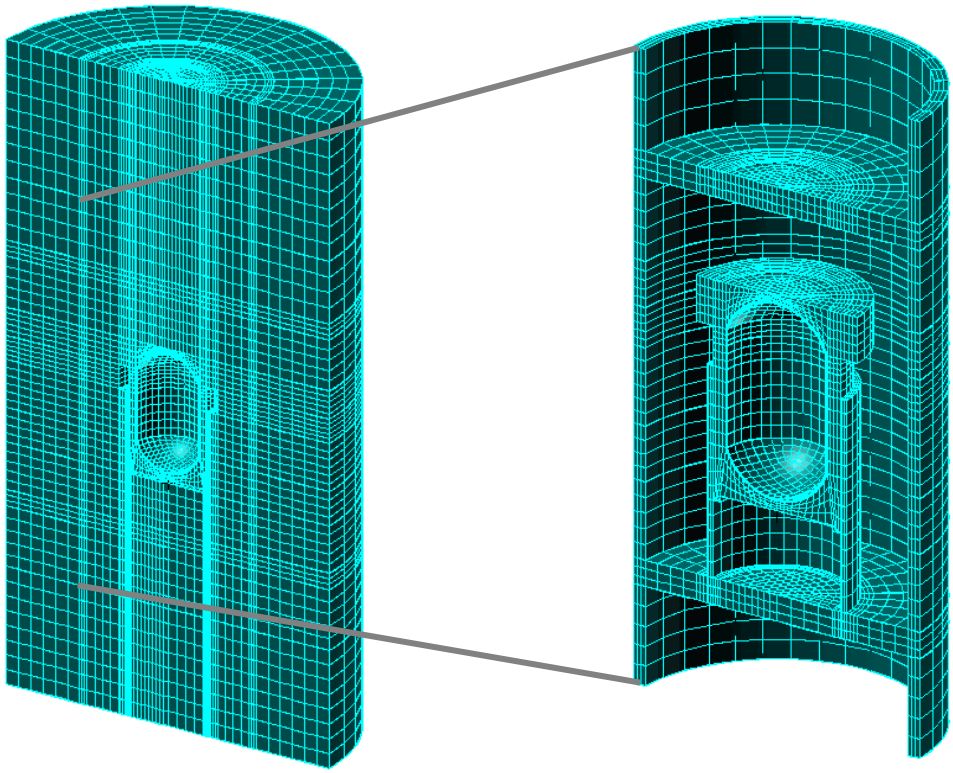

Figure 3-3. Finite Element Mesh of the PAT-1 Half-Symmetry Thermal Model and Enlarged Load Spreader, Copper Cylinder, TB-1, and T-Ampoule

Table 3-6. Boundary Conditions Used for the "Heat" NCT Thermal Evaluation

Boundary Condition	Application Region	Value Used
Environment Temperature	External node representing environment	54.4 °C (130°F)
Convection	Entire outer surface of the package	3.5 W/m^2-K (0.62 Btu/hr-ft^2-°F)
Radiation	Entire outer surface of the package	Package surface emissivity of 0.2,* Environment emissivity of 1
Insolation (Solar Flux averaged over 24 hours)	Curved surfaces	193.83 W/m^2 (61.44 Btu/hr-ft^2)
	Flat surfaces transported vertically (package ends)	96.92 W/m^2 (30.72 Btu/hr-ft^2)
Internal heat Flux (Decay heat)	Small region described in Section 3.1.2 of this addendum	16,680 W/m^2 (5287.5 Btu/hr-ft^2)

* From Table 3.2 in the SAR[1]

In addition to the "heat" NCT analysis, the package has to be able to maintain containment when exposed to an ambient temperature of -40°C (-40°F) in still air and shade as specified in 10 CFR 71.71(c)(2).[2] The results of exposing PAT-1 to these conditions are discussed in Section 3.3.1 of this addendum.

3.3.1 Heat and Cold

The finite element model described above was used for the NCT analysis. First, the model was verified by simulating both the steady-state test and the transient NCT analysis described in the SAR[1]. These models evenly distributed the 25W (85.3 Btu/hr) internal heat load and applied it to the inside wall of the TB-1. The results from this validation exercise are presented in Section 3.3.1.1 of this addendum. Once the model was verified against the results in the SAR,[1] the concentrated internal heat load described in Section 3.1.2 of this addendum was applied to the inner wall of the T-Ampoule. These results are presented in Section 3.3.1.2. of this addendum

3.3.1.1 Model Verification

The FE model described in Section 3.3 of this addendum was verified by simulating both the steady-state test and the transient NCT analysis described in the SAR.[1] The intent of this exercise was to verify the computer model against the data available in the SAR.[1] The validated model was then used to analyze the thermal response of the package with the plutonium metal content. These models evenly distributed the 25W (85.3 Btu/hr) internal heat load and applied it to the inside wall of the TB-1, as was the case for the models in the SAR.[1]

First, the computer model was verified against a low-temperature thermal test that was performed and presented in the SAR.[1] This test was performed to empirically determine the effective thermal resistance values for PAT-1 components. While boundary conditions are not well known, it is understood that a PAT-1 package was placed in a temperature-controlled chamber maintained at approximately 93°C (200°F). An internal heater was maintained at 25 watts (85.3 Btu/hr) using a variable resistance power supply. Transient response was measured with thermocouples placed at key locations within and outside the package. These data are documented in Sections 3.4.1.2 and Appendix 3-A of the SAR.[1] The results of the verification analysis are presented in Figure 3-4. Temperature results after 50 hours favorably compare with those reported in Table 3-A.1 of Appendix 3-A in the SAR,[1] as illustrated in Table 3-7 of this addendum. Figure 3-4 also favorably compares with Figure 3.4 in the SAR.[1] The results from this validation exercise demonstrate that the geometry representation, material properties, and finite element representation are adequate to predict the performance of the PAT-1 package when exposed to similar thermal loads.

Second, the computer model was verified against the transient NCT analysis results presented in the SAR.[1] This included variable insolation heating (over time and position) as described in Section 3.4.1.2 in the SAR.[1] All boundary conditions were applied as described in that section of the SAR.[1] In order to model those conditions adequately, the half-symmetry model was mirror-copied to make a full three-dimensional model of the package. The results from this verification exercise, presented in Figures 3-5 and 3-6, compare favorably with the results presented in the SAR.[1] The data documented in Figure 3-6 is in agreement with the data shown in Figure 3.5 of the SAR.[1] This indicates proper three-dimensional modeling of the package. The three-dimensional temperature distribution of the package at the time just before sundown (the most severe case) is shown in Figure 3-7. This temperature distribution shows a peak outer skin temperature of 116°C (241°F), which is approximately 9°C (17°F) hotter than the maximum surface temperature reported in SAR,[1] Section 3.4.1.2.

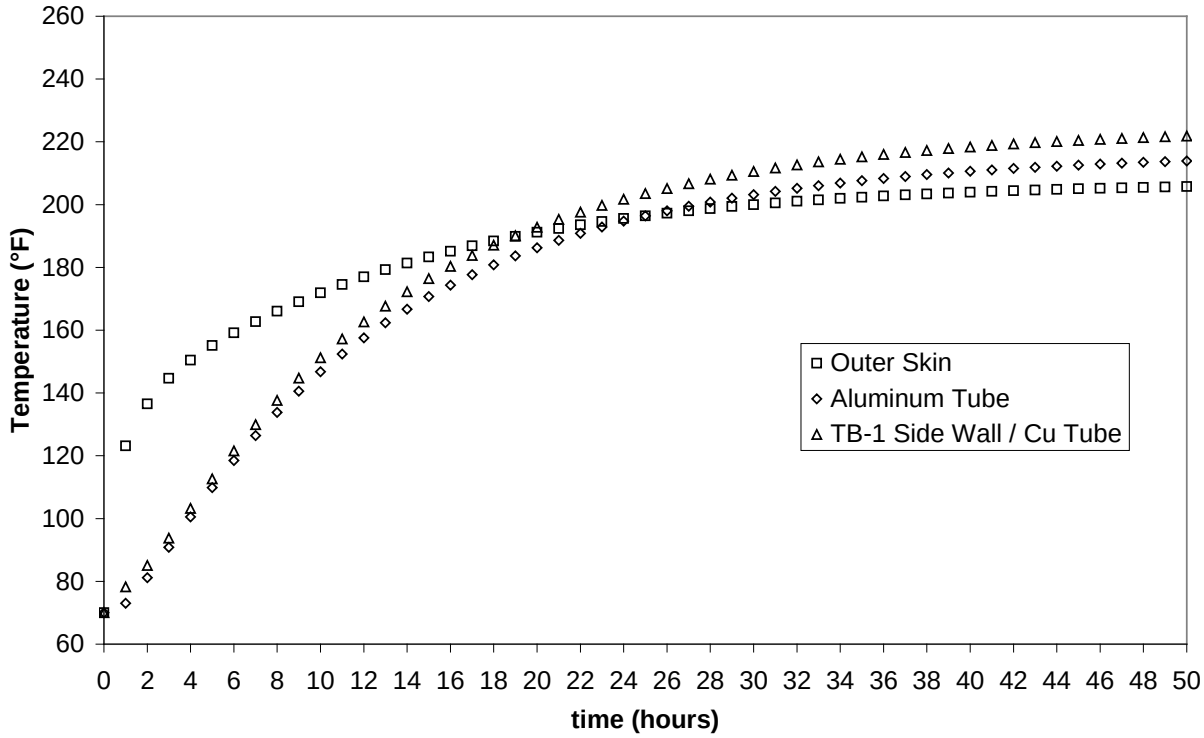

Figure 3-4. Low-Temperature Thermal Test Simulation Results. (°C=[°F-32]/1.8)

Table 3-7. Comparison of Test and Analysis Temperatures – Low Temperature Test

Location	Steady-State Temperature – Test Data	Steady-State Temperature – Analysis Data at Package Mid-Height
Cu Tube	105°C (221°F)	105.6°C (222°F)
Al Tube	100°C (212°F)	101°C (214°F)
Outer Skin	93°C (200°F)	96.6°C (206°F)

Third, the boundary conditions in the computer model were changed to reflect those specified in 10 CFR 71.71[2] in a steady-state simulation and to verify how the package response under these conditions compares to the transient method used in the SAR.[1] The intent of this exercise was to determine if the new analysis for this addendum is still bounding when using the steady-state method. The results from this exercise are presented in Figures 3-7 and 3-8. A comparison of the results in these two figures with those obtained from the transient simulation described above indicate that while the outer temperatures (maximums and distributions) are different, the steady-state analysis thoroughly envelops the transient response of the TB-1 and its surrounding regions. Therefore, it was decided to run a steady-state NCT analysis of the PAT-1 with the new contents configuration. The results from the steady-state analysis for this addendum are presented in Section 3.3.1.2.

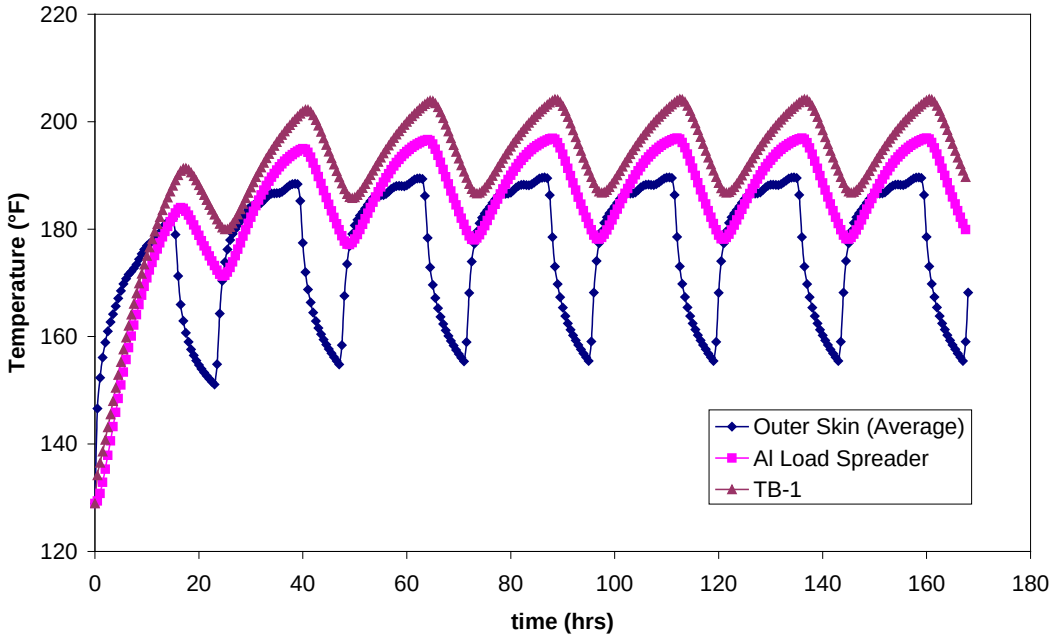

Figure 3-5. Seven-day Thermal Cycling for Quasi-Steady-State Analysis – Package Mid-Height Response (°C=[°F-32]/1.8)

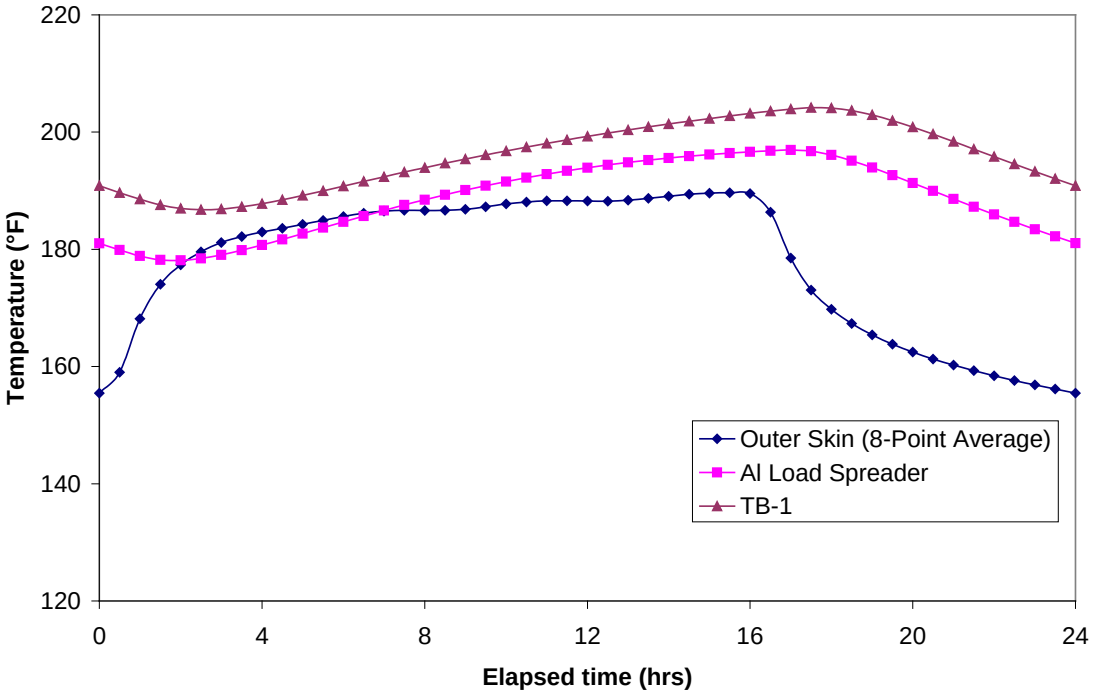

Figure 3-6. NCT Daily Thermal Cycle (Quasi-Steady-State NCT Solution) – Package Mid-Height Response (°C=[°F-32]/1.8)

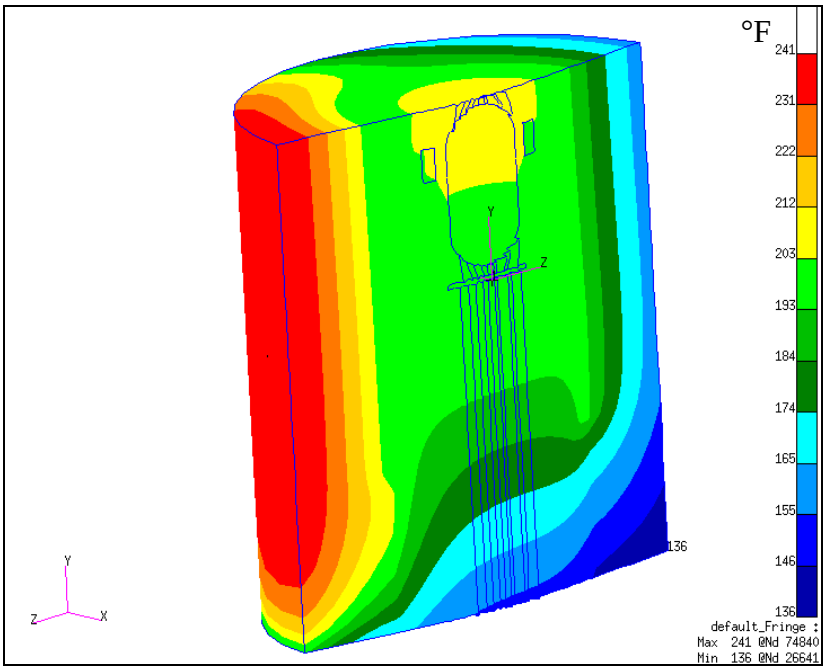

Figure 3-7. Temperature Distribution of PAT-1 Just Before Sundown – Most Severe Case of Transient NCT SAR[1] Analysis (Plot of ¼ of Package, °C=[°F-32]/1.8)

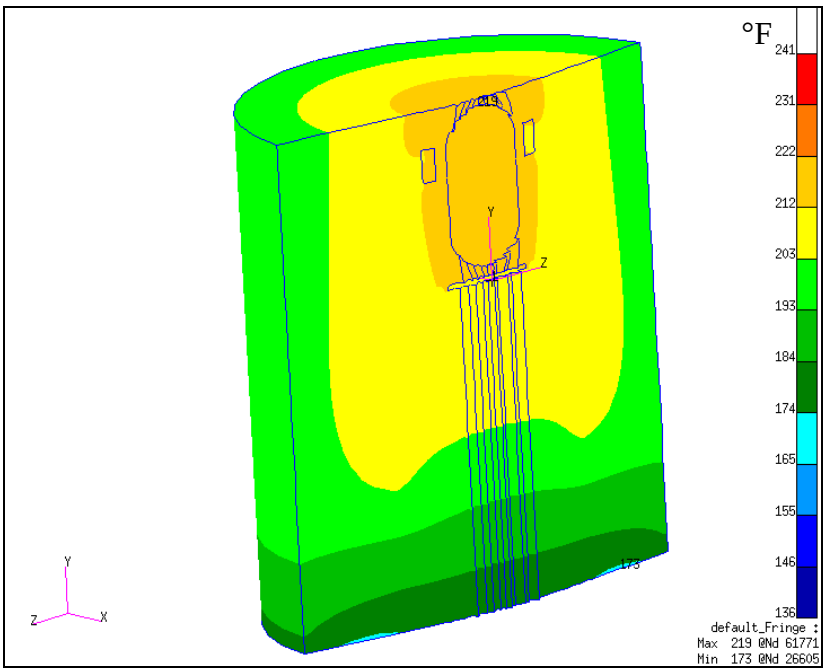

Figure 3-8. Temperature Distribution of PAT-1 – Steady-State NCT SAR[1] Analysis (Plot of ¼ of Package, °C=[°F-32]/1.8)

3.3.1.2 Addendum Analysis

The results from the NCT steady-state analysis of the package with the conservative internal heat load configuration of the new plutonium metal contents are presented in Figure 3-9. Note that the scale of the temperature distribution for this figure (and others in this section) is different from those previously shown. The temperature distribution shown in Figure 3-9 clearly illustrates the effect of the very concentrated heat applied to the seal region as described in Section 3.1.2 of this addendum. The T-Ampoule seal temperature was conservatively assumed to be the inside wall temperature of the T-Ampoule. This is conservative because the T-Ampoule closure was not explicitly modeled; instead the wall thickness of the T-Ampoule was assumed to be constant everywhere and therefore, that seal region had less thermal mass. This allows for more direct heating of the T-Ampoule seal, as energy that would be absorbed by the additional titanium in the vicinity of the seal is neglected and the heat path from the heated surface to the seal is shorter. The maximum T-Ampoule "seal" temperature is approximately 122°C (251°F) even in the very conservative internal heat load scenario. Therefore, the performance of the elastomeric O-ring in the T-Ampoule is not degraded and maintains product quality, as this temperature is within the operating range specified by the manufacturer. The maximum seal region temperature of the TB-1 was 114°C (238°F). This temperature is within the operating temperature range of the metallic seal. Therefore, the TB-1 is able to maintain containment.

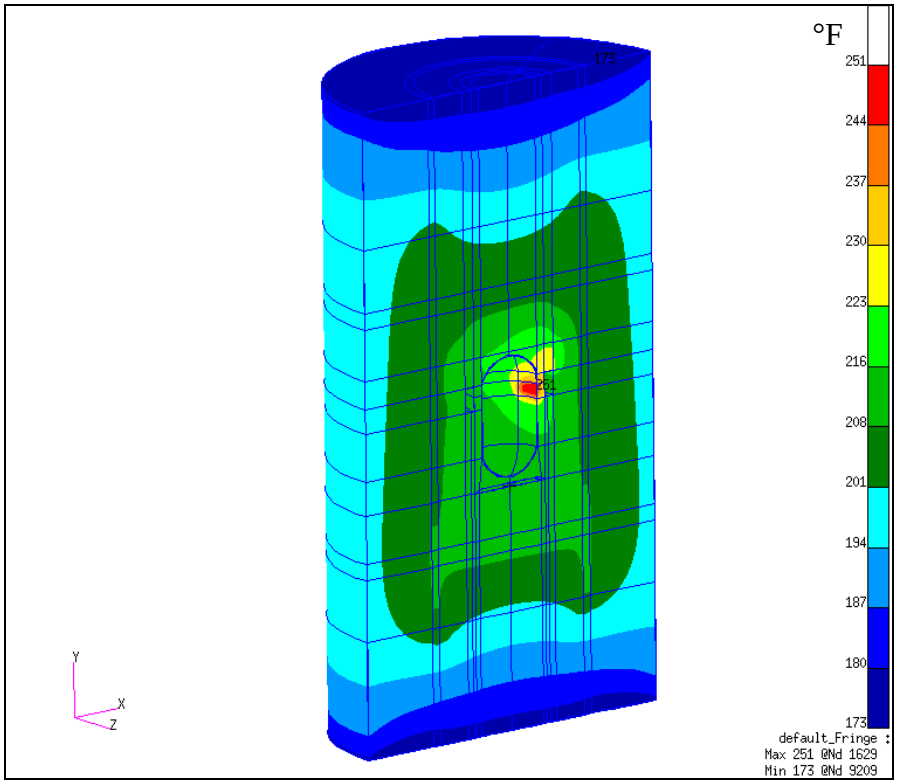

Figure 3-9. NCT Steady-State Temperature Distribution (°C=[°F-32]/1.8)

Regulatory requirements in 10 CFR 71.71(c)(2)[2] specify that the package must be capable of maintaining containment when it is exposed to an ambient temperature of -40°C (-40°F) in still air and shade. If one assumes no internal heating, the minimum temperature any PAT-1 package

component could reach is -40°C (-40°F). As discussed in Section 3.4.6 of the SAR,[1] the copper seal used in the TB-1 is unaffected at this low temperature. Therefore, the PAT-1 can maintain containment at this low temperature extreme even without taking credit for any decay heat of the contents, which will definitely heat the seal region of the TB-1 to above -40°C (-40°F).

Since the results in Figure 3-9 show parts of the outer surface at temperatures above 85°C (185°F), an additional analysis was performed assuming the package is in the shade (no insolation), still air, and exposed to the conservative ambient temperature of 55°C (130°F). This was done to demonstrate compliance with 10 CFR 71.43(g),[2] which specifies that any accessible surface of a package must not exceed 85°C (185°F) in an exclusive use shipment. The results from this analysis are presented in Figure 3-10. Compliance with 10 CFR 71.43(g) is demonstrated, since the maximum outer surface temperature of the package is less than 58°C (137°F). The somewhat "skewed" temperature distribution seen in Figure 3-10(b) is the result of the concentrated internal heating of the package.

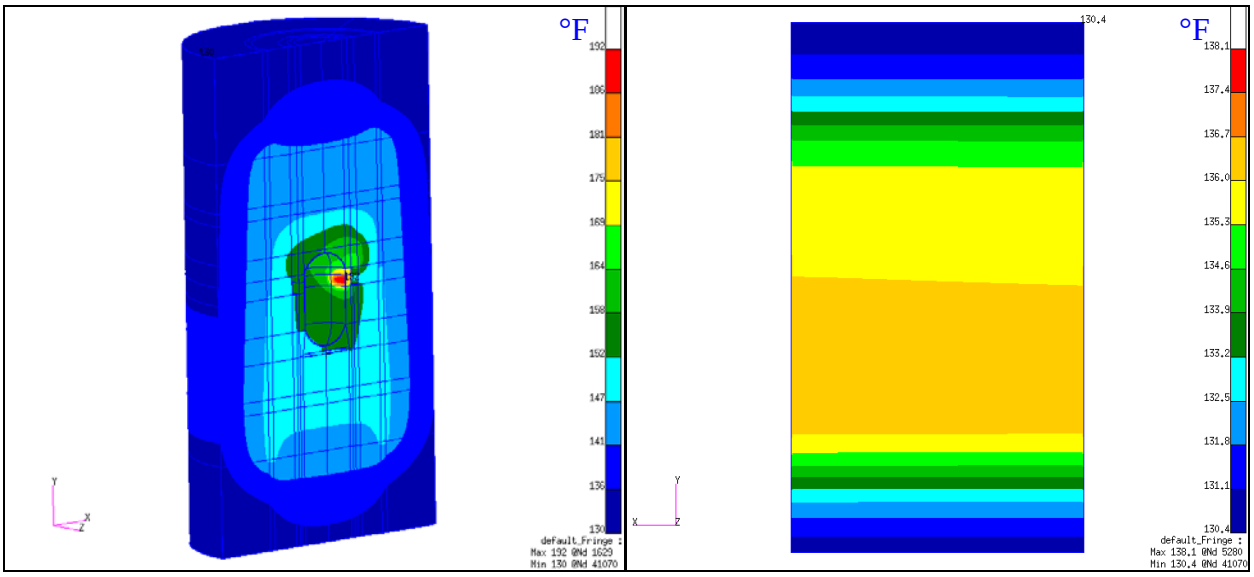

(a) Internal Temperatures **(b) Outer Surface Temperatures**

Figure 3-10. Steady-State Analysis in the Shade – 10 CFR 71.43(g) (°C=[°F-32]/1.8)

3.3.2 Maximum Normal Operating Pressure

The maximum normal operating pressure (MNOP) that may occur within the TB-1 is estimated to be 29 kPa (4.2 psig) (see Section 4 of this addendum). This was calculated using the average internal surface temperature of the T-Ampoule as the average temperature of the gas inside the TB-1, which is 103.3°C (218°F) and the contribution to the internal pressure over time due to alpha decay. The MNOP was then estimated as $P_{gauge} = (P_{initial} + P_{alpha_decay})*(T_2/T_1) - 1atm = [(1$ atm + 0.005 atm) * (678°R / 530°R) -1 atm] = 0.286 atm or ~ 29 kPa (4.2 psig), assuming initial fill of the TB-1 is done with gas at a room temperature of 21°C (70ºF) and in an environment with an atmospheric pressure of one.

3.4 Thermal Evaluation under HAC

The P/Thermal FE model that was used for the NCT analysis was also used for the HAC analysis. Since the deformations shown in the SAR[1] after the package was dropped from 30 feet are minimal, the computer model used for the HAC thermal evaluation represents an undamaged package. Boundary conditions were modified to meet those specified in 10 CFR 71.73(c)(4).[2] In addition, the same model was used in a model verification exercise to simulate the 52-minute fire test documented in the SAR.[1]

In the SAR,[1] a description of a longer-than-regulatory fire test and results are presented. The PAT-1 package used for the test did not have internal heating. The SAR[1] does not indicate the temperature distribution or overall temperature of the package prior to the test. For the purpose of model verification, an initial uniform temperature of 27°C (80°F) was assumed within the PAT-1 package and no internal heating was applied. The boundary conditions used are summarized in Table 3-8 of this addendum. The estimation for the convection heat transfer coefficients in this table is presented following the table. Note that for the purpose of this model verification exercise, the average temperature of 982°C (1800°F) on the thin-walled AQ-1 drum reported in Table 3.4 in the SAR[1] was used as the effective fire temperature.

Table 3-8. Boundary Conditions Used for the Transient Model Verification Exercise

Boundary Condition	Application Region	Value Used During 52-Minute Fire	Value Used After Fire (Cool-down)
Environment Temperature	External node representing environment	982°C (1800°F)*	27°C (80°F)**
Convection	Entire outer surface of the package	11.5 W/m^2-K (2.03 Btu/hr-ft^2-°F)	3.5 W/m^2-K (0.62 Btu/hr-ft^2-°F)
Radiation	Entire outer surface of the package (exchange with environment node)	Package surface emissivity of 0.8, Fire emissivity of 1	Package surface emissivity of 0.2,*** Environment emissivity of 1
Internal Heat Flux (Decay Heat)	N/A	0	0

*From Table 3.4 in the SAR[1]
**Assumed ambient temperature
***From Table 3.2 in the SAR[1]

Values for convection heat transfer coefficients were estimated using correlations and verified with typically used values. For the convection heat transfer coefficient applied to the package surface during the fire (h_{fire}), a simplified temperature-only dependent correlation for a horizontal cylinder with turbulent flow as employed in the TOPAZ heat transfer code[10] was used. That is,

$$h_{fire} = 1.24*(T_{ambient} - T_{surface})^{1/3} \text{ W/m}^2\text{-K}$$

where $T_{ambient}$ is the temperature of the environment around the package and $T_{surface}$ is the outer surface temperature of PAT-1, with both temperatures in °C or Kelvin.

Assuming
$T_{ambient}$ = 1475°F (800°C) (fire temperature in 10 CFR 71.73)
$T_{surface}$ = 176°F (80°C) (value obtained from NCT solution in the SAR[1])

$$h_{fire} = 1.24*(800°C - 80°C)^{1/3} \text{ W/m}^2\text{-K}$$

$$h_{fire} = 11.11 \text{ W/m}^2\text{-K or } 1.96 \text{ Btu/hr-ft}^2\text{-°F}$$

This value of forced convection coefficient was corroborated using a more complex correlation proposed by Churchill and Bernstein[12] and experimental open-pool fire velocity measurements in Reference 13. In calm wind conditions for open-pool fires, vertical gas velocities are typically in the range of 5-10 m/s (16.4-32.8 ft/s) approximately 2 meters (6.56 ft) above the pool, but decrease to about 1 m/s (3.28 ft/s) near the surface of the pool.[13] Table 3-9 of this addendum presents typical values of the Grashof number (Gr_D) and the Reynolds number (Re_D) using a 5 m/s (16.4 ft/s) vertical gas velocity. To obtain these values, the temperature of the fire was assumed to be 800°C (1475°F) and air properties were used.

When $Gr_D/(Re_D)^2$ is less than 1, forced convection dominates. Therefore, the correlation suggested by Churchill and Bernstein for forced convection applies and was used to obtain an average convection coefficient:

$$\overline{Nu}_D = 0.3 + \frac{0.62\,\mathrm{Re}_D^{1/2}\,\mathrm{Pr}^{1/3}}{\left[1+(0.4/\mathrm{Pr})^{2/3}\right]^{1/4}}\left[1+\left(\frac{\mathrm{Re}_D}{282{,}000}\right)^{5/8}\right]^{4/5} \qquad (3\text{-}6)$$

where $\overline{Nu}_D$ is the Nusselt number and Pr is the Prandtl number. The convective coefficient, h, is equal to $\overline{Nu}_D k/D$, where k is the thermal conductivity of air and D is the diameter of the package. As demonstrated in Table 3-9 of this addendum the convection heat transfer coefficient is highest at the beginning of the fire when the temperature difference between the flame and the external wall of the cylinder is highest.

Table 3-9. Grashof, Reynolds, Nusselt Numbers for Calm Wind, Open-Pool Fire Conditions

Surface Temperature, Ts	Gr_D	Re_D	Gr_D/Re_D^2	Nu_D (Pr=0.7 for Air)	Convection Coefficient, h W/m^2-K [Btu/hr-ft^2-°F]
80°C [176°F]	2.39E+08	32870	0.22	106.1	10.0 [1.76]
527°C [981°F]	2.39E+07	21166	0.06	81.8	9.5 [1.67]
800°C [1472°F]	0	15102	0	67.4	8.7 [1.53]

Given that the value of h_{fire} using the correlation suggested by Churchill and Bernstein is between 8.7 and 10 and the simplified correlation from Shapiro and Edwards[10] is 11.11, a conservative heat transfer coefficient of **h_{fire} = 11.5 W/m^2-K (2.03 Btu/hr-ft^2-°F)** was used in the model.

The same simplified temperature- and diameter-dependent correlation for a horizontal cylinder with laminar flow that was used to calculate the natural convection coefficient for NCT in Section 3.3 of this addendum was used to estimate the natural convection coefficient for the modeling of the cool-down process after the fire. That is:

$$h_{natural} = 1.32*[(T_{surface} - T_{ambient})/Diameter_{cylinder}]^{0.25}\ W/m^2\text{-}K \quad (3\text{-}7)$$

Assuming
$T_{surface}$ = 1475°F (800°C) (assuming outer surface at prescribed regulatory fire temperature for bounding, maximum value calculation)
$T_{ambient}$ = 100°F (38°C) (ambient temperature in 10 CFR 71.71[2])
$Diameter_{cylinder}$ = 20 in. (0.5588 m) (PAT-1 approximate external diameter)

$$h_{natural} = 1.32*[(800°C - 38°C)/0.5588\ m]^{0.25}\ W/m^2\text{-}K \quad (3\text{-}8)$$

$$h_{natural} = 8\ W/m^2\text{-}K \text{ or } 1.4\ Btu/hr\text{-}ft^2\text{-}°F \quad (3\text{-}9)$$

This estimated maximum value of $h_{natural}$ is in the mid range of typical natural convection heat transfer coefficients for gases.[11] However, a more conservative value of **$h_{natural}$ = 3.5 W/m^2-K (0.62 Btu/hr-ft^2-°F)** (the same value used in the evaluation of NCT) was assumed for the cool-down calculation.

The results from the verification model are presented in Figures 3-11 through 3-15. Figures 3-11 and 3-12 show the temperature distribution of the overall package and the internal components at the end of the 52-minute fire. Figures 3-13 and 3-14 are similar to the previous two, but show the temperature distribution at the time when the internal temperature of the TB-1 peaked (300 minutes after the fire). The plot in Figure 3-15 illustrates the temperature history of the package at selected locations.

When the simulated temperature response was compared to the results of the 52-minute fire test discussed in the SAR,[1] it was found that the computer prediction overestimated the thermal response of the package. The spatial average temperature of the TB-1 at the time the peak temperature occurred was 100°C (212°F). This is 7°C (12°F) hotter than the average TB-1 temperature reported in the SAR.[1] Since the model in this verification exercise overestimated the TB-1 average temperature, the simulation of the package response to the HAC with the concentrated heat is also overestimated. Therefore, it is conservative to use this model to estimate the thermal response of the package configuration for this addendum. The results are presented in the following sections.

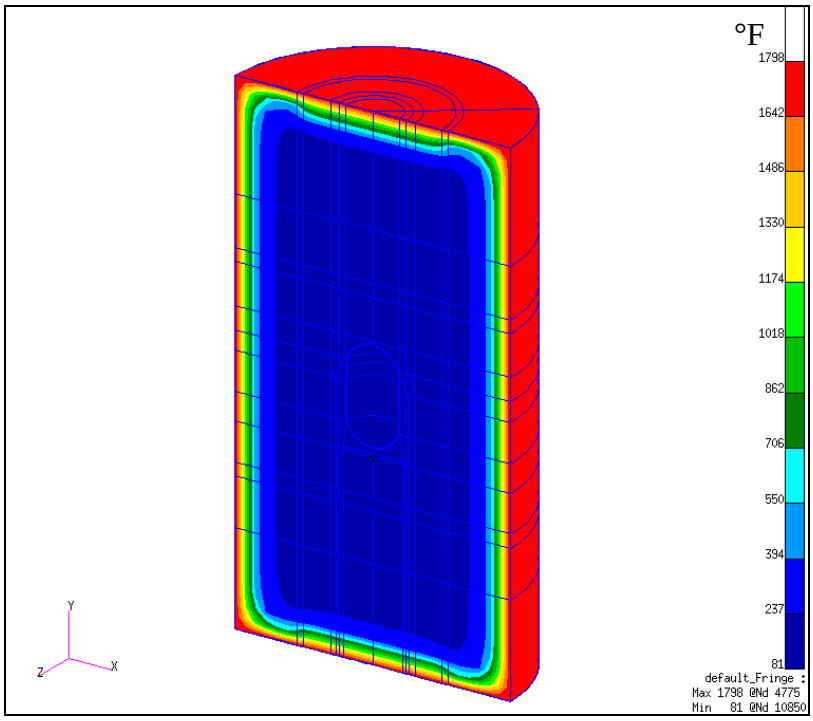

Figure 3-11. Temperature Distribution of the Verification Model at the End of the 52 Minute Fire — Complete Model (°C=[°F-32]/1.8)

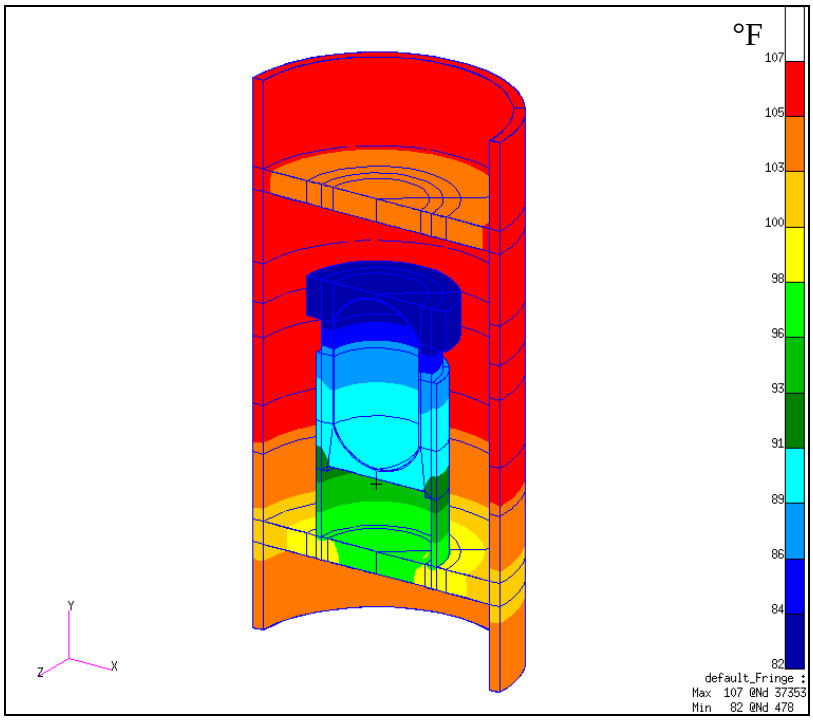

Figure 3-12. Temperature Distribution of the Verification Model at the End of the 52 Minute Fire — T-Ampoule, TB-1, Heat Transfer Cu Cylinder, and Aluminum Load Spreader (°C=[°F-32]/1.8)

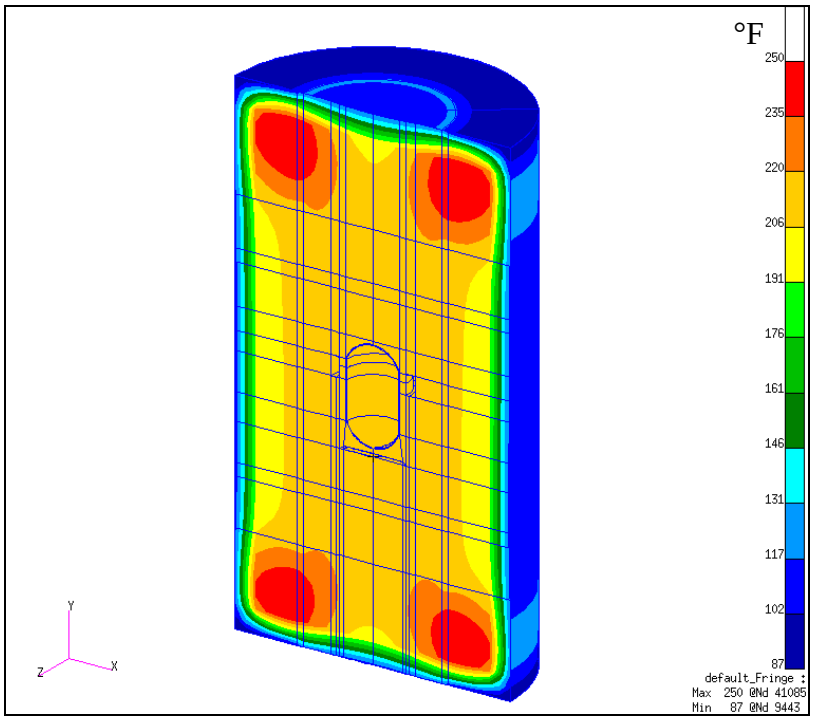

Figure 3-13. Temperature Distribution of the Verification Model at t=352 Minutes (300 Minutes after the 52 Minute Fire) — Complete Model (°C=[°F-32]/1.8)

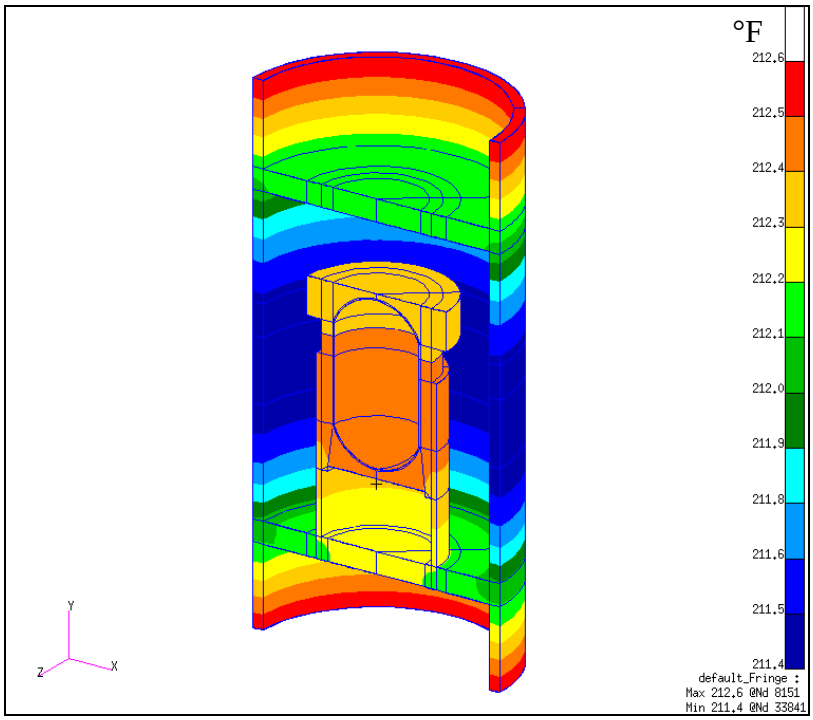

Figure 3-14. Temperature Distribution of the Verification Model at t=352 Minutes (300 Minutes after the 52 Minute Fire) — T-Ampoule, TB-1, Heat Transfer Cu Cylinder, and Aluminum Load Spreader (°C=[°F-32]/1.8)

3.4.1 Initial Conditions

The initial condition for the transient thermal analysis described in 10 CFR 71.73[2] is the temperature distribution calculated for the NCT. This initial temperature distribution is shown in Figure 3-9.

3.4.2 Hypothetical Accident Conditions (HAC)

The PAT-1 package model was subjected to the thermal transient conditions specified in 10 CFR 71.73[2] to evaluate whether the TB-1 can maintain containment and the T-Ampoule maintain seal (for product quality, not regulatory purpose) during and after a HAC fire event. The boundary conditions that were used in the model are summarized in Table 3-10 of this addendum. Note that only two boundary conditions were changed between this model and the one that was run for the 52-minute fire test verification exercise. That is, the fire duration was set to 30 minutes, and the same concentrated internal heat load applied to the NCT model was also used. As in the SAR,[1] the fire temperature was conservatively assumed to be 1010°C (1850°F) and the environment temperature for the cool-down period was conservatively assumed to be 54.4°C (130°F).

For the simulation of the HAC, the effect of a vertical and a horizontal package orientation in the fire were considered to determine the most damaging configuration. The calculations presented in Section 3.5.4 show that the package would receive more heat during HAC if it is positioned horizontally in the fire. Thus that conservative configuration was assumed for the fire analysis summarized in this section of the Addendum. Section 3.5.4 also shows that the value used for the cool-down is bounding.

The results from the simulation of the 10 CFR 71.73(c)(4)[2] environment are presented in Figures 3-16 through 3-20. Figures 3-16 and 3-17 show the temperature distribution of the overall package and the internal components at the end of the 30-minute regulatory fire. Figures 3-18 and 3-19 are similar to the previous two but show the temperature distribution at the time when the internal temperature of the TB-1 peaked (260 minutes after the fire). The plot in Figure 3-20 illustrates the temperature history of the package at selected locations.

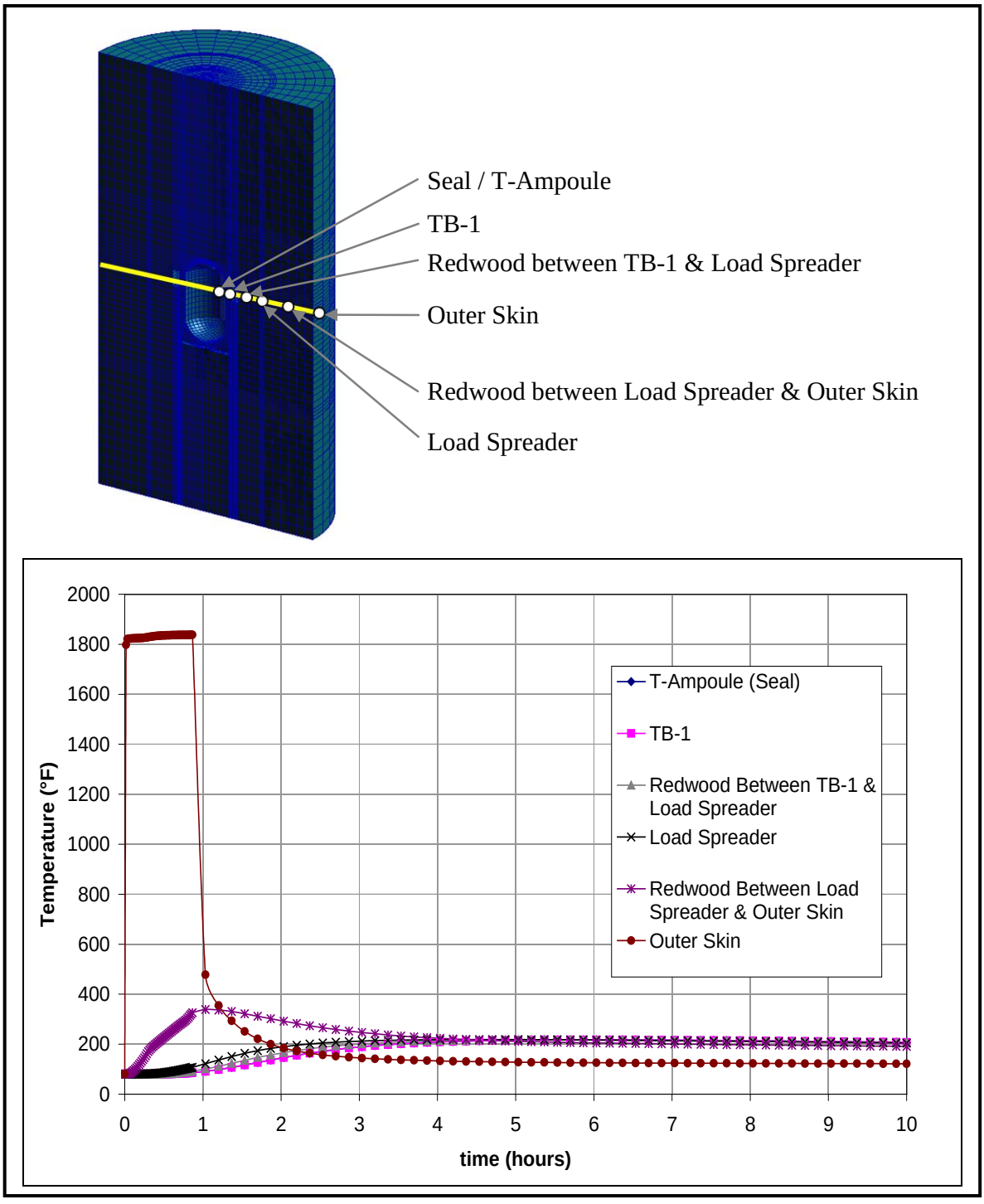

Figure 3-15. Temperature History at T-Ampoule Seal Height for the 52-Minute Fire Model Verification Exercise (°C=[°F-32]/1.8). Note: In the schematic above the plot, the reference yellow line crosses the cask at the T-Ampoule-seal height and the white dots are the approximate locations of the temperature history lines in the plot. The "T-Ampoule (Seal)" curve is completely covered by the "TB-1" curve.

Table 3-10. Boundary Conditions Used for the HAC Thermal Evaluation

Boundary Condition	Application Region	Value Used During 30-minute Fire	Value Used After Fire (Cool-down)
Environment Temperature	External node representing environment	1010°C (1850°F)	54°C (130°F)
Convection	Entire outer surface of the package	11.5 W/m^2-K (2.03 Btu/hr-ft^2-°F)	3.5 W/m^2-K (0.62 Btu/hr-ft^2-°F)
Radiation	Entire outer surface of the package	Package surface emissivity of 0.8, Fire emissivity of 1	Package surface emissivity of 0.2,* Environment emissivity of 1
Internal Heat Flux (Decay Heat)	Small region described in Section 3.1.2 of this addendum	16,680 W/m^2 (5287.5 Btu/hr-ft^2)	16,680 W/m^2 (5287.5 Btu/hr-ft^2)

* From Table 3.2 in the SAR[1]

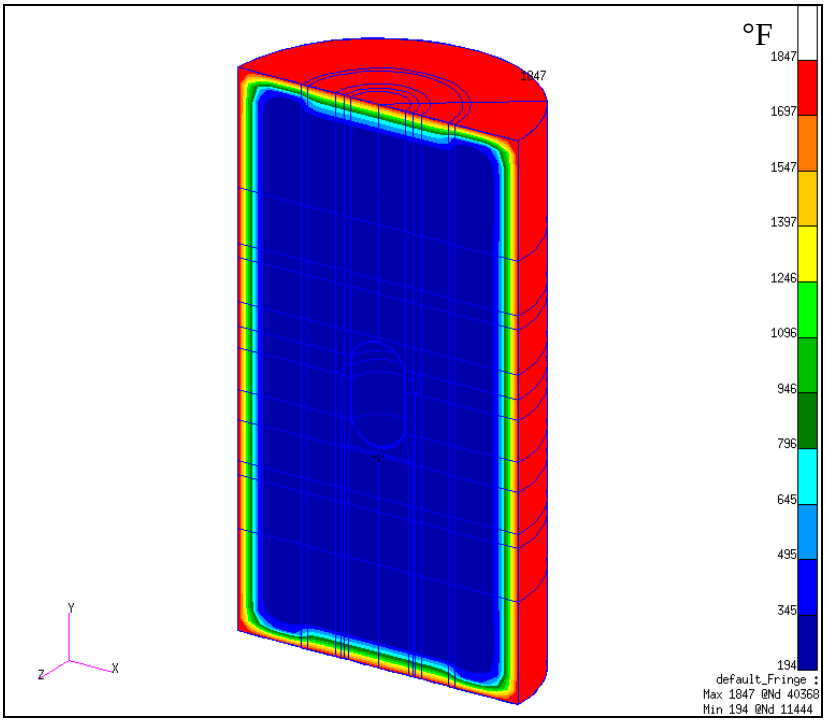

Figure 3-16. Temperature Distribution at the End of the 30-Minute Regulatory Fire — Complete Model (°C=[°F-32]/1.8)

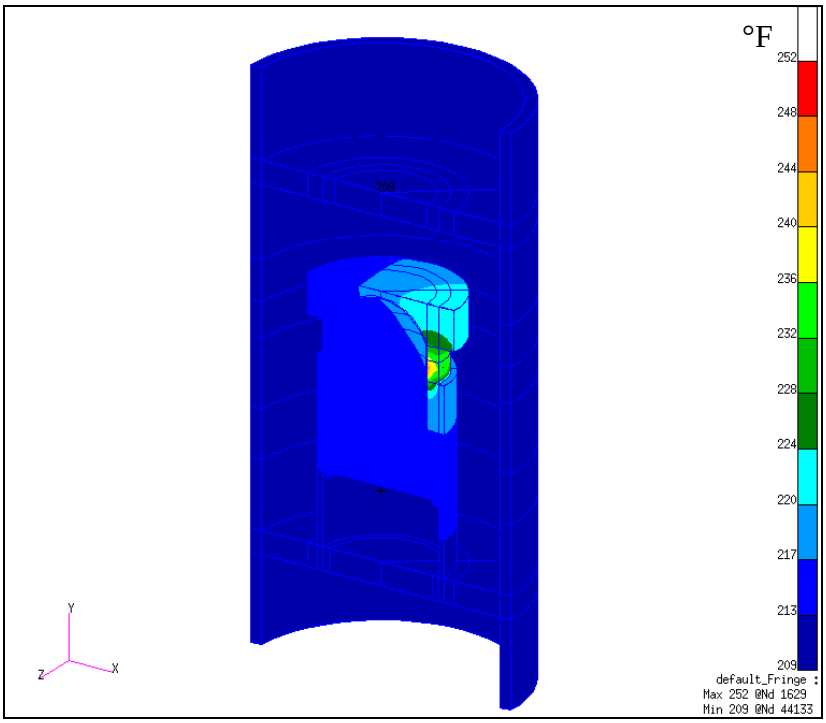

Figure 3-17. Temperature Distribution at the End of the 30-Minute Regulatory Fire — T-Ampoule, TB-1, Heat Transfer Cu Cylinder, and Aluminum Load Spreader (°C=[°F-32]/1.8)

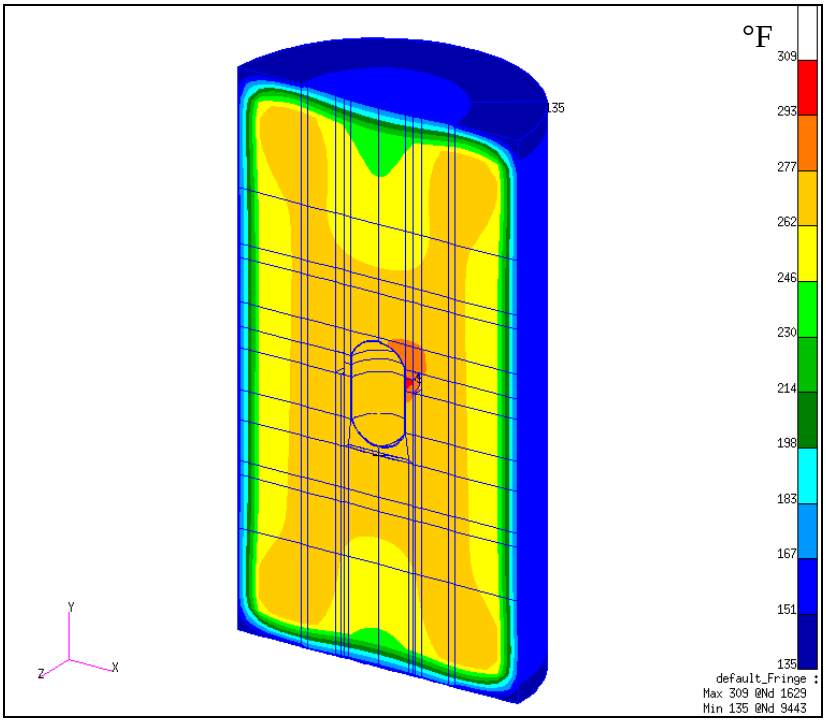

Figure 3-18. Temperature Distribution at t=290 Minutes (260 Minutes after the 30-Minute Fire) — Complete Model (°C=[°F-32]/1.8)

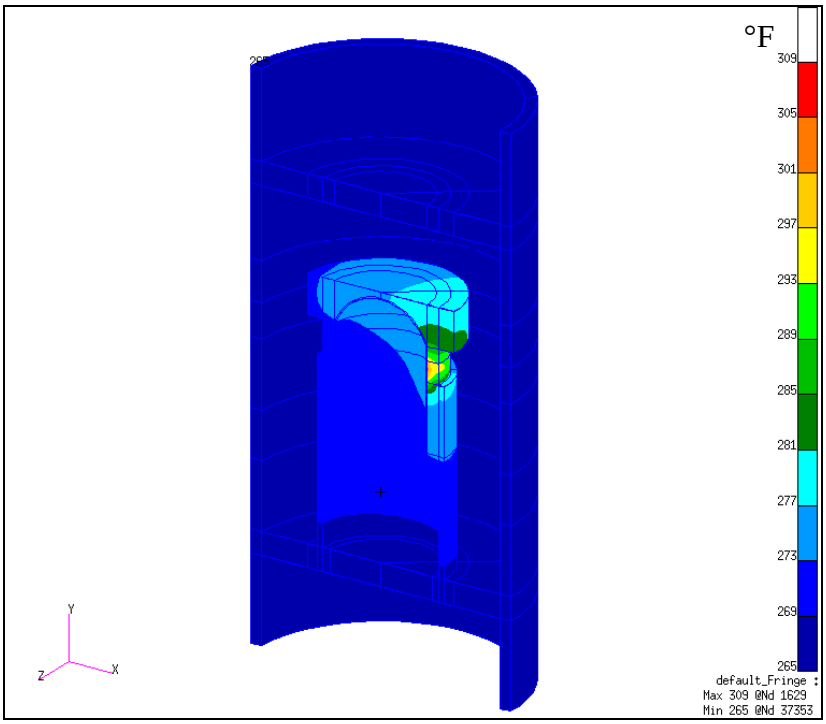

Figure 3-19. Temperature Distribution at t=290 Minutes (260 Minutes after the 30-Minute Fire) — T-Ampoule, TB-1, Heat Transfer Cu Cylinder, and Aluminum Load Spreader (°C=[°F-32]/1.8)

3.4.3 Maximum Temperatures and Pressure

Results from the hypothetical accident conditions evaluation of the AQ–1, TB-1, and the T-Ampoule, assuming the bounding concentrated internal heat described in Section 3.1.2 of this addendum and using the conservative transient computer model described in Section 3.4 of this addendum, are summarized in Table 3-11 of this addendum.

The components listed in this table did not reach temperatures of concern. Only the redwood regions closer to the outer skin of the package are expected to degrade (see Section 3.2.1 of the Addendum). Nevertheless, PAT-1 protects the package contents during and after the exposure to a severe fire environment, as required by 10 CFR 71.73.

The HAC evaluation indicated a peak T-Ampoule seal temperature of 153°C (308°F) and a peak TB-1 (and seal) temperature of 147°C (296°F). This TB-1 seal temperature is 38°C (69°F) higher than that reported as the TB-1 temperature in Section 3.5.1.1 of the PAT-1 SAR[1] and is, once again, considered to be overestimated (or conservative) due to the concentrated heat loading assumption. Nevertheless, this temperature does not exceed the limit temperature of the copper seal. Therefore, the TB-1 is able to maintain containment. In addition, the T-Ampoule is also able to maintain a seal for product quality.

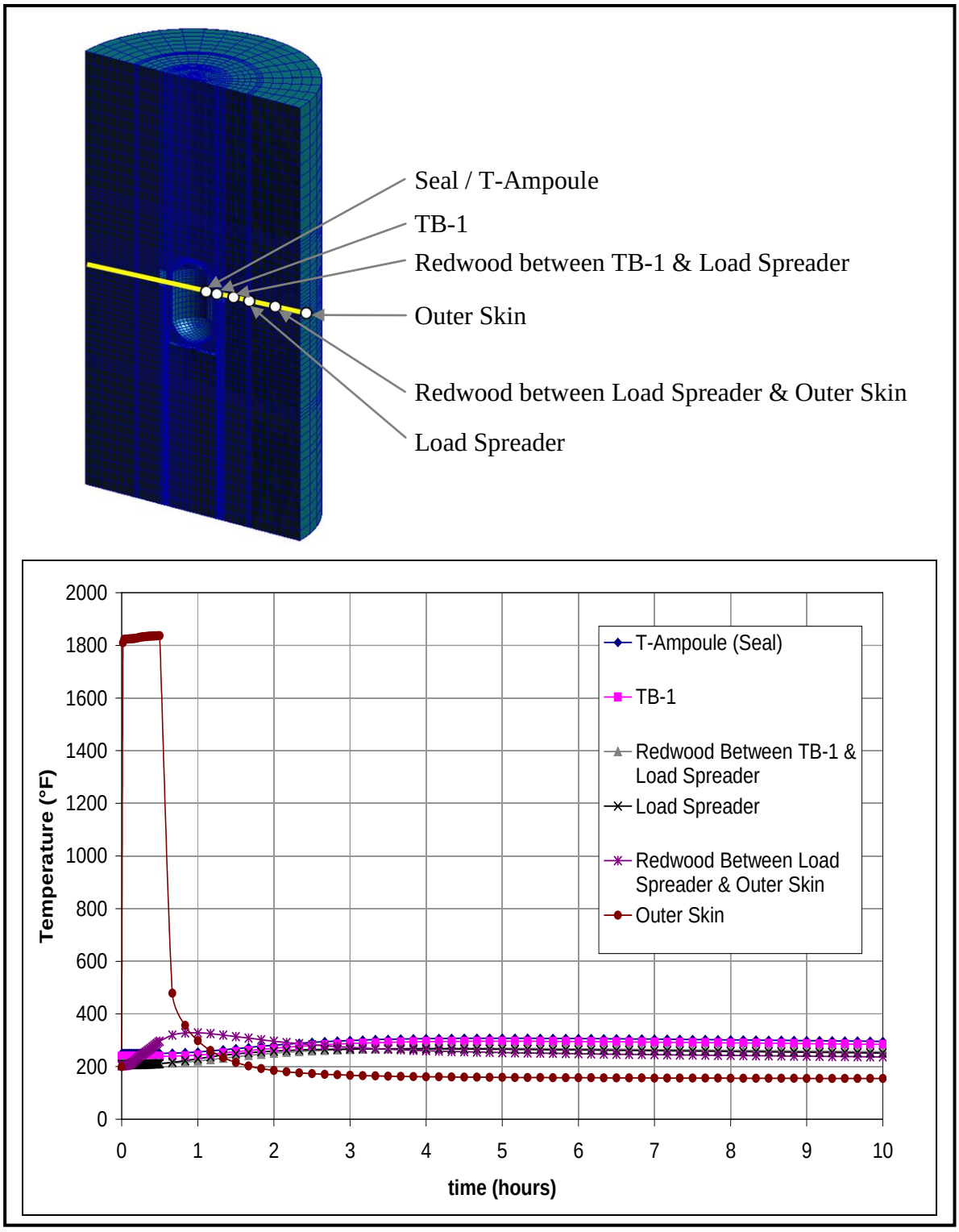

Figure 3-20. Temperature History at T-Ampoule Seal Height for the 30-Minute Regulatory Fire (°C=[°F-32]/1.8). Note: In the schematic above the plot, the reference yellow line crosses the cask at T-Ampoule-seal height and the white dots are the approximate locations of the temperature history lines in the plot.

Table 3-11. Summary of Maximum Temperatures and Times for the HAC

Component	HAC Maximum Temperature and Time to Reach Temperature
T-Ampoule (Seal)	153°C (308°F) @ 260 minutes after the fire
TB-1 (and TB-1 seal)*	147°C (296°F) @ 260 minutes after the 30-minute fire
Center of Redwood between TB-1 and Load Spreader	132°C (270°F) @ 240 minutes after the 30-minute fire
Aluminum Load Spreader	131°C (267°F) @ 190 minutes after the 30-minute fire
Center of Redwood between Load Spreader and Outer Skin	164°C (328°F) @ 30 minutes after the 30-minute fire
Stainless Steel Outer Drum	1003°C (1837°F) @ end of fire

*Maximum seal temperature was conservatively taken as the TB-1 maximum temperature.

The average T-Ampoule internal surface temperature was 136°C (276°F). Assuming the gas inside the TB-1 is at this average temperature, the maximum internal pressure that the TB-1 could experience under HAC can be estimated. When calculating this pressure, it was also assumed that the TB-1 was initially loaded at a room temperature of 21°C (70°F) and in a pressure environment of 1 atmosphere. Additionally, pressure generation due to alpha decay as calculated in Section 4 of this addendum was included in the total pressure calculation. Thus:

$$P_{TB\text{-}1@276°F\text{-}gauge} = (P_{initial} + P_{alpha_decay})*(T_2/T_1) - 1atm$$

$$= (1\ atm + 0.005\ atm) * (736°R/530°R) - 1atm$$

$$= 0.4\ atm \text{ or } \sim 40\ kPa\ (5.8\ psig) \qquad (3\text{-}10)$$

In summary, these results show that the PAT–1 provides containment for the proposed new payload inside the TB-1 and adequately contains the material inside the T-Ampoule, as maximum seal temperatures are within the service temperature range specified in Table 3-5 and the TB-1 can withstand the pressure that would arise during and after the HAC fire event. Additionally, the eutectic prevention barrier is retained because the T-Ampoule is constructed of titanium 6Al-4V alloy and can withstand the temperatures and pressures observed under the 10 CFR 71[2] HAC, as documented in Section 2 of this addendum.

3.4.4 Maximum Thermal Stresses

The maximum thermal stresses are determined from results of the differential thermal expansion analysis conducted and documented in Section 2.7.4.2 of this addendum. Since the American Society of Mechanical Engineers (ASME) Boiler and Pressure Vessel (B&PV) code does not provide the coefficient of thermal expansion (α) for Ti-6Al-4V, the value listed in the MIL-HDBK-5E[14] (9.18×10^{-6} m/m/°C [5.1×10^{-6} in/in/°F]) was used in this analysis.

A conservative estimate of the T-Ampoule maximum expansion can be calculated by assuming the T-Ampoule is a 0.2 m (7.418 in.) long cylinder (the actual T-Ampoule is capped) with a diameter of 0.11 m (4.22 in). Assuming a temperature increase of (153°C – 21.1°C) = 132°C

([308°F – 70°F] = 238°F), the expansion produced equals $\alpha \Delta TL$, or 0.23 mm (0.009 in.) in the longitudinal direction and 0.41 mm (0.0161 in.) in circumference (or 0.13 mm [0.0051 in.] in diameter). Since the gap between the T-Ampoule and the TB-1 is 0.381 mm (0.015 in.) around the entire perimeter, the T-Ampoule will not expand enough to induce any stress on the TB-1, even if thermal expansion of the TB-1 is ignored.

3.4.5 Hypothetical Accident Conditions for Fissile Material Packages for Air Transport

Thermal tests that meet the specifications in 10 CFR 71.64[2] were conducted on the PAT-1 and are documented in Chapter 3 of the SAR[1]. Physical tests were the primary means used to demonstrate that the PAT-1 package met the requirements of the NRC Qualification Criteria (10 CFR 71.74[2]). The purpose of the assessment documented in Section 3.6 of the SAR[1] was to demonstrate that the maximum TB-1 temperature (reported in Section 3.6.3 of the SAR[1]) used in Section 4.4.2 of the SAR[1] was a reasonable upper limit for bounding the results.

The package temperatures cited in Section 3.6.3 of the SAR[1] stated the following: "Based on the analysis and test results in Sections 3.6.1.1 and 3.6.1.2, the TB-1 is estimated to have attained a maximum temperature of approximately 582°C (1080ºF) during the thermal test specified in the NRC Qualification Criteria." This maximum temperature is not affected by any of the packing or content modifications presented in this addendum. That is, the maximum internal heat generation of the content remains the same (25 watts [85.3 Btu/hr]) and the design of the TB-1 and the rest of the packaging outward of the TB-1 is the same as evaluated in the SAR.[1] Therefore, the maximum temperature of the TB-1 used for this addendum, for the calculation of loads due to internal pressure and thermal expansion during the plutonium aircraft fire environment is 582°C (1080ºF).

At the maximum temperature of the TB-1 after the plutonium aircraft accident fire, there is a potential for plutonium metal to form eutectics with certain metals such as iron in the TB-1. The materials that were selected for the components within the TB-1 were based on the resistance to eutectic formation with plutonium. The melting temperatures for different material combinations are presented in Section 3.5.3 of this addendum. Given that the melting point of the plutonium-iron eutectic is lower than the maximum TB-1 temperature in the plutonium air transport thermal evaluation, the titanium T-Ampoule is used as a barrier between the plutonium metal and the PH13-8Mo material in the TB-1. The structural analysis documented in Section 2 of this addendum demonstrates that the T-Ampoule wall will not be breached as a result of NCT, HAC, or the accident conditions for air transport of plutonium. Thus, the formation of a Pu-Fe eutectic as a result of the thermal conditions resulting from a 10 CFR 71.74 specified fire is not possible because of the separation between the Pu content and the Fe in the TB-1 provided by the T-Ampoule wall. The service temperatures of all components (T-Ampoule and its packing within the TB-1) shown in Table 3-5 in this addendum, which were derived in part from the eutectic evaluation in Section 3.5.3 in this addendum, are all above 582°C (1080ºF).

In addition to the Pu-Fe eutectic potential discussed above, a plutonium-beryllium eutectic may also form. The melting point of this Pu-Be eutectic is 595°C (1103ºF) (see Section 3.5.3 in this addendum). This is 13ºC (23ºF) higher than the highest temperature excursion that occurs in the system.

The maximum internal pressure that may occur within the TB-1 during the air transport thermal evaluation is 7.55 MPa (1095 psig) (see Section 4 and 2.12.8 of this addendum). This was calculated by adding the pressure generated from the decomposition of the O-rings in the SC-1 configuration, which includes the elastomeric seal of the T-Ampoule and three SC-1s (highest amount of elastomeric material), which yielded a pressure of 599.2 psi (from Section 2.12.8 of this addendum), the pressure generated from the decomposition of the ancillary plastic (468 psi from Table 11 in Section 2.12.8), the pressure generated due to the change in temperature of the initial fill gas (42.3 psi), and the pressure from gas generation from alpha decay of plutonium [0.173 psi (from Table 11 in 2.12.8)]. This maximum pressure of 1110 psia is equal to the maximum TB-1 pressure stipulated in the PAT-1 SAR[1] (1095.3 psig, see Section 4.3.1 and 2.12.8 of this addendum). Therefore, the TB-1 is capable of sustaining this maximum pressure observed during the plutonium air transport fire accident condition without rupturing. Note that the T-Ampoule will not retain any pressure because its elastomeric O-ring can extrude out of the O-ring groove and no longer maintain a seal at temperatures above its service temperature of 204ºC (400ºF).

The thermal expansion calculation in Section 2.8.6 of this addendum demonstrates that no stresses will be induced in the TB-1 by differential thermal expansion resulting from the air transport fire accident.

The analysis in this section demonstrates that the replacement of the PC-1 inner container (with its packing and contents) with the T-Ampoule inner container (with its packing and contents) does not alter the thermal performance of the PAT-1. Therefore, the discussion in Section 3.6 of the SAR[1] regarding the ability of the package to meet the requirements in the plutonium air transport regulations due to thermal loads remains valid. That is, the performance of the PAT-1 with the T-Ampoule (with its packing and contents) inside the TB-1 is bounded by the tests presented in the SAR[1] and therefore the TB-1 maintains containment.

3.5 Appendix

3.5.1 References

1. United States. Nuclear Regulatory Commission. NUREG-0361. "Safety Analysis Report for the Plutonium Air Transportable Package, Model PAT-1." Washington, D.C. 1978.

2. United States. Nuclear Regulatory Commission. Code of Federal Regulations, 10 CFR 64, 71, 73, and 74. January 1, 2009.

3. White, R.H., and E.L. Schaffer. "Application of CMA Program to Wood Charring," *Fire Technology*. Volume 14, Number 4 (1978): 279-290.

4. MSC Patran Thermal 2005 r2. MSC Software Corporation. <www.mscsoftware.com.>

5. Touloukian, Y.S., "Thermophysical Properties of High-Temperature Solid Materials." (1967).

6. Schorsch, R.H., "Engineering Properties of Selected Materials." (1966).

7. Hodge, A.W. and D.J. Maykuth. "Properties of New High-Temperature Titanium Alloys," DMIC Memo 230, Defense Metals Information Center, Battelle Memorial Institute, Columbus Ohio. February 1968.

8. Boivineau, M., C. Cagran, D. Doytier, V. Eyraud, M.-H. Nadal, B. Wilthan, and G. Pottlacher, "Thermophysical Properties of Solid and Liquid Ti-6Al-4V (TA6V) Alloy," International Journal of Thermophysics, Vol. 27, No. 2, March 2006.

9. Mason, R.E. and S.P. Willson, "Eutectic Analysis of Ti-6Al-4V with Plutonium and Copper," LA-UR-08-07663. Los Alamos National Laboratory. Los Alamos, NM. 2008. (Presented in Appendix 3.5.3).

10. Shapiro, A.B. and A.L. Edwards. "TOPAZ2D Heat Transfer Code Users Manual and Property Data Base," UCRL-ID--104558. Lawrence Livermore National Laboratory. Livermore, CA. 1990.

11. Incropera, F.P. and D.P. DeWitt. "Fundamentals of Heat and Mass Transfer, 4th ed.," New Jersey: Wiley & Sons, Inc., 1996.

12. Churchill, S.W. and J. M. Bernstein. *Heat Transfer*. 99, 300. (1977).

13. Nakos, J.T., "Uncertainty Analysis of Steady-State Incident Heat Flux Measurements in Hydrocarbon Fuel Fires," SAND2005-7144. Sandia National Laboratories. Albuquerque, NM. December 2004.

14. Department of Defense. *Military Standardization Handbook: Metallic Materials and Elements for Aerospace Vehicle Structures.* MIL-HDBK-5E: May 1988.

3.5.2 Viton® O-Ring Technical Information

Technical Information

Rev. 6, November 2005

Viton® fluoroelastomer

From DuPont Performance Elastomers

Selection Guide

Introduction

Viton® fluoroelastomer was introduced in 1957 to meet the needs of the aerospace industry for a high-performance seal elastomer. Since then, the use of Viton® fluoroelastomer has expanded to many other industries, especially in the automotive, fluid power, appliance, and chemical fields. With over 40 years of proven performance, Viton® fluoroelastomer has developed a reputation for outstanding performance in high temperature and extremely corrosive environments.

Valuable Properties of Viton® Fluoroelastomer

Vulcanizates based on Viton® provide an exceptional balance of physical property characteristics, including the following features:

- Resistance to temperature extremes:

Heat—Compared to most other elastomers, Viton® is better able to withstands high temperature, while simultaneously retaining its good mechanical properties. Oil and chemical resistance are also essentially unaffected by elevated temperatures. Compounds of Viton® remain substantially elastic substantially indefinitely when exposed to laboratory air oven aging up to 204°C or to intermittent exposures up to 316°C. High temperature service limits are generally considered to be:

3,000 hr at 232°C
1,000 hr at 260°C
240 hr at 288°C
48 hr at 316°C

Cold—Viton® is generally serviceable in dynamic applications to temperatures of –18 to –23°C. Special formulations permit its use in static applications down to –54°C. Also, Viton® has proven to be satisfactory for static seals used under conditions approaching absolute zero. Viton® is characterized by its;

- Resistance to degradation by a greater variety of fluids and chemicals than any nonfluorinated elastomer. Excellent resistance to oils, fuels, lubricants, and most mineral acids.
- Extremely low permeability to a broad range of substances, including particularly good performance in oxygenated automotive fuels.
- Resistance to aliphatic, aromatic hydrocarbons that dissolve other rubbers.
- Exceptionally good resistance to compression set, even at high temperatures.
- Exceptionally good resistance to atmospheric oxidation, sun, and weather. Excellent resistance to fungus and mold.
- Good electrical properties in low voltage, low frequency applications.
- Low burning characteristics; inherently more resistant to burning than other, non-fluorinated hydrocarbon rubbers.

Safety and Handling

As with many polymers, minute quantities of potentially irritating or harmful gases may diffuse from uncured Viton® even at room temperature. Therefore, all containers should be opened and used only in well-ventilated areas. In case of eye contact, immediately flush the eyes for at least 15 min with water. Always wash contacted skin with soap and water after handling Viton®.

Potential hazards, including the evolution of toxic vapors, may arise during compounding, processing, and curing of the raw polymers into finished products or under high-temperature service conditions. Therefore, before handling or processing Viton®, make sure that you read and follow the recommendations in the DuPont Performance Elastomers bulletin "Handling Precautions for Viton® and Related Chemicals."

Compounding ingredients and solvents that are used with Viton® to prepare finished products may present hazards in handling and use. Before proceeding with any compounding or processing work, consult and follow label directions and handling precautions from suppliers of all ingredients.

The Various Families and Types of Viton® Fluoroelastomer

Standard types of Viton® fluoroelastomer products are designated as A, B, or F according to their relative resistance to attack by fluids and chemicals. The differences in fluid resistance are the result of different levels of fluorine in the polymer, which is determined by the types and relative amounts of copolymerized monomers that comprise the polymer.

In general, Viton® exhibits outstanding resistance to attack from a wide variety of fluids, including mineral acids and aliphatic and aromatic hydrocarbons. The higher the fluorine content of the polymer, the less will be the effect, as measured by volume increase, for example. The most significant differences between A, B and F types of Viton®, in terms of resistance to volume change or retention of physical properties, are exhibited in low molecular weight, oxygenated solvents (such as methanol and methyl t-butyl ether).

As mentioned above, the fluid resistance of Viton® A, B, and F types improves with increasing fluorine levels. This is shown in Table 1 (note the volume increase after aging in methanol at 23°C). As the fluorine content increases, however, the low temperature flexibility of the polymer decreases, and a compromise must be made between fluid resistance and low temperature flexibility of the final vulcanizate.

For those applications that require the best performance in both fluid resistance and low temperature flexibility a number of specialty types of Viton® were developed that contain a copolymerized fluorinated vinyl ether monomer. Polymers that contain this monomer exhibit significantly improved low temperature flexibility, compared to standard types of fluoroelastomer.

Viton® GLT introduced in 1976, was the first commercial fluoroelastomer to incorporate this fluorinated vinyl ether monomer. This polymer provides the same excellent resistance to heat and fluids that is typical of the A types of Viton® fluoroelastomer. Viton® GFLT, like Viton® GLT, exhibits significantly improved low temperature flex characteristics compared to standard types of fluoroelastomer. In addition, Viton® GFLT provides the same superior resistance to fluids that is typical of the F types of Viton® fluoroelastomer.

Types of Viton® Extreme™

Fluoroelastomers that contain copolymerized vinylidene fluoride(VF2) are subject to attack by high pH materials, including caustics and amines. In addition, standard fluoroelastomers are not resistant to low molecular weight carbonyl compounds, such as methyl ethyl ketone, acetone, or methyl tertiarybutyl ether.

Viton® Extreme™ ETP-600S is a copolymer of ethylene, tetrafluoroethylene (TFE), and perfluoromethylvinyl ether (PMVE). This unique combination of monomers provides outstanding resistance to fluids and is an example of an ETP polymer. The ETP types of Viton® exhibit the same excellent resistance to acids and hydrocarbons typical of A, B and F types of Viton®. Unlike conventional fluoroelastomers, however, ETP types of Viton® also provide excellent resistance to low molecular weight esters, ketones, and aldehydes. In addition, these unique polymers are inherently resistant to attack by base, and thus provide excellent resistance to volume swell and property loss in highly caustic solutions and amines.

Additional information regarding performance differences between the various families and types of Viton® fluoroelastomer is presented in Tables 3–6 to assist in selecting the particular grade of

Viton® that is best suited for both a given end-use application and for a specific manufacturing process.

Table 1
Polymer Fluorine Content versus Fluid Resistance and Low Temperature Flexibility

	Standard Types			Specialty Types		
	A	B	F	GLT-S	GFLT-S	ETP-S
Nominal Polymer Fluorine Content, wt%	66	68	70	64	67	67
Percent Volume Change in Fuel C, 168 hr at 23°C*	4	3	2	5	2	4
Percent Volume Change in Methanol, 168 hr at 23°C*	90	40	5	90	5	5
Percent Volume Change in Methyl ethyl Ketone, 168 hr at 23°C*	>200	>200	>200	>200	>200	19
Percent Volume Change in 30% Potassium Hydroxide, 168 hr at 70°C*	(Samples too swollen and degraded to test)					14
Low Temperature Flexibility, TR-10, °C*	-17	-13	-6	-30	-24	-12

*Nominal values, based on results typical of those obtained from testing a standard, 30 phr MT (N990) carbon black-filled, 75 durometer vulcanizate. These are not intended to serve as specifications.

Curing Systems for Viton® Fluoroelastomer

In addition to inherent differences between the various types and families of Viton® fluoroelastomer, a number of compounding variables have major effects on the physical property characteristics of the final vulcanizates. One very important variable is the crosslinking or curing system that is used to vulcanize the elastomer.

Diamine curatives were introduced in 1957 for crosslinking Viton® A. While these diamine curatives are relatively slow curing, and do not provide the best possible resistance to compression set, they do offer unique advantages. For example, compounds cured with diamines exhibit excellent adhesion to metal inserts and high hot tensile strength.

Most fluoroelastomers are crosslinked with Bisphenol AF, a curative introduced in 1970, in the first commercial curative-containing precompound, Viton® E-60C. Compounds of Viton® that use this curative exhibit fast rates of cure and excellent scorch safety and resistance to compression set.

In 1987, an improved bisphenol curative was introduced, which was made available in several different precompounds. The modified system provides faster cure rates, improved mold release, and slightly better resistance to compression set, compared to the original bisphenol cure system used in Viton® E-60C and E-430. Additional precompounds of Viton®, incorporating this modified curative, were introduced in 1993, including Viton® A-331C, A-361C, B-601C, and B-651C. A brief description of all these products can be found in Table 6.

In 1976, efficient peroxide curing of fluoroelastomers was made possible for the first time with the introduction of Viton® GLT. The peroxide cure system provides fast cure rates and excellent physical properties in polymers such as GLT and GFLT which cannot be readily cured with either diamine or bisphenol crosslinking systems. In the case of polymers such as Viton® GF, GBL-200, and GBL-900, the peroxide cure provides enhanced resistance to aggressive automotive lubricating oils and steam and acids. Generally, vulcanizates of Viton® fluoroelastomers cured with peroxide do not show any significant difference in resistance to other fluids and chemicals compared to the same polymer cured with bisphenol.

In 2003, a series of peroxide-cure types of Viton® made with Advanced Polymer Architecture was introduced. These polymers, designated as APA polymers by having an "S" suffix on the product name, incorporate a significantly improved cure site. As a result, they provide substantially better processing and physical properties, compared to the original, non-APA peroxide-cure types of Viton®. A comparison of the various processing and physical property characteristics of compounds using the various cure systems is shown in Table 2.

Table 2
A Comparison of Cure Systems Used in Crosslinking Viton®

Property, Processing Characteristic	Type of Cure System		
	Diamine	Bisphenol	Peroxide*
Processing Safety (Scorch)	P-F	E	E
Fast Cure Rate	P-F	E	E
Mold Release/Mold Fouling	P	G-E	G-E
Adhesion to Metal Inserts	E	G	G
Compression Set Resistance	P	E	E
Steam, Water, Acid Resistance	F	G	E
Flex Fatigue Resistance	G	G	G

Rating: E=Excellent G=Good F=Fair P=Poor
*Luperco 101-XL (trademark of Pennwalt Corporation) and Varox Powder (trademark of R.T. Vanderbilt Co., Inc.) are commonly used.

Selecting a Specific Type of Viton® Fluoroelastomer
Inherent Physical Property Differences Between Types/Families of Viton® Products

The physical properties of vulcanizates based on Viton® fluoroelastomers are determined to a large extent by the type and amount of the filler(s) and curative(s) used in the formulation, and by the temperature and duration of the curing cycle used in their manufacture.

In terms of resistance to compression set, low temperature flexibility, and resistance to certain classes of fluids, however, some inherent differences exist among the various families of Viton® fluoroelastomers. These are the result of differences in the relative amount and type of monomers used in the manufacture of the various types of Viton® fluoroelastomers.

The differences in physical property characteristics which exist between various types and families of Viton® fluoroelastomer products are outlined in general terms in Table 3.

As an example, resistance to compression set is an important property for seals and if this property were considered to be the most important feature for a particular part, then one of the A-types of Viton® might be the best choice for the application. However, if resistance to the widest possible range of fluids is a more important consideration then an F-type Viton® fluoroelastomer might well be a better choice for that particular end-use application. Further, if both fluid resistance and low temperature flexibility are equally important requirements for maximizing the end-use suitability of a given part GFLT-types of Viton® would represent the best overall choice.

Table 3
Physical Property Differences Between Types/Families of Viton® Products

Type of Viton® Fluoroelastomer	Resistance to Compression Set	General Fluids/ Chemical Resistance*	Low Temperature Flexibility**
A	1	3	3
B, GBL-S	2	3	3
F, GF-S	3	2	3
GLT-S	2	3	1
GFLT-S	2	2	2
ETP-S	3	1	3

1=Excellent—Best performance capability of all types; 2=Very Good; 3=Good—Sufficient for all typical fluoroelastomer applications
*See *Table 4* for a detailed guide to choosing the best type of Viton® fluoroelastomer, relative to specific classes of fluids and chemicals.
**Flexibility, as measured by Temperature of Retraction (TR-10), Gehman Torsional Modulus, Glass Transition (Tg), or Clash-Berg Temperature. Brittle-Point tests are a measure of impact resistance only and do not correlate at all with the low temperature sealing capability of a vulcanizate.

Selecting a Specific Type of Viton® Fluoroelastomer
Differences in Fluid Resistance Between Types of Viton® Products

As in the case of physical properties, different polymer compositions will result in inherent differences with regard to fluid resistance.

Table 4 outlines the differences that exist between types of Viton® products, in terms of their resistance to various classes of fluids and chemicals.

Because as certain types of Viton® products may exhibit performance that is superior to other types in one regard, but not quite as good in some other aspect, it is important to consider the requirements of the part to be manufactured, in terms of both physical property requirements and fluid or chemical resistance needs.

Using Tables 3 and 4, the compounder can select the best type of Viton® product for a given end-use application, based on the best combination of physical property and fluid resistance characteristics.

Table 4
Differences in Fluid Resistance Between Types of Viton® Fluoroelastomer

	Type of Viton® Fluoroelastomer							
	A	B	F	GBL-S	GF-S	GLT-S	GFLT-S	ETP-S
	Cure System							
	Bisphenol			Peroxide				
Hydrocarbon Automotive, Aviation Fuels	1	1	1	1	1	1	1	1
Oxygenated Automotive Fuels (containing MeOH, EtOH, MTBE, etc.)	NR	2	1	2	1	NR	1	1
Reciprocating Engine Lubricating Oils (SE-SF Grades)	2	1	1	1	1	1	1	1
Reciprocating Engine Lubricating Oils (SG-SH Grades)	3	2	2	1	1	1	1	1
Aliphatic Hydrocarbon Process Fluids, Chemicals	1	1	1	1	1	2	1	1
Aromatic Hydrocarbon Process Fluids, Chemicals	2	2	1	1	1	2	1	1
Aqueous Fluids: Water, Steam, Mineral Acids (H_2SO_4, HNO_3, HCl, etc.)	3	2	2	1	1	1	1	1
Amines, High pH Caustics (KOH, NaOH, etc.)	NR	NR	NR	3	3	3	3	1
Low Molecular Weight Carbonyls (MTBE, MEK, MIBK, etc.)	NR	NR	NR	NR	NR	NR	NR	1

1=Excellent—Best choice of Viton® type(s) for service in this class of fluid/chemical; minimal volume increase, change in physical properties.
2=Very Good—Good serviceability in this class of fluid/chemical; small amounts of volume increase and/or changes in physical properties.
3=Good—Suitable for use in this class of fluid/chemical; acceptable amounts of volume increase and/or changes in physical properties.
NR=Not Recommended—Excessive volume increase or change in physical properties.

6

Viton® Product Naming System

With the introduction of six improved processing precompounds in 1993, a new nomenclature system was adopted for Viton® fluoroelastomer products. The new system incorporates the following information in a product name:

- Nominal Mooney Viscosity
- Family type (relative fluid resistance)
- Relative state of cure (relative level of crosslinking agent present in curative-containing precompounds)
- An indication of whether the product can be crosslinked using a peroxide cure system
- An indication of whether the product is a gum polymer or a precompound, which contains a preset, carefully controlled amount of bisphenol crosslinking system.

Each character in the product name indicates a specific characteristic as outlined below:

1st Character (Letter)

- Represents the Viton® fluoroelastomer family--A, B, F, or ETP.
- A "G" prefix, in addition to a family prefix, indicates that the polymer can be crosslinked with the peroxide cure system.
- An "L" designation indicates that the A, B, or F type polymer provides slightly improved low temperature flexibility characteristics versus other polymers within the same family. An "LT" designation indicates a more significant improvement in low temperature performance criteria.

2nd Character (Number)

Represents nominal Mooney Viscosity of the product—ML 1 + 10 at 121°C.

3rd Character (Number)

Represents the relative level of curative in a precompound on a scale of 10 → 1 (10 is represented by 0);

0 = High curative level (for optimum compression set)

9 → 2 = Intermediate, decreasing levels of curative (increased elongation at break, tear resistance)

1 = Low curative level (for optimum tear, flex resistance)

4th Character (Number)

Represents a slightly different version of a particular precompound.

5th Character (Letter)

- Absence of a letter suffix indicates that the product is a gum polymer only and contains no curatives (may contain process aid).
- "C" indicates that the product is a precompound, containing accelerator and curative.
- "S" indicates that the product incorporates Viton® made with Advanced Polymer Architecture technology

Choosing a Viton® Product for Use in a Particular Type of Manufacturing Process

The Viton® product line includes a wide variety of different types of fluoroelastomer products, which exhibit some inherent differences in their end-use capabilities (see Tables 3 and 4). In addition, a broad range of viscosities is offered for most types of Viton®, providing a wide degree of utility in various manufacturing processes.

Having selected a given class of Viton® products for an end use, the compounder must then choose which particular Viton® product is best suited for use in a specific manufacturing process.

The Viton® - Application Guide (Table 5) lists the Viton® products that are recommended for particular end-use applications, according to the various processes that are most commonly used in their manufacture.

The Viton® - Product Listing (Table 6) provides more specific information about the various individual Viton® products. Contact your DuPont Performance Elastomers sales or technical representative to obtain more detailed information or data on specific Viton® products.

How to Use the Viton® Application Guide

The Viton® - Application Guide (Table 5) has been designed to facilitate choice of the type of Viton® that is best suited for meeting both the property requirements of the intended end use and the needs of the production method used to manufacture the finished product.

The guide is divided into five general categories (columns) of end-use products, differentiated primarily by physical form:

- Sheet form goods, such as gaskets, diaphragms, etc.
- Simple shapes, such as O-rings, V-rings, etc., which do not typically require high levels of demolding tear resistance, but which generally require high states of cure to obtain the best compression set possible.
- Complicated molded shapes, such as shaft seals or valve stem seals, which require good hot tear upon demolding do to the undercuts in the molds used to form such parts and good adhesion to metal inserts (obtained during the vulcanization of the parts).
- Complicated molded shapes that do not involve adhesion to metal inserts during vulcanization, but which require good resistance to tear during demolding. Carburetor roll-over cages, boots, and reed valves are examples of such parts.
- Extruded shapes, such as rod, tubing, or hose constructions.

Each general end-use category listed is divided into four columns, each listing Viton® products within a specific family or type of Viton® fluoroelastomer—A, B, F, and specialty types.

The guide is further divided into the five major types of process (rows) by which these general end-use categories might be produced:

- Compression molding
- Transfer molding
- Injection molding
- Extrusion
- Calendering

Within the blocks formed by the "intersection" of a given end-use category (column) and the process type by which the end products will be manufactured (row), we have listed the types of Viton® that we believe are appropriate choices for meeting the physical property requirements of the finished product and that are best suited for the chosen manufacturing process.

The Viton® products we believe will provide the best combination of end-use physical properties, together with the best processing characteristics for given methods of manufacture, are listed in bold type.

Additional details for specific types of Viton® can be found in the Viton® Product Listing and in product-specific data sheets.

8

Table 5
Viton® Fluoroelastomer Application Guide

Manufacturing Process	Reinforced/Unreinforced Sheet Stock (Gaskets, Diaphragms, etc.)				Molded (Non-Bonded), Simple Shapes (O-Rings, V-Rings, etc.)			
	Viton® Types							
	A	B	F	Specialty	A	B	F	Specialty
Compression Molding	A-331C A-361C A-401C A-601C A-500 A-700 AL-600	B-435C B-601C B-651C GBL-600S B-600	F-605C GF-600S	GLT-600S GBLT-600S GFLT-600S ETP-600S	A-401C A-331C A-601C A-500 A-HV A-700 AL-600	B-601C B-651C GBL-600S B-600	F-605C GF-600S	GLT-600S GBLT-600S GFLT-600S ETP-600S
Transfer Molding	A-201C A-331C A-361C A-401C A-200 AL-300	B-435C GBL-200S B-202	F-605C GF-200S	GLT-200S GBLT-200S GFLT-200S ETP-600S	A-201C A-331C A-361C A-200 AL-300	B-651C GBL-200S B-202	F-605C GF-200S	GLT-200S GBLT-200S GFLT-200S ETP-600S
Injection Molding	A-201C A-331C A-361C A-200 AL-300	B-435C GBL-200S B-202	GF-200S	GLT-200S GBLT-200S GFLT-200S	A-201C A-331C A-361C A-100 A-200 A-500 AL-300	B-601C B-651C GBL-200S B-202	F-605C GF-200S	GLT-200S GBLT-200S GFLT-200S ETP-600S
Calendering	A-201C A-401C A-331C A-361C AL-300	B-435C B-601C B-651C GBL-200S GBL-600S B-202 B-600	F-605C GF-200S GF-600S	GLT-200S GLT-600S GBLT-200S GBLT-600S GFLT-200S GFLT-600S ETP-600S				
	Molded (Bonded), Complicated Shapes (Valve Stem, Shaft Seals, etc.)				Molded (Non-Bonded), Complicated Shapes (Boots, Valves, etc.)			
Compression Molding	A-361C A-500 A-700 AHV AL-600	B-435C B-651C GBL-600S B-600	F-605C/GF-200S GF-200S GF-600S	GLT-200S GLT-600S GBLT-200S GBLT-600S GFLT-200S GFLT-600S ETP-600S	A-331C A-401C/A-500 A-601C/A-200 A-361C A-700 AHV AL-600	B-435C B-651C GBL-600S B-600	F-605C/GF-600S GF-600S	GLT-600S GBLT-600S GFLT-600S ETP-600S
Transfer Molding	A-361C A-200 A-500 AL-300	B-435C GBL-200S B-202	GF-200S	GLT-200S GBLT-200S GFLT-200S ETP-600S	A-200 A-331C A-361C A-200 A-500 AL-300	B-435C B-651C GBL-200S B-600	F-605C/ GF-200S GF-300	GLT-200S GBLT-200S GFLT-200S ETP-600S
Injection Molding	A-361C A-100 A-200 A-500 AL-300	B-435C B-651C GBL-200S B-202	F-605C/ GF-200S GF-200S	GLT-200S GBLT-200S GFLT-200S	A-200 A-331C A-361C A-200 A-500 AL-300	B-435C B-651C GBL-200S B-202	F-605C/ GF-200S GF-200S	GLT-200S GBLT-200S GFLT-200S

Table 5
Viton® Fluoroelastomer Application Guide *(cont'd.)*

Manufacturing Process	Extruded Goods (Hose, Tubing, Extruded Profiles, etc.) Viton® Types			
	A	B	F	Specialty
Extrusion	A-201C A-401C A-361C A-200 A-500 AL-300	B-435C B-651C GBL-200S B-202 B-600	F-605C GF-200S	GLT-200S GBLT-200S GFLT-200S ETP-600S

Table 6
Viton® Fluoroelastomer Product Listing

	Polymer Properties			Nominal Physical Properties*				
Viton® Product Type	Nominal Viscosity, ML1 + 10 at 121°C	Specific Gravity	Polymer Fluorine Content, %	Compression Set, % 70 hr/200°C	Temperature of Retraction (TR-10) °C	Volume Increase, After 7 days/ MeOH/23°C	Viton® Fluoroelastomer Product Description	Viton® Fluoroelastomer Product Suggested Uses/ Applications
A-Types: Curative-Containing Precompounds								
A-201C	20	1.81	66.0	15	-17	+75 to 105%	Fast cure rate, excellent injection molding rheology, mold release	FDA-compliant**: injection molding, O-rings, gaskets, extruded shapes
A-331C	30	1.81	66.0	20	-17	+75 to 105%	Excellent mold flow, high elongation/tear resistance	Compression—injection molding of complex shapes, requiring maximum hot tear
A-361C	30	1.81	66.0	20	-17	+75 to 105%	Excellent mold flow, tear resistance, bonding to metal inserts	Compression—injection molding of complex shapes, bonded metal inserts
A-401C	40	1.81	66.0	15	-17	+75 to 105%	Excellent rheology at high shear rates, excellent resistance to compression set	FDA-compliant**: compression, transfer, or injection molding of O-rings
A-601C	60	1.81	66.0	12	-17	+75 to 105%	High viscosity, high state of cure; optimum resistance to compression set	FDA-compliant**: compression molding of O-rings, simple shapes

*Nominal physical properties typical of those that can be expected of vulcanizates based on the specific type of Viton® noted, in a 70A hardness, MT carbon black-filled formulation. These are not intended to serve as specifications.
**Curative-containing precompounds, and polymers + VC-50 (at levels less than or equal to 2.50 phr rubber) have been determined to be in compliance with FDA 21 CFR-177.2600—Rubber Articles for Repeated Food Contact.

10

Table 6
Viton® Fluoroelastomer Product Listing *(cont'd.)*

	Polymer Properties			Nominal Physical Properties*				
Viton® Product Type	Nominal Viscosity, ML1 + 10 at 121°C	Specific Gravity	Polymer Fluorine Content, %	Compression Set, % 70 hr/200°C	Temperature of Retraction (TR-10) °C	Volume Increase, After 7 days/ MeOH/23°C	Viton® Fluoroelastomer Product Description	Viton® Fluoroelastomer Product Suggested Uses/ Applications
A-Types: Gum Polymers								
A-100	10	1.82	66.0	15	-17	+75 to 105%	Ultra-low viscosity: excellent polymer rheology	Coatings, viscosity modifier for higher viscosity types
A-200	20	1.82	66.0	15	-17	+75 to 105%	Low viscosity: excellent polymer rheology	FDA-compliant**, cured w. VC-50: injection molding applications
A-500	50	1.82	66.0	15	-17	+75 to 105%	Intermediate viscosity: excellent polymer rheology	FDA-compliant**, cured w. VC-50: compression, transfer, injection molding
A-700	70	1.82	66.0	15	-17	+75 to 105%	High viscosity: excellent physical properties	FDA-compliant**, cured w. VC-50: compression, transfer, injection molding
A-HV	160	1.82	66.0	15	-17	+75 to 105%	Ultra-high viscosity: excellent physical properties	FDA-compliant**, cured w. VC-50: compression molding, high strength vulcanizates
AL-300	30	1.77	66.0	25	-19	+75 to 105%	Slightly improved low temperature flexibility. Low viscosity	Transfer, or injection molded goods, where A-types are marginal in low-temperature flexibility
AL-600	60	1.77	66.0	20	-19	+75 to 105%	Slightly improved low temperature flexibility. Medium viscosity	General molded goods, where A-types are marginal in low-temperature flexibility

*Nominal physical properties typical of those that can be expected of vulcanizates based on the specific type of Viton® noted, in a 70A hardness, MT carbon black-filled formulation. These are not intended to serve as specifications.
**Various types of Viton® curative-containing precompounds have been determined to be in compliance with FDA 21 CFR-177.2600—Rubber Articles for Repeated Food Contact.

11

Table 6
Viton® Fluoroelastomer Product Listing *(cont'd.)*

	Polymer Properties			Nominal Physical Properties*				
Viton® Product Type	Nominal Viscosity, ML1 + 10 at 121°C	Specific Gravity	Polymer Fluorine Content, %	Compression Set, % 70 hr/200°C	Temperature of Retraction (TR-10) °C	Volume Increase, After 7 days/ MeOH/23°C	Viton® Fluoroelastomer Product Description	Viton® Fluoroelastomer Product Suggested Uses/ Applications
B-Types: Curative-Containing Precompounds								
B-435C	40	1.85	68.5	25	-14	+35 to 45%	Improved processing/mold release/bonding vs. B-641C, B-651C	Injection—compression molding of metal-bonded parts
B-601C	60	1.85	68.5	20	-14	+35 to 45%	Excellent balance of resistance to compression set/fluids	FDA-compliant**: compression – injection molding of O-rings, simple shapes
B-651C	60	1.85	68.5	30	-14	+35 to 45%	Excellent mold flow, very good tear resistance, bonding to metal inserts	Compression – injection molding of complex shapes, bonded metal inserts
B-Types: Gum Polymers								
GBL-200S	20-30	1.85	67.0	30	-16	+40 to 50%	Excellent resistance to automotive lubricating oils, aqueous fluids	FDA Compliant** Transfer – compression molding auto lubricating oil, coolant system seals
GBL-600S	65	1.85	67.0	30	-16	+40 to 50%	Excellent resistance to automotive lubricating oils, aqueous fluids	FDA Compliant** Compression molding automotive lubricating oil, coolant system seals
B-202	20	1.86	68.5	25	-14	+35 to 45%	Excellent extrudability; lower MeOH permeability than A-types	FDA-compliant**: high shear extrusion applications—fuel hose veneer, coatings
B-600	60	1.86	68.5	20	-14	+35 to 45%	Intermediate viscosity, excellent polymer rheology, superior fluids resistance	FDA-compliant**: compression, transfer, and injection molding

*Nominal physical properties typical of those that can be expected of vulcanizates based on the specific type of Viton® noted, in a 70A hardness, MT carbon black-filled formulation. These are not intended to serve as specifications.
**Various types of Viton® curative-containing precompounds have been determined to be in compliance with FDA 21 CFR-177.2600—Rubber Articles for Repeated Food Contact.

12

Table 6
Viton® Fluoroelastomer Product Listing *(cont'd.)*

	Polymer Properties			Nominal Physical Properties*				
Viton® Product Type	Nominal Viscosity, ML1 + 10 at 121°C	Specific Gravity	Polymer Fluorine Content, %	Compression Set, % 70 hr/200°C	Temperature of Retraction (TR-10) °C	Volume Increase, After 7 days/ MeOH/23°C	Viton® Fluoroelastomer Product Description	Viton® Fluoroelastomer Product Suggested Uses/ Applications
F-Types: Curative-Containing Precompounds								
F-605C	60	1.90	69.5	30	-8	+5 to 10%	Improved polymer base vs. F-601C—improved rheology, compression set	FDA-compliant**: compression molded goods requiring best fluids resistance
F-Types: Gum Polymers								
GF-200S	25-30	1.91	70.0	35	-6	+3 to 5%	Low viscosity version of GF-600S	FDA-compliant**: Injection transfer, or compression molded goods requiring best fluids resistance
GF-600S	65	1.91	70.0	35	-6	+3 to 5%	Superior resistance to broad range of fluids and chemicals, including MeOH	FDA-compliant**: Compression molded goods requiring best fluids resistance
Low-Temperature Types of Viton® Polymer								
GLT Types								
GLT-200S	25-30	1.78	64.0	30	-30	+75 to 105%	20-30 Mooney GLT: best FKM low-temperature flexibility	FDA Compliant** Injection – transfer molded automotive fuel, chemical, petroleum industry seals
GLT-600s	65	1.78	64.0	35	-30	+75 to 105%	Medium viscosity version of GLT	FDA Compliant** Transfer – compression molded automotive fuel, chemical, petroleum industry seals
GBLT Types								
GBLT-200S	25-30	1.80	65.0	40	-26	+65 to 90%	Low-temperature flexibility/fluid resistance intermediate between GLT/GFLT types	Fuel systems parts: resistance to low oxygenates, low-temperature flexibility
GBLT-600S	65	1.80	65.0	35	-26	+65 to 90%	Low-temperature flexibility/fluid resistance intermediate between GLT/GFLT types	Fuel systems parts: resistance to low oxygenates, low-temperature flexibility

*Nominal physical properties typical of those that can be expected of vulcanizates based on the specific type of Viton® noted, in a 70A hardness, MT carbon black-filled formulation. These are not intended to serve as specifications.

**Various types of Viton® curative-containing precompounds have been determined to be in compliance with FDA 21 CFR-177.2600—Rubber Articles for Repeated Food Contact.

13

Table 6
Viton® Fluoroelastomer Product Listing *(cont'd.)*

	Polymer Properties			Nominal Physical Properties*				
Viton® Product Type	Nominal Viscosity, ML1 + 10 at 121°C	Specific Gravity	Polymer Fluorine Content, %	Compression Set, % 70 hr/200°C	Temperature of Retraction (TR-10) °C	Volume Increase, After 7 days/ MeOH/23°C	Viton® Fluoroelastomer Product Description	Viton® Fluoroelastomer Product Suggested Uses/ Applications
GFLT Types								
GFLT-200S	25-30	1.86	66.5	35	-24	+5 to 10%	30 ML GFLT: best combination of low-temperature flexibility/fluids resistance	Bonded fuel systems parts: resistance to oxygenates, low-temperature flexibility
GFLT-600S	65	1.86	66.5	40	-24	+5 to 10%	65 ML GFLT: best combination of low-temperature flexibility/fluids resistance	Bonded fuel systems parts: resistance to oxygenates, low-temperature flexibility
Viton® Extreme™ Types								
ETP-600S	60	1.82	67.0	40	-12	+10 to 15%	Outstanding resistance to fluids/chemicals, including low molecular weight acids, aldehydes, ketones	FDA-compliant**: Transfer – compression molded seals, gaskets

*Nominal physical properties typical of those that can be expected of vulcanizates based on the specific type of Viton® noted, in a 70A hardness, MT carbon black-filled formulation. These are not intended to serve as specifications.

**Various types of Viton® curative-containing precompounds have been determined to be in compliance with FDA 21 CFR-177.2600—Rubber Articles for Repeated Food Contact.

Applications

Automotive

Parts produced from Viton® fluoroelastomer are widely used in the automotive industry because of their outstanding heat and fluid resistance. They are used in the following areas:

Powertrain Systems

- Crankshaft seals, Valve stem seals, Transmission seals
- Air Intake Manifold gaskets

Fuel Systems

- Veneered fuel hose
- In-tank fuel hose and tubing
- Pump seals, Diaphragms and Injector O-rings
- Accelerator pump cups
- Filter caps and filter seals
- Fuel sender seals, Carburetor needle tips

Appliances

The heat and fluid resistance of Viton® fluoroelastomer, coupled with its good mechanical strength, makes it a natural choice for many appliance parts. The use of seals and gaskets of Viton® has resulted in design of appliances in challenging environments. Here are some typical success stories:

- In one commercial automatic dry cleaning machine, no less than 107 components are made of Viton®: door seals, sleeve-type duct couplings, shaft seals, O-rings, and various static gaskets. They perform in an atmosphere of perchloroethylene fumes at temperatures up to 88°C, conditions that would quickly degrade other elastomers.
- A fluid-activated diaphragm-type thermostat for gas or electric ranges owes its success to the designer's choice of Viton® for the actuator element. Because Viton® adheres well to brass is virtually impermeable to and is not swelled or deteriorated by the fluids used, can withstand operating temperatures of 149 to 204°C, and has the mechanical strength to resist repeated flexing.

Chemical Industry

Viton® fluoroelastomer is essentially a universal seal for chemical process equipment. Its application in the chemical industry is illustrated by the following examples:

- In a pumping station that handles more than 80 different solvents, oils, and chemicals, seals of Viton® are used in the piping's swivel and telescoping joints. When these joints were inspected after two years' service, they were found to be as good as new.
- Valves lined with Viton® reduce heat and corrosion worries in many plants.
- Hose made of Viton® transfers solvents and reactive petrochemicals to and from processing and distribution facilities. There are installations on ocean tankers as well as on highway trailers.
- Processing rolls for hot or corrosive service are covered with Viton®.
- Flange gaskets for glass-bodied valves in a paper bleaching plant are of Viton®.
- Viton® replaced caulking on a process equipment enclosure, previously plagued with hot solvent leaks, and saved $4,000 per year in maintenance costs.
- Aerosol-propelled solvent solutions of Viton® are sprayed on chemical process equipment as multi-purpose maintenance coatings.

Industrial Use

The good mechanical properties of Viton® fluoroelastomer have permitted it to replace conventional elastomers in a range of applications that cut across industry lines. To cite a few:

- Stable-dimensioned O-rings in the meters of automatic gasoline blending pumps
- High vacuum seals for the world's most powerful proton accelerator
- Heat- and corrosion-resistant expansion joints for a utility company's stack gas exhaust ducts
- Tubing and seals for a variety of top-quality industrial instruments
- Compression pads for heavy-duty vibration mounts used for portable missile ground control apparatus
- Conveyor rolls for a solvent cleaning machine
- Packing rings for hydraulic activators on steel mill ladles
- Clamp cushions for parts dipped in 285°C solder
- Jacketing for steel mill signal cable
- Deflector rolls on high-speed tinplating lines
- Precision-molded balls for check valves in oil or chemical service
- O-ring seals for test equipment in an automotive manufacturer's experimental lab

Aerospace

Reliability of materials under extreme exposure conditions is a prime requisite in this field. Aircraft designers report that O-rings of Viton® fluoroelastomer have a useful thermal range of –54 to 316°C and that Viton® exhibits "long and consistent life," even at the upper end of this range. Higher temperatures can be tolerated for short periods. Viton® also resists the effects of thermal cycling, encountered in rapid ascent to and descent from the stratosphere. Other desirable characteristics of Viton® that are pertinent to aerospace applications are its excellent abrasion resistance and its ability to seal against "hard" vacuum, as low as 10^{-9} mm Hg (133 nPa), absolute.

The high-performance properties of Viton® have been demonstrated in these typical aircraft and missile components:

- O-rings and Manifold gaskets
- Coated fabric covers for jet engine exhausts between flights
- Firewall seals
- Abrasion-resistant solution coating over braid-sheathed ignition cable
- Clips for jet engine wiring harnesses
- Tire valve stem seals
- Siphon hose for hot engine lubricants

Fluid Power

Designers and engineers are discovering that seals of Viton® fluoroelastomer work better and last longer than any other rubber in most fluid power applications. Viton® seals effectively up to 204°C and is unaffected by most hydraulic fluids, including the fire-resistant types. Seals of Viton® can also cut maintenance costs under more moderate service conditions (below 121°C) by providing longer, uninterrupted seal reliability.

Some applications in which seals of Viton® can reduce fluid loss and minimize downtime include the following:

- Actuators are the hydraulic components most likely to develop small, steady leaks when rubber seals wear and lose resilience, which can be extremely expensive. In a working year, day-to-day leakage from the average hydraulic system wastes enough fluid to completely fill the system more than four times. Viton® prevents or reduces leakage by maintaining its toughness and resilience longer than other rubber seal materials under normal fluid power conditions.
- In pumps, poor sealing performance increases operating costs by wasting power. When internal seals lose resilience and allow more slippage than the pump design permits, power is wasted. When seals swell and drag, power is wasted. Seals of Viton® keep their resilience and don't swell, thus preventing power waste and helping hold down operating costs.

Test Procedures

Property Measured	Test Procedure
Compression Set	ASTM D3955, Method B (25% deflection)
Compression Set—Low Temperature	ASTM D1299, Method B (25% deflection)
Compression Set, O-Rings	ASTM D1414
Hardness	ASTM D2240, durometer A
Mooney Scorch	ASTM D1646, using the small rotor. Minimum viscosity and time to a 1-, 5-, or a 10-unit rise are reported.
Mooney Viscosity	ASTM D1646, ten pass 100°C and 121°C
ODR (vulcanization characteristics measured with an oscillating disk cure meter)	ASTM D2084
Property Change After Oven Heat-Aging	ASTM D573
Stress/Strain Properties 100% Modulus Tensile Strength Elongation at Break	ASTM D412, pulled at 8.5mm/s (20 in/min.)
Stiffness, Torsional, Clash-Berg	ASTM D1043
Temperature Retraction	ASTM D1329
Volume Change in Fluids	ASTM D471

*Note: Test temperature is 24°C, except where specified otherwise

For further information please contact one of the offices below, or visit our website at
www.dupontelastomers.com/viton

Global Headquarters – Wilmington, DE USA
Tel. +1-800-853-5515
+1-302-792-4000
Fax +1-302-792-4450

European Headquarters - Geneva
Tel. +41-22-717-4000
Fax +41-22-717-4001

South & Central America Headquarters - Brazil
Tel. +55-11-4166-8978
Fax +55-11-4166-8989

Asia Pacific Headquarters - Singapore
Tel. +65-6275-9383
Fax +65-6275-9395

Japan Headquarters – Tokyo
Tel. +81-3-5521-2990
Fax +81-3-5521-2991

The information set forth herein is furnished free of charge and is based on technical data that DuPont Performance Elastomers believes to be reliable. It is intended for use by persons having technical skill, at their own discretion and risk. Handling precaution information is given with the understanding that those using it will satisfy themselves that their particular conditions of use present no health or safety hazards. Since conditions of product use and disposal are outside our control, we make no warranties, express or implied, and assume no liability in connection with any use of this information. As with any material, evaluation of any compound under end-use conditions prior to specification is essential. Nothing herein is to be taken as a license to operate or a recommendation to infringe on patents.

Caution: Do not use in medical applications involving permanent implantation in the human body. For other medical applications, discuss with your DuPont Performance Elastomers customer service representative and read Medical Caution Statement H-69237.

DuPont™ is a trademark of DuPont and its affiliates.

Viton® and Viton® Extreme™ are trademarks or registered trademarks of DuPont Performance Elastomers.

Copyright © 1998, 2004, 2005 DuPont Performance Elastomers. All Rights Reserved.

(11/05) Printed in U.S.A.
Reorder no: VTE-H68134-00-F1105

DuPont Performance Elastomers

3.5.3 Eutectic Analysis of Ti-6Al-4V with Plutonium and Copper

LA-UR 08-07663

Plutonium Metal Compatibility with Materials of the Ti-6Al-4V Packaging System

Prepared by:
Richard E. Mason, PMT-1
and
Stephen P. Willson, PMT-1

2 December 2008

Los Alamos National Laboratory, an affirmative action/equal opportunity employer, is operated by the Los Alamos National Security, LLC for the National Nuclear Security Administration of the U.S. Department of Energy under contract DE-AC52-06NA25396. By acceptance of this article, the publisher recognizes that the U.S. Government retains a nonexclusive, royalty-free license to publish or reproduce the published form of this contribution, or to allow others to do so, for U.S. Government purposes. Los Alamos National Laboratory requests that the publisher identify this article as work performed under the auspices of the U.S. Department of Energy. Los Alamos National Laboratory strongly supports academic freedom and a researcher's right to publish; as an institution, however, the Laboratory does not endorse the viewpoint of a publication or guarantee its technical correctness.

1

LA-UR-08-07663

Abstract

This technical basis report considers phase stability of plutonium metal encapsulated in a Ti-6Al-4V ampoule. The maximum temperature that these materials will be exposed to is 582°C. The plutonium metal may also be encapsulated in tantalum foil plus beryllium is potentially in contact with the plutonium. It is concluded by analysis of phase diagrams and composition of materials for all possible binary systems that no liquid phases are expected in this system at 582°C. Furthermore, it is anticipated that the lowest melting point phase that may form within this system is 595°C – the plutonium/beryllium eutectic temperature. This is 13°C higher than the highest temperature excursion considered for the system. This is not a large margin but the 595°C value is a conservative estimate, thus the system in a transient reaching 582°C is still considered safe. Review of the ternary phase diagrams available in the literature involving components of this system supports the conclusions drawn from the binary systems, however, the ternary systems are limited and this is a much more complex system than reviewed in the binary or ternary systems available in the literature.

LA-UR-08-07663

Table of Contents

INTRODUCTION **4**

INTERFACIAL REACTION ZONES **6**

Aluminum *6*
Beryllium *8*
Copper *10*
Gallium *11*
Plutonium *12*
Tantalum, Titanium, and Vanadium *13*
Binary interaction summary *13*

INVESTIGATION OF TERNARY SYSTEMS **14**

ADDITIONAL CHEMICAL REACTION **15**

CONCLUSIONS **15**

REFERENCES **15**

LA-UR-08-07663

Introduction

The PAT-1 (Plutonium Air Transport) package was originally designed to transport plutonium oxide across the country and to other countries that process plutonium oxide. The TB-1 containment vessel was designed to contain this material. The TB-1 vessel is stainless steel. Because of the need to air transport alpha and delta-stabilized plutonium metal, the container or ampoule inside the TB-1 containment vessel is newly constructed of the Ti-6Al-4V alloy to protect the TB-1 vessel from attack by plutonium. This analysis focuses on binary eutectic compositions that could form in a hypothetical accident scenario in which the TB-1 vessel attains a maximum temperature of 582°C and is exposed to this temperature for up to four days. Within the liner is a copper foam support structure of ≥99.99% copper, and an alpha or delta-stabilized plutonium metal sample. Plutonium metal is loaded into the copper foam and the combined package is loaded into the Ti-6Al-4V liner in an inert atmosphere glove box. The interior void space of the liner is flushed with helium, then sealed and leak-checked.

The melting points of pure metals considered for this analysis are presented in Table 1.[Lide 1991] A summary of the lowest melting points for the possible binary systems has been taken from the binary phase diagrams, and assembled in Table 2.

Table 1. Melting points of pure metals considered in this system.

Element	Melt Temperature (°C)
Aluminum	660
Beryllium	1287
Copper	1085
Gallium	30
Plutonium	640
Tantalum	3017
Titanium	1668
Vanadium	1910

LA-UR-08-07663

Table 2. Lowest melting points and compositions derived from binary phase diagrams.

System	Lowest Melting Point (°C)
Ti6Al4V	1604°C
Aluminum – Beryllium	644°C eutectic
Aluminum – Copper	548°C at compositions between pure aluminum and about 45 atom percent aluminum, 660C for copper alloying with aluminum up to about 3 weight percent Al, greater than 600°C for aluminum alloying with copper up to 25 weight percent Cu
Aluminum – Gallium	26.3°C eutectic
Aluminum – Plutonium	640°C for pure Pu
Aluminum – Tantalum	660C for pure Al
Aluminum – Titanium	660°C for pure Al
Aluminum – Vanadium	660°C for pure Al
Aluminum – Beryllium	644°C eutectic
Beryllium – Copper	The congruent melt temperature of 858°C is the lowest melt temperature in the binary system
Beryllium – Gallium	30°C the gallium melt temperature. The gallium melts and there is minimal solution of the beryllium below 600°C
Beryllium – Plutonium	The additions of small amounts of beryllium may lower the plutonium rich metal to a melt temperature of 595°C
Beryllium – Tantalum	1287°C as there was no binary phase diagram found
Beryllium – Titanium	1287°C of pure Beryllium
Beryllium – Vanadium	1287°C of pure Beryllium
Copper – Gallium	625°C for phases containing greater than 55 atom percent gallium
Copper – Plutonium	626°C for 6 atom% Cu, 1.7 wt% Cu
Copper – Tantalum	1085°C of pure Cu
Copper – Titanium	880°C for 27 atom% Ti, 22 wt% Ti
Copper – Vanadium	1085°C for pure Cu
Titanium – Vanadium	>1600°C for 30 wt% V
Gallium – Aluminum	Compositions above 2 atom% (5 wt%) gallium are liquid at 625°C
Gallium – Copper	Compositions above 55 atom% gallium (57 wt%) are liquid at 625°C
Gallium – Plutonium	Compositions above 75 atom% gallium (47 wt%) are liquid at 625°C
Gallium – Titanium	Compositions above 99 atom% gallium (99 wt%) are liquid at 625°C
Gallium – Vanadium	Compositions above 97 atom% gallium (98 wt%) are liquid at 625°C
Plutonium – Tantalum	640°C of pure Pu
Plutonium – Titanium	640°C of pure Pu
Plutonium – Vanadium	625°C for < 2 wt% V
Tantalum – Titanium	1668°C for pure Ti
Tantalum – Vanadium	1910°C for pure V
Titanium – Vanadium	1668°C for pure Ti

LA-UR-08-07663

Interfacial Reaction Zones

Reactions between metals of the Ti-6Al-4V alloy with the contents it will hold are restricted to contact zones between different metal compositions. Because none of the major individual starting materials reach their melting points during a 582°C temperature excursion, formation of new phases must depend upon solid state transport of material from one of the original phases into another. The original starting materials are not pure materials. Gallium is never in the system as a metal but is dissolved in plutonium and the gallium-plutonium alloy has a melting point well above 582°C. Redistribution of the gallium into a pure metal will not be an issue. Gallium can only influence the performace of the materials in this system if it diffuses to another metal or alloy. Material transport will only occur between phases that are in mechanical contact. Transport will be substantially impeded by the presence of thin surface oxide layers, which will be present on the titanium alloy, the copper, the beryllium and the plutonium. Formation of any new phases in the container, eutectic or otherwise, is explicitly dependent upon sufficient solid state mass transport, which depends on solid state solubility of the components, intimacy of contact between the components, and the time the system is held at the elevated temperature. The kinetic data that would be required to quantitatively address solid state diffusion between the plutonium, the beryllium, the copper, and the titanium ampoule is not available. Qualitative conclusions are drawn based on the available phase diagrams, which capture the thermodynamically stable compositions of binary systems, at a given temperature.

When an alloy is in contact with another metal composition, solid state transport will be different for the different components of the alloy, resulting in preferential reaction with one component, and changing the resultant concentrations of both phases by enriching one and depleting the other with respect to the most mobile component. Contact reaction zones are discussed by reference to binary phase diagrams. At the low temperature of 582°C diffusion will be slow and the integrity of the ampoule alloy will only be compromised if a liquid was to form. As long as all component combinations do not form a liquid, the ampoule will remain intact and contain the material shipped.

Aluminum

Aluminum contact with components of the Ti-6Al-4V packaging system

Aluminum is initially present at only 10 atom percent in the titanium alloy. Although aluminum binaries with the elements of this system are considered, it is improbable that interactions with aluminum alone and the other components would ever occur. The aluminum is alloyed with titanium and vanadium and all three form high temperature alloys with all of the components expected in a shipment of plutonium metal.

Aluminum contact with beryllium

The aluminum-beryllium system forms a eutectic at 644°C, 16°C below the melt temperature of pure aluminum. There are no intermediate phases thus liquid aluminum

will exist above this temperature. This temperature is higher than the maximum temperature considered for safe operation of this system..[Landolt-Bornstein 1992]

Aluminum contact with copper

The aluminum-copper system is complex with a eutectic melt temperature of 548°C at 66.8 weight percent aluminum.[Landolt-Bornstein 1992] The 548°C solidus extends from about 5.6 weight percent aluminum to about 45 weight percent aluminum. The solidus temperatures between pure copper and 45 weight percent aluminum are much higher temperatures and with five intermediate phases in the system. Aluminum is an alloying element in copper is solid at 600C up to about 25 weight percent aluminum. This is not an issue because the aluminum is a minor alloy constituent and as titanium content increases the melt temperature of the copper-titanium-aluminum will likely increase. For alloy compositions with aluminum content greater than 45 weight percent aluminum, the melt temperature is much greater than 600°C and more than 5 weight percent aluminum would have to diffuse into the copper for the melt temperature to be lower than 600°C. Significant aluminum would have to diffuse out of the ampoule alloy into the copper or aluminum into the copper. Both are impractical at the maximum temperature that these materials could be exposed to.

Aluminum contact with gallium

Gallium metal melts at 29°C and the aluminum-gallium binary is a eutectic binary system. There are no intermediate phases in this system. This binary system is a simple eutectic system with eutectic temperature at 26.6°.[Landolt-Bornstein 1992] The liquidus is well known but the boundaries of the solid phases are not well known. The solubility of aluminum in gallium metal is very low. The maximum solubility of gallium in aluminum metal is approximately 9 atom percent and the aluminum is solid at 600C up to about 7 atom percent gallium. The formation of a separate gallium-aluminum phase is not credible because both gallium and aluminum are soluble in plutonium at the compositions present and at temperatures below the melting point of plutonium. It is impractical for an alloy composition to form that would be liquid because it would simultaneously require local concentration of the aluminum to 98 atom percent. This phase is highly unlikely.

Aluminum contact with plutonium

Aluminum forms five intermediate phases with plutonium with $PuAl_2$ being the dominant intermediate phase melting at 1540±50°C. The compound Pu_3Al of the plutonium rich compositions is formed by a very sluggish peritectoid reaction between the plutonium delta phase and PuAl. [Wick 1980] Aluminum goes into solid solution with plutonium up to 10 atom percent aluminum. As the content of aluminum increases the melt temperature increases up to the $PuAl_2$ solidus at 801°C.[Wick 1980] In this binary system the combination of the two elements increases the melt temperature.

Aluminum contact with tantalum

Aluminum and tantalum form four intermediate phases. With the addition of a small amount of tantalum to the aluminum the melt temperature of aluminum metal is raised about eight degrees and the solidus exists to 25 atom percent aluminum. At 25 atom percent aluminum Al_3Ta is the solid and it melts at about 1629°C. On the tantalum rich

LA-UR-08-07663

side of Al_3Ta the solidus temperature is a bit lower but remains close to 1629°C until the intermittent phase Al_3Ta_2 is reached where the solidus temperature is a few degrees lower. Thereafter, as the concentration of tantalum increased the solidus temperature increases.[Landolt-Bornstein 1992] Again the melting temperatures of the intermediate phases are much above the maximum temperature this system will be exposed to thus the combination of these two elements will not negatively affect the safe operation of this system but will more likely decrease the likelihood of liquid formation.

Aluminum contact with titanium
At aluminum concentrations between pure and 25 atom percent aluminum the solidus is 665°C. That is, with the addition of a small amount of titanium to the aluminum the melt temperature of aluminum metal is raised about five degrees and remains the solidus to 25 atom percent aluminum. The Al_3Ti melts at about 1387°C.[Landolt-Bornstein 1992] Again the melt temperatures of the intermediate phases are much above the maximum temperature this system will be exposed to thus the combination of these two elements will not affect the safe operation of this system.

Aluminum contact with Vanadium
Aluminum and Vanadium form five intermediate phases. With the addition of a small amount of tantalum to the aluminum the melt temperature of aluminum metal is raised about two degrees and remains the solidus to about 8 atom percent aluminum. As each intermediate phase is reached the solidus temperature is increased as the concentration of Vanadium increases.[Landolt-Bornstein 1992] Again the melting temperatures of the intermediate phases are much above the maximum temperature this system will be exposed to thus the combination of these two elements will not affect the safe operation of this system.

Beryllium

Beryllium and plutonium may contact the Ti-6Al-4V container if they are not wrapped with tantalum foil and either metal penetrates the copper foam. Tantalum may also be wrapped around the beryllium and/or plutonium pieces and in this case these materials would have to penetrate the tantalum wrapping material and then the copper foam before reaching the ampoule alloy.

Beryllium contact with copper
Beryllium and copper alloys are commonly used alloying elements. An alloy of beryllium and copper with 24 atom percent copper melts at 966°C.[Landolt-Bornstein 1992] This is the lowest melting alloy in this binary system with all other compositions and phases melting at higher temperatures. The combination of beryllium and copper will not compromise the safe use of this system.

LA-UR-08-07663

Beryllium contact with gallium
Beryllium and gallium do not form intermediate phases, consequently, at temperatures above gallium's melting point of 30°C and below 600°C there is minimal mixing of the two materials.[Landolt-Bornstein 1992] If the two materials were to interact, then above 30°C the gallium will be liquid at the grain boundaries causing a decrease in mechanical strength of the beryllium. Interaction of these two components of the system is an improbable scenario because the gallium in the plutonium is in solid solution and only at quantities less than 10 atom percent.

Beryllium contact with plutonium
The main feature of the beryllium-plutonium system is one intermediate compound $PuBe_{13}$ which has a higher melt temperature than either pure constituent at 1950±50°C. The eutectic at 96 atom percent plutonium probably lowers the melt temperature only 10°C. [Wick 1980] However, one experimenter reported the eutectic melt temperature lowered by as much as 45°C. Although, Wick et al. report that a melt temperature drop of 10°C is most accurate the worse case would be the 45°C decrease from 640C of plutonium metal or a melt temperature of 595°C. At 582°C the components are still solid but close to a potential melt temperature.[Wick 1980] This is the lowest melting material or alloy of the systems considered. It is a combination of material that could be present in an accident.

Beryllium contact with tantalum
The phase equilibria are not know.[Landolt-Bornstein 1992] In a sample containing 0.05 atom percent tantalum after solidification from the melt the solidified microstructure indicated a eutectic phase and several intermediate phases with one having a melting temperature of $Be_{12}Ta$ at 1850°C and for $Be_{17}Ta_2$ a melting temperature of 1980°C.

Beryllium contact with titanium
There are four or more intermediate compounds in this system with an eutectic at 70 atom percent titanium and at a temperature of 980°C. [Murray 1987 & Ohnuma 2004] Should the beryllium penetrate the copper, the beryllium could be mechanically mixed with the titanium at the surfaces of the pieces. Even mixed the eutectic temperature is not reached and the containment not affected.

Beryllium contact with vanadium
There are three or more intermediate compounds in this system. The solidus temperature is raised more than 230°C when the vanadium content exceeds about 7 atom percent.[Landolt-Bornstein 1992] Vanadium is only 4 atom percent in the ampoule alloy but its contribution to any alloy of these systems would be to increase the melt temperature. Should the beryllium penetrate the copper beryllium could be mechanically mixed with the titanium at the surfaces of the pieces. Even mixed the eutectic temperature is not reached and the containment not affected.

LA-UR-08-07663

Copper

It is not expected that a liquid phase will form at this interface at the highest temperature of any hypothetical accident (582°C). Because the copper surrounds the metal as the structural matrix to hold the plutonium metal in favored positions within the ampoule, it is the first to interact with the plutonium, beryllium or tantalum that the plutonium metal is wrapped in. At 582°C, both copper and the titanium alloy ampoule are solid and 582°C is well below their respective melting points. Aluminum-copper compositions with more than 64 atom percent (43 weight percent) aluminum will melt at 625°C, which is also the melting point of the plutonium-vanadium eutectic, considered later in this report. Aluminum is present in the titanium alloy at a concentration of 10 atom percent. In order to form a melting composition with copper at 625°C, it needs to attain a concentration within the copper of 64 atom percent or greater. Solid state transport on the scale required for formation of a low melting phase (below 625°C) at this boundary in four days is not expected.

Copper contact with gallium

Gallium is in solid solution in copper up to about 19 to 20 atomic percent gallium with the alloying of these two metals lowering the melt temperature to about 900°C at 20 percent gallium.[Landolt-Bornstein 1992] Solid state transport of gallium from a 10 atom percent gallium-plutonium alloy into pure copper sufficient to form a 20 atom percent gallium-copper alloy is improbable. Incorporation of enough gallium into the copper at 582°C to form a liquid phase requires passage through five successive solid state phases. Formation of each of these phases requires a microstructure rearrangement before more gallium atoms can be incorporated, thus reduction of melting temperatures due to the combination of these two metals is very unlikely.

Copper contact with Plutonium

The plutonium rich component of the binary phase has a eutectic at about 6 atom percent copper and a temperature of 625°C. [Wick 1980 & Copper 2000] It is not expected that a liquid phase will form at this interface at a temperature of 582°C. First consider possible reaction of copper with alpha plutonium. Due to the softening of plutonium metal near its melting point, 640°C, and the roughly 5% expansion of alpha plutonium upon conversion to epsilon plutonium it is possible that alpha plutonium samples will tightly contact the copper foam, and reaction will occur at the interface. The progression of the reaction will be limited by the temperature actually reached, and by the time held at that temperature. The plutonium-copper eutectic composition will not melt at 582°C.

Copper contact with Tantalum

The mutual solubility of copper and tantalum is negligibly small and intermediate phases do not exist.[Landolt-Bornstein 1992] Copper and tantalum are immiscible at temperatures lower than 1083°C. Even the solubility of tantalum in liquid copper above the melting point is small. The solubility of Ta in liquid copper amounts to 0.0088 atom percent tantalum at 1200°C. Combining these two materials in this storage system will not lower the melting temperatures of the materials and are of no consequence to the safety of the system but may enhance the safety margin.

LA-UR-08-07663

Copper contact with titanium
The copper-titanium system is also a complex binary system with five intermediate phases and a eutectic at 860°C and 27 atom percent titanium.[Landolt-Bornstein 1992] Combining these two materials in this storage system will not lower the melting temperatures of the materials and are of no consequence to the safety of the system but may enhance the safety margin.

Copper contact with vanadium
The copper vanadium system is a simple eutectic system. The eutectic is on the vanadium rich side at about 15 atom percent copper and a eutectic temperature of 1530°C.[Landolt-Bornstein 1992] Combining these two materials in this storage system will not lower the melting temperatures of the materials and are of no consequence to the safety of the system but may enhance the safety margin.

Gallium

Gallium has an extremely low melting temperature when compared to the other metals in the ampoule material and the material to be shipped. The gallium is soluble in the plutonium and is a component of the plutonium up to 10 atom percent. The only thermodynamic driver of this conversion is the leaching ability of other metals from the plutonium-gallium alloy. Gallium is soluble in the plutonium epsilon phase and will not segregate to the interface and is consequently not easily leachable from the plutonium should one of the other elements have a higher affinity to alloy gallium than plutonium.

Gallium contact with Plutonium
The gallium is soluble in the plutonium up to about 10 atom percent gallium in the plutonium. The delta phase of plutonium is stabilized at room temperature by the addition of less than 10 atom% gallium. [Wick 1980] Because delta plutonium contracts upon conversion to epsilon, it will not experience increased pressure at the interface upon heating. Up to 20 atom percent gallium is soluble in the plutonium epsilon phase, so there will be no segregation of gallium upon transition to epsilon plutonium. A liquid phase will not form in the plutonium rich material until the melt temperature of plutonium is reached. There is also no driver for the gallium to segregate since it is already in solid solution

Gallium in contact with tantalum
There are four intermediate phases in this binary system and with increasing tantalum the solidus increases with each intermediate phase. The liquidus remains at 29°C until the intermediate Ga_3Ta is reached.[Landolt-Bornstein 1992] The phase relations in this system are not sufficient to give additional detail. Given sufficient gallium in the system this combination could compromise the safety of the system but there is simply insufficient gallium in the entire mass of plutonium metal to compromise the container.

Gallium in contact with titanium

LA-UR-08-07663

The gallium-titanium system requires more than 99 atom percent gallium in order to form a phase that melts at 625°C.[Landolt-Bornstein 1992] Because the gallium is soluble and stable at lower concentrations, formation of a phase with such high gallium content, nearly pure gallium is not expected to occur. Formation of a molten phase of either gallium-titanium or gallium-vanadium is unlikely given the available quantity of gallium and the thermodynamic stability of lower concentration solid phases.

Gallium in contact with Vanadium
There are four intermediate phases in this binary system and with increasing vanadium the solidus increases with each intermediate phase. The solidus remains at 29°C until the intermediate Ga_4V_8 is reached where the solidus on the vanadium rich side of this intermediate compound is 500°C. The gallium-vanadium compositions require more than 84 atom percent of gallium in order to form a phase that melts at 625°C.[Landolt-Bornstein 1992] Given sufficient gallium in the system this combination could compromise the safety of the system but there is simply insufficient gallium in the entire mass of plutonium metal to compromise the container.

Plutonium

It is not expected that a liquid phase will form at this interface. In the event that plutonium is sheared from the bulk and contacts the Ti-6Al-4V liner, consideration must be given to the interfacial reaction zone. The possible binary compositions of interest for contact between the liner and alpha plutonium include plutonium-aluminum, plutonium-titanium, and plutonium-vanadium. In the case of both plutonium-aluminum and plutonium-titanium, the melting point is increased relative to that of pure plutonium for all concentrations.

Plutonium contact with tantalum
This combination of materials is very stable and will not negatively impact the safe operation of the system. Tantalum and plutonium form a eutectic very close to pure plutonium. The eutectic reduces the melt temperature by only a degree or two. At temperatures above the 640°C solid tantalum can contain increasing plutonium up to about 25% plutonium near 2550°C.[Boxi 1991] There is also significant solubility of plutonium in the tantalum metal at temperatures above the plutonium melt temperature but limited solubility of plutonium in tantalum at temperatures below 640°C. [Wick 1980] Consequently, pure plutonium stored in pure tantalum foil is compatible at temperatures below plutonium's melting temperature. Above plutonium's melt temperature there is little reaction except that as the temperature rises an increasing amount of plutonium will diffuse into the tantalum metal matrix.

Plutonium contact with titanium
There are no intermediate phases in the binary system. A peritectiod composition at 6.5 atom percent titanium increases the solubility of titanium in the plutonium metal to a maximum of 25 atom percent at 770°C. Above the melting temperature of plutonium the liquid plutonium will combine with the tantalum to form a solid mixture up to 770°C, the highest solidus temperature in the system.[Landolt-Bornstein 1992] This reaction would stabilize the system in a high temperature transient situation.

LA-UR-08-07663

Plutonium contact with vanadium
The plutonium-vanadium eutectic composition forms with less than 2 weight percent vanadium resulting in a solidus temperature of 625°C from 2 to 100 weight percent vanadium. At all concentrations of more than 2 wt% vanadium in plutonium, and at a temperature of 625°C or higher, the plutonium-vanadium system exhibits a liquid phase.[Landolt-Bornstein 1992] At all compositions, at temperatures less than 625°C, only solid phases are present. If mobility into the solid plutonium metal leaves the ampoule alloy depleted in one of its other constituents, the melting point of the liner in the depleted zone will be increased.

Tantalum, Titanium, and Vanadium

Vanadium and aluminum are the minor constituents of the alloy of the ampoule at 10 atom percent or less. Consequently, titanium will probably dominate the interactions of the container with the packaged material. When tantalum is used to wrap the plutonium metal it too will be a major contributor to the performance of the shipping container during the transient. Interaction between or alloying of these four components aluminum, tantalum, titanium and vanadium produce material that will probably not form lower melt temperature

Tantalum contact with titanium
The Ti-Ta binary phase diagram is characterized by an isomorphous body centered cubic phase field extending from pure titanium at elevated temperatures to pure tantalum with limited mutual solubilities.[Landolt-Bornstein 1992] Since there are no intermediate phases and the solidus is essentially linear between the melt temperature of titanium (1670°C) and tantalum (3017°C), a combination of these metals with other compound will probably increase the melt temperature of the system.

Tantalum contact with Vanadium
There are no intermediate phases and the solidus and liquidus increase from the 1910°C melt temperature to the 3017°C melt temperature of tantalum. Addition of any of these two metals will likely increase the melt temperature of the resulting mixture.

Titanium contact with Vanadium
There are three intermediate phases and the solidus and liquidus increase from the 1668°C titanium melt temperature to the 1910°C melt temperature of vanadium.[Landolt-Bornstein 1992] Addition of any of these two metals will likely increase the melt temperature of the resulting mixture of container and package materials.

Binary interaction summary

The lowest melt temperature is 595°C between the plutonium and beryllium with the next lowest between the plutonium-vanadium eutectic at 625°C. The 595°C temperature may be a low estimate because of impurities in the material tested with the melt temperature of the beryllium-plutonium probably closer to 630°C. However, for safety evaluations this is the worst case temperature.

LA-UR-08-07663

The lowest melting phase with plutonium/vanadium liner contact is 625°C, and is unlikely to form based on the absence of a clean contact surface under pressure between the plutonium and the liner. The melting temperature of this eutectic is 43°C higher than that of the proposed high temperature excursion.

Addition of the beryllium to the system brings the melt temperature close to the maximum temperature that the ampoule may be exposed to. If all the components internal to the titanium ampoule are combined and intimately mixed, that is, plutonium, beryllium, gallium, tantalum, and copper are completely alloyed, the melt temperature could be lower than 582°C. There is no data to show otherwise and 595°C is close to this temperature. However, it is unlikely and impractical to intimately mix these components together by mechanical impact and then expose them to temperatures above the binary melting points. Significant work on this complex metal alloy system would be required if a mechanism could be hypothesized to form such an alloy by impact of separate alloys and metals but it is not considered plausible.

Investigation of Ternary Systems

Published information was available for eleven of the possible ternary systems considered.[Petzow 1992 & Villars 1995] The Ti-6Al-4V alloy was designed to be solid to 1604°C. The tantalum-titanium-aluminum system is solid above 1100C.[Weaver 1995] It is generally true that for the ternary phase diagrams reviewed, there was little new information with respect to melting temperatures that was not captured by the binary diagrams. Expected compositions are those that do not require achieving large concentrations of a particular element in a phase against a strong concentration gradient. For example, given that aluminum begins at 10 atom percent in the titanium alloy used, it is considered unlikely that it would achieve concentrations of 20 atom percent or more in another phase. The same rule is applied with respect to the vanadium and gallium components, both of which begin at low concentrations in their respective thermodynamically stable alloys.

Reviewed binary and ternary systems that possess a liquid component at temperatures below 625°C are those with high concentrations of aluminum and gallium (greater than 50 atom percent combined aluminum and gallium content). It is considered improbable that with less than 9 atom percent gallium in the plutonium and 10 atom percent aluminum in the titanium alloy, any phases will form containing more than 50 atom percent combined gallium and aluminum.

In both titanium and plutonium, aluminum and gallium may substitute for each other, partially or completely, without altering the observed phase. Several of the ternary systems reviewed show no ternary phases, only mixtures of binary phases, all of which have already been captured by the preceding review of binary phase diagrams. The only ternary diagram available that contained plutonium was the aluminum-gallium-plutonium diagram.

Conclusions drawn by reference to the binary phase diagrams are consistent with the information present in the ten available ternary phase diagrams.

Additional Chemical Reaction

Finely divided metals tend to oxidize rapidly in air due to the high surface area relative to mass of metal present. The oxidation reaction for a metal is generally exothermic, and in the event of finely divided powders in air, can often result in pyrophoricity. During the proposed accident scenario for this analysis, the system containment is not mechanically breached, and an inert environment is maintained. The small amount of oxygen in the system will exist as oxide on the various system components, rather than as gaseous oxygen. In the event that small particles are generated within the titanium alloy ampoule, they will not ignite due to an absence of oxygen necessary for the reaction. The initial system components are bulk metal materials. These are not pyrophoric.

Conclusions

All of the expected phases formed from the original materials at a temperature of 582°C are solid. The lowest probable binary phase melting point is 595°C (plutonium-Beryllium). The second lowest probable binary phase melting point is 625°C (plutonium-vanadium) and the third lowest melting point is 626°C (plutonium-copper). The lowest is possible if other impurities not considered in this technical basis were present. It is anticipated that the second and third lowest compositions will not form due to the presence of surface oxide layers on the initial components of the system. A review of available ternary phase diagrams supports the conclusions drawn from the binary phase diagrams. However, the many combinations of the product materials and the container materials make it impossible to absolutely rule out a lowering of the melting point due to mechanical mixing that could occur in a severe impact and post impact fire until some testing verification on the materials are conducted.

References

Boxi, H.C., Massalski, T.B., and Rizzo, H.F., 1991, *The Pu-Ta (Plutonium-Tantalum) System*, Journal of Phase Equilibria, 12 No. 5 pp 593

Brandes, E. A., ed. 1983. Smithells Metals Reference Book, Sixth Edition. Ch. 11.

Kaufmann, A.R., Gordon, P., Lillie, D.W. 1950, ASM Trans. Q. **42** p 801.

Cooper, N. G., ed. 2000. *Challenges in Plutonium Science, Volume II.* Plutonium and Its Alloys. pp. 291-335.

Landolt-Bornstein – Group IV Physical Chemistry Volumes 5b and 5j (1992)

Lide, D. R., ed. 1991. *CRC Handbook of Chemistry and Physics*, pp. 4-122, 4-123.

LA-UR-08-07663

Murray, J.L., 1987, The Be-Ti (Beryllium-Titanium) System, *Phase Diagrams of Binary Titanium Alloys,* J.L. Murray, Ed., ASM International, p 40-43

Ohnuma, I.; Kainuma, R.; Uda, M.; Iwadachi, T.; Uchida, M., Kawamura, H., and Ishida, K., 2003 "Phase Equilibria in the Be-V and Be-Ti Binary Systems," *Proc. Sixth International Workshop on Beryllium Technology for Fusion, 2003*, Japan. Atom. Energy Res. Inst.,

Petzow, G., Effenberg, G., ed., 1992, *Ternary Alloys.* VCH Publishers, NY, NY: ASM International.

Villars, P.; Prince, A.; Okamoto, H., 1995. *Handbook of Ternary Alloy Phase Diagrams.* Materials Park, OH: ASM International.

Weaver, M.L. and Kaufman, M.J., 1995 "Phase Relationships and Transformations in the Ternary Aluminum-Titanium-Tantalum system," *Acta metall, mater.* Vol. 43, No. 7, pp. 2625-2640.

Wick, O. J., ed. 1980. *Plutonium Handbook.* Chaps. 7 and 12-3. La Grange Park, IL: American Nuclear Society

3.5.4 Determination of Most Damaging Package Orientation for HAC Analysis

This section of the Appendix contains a summary of the calculations used to determine which package orientation is the most thermally damaging configuration for the HAC analysis. The PAT-1 package was considered as a cylinder exposed to a fully-engulfing, uniform temperature, fire and to an open (cool) environment in both the vertical and the horizontal orientations. In both orientations, the maximum heat flux exchange between the package and the environment occurs soon after the fire starts or soon after the fire is extinguished. Assuming a fire environment temperature of 800°C (1472°F), an ambient temperature of 38°C (100°F), and equal view factor and emissivity for both orientations, the difference in absorbed or released heat flux between a vertically- and a horizontally-oriented package would be a function of the convective heat flux exchange only. Whether the package is heating or cooling, or in the vertical or horizontal positions, the model assumes the following dimensions, thermal conditions, and gas properties:

Parameters	Values
Hot temperature	$T_h := 1073K$
Cold temperature	$T_c := 311K$
Flow velocity during fire	$V = 5\frac{m}{s}$
Diameter of package	$D := 0.5715m$
Length of package	$L := 1.08585m$
Conductivity of the fluid (Air)	$k_f := 52 \cdot 10^{-3}\frac{W}{m \cdot K}$
Kinematic viscosity of fluid (Air)	$\nu := 68 \times 10^{-6}\frac{m^2}{s}$
Thermal diffusivity (Air)	$\alpha := 98 \times 10^{-6}\frac{m^2}{s}$
Prandtl Number	$Pr := \frac{\nu}{\alpha} = 0.694$
Area of cylindrical sides	$A_{cyl} := \pi \cdot D \cdot L = 1.95m^2$
Area of cylindrical ends	$A_{ends} := \frac{\pi \cdot D^2}{4} = 0.257m^2$

During the fire, convection is predominately considered to be forced convection as suggested by the ratio of Gr/Re^2 given in Table 3-9 of the Addendum. This ratio is much less than one; hence, only force convection is considered. On the other hand, during the cool-down process, convection is predominately free convection since the buoyancy forces are weak with no imposed flow. Therefore, there are four cases that need to be considered to determine which package orientation is the most thermally damaging configuration for the PAT-1:

1. Horizontal orientation with force convection during the fire
2. Vertical orientation with force convection during the fire
3. Horizontal orientation with free convection during the cool down period
4. Vertical orientation with free convection during the cool down period

In Case 1, the package is in the horizontal position and gas flows around the perimeter of the cylinder and across the vertical flat ends with an imposed velocity of 5 m/s (16.4 ft/s). In Case 2, the package is in the vertical position and gas "impinges" on the bottom (flat end) of the cylinder and flows across the vertical cylinder walls at an imposed velocity of 5 m/s (16 ft/s). In both cases, the maximum convection heat transfer will occur initially during the fire when the temperature of the fire is much greater than that of the package. For both of these cases, the following Nusselt (Nu_{avg}) number correlation is used to determine the effective convective heat transfer coefficient:

$$Nu_{avg}(C, m, Re, Pr) := C \cdot Re^{m} \cdot Pr^{\frac{1}{3}},$$

where *C* and *m* are experimentally determined coefficients; *Re* is the Reynolds number; and *Pr* is the Prandtl number. The coefficients *C* and *m* vary with the relative orientation between the flow and the object and with the geometry of the object. Values for *C* and *m* are given in Incropera and Dewitt (1996) and in Kobus and Shumway (2006).

The equations below show the calculations performed to obtain the effective convection heat transfer coefficient for Case 1. The effective convective heat transfer coefficient was obtained by assuming the same temperature difference for all surfaces (i.e., T_h-T_s).

$Re := \frac{V \cdot D}{\nu} = 4.202 \times 10^4$	
$Nu_{cyl} := Nu_{avg}(0.027, 0.805, Re, Pr) = 125.996$	$Nu_{ends} := Nu_{avg}(0.68, 0.5, Re, Pr) = 123.408$
$h_{cyl} := \frac{k_f \cdot Nu_{cyl}}{D} = 11.464 \frac{W}{m^2 \cdot K}$	$h_{ends} := \frac{k_f \cdot Nu_{ends}}{D} = 11.229 \cdot \frac{W}{m^2 \cdot K}$
$h_{hor_eff} := \frac{h_{cyl} \cdot A_{cyl} + 2 \cdot h_{ends} \cdot A_{ends}}{A_{cyl} + 2 \cdot A_{ends}} = 11.415 \cdot \frac{W}{m^2 \cdot K}$	

The following equations show the calculations performed to obtain the effective convection heat transfer coefficient for Case 2. Note that the top (flat) end of the vertical cylinder is conservatively assumed to have the same convective heat transfer coefficient as the bottom ("impinged") flat end.

$Re_{cyl} := \frac{V \cdot L}{\nu} = 7.984 \times 10^4$	$Re_{end_btm} := \frac{V \cdot D}{\nu} = 4.202 \times 10^4$
$Nu_{cyl} := Nu_{avg}(0.68, 0.5, Re_{cyl}, Pr) = 170.10$	$Nu_{end_btm} := Nu_{avg}(0.966, 0.46, Re_{end_btm}, Pr) = 114.5$
$h_{cyl} := \frac{k_f \cdot Nu_{cyl}}{L} = 8.146 \cdot \frac{W}{m^2 \cdot K}$	$h_{end_btm} := \frac{k_f \cdot Nu_{end_btm}}{D} = 10.42 \cdot \frac{W}{m^2 \cdot K}$
$h_{ver_eff} := \frac{h_{cyl} \cdot A_{cyl} + 2 \cdot h_{end_btm} \cdot A_{ends}}{A_{cyl} + 2A_{ends}} = 8.62 \cdot \frac{W}{m^2 \cdot K}$	

In Case 3 and Case 4, free convection dominates since the package is allowed to cool naturally. In both cases, the maximum free convection heat transfer will occur immediately after the fire which is when the temperature of the package is much higher than that of the environment. The following Nu_{avg} correlations are used to determine the effective convective heat transfer coefficient for both of these cases:

Nusselt number for free flow across a cylinder

$$Nu_{cyl}(Ra, Pr) := \left[0.60 + \frac{0.387 \cdot Ra^{\frac{1}{6}}}{\left[1 + \left(\frac{0.559}{Pr} \right)^{\frac{9}{16}} \right]^{\frac{8}{27}}} \right]^2$$

Nusselt number for free flow across a plate

$$Nu_{plate}(Ra, Pr) := \left[0.825 + \frac{0.387 \cdot Ra^{\frac{1}{6}}}{\left[1 + \left(\frac{0.492}{Pr} \right)^{\frac{9}{16}} \right]^{\frac{8}{27}}} \right]^2$$

Nusselt number for free flow perpendicular to a circular plate

$$Nu_{cyl_ends}(C, m, Ra) := C \cdot Ra^m$$

where *Ra* is the Raleigh number, and *C* and *m* are empirical constants determined from experiments. The constants *C* and *m* vary with the relative orientation between the flow and the object. Values for *C* and *m* are given in Incropera and Dewitt (1996).

The equations below show the calculations performed to obtain the effective convection heat transfer coefficient for Case 3.

$Gr := \frac{g \cdot (T_h - T_c) \cdot D^3}{\frac{(T_c + T_h)}{2} \cdot \nu^2} = 4.4 \times 10^8$	$Ra := Gr \cdot Pr = 3 \times 10^8$
$Nu_{hcyl} := Nu_{cyl}(Ra, Pr) = 79.354$	$Nu_{ends} := Nu_{plate}(Ra, Pr) = 84.915$
$h_{hcyl} := \frac{Nu_{hcyl} \cdot k_f}{D} = 7.22 \cdot \frac{W}{m^2 \cdot K}$	$h_{ends} := \frac{Nu_{ends} \cdot k_f}{D} = 7.726 \cdot \frac{W}{m^2 \cdot K}$
$h_{hor_eff} := \frac{h_{hcyl} \cdot A_{cyl} + 2 \cdot h_{ends} \cdot A_{ends}}{A_{cyl} + 2A_{ends}} = 7.326 \cdot \frac{W}{m^2 \cdot K}$	

The following equations show the calculations performed to obtain the effective convection heat transfer coefficient for Case 4. Note that the Nusselt number for flow over a plate was used for the cylindrical sides of the package. This assumption is valid as long as the ratio of D/L is greater or equal to the ratio of $35/Gr^{0.25}$.

$Gr_{vcyl} := \frac{g \cdot (T_h - T_c) \cdot L^3}{\frac{(T_h + T_c)}{2} \cdot \nu^2} = 3 \times 10^9$	$Gr_{ends} := \frac{g \cdot (T_h - T_c) \cdot D^3}{\frac{(T_h + T_c)}{2} \cdot \nu^2} = 4.4 \times 10^8$
$Ra_{vcyl} := Gr_{vcyl} \cdot Pr = 2.1 \times 10^9$	$Ra_{ends} := Gr_{ends} \cdot Pr = 3 \times 10^8$
$\frac{D}{L} \geq \frac{35}{Gr_{vcyl}^{\frac{1}{4}}}$	Since D/L is greater than the ratio of $35/Gr^{0.25}$, the vertical plate correlation can be used for the vertical walls of the cylinder.
$Nu_{vcyl} := Nu_{plate}(Ra_{vcyl}, Pr) = 153.5$	$h_{vcyl} := \frac{Nu_{vcyl} \cdot k_f}{L} = 7.4 \cdot \frac{W}{m^2 \cdot K}$
$Nu_{btm_end} := Nu_{cyl_ends}(0.27, 0.25, Ra_{ends}) = 35.6$	$h_{btm_end} := \frac{Nu_{btm_end} \cdot k_f}{D} = 3.2 \cdot \frac{W}{m^2 \cdot K}$
$Nu_{top_end} := Nu_{cyl_ends}(0.54, 0.25, Ra_{ends}) = 71.2$	$h_{top_end} := \frac{Nu_{top_end} \cdot k_f}{D} = 6.5 \frac{kg}{K \cdot s^3}$
$h_{ver_eff} := \frac{h_{vcyl} \cdot A_{cyl} + h_{btm_end} \cdot A_{ends} + h_{top_end} \cdot A_{ends}}{A_{cyl} + 2 \cdot A_{ends}} = 6.8 \cdot \frac{W}{m^2 \cdot K}$	

In all cases, the difference between the vertical and the horizontal orientation was minimal, with the horizontal orientation being slightly more severe for the package. That is, the horizontal configuration provides the highest convection during the fire and the lowest convection during the cool-down.

For the HAC analysis in the Addendum, a value of 11.5 W/m^2-K (2.03 Btu/hr-ft^2-°F) was used during the regulatory fire analysis and a value of 3.5 W/m^2-K (0.62 Btu/hr-ft2-°F) was used during the cool-down period. The values used in the analyses described in the Addendum are conservative, as they bound all values that are presented in this section. That is, a higher convection heat transfer coefficient than those calculated in this section was used for the fire analysis and a lower convection heat transfer coefficient than those calculated in this section was used for the cool-down process.

References:

1. Incropera, F.P. and D.P. DeWitt. “Fundamentals of Heat and Mass Transfer, 4th ed.,” New Jersey: Wiley & Sons, Inc., 1996.
2. Kobus, C.J. and G. Shumway. “An experimental investigation into impinging forced convection heat transfer from stationary isothermal circular disks,”International J. of Heat and Mass Transfer 49 (2006), pp. 411–414.

4. CONTAINMENT

The Plutonium Air Transportable Package, Model PAT-1, is certified under Title 10 Code of Federal Regulations, Part 71,[1] by the U.S. Nuclear Regulatory Commission (NRC) per Certificate of Compliance (CoC) USA/0361/B(U)F-96 (current Revision 9).[2] The current authorized contents are plutonium oxide (PuO_2) and its daughter products, or a mixture of PuO_2 and uranium oxide (UO_2) and its daughter products. The (-96) in the certificate of compliance number indicates that the NRC has evaluated the PAT-1 against the current regulations (including 10 CFR 71.63) and determined that the package satisfies the current regulations.

The purpose of this addendum is to incorporate plutonium metal as a new payload for the PAT-1 package and to demonstrate that the package with the new *T-Ampoule Assembly*[A] (Drawing 2A0261, designated the T-Ampoule) and packing within the TB-1 *Containment Vessel* (Drawing 1017, designated TB-1) meet the current containment requirements in 10 CFR 71.[3] The 71.63 requirement is satisfied for the PAT-1 with the T-Ampoule and its packing material configuration because the plutonium metal payload contents are solid, pure or alloyed plutonium metal contents or Pu/Be composite samples.

The CoC[2] describes the TB-1 as a stainless steel containment vessel surrounded by a stainless steel and redwood overpack (*Overpack, AQ*, Drawing 1002, designated AQ-1). The plutonium oxide contents are sealed within a stainless steel product can (designated PC-1). The CoC does not identify the PC-1 as a "containment vessel," but as a "sealed … product can." For the plutonium metal content packaging configuration described in this addendum, the PC-1, aluminum honeycomb top spacer and packing material is replaced with a T-Ampoule, *Ring, Filler* (Drawing 2A0262, designated Ring Filler) and packing material which provides a eutectic prevention barrier between the TB-1 and the plutonium metal content. The T-Ampoule provides the following:

- A eutectic prevention barrier between the stainless steel TB-1 and the plutonium metal payload for NCT, HAC, and air transport accident conditions.
- A T-Ampoule seal area that is not significantly deformed (see Sections 2 and 3 of this addendum) nor a seal temperature that exceeds the allowable temperature of the gasket material during NCT or HAC. The T-Ampoule is expected to remain sealed during NCT and HAC, like the PC-1.
- A retained eutectic prevention barrier function following the air transport accident condition drops and fire. Although the O-ring in the T-Ampoule would be expected to fail in the 10 CFR 71.74 air transport of plutonium fire test, the T-Ampoule is shown in Sections 2 and 3 of this addendum to remain intact (no significant deformation in the seal area and no breaches). The T-Ampoule is more robust than the PC-1.

The documentation and analysis in this section and other sections of this addendum demonstrate that the replacing the PC-1 with oxide content and associated packing material with the T-Ampoule with plutonium metal content and associated packing material satisfies the

[A] The drawing titles are in italics and are used interchangeably with the designated names in this addendum. See Section 1.3.2 in this addendum and Chapter 9 in the SAR[4] for drawing number, title, and revision.

requirements specified in 10 CFR 71.19(d). That is, the modifications of the PAT-1 described in this addendum are not significant with respect to the design, operating characteristics, safe performance of the containment system, or prevention of criticality when the package is subjected to the tests specified in 10 CFR 71.71, 71.73, and 71.74.

4.1 Description of the Containment System

The CoC USA/0361/B(U)F-96[2] defines the TB-1 as the containment vessel for the PAT-1 for the current PuO_2 and its daughter products and UO_2 and its daughter products as authorized contents. The description of the TB-1 containment vessel is provided in Sections 1 and 9 of the SAR.[4] For this plutonium metals addendum, the TB-1 containment vessel (see Figure 4-1) provides the containment boundary for the proposed metal contents as it did for the oxide contents. The T-Ampoule replaces the PC-1. The TB-1 O-ring is not used for the plutonium metal shipments.

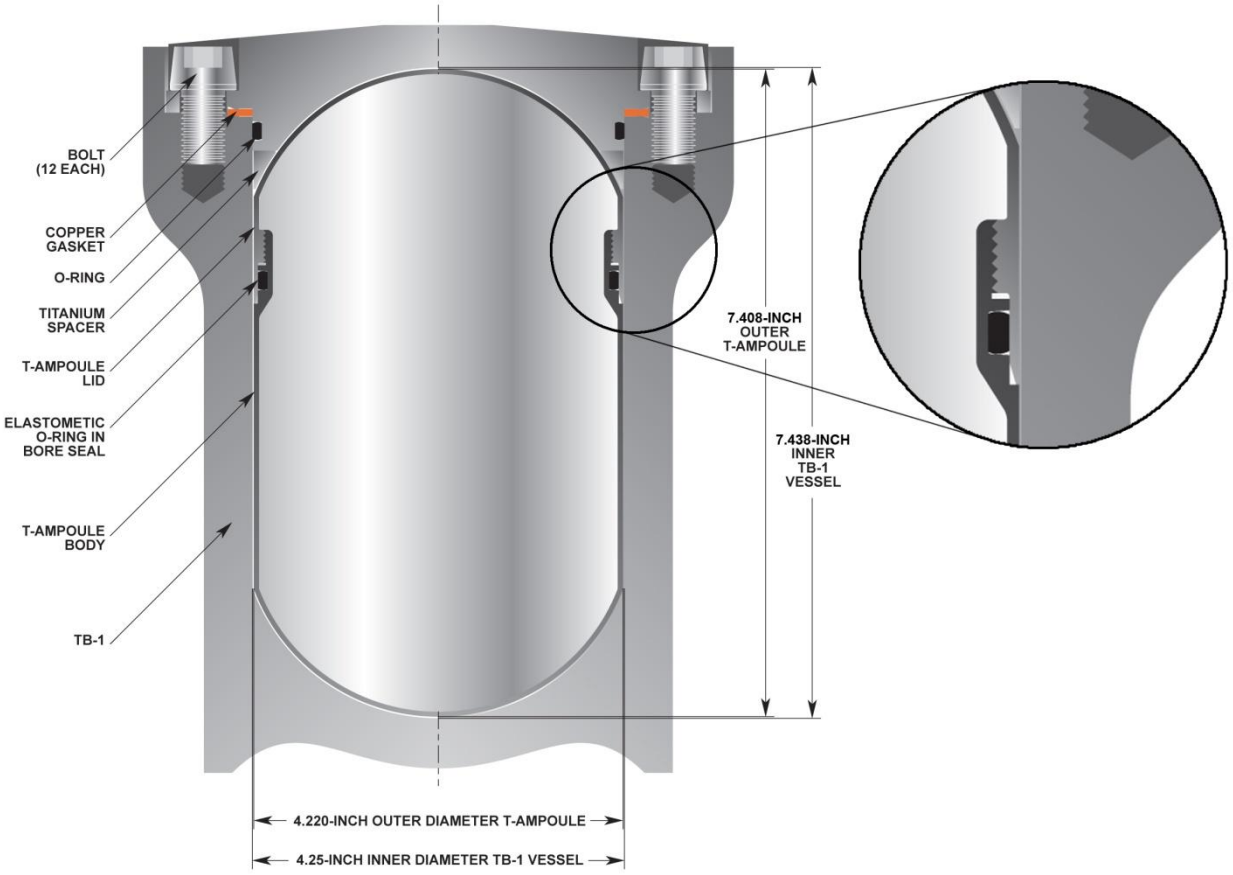

Figure 4-1. TB-1 Containment Vessel and T-Ampoule Contents Container

Table 4-1 of the SAR[4] summarizes the results of the post-test assessment of PAT-1 containment of its surrogate PuO_2 powder contents during the three transport tests (10 CFR 71.71, 10 CFR 71.73, and 10 CFR 71.74) and demonstrates that the containment criteria are met.

Table 4-1. PAT-1 Package Post-Test Containment

			Post Test Results	
Component	**Test Condition**	**Regulatory Acceptance Standard**	**Helium Leak-Rate (atm-cc/sec)**	**Maximum Mass of Powder Release[b] (mg)**
TB-1	NCT (71.71)	10^{-6} A_2/hr	Less than 1×10^{-10}	0
	HAC (71.73)	A_2/week	Less than 1×10^{-10}	0
	Plutonium Air Transport (71.74)	A_2/week[a]	Less than 4.5×10^{-5}	0.17

[a] For a typical mixture of plutonium oxide (PuO_2) powder, an A_2 quantity is approximately 2.55 mg.
[b] Depleted uranium oxide powder was used as the surrogate for plutonium oxide powder during PAT-1 testing. From the SAR, the bounding magnitude of potential PuO_2 powder leakage from the TB-1 vessel would be less than 0.17 mg in one week.

Section 4.5.5 provides a determination of A_2 for the PAT-1 package with plutonium metal in its most dispersible form as contents and Section 4.5.6 provides calculations of the PAT-1 containment vessel's regulatory reference air leakage rates.

The containment criteria for radioactive, fissile material packages are given in 10 CFR 71.51(a)(1) for NCT ($\leq 10^{-6}$ A_2/h), in 71.51(a)(2) for HAC ($\leq A_2$ in a week), and 71.64(a)(1)(i) for accident conditions for air transport of plutonium ($\leq A_2$ in a week). In Section 4.5.5, the A_2 value for the mixture of isotopes was determined to establish the content containment criteria and to determine the maximum release quantity that is allowed by the regulations. The A_2 values of the plutonium content to be shipped were evaluated based on the mass and weight percents of materials shown in Section 1.2.2. The analysis in Section 4.5.5 was conducted to establish an upper limit for the total activity and the maximum number of A_2s proposed for transport in the PAT-1 package. The values were determined using a maximum of 1300 g of plutonium as a bounding condition.

The PAT-1 leak-testing requirements of the containment boundary are based on the smallest maximum allowable leakage rate generated from the maximum plutonium content defined in Table 4.5.5.1 given the allowable leak rates defined in ANSI N14.5-1997, which defines the maximum allowable leakage rate based on the maximum allowable release rate. L_N, L_A, and L_{PA} are the maximum allowable seal leakage rates for NCT, HAC, and accident conditions for air transport of plutonium (ACATP). The worst case maximum allowable leakage rates are used to calculate an equivalent leakage hole diameter following ANSI N14.5-1997, Appendix B, for each condition of transport. This leakage hole diameter is used to calculate a reference air and helium leakage rate for leak testing. The bounding mass for the plutonium content of 1300 g was used in this calculation; note that a 831 g weight limit for the plutonium hollow cylinder was used in the structural analysis and is the maximum plutonium metal content for certification. The use of 1300 g was conservative; the maximum allowable leak rates are calculated using this maximum content mass in a much more dispersive form (oxide powder) for additional conservatism at the highest calculated pressures (assuming the maximum amount of material for disposition) and temperatures as analyzed in Section 2.12.8.

The regulatory leakage criteria for 1300 g plutonium (bounding case for containment analysis assuming oxide) are shown in Table 4-2 in this addendum.

In accordance with Table 4-1 of the SAR, the highest measured helium leakage rate following the accident conditions for air transport of plutonium was 4.5×10^{-5} cc/s. This leakage rate is considerably lower than the calculated maximum allowable regulatory leakage rate requirement of 1.4703×10^{-3} ref cc/s (see Table 4-2 in this addendum) for ACATP at 1110 psia, 1080ºF. These results are from Table 4.5.6.1 (of Section 4.5.6 in this addendum). It can be concluded that the TB-1 containment vessel inside of the PAT-1 package maintains containment for NCT, HAC, and Accident conditions for air transport of plutonium.

The mass release during the Accident conditions for air transport of plutonium was calculated in Section 4.5.6. For the 1300 g bounding case, the allowable mass release for no decay of Pu-241 is 2.7634×10^{-1} g and for complete decay of Pu-241 to Am-241 is 2.3336×10^{-1} g. The maximum amount of powder released shown in Table 4-1 above after the Accident conditions for air transport of plutonium test was less than 0.17 mg.

Table 4-2. Regulatory Leakage Criteria for 1300 g Plutonium (Bounding Case)

Isotopic Distribution	Ancillary plastic composition	NCT [a]		HAC [a]		ACATP	
		$L_{R,N\text{-}air}$ (ref-cm^3/s)	$L_{R,N\text{-}He}$ (cm^3/s)	$L_{R,A\text{-}air}$ (ref-cm^3/s)	$L_{R,A\text{-}He}$ (cm^3/s)	$L_{R,PA\text{-}air}$ (ref-cm^3/s)	$L_{R,PA\text{-}He}$ (cm^3/s)
No Pu-241 decay	polyethylene terephthalate	5.1244 E-06	8.8373 E-06	9.4686 E-02	9.8072 E-02	1.7546E-03	2.0876E-03
	polyethylene	5.1244 E-06	8.8373 E-06	9.4686 E-02	9.8072 E-02	1.7339E-03	2.0642E-03
	polyvinyl chloride	5.1244 E-06	8.8373 E-06	9.4686 E-02	9.8072 E-02	1.7487E-03	2.0810E-03
	polytetrafluoroethylene	5.1244 E-06	8.8373 E-06	9.4686 E-02	9.8072 E-02	2.1844E-03	2.5725E-03
Complete Pu-241 decay to Am-241	polyethylene terephthalate	4.2787 E-06	7.4737 E-06	7.9817 E-02	8.3008 E-02	1.4703E-03	1.7873E-03
	polyethylene	4.2787 E-06	7.4737 E-06	7.9817 E-02	8.3008 E-02	1.4729E-03	1.7673E-03
	polyvinyl chloride	4.2787 E-06	7.4737 E-06	7.9817 E-02	8.3008 E-02	1.4854E-03	1.7816E-03
	polytetrafluoroethylene	4.2787 E-06	7.4737 E-06	7.9817 E-02	8.3008 E-02	1.8549E-03	2.2012E-03

[a] Since temperatures associated with pyrolysis of the ancillary plastics are not reached during NCT and HAC, the various plastics have no affect on the regulatory leakage criteria at those conditions.

4.1.1 Special Requirements for Plutonium

The proposed plutonium metal contents meet the current requirements set forth in 10 CFR 71.[3] In 10 CFR 71.63, "Shipments containing plutonium must be made with contents in solid form, if the contents contain greater than 0.74 TBq (20 Ci) of plutonium." This requirement is satisfied for the PAT-1 with the T-Ampoule and its packing because the proposed plutonium metal payload contents are solid, pure or alloyed plutonium metal or Pu/Be composite samples.

The PAT-1 Certificate of Compliance[2] (CoC) (USA/0361/B(U)F-96) (current Revision 9) in Item 5. (a) Packaging, (2) includes the description of the PAT-1,

"A stainless steel containment vessel (designated TB-1) surrounded by a stainless steel and redwood overpack (designated AQ-1). The contents are sealed within a stainless steel product can (designated PC-1) inside the containment vessel."

The "-96" in the certificate of compliance number indicates that the NRC has evaluated the PAT-1 against the current regulations (including 10 CFR 71.63) and determined that the package satisfies the current regulations. The CoC[2] identifies the TB-1 as the containment vessel.

For this addendum, the PAT-1 is unchanged from the inside surface of the TB-1 containment vessel to the outside surface of the AQ-1 overpack. The only change to the PAT-1 package is replacement of the PC-1 and its contents, top spacer and packing material with the T-Ampoule and its contents, Ring Filler and packing material. The T-Ampoule, a titanium container, provides eutectic prevention for the metal payload.

The proposed contents include plutonium metal in the form of hollow cylinders, disks, plates, solid cylinders and test samples. The plutonium metal contents are typically loaded into the T-Ampoule in a glove box containing a limited quantity of oxygen and moisture ($\leq$ 100 ppm). Prior to loading, the contents are brushed clean to remove any oxide present on the surface. The quantity of oxide that could form in the T-Ampoule during transport is limited by less than 100 ppm concentration of oxygen and moisture in the glove box atmosphere. The estimate of oxide formation due to this atmosphere is provided in Section 4.5.2.1 and is approximately 1.64 mg (3.62 E-6 lb). If the atmosphere is assumed to be air and because this is an oxygen-limited system, the estimated quantity of oxide formed on the metal contents is 3.46 g, the activity of PuO_2 formed is 3.74 Ci if no decay is assumed (100% Pu-241), and 0.397 Ci if 100% decay is assumed (100% Am-241). If the metal contents are not cleaned sufficiently, conservative estimates that double the quantity of oxide could be present on the metal, 6.92 g, which is less than 8 Ci.

The function of the T-Ampoule is to provide a safety barrier that prevents the formation of a eutectic between the plutonium metal contents and the iron in the TB-1 containment vessel. The structural analyses in Section 2 of this addendum demonstrate that the bore seal area (see Figure 4-1) of the T-Ampoule is not significantly deformed and is expected to remain intact for all accident conditions analyzed. It can be concluded from these analyses that the T-Ampoule is more robust than the PC-1.

The PC-1 Product Can used for the oxide shipment must not be used for the metal shipment since the iron in the can could possibly form a eutectic with the plutonium metal contents. The titanium material for the T-Ampoule was selected to provide a eutectic prevention barrier between the metallic Pu contents and the TB-1 containment vessel. The *Body, T-Ampoule* (Drawing 2A0259, designated T-Ampoule Body) and *Lid, T-Ampoule* (Drawing 2A0260, designated T-Ampoule Lid) are fabricated from a solid block of Ti-6Al-4V Grade 5 alloy. There are no welds, penetrations, valves, or pressure relief devices in the T-Ampoule. Once placed within the TB-1, the T-Ampoule cannot be opened unintentionally. The clearance between the T-Ampoule and the TB-1 is 0.038 cm (0.015 in.) all around; thus, both walls have immediate contact to resist the impact forces created by the deceleration of the internal Pu contents during the impact accident environment. The sample containers (*Sample Container-1 [SC-1] Assembly*, Drawing 2A0268, designated SC-1, and *Sample Container-2 [SC-2] Assembly*, Drawing 2A0265, designated SC-2) and structure (*Inner Cradle*, Drawing 2A0385, designated Inner Cradle) are also constructed of Ti-6Al-4V Grade 5 alloy that is resistant to the formation of eutectics with the plutonium metal content. Tantalum foil, which may be used to wrap and protect the samples from contamination, was selected for its resistance to eutectic formation.

The shielding evaluation in Section 5 of this addendum demonstrates that the package with plutonium metal contents complies with the dose rate limits of 10 CFR 71.47(a) (non-exclusive use) for the normal conditions of transport (NCT) and 10 CFR 71.51(a)(2) for hypothetical accident conditions (HAC). The criticality evaluation in Section 6 of this addendum demonstrates that the package with plutonium metal contents remains subcritical under NCT and HAC and has a CSI value of 0.1 per 10 CFR 71.59.

The modifications to the PAT-1 package are not significant with respect to design, operating characteristics, or safe operation of the PAT-1 package when subjected to the tests specified in 10 CFR 71.71 and 10 CFR 71.73:

- The PAT-1 package is unchanged from the inside surface of the TB-1 containment vessel to the outside surface of the AQ-1 overpack.
- The T-Ampoule and its contents, Ring Filler and packing material replace the PC-1 and its contents, top spacer and packing material and provide protection for its metal contents.
- The T-Ampoule is a eutectic prevention barrier between the plutonium metal contents and the stainless steel TB-1 containment vessel. The structural analysis in Section 2 of this addendum demonstrates that the T-Ampoule does not breach during the 10 CFR 71.71, 10 CFR 71.73, and 10 CFR 71.74 structural evaluations, thus maintaining its eutectic function.
- The structural analyses in Section 2 demonstrated that the TB-1 met containment requirements. The TB-1's containment capability will be unaffected by the addition of metals contents through the plutonium air transport tests.
- The packing materials within the T-Ampoule are also not susceptible to eutectic formation with plutonium metal.
- The structural analysis in Section 2, the thermal analysis in Section 3, the shielding analysis in Section 5, and the criticality analysis in Section 6 of this addendum show that the requirements of 10 CFR 71.19(d) are met because the modifications to PAT-1

package are not significant with respect to the design, operating characteristics, or safe performance of the package design when subjected to the tests specified in 10 CFR 71.71 and 10 CFR 71.73.

4.1.2 Plutonium Metal Contents

The proposed plutonium metal contents include:

- Electro-Refined (ER) Pu (Purity ≥ 99.8% Pu 239).
- Pu of various ages containing stabilization alloys such as gallium (Ga).
- Composite samples consisting of Pu and beryllium (Be) separated by an alpha barrier (Ti) to preclude neutron generation.
- The forms of the metal include hollow cylinders, cylinders, discs, strips, etc.
- The container configurations within the TB-1 containment vessel are:
- T-Ampoule for bulk metal hollow cylinders and sample containers; and
- Sample containers (SC-1 and SC-2) carried within the Inner Cradle of the T-Ampoule for smaller metal samples.

The isotopic compositions, masses, A_2 values, decay heat, activities, and impurities for ER plutonium metal, alloyed plutonium metal, and bonded plutonium metal are presented below.

4.1.2.1 ER Plutonium Metal[5]

The maximum ER content is 831 g (1.83 lb) for an isotopic composition that assumes no Pu-241 decay (see Table 4-3). The ER metal mass estimates for 3000 A_2 range from 831 g (1.83 lb) assuming no Pu-241 decay (Table 4-3), and 707 g (1.56 lb) assuming 100% Pu-241 decay (see Table 4-4). Table 4-4 assumes that all of the Pu-241 has decayed to Am-241 which results in the 707 g quantity for 3000 A_2. Note that Table 4-4 is used for comparative purposes only to determine the effect of assuming 100% Pu-241 decay to Am-241. The ER metal will be manufactured and shipped prior to significant Pu-241 decay. The minimum ER cylinder weight as documented in Table 1-1 of Section 1 is 731 g.

Table 4-3. 831 g (1.83 lb): 3,000 A_2 Quantity of ER Plutonium Metal Assuming No Pu-241 Decay to Am-241

831 grams: 3,000 A_2 quantity of ER Pu metal assuming 0% Pu241 decay to Am241									
Metal Mass (g) (max)	Mass % (max)	Grams (max)	LANL Specification 55Y-638728	Isotope	Pu Isotopic % (max)	Pu Isotopic mass (g)	Decay Heat (W)	Activity (Ci)	A_2
831.00	Plutonium 99.84%	Plutonium 829.67		Pu238	0.05%	0.41	2.35E-01	7.05E+00	2.61E+02
				Pu239*	92.35%	766.20	1.46E+00	4.75E+01	1.76E+03
				Pu240	6.50%	53.93	3.83E-01	1.24E+01	4.59E+02
				Pu241	1.00%	8.30	1.04E-01	8.30E+02	5.19E+02
				Pu242	0.10%	0.83	8.30E-05	3.24E-03	1.20E-01
				Am241	0.00%	0.00	0.00E+00	0.00E+00	0.00E+00
	Impurities 0.16%	Impurities 1.33		Impurities: N/A					
* stated as % balance						Total:	2.18E+00	8.97E+02	3.00E+03

Table 4-4. 707 g (1.56 lb): 3,000 A_2 Quantity of ER Plutonium Metal Assuming 100% Pu-241 Decay to Am-241

707 grams: 3,000 A_2 quantity of ER Pu metal assuming 100% Pu241 decay to Am241									
Metal Mass (g) (max)	Mass % (max)	Grams (max)	LANL Specification 55Y-638728	Isotope	Pu Isotopic % (max)	Pu Isotopic mass (g)	Decay Heat (W)	Activity (Ci)	A_2
707.00	Plutonium 99.84%	Plutonium 705.87		Pu238	0.05%	0.35	2.00E-01	6.00E+00	2.22E+02
				Pu239*	92.35%	651.87	1.24E+00	4.04E+01	1.50E+03
				Pu240	6.50%	45.88	3.26E-01	1.06E+01	3.91E+02
				Pu241	0.00%	0.00	0.00E+00	0.00E+00	0.00E+00
				Pu242	0.10%	0.71	7.06E-05	2.75E-03	1.02E-01
				Am241	1.00%	7.06	8.10E-01	2.40E+01	8.89E+02
	Impurities 0.16%	Impurities 1.13		Impurities: N/A					
* stated as % balance						Total:	2.57E+00	8.10E+01	3.00E+03
Note: Table shown for comparative purposes only. ER metal will be manufactured and shipped prior to significant Pu241 decay									

4.1.2.2 Alloyed Plutonium Metal[5]

The maximum contents in two SC-2 sample containers within the T-Ampoule are 676 g (1.49 lb). A_2 calculations were performed assuming 100% Pu-241 decay to Am-241 (2840 A_2) (see Table 4-5) and No Pu-241 decay (2410 A_2) (see Table 4-6). Alloyed plutonium metal may be shipped in a hollow log form in the T-Ampoule if the requirements in Table 1-1 of this addendum and the shipper are met.

Table 4-5. 676 g (1.49 lb): Alloyed Plutonium Metal Assuming 100% Pu-241 Decay to Am-241

676 grams: Alloyed Pu metal assuming 100% Pu241 decay to Am241									
Metal Mass (g) (max)	Mass % (max)	Grams (max)	LANL Specification 55Y-638728	Isotope	Pu Isotopic % (max)	Pu Isotopic mass (g)	Decay Heat (W)	Activity (Ci)	A_2
676.00	Plutonium 98.84%	Plutonium 668.16		Pu238	0.05%	0.33	1.89E-01	5.68E+00	2.10E+02
				Pu239*	92.35%	617.04	1.17E+00	3.83E+01	1.42E+03
				Pu240	6.50%	43.43	3.08E-01	9.99E+00	3.70E+02
				Pu241	0.00%	0.00	0.00E+00	0.00E+00	0.00E+00
				Pu242	0.10%	0.67	6.68E-05	2.61E-03	9.65E-02
				Am241	1.00%	6.68	7.67E-01	2.27E+01	8.41E+02
	Impurities 0.16%	Impurities 1.08		Impurities: N/A					
	Gallium 1.00%	Gallium 6.76		Gallium: N/A					
* stated as % balance					Total:		2.44E+00	7.66E+01	2.84E+03

Table 4-6. 676 g (1.49 lb): Alloyed Plutonium Metal Assuming No Pu-241 Decay to Am-241

676 grams: Alloyed Pu metal assuming 0% Pu241 decay to Am241									
Metal Mass (g) (max)	Mass % (max)	Grams (max)	LANL Specification 55Y-638728	Isotope	Pu Isotopic % (max)	Pu Isotopic mass (g)	Decay Heat (W)	Activity (Ci)	A_2
676.00	Plutonium 98.84%	Plutonium 668.16		Pu238	0.05%	0.33	1.89E-01	5.68E+00	2.10E+02
				Pu239*	92.35%	617.04	1.17E+00	3.83E+01	1.42E+03
				Pu240	6.50%	43.43	3.08E-01	9.99E+00	3.70E+02
				Pu241	1.00%	6.68	8.35E-02	6.68E+02	4.18E+02
				Pu242	0.10%	0.67	6.68E-05	2.61E-03	9.65E-02
				Am241	0.00%	0.00	0.00E+00	0.00E+00	0.00E+00
	Impurities 0.16%	Impurities 1.08		Impurities: N/A					
	Gallium 1.00%	Gallium 6.76		Gallium: N/A					
* stated as % balance					Total:		1.75E+00	7.22E+02	2.41E+03

4.1.2.3 Bonded Plutonium Metal[5]

A 60 g (0.13 lb) bonded 16.85 mm diameter × 16.85 mm height Pu/Be metal cylinder (or a number of smaller cylinders [up to 25 5.1 mm diameter × 5.1 mm height cylinders] as described in Table 1.1, Section 1 of this addendum) may each be shipped in the SC-1 sample container for a total payload weight of 180 g (0.39 lb) (657 A_2) or in the SC-2 sample container for a total payload weight of 120 g (0.26 lb) within the T-Ampoule. The composite payload weight is limited to 60 grams or less in each sample container. See Table 4-7 for estimate of curies, number of A_2, decay heat, weight, and isotopic composition of the Pu/Be material based upon a disk configuration.

Table 4-7. 60 g (0.13 lb): Bonded Pu/Be Metal Disk Assuming 100% Pu-241 Decay to Am-241

60 grams: Bonded Pu/Be metal disc assuming 100% Pu241 decay to Am241										
Composite %	Metal Mass (g) (max)	Mass % (max)	Grams (max)	LANL Specification 55Y-638728	Isotope	Pu Isotopic % (max)	Pu Isotopic mass (g)	Decay Heat (W)	Activity (Ci)	A_2
Pu metal 87.00%	52.20	MT52 Plutonium 98.84%	MT52 Plutonium 51.59		Pu238	0.05%	0.03	1.46E-02	4.39E-01	1.62E+01
					Pu239*	92.35%	47.65	9.05E-02	2.95E+00	1.09E+02
					Pu240	6.50%	3.35	2.38E-02	7.71E-01	2.86E+01
					Pu241	0.00%	0.00	0.00E+00	0.00E+00	0.00E+00
					Pu242	0.10%	0.05	5.16E-06	2.01E-04	7.45E-03
					Am241	1.00%	0.52	5.92E-02	1.75E+00	6.50E+01
		Impurities 0.16%	Impurities 0.08		Impurities: N/A					
		Gallium 1.00%	Gallium 0.52	Gallium: N/A						
Beryllium 13.00%	7.80	Beryllium 13.00%	Beryllium 7.80	Beryllium: N/A						
Alpha Barrier 0.00%	0.00	Alpha Barrier 0.00%	Alpha Barrier 0.00	Assumes no alpha barrier to yield maximum dose						
100.00%	60.00	◄◄◄ Totals ►►►						1.88E-01	5.92E+00	2.19E+02
*stated as % balance										

4.2 Containment under Normal Conditions of Transport (NCT)

The TB-1 containment vessel meets the regulatory acceptance standard for NCT of 10^{-6} A_2/hr as demonstrated in Table 4-1. The T-Ampoule is not a containment vessel under NCT.

The thermal analysis in Section 3.3 of this addendum, which analyzed a localized 25-watt (85.3 Btu/hr) thermal source against the O-ring seal of the T-Ampoule, indicated an average temperature of 103.3°C (218°F).

The internal pressure within the TB-1 during NCT with an internal heat generation of 25 watts (85.3 Btu/hr) from the plutonium metal contents indicated a maximum pressure of 18.8 psia, due to the temperature difference. The calculation assumes an initial room temperature of 20°C (70°F), then:

$$P2 = 1atm*(678/530R) = 1.28 \text{ atm or } \sim 18.8 \text{ psia}$$

To determine the pressure generated from the alpha decay of plutonium, the TB-1 was assumed to be filled at ambient temperature and to reach the NCT temperature quickly (see Section 4.5.3). The helium pressure, shown below, is thus:

$$P_{He} = n_{He}*(RT/V)$$

where $n_{He} = gm_{He}/4$

T = the NCT average temperature in Kelvin (absolute)
V = 1.252 liters

R = 0.082 l-atm/mole-K, the gas constant
Pressure in psi = 14.7*Pressure in atmospheres
The pressure from helium (He) generation for 1300 g Pu (for conservatism) at NCT temperature via alpha decay is 0.067 psia.

The total pressure as the result of internal heat generation and alpha decay is 18.9 psia, or 4.2 psig, which defines the maximum normal operating pressure (MNOP) for the TB-1.

The MNOP of 4.2 psig (18.9 psia) calculated above is slightly less than that calculated for the PuO_2 contents in the SAR (34.3 psia) since a small quantity of moisture was assumed to be present in the PuO_2 within the TB-1.

4.3 Containment under Hypothetical Accident Conditions (HAC)

The TB-1 meets the regulatory acceptance standard for HAC of A_2 in a week as documented in Table 4-1. The T-Ampoule is not a containment vessel under HAC.

The thermal analysis in Section 3.4 of this addendum includes localized heating produced by the plutonium metal contents, and the HAC evaluation indicated that the average temperature is 136°C (276°F) in the T-Ampoule. The temperature of the T-Ampoule seal does not exceed the manufacturer's specification for the operating range of the seal material (204°C [400°F]).

The pressure calculated within the TB-1 as the result of internal heat generation of 25 watts from the plutonium metal contents and the HAC indicated that the maximum pressure is 20.4 psi. The calculation assumes an initial room temperature of 21°C (70°F), then:

$$P2 = 1atm*(736R/530R) = 1.39 \text{ atm or } \sim 20.4 \text{ psia}$$

Pressure from He generation for 1300 g of Pu metal (for conservatism) via alpha decay is 0.073 psia from Section 4.5.3 of this addendum.

The total pressure as a result of internal heat generation and alpha decay is 20.5 psia. The pressure of 20.5 psia is less than the HAC pressure reported in the SAR[4] (38.7 psia [Section 3.5.4 of the SAR[4]]).

4.3.1 Containment under Plutonium Air Transport Fire Test

The TB-1 meets the regulatory acceptance standard for the plutonium air transport tests of A_2 in a week as documented in Table 4-1. The T-Ampoule is not a containment vessel under the plutonium air transport conditions.

In Section 2.12.8, an initial calculation was performed using an air-filled TB-1 as a realistic starting assumption to examine the rise in pressure from decomposition of the elastomeric O-rings within the T-Ampoule and two SC-2 or three SC-1 sample containers and a range of weights for ancillary plastics. The three SC-1 configurations and the selected 70 gram quantity of HDPE yielded the highest pressure rise of 572 psia. Including the rise in pressure from ambient temperature to 582ºC (1080ºF) of 42.7 psia and the helium pressure generation from 1300 g of plutonium (for conservatism) from alpha decay of 0.11 psia, the total pressure within

the TB-1 is 615 psia. The PAT-1 SAR,[4] Section 4.4.2 stipulates that the maximum allowable TB-1 pressure during the post-fire plutonium air transport accident condition was 1,110 psia.

A subsequent calculation was performed in Section 2.12.8 which assumed the no-char assumption for O-ring decomposition in LA-UR-10-05846 in Section 4.5.4. The no-char assumption was also used for decomposition of the ancillary plastic. The pressures from the original atmosphere, helium generation from alpha decay, O-ring decomposition and the pressure from ancillary plastics were set equal to 1110 psia, the pressure of the TB-1 from the post-fire plutonium air transport accident condition. The resulting ancillary plastic pressure was then used to determine the masses of the plastics that could be used within the TB-1. The various pressures from the components are reported in Table 11 in Section 2.12.8.

The results of the highly conservative calculation of the thermal degradation of *Viton A® O-rings* and ancillary plastic in Section 2.12.8 used the maximum internal pressure of 1110 psia. Therefore, this will be the pressure for plutonium air transport fire test for plutonium metals.

In summary, the TB-1 structure is unaffected by the impact and thermal environments and maintains its containment integrity for NCT, HAC, and the accident conditions for air transport of plutonium.

4.4 Leakage Rate Tests for Type B Packages

The leakage rate tests for the TB-1, which is the primary containment vessel, is described in Sections 7 and 8.

4.5 Appendix

4.5.1 References

1. United States. Nuclear Regulatory Commission. Code of Federal Regulations. 10 CFR 71. "Packaging and Transportation of Radioactive Material." January 1, 2009.

2. United States. Nuclear Regulatory Commission. "Certificate of Compliance for Radioactive Material Packages." Certificate Number 0361, Revision Number 9, Docket Number 71-0361, Package Identification Number USA/0361/B(U)F-96. March 4, 2009.

3. United States. Nuclear Regulatory Commission. Code of Federal Regulations. 10 CFR 71.63. "Special requirements for plutonium shipments," as published in 69 FR 3795. January 26, 2004.

4. United States. Nuclear Regulatory Commission. NUREG-0361, "Safety Analysis Report for the Plutonium Air Transportable Package, Model PAT-1." Washington, D.C. 1978.

5. Caviness, M. L., and J.B. Rubin. "Authorized Contents Proposed for the Plutonium Air Transporter (PAT-1) Packaging (U)," LA-UR-08-05154. Los Alamos National Laboratory. Los Alamos, NM: August 7, 2008.

6. Rubin, J. B. "Thermal Decomposition of Viton® O-rings for the PAT-1 Packaging Accident Scenario," LA-UR-10-05846. Los Alamos National Laboratory. Los Alamos, NM: August 31, 2010.

4.5.2 PAT-1 Contents

LA-UR-08-05154

Approved for public release; distribution is unlimited.

Title:	Authorized Contents Proposed for the Plutonium Air Transporter (PAT-1) Packaging (U)
Author(s):	Michael L. Caviness, PMT-3 Jim B. Rubin, PMT-2
Intended for:	Development of an application to the US Nuclear Regulatory Commission for the transport of plutonium metal by air in the Plutonium Air Transporter (PAT-1) packaging

Los Alamos National Laboratory, an affirmative action/equal opportunity employer, is operated by the Los Alamos National Security, LLC for the National Nuclear Security Administration of the U.S. Department of Energy under contract DE-AC52-06NA25396. By acceptance of this article, the publisher recognizes that the U.S. Government retains a nonexclusive, royalty-free license to publish or reproduce the published form of this contribution, or to allow others to do so, for U.S. Government purposes. Los Alamos National Laboratory requests that the publisher identify this article as work performed under the auspices of the U.S. Department of Energy. Los Alamos National Laboratory strongly supports academic freedom and a researcher's right to publish; as an institution, however, the Laboratory does not endorse the viewpoint of a publication or guarantee its technical correctness.

Form 836 (7/06)

Authorized Contents Proposed for the Plutonium Air Transporter (PAT-1) Packaging

Authors: Michael Caviness, PMT-3, Nuclear Materials Management

Jim Rubin, PMT-2, Actinide Process Chemistry

PAT-1 Packaging Assembly

Page 1 of 5

ELECTRO-REFINED PLUTONUM METAL

1,300 grams: Maximum quantity of Electro-refined (ER) Pu metal excluding Pu241 decay

Metal Mass (g) (max)	Mass % (max)	Grams (max)		Isotope	Pu Isotopic % (max)	Pu Isotopic mass (g)	Decay Heat (W)	Activity (Ci)	A_2
1,300.00	Plutonium 99.84%	Plutonium 1297.92	LANL Specification 55Y-638728	Pu238	0.05%	0.65	3.68E-01	1.10 E+01	4.09 E+02
				Pu239*	92.35%	1198.63	2.28E+00	7.43 E+01	2.75 E+03
				Pu240	6.50%	84.36	5.99E-01	1.94 E+01	7.19 E+02
				Pu241	1.00%	12.98	1.62E-01	1.30 E+03	8.11 E+02
				Pu242	0.10%	1.30	1.30E-04	5.06 E-03	1.87 E-01
				Am241	0.00%	0.00	0.00E+00	0.00 E+00	0.00E +00
	Impurities 0.16%	Impurities 2.08		Impurities: N/A					
* stated as % balance						Total:	3.41E+00	1.40E+ 03	4.69E +03

Reference Values	
Decay Heat	
Isotope	Watts/ gram
Pu238	5.67E-01
Pu239	1.90E-03
Pu240	7.10E-03
Pu241	1.25E-02
Pu242	1.00E-04
Am241	1.15E-01
DOE-STD-3013-00, Table B-5	

831 grams: 3,000 A_2 quantity of ER Pu metal assuming 0% Pu241 decay to Am241

Metal Mass (g) (max)	Mass % (max)	Grams (max)		Isotope	Pu Isotopic % (max)	Pu Isotopic mass (g)	Decay Heat (W)	Activity (Ci)	A_2
831.00	Plutonium 99.84%	Plutonium 829.67	LANL Specification 55Y-638728	Pu238	0.05%	0.41	2.35E-01	7.05 E+00	2.61 E+02
				Pu239*	92.35%	766.20	1.46E+00	4.75 E+01	1.76 E+03
				Pu240	6.50%	53.93	3.83E-01	1.24 E+01	4.59 E+02
				Pu241	1.00%	8.30	1.04E-01	8.30 E+02	5.19 E+02
				Pu242	0.10%	0.83	8.30E-05	3.24 E-03	1.20 E-01
				Am241	0.00%	0.00	0.00E+00	0.00 E+00	0.00 E+00
	Impurities 0.16%	Impurities 1.33		Impurities: N/A					
* stated as % balance						Total:	2.18E+00	8.97 E+02	3.00 E+03

Reference Values		
A_2 values of radionuclides		
Isotope	A_2 (Ci)	Ci/g
Pu238	2.70E-02	1.70 E+01
Pu239	2.70E-02	6.20 E-02
Pu240	2.70E-02	2.30 E-01
Pu241	1.60E+00	1.00 E+02
Pu242	2.70E-02	3.90 E-03
Am241	2.70E-02	3.40 E+00
49 CFR 173.435, Table of A1 and A2 Values for Radionuclides		

707 grams: 3,000 A_2 quantity of ER Pu metal assuming 100% Pu241 decay to Am241

Metal Mass (g) (max)	Mass % (max)	Grams (max)		Isotope	Pu Isotopic % (max)	Pu Isotopic mass (g)	Decay Heat (W)	Activity (Ci)	A_2
707.00	Plutonium 99.84%	Plutonium 705.87	LANL Specification 55Y-638728	Pu238	0.05%	0.35	2.00E-01	6.00 E+00	2.22 E+02
				Pu239*	92.35%	651.87	1.24E+00	4.04 E+01	1.50 E+03
				Pu240	6.50%	45.88	3.26E-01	1.06 E+01	3.91 E+02
				Pu241	0.00%	0.00	0.00E+00	0.00 E+00	0.00 E+00
				Pu242	0.10%	0.71	7.06E-05	2.75 E-03	1.02 E-01
				Am241	1.00%	7.06	8.10E-01	2.40 E+01	8.89 E+02
	Impurities 0.16%	Impurities 1.13		Impurities: N/A					
* stated as % balance						Total:	2.57E+00	8.10 E+01	3.00 E+03

Note: Table shown for comparative purposes only. ER metal will be manufactured and shipped prior to significant Pu241 decay

Impurity Limits (max)		
Values in parts per million (ppm)		
Al: 100	Fe: 200	Ta: 100
Am: 200	Ga: 300	Th: 100
B: 50	Mg: 500	Ti: 100
Be: 3	Mn: 100	U: 100
C: 200	Ni: 100	W: 200
Ca: 500	Np: 100	Zn: 100
Cd: 10	Pb: 100	
Cr: 100	Si: 100	
Cu: 100	Sn: 100	
LANL Specification 55Y-638728		

ALLOYED PLUTONUM METAL

676 grams: Alloyed Pu metal assuming 0% Pu241 decay to Am241

Metal Mass (g) (max)	Mass % (max)	Grams (max)		Isotope	Pu Isotopic % (max)	Pu Isotopic mass (g)	Decay Heat (W)	Activity (Ci)	A_2
676.00	Plutonium 98.84%	Plutonium 668.16	LANL Specification 55Y-638728	Pu238	0.05%	0.33	1.89E-01	5.68 E+00	2.10 E+02
				Pu239*	92.35%	617.04	1.17E+00	3.83 E+01	1.42 E+03
				Pu240	6.50%	43.43	3.08E-01	9.99 E+00	3.70 E+02
				Pu241	1.00%	6.68	8.35E-02	6.68 E+02	4.18 E+02
				Pu242	0.10%	0.67	6.68E-05	2.61 E-03	9.65 E-02
				Am241	0.00%	0.00	0.00E+00	0.00 E+00	0.00 E+00
	Impurities 0.16%	Impurities 1.08		Impurities: N/A					
	Gallium 1.00%	Gallium 6.76		Gallium: N/A					
* stated as % balance						Total:	1.75E+00	7.22 E+02	2.41 E+03

Reference Values	
Decay Heat	
Isotope	Watts/ gram
Pu238	5.67E-01
Pu239	1.90E-03
Pu240	7.10E-03
Pu241	1.25E-02
Pu242	1.00E-04
Am241	1.15E-01
DOE-STD-3013-00, Table B-5	

676 grams: Alloyed Pu metal assuming 100% Pu241 decay to Am241

Metal Mass (g) (max)	Mass % (max)	Grams (max)		Isotope	Pu Isotopic % (max)	Pu Isotopic mass (g)	Decay Heat (W)	Activity (Ci)	A_2
676.00	Plutonium 98.84%	Plutonium 668.16	LANL Specification 55Y-638728	Pu238	0.05%	0.33	1.89E-01	5.68 E+00	2.10 E+02
				Pu239*	92.35%	617.04	1.17E+00	3.83 E+01	1.42 E+03
				Pu240	6.50%	43.43	3.08E-01	9.99 E+00	3.70 E+02
				Pu241	0.00%	0.00	0.00E+00	0.00 E+00	0.00 E+00
				Pu242	0.10%	0.67	6.68E-05	2.61 E-03	9.65 E-02
				Am241	1.00%	6.68	7.67E-01	2.27 E+01	8.41 E+02
	Impurities 0.16%	Impurities 1.08		Impurities: N/A					
	Gallium 1.00%	Gallium 6.76		Gallium: N/A					
* stated as % balance						Total:	2.44E+00	7.66 E+01	2.84 E+03

Reference Values		
A_2 values of radionuclides		
Isotope	A_2 (Ci)	Ci/g
Pu238	2.70 E-02	1.70 E+01
Pu239	2.70 E-02	6.20 E-02
Pu240	2.70 E-02	2.30 E-01
Pu241	1.60 E+00	1.00 E+02
Pu242	2.70 E-02	3.90 E-03
Am241	2.70 E-02	3.40 E+00
49 CFR 173.435, Table of A1 and A2 Values for Radionuclides		

Impurity Limits (max)		
Values in parts per million (ppm)		
Al: 100	Fe: 200	Ta: 100
Am: 200	Ga: N/A	Th: 100
B: 50	Mg: 500	Ti: N/A
Be: N/A	Mn: 100	U: 100
C: 200	Ni: 100	W: 200
Ca: 500	Np: 100	Zn: 100
Cd: 10	Pb: 100	
Cr: 100	Si: 100	
Cu: 100	Sn: 100	
LANL Specification 55Y-638728		

BONDED PLUTONUM METAL

60 grams: Bonded Pu/Be metal disc assuming 100% Pu241 decay to Am241

Com-posite %	Metal Mass (g) (max)	Mass % (max)	Grams (max)	LANL Specification 55Y-638728	Isotope	Pu Isotopic % (max)	Pu Isotopic mass (g)	Decay Heat (W)	Activity (Ci)	A_2
Pu metal 87.00%	52.20	MT52 Plutonium 98.84%	MT52 Plutonium 51.59		Pu238	0.05%	0.03	1.46E-02	4.39 E-01	1.62 E+01
					Pu239*	92.35%	47.65	9.05E-02	2.95 E+00	1.09 E+02
					Pu240	6.50%	3.35	2.38E-02	7.71 E-01	2.86 E+01
					Pu241	0.00%	0.00	0.00E+00	0.00 E+00	0.00 E+00
					Pu242	0.10%	0.05	5.16E-06	2.01 E-04	7.45 E-03
					Am241	1.00%	0.52	5.92E-02	1.75 E+00	6.50 E+01
		Impurities 0.16%	Impurities 0.08		Impurities: N/A					
		Gallium 1.00%	Gallium 0.52		Gallium: N/A					
Beryllium 13.00%	7.80	Beryllium 13.00%	Beryllium 7.80		Beryllium: N/A					
Alpha Barrier 0.00%	0.00	Alpha Barrier 0.00%	Alpha Barrier 0.00		Assumes no alpha barrier to yield maximum dose					
100.00%	60.00	◄◄◄ Totals ►►►						1.88E-01	5.92 E+00	2.19 E+02
*stated as % balance										

Reference Values

Decay Heat

Isotope	Watts/ gram
Pu238	5.67E-01
Pu239	1.90E-03
Pu240	7.10E-03
Pu241	1.25E-02
Pu242	1.00E-04
Am241	1.15E-01

DOE-STD-3013-00, Table B-5

Reference Values

A_2 values of radionuclides

Isotope	A_2 (Ci)	Ci/g
Pu238	2.70 E-02	1.70 E+01
Pu239	2.70 E-02	6.20E -02
Pu240	2.70 E-02	2.30 E-01
Pu241	1.60 E+00	1.00 E+02
Pu242	2.70 E-02	3.90 E-03
Am241	2.70 E-02	3.40 E+00

49 CFR 173.435, Table of A1 and A2 Values for Radionuclides

Dose rate calculations:

Total (max) dose (5X)	Surface	0.3m (1ft)	1.0m (3.3 ft)
	9.72E+03	2.65E-01	2.45E-02

The maximum dose rates stated above assumes the following: 1) three bonded Pu/Be disks are assumed to preferentially stack during HAC conditions (see layout at right), 2) the alpha barrier between the 3 bonded Pu/Be disks are conservatively ignored, 3) the 3 bonded Pu/Be disks without alpha barriers yield 5 instances of Pu/Be contact surfaces, and 4) the dose rate is calculated for 5X a given Pu/Be surface area of an undefined disk diameter (max)***.

*** The bonded Pu/Be disk diameter is not stated due to a security classification determination. The information (disk diameter) is available through classified communication.

Unit dose (mrem/h/cm2) provided in LANL Memorandum, RP-3-08-32, Crawford to Caviness, Subject: MT52-Be Interface Disc Dose Calculations

Configuration Layout

The following configuration shows 3 bonded Pu/Be disks preferentially stacked with the alpha barriers conservatively removed to yield 5 instances of Pu/Be contact surfaces.

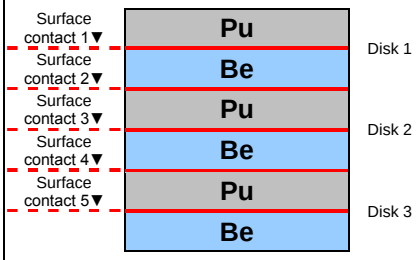

Impurity Limits (max)

Values in parts per million (ppm)

Al: 100	Fe: 200	Ta: 100
Am: 200	Ga: N/A	Th: 100
B: 50	Mg: 500	Ti: N/A
Be: N/A	Mn: 100	U: 100
C: 200	Ni: 100	W: 200
Ca: 500	Np: 100	Zn: 100
Cd: 10	Pb: 100	
Cr: 100	Si: 100	
Cu: 100	Sn: 100	

LANL Specification 55Y-638728

Maximum PU Oxide and Curies (CI) formed in the TB-1 with a 21% Oxygen

Oxide and Curie Values					
No Pu-241decay (100% Pu-241)			100% Pu-241decay (100% Am-241)		
Isotope	Oxide (g)	Curies	Isotope	Oxide (g)	Curies
Pu-238	1.73E-03	2.94E-02	Pu-238	1.73E-03	2.94E-02
Pu-239	3.20E+00	1.98E-01	Pu-239	3.20E+00	1.98E-01
Pu-240	2.25E-01	5.17E-02	Pu-240	2.25E-01	5.17E-02
Pu-241	3.46E-02	3.46E+00	Pu-241	0.00E+00	0.00E+00
Pu-242	3.46E-03	1.35E-05	Pu-242	3.50E-03	1.37E-05
Am-241	0.00E+00	0.00E+00	Am-241	3.46E-02	1.18E-01
Total:	3.46E+00	3.74E+00	Total:	3.46E+00	3.97E-01

Isotopic % (max)	
Pu-238	0.05%
Pu-239	92.35%
Pu-240	6.50%
Pu-241	100%
Pu-242	0.10%
Am-241	0.00%
LANL Specification 55Y-638728	

Reference Values		
radionuclides		
Isotope	A_2(Ci)	Ci/g
Pu-238	2.70E-02	17.0E+01
Pu-239	2.70E-02	6.20E-02
Pu-240	2.70E-02	2.30E-01
Pu-241	1.60E+00	1.00E+02
Pu-242	2.70E-02	3.90E-03
Am-241	2.70E-02	3.40E+00
49 CFR 173.435, Table of A_1 and A_2 Values for Radionuclides		

Basis of Calculated Values			
Variable:	Variable Unit:	Value	Definition of value
pressure inside of TB-1, P	atmosphere (atm)	0.21	1 atmosphere pressure at 21% O_2 in TB-1
Internal volume of TB-1, V	cubic centimeters (cm^3)	1460.00	internal volume of TB-1 without contents as stated in the PAT-1 SAR
universal gas constant, R	constant	82.06	gas constant values based on pressure and volume units
temperature, T	kelvin (K)	298.00	assumes room temperature of 25°C
O_2 in TB-1 internal volume, n	moles	0.013	n = PV/RT (ideal gas law is suitable since the compressibility factor (Z) for air at 1.01 bar and 15°C (59°F) is 0.9992)
PuO_2 formed from O_2 in the TB-1, m	moles	0.013	$Pu(s) + O_2(g) \rightarrow PuO_2(s)$
Molar mass PuO_2, M	constant	276	grams per mole (assuming molar mass of Pu = 244)
PuO_2 formed, g	grams (g)	3.46	grams of PuO_2 formed when all O_2 reacts completely in the sealed TB-1

Basis of Calculated Values			
Variable:	Variable Unit:	Value	Definition of value
pressure inside of TB-1, P	atmosphere (atm)	0.00010	1 atmosphere pressure at 100 ppm O_2 in TB-1
Internal volume of TB-1, V	cubic centimeters (cm^3)	1460.00	internal volume of TB-1 without contents as stated in the PAT-1 SAR
universal gas constant, R	constant	82.06	gas constant values based on pressure and volume units
temperature, T	kelvin (K)	298.00	assumes room temperature of 25°C
O_2 in TB-1 internal volume, n	moles	5.97E-06	n = PV/RT (ideal gas law is suitable since the compressibility factor (Z) for air at 1.01 bar and 15°C (59°F) is 0.9992)
PuO_2 formed from O_2 in the TB-1, m	moles	5.97E-06	$Pu(s) + O_2(g) \rightarrow PuO_2(s)$
Molar mass PuO_2, M	constant	276.06	grams per mole (assuming molar mass of Pu = 244)
PuO_2 formed, g	grams (g)	1.65E-03	grams of PuO_2 formed when all O_2 reacts completely in the sealed TB-1

4.5.2.1 Summary of Maximum Pu Oxide and Curies (Ci) Formed in the TB-1 with 21% and 100 ppm Oxygen:

An analysis[1] was performed to determine the maximum quantity of PuO_2 that would form on the plutonium metal content contained within the TB-1 containment vessel. The table on Page 5 of 5 in LA-UR-08-05154 in this appendix presents the analysis methodology for calculating the quantities of oxides formed. The TB-1, which is normally filled with glove box atmosphere, was assumed to contain 1 atmosphere of air at 21% O_2. Using a TB-1 conservative internal empty volume of 1460 cm^3 (89.19 in^3) and the Ideal Gas Law, there are 0.013 moles of O_2 in the internal volume and 0.013 moles of PuO_2 in the TB-1. The molar mass of PuO_2 is 276 g/mole assuming a molar mass of Pu = 244. The quantity of PuO_2 formed is 3.46 g when all of the O_2 reacts completely inside of a sealed TB-1. Because this is an oxygen-limited system, no more than 3.46 g (0.0076 lb) of PuO_2 are formed when all of the O_2 completely reacts inside of a sealed TB-1 containment vessel.

If a glove box atmosphere (assume all 100 ppm oxygen in an inert atmosphere) is assumed within the TB-1, the quantity of PuO_2 formed on the surface of the plutonium metal content is 1.64 mg (3.62 E-6 lb).

To determine the isotopic composition of the PuO_2 that was formed, Los Alamos National Laboratory (LANL) Specification 55Y-638728[4] on Page 5 of 5 in LA-UR-08-0514 in this appendix presents the maximum isotopic composition for the Pu contents. Included in the table are oxide and curie values assuming no decay (100% Pu-241) and 100% Pu-241 decay to Am-241.

The above calculations provide estimates of the amount of oxides formed due to the oxygen present in the T-Ampoule from the glovebox atmosphere and assumption of air. The oxide formation does not affect the safety of the package since the containment analysis assumed that all of the plutonium material was in its most dispersible form.

4.5.2.2 Reference

1. Caviness, M. L., and J.B. Rubin. “Authorized Contents Proposed for the Plutonium Air Transporter (PAT-1) Packaging (U),” LA-UR-08-05154. Los Alamos National Laboratory. Los Alamos, NM: August 7, 2008.

4.5.3 Helium Generation

PAT-1 Analyses for Helium Generation

Ruth F. Weiner

Sandia National Laboratories

Calculation of Helium Production

A helium is produced when an alpha particle, which is a helium nucleus, picks up an electron. The production rate of helium is thus directly proportional to the production rate of alpha particles. The production rate of alpha particles is equal to the rate of decay of alpha emitters: each decay results in an alpha particle. The basic equation for radioactive decay is

$$N = N_0 \exp(-\lambda t) \qquad (1)$$

Where N = the number of atoms of the radionuclide at time t
N_0= the number of atoms of the radionuclide at time t=0
$\lambda = \ln 2/t_{1/2}$; $t_{1/2}$ is the half life of the radionuclide

When a radionuclide emits an alpha particle, the atomic number decreases by 2 and the mass number decreases by 4, because an alpha particle is a helium nucleus: ${}_2He^4$. The radionuclides in delta plutonium emit alpha particles by the following equations:

${}_{94}Pu^{238} = \alpha + {}_{92}U^{234}$
${}_{94}Pu^{239} = \alpha + {}_{92}U^{235}$
${}_{94}Pu^{240} = \alpha + {}_{92}U^{236}$
${}_{94}Pu^{242} = \alpha + {}_{92}U^{238}$

However, ${}_{94}Pu^{241}$ is a beta emitter and decays by the equation ${}_{94}Pu^{241} = \beta^- + {}_{95}Am^{241}$ since a beta particle is the same as an electron. ${}_{95}Am^{241}$ decays by emitting an alpha particle by the equation ${}_{95}Am^{241} = \alpha + {}_{93}Np^{237}$

Table1 gives the radioactive composition of delta plutonium and the half-lives of each radioactive component:

Table 1. Radioactive Composition of Delta and Half-Lives of Each Radioactive Component

Element	Atomic mass	gm/gm delta[1]	$t_{1/2}$ (yr)	$t_{1/2}$ sec	λ	Bq/gm delta	Ci/gm delta
Pu	238	0.0001	87.7	2.77E+09	2.51E-10	6.34E+07	1.71E-03
Pu	239	0.9378	24100	7.60E+11	9.12E-13	2.15E+09	5.82E-02
Pu	240	0.06	6560	2.07E+11	3.35E-12	5.04E+08	1.36E-02
Pu	241	0.002	14.4	4.54E+08	1.53E-09	7.62E+09	2.06E-01
Pu	242	0.0002	3.75E+05	1.18E+13	5.86E-14	2.92E+04	7.88E-07
Am	241	0	432	1.36E+10	5.09E-11	0	0
U	234	0	2.46E+05	7.76E+12	8.93E-14	0	0

One Becquerel (Bq) is = sec^{-1}. The numbers in the last column were obtained by the equation that converts mass to radioactivity:

$$Bq = \frac{(ln2)(6.02\ x\ 10^{23})\left(\frac{gm}{gm\ atomic\ wt}\right)}{t_{1/2}} \qquad (2)$$

Where Bq = the radioactivity in sec^{-1}; one curie (Ci) = 3.7×10^{10} Bq.

6.02×10^{23} is Avogadro's number, the number of atoms in one gram atomic weight
$t_{1/2}$ = half life of the radionuclide in seconds.
$\ln(2)/t_{1/2} = \lambda$

So that, e.g.,

$6.34\ x\ 10^{7} = \lambda\ (6.02 \times 10^{23})(0.0001/238) = (2.51 \times 10^{-10})\ (6.02 \times 10^{23})(0.0001/238)$

The last column in Table 1 thus gives the initial activity—the N_0—of each radionuclide.

$_{95}Am^{241}$ builds up as $_{94}Pu^{241}$ decays, by the first Bateman equation

$$N_{Am}(t) = N_{Pu}(t) * \left(\frac{\lambda_{Pu}}{\lambda_{Am} - \lambda_{Pu}}\right) * \{exp(-\lambda_{Pu}t) - exp(-\lambda_{Am}t)\}$$

Where $N_{Am}(t)$ = the number of $_{95}Am^{241}$ atoms at time t

$N_{Pu}(t)$ = the number of $_{94}Pu^{241}$ atoms at time t

Am refers to $^{95}Am^{241}$

Pu refers to $_{94}Pu^{241}$

$_{92}U^{234}$ builds up by a similar equation. Because of its long half-life, however, its alpha decay does not contribute significantly to helium production.

Conversion from radioactivity to weight can be done in two ways—by using Equation (2) or by calculating Bq/gm delta or Ci/gm delta from Table 1 (which is based on Equation (2)). The latter was used, resulting in Table 2. The values for $_{95}Am^{241}$ and $_{92}U^{234}$ were calculated using Equation (2).

Table 2. Weight Conversions

Element	gm/gm delta	Ci/gm delta	Ci/gm
Pu-238	0.0001	1.71E-03	1.71E-03
Pu-239	0.9378	5.82E-02	6.21E-02
Pu-240	0.06	1.36E-02	2.27E-01
Pu-241	0.002	2.06E-01	1.03E+02
Pu-242	0.0002	7.88E-07	3.94E-03
Am-241	0	0	3.43
U-234	0	0	6.21E-03

Every decay produces an alpha particle and every alpha particle becomes a helium atom. Equation (1) allows calculation of decay of each radionuclide, and Equation (2) relates that decay to loss of mass of that radionuclide. Because of conservation of mass, the mass of He produced is equal to the total loss of mass of the decaying radionuclides, or

$$gm(He_t) = gm(delta_{t=0})-\{gm(Pu\text{-}238_t)+gm(Pu\text{-}239_t)+gm(Pu\text{-}240_t)+gm(Pu\text{-}241_t)+ gm(Pu\text{-}242_t)+ gm(Am\text{-}241_t)+ gm(U\text{-}234_t)\} \quad (3)$$

where the subscript t is time.

Calculation of Gas Pressure

The basic equation is the Ideal Gas Law:

$$pV = nRT$$
$$p = nRT/V \quad (4)$$

where p = total pressure in the volume V
V = void volume
T = absolute temperature (K)
N = number of moles of gas
R = the gas constant, 0.082 liter-atm/mole-K

Calculations were done using liters, atmospheres, etc., and converted to psia at the end. Conversions used were:

1 mole He = 4 grams
$n(He_t) = gm(He_t)/4$
$gm(He_t)$: from Equation (3).
K = °C + 273
1 atm = 14.7 psia

Since the container was initially filled at atmospheric pressure, the total pressure in atmospheres at any time t, at a particular volume and temperature, is

$$p_t = 1 + p(He_t) = 1 + n(He_t)*RT/V \quad (5)$$

The TB-1 and the TB-1 internal configurations were considered. From Table 3, the SC-1 and SC-2 quantities were less the 831 g Electro-Refined (ER) Pu hollow cylinder. The 1300 gram Pu metal hollow cylinder represents an upper limit of the quantity of Pu metal considered for the PAT-1 and is presented for reference. Consequently, pressure calculations for alpha decay were only performed for the 831 and 1300 gram amounts. The temperatures considered were the "normal" extremes, -40ºC (-40ºF) NCT temperature (104ºC), 136ºC (276ºF) HAC fire temperature, and 582ºC (1080ºF) in the accident conditions of plutonium air transport fire. A calculation at room temperature (21ºC) was provided for reference.

Containments were assumed to be loaded at 1 atmosphere pressure (14.7 psi). Table 3 presents RT/V at these temperatures and volumes.

A 1300 g evaluation is provided for reference in Tables 3, 5, and 7; 831 g is the maximum plutonium content for this addendum. Helium generation was calculated from the mass loss of

the Pu isotopic mixture. Table 4 shows the helium generation, per g of plutonium isotopic mixture, for the first year.

Table 3. RT/V for TB-1 Containment

	Maximum Plutonium Mass (g)	676.00	523.00	831.00	1300.00
		Void Volume TB-1 Containment Boundary (liters)			
		1.1103	1.1112	1.2749	1.2519
Deg C	**Deg K**	**P=RT/V(atm/mole)[a]**			
104	377	27.84	27.82	24.25	24.69
-40	233	17.21	17.19	14.99	15.26
136	409	30.21	30.18	26.31	26.79
20	293	21.64	21.62	18.85	19.19
582	855	63.15	63.09	54.99	56.00

[a]R=0.082 liter-atm/mole-deg

Table 4. Helium Generation Per Gram of Pu Isotopic Mixture for One Year

Time (weeks)	gm Pu	gm He	moles He	Time (weeks)	gm Pu	gm He	moles He
0	1.00E+00	0.00E+00	0.00E+00	28	1.00E+00	3.06E-07	7.65E-08
2	1.00E+00	2.19E-08	5.46E-09	30	1.00E+00	3.28E-07	8.20E-08
4	1.00E+00	4.37E-08	1.09E-08	32	1.00E+00	3.50E-07	8.74E-08
6	1.00E+00	6.56E-08	1.64E-08	34	1.00E+00	3.72E-07	9.29E-08
8	1.00E+00	8.74E-08	2.19E-08	36	1.00E+00	3.93E-07	9.83E-08
10	1.00E+00	1.09E-07	2.73E-08	38	1.00E+00	4.15E-07	1.04E-07
12	1.00E+00	1.31E-07	3.28E-08	40	1.00E+00	4.37E-07	1.09E-07
14	1.00E+00	1.53E-07	3.82E-08	42	1.00E+00	4.59E-07	1.15E-07
16	1.00E+00	1.75E-07	4.37E-08	44	1.00E+00	4.81E-07	1.20E-07
18	1.00E+00	1.97E-07	4.92E-08	46	1.00E+00	5.03E-07	1.26E-07
20	1.00E+00	2.19E-07	5.46E-08	48	1.00E+00	5.24E-07	1.31E-07
22	1.00E+00	2.40E-07	6.01E-08	50	1.00E+00	5.46E-07	1.37E-07
24	1.00E+00	2.62E-07	6.56E-08	52	1.00E+00	5.68E-07	1.42E-07
26	1.00E+00	2.84E-07	7.10E-08				

The partial pressure of helium and the total pressure in the containment depend on the containment volume and on the temperature. The total pressure is the sum of the partial pressure of helium and the pressure at which the containment was loaded; the latter is assumed to be one atmosphere (14.7 psi).

The container was assumed to be filled at ambient temperature (294 K or 21 deg. C) and to reach the indicated temperature quickly. At two weeks the indicated temperature would have been reached. The helium pressure, shown in Table 3, is thus:

$$P_{He} = n_{He}*(RT/V)$$

where $n_{He} = gm_{He}/4$

T= the final average temperature in Kelvin (absolute)
V = 1.252 liters
R = 0.082 l-atm/mole K, the gas constant.
Pressure in psi= 14.7*Pressure in atmospheres

Table 5 shows helium pressure increase in atm and psi in the TB-1 in weeks up to one year assuming 1300 g Pu content.

Table 5. Helium Pressure Increase in TB-1, Void Volume 1.252 Liters, for 1300 g Pu

	deg C	104	-40	136	582	104	-40	136	582
	Kelvin	377	233	409	855	377	233	409	855
	RT/V	24.69	15.26	26.79	56.18	24.69	15.26	26.79	56.18
	gm Pu	1300.0	1300.0	1300.0	1300.0	1300.0	1300.0	1300.0	1300.0
Weeks	**mole He/gm**	**Atmospheres**				**PSI**			
0	0.000	0.000	0.000	0.000	0.000	0.000	0.000	0.000	0.000
2	5.46E-09	1.75E-04	1.08E-04	1.90E-04	3.98E-04	2.58E-03	1.59E-03	2.80E-03	5.85E-03
4	1.09E-08	3.51E-04	2.17E-04	3.81E-04	7.96E-04	5.16E-03	3.19E-03	5.59E-03	1.17E-02
6	1.64E-08	5.26E-04	3.25E-04	5.71E-04	1.19E-03	7.74E-03	4.78E-03	8.39E-03	1.75E-02
8	2.19E-08	7.02E-04	4.34E-04	7.61E-04	1.59E-03	1.03E-02	6.37E-03	1.12E-02	2.34E-02
10	2.73E-08	8.77E-04	5.42E-04	9.51E-04	1.99E-03	1.29E-02	7.97E-03	1.40E-02	2.92E-02
12	3.28E-08	1.05E-03	6.50E-04	1.14E-03	2.39E-03	1.55E-02	9.56E-03	1.68E-02	3.51E-02
14	3.82E-08	1.23E-03	7.59E-04	1.33E-03	2.78E-03	1.80E-02	1.12E-02	1.96E-02	4.09E-02
16	4.37E-08	1.40E-03	8.67E-04	1.52E-03	3.18E-03	2.06E-02	1.27E-02	2.24E-02	4.68E-02
18	4.92E-08	1.58E-03	9.76E-04	1.71E-03	3.58E-03	2.32E-02	1.43E-02	2.52E-02	5.26E-02
20	5.46E-08	1.75E-03	1.08E-03	1.90E-03	3.98E-03	2.58E-02	1.59E-02	2.80E-02	5.85E-02
22	6.01E-08	1.93E-03	1.19E-03	2.09E-03	4.38E-03	2.84E-02	1.75E-02	3.08E-02	6.43E-02
24	6.56E-08	2.10E-03	1.30E-03	2.28E-03	4.77E-03	3.09E-02	1.91E-02	3.36E-02	7.02E-02
26	7.10E-08	2.28E-03	1.41E-03	2.47E-03	5.17E-03	3.35E-02	2.07E-02	3.64E-02	7.60E-02
28	7.65E-08	2.46E-03	1.52E-03	2.66E-03	5.57E-03	3.61E-02	2.23E-02	3.92E-02	8.19E-02
30	8.20E-08	2.63E-03	1.63E-03	2.85E-03	5.97E-03	3.87E-02	2.39E-02	4.20E-02	8.77E-02
32	8.74E-08	2.81E-03	1.73E-03	3.04E-03	6.36E-03	4.13E-02	2.55E-02	4.48E-02	9.36E-02
34	9.29E-08	2.98E-03	1.84E-03	3.23E-03	6.76E-03	4.38E-02	2.71E-02	4.76E-02	9.94E-02
36	9.83E-08	3.16E-03	1.95E-03	3.43E-03	7.16E-03	4.64E-02	2.87E-02	5.03E-02	1.05E-01
38	1.04E-07	3.33E-03	2.06E-03	3.62E-03	7.56E-03	4.90E-02	3.03E-02	5.31E-02	1.11E-01
40	1.09E-07	3.51E-03	2.17E-03	3.81E-03	7.96E-03	5.16E-02	3.19E-02	5.59E-02	1.17E-01
42	1.15E-07	3.68E-03	2.28E-03	4.00E-03	8.35E-03	5.41E-02	3.35E-02	5.87E-02	1.23E-01
44	1.20E-07	3.86E-03	2.38E-03	4.19E-03	8.75E-03	5.67E-02	3.51E-02	6.15E-02	1.29E-01
46	1.26E-07	4.03E-03	2.49E-03	4.38E-03	9.15E-03	5.93E-02	3.66E-02	6.43E-02	1.34E-01
48	1.31E-07	4.21E-03	2.60E-03	4.57E-03	9.55E-03	6.19E-02	3.82E-02	6.71E-02	1.40E-01
50	1.37E-07	4.38E-03	2.71E-03	4.76E-03	9.94E-03	6.45E-02	3.98E-02	6.99E-02	1.46E-01
52	1.42E-07	4.56E-03	2.82E-03	4.95E-03	1.03E-02	6.70E-02	4.14E-02	7.27E-02	1.52E-01

Table 6 shows the helium pressure increase in atm and psi in the TB-1, in weeks up to one year assuming an 831 g Pu content.

Table 6. Helium Pressure in TB-1, Void Volume 1.275 Liters, for 831 g Pu

	deg C	104	-40	136	582	104	-40	136	582
	deg K	377	233	409	855	377	233	409	855
	RT/V	24.25	14.99	26.31	54.99	24.25	14.99	26.31	54.99
	gm Pu	831	831	831	831	831	831	831	831
Weeks	mole He/gm	Atmospheres				PSI			
0	0.00	0.00	0.00	0.00	0.00	0.0000	0.0000	0.0000	0.000
2	5.46E-09	1.10E-04	6.80E-05	1.19E-04	2.50E-04	0.0016	0.0010	0.0018	0.004
4	1.09E-08	2.20E-04	1.36E-04	2.39E-04	4.99E-04	0.0032	0.0020	0.0035	0.007
6	1.64E-08	3.30E-04	2.04E-04	3.58E-04	7.49E-04	0.0049	0.0030	0.0053	0.011
8	2.19E-08	4.40E-04	2.72E-04	4.78E-04	9.99E-04	0.0065	0.0040	0.0070	0.015
10	2.73E-08	5.50E-04	3.40E-04	5.97E-04	1.25E-03	0.0081	0.0050	0.0088	0.018
12	3.28E-08	6.61E-04	4.08E-04	7.17E-04	1.50E-03	0.0097	0.0060	0.0105	0.022
14	3.82E-08	7.71E-04	4.76E-04	8.36E-04	1.75E-03	0.0113	0.0070	0.0123	0.026
16	4.37E-08	8.81E-04	5.44E-04	9.56E-04	2.00E-03	0.0129	0.0080	0.0140	0.029
18	4.92E-08	9.91E-04	6.12E-04	1.07E-03	2.25E-03	0.0146	0.0090	0.0158	0.033
20	5.46E-08	1.10E-03	6.80E-04	1.19E-03	2.50E-03	0.0162	0.0100	0.0176	0.037
22	6.01E-08	1.21E-03	7.48E-04	1.31E-03	2.75E-03	0.0178	0.0110	0.0193	0.040
24	6.56E-08	1.32E-03	8.17E-04	1.43E-03	3.00E-03	0.0194	0.0120	0.0211	0.044
26	7.10E-08	1.43E-03	8.85E-04	1.55E-03	3.25E-03	0.0210	0.0130	0.0228	0.048
28	7.65E-08	1.54E-03	9.53E-04	1.67E-03	3.50E-03	0.0227	0.0140	0.0246	0.051
30	8.20E-08	1.65E-03	1.02E-03	1.79E-03	3.75E-03	0.0243	0.0150	0.0263	0.055
32	8.74E-08	1.76E-03	1.09E-03	1.91E-03	3.99E-03	0.0259	0.0160	0.0281	0.059
34	9.29E-08	1.87E-03	1.16E-03	2.03E-03	4.24E-03	0.0275	0.0170	0.0298	0.062
36	9.83E-08	1.98E-03	1.22E-03	2.15E-03	4.49E-03	0.0291	0.0180	0.0316	0.066
38	1.04E-07	2.09E-03	1.29E-03	2.27E-03	4.74E-03	0.0307	0.0190	0.0334	0.070
40	1.09E-07	2.20E-03	1.36E-03	2.39E-03	4.99E-03	0.0324	0.0200	0.0351	0.073
42	1.15E-07	2.31E-03	1.43E-03	2.51E-03	5.24E-03	0.0340	0.0210	0.0369	0.077
44	1.20E-07	2.42E-03	1.50E-03	2.63E-03	5.49E-03	0.0356	0.0220	0.0386	0.081
46	1.26E-07	2.53E-03	1.56E-03	2.75E-03	5.74E-03	0.0372	0.0230	0.0404	0.084
48	1.31E-07	2.64E-03	1.63E-03	2.87E-03	5.99E-03	0.0388	0.0240	0.0421	0.088
50	1.37E-07	2.75E-03	1.70E-03	2.99E-03	6.24E-03	0.0405	0.0250	0.0439	0.092
52	1.42E-07	2.86E-03	1.77E-03	3.11E-03	6.49E-03	0.0421	0.0260	0.0456	0.095

Table 7 presents helium pressure increase for all four masses of Pu at ambient temperature (21°C; 294 K) with their respective void volumes.

Table 7. Helium Pressure Increase in TB-1, Void Volume at 21 degrees C (294 K)

	V (liters	1.1103	1.1112	1.2749	1.2519	1.1103	1.1112	1.2749	1.2519
	RT/V	21.71	21.70	18.91	19.26	21.71	21.70	18.91	19.26
	gm Pu	676.00	523.00	831.00	1300.00	676.00	523.00	831.00	1300.0
Week	mole He/gm	Atmospheres				PSI			
0	0.00	0.00	0.00	0.00	0.00	0.00	0.00	0.00	0.00
2	5.46E-09	8.02E-05	6.20E-05	8.59E-05	1.37E-04	1.18E-03	9.11E-04	1.26E-03	2.01E-03
4	1.09E-08	1.60E-04	1.24E-04	1.72E-04	2.74E-04	2.36E-03	1.82E-03	2.52E-03	4.02E-03
6	1.64E-08	2.41E-04	1.86E-04	2.58E-04	4.10E-04	3.54E-03	2.73E-03	3.79E-03	6.03E-03
8	2.19E-08	3.21E-04	2.48E-04	3.43E-04	5.47E-04	4.72E-03	3.65E-03	5.05E-03	8.04E-03
10	2.73E-08	4.01E-04	3.10E-04	4.29E-04	6.84E-04	5.89E-03	4.56E-03	6.31E-03	1.01E-02
12	3.28E-08	4.81E-04	3.72E-04	5.15E-04	8.21E-04	7.07E-03	5.47E-03	7.57E-03	1.21E-02
14	3.82E-08	5.61E-04	4.34E-04	6.01E-04	9.57E-04	8.25E-03	6.38E-03	8.83E-03	1.41E-02
16	4.37E-08	6.42E-04	4.96E-04	6.87E-04	1.09E-03	9.43E-03	7.29E-03	1.01E-02	1.61E-02
18	4.92E-08	7.22E-04	5.58E-04	7.73E-04	1.23E-03	1.06E-02	8.20E-03	1.14E-02	1.81E-02
20	5.46E-08	8.02E-04	6.20E-04	8.59E-04	1.37E-03	1.18E-02	9.11E-03	1.26E-02	2.01E-02
22	6.01E-08	8.82E-04	6.82E-04	9.44E-04	1.50E-03	1.30E-02	1.00E-02	1.39E-02	2.21E-02
24	6.56E-08	9.62E-04	7.44E-04	1.03E-03	1.64E-03	1.41E-02	1.09E-02	1.51E-02	2.41E-02
26	7.10E-08	1.04E-03	8.06E-04	1.12E-03	1.78E-03	1.53E-02	1.18E-02	1.64E-02	2.61E-02
28	7.65E-08	1.12E-03	8.68E-04	1.20E-03	1.91E-03	1.65E-02	1.28E-02	1.77E-02	2.81E-02
30	8.20E-08	1.20E-03	9.30E-04	1.29E-03	2.05E-03	1.77E-02	1.37E-02	1.89E-02	3.02E-02
32	8.74E-08	1.28E-03	9.92E-04	1.37E-03	2.19E-03	1.89E-02	1.46E-02	2.02E-02	3.22E-02
34	9.29E-08	1.36E-03	1.05E-03	1.46E-03	2.33E-03	2.00E-02	1.55E-02	2.15E-02	3.42E-02
36	9.83E-08	1.44E-03	1.12E-03	1.55E-03	2.46E-03	2.12E-02	1.64E-02	2.27E-02	3.62E-02
38	1.04E-07	1.52E-03	1.18E-03	1.63E-03	2.60E-03	2.24E-02	1.73E-02	2.40E-02	3.82E-02
40	1.09E-07	1.60E-03	1.24E-03	1.72E-03	2.74E-03	2.36E-02	1.82E-02	2.52E-02	4.02E-02
42	1.15E-07	1.68E-03	1.30E-03	1.80E-03	2.87E-03	2.48E-02	1.91E-02	2.65E-02	4.22E-02
44	1.20E-07	1.76E-03	1.36E-03	1.89E-03	3.01E-03	2.59E-02	2.00E-02	2.78E-02	4.42E-02
46	1.26E-07	1.84E-03	1.43E-03	1.97E-03	3.15E-03	2.71E-02	2.10E-02	2.90E-02	4.62E-02
48	1.31E-07	1.92E-03	1.49E-03	2.06E-03	3.28E-03	2.83E-02	2.19E-02	3.03E-02	4.83E-02
50	1.37E-07	2.00E-03	1.55E-03	2.15E-03	3.42E-03	2.95E-02	2.28E-02	3.16E-02	5.03E-02
52	1.42E-07	2.08E-03	1.61E-03	2.23E-03	3.56E-03	3.06E-02	2.37E-02	3.28E-02	5.23E-02

4.5.3.1 Reference

1. Caviness, M., LANL Content Description for PAT-1 PACKAGING, Updated August 9, 2007.

4.5.4 O-Ring Decomposition

LA-UR-10-05846

Approved for public release; distribution is unlimited.

Title:	Thermal Decomposition of Viton® O-rings for the PAT-1 Packaging Accident Scenario
Author(s):	J.B. Rubin
Intended for:	Support an amendment application to the US Nuclear Regulatory Commission for the PAT-1 packaging

Los Alamos NATIONAL LABORATORY EST. 1943

Los Alamos National Laboratory, an affirmative action/equal opportunity employer, is operated by the Los Alamos National Security, LLC for the National Nuclear Security Administration of the U.S. Department of Energy under contract DE-AC52-06NA25396. By acceptance of this article, the publisher recognizes that the U.S. Government retains a nonexclusive, royalty-free license to publish or reproduce the published form of this contribution, or to allow others to do so, for U.S. Government purposes. Los Alamos National Laboratory requests that the publisher identify this article as work performed under the auspices of the U.S. Department of Energy. Los Alamos National Laboratory strongly supports academic freedom and a researcher's right to publish; as an institution, however, the Laboratory does not endorse the viewpoint of a publication or guarantee its technical correctness.

Form 836 (7/06)

Abstract

As part of the submission package to the NRC to amend the approved contents for the PAT-1 container, a calculation was necessary to determine the theoretical pressure rise in the PAT-1 containment vessel (TB-1) due to the thermal decomposition of O-rings within the container. These o-rings are composed of Viton®A, whose number and mass are determined by the internal packing configuration. This report contains a conservative calculation of the decomposition of these O-rings, in the theoretical accident conditions defined by the PAT-1 SARP. The calculation assumes a scenario whereby the O-ring material is completely volatized, using a reaction scheme which generates the maximum number of gaseous reaction products, and the maximum pressure rise within the TB-1. The results show that even for the case of complete thermal decomposition to gaseous products, the total pressure rise inside of the TB-1 containment vessel is less than the maximum allowable, as defined in the PAT-1 SARP.

The o-rings are treated as tori, with a volume given by

$$V = (2\pi R)(\pi r^2) \quad (1)$$

where r is the radius of the cross-sectional area of the torus and R is the distance from the center of the torus to the center of the cross sectional area, Figure 1 :

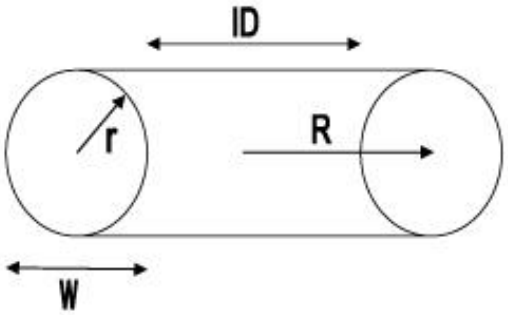

Figure 1. Cross section of a torus, showing the dimensional relations to Eq. (1).

Table 1. Dimensions and volumes of Viton A® O-rings contained within the TB-1 for the Packing Configurations described in Table 3 and shown schematically in Figure 2.

O-ring location	O-ring Size Standard[i]	w (in)	r (in)	ID (in)	R (in)	Volume (in^3)	Volume (cm^3)
T-Ampoule[ii]	241	0.139	0.070	3.859	2.000	0.1906	3.1233
SC-1/2	147	0.103	0.052	2.675	1.389	0.0727	1.1916
Packing Configuration #1							
T-Ampoule	241	0.139	0.070	3.859	2.000	0.1906	3.1233
					Total	**0.1906**	**3.1233**
Packing Configuration #2							
T-Ampoule	241	0.139	0.070	3.859	2.000	0.1906	3.1233
SC-2	147	0.103	0.052	2.675	1.389	0.0727	1.1916
SC-2	147	0.103	0.052	2.675	1.389	0.0727	1.1916
					Total	**0.3360**	**5.5065**
Packing Configuration #3							
T-Ampoule	241	0.139	0.070	3.859	2.000	0.1906	3.1233
SC-1	147	0.103	0.052	2.675	1.389	0.0727	1.1916
SC-1	147	0.103	0.052	2.675	1.389	0.0727	1.1916
SC-1	147	0.103	0.052	2.675	1.389	0.0727	1.1916
					Total	**0.4087**	**6.6981**

Table 1 gives the relevant dimensions (w, r and R as defined in Figure 1) of the O-rings, while the ID and w are provided from SAE AS568C "Aerospace Size Standard for O-rings". From these dimensions, the volume of each O-ring is calculated using Eq. (1) and compared to the values given in the SAE AS568C standard (as verification that the volume of each O-ring is accurate). From these individual O-ring volumes, the total O-ring (volume) inventory in the TB-1, for each of the three packing configurations, is obtained. ***Note that the TB-1 O-ring is not used for the plutonium metal shipments and is not included in the volume calculation.***

Based on literature review, the reaction products produced by pyrolysis of Viton A® in air is similar to that of pyrolysis of PTFE in air, namely, CO, CO_2, COF_2, HF, CF_4, C_2F_4, C_3F_6, C_3F_6, C_4F_8. This is to be expected since the atomic species present in the two fluoropolymers are nominally similar, both composed largely of carbon and fluorine. Once volatilized, these atomic species will re-form into other molecular species having stoichiometries determined by the prevailing thermodynamic conditions in the gas phase.

Viton A® is a vinylidene fluoride/hexafluoropropylene copolymer, manufactured by DuPont Corporation, with a nominal composition of 78 wt% CF_2CH_2 and 22 wt% C_3F_6 [iii]. (By comparison, PTFE has a nominal composition of 100 wt% C_2F_4. In the case of PTFE, the hydrogenous compounds observed on pyrolysis would obtain the necessary hydrogen from water vapor, which is invariably present during air oxidation.[iv]) It is noted that air oxidation of

PTFE can result in significant fractions of higher molecular weight products, such as COF_2,[v] relative to the oxidative pyrolysis of Viton A® (which produces larger fractions of HF and CF_4). In order to be ***conservative***, we will assume that the pyrolysis products of Viton A® are composed of lower molecular weight products, resulting in the greatest number of moles of gaseous reaction product, and therefore the largest pressure increase. Consequently, for gas generation calculations, we will assume that the maximum amount of HF(g) is formed, since this specie would form the greatest amount of product, on a molar basis, from the degradation products, and therefore represents the maximum pressure contribution of any (single) pyrolysis product. It is further assumed that any fluorine in excess of that taken up in the formation of HF(g) will react with carbon to form the maximum amount of CF_4(g).

It is known that Viton A® contains inorganic fillers, such as metal oxides and diatomaceous earth, to aid in processing.[vi,vii] Again, to be ***conservative***, no credit is given for any non-volatile components within the elastomer.

In the following section, a calculation will be given of the pressure rise due to O-ring degradation for Packing Configuration #3, which includes four O-rings, as shown in Table 1. Table 2 gives the results of this calculation, as well as the results for Packing Configurations 1 & 2.

The basis of the calculation assumes the sequential formation of

(1) HF, to completely account for the hydrogen present in the original O-ring material, then

(2) saturated fluorocarbon (CF_4), to account for the excess amount of fluorine over that taken up by HF formation, followed lastly by

(3) either CO(g) or CO_2(g), to account for the excess amount of carbon remaining after accounting for the hydrogen and fluorine present in the original O-ring(s).

This reaction scheme results in the maximum number of moles of gaseous reaction products, thereby generating the highest amount of internal pressure in the TB-1 unoccupied volume. This is the most conservative case.

For Packing Configuration #3, the total elastomer volume is 6.698 cm^3 (Table 1). Assuming an elastomer specific gravity of 1.8 g/cm^3,[vii] we have 12.057 g of elastomer material, or 9.404 g (0.147 moles) CF_2CH_2 and 2.652 g (0.018 moles) C_3F_6. The overall decomposition reaction, based on the assumed decomposition products is therefore

$$0.147\ CF_2CH_2(s) + 0.018\ C_3F_6(s) \rightarrow 0.320\ C(s) + 0.294\ HF(g) + 0.027\ CF_4(g) \quad (2a)$$

$$0.320\ C(s) + 0.160\ O_2\ (g) \rightarrow 0.320\ CO_2\ (g) \text{ or } 0.320\ CO(g) \quad (2b)$$

For the elastomer inventory in Packing Configuration #3, we have

$$9.404\ g\ CF_2CH_2\left(\frac{37.996\ g\ F}{64.034\ g\ CF_2CH_2}\right) = 5.580\ g\ F \quad (3)$$

$$9.404\ g\ CF_2CH_2\left(\frac{2.016\ g\ H}{64.034\ g\ CF_2CH_2}\right) = 0.296\ g\ H \quad (4)$$

$$9.404\ g\ CF_2CH_2\left(\frac{24.022\ g\ C}{64.034\ g\ CF_2CH_2}\right) = 3.528\ g\ C \quad (5)$$

plus

$$2.652\ g\ C_3F_6\left(\frac{113.988\ g\ F}{150.021\ g\ C_3F_6}\right) = 2.015\ g\ F \quad (6)$$

$$2.652\ g\ C_3F_6\left(\frac{36.033\ g\ C}{150.021\ g\ C_3F_6}\right) = 0.637\ g\ C \quad (7)$$

or

$$7.596\ g\ F \quad (8)$$

$$4.165\ g\ C \quad (9)$$

$$0.296\ g\ H \quad (10)$$

If we assume that all available hydrogen and fluorine are liberated and form the maximum ***moles*** of gaseous products, we would have

$\left(\frac{0.296\ g\ H}{1.008\ g/mole\ H}\right) = 0.294$ moles hydrogen available for HF generation, and

$\left(\frac{7.595\ g\ F}{18.998\ g/mole\ F}\right) = 0.400$ moles total fluorine minus the 0.294 moles of fluorine in HF, leaving 0.106 moles of fluorine available for CF_4(g) generation, or 0.027 moles CF_4(g). If these reaction products add incrementally, and ideally, then we would have 0.294 moles HF(g) + 0.027 mole CF_4(g), or a total of 0.320 moles of gaseous [HF(g) + CF_4(g)] reaction products. For an unoccupied internal TB-1 volume of 1103.01 cm^3 (see Packing Configuration #3 in Table 3), and T = 1080°F (582.2°C, 855.4 K) for the PAT-1 hypothetical accident condition, there would be a pressure increase of[x]

$$P = \frac{(0.320\ \text{mole})\left(82.056\ {}^{\text{atm cm}^3}\!/_{\text{mole K}}\right)(855.4\ \text{K})}{1103.01\ \text{cm}^3} = 20.38\ \text{atm} \qquad (11)$$

or 299.49 psi due to the assumed o-ring degradation products. Once the hydrogen and fluorine are consumed in the formation of HF(g) and CF_4(g), there is a theoretical excess of $\left(\frac{4.165\ \text{g C}}{12.011\ {}^{\text{g}}\!/_{\text{mole}}}\right) = 0.347$ moles of carbon in the virgin elastomer minus 0.027 moles carbon in CF_4, or 0.320 moles.

At this point we could assume that (1) the theoretical excess of carbon will remain as solid, unreactive char, or that (2) the excess carbon can be further reacted with oxygen to form CO(g) or CO_2(g) (the formation of either CO(g) or CO_2(g) would produce the same number of **moles** of gaseous reaction products and therefore, in the ideal gas case, an equal pressure contribution).

The formation of residual carbon char, as opposed to the formation of CO(g) or CO_2(g), would be supported based on (a) any oxygen present at the time of initial packaging is scavenged completely by the formation of plutonium oxide, and (b) the TB-1 remains intact at the theoretical accident conditions. Solid char is experimentally observed, even in the oxidative thermal decomposition of fluoroelastomers.[x,xi,xii] Further, for studies of the thermal degradation of Viton®A in non-oxidizing environments, an incomplete volatilization of the polymer is evidenced by a low yield of fluorine with respect to the theoretical quantity.[xii] However, for the purposes of a ***conservative*** estimate, we assume the case where additional oxygen were to be made available in the TB-1 and sample containers, in a quantity sufficient to react completely with the excess carbon from the elastomer, to produce CO(g) or CO_2 (g). Such a reaction would increase the overall moles of gaseous reaction products to 0.320 moles [HF(g) + CF_4(g)] + 0.320 moles [CO(g) or CO_2(g)], thereby (approximately) doubling the overall pressure rise from 20.38 atm to 40.76 atm, or 598.98 psi.

Table 2 summarizes the calculation given above, which, again, represents the elastomer inventory in Packaging Configuration #3, along with a similar calculation of the remaining two Packing Configurations, which have a reduced elastomer loading.

Table 2. Calculation of elastomer degradation products for the three Packing Configurations described in Table 1 and shown schematically in Figure 2. The summation in the right-hand column of each row is the total number of moles assuming that the excess carbon reacts completely to form gaseous product, either CO(g) or CO_2(g).

Packing Configuration #1 (3.1233 cm^3 of Viton®A)	4.385 g (0.068 moles) CF_2CH_2 1.237 g (0.008 moles) C_3F_6	0.138 g (0.137 moles) H 3.542 g (0.186 moles) F 1.942 g (0.162 moles) C	0.137 moles HF(g) 0.012 moles CF_4(g) 0.149 moles CO(g) ***Σ = 0.299 moles***
Packing Configuration #2 (5.5065 cm^3 of Viton®A)	7.731 g (0.121 moles) CF_2CH_2 2.181 g (0.015 moles) C_3F_6	0.243 g (0.241 moles) H 6.244 g (0.329 moles) F 3.424 g (0.285 moles) C	0.241 moles HF(g) 0.022 moles CF_4(g) 0.263 moles CO(g) ***Σ = 0.527 moles***
Packing Configuration #3 (6.6981 cm^3 of Viton®A)	9.404 g (0.147 moles) CF_2CH_2 2.652 g (0.018 moles) C_3F_6	0.296 g (0.294 moles) H 7.596 g (0.400 moles) F 4.165 g (0.347 moles) C	0.294 moles HF(g) 0.027 moles CF_4(g) 0.320 moles CO(g) ***Σ = 0.640 moles***

Table 3 gives the overall pressure rise calculation for the three Packing Configurations, using the appropriate O-ring inventory (Table 1) and unoccupied TB-1 volume (Table 3) for each Configuration.

Table 3. Internal volume of the TB-1 container (top line), and solid volumes of T-ampoule, filler ring, sample containers (SC-1 or SC-2) and Pu metal payloads for each Packing Configuration (volume of O-ring lubricant and optional tantalum foil are not included). The amount of lubricant on the O-ring would be minimal to permit joining the lid to the body of the T-Ampoule or sample containers. Column 4 gives the pressure rise for the case of complete volatilization of all contained o-ring materials. Column 5 is a summation of the pressure rise from Column 4 plus an additional 2.9 atmospheres, due to an initial 1 atm of pressure assumed to be present in the TB-1 at the time of packaging, and then heated from ambient to 582.2 K during the accident scenario.

components	Volume (in^3)	Volume (cm^3)	Pressure rise (**psi**)	Pressure rise (**psia**)
Empty TB-1	89.10	1460.09		
Packing Configuration #1				
T-ampoule	7.83	128.31		
Filler ring	0.90	14.75		
Pu cylinder 831 g	2.57	42.11		
Unoccupied TB-1 volume	**77.80**	**1274.91**	**241.63**	**284.25**
Packing Configuration #2				
T-ampoule	7.83	128.31		
Filler ring	0.90	14.75		
SC-2	2.75	45.06		
SC-2	2.75	45.06		
SC-2 Cradle Assembly	4.90	80.30		
Pu cylinder 1.1" Ø x 1.1" h	1.05	17.21		
Pu cylinder 1.1" Ø x 1.1" h	1.05	17.21		
Unoccupied TB-1 volume	**67.87**	**1112.19**	**488.33**	**530.94**
Packing Configuration #3				
T-ampoule	7.83	128.31		
Filler ring	0.90	14.75		
SC-1	2.15	35.23		
SC-1	2.15	35.23		
SC-1	2.15	35.23		
SC-1 Cradle Assembly	5.02	82.26		
Pu cylinder 0.88"Ø x 0.88" h	0.53	8.69		
Pu cylinder 0.88"Ø x 0.88" h	0.53	8.69		
Pu cylinder 0.88"Ø x 0.88" h	0.53	8.69		
Unoccupied TB-1 volume	**67.31**	**1103.01**	**598.94**	**641.56**

The PAT-1 SARP (section 4.4.2) stipulates that the maximum allowable internal TB-1 pressure, in the theoretical accident conditions, must remain less than 1,110 psia. The results of this highly conservative calculation of the thermal degradation of Viton® A in the theoretical accident conditions show that this maximum internal pressure is not exceeded for any of the three Packing Configurations.

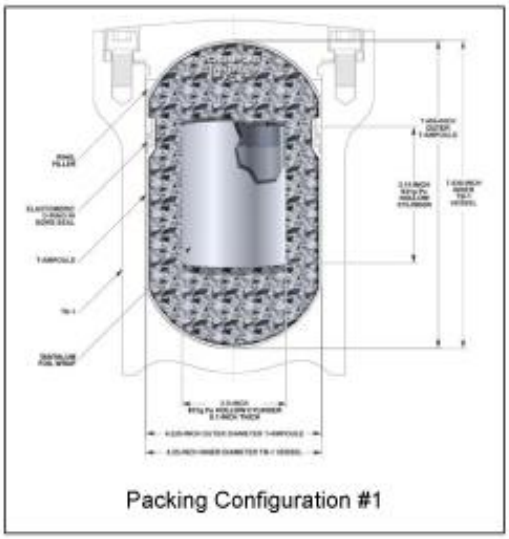

Packing Configuration #1

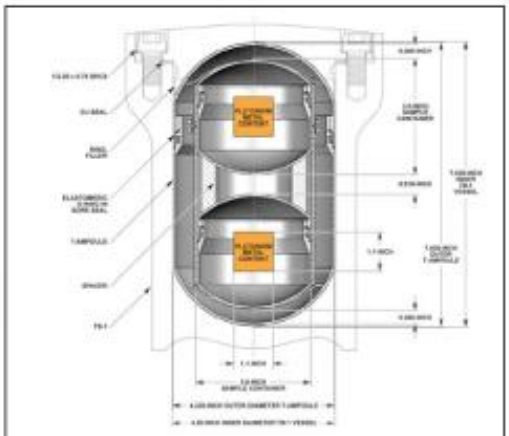

Packing Configuration #2

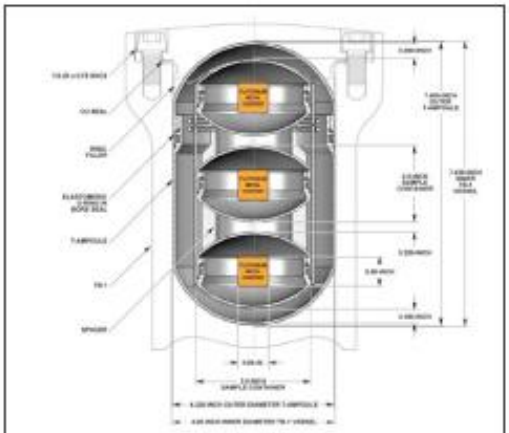

Packing Configuration #3

Figure 2. Schematic illustration of the Packing Configurations of the TB-1.

[i]. From SAE AS568C, "Aerospace Size Standard for O-rings". ID, w, and Volume are provided from Table 1, r and R are derived.

[ii]. The TB-1 O-ring is not used for plutonium metal shipments.

[iii]. A.K. Burnham and R.K. Weese, "Kinetics of thermal degradation of explosive binders Viton A, Estane, and Kel-F", Thermochimica Acta 426 (2005) pp. 85–92.

[iv]. H. Arito and R. Soda "Pyrolysis Products of Polytetrafluoroethylene and Polytetrafluoroethylenepropylene with Reference to Inhalation Toxicology", Korean J. Chem. Eng. 12 (1995) pp. 247-255.

[v]. L.D. Scheel, W.C. Lane and W.E. Colemen, "The Toxicity of Polytetraethylene Pyrolysis Products- Including Carbonyl Fluoride and a Reaction Product, Silicon Tetrafluoride", Amer. Ind. Hygiene Ass. 29 (1968) pp. 41-48.

[vi]. J. F. Smith and G. T. Perkins, "The Mechanism of Post Cure of Viton A* Fluorocarbon Elastomer", J. Appl. Polym. Sci. 16 (1961) pp. 460-467.

[vii]. Technical Information - Viton® fluoroelastomer Fluid Resistance Guide (DuPont Dow Elastomers, 1998).

[viii]. Technical Information - Viton® A-100 (DuPont Dow Elastomers, 2003).

[ix]. The ideal gas law gives relates pressure, as a function of temperature and volume, as $P = nRT/V$. If temperature (T) is expressed in Kelvin, volume (V) is expressed in cm^3, and mass (n) in moles, then the pressure can be expressed in units of atmospheres (atm) using a conversion factor of $\left(82.056 \; {atm\,cm^3}/{mole\,K}\right)$.

[x]. Analytical Pyrolysis of Synthetic Organic Polymers, ed. by Şerban Moldoveanu (2005) p.289.

[xi]. I. Lee, R.R. Reed, V.L. Brady, and S.A. Finnegan, "Energy release in the reaction of metal powders with fluorine containing polymers", J. Thermal Anal. 49 (1997) pp. 1699-1705.

[xii]. A.E. Venger, et al., "Thermogravimetric Study of the Thermal Decomposition of poly(tetrafluoroethylene) under Nonisothermal Conditions", Vestsi Akademii Navuk BSSR, Seryya Fizika-Energetychnykh Navuk 2 (1976) pp. 65.

[xiii]. G. J. Knight and W. W. Wright, "The Thermal Degradation of Hydrofluoro Polymers", J. Appl. Polym. Sci. 16 (1972) pp. 683-693.

4.5.5 Determination of A_2 for the PAT 1 Package with Plutonium Contents

Prepared by Monty L. Goins and reviewed by Drew Winder, both of B&W Y-12 Technical Services, L.L.C., on November 23, 2010.

Introduction

The containment criteria for radioactive, fissile material packages are given in 10 CFR 71.51(a)(1) for Normal Conditions of Transport (NCT) ($\leq 10^{-6}$ A_2/h), in 71.51(a)(2) for Hypothetical Accident Conditions (HAC) ($\leq A_2$ in a week), and 71.64(a)(1)(i) for Accident conditions for air transport of plutonium ($\leq A_2$ in a week). The A_2 value for this mixture of radioisotopes must be determined to establish the content containment criteria and to determine the maximum release quantity that is allowed by the regulations. These values for a mixture of isotopes are determined by the methodology given in 10 CFR 71, Appendix A, "Determination of A_1 and A_2," Section IV. The results of these analyses are used to demonstrate compliance of the PAT-1 package with the containment requirements of 10 CFR 71.

Scope

The A_2 value of the plutonium content to be shipped is evaluated based on the mass and weight percents of materials shown in Tables 4.5.5.1 and 4.5.5.2 defined in Section 1.2.2 of the addendum. The analysis documented in this section was conducted to establish the upper limit for the total activity and the maximum number of A_2s proposed for transport in the PAT-1 package. The maximum activity [53.281 TBq (1440.02 Ci)] occurs at initial fabrication. However, the maximum activity-to-A_2 value (5.5708 H 10^3) of the contents occurs when the Pu-241 fully decays to Am-241. These values have been determined using a maximum of 1300 gram of plutonium. By applying the weight percents of isotopes shown in Tables 4.5.5.1 and 4.5.5.2, the maximum activity, minimum A_2 value, and the minimum leakage requirements were determined for the proposed contents and are summarized in Tables 4.5.5.3, 4.5.5.4, and 4.5.5.5. The mass and isotopic concentrations used for the proposed content do not take into consideration limits based on shielding, criticality or structural.

According to 10 CFR 71, Appendix A, parent and daughter nuclides are considered to be a mixture of different nuclides than those of the parent nuclide. The radioactive decay of uranium (refer to the decay chains presented by Dr. David C. Kocher, *Radioactive Decay Data Tables* [Kocher 1981]) creates isotopes that will accumulate enough activity to exceed their respective criteria for limited quantities (*Shippers–General Requirements for Shipments and Packagings* [49 CFR 173.425], Table 4, "Activity Limits for Limited Quantities, Instruments, and Articles") and for Type A quantities of radionuclides (10 CFR 71, Table A-1, "A_1 and A_2 Values for Radionuclides"). Furthermore, the A_2 value for the mixture will change over time as a result of radioactive decay. The analysis below shows that the A_2 value for this mixture reaches a minimum when the Pu-241 is fully decayed to Am-241.

Analysis

Mass Tables. The mass and weight fractions for the isotopes used in the containment calculations are presented in Tables 4.5.5.1 and 4.5.5.2.

Table 4.5.5.1. Isotopic mass and weight percent for the Plutonium contents [a]

Nuclide	Weight percent	Mass (g)
Pu-238	0.050000	0.650000
Pu-239	92.350000	1200.550000
Pu-240	6.500000	84.500000
Pu-241	1.000000	13.000000
Pu-242	0.100000	1.300000
Am-241	0.000000	0.000000
Total	100.000000	1300.000000

[a] Entire weight of contents is assumed to be plutonium. Maximum content mass is assumed to be 1300 grams.

Table 4.5.5.2. Isotopic mass and weight percent for the Plutonium contents with full Pu-241 decay to Am-241[a]

Nuclide	Weight percent	Mass (g)
Pu-238	0.050000	0.650000
Pu-239	92.350000	1200.550000
Pu-240	6.500000	84.500000
Pu-241	0.000000	0.000000
Pu-242	0.100000	1.300000
Am-241	1.000000	13.000000
Total	100.000000	1300.000000

[a] Entire weight of contents is assumed to be plutonium. Maximum content mass is assumed to be 1300 grams.

Table 4.5.5.3. A_2 value and activity calculation for 1300 g of radioactive material at 0 years

Isotope	Mass (g)	Specific activity (TBq/g)	Activity (TBq)	A_2 (TBq)	f(i) (TBq/TBq)	f(i) / A_2 (1/TBq)
Pb-210	0.00000	2.8000E+00	0.0000E+00	5.0000E-02	0.0000E+00	0.0000E+00
Pb-212	0.00000	5.1000E+04	0.0000E+00	2.0000E-01	0.0000E+00	0.0000E+00
Bi-210	0.00000	4.6000E+03	0.0000E+00	6.0000E-01	0.0000E+00	0.0000E+00
Bi-212	0.00000	5.4000E+05	0.0000E+00	6.0000E-01	0.0000E+00	0.0000E+00
Po-210	0.00000	1.7000E+02	0.0000E+00	2.0000E-02	0.0000E+00	0.0000E+00
Rn-222	0.00000	5.7000E+03	0.0000E+00	4.0000E-03	0.0000E+00	0.0000E+00
Ra-223	0.00000	1.9000E+03	0.0000E+00	7.0000E-03	0.0000E+00	0.0000E+00
Ra-224	0.00000	5.9000E+03	0.0000E+00	2.0000E-02	0.0000E+00	0.0000E+00
Ra-225	0.00000	1.5000E+03	0.0000E+00	4.0000E-03	0.0000E+00	0.0000E+00
Ra-226	0.00000	3.7000E-02	0.0000E+00	3.0000E-03	0.0000E+00	0.0000E+00
Ra-228	0.00000	1.0000E+01	0.0000E+00	2.0000E-02	0.0000E+00	0.0000E+00
Ac-225	0.00000	2.1000E+03	0.0000E+00	6.0000E-03	0.0000E+00	0.0000E+00
Ac-227	0.00000	2.7000E+00	0.0000E+00	9.0000E-05	0.0000E+00	0.0000E+00
Ac-228	0.00000	8.4000E+04	0.0000E+00	5.0000E-01	0.0000E+00	0.0000E+00
Th-227	0.00000	1.1000E+03	0.0000E+00	5.0000E-03	0.0000E+00	0.0000E+00
Th-228	0.00000	3.0000E+01	0.0000E+00	1.0000E-03	0.0000E+00	0.0000E+00
Th-229	0.00000	7.9000E-03	0.0000E+00	5.0000E-04	0.0000E+00	0.0000E+00
Th-230	0.00000	7.6000E-04	0.0000E+00	1.0000E-03	0.0000E+00	0.0000E+00
Th-231	0.00000	2.0000E+04	0.0000E+00	2.0000E-02	0.0000E+00	0.0000E+00
Th-232	0.00000	4.0000E-09	0.0000E+00	1.0000E+75	0.0000E+00	0.0000E+00
Pa-231	0.00000	1.7000E-03	0.0000E+00	4.0000E-04	0.0000E+00	0.0000E+00
Pa-233	0.00000	7.7000E+02	0.0000E+00	7.0000E-01	0.0000E+00	0.0000E+00
U-232	0.00000	8.3000E-01	0.0000E+00	1.0000E-03	0.0000E+00	0.0000E+00
U-233	0.00000	3.6000E-04	0.0000E+00	6.0000E-03	0.0000E+00	0.0000E+00
U-234	0.00000	2.3000E-04	0.0000E+00	6.0000E-03	0.0000E+00	0.0000E+00
U-235	0.00000	8.0000E-08	0.0000E+00	1.0000E+75	0.0000E+00	0.0000E+00
U-236	0.00000	2.4000E-06	0.0000E+00	6.0000E-03	0.0000E+00	0.0000E+00
Np-237	0.00000	2.6000E-05	0.0000E+00	2.0000E-03	0.0000E+00	0.0000E+00
Pu-236	0.00000	2.0000E+01	0.0000E+00	3.0000E-03	0.0000E+00	0.0000E+00
Pu-238	0.65000	6.3000E-01	4.0950E-01	1.0000E-03	7.6857E-03	7.6857E+00
Pu-239	1200.5500	2.3000E-03	2.7613E+00	1.0000E-03	5.1825E-02	5.1825E+01
Pu-240	84.50000	8.4000E-03	7.0980E-01	1.0000E-03	1.3322E-02	1.3322E+01
Pu-241	13.0000	3.8000E+00	4.9400E+01	6.0000E-02	9.2716E-01	1.5453E+01
Pu-242	1.30000	1.5000E-04	1.9500E-04	1.0000E-03	3.6599E-06	3.6599E-03
Mass =	**1300.0000**	**ACTIVITY SUM =**	**5.3281E+01**		**SUM OF F_I/A_2 =**	**8.8289E+01**

$$(\text{mixture}) = \frac{1}{3f(i) / A_2} = \frac{1}{8.8289 \text{ H } 10^{1} \text{ (1/TBq)}} = 1.1326 \text{ H } 10^{-2} \text{ TBq}$$

Table 4.5.5.4. A_2 value and activity calculation for 1300 g of radioactive material with full Pu-241 decay to Am-241

Isotope	Mass (g)	Specific activity (TBq/g)	Activity (TBq)	A_2 (TBq)	f(i) (TBq/TBq)	f(i) / A_2 (1/TBq)
Pb-210	0.00000	2.8000E+00	0.0000E+00	5.0000E-02	0.0000E+00	0.0000E+00
Pb-212	0.00000	5.1000E+04	0.0000E+00	2.0000E-01	0.0000E+00	0.0000E+00
Bi-210	0.00000	4.6000E+03	0.0000E+00	6.0000E-01	0.0000E+00	0.0000E+00
Bi-212	0.00000	5.4000E+05	0.0000E+00	6.0000E-01	0.0000E+00	0.0000E+00
Po-210	0.00000	1.7000E+02	0.0000E+00	2.0000E-02	0.0000E+00	0.0000E+00
Rn-222	0.00000	5.7000E+03	0.0000E+00	4.0000E-03	0.0000E+00	0.0000E+00
Ra-223	0.00000	1.9000E+03	0.0000E+00	7.0000E-03	0.0000E+00	0.0000E+00
Ra-224	0.00000	5.9000E+03	0.0000E+00	2.0000E-02	0.0000E+00	0.0000E+00
Ra-225	0.00000	1.5000E+03	0.0000E+00	4.0000E-03	0.0000E+00	0.0000E+00
Ra-226	0.00000	3.7000E-02	0.0000E+00	3.0000E-03	0.0000E+00	0.0000E+00
Ra-228	0.00000	1.0000E+01	0.0000E+00	2.0000E-02	0.0000E+00	0.0000E+00
Ac-225	0.00000	2.1000E+03	0.0000E+00	6.0000E-03	0.0000E+00	0.0000E+00
Ac-227	0.00000	2.7000E+00	0.0000E+00	9.0000E-05	0.0000E+00	0.0000E+00
Ac-228	0.00000	8.4000E+04	0.0000E+00	5.0000E-01	0.0000E+00	0.0000E+00
Th-227	0.00000	1.1000E+03	0.0000E+00	5.0000E-03	0.0000E+00	0.0000E+00
Th-228	0.00000	3.0000E+01	0.0000E+00	1.0000E-03	0.0000E+00	0.0000E+00
Th-229	0.00000	7.9000E-03	0.0000E+00	5.0000E-04	0.0000E+00	0.0000E+00
Th-230	0.00000	7.6000E-04	0.0000E+00	1.0000E-03	0.0000E+00	0.0000E+00
Th-231	0.00000	2.0000E+04	0.0000E+00	2.0000E-02	0.0000E+00	0.0000E+00
Th-232	0.00000	4.0000E-09	0.0000E+00	1.0000E+75	0.0000E+00	0.0000E+00
Pa-231	0.00000	1.7000E-03	0.0000E+00	4.0000E-04	0.0000E+00	0.0000E+00
Pa-233	0.00000	7.7000E+02	0.0000E+00	7.0000E-01	0.0000E+00	0.0000E+00
U-232	0.00000	8.3000E-01	0.0000E+00	1.0000E-03	0.0000E+00	0.0000E+00
U-233	0.00000	3.6000E-04	0.0000E+00	6.0000E-03	0.0000E+00	0.0000E+00
U-234	0.00000	2.3000E-04	0.0000E+00	6.0000E-03	0.0000E+00	0.0000E+00
U-235	0.00000	8.0000E-08	0.0000E+00	1.0000E+75	0.0000E+00	0.0000E+00
U-236	0.00000	2.4000E-06	0.0000E+00	6.0000E-03	0.0000E+00	0.0000E+00
Np-237	0.00000	2.6000E-05	0.0000E+00	2.0000E-03	0.0000E+00	0.0000E+00
Pu-236	0.00000	2.0000E+01	0.0000E+00	3.0000E-03	0.0000E+00	0.0000E+00
Pu-238	0.65000	6.3000E-01	4.0950E-01	1.0000E-03	7.3509E-02	7.3509E+01
Pu-239	1200.5500	2.3000E-03	2.7613E+00	1.0000E-03	4.9567E-01	4.9567E+02
Pu-240	84.50000	8.4000E-03	7.0980E-01	1.0000E-03	1.2742E-01	1.2742E+02
Pu-241	0.0000	3.8000E+00	0.0000E+00	6.0000E-02	0.0000E+00	0.0000E+00
Pu-242	1.30000	1.5000E-04	1.9500E-04	1.0000E-03	3.5004E-05	3.5004E-02
Am-241	13.0000	1.3000E-01	1.6900E+00	1.0000E-03	3.0337E-01	3.0337E+02
Mass =	**1300.0000**	**Activity sum =**	**5.5708E+00**		**Sum of f_i/A_2 =**	**1.0000E+03**

$$A_2\,(\text{mixture}) = \frac{1}{3f(i) / A_2} = \frac{1}{1.0000\ \text{H}\ 10^{3}\ (1/\text{TBq})} = 1.0000\ \text{H}\ 10^{-3}\ \text{TBq}$$

The total number of A_2 proposed for shipment is equal to the ratio of total activity divided by the A_2 of this particular mixture as shown in Table 4.5.5.5.

Table 4.5.5.5. Activity, A_2 value, and number of A_2 proposed for transport

Isotopic distribution	Activity (TBq)	A_2 (TBq)	Act / A_2
Full Pu-241 (see Table 4.5.5.1)	5.3281E+01	1.1326E-02	4.7042E+03
Full Am-241 (see Table 4.5.5.2)	5.5708E+00	1.0000E-03	5.5708E+03

4.5.6 Calculation of the PAT-1 Containment Vessel's Regulatory Reference Air Leakage Rates

Prepared by Monty L. Goins and reviewed by Drew Winder, both of B & W Y-12 Technical Services, L.L.C., on November 23, 2010.

Introduction

The PAT-1 leak-testing requirements of the containment boundary are based on the smallest maximum allowable leakage rate generated from the maximum plutonium content defined in Tables 4.5.5.1 and 4.5.5.2. Section 5 of ANSI N14.5-1997 defines the maximum allowable leakage rate based on the maximum allowable release rate. These leakage rates, L_N , L_A , and L_{PA} , are the maximum allowable seal leakage rates for Normal Conditions of Transport (NCT), Hypothetical Accident Conditions (HAC), and Accident condition for air transport of plutonium (ACATP). The worst-case maximum allowable leakage rates are used to calculate an equivalent leakage hole diameter following ANSI N14.5-1997, Appendix B, for each condition of transport. This leakage hole diameter is used to calculate a reference air and a helium leakage rate for leak testing. A bounding mass for the plutonium content of 1300 gram is used in this calculation to certify the PAT-1 package for shipment. The maximum allowable leakage rates are calculated using this maximum content mass in a much more dispersive form (oxide powder) at the highest calculated pressures and temperatures. This section shows the following procedure used to calculate the leak criteria for the plutonium constituents at initial fabrication. Table 4.5.6.1 shows the results of using this procedure for both set of isotopic distributions.

Plutonium Content with no Pu-241 decay

Calculate R_N , R_A, and R_{PA}:

where

R_N = allowable release rate for normal conditions of transport;
R_A = allowable release rate for hypothetical accident condition, and
R_{PA} = allowable release rate for accident condition for air transport of plutonium.

The maximum allowable release rate is based on using A_2.

A_2 = 1.1326×10^{-2} TBq, (3.0611×10^{-1} Ci). Table 4.5.5.5

The containment requirements for NCT, HAC, and ACATP are:

R_N = $A_2 \times 10^{-6}$ TBq/h = $A_2 \times 2.78 \times 10^{-10}$ TBq/s, ANSI N14.5-1997 (Eq. 1)
= $1.1326 \times 10^{-2} \times 2.78 \times 10^{-10}$ TBq/s,
= 3.1488×10^{-12} TBq/s, (8.5102 H 10^{-11} Ci/s).

R_A = A_2 (TBq/week),
= $A_2 \times 1.65 \times 10^{-6}$ (TBq/s), ANSI N14.5-1997 (Eq. 2)
= $1.1326 \times 10^{-2} \times 1.65 \times 10^{-6}$ TBq/s,
= 1.8689×10^{-8} TBq/s, (5.0510×10^{-7} Ci/s). or limited to 10 A2 /week of 85Kr

R_{PA} = A_2 (TBq/week),
= $A_2 \times 1.65 \times 10^{-6}$ (TBq/s), ANSI N14.5-1997 (Eq. 2)
= $1.1326 \times 10^{-2} \times 1.65 \times 10^{-6}$ TBq/s,

= 1.8689×10^{-8} TBq/s, (5.0510×10^{-7} Ci/s).

Following ANSI N14.5-1997, the medium aerosol activity must be calculated to determine the leakage rates.

m	=	total nuclide mass in the package available for release (g),
TotA	=	total activity in the package available for release (TBq),
TSA	=	total specific activity in the package available for release (TBq/g).

For the plutonium content:

TSA	=	TotA / m,	
TSA	=	5.3281×10^{1} (TBq) / 1300 (g),	Table 4.5.5.5
TSA	=	4.0985×10^{-2} TBq/g.	

ρ_P = 9×10^{-6} g/cm^3. The maximum density of powder aerosols in the fill gas Curren, W.D. and R.D. Bond, 1980, *Leakage of Radioactive Powders from Containers*.

For the packaging arrangement:

C_N	=	activity per unit volume of medium that could escape from the containment system (TBq/cm^3).	
C_N	=	TSA $\times$ ρ_P,	
	=	4.0985×10^{-2} (TBq/g) $\times$ 9×10^{-6} (g/cm^3),	
C_N	=	3.6887×10^{-7} TBq/cm^3.	NCT

Using Curren's maximum aerosol density, $C_A = C_N = C_{PA}$:

C_A	=	activity per unit volume of exiting gas (TBq/cm^3),	HAC
C_A	=	3.6887×10^{-7} TBq/cm^3.	

C_{PA}	=	activity per unit volume of exiting gas (TBq/cm^3),	ACATP
C_{PA}	=	3.6887×10^{-7} TBq/cm^3.	

Section 6.1 of ANSI N14.5-1997 calculates L_N with (Eq. 3) and L_A, and L_{PA} with (Eq. 4). L_N, L_A, and L_{PA} are the maximum allowable leakage rates for the containment vessel fill gas aerosol during NCT, HAC, and ACATP, respectively.

L_N	=	maximum allowable leakage rate for the medium for NCT (TBq/cm^3),	
L_N	=	R_N / C_N,	ANSI N14.5-1997 (Eq. 3)
L_N	=	3.1488×10^{-12} (TBq/s) / 3.6887×10^{-7} (TBq/cm^3),	
L_N	=	8.5363×10^{-6} cm^3/s.	

L_A	=	maximum allowable leakage rate for the medium for HAC (TBq/cm^3),
L_A	=	R_A / C_A,
L_A	=	1.8689×10^{-8} (TBq/s) / 3.6887×10^{-7} (TBq/cm^3),
L_A	=	5.0665×10^{-2} cm^3/s.

L_{PA} = maximum allowable leakage rate for the medium for ACATP (TBq/cm^3),

L_{PA} = R_{PA} / C_{PA},
L_{PA} = 1.8689×10^{-8} (TBq/s) / 3.6887×10^{-7} (TBq/cm^3),
L_{PA} = 5.0665×10^{-2} cm^3/s.

L_N , L_A, and L_{PA} correspond to the upstream volumetric leakage rate (L_u) at the upstream pressure (P_u) in the ANSI N14.5-1997 formulas for use later in this section. The reference air leakage rates $L_{R,N}$. $L_{R,A}$, and $L_{R,PA}$ for NCT, HAC, and ACATP based on the L_N, L_A, and L_{PA} are then calculated using the maximum temperatures and pressure combinations from Sections 4.2, 4.3, and 4.3.1.

Determination of the Leakage Test Procedure Requirements for the Plutonium Content

This calculation will examine the most conservative effects of a fully loaded containment vessel with a plutonium mass of 1300 gram. The smallest allowable leakage values are shown in Table 4.5.6.1. The A_2 value and the maximum content activity-to-A_2 value ratio for this mixture were calculated in Section 4.5.5 and summarized in Table 4.5.5.5. As calculated in Section 4.5.5, the A_2 value and the maximum content activity-to-A_2 ratio used in the following calculations occur at initial fabrication and are 1.1326×10^{-2} TBq (3.0611×10^{-1} Ci) and 4.7042×10^{3} respectively. These values are used to determine the leakage test procedural requirements when packaging the TB-1 containment vessel.

The following analysis determines the maximum allowable seal air reference leakage rate for NCT, HAC, and ACATP. The ANSI N14.5-1997 recommended method using a straight circular tube to model the leakage path is applied. Using this Astandard@ leakage hole model permits the calculation of equivalent reference leakage rates from which leak-test requirements can be established. Viscosity data for air and helium used in the following analyses were obtained from curve fitting routines at specific temperatures based on viscosity data for air (Handbook of Chemistry and Physics, 55th ed.) and helium (NBS Technical Note 631).

L_N and L_A correspond to the upstream volumetric leakage rate (L_u) at the upstream pressure (P_u).

L_N = 8.5363×10^{-6} cm^3/s,
L_A = 5.0665×10^{-2} cm^3/s,
L_{PA} = 5.0665×10^{-2} cm^3/s.

Find the maximum pressure and temperature in the containment vessel:
Converting the temperature to degrees Kelvin:

T = 273.15 + T(°C),
T = 273.15 + 5 / 9 (°F - 32) (K).

T_N = 273.15 + 5 / 9 (218.00°F - 32) (K), (T = 218.00°F)
T_N = 376.48 K. NCT (Section 4.2)

T_A = 273.15 + 5 / 9 (276.00°F - 32) (K), (T = 276.00°F)
T_A = 408.71 K. HAC (Section 4.3)

T_{PA} = 273.15 + 5 / 9 (1080.00°F - 32) (K), (T = 1080°F)
T_{PA} = 855.37 K. ACATP (Section 4.3.1)

Converting the pressures from psia to atmospheres:

P_N	=	P (psia) / 14.696 (psia/atm),	where P is the pressure in Section 4.2
P_N	=	18.872 (psia) / 14.696 (psia/atm),	for NCT
P_N	=	1.2842 atm.	

P_A	=	P (psia) / 14.696 (psia/atm),	where P is the pressure in Section 4.3
P_A	=	20.486 (psia) / 14.696 (psia/atm),	for HAC
P_A	=	1.3940 atm.	

For ACATP conditions, a pressure of 1110 psia will be analyzed:

P_{PA}	=	P (psia) / 14.696 (psia/atm),	where P is the pressure in Section 4.3.1
P_{PA}	=	1110 (psia) / 14.696 (psia/atm),	for ACATP
P_{PA}	=	75.5308 atm.	

The molar gas percentages, determined later in this section for ACATP at 1110 psia, will be used for the P_{PA} analysis during ACATP.

NCT Leakage Hole Diameter for the Plutonium Content

The following calculations determine the leakage hole diameter that generates the maximum allowable leakage rate during NCT. To keep these calculations conservative, the maximum values for temperature and pressure were used as steady-state conditions for NCT. According to Section 4.1.1, the gas inside the containment vessel may consist of nitrogen/helium/argon with a maximum 100 parts per million of oxygen. Based on sample calculations, the lowest regulatory leakage rate was predicted with 100 percent helium in the void volumes of the TB-1 containment vessel and T-Ampoule. The leak path length was assumed to be 0.022 inches (0.056 cm) based on the length of the copper gasket seal compression.

Input data for NCT with 100% helium gas:

L_N	=	8.5363×10^{-6} cm^3/s,	Maximum upstream leakage
P_u	=	1.2842 atm,	Upstream pressure = 18.872 psia
P_d	=	0.2382 atm,	Downstream pressure = 3.5 psia, per 10 CFR 71.71(3)
a	=	0.056 cm,	Leak path length (copper gasket seal compression)
T	=	376.48 K,	Fill gas temperature = 218.00EF
μ	=	0.02310 cP,	Viscosity at temperature
M	=	4.0 g/g-mole.	Molecular weight of fill gas

The average pressure is:

P_a	=	$(P_u + P_d)/2$,	
	=	(1.2842 + 0.2382) / 2,	
P_a	=	0.7612 atm.	Average pressure during NCT

According to ANSI N14.5-1997, the flow leakage hole diameter is unknown. Therefore, the mass-like leakage flow rate must be calculated to calculate the average leakage flow rate.

Q is the mass-like leakage for flow using the upstream leakage, L_u, and pressure, P_u:

$Q = P_u L_u$, (Eq. B1)
$L_u = L_N$. NCT leakage

$Q = (1.2842)(atm)\ (8.5363 \times 10^{-6})(cm^3/s)$,
$Q = 1.0962 \times 10^{-5}$ atm-cm^3/s. NCT mass-like leakage rate

$Q = P_a L_a$, (Eq. B1)
$L_a = Q / P_a = 1.0692 \times 10^{-5}$ (atm-cm^3/s) / (0.7612)(atm),
$L_a = 1.4403 \times 10^{-5}\ \ 10^{-5}\ cm^3/s$. NCT average leakage rate

Solve equations B2BB4 from ANSI N14.5-1997:

$L_a = (F_c + F_m)\ (P_u - P_d)\ cm^3/s$, (Eq. B2)
$L_a = (F_c + F_m)\ (1.2842 - 0.2382)$,
$L_a = (1.0460)\ (F_c + F_m)\ cm^3/s$.

$F_c = (2.49 \times 10^6)\ D^4 / (a\ \mu)\ (cm^3/atm\text{-}s)$, (Eq. B3)
$F_c = (2.49 \times 10^6)\ D^4 / (\ (0.056)\ (0.02310)\ )$,
$F_c = (1.9245 \times 10^9)\ D^4\ cm^3/atm\text{-}s$.

$F_m = (3.81 \times 10^3)\ D^3\ (T / M)^{.5} / (a\ P_a)\ (cm^3/atm\text{-}s)$, (Eq. B4)
$F_m = (3.81 \times 10^3)\ D^3\ (376.48 / 4.0)^{.5} / (\ (0.056)\ (0.7612)\ )$,
$F_m = (8.6717 \times 10^5)\ D^3\ cm^3/atm\text{-}s$.

From the mass-like leakage calculation:

$L_a = 1.4403 \times 10^{-5}\ cm^3/s$. NCT average leakage rate

Find the leakage hole diameter that sets:

$L_2 = L_a$.

Using the equations:

$L_2 = (1.0460)\ (F_c + F_m)\ cm^3/s$,
$F_c = (1.9245 \times 10^9)\ D^4\ cm^3/atm\text{-}s$,
$F_m = (8.6717 \times 10^5)\ D^3\ cm^3/atm\text{-}s$.

To get a better guess on a new D use:

$D = D_2\ (L_a / L_2)^{0.252}$.

Now a guess must be made for D_2 to solve Eq. B2 for NCT:

D_2 = 0.001 cm, and solve for $L_a = 1.4403 \times 10\text{-}^5\ cm^3/s$. NCT average leakage rate

Diameter	F_c	F_m	L_2	L_a / L_2
1.0000E-03	1.9245E-03	8.6717E-04	2.9201E-03	0.0049
2.6221E-04	9.0966E-06	1.5632E-05	2.5867E-05	0.5568
2.2623E-04	5.0410E-06	1.0041E-05	1.5775E-05	0.9129
2.2110E-04	4.5987E-06	9.3723E-06	1.4614E-05	0.9855
2.2028E-04	4.5315E-06	9.2693E-06	1.4436E-05	0.9976
2.2015E-04	4.5207E-06	9.2528E-06	1.4407E-05	0.9996
2.2013E-04	4.5190E-06	9.2502E-06	1.4403E-05	0.9999
2.2013E-04	4.5187E-06	9.2498E-06	1.4402E-05	1.0000

The NCT leakage hole diameter for the plutonium content:

$D = 2.2013 \times 10^{-4}$ cm. NCT diameter

NCT Reference Air Leakage Rate for the Plutonium Content

The leakage hole diameter found for the maximum allowable leakage rate for NCT will be used to determine the reference air leakage rate. O-ring seal leakage testing must ensure that no leakage is greater than the leakage generated by the hole diameter $D = 2.2013 \times 10^{-4}$ cm. Therefore, the NCT reference leakage flow rate ($L_{R, N}$) must be calculated to determine the allowable test leakage rate.

Input data for NCT reference air leakage rate:

$D = 2.2013 \times 10^{-4}$ cm, From NCT
$a = 0.056$ cm, Leak path length (copper gasket seal compression),
$P_u = 1.0$ atm, Upstream pressure
$P_d = 0.01$ atm, Downstream pressure
$T = 298$ K, Fill gas temperature, 77°F
$M = 29$ g/g-mole, Molecular weight of air
$\mu = 0.0185$ cP, Viscosity of air at reference temperature

Calculate P_a:

$P_a = (P_u + P_d) / 2$,
$= (1.0 + 0.01) /2$,
$P_a = 0.505$ atm. NCT average pressure

$F_c = (2.49 \times 10^6) D^4 / (a \mu)$ (cm^3/atm-s), (Eq. B3)
$F_c = (2.49 \times 10^6) (2.2013 \times 10^{-4})^4 / ((0.056) (0.0185))$,
$F_c = (2.4035 \times 10^9) (2.2013 \times 10^{-4})^4$,
$F_c = 5.6433 \times 10^{-6}$ cm^3/atm-s.

$F_m = (3.81 \times 10^3) D^3 (T / M)^5 / (a P_a)$ (cm^3/atm-s), (Eq. B4)

$F_m = (3.81 \times 10^3) (2.2013 \times 10^{-4})^3 (298 / 29)^5 / ((0.056) (0.505)),$
$F_m = (4.3187 \times 10^5) (2.2013 \times 10^{-4})^3,$
$F_m = 4.6066 \times 10^{-6}$ cm^3/atm-s.

$L_u = (F_c + F_m) (P_u - P_d) (P_a / P_u)$ (cm^3/s), (Eq. B5)
$L_u = (5.6433 \times 10^{-6} + 4.6066$ H $10^{!6})$(cm^3/atm-s) (1.0 - 0.01)(atm) (0.505 / 1.0),
$L_u = (1.0250 \times 10^{-6})$(cm^3/atm-s) (0.49995)(atm),
$L_u = 5.1244 \times 10^{-6}$ cm^3/s.

The reference air leakage rate as defined in ANSI N14.5-1997, Section B.3, is the upstream leakage in air.

$L_{R,N\text{-}Air} = 5.1244 \times 10^{-6}$ ref-cm^3/s. plutonium content

The same equations can be used to calculate an allowable leakage rate using helium for leak testing.

M = 4 g/g-mole, Molecular weight of helium
μ = 0.0198 cP. Viscosity of helium at temperature

$F_c = (2.49 \times 10^6) D^4 / (a \mu)$ (cm^3/atm-s), (Eq. B3)
$F_c = (2.49 \times 10^6) (2.2013 \times 10^{-4})^4 / ((0.056) (0.0198)),$
$F_c = (2.2457 \times 10^9) (2.2013$ H$\times 10^{-4})^4,$
$F_c = 5.2728 \times 10^{-6}$ cm^3/atm-s.

$F_m = (3.81 \times 10^3) D^3 (T / M)^5 / (a P_a)$ (cm^3/atm-s), (Eq. B4)
$F_m = (3.81 \times 10^3) (2.2013 \times 10^{-4})^3 (298 / 4.0)^{.5} / ((0.056) (0.505)),$
$F_m = (1.1629 \times 10^6) (2.2013 \times 10^{-4})^3,$
$F_m = 1.2404 \times 10^{-5}$ cm^3/atm-s.

$L_u = (F_c + F_m) (P_u - P_d) (P_a / P_u)$ (cm^3/s), (Eq. B5)
$L_u = (5.2728 \times 10^{-6} + 1.2404 \times 10^{-5})$(cm^3/atm-s) (1.0 - 0.01)(atm) (0.505 / 1.0),
$L_u = (1.7676 \times 10^{-5})$(cm^3/atm-s) (0.49995)(atm),
$L_u = 8.8373 \times 10^{-6}$ cm^3/s.

The allowable leakage rate using helium for leak testing is:

$L_{R,N\text{-}He} = 8.8373 \times 10^{-6}$ cm^3/s. NCT helium test value

HAC Leakage Hole Diameter for the Plutonium Content

The calculation of a maximum allowable leakage rate hole diameter is based on the temperature and pressure of the fill gas aerosol for HAC, assuming the content is in an oxide powder form. Keeping this calculation conservative, the maximum values for temperature and pressure were used as steady-state conditions for a week. The maximum values were generated during the 30-min burn test for HAC.

Input data for HAC:

L_A = 5.0665 H 10^{-2} cm^3/s, Maximum exit leakage
P_u = 1.3940 atm, Upstream pressure = 20.486 psia
P_d = 1.0 atm, Downstream pressure

T	=	408.71 K,	Fill gas temperature = 276°F
μ	=	0.02442 cP,	Viscosity of gas mixture at temperature
M	=	29 g/g-mole,	Molecular weight of gas mixture
a	=	0.056 cm.	Leak path length (copper gasket seal compression)

$P_a = (P_u + P_d) / 2$

$= (1.3940 + 1.0) / 2,$ HAC average pressure

$P_a = 1.1970$ atm.

Q is the mass-like leakage for flow using the upstream leakage, L_u, and pressure, P_u:

$Q = P_u L_u,$ (Eq. B1)

$L_u = L_A.$ HAC leakage

$Q = (1.3940)(\text{atm})\ (5.0665 \times 10^{-2})(\text{cm}^3/\text{s}),$

$Q = 7.0626 \times 10^{-2}\ \text{atm-cm}^3/\text{s}.$ HAC mass-like leakage rate

$Q = P_a L_a,$ (Eq. B1)

$L_a = Q / P_a$

$L_a = 7.0626 \times 10^{-2}\ (\text{atm-cm}^3/\text{s}) / (1.1970)(\text{atm}),$

$L_a = 5.9003 \times 10^{-2}\ \text{cm}^3/\text{s}.$ HAC average leakage rate

Solve equations B2BB4 from ANSI N14.5-1997:

$L_a = (F_c + F_m)\ (P_u - P_d)\ (\text{cm}^3/\text{s}),$ (Eq. B2)

$L_a = (F_c + F_m)\ (1.3940 - 1.0),$

$L_a = 0.3940\ (F_c + F_m)\ \text{cm}^3/\text{s}.$

$F_c = (2.49 \times 10^6)\ D^4 / (a\ \mu)\ (\text{cm}^3/\text{atm-s}),$ (Eq. B3)

$F_c = (2.49 \times 10^6)\ D^4 / ((0.056)\ (0.02442)),$

$F_c = (1.8211 \times 10^9)\ D^4\ \text{cm}^3/\text{atm-s}.$

$F_m = (3.81 \times 10^3)\ D^3\ (T / M)^{.5} / (a\ P_a)\ (\text{cm}^3/\text{atm-s}),$ (Eq. B4)

$F_m = (3.81 \times 10^3)\ D^3\ (408.71 / 4.0)^{.5} / ((0.056)\ (1.1970)),$

$F_m = (5.7454 \times 10^5)\ D^3\ \text{cm}^3/\text{atm-s}.$

From the mass-like leakage calculation:

$L_a = 5.9003\ H\ 10^{-2}\ \text{cm}^3/\text{s}.$ HAC average leakage rate

Find the leakage hole diameter that sets:

$L_2 = L_a.$

Using the equations:

$L_2 = 0.3940(F_c + F_m)\ \text{cm}^3/\text{s},$

$F_c = (1.8211 \times 10^9)\ D^4\ \text{cm}^3/\text{atm-s},$

$F_m = (5.7454 \times 10^5)\ D^3\ \text{cm}^3/\text{atm-s}.$

To get a better guess on a new D use:

$D = D_2 (L_a / L_2)^{0.252}$.

Now a guess must be made for D_2 to solve Eq. B2 for HAC:

D_2 = 0.001 (cm), and solve for L_a = 5.9003 H 10^{-2} (cm^3/s). HAC average leakage rate

Diameter	F_c	F_m	L_2	L_a / L_2
1.0000E-02	1.8211E+01	5.7454E-01	7.4014E+01	0.00797
2.9593E-03	1.3967E-02	1.4890E-02	6.0896E-02	0.96891
2.9359E-03	1.3530E-02	1.4539E-03	5.9034E-02	0.99948
2.9355E-03	1.3523E-02	1.4533E-03	5.9004E-02	0.99999
2.9355E-03	1.3523E-02	1.4533E-03	5.9003E-02	1.00000

The HAC leakage hole diameter for the Plutonium content is:

D = 2.9355 H 10^{-3} cm. HAC diameter

HAC Reference Air Leakage Rate for Plutonium Content

The leakage hole diameter found for the maximum allowable leakage rate for HAC will be used to determine the reference air leakage rate. O-ring seal leakage testing must assure that no leakage is greater than the leakage generated by the hole diameter D = 2.9355 × 10^{-3} cm. Therefore, the HAC reference air leakage rate ($L_{R, A}$) must be calculated to determine the acceptable test leakage rate for post-HAC leakage testing.

Input data for HAC reference air leakage rate:

D	=	2.9355 × 10^{-3} cm,	From the HAC of transport
a	=	0.056 cm,	Leak path length (copper gasket seal compression)
P_u	=	1.0 atm,	Upstream pressure
P_d	=	0.01 atm,	Downstream pressure
T	=	298 K,	Fill gas temperature, 77EF
M	=	29 g/g-mole,	Molecular weight of air
μ	=	0.0185 cP.	Viscosity at temperature

Calculate P_a:

$P_a = (P_u + P_d) / 2$

$= 0.505$ atm. HAC average pressure

$F_c = (2.49 \times 10^6) D^4 / (a \mu)$ (cm^3/atm-s), (Eq. B3)

$F_c = (2.49 \times 10^6) (2.9355 \times 10^{-3})^4 / ((0.056) (0.0185))$,

$F_c = (2.4035 \times 10^9) (2.9355 \times 10^{-3})^4$,

F_c = 1.7847×10^{-1} cm^3/atm-s.

F_m = $(3.81 \times 10^3) D^3 (T / M)^{.5} / (a P_a)$ (cm^3/atm-s), (Eq. B4)
F_m = $(3.81 \times 10^3) (2.9355 \times 10^{-3})^3 (298 / 29)^{.5} / ((0.056) (0.505))$,
F_m = $(4.3187 \times 10^5) (2.9355 \times 10^{-3})^3$,
F_m = 1.0924×10^{-2} cm^3/atm-s.

L_u = $(F_c + F_m) (P_u - P_d) (P_a / P_u)$ (cm^3/s), (Eq. B5)
L_u = $(1.7847 \times 10^{-1} + 1.0924 \times 10^{-2})$($cm^3$/atm-s) (1.0 - 0.01)(atm) (0.505 / 1.0),
L_u = (1.8939×10^{-1})(cm^3/atm-s) (0.49995)(atm),
L_u = 9.4686×10^{-2} cm^3/s.

The HAC reference air leakage rate as defined in ANSI N14.5-1997, Section B.3, is the upstream leakage in air.

$L_{R,A\text{-}Air}$ = 9.4686×10^{-2} ref-cm^3/s. for plutonium content

The same equations can be used to calculate an allowable leakage rate using helium for leak testing.

M = 4 g/g-mole, Molecular weight of helium
μ = 0.0198 cP. Viscosity of helium at temperature

F_c = $(2.49 \times 10^6) D^4 / (a \mu)$ (cm^3/atm-s), (Eq. B3)
F_c = $(2.49 \times 10^6) (2.9355 \text{ H } 10^{-3} \text{ cm})^4 / ((0.056) (0.0198))$,
F_c = $(2.2457 \times 10^9) (2.9355 \text{ H } 10^{-3} \text{ cm})^4$,
F_c = 1.6675×10^{-1} cm^3/atm-s.

F_m = $(3.81 \times 10^3) D^3 (T / M)^{0.5} / (a P_a)$ (cm^3/atm-s), (Eq. B4)
F_m = $(3.81 \times 10^3) (2.9355 \times 10^{-3} \text{ cm})^3 (298 / 4)^{.5} / ((0.056) (0.505))$,
F_m = $(1.1629 \times 10^6) (2.9355 \times 10^{-3} \text{ cm})^3$,
F_m = 2.9415×10^{-2} cm^3/atm-s.

L_u = $(F_c + F_m) (P_u - P_d) (P_a / P_u)$ (cm^3/s), (Eq. B5)
L_u = $(1.6675 \times 10^{-1} + 2.9415 \times 10^{-2})$($cm^3$/atm-s) (1.0 - 0.01)(atm) (0.505 / 1.0),
L_u = (1.9617×10^{-1})(cm^3/atm-s) (0.49995)(atm),
L_u = $9.8072 \times 10^{!2}$ cm^3/s.

The allowable leakage rate using helium for leak testing for HAC is:

$L_{R,A\text{-}He}$ = 9.8072×10^{-2} cm^3/s. HAC helium test value

Accident Condition for Air Transport of Plutonium (ACATP)

The calculation of a maximum allowable leakage rate hole diameter is based on the temperature and pressure of the fill gas aerosol for ACATP, assuming the content is in an oxide powder form. Keeping this calculation conservative, the maximum values for temperature and pressure were used as steady-state conditions for a week. The maximum values were generated during the 60-min burn test for ACATP [10 CFR 71.74(a)(5)]. In accordance with 4.5.3, 1.42 H 10^{-7} moles of He gas are generated per gram of plutonium in one year. Therefore, using 1300 grams of plutonium, 1.846 H 10^{-4} moles of helium is generated in one year. The basic assumption for the packaging assumed that the contents are

assembled inside a glove box filled with an inert gas. Using helium as the inert gases will lower the regulatory leakage criteria. Therefore, the 1103.01 cm^3 of void volume would contain 0.0452 moles of helium. According to the O-ring decomposition and pyrolysis of ancillary plastic analysis shown in Section 2.12.8, the following molar quantity of gases (shown in the table below) are created during ACATP for each proposed ancillary plastic type.

Common Name	Units	**Metalized PET**	**Polyethylene**	**PVC**	**Teflon (PTFE)**
Chemical name of monomer		Polyethylene terephthalate	Polyethylene	Polyvinyl chloride	polytetrafluoro-ethylene
Monomer formula		$C_{10}H_8O_4$	CH_2	C_2H_4Cl	C_2F_4
Allowable mass (plastic only)	**g**	**6.9**	**3.5**	**12.2**	**12.5**
Molar Contribution (mol)					
Original Atmosphere	mol	0.0452	0.0452	0.0452	0.0452
O-ring Thermal Decomposition					
HF	mol	0.2940	0.2940	0.2940	0.2940
CF_4	mol	0.0270	0.0270	0.0270	0.0270
CO_2	mol	0.3200	0.3200	0.3200	0.3200
Helium generated from alpha decay	mol	0.0002	0.0002	0.0002	0.0002
Subtotal of all above sources	mol	**0.6864**	**0.6864**	**0.6864**	**0.6864**
Ancillary Plastic -- thermal decomposition and oxidation					
CO_2	mol	0.3577	0.2504	0.2504	0.2504
H_2O	mol	0.1431	0.2504	0.1878	
Cl_2	mol			0.0626	
F_2	mol				0.2504
Total	mol	**1.1872**	**1.1872**	**1.1872**	**1.1872**

This table represents four different packaging scenarios. The gases in each scenario are assumed perfectly mixed generating the following gas percentages:

	Shipping arrangement ancillary plastic material (percent of total gas mixture)			
Gas constituents	Polyethylene terephthalate	Polyethylene	Polyvinyl chloride	Polytetrafluoroethylene
He	3.8241	3.8241	3.8241	3.8241
HF	24.7642	24.7642	24.7642	24.7642
CF_4	2.2743	2.2743	2.2743	2.2743
CO_2	57.0838	48.0458	48.0458	48.0458
H_2O	12.0536	21.0916	15.8187	0.0000
Cl_2	0.0000	0.0000	5.2729	0.0000
F_2	0.0000	0.0000	0.0000	21.0916
Total	100.0000	100.0000	100.0000	100.0000

Normally, the leakage hole length, a, is assumed to be the basic diameter of the O-ring seal. In this case where the seal is created by deformation into a copper gasket, the value for "a", is the indentation depth into the copper gasket of 0.022 inches (0.056 cm.). Varying this value by a factor of 10 will increase the leakage rates by approximately the same factor. The following calculations are shown for the case where the Pu-241 has not decayed to Am-241 and the ancillary plastic is metalized PET. Table 4.5.6.1 summarizes the results for both decay conditions with the various gas mixtures.

Input data for ACATP:

L_{PA}	=	5.0665×10^{-2} cm^3/s,	Maximum exit leakage
P_u	=	75.5308 atm,	Upstream pressure = 1110 psia (P_{PA})
P_d	=	1.0 atm,	Downstream pressure
T	=	855.37 K,	Fill gas temperature = 1080°F
μ	=	0.04168 cP,	Viscosity of gas mixture at temperature
M	=	34.40 g/g-mole,	Molecular weight of gas mixture
a	=	0.056 cm.	Leak path length (copper gasket seal compression)

$P_a = (P_u + P_d) / 2$

$= (75.5308 + 1.0) / 2,$ ACATP average pressure

$P_a = 38.2654$ atm.

Q is the mass-like leakage for flow using the upstream leakage, L_u, and pressure, P_u:

$Q = P_u L_u,$ (Eq. B1)

$L_u = L_A.$ ACATP leakage

$Q = (75.5308)(\text{atm})\ (5.0665 \text{ H } 10^{-2})(\text{cm}^3/\text{s}),$

$Q = 3.8268$ atm-cm^3/s. ACATP mass-like leakage rate

$Q = P_a L_a,$ (Eq. B1)

$L_a = Q / P_a$

$L_a = 3.8268$ (atm-cm^3/s) / (38.2654)(atm),

$L_a = 1.0001 \text{ H } 10^{-1}$ cm^3/s. ACATP average leakage rate

Solve equations B2BB4 from ANSI N14.5-1997:

$L_a = (F_c + F_m)(P_u - P_d)$ (cm^3/s), (Eq. B2)

$L_a = (F_c + F_m)(75.5308 - 1.0),$

$L_a = 74.5308 (F_c + F_m)$ cm^3/s.

$F_c = (2.49 \times 10^6) D^4 / (a \mu)$ (cm^3/atm-s), (Eq. B3)

$F_c = (2.49 \times 10^6) D^4 / ((0.056)(0.04168)),$

$F_c = (1.0668 \times 10^9) D^4$ cm^3/atm-s.

$F_m = (3.81 \times 10^3) D^3 (T / M)^{.5} / (a P_a)$ (cm^3/atm-s), (Eq. B4)

$F_m = (3.81 \times 10^3) D^3 (855.37 / 34.40)^{.5} / ((0.056)(38.2654)),$

$F_m = (8.8665 \times 10^3) D^3$ cm^3/atm-s.

From the mass-like leakage calculation:

$L_a = 1.0001 \text{ H } 10^{-1}$ cm^3/s. ACATP average leakage rate

Find the leakage hole diameter that sets:

$L_2 = L_a.$

Using the equations:

L_2 = 74.5308 (F_c + F_m) cm^3/s,
F_c = (1.0668×10^9) D^4 cm^3/atm-s,
F_m = (8.8665×10^3) D^3 cm^3/atm-s.

To get a better guess on a new D use:

D = $D_2 (L_a / L_2)^{0.252}$.

Now a guess must be made for D_2 to solve Eq. B2 for ACATP:

D_2 = 0.01 (cm), and solve for L_a = 1.0001 H 10^{-1} (cm^3/s). ACATP average leakage rate

Diameter	**F_c**	**F_m**	**L_2**	**L_a / L_2**
1.0000E-02	1.0668E+01	8.8665E-03	7.9574E+02	0.00013
1.0400E-03	1.2477E-03	9.9722E-06	9.3738E-02	1.06687
1.0571E-03	1.3319E-03	1.0472E-05	1.0005E-01	0.99961
1.0569E-03	1.3313E-03	1.0469E-05	1.0001E-01	1.00000

The ACATP leakage hole diameter for the Plutonium content is:

D = 1.0569 H 10^{l3} cm. ACATP diameter

ACATP Reference Air Leakage Rate for Plutonium Content

The leakage hole diameter found for the maximum allowable leakage rate for ACATP will be used to determine the reference air leakage rate. O-ring seal leakage testing must assure that no leakage is greater than the leakage generated by the hole diameter D = 1.0569×10^{-3} cm. Therefore, the ACATP reference air leakage rate ($L_{R, PA-AIR}$) must be calculated to determine the acceptable test leakage rate for post-ACATP leakage testing.

Input data for ACATP reference air leakage rate:

D = 1.0569×10^{-3} cm, From the ACATP of transport
a = 0.056 cm, Leak path length (copper gasket seal compression)
P_u = 1.0 atm, Upstream pressure
P_d = 0.01 atm, Downstream pressure
T = 298 K, Fill gas temperature, 77°F
M = 29 g/g-mole, Molecular weight of air
μ = 0.0185 cP. Viscosity at temperature

Calculate P_a:

$P_a = (P_u + P_d) / 2$
$= 0.505$ atm. ACATP average pressure

$F_c = (2.49 \times 10^6) D^4 / (a \mu) (cm^3/atm\text{-}s),$ (Eq. B3)
$F_c = (2.49 \times 10^6) (1.0569 \times 10^{-3})^4 / ((0.056) (0.0185)),$
$F_c = (2.4035 \times 10^9) (1.0569 \times 10^{-3})^4,$
$F_c = 2.9995 H \times 10^{-3} \ cm^3/atm\text{-}s.$

$F_m = (3.81 \times 10^3) D^3 (T / M)^{.5} / (a P_a) (cm^3/atm\text{-}s),$ (Eq. B4)
$F_m = (3.81 \times 10^3) (1.0569 \times 10^{-3})^3 (298 / 29)^{.5} / ((0.056) (0.505)),$
$F_m = (4.3187 \times 10^5) (1.0569 \times 10^{-3})^3,$
$F_m = 5.0994 \times 10^{-4} \ cm^3/atm\text{-}s.$

$L_u = (F_c + F_m) (P_u - P_d) (P_a / P_u) (cm^3/s),$ (Eq. B5)
$L_u = (2.9995 \times 10^{-3} + 5.0994 \times 10^{-4}) (cm^3/atm\text{-}s) (1.0 - 0.01)(atm) (0.505 / 1.0),$
$L_u = (3.5095 \times 10^{-3}) (cm^3/atm\text{-}s) (0.49995)(atm),$
$L_u = 1.7546 \times 10^{-3} \ cm^3/s.$

The ACATP reference air leakage rate as defined in ANSI N14.5-1997, Section B.3, is the upstream leakage in air.

$L_{R,PA\text{-}AIR} = 1.7546 \times 10^{-3}$ ref-$cm^3/s.$ for plutonium content

The same equations can be used to calculate an allowable leakage rate using helium for leak testing.

$M = 4$ g/g-mole, Molecular weight of helium

$\mu = 0.0198$ cP. Viscosity of helium at temperature

$F_c = (2.49 \times 10^6) D^4 / (a \mu) (cm^3/atm\text{-}s),$ (Eq. B3)
$F_c = (2.49 \times 10^6) (1.0569 \text{ H } 10^{-3} cm)^4 / ((0.056) (0.0198)),$
$F_c = (2.2457 \times 10^9) (1.0569 \times 10^{-3} cm)^4,$
$F_c = 2.8026 \times 10^{-3} \ cm^3/atm\text{-}s.$

$F_m = (3.81 \times 10^3) D^3 (T / M)^{0.5} / (a P_a) (cm^3/atm\text{-}s),$ (Eq. B4)
$F_m = (3.81 \times \text{H } 10^3) (1.0569 \times 10^{-3} cm)^3 (298 / 4)^{.5} / ((0.056) (0.505)),$
$F_m = (1.1629 \times 10^6) (1.0569 \text{ H } 10^{-3} cm)^3,$
$F_m = 1.3730 \times 10^{-3} \ cm^3/atm\text{-}s.$

$L_u = (F_c + F_m) (P_u - P_d) (P_a / P_u) (cm^3/s),$ (Eq. B5)
$L_u = (2.8026 \times 10^{-3} + 1.3730 \times 10^{-3}) (cm^3/atm\text{-}s) (1.0 - 0.01)(atm) (0.505 / 1.0),$
$L_u = (4.1757 \times 10^{-3}) (cm^3/atm\text{-}s) (0.49995)(atm),$
$L_u = 2.0876 \times 10^{-3} \ cm^3/s.$

The allowable leakage rate using helium for leak testing for ACATP is:

$L_{R,PA\text{-}He} = 2.0876 \times 10^{-3} \ cm^3/s.$ ACATP helium test value

In accordance with Table 4.2 of the SAR, the highest measured air leakage rate following the ACATP conditions was 4.5 H 10^{-5} cc/sec at atmosphere conditions (atm cc/s). This leakage rate is considerably lower than the calculated maximum allowable regulatory leakage rate requirement of 1.4703×10^{-3} ref cc/s shown in Table 4.5.6.1. Therefore, the TB-1 containment vessel inside the PAT-1 shipping package maintains containment for NCT, HAC, and ACATP conditions.

Mass Release During ACATP

To determine the amount of material that leaks out of the containment boundary in one week under ACATP conditions, the measured volumetric leakage rate shown in Table 4.2 (4.5×10^{-5} cm^3/s) is multiplied by the aerosol mass density (9.0×10^{-6} g/cm^3) and by time (6.048×10^5 sec/week). You obtain a mass release of approximately 2.45×10^{-4} grams in one week. This release amount disregards orifice size and particle size limits.

The regulatory release mass limit for the material in the containment vessel is calculated by using the regulatory activity limit of an A_2 in one week divided by the specific activity of the mixture. Assuming a homogenous mixture, the material leaving the containment vessel has a specific activity determined by dividing the total activity (TBq) by the total mass (grams) or TBq/gram. Therefore, the allowable mass release is then the A_2 in a week (TBq/week) divided by the specific activity of the mixture (TBq/gram) or grams/week. Using this approach for the material that has no Pu-241 decay and Table 4.5.5.3, you obtain an activity release rate of 1.1326×10^{-2} TBq/week; total activity of 53.2808 TBq; total mass of 1300 grams; a specific activity of 4.0985×10^{-2} TBq/g; and finally an allowable mass release of 2.7634×10^{-1} grams. Again using this approach for the material with total Pu-241 decay to Am-241 and Table 4.5.5.4, you obtain an allowable mass release of 2.3336×10^{-1} grams. Since both of these material conditions release much less than the regulatory allowable mass release, the TB-1 containment vessel inside the PAT-1 shipping package maintains containment during ACATP conditions.

Table 4.5.6.1 Regulatory Leakage Criteria for 1300 g plutonium

Isotopic Distribution	Ancillary plastic composition	NCT [a]		HAC [a]		ACATP	
		$L_{R,N\text{-}air}$ (ref-cm^3/s)	$L_{R,N\text{-}He}$ (cm^3/s)	$L_{R,A\text{-}air}$ (ref-cm^3/s)	$L_{R,A\text{-}He}$ (cm^3/s)	$L_{R,PA\text{-}air}$ (ref-cm^3/s)	$L_{R,PA\text{-}He}$ (cm^3/s)
No Pu-241 decay	polyethylene terephthalate	5.1244 E-06	8.8373 E-06	9.4686 E-02	9.8072 E-02	1.7546E-03	2.0876E-03
	polyethylene	5.1244 E-06	8.8373 E-06	9.4686 E-02	9.8072 E-02	1.7339E-03	2.0642E-03
	polyvinyl chloride	5.1244 E-06	8.8373 E-06	9.4686 E-02	9.8072 E-02	1.7487E-03	2.0810E-03
	polytetrafluoroethylene	5.1244 E-06	8.8373 E-06	9.4686 E-02	9.8072 E-02	2.1844E-03	2.5725E-03
Complete Pu-241 decay to Am-241	polyethylene terephthalate	4.2787 E-06	7.4737 E-06	7.9817 E-02	8.3008 E-02	1.4703E-03	1.7873E-03
	polyethylene	4.2787 E-06	7.4737 E-06	7.9817 E-02	8.3008 E-02	1.4729E-03	1.7673E-03
	polyvinyl chloride	4.2787 E-06	7.4737 E-06	7.9817 E-02	8.3008 E-02	1.4854E-03	1.7816E-03
	polytetrafluoroethylene	4.2787 E-06	7.4737 E-06	7.9817 E-02	8.3008 E-02	1.8549E-03	2.2012E-03

[a] Since temperatures associated with pyrolysis of the ancillary plastics are not reached during NCT and HAC, the various plastics have no affect on the regulatory leakage criteria at those conditions.

4.5.7 References for Sections 4.5.5 and 4.5.6

10 CFR 71, *Packaging and Transportation of Radioactive Material,* Jan. 1, 2010.

49 CFR 173, *Shippers—General Requirements for Shipments and Packagings,* Oct. 1, 2010.

ANSI N14.5-1997, *Radioactive Materials—Leakage Tests on Packages for Shipment*, American Natl. Standards Institute, Feb. 5, 1998.

Curren, W. D. and R. D. Bond, *Leakage of Radioactive Powders from Containers*, Proceedings of the Sixth International Symposium on Packaging and Transportation of Radioactive Material: PATRAM '80, West Berlin, F.R.G., November 10–14, 1980, pp. 463–471.

Kocher, D. C., *Radioactive Decay Data Tables, A Handbook of Decay Data for Application to Radiation Dosimetry and Radiological Assessments*, DOE/TIC-11026, U.S. DOE, Office of Scientific and Technical Information, 1981.

R.H. Perry, D.W. Green, and J.O. Maloney, *Perry's Chemical Engineers' Handbook*, 7th edition, 1997, p. 2-363)

R.D. McCarty Cryogenics Division, *National Bureau of Standards Technical Note 631*, "Thermophysical Properties of Helium-43 from 2 to 1500 K with Pressures to 100 Atmospheres," pg 49, Nov. 1972.

Robert C. Weast, Ph. D., *Handbook of Chemistry and Physics*, 55th ed., pg. F-13, 1974.

This page intentionally left blank

5. SHIELDING EVALUATION

This section describes the shielding evaluation for incorporating plutonium (Pu) metal contents as a new payload into the PAT-1 package. The Pu metal is packed in an inner container (*T- Ampoule Assembly,*[A] Drawing 2A0261, designated the T-Ampoule) that replaces the PC-1 inner container. The T-Ampoule and associated Pu metal content packing configurations are described in Section 1.2.1 and Section 1.2.2 of this addendum, respectively.

To demonstrate compliance with the dose rate limits of 10 CFR 71.47(a) (non-exclusive use) for normal conditions of transport (NCT) and 10 CFR 71.51(a)(2) for hypothetical accident conditions (HAC), an evaluation of the shielding performance of the Plutonium Air Transportation (PAT-1) package has been completed. The evaluation assumes a package loaded with up to 1.3 kg* of Pu metal or plutonium/beryllium (Pu/Be) sources with a total mass of 200 g* or less of Pu; a combined Pu/Be contact surface area of 91 cm^2 or less; and an isotopic Pu composition, including allowance for decay, such that the total neutron source from the (α,n) reaction with beryllium (Be) metal does not exceed 363 n/s/cm^2 (see Table 5-13). A detailed description of the shielding characteristics of the PAT-1 packaging is provided in Section 5.4 of the SAR.[1]

5.1 Description of Shielding Design

5.1.1 Design Features

The shielding design features of the PAT-1 include the stainless steel overpack drum (*Overpack, AQ,*[A] Drawing 1002 in the SAR,[1] designated the AQ-1); the stainless steel (PH13-8Mo) TB-1 *Containment Vessel* (Drawing 1017, designated the TB-1); and the titanium ampoule (*T-Ampoule Assembly*, Drawing 2A0261, designated the T-Ampoule), which secures the contents inside the containment vessel. In addition, the aluminum (Al) load spreader assembly, the copper heat conductor tube, and the redwood assemblies (both inner and outer) provide minimal additional shielding. While these additional features are largely designed for other purposes, they perform a dual role as shielding features. The lid and the bottom of the overpack drum, the containment vessel, and the T-Ampoule provide shielding in the axial direction. Shielding credit is not taken for the T-Ampoule (or for packing materials contained therein), the inner redwood assembly, or the thicker portions of the TB-1 vessel.

The stainless steel 304 materials are fabricated with a density of 7.9 g/cm^3 with the exception of the TB-1 containment vessel, which is fabricated with a PH13-8Mo material[2] with a density of 7.5 g/cm^3. The copper tube is fabricated from pure copper metal with a density of 8.94 g/cm^3, and the Al load spreader is fabricated from Al 6061 with a density of 2.6989 g/cm^3. The redwood is assumed to be cellulose ($C_6H_{10}O_5$)[3, 4] with a density of 0.36 g/cm^3.

[A] The drawing titles are in italics and are used interchangeably with the designated names in this addendum. See Section 1.3.2 in this addendum and Chapter 9 of the SAR[1] for drawing number, title, and revision.

* The plutonium quantities analyzed in this shielding section represent a conservative upper bound for analysis and are higher than the payload quantities shown in Table 1-1 of Section 1 of this addendum.

The shielding design requirements for these packages are minimal due to high purification and relatively low specific activity of the desired contents. Thus, with generous bounding assumptions on the source magnitude, the dose rates are still demonstrated to be small fractions of the regulatory limits.

5.1.2 Summary Table of Maximum Radiation Levels

The dose rates shown in Table 5-1 indicate that the PAT-1 meets regulatory dose limits as specified in the respective 10 CFR sections under NCT and HAC for nonexclusive use. The analysis for the limiting contents is based on the natural radioactivity produced from the decay of 1300 g of plutonium metal under bounding conditions that include peak dose rates due to decay (Pu shelf-life after separation), worst-case scenario for the various isotopes of Pu, and (α,n) production from an oxide matrix instead of a metal matrix. Details of the source generation and shielding analyses for the limiting contents are described in Sections 5.2 and 5.3, respectively. Description of an alternate content of Pu/Be sources is described in Section 5.5.3. It is shown in this section that Pu/Be is not the limiting content.

Table 5-1. Summary Table of External Radiation Levels (Non-Exclusive Use)

NCT	Package Surface mSv/h (mrem/h)			1 Meter from Package Surface mSv/h (mrem/h)		
Radiation	**Top**	**Side**	**Bottom**	**Top**	**Side**	**Bottom**
Gamma	0.060 (6.0)[a]	0.277 (27.7)	0.055 (5.5)[a]	0.006 (0.6)[a]	0.015 (1.5)	0.006 (0.6)[a]
Neutron	0.036 (3.6)[a]	0.319 (31.9)	0.038 (3.8)[a]	0.003 (0.3)[a]	0.014 (1.4)[a]	0.003 (0.3)[a]
Total	0.096 (9.6)[a]	0.596 (59.6)	0.093 (9.3)[a]	0.009 (0.9)[a]	0.029 (2.9)	0.009 (0.9)[a]
10 CFR 71.47(a) Limit	2 (200)	2 (200)	2 (200)	0.1 (10)[b]	0.1 (10)[b]	0.1 (10)[b]

[a] Monte Carlo statistics of 5% or less; all others 1% or less.
[b] Transport index may not exceed 10.

HAC	1 Meter from Package Surface mSv/h (mrem/h)		
Radiation	**Top**	**Side**	**Bottom**
Gamma	0.024 (2.4)	0.035 (3.5)	0.021 (2.1)
Neutron	0.015 (1.5)	0.018 (1.8)	0.014 (1.4)
Total	0.039 (3.9)	0.053 (5.3)	0.035 (3.5)
10 CFR 71.51(a)(2) Limit	10 (1000)	10 (1000)	10 (1000)

5.2 Source Specification

Because of the variety of contents envisioned for the PAT-1, a procedure to determine and generate bounding sources was developed that allows for a great deal of flexibility of allowed package contents. The gamma and neutron sources are based on a limiting Pu isotopic vector (see Table 5-2) that should allow for almost any form of plutonium metal to be loaded into the package, subject only to the mass and heat constraints of 1300 g of Pu and 25 watts, respectively.

The Pu isotopic distribution (Pu isotope versus mass fraction seen in Table 5-2) was generated through simulation of all conceivable routes of Pu production from different reactor types. The package was limited to 1300 g and a heat load of 25 watts although the isotopes for the radiation source are based on 2197 g with a heat load of 40 watts. For each isotope, the largest weight percent was selected across all the reactor types; taking the largest weight percent for each isotope regardless of other restrictions results in a total that exceeds 100 weight percent (wt %). The source definition is the upper bound of the actual source and therefore, yields an overestimate of the expected package doses. The analysis to support these Pu isotopic values is further described in Section 5.5.2.

Table 5-2. Plutonium Isotopics Used for Source Generation

Isotope	Mass Fraction	Mass (g)
Pu-236	2.0E−07	0.00026
Pu-238	0.04	52
Pu-239	1.00	1300
Pu-240	0.40	520
Pu-241	0.15	<195[a]
Pu-242	0.10	130
Am-241	0.15[a]	<195[a]
Total	1.69[b]	2197

[a] The initial Am-241 is assumed to be zero, with 195 g of Pu-241. The time-varying source is optimized such that the maximum dose is computed with respect to the decay of Pu-241 to Am-241.

[b] As a conservative assumption, the mass fractions used to generate the radiation source are allowed to exceed unity. The package is limited to 831 g (1300 g was used as an upper bound), although the isotopics for the radiation source are based on 2197 g. In addition, the allowed heat load is limited to 25 watts, while the radiation source used in this analysis is based on isotopics that would generate about 40 watts of heat.

5.2.1 Gamma Source

The gamma source arises from the beta and gamma decay of the Pu isotopes, each of which has distinct time and energy characteristics. The specific radiation characteristics of each of these isotopes are discussed further in Section 5.5.2. From this analysis, a gamma source is derived that bounds all realistic forms of plutonium metal. This source is given in Table 5-3 in the SCALE 18 group structure. This source corresponds to 2197 g of Pu (1300 g of Pu with the mass fractions specified in Table 5-2) and a decay time since Pu separation of 18.0 years (referred to as the shelf-life). While this decay time does not represent the peak source, it does represent the peak dose rate due to the dominance of the high-energy photons from the decay of Pu-236, which peaks at 18.0 years. In contrast, the lower-energy photons from predominately Pu/Am-241 have a very broad peak of about 75 years (see Figure 5-3).

5.2.2 Neutron Source

The neutron source consists of spontaneous fission and (α,n) components, as shown in Table 5-4. The spontaneous fission component is invariant relative to the Pu matrix material (oxide or metal), is uniquely defined for each isotope, and decreases slightly with decay time. The (α,n) component is a function of the impurities in the Pu matrix and exhibits a broad peak with decay

due to the variation of the Pu/Am-241 concentrations (see Figure 5-3). The (α,n) component of the neutron spectrum, shown in Table 5-4, is based on an oxide matrix and represents a bound of the contents for a metal matrix (see Section 5.5.2). Both components of the neutron source shown are for a Pu decay time of 30 years, which corresponds to the peak source and dose with respect to the decay time.

Table 5-3. Gamma-Ray Source Used in the Shielding Analysis (2197 g Pu)

Energy Group	Energy Boundaries (MeV)	Photons/s
1	10	6.691E+02
2	8	3.182E+03
3	6.5	1.645E+04
4	5	4.162E+04
5	4	1.255E+05
6	3	6.089E+07
7	2.5	2.481E+05
8	2	7.277E+05
9	1.66	3.519E+06
10	1.33	2.546E+06
11	1	1.201E+07
12	0.8	1.396E+08
13	0.6	1.404E+08
14	0.4	4.397E+08
15	0.3	1.636E+09
16	0.2	7.217E+09
17	0.1	4.048E+12
18	0.05	5.459E+12
Total		9.517E+12

5.3 Shielding Model

5.3.1 Configuration of Source and Shielding

A slice of the three-dimensional shielding model used for the NCT evaluation is shown in Figure 5-1. This model is constructed with the dimensions given in Table 5-5 and contains the materials as described in Table 5-6. The dimensions correspond to those from the reference drawings with nominal dimensions used where given. The use of nominal dimensions is appropriate for this analysis since the package materials are not designed as shielding bodies and, therefore, produce minimal shielding effects. In addition, the inner redwood assembly, inner can assembly, T-Ampoule, and thicker regions along the side of the TB-1 containment vessel are assumed to be void in the shielding model. Since the geometry of the source material is variable, analyses were

performed to conservatively bound the configuration and magnitude of the source. The bounding of the source magnitude was previously discussed in Section 5.2.

Table 5-4. Neutron Source Used in the Shielding Analysis (2197 g Pu)

Energy Group	Energy Boundaries (eV)	Spontaneous Fission (neutrons/s)	(α,n) Source (neutrons/s)	Total (neutrons/s)
1	2.000E+7	1.161E+04	0.0	1.161E+04
2	6.434E+6	1.632E+05	2.658E+05	4.290E+05
3	3.000E+6	2.024E+05	5.305E+05	7.330E+05
4	1.850E+6	1.154E+05	1.185E+05	2.340E+05
5	1.400E+6	1.486E+05	7.443E+04	2.231E+05
6	9.000E+5	1.517E+05	5.428E+04	2.060E+05
7	4.000E+5	7.012E+04	2.719E+04	9.731E+04
8	1.000E+5	1.034E+04	4.798E+03	1.513E+04
9	1.700E+4	7.403E+02	3.497E+02	1.090E+03
10	3.000E+3	5.486E+01	2.255E+01	7.740E+01
11	5.500E+2	4.314E+00	1.855E+00	6.169E+00
12	1.000E+2	3.031E-01	1.385E-01	4.415E-01
13	3.000E+1	4.813E-02	2.516E-03	5.065E-02
14	1.000E+1	9.546E-03	8.739E-04	1.042E-02
15	3.05	1.081E-03	1.607E-04	1.242E-03
16	1.77	3.179E-04	5.900E-05	3.769E-04
17	1.30	1.025E-04	2.134E-05	1.238E-04
18	1.13	7.345E-05	1.632E-05	8.976E-05
19	1.00	1.040E-04	2.510E-05	1.291E-04
20	0.80	1.698E-04	5.021E-05	2.200E-04
21	0.40	2.504E-05	9.414E-06	3.445E-05
22	0.33	2.923E-05	1.255E-05	4.179E-05
23	0.23	2.847E-05	8.945E-06	3.742E-05
24	0.10	8.138E-06	0.0	8.138E-06
25	0.05	2.565E-06	0.0	2.565E-06
26	0.03	2.095E-06	0.0	2.095E-06
27	0.01	1.121E-06	0.0	1.121E-06
Total		**8.743E+05**	1.076E+06	1.950E+06

The shape of the source in this scenario determines the (1) degree to which the source particles are self-shielded for gamma emissions and (2) the magnitude of the neutron source multiplication due to fission. The bounding source geometry is determined from a series of three assumed source geometries (see Section 5.4.4):

- A full-density, solid sphere with a radius of 2.63 cm
- A reduced-density, smeared source that completely fills the central region shown in Figure 5-1
- A full-density, thin, hollow cylinder with inner and outer radii of 5.249 and 5.4 cm, respectively, and a height of 15.11 cm (the central cylindrical region shown in Figure 5-1**).**

Each of these three geometries is assumed to contain 1300 g of plutonium metal. The full-density models assume the use of plutonium metal with a density of 17.0 g/cm^3 (see Table 5-6 for material reference and discussion below). The bounding source geometry for the neutron dose is the solid, maximum-density sphere with the sphere moved outward so that it touches the inside surface of the TB-1 vessel. The bounding source geometry for the gamma doses is the smeared geometry, which minimizes the self-shielding effect and also moves the source material closer to the detector locations. The maximum total side dose (neutron plus gamma components) is simulated using the smeared geometry model for the gamma contribution and an intermediate full-density off-center sphere (density of 17 g/cm^3) for the neutron contribution; the predicted total doses using this hybrid approach are some 20% greater than those using consistent neutron/gamma contributions for the various geometry/density models. The top and bottom dose values reported in Table 5-1 are based on the reduced-density, smeared Pu source model only since these values are not limiting.

Spot checks were completed for the top and bottom geometries to ensure that the peak source geometries were evaluated. The shielding source model for the HAC is the same as the NCT reduced-density smeared source model with only the central Pu region and the TB-1 containment vessel remaining.

5.3.2 Material Properties

The constituents of the materials used in the shielding calculations are shown in Table 5-6. All materials are used at their stated densities, although the plutonium metal density is modified by the ratio of the full-density volume to the smeared-density volume used in the reduced-density source model that bounds the shielding results. The density for this case follows.

The volume of the bottom curved region (204.2 cm^3) is taken from Section 6.9.2. The cylindrical volume is given below and differs from that in Section 6.9.2 since a minimum thickness of the TB-1 lid is assumed here.

$$\text{Smeared-plutonium-source density} = 1300\ \text{g} / ([\pi * 5.4^2 * 15.11] + 204.2)\ \text{cm}^3 = 0.818\ \text{g/cm}^3$$

The non-Pu materials use the SCALE standard definitions for the isotopic compositions, while selecting the minimal density from other sources, if available. The references used for each material are also presented in Table 5-6.

5.4 Shielding Evaluation

5.4.1 Methods

The shielding evaluation is performed by calculating the dose rates at the top, bottom, and radial directions of the PAT-1 package to verify compliance with the 10 CFR Part 71 nonexclusive dose rates during NCT. The dose rates are 2 mSv/h (200 mrem/h) at the package surface and 0.01mSv/h (10 mrem/h) at 1m from the accessible package surface under NCT, and 10 mSv/h (1000 mrem/h) at 1m, the 10 CFR Part 71 dose rate limit, under HAC.

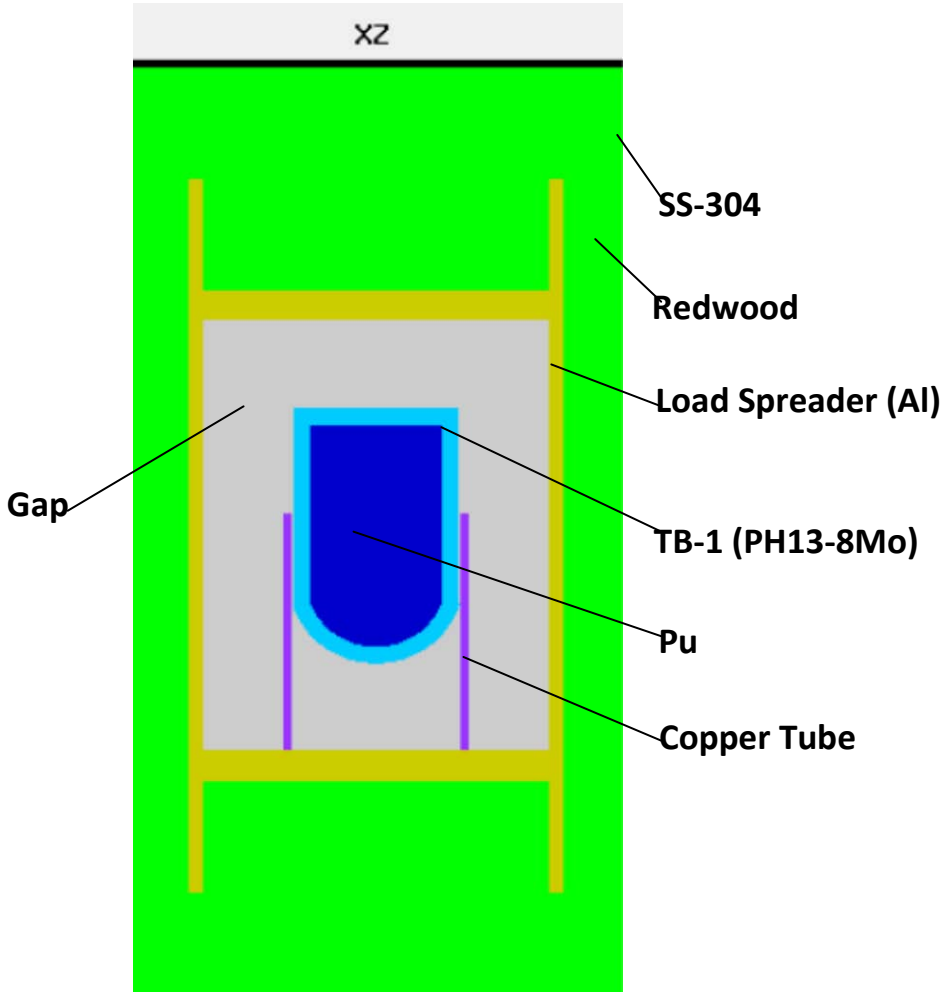

Figure 5-1. Cylindrical Shielding Model of PAT-1 Used in This Analysis (see Table 5-6 for Dimensional Information)

The evaluation has been performed for the PAT-1 package containing up to 1300g of plutonium metal. The Shielding Analysis Sequence #4 (SAS4)[3] code was utilized to determine the dose rate at the surface and at 1 m from the surface, in both the axial and radial directions, for

bounding gamma and neutron sources. The dose locations evaluated in this scenario are shown in Figure 5-2. As shown in Table 5-1, the surface side dose is the most restrictive and is composed almost equally of gamma and neutron dose components.

The spatial distribution for each source used in these analyses was uniform within each of the defining cylindrical or spherical volumes (i.e., reduced-density, smeared cylinder; full-density annular cylinder; full-density sphere), as described in Section 5.3.1.

Table 5-5. Dimensions of Materials Regions Used in Shielding Analyses

Body	Radius (cm)	Bottom location (cm)	Height (cm)	Description
1 – cylinder	5.40	–5.64	15.11	cylindrical inside of TB-1
2 – sphere	5.72	–3.74 [a]	—	curved inside of TB-1
3 – cylinder	6.795	–5.64	16.71	outside of TB-1
4 – sphere	7.12	–3.74 [a]	—	curved outside of TB-1
5 – cylinder	10.0	–5.64	16.71	dummy piece for geometry
6 – cylinder	6.875	–10.86	21.93	void outside TB-1
7 – cylinder	6.875	–18.25	7.39	wood block below TB-1
8 – cylinder	7.52	–18.25	20.32	copper tube
9 – cylinder	8.74	2.07	9.00	void for thicker TB-1 region
10 – cylinder	13.97	–18.25	36.79	wood inside Al spreader
11 – cylinder	13.97	–20.79	41.87	upper and lower Al spreader
12 – cylinder	13.97	–30.35	60.81	top and bottom wood inside Al
13 – cylinder	15.24	–30.35	60.81	Al on outside of spreader
14 – cylinder	28.58	–48.69	99.13	wood inside drum
15 – cylinder	28.73	–48.84	99.43	steel drum

[a] For spherical bodies, this value is the z location of the sphere; all bodies shown are centered at x and y = 0.

All shielding calculations were performed with the SCALE 5.1 version of the SAS4. This sequence consists of multiple codes executed from a single input stream. The individual modules used are the:

- BONAMI and NITAWL codes, which process the cross sections into formats the subsequent shielding codes can utilize.
- XSDRNPM one-dimensional discrete ordinates code, which is run in the adjoint mode to automatically generate biasing parameters for the final shielding analysis.
- MORSE-SGC, which is the Monte Carlo shielding code that quantifies the fluxes and dose rates at desired locations in the geometry.

Unless otherwise noted, all results reported in Table 5-1 are converged to a Monte Carlo statistical value of 1% or less at the 1 sigma level, indicating that the results are well converged.

This degree of convergence is aided by the automated bias generation built into the SAS4 sequence. Automated biasing as implemented in SAS4 gives rise to some inherent geometry limitations (e.g., axially symmetric models). Section 5.5.4 contains a discussion of how these limitations were overcome.

Table 5-6. Elemental Compositions Used in Shielding Analysis

Material	Density (g/cm^3)	Composition, wt % (atoms/barn-cm)		
PH13-8Mo[2]	7.74 (7.5 used)	Cr	12.75	(1.10753E-02)
		Ni	8.00	(6.15690E-03)
		Al	1.13	(1.88319E-03)
		Mo	2.25	(1.05924E-03)
		Fe	75.88	(6.13662E-02)
Redwood[3,4]	0.36	H	6.2	(1.33725E-02)
		C	44.4	(8.02350E-03)
		O	49.4	(6.68625E-02)
Aluminum[3,5]	2.6989	Al	100.0	(6.02375E-02)
304 Stainless Steel[3,5]	7.9	C	0.080	(3.16873E-04)
		Si	1.000	(1.69394E-03)
		Cr	19.000	(1.73846E-02)
		Mn	2.000	(1.73195E-03)
		Fe	68.375	(5.82497E-02)
		Ni	9.500	(7.70121E-03)
		P	0.045	(6.91181E-05)
Copper[5]	8.94	Cu	100.0	(8.47233E-02)
Plutonium metal[6]	15-19.7 (17.0 used)	Pu-239	100.0	(4.28259E-02)

The following is a complete list of the conservative assumptions and techniques used in this analysis to ensure that the results generated bound those of the actual contents under any circumstances.

1. The source is generated based on an extremely pessimistic representation of the Pu isotopes. The use of a burned reactor-grade Pu vector allows for isotopes other than Pu-239 to contribute significantly to the total source. The expected use of components more in line with weapons-grade Pu (higher Pu-239; lower for other isotopes) should produce radiation levels much lower than those assumed in this analysis. See estimates of this effect in Section 5.5.2.

2. The metal matrix anticipated for shipments using this package should have a neutron source that is significantly lower than the oxide matrix that was used for all source calculations (see Section 5.5.2).

3. The source generation scenario is based on a Pu mass 60% greater than allowed and a heat generation rate also 60% greater than the allowed rate, ensuring that doses are bounding. However, the actual mass of Pu in the package for self-shielding purposes is only 1300 g.

4. The shape of the source was varied to determine the configuration that produced the maximum dose for the bounding source spectrum described above and in Section 5.2.

5. The time variation of the source spectrum and magnitude was analyzed to select a decay time that produced bounding dose rates over any possible decay time.

6. The shielding analysis assumed the minimum Pu density expected for the various forms of plutonium metal.

7. The T-Ampoule, the thicker steel portions of the TB-1 containment vessel, and the inner redwood assembly were omitted from the shielding analysis. The structural material densities were the minimum values found in the literature.

In the model, the dose at a given location is obtained by assuming "point detectors," which allow the dose at a specific point in space to be tabulated. Dose estimation via point detectors is less efficient than that based on radiation tracking across a specified surface length or area, but it allows for greater detail in the reported results. In each case, a series of point detectors were placed side-by-side to determine the location of the peak dose. In most cases, the peak dose was at the location corresponding to or in alignment with the center of the source region. The point locations shown in Figure 5-2 indicate where the point detectors were placed for the various locations reported in Table 5-1. The use of point detectors directly on the outermost shielding surface is limited; standard practice is to move the point detectors about 1 cm off the surface. The 1-m detectors are located precisely 1 m from the outermost shielding surface. For the HAC cases, only the contents and the TB-1 containment vessel were modeled, with the 1-m detectors placed at a distance of precisely 1 m from the outermost surface of the TB-1 body.

The cross section set used for all analyses was the SCALE 27N-18COUPLE library. This is the recommended library for all shielding calculations using the SCALE system.

5.4.2 Input and Output Data

A listing of the input data for the ORIGEN-S source generation is shown in Section 5.5.4. The output of this source generation calculation is automatically written onto a file named *ft71f001* and subsequently read in by the shielding analysis modules. SAS4 inputs for the shielding study of the radial neutron and gamma doses are also given in Section 5.5.4. SAS4 utilizes an automated bias parameter generator, which typically allows for both neutron and gamma problems to converge rapidly. In all cases, the results given in Table 5-1 are converged to 1% or less unless otherwise noted.

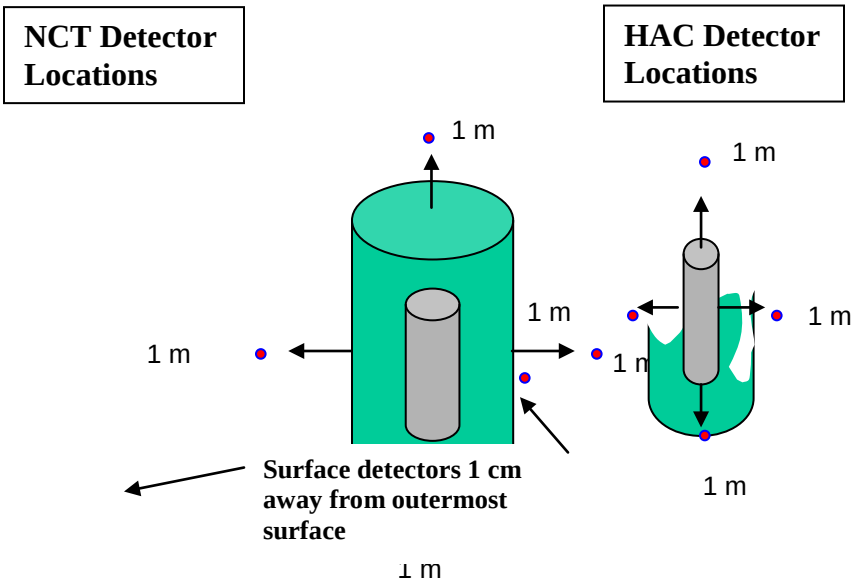

Figure 5-2. Dose Locations Analyzed for the PAT-1 Package

5.4.3 Flux-to-Dose-Rate Conversion

ANSI/ANS-6.1.1-1977 flux-to-dose-rate conversion factors are used in the SAS4 shielding calculations. These factors are provided in Tables 5-7 and 5-8 for neutrons in the SCALE 27 neutron group structure and gamma radiation in the SCALE 18 group gamma structure.

5.4.4 External Radiation Levels

Radiation levels corresponding to up to 1300 g of plutonium metal loaded in the PAT-1 package have been predicted in this section. The methods and techniques are based on current-generation, well-known, and approved codes and procedures and should be accurate to within 10–20%. A number of bounding approximations included in each phase of the analysis should ensure that the predicted results are larger than any actual radiation levels and, therefore, allow a high level of assurance that an actual shipment should pass the dose-measurement tests at the time approved contents are shipped. While no measurements of sufficient quality exist to serve as benchmarks for expected dose rates near plutonium metal components, the results reported herein are consistent with previous analyses[7] performed prior to certification of Pu oxide contents in the same PAT-1 package. The sources and final dose predictions from that study differ only within a factor of 2 from those in this study, even though the techniques and underlying data sets have been updated since the previous study.

A comparison of dose predictions at the top, side, and bottom package locations (both at the surface and at 1 m) indicates very consistent relative dose values: the package surface values are a factor of 5 greater along the side than those along the top and bottom. At 1 m , this factor of 5 is reduced to approximately 3 (as expected), as the distributed Pu source will begin to approximate a point source as the distance from the package increases. The top and bottom doses are also consistent with each other as expected from a visual examination of Figure 5-1, which shows similar top and bottom geometries and similar distances from the package contents to the exterior surface locations.

Although not included in the analyses, the effect of ground scatter during the loading process should only be approximately 10–20%, which is readily bounded by the conservatisms included in the analysis.

The bounding source configuration was found to be the reduced-density, smeared Pu source that completely filled the inside of the TB-1 containment vessel volume. This conclusion is based on the analysis of five other source configurations described as follows:

Table 5-7. Neutron Flux-to-Dose Conversion Factors Used in Shielding Analysis

Group Number	Energy Bounds (eV)	Dose Factor (rem/h/neutrons/cm^2/s)
1	2.000E+07	1.492E-04
2	6.434E+06	1.446E-04
3	3.000E+06	1.270E-04
4	1.850E+06	1.281E-04
5	1.400E+06	1.298E-04
6	9.000E+05	1.028E-04
7	4.000E+05	5.118E-05
8	1.000E+05	1.232E-05
9	1.700E+04	3.837E-06
10	3.000E+03	3.725E-06
11	5.500E+02	4.015E-06
12	1.000E+02	4.293E-06
13	3.000E+01	4.474E-06
14	1.000E+01	4.568E-06
15	3.050E+00	4.558E-06
16	1.770E+00	4.519E-06
17	1.300E+00	4.488E-06
18	1.130E+00	4.466E-06
19	1.000E+00	4.435E-06
20	8.000E-01	4.327E-06
21	4.000E-01	4.197E-06
22	3.250E-01	4.098E-06
23	2.250E-01	3.839E-06
24	1.000E-01	3.675E-06
25	5.000E-02	3.675E-06
26	3.000E-02	3.675E-06
27	1.000E-02	3.675E-06

- A full-density, solid sphere of radius 2.63 cm located at the center of the TB-1 volume
- A solid sphere moved to the TB-1 vessel inner wall
- Three hollow cylindrical configurations with various radii and heights

The three hollow cylindrical sources are described as a small cylinder; a large cylinder; and a large, thin cylinder. The first two are actual components under consideration for loading. The

third is a hypothetical cylinder with an outer radius of 5.4 cm, which coincides with the inner radius of the TB-1 vessel, and a height of 15.11 cm, which is the complete height of the cylindrical section inside the TB-1 vessel. The inner radius was calculated to be 5.249 cm, which corresponds to 1300 g of plutonium metal at a density of 17.0 g/cm^3. The complete set of results for the side surface of the package is shown in Table 5-9. These results show that the reduced- density, smeared cylinder is the bounding source geometry; however, the results also show very little sensitivity of the total dose to the source configuration. Hence, for the top and bottom dose locations, only the reduced-density, smeared cylinder source configuration was analyzed.

Table 5-8. Gamma Flux-to-Dose Conversion Factors Used in Shielding Analysis

Group Number	Energy Bounds (eV)	Dose Factor (rem/h/photon/cm^2/s)
1	1.000E+07	8.772E-06
2	8.000E+06	7.478E-06
3	6.500E+06	6.375E-06
4	5.000E+06	5.414E-06
5	4.000E+06	4.622E-06
6	3.000E+06	3.960E-06
7	2.500E+06	3.469E-06
8	2.000E+06	3.019E-06
9	1.660E+06	2.628E-06
10	1.330E+06	2.205E-06
11	1.000E+06	1.833E-06
12	8.000E+05	1.523E-06
13	6.000E+05	1.172E-06
14	4.000E+05	8.759E-07
15	3.000E+05	6.306E-07
16	2.000E+05	3.834E-07
17	1.000E+05	2.669E-07
18	5.000E+04	9.347E-07

Table 5-9. Source Geometry Optimization Dose Results (at PAT-1 Side Surface)

Source Configuration	Neutron Dose (mrem/h)	Gamma Dose (mrem/h)	Total Dose (mrem/h)
reduced-density, smeared cylinder	18.9	27.7	46.6
centered sphere	26.1	10.3	36.4
off-center sphere	31.9	11.1	43.0
large cylinder	20.3	20.5	40.8
small cylinder	20.3	16.9	37.2
Large, thin cylinder	20.2	25.6	45.8

Dose profiles were generated for each separate analysis. In all cases the peak dose occurs at the center point of the source region or just off the center point (due to the influence of the copper pipe in the radial calculations). These are the expected results for a uniformly distributed source and indicate no streaming through various regions of the PAT-1 geometry.

5.5 Appendix

5.5.1 References

1. United States. Nuclear Regulatory Commission. NUREG-0361, "Safety Analysis Report for the Plutonium Air Transportable Package, Model PAT-1." Washington, D.C. 1978.

2. Brown, Jr., W. F. and S. J. Setlak. *Aerospace Structural Metals Handbook, 37th Edition*, CINDAS/USAF CRDA Handbooks Operation, Purdue University, West Lafayette, IN. 2001.

3. SCALE-5.1, "A Modular Code System for Performing Standardized Computer Analyses for Licensing Evaluation for Workstations and Personal Computers, CCC-545," Oak Ridge National Laboratory. Oak Ridge, TN.

4. United States. Dept. of Agriculture. Alden, H. A., "Softwoods of North America," September 1997.

5. Davis, J.R., ed. *ASM Specialty Handbook: Copper and Copper Alloys*. p. 446-452, ASM International, 2001.

6. "LANL Content Description for PAT-1 Packaging," Los Alamos National Laboratory. Los Alamos, NM: August 9, 2007.

7. United States. Nuclear Regulatory Commission. NUREG/CR-0030 (SAND76-0587), "PARC (Plutonium Accident Resistant Container) Program Research, Design, and Development." Reprinted January 1983.

8. PAT-1 Content impurity description transmitted from SNL to ORNL on October 18, 2007.

9. Wilson, W.B., et al. "SOURCES 4C: A Code for Calculating (α,n), Spontaneous Fission, and Delayed Neutron Sources and Spectra," LA-UR-02-1839: Los Alamos National Laboratory. Los Alamos, NM: April 2002.

10. Caviness, M. L., and J.B. Rubin. "Authorized Contents Proposed for the Plutonium Air Transporter (PAT-1) Packaging (U)," LA-UR-08-05154. Los Alamos National Laboratory. Los Alamos, NM: August 7, 2008.

5.5.2 Summary of Source Bounding Analyses

The isotopes of concern in generating a radioactive source for Pu are Pu-236, Pu-238, Pu-239, Pu-240, Pu-241, and Pu-242. Each of these have very different behaviors with respect to neutron and photon emissions and their variation over time since purification of the Pu product (referred to as either decay time or shelf-life). The key parameters of the neutron source, photon source, and decay heat per gram of each of these isotopes are given in Figures 5-3 through 5-5.

These values indicate that the primary contributors (per unit mass) to the photon source are, in order, Pu-236, Pu-238, and Pu-241. Of these, Pu-241 is typically the most abundant isotope. The primary contributors to the neutron source are the same three isotopes. The specific decay heat values from Figure 5-5 are 18.2, 0.57, 1.9E-3, 7.1E-3, 0.10, and 1.2E-4 watts/g for Pu-236,

Pu-238, Pu-239, Pu-240, Pu-241, and Pu-242, respectively. The value for Pu-241 corresponds to the peak time-varying value and can be used per gram of both Pu-241 and Am-241.

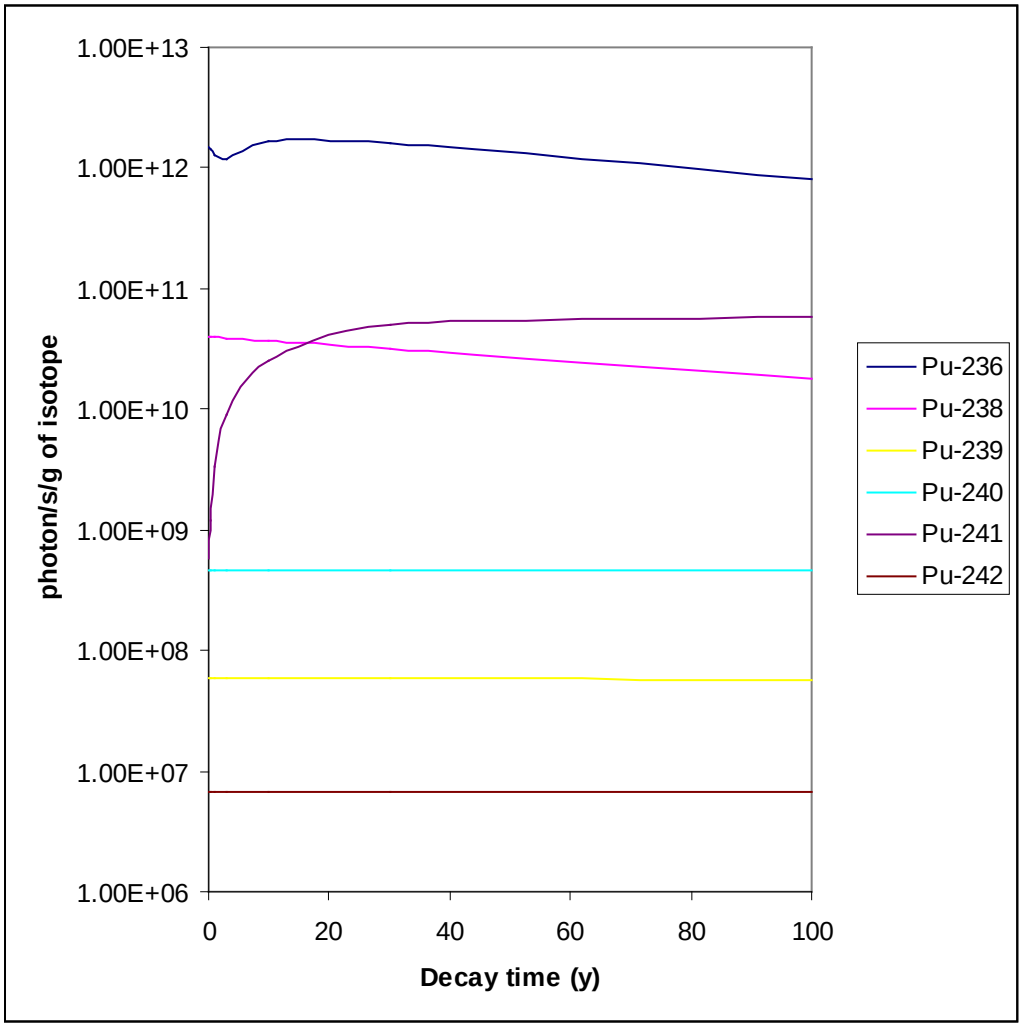

Figure 5-3. Photon Source per Gram of Each Isotope of Pu Initially Present (Note That Pu-241 Data Includes Buildup of Am-241)

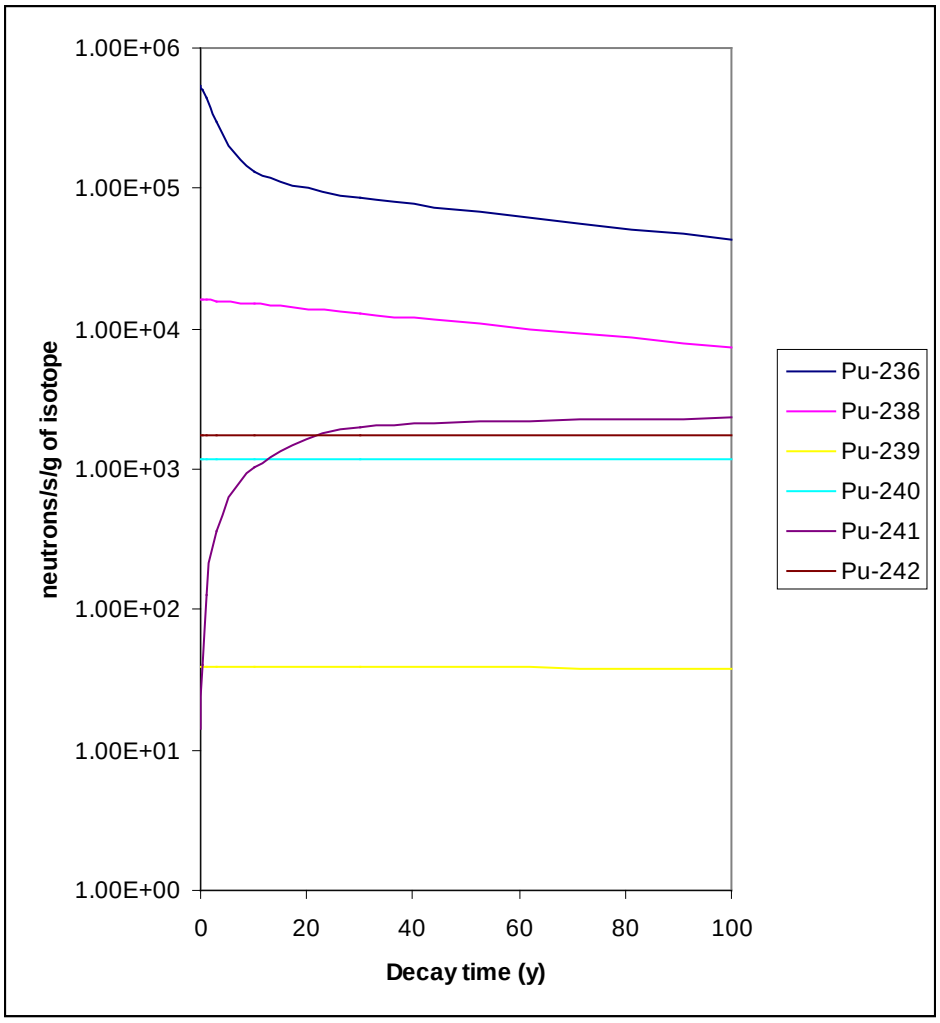

Figure 5-4. Neutron Source per Gram of Each Isotope of Pu Initially Present (Includes Both Spontaneous Fission and (α,n) Components with an Oxide Matrix; Also Note That Pu-241 Data Includes Buildup of Am-241)

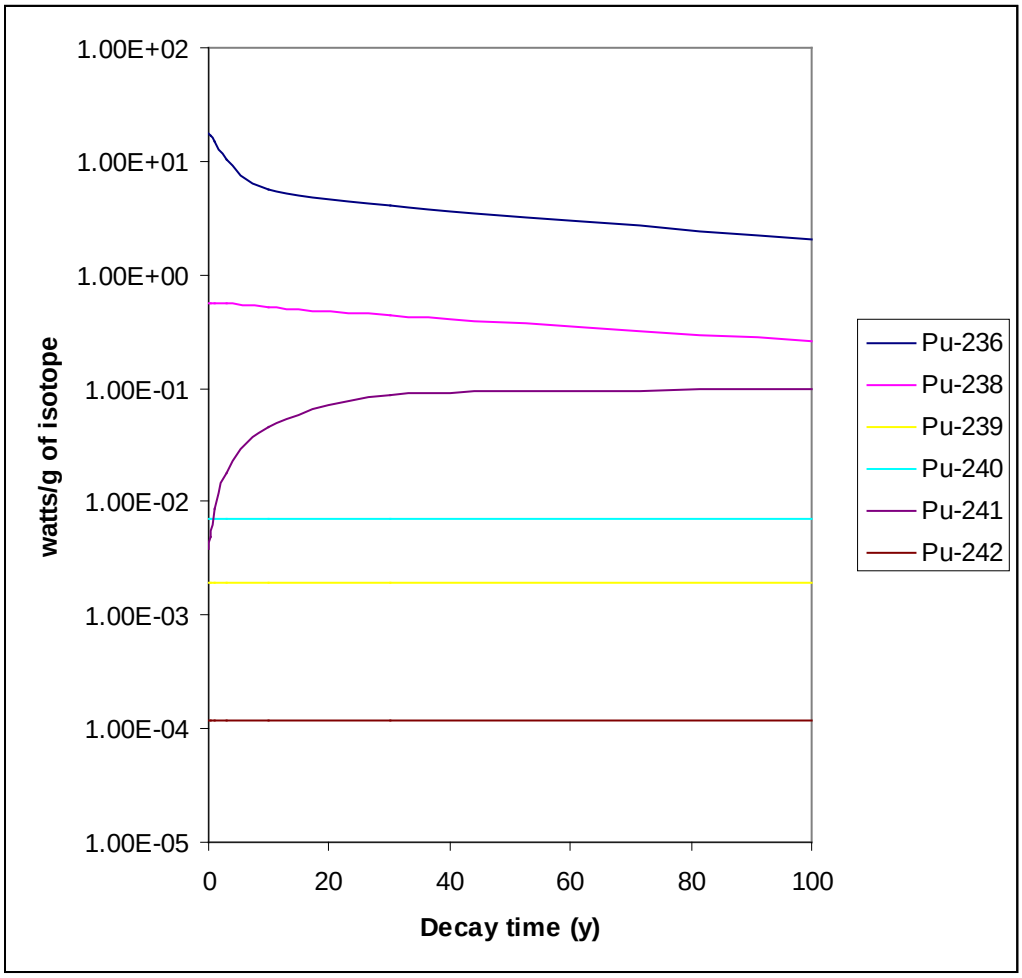

Figure 5-5. Watts per Gram of Each Isotope of Pu Initially Present (Note That Pu-241 Data Includes Buildup of Am-241)

In order to bound the Pu sources in this study, a series of seven depletion calculations were performed using the SCALE depletion code ORIGEN-ARP.[3] The ORIGEN-ARP code uses the same ORIGEN-S code used to generate the neutron, photon, and decay heat values presented in Figures 5-3 to 5-5. The ARP portion of ORIGEN-ARP takes reactor-based cross sections tabulated for each reactor system and automatically interpolates to the desired burnup and enrichment values appropriate for a given level of depletion. Three reactor systems were selected for this study: a pressurized water reactor (PWR, Westinghouse 17×17 lattice), a CANDU (Canadian design power reactor), and the Hanford N Reactor (a government reactor primarily designed for Pu production). A total of seven depletion scenarios were performed for these systems as defined in Table 5-10, corresponding to medium and high burnups for the PWR and CANDU designs and to a low, medium, and high burnup for the N reactor. The goal of these studies is to predict the full range of Pu isotopes that would result from these scenarios. The resulting Pu isotope values are given in Table 5-10 for each scenario.

Table 5-10. Pu Isotope Wt % Under Various Depletion Scenarios

Isotope	PWR (35 GWd/t)	PWR (60 GWd/t)	CANDU (5 GWd/t)	CANDU (10 GWd/t)	N_Reactor (2 GWd/t)	N_Reactor (5 GWd/t)	N_Reactor (10 GWd/t)
Pu-236	2.4E–6	1.6E–5	8.5E–8	2.5E–7	2.0E–8	1.0E–7	2.2E–7
Pu-238	0.49	3.6	0.05	0.15	0.01	0.05	0.12
Pu-239	74.9	49.3	75.4	59.5	93.6	83.9	76.7
Pu-240	15.2	23.7	20.2	30.7	5.8	12.8	17.6
Pu-241	8.4	15.2	3.7	6.9	0.6	3.0	5.0
Pu-242	1.1	8.2	0.6	2.8	0.02	0.2	0.6
Total	100	100	100	100	100	100	100

From these individual results, the following Pu isotope definition is generated that bounds all the above scenarios. The maximum weight percent from each isotope in Table 5-10 is used to define the mass fractions given in Table 5-11 (for Pu-236, the value of 1.6E-5 is divided by 100 and rounded to 2E-7). The use of this Pu isotope definition should allow any realistic Pu production scenario to be accounted for.

In order to estimate the amount of overprediction for the bounding radiation sources, the bounding neutron and gamma sources are presented in Table 5-12 along with predicted sources based on the "N_Reactor 2 GWd/t" case shown in Table 5-10. The Pu isotopic distributions from this case correspond closely with typical weapons-grade plutonium metal along with corresponding impurities.[6, 8]

5.5.3 Analysis of Pu/Be Source Contents

An alternate content of Pu/Be sources is desired for the PAT-1 package. This section separately analyzes the shielding concerns related to this content.

The radiation emitted from a Pu/Be source, both neutron source magnitude and energy spectrum, is estimated using the SOURCE4C[9] code. The source configuration used in this study is an interface source, where α particles emitted from the Pu and americium (Am) materials produce neutrons via interaction with the Be material along a common interface. The source from such a calculation is tabulated as n/s/cm^2, with the source directly proportional to the contact surface area between the two materials. For the materials expected to be shipped in this package, there is also an alpha barrier, which places another material between the Pu and Be, effectively making the neutron source much smaller. The influence of alpha barriers is conservatively ignored in these source estimates.

The neutron source used in the Pu/Be source study is given in Tables 5-13 and 5-14. The assumed Pu and Am isotopes are taken from Reference 10 and correspond to the expected material to be shipped; as a bound on the source magnitude, the Pu-241 is assumed to be completely decayed to Am-241. The neutron source spectrum is shown in Table 5-14.

The impurity content of the plutonium metal used for the Pu/Be sources is given in Reference 10; however, for this study the impurities were replaced with plutonium metal to maximize the quantity of α-producing material present in the calculations.

Table 5-11. Bounding Pu Isotope Mass Fraction Used in This Study

Isotope	Mass Fraction	Mass (g)
Pu-236	2E−7	0.00026
Pu-238	0.04	52
Pu-239	1.00	1300
Pu-240	0.40	520
Pu-241	0.15	<195[a]
Pu-242	0.10	130
Am-241	0.15 [a]	<195 [a]
Total	1.69 [b]	2197

[a] The initial Am-241 is assumed to be zero, with 195 g of Pu-241. The time-varying source is optimized such that the maximum dose is computed with respect to the decay of Pu-241 to Am-241.

b As a conservative assumption, the mass fractions are allowed to exceed unity. The package is limited to 1300 g, although the source is based on 2197 g. In addition, the heat load is limited to 25 watts, while the source is based on a heating of about 40 watts.

Table 5-12. Estimation of Degree of Overprediction in Bounding Pu Source Used in This Study

Case	Neutron Source (neutrons/s)	Gamma Source (photons/s)
Bounding source	1.950E+6	9.517E+12
Typical source[a]	3.241E+5	2.623E+11
Ratio bounding/typical	6.0	36.3

[a] Case based on 1300 g of Pu with isotopic distribution corresponding to source scenario "N_Reactor 2 GWd/t" in Table 5-12 with the following impurities: 200 ppm each of Be, Li, B, F, Al, and Si; 300 ppm of Na; 500 ppm each of C and Mg.

In order to arrive at the total neutron source to be used in these shielding studies, the per-unit-area sources given in Table 5-13 require a bounding contact surface area. The value used in this study assumes that the diameter of the TB-1 container (a radius of 5.4 cm is given in Table 5-5) provides a bounding surface area of 91 cm^2. Thus, the sources loaded into the PAT-1 package under this analysis must have total contact surface areas equal to or less than this area.

Table 5-13. Pu/Be Source Specification Used in This Study

Isotope	Mass Fraction	Atom Fraction	Neutron Source for Pure Isotope (n/s/cm^2)
Pu-238	0.0005	0.0005	65,000
Pu-239	0.9235	0.9238	171.85
Pu-240	0.0650	0.0648	637.58
Pu-241	0.0000 [a]	0.0000	5.36
Pu-242	0.0010	0.0010	8.53
Am-241	0.0100	0.0099	13,000
Total	1.0000	1.0000	363 [b]

[a] The Pu-241 is assumed to be completely decayed to Am-241 to bound the source for the typical material isotopes expected to be shipped.

[b] This neutron source value is the basis for the Pu/Be source shielding calculations in this section. The value is obtained by multiplying the mass fraction values in column 2 by the neutron source for pure isotope values in column 4 and summing over all isotopes. A source with mass fractions that differ from those in this table can be shipped if the estimated source is less than this value with allowance for decay. Typical Pu/Be source materials should fit this specification provided the Pu-238 content is 0.4 wt % or less.

The mass of Pu material loaded into the package must also be bounded: the same value used in the criticality analysis, 200 g of plutonium metal, is assumed. Using a mass of 200 g and the default full density of α-phase plutonium metal (Reference 2 gives a density of 19.84 g/cc), the dimensions of this sphere can be calculated for use in the shielding studies: a sphere of full-density, α-phase plutonium metal with a mass of 200 g will have a radius of 1.34 cm. A spherical source of this dimension with offset distances corresponding to the package surface and 1 m from the package surface was used in the shielding analyses.

As described above, the shielding model for the Pu/Be source study was a sphere with radius of 1.34 cm containing full–density, α-phase plutonium metal. The rest of the PAT-1 package is conservatively omitted from the analysis. The offset distances used for the package surface and 1-m dose values were determined from the values in Table 5-5; the minimum distance from a source to the surface detector along the cask side is specified as the difference in radii for bodies 15 and 1 (28.73 – 5.4 = 23.33 cm). Along the cask bottom, the minimum source-to-detector distance is specified as the difference in bottom locations for bodies 11 and 15 (48.84 – 20.79 = 28.05 cm). Along the cask top, the minimum source-to-detector distance is specified as the differences in the top boundaries for bodies 11 and 15 (99.43 – 48.84 – 41.87 + 20.79 = 29.51 cm). These top and bottom distances assume that the source rests on the Al spacer material, which is conservative. In addition, because the side detector locations are closer to the source than the top and bottom locations, the side locations are used for side, top, and bottom dose estimates. The 1-m dose location for side, top, and bottom locations is therefore 123.33 cm. These locations are actually minimum distances from the outer surface of the spherical source touching these named bodies, but for conservatism, the code input assumes these distances are from the source center, not the edge.

Table 5-14. Neutron Source Spectrum Used in the Pu/Be Source Shielding Analysis

Energy Group	Energy Boundaries (eV)	(α,n) Source Spectrum
1	2.000E+7	2.90211E-01
2	6.434E+6	4.11765E-01
3	3.000E+6	2.26912E-01
4	1.850E+6	1.91999E-02
5	1.400E+6	2.54550E-02
6	9.000E+5	2.39615E-02
7	4.000E+5	2.58964E-03
8	1.000E+5	8.56173E-05
9	1.700E+4	3.16844E-06
10	3.000E+3	4.29906E-08
11	5.500E+2	0.0
12	1.000E+2	0.0
13	3.000E+1	0.0
14	1.000E+1	0.0
15	3.05	0.0
16	1.77	0.0
17	1.30	0.0
18	1.13	0.0
19	1.00	0.0
20	0.80	0.0
21	0.40	0.0
22	0.33	0.0
23	0.23	0.0
24	0.10	0.0
25	0.05	0.0
26	0.03	0.0
27	0.01	0.0
	0.00001	
Total		1.000E+00

The SAS1 module of the SCALE system, version 5.1[3] was used to quantify the dose rates from a Pu/Be source using the source and geometry described above. Briefly, the SAS1 shielding model for both NCT and HAC consisted of an unshielded Pu sphere with a mass of 200 g. The NCT and HAC dose locations were specified as the minimum source-to-detector locations possible. The SAS1 code explicitly accounts for both secondary gamma radiation and subcritical source multiplication. The cross section library was the same SCALE 27N-18COUPLE library used for the other source configurations described in Section 5.4. The flux-to-dose conversion

factors were also the same used for the other source calculations, the ANSI/ANS 6.1.1-1977 standard. See Section 5.5.4 for a listing of the inputs for SAS1 and SOURCES4C.

The results for the Pu/Be source analysis are given in Table 5-15. The full-density results under conservative conditions show that the doses from the Pu/Be sources described herein are well below those of the other contents considered in Sections 5.2 through 5.4. The maximum total doses for the Pu/Be sources shown in Table 5-15 are 28, 41, and 88 times less than the limiting cases shown in Table 5-1 for NCT surface, NCT 1-m, and HAC 1-m locations respectively. The plutonium metal used in the Pu/Be sources also has a natural component of radiation; however, the Pu mass limit of 200 g for the Pu/Be sources is a factor of 6 lower in mass than the metal-only limits. The conservatisms built into this Pu/Be source analysis include the following:

1. PAT-1 packaging is ignored.

2. Both sides of a Pu/Be disk are assumed to have contact surface areas.

3. Complete decay of Pu-241 to Am-241 is assumed.

4. The minimum source-to-detector distance is used for the surface and 1-m dose locations. The center of the source is assumed to contact the innermost package boundary.

5. No α barrier is included in the calculations, although one is physically present in the sources to be shipped.

6. Comparisons of void source material to full-density sources in the shielding analysis indicate that doses for full-density material are higher due to source multiplication. Comparison of α- and δ-phase Pu also indicated that higher densities produced higher dose estimates.

7. In the shielding model, the source containing Pu was assumed to contain 100% Pu-239 to maximize the source subcritical multiplication.

It can therefore be concluded that the addition of Pu/Be sources as allowable contents of the PAT-1 package have no influence on the limiting dose results given in Table 5-1.

Table 5-15. Dose Results for Pu/Be Source Content

Case description	Detector location for top, bottom, or side geometry	Neutron dose (gamma dose) mrem/h	Total dose, doubled[a] mrem/h
Full-density, α-phase Pu	surface	0.838 (0.004)	1.68
	1 m	0.030 (0.0001)	0.06
Voided source	surface	0.680 (1e-8)	1.36
	1 m	0.024 (1e-9)	0.05

[a] Dose rates for a doubled case are given to account for the possible rearrangement of multiple Pu/Be sources such that both sides of the Pu surface come in contact with the Be material, doubling the radiation emitted. The comparison of doubled doses to regulatory limits effectively allows the summing of contact surface areas from multiple disks without regard to possible restacking. For example, while a single disk would only have a surface area corresponding to the actual contact area between the Pu and Be, two disks could properly align such that there were three contact surfaces, and three disks could properly align such that there were five contact surfaces. By applying a factor of two, only the actual contact areas for individual sources or multiple sources need to be considered.

5.5.4 List of Various Code Inputs

The ORIGEN-S computer code calculates the neutron and gamma source based on the initial loadings of each isotope as specified in Table 5-2. The code then generates the neutron and gamma spectrum in the specified SCALE 27 neutron and 18 gamma group structures for a series of decay times. The case below determines the sources at the following decay times: 0.1, 0.3, 1, 3, 10, 18, 30, 50, 75, and 100 years.

Code Listing 5-1 ORIGEN-S Input

```
'This SCALE input file was generated by
'OrigenArp Version  5.1 October 27, 2006
#origens
0$$ a11 71 e t
Decay Case
3$$ 21 1 1 27 a16 2 a33 18 e t
35$$ 0 t
54$$ a8 1 a11 0  e
56$$ a2 10 a6 1 a10 0 a13 6 a14 5 a15 3 a17 2 e
57** 0 a3 1e-05 e
95$$ 0 t
Case 1
0 MTU
60** 0.1 0.3 1 3 10 18 30 50 75 100
61** f0.05
65$$
'Gram-Atoms   Grams   Curies   Watts-All   Watts-Gamma
 3z   1   0   0   3z   3z   3z   6z
 3z   1   0   0   3z   3z   3z   6z
 3z   1   0   0   3z   3z   3z   6z
81$$ 2 0 26 1 a7 200 e
82$$ 2 2 2 2 2 2 2 2 2 2 e
83**
 1.0000000e+07 8.0000000e+06 6.5000000e+06 5.0000000e+06 4.0000000e+06
```

```
 3.0000000e+06 2.5000000e+06 2.0000000e+06 1.6600000e+06 1.3300000e+06
 1.0000000e+06 8.0000000e+05 6.0000000e+05 4.0000000e+05 3.0000000e+05
 2.0000000e+05 1.0000000e+05 5.0000000e+04 1.0000000e+04 e
84**
 2.0000000e+07 6.4340000e+06 3.0000000e+06 1.8500000e+06
 1.4000000e+06 9.0000000e+05 4.0000000e+05 1.0000000e+05 1.7000000e+04
 3.0000000e+03 5.5000000e+02 1.0000000e+02 3.0000000e+01 1.0000000e+01
 3.0499900e+00 1.7700000e+00 1.2999900e+00 1.1299900e+00 1.0000000e+00
 8.0000000e-01 4.0000000e-01 3.2500000e-01 2.2500000e-01 9.9999850e-02
 5.0000000e-02 3.0000000e-02 9.9999980e-03 1.0000000e-05 e
 73$$ 942360 942380 942390 942400 942410 942420
74** 0.00026 52 1300 520 195 130
75$$ 2 2 2 2 2 2
t
56$$ 0 0 a10  1 e t
56$$ 0 0 a10  2 e t
56$$ 0 0 a10  3 e t
56$$ 0 0 a10  4 e t
56$$ 0 0 a10  5 e t
56$$ 0 0 a10  6 e t
56$$ 0 0 a10  7 e t
56$$ 0 0 a10  8 e t
56$$ 0 0 a10  9 e t
56$$ 0 0 a10  10 e t
56$$ f0 t
end
=opus
LIBUNIT=21
TYPARAMS=NUCLIDES
UNITS=WATTS
LIBTYPE=ALL
TIME=YEARS
NPOSITION=1 2 3 4 5 6 7 8 9 10 end
End
=shell
[command to copy file ft71f001 to a local directory]
end
```

The Shielding Analysis Sequence #4 (SAS4) code reads the shielding problem definitions from a single input stream, then proceeds to automatically execute the BONAMI, NITAWL, XSDRNPM, and MORSE-SCG computer codes in sequence. The SCALE driver software reads the single input stream and prepares individual inputs for each of the above codes, automatically executes each code, and then collects all output into a common output file. The source file written by the ORIGEN-S code with the input stream shown in Code Listing 5-1 is copied into the ft30f001 file just prior to execution as described in the first `=shell` input shown in Code Listing 5-2.

The input options for SAS4 were carefully chosen to ensure accurate dose estimates. The radial calculations along the package side utilize the IDR=0 option with full automated biasing as well as point detectors because the code is fully applicable under these conditions. The axial calculations for the package top and bottom used the IDR=2 option and effectively turned off the automated biasing (note all void materials in the one-dimensional adjoint model). The axial biasing produces inaccurate results for a nonsymmetric axial model because the SAS4 code is designed to bias particles in opposite directions above and below the model axial centerline. The effective removal of the automated biasing allows the underlying MORSE-SCG code to run

without the axial symmetry requirement. The accuracy of these results was tested by comparison to another SCALE module under development that removes these limitations.

Code Listing 5-2 SAS4 Input Stream for NCT Reduced-Density Smeared Cylinder Source (radial side gamma)

```
=shell
[copy ORIGEN-S ft71f001 output file previously saved to file named ft30f001]
end
'Input generated by Espn 5.1 Compiled on 8-07-2006
=sas4     parm=size=1000000
pat-1 pu large cyl 3d case
27n-18couple  infhommedium
 pu 1 den=0.818 1 300 end
 redwood 3 den=0.36 1 300 end
 aluminum 4 den=2.6989 1 300 end
 ss304 5 den=7.9 1 300 end
 copper 6 den=8.94 1 300 end
 mgconcrete 7 1 300 end
 arbmph13-8mo 7.5 5 0 0 0 24000 12.75 28000 8 13000 1.125 42000 2.25
 26000 75.875 2 1 300 end
end comp
 izm=6 mhw=2 frd=5.4  end
 5.4 6.8 13.97 15.24 28.58 28.73   end
 1 2 0 4 3 5   end
xend
 ran=000003600621 tim=1200 nst=4000 nmt=12000 nit=900 nco=4 ist=0 ipr=0
 iso=0 nod=16 sfa=9.517e+12 igo=4 inb=0 ine=0 mfu=2 isp=6 ipf=0 isd=4
 nda=1000  end
 det 30 0 0 30 0 2 30 0 4 30 0 6 30 0 8 30 0 10 30 0 15 30 0 20
    128.7 0 0 128.7 0 5 128.7 0 10 128.7 0 15 128.7 0 20 128.7 0 25 128.7 0 30
    128.7 0 35 end
 sxy 1 -5.4 5.4 -5.4 5.4 0 10 100 100 100 100   end
gend
shielding problem
 0 0 0 0
 rcc 0 0 -5.64 0 0 15.11 5.40
 sph 0 0 -3.74 5.72
 rcc 0 0 -5.64 0 0 16.71 6.795
 sph 0 0 -3.74 7.12
 rcc 0 0 -5.64 0 0 16.71 10
 rcc 0 0 -10.86 0 0 21.93 6.875
 rcc 0 0 -18.25 0 0  7.39 6.875
 rcc 0 0 -18.25 0 0 20.32 7.52
 rcc 0 0 2.07 0 0 9 8.74
 rcc 0 0 -18.25 0 0 36.79 13.97
 rcc 0 0 -20.79 0 0 41.87 13.97
 rcc 0 0 -30.35 0 0 60.81 13.97
 rcc 0 0 -30.35 0 0 60.81 15.24
 rcc 0 0 -48.69 0 0 99.13 28.58
 rcc 0 0 -48.84 0 0 99.43 28.73
 sph 0 0 0 300
 rcc 0 0 -2.936 0 0 5.872 4.032
 rcc 0 0 -2.936 0 0 5.872 4.445
  end
 src +1
 src +2 -3
 tb1 +3 -1
 tb1 +4 -2 -5
 vod +6 -5 -4 or 6 5 8 -3
 wod +7 -6
```

```
 cop +8 -7 -6
 vod +9 -3
 wod +10 -9 -8
 alu +11 -10
 wod +12 -11
 alu +13 -12
 wod +14 -13
 drm +15 -14
 vod +16 -15
 exv -16
  end
 1 1 1 1 1 1 1 1 1 1 1 1 1 1 1
 0 0 0 0 0 0 0 0 0 0 0 0 0 0 0
 1 1 2 2 1000 1000 6 1000 1000 4 3 4 3 5 1000 0
 0

End
```

Code Listing 5-3 SAS4 Input Stream for NCT Reduced-Density Smeared Cylinder Source (radial side neutron)

```
=shell
[copy ORIGEN-S ft71f001 output file previously saved to file named ft30f001]
end
'Input generated by Espn 5.1 Compiled on 8-07-2006
=sas4     parm=size=1000000
pat-1 pu large cyl 3d case
27n-18couple  infhommedium
 pu 1 den=0.818 1 300 end
 redwood 3 den=0.36 1 300 end
 aluminum 4 den=2.6989 1 300 end
 ss304 5 den=7.9 1 300 end
 copper 6 den=8.94 1 300 end
 mgconcrete 7 1 300 end
 arbmph13-8mo 7.5 5 0 0 0 24000 12.75 28000 8 13000 1.125 42000 2.25
 26000 75.875 2 1 300 end
end comp
ity=1 irf=9029 izm=6 mhw=2 frd=5.4  end
 5.4 6.8 13.97 15.24 28.58 28.73   end
 1 2 0 4 3 5   end
xend
 ran=000003600621 tim=1200 nst=4000 nmt=12000 nit=200 nco=4 ist=0 ipr=0
 iso=0 nod=16 sfa=1.95e+6 igo=4 inb=0 ine=0 mfu=2 isp=7 ipf=0 isd=4
 nda=1000  end
 det 30 0 0 30 0 2 30 0 4 30 0 6 30 0 8 30 0 10 30 0 15 30 0 20
    128.7 0 0 128.7 0 5 128.7 0 10 128.7 0 15 128.7 0 20 128.7 0 25 128.7 0 30
    128.7 0 35 end
 sxy 1 -5.4 5.4 -5.4 5.4 0 10 100 100 100 100   end
gend
shielding problem
 0 0 0 0
 rcc 0 0 -5.64 0 0 15.11 5.40
 sph 0 0 -3.74 5.72
 rcc 0 0 -5.64 0 0 16.71 6.795
 sph 0 0 -3.74 7.12
 rcc 0 0 -5.64 0 0 16.71 10
 rcc 0 0 -10.86 0 0 21.93 6.875
 rcc 0 0 -18.25 0 0  7.39 6.875
 rcc 0 0 -18.25 0 0 20.32 7.52
 rcc 0 0 2.07 0 0 9 8.74
 rcc 0 0 -18.25 0 0 36.79 13.97
 rcc 0 0 -20.79 0 0 41.87 13.97
```

```
 rcc 0 0 -30.35 0 0 60.81 13.97
 rcc 0 0 -30.35 0 0 60.81 15.24
 rcc 0 0 -48.69 0 0 99.13 28.58
 rcc 0 0 -48.84 0 0 99.43 28.73
 sph 0 0 0 300
 rcc 0 0 -2.936 0 0 5.872 4.032
 rcc 0 0 -2.936 0 0 5.872 4.445
  end
 src +1
 src +2 -3
 tb1 +3 -1
 tb1 +4 -2 -5
 vod +6 -5 -4 or 6 5 8 -3
 wod +7 -6
 cop +8 -7 -6
 vod +9 -3
 wod +10 -9 -8
 alu +11 -10
 wod +12 -11
 alu +13 -12
 wod +14 -13
 drm +15 -14
 vod +16 -15
 exv -16
  end
 1 1 1 1 1 1 1 1 1 1 1 1 1 1 1
 0 0 0 0 0 0 0 0 0 0 0 0 0 0 0
 1 1 2 2 1000 1000 6 1000 1000 4 3 4 3 5 1000 0
 0

End
```

Code Listing 5-4 SAS4 Input Stream for NCT Reduced-Density Smeared Cylinder Source (axial top neutron)

```
=shell
[copy ORIGEN-S ft71f001 output file previously saved to file named ft30f001]
end
'Input generated by Espn 5.1 Compiled on 8-07-2006
=sas4     parm=size=1000000
pat-1 pu large cyl top 3d case
27n-18couple  infhommedium
 pu 1 den=0.818 1 300 end
 redwood 3 den=0.36 1 300 end
 aluminum 4 den=2.6989 1 300 end
 ss304 5 den=7.9 1 300 end
 copper 6 den=8.94 1 300 end
 mgconcrete 7 1 300 end
 arbmph13-8mo 7.5 5 0 0 0 24000 12.75 28000 8 13000 1.125 42000 2.25
 26000 75.875 2 1 300 end
end comp
idr=2 ity=1 irf=9029 izm=6 mhw=2 frd=5.4  end
 9.46 11.06 18.54 21.08 50.44 50.59   end
 0 0 0 0 0 0   end
xend
 ran=000003600621 tim=1200 nst=4000 nmt=12000 nit=1000 nco=4 ist=0 ipr=0
 iso=0 nod=7 sfa=1.95e+6 igo=4 inb=0 ine=0 mfu=2 isp=7 ipf=0 isd=4
 nda=1000  end
 det 0 0 52 2 0 52 4 0 52 6 0 52
     0 0 150.59 5 0 150.59 10 0 150.59 end
 sxy 1 -5.4 5.4 -5.4 5.4 0 10 100 100 100 100   end
gend
```

```
shielding problem
 0 0 0 0
 rcc 0 0 -5.64 0 0 15.11 5.40
 sph 0 0 -3.74 5.72
 rcc 0 0 -5.64 0 0 16.71 6.795
 sph 0 0 -3.74 7.12
 rcc 0 0 -5.64 0 0 16.71 10
 rcc 0 0 -10.86 0 0 21.93 6.875
 rcc 0 0 -18.25 0 0  7.39 6.875
 rcc 0 0 -18.25 0 0 20.32 7.52
 rcc 0 0 2.07 0 0 9 8.74
 rcc 0 0 -18.25 0 0 36.79 13.97
 rcc 0 0 -20.79 0 0 41.87 13.97
 rcc 0 0 -30.35 0 0 60.81 13.97
 rcc 0 0 -30.35 0 0 60.81 15.24
 rcc 0 0 -48.69 0 0 99.13 28.58
 rcc 0 0 -48.84 0 0 99.43 28.73
 sph 0 0 0 300
 rcc 0 0 -2.936 0 0 5.872 4.032
 rcc 0 0 -2.936 0 0 5.872 4.445
  end
 src +1
 src +2 -3
 tb1 +3 -1
 tb1 +4 -2 -5
 vod +6 -5 -4 or 6 5 8 -3
 wod +7 -6
 cop +8 -7 -6
 vod +9 -3
 wod +10 -9 -8
 alu +11 -10
 wod +12 -11
 alu +13 -12
 wod +14 -13
 drm +15 -14
 vod +16 -15
 exv -16
  end
 1 1 1 1 1 1 1 1 1 1 1 1 1 1 1
 0 0 0 0 0 0 0 0 0 0 0 0 0 0 0
 1 1 2 2 1000 1000 6 1000 1000 4 3 4 3 5 1000 0
 0

end
```

Code Listing 5-5 SAS4 Input Stream for HAC Reduced-Density Smeared Cylinder Source (radial gamma)

```
=shell
[copy ORIGEN-S ft71f001 output file previously saved to file named ft30f001]
end
'Input generated by Espn 5.1 Compiled on 8-07-2006
=sas4     parm=size=1000000
pat-1 pu large cyl 3d case
27n-18couple  infhommedium
 pu 1 den=0.818 1 300 end
 redwood 3 den=0.36 1 300 end
 aluminum 4 den=2.6989 1 300 end
 ss304 5 den=7.9 1 300 end
 copper 6 den=8.94 1 300 end
 mgconcrete 7 1 300 end
 arbmph13-8mo 7.5 5 0 0 0 24000 12.75 28000 8 13000 1.125 42000 2.25
```

```
 26000 75.875 2 1 300 end
end comp
 izm=6 mhw=2 frd=5.4  end
 5.4 6.8 13.97 15.24 28.58 28.73   end
 1 2 0 0 0 0   end
xend
 ran=000003600621 tim=1200 nst=4000 nmt=12000 nit=900 nco=4 ist=0 ipr=0
 iso=0 nod=10 sfa=9.517e+12 igo=4 inb=0 ine=0 mfu=2 isp=6 ipf=0 isd=4
 nda=1000  end
 det 106.8 0 0 106.8 0 5 106.8 0 10 106.8 0 15 106.8 0 20 106.8 0 25 106.8 0 30
    106.8 0 35  0 0 -110.98  0 0 111.06 end
 sxy 1 -5.4 5.4 -5.4 5.4 0 10 100 100 100 100   end
gend
shielding problem
 0 0 0 0
 rcc 0 0 -5.64 0 0 15.11 5.40
 sph 0 0 -3.74 5.72
 rcc 0 0 -5.64 0 0 16.71 6.795
 sph 0 0 -3.74 7.12
 rcc 0 0 -5.64 0 0 16.71 10
 rcc 0 0 -10.86 0 0 21.93 6.875
 rcc 0 0 -18.25 0 0  7.39 6.875
 rcc 0 0 -18.25 0 0 20.32 7.52
 rcc 0 0 2.07 0 0 9 8.74
 rcc 0 0 -18.25 0 0 36.79 13.97
 rcc 0 0 -20.79 0 0 41.87 13.97
 rcc 0 0 -30.35 0 0 60.81 13.97
 rcc 0 0 -30.35 0 0 60.81 15.24
 rcc 0 0 -48.69 0 0 99.13 28.58
 rcc 0 0 -48.84 0 0 99.43 28.73
 sph 0 0 0 300
 rcc 0 0 -2.936 0 0 5.872 4.032
 rcc 0 0 -2.936 0 0 5.872 4.445
  end
 src +1
 src +2 -3
 tb1 +3 -1
 tb1 +4 -2 -5
 vod +6 -5 -4 or 6 5 8 -3
 wod +7 -6
 cop +8 -7 -6
 vod +9 -3
 wod +10 -9 -8
 alu +11 -10
 wod +12 -11
 alu +13 -12
 wod +14 -13
 drm +15 -14
 vod +16 -15
 exv -16
  end
 1 1 1 1 1 1 1 1 1 1 1 1 1 1 1
 0 0 0 0 0 0 0 0 0 0 0 0 0 0 0
 1 1 2 2 1000 1000 1000 1000 1000 1000 1000 1000 1000 1000 1000 0
 0

end
```

The Shielding Analysis Sequence #1 (SAS1) code reads the shielding problem definitions from a single input stream, then proceeds to automatically execute the BONAMI, NITAWL, XSDRNPM, and XSDOSE computer codes in sequence. The SCALE driver software reads the single input stream and prepares individual inputs for each of the above codes, automatically

executes each code, and then collects all output into a common output file. The (α,n) source description written by the SOURCES4C code with the input stream shown in Code Listing 5-6 is entered by hand into the SAS1 input stream.

Code Listing 5-6 SAS1 Input Stream for Pu/Be spherical source with full density alpha-Pu metal

```
=sas1   parm=nitawl
pube neutron source alpha phase - no void
27n-18couple  infhommedium
plutoniumalp 1 1.0 293 end
end comp
end
last
neutron case
spherical
1 1.34 1 -1 0 0 3304 0
end zone
2.90211e-1 4.11765e-1 2.26912e-1 1.91999e-2 2.54550e-2
2.39615e-2 2.58964e-3 8.56173e-5 3.16844e-6 4.29906e-8
17z  18z
ndetec=2
read xsdose
23.33 123.33
end
```

The SOURCES4C code is designed to predict the (α,n) source generation for homogenous and interface problems. This analysis uses the interface option to determine the (α ,n) source per unit area of contact between the α generator and a target nucleus. In this case, the α generator is plutonium metal and the target material is Be. The code can output the neutron source in any group structure; in this case, the 27-group structure used in SCALE is specified and the source spectrum from SOURCES4C is used directly in the SAS1 case shown above.

Code Listing 5-7 SOURCES4C Input Stream for Pu-Be Interface Source Problem

```
WPu-Be Interface Problem
2 2 1
2 0 6.50 0.0000001
  94 0.99
  95 0.01
100
5
  942380 0.0005
  942390 0.9238
  942400 0.0648
  942420 0.0010
  952410 0.0099
target is composed of Be
1 0
  4 1.0
-27 20.0 1e-11
20 6.43 3 1.85 1.4 0.9 0.4 0.1 0.017 0.003 0.00055
1e-4 3e-5 1e-5 3.05e-6 1.77e-6 1.3e-6 1.13e-6 1e-6
8e-7 4e-7 3.25e-7 2.25e-7 1e-7 5e-8 3e-8 1e-8
1 4000
  40090 1.0
```

This page intentionally left blank

6. CRITICALITY EVALUATION

This section describes the criticality evaluation for incorporating plutonium (Pu) metal as a new payload for the PAT-1 package. The Pu metal is packed in an inner container (*T-Ampoule Assembly,*[*] Drawing 2A0261, designated the T-Ampoule) that replaces the PC-1 inner container. The T-Ampoule and associated Pu metal content packing configurations are described in Section 1.2.1 and Section 1.2.2 of this addendum, respectively.

This section was written to meet the applicable requirements of 10 CFR Part 71, "*Packaging and Transportation of Radioactive Material*," and to be consistent with the guidance provided in U.S. Nuclear Regulatory Commission, Office of Nuclear Regulatory Research, Regulatory Guide 7.9, Rev. 2, "*Standard Format and Content of Part 71 Applications for Approval of Packages for Radioactive Material*," dated March 2005. The section also considers the recommendations provided in NUREG/CR-5661, ORNL/TM-11936, "*Recommendations for Preparing the Criticality Safety Evaluation of Transportation Packages*," U.S. Nuclear Regulatory Commission, Oak Ridge National Laboratory, March 1997.[1]

6.1 Description of Criticality Design

6.1.1 Design Features

The primary feature important for criticality control is the ability of the TB-1 containment vessel to retain the fissile material under normal and hypothetical accident conditions (HAC). Retention of the fissile material within the approximately 1.5–liter (0.4 gallon) inner volume of the TB-1 limits the quantity of water available for neutron moderation. As discussed in Sections 4.2 and 4.3 of this addendum, containment integrity is maintained for both normal conditions of transport and under hypothetical accident conditions. No credit is taken in the criticality safety analysis for containment integrity of material packages designed to be transported by air.

Credit is taken for some spacing provided by the package in the criticality safety analysis of package arrays for normal conditions of transport and under hypothetical accident conditions. No criticality control credit is taken for the packaging inside the TB-1. Such packaging may include sample holders and containers, structural supports, tantalum foil, plastic bagging, etc. Instead, the criticality analysis for all normal and hypothetical accident conditions considered optimum water moderation to the extent achievable within the TB-1 containment vessel. This approach eliminates the need for controls limiting the quantity of hydrogenous packaging materials (e.g., plastic bagging) that may be used within the TB-1 containment vessel.

The optimum H/Pu ratio cannot be achieved within the TB-1 unless plutonium (Pu) quantities are less than 1300 g (2.87 lb) . Note that a plutonium quantity of 1300 g represents a conservative upper bound for analysis and is greater than the payload quantities shown in Table 1-1 of Section 1.2.2.1 of this addendum. Results presented later in this section show that removing Pu and adding water results in significantly lower k_{eff} values.

[*] Note: The drawing titles are in italics and are used interchangeably with the designated names in this addendum. See Section 1.3.2 in this addendum and Chapter 9 in the SAR[2] for drawing number, title, and revision.

6.1.2 Summary Table of Criticality Evaluation

Table 6-1 is a summary table of the criticality evaluation.

Table 6-1. Summary Table of Criticality Evaluation Results

Case	Number of Packages	Internal Moderation[a]	Array size	$k_{eff} \pm \sigma$[b]	Bias[c] (Δk)	Upper Subcritical Limit[d]
cv001	1	0	1[e]	0.6565 ± 0.0005	0	0.8893
cv031	1	0.956	1[e]	0.7076 ± 0.0006	0	0.9383
fhlsf001	2646	0	19 × 15.5 × 9[f]	0.6509 ± 0.0005	0	0.8893
fslsf031	2601	0.956	17 × 17 × 9[g]	0.6337 ± 0.0005	0	0.9396
hexsdry	1152	0.956	18 × 10.7 × 6[h]	0.7027 ± 0.0007	0	0.9351
hexs100	1152	0.956	18 × 10.7 × 6[h]	0.7154 ± 0.0005	0	0.9396
sph14	1	0.956	1[i]	0.7147 ± 0.0005	0	0.9383

[a] Internal moderation is the specific gravity of the water mixed with the Pu-239.
[b] KENO V.a calculated k_{eff} and one standard deviation values.
[c] As noted in Section 6.8.2.7, the average k_{eff} value for each validation set was greater than 1.0, resulting in positive biases, which were discarded (i.e., no credit taken for positive bias).
[d] From Section 6.8.2.7, Table 6-7.
[e] Normal conditions, single package, see Section 6.3.4.1.
[f] Normal conditions, close-packed hexagonal-pitched array, see Section 6.3.4.2 and Figure 6-10.
[g] Normal conditions, close-packed square-pitched array, see Section 6.3.4.2.
[h] HAC, close-packed hexagonal-pitched array. See Section 6.3.4.3 and Figure 6-12.
[i] Expanded HAC, single package for air transport. See Section 6.3.4.4.

6.1.3 Criticality Safety Index

From preliminary scoping calculations, it was concluded that an infinite array of damaged packages, as described in Section 6.3.1.3, would not be subcritical under optimum moderation conditions. Consequently, a criticality safety index (CSI) value of zero is unattainable. Per 10 CFR 71.59(b), the smallest allowed CSI above zero is 0.1. Assignment of a 0.1 CSI requires an N value of 500, and that 2500 (= 5 × N) undamaged packages, with nothing between the packages, be subcritical and that 1000 (= 2 × N) damaged packages would be subcritical with optimum interspersed hydrogenous moderation.

The CSI for the package was calculated as prescribed by 10 CFR 71.59. The evaluation in Section 6.5 shows that an array of more than 2500 undamaged packages, with nothing between the packages, is subcritical. Thus the value of "N" identified in 10 CFR 71.59 is 500, calculated as 2500 divided by 5. The evaluation in Section 6.6 shows that an array of greater than 2 times N (or 1000) damaged packages would be subcritical with optimum interspersed hydrogenous moderation. As per 10 CFR 71.59, the CSI value is 0.1, which is calculated as 50 divided by N (N=500).

6.2 Fissile Material Contents

6.2.1 Plutonium Metal – General Form

The fissile material loaded into the package will include up to 1300 g (2.87 lb) of plutonium metal. There are no criticality controls on the form or number of pieces of plutonium metal.

There are no criticality controls on the isotopic composition of the Pu. It is assumed, however, that the Pu-240 content exceeds the Pu-241 content. With this assumption, the fissile material is conservatively modeled as 100% Pu-239. The justification for this assumption is that the presence of Pu-241 content greater than Pu-240 content would require expensive isotopic enrichment, generating only milligrams of Pu enriched in Pu-241. The vast majority of Pu present in the world today meets this isotopic composition assumption. Note that of the Pu nuclides that may be present, Pu-241 has the shortest half-life (14.4 years). It then decays to americium (Am-)241, which is included in the Pu mass. Counting the Am-241 as Pu-239 is conservative because it is a parasitic neutron absorber in well moderated systems and, in unmoderated systems, requiring a larger mass (~ 34 kg [75 lb] Am-241) than Pu-239 (~ 5 kg [11 lb] Pu-239) to achieve criticality.

The Pu may be alloyed with other non-neutron-multiplying metals and may also contain trace impurities, typically small fractions of a percent, both of which are conservatively omitted for the criticality analysis. It is conservative to ignore these impurities, which are frequently parasitic neutron absorbers, because modeling them would either have no effect or would reduce k_{eff} (resulting from neutron absorption and scattering). Modeling the presence of alloyed metals and impurities would decrease the density of the fissile material and thus, decrease the volume available for water inside the TB-1 containment vessel. Replacing water with nonfissile alloys or impurities results in lower k_{eff} values for the limiting cases.

There are no criticality controls for the fissile material dimensions other than that it must fit within the TB-1 containment vessel.

There are no criticality controls for the fissile material density. Consequently, the plutonium metal may have a density up to the maximum theoretical density for alpha phase plutonium metal, which is 19.84 g [0.044 lb] Pu/cm^3 The criticality analysis considers the full range of Pu density.

While it is anticipated that the Pu will have very low moisture content, no criticality control for the Pu moisture content is required, because it is considered in the criticality analysis that the containment vessel may be fully flooded with water and the Pu may be mixed with and surrounded by water for all normal conditions of transport and hypothetical accident conditions. The water in the TB-1 vessel is included as a bounding model for packaging that may be in the TB-1.

For use of the general-forms Pu loading limit (1300 g [2.87 lb] Pu maximum), presence of neutron-multiplying materials (e.g., beryllium (Be), normal or depleted uranium) within the TB-1 vessel is not permitted.

6.2.2 Plutonium Metal – Pu/Be Sources

Loading of the TB-1 vessel may include Pu/Be sources, subject to the following limits/restrictions:

- The maximum mass of Pu metal or alloy present is 200 g (0.44 lb), as one or more pieces/parts with no restriction on shape or density. The primary Pu isotope present is Pu-239 and the Pu-240 content must exceed the Pu-241 content.

- The maximum mass of beryllium present is 30 g (0.066 lb) and (except for the Pu) no other neutron multiplying materials (e.g., normal or depleted uranium) are permitted within the TB-1 vessel.

As for the general-form Pu contents, the Nuclear Criticality Safety (NCS) evaluation for the Pu/Be sources assumes that the TB-1 containment vessel contents may include water (up to full flooding) for all normal conditions of transport and hypothetical accident conditions. Thus, the NCS evaluation for Pu/Be source contents assumes a model which bounds packaging material that may be present as part of the Pu/Be source loading. Note that the quantity of Pu/Be evaluated in this section is an upper bound for analysis and is less than that specified in Table 1-1 of Section 1.2.2.1 of this addendum.

6.3 General Considerations

6.3.1 Model Configuration

Of the two permitted loadings for the PAT-1 package (Pu metal in general form or Pu/Be sources), the general-form 1300 g (2.87 lb) Pu metal limit is the limiting case for NCS evaluation purposes. For Pu/Be source loadings, both the Pu and Be are restricted to much smaller mass limits (200 g [0.44 lb] Pu alloy, 30 g [0.066 lb] Be). If the Be is replaced with Pu metal on either a mass or volume basis (for NCS modeling purposes), the resulting NCS models contain far less than the 1300 g (2.87 lb) Pu general-form metal loading limit. Thus, this and subsequent Section 6 sections evaluate the PAT-1 package with 1300 g (2.87 lb) Pu metal as the most reactive, most limiting case for NCS purposes. Section 6.9.6 provides additional justification that the Pu/Be source loading is bounded by considerations for the 1300 g (2.87 lb) general-form Pu metal loading.

Several computational models were used in the criticality analysis. The package models include a detailed model constructed using nominal dimensions, five variations of a simplified model, and two post-testing simplified models used for analysis of HAC. In the base simplified model (Model 1), the steel outer container, redwood, and steel TB-1 containment vessel are modeled. Variations on the base simplified model include:

- Models in which the redwood density was varied ±20% of the nominal redwood density;

- A model in which the redwood is replaced with full density water; and

- A model in which the outer container steel, redwood, and TB-1 steel are all replaced with water.

A detailed model was used to confirm that the simplified models in which the redwood is replaced with water are conservative representations of the PAT-1 package. These models are discussed in Sections 6.3.1.1 and 6.3.1.2. The post-testing simplified models used to analyze damaged package arrays from a hypothetical accident condition are discussed in Section 6.3.1.3.

Except for a few sensitivity calculations, in which water inside the TB-1 but outside a plutonium metal sphere was removed to quantify the reactivity worth of that water, all calculations were performed with the maximum quantity of water that could fit in the TB-1, given the quantity of Pu also present. The maximum quantity of water was included to provide a conservative model for the packaging, some of which may be hydrogenous, within the TB-1. Comparison of cases *sudma* and *sudmb* show that, for this particular model, removing the water in the TB-1 reduced k_{eff} by nearly 10% Δk. The calculations generated to support the criticality analysis show that, due to the limited TB-1 internal volume, the Pu is under moderated in all cases. Other than case *sudma*, all cases included the maximum quantity of water that could fit within the TB-1, given the quantity of plutonium present. Section 6.9.4 includes a list of the cases, excluding the Pu/Be scoping calculations described in Section 6.9.6, used to support the criticality analysis.

6.3.1.1 Detailed Model

A detailed package model was generated using the nominal dimensions and material descriptions provided in the reference drawings.[4–30] Figure 6-1 shows a cutaway view of the detailed model. The load spreader assembly[19] includes a cadmium-plated copper cylinder. The cadmium plating is not modeled. Omitting the cadmium is conservative because it is a strong thermal neutron absorber. Several minor simplifications were made, such as omitting glue, bolts, and other fasteners used to assemble the package.

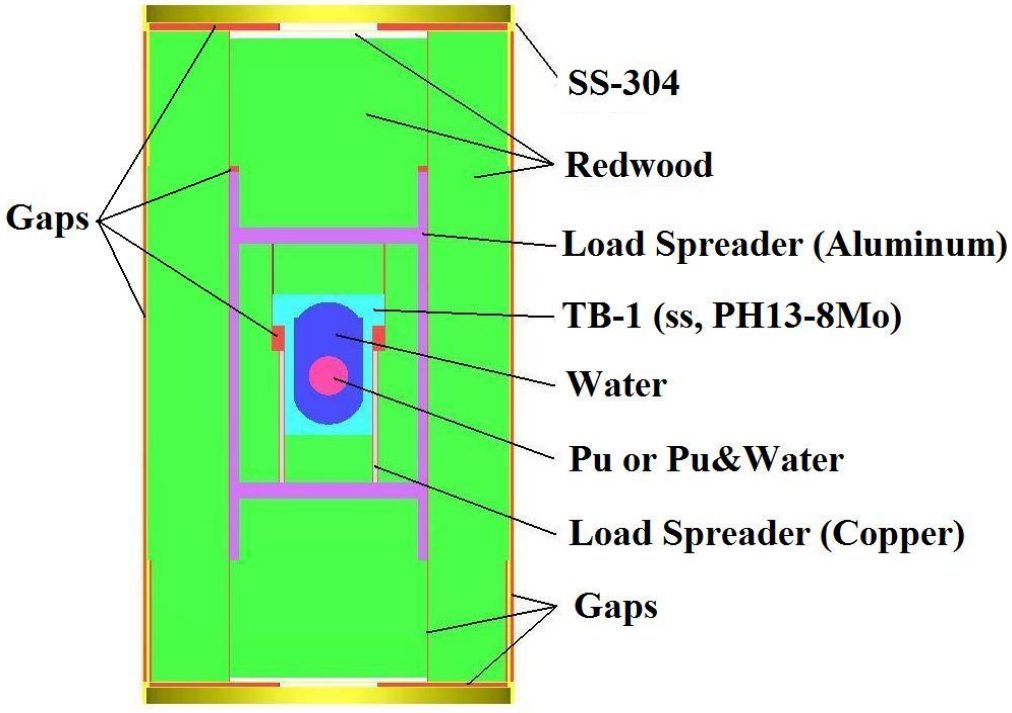

Figure 6-1. Detailed Model of a Single Package

This detailed model was prepared to confirm that the simplified models, which were used to perform most of the parametric studies, are adequately conservative.

6.3.1.2 Simplified Models

The criticality analysis of the single-package normal conditions of transport, single-package hypothetical accident conditions, and normal conditions of transport arrays is based primarily on simplified model calculations. The simplified models were developed using dimensions and materials described in References 4 through 30, and are shown in Figure 6-2. The simplified models were developed as follows:

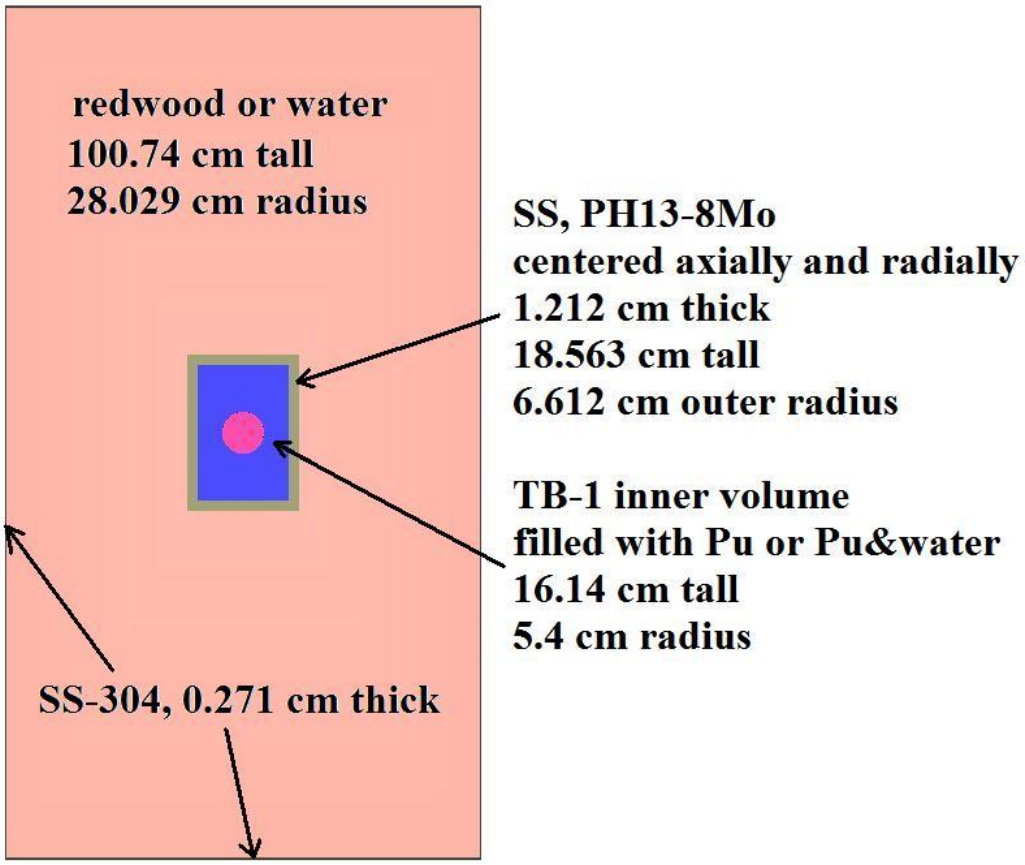

Figure 6-2. Simplified Model of a Single Package

The maximum volume inside the TB-1 containment vessel was calculated to be 1478cm^3 (90.22 in^3). Using the maximum internal volume maximizes the quantity of water that may be present in the fissile material to moderate neutrons. The calculation of this volume is described in Section 45. Use of other containers and supporting structures within the TB-1 are anticipated. If modeled, these other materials would reduce the quantity of water that could be present within the TB-1. As shown in the calculation results and plots presented throughout this section, maximizing the quantity of water mixed with the plutonium within the TB-1 results in a maximum k_{eff} value. The inner volume of the TB-1 was modeled as a cylinder with a radius of 5.400 cm (2.126 in.) and a height of 16.14 cm (6.354 in.). The radius is equivalent to the maximum internal radius for the TB-1, and the height is set so that the maximum internal volume is 1478 cm^3 (90.22 in^3).

The fissile material inside the TB-1 containment vessel is modeled as various mixtures of Pu-239 metal and water. At a density of 19.84 g/cm^3 (0.717 lb/in^3), the 1300 g (2.87 lb) of Pu-239 fills 65.52 cm^3 (3.99 in^3) of the interior volume, leaving 1412 cm^3 (86.16 in^3) of TB-1 internal volume that is modeled as filled with water. The criticality analysis considers various arrangements of the plutonium metal/water mixture surrounded by any unused water. Any of the 1412 cm^3 (86.16 in^3) of water not used in the plutonium metal/water mixture fills the remainder of the TB-1 interior.

The TB-1 containment vessel was modeled as a simple cylinder around the volume described in Figure 6-2. The wall thickness used for the top, bottom, and side was 1.212 cm (0.477 in.). This dimension is the minimum steel thickness identified from the reference drawings and is the minimum distance through the center of the TB-1 lid.

The PAT-1 package includes an internal structure referred to as the load spreader assembly. These components are constructed of aluminum and cadmium-plated copper. In the simplified models, these components and the small gaps between components are replaced with redwood or water, depending on the analysis. See Figure 6-1.

The TB-1 is modeled as surrounded by redwood or water to the minimum outer dimensions of the redwood specified by the reference drawings. The minimum dimensions were used to minimize the center-to-center spacing between drums in array calculations. The TB-1 is surrounded by a cylinder of redwood or water with a radius of 28.029 cm (11.04 in.) and a height of 100.7 cm (39.66 in.).

A review of Reference Drawings[4–30] reveals that the outer steel package is composed of two or more layers of 16-gauge, Type 304 stainless steel. The nominal and minimum thicknesses for 16 gauge steel are 0.15189 cm (0.598 in.) and 0.13538 cm (0.533 in.), respectively.[31] The last layer of the simplified package model is steel wrapped tightly around the enclosed wood or water region. A steel thickness of 0.271 cm (0.1063 in.) was used in the simplified model. This represents the minimum thickness for two sheets of 16-gauge steel.

For the simplified model used in array calculations, the total package height is 101.28 cm (39.87 in.) and the outer diameter is 56.60 cm (22.28 in.). The drawings describe the package as being approximately 108.58 cm (42.75 in.) tall and the drum body having an outer diameter of approximately 57.15 cm (22.50 in.). The simplified model does not include the top and bottom drum closure rings and does not model the space between the outer covers and the liners on both ends. Omitting these features is conservative because the height and diameter reductions result in more tightly packed arrays, minimizing neutron leakage from arrays.

The conditions of reflection outside the package model vary with the analysis for which the model is being used. For example, full density water reflection is used for the single package analysis. In analysis of arrays for normal conditions of transport, nothing exists between the packages, and the outside of the arrays are reflected with full density water.

For the single-package analysis, calculations performed included a series (Cases *cv001* through *cv038*) in which the outer drum steel and TB-1 steel were replaced with full density water that

extended axially and radially 30 cm (11.81 in.) beyond the Pu and water contained within the TB-1.

For discussion purposes, the simplified model variations used in the analysis are identified as follows.

Model 1: Base model, redwood modeled at 100% nominal density, TB-1 steel modeled, outer container steel modeled.

Model 2: Similar to Model 1, except redwood modeled at 80% of nominal density.

Model 3: Similar to Model 1, except redwood modeled at 120% of nominal density.

Model 4: Similar to Model 1, except redwood replaced with full density water.

Model 5: Similar to Model 1, except redwood, TB-1 steel, and outer container steel all replaced with full density water extending axially and radially 30 cm (11.81 in.) beyond the Pu and water contained within the TB-1. This model was used only in the single package analysis.

6.3.1.3 Damaged Container Models

Damaged container models were created for end-impact and side-impact test cases. Dimensions for the end-impact case were taken from Figures 2.18 and 2.30 of NUREG-0361.[2] Dimensions for the side-impact case were taken from Figure 2.24 of NUREG-0361.[2]

The model for the end-impact case is basically the normal case simplified model described above, except the outer drum has been shortened from 101.28 cm (39.87 in.) long to 76.2 cm (30 in.) long and the top of the TB-1 containment vessel is located 19.05 cm (7.5 in.) from the top end of the drum. The redwood is modeled with varying densities of water to simulate combustion of the redwood and potential postfire flooding. This model is shown in Figure 6-3.

The model of the side-impact case is a half-cylinder that is 101.28 cm (39.87 in.) long and has an outer diameter of 74.93 cm (29.5 in.). The undamaged TB-1 containment vessel is centered axially and is located immediately adjacent to the center of the flattened side of the drum. The redwood is modeled with varying densities of water to simulate combustion of the redwood and potential postfire flooding. This model is shown in Figure 6-4.

A final damaged container model was created to support evaluation of 10 CFR 71.55, "*General requirements for fissile material packages*," paragraph (f), which covers fissile material packages transported by air. To meet the requirements of this section, calculations were performed with the TB-1 contents (1300 g [2.87 lb] of Pu-239 and up to 1412 cm^3 [86.16 in^3] of water) in spheres of varying radii reflected by 20 cm (7.9 in.) of water. The purpose of this model is to show that, provided there is no leakage of water into the TB-1 containment vessel, a single package is subcritical without taking credit for the geometry of the package or the continued presence of any package structural materials. This analysis is discussed in Section 6.7. This model is shown in Figure 6-5.

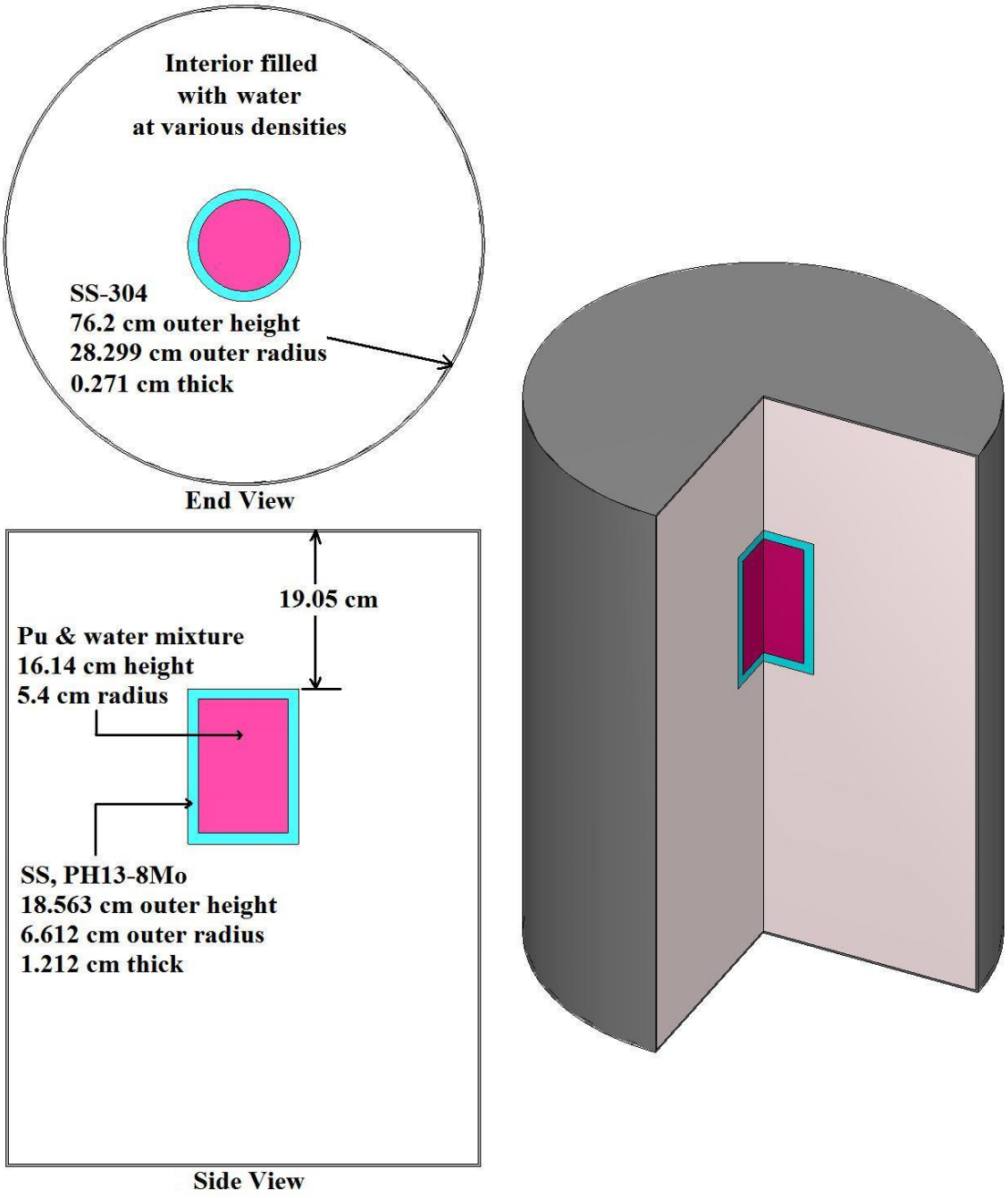

Figure 6-3. End-Impact Damaged Package Model

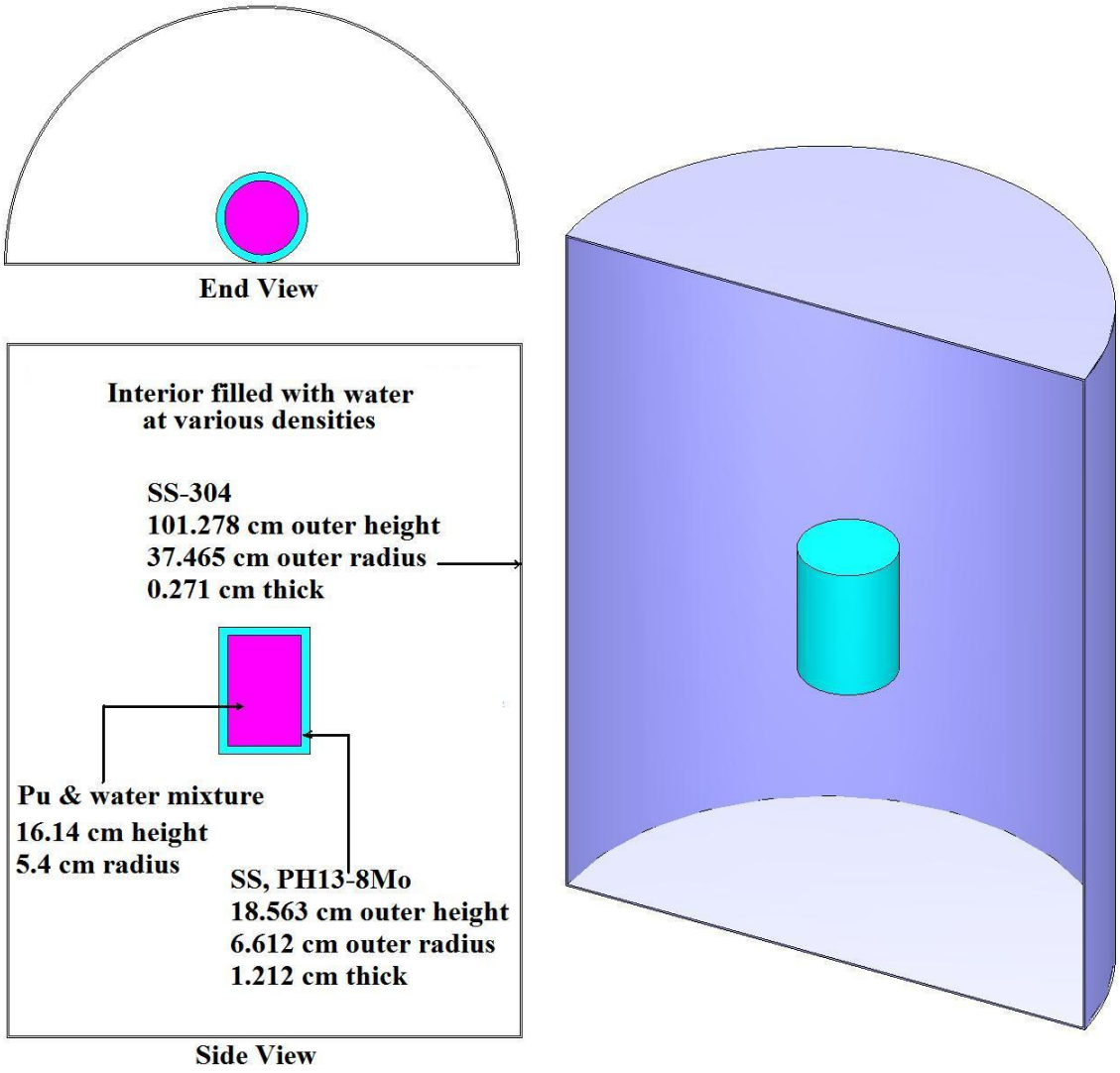

Figure 6-4. Side-Impact Damaged Package Model

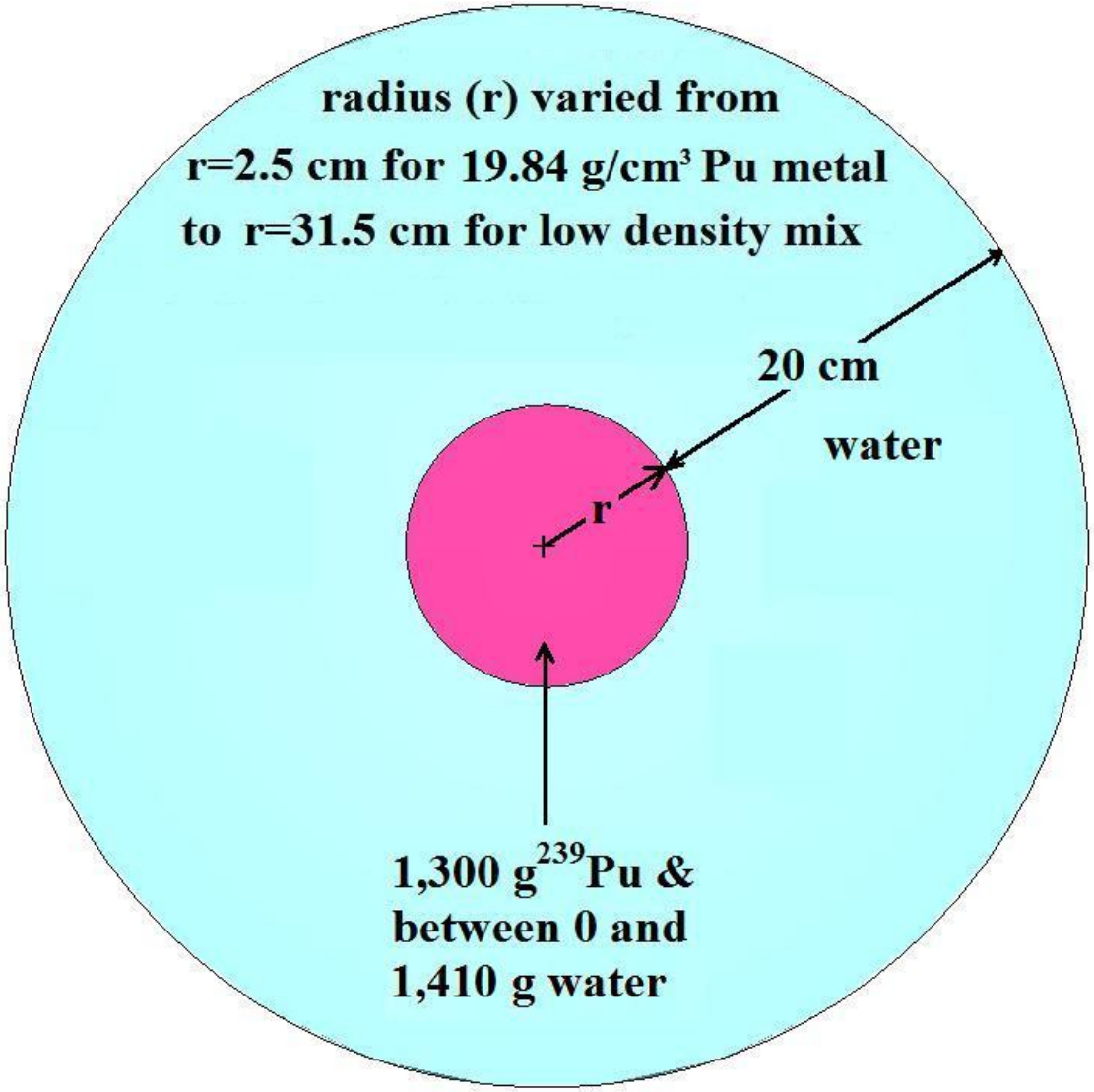

Figure 6-5. HAC Single Package Model for 10 CFR 71.55(f) Analysis

6.3.2 Material Properties

The materials used in the criticality analysis are described in this section. Table 6-2 shows the weight and densities for the materials used in the criticality analysis models.

Table 6-2. Material Specifications

Material	Density (g/cm^3)	Constituent	Atomic Density (atoms/b-cm)
Pu-239 metal	19.84	Pu-239 metal	4.9980E–02
Pu-239 and Water Mixture	1.8331		
(H/Pu atom ratio = 28.8)		Pu-239 (0.8794 g/cm^3)	2.2155E–03
(limiting case composition)		H (0.9537 g/cm^3 water)	6.3793E–02
		O (0.9537 g/cm^3 water)	3.1896E–02

Table 6-2. Material Specifications (Continued)

Material	Density (g/cm^3)	Constituent		Atomic Density (atoms/b-cm)
Full Density Water	0.9979			
		H		6.6752E−02
		O		3.3376E−02
PH13-8Mo Stainless Steel	7.74			
		Fe	(75.775 wt %)	6.3246E−02
		Cr	(12.75 wt %)	1.1430E−02
		Ni	(8 wt %)	6.3532E−03
		Mo	(2.25 wt %)	1.0931E−03
		Al	(1.125 wt %)	1.9435E−03
		Mn	(0.1 wt %)	8.4843E−05
Redwood ($C_6H_{10}O_5$)	0.387			
(± 20% density considered)		H		1.4375E−02
		C		8.6253E−03
		O		7.1877E−03
Stainless Steel-304	7.94			
		C	(0.08 wt %)	3.1848E−04
		Si	(1 wt %)	1.7025E−03
		P	(0.045 wt %)	6.9468E−05
		Cr	(19 wt %)	1.7472E−02
		Mn	(2 wt %)	1.7407E−03
		Fe	(68.375 wt %)	5.8546E−02
		Ni	(9.5 wt %)	7.7401E−03
Aluminum	2.702	Al		6.0307E−02
Copper	8.92	Cu		8.4534E−02

The criticality analysis of the hypothetical accident conditions evaluates the loss of redwood packaging material during a fire by replacing the redwood and charred redwood with water with densities that vary from zero to full density (see Table 6-2). The only other package materials included in the HAC models are the TB-1 containment vessel and the stainless steel outer drum. The aluminum and copper included in the detailed model described in Section 6.3.1.1 are not included in the HAC models. The TB-1 containment vessel is not significantly affected by the HAC conditions. Changes to the stainless steel outer drum shape and dimensions are modeled, as described in Section 6.3.1.3, consistent with the results of prior HAC testing.

6.3.2.1 Fissile Material

The fissile material is comprised of Pu-239 metal mixed with water at varying concentrations. The default Pu density in the SCALE standard composition library[3] is 1.0 g Pu/cm^3 (0.036 lb Pu/$in.^3$). Consequently, the desired Pu density is entered as a density multiplier in the

composition input data. The calculations use Pu-239 densities ranging from 19.84g/cm^3 (0.717 lb/in.^{3}) down to 0.00992 g/cm^3 (0.000358 lb/in.^{3}).

The default water density in the SCALE standard composition library is 0.99793 g/cm^3 (0.036053 lb/in.^{3}) when the 238 group ENDF/B-VI nuclear data library is used. Water with densities ranging from full density to effectively zero density is mixed with the Pu-239 in the TB-1 containment vessel. Within the Pu region, the remaining non-Pu volume fraction is modeled as being filled with water. The water volume fraction in the mixture is, thus calculated as one minus the ratio of the desired Pu-239 density divided by 19.84 g/cm^3 (0.717 lb/in.^{3}). For example, if the mixture will have Pu-239 at 1.000 g/cm^3 (0.036 lb/in.^{3}), the volume fraction for the water is then calculated to be 0.9496 (= 1.0 – 1.000/19.84). This value is entered in the Mixture 1 composition data as the density multiplier for water.

When the Pu-239 is mixed with the maximum quantity of water, completely filling the interior of the TB-1, the Pu-239 density is:

$$1300 \text{ g Pu-239}/1478 \text{ cm}^3 = 0.8794 \text{ g Pu-239 /cm}^3.$$

In this case, the volume fraction for the water mixed with the Pu-239 is calculated as

$$1.0 - 0.8794/19.84 = 0.9557.$$

For this case, the SCALE inputs would be density multipliers of 0.8794 for Pu-239 and 0.9557 for the intermixed water. These inputs would result in a mixture with a Pu-239 density of 0.8794 g Pu-239/cm^3 (0.0318 lb Pu-239/ in.^{3}) and water at 0.9537 g water/cm^3 (0.0344 lb water/in.^{3}).

From page 8 of LA-12808, "Nuclear Criticality Safety Guide,"[32] *"With the exception of uranium enriched to less than about 6 weight percent (wt%) ^{235}U, subcritical masses for solutions apply conservatively to other distributions in water at the same hydrogen-to-fissile atomic ratio."* For Pu-239, the homogeneous metal/water mixture bounds all heterogeneous mixtures. Consequently, except for cases with H/Pu of zero, all cases use a homogeneous plutonium metal and water mixture.

6.3.2.2 Water

The models use water at various densities, from effectively zero density up to full density water. The default water density provided by the SCALE standard composition library when ENDF/B-VI cross sections are used is 0.99793 g/cm^3 (0.36053 lb/in.^{3}). Note: that a slightly different value (0.9982 g/cm^3 [0.3606 lb/in.^{3}]) is reported in the SCALE 5.1 documentation.[3] The difference is due to a slight change in the oxygen atomic weight in the ENDV/B-VI nuclear data evaluation. The SCALE input used for H_2O is a density multiplier on the default density. A density multiplier value of 1.0 translates to a water density of 0.99793 g/cm^3 (0.36053 lb/in.^{3}).

6.3.2.3 Stainless Steel PH 13-8 Mo

The TB-1 containment vessel and lid are made of stainless steel alloy PH13-8 Mo. Table 1.041 of the *Aerospace Structural Metals Handbook*[33] describes the composition of PH13-8Mo as shown in the Min. and Max. columns of Table 6-3. Except for hydrogen, the trace constituents

below manganese are absorbers and weak moderators. Even at their maximum values, the presence of these elements has an insignificant effect on k_{eff}. Consequently, trace elements below manganese were omitted.

Table 6-3. Stainless Steel PH 13-8 Mo Composition (wt %)

Element	Min.	Max.	Modeled
Chromium	12.25	13.25	12.75
Nickel	7.5	8.5	8
Molybdenum	2	2.5	2.25
Aluminum	0.9	1.35	1.125
Manganese	—	0.1	0.1
Silicon	—	0.1	0
Carbon	—	0.05	0
Nitrogen	—	0.01	0
Phosphorus	—	0.01	0
Sulfur	—	0.01	0
Oxygen	—	0.005	0
Hydrogen	—	0.0025	0
Iron	Remainder		75.78

PH13-8Mo density information is limited. The analysis reported in Chapter 5 of NUREG-0361[2] used a value of 7.76 g/cm^3 (0.28 lb/in.^{3}). Chapter 6 of the same report used atom densities equivalent to 7.843 g/cm^3 (0.283 lb/in.^{3}). Table 2.021 of the *Aerospace Structural Metals Handbook*[33] provides densities for PH13-8Mo stainless steel ranging from 7.74 to 7.76 g/cm^3 (0.2796 to 0.2803 lb/in.^{3}). A density of 7.74 g/cm^3 (0.2796 lb/in.^{3}) is used in the calculations. The lower 7.74 g/cm^3 (0.2796 lb/in.^{3}) value was used to minimize the quantity of steel present in array calculations. The steel is modeled as water in the limiting cases for the single-package analyses.

Sensitivity calculations were performed using two of the side-impact hypothetical accident condition models, and with the steel density varied ±2% of the 7.74 g/cm^3 (0.2796 lb/in.^{3}) value. Results from these calculations are presented in Figure 6-6. This figure shows that for PAT-1 models in which the redwood is modeled as full density water, the k_{eff} value of the system is insensitive to the steel density. The figure also shows that for systems where the redwood is missing, such as some of the hypothetical accident cases, k_{eff} value increases slightly with increased steel density. From the sensitivity data, increasing the density from 7.74 to 7.76 increases k_{eff} less than 0.02% Δk.

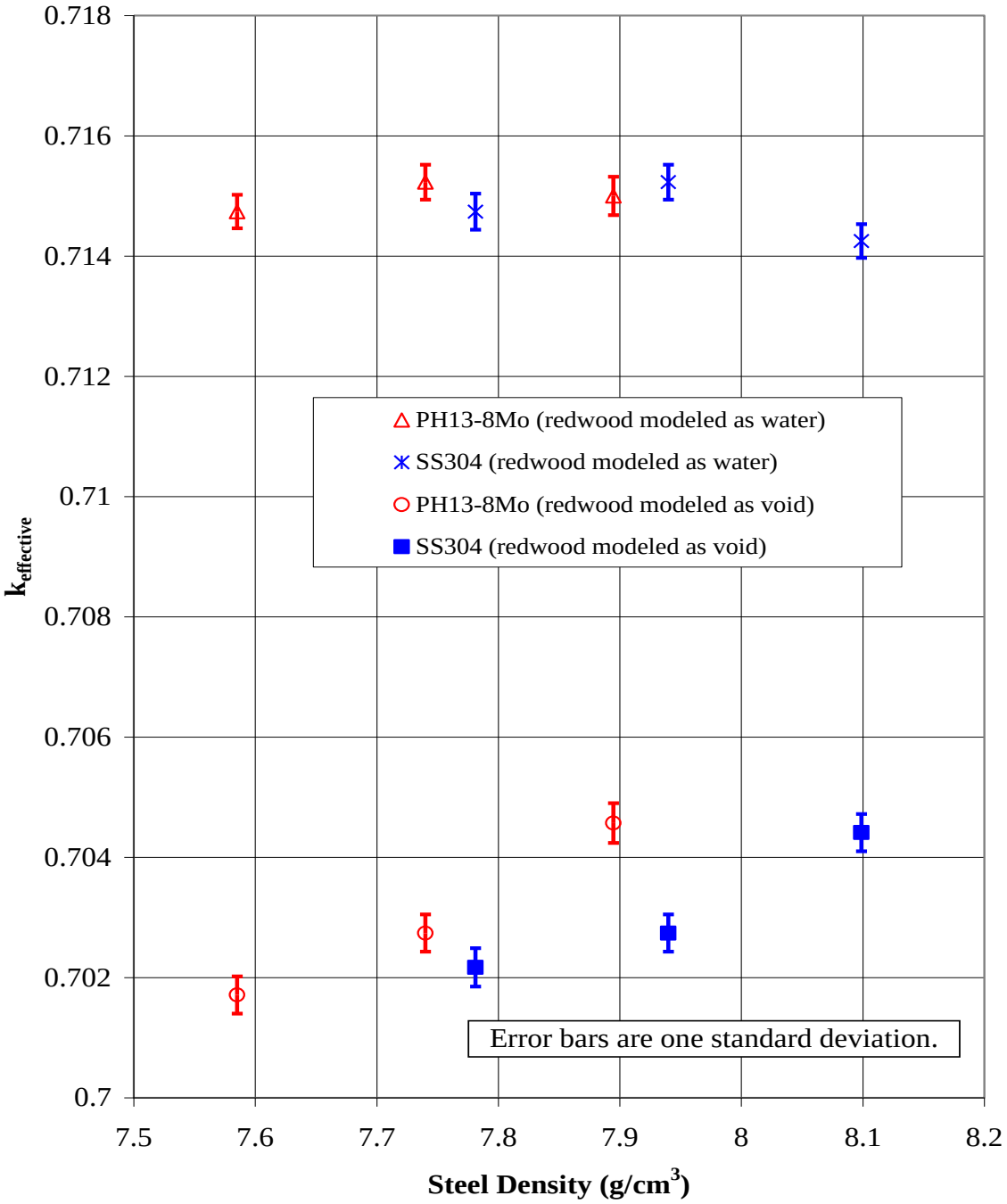

Figure 6-6. Sensitivity of k_{eff} to Steel Density

6.3.2.4 Redwood

Most of the space between the TB-1 containment vessel and the outer steel drum is filled with redwood. The Standard Composition Library[3] in SCALE includes a model for redwood with a default density of 0.3868 g/cm^3 (0.01397 lb/in.^{3}). An informal review of the literature found redwood densities ranging from 0.34 to 0.45 g/cm^3 (0.01228 to 0.01626 lb/in.^{3}), depending on whether the redwood was from new growth or old growth and how much moisture was retained. The models used in the criticality analysis use the SCALE default redwood density. Calculations

were also performed at ±20% of the default density. Results from these calculations are presented in the figures of Section 6.3.4.

6.3.2.5 Aluminum

The detailed model included modeling of the load spreader, which is constructed of aluminum and cadmium-plated copper. The detailed model used aluminum with a density of 2.702 g/cm^3 (0.976 lb/in.^{3}), which is the maximum theoretical density for aluminum provided in the 74th edition of the CRC Handbook of Chemistry and Physics.[34]

6.3.2.6 Copper

The detailed model included modeling of the load spreader, which is constructed of aluminum and cadmium-plated copper. The detailed model used copper at a density of 8.92 g/cm^3 (0.32 lb/in.^{3}), which is the maximum theoretical density for copper provided in the 74th edition of the CRC Handbook of Chemistry and Physics.[34] The cadmium plating on the copper was conservatively omitted from the load spreader model. This is conservative because Cd is a strong thermal neutron absorber.

6.3.2.7 Stainless Steel 304

The outer steel drum and liner are constructed of stainless steel-304 (ss304). Except for the sensitivity cases, the models used the standard ss304 provided by the SCALE Standard Composition Library.[3] The SCALE ss304 has a density of 7.94 g/cm^3 (0.29 lb/in.^{3}) and has the following composition: 68.375 wt % iron, 19 wt % chromium, 9.5 wt % nickel, 2 wt % manganese, 1 wt % silicon, 0.08 wt % carbon, and 0.045 wt % phosphorus. This composition is close that provided for ss304 on page 12-161 of the 74th edition of the CRC Handbook of Chemistry and Physics.[34] The only difference being that the mid-range value provided in the CRC for nickel is 10.0 wt % rather than the 9.5wt% used in the SCALE ss304. On page 12-160, the CRC Handbook of Chemistry and Physics[34] provides a density of 7.9 g/cm^3 (0.286 lb/in.^{3}) for ss304. Sensitivity cases, ±2% on ss304 density, were run for two of the most limiting cases containing ss304. The results of the sensitivity study are presented in Figure 6-6. These results show that the k_{eff} value is insensitive to the steel density when the redwood is modeled as full density water and that changing the density from 7.94 g/cm^3 (0.29 lb/in.^{3}) to 7.90 g/cm^3 (0.286 lb/in.^{3}) reduces system reactivity by about 0.03% Δk when the redwood is modeled as void.

6.3.3 Computer Codes and Cross-Section Libraries

The SCALE 5.1 computer software package[35] was used for all analysis and validation calculations. Criticality calculations were performed using the CSAS25[36] sequence and the SCALE 238-energy-group ENDF/B-VI nuclear data (SCALE 5.1 library id = v6-238). The CSAS25 sequence used BONAMI for incorporating problem specific unresolved resonance data, CENTRM/PMC for the resolved resonance data, and KENO V.a for k_{eff} calculation. The SCALE 5.1 computer software package is a well-established analysis tool for criticality evaluation of fissile material packages. The SCALE ENDF/B-VI 238-energy-group cross-section library is the most modern nuclear data set publicly distributed with SCALE 5.1.

All calculations were initially performed on the "nuc" cluster of workstations identified as nuc1 through nuc30. The nuc workstations are DEC Alpha workstations running Tru64 UNIX, version 5.1. All k_{eff} calculations for the limiting safety analysis models and validation set critical

experiments were run on the nuc cluster. In connection with the revision of Section 6 to incorporate Pu/Be source limits, some TSUNAMI and direct perturbation cases were run on the "cpile2" cluster, nodes 1 – 6. The first 6 nodes of the cpile2 cluster, nodes 1 – 6, have an AMD Opteron™ Processor 246 running the GNU/Linux 2 operating system. The SCALE 5.1 software used for the PAT-1 work was in a directory tree starting at /projects/ymp/scale5.1/ and is controlled under a quality assurance plan, software quality assurance plans, and requirements consistent with 10 CFR 71, Subpart H, "Quality Assurance."

Criticality calculations were performed using at least 3,000 neutrons per generation. The number of generations requested was either 1,050 or 3,050, with at least the first 50 generations being discarded. The KENO V.a "sig" input parameter was used to terminate calculations when the standard deviation of the mean k_{eff} value reached a value of 0.0005. The default starting neutron distribution was used. Neutrons were started uniformly in fissile material for the initial generation. All reflectors were modeled explicitly and no albedo or "bias" data were used.

The convergence plots for each of the limiting cases were reviewed to verify convergence. Trend plots of k_{eff} values were reviewed to identify any cases that may not be converged. Cases with poor convergence or that failed the KENO internal normality tests were rerun with a different number of neutrons per generation, effectively changing the random number sequence of the Monte Carlo method calculations.

The validation study used the SCALE 5.1 TSUNAMI[37, 38] sensitivity and uncertainty analysis tools to assess the similarity of the safety analysis cases and the validation study critical experiments. TSUNAMI-3D[37] was used to generate a set of nuclide- and reaction-specific k_{eff} sensitivity neutron energy-dependent profiles for each limiting safety analysis case and for each critical experiment used in the validation study. The TSUNAMI-3D calculations were performed using the SCALE ENDF/B-VI 238-energy-group cross-section library.

The TSUNAMI-IP[38] module was used to compare the safety analysis cases with critical experiment models. TSUNAMI-IP used the SCALE 5.1 44-group ENDF/B-VI recommended covariance data set (SCALE 5.1 library id = 44groupv6rec). The c_k parameter, average lethargy of fission (EALF), and H/Pu were used to quantify similarity between limiting safety cases and the critical experiments used in the validation. Details are provided in Section 6.8. The 44-neutron-energy-group structure is a subset of the 238-group structure used in the cross-section library that is used for all neutron transport calculations. When the 44-group covariance data is used with the 238-group cross-section library, all of the fine groups within each of the 44 groups use the same 44-group covariance data.

6.3.4 Demonstration of Maximum Reactivity

The purpose of this section is to identify the configuration of maximum reactivity for:

- Section 6.3.4.1 a single package under normal conditions of transport (NCT) and HAC
- Section 6.3.4.2 an array of 5*N undamaged packages under NCT
- Section 6.3.4.3 an array of 2* N damaged packages under HAC

- Section 6.3.4.4 a single package under the expanded HAC specified by 10 CFR 71.55(f)

6.3.4.1 Single Package Under Normal Conditions of Transport and Hypothetical Accident Conditions

The purpose of this section is to identify and demonstrate the maximum reactivity configurations for a single package under normal and hypothetical accident conditions. To support this analysis, simplified and detailed models were created and used in parametric studies.

A parametric study was performed using five variations of the simplified model to show the impact on k_{eff} from various modeling approximations. The results of this study are shown in Figure 6-7 and in the list of calculations provided in Section 6.9.4.1 of this addendum.

Three curve segments are plotted for each of the five simplified model variations described as Models 1 through 5 in Section 6.3.1.2. The left-most segments cover the H/Pu range of 0 to 12.1. In this range, the results are for 1300 g (2.87 lb) of Pu or Pu-water in spheres of increasing radii ranging from the minimum 2.50 cm (0.98 in.), for unmoderated maximum theoretical density plutonium metal, to 5.40 cm (2.13 in.), for a sphere that is the maximum size that could fit within the TB-1 containment vessel. The second set of segments cover the H/Pu range from 5.34 through 28.8. In this range, the results are for a 1300 g (2.87 lb) plutonium and water cylinder with an outer radius of 5.40 cm (2.13 in.) and with height varying from 3.58 to 16.14 cm (1.41 to 6.35 in.), which completely fills the interior of the TB-1 containment vessel. The right-most segments curve cover the H/Pu range from 28.8 through 132.2 and show the impact of replacing Pu with water in the TB-1. All simplified model results show one maxima at a H/Pu ratio equal to zero (maximum theoretical density plutonium metal sphere surrounded by water in the TB-1) and another at a H/Pu ratio equal to 28.8, where the 1300 g (2.87 lb) of Pu are spread throughout the TB-1 and mixed with the maximum quantity of water that could fit within the TB-1, considering the presence of 1300 g (2.87 lb) of Pu.

The curves for simplified Models 1, 2, and 3 show the sensitivity of k_{eff} to the density of the redwood. As discussed in Section 6.3.2, the density of the redwood may vary considerably. The black (Model 3) and purple (Model 2) curves show the effect on k_{eff} from the variation of the redwood density by ±20% around the nominal 0.387 g redwood/cm^3 (1.139 lb/in.^{3}). Model 1 has nominal redwood density. Model 2 has 80% of nominal redwood density. Model 3 has 120% of nominal redwood density. The red curve (Model 4) shows the effect on k_{eff} from the replacement of the redwood with full density water. The blue curve (Model 5) shows the effect on k_{eff} from the replacement of both the redwood and steel with water. It is concluded from this study that the maximum k_{eff} value is generated by the simplified model case *cv031*, in which the redwood and steel were replaced with full density water and the 1300 g (2.87 lb) of Pu is spread throughout the inside of the TB-1 containment vessel and mixed with the maximum quantity of water that could also be present in the TB-1 (i.e., the peak of the Model 5 curve at H/Pu = 28.8).

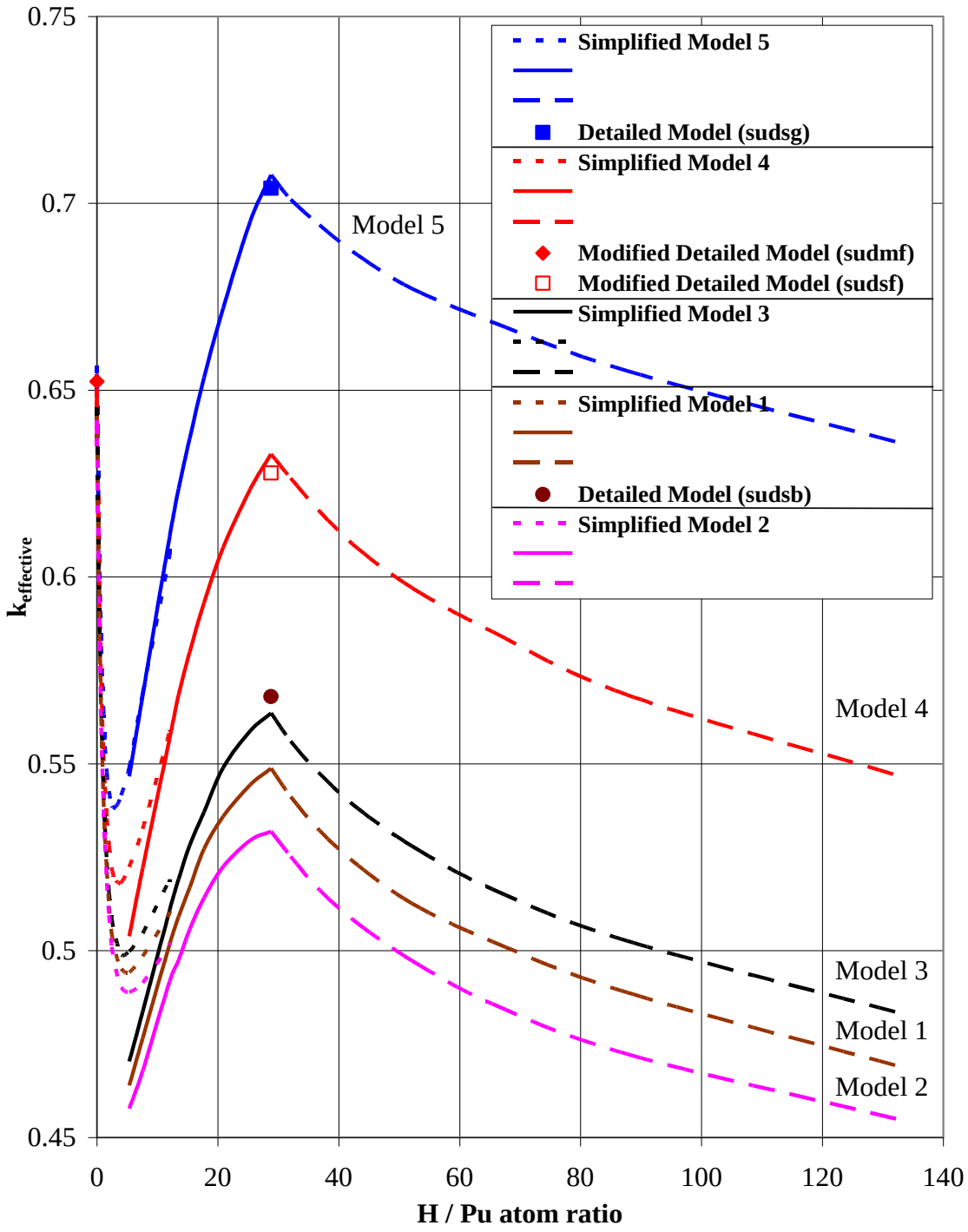

Figure 6-7. Single Package Moderation Study

Impact of Modeling Simplifications

Additional calculations were performed with a detailed model (see Figure 6-1) to show that the simplified model results bound the detailed model results and to show the impact of various modeling approximations.

In the first series of additional detailed model calculations, the package payload is a 1300 g (2.87 lb) plutonium metal sphere (H/Pu = 0) in the middle of the TB-1 containment vessel. The results from the first series are presented in Table 6-4. The results from case *sudmf* is plotted in Figure 6-7 as "Modified Detailed Model (sudmf)." This modified detailed model yielded a k_{eff} of 0.6523 ± 0.0005, which is lower than the k_{eff} of 0.6565 ± 0.0005 produced by simplified Model 5 (blue curve in Figure 6-7) with an H/Pu of zero.

Table 6-4. Detailed Model, Plutonium Metal Sphere, Modeling Impact Study

Case	k_{eff}	σ	Case Description
sudma	0.5525	0.0005	Detailed model with no water in TB-1 or in gaps. Redwood, aluminum, copper, and steel modeled.
sudmb	0.6492	0.0005	Case *sudma* with TB-1 filled with water
sudmwoodm	0.6486	0.0005	Case *sudmb* with redwood density decreased 20%
sudmwoodp	0.6500	0.0005	Case *sudmb* with redwood density increased 20%
sudmc	0.6504	0.0005	Case *sudmb* with gaps filled with water
sudmd	0.6499	0.0005	Case *sudmc* with copper changed to water
sudme	0.6489	0.0005	Case *sudmd* with aluminum changed to water
sudmf	0.6523	0.0005	Case *sudme* with redwood changed to water

In a second series of detailed model calculations, the package payload is 1300 g (2.87 lb) Pu mixed with 1412 g (3.113 lb) of water in the TB-1 containment vessel (H/Pu = 28.8). The results are presented in Table 6-5. The results from cases *sudsb*, *sudsf*, and *sudsg* are plotted on Figure 6-7 as "Detailed Model sudsb," "Detailed Model sudsf," and "Detailed Model sudsg," respectively. Calculations *sudmf* and *sudsf* produce k_{eff} values that are similar to those from simplified Model 4 in which the redwood, gaps, copper, and aluminum have all been replaced with water. Calculation *sudsg* produce a k_{eff} value (0.7040 ± 0.0005) that is a slightly lower than the peak k_{eff} value (0.7076 ± 0.0006) from the simplified Model 5 at an H/Pu of 28.8.

It is concluded from the results presented in Figure 6-7 that analysis case *cv031*, in which the wood, steel, aluminum, copper, and gaps are modeled as water, yields the maximum k_{eff} value (0.7076 ± 0.0006) for a single package under normal conditions of transport. Furthermore, because this case already includes the maximum quantity of water possible within the TB-1 containment vessel and the maximum flooding of the package outside the TB-1, it also yields the maximum k_{eff} value for a single package under hypothetical accident conditions. Figure 6-7 also shows that removing water from inside the TB-1 containment vessel results in a decreased k_{eff} value and that removing Pu from the TB-1 vessel to make room to add water also results in a decreased k_{eff} value.

A note of interest: is the relationship between the detailed model (with steel, redwood, copper, and aluminum modeled) results and the simplified model (with steel and redwood modeled) results. In Figure 6-7, the brown dot representing detailed model case *sudsb* is significantly higher than the simplified Model 1 result at an H/Pu of 28.8. A similar trend is seen in Figure 6-9 between the detailed model results and the simplified Model 1 results.

Table 6-5. Detailed Model, Plutonium and Water Solution Cylinder, Modeling Impact Study

Case	k_{eff}	σ	Case Description
sudsb	0.56797	0.0005	Detailed model with no water in gaps. Redwood, aluminum, copper, and steel modeled.
sudswoodm	0.5599	0.0005	Case *sudsb* with redwood density decreased 20%
sudswoodp	0.5761	0.0005	Case *sudsb* with redwood density increased 20%
sudsc	0.5911	0.0005	Case *sudsb* with gaps filled with water
sudsd	0.5920	0.0005	Case *sudsc* with copper changed to water
sudse	0.5932	0.0005	Case *sudsd* with aluminum changed to water
sudsf	0.6278	0.0005	Case *sudse* with redwood changed to water
sudsg	0.7040	0.0005	Case *sudsf* with all steel changed to water

The results in Table 6-5 show if the copper or aluminum is replaced in the detailed model with water, k_{eff} decreases. This is somewhat counterintuitive. This effect is likely due to the much larger total neutron cross section that hydrogen has and the physical locations of the copper and aluminum components. The additional moderation provided by replacing the copper or aluminum with water at the locations of the copper and aluminum components appears to decrease the fraction of neutrons that can migrate back to the Pu. Figure 6-7 and Figure 6-9 show that the simplified Models 4 and 5, in which the redwood, copper, and aluminum have been replaced with water, yield significantly higher k_{eff} values than simplified Models 1, 2, and 3 and the detailed model. Figure 6-7 also shows the results at an H/Pu of 28.8 for a detailed model in which the redwood, copper, aluminum, and gaps have been changed to water (case *sudsf*) and where the TB-1 steel and outer container steel have been changed to water (case *sudsg*). These modified details yield k_{eff} values that are slightly lower than the simplified model results. It is concluded that simplified Models 4 and 5 provide conservative representations of the PAT-1 package.

6.3.4.2 Array of Packages Under Normal Conditions of Transport

Title 10 CFR 71.59(a)(1) requires that a water reflected array of five times "N" undamaged packages with nothing between the packages would be subcritical. From Section 6.1.3, the value of N is 500, thus it must be shown that 2500 undamaged packages would be subcritical. Calculations were performed with packages in both square and hexagonal pitched arrays with the package contents varied from a 1300 g (2.87 lb) plutonium metal sphere to a 1300 g (2.87 lb) Pu-water mixture spread throughout the interior of the TB-1 containment vessel. Additional calculations were also performed to show that removing Pu to make room for additional water would result in a lower k_{eff} value.

Using a square-pitched array in a 17 × 17 × 9 arrangement, results in a near cuboidal arrangement of 2,601 packages. The space between packages is modeled as void per 10 CFR 71.59(a)(1) and a 30-cm-thick (11.8 in.) layer of water surrounds the array on all sides. Figure 6-8 shows a cutaway view of the array model. The series of calculations were performed on both detailed and simplified models.

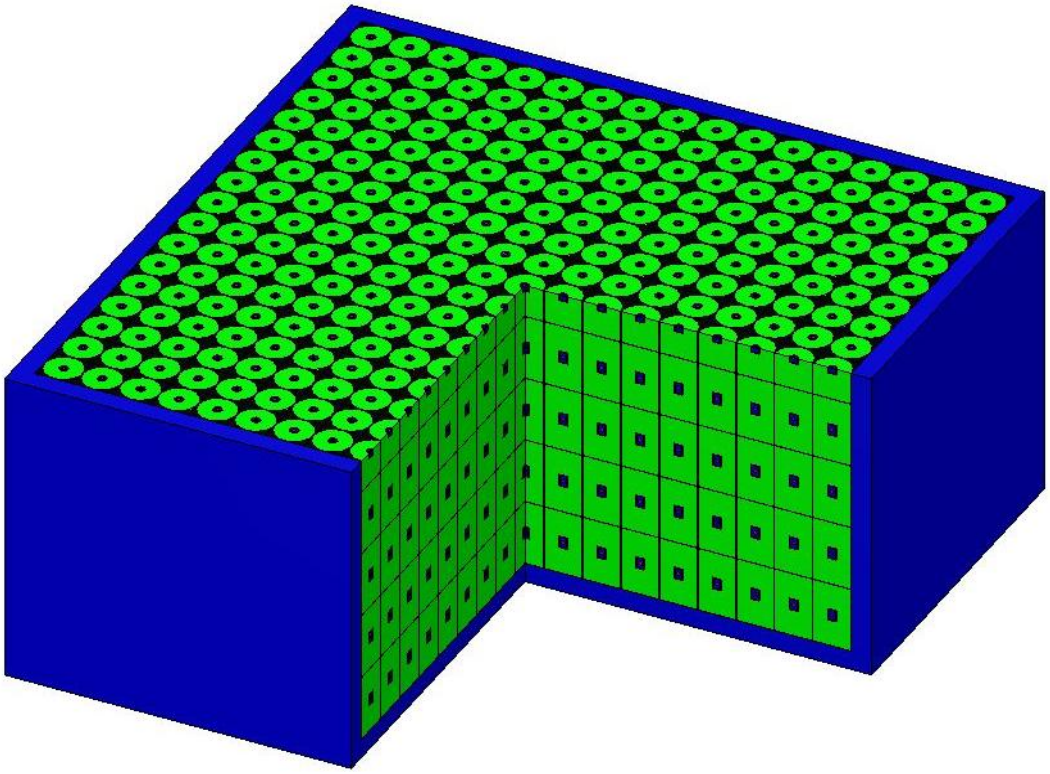

Figure 6-8. Normal Conditions of Transport – Square-Pitched Array

Figure 6-9 and the table in Section 6.9.4.2 show the results of the series of calculations with simplified and detailed models in a square-pitched array. Calculations were performed for H/Pu ratios ranging from zero to 132.2. Three curve segments are plotted for each of four simplified model variations, described as Models 1 through 4 in Section 6.3.1.2, and for an array of detailed models, described in Section 6.3.1.1.

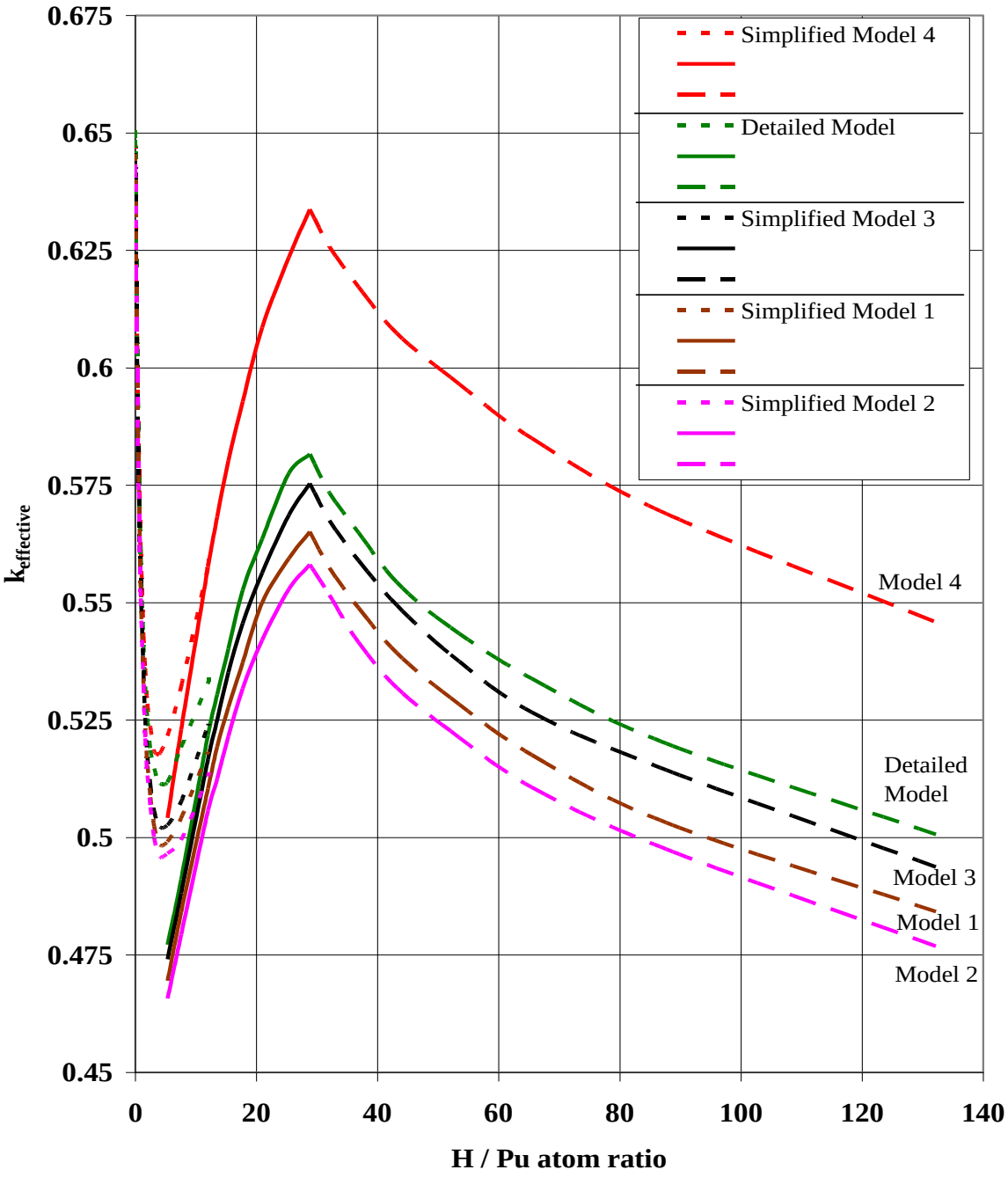

Figure 6-9. Normal Conditions of Transport – Square-Pitched Array Results

The left-most segment for each curve covers the H/Pu range of 0 to 12.1. In this range, the results are for 1300 g (2.87 lb) Pu or Pu-water spheres of increasing radii ranging from the minimum 2.50 cm (0.98 in.), for unmoderated maximum theoretical density plutonium metal, to 5.40 cm, for a sphere that is the maximum size that could fit within the TB-1 containment vessel. The second segment of each curve covers the H/Pu range from 5.34 through 28.8. In this range, the results are for a 1300 g (2.87 lb) Pu-water cylinder with an outer radius of 5.40 cm and with height varying from 3.58 to 16.14 cm (1.41 to 6.35 in.), which completely fills the interior of the TB-1 containment vessel. The right-most segment of each curve covers the H/Pu range from

28.8 through 132.2 and shows the effect on k_{eff} of removing Pu and adding water into the TB-1. The model results all show one maxima at a H/Pu ratio equal to zero and another at a H/Pu ratio equal to 28.8, where the 1300 g (2.87 lb) of Pu are spread throughout the TB-1 and mixed with the maximum quantity of water that could fit within the TB-1 considering the presence of 1,300 g of Pu.

For all models, the highest k_{eff} values were generated with the 1300 g (2.87 lb) plutonium metal sphere in the TB-1 containment vessel with the remainder of the containment vessel filled with water. The detailed model and the simplified model with redwood replaced by water yielded statistically equivalent k_{eff} values (i.e., 0.6505 ± 0.0005 for the detailed model and 0.6504 ± 0.0005 for Simplified Model 4) at the H/Pu of zero. These were the highest k_{eff} values generated for the square-pitched arrays.

The series of calculations were also performed with the simplified model packages in a close-packed hexagonal array. The array model includes 2,646 packages in a near cuboidal shaped array as shown in Figure 6-10.

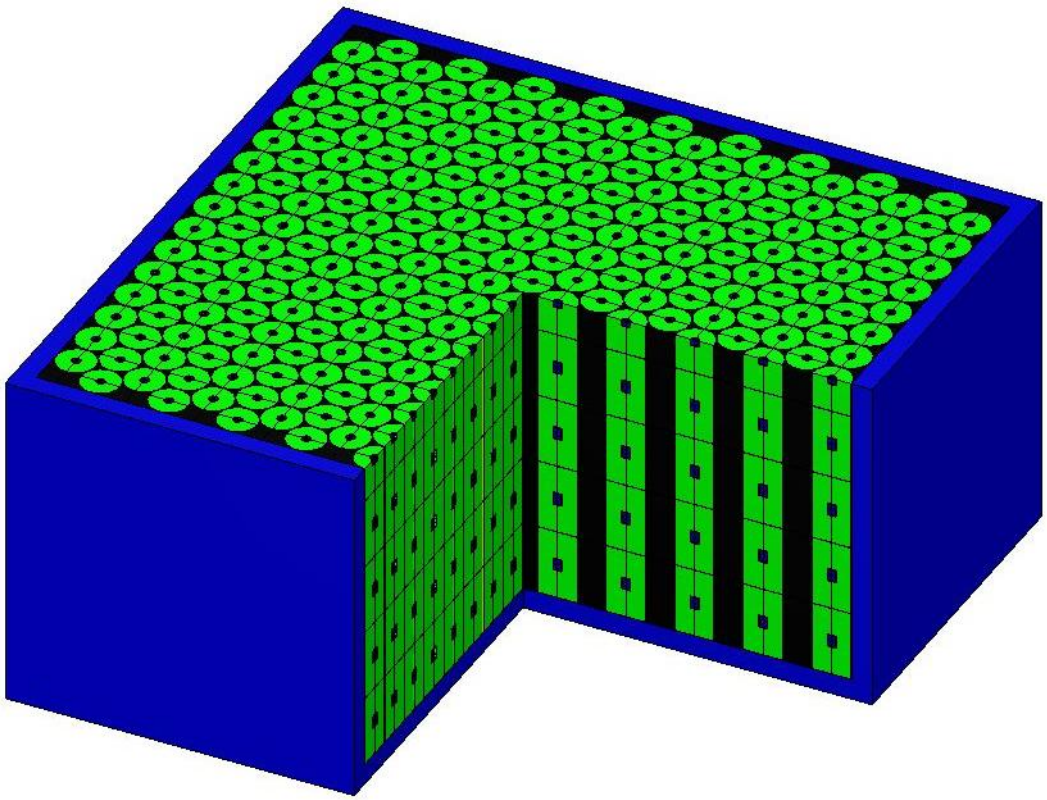

Figure 6-10. Normal Conditions of Transport – Hexagonal-Pitched Array

Figure 6-11 shows the results of series of calculations with simplified models. Calculations were performed for H/Pu ratios ranging from zero to 132.2. Three curve segments are plotted for each of four simplified model variations, described as Models 1 through 4 in Section 6.3.1.2.

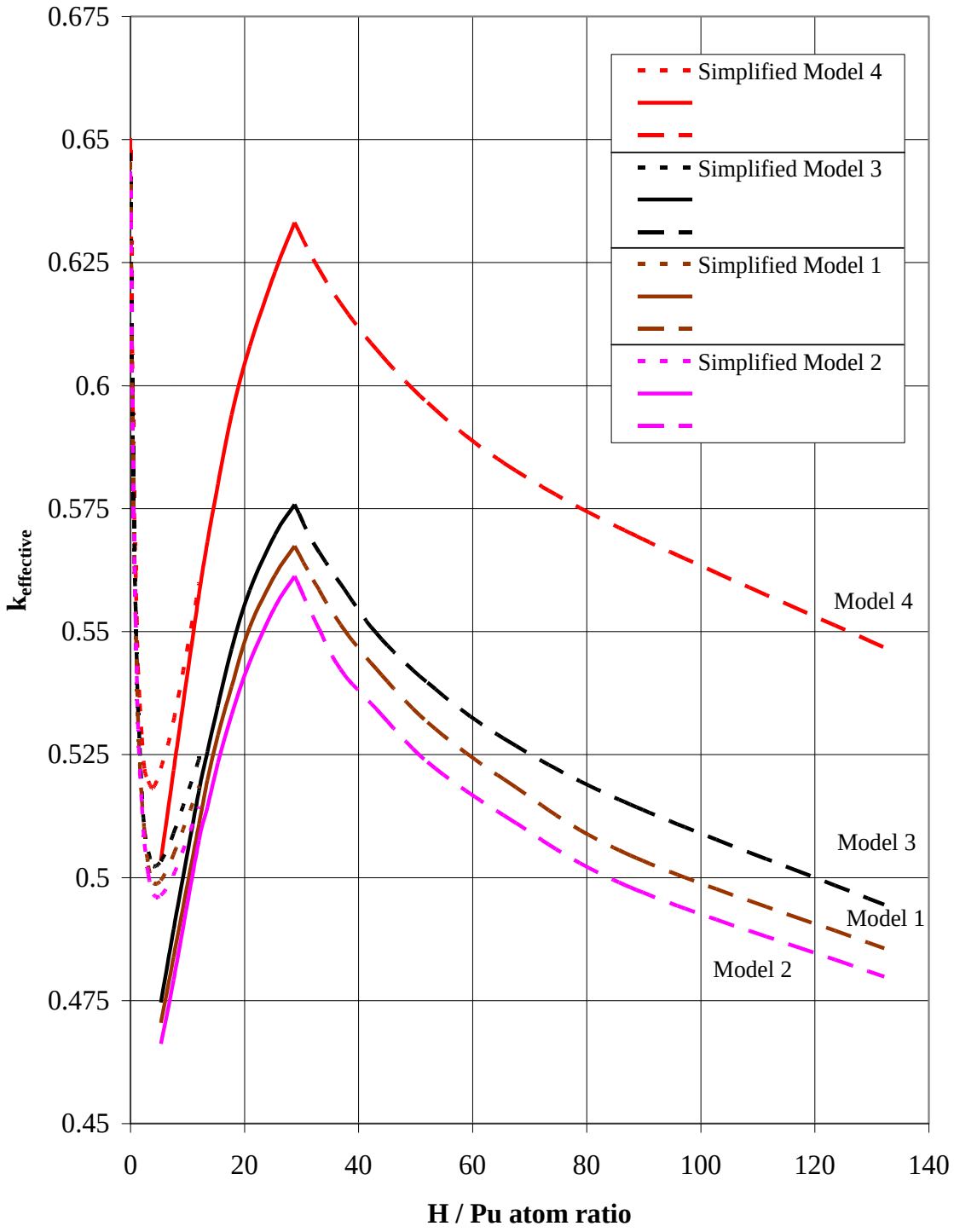

Figure 6-11. Normal Conditions of Transport – Hexagonal-Pitched Array Results

The left-most segment for each curve covers the H/Pu range of 0 to 12.1. In this range, the results are for 1300 g (2.87 lb) Pu or Pu -water spheres of increasing radii ranging from the minimum 2.50 cm (0.98 in.), for unmoderated maximum theoretical density plutonium metal, to 5.40 cm (2.13 in.), for a sphere that is the maximum size that could fit within the TB-1 containment vessel. The second segment of each curve covers the H/Pu range from 5.34 through

28.8. In this range, the results are for a 1300 g (2.87 lb) Pu -water cylinder with an outer radius of 5.40 cm (2.3 in.) and with height varying from 3.58 to 16.14 cm (1.41 to 6.35 in.), which completely fills the interior of the TB-1 containment vessel. The right-most segment of each curve covers the H/Pu range from 28.8 through 132.2 and shows the effect on k_{eff} of removing Pu and adding water into the TB-1. The model results all show one maxima at a H/Pu ratio equal to zero and another at a H/Pu ratio equal to 28.8, where the 1300 g (2.87 lb) of Pu are spread throughout the TB-1 and mixed with the maximum quantity of water that could fit within the TB-1, considering the presence of 1300 g (2.87 lb) of Pu.

For all models, the highest k_{eff} values were generated with the 1300 g (2.87 lb) plutonium metal sphere in the TB-1 containment vessel with the remainder of the containment vessel filled with water. The Simplified Model 4, with redwood replaced by water, and at an H/Pu ratio of zero, yielded the highest k_{eff} value, 0.6509 ± 0.0005. While this k_{eff} value is slightly higher than the value for the square-pitched array of packages, it is statistically the same. This indicates that, with the redwood zone modeled as full density water, the maximum k_{eff} value is not sensitive to the number or arrangement of the surrounding packages.

The NCT array analysis was performed with redwood at nominal and ±20% density and full density water to ensure that the NCT array model was conservative. The results presented in Figure 6-9 and Figure 6-11 clearly show this is the case for all configurations except the single solid metal Pu sphere. As shown by comparing the results in Section 6.9.4.2, replacing the redwood with water is conservative even for the metal sphere cases. The NCT arrays with full density water replacing the redwood yields a higher array k_{eff} than does the same array with the redwood modeled.

The maximum k_{eff} value for an array under normal conditions of transport is 0.6509 ± 0.0005 for Simplified Model 4 with each package containing a 1300 g (2.87 lb) Pu metal sphere and arranged in hexagonal-pitched arrangement of 2646 packages (Case *fhlsf001*).

6.3.4.3 Array of Packages Under Hypothetical Accident Conditions

Title 10 CFR 71.59(a)(2) requires that a water reflected array of two times "N" damaged packages with optimum interspersed moderation between the packages would be subcritical. From Section 6.1.3, the value of N is 500, thus, it must be shown that 1000 damaged packages would be subcritical. Two different damaged container models described in Section 6.3.1.3 were evaluated: one for an end-impact case (see Figure 6-3) and one for a side-impact case (see Figure 6-4). Calculations were performed with both damaged-container models in various arrangements of varying numbers of packages to identify which damaged container and which arrangement produced the highest k_{eff} values. In all cases, the number of rows, columns, and layers were set to produce a nearly cubic array of packages. The intent of this study is to show which damaged container model in which arrangement of 1000 packages produces the highest k_{eff} value. The results of this study are presented in Figure 6-19. All calculations used in the analysis of package arrays under HACs are listed in the Section 6.9.4.3 table.

Four different array arrangements were considered for the side-impact damaged container model. The most limiting array involved pairs of damaged packages oriented so that their flat sides were together. Pairs of damaged packages were then placed in a hexagonal-pitch array. Figure 6-12

shows an overhead view of one of these arrays. The array is enclosed on three sides by a 30-cm-thick (11.8 in.) water reflector. A reflective boundary condition is used on the other three sides.

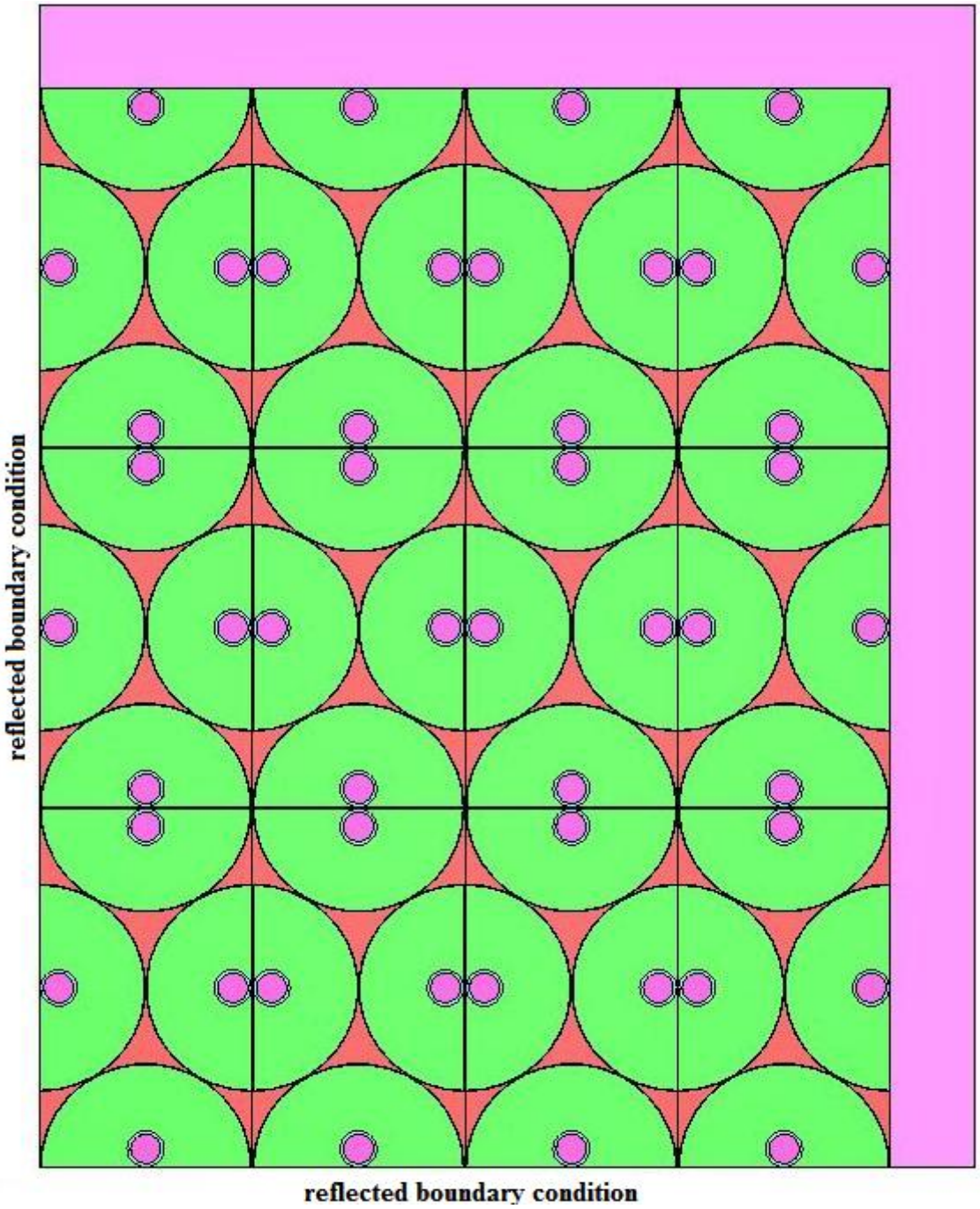

Figure 6-12. Damaged Packages – Side-Impact Hexagonal-Pitch Array, Top View

Calculations were also performed for an array of damaged packages arranged such that each pair of damaged packages was arranged in a square-pitch as shown in Figure 6-13. Figure 6-14 and Figure 6-15 show arrays in which damaged packages were oriented to try to locally increase the fissile material density within the array.

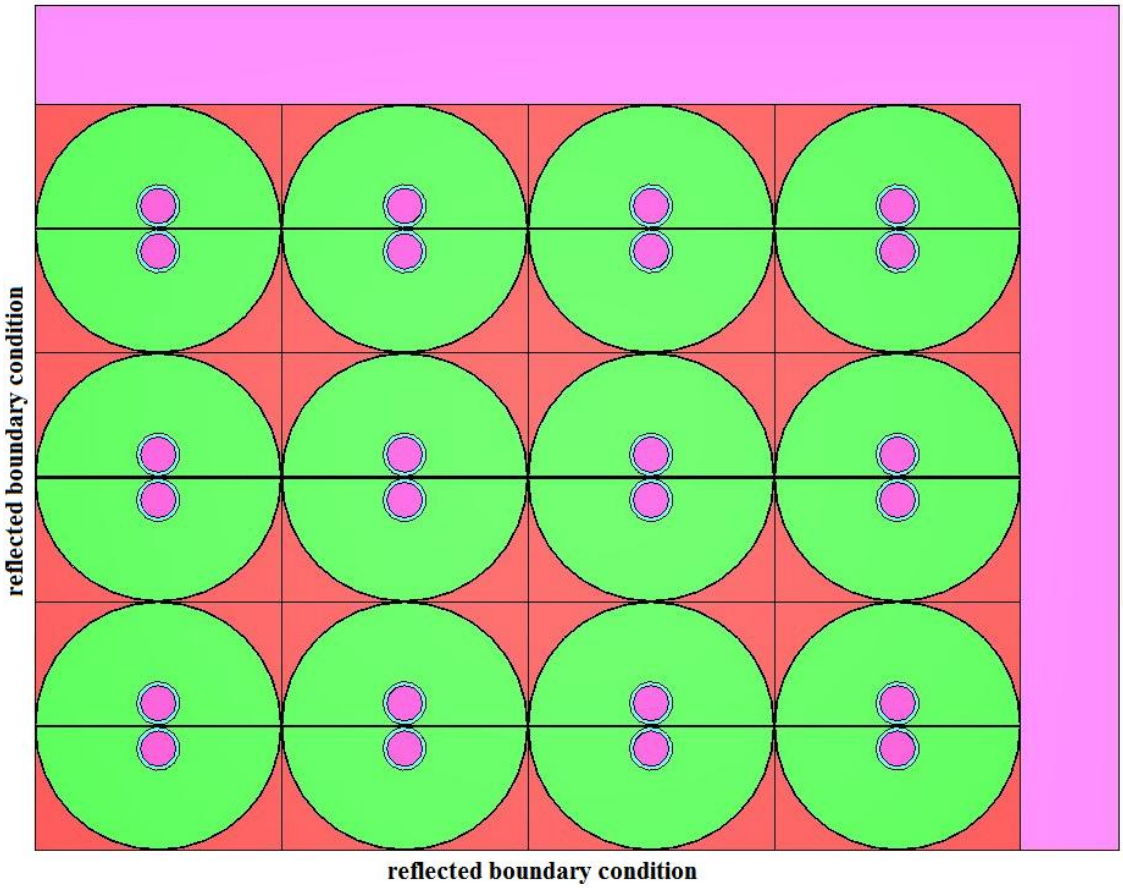

Figure 6-13. Damaged Packages – Side-Impact Square-Pitch Array, Top View

Two types of arrays of end-impact damaged packages were also considered. In both cases, the damaged drums are arranged horizontally in a close-packed hexagonal array. In one type of end-impact damaged package array, each vertical layer is repeated. In the other type, the packages are turned upside-down in alternating layers to minimize the spacing between the fissile material in every other layer. Side views of these two arrangements are provided in Figure 6-17Figure 6-16 and Figure 6-17. A top view is shown in Figure 6-18.

Calculations were performed with both damaged-container models in various arrangements of varying numbers of packages to identify which damaged container and which arrangement produced the highest k_{eff} values. In all cases, the number of rows, columns, and layers were set to produce a nearly cubic array of packages. The intent of this study is to show which damaged container model in which arrangement of 1000 packages produces the highest k_{eff} value. The results of this study are presented in Figure 6-19. In this study, the redwood, aluminum, and copper are modeled as void to maximize interaction between units. Based on the study results, it is concluded that the close-packed hexagonal array of side-impact damaged drums yields the highest k_{eff} values for array sizes of 1000 damaged packages.

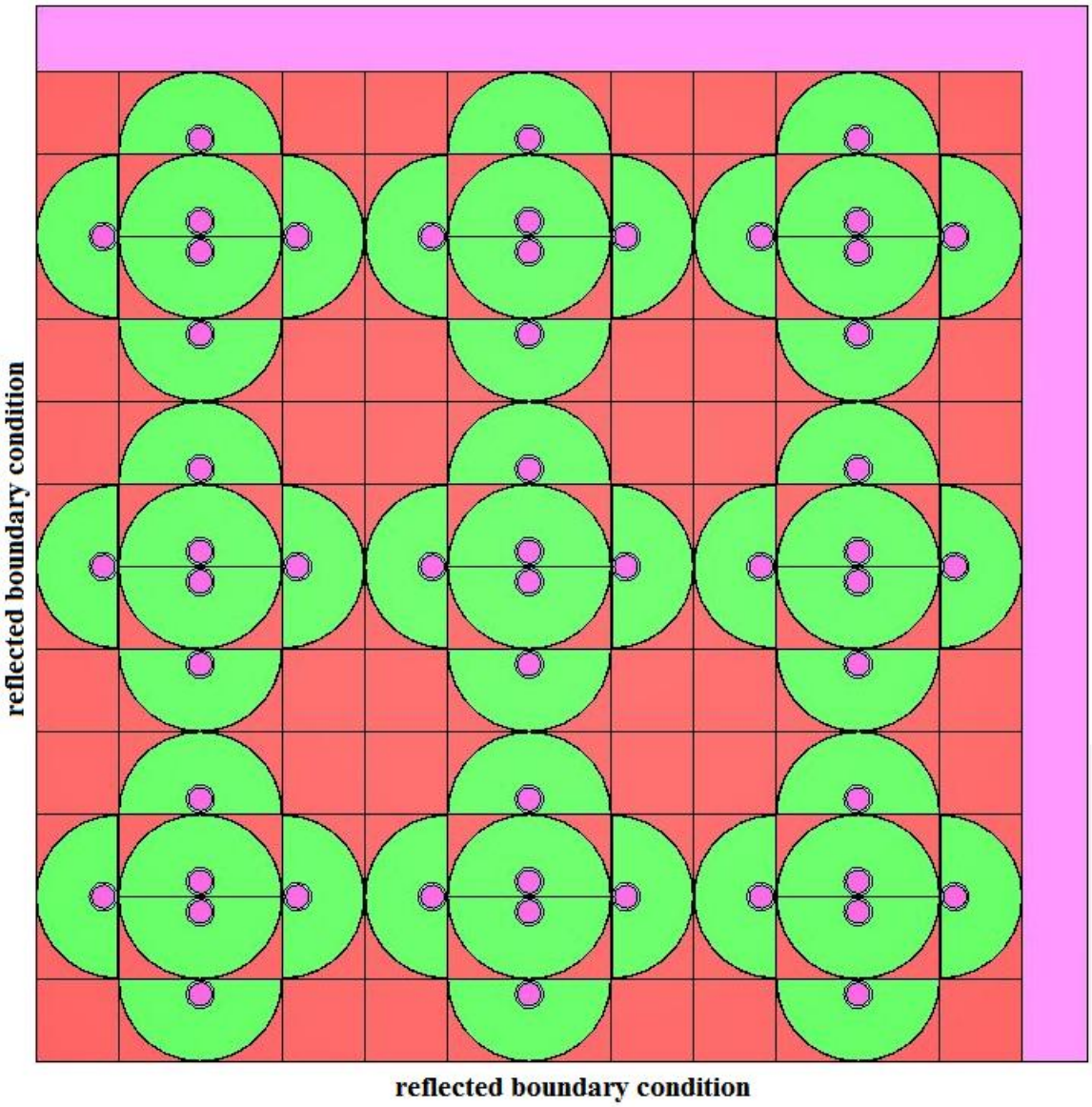

Figure 6-14. Damaged Packages – Side-Impact Nested Arrangement No. 1, Top View

The tests performed on the damaged package included a fire test that resulted in burning and loss of some of the redwood. The criticality analysis considers that some or all of the redwood may be lost and may be replaced with water. This bounds the entire range (0 to 100%) of wood and/or water that could be present following hypothetical accident conditions. A series of calculations were performed to identify the optimum level of moderation in the redwood package zone. Figure 6-20 presents the results of a study identifying the optimum quantity of moderator to place in the charred redwood zone. Calculations were performed for the two combinations of Pu-water in the TB-1 that produced maxima in the normal conditions array calculations. These were with a 1300 g (2.87 lb) Pu sphere inside a flooded TB-1 container and with the 1300 g (2.87 lb) of Pu intimately mixed with the 1412 g of water that could be in the TB-1. Calculations were performed for the side-impact damaged drums in the close-packed hexagonal and square-pitched arrays. Each series of calculations was performed with the redwood zone replaced with water varying from 0% to 100% density.

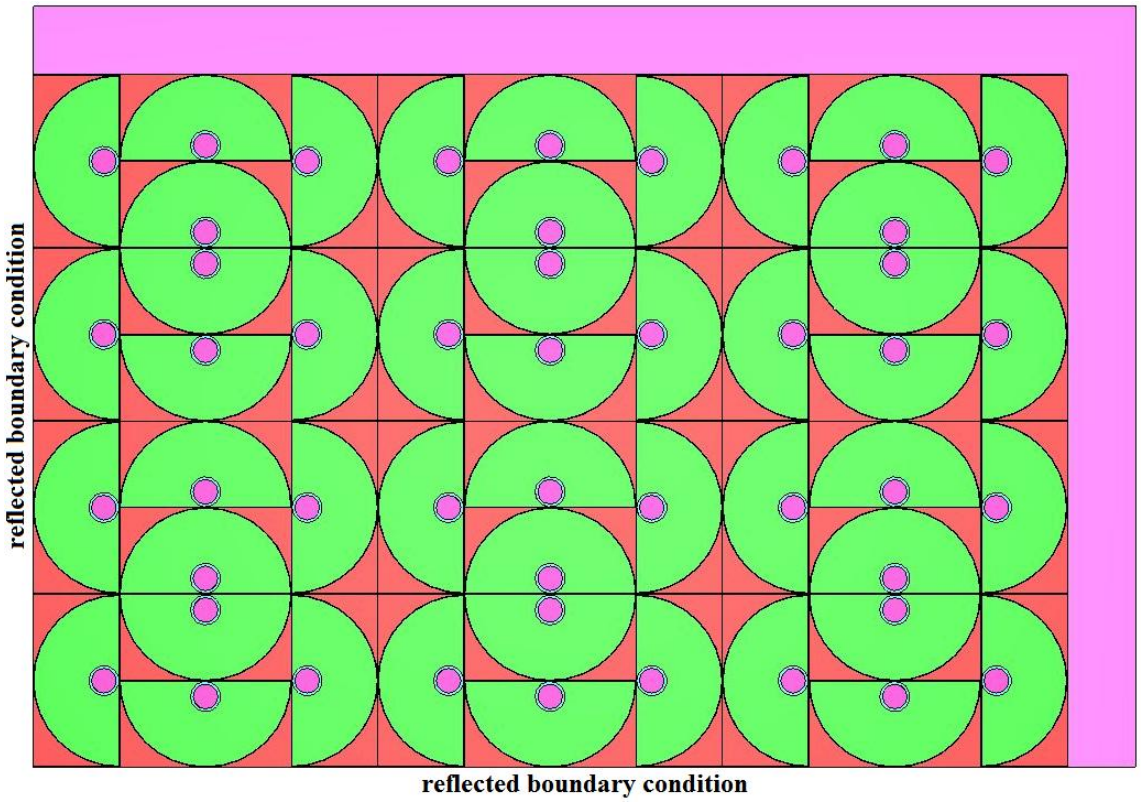

Figure 6-15. Damaged Packages – Side-Impact Nested Arrangement No. 2, Top View

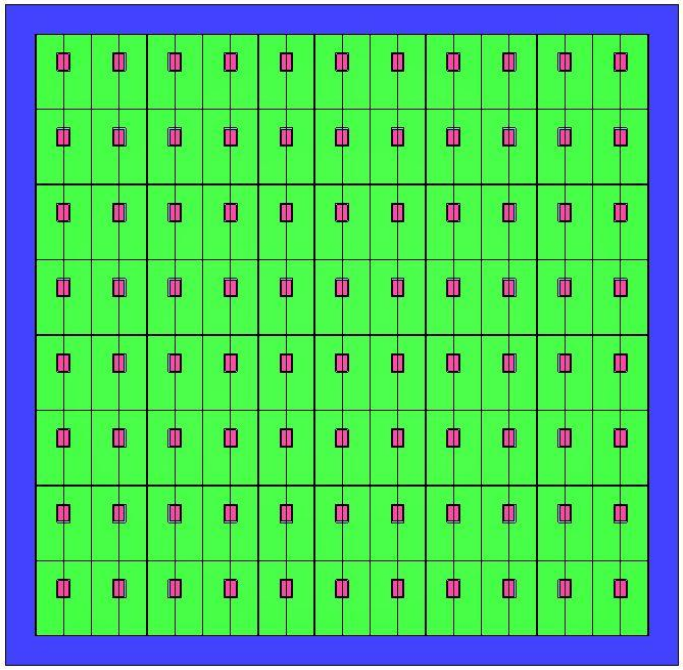

Figure 6-16. Damaged Packages – End-Impact Array, Repeated Layers, Side View

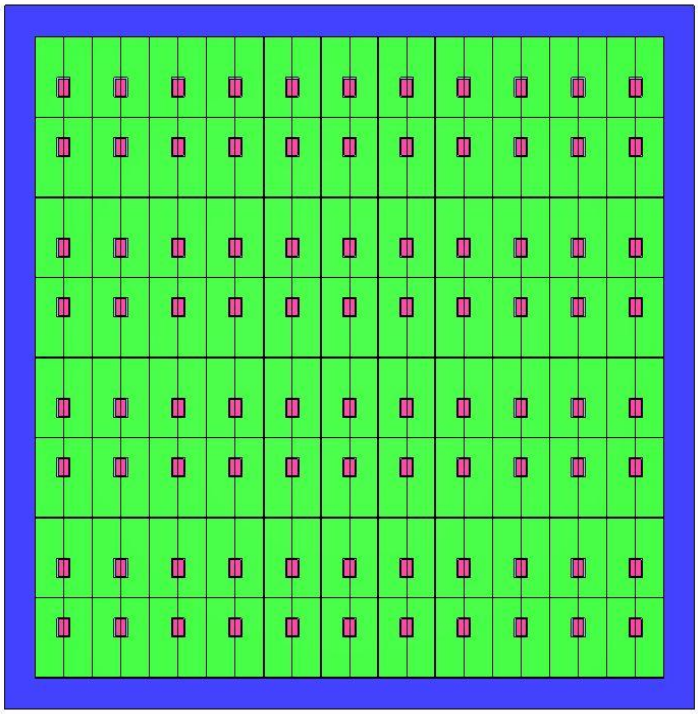

Figure 6-17. Damaged Packages – End-Impact Array, Alternating Layers, Side View

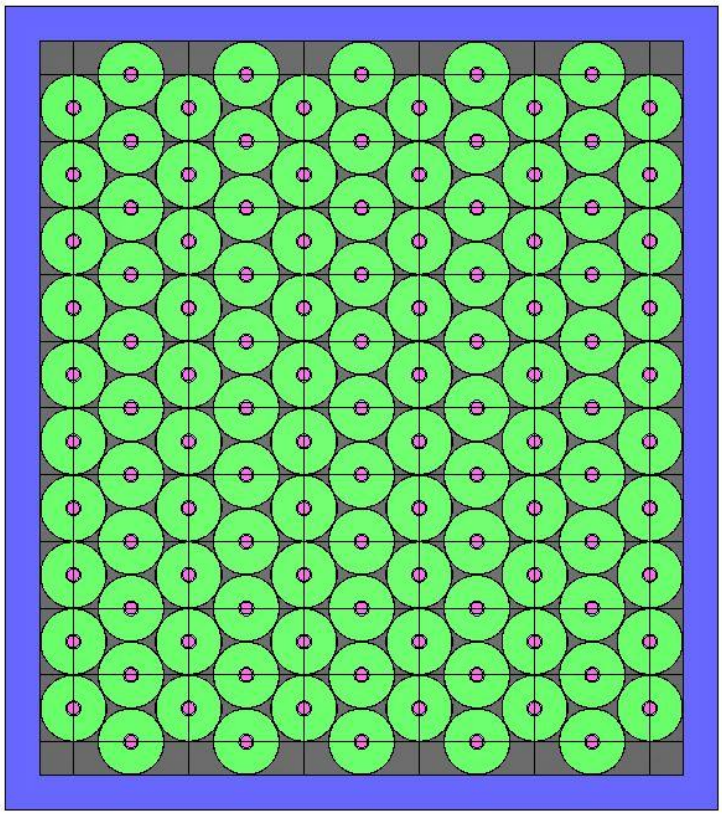

Figure 6-18. Damaged Packages – End-Impact Arrays, Repeated and Alternating Layers, Top View

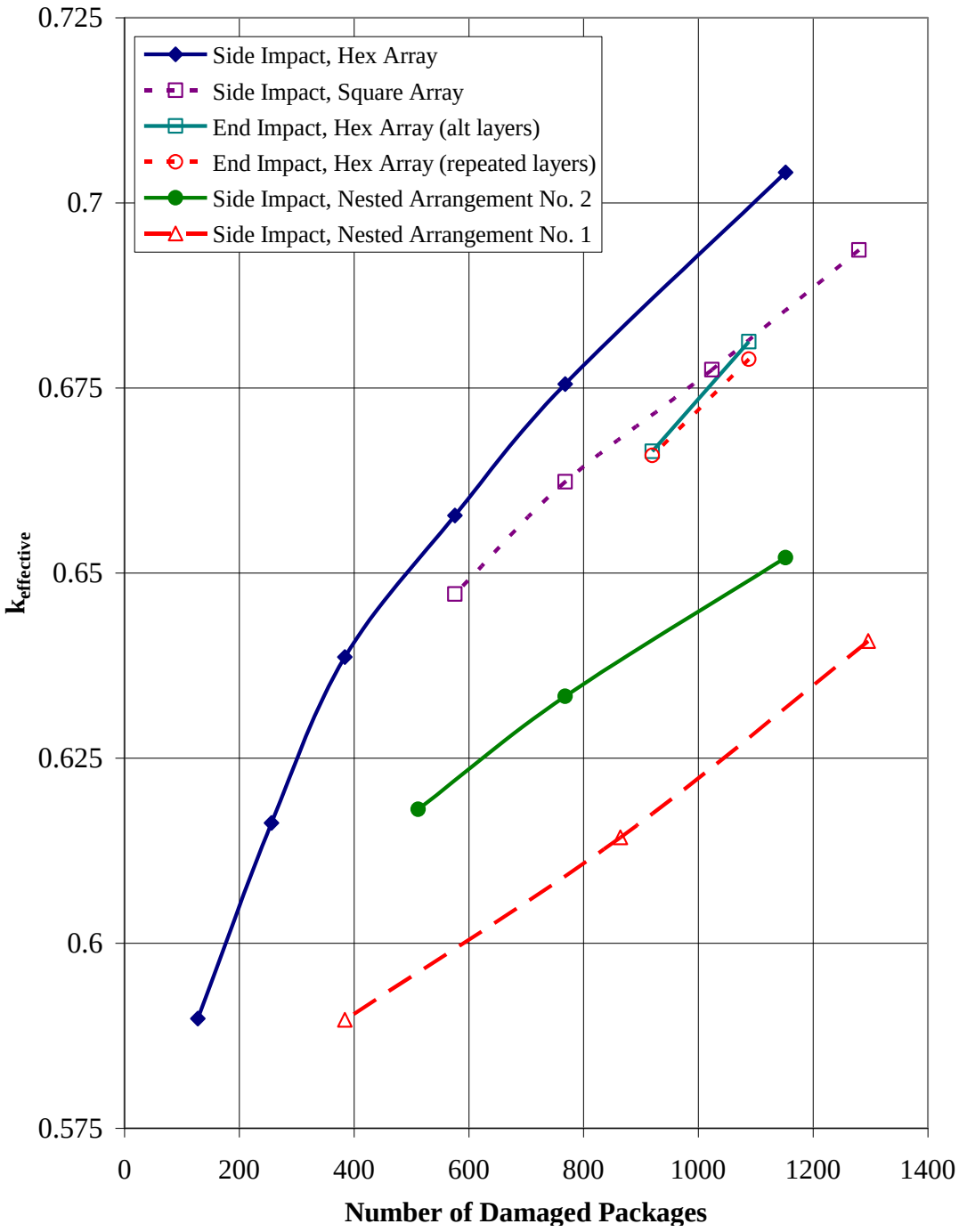

Figure 6-19. Damaged Package Array Study

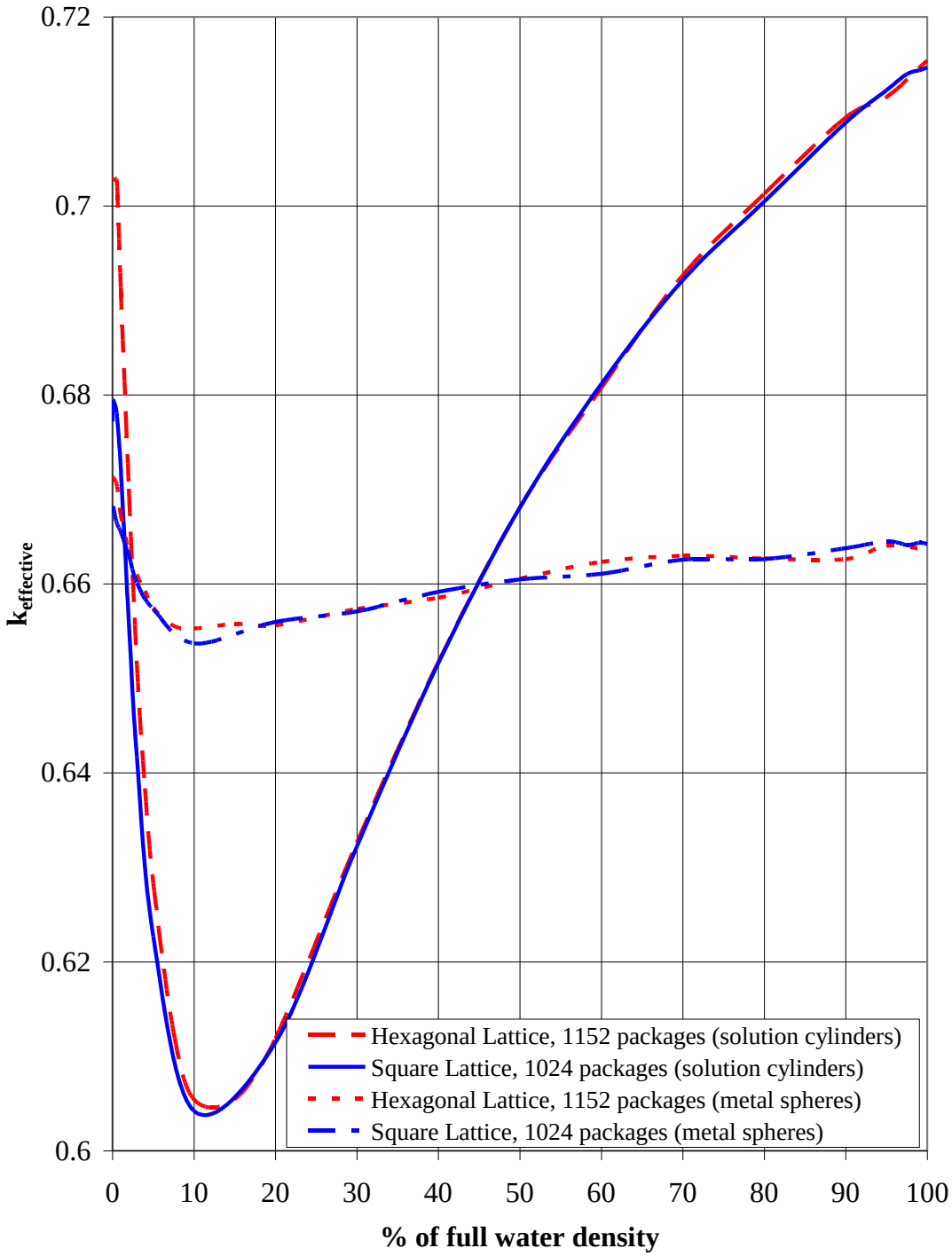

Figure 6-20. Damaged Package Array Internal (redwood zone) Moderation Study

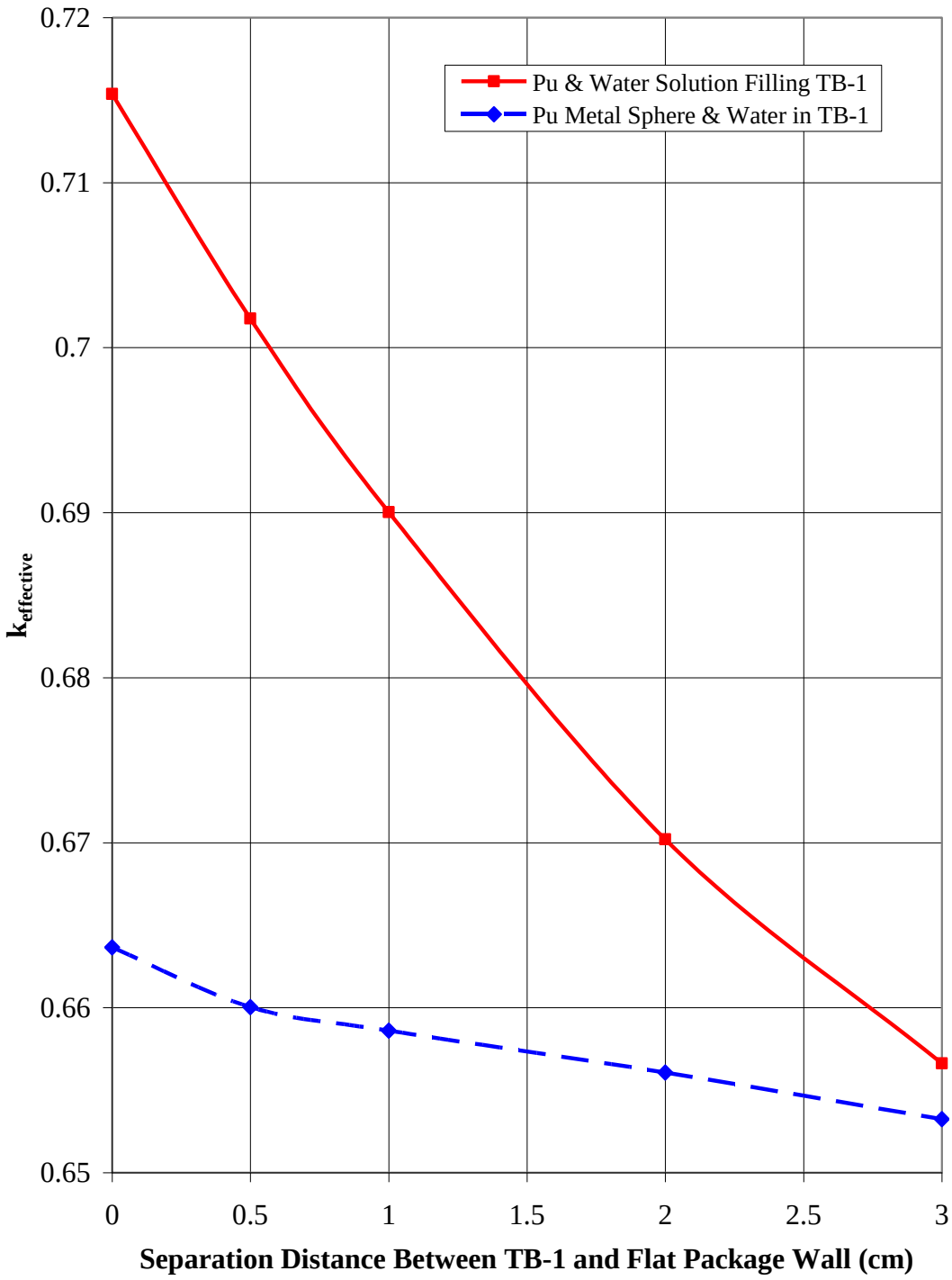

Figure 6-21. Damaged Package TB-1 Location Study

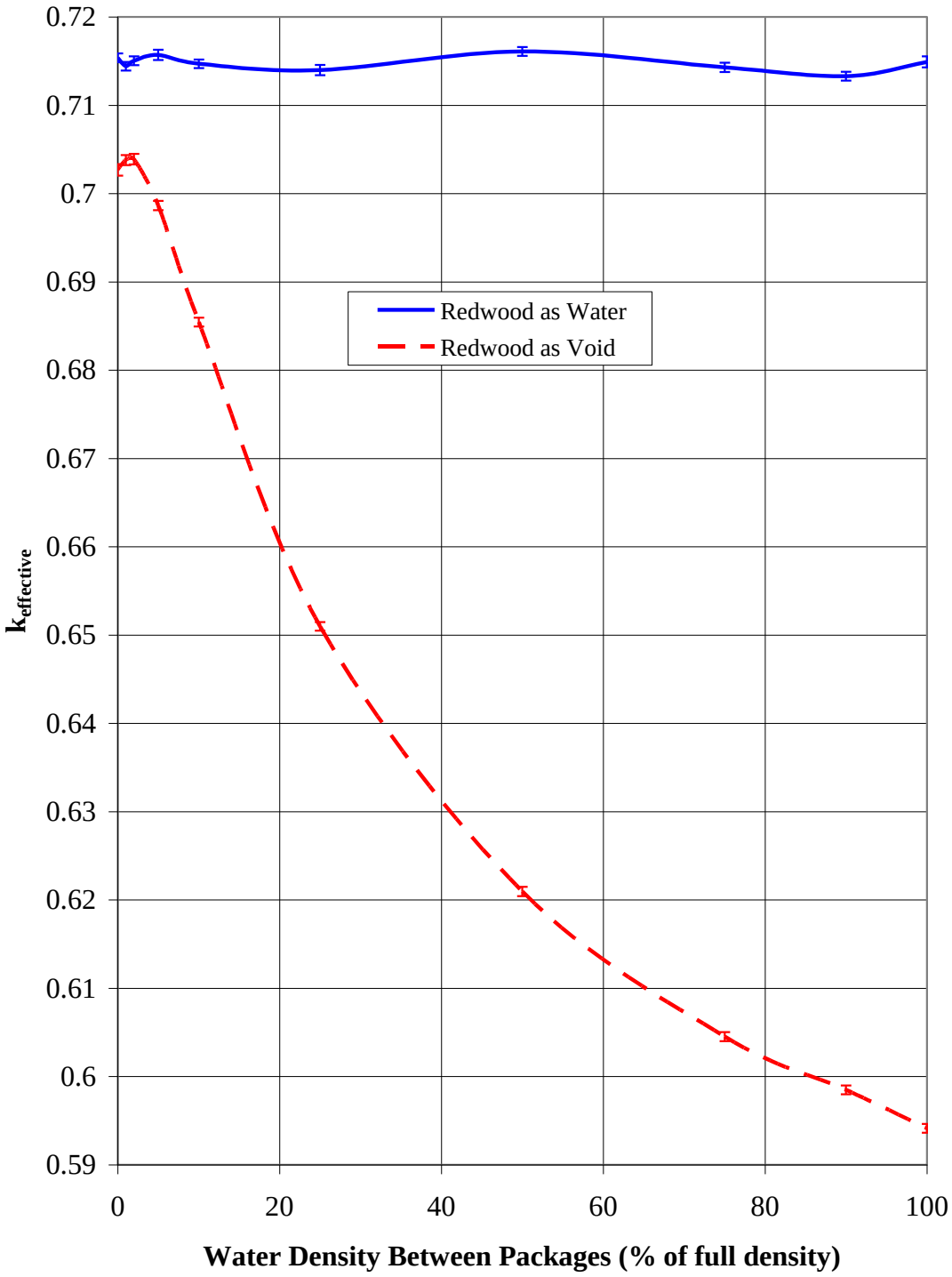

Figure 6-22. Damaged Package External Moderation Study

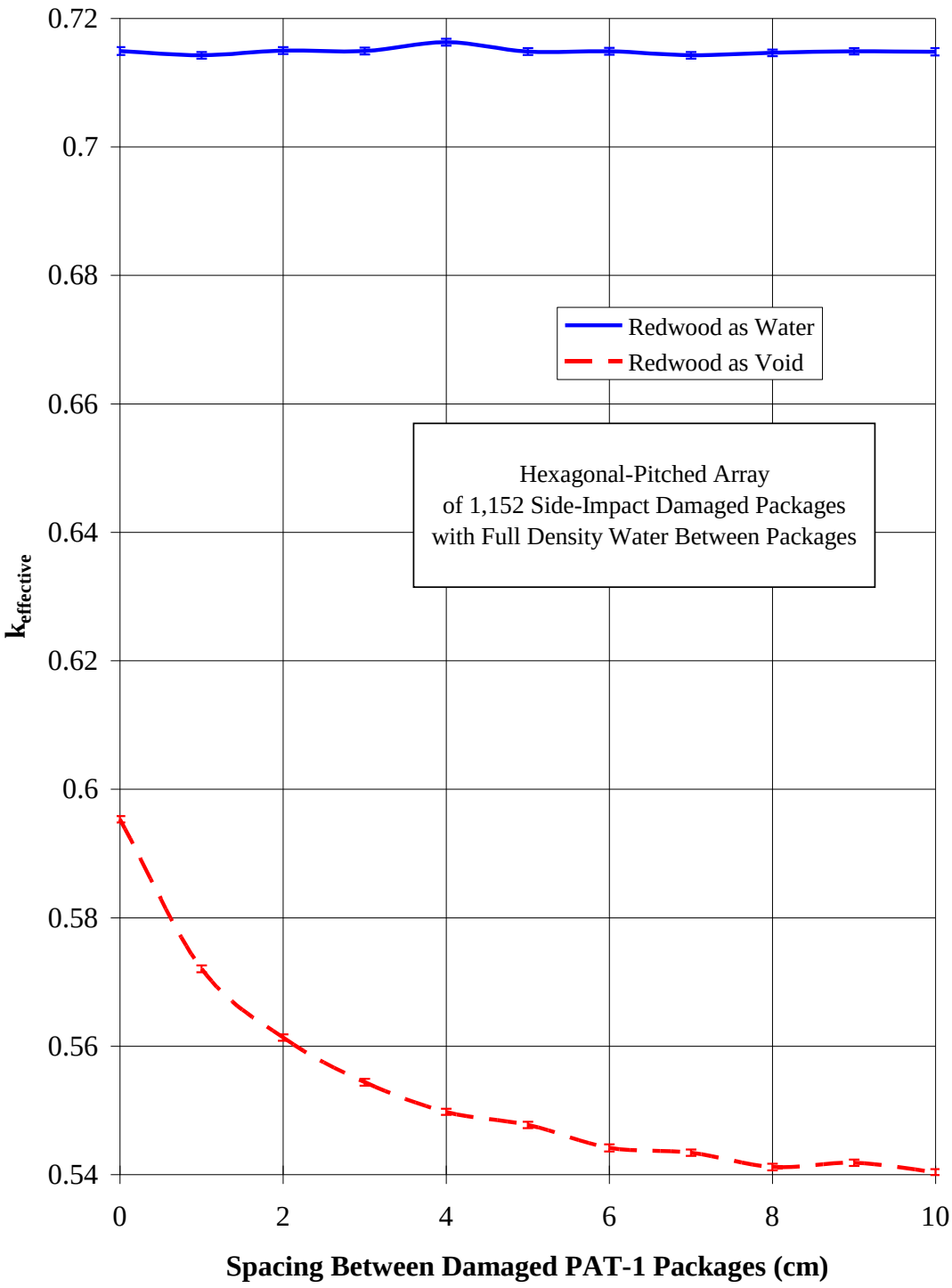

Figure 6-23. Damaged Package External Moderation Study (Package Spacing Varied)

This study shows that the highest k_{eff} value would be obtained with 1300 g (2.87 lb) Pu mixed with 1412 g of water in the TB-1 and with all of the wood replaced with full density water. Because this is the limiting hypothetical accident condition case, an additional study was performed with the side-impact damaged package array to demonstrate that the highest k_{eff} value was obtained with the TB-1 immediately adjacent to the flat side of the package. Figure 6-21 shows the results of calculations in which the TB-1 containment vessel was moved away from the flat side of the package. The redwood zone was modeled as full density water in these calculations. Note: from Figure 6-21 that the highest k_{eff} value is obtained with the TB-1 containment vessel immediately adjacent to the flat side of the package.

Consideration of optimum moderation between packages is also required. Figure 6-22 shows the results of a study in which water with density varying between 0% and 100% was placed between the packages. Figure 6-23 shows the results of a study in which full density water is placed between packages and the distance between packages is varied from 0 to 10 cm (0 to 3.9 in.). Calculations were performed with models for both of the maxima shown in Figure 6-21, namely the redwood modeled as either void or full density water. For the series in which the redwood was modeled as full density water, the water between the drums has no impact on the value of k_{eff}. The minor variation in the curve is due solely to variation introduced by the Mont Carlo method. For the series in which the redwood is modeled as void, adding water between the packages significantly reduces the k_{eff} value.

Considering the discussion provided above, the configuration producing the maximum k_{eff} value for the hypothetical accident conditions is case *hexs100*. This model has 1300 g (2.87 lb) Pu mixed with 1412 g (3.113 lb) of water in the TB-1 containment vessels in 1152 side-impact damaged packages arranged, touching, as shown in Figure 6-12. In this model, the redwood, aluminum, copper, and gaps inside the PAT-1 are modeled as full density water. Optimum moderation between containers was studied and found to have no impact.

6.3.4.4 Single Package Under Expanded Hypothetical Accident Conditions of 10 CFR 71.55(f)

Title 10 CFR 71.55(f) addresses additional requirements applicable to fissile material packages designed to be transported by air. The specifications in 10 CFR 71.55(f) permit use of an assumption that there is no water in-leakage. Considering this assumption, and due to the limited quantity of Pu and hydrogenous packaging that could be present in the TB-1 containment vessel, the analysis in this section shows that criticality cannot be achieved with a single package. Note: that the up to 1412 g (3.113 lb) of water that may be inside the TB-1 vessel is a bounding model for the presence of hydrogenous and other nonneutron multiplying packaging materials. This does not represent water that has leaked into the TB-1.

The criticality analysis considers the remainder of the volume within the TB-1 that is not filled by the Pu may be filled with full density water. This is a bounding model for the packaging materials that could be inside the TB-1. As shown in Section 45, the internal volume of the TB-1 containment vessel is no greater than 1478 cm^3. Because 1300 g (2.87 lb) Pu fills a minimum of 65.6 cm^3 (4.003 $in.^3$), there could be up to 1412 cm^3 (90.19 $in.^3$) of water in the TB-1. Because the package will have, at most, 1300 g (2.87 lb) Pu, a simple conservative analysis approach is used to show that a single damaged package remains subcritical. A series of calculations was performed where the 1300 g (2.87 lb) of Pu were mixed with from 0 to 1412 g (0 to 3.113 lb) of water. The radius of the Pu-water mixture sphere was varied from 2.5 cm

(0.98 in.) for a plutonium metal sphere, to 7.07 cm (2.78 in.) for the smallest sphere that can contain 1300 g (2.87 lb) Pu and 1412 g (3.113 lb) of water, and beyond. As required by 10 CFR 71.55(f)(1), the sphere is reflected by 20 cm (7.8 in.) of water.

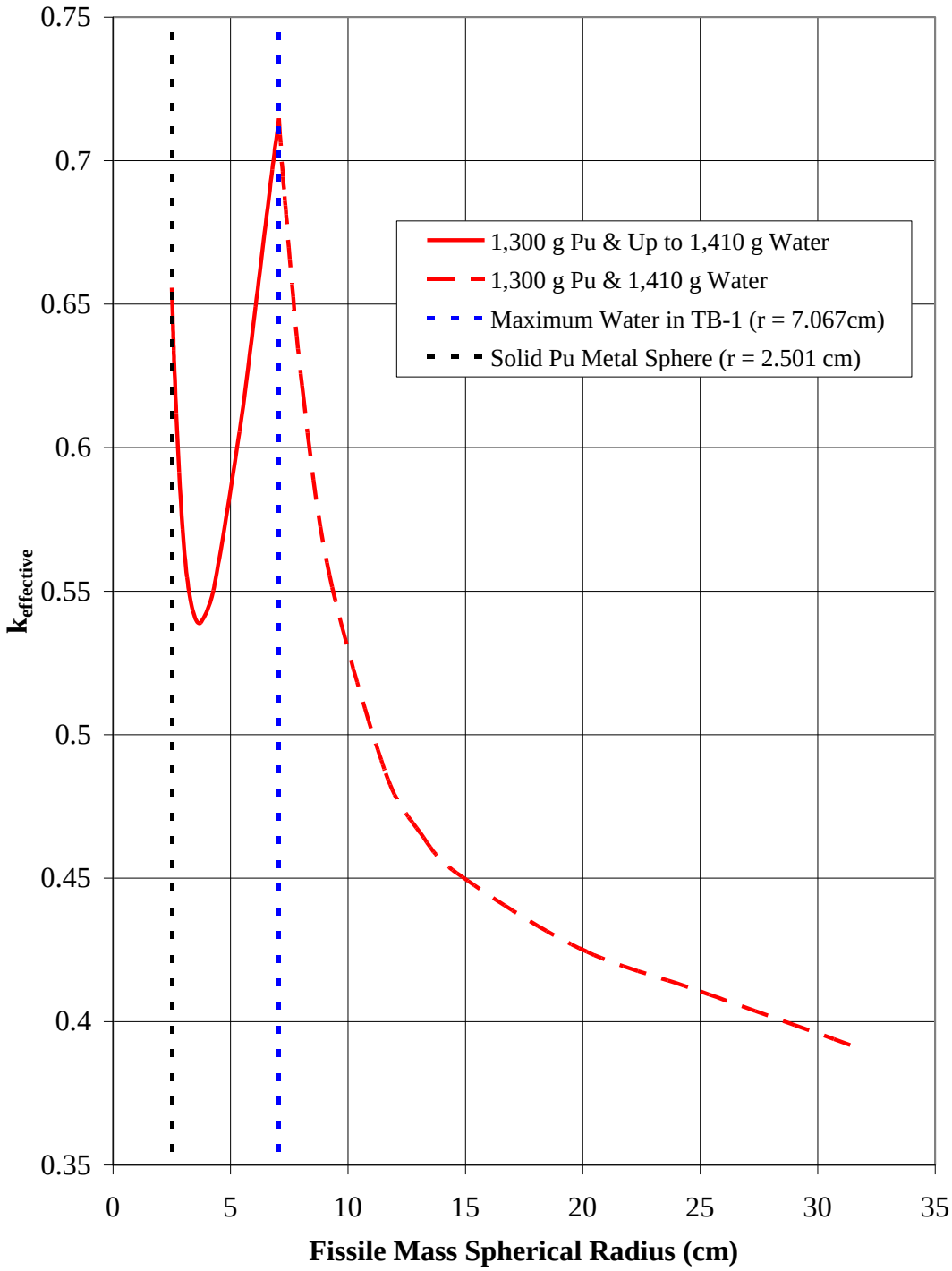

Figure 6-24. Single Package HAC for Air Transport

The results of this study are presented in Figure 6-24. The maximum k_{eff} value of 0.7147 ± 0.0005 was generated by case *sph14*. This analytical approach takes no credit for the dimensions or presence of any structural materials. Consequently, the results of the various tests specified by 10 CFR 71.55(f) do not affect the analysis. The analysis reported in this section takes no credit for the continued presence of any package materials or any package dimensions. The analysis documented in this section is different from the analysis that was presented in Section 6.3.4.1, because this analysis takes credit for the maximum internal diameter of the TB-1 containment vessel.

6.4 Single Package Evaluation

6.4.1 Configuration

The purpose of this section is to demonstrate that a single package is subcritical under both normal conditions of transport and HAC, as specified in 10 CFR 71.55(b) and 10 CFR 71.55(d)(2)-(d)(4). The limiting configuration for these conditions was demonstrated in Section 6.3.4.1.

From Section 1.2.1 of Reference 2, the PAT-1 container is 108 cm (42.52 in.) long and has a diameter of 62.2 cm (24.49 in.). From Section 6.3.1.2, the simplified model is 101.28 cm long and has a diameter of 56.6 cm (22.28 in.). The criteria specified in 10 CFR 71.55(d)(4)(i) and (ii)–consideration of a 5% reduction in volume and spacing–are met because the evaluation model has a diameter that is 9% smaller than the actual package and is 6% shorter than the actual package. The volume of the simplified model is 22% smaller than the actual package. Consequently, criticality safety has been evaluated with a 5% reduction in packaging volume and a 5% reduction in the effective spacing between fissile contents and the outer surface of the packaging. The criteria specified in 10 CFR 71.55(d)(4)(iii) is met because there are no apertures in the outer surface of the packaging large enough to permit entry of a 10 cm (4 in.) cube.

The bounding model adopted for the single package evaluation is the simplified model described in Section 6.3.1 with the wood and outer steel container replaced with water. As demonstrated in Section 6.3.4.1, the case *cv031* yielded the highest k_{eff} value. In this calculation, 1300 g (2.87 lb) of Pu-239 was spread throughout the internal volume of the TB-1 containment vessel and mixed homogenously with 1412 g (3.113 lb) of water. This model was reflected by 30 cm (11.8 in.) of full density water.

This model is bounding for both the single package normal conditions of transport and hypothetical accident conditions, because the TB-1 containment vessel already holds as much water as it can. No further in-leakage is possible. In the bounding case, the redwood, load spreader, gaps, and outer steel drum are modeled as full density water. Consequently, no further in-leakage into the package is possible. As seen in Figure 6-7, the model yields a far higher k_{eff} value when the steel and redwood are modeled as full density water than when they are modeled as steel and redwood. As described in NUREG-0361,[2] the test specified for normal conditions of transport had negligible effect on the package geometry. Additional discussion is provided in Section 6.3.4.1 supporting the concept that this model is the bounding model for both normal conditions of transport and hypothetical accident conditions.

6.4.2 Results

The maximum k_{eff} value of 0.7076 ± 0.0006 was produced by Case *cv031,* in which 1300 g (2.87 lb) of Pu-239 was spread throughout the internal volume of the TB-1 containment vessel and mixed homogenously with 1412 g (3.113 lb) of water. As determined in Section 6.8.2.5, an upper subcritical limit (USL) of 0.9456 is applicable to this case. Because the calculated k_{eff} value plus two standard deviations is less than the USL, a single package is subcritical under both normal conditions of transport and the single package hypothetical accident conditions.

6.5 Evaluation of Package Arrays under Normal Conditions of Transport

6.5.1 Configuration

The purpose of this section is to demonstrate that 2500 (5 × N, where N = 500) packages with nothing between the packages are subcritical. The limiting configuration for these conditions was demonstrated in Section 6.3.4.2.

As shown in Section 6.3.4.2, each package in the selected limiting configuration has a 1300 g (2.87 lb) Pu-239 metal sphere surrounded by 1412 g of water inside the TB-1 containment vessel. The "simplified" model shown in Figure 6-2 was used, with the redwood modeled as full density water. The model has 2646 packages in a 19 × 15.5 × 9 hexagonal-pitched array with 30 cm (11.8 in.) of close-fitting full density water around the outside of the array.

6.5.2 Results

The maximum k_{eff} value of 0.6509 ± 0.0005 was produced by case *fhlsf001*. As determined in Section 6.8.2.3, a USL of 0.8893 is applicable to this case. Because the calculated k_{eff} value plus two standard deviations is less than the USL, an array of 2646 packages is subcritical under normal conditions of transport. Thus a smaller array of 2500 packages is also subcritical under normal conditions of transport.

6.6 Package Arrays under Hypothetical Accident Conditions

6.6.1 Configuration

The purpose of this section is to demonstrate that 1000 (2 × N, where N = 500) damaged packages are subcritical. The limiting configuration for these conditions was demonstrated in Section 6.3.4.3.

As was shown in Section 6.3.4.3, each package in the selected limiting configuration has 1300 g (2.87 lb) Pu-239 metal homogenously mixed with 1412 g (3.113 lb) of water inside the TB-1 containment vessel. The "side impact" model shown in Figure 6-4 was used, with the redwood modeled as full density water. The model has 1152 packages arranged in a near cubic array. Pairs of packages are arranged in a tight-fitting hexagonal array. Figure 6-12 shows how the packages are arranged in each of the six layers. Note: that this model uses a reflective boundary condition along the bottom and left-hand side of the figure such that each of the six layers has four times as many packages than are shown in the figure. As was shown in Section 6.3.4.3, optimum interspersed moderation is achieved with nothing present between the packages. A close-fitting 30-cm-thick (11.8-in.-thick) full-density-water reflector completely encloses the array.

6.6.2 Results

The maximum k_{eff} value of 0.7154 ± 0.0005 was produced by case *hexs100*. As determined in Section 6.8.2.4, a USL of 0.9396 is applicable to this case. Because the calculated k_{eff} value plus two standard deviations is less than the USL, an array of 1152 packages is subcritical under hypothetical accident conditions. Thus, a smaller array of 1000 packages is also subcritical under hypothetical accident conditions.

6.7 Fissile Material Packages for Air Transport

6.7.1 Configuration

The purpose of this section is to demonstrate that a single package, subjected to the additional tests and conditions specified in 10 CFR 71.55(f) for fissile material package designs to be transported by air, would be subcritical. As shown in Section 6.3.4.4, the limiting configuration is a sphere with a radius of 7.067 cm, containing 1300 g (2.87 lb) of Pu-239 mixed homogenously with 1412 g of water, and reflected by 20 cm of water.

6.7.2 Results

The maximum k_{eff} value of 0.7147 ± 0.0005 was produced by case *sph14*. As determined in Section 6.8.2.5, a USL of 0.9462 is applicable to this case. Because the calculated k_{eff} value plus two standard deviations is less than the USL, a single package, with no water in-leakage, is subcritical without taking any credit for packaging materials and dimensions.

6.8 Benchmark Evaluations

The purpose of the benchmark evaluations is to validate the computational method used to calculate the neutron multiplication factors (e.g., k_{eff} values) for the limiting safety calculations involving plutonium metal and packaging materials that comprise a loaded PAT-1 package and water that is placed in and around the PAT-1 packages for the safety analysis. Validation is completed using the same computational methods to model critical configurations, which are similar to the limiting safety calculations, and performing statistical analyses to determine upper subcritical limits applicable to the safety calculations. The computational method is described in Section 6.3.3.

The process used to validate the computational method for the PAT-1 packages is comprised of the following steps:

1. Identify the limiting application systems and the ranges of parameters and conditions for which the validation will apply.

2. Select critical benchmark configurations for consideration based on similarities in physical characteristics between the limiting application systems and critical benchmark configurations.

3. Identify applicable critical benchmark configurations based on neutronic similarity between the application systems and the selected critical benchmark configurations, as determined by comparing characteristic parameters such as the hydrogen to Pu-239 atom

ratio (H/Pu) and the energy of average lethargy of neutrons causing fission (EALF) and by using the SCALE 5.1 sensitivity/uncertainty computational tools (TSUNAMI).[37, 38]

4. Use the results from the critical experiment models to determine the USLs that are applicable to the limiting applications using accepted statistical analysis techniques and industry tools. Only critical experiments that have neutronic similarities–that is, similar material compositions, neutron spectra, and leakage–with the application systems are used in the determination of the USLs. As is described in Section 6.8.2, the USLs include bias, bias uncertainty, administrative margin, and any additional margin that may be required by the statistical technique used to derive the USLs.

6.8.1 Applicability of Benchmark Experiments

All critical configurations used in the benchmark evaluation were selected from the *International Handbook of Evaluated Criticality Safety Benchmark Experiments* (IHECSBE) from the Nuclear Energy Agency of the Organization for Economic Co-operation and Development (OECD-NEA).[39] The IHECSBE contains evaluations of criticality benchmark experiments that have been peer reviewed by an international group of experts. Each evaluation contains a detailed description of the critical configuration with an extensive analysis of any assumptions and biases resulting from the difference between the actual experimental configuration and its description.

CSAS25/KENO V.a[3534, 36] models of a large portion of the critical benchmark configurations in the evaluated experiments contained in the IHECSBE have been created by Oak Ridge National Laboratory (ORNL) staff. TSUNAMI-3D[37] was used to perform sensitivity analysis for each of these critical configurations. TSUNAMI-3D uses flux moment data, generated by forward and adjoint Monte Carlo calculations, in a first-order linear perturbation theory method to calculate energy-, nuclide-, reaction-, and mixture-dependent k_{eff} sensitivity data. As part of the PAT-1 validation study, TSUNAMI-IP[38] was used to compare the k_{eff} sensitivity data of the safety calculations to the sensitivity data for about 240 Pu-critical experiment configurations. TSUNAMI-IP yields a correlation coefficient, c_k, which is a measure of how similar each critical configuration is to each of the limiting safety applications. The correlation coefficients were used to identify 125 critical configurations that are most similar to the limiting safety applications. These critical configurations include the following: 7 plutonium metal spherical assemblies with and without a reflector; 29 Pu-polystyrene slabs with and without a reflector; and 89 Pu solutions in spheres or cylinders. The 125 critical benchmark configurations, the evaluated experiment they are from, and brief descriptions are listed in Section 6.9.3.

The similarity or applicability of critical configurations to specific criticality analysis cases was assessed by comparing characteristic neutron parameters (EALF, H/Pu, and c_k) for the safety analysis cases with those from the critical configurations. The energy from average lethargy of neutrons causing fission (EALF) values were extracted from the KENO V.a output. The H/Pu ratios were calculated from the composition information for the mixture containing the Pu. Ideally, the sets of validation experiments should have EALF and H/Pu values bounding the analysis cases and have data points near the EALF and H/Pu values for the safety applications. The c_k parameter provides a more detailed neutronic comparison of the safety cases and validation experiments. A c_k of 1 indicates perfect similarity, and a c_k value greater than 0.9 indicates good similarity for validation purposes. More details are provided below on performing similarity analysis using the SCALE 5.1 sensitivity and uncertainty tools.

TSUNAMI-3D calculations were performed for the set of 11 application models that are representative of the limiting normal and hypothetical accident conditions. A brief description of each application is provided below with its acronym.

- *cv001* – The application consists of a single sphere consisting of 1300 g (2.87 lb) of Pu-239 metal centered in a cylinder of water approximately the volume of a PAT-1 package.

- *cv031* – The application consists of a single cylinder containing a Pu-239 metal-water mixture having 1300 g (2.87 lb) of Pu homogeneously mixed with sufficient water to fill the inside volume of a TB-1 container. This Pu-water cylinder is then centered in a cylinder of water approximately the volume of a PAT-1 package.

- *sph14* – The application consists of a single sphere containing a Pu-239 metal-water mixture having 1300 g (2.87 lb) of Pu-239 homogeneously mixed with sufficient water to fill the inside volume of a TB-1 container reflected by 20 cm (7.87 in.) of water.

- *fhlsf001* – The application consists of a roughly cubic-shaped hexagonal-pitch array of 2646 PAT-1 packages, with each position containing the following geometry. The innermost region contains a 1300 g (2.87 lb) Pu-239 metal sphere centered in a water cylinder representing the inside of a TB-1 container. This is centered in a steel cylinder representing the TB-1 container. The space between the TB-1 container and outer PAT-1 container is filled with water. The water is surrounded by a steel cylinder representing a PAT-1 outer container. The space between PAT-1 packages is void and a 30-cm-thick (11.81-in.-thick) water reflector surrounds the array on all sides.

- *fhlsf031* – The application consists of a roughly cubic-shaped hexagonal-pitch array of 2646 PAT-1 packages, with each position containing the following geometry. The innermost region contains a Pu-239 metal-water mixture having 1300 g (2.87 lb) of Pu-239 homogeneously mixed with sufficient water to fill the inside volume of a TB-1 container. This is centered in a steel cylinder representing a TB-1 container. The space between the TB-1 container and outer PAT-1 outer container is filled with water. The water is surrounded by a steel cylinder representing a PAT-1 outer container. The space between PAT-1 packages is void and a 30-cm-thick (11.81-in.-thick) water reflector surrounds the array on all sides.

- *fslsf001* – The application consists of a 17×17×9 square-pitched array of 2601 PAT-1 packages, with each position containing the following geometry. The innermost region contains a 1300 g (2.87 lb) Pu-239 metal sphere centered in a water cylinder representing the inside of a TB-1 container. This is centered in a steel cylinder representing a TB-1 container. The space between the TB-1 container and outer PAT-1 container is filled with water. The water is surrounded by a steel cylinder representing a PAT-1 outer container. The space between PAT-1 packages is void and a 30-cm-thick (11.81-in.-thick) water reflector surrounds the array on all sides.

- *fslsf031* – The application consists of a 17×17×9 square-pitched array of 2601 PAT-1 packages, with each position containing the following geometry. The innermost region

contains a Pu-239 metal/water mixture having 1300 g (2.87 lb) of Pu-239 homogeneously mixed with sufficient water to fill the inside volume of a TB-1 container. This is centered in a steel cylinder representing a TB-1 container. The space between the TB-1 container and outer PAT-1 container is filled with water. The water is surrounded by a steel cylinder representing a PAT-1 outer container. The space between PAT-1 packages is void, and a 30-cm-thick (11.81-in.-thick) water reflector surrounds the array on all sides.

- *hexs100* – A roughly cubic-shaped hexagonal-pitch array representing 1152 damaged PAT-1 packages. Each container holds a Pu-239 metal-water cylinder having 1300 g (2.87 lb) of Pu-239 homogeneously mixed with sufficient water to fill the inside volume of a TB-1 container. This is centered in a steel cylinder representing a TB-1 container. The outer PAT-1 container is a steel hemicylinder, representing a smashed container. The containers are then stacked flat side to flat side and loaded into a hexagonal array with each row rotated 90 degrees. The TB-1 container is located inside and immediately adjacent to the center of the damaged outer drum's flat side. The space between the TB-1 container and the damaged outer PAT-1 container is filled with water. The space between PAT-1 packages is void. A 30-cm-thick (11.81-in.-thick) water reflector surrounds the array on all positive faces (i.e., +x, +y, and +z). The model uses specular reflection on all negative faces.

- *hexsdry* – A roughly cubic-shaped hexagonal-pitch array representing 1152 damaged PAT-1 packages. Each container holds a Pu-239 metal/water cylinder having 1300 g (2.87 lb) of plutonium homogeneously mixed with sufficient water to fill the inside volume of a TB-1 container. This is centered in a steel cylinder representing a TB-1 container. The outer PAT-1 container is a steel hemicylinder, representing a smashed container. The containers are then stacked flat side to flat side and loaded into a hexagonal array with each row rotated 90 degrees. The TB-1 container is located inside and immediately adjacent to the center of the flat side of the damaged outer drum. The space between the TB-1 container and outer PAT-1 container is void. The space between PAT-1 packages is void. A 30-cm-thick (11.81-in.-thick) water reflector surrounds the array on all positive faces. The model uses specular reflection on all negative faces.

- *octs100* – A 4×8×4 square-pitched lattice representing 1024 damaged PAT-1 packages. Each container holds a Pu-239 metal/water cylinder having 1300 g (2.87 lb) of Pu-239 homogeneously mixed with sufficient water to fill the inside volume of a TB-1 container. This is centered in a steel cylinder representing a TB-1 container. The outer PAT-1 container is a hemicylinder, representing a smashed container. The containers are then stacked flat side to flat side and loaded into a square-pitched array. The TB-1 container is located inside and immediately adjacent to the center of the damaged outer drum's flat side. The space between the TB-1 container and outer PAT-1 container is filled with water. The space between PAT-1 packages is void. A 30-cm-thick (11.81-in.-thick) water reflector surrounds the array on all positive faces and specular reflection is used on all negative faces.

- *octsdry* – A 4×8×4 square pitched lattice representing 1024 damaged PAT-1 packages. Each container holds a Pu-239 metal/water cylinder having 1300 g (2.87 lb) of Pu-239 homogeneously mixed with sufficient water to fill the inside volume of a TB-1 container.

This is centered in a steel cylinder representing a TB-1 container. The outer PAT-1 container is a hemicylinder, representing a smashed container. The containers are then stacked flat side to flat side and loaded into a square-pitched array. The TB-1 container is located inside and immediately adjacent to the center of the damaged outer drum's flat side. The space between the TB-1 container and outer PAT-1 container is filled with void. The space between PAT-1 packages is void. A 30-cm-thick (11.81-in.-thick) water reflector surrounds the array on all positive faces and specular reflection is used on all negative faces.

The convergence of each of the CSAS25/KENO V.a and TSUNAMI-3D calculations for the set of 125 critical benchmark configurations and the 11 applications were assessed by reviewing the plot of average k_{eff} by generation run and the plot of average k_{eff} by generation skipped. No trends were observed in these plots that would be indicative of poor convergence. In addition, the frequency distribution plots were examined. These frequency distribution plots show single k_{eff} peaks, which is also an indication of convergence. The k_{eff} results of KENO V.a forward and adjoint calculations, which are used in the S/U (TSUNAMI-3D) analysis, were adequately similar, varying by less than 1% for most cases.

Although each application was examined individually, they were divided into four general groups with the members of each group having very similar neutronic characteristics. A short description of the types of critical benchmark configurations used to validate each group of applications is provided below. Table 6-6 provides a synopsis of each application and the critical benchmark configurations used for their validation.

- Metal Pu Spheres (*cv001, fhlsf001, fslsf001*) – These applications contain 1300 g (2.87 lb) plutonium metal spheres surrounded by water. The EALF of these three applications is between 54 and 80 keV. The critical benchmark configurations that best represent these applications are from the Plutonium Metal Fast (PMF) experiments and Plutonium Compound Mixed (PCM) experiments whose EALF values range from 1.76 keV to 1.27 Mev.

- Solution Lattices (*fhlsf031, fslsf031, hexs100, octs100*) – These applications contain Pu-water solutions surrounded by water in either a hexagonal or rectangular pitched lattice. The lattice is reflected by 30 cm (11.81 in.) of water.

- The EALF of these four applications is between 2.54 and 2.70 eV. The critical benchmark configurations that best represent these applications are primarily from the Plutonium Solution Thermal (PST) experiments and a few PCM experiments whose EALF values range from 0.147 to 6.446 eV.

- Single Solution Units (*cv031, sph14*) – These applications contain plutonium-water solutions surrounded by water. The EALF of the two applications is 1.094 and 1.259 eV respectively. The critical benchmark configurations that best represent these applications are from the PST experiments whose EALF values range from 0.112 to 5.405 eV.

Table 6-6. Summary of Similarity Between Benchmark Configurations and Applications

Application Name	Application			Critical Benchmark Configurations			
	k_{eff}	EALF (eV)	H/Pu	N[a]	EALF (eV)	H/Pu Ratio	c_k Values
cv001	0.6565	5.470E4	0.0	13	1.76E3 – 1.27E6	0.00 – 0.05	0.9158 – 0.9948
fhlsf001	0.6509	8.034E4	0.0	13	1.76E3 – 1.27E6	0.00 – 0.05	0.9178 – 0.9960
fslsf001	0.6504	7.957E4	0.0	13	1.76E3 – 1.27E6	0.00 – 0.05	0.9176 – 0.9958
fhlsf031	0.6324	2.682	28.8	60	0.147 – 6.446	15.46 – 220.19	0.8933 – 0.9362
fslsf031	0.6337	2.692	28.8	60	0.147 – 6.446	15.46 – 220.19	0.8903 – 0.9334
hexs100	0.7154	2.544	28.8	60	0.147 – 6.446	15.46 – 220.19	0.8979 – 0.9517
octs100	0.7147	2.531	28.8	60	0.147 – 6.446	15.46 – 220.19	0.8974 – 0.9505
cv031	0.7076	1.091	28.8	95	0.112 – 5.405	15.46 – 258.46	0.9018 – 0.9604
sph14	0.7147	1.255	28.8	95	0.112 – 5.405	15.46 – 258.46	0.9088 – 0.9588
hexsdry	0.7027	4.845	28.8	33	0.254 – 37.727	15.46 – 131.30	0.9059 – 0.9741
octsdry	0.6772	5.020	28.8	33	0.254 – 37.727	15.46 – 131.30	0.9025 – 0.9706

[a] Number of critical configurations in validation set.

- Dry Lattices (*hexsdry*, *octsdry*) – These applications contain plutonium-water solutions with no surrounding hydrogenous material. The array, however, is surrounded by 30 cm of water. The EALF is 4.864 and 5.042 eV respectively. The critical benchmark configurations that best represent these applications are primarily from the PCM experiments and a few PST experiments whose EALF values range from 0.254 to 37.727 eV.

TSUNAMI-3D was used to calculate the sensitivity profiles used in the assessment of the similarity of the safety analysis models and the critical experiment models. When using TSUNAMI-3D the analyst selects from several analysis approaches depending upon the nature and complexity of the problem. The analyst verifies that a correct analytical approach was used by performing direct perturbation calculations. These calculations involve running additional k_{eff} calculations with the densities of selected nuclides or mixtures varied to show effect of these changes on system k_{eff}. The direct perturbation results are then compared with the TSUNAMI sensitivity analysis results, confirming that an appropriate analytical approach was used. Generally, it is not necessary to perform direct perturbation calculations for all nuclides in a problem. Typically, direct perturbations calculations are performed for the primary fissile nuclide and the primary neutron moderator. It is not necessary to perform direct perturbation calculations for every nuclide mixed in with the primary fissile nuclide or mixed in with the primary moderator because checking those two nuclides ensures that the forward and adjoint neutron transport solutions used in the TSUNAMI calculation are adequately converged and the problem has enough spatial resolution to adequately capture local variations. Additional direct

perturbation calculations may also be performed for other key model features, such as neutron poison panels in a spent fuel storage rack.

To verify the TSUNAMI-3D sensitivity analysis, a representative sample of the critical benchmark configuration set was selected for direct perturbation analysis. The 15 critical benchmark configurations in this sample were analyzed by increasing and decreasing the Pu-239 concentration and, where possible, the hydrogen concentration such that the resulting k_{eff} values span approximately 10 standard deviations. The sensitivities from the direct perturbation results were then compared to the sensitivities produced by TSUNAMI-3D. For the critical benchmark configurations, the direct perturbation sensitivities compare to the TSUNAMI sensitivities within approximately 2 standard deviations in all but one case as shown in Section 6.9.3. Thus, the direct perturbation results confirm that the TSUNAMI-3D calculations were performed properly.

The TSUNAMI-3D sensitivity analyses for each of the 11 applications were also verified using direct perturbation analysis. The applications were analyzed by increasing and decreasing the Pu-239 concentration and water concentration such that the resulting k_{eff} values span approximately 10 standard deviations. The sensitivities from the direct perturbation results were then compared to the sensitivities produced by TSUNAMI-3D. For the set of 11 applications, the direct perturbation sensitivities compare to the TSUNAMI sensitivities within 2 standard deviations for all cases as shown in Table 6-10 in Section 6.9.3. Thus, the direct perturbation results confirm that the TSUNAMI-3D calculations were performed properly.

The similarity of the critical benchmark configurations to each application was evaluated by comparing the EALF values and H/Pu ratios of the critical experiments to the values from the applications. The application EALF and H/Pu values are similar to the values from the critical configurations. Similarity was also evaluated by examining the c_k values produced when comparing the available critical benchmark configurations to each application using TSUNAMI-IP.[38] The value of the TSUNAMI global integral index, c_k, measures the correlation of sensitivity and nuclear data uncertainty between systems. Systems that have highly correlated sensitivities and nuclear data uncertainties should exhibit similar calculation biases, because the sensitivity is a measure of system response to data variation or data errors. A c_k value of 1.0 indicates that the experiment and application are identical in terms of sensitivity and uncertainty data. Critical benchmark configurations, with correlation coefficient (c_k) values greater than 0.8, are considered marginally applicable.[44] Critical configurations, with c_k values greater than 0.9, are considered applicable to the validation of the application.

The applications were sorted into groups based on their similarity in nuclear parameters and sensitivities to the critical benchmark configurations. A set of critical benchmark configurations having the highest c_k values was selected for each application to be included in the validation. The EALF and H/Pu ratios of the critical benchmark configurations with the highest c_k values were then checked to see if they encompassed the application. The goal was to have as many as possible critical benchmark configurations in the validation for each application that had c_k values greater than 0.9. The set of critical benchmark configurations were then collected for each group. Section 6.9.3 contains lists of the critical benchmark configurations that have the highest c_k values of all the available Pu configurations relative to the applications.

Comparison of the EALF values, H/Pu ratios, and c_k values indicate that the critical configurations in the validation sets for the applications are similar to the associated applications as indicated primarily by the high c_k values.

Table 6-6 summarizes of the nuclear parameters of the applications and critical benchmark configurations used for each validation. Note that the validation sets for 5 of the 1 applications included fewer than 50 critical configurations. This is acceptable because the Distribution-Free Tolerance Limit Method used for the USL calculation in these sets is designed to be used with as few as 10 data points.

6.8.2 Bias Determination

This section describes the methods used to determine an USL for the applications evaluated in this report based on the critical benchmark configurations chosen as representative of the applications. Bias and bias uncertainty over the area of applicability of critical experiments are determined using the guidance in ANSI/ANS 8.1-1998, ANSI/ANS 8.17-2004, and ANSI/ANS 8.24-2007. The accuracy of the computational method and cross section data is established by evaluating critical experiments. Computational bias is the difference between calculated and experimental results. The uncertainty in bias is an allowance for uncertainties in the experiment conditions, the lack of accuracy and precision in the calculational method, and, if necessary, the extension of the area of applicability.

Generally, the bias and bias uncertainty are expected to be functions of various physical or neutronic parameters that can be determined using trending analyses. This technique can be applied to establish bias and bias uncertainty because k_{eff} values often exhibit an increasing or decreasing trend as a function of parameters such as fissile material concentration, hydrogen-to-fissile material ratio, EALF, sensitivity coefficient, etc., that can be distinguished from random behavior.

Statistical techniques exist for evaluating the bias and bias uncertainty, and for establishing limits that can reliably be used to predict subcriticality, such as tolerance band, single-sided tolerance limit, and distribution-free tolerance limit (nonparametric) methods.[40,41,42,43] These methods use bias and the bias uncertainty in combination with additional considerations (e.g., administrative margins, where applicable) to establish a critical limit (CL) (single value or a function, depending on the method applied) above which a desired fraction of the true population of k_{eff} values calculated for critical systems is expected to lie, with a prescribed confidence and within the area of applicability. The parametric methods typically require that the k_{eff} values for the applicable critical experiments form a normal distribution. When the k_{eff} values for the critical experiments are not normally distributed about a mean value, a nonparametric statistical treatment (i.e., distribution-free methods) should be used.[43]

The level of subcriticality required to maintain safety is calculated based on Section 5.1 of ANSI/ANS 8.17. For an application or system to be considered subcritical, the calculated multiplication factor for the system, k_s, must be less than or equal to an established maximum allowable multiplication factor based on benchmark calculations and uncertainty terms, as shown in Equation 6-1.

$$k_s \leq k_c - \Delta k_s - \Delta k_c - \Delta k_m \qquad \text{(Eq. 6-1)}$$

where

k_s = multiplication factor k_{eff} for the application or system for which subcriticality must be maintained;
k_c = the mean value of k_{eff} resulting from the calculation of benchmark criticality experiments using a specific calculational method and data;
Δk_s = uncertainty in the value of k_s;
Δk_c = uncertainty in the value of k_c;
Δk_m = an additional margin to ensure subcriticality.

The value of Δk_m is often referred to as the administrative margin and assigned an arbitrary limit of 0.05. This value is set in Method 1 and calculated in Method 2 of USLSTATS.[40]

If calculational bias, β, is defined as $\beta = k_c - 1.0$, then the uncertainty in the calculational bias is identical to the uncertainty in k_c, (i.e., $\Delta\beta = \Delta k_c$). The bias is defined as negative if $k_c \leq 1$ and positive if $k_c \geq 1$. By convention, a positive bias is never allowed; if $k_c \geq 1$, then k_c is set equal to 1.0.

The values of k_c and β may not be constant, but instead may vary over some parameter (e.g., EALF, H/Pu, correlation coefficient, etc.). In this case $k_c(x)$ and $\beta(x)$ are determined using a least squares fit over the calculated k_{eff} values as a function of the parameters of interest, x. Positive biases are not considered by setting $k_c(x) = 1.0$ wherever it is greater than 1.0.

Based on the criteria for subcriticality set forth in ANSI/ANS-8.17 and what is above, a USL can be determined using a set of critical experiment benchmarks. The USL is determined such that there is a high degree of confidence that a calculated result is subcritical; i.e., an application or system is considered subcritical with a high degree of certainty if a calculated k_{eff} plus calculational uncertainties lies at or below this limit ($k_s + \Delta k_s < \text{USL}$). Thus, the USL is the magnitude of the sum of the biases, uncertainties, and administrative and/or statistical margins applied to a set of critical benchmarks, such that with a high degree of confidence:

$$\text{USL} = 1.0 - \Delta k_m + \beta(x) - \Delta\beta(x). \qquad \text{(Eq. 6-2)}$$

Only the distribution-free tolerance method and the confidence band with administrative margin were used and are described in Sections 6.8.2.1 and 6.8.2.2, respectively. Derivation of USLs for each of the application groups is discussed in Sections 6.8.2.3 through 6.8.2.6. The results are summarized in Section 6.8.2.7.

6.8.2.1 Distribution-Free Tolerance Limit Method

The distribution-free tolerance limit method[43] is typically used to calculate a lower band threshold limit (LBTL) when the k_{eff} values for the critical experiments do not pass tests for normality.[43] This method involves sorting all k_{eff} values for the applicable critical experiments in ascending order and determining the degree of confidence for the fraction of the true population that lies above the smallest observed value. The percent confidence that a fraction of the population of k_{eff} values calculated for critical systems is above the lowest observed value can be determined using the following equation:

$$\beta = 1 - \sum_{j=0}^{m-1} \frac{n!}{j!(n-1)!}(1-q)^j q^{(n-j)}, \qquad \text{(Eq. 6-3)}$$

where

n = sample size (number of k_{eff} values),
m = rank order of the smallest k_{eff} value, and
q = the desired population fraction above the smallest k_{eff} value (normally 0.95).

For a desired population fraction of 0.95 and a rank order of 1 (the lowest data sample), Equation 6-3 reduces to

$$\beta = 1 - q^n = 1 - 0.95^n \qquad \text{(Eq. 6-4)}$$

The nonparametric margin is determined by first calculating β using Equation 6-4. The nonparametric margin is then determined using Table 2.2 in Reference 43. The single-valued *LBTL* function for nonparametric data analysis is then determined as follows:

LBTL = smallest k_{eff} – uncertainty for smallest k_{eff} – nonparametric margin. (Eq. 6-5)

Note that the confidence value determined by Equations 6-3 and 6-4 increases with increasing sample size and the nonparametric margin, in Equation 6-5, is used to account for small sample size.

6.8.2.2 USL Method 1: Confidence Band with Administrative Margin

The USLSTATS code, documented in Section 4 and Appendix C of Reference 40, Method 1 applies a statistical calculation of the bias and its uncertainty plus an administrative margin to a linear fit of the critical experimental benchmark data. The approach to this method is to first calculate a linear fit of the critical experiments, $k_c(x)$. To remove any positive bias, $k_c(x)$ is reset such that $k_c(x) = 1.0$ anywhere $k_c(x) > 1.0$. A confidence band for a single additional calculation is then determined. The width of this band is determined statistically based on the existing data and a specified level of confidence; the greater the standard deviation in the data or the larger the confidence desired, the larger the band width. This confidence band, W, accounts for uncertainties in the experiments, cross sections, and calculational method, and is therefore a statistical basis of Δβ, the uncertainty in the value of β. W is defined for a confidence level of $(1 - \gamma)$ using the relation

$$W = \max\{w(x)|_{x\min, x\max}\} \qquad \text{(Eq. 6-6)}$$

where

$$w(x) = t_{1-\gamma} s_p \left[1 + \frac{1}{n} + \frac{(x - \bar{x})^2}{\sum_{i=1,n}(x_i - \bar{x})^2}\right]^{\frac{1}{2}} \qquad \text{(Eq. 6-7)}$$

and

n = the number of critical calculations used in establishing $k_c(x)$,
$t_{1-\gamma}$ = the Student-t distribution statistic for 1-γ and n-2 degrees of freedom
S_p = the pooled standard deviation for the set of criticality calculations, and
x = the mean value of parameter x in the set of calculations.

Typically, W is determined at the 95% confidence level. For transport and storage packages, an administrative margin, Δk_m, 0.05 Δk is typically used.

Using the above formulas, the USL Method 1 is defined as

$$USL_1(x) = 1 - \Delta k_m - W + \beta(x). \quad \text{(Eq. 6-8)}$$

With one exception, the USLSTATS inputs are described in Appendix C of Reference 40. The exception is that the first word in the title must be "tsunami" when the trending parameter is c_k. Without this input, USLSTATS will not permit extrapolation of the USLs. When "tsunami" is included as the first word on the first line, USLSTATS will extrapolate to a c_k value of 1.0. The other input parameters used were as follows:

P	= 0.999	=	proportion of population falling above the lower tolerance level
$1 - \gamma$	= 0.95	=	confidence on fit
α	= 0.95	=	confidence on proportion P
x_{min}	= 0	=	minimum value of trending parameter
x_{max}	= 1.0	=	maximum value of trending parameter
σ_{sample}	= -1	=	estimated average standard deviation of all input values of k_{eff} a "-1" value directs USLSTATS to use third column of experiment-specific input
Δk_m	= 0.05	=	administrative margin used to ensure subcriticality

The remainder of the input is provided as three pieces of data for each critical configuration on individual lines. The first input is the value of the trending parameter. The second input is the calculated k_{eff} value divided by the expected k_{eff} value. The expected value is taken from the IHECSBE[39] and includes biases for simplifications used in describing the critical configuration. These expected and calculated k_{eff} values are provided in Section 6.9.3. The third parameter is the uncertainty in the calculated k_{eff} values. A USLSTATS input deck for application *cv031* is included in Section 6.9.5.5.

6.8.2.3 Metal Sphere Applications

The METAL SPHERE applications consist of three cases: *cv001, fhlsf001,* and *fslsf001*. A set of 13 selected, critical benchmark configurations are well correlated to the three applications from a neutronic perspective as represented by the range of c_k values calculated using TSUNAMI. The c_k values for the *cv001* application range from 0.916 to 0.995, the *fhlsf001* application range from 0.918 to 0.996, and the *fslsf001* application range from 0.918 to 0.996. Values above 0.9 indicate a high correlation between cases. The EALF and the H/Pu ratio of the three applications are contained within the range of these values from the set of critical benchmark configurations used in the validation. The EALF values of the three applications are 5.470e4, 8.034e4, and 7.957e4 eV; whereas the range of EALF values for the set of critical

benchmark configurations is 1.76e3 to 1.27e6 eV. The H/Pu ratios of the three applications are 0.0 where as the range of H/Pu ratios for the critical benchmarks ranges from 0.0 to 0.05. Both the H/Pu ratio and EALF for the three applications are bounded by the selected cases that have c_k values above 0.9.

The normality of the distribution of the k_{eff} values for the group of critical benchmark configurations used to validate the METAL SPHERE applications was checked using the Shapiro-Wilk Test.[43] This test was used because of the small number of samples in this group—only 13 critical benchmark configurations. The Chi-Squared (χ^2) Test implemented in USLSTATS requires a minimum of 25 samples. The test calculated W = 0.8546, which is less than the value from Table A.5 of Reference 43, which for $\alpha = 0.05$ and n = 13 is $W_t = 0.866$. This indicates the sample distribution test is not normally distributed. As is shown in Figure 6-25, the distribution has two peaks. For the samples to pass a normality test, the calculated W must be greater than the W test value from Table A.5 of Reference 43 for a given α and n.

Because the data is not normally distributed, the distribution-free tolerance limit method is used. The nonparametric margin is determined using Equation 6-3. Given a population (n) of 13 and a desired population fraction (q) of 0.95 the degree of confidence is calculated to be 48.6%. From Table 2.2 of Reference 43, a nonparametric margin of 0.05 needs to be included in the calculation of the USL. The resulting USL is 0.8893, which is calculated as follows:

USL = lowest k_{eff} value-combined Monte Carlo and experimental uncertainty-administrative margin-nonparametric margin

$$USL = 0.9916 - (0.0005^2 + 0.0022^2)^{0.5} - 0.05 - 0.05 = 0.8893$$

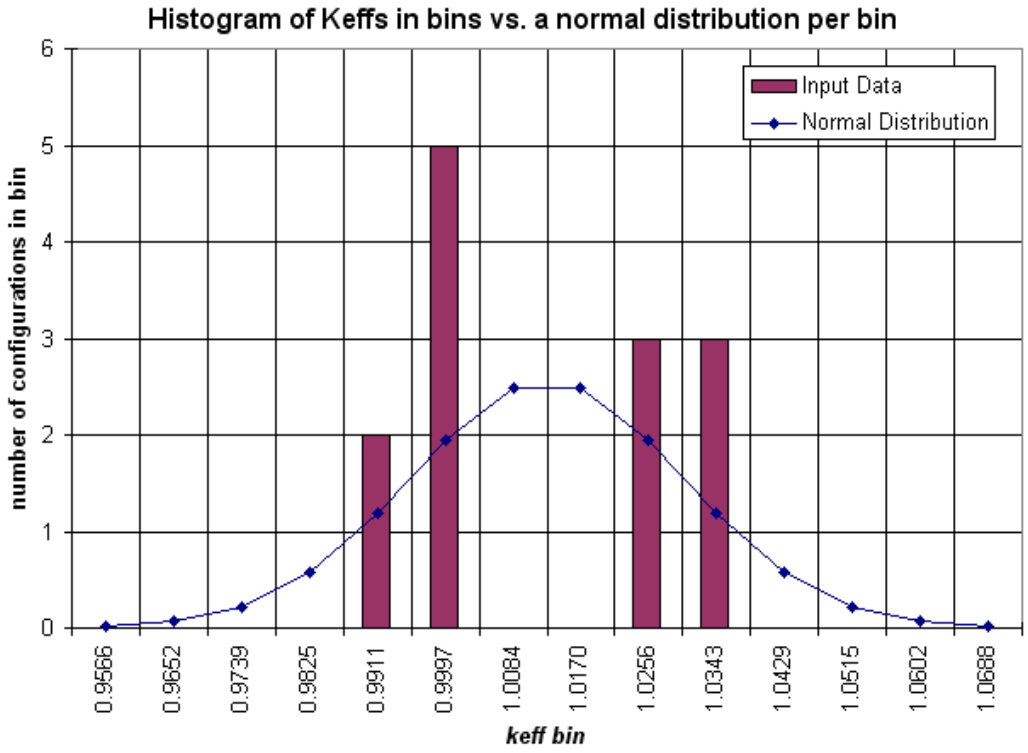

Figure 6-25. Pu Metal Sphere Critical Benchmark Histogram

6.8.2.4 Solution Lattice Applications

The SOLUTION LATTICE applications include four cases: *fhlsf031, fslsf031, hexs100,* and *octs100*. A set of 60 selected critical benchmark configurations are well correlated to the four applications from a neutronic perspective as represented by the range of c_k values calculated using TSUNAMI. The c_k values for the *fhlsf031* application range from 0.893 to 0.936, the *fslsf031* application range from 0.890 to 0.933, the *hexs100* application range from 0.898 to 0.952 and the *octs100* application range from 0.897 to 0.950. Values above 0.9 indicate a high correlation between cases. The EALF and the H/Pu ratio of the four applications are contained within the range of these values from the set of critical benchmark configurations used in the validation. The EALF values of the four applications are 2.682, 2.692, 2.544, and 2.531 eV; whereas the range of EALF values for the benchmark configurations is 0.147 to 6.446 eV. The H/Pu ratios of the four applications are 28.8 where as the range of H/Pu ratios for the benchmark configurations is 15.46 to 220.19. Both the H/Pu ratio and EALF for the four applications are bounded by the selected cases that have c_k values of approximately 0.9 or above.

The normality of the k_{eff} values for the group of critical benchmark configuration used to validate the SOLUTION LATTICE applications was checked using the χ^2 test. The test determined that the samples are not normally distributed. A visual inspection of the k_{eff} distribution, shown in Figure 6-26, shows a pronounced single peak with a long tail on the side with increasing k_{eff} and a very short tail on the side with decreasing k_{eff}.

Because the data is not normally distributed, the USL is determined using the distribution-free tolerance limit method described in Section 6.8.2.1. A nonparametric margin is determined using Equation 6-3. Given a population (n) of 60 and a desired population fraction (q) of 0.95, the degree of confidence is calculated to be 95.4%. From Table 2.2 of Reference 43, no additional nonparametric margin is needed to obtain a 95% confidence for 95% of the population. The resulting USL is 0.9396, which is calculated as follows:

USL = lowest k_{eff} value-combined Monte Carlo and experimental uncertainty-administrative margin-nonparametric margin

$$USL = 0.9956 - (0.0005^2 + 0.0060^2)^{0.5} - 0.05 - 0.0 = 0.9396$$

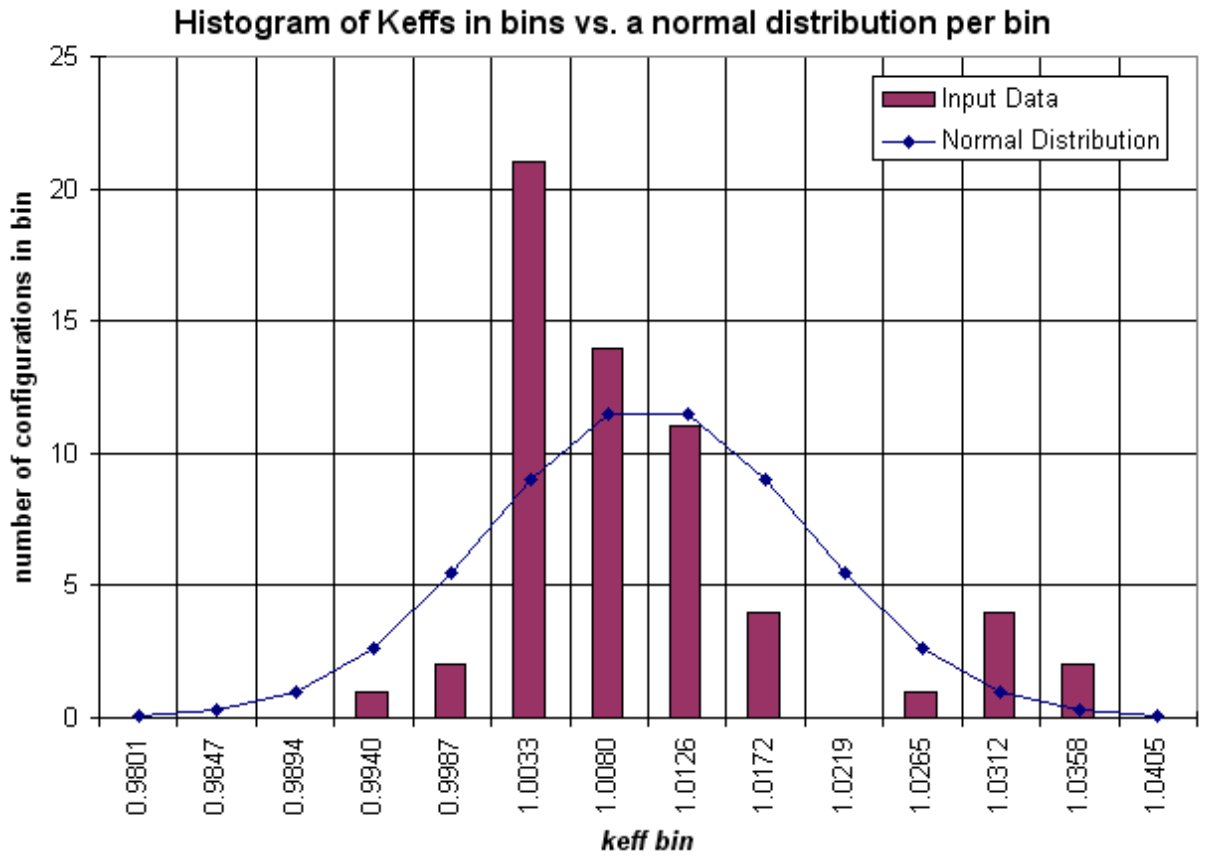

Figure 6-26. Solution Lattice Critical Benchmark Histogram

6.8.2.5 Single Unit Solution Applications

The SINGLE UNIT SOLUTION applications consist of two cases: *cv031* and *sph14*. A set of 95 selected critical benchmark configurations are well-correlated to the two applications from a neutronic perspective as represented by the range of c_k values calculated using TSUNAMI. The c_k values for the *cv031* application range from 0.902 to 0.961 and for the *sph14* application from 0.909 to 0.959. Values above 0.9 indicate a high correlation between cases. The EALF and the H/Pu ratio of the two applications are contained within the range of these values from the set of critical benchmark configurations used in the validation. The EALF values of the two applications are 1.091 and 1.255 eV; whereas the range of EALF values for the benchmark configurations is 0.112 to 5.405 eV. The H/Pu ratios of the two applications are 28.8 where as the range of H/Pu ratios for the benchmark configurations is 15.46 to 258.46. Both the H/Pu ratio and EALF for the two applications are bounded by the selected cases that have c_k values above 0.9 for both applications.

The normality of the k_{eff} values for the group of critical benchmark configuration used to validate the SOLUTION LATTICE applications was checked using the χ^2 test. The test determined that the 95 samples are not normally distributed. A visual inspection of the k_{eff} distribution, shown in Figure 6-27, shows a pronounced single peak with a long tail on the side, and increasing k_{eff} and a very short tail on the side with decreasing k_{eff}.

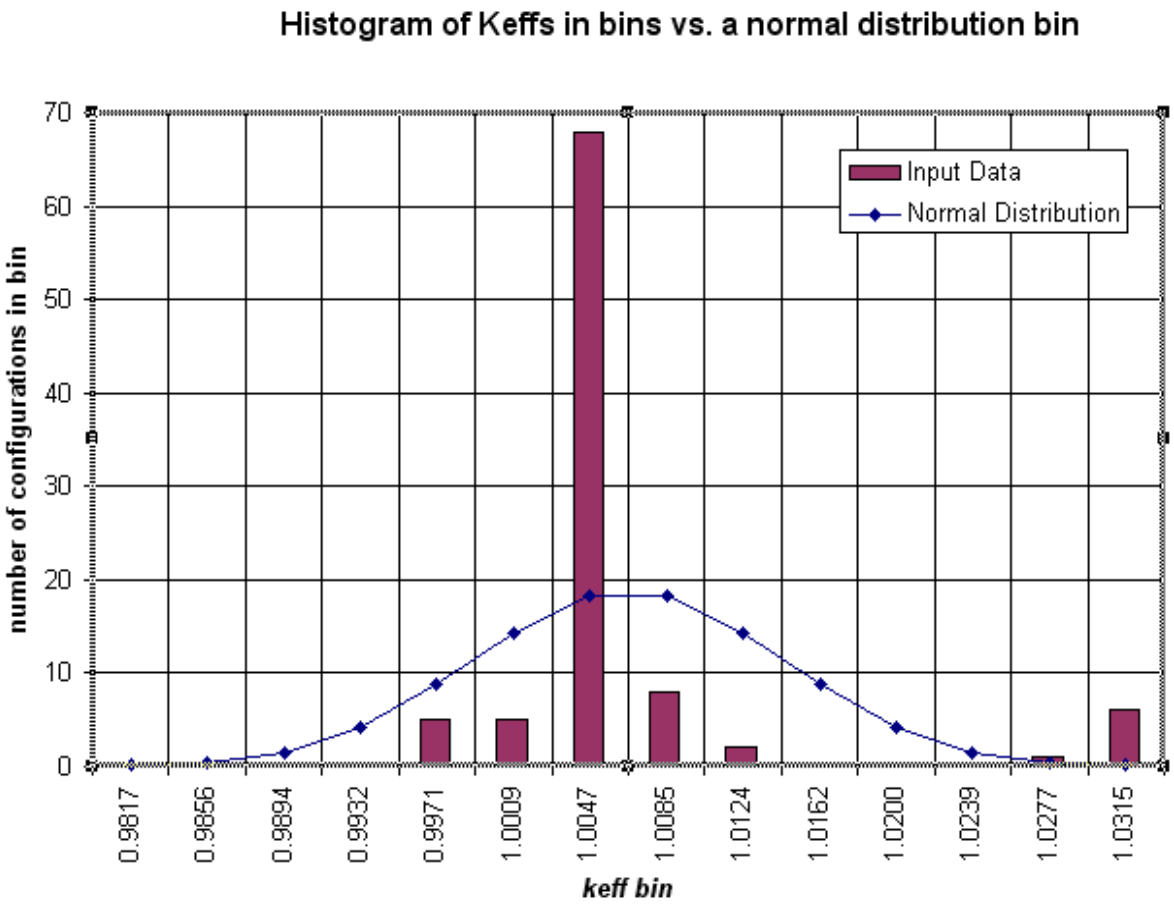

Figure 6-27. Single Unit Solution Critical Benchmark Histogram

Because the data is not normally distributed, the USL is determined using the distribution-free tolerance limit method described in Section 6.8.2.1. A nonparametric margin is determined using Equation 6-3. Given a population (n) of 95 and a desired population fraction (q) of 0.95 the degree of confidence is calculated to be 99.2%. From Table 2.2 of Reference 43, no additional nonparametric margin is needed to obtain a 95% confidence for 95% of the population. The resulting USL is 0.9383, which is calculated as follows:

USL = lowest k_{eff} value-combined Monte Carlo and experimental uncertainty-administrative margin-nonparametric margin

USL = $0.9956 - (0.0005^2 + 0.0073^2)^{0.5} - 0.05 - 0.0 = 0.9383$

6.8.2.6 Dry Lattice Applications

The DRY LATTICE applications consist of two cases: *hexsdry* and *octsdry*. A set of 33 selected critical benchmark configurations are well-correlated to the two applications from a neutronic perspective as represented by the range of c_k values calculated using TSUNAMI. The c_k values for the *hexsdry* application range from 0.906 to 0.974 and for the *octsdry* application from 0.903 to 0.971. Values above 0.9 indicate a high correlation between cases. In addition, the EALF and the H/Pu ratio of the selected benchmark applications span the range of these values from the set

of critical benchmark configurations used in the validation. The EALF values of the two applications are 4.864 and 5.042 eV, whereas the range of EALF values for the benchmark configurations is 0.254 to 37.727 eV. The H/Pu ratios of the two applications are 28.8, where as the range of H/Pu ratios for the benchmark configurations is 15.46 to 131.3. Both the H/Pu ratio and EALF for the two applications are bounded by the selected cases that have c_k values above 0.9 for both applications.

The normality of the k_{eff} values for the group of critical benchmark configurations used to validate the DRY LATTICE applications was checked using the χ^2 test. The test determined that the 33 samples are not normally distributed with some bins not containing the required 5 values. The normality was then checked using the Shapiro-Wilk test.[43] The Shapiro-Wilk test is a more mathematically rigorous test of normality than the χ^2 test. The Shapiro-Wilk test calculated W=0.941546, which is greater than the value from Table A.5 of Reference 43, which for α = 0.05 and n = 33 is W_t = 0.931. A visual inspection of the k_{eff} distribution in Figure 6-28 shows a peak in the center with approximately equal tails on each side. This indicates the sample distribution is normally distributed.

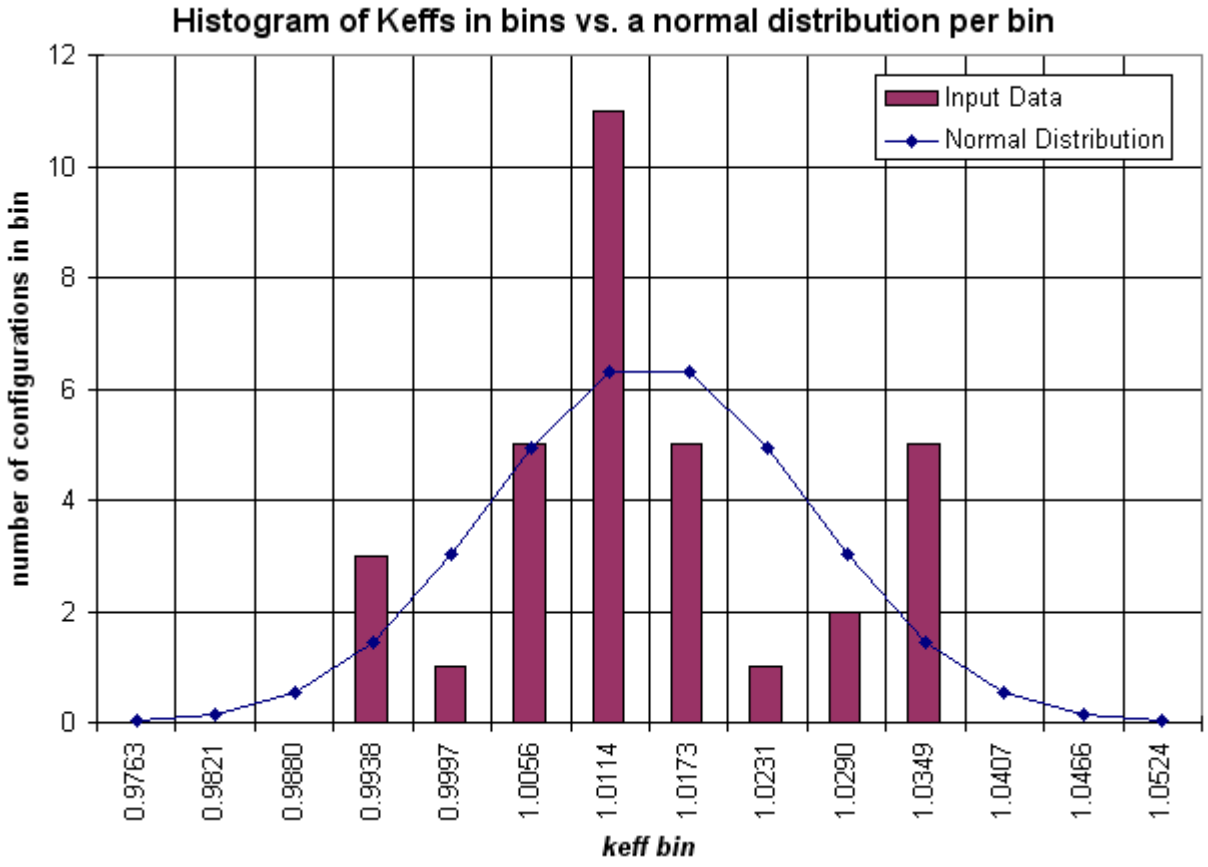

Figure 6-28. Dry Lattice Critical Benchmark Histogram

Trending was done using the c_k values of the critical benchmark configurations for each of the dry lattice applications using the USLSTATS code distributed with SCALE 5.1. This version of USLSTATS permits extrapolation of the USL-1 to a c_k value of 1.0, which is the c_k of the application. The inputs used for USLSTATS are described in Section 6.8.2.2.

USLSTATS is used to calculate an upper subcritical limit for each application using the set of critical benchmark configurations and c_k values as the trending parameter. Figure 6-29 and Figure 6-30 show the results of the USLSTATS analysis for *hexsdy* and *octsdry*. The c_k values have a positive slope as c_k approach 1.0. The linear fit of k_{eff} is above 1.0 throughout the range. Credit is not taken for the positive bias. Based on the analysis, the USL can be established as USL = 0.9351 for *hexsdry* and USL = 0.9352 for *octsdry*.

6.8.2.7 Results Summary

Based on the above data, an USL and bias can be determined for each application. An administrative margin of 0.05 is used for all applications. The USL and bias was determined using nonparametric methods for 9 of the 11 applications because the k_{eff} values of the applicable critical benchmark configurations did not fit a normal distribution. For these nine applications, a nonparametric margin was determined using the number of benchmark configurations to validate the application and a desired population fraction of 0.95 above the minimum k_{eff}. The USL is then determined by subtracting the administrative margin, the nonparametric margin, and 2 standard deviations from the minimum k_{eff} value.

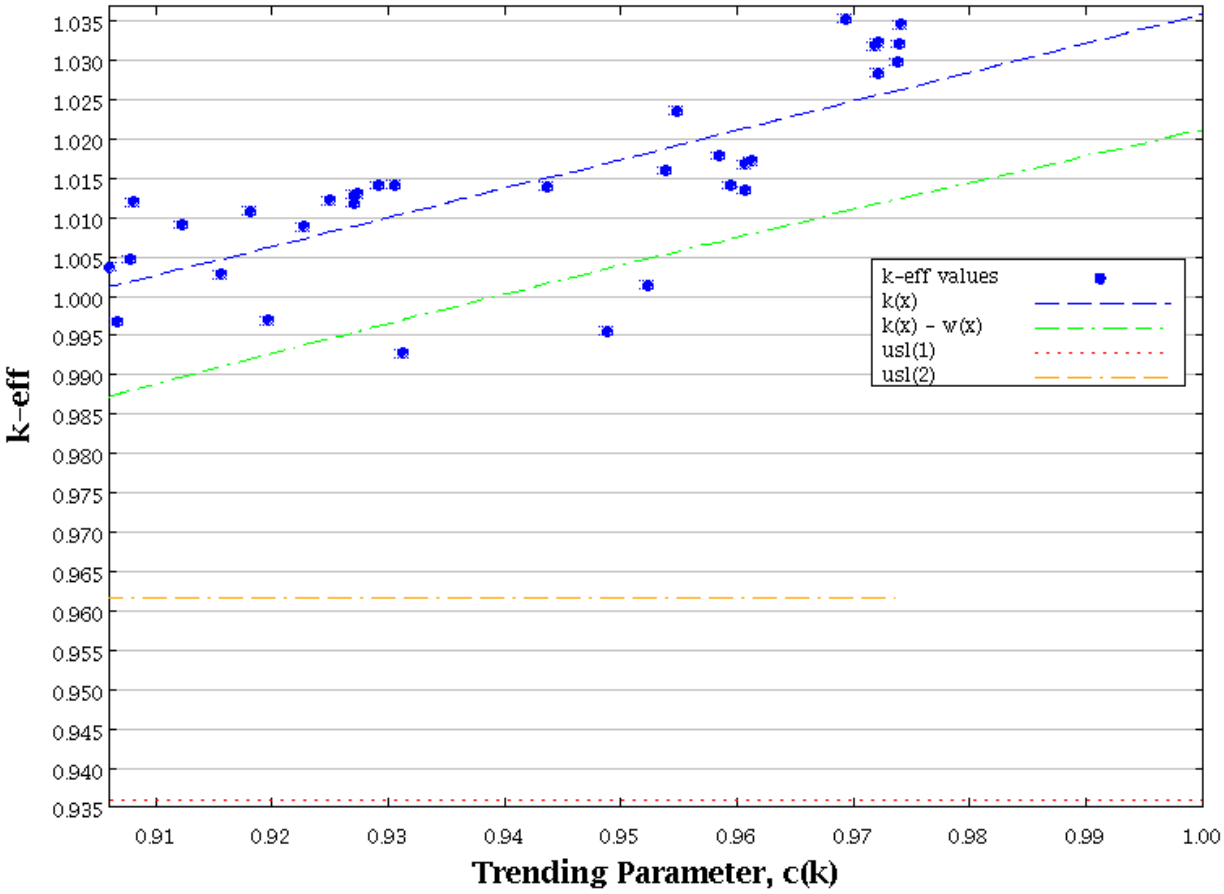

Figure 6-29. USLSTATS Plot for HEXSDRY Application of ck vs. k_{eff}

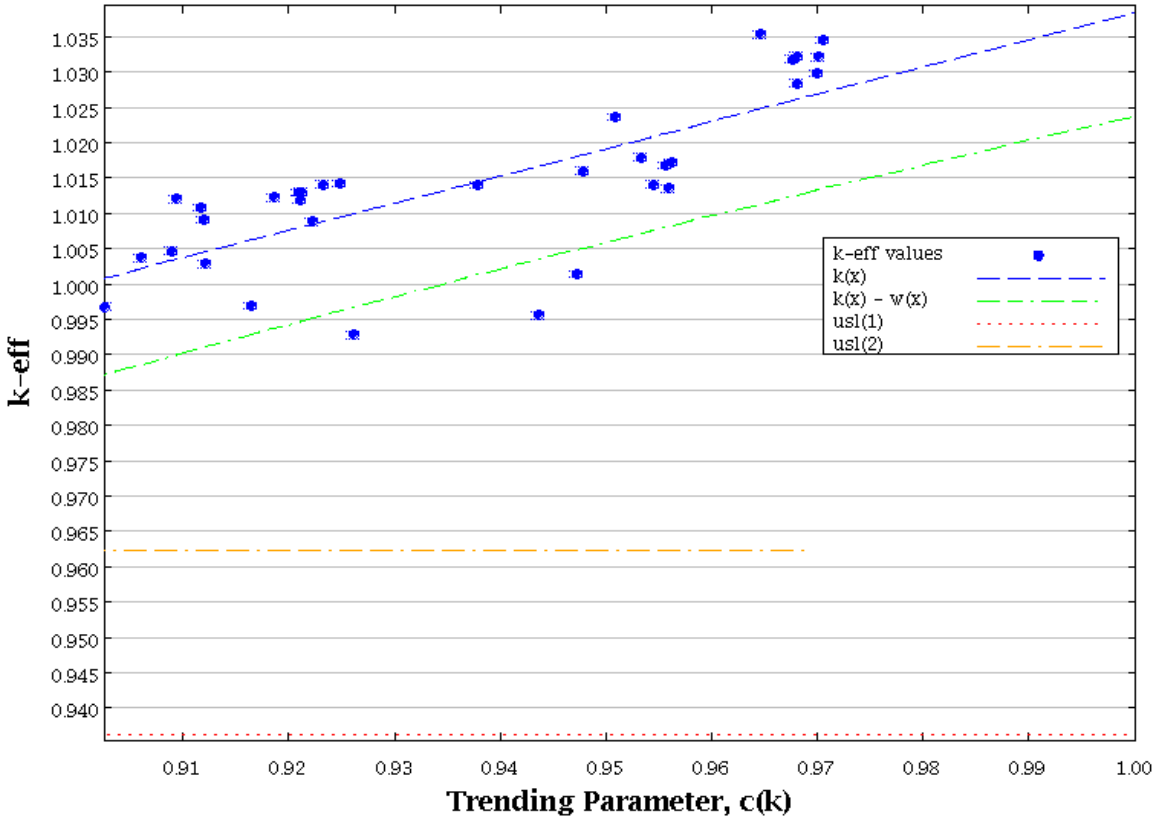

Figure 6-30. USLSTATS Plot for OCTSDRY Application of ck vs. k_{eff}

Table 6-7. USL and Bias Data Summary

Application Name	Method Used	NPM	Minimum k_{eff}	USL	Bias
cv001	Nonparametric	0.05	0.9916	0.8893	0
fhlsf001	Nonparametric	0.05	0.9916	0.8893	0
fslsf001	Nonparametric	0.05	0.9916	0.8893	0
fhlsf031	Nonparametric	0.0	0.9956	0.9396	0
fslsf031	Nonparametric	0.0	0.9956	0.9396	0
hexs100	Nonparametric	0.0	0.9956	0.9396	0
octs100	Nonparametric	0.0	0.9956	0.9396	0
cv031	Nonparametric	0.0	0.9958	0.9383	0
sph14	Nonparametric	0.0	0.9958	0.9383	0
hexsdry	USLSTATS	N/A	N/A	0.9351	0
octsdry	USLSTATS	N/A	N/A	0.9352	0

All cases use an administrative margin of 0.05.
USL for nonparametric cases = min $k_{eff} - [(\sigma_{exp})^2 + (\sigma_{MC})^2]^{0.5} - 0.05 - \text{NPM}$.
USL for parametric cases is USL Method 1 is determined using USLSTATS.
All cases are run to a $\sigma = 0.0005$.
Positive biases (average calculated k_{eff} value > 1) are discarded.

For the two applications where the critical configuration k_{eff} values tested as a normal distribution, the USL was calculated using USLSTATS. The method used in USLSTATS is described in Section 6.8.2.1. An administrative margin of 0.05 was included in the calculations. The reported USL is USL Method 1, which is the confidence band with administrative margin. The bias for the *hexsdry* and *octsdry* applications is zero because the fits of k_{eff} for the critical configurations were above 1.0 throughout their ranges. No credit is taken for such positive biases.

6.9 Appendices

Consistent with the guidance from the U.S. Nuclear Regulatory Commission, Office of Nuclear Regulatory Research, Regulatory Guide 7.9, Rev. 2, "*Standard Format and Content of Part 71 Applications for Approval of Packages for Radioactive Material*," March 2005, this section includes supplemental information.

6.9.1 References

1. United States. Nuclear Regulatory Commission. NUREG/CR-5661, ORNL/TM-11936. Dyer, H. R. and C. V. Parks. "Recommendations for Preparing the Criticality Safety Evaluation of Transportation Packages," Oak Ridge National Laboratory, March 1997.

2. United States. Nuclear Regulatory Commission. NUREG-0361. "Safety Analysis Report for the Plutonium Air Transportable Package, Model PAT-1." Washington, D.C. 1978..

3. Petrie, L. M., P. B. Fox, and K. Lucius, "Standard Composition Library," Vol. III, Sect. M8 in *SCALE: A Modular Code System for Performing Standardized Computer Analyses for Licensing Evaluations*, ORNL/TM-2005/39, Version 5.1, Vols. I–III, November 2006. Available from Radiation Safety Information Computational Center at Oak Ridge National Laboratory as CCC-732.

4. Drawing 1001, Issue A, "PAT-1 ASSEMBLY." May 9, 1978.

5. Drawing 1002, Issue A, "OVERPACK, AO." May 9, 1978.

6. Drawing 1003, Issue A, "CONTAINER SUBASSEMBLY." May 9, 1978.

7. Drawing 1004, Issue B, "DRUM." July 11, 1990.

8. Drawing 1005, Issue A, "COVER, MODIFIED." May 9, 1978.

9. Drawing 1006, Issue A, "RING, CLAMP, MODIFIED." May 9, 1978.

10. Drawing 1007, Issue A, "COVER,LINER." May 8, 1978.

11. Drawing 1008, Issue A, "CYLINDER, WOOD." May 8, 1978.

12. Drawing 1009, Issue B, "CYLINDER, WOOD." July 9, 1990.

13. Drawing 1010, Issue A, "PLUG, WOOD, FIXED." May 9, 1978.

14. Drawing 1011, Issue A, "CYLINDER, WOOD." May 8, 1978.

15. Drawing 1012, Issue A, "PLUG, WOOD, FIXED." May 8, 1978.

16. Drawing 1013, Issue B, "PLUG, WOOD, REMOVABLE." July 5, 1990.

17. Drawing 1014, Issue A, "PLUG, WOOD, REMOVABLE." May 9, 1978.

18. Drawing 1015, Issue A, "SPACER, TOP." May 9, 1978.

19. Drawing 1016, Issue B, "LOAD SPREADER ASSEMBLY." July 9, 1990.

20. Drawing 1017, Issue B, "CONTAINMENT VESSEL." July 19, 1990.

21. Drawing 1018, Issue B, "BOLD, SOCKET, HEAD SPECIAL .500-20." July 10, 1990.

22. Drawing 1019, Issue B, "GASKET COPPER." July 10, 1990.

23. Drawing 1020, Issue B, "LID, TB." July 18, 1990.

24. Drawing 1021, Issue A, "FORGING, TB LID." May 9, 1978.

25. Drawing 1022, Issue B, "BODY, TB." July 16, 1990.

26. Drawing 1023, Issue A, "FORGING, TB BODY." May 9, 1978.

27. Drawing 1024, Issue B, "CAN ASSEMBLY." June 1, 1978.

28. Drawing 1025, Issue A, "CYLINDER, LINER." May 9, 1978.

29. Drawing 1026, Issue A, "PAD, INSULATION." May 9, 1978.

30. Drawing 1027, Issue A, "PAD INSULATION." May 9, 1978.

31. No current standard specifies the minimum thickness for 16-gauge steel. The value used was cited as the minimum thickness for 16-gauge steel used in DOT 17C and 17H drums. These standards are ANSI/ASC MH2-1985(3.4), "American National Standard for 55-Gallon (208-Liter) Tight-Head Steel (Double-Seam Chime) Drums (DOT-17C) and ANS MH2-1991 (3.8), "American National Standard for 55-Gallon (208-Liter) Full-Removable-Head Steel (Round-Seam Chime) Drums (DOT-17H, UFC-Rule 40, NMFC-Item260). Considering their past use in similar applications, the specified 16 gauge minimum steel thickness is a reasonable value for the minimum steel thickness.

32. Los Alamos National Laboratory, ed. Pruvost, N. L. and Paxton, H. C.: *Nuclear Criticality Safety Guide*. LA-12808 (UC-714), September 1996.

33. Brown, Jr., W. F. and S. J. Setlak, *Aerospace Structural Metals Handbook, 37th Edition*, CINDAS/USAF CRDA Handbooks Operation, Purdue University, West Lafayette, IN. 2001.

34. *Handbook of Chemistry and Physics, 74th Edition.* CRC Press, Inc. Boca Raton, FL. 1993. [Page 4-83]

35. *SCALE: A Modular Code System for Performing Standardized Computer Analyses for Licensing Evaluations*, ORNL/TM-2005/39, Version 5.1, Vols. I–III, November 2006. Available from Radiation Safety Information Computational Center at Oak Ridge National Laboratory as CCC-732.

36. Goluoglu, S., N. F. Landers, L. M. Petrie, and D. F. Hollenbach, "CSAS: Control Module for Enhanced Criticality Safety Analysis Sequences," Vol. I, Sect. C4 in *SCALE: A Modular Code System for Performing Standardized Computer Analyses for Licensing Evaluations*, ORNL/TM-2005/39, Version 5.1, Vols. I–III, November 2006. Available from Radiation Safety Information Computational Center at Oak Ridge National Laboratory as CCC-732.

37. Rearden, B. T., "TSUNAMI-3D: Control Module for Three-Dimensional Cross-Section Sensitivity and Uncertainty Analysis for Criticality," Vol. I, Sect. C9 in *SCALE: A Modular Code System for Performing Standardized Computer Analyses for Licensing Evaluations*, ORNL/TM-2005/39, Version 5.1, Vols. I–III, November 2006. Available from Radiation Safety Information Computational Center at Oak Ridge National Laboratory as CCC-732.

38. Rearden, B. T., "TSUNAMI Utility Modules," Vol. III, Sect. M18.1 in *SCALE: A Modular Code System for Performing Standardized Computer Analyses for Licensing Evaluations*, ORNL/TM-2005/39, Version 5.1, Vols. I–III, November 2006. Available from Radiation Safety Information Computational Center at Oak Ridge National Laboratory as CCC-732.

39. *International Handbook of Evaluated Criticality Safety Benchmark Experiments*. NEA/NSC/DOC(95)03, NEA Nuclear Science Committee. September 2007.

40. United States. Nuclear Regulatory Commission. NUREG/CR-6361 (ORNL/TM-13211). Lichtenwalter, J. J., S. M. Bowman, M. D. DeHart, and C. M. Hopper. "Criticality Benchmark Guide for Light-Water-Reactor Fuel in Transportation and Storage Packages." Oak Ridge National Laboratory. March 1997.

41. Bowden, D. C. and F. A. Graybill, "Confidence Bands of Uniform and Proportional Width for Linear Models," *Am. Stat. Assoc. J.*, 61, 182. March 1966.

42. Johnson, N. L., Ed., "Query" *Technometrics*, 10, 207–209. February 1968.

43. United States. Nuclear Regulatory Commission. NUREG/CR-6698. "Guide for Validation of Nuclear Criticality Safety Calculational Methodology." Washington D.C.: January 2001.

44. Broadhead, B. L., B. T. Rearden, C. M. Hopper, J. J. Wagschal, and C. V. Parks, "Sensitivity and Uncertainty-Based Criticality Safety Validation Techniques," *Nuc. Sci. Eng*. 146, 340–366. 2004.

45. Oberg, E., F. D. Jones, H. L. Horton, and H. H. Ryffel, "Machinery's Handbook, 24th Edition." Industrial Press Inc.: New York. 1992.

6.9.2 TB-1 Containment Vessel Inner Volume

A key parameter of the criticality analysis is the maximum quantity of water that could be present within the TB-1 containment vessel. Since this component has a rather complicated internal shape, the calculation of its internal volume is presented in this section.

The TB-1 containment vessel is shown in Drawing 1017.[20] The volume can be divided into three sub-volumes. Most of the volume is in the straight right-circular cylinder that extends from the bottom spherical section up to the bottom edge of the lid. As indicated in Drawing 1022,[25] the bottom is a spherical section. As indicated in Drawing 1020,[23] the recess in the lid is also a spherical section.

Equations and figure provided in the Machinery's Handbook [Reference 45, page 66] for calculating volumes of spherical segments are reproduced in Figure 6-31.

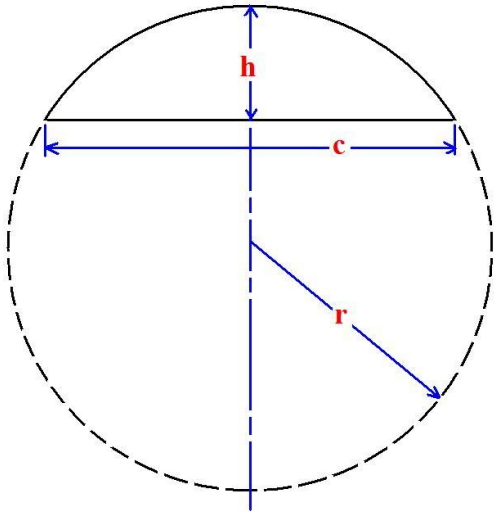

V = volume

$$V = 3.1416\, h^2 \left(r - \frac{h}{3} \right)$$

$$V = 3.1416\, h \left(\frac{c^2}{8} + \frac{h^2}{6} \right)$$

$$c = 2\sqrt{h(2r - h)}$$

$$r = \frac{c^2 + 4h^2}{8h}$$

Figure 6-31. Spherical Segment Volume Calculations

The volume in the bottom of the TB-1 can be calculated using information from Drawing 1022:[25]

h 25+0.005 – 5.450 + 4.700 = 1.505"
c = 4.250 + 0.0022 = 4.2522"
V_{bottom} = 3.1416*1.505*(4.2522^2/8 + 1.505^2/6) = 12.471 in^3

The volume of the central cylinder can be calculated using information from Drawings 1020[23] and 1022:[25]

V = π * r^2 * L
r = (4.250+0.0022)/2 = 2.1261"
L = 5.450 + 0.010 – 0.437+0.010 – 0.047 + 0.002 + 0.080 +0.002
L = 5.070"
V_{middle} = π * 2.1261^2 * 5.070 = 71.999 in^3

The volume in the lid is calculated using information from Drawing 1020:[23]

$h = 0.437 + 0.01 + 0.513+0.01 = 0.970$”
$r = 2.25 + 0.02 = 2.27$”
$V_{top} = 3.1416*0.97^2*(2.27-0.97/3) = 5.754\ in^3$

The total volume is then the sum of the partial volumes:

$$V = 12.471 + 71.999 + 5.754 = 90.22\ in^3 = 1478\ cm^3$$

Thus the maximum internal volume of the TB-1 containment vessel is 1478 cm^3. The Pu, any packaging, and other internal containment and support structures must fit within this volume.

6.9.3 Applicability of Benchmark Experiments

Table 6-8 lists all of the validation cases used in this evaluation. There are 125 cases considered in this validation. All cases contain plutonium as the primary fissile material and are either fast metal, intermediate spectrum Pu/Polystyrene blocks or thermal solution cases. The standard deviation for all the calculated k_{eff} values is 0.0005.

Table 6-8. List of Validation Critical Configurations

IHECSBE Identifier	Case	Description	Benchmark		Calculated	
			k_{eff}	±σ	k_{eff}	EALF
pcm*001	1	PuO_2 –Polystyrene Slab	0.9986	0.0041	1.02438	9.73E+05
	3		0.9990	0.0047	1.02356	30.518
	4		1.0000	0.0033	0.99275	37.727
	5		0.9989	0.0053	1.01403	1.468
pcm002	1	Plexiglas Reflected PuO_2 –Polystyrene Slabs	0.9990	0.0046	1.03757	4.56E+03
	2		0.9990	0.0046	1.03641	3.98E+03
	3		0.9990	0.0046	1.03179	3.26E+03
	4		0.9990	0.0046	1.02547	2.42E+03
	5		0.9990	0.0046	1.02328	1.76E+03
	10		1.0000	0.0044	1.03534	4.026
	11		1.0000	0.0044	1.03184	4.405
	12		1.0000	0.0044	1.03209	4.970
	13		1.0000	0.0044	1.02982	5.262
	14		1.0000	0.0044	1.03451	5.405
	15		1.0000	0.0044	1.03220	5.366
	16		1.0000	0.0044	1.02841	4.998
	17		0.9988	0.0044	1.01596	4.762
	18		0.9988	0.0044	1.01408	5.998
	19		0.9988	0.0044	1.01680	6.268
	20		0.9988	0.0044	1.01355	6.446
	21		0.9988	0.0044	1.01719	6.400

Table 6-8. List of Validation Critical Configurations

IHECSBE Identifier	Case	Description	Benchmark		Calculated	
			k_{eff}	±σ	k_{eff}	EALF
	22		0.9988	0.0044	1.01789	6.241
	23		1.0000	0.0046	1.01077	0.663
	24		1.0000	0.0046	1.01215	0.673
	25		1.0000	0.0046	1.01189	0.684
	26		1.0000	0.0046	1.01298	0.689
	27		1.0000	0.0046	1.01294	0.700
	28		1.0000	0.0046	1.01412	0.703
	29		1.0000	0.0046	1.01424	0.708
pmf*002	1	Bare Pu metal sphere	1.0000	0.0020	0.99666	1.27E+06
pmf011	1	H_2O reflected Pu metal sphere	1.0000	0.0010	0.99746	8.37E+04
pmf022	1	Bare Pu metal spherical ass.	1.0000	0.0021	0.99409	1.23E+06
pmf024	1	Poly Refl Spherical Assembly	1.0000	0.0020	0.99872	6.31E+05
pmf027	1	Poly Refl Spherical Assembly	1.0000	0.0022	1.00215	7.02E+04
pmf029	1	Bare Pu Spherical Assembly	1.0000	0.0022	0.99155	1.26E+06
pmf031	1	Poly Refl Spherical Assembly	1.0000	0.0021	1.00215	1.85E+05
pst*001	4	Water Reflected filled 29.21 cm (11.5in.) Pu Nitrate solution spheres	1.0000	0.0050	1.00433	0.147
	5		1.0000	0.0050	1.00819	0.155
	6		1.0000	0.0050	1.00882	0.337
pst007	2	Water reflected partially filled 29.21 cm (11.5in.) Pu Nitrate sol. Spheres	1.0000	0.0047	1.00909	0.267
	3		1.0000	0.0047	1.00375	0.254
	8		1.0000	0.0047	0.99874	0.112
pst014	3	Interacting 30 cm (11.81 in.) diameter cylinders of Pu Nitrate solution (115.1 g Pu/l [0.9605 lb/gal]) in air	0.9980	0.0032	1.00489	0.162
	4		0.9980	0.0032	1.00520	0.162
	6		0.9980	0.0032	1.00533	0.162
	8		0.9980	0.0032	1.00292	0.163
	9		0.9980	0.0032	1.00336	0.162
	10		0.9980	0.0032	1.00470	0.162
	11		0.9980	0.0032	1.00475	0.162
	12		0.9980	0.0032	1.00440	0.162
	14		0.9980	0.0043	1.00461	0.163
	16		0.9980	0.0043	1.00416	0.162
	17		0.9980	0.0043	1.00372	0.162
	20		0.9980	0.0043	1.00455	0.162
	22		0.9980	0.0043	1.00405	0.162
	23		0.9980	0.0043	1.00358	0.162
	25		0.9980	0.0043	1.00367	0.163
	26		0.9980	0.0043	1.00279	0.162
	27		0.9980	0.0043	1.00479	0.162

Table 6-8. List of Validation Critical Configurations

IHECSBE Identifier	Case	Description	Benchmark		Calculated	
			k_{eff}	±σ	k_{eff}	EALF
	28		0.9980	0.0043	1.00403	0.162
	29		0.9980	0.0043	1.00392	0.162
	30		0.9980	0.0043	1.00519	0.163
	31		0.9980	0.0043	1.00260	0.163
	32		0.9980	0.0043	1.00296	0.163
	33		0.9980	0.0043	1.00340	0.163
	34		0.9980	0.0043	1.00408	0.162
	35		0.9980	0.0043	1.00533	0.162
pst015	1	Interacting 30 cm (11.81 in.) diameter cylinders of Pu Nitrate solution (152.5 g Pu/l [1.273 lb/gal]) in air	0.9980	0.0038	1.00653	0.230
	2		0.9980	0.0038	1.00642	0.229
	3		0.9980	0.0038	1.00535	0.229
	4		0.9980	0.0038	1.00597	0.229
	5		0.9980	0.0038	1.00658	0.228
	6		0.9980	0.0038	1.00733	0.228
	7		0.9971	0.0047	1.00753	0.230
	8		0.9971	0.0047	1.00520	0.230
	9		0.9971	0.0047	1.00625	0.229
	10		0.9971	0.0047	1.00457	0.228
	11		0.9971	0.0047	1.00329	0.231
	12		0.9971	0.0047	1.00475	0.230
	13		0.9971	0.0047	1.00501	0.229
	14		0.9971	0.0047	1.00636	0.228
	15		0.9971	0.0047	1.00765	0.231
	16		0.9971	0.0047	1.00520	0.230
	17		0.9971	0.0047	1.00472	0.229
pst016	1	Interacting 30 cm (11.81 in.) and 25.6 cm (10.01in.) diameter cylinders of Pu Nitrate solution (152.5 and 115.1 g Pu/l [1.273 and 0.9605 lb/gal) and nitric acid (2N) in air	0.9980	0.0043	1.00555	0.230
	2		0.9980	0.0043	1.00501	0.229
	3		0.9980	0.0043	1.00672	0.229
	4		0.9980	0.0043	1.00696	0.228
	5		0.9969	0.0038	1.00372	0.163
	6		0.9969	0.0038	1.00502	0.162
	7		0.9969	0.0038	1.00582	0.162
	8		0.9969	0.0038	1.00492	0.162
	9		0.9963	0.0033	1.00541	0.161
	10		0.9963	0.0033	1.00564	0.161
	11		0.9963	0.0033	1.00658	0.162
pst017	1	Interacting 30 cm (11.81 in.) and 25.6cm (10.01 in.) diameter	0.9969	0.0038	1.00379	0.162
	2		0.9969	0.0038	1.00490	0.162

Table 6-8. List of Validation Critical Configurations

IHECSBE Identifier	Case	Description	Benchmark		Calculated	
			k_{eff}	±σ	k_{eff}	EALF
	3	cylinders of Pu Nitrate solution (115.1 g Pu/l [0.9605 lb/gal]) in air I	0.9969	0.0038	1.00346	0.162
	4		0.9969	0.0038	1.00499	0.162
	5		0.9969	0.0038	1.00452	0.162
	6		0.9969	0.0038	1.00461	0.162
	7		0.9969	0.0038	1.00422	0.162
	8		0.9969	0.0038	1.00485	0.162
	9		0.9969	0.0038	1.00389	0.162
	10		0.9969	0.0038	1.00441	0.162
	11		0.9969	0.0038	1.00387	0.162
	12		0.9969	0.0038	1.00536	0.162
	13		0.9969	0.0038	1.00454	0.162
	14		0.9969	0.0038	1.00545	0.162
	15		0.9969	0.0038	1.00497	0.162
	16		0.9969	0.0038	1.00506	0.162
	17		0.9969	0.0038	1.00568	0.162
	18		0.9969	0.0038	1.00465	0.162
pst020	9	Pu Nitrate solution sphere	1.0000	0.0059	0.99773	0.074
pst021	3	Pu Nitrate solution sphere	1.0000	0.0065	1.01198	0.302
	8		1.0000	0.0065	1.00474	0.302
pst024	3	Polyethylene reflected Pu Nitrate solution slab	1.0000	0.0062	1.00277	0.444
	6		1.0000	0.0077	1.00136	1.607
	16		1.0000	0.0053	1.00457	0.287
pst025	22	Water reflected Pu Nitrate solution slab	1.0000	0.0044	0.99944	0.240
	31		1.0000	0.0048	0.99675	0.353
	42		1.0000	0.0060	0.99558	1.142
pst026	12	Unreflected Pu Nitrate solution slab	1.0000	0.0047	1.00047	0.239
	16		1.0000	0.0044	0.99735	0.312
	19		1.0000	0.0049	0.99688	0.503

All k_{eff} values were calculated with a standard deviation of 0.0005.

Table 6-9. Comparison of Tsunami Sensitivities and Direct Perturbation Sensitivities for a Representative Selection of Benchmark Critical Configurations

Case	Perturbed Material	Direct Perturbation		TSUNAMI		Number Std. Dev. Apart
		Sensitivity	Sigma	Sensitivity	Sigma	
pcm001c01	H	0.0020	0.0007	0.0014	0.0001	0.94
	Pu-239	0.6016	0.0846	0.6410	0.0017	0.47
pcm001c05	H	0.4158	0.0374	0.2956	0.0092	2.67
	Pu-239	0.1326	0.0171	0.1126	0.0008	1.17
pcm002c01	H	0.0002	0.0007	0.0015	0.0001	1.88
	Pu-239	0.3442	0.0477	0.3856	0.0092	0.85
pcm002c20	H	0.2592	0.0311	0.2390	0.0056	0.64
	Pu-239	0.1804	0.0244	0.1813	0.0009	0.04
pcm002c24	H	0.2673	0.0139	0.2715	0.0048	0.28
	Pu-239	0.1128	0.0059	0.1061	0.0006	1.14
pmf002c01	H	N/A	N/A	N/A	N/A	N/A
	Pu-239	0.6986	0.0869	0.6881	0.0016	0.12
pmf011c01	H	N/A	N/A	N/A	N/A	N/A
	Pu-239	0.6529	0.0868	0.6501	0.0014	0.03
pmf024c01	H	N/A	N/A	N/A	N/A	N/A
	Pu-239	0.7585	0.0867	0.7754	0.0015	0.20
pst001c05	H	0.4075	0.0573	0.4840	0.0074	1.32
	Pu-239	0.0742	0.0104	0.0751	0.0004	0.08
pst014c03	H	0.5493	0.0690	0.6034	0.0047	0.78
	Pu-239	0.0801	0.0108	0.07996	0.0005	0.01
pst015c01	H	0.5613	0.0688	0.5996	0.0039	0.55
	Pu-239	0.0613	0.0098	0.0708	0.0004	0.96
pst024c03	H	0.4644	0.0494	0.3894	0.0093	1.49
	Pu-239	0.0863	0.0133	0.0974	0.0009	0.83
pst024c06	H	0.3395	0.0433	0.3483	0.0090	0.20
	Pu-239	0.1151	0.0165	0.1214	0.0008	0.38
pst024c16	H	0.3605	0.0493	0.4074	0.0106	0.93
	Pu-239	0.1159	0.0138	0.1021	0.0010	1.00
pst025c31	H	0.3530	0.0435	0.3452	0.0061	0.18
	Pu-239	0.0920	0.0129	0.0953	0.0007	0.26

pcm = PU-COMP-MIXED
pmf = PU-MET-FAST
pst = PU-SOL-THERM

Table 6-10. Comparison of Direct Perturbation Sensitivities and Tsunami Sensitivities for the 11 Representative Applications

Case	Perturbed Material	Direct Perturbation		TSUNAMI		Number Std. Dev. Apart
		Sensitivity	Sigma	Sensitivity	Sigma	
cv001	Pu-239	0.6857	0.1051	0.8527	0.1390	0.96
	H_2O	0.1539	0.0215	0.1977	0.0654	0.64
cv031	Pu-239	0.0970	0.0173	0.0944	0.0306	0.07
	H_2O	0.8443	0.0999	0.9643	0.3201	0.36
fhlsf001	Pu-239	0.7719	0.1032	0.7434	0.0017	0.28
	H_2O	0.1778	0.0059	0.1382	0.0234	1.63
fhlsf031	Pu-239	0.1204	0.0272	0.1451	0.0057	0.89
	H_2O	0.8882	0.1089	0.6675	0.0781	1.65
fslsf001	Pu-239	0.7183	0.1060	0.7418	0.0018	0.22
	H_2O	0.1836	0.0212	0.1441	0.0226	1.28
fslsf031	Pu-239	0.1590	0.0272	0.1304	0.0020	1.05
	H_2O	0.7623	0.1117	0.6070	0.0297	1.34
hexs100	Pu-239	0.1329	0.0247	0.1302	0.0013	0.11
	H_2O	0.8358	0.0940	0.5574	0.1259	1.77
hexsdry	Pu-239	0.2105	0.0805	0.1524	0.0006	0.72
	H_2O	0.7135	0.0654	0.7153	0.0060	0.03
octs100	Pu-239	0.1469	0.0235	0.1368	0.0025	0.43
	H_2O	0.5071	0.0965	0.5577	0.0357	0.49
octsdry	Pu-239	0.0944	0.0835	0.1549	0.0006	0.72
	H_2O	0.8289	0.0644	0.7584	0.0065	1.09
sph14	Pu-239	0.1633	0.0241	0.1212	0.0120	1.56
	H_2O	0.9150	0.0963	0.6715	0.1178	1.60

Table 6-11. Comparison of METAL SPHERE Applications to Critical Benchmarks

IHECSBE Identifier	Case	*cv001* c_k	*fhslf001* c_k	*fslsf001* c_k	EALF (eV)	H/Pu	k_{eff}
pcm001	1	0.9686	0.9684	0.9682	9.73E+05	0.05	1.02438
pcm002	1	0.9427	0.9440	0.9439	4.56E+03	0.05	1.03757
	2	0.9390	0.9404	0.9402	3.98E+03	0.05	1.03641
	3	0.9345	0.9361	0.9359	3.26E+03	0.05	1.03179
	4	0.9260	0.9277	0.9275	2.42E+03	0.05	1.02547
	5	0.9158	0.9178	0.9176	1.76E+03	0.05	1.02328

Table 6-11. Comparison of METAL SPHERE Applications to Critical Benchmarks

IHECSBE Identifier	Case	*cv001* c_k	*fhslf001* c_k	*fslsf001* c_k	EALF (eV)	H/Pu	k_{eff}
pmf002	1	0.9699	0.9714	0.9709	1.27E+06	0.00	0.99666
pmf011	1	0.9948	0.9960	0.9958	8.37E+04	0.00	0.99746
pmf022	1	0.9856	0.9871	0.9866	1.23E+06	0.00	0.99409
pmf024	1	0.9917	0.9930	0.9927	6.31E+05	0.00	0.99872
pmf027	1	0.9916	0.9930	0.9928	7.02E+04	0.00	1.00215
pmf029	1	0.9822	0.9837	0.9832	1.26E+06	0.02	0.99155
pmf031	1	0.9915	0.9929	0.9926	1.85E+05	0.02	1.00215

All k_{eff} values were calculated with a standard deviation of 0.0005.
For all applications H/ Pu = 0.0
EALF values for the above applications is as follows:
Case cv001: 5.449E+04 eV
Case fhlsf001: 7.872E+04 eV
Case fslsf001: 7.976E+04 eV

Table 6-12. Comparison of SOLUTION LATTICE Applications to Critical Benchmarks

IHECSBE Identifier	Case	*fhlsf031* c_k	*fslsf031* c_k	*hexs100* c_k	*octs100* c_k	EALF (eV)	H/Pu Ratio	k_{eff}
pcm001	5	0.9102	0.9078	0.9324	0.9307	1.468	65.37	1.01403
pcm002	10	0.9296	0.9262	0.9471	0.9457	4.026	15.46	1.03534
	11	0.9328	0.9297	0.9494	0.9480	4.405	15.46	1.03184
	12	0.9362	0.9334	0.9517	0.9505	4.970	15.46	1.03209
	13	0.9345	0.9317	0.9499	0.9487	5.262	15.46	1.02982
	14	0.9353	0.9325	0.9500	0.9489	5.405	15.46	1.03451
	15	0.9307	0.9276	0.9465	0.9452	5.366	15.46	1.03220
	16	0.9315	0.9286	0.9478	0.9465	4.998	15.46	1.02841
	17	0.9101	0.9069	0.9311	0.9297	4.762	16.40	1.01596
	18	0.9140	0.9100	0.9318	0.9306	5.998	16.40	1.01408
	19	0.9180	0.9150	0.9365	0.9353	6.268	16.40	1.01680
	20	0.9148	0.9109	0.9318	0.9307	6.446	16.40	1.01355
	21	0.9187	0.9157	0.9369	0.9358	6.400	16.40	1.01719
	22	0.9111	0.9071	0.9292	0.9280	6.241	16.40	1.01789
	23	0.8933	0.8903	0.9159	0.9141	0.663	65.37	1.01077
	24	0.8979	0.8940	0.9196	0.9178	0.673	65.37	1.01215
	25	0.9007	0.8970	0.9220	0.9202	0.684	65.37	1.01189
	26	0.9007	0.8969	0.9220	0.9202	0.689	65.37	1.01298

Table 6-12. Comparison of SOLUTION LATTICE Applications to Critical Benchmarks

IHECSBE Identifier	Case	*fhlsf031* c_k	*fslsf031* c_k	*hexs100* c_k	*octs100* c_k	EALF (eV)	H/Pu Ratio	k_{eff}
	27	0.8996	0.8957	0.9211	0.9194	0.700	65.37	1.01294
	28	0.9024	0.8987	0.9236	0.9218	0.703	65.37	1.01412
	29	0.9043	0.9008	0.9252	0.9235	0.708	65.37	1.01424
pst001	4	0.8973	0.8953	0.9000	0.8994	0.147	190.43	1.00433
	5	0.8999	0.8978	0.9030	0.9024	0.155	180.16	1.00819
	6	0.9340	0.9319	0.9409	0.9400	0.337	91.19	1.00882
pst007	2	0.9262	0.9234	0.9318	0.9309	0.267	109.55	1.00909
	3	0.9235	0.9216	0.9290	0.9282	0.254	113.97	1.00375
pst014	11	0.8985	0.8985	0.9024	0.9017	0.162	220.19	1.00475
pst015	1	0.9100	0.9069	0.9141	0.9132	0.230	162.67	1.00653
	2	0.9107	0.9077	0.9143	0.9135	0.229	162.67	1.00642
	3	0.9115	0.9085	0.9146	0.9138	0.229	162.67	1.00535
	4	0.9119	0.9090	0.9148	0.9140	0.229	162.67	1.00597
	5	0.9118	0.9089	0.9147	0.9139	0.228	162.67	1.00658
	6	0.9126	0.9097	0.9151	0.9144	0.228	162.67	1.00733
	7	0.9084	0.9055	0.9145	0.9135	0.230	162.67	1.00753
	8	0.9097	0.9066	0.9141	0.9132	0.230	162.67	1.00520
	9	0.9113	0.9083	0.9146	0.9138	0.229	162.67	1.00625
	10	0.9126	0.9097	0.9152	0.9144	0.228	162.67	1.00457
	11	0.9095	0.9065	0.9145	0.9136	0.231	162.67	1.00329
	12	0.9107	0.9077	0.9145	0.9137	0.230	162.67	1.00475
	13	0.9117	0.9087	0.9148	0.9140	0.229	162.67	1.00501
	14	0.9124	0.9095	0.9151	0.9143	0.228	162.67	1.00636
	15	0.9071	0.9042	0.9140	0.9130	0.231	162.67	1.00765
	16	0.9096	0.9066	0.9143	0.9134	0.230	162.67	1.00520
	17	0.9112	0.9082	0.9146	0.9138	0.229	162.67	1.00472
pst016	1	0.9112	0.9081	0.9145	0.9137	0.230	162.66	1.00555
	2	0.9125	0.9096	0.9150	0.9143	0.229	162.66	1.00501
	3	0.9126	0.9097	0.9151	0.9143	0.229	162.66	1.00672
	4	0.9127	0.9099	0.9151	0.9144	0.228	162.66	1.00696
	8	0.8989	0.8989	0.9025	0.9019	0.162	220.20	1.00492
pst017	1	0.8977	0.8948	0.8980	0.8974	0.162	220.19	1.00379
	2	0.8985	0.8962	0.8998	0.8992	0.162	220.19	1.00490
	5	0.8973	0.8944	0.8979	0.8974	0.162	220.19	1.00452
	7	0.8974	0.8947	0.8987	0.8981	0.162	220.19	1.00422
pst021	3	0.9233	0.9203	0.9258	0.9251	0.302	131.30	1.01198

Table 6-12. Comparison of SOLUTION LATTICE Applications to Critical Benchmarks

IHECSBE Identifier	Case	*fhlsf031* c_k	*fslsf031* c_k	*hexs100* c_k	*octs100* c_k	EALF (eV)	H/Pu Ratio	k_{eff}
	8	0.9234	0.9204	0.9258	0.9251	0.302	131.30	1.00474
pst024	3	0.9065	0.9025	0.9213	0.9198	0.444	115.40	1.00277
	6	0.9190	0.9141	0.9376	0.9360	1.607	59.25	1.00136
pst025	31	0.9034	0.8987	0.9187	0.9172	0.353	115.40	0.99675
	42	0.9233	0.9179	0.9412	0.9398	1.142	59.25	0.99558
pst026	19	0.9090	0.9050	0.9232	0.9217	0.503	115.40	0.99688

All k_{eff} values were calculated with a standard deviation of 0.0005.
For all applications H/ Pu = 28.79
EALF values for the above applications is as follows:
Case fhlsf031: 2.693 eV
Case fslsf031: 2.695 eV
Case hexs100: 2.548 eV
Case octs100: 2.547 eV

Table 6-13. Comparison of SINGLE UNIT SOLUTION Applications to Critical Benchmarks

IHECSBE	Case	*cv031* c_k	*sph14* c_k	EALF (eV)	H / Pu	k_{eff}
pcm002	10	0.9067	0.9282	4.026	15.46	1.03534
	11	0.9091	0.9309	4.405	15.46	1.03184
	12	0.9118	0.9339	4.970	15.46	1.03209
	13	0.9081	0.9308	5.262	15.46	1.02982
	14	0.9083	0.9311	5.405	15.46	1.03451
	15	0.9025	0.9257	5.366	15.46	1.03220
	16	0.9046	0.9276	4.998	15.46	1.02841
	29	0.9018	0.9168	0.708	65.37	1.01424
pst001	4	0.9388	0.9314	0.147	190.43	1.00433
	5	0.9401	0.9333	0.155	180.16	1.00819
	6	0.9583	0.9588	0.337	91.19	1.00882
pst007	2	0.9558	0.9530	0.267	109.55	1.00909
	3	0.9534	0.9515	0.254	113.97	1.00375
	8	0.9292	0.9194	0.112	258.46	0.99874
pst014	3	0.9438	0.9340	0.162	220.19	1.00489
	4	0.9446	0.9346	0.162	220.19	1.00520
	6	0.9451	0.9351	0.162	220.19	1.00533
	8	0.9411	0.9320	0.163	220.19	1.00292

Table 6-13. Comparison of SINGLE UNIT SOLUTION Applications to Critical Benchmarks

IHECSBE	Case	*cv031* c_k	*sph14* c_k	EALF (eV)	H / Pu	k_{eff}
	9	0.9432	0.9335	0.162	220.19	1.00336
	10	0.9440	0.9342	0.162	220.19	1.00470
	11	0.9380	0.9351	0.162	220.19	1.00475
	12	0.9453	0.9352	0.162	220.19	1.00440
	14	0.9411	0.9320	0.163	220.19	1.00461
	16	0.9447	0.9348	0.162	220.19	1.00416
	17	0.9450	0.9351	0.162	220.19	1.00372
	20	0.9435	0.9338	0.162	220.19	1.00455
	22	0.9449	0.9349	0.162	220.19	1.00405
	23	0.9454	0.9353	0.162	220.19	1.00358
	25	0.9397	0.9310	0.163	220.19	1.00367
	26	0.9428	0.9333	0.162	220.19	1.00279
	27	0.9448	0.9349	0.162	220.19	1.00479
	28	0.9447	0.9347	0.162	220.19	1.00403
	29	0.9452	0.9352	0.162	220.19	1.00392
	30	0.9381	0.9298	0.163	220.19	1.00519
	31	0.9399	0.9313	0.163	220.19	1.00260
	32	0.9412	0.9320	0.163	220.19	1.00296
	33	0.9421	0.9328	0.163	220.19	1.00340
	34	0.9432	0.9336	0.162	220.19	1.00408
	35	0.9435	0.9338	0.162	220.19	1.00533
pst015	1	0.9494	0.9432	0.230	162.67	1.00653
	2	0.9506	0.9442	0.229	162.67	1.00642
	3	0.9518	0.9451	0.229	162.67	1.00535
	4	0.9523	0.9456	0.229	162.67	1.00597
	5	0.9522	0.9456	0.228	162.67	1.00658
	6	0.9533	0.9465	0.228	162.67	1.00733
	7	0.9444	0.9403	0.230	162.67	1.00753
	8	0.9487	0.9428	0.230	162.67	1.00520
	9	0.9513	0.9448	0.229	162.67	1.00625
	10	0.9532	0.9464	0.228	162.67	1.00457
	11	0.9471	0.9420	0.231	162.67	1.00329
	12	0.9502	0.9440	0.230	162.67	1.00475
	13	0.9518	0.9453	0.229	162.67	1.00501
	14	0.9530	0.9462	0.228	162.67	1.00636

Table 6-13. Comparison of SINGLE UNIT SOLUTION Applications to Critical Benchmarks

IHECSBE	Case	*cv031* c_k	*sph14* c_k	EALF (eV)	H / Pu	k_{eff}
	15	0.9423	0.9387	0.231	162.67	1.00765
	16	0.9481	0.9425	0.230	162.67	1.00520
	17	0.9511	0.9447	0.229	162.67	1.00472
pst016	1	0.9511	0.9446	0.230	162.66	1.00555
	2	0.9532	0.9463	0.229	162.66	1.00501
	3	0.9533	0.9465	0.229	162.66	1.00672
	4	0.9535	0.9466	0.228	162.66	1.00696
	5	0.9431	0.9334	0.163	220.20	1.00372
	6	0.9443	0.9344	0.162	220.20	1.00502
	7	0.9456	0.9355	0.162	220.20	1.00582
	8	0.9387	0.9357	0.162	220.20	1.00492
	9	0.9453	0.9352	0.161	220.20	1.00541
	10	0.9457	0.9356	0.161	220.20	1.00564
	11	0.9456	0.9355	0.162	220.20	1.00658
pst017	1	0.9460	0.9358	0.162	220.19	1.00379
	2	0.9446	0.9362	0.162	220.19	1.00490
	3	0.9457	0.9356	0.162	220.19	1.00346
	4	0.9451	0.9352	0.162	220.19	1.00499
	5	0.9453	0.9354	0.162	220.19	1.00452
	6	0.9456	0.9355	0.162	220.19	1.00461
	7	0.9442	0.9351	0.162	220.19	1.00422
	8	0.9452	0.9352	0.162	220.19	1.00485
	9	0.9454	0.9353	0.162	220.19	1.00389
	10	0.9448	0.9348	0.162	220.19	1.00441
	11	0.9458	0.9357	0.162	220.19	1.00387
	12	0.9453	0.9352	0.162	220.19	1.00536
	13	0.9450	0.9350	0.162	220.19	1.00454
	14	0.9446	0.9347	0.162	220.19	1.00545
	15	0.9453	0.9352	0.162	220.19	1.00497
	16	0.9453	0.9352	0.162	220.19	1.00506
	17	0.9455	0.9354	0.162	220.19	1.00568
	18	0.9453	0.9352	0.162	220.19	1.00465
pst021	3	0.9601	0.9546	0.302	131.30	1.01198
	8	0.9604	0.9548	0.302	131.30	1.00474
pst024	3	0.9205	0.9260	0.444	115.40	1.00277

Table 6-13. Comparison of SINGLE UNIT SOLUTION Applications to Critical Benchmarks

IHECSBE	Case	*cv031* c_k	*sph14* c_k	EALF (eV)	H / Pu	k_{eff}
	6	0.9085	0.9240	1.607	59.25	1.00136
	16	0.9068	0.9088	0.287	161.28	1.00457
pst025	31	0.9127	0.9165	0.353	115.40	0.99675
	42	0.9119	0.9251	1.142	59.25	0.99558
pst026	12	0.9157	0.9147	0.239	189.80	1.00047
	16	0.9074	0.9099	0.312	161.28	0.99735
	19	0.9240	0.9297	0.503	115.40	0.99688

All k_{eff} values were calculated with a standard deviation of 0.0005.
For all applications H/ Pu = 28.79
EALF values for the above applications is as follows:
Case cv031: 1.094 eV
Case sph14: 1.259 eV

Table 6-14. Comparison of DRY LATTICE Applications to Critical Benchmarks

IHECSBE Identifier	Case	*Hexsdry* c_k	*Octsdry* c_k	EALF (eV)	H / Pu	k_{eff}
pcm001	3	0.9549	0.9509	30.518	15.46	1.02356
	4	0.9313	0.9262	37.727	16.40	0.99275
	5	0.9437	0.9378	1.468	65.37	1.01403
pcm002	10	0.9693	0.9646	4.026	15.46	1.03534
	11	0.9718	0.9676	4.405	15.46	1.03184
	12	0.9739	0.9701	4.970	15.46	1.03209
	13	0.9738	0.9700	5.262	15.46	1.02982
	14	0.9741	0.9706	5.405	15.46	1.03451
	15	0.9721	0.9681	5.366	15.46	1.03220
	16	0.9722	0.9681	4.998	15.46	1.02841
	17	0.9538	0.9479	4.762	16.40	1.01596
	18	0.9594	0.9545	5.998	16.40	1.01408
	19	0.9607	0.9557	6.268	16.40	1.01680
	20	0.9607	0.9560	6.446	16.40	1.01355
	21	0.9612	0.9563	6.400	16.40	1.01719
	22	0.9584	0.9534	6.241	16.40	1.01789
	23	0.9181	0.9117	0.663	65.37	1.01077
	24	0.9249	0.9187	0.673	65.37	1.01215
	25	0.9270	0.9211	0.684	65.37	1.01189
	26	0.9273	0.9213	0.689	65.37	1.01298
	27	0.9271	0.9210	0.700	65.37	1.01294
	28	0.9292	0.9233	0.703	65.37	1.01412
	29	0.9306	0.9248	0.708	65.37	1.01424
pst001	6	0.9227	0.9223	0.337	91.19	1.00882
pst007	2	0.9122	0.9120	0.267	109.55	1.00909
	3	0.9059	0.9060	0.254	113.97	1.00375
pst021	3	0.9081	0.9093	0.302	131.30	1.01198
	8	0.9078	0.9090	0.302	131.30	1.00474
pst024	3	0.9156	0.9121	0.444	115.40	1.00277
	6	0.9523	0.9473	1.607	59.25	1.00136
pst025	31	0.9067	0.9025	0.353	115.40	0.99675
	42	0.9488	0.9437	1.142	59.25	0.99558
pst026	19	0.9196	0.9164	0.503	115.40	0.99688

All k_{eff} values were calculated with a standard deviation of 0.0005.
For all applications H/ Pu = 28.79
EALF values for the applications are as follows: Case *hexsdry*: 4.864 eV
Case *octsdry*: 5.042 eV

6.9.4 Calculation Results

6.9.4.1 Calculations Supporting Single Package Analysis

Table 6-15 lists calculations performed to support the standard single package analysis for normal conditions of transport and hypothetical accident conditions.

Table 6-15. Tabulation of Calculations Supporting the Standard Single Package Analysis for Normal Conditions of Transport and Hypothetical Accident Conditions

Case Name	k_{eff}	σ	Model Type	Description	H/Pu	Case location
Sudma	0.55252	0.00049	detailed	Pu metal sphere, no water in TB-1	0	/pat1/apps/normsp/detailed/met/
sudmb	0.64919	0.00049	detailed	Pu metal sphere reflected by water in TB-1	0	/pat1/apps/normsp/detailed/met/
sudmwoodm	0.64857	0.00050	detailed	sudmb with 80% of redwood density	0	/pat1/apps/normsp/detailed/met/
sudmwoodp	0.65003	0.00049	detailed	sudmb with 120% of redwood density	0	/pat1/apps/normsp/detailed/met/
sudmc	0.65037	0.00049	detailed	sudmb with gaps filled with water	0	/pat1/apps/normsp/detailed/met/
sudmd	0.64988	0.00049	detailed	sudmc with copper changed to water	0	/pat1/apps/normsp/detailed/met/
sudme	0.64889	0.00050	detailed	sudmd with aluminum changed to water	0	/pat1/apps/normsp/detailed/met/
sudmf	0.65231	0.00050	detailed	sudme with redwood changed to water	0	/pat1/apps/normsp/detailed/met/
sudsb	0.56797	0.00051	detailed	Pu-water in TB-1	28.8	/pat1/apps/normsp/detailed/soln/
sudswoodm	0.55988	0.00053	detailed	sudsb with 80% of redwood density	28.8	/pat1/apps/normsp/detailed/soln/
sudswoodp	0.57611	0.00049	detailed	sudsb with 120% of redwood density	28.8	/pat1/apps/normsp/detailed/soln/
sudsc	0.59112	0.00050	detailed	sudsb with gaps filled with water	28.8	/pat1/apps/normsp/detailed/soln/
sudsd	0.59200	0.00050	detailed	sudsc with copper changed to water	28.8	/pat1/apps/normsp/detailed/soln/
sudse	0.59316	0.00049	detailed	sudsd with aluminum changed to water	28.8	/pat1/apps/normsp/detailed/soln/
sudsf	0.62781	0.00052	detailed	sudse with redwood changed to water	28.8	/pat1/apps/normsp/detailed/soln/
sudsg	0.70400	0.00050	detailed	sudsf with steel changed to water	28.8	/pat1/apps/normsp/detailed/soln/
cv001[a]	0.65648	0.00046	simplified	redwood and outer steel drum modeled as water	0	/pat1/apps/normsp/simple/cv/
cv002	0.65418	0.00049	simplified	redwood and outer steel drum modeled as water	0.013	/pat1/apps/normsp/simple/cv/
cv003	0.65184	0.00048	simplified	redwood and outer steel drum modeled as water	0.027	/pat1/apps/normsp/simple/cv/
cv004	0.64541	0.00049	simplified	redwood and outer steel drum modeled as water	0.070	/pat1/apps/normsp/simple/cv/
cv005	0.63449	0.00050	simplified	redwood and outer steel drum modeled as water	0.15	/pat1/apps/normsp/simple/cv/
cv006	0.62351	0.00049	simplified	redwood and outer steel drum modeled as water	0.24	/pat1/apps/normsp/simple/cv/
cv007	0.61203	0.00049	simplified	redwood and outer steel drum modeled as water	0.33	/pat1/apps/normsp/simple/cv/
cv008	0.60147	0.00050	simplified	redwood and outer steel drum modeled as water	0.45	/pat1/apps/normsp/simple/cv/

Table 6-15. Tabulation of Calculations Supporting the Standard Single Package Analysis for Normal Conditions of Transport and Hypothetical Accident Conditions

Case Name	k_{eff}	σ	Model Type	Description	H/Pu	Case location
cv009	0.59098	0.00049	simplified	redwood and outer steel drum modeled as water	0.57	/pat1/apps/normsp/simple/cv/
cv010	0.58139	0.00045	simplified	redwood and outer steel drum modeled as water	0.72	/pat1/apps/normsp/simple/cv/
cv011	0.57148	0.00049	simplified	redwood and outer steel drum modeled as water	0.89	/pat1/apps/normsp/simple/cv/
cv012	0.56435	0.00049	simplified	redwood and outer steel drum modeled as water	1.09	/pat1/apps/normsp/simple/cv/
cv013	0.55469	0.00050	simplified	redwood and outer steel drum modeled as water	1.34	/pat1/apps/normsp/simple/cv/
cv014	0.54769	0.00050	simplified	redwood and outer steel drum modeled as water	1.63	/pat1/apps/normsp/simple/cv/
cv015	0.54270	0.00050	simplified	redwood and outer steel drum modeled as water	2.00	/pat1/apps/normsp/simple/cv/
cv016	0.53871	0.00050	simplified	redwood and outer steel drum modeled as water	2.48	/pat1/apps/normsp/simple/cv/
cv017	0.53848	0.00049	simplified	redwood and outer steel drum modeled as water	3.12	/pat1/apps/normsp/simple/cv/
cv018	0.54156	0.00050	simplified	redwood and outer steel drum modeled as water	4.01	/pat1/apps/normsp/simple/cv/
cv019	0.54894	0.00049	simplified	redwood and outer steel drum modeled as water	5.34	/pat1/apps/normsp/simple/cv/
cv020	0.56885	0.00049	simplified	redwood and outer steel drum modeled as water	7.57	/pat1/apps/normsp/simple/cv/
cv021	0.60586	0.00050	simplified	redwood and outer steel drum modeled as water	12.0	/pat1/apps/normsp/simple/cv/
cv022	0.60740	0.00054	simplified	redwood and outer steel drum modeled as water	12.1	/pat1/apps/normsp/simple/cv/
cv023	0.54664	0.00049	simplified	redwood and outer steel drum modeled as water	5.34	/pat1/apps/normsp/simple/cv/
cv024	0.56835	0.00050	simplified	redwood and outer steel drum modeled as water	7.57	/pat1/apps/normsp/simple/cv/
cv025	0.61086	0.00050	simplified	redwood and outer steel drum modeled as water	12.0	/pat1/apps/normsp/simple/cv/
cv026	0.62366	0.00049	simplified	redwood and outer steel drum modeled as water	13.5	/pat1/apps/normsp/simple/cv/
cv027	0.63709	0.00049	simplified	redwood and outer steel drum modeled as water	15.4	/pat1/apps/normsp/simple/cv/
cv028	0.65343	0.00049	simplified	redwood and outer steel drum modeled as water	17.7	/pat1/apps/normsp/simple/cv/
cv029	0.67196	0.00053	simplified	redwood and outer steel drum modeled as water	20.9	/pat1/apps/normsp/simple/cv/
cv030	0.69513	0.00057	simplified	redwood and outer steel drum modeled as water	25.4	/pat1/apps/normsp/simple/cv/
cv031[a]	0.70756	0.00055	simplified	redwood and outer steel drum modeled as water	28.8	/pat1/apps/normsp/simple/cv/
cv032	0.70106	0.00054	simplified	redwood and outer steel drum modeled as water	32.0	/pat1/apps/normsp/simple/cv/

Table 6-15. Tabulation of Calculations Supporting the Standard Single Package Analysis for Normal Conditions of Transport and Hypothetical Accident Conditions

Case Name	k_{eff}	σ	Model Type	Description	H/Pu	Case location
cv033	0.69423	0.00050	simplified	redwood and outer steel drum modeled as water	36.8	/pat1/apps/normsp/simple/cv/
cv034	0.68607	0.00051	simplified	redwood and outer steel drum modeled as water	43.2	/pat1/apps/normsp/simple/cv/
cv035	0.67715	0.00051	simplified	redwood and outer steel drum modeled as water	52.1	/pat1/apps/normsp/simple/cv/
cv036	0.66815	0.00052	simplified	redwood and outer steel drum modeled as water	65.4	/pat1/apps/normsp/simple/cv/
cv037	0.65515	0.00050	simplified	redwood and outer steel drum modeled as water	87.7	/pat1/apps/normsp/simple/cv/
cv038	0.63611	0.00053	simplified	redwood and outer steel drum modeled as water	132.2	/pat1/apps/normsp/simple/cv/
sp001	0.64320	0.00049	simplified	nominal redwood & steel modeled	0	/pat1/apps/normsp/simple/rdwood/
sp002	0.64219	0.00049	simplified	nominal redwood & steel modeled	0.013	/pat1/apps/normsp/simple/rdwood/
sp003	0.63869	0.00050	simplified	nominal redwood & steel modeled	0.027	/pat1/apps/normsp/simple/rdwood/
sp004	0.63183	0.00049	simplified	nominal redwood & steel modeled	0.070	/pat1/apps/normsp/simple/rdwood/
sp005	0.62057	0.00049	simplified	nominal redwood & steel modeled	0.15	/pat1/apps/normsp/simple/rdwood/
sp006	0.60807	0.00049	simplified	nominal redwood & steel modeled	0.24	/pat1/apps/normsp/simple/rdwood/
sp007	0.59672	0.00049	simplified	nominal redwood & steel modeled	0.33	/pat1/apps/normsp/simple/rdwood/
sp008	0.58466	0.00049	simplified	nominal redwood & steel modeled	0.45	/pat1/apps/normsp/simple/rdwood/
sp009	0.57386	0.00049	simplified	nominal redwood & steel modeled	0.57	/pat1/apps/normsp/simple/rdwood/
sp010	0.56209	0.00048	simplified	nominal redwood & steel modeled	0.72	/pat1/apps/normsp/simple/rdwood/
sp011	0.55118	0.00049	simplified	nominal redwood & steel modeled	0.89	/pat1/apps/normsp/simple/rdwood/
sp012	0.54046	0.00049	simplified	nominal redwood & steel modeled	1.09	/pat1/apps/normsp/simple/rdwood/
sp013	0.53048	0.00049	simplified	nominal redwood & steel modeled	1.34	/pat1/apps/normsp/simple/rdwood/
sp014	0.52122	0.00050	simplified	nominal redwood & steel modeled	1.63	/pat1/apps/normsp/simple/rdwood/
sp015	0.51185	0.00049	simplified	nominal redwood & steel modeled	2.00	/pat1/apps/normsp/simple/rdwood/
sp016	0.50434	0.00050	simplified	nominal redwood & steel modeled	2.48	/pat1/apps/normsp/simple/rdwood/
sp017	0.49909	0.00050	simplified	nominal redwood & steel modeled	3.12	/pat1/apps/normsp/simple/rdwood/
sp018	0.49516	0.00049	simplified	nominal redwood & steel modeled	4.01	/pat1/apps/normsp/simple/rdwood/

Table 6-15. Tabulation of Calculations Supporting the Standard Single Package Analysis for Normal Conditions of Transport and Hypothetical Accident Conditions

Case Name	k_{eff}	σ	Model Type	Description	H/Pu	Case location
sp019	0.49425	0.00047	simplified	nominal redwood & steel modeled	5.34	/pat1/apps/normsp/simple/rdwood/
sp020	0.49848	0.00049	simplified	nominal redwood & steel modeled	7.57	/pat1/apps/normsp/simple/rdwood/
sp021	0.51005	0.00050	simplified	nominal redwood & steel modeled	12.0	/pat1/apps/normsp/simple/rdwood/
sp022	0.51044	0.00049	simplified	nominal redwood & steel modeled	12.1	/pat1/apps/normsp/simple/rdwood/
sp023	0.46393	0.00049	simplified	nominal redwood & steel modeled	5.34	/pat1/apps/normsp/simple/rdwood/
sp024	0.47663	0.00049	simplified	nominal redwood & steel modeled	7.57	/pat1/apps/normsp/simple/rdwood/
sp025	0.50178	0.00049	simplified	nominal redwood & steel modeled	12.0	/pat1/apps/normsp/simple/rdwood/
sp026	0.50911	0.00049	simplified	nominal redwood & steel modeled	13.5	/pat1/apps/normsp/simple/rdwood/
sp027	0.51691	0.00050	simplified	nominal redwood & steel modeled	15.4	/pat1/apps/normsp/simple/rdwood/
sp028	0.52725	0.00049	simplified	nominal redwood & steel modeled	17.7	/pat1/apps/normsp/simple/rdwood/
sp029	0.53595	0.00047	simplified	nominal redwood & steel modeled	20.9	/pat1/apps/normsp/simple/rdwood/
sp030	0.54436	0.00049	simplified	nominal redwood & steel modeled	25.4	/pat1/apps/normsp/simple/rdwood/
sp031	0.54872	0.00053	simplified	nominal redwood & steel modeled	28.8	/pat1/apps/normsp/simple/rdwood/
sp032	0.54122	0.00053	simplified	nominal redwood & steel modeled	32.0	/pat1/apps/normsp/simple/rdwood/
sp033	0.53213	0.00049	simplified	nominal redwood & steel modeled	36.8	/pat1/apps/normsp/simple/rdwood/
sp034	0.52280	0.00049	simplified	nominal redwood & steel modeled	43.2	/pat1/apps/normsp/simple/rdwood/
sp035	0.51265	0.00054	simplified	nominal redwood & steel modeled	52.1	/pat1/apps/normsp/simple/rdwood/
sp036	0.50240	0.00049	simplified	nominal redwood & steel modeled	65.4	/pat1/apps/normsp/simple/rdwood/
sp037	0.48877	0.00050	simplified	nominal redwood & steel modeled	87.7	/pat1/apps/normsp/simple/rdwood/
sp038	0.46921	0.00049	simplified	nominal redwood & steel modeled	132.2	/pat1/apps/normsp/simple/rdwood/
rwh001	0.64527	0.00049	simplified	120% redwood density	0	/pat1/apps/normsp/simple/rdwood+/
rwh002	0.64286	0.00050	simplified	120% redwood density	0.013	/pat1/apps/normsp/simple/rdwood+/
rwh003	0.64097	0.00050	simplified	120% redwood density	0.027	/pat1/apps/normsp/simple/rdwood+/
rwh004	0.63332	0.00050	simplified	120% redwood density	0.070	/pat1/apps/normsp/simple/rdwood+/

Table 6-15. Tabulation of Calculations Supporting the Standard Single Package Analysis for Normal Conditions of Transport and Hypothetical Accident Conditions

Case Name	k_{eff}	σ	Model Type	Description	H/Pu	Case location
rwh005	0.62197	0.00049	simplified	120% redwood density	0.15	/pat1/apps/normsp/simple/rdwood+/
rwh006	0.60969	0.00049	simplified	120% redwood density	0.24	/pat1/apps/normsp/simple/rdwood+/
rwh007	0.59769	0.00049	simplified	120% redwood density	0.33	/pat1/apps/normsp/simple/rdwood+/
rwh008	0.58662	0.00049	simplified	120% redwood density	0.45	/pat1/apps/normsp/simple/rdwood+/
rwh009	0.57499	0.00049	simplified	120% redwood density	0.57	/pat1/apps/normsp/simple/rdwood+/
rwh010	0.56412	0.00050	simplified	120% redwood density	0.72	/pat1/apps/normsp/simple/rdwood+/
rwh011	0.55307	0.00050	simplified	120% redwood density	0.89	/pat1/apps/normsp/simple/rdwood+/
rwh012	0.54232	0.00049	simplified	120% redwood density	1.09	/pat1/apps/normsp/simple/rdwood+/
rwh013	0.53303	0.00050	simplified	120% redwood density	1.34	/pat1/apps/normsp/simple/rdwood+/
rwh014	0.52358	0.00049	simplified	120% redwood density	1.63	/pat1/apps/normsp/simple/rdwood+/
rwh015	0.51553	0.00049	simplified	120% redwood density	2.00	/pat1/apps/normsp/simple/rdwood+/
rwh016	0.50835	0.00050	simplified	120% redwood density	2.48	/pat1/apps/normsp/simple/rdwood+/
rwh017	0.50323	0.00050	simplified	120% redwood density	3.12	/pat1/apps/normsp/simple/rdwood+/
rwh018	0.49883	0.00050	simplified	120% redwood density	4.01	/pat1/apps/normsp/simple/rdwood+/
rwh019	0.49978	0.00049	simplified	120% redwood density	5.34	/pat1/apps/normsp/simple/rdwood+/
rwh020	0.50463	0.00047	simplified	120% redwood density	7.57	/pat1/apps/normsp/simple/rdwood+/
rwh021	0.51893	0.00049	simplified	120% redwood density	12.0	/pat1/apps/normsp/simple/rdwood+/
rwh022	0.51840	0.00048	simplified	120% redwood density	12.1	/pat1/apps/normsp/simple/rdwood+/
rwh023	0.47035	0.00049	simplified	120% redwood density	5.34	/pat1/apps/normsp/simple/rdwood+/
rwh024	0.48375	0.00050	simplified	120% redwood density	7.57	/pat1/apps/normsp/simple/rdwood+/
rwh025	0.51085	0.00049	simplified	120% redwood density	12.0	/pat1/apps/normsp/simple/rdwood+/
rwh026	0.51912	0.00049	simplified	120% redwood density	13.5	/pat1/apps/normsp/simple/rdwood+/
rwh027	0.52822	0.00049	simplified	120% redwood density	15.4	/pat1/apps/normsp/simple/rdwood+/
rwh028	0.53713	0.00050	simplified	120% redwood density	17.7	/pat1/apps/normsp/simple/rdwood+/

Table 6-15. Tabulation of Calculations Supporting the Standard Single Package Analysis for Normal Conditions of Transport and Hypothetical Accident Conditions

Case Name	k_{eff}	σ	Model Type	Description	H/Pu	Case location
rwh029	0.54898	0.00049	simplified	120% redwood density	20.9	/pat1/apps/normsp/simple/rdwood+/
rwh030	0.55880	0.00048	simplified	120% redwood density	25.4	/pat1/apps/normsp/simple/rdwood+/
rwh031	0.56354	0.00049	simplified	120% redwood density	28.8	/pat1/apps/normsp/simple/rdwood+/
rwh032	0.55604	0.00049	simplified	120% redwood density	32.0	/pat1/apps/normsp/simple/rdwood+/
rwh033	0.54737	0.00050	simplified	120% redwood density	36.8	/pat1/apps/normsp/simple/rdwood+/
rwh034	0.53800	0.00049	simplified	120% redwood density	43.2	/pat1/apps/normsp/simple/rdwood+/
rwh035	0.52800	0.00049	simplified	120% redwood density	52.1	/pat1/apps/normsp/simple/rdwood+/
rwh036	0.51637	0.00051	simplified	120% redwood density	65.4	/pat1/apps/normsp/simple/rdwood+/
rwh037	0.50261	0.00049	simplified	120% redwood density	87.7	/pat1/apps/normsp/simple/rdwood+/
rwh038	0.48353	0.00048	simplified	120% redwood density	132.2	/pat1/apps/normsp/simple/rdwood+/
rwl001	0.64199	0.00050	simplified	80% redwood density	0	/pat1/apps/normsp/simple/rdwood-/
rwl002	0.64025	0.00050	simplified	80% redwood density	0.013	/pat1/apps/normsp/simple/rdwood-/
rwl003	0.63708	0.00050	simplified	80% redwood density	0.027	/pat1/apps/normsp/simple/rdwood-/
rwl004	0.63111	0.00050	simplified	80% redwood density	0.070	/pat1/apps/normsp/simple/rdwood-/
rwl005	0.61906	0.00049	simplified	80% redwood density	0.15	/pat1/apps/normsp/simple/rdwood-/
rwl006	0.60665	0.00049	simplified	80% redwood density	0.24	/pat1/apps/normsp/simple/rdwood-/
rwl007	0.59477	0.00050	simplified	80% redwood density	0.33	/pat1/apps/normsp/simple/rdwood-/
rwl008	0.58214	0.00049	simplified	80% redwood density	0.45	/pat1/apps/normsp/simple/rdwood-/
rwl009	0.57065	0.00050	simplified	80% redwood density	0.57	/pat1/apps/normsp/simple/rdwood-/
rwl010	0.55970	0.00050	simplified	80% redwood density	0.72	/pat1/apps/normsp/simple/rdwood-/
rwl011	0.54871	0.00050	simplified	80% redwood density	0.89	/pat1/apps/normsp/simple/rdwood-/
rwl012	0.53773	0.00048	simplified	80% redwood density	1.09	/pat1/apps/normsp/simple/rdwood-/
rwl013	0.52837	0.00050	simplified	80% redwood density	1.34	/pat1/apps/normsp/simple/rdwood-/
rwl014	0.51804	0.00050	simplified	80% redwood density	1.63	/pat1/apps/normsp/simple/rdwood-/

Table 6-15. Tabulation of Calculations Supporting the Standard Single Package Analysis for Normal Conditions of Transport and Hypothetical Accident Conditions

Case Name	k_{eff}	σ	Model Type	Description	H/Pu	Case location
rwl015	0.50939	0.00049	simplified	80% redwood density	2.00	/pat1/apps/normsp/simple/rdwood-/
rwl016	0.50098	0.00049	simplified	80% redwood density	2.48	/pat1/apps/normsp/simple/rdwood-/
rwl017	0.49512	0.00050	simplified	80% redwood density	3.12	/pat1/apps/normsp/simple/rdwood-/
rwl018	0.49014	0.00049	simplified	80% redwood density	4.01	/pat1/apps/normsp/simple/rdwood-/
rwl019	0.48891	0.00049	simplified	80% redwood density	5.34	/pat1/apps/normsp/simple/rdwood-/
rwl020	0.49139	0.00050	simplified	80% redwood density	7.57	/pat1/apps/normsp/simple/rdwood-/
rwl021	0.50138	0.00052	simplified	80% redwood density	12.0	/pat1/apps/normsp/simple/rdwood-/
rwl022	0.50208	0.00050	simplified	80% redwood density	12.1	/pat1/apps/normsp/simple/rdwood-/
rwl023	0.45772	0.00049	simplified	80% redwood density	5.34	/pat1/apps/normsp/simple/rdwood-/
rwl024	0.46789	0.00049	simplified	80% redwood density	7.57	/pat1/apps/normsp/simple/rdwood-/
rwl025	0.49183	0.00050	simplified	80% redwood density	12.0	/pat1/apps/normsp/simple/rdwood-/
rwl026	0.49746	0.00049	simplified	80% redwood density	13.5	/pat1/apps/normsp/simple/rdwood-/
rwl027	0.50572	0.00050	simplified	80% redwood density	15.4	/pat1/apps/normsp/simple/rdwood-/
rwl028	0.51415	0.00050	simplified	80% redwood density	17.7	/pat1/apps/normsp/simple/rdwood-/
rwl029	0.52251	0.00049	simplified	80% redwood density	20.9	/pat1/apps/normsp/simple/rdwood-/
rwl030	0.52951	0.00050	simplified	80% redwood density	25.4	/pat1/apps/normsp/simple/rdwood-/
rwl031	0.53188	0.00050	simplified	80% redwood density	28.8	/pat1/apps/normsp/simple/rdwood-/
rwl032	0.52522	0.00057	simplified	80% redwood density	32.0	/pat1/apps/normsp/simple/rdwood-/
rwl033	0.51621	0.00049	simplified	80% redwood density	36.8	/pat1/apps/normsp/simple/rdwood-/
rwl034	0.50720	0.00052	simplified	80% redwood density	43.2	/pat1/apps/normsp/simple/rdwood-/
rwl035	0.49733	0.00049	simplified	80% redwood density	52.1	/pat1/apps/normsp/simple/rdwood-/
rwl036	0.48574	0.00053	simplified	80% redwood density	65.4	/pat1/apps/normsp/simple/rdwood-/
rwl037	0.47230	0.00049	simplified	80% redwood density	87.7	/pat1/apps/normsp/simple/rdwood-/
rwl038	0.45497	0.00049	simplified	80% redwood density	132.2	/pat1/apps/normsp/simple/rdwood-/

Table 6-15. Tabulation of Calculations Supporting the Standard Single Package Analysis for Normal Conditions of Transport and Hypothetical Accident Conditions

Case Name	k_{eff}	σ	Model Type	Description	H/Pu	Case location
spw001	0.65033	0.00050	simplified	redwood modeled as water	0	/pat1/apps/normsp/simple/h2owood/
spw002	0.64843	0.00049	simplified	redwood modeled as water	0.013	/pat1/apps/normsp/simple/h2owood/
spw003	0.64700	0.00049	simplified	redwood modeled as water	0.027	/pat1/apps/normsp/simple/h2owood/
spw004	0.63908	0.00049	simplified	redwood modeled as water	0.070	/pat1/apps/normsp/simple/h2owood/
spw005	0.62742	0.00050	simplified	redwood modeled as water	0.15	/pat1/apps/normsp/simple/h2owood/
spw006	0.61727	0.00049	simplified	redwood modeled as water	0.24	/pat1/apps/normsp/simple/h2owood/
spw007	0.60483	0.00049	simplified	redwood modeled as water	0.33	/pat1/apps/normsp/simple/h2owood/
spw008	0.59386	0.00050	simplified	redwood modeled as water	0.45	/pat1/apps/normsp/simple/h2owood/
spw009	0.58271	0.00049	simplified	redwood modeled as water	0.57	/pat1/apps/normsp/simple/h2owood/
spw010	0.57190	0.00049	simplified	redwood modeled as water	0.72	/pat1/apps/normsp/simple/h2owood/
spw011	0.56188	0.00049	simplified	redwood modeled as water	0.89	/pat1/apps/normsp/simple/h2owood/
spw012	0.55272	0.00049	simplified	redwood modeled as water	1.09	/pat1/apps/normsp/simple/h2owood/
spw013	0.54391	0.00049	simplified	redwood modeled as water	1.34	/pat1/apps/normsp/simple/h2owood/
spw014	0.53537	0.00049	simplified	redwood modeled as water	1.63	/pat1/apps/normsp/simple/h2owood/
spw015	0.52825	0.00049	simplified	redwood modeled as water	2.00	/pat1/apps/normsp/simple/h2owood/
spw016	0.52190	0.00050	simplified	redwood modeled as water	2.48	/pat1/apps/normsp/simple/h2owood/
spw017	0.51869	0.00050	simplified	redwood modeled as water	3.12	/pat1/apps/normsp/simple/h2owood/
spw018	0.51825	0.00049	simplified	redwood modeled as water	4.01	/pat1/apps/normsp/simple/h2owood/
spw019	0.52240	0.00049	simplified	redwood modeled as water	5.34	/pat1/apps/normsp/simple/h2owood/
spw020	0.53256	0.00050	simplified	redwood modeled as water	7.57	/pat1/apps/normsp/simple/h2owood/
spw021	0.55865	0.00050	simplified	redwood modeled as water	12.0	/pat1/apps/normsp/simple/h2owood/
spw022	0.55901	0.00049	simplified	redwood modeled as water	12.1	/pat1/apps/normsp/simple/h2owood/
spw023	0.50382	0.00049	simplified	redwood modeled as water	5.34	/pat1/apps/normsp/simple/h2owood/
spw024	0.52217	0.00046	simplified	redwood modeled as water	7.57	/pat1/apps/normsp/simple/h2owood/

Table 6-15. Tabulation of Calculations Supporting the Standard Single Package Analysis for Normal Conditions of Transport and Hypothetical Accident Conditions

Case Name	k_{eff}	σ	Model Type	Description	H/Pu	Case location
spw025	0.55687	0.00049	simplified	redwood modeled as water	12.0	/pat1/apps/normsp/simple/h2owood/
spw026	0.56847	0.00050	simplified	redwood modeled as water	13.5	/pat1/apps/normsp/simple/h2owood/
spw027	0.57991	0.00050	simplified	redwood modeled as water	15.4	/pat1/apps/normsp/simple/h2owood/
spw028	0.59315	0.00049	simplified	redwood modeled as water	17.7	/pat1/apps/normsp/simple/h2owood/
spw029	0.60796	0.00049	simplified	redwood modeled as water	20.9	/pat1/apps/normsp/simple/h2owood/
spw030	0.62351	0.00049	simplified	redwood modeled as water	25.4	/pat1/apps/normsp/simple/h2owood/
spw031	0.63291	0.00050	simplified	redwood modeled as water	28.8	/pat1/apps/normsp/simple/h2owood/
spw032	0.62643	0.00050	simplified	redwood modeled as water	32.0	/pat1/apps/normsp/simple/h2owood/
spw033	0.61758	0.00050	simplified	redwood modeled as water	36.8	/pat1/apps/normsp/simple/h2owood/
spw034	0.60761	0.00049	simplified	redwood modeled as water	43.2	/pat1/apps/normsp/simple/h2owood/
spw035	0.59709	0.00051	simplified	redwood modeled as water	52.1	/pat1/apps/normsp/simple/h2owood/
spw036	0.58537	0.00051	simplified	redwood modeled as water	65.4	/pat1/apps/normsp/simple/h2owood/
spw037	0.56841	0.00050	simplified	redwood modeled as water	87.7	/pat1/apps/normsp/simple/h2owood/
spw038	0.54692	0.00051	simplified	redwood modeled as water	132.2	/pat1/apps/normsp/simple/h2owood/

[a] Limiting cases listed in Table 6-1.

6.9.4.2 Calculations Supporting Normal Conditions of Transport Array Analysis

Table 6-16 lists calculations performed to support the analysis of arrays of undamaged packages.

Note that some case names were used multiple times. Refer to the case description and file location to differentiate cases.

Table 6-16. Tabulation of Calculations Supporting the Analysis of Arrays of Undamaged Packages

Case Name	k_{eff}	σ	Package Model Type	Array Type	Description	H/Pu	Location
fsld001	0.65045	0.00049	detailed	square	Base detailed model	0	/pat1/apps/normarray/detail/fsld/
fsld002	0.64841	0.00050	detailed	square	Base detailed model	0.013	/pat1/apps/normarray/detail/fsld/
fsld003	0.64611	0.00050	detailed	square	Base detailed model	0.027	/pat1/apps/normarray/detail/fsld/
fsld004	0.63833	0.00049	detailed	square	Base detailed model	0.070	/pat1/apps/normarray/detail/fsld/
fsld005	0.62772	0.00050	detailed	square	Base detailed model	0.15	/pat1/apps/normarray/detail/fsld/
fsld006	0.61627	0.00050	detailed	square	Base detailed model	0.24	/pat1/apps/normarray/detail/fsld/
fsld007	0.60399	0.00049	detailed	square	Base detailed model	0.33	/pat1/apps/normarray/detail/fsld/
fsld008	0.59302	0.00049	detailed	square	Base detailed model	0.45	/pat1/apps/normarray/detail/fsld/
fsld009	0.58156	0.00049	detailed	square	Base detailed model	0.57	/pat1/apps/normarray/detail/fsld/
fsld010	0.57146	0.00046	detailed	square	Base detailed model	0.72	/pat1/apps/normarray/detail/fsld/
fsld011	0.55968	0.00048	detailed	square	Base detailed model	0.89	/pat1/apps/normarray/detail/fsld/
fsld012	0.55046	0.00048	detailed	square	Base detailed model	1.09	/pat1/apps/normarray/detail/fsld/
fsld013	0.54098	0.00050	detailed	square	Base detailed model	1.34	/pat1/apps/normarray/detail/fsld/
fsld014	0.53212	0.00049	detailed	square	Base detailed model	1.63	/pat1/apps/normarray/detail/fsld/
fsld015	0.52530	0.00050	detailed	square	Base detailed model	2.00	/pat1/apps/normarray/detail/fsld/
fsld016	0.51857	0.00050	detailed	square	Base detailed model	2.48	/pat1/apps/normarray/detail/fsld/
fsld017	0.51468	0.00046	detailed	square	Base detailed model	3.12	/pat1/apps/normarray/detail/fsld/
fsld018	0.51149	0.00050	detailed	square	Base detailed model	4.01	/pat1/apps/normarray/detail/fsld/
fsld019	0.51174	0.00050	detailed	square	Base detailed model	5.34	/pat1/apps/normarray/detail/fsld/
fsld020	0.51919	0.00050	detailed	square	Base detailed model	7.57	/pat1/apps/normarray/detail/fsld/
fsld021	0.53283	0.00049	detailed	square	Base detailed model	12.0	/pat1/apps/normarray/detail/fsld/
fsld022	0.53398	0.00050	detailed	square	Base detailed model	12.1	/pat1/apps/normarray/detail/fsld/
fsld023	0.47720	0.00049	detailed	square	Base detailed model	5.34	/pat1/apps/normarray/detail/fsld/
fsld024	0.49116	0.00050	detailed	square	Base detailed model	7.57	/pat1/apps/normarray/detail/fsld/
fsld025	0.52185	0.00050	detailed	square	Base detailed model	12.0	/pat1/apps/normarray/detail/fsld/
fsld026	0.53042	0.00049	detailed	square	Base detailed model	13.5	/pat1/apps/normarray/detail/fsld/

Table 6-16. Tabulation of Calculations Supporting the Analysis of Arrays of Undamaged Packages

Case Name	k_{eff}	σ	Package Model Type	Array Type	Description	H/Pu	Location
fsld027	0.54015	0.00049	detailed	square	Base detailed model	15.4	/pat1/apps/normarray/detail/fsld/
fsld028	0.55270	0.00049	detailed	square	Base detailed model	17.7	/pat1/apps/normarray/detail/fsld/
fsld029	0.56357	0.00049	detailed	square	Base detailed model	20.9	/pat1/apps/normarray/detail/fsld/
fsld030	0.57757	0.00051	detailed	square	Base detailed model	25.4	/pat1/apps/normarray/detail/fsld/
fsld031	0.58160	0.00049	detailed	square	Base detailed model	28.8	/pat1/apps/normarray/detail/fsld/
fsld032	0.57339	0.00053	detailed	square	Base detailed model	32.0	/pat1/apps/normarray/detail/fsld/
fsld033	0.56487	0.00061	detailed	square	Base detailed model	36.8	/pat1/apps/normarray/detail/fsld/
fsld034	0.55433	0.00050	detailed	square	Base detailed model	43.2	/pat1/apps/normarray/detail/fsld/
fsld035	0.54470	0.00049	detailed	square	Base detailed model	52.1	/pat1/apps/normarray/detail/fsld/
fsld036	0.53388	0.00053	detailed	square	Base detailed model	65.4	/pat1/apps/normarray/detail/fsld/
fsld037	0.51999	0.00053	detailed	square	Base detailed model	87.7	/pat1/apps/normarray/detail/fsld/
fsld038	0.50063	0.00050	detailed	square	Base detailed model	132.2	/pat1/apps/normarray/detail/fsld/
fsld001a	0.65125	0.00049	detailed	square	base detailed model, Gap -> redwood	0.0	/pat1/apps/normarray/detail/swap/
fsld001b	0.64857	0.00049	detailed	square	fsld001a with copper -> redwood	0.0	/pat1/apps/normarray/detail/swap/
fsld001c	0.64787	0.00050	detailed	square	fsld001b with aluminum -> redwood	0.0	/pat1/apps/normarray/detail/swap/
fsld001d	0.65266	0.00048	detailed	square	fsld001c with redwood -> water	0.0	/pat1/apps/normarray/detail/swap/
fsld031a	0.58653	0.00050	detailed	square	base detailed model, Gap -> redwood	28.8	/pat1/apps/normarray/detail/swap/
fsld031b	0.57760	0.00053	detailed	square	fsld031a with copper -> redwood	28.8	/pat1/apps/normarray/detail/swap/
fsld031c	0.57512	0.00056	detailed	square	fsld031b with aluminum -> redwood	28.8	/pat1/apps/normarray/detail/swap/
fsld031d	0.62750	0.00050	detailed	square	fsld031c with redwood -> water	28.8	/pat1/apps/normarray/detail/swap/
fslw001	0.64556	0.00050	simplified	square	base simplified model	0	/pat1/apps/normarray/square/wood/
fslw002	0.64345	0.00049	simplified	square	base simplified model	0.013	/pat1/apps/normarray/square/wood/
fslw003	0.64008	0.00050	simplified	square	base simplified model	0.027	/pat1/apps/normarray/square/wood/
fslw004	0.63367	0.00050	simplified	square	base simplified model	0.070	/pat1/apps/normarray/square/wood/
fslw005	0.62197	0.00049	simplified	square	base simplified model	0.15	/pat1/apps/normarray/square/wood/
fslw006	0.60997	0.00049	simplified	square	base simplified model	0.24	/pat1/apps/normarray/square/wood/

Table 6-16. Tabulation of Calculations Supporting the Analysis of Arrays of Undamaged Packages

Case Name	k_{eff}	σ	Package Model Type	Array Type	Description	H/Pu	Location
fslw007	0.59731	0.00050	simplified	square	base simplified model	0.33	/pat1/apps/normarray/square/wood/
fslw008	0.58659	0.00050	simplified	square	base simplified model	0.45	/pat1/apps/normarray/square/wood/
fslw009	0.57517	0.00050	simplified	square	base simplified model	0.57	/pat1/apps/normarray/square/wood/
fslw010	0.56406	0.00050	simplified	square	base simplified model	0.72	/pat1/apps/normarray/square/wood/
fslw011	0.55274	0.00050	simplified	square	base simplified model	0.89	/pat1/apps/normarray/square/wood/
fslw012	0.54323	0.00048	simplified	square	base simplified model	1.09	/pat1/apps/normarray/square/wood/
fslw013	0.53268	0.00050	simplified	square	base simplified model	1.34	/pat1/apps/normarray/square/wood/
fslw014	0.52321	0.00049	simplified	square	base simplified model	1.63	/pat1/apps/normarray/square/wood/
fslw015	0.51526	0.00049	simplified	square	base simplified model	2.00	/pat1/apps/normarray/square/wood/
fslw016	0.50857	0.00050	simplified	square	base simplified model	2.48	/pat1/apps/normarray/square/wood/
fslw017	0.50236	0.00050	simplified	square	base simplified model	3.12	/pat1/apps/normarray/square/wood/
fslw018	0.49835	0.00050	simplified	square	base simplified model	4.01	/pat1/apps/normarray/square/wood/
fslw019	0.49909	0.00046	simplified	square	base simplified model	5.34	/pat1/apps/normarray/square/wood/
fslw020	0.50414	0.00049	simplified	square	base simplified model	7.57	/pat1/apps/normarray/square/wood/
fslw021	0.51817	0.00049	simplified	square	base simplified model	12.0	/pat1/apps/normarray/square/wood/
fslw022	0.51808	0.00049	simplified	square	base simplified model	12.1	/pat1/apps/normarray/square/wood/
fslw023	0.46952	0.00050	simplified	square	base simplified model	5.34	/pat1/apps/normarray/square/wood/
fslw024	0.48411	0.00050	simplified	square	base simplified model	7.57	/pat1/apps/normarray/square/wood/
fslw025	0.51041	0.00050	simplified	square	base simplified model	12.0	/pat1/apps/normarray/square/wood/
fslw026	0.51930	0.00049	simplified	square	base simplified model	13.5	/pat1/apps/normarray/square/wood/
fslw027	0.52770	0.00050	simplified	square	base simplified model	15.4	/pat1/apps/normarray/square/wood/
fslw028	0.53726	0.00049	simplified	square	base simplified model	17.7	/pat1/apps/normarray/square/wood/
fslw029	0.55000	0.00051	simplified	square	base simplified model	20.9	/pat1/apps/normarray/square/wood/
fslw030	0.55945	0.00049	simplified	square	base simplified model	25.4	/pat1/apps/normarray/square/wood/
fslw031	0.56510	0.00052	simplified	square	base simplified model	28.8	/pat1/apps/normarray/square/wood/
fslw032	0.55740	0.00051	simplified	square	base simplified model	32.0	/pat1/apps/normarray/square/wood/

Table 6-16. Tabulation of Calculations Supporting the Analysis of Arrays of Undamaged Packages

Case Name	k_{eff}	σ	Package Model Type	Array Type	Description	H/Pu	Location
fslw033	0.54891	0.00051	simplified	square	base simplified model	36.8	/pat1/apps/normarray/square/wood/
fslw034	0.53927	0.00050	simplified	square	base simplified model	43.2	/pat1/apps/normarray/square/wood/
fslw035	0.52975	0.00050	simplified	square	base simplified model	52.1	/pat1/apps/normarray/square/wood/
fslw036	0.51761	0.00050	simplified	square	base simplified model	65.4	/pat1/apps/normarray/square/wood/
fslw037	0.50314	0.00049	simplified	square	base simplified model	87.7	/pat1/apps/normarray/square/wood/
fslw038	0.48423	0.00051	simplified	square	base simplified model	132.2	/pat1/apps/normarray/square/wood/
fslw+001	0.64568	0.00050	simplified	square	120% redwood density	0	/pat1/apps/normarray/square/wood+/
fslw+002	0.64401	0.00050	simplified	square	120% redwood density	0.013	/pat1/apps/normarray/square/wood+/
fslw+003	0.64154	0.00050	simplified	square	120% redwood density	0.027	/pat1/apps/normarray/square/wood+/
fslw+004	0.63415	0.00049	simplified	square	120% redwood density	0.070	/pat1/apps/normarray/square/wood+/
fslw+005	0.62300	0.00050	simplified	square	120% redwood density	0.15	/pat1/apps/normarray/square/wood+/
fslw+006	0.61131	0.00049	simplified	square	120% redwood density	0.24	/pat1/apps/normarray/square/wood+/
fslw+007	0.59906	0.00049	simplified	square	120% redwood density	0.33	/pat1/apps/normarray/square/wood+/
fslw+008	0.58795	0.00049	simplified	square	120% redwood density	0.45	/pat1/apps/normarray/square/wood+/
fslw+009	0.57705	0.00049	simplified	square	120% redwood density	0.57	/pat1/apps/normarray/square/wood+/
fslw+010	0.56459	0.00049	simplified	square	120% redwood density	0.72	/pat1/apps/normarray/square/wood+/
fslw+011	0.55413	0.00048	simplified	square	120% redwood density	0.89	/pat1/apps/normarray/square/wood+/
fslw+012	0.54491	0.00045	simplified	square	120% redwood density	1.09	/pat1/apps/normarray/square/wood+/
fslw+013	0.53489	0.00050	simplified	square	120% redwood density	1.34	/pat1/apps/normarray/square/wood+/
fslw+014	0.52548	0.00048	simplified	square	120% redwood density	1.63	/pat1/apps/normarray/square/wood+/
fslw+015	0.51717	0.00050	simplified	square	120% redwood density	2.00	/pat1/apps/normarray/square/wood+/
fslw+016	0.51105	0.00049	simplified	square	120% redwood density	2.48	/pat1/apps/normarray/square/wood+/
fslw+017	0.50560	0.00050	simplified	square	120% redwood density	3.12	/pat1/apps/normarray/square/wood+/
fslw+018	0.50222	0.00047	simplified	square	120% redwood density	4.01	/pat1/apps/normarray/square/wood+/
fslw+019	0.50263	0.00049	simplified	square	120% redwood density	5.34	/pat1/apps/normarray/square/wood+/
fslw+020	0.50756	0.00050	simplified	square	120% redwood density	7.57	/pat1/apps/normarray/square/wood+/

Table 6-16. Tabulation of Calculations Supporting the Analysis of Arrays of Undamaged Packages

Case Name	k_{eff}	σ	Package Model Type	Array Type	Description	H/Pu	Location
fslw+021	0.52384	0.00050	simplified	square	120% redwood density	12.0	/pat1/apps/normarray/square/wood+/
fslw+022	0.52420	0.00048	simplified	square	120% redwood density	12.1	/pat1/apps/normarray/square/wood+/
fslw+023	0.47407	0.00050	simplified	square	120% redwood density	5.34	/pat1/apps/normarray/square/wood+/
fslw+024	0.48817	0.00050	simplified	square	120% redwood density	7.57	/pat1/apps/normarray/square/wood+/
fslw+025	0.51666	0.00049	simplified	square	120% redwood density	12.0	/pat1/apps/normarray/square/wood+/
fslw+026	0.52504	0.00049	simplified	square	120% redwood density	13.5	/pat1/apps/normarray/square/wood+/
fslw+027	0.53514	0.00049	simplified	square	120% redwood density	15.4	/pat1/apps/normarray/square/wood+/
fslw+028	0.54560	0.00050	simplified	square	120% redwood density	17.7	/pat1/apps/normarray/square/wood+/
fslw+029	0.55633	0.00049	simplified	square	120% redwood density	20.9	/pat1/apps/normarray/square/wood+/
fslw+030	0.56867	0.00050	simplified	square	120% redwood density	25.4	/pat1/apps/normarray/square/wood+/
fslw+031	0.57535	0.00050	simplified	square	120% redwood density	28.8	/pat1/apps/normarray/square/wood+/
fslw+032	0.56751	0.00050	simplified	square	120% redwood density	32.0	/pat1/apps/normarray/square/wood+/
fslw+033	0.55898	0.00049	simplified	square	120% redwood density	36.8	/pat1/apps/normarray/square/wood+/
fslw+034	0.54947	0.00050	simplified	square	120% redwood density	43.2	/pat1/apps/normarray/square/wood+/
fslw+035	0.53894	0.00052	simplified	square	120% redwood density	52.1	/pat1/apps/normarray/square/wood+/
fslw+036	0.52669	0.00050	simplified	square	120% redwood density	65.4	/pat1/apps/normarray/square/wood+/
fslw+037	0.51434	0.00049	simplified	square	120% redwood density	87.7	/pat1/apps/normarray/square/wood+/
fslw+038	0.49369	0.00050	simplified	square	120% redwood density	132.2	/pat1/apps/normarray/square/wood+/
fslw-001	0.64322	0.00049	simplified	square	80% redwood density	0	/pat1/apps/normarray/square/wood-/
fslw-002	0.64209	0.00049	simplified	square	80% redwood density	0.013	/pat1/apps/normarray/square/wood-/
fslw-003	0.63918	0.00049	simplified	square	80% redwood density	0.027	/pat1/apps/normarray/square/wood-/
fslw-004	0.63135	0.00049	simplified	square	80% redwood density	0.070	/pat1/apps/normarray/square/wood-/
fslw-005	0.62016	0.00049	simplified	square	80% redwood density	0.15	/pat1/apps/normarray/square/wood-/
fslw-006	0.60936	0.00051	simplified	square	80% redwood density	0.24	/pat1/apps/normarray/square/wood-/
fslw-007	0.59841	0.00050	simplified	square	80% redwood density	0.33	/pat1/apps/normarray/square/wood-/
fslw-008	0.58495	0.00049	simplified	square	80% redwood density	0.45	/pat1/apps/normarray/square/wood-/

Table 6-16. Tabulation of Calculations Supporting the Analysis of Arrays of Undamaged Packages

Case Name	k_{eff}	σ	Package Model Type	Array Type	Description	H/Pu	Location
fslw-009	0.57363	0.00049	simplified	square	80% redwood density	0.57	/pat1/apps/normarray/square/wood-/
fslw-010	0.56234	0.00047	simplified	square	80% redwood density	0.72	/pat1/apps/normarray/square/wood-/
fslw-011	0.55087	0.00049	simplified	square	80% redwood density	0.89	/pat1/apps/normarray/square/wood-/
fslw-012	0.54208	0.00049	simplified	square	80% redwood density	1.09	/pat1/apps/normarray/square/wood-/
fslw-013	0.53233	0.00047	simplified	square	80% redwood density	1.34	/pat1/apps/normarray/square/wood-/
fslw-014	0.52107	0.00049	simplified	square	80% redwood density	1.63	/pat1/apps/normarray/square/wood-/
fslw-015	0.51317	0.00048	simplified	square	80% redwood density	2.00	/pat1/apps/normarray/square/wood-/
fslw-016	0.50645	0.00049	simplified	square	80% redwood density	2.48	/pat1/apps/normarray/square/wood-/
fslw-017	0.49987	0.00049	simplified	square	80% redwood density	3.12	/pat1/apps/normarray/square/wood-/
fslw-018	0.49590	0.00049	simplified	square	80% redwood density	4.01	/pat1/apps/normarray/square/wood-/
fslw-019	0.49662	0.00049	simplified	square	80% redwood density	5.34	/pat1/apps/normarray/square/wood-/
fslw-020	0.49943	0.00049	simplified	square	80% redwood density	7.57	/pat1/apps/normarray/square/wood-/
fslw-021	0.51299	0.00049	simplified	square	80% redwood density	12.0	/pat1/apps/normarray/square/wood-/
fslw-022	0.51393	0.00049	simplified	square	80% redwood density	12.1	/pat1/apps/normarray/square/wood-/
fslw-023	0.46574	0.00049	simplified	square	80% redwood density	5.34	/pat1/apps/normarray/square/wood-/
fslw-024	0.47934	0.00049	simplified	square	80% redwood density	7.57	/pat1/apps/normarray/square/wood-/
fslw-025	0.50573	0.00049	simplified	square	80% redwood density	12.0	/pat1/apps/normarray/square/wood-/
fslw-026	0.51249	0.00049	simplified	square	80% redwood density	13.5	/pat1/apps/normarray/square/wood-/
fslw-027	0.52155	0.00050	simplified	square	80% redwood density	15.4	/pat1/apps/normarray/square/wood-/
fslw-028	0.53176	0.00049	simplified	square	80% redwood density	17.7	/pat1/apps/normarray/square/wood-/
fslw-029	0.54201	0.00051	simplified	square	80% redwood density	20.9	/pat1/apps/normarray/square/wood-/
fslw-030	0.55290	0.00050	simplified	square	80% redwood density	25.4	/pat1/apps/normarray/square/wood-/
fslw-031	0.55812	0.00050	simplified	square	80% redwood density	28.8	/pat1/apps/normarray/square/wood-/
fslw-032	0.55161	0.00050	simplified	square	80% redwood density	32.0	/pat1/apps/normarray/square/wood-/
fslw-033	0.54153	0.00051	simplified	square	80% redwood density	36.8	/pat1/apps/normarray/square/wood-/
fslw-034	0.53183	0.00051	simplified	square	80% redwood density	43.2	/pat1/apps/normarray/square/wood-/

Table 6-16. Tabulation of Calculations Supporting the Analysis of Arrays of Undamaged Packages

Case Name	k_{eff}	σ	Package Model Type	Array Type	Description	H/Pu	Location
fslw-035	0.52267	0.00049	simplified	square	80% redwood density	52.1	/pat1/apps/normarray/square/wood-/
fslw-036	0.51073	0.00050	simplified	square	80% redwood density	65.4	/pat1/apps/normarray/square/wood-/
fslw-037	0.49751	0.00050	simplified	square	80% redwood density	87.7	/pat1/apps/normarray/square/wood-/
fslw-038	0.47683	0.00050	simplified	square	80% redwood density	132.2	/pat1/apps/normarray/square/wood-/
fslsf001	0.65043	0.00049	simplified	square	redwood -> water, steel modeled	0	/pat1/apps/normarray/square/water/
fslsf002	0.64824	0.00049	simplified	square	redwood -> water, steel modeled	0.013	/pat1/apps/normarray/square/water/
fslsf003	0.64602	0.00050	simplified	square	redwood -> water, steel modeled	0.027	/pat1/apps/normarray/square/water/
fslsf004	0.63965	0.00049	simplified	square	redwood -> water, steel modeled	0.070	/pat1/apps/normarray/square/water/
fslsf005	0.62794	0.00050	simplified	square	redwood -> water, steel modeled	0.15	/pat1/apps/normarray/square/water/
fslsf006	0.61670	0.00050	simplified	square	redwood -> water, steel modeled	0.24	/pat1/apps/normarray/square/water/
fslsf007	0.60480	0.00050	simplified	square	redwood -> water, steel modeled	0.33	/pat1/apps/normarray/square/water/
fslsf008	0.59330	0.00049	simplified	square	redwood -> water, steel modeled	0.45	/pat1/apps/normarray/square/water/
fslsf009	0.58317	0.00049	simplified	square	redwood -> water, steel modeled	0.57	/pat1/apps/normarray/square/water/
fslsf010	0.57226	0.00050	simplified	square	redwood -> water, steel modeled	0.72	/pat1/apps/normarray/square/water/
fslsf011	0.56133	0.00050	simplified	square	redwood -> water, steel modeled	0.89	/pat1/apps/normarray/square/water/
fslsf012	0.55309	0.00050	simplified	square	redwood -> water, steel modeled	1.09	/pat1/apps/normarray/square/water/
fslsf013	0.54294	0.00050	simplified	square	redwood -> water, steel modeled	1.34	/pat1/apps/normarray/square/water/
fslsf014	0.53598	0.00050	simplified	square	redwood -> water, steel modeled	1.63	/pat1/apps/normarray/square/water/
fslsf015	0.52848	0.00050	simplified	square	redwood -> water, steel modeled	2.00	/pat1/apps/normarray/square/water/
fslsf016	0.52345	0.00049	simplified	square	redwood -> water, steel modeled	2.48	/pat1/apps/normarray/square/water/
fslsf017	0.51828	0.00050	simplified	square	redwood -> water, steel modeled	3.12	/pat1/apps/normarray/square/water/
fslsf018	0.51784	0.00049	simplified	square	redwood -> water, steel modeled	4.01	/pat1/apps/normarray/square/water/
fslsf019	0.52162	0.00049	simplified	square	redwood -> water, steel modeled	5.34	/pat1/apps/normarray/square/water/
fslsf020	0.53219	0.00050	simplified	square	redwood -> water, steel modeled	7.57	/pat1/apps/normarray/square/water/
fslsf021	0.55776	0.00049	simplified	square	redwood -> water, steel modeled	12.0	/pat1/apps/normarray/square/water/
fslsf022	0.56011	0.00050	simplified	square	redwood -> water, steel modeled	12.1	/pat1/apps/normarray/square/water/

Table 6-16. Tabulation of Calculations Supporting the Analysis of Arrays of Undamaged Packages

Case Name	k_{eff}	σ	Package Model Type	Array Type	Description	H/Pu	Location
fslsf023	0.50415	0.00050	simplified	square	redwood -> water, steel modeled	5.34	/pat1/apps/normarray/square/water/
fslsf024	0.52298	0.00050	simplified	square	redwood -> water, steel modeled	7.57	/pat1/apps/normarray/square/water/
fslsf025	0.55762	0.00049	simplified	square	redwood -> water, steel modeled	12.0	/pat1/apps/normarray/square/water/
fslsf026	0.56821	0.00050	simplified	square	redwood -> water, steel modeled	13.5	/pat1/apps/normarray/square/water/
fslsf027	0.58015	0.00049	simplified	square	redwood -> water, steel modeled	15.4	/pat1/apps/normarray/square/water/
fslsf028	0.59283	0.00050	simplified	square	redwood -> water, steel modeled	17.7	/pat1/apps/normarray/square/water/
fslsf029	0.60854	0.00053	simplified	square	redwood -> water, steel modeled	20.9	/pat1/apps/normarray/square/water/
fslsf030	0.62355	0.00049	simplified	square	redwood -> water, steel modeled	25.4	/pat1/apps/normarray/square/water/
fslsf031[a]	0.63371	0.00050	simplified	square	redwood -> water, steel modeled	28.8	/pat1/apps/normarray/square/water/
fslsf032	0.62580	0.00050	simplified	square	redwood -> water, steel modeled	32.0	/pat1/apps/normarray/square/water/
fslsf033	0.61719	0.00049	simplified	square	redwood -> water, steel modeled	36.8	/pat1/apps/normarray/square/water/
fslsf034	0.60732	0.00050	simplified	square	redwood -> water, steel modeled	43.2	/pat1/apps/normarray/square/water/
fslsf035	0.59799	0.00055	simplified	square	redwood -> water, steel modeled	52.1	/pat1/apps/normarray/square/water/
fslsf036	0.58499	0.00050	simplified	square	redwood -> water, steel modeled	65.4	/pat1/apps/normarray/square/water/
fslsf037	0.56893	0.00053	simplified	square	redwood -> water, steel modeled	87.7	/pat1/apps/normarray/square/water/
fslsf038	0.54583	0.00050	simplified	square	redwood -> water, steel modeled	132.2	/pat1/apps/normarray/square/water/
fhlsf001	0.64477	0.00046	simplified	hexagonal	base simplified model	0	/pat1/apps/normarray/hex/wood/
fhlsf002	0.64302	0.00050	simplified	hexagonal	base simplified model	0.013	/pat1/apps/normarray/hex/wood/
fhlsf003	0.64060	0.00049	simplified	hexagonal	base simplified model	0.027	/pat1/apps/normarray/hex/wood/
fhlsf004	0.63350	0.00049	simplified	hexagonal	base simplified model	0.070	/pat1/apps/normarray/hex/wood/
fhlsf005	0.62093	0.00049	simplified	hexagonal	base simplified model	0.15	/pat1/apps/normarray/hex/wood/
fhlsf006	0.61030	0.00050	simplified	hexagonal	base simplified model	0.24	/pat1/apps/normarray/hex/wood/
fhlsf007	0.59855	0.00050	simplified	hexagonal	base simplified model	0.33	/pat1/apps/normarray/hex/wood/
fhlsf008	0.58671	0.00049	simplified	hexagonal	base simplified model	0.45	/pat1/apps/normarray/hex/wood/
fhlsf009	0.57560	0.00049	simplified	hexagonal	base simplified model	0.57	/pat1/apps/normarray/hex/wood/
fhlsf010	0.56323	0.00049	simplified	hexagonal	base simplified model	0.72	/pat1/apps/normarray/hex/wood/

Table 6-16. Tabulation of Calculations Supporting the Analysis of Arrays of Undamaged Packages

Case Name	k_{eff}	σ	Package Model Type	Array Type	Description	H/Pu	Location
fhlsf011	0.55382	0.00049	simplified	hexagonal	base simplified model	0.89	/pat1/apps/normarray/hex/wood/
fhlsf012	0.54309	0.00050	simplified	hexagonal	base simplified model	1.09	/pat1/apps/normarray/hex/wood/
fhlsf013	0.53321	0.00049	simplified	hexagonal	base simplified model	1.34	/pat1/apps/normarray/hex/wood/
fhlsf014	0.52341	0.00046	simplified	hexagonal	base simplified model	1.63	/pat1/apps/normarray/hex/wood/
fhlsf015	0.51540	0.00049	simplified	hexagonal	base simplified model	2.00	/pat1/apps/normarray/hex/wood/
fhlsf016	0.50797	0.00049	simplified	hexagonal	base simplified model	2.48	/pat1/apps/normarray/hex/wood/
fhlsf017	0.50226	0.00050	simplified	hexagonal	base simplified model	3.12	/pat1/apps/normarray/hex/wood/
fhlsf018	0.49941	0.00049	simplified	hexagonal	base simplified model	4.01	/pat1/apps/normarray/hex/wood/
fhlsf019	0.49842	0.00050	simplified	hexagonal	base simplified model	5.34	/pat1/apps/normarray/hex/wood/
fhlsf020	0.50482	0.00049	simplified	hexagonal	base simplified model	7.57	/pat1/apps/normarray/hex/wood/
fhlsf021	0.51877	0.00049	simplified	hexagonal	base simplified model	12.0	/pat1/apps/normarray/hex/wood/
fhlsf022	0.51934	0.00050	simplified	hexagonal	base simplified model	12.1	/pat1/apps/normarray/hex/wood/
fhlsf023	0.46992	0.00049	simplified	hexagonal	base simplified model	5.34	/pat1/apps/normarray/hex/wood/
fhlsf024	0.48301	0.00050	simplified	hexagonal	base simplified model	7.57	/pat1/apps/normarray/hex/wood/
fhlsf025	0.51101	0.00050	simplified	hexagonal	base simplified model	12.0	/pat1/apps/normarray/hex/wood/
fhlsf026	0.51898	0.00047	simplified	hexagonal	base simplified model	13.5	/pat1/apps/normarray/hex/wood/
fhlsf027	0.52944	0.00049	simplified	hexagonal	base simplified model	15.4	/pat1/apps/normarray/hex/wood/
fhlsf028	0.53935	0.00049	simplified	hexagonal	base simplified model	17.7	/pat1/apps/normarray/hex/wood/
fhlsf029	0.55131	0.00049	simplified	hexagonal	base simplified model	20.9	/pat1/apps/normarray/hex/wood/
fhlsf030	0.56197	0.00049	simplified	hexagonal	base simplified model	25.4	/pat1/apps/normarray/hex/wood/
fhlsf031	0.56731	0.00049	simplified	hexagonal	base simplified model	28.8	/pat1/apps/normarray/hex/wood/
fhlsf032	0.55967	0.00050	simplified	hexagonal	base simplified model	32.0	/pat1/apps/normarray/hex/wood/
fhlsf033	0.55178	0.00049	simplified	hexagonal	base simplified model	36.8	/pat1/apps/normarray/hex/wood/
fhlsf034	0.54092	0.00050	simplified	hexagonal	base simplified model	43.2	/pat1/apps/normarray/hex/wood/
fhlsf035	0.53123	0.00049	simplified	hexagonal	base simplified model	52.1	/pat1/apps/normarray/hex/wood/
fhlsf036	0.51910	0.00050	simplified	hexagonal	base simplified model	65.4	/pat1/apps/normarray/hex/wood/

Table 6-16. Tabulation of Calculations Supporting the Analysis of Arrays of Undamaged Packages

Case Name	k_{eff}	σ	Package Model Type	Array Type	Description	H/Pu	Location
fhlsf037	0.50549	0.00050	simplified	hexagonal	base simplified model	87.7	/pat1/apps/normarray/hex/wood/
fhlsf038	0.48705	0.00049	simplified	hexagonal	base simplified model	132.2	/pat1/apps/normarray/hex/wood/
fhlsf001	0.64580	0.00050	simplified	hexagonal	120% redwood density	0	/pat1/apps/normarray/hex/woodp/
fhlsf002	0.64354	0.00049	simplified	hexagonal	120% redwood density	0.013	/pat1/apps/normarray/hex/woodp/
fhlsf003	0.64179	0.00049	simplified	hexagonal	120% redwood density	0.027	/pat1/apps/normarray/hex/woodp/
fhlsf004	0.63556	0.00050	simplified	hexagonal	120% redwood density	0.070	/pat1/apps/normarray/hex/woodp/
fhlsf005	0.62339	0.00049	simplified	hexagonal	120% redwood density	0.15	/pat1/apps/normarray/hex/woodp/
fhlsf006	0.61212	0.00049	simplified	hexagonal	120% redwood density	0.24	/pat1/apps/normarray/hex/woodp/
fhlsf007	0.59963	0.00050	simplified	hexagonal	120% redwood density	0.33	/pat1/apps/normarray/hex/woodp/
fhlsf008	0.58871	0.00048	simplified	hexagonal	120% redwood density	0.45	/pat1/apps/normarray/hex/woodp/
fhlsf009	0.57679	0.00050	simplified	hexagonal	120% redwood density	0.57	/pat1/apps/normarray/hex/woodp/
fhlsf010	0.56523	0.00050	simplified	hexagonal	120% redwood density	0.72	/pat1/apps/normarray/hex/woodp/
fhlsf011	0.55469	0.00050	simplified	hexagonal	120% redwood density	0.89	/pat1/apps/normarray/hex/woodp/
fhlsf012	0.54377	0.00049	simplified	hexagonal	120% redwood density	1.09	/pat1/apps/normarray/hex/woodp/
fhlsf013	0.53468	0.00049	simplified	hexagonal	120% redwood density	1.34	/pat1/apps/normarray/hex/woodp/
fhlsf014	0.52574	0.00049	simplified	hexagonal	120% redwood density	1.63	/pat1/apps/normarray/hex/woodp/
fhlsf015	0.51752	0.00050	simplified	hexagonal	120% redwood density	2.00	/pat1/apps/normarray/hex/woodp/
fhlsf016	0.51053	0.00050	simplified	hexagonal	120% redwood density	2.48	/pat1/apps/normarray/hex/woodp/
fhlsf017r1	0.50524	0.00049	simplified	hexagonal	120% redwood density	3.12	/pat1/apps/normarray/hex/woodp/
fhlsf018	0.50272	0.00050	simplified	hexagonal	120% redwood density	4.01	/pat1/apps/normarray/hex/woodp/
fhlsf019	0.50388	0.00050	simplified	hexagonal	120% redwood density	5.34	/pat1/apps/normarray/hex/woodp/
fhlsf020	0.50898	0.00048	simplified	hexagonal	120% redwood density	7.57	/pat1/apps/normarray/hex/woodp/
fhlsf021	0.52383	0.00049	simplified	hexagonal	120% redwood density	12.0	/pat1/apps/normarray/hex/woodp/
fhlsf022	0.52515	0.00050	simplified	hexagonal	120% redwood density	12.1	/pat1/apps/normarray/hex/woodp/
fhlsf023	0.47521	0.00049	simplified	hexagonal	120% redwood density	5.34	/pat1/apps/normarray/hex/woodp/
fhlsf024	0.48937	0.00050	simplified	hexagonal	120% redwood density	7.57	/pat1/apps/normarray/hex/woodp/

Table 6-16. Tabulation of Calculations Supporting the Analysis of Arrays of Undamaged Packages

Case Name	k_{eff}	σ	Package Model Type	Array Type	Description	H/Pu	Location
fhlsf025	0.51784	0.00050	simplified	hexagonal	120% redwood density	12.0	/pat1/apps/normarray/hex/woodp/
fhlsf026	0.52630	0.00050	simplified	hexagonal	120% redwood density	13.5	/pat1/apps/normarray/hex/woodp/
fhlsf027	0.53525	0.00049	simplified	hexagonal	120% redwood density	15.4	/pat1/apps/normarray/hex/woodp/
fhlsf028	0.54683	0.00049	simplified	hexagonal	120% redwood density	17.7	/pat1/apps/normarray/hex/woodp/
fhlsf029	0.55869	0.00050	simplified	hexagonal	120% redwood density	20.9	/pat1/apps/normarray/hex/woodp/
fhlsf030	0.56901	0.00049	simplified	hexagonal	120% redwood density	25.4	/pat1/apps/normarray/hex/woodp/
fhlsf031	0.57554	0.00049	simplified	hexagonal	120% redwood density	28.8	/pat1/apps/normarray/hex/woodp/
fhlsf032	0.56919	0.00049	simplified	hexagonal	120% redwood density	32.0	/pat1/apps/normarray/hex/woodp/
fhlsf033	0.55945	0.00049	simplified	hexagonal	120% redwood density	36.8	/pat1/apps/normarray/hex/woodp/
fhlsf034	0.55105	0.00050	simplified	hexagonal	120% redwood density	43.2	/pat1/apps/normarray/hex/woodp/
fhlsf035	0.54102	0.00049	simplified	hexagonal	120% redwood density	52.1	/pat1/apps/normarray/hex/woodp/
fhlsf036	0.52769	0.00050	simplified	hexagonal	120% redwood density	65.4	/pat1/apps/normarray/hex/woodp/
fhlsf037	0.51388	0.00049	simplified	hexagonal	120% redwood density	87.7	/pat1/apps/normarray/hex/woodp/
fhlsf038	0.49489	0.00048	simplified	hexagonal	120% redwood density	132.2	/pat1/apps/normarray/hex/woodp/
fhlsf001	0.64316	0.00050	simplified	hexagonal	80% redwood density	0	/pat1/apps/normarray/hex/woodm/
fhlsf002	0.64231	0.00050	simplified	hexagonal	80% redwood density	0.013	/pat1/apps/normarray/hex/woodm/
fhlsf003	0.63914	0.00049	simplified	hexagonal	80% redwood density	0.027	/pat1/apps/normarray/hex/woodm/
fhlsf004	0.63221	0.00049	simplified	hexagonal	80% redwood density	0.070	/pat1/apps/normarray/hex/woodm/
fhlsf005	0.62042	0.00048	simplified	hexagonal	80% redwood density	0.15	/pat1/apps/normarray/hex/woodm/
fhlsf006	0.60825	0.00049	simplified	hexagonal	80% redwood density	0.24	/pat1/apps/normarray/hex/woodm/
fhlsf007	0.59688	0.00050	simplified	hexagonal	80% redwood density	0.33	/pat1/apps/normarray/hex/woodm/
fhlsf008	0.58585	0.00049	simplified	hexagonal	80% redwood density	0.45	/pat1/apps/normarray/hex/woodm/
fhlsf009	0.57398	0.00049	simplified	hexagonal	80% redwood density	0.57	/pat1/apps/normarray/hex/woodm/
fhlsf010	0.56363	0.00050	simplified	hexagonal	80% redwood density	0.72	/pat1/apps/normarray/hex/woodm/
fhlsf011	0.55205	0.00049	simplified	hexagonal	80% redwood density	0.89	/pat1/apps/normarray/hex/woodm/
fhlsf012	0.54133	0.00050	simplified	hexagonal	80% redwood density	1.09	/pat1/apps/normarray/hex/woodm/

Table 6-16. Tabulation of Calculations Supporting the Analysis of Arrays of Undamaged Packages

Case Name	k_{eff}	σ	Package Model Type	Array Type	Description	H/Pu	Location
fhlsf013	0.53164	0.00050	simplified	hexagonal	80% redwood density	1.34	/pat1/apps/normarray/hex/woodm/
fhlsf014	0.52125	0.00048	simplified	hexagonal	80% redwood density	1.63	/pat1/apps/normarray/hex/woodm/
fhlsf015	0.51309	0.00049	simplified	hexagonal	80% redwood density	2.00	/pat1/apps/normarray/hex/woodm/
fhlsf016	0.50720	0.00050	simplified	hexagonal	80% redwood density	2.48	/pat1/apps/normarray/hex/woodm/
fhlsf017	0.50025	0.00050	simplified	hexagonal	80% redwood density	3.12	/pat1/apps/normarray/hex/woodm/
fhlsf018	0.49739	0.00049	simplified	hexagonal	80% redwood density	4.01	/pat1/apps/normarray/hex/woodm/
fhlsf019	0.49650	0.00049	simplified	hexagonal	80% redwood density	5.34	/pat1/apps/normarray/hex/woodm/
fhlsf020	0.50184	0.00048	simplified	hexagonal	80% redwood density	7.57	/pat1/apps/normarray/hex/woodm/
fhlsf021	0.51472	0.00049	simplified	hexagonal	80% redwood density	12.0	/pat1/apps/normarray/hex/woodm/
fhlsf022	0.51465	0.00049	simplified	hexagonal	80% redwood density	12.1	/pat1/apps/normarray/hex/woodm/
fhlsf023	0.46681	0.00050	simplified	hexagonal	80% redwood density	5.34	/pat1/apps/normarray/hex/woodm/
fhlsf024	0.47993	0.00048	simplified	hexagonal	80% redwood density	7.57	/pat1/apps/normarray/hex/woodm/
fhlsf025	0.50549	0.00049	simplified	hexagonal	80% redwood density	12.0	/pat1/apps/normarray/hex/woodm/
fhlsf026	0.51495	0.00050	simplified	hexagonal	80% redwood density	13.5	/pat1/apps/normarray/hex/woodm/
fhlsf027	0.52304	0.00049	simplified	hexagonal	80% redwood density	15.4	/pat1/apps/normarray/hex/woodm/
fhlsf028	0.53359	0.00050	simplified	hexagonal	80% redwood density	17.7	/pat1/apps/normarray/hex/woodm/
fhlsf029	0.54539	0.00050	simplified	hexagonal	80% redwood density	20.9	/pat1/apps/normarray/hex/woodm/
fhlsf030	0.55441	0.00050	simplified	hexagonal	80% redwood density	25.4	/pat1/apps/normarray/hex/woodm/
fhlsf031	0.56076	0.00048	simplified	hexagonal	80% redwood density	28.8	/pat1/apps/normarray/hex/woodm/
fhlsf032	0.55336	0.00048	simplified	hexagonal	80% redwood density	32.0	/pat1/apps/normarray/hex/woodm/
fhlsf033	0.54346	0.00050	simplified	hexagonal	80% redwood density	36.8	/pat1/apps/normarray/hex/woodm/
fhlsf034	0.53431	0.00049	simplified	hexagonal	80% redwood density	43.2	/pat1/apps/normarray/hex/woodm/
fhlsf035	0.52422	0.00049	simplified	hexagonal	80% redwood density	52.1	/pat1/apps/normarray/hex/woodm/
fhlsf036	0.51261	0.00049	simplified	hexagonal	80% redwood density	65.4	/pat1/apps/normarray/hex/woodm/
fhlsf037	0.49912	0.00050	simplified	hexagonal	80% redwood density	87.7	/pat1/apps/normarray/hex/woodm/
fhlsf038	0.47869	0.00050	simplified	hexagonal	80% redwood density	132.2	/pat1/apps/normarray/hex/woodm/

Table 6-16. Tabulation of Calculations Supporting the Analysis of Arrays of Undamaged Packages

Case Name	k_{eff}	σ	Package Model Type	Array Type	Description	H/Pu	Location
fhlsf001[a]	0.65094	0.00049	simplified	hexagonal	redwood -> water, steel modeled	0	/pat1/apps/normarray/hex/water/
fhlsf002	0.64849	0.00049	simplified	hexagonal	redwood -> water, steel modeled	0.013	/pat1/apps/normarray/hex/water/
fhlsf003	0.64581	0.00047	simplified	hexagonal	redwood -> water, steel modeled	0.027	/pat1/apps/normarray/hex/water/
fhlsf004	0.63992	0.00050	simplified	hexagonal	redwood -> water, steel modeled	0.070	/pat1/apps/normarray/hex/water/
fhlsf005	0.62683	0.00049	simplified	hexagonal	redwood -> water, steel modeled	0.15	/pat1/apps/normarray/hex/water/
fhlsf006	0.61620	0.00049	simplified	hexagonal	redwood -> water, steel modeled	0.24	/pat1/apps/normarray/hex/water/
fhlsf007	0.60544	0.00049	simplified	hexagonal	redwood -> water, steel modeled	0.33	/pat1/apps/normarray/hex/water/
fhlsf008	0.59378	0.00050	simplified	hexagonal	redwood -> water, steel modeled	0.45	/pat1/apps/normarray/hex/water/
fhlsf009	0.58304	0.00049	simplified	hexagonal	redwood -> water, steel modeled	0.57	/pat1/apps/normarray/hex/water/
fhlsf010	0.57217	0.00050	simplified	hexagonal	redwood -> water, steel modeled	0.72	/pat1/apps/normarray/hex/water/
fhlsf011	0.56250	0.00050	simplified	hexagonal	redwood -> water, steel modeled	0.89	/pat1/apps/normarray/hex/water/
fhlsf012	0.55238	0.00050	simplified	hexagonal	redwood -> water, steel modeled	1.09	/pat1/apps/normarray/hex/water/
fhlsf013	0.54361	0.00049	simplified	hexagonal	redwood -> water, steel modeled	1.34	/pat1/apps/normarray/hex/water/
fhlsf014	0.53538	0.00049	simplified	hexagonal	redwood -> water, steel modeled	1.63	/pat1/apps/normarray/hex/water/
fhlsf015	0.52817	0.00050	simplified	hexagonal	redwood -> water, steel modeled	2.00	/pat1/apps/normarray/hex/water/
fhlsf016	0.52190	0.00049	simplified	hexagonal	redwood -> water, steel modeled	2.48	/pat1/apps/normarray/hex/water/
fhlsf017	0.51867	0.00050	simplified	hexagonal	redwood -> water, steel modeled	3.12	/pat1/apps/normarray/hex/water/
fhlsf018	0.51768	0.00049	simplified	hexagonal	redwood -> water, steel modeled	4.01	/pat1/apps/normarray/hex/water/
fhlsf019	0.52126	0.00050	simplified	hexagonal	redwood -> water, steel modeled	5.34	/pat1/apps/normarray/hex/water/
fhlsf020	0.53261	0.00049	simplified	hexagonal	redwood -> water, steel modeled	7.57	/pat1/apps/normarray/hex/water/
fhlsf021	0.55883	0.00050	simplified	hexagonal	redwood -> water, steel modeled	12.0	/pat1/apps/normarray/hex/water/
fhlsf022	0.55958	0.00050	simplified	hexagonal	redwood -> water, steel modeled	12.1	/pat1/apps/normarray/hex/water/
fhlsf023	0.50296	0.00049	simplified	hexagonal	redwood -> water, steel modeled	5.34	/pat1/apps/normarray/hex/water/
fhlsf024	0.52189	0.00049	simplified	hexagonal	redwood -> water, steel modeled	7.57	/pat1/apps/normarray/hex/water/
fhlsf025	0.55819	0.00050	simplified	hexagonal	redwood -> water, steel modeled	12.0	/pat1/apps/normarray/hex/water/
fhlsf026	0.56757	0.00050	simplified	hexagonal	redwood -> water, steel modeled	13.5	/pat1/apps/normarray/hex/water/

Table 6-16. Tabulation of Calculations Supporting the Analysis of Arrays of Undamaged Packages

Case Name	k_{eff}	σ	Package Model Type	Array Type	Description	H/Pu	Location
fhlsf027	0.57968	0.00049	simplified	hexagonal	redwood -> water, steel modeled	15.4	/pat1/apps/normarray/hex/water/
fhlsf028	0.59359	0.00049	simplified	hexagonal	redwood -> water, steel modeled	17.7	/pat1/apps/normarray/hex/water/
fhlsf029	0.60825	0.00049	simplified	hexagonal	redwood -> water, steel modeled	20.9	/pat1/apps/normarray/hex/water/
fhlsf030	0.62311	0.00049	simplified	hexagonal	redwood -> water, steel modeled	25.4	/pat1/apps/normarray/hex/water/
fhlsf031	0.63235	0.00050	simplified	hexagonal	redwood -> water, steel modeled	28.8	/pat1/apps/normarray/hex/water/
fhlsf032	0.62619	0.00049	simplified	hexagonal	redwood -> water, steel modeled	32.0	/pat1/apps/normarray/hex/water/
fhlsf033	0.61657	0.00050	simplified	hexagonal	redwood -> water, steel modeled	36.8	/pat1/apps/normarray/hex/water/
fhlsf034	0.60778	0.00050	simplified	hexagonal	redwood -> water, steel modeled	43.2	/pat1/apps/normarray/hex/water/
fhlsf035	0.59750	0.00049	simplified	hexagonal	redwood -> water, steel modeled	52.1	/pat1/apps/normarray/hex/water/
fhlsf036	0.58477	0.00049	simplified	hexagonal	redwood -> water, steel modeled	65.4	/pat1/apps/normarray/hex/water/
fhlsf037	0.56890	0.00050	simplified	hexagonal	redwood -> water, steel modeled	87.7	/pat1/apps/normarray/hex/water/
fhlsf038	0.54643	0.00049	simplified	hexagonal	redwood -> water, steel modeled	132.2	/pat1/apps/normarray/hex/water/

[a] Limiting cases listed in Table 6-1.

6.9.4.3 Calculations Supporting Hypothetical Accident Conditions Array Analysis

Table 6-17 lists calculations performed to support the analysis of damaged package arrays.

Table 6-17. Tabulation of Calculations Supporting the Analysis of Arrays of Damaged Packages

Case Name	k_{eff}	σ	Package Model Type	H/Pu	Water Density Fraction in Wood Zone	Array Type	Number of Packages	Description	Locations
enda1088	0.67887	0.00049	end	28.8	0	hex	1088	identical repeated layers	/pat1/apps/hacarray/arraystudy/
enda1088m	0.65085	0.00050	end	0	0	hex	1088	enda1088 with Pu metal spheres	/pat1/apps/hacarray/arraystudy/
enda920	0.66587	0.00049	end	28.8	0	hex	920	identical repeated layers	/pat1/apps/hacarray/arraystudy/
endb1088	0.68125	0.00049	end	28.8	0	hex	1088	alternating layers, bringing pairs of TB-1s closer	/pat1/apps/hacarray/arraystudy/
endb920	0.66644	0.00049	end	28.8	0	hex	920	alternating layers, bringing pairs of TB-1s closer	/pat1/apps/hacarray/arraystudy/
hex0	0.70411	0.00056	side	28.8	0	hex	1152	varying number of packages with air between	/pat1/apps/hacarray/arraystudy/
hex0a	0.65776	0.00054	side	28.8	0	hex	576	varying number of packages with air between	/pat1/apps/hacarray/arraystudy/
hex0b	0.67551	0.00054	side	28.8	0	hex	768	varying number of packages with air between	/pat1/apps/hacarray/arraystudy/
hex0c	0.63864	0.00053	side	28.8	0	hex	384	varying number of packages with air between	/pat1/apps/hacarray/arraystudy/
hex0d	0.61622	0.00056	side	28.8	0	hex	256	varying number of packages with air between	/pat1/apps/hacarray/arraystudy/
hex0e	0.58981	0.00059	side	28.8	0	hex	128	varying number of packages with air between	/pat1/apps/hacarray/arraystudy/
hex0met	0.67138	0.00049	side	0	0	hex	1152	hex0 with Pu metal spheres	/pat1/apps/hacarray/arraystudy/
hex100	0.71538	0.00050	side	28.8	1	hex	1152	varying number of packages with water between	/pat1/apps/hacarray/arraystudy/
hex100a	0.71524	0.00051	side	28.8	1	hex	576	varying number of packages with water between	/pat1/apps/hacarray/arraystudy/
hex100b	0.71456	0.00049	side	28.8	1	hex	768	varying number of packages with water between	/pat1/apps/hacarray/arraystudy/
hex100c	0.71449	0.00056	side	28.8	1	hex	384	varying number of packages with water between	/pat1/apps/hacarray/arraystudy/
hex100d	0.71498	0.00049	side	28.8	1	hex	256	varying number of packages with water between	/pat1/apps/hacarray/arraystudy/
hex100e	0.71481	0.00056	side	28.8	1	hex	128	varying number of packages with water between	/pat1/apps/hacarray/arraystudy/
hex100met	0.66365	0.00049	side	0	1	hex	1152	hex100 with Pu metal spheres	/pat1/apps/hacarray/arraystudy/
nest1a	0.58966	0.00051	side	28.8	0	nest-1	384	varying number of packages with air between	/pat1/apps/hacarray/arraystudy/
nest1b	0.61431	0.00053	side	28.8	0	nest-1	864	varying number of packages with air between	/pat1/apps/hacarray/arraystudy/
nest1c	0.64080	0.00053	side	28.8	0	nest-1	1296	varying number of packages with air between	/pat1/apps/hacarray/arraystudy/
nest1met	0.66557	0.00049	side	0	0	nest-1	384	nest1a with Pu metal spheres	/pat1/apps/hacarray/arraystudy/
nest1metc	0.66991	0.00050	side	0	0	nest-1	1296	nest1c with Pu metal spheres	/pat1/apps/hacarray/arraystudy/
nest2a	0.61807	0.00053	side	28.8	0	nest-2	512	varying number of packages with air between	/pat1/apps/hacarray/arraystudy/
nest2b	0.65206	0.00050	side	28.8	0	nest-2	1152	varying number of packages with air between	/pat1/apps/hacarray/arraystudy/
nest2c	0.63333	0.00050	side	28.8	0	nest-2	768	varying number of packages with air between	/pat1/apps/hacarray/arraystudy/
nest2met	0.66594	0.00051	side	0	0	nest-2	512	nest2a with Pu metal spheres	/pat1/apps/hacarray/arraystudy/

Table 6-17. Tabulation of Calculations Supporting the Analysis of Arrays of Damaged Packages

Case Name	k_{eff}	σ	Package Model Type	H/Pu	Water Density Fraction in Wood Zone	Array Type	Number of Packages	Description	Locations
nest2metb	0.67004	0.00050	side	0	0	nest-2	1152	nest2b with Pu metal spheres	/pat1/apps/hacarray/arraystudy/
octa	0.67746	0.00052	side	28.8	0	square	1024	varying number of packages with air between	/pat1/apps/hacarray/arraystudy/
octb	0.66231	0.00049	side	28.8	0	square	768	varying number of packages with air between	/pat1/apps/hacarray/arraystudy/
octc	0.64717	0.00049	side	28.8	0	square	576	varying number of packages with air between	/pat1/apps/hacarray/arraystudy/
octd	0.69364	0.00053	side	28.8	0	square	1280	varying number of packages with air between	/pat1/apps/hacarray/arraystudy/
octmet	0.67989	0.00050	side	0	0	square	1024	octa with Pu metal spheres	/pat1/apps/hacarray/arraystudy/
hexsdry[a]	0.70268	0.00065	side	28.8	0	hex	1152	Varying water density in redwood zone	/pat1/apps/hacarray/sideimpact/hexstudy/hexsol/
hexs0005	0.70279	0.00053	side	28.8	0.005	hex	1152	Varying water density in redwood zone	/pat1/apps/hacarray/sideimpact/hexstudy/hexsol/
hexs001	0.69192	0.00055	side	28.8	0.01	hex	1152	Varying water density in redwood zone	/pat1/apps/hacarray/sideimpact/hexstudy/hexsol/
hexs002	0.67005	0.00055	side	28.8	0.02	hex	1152	Varying water density in redwood zone	/pat1/apps/hacarray/sideimpact/hexstudy/hexsol/
hexs003	0.65145	0.00049	side	28.8	0.03	hex	1152	Varying water density in redwood zone	/pat1/apps/hacarray/sideimpact/hexstudy/hexsol/
hexs004	0.63834	0.00052	side	28.8	0.04	hex	1152	Varying water density in redwood zone	/pat1/apps/hacarray/sideimpact/hexstudy/hexsol/
hexs005	0.62834	0.00050	side	28.8	0.05	hex	1152	Varying water density in redwood zone	/pat1/apps/hacarray/sideimpact/hexstudy/hexsol/
hexs0075	0.61259	0.00052	side	28.8	0.075	hex	1152	Varying water density in redwood zone	/pat1/apps/hacarray/sideimpact/hexstudy/hexsol/
hexs010	0.60541	0.00049	side	28.8	0.1	hex	1152	Varying water density in redwood zone	/pat1/apps/hacarray/sideimpact/hexstudy/hexsol/
hexs015	0.60543	0.00050	side	28.8	0.15	hex	1152	Varying water density in redwood zone	/pat1/apps/hacarray/sideimpact/hexstudy/hexsol/
hexs020	0.61187	0.00052	side	28.8	0.2	hex	1152	Varying water density in redwood zone	/pat1/apps/hacarray/sideimpact/hexstudy/hexsol/
hexs030	0.63261	0.00050	side	28.8	0.3	hex	1152	Varying water density in redwood zone	/pat1/apps/hacarray/sideimpact/hexstudy/hexsol/
hexs040	0.65171	0.00055	side	28.8	0.4	hex	1152	Varying water density in redwood zone	/pat1/apps/hacarray/sideimpact/hexstudy/hexsol/
hexs050	0.66806	0.00050	side	28.8	0.5	hex	1152	Varying water density in redwood zone	/pat1/apps/hacarray/sideimpact/hexstudy/hexsol/
hexs060	0.68073	0.00050	side	28.8	0.6	hex	1152	Varying water density in redwood zone	/pat1/apps/hacarray/sideimpact/hexstudy/hexsol/
hexs070	0.69265	0.00054	side	28.8	0.7	hex	1152	Varying water density in redwood zone	/pat1/apps/hacarray/sideimpact/hexstudy/hexsol/
hexs080	0.70127	0.00049	side	28.8	0.8	hex	1152	Varying water density in redwood zone	/pat1/apps/hacarray/sideimpact/hexstudy/hexsol/
hexs090	0.70936	0.00053	side	28.8	0.9	hex	1152	Varying water density in redwood zone	/pat1/apps/hacarray/sideimpact/hexstudy/hexsol/
hexs095	0.71150	0.00049	side	28.8	0.95	hex	1152	Varying water density in redwood zone	/pat1/apps/hacarray/sideimpact/hexstudy/hexsol/
hexs100[a]	0.71538	0.00050	side	28.8	1	hex	1152	Varying water density in redwood zone	/pat1/apps/hacarray/sideimpact/hexstudy/hexsol/
hexs100_1	0.69003	0.00051	side	28.8	1	hex	1152	TB-1s moved 1 cm from flat side of package	/pat1/apps/hacarray/sideimpact/hexstudy/hexsol/
hexs100_2	0.67021	0.00050	side	28.8	1	hex	1152	TB-1s moved 2 cm from flat side of package	/pat1/apps/hacarray/sideimpact/hexstudy/hexsol/

Table 6-17. Tabulation of Calculations Supporting the Analysis of Arrays of Damaged Packages

Case Name	k_{eff}	σ	Package Model Type	H/Pu	Water Density Fraction in Wood Zone	Array Type	Number of Packages	Description	Locations
hexs100_3	0.65663	0.00049	side	28.8	1	hex	1152	TB-1s moved 3 cm from flat side of package	/pat1/apps/hacarray/sideimpact/hexstudy/hexsol/
hexs100_p5	0.70177	0.00054	side	28.8	1	hex	1152	TB-1s moved 0.5 cm from flat side of package	/pat1/apps/hacarray/sideimpact/hexstudy/hexsol/
hexs100	0.71523	0.00029	side	28.8	1	hex	1152	Rerun for tighter convergence for sens study	/pat1/apps/hacarray/sideimpact/hexstudy/hexsol/sens_study/
Hexsdry	0.70274	0.00031	side	28.8	0	hex	1152	Rerun for tighter convergence for sens study	/pat1/apps/hacarray/sideimpact/hexstudy/hexsol/sens_study/
ph13m2	0.70171	0.00031	side	28.8	0	hex	1152	hexsdry with TB-1 steel at 98% density	/pat1/apps/hacarray/sideimpact/hexstudy/hexsol/sens_study/dry/
ph13p2	0.70457	0.00033	side	28.8	0	hex	1152	hexsdry with TB-1 steel at 102% density	/pat1/apps/hacarray/sideimpact/hexstudy/hexsol/sens_study/dry/
ss304m2	0.70217	0.00032	side	28.8	0	hex	1152	hexsdry with drum steel at 98% density	/pat1/apps/hacarray/sideimpact/hexstudy/hexsol/sens_study/dry/
ss304p2	0.70441	0.00031	side	28.8	0	hex	1152	hexsdry with drum steel at 102% density	/pat1/apps/hacarray/sideimpact/hexstudy/hexsol/sens_study/dry/
ph13m2	0.71474	0.00028	side	28.8	1	hex	1152	hexs100 with TB-1 steel at 98% density	/pat1/apps/hacarray/sideimpact/hexstudy/hexsol/sens_study/wet/
ph13p2	0.71500	0.00032	side	28.8	1	hex	1152	hexs100 with TB-1 steel at 102% density	/pat1/apps/hacarray/sideimpact/hexstudy/hexsol/sens_study/wet/
ss304m2	0.71474	0.00030	side	28.8	1	hex	1152	hexs100 with drum steel at 98% density	/pat1/apps/hacarray/sideimpact/hexstudy/hexsol/sens_study/wet/
ss304p2	0.71425	0.00028	side	28.8	1	hex	1152	hexs100 with drum steel at 102% density	/pat1/apps/hacarray/sideimpact/hexstudy/hexsol/sens_study/wet/
Hexmdry	0.67134	0.00049	side	0	0	hex	1152	Varying water density in redwood zone	/pat1/apps/hacarray/sideimpact/hexstudy/hexmet/
hexm0005	0.67054	0.00049	side	0	0.005	hex	1152	Varying water density in redwood zone	/pat1/apps/hacarray/sideimpact/hexstudy/hexmet/
hexm001	0.66744	0.00050	side	0	0.01	hex	1152	Varying water density in redwood zone	/pat1/apps/hacarray/sideimpact/hexstudy/hexmet/
hexm002	0.66340	0.00049	side	0	0.02	hex	1152	Varying water density in redwood zone	/pat1/apps/hacarray/sideimpact/hexstudy/hexmet/
hexm003	0.66093	0.00049	side	0	0.03	hex	1152	Varying water density in redwood zone	/pat1/apps/hacarray/sideimpact/hexstudy/hexmet/
hexm004	0.65925	0.00050	side	0	0.04	hex	1152	Varying water density in redwood zone	/pat1/apps/hacarray/sideimpact/hexstudy/hexmet/
hexm005	0.65746	0.00050	side	0	0.05	hex	1152	Varying water density in redwood zone	/pat1/apps/hacarray/sideimpact/hexstudy/hexmet/
hexm0075	0.65555	0.00049	side	0	0.075	hex	1152	Varying water density in redwood zone	/pat1/apps/hacarray/sideimpact/hexstudy/hexmet/
hexm010	0.65528	0.00049	side	0	0.1	hex	1152	Varying water density in redwood zone	/pat1/apps/hacarray/sideimpact/hexstudy/hexmet/

Table 6-17. Tabulation of Calculations Supporting the Analysis of Arrays of Damaged Packages

Case Name	k_{eff}	σ	Package Model Type	H/Pu	Water Density Fraction in Wood Zone	Array Type	Number of Packages	Description	Locations
hexm015	0.65577	0.00049	side	0	0.15	hex	1152	Varying water density in redwood zone	/pat1/apps/hacarray/sideimpact/hexstudy/hexmet/
hexm020	0.65561	0.00048	side	0	0.2	hex	1152	Varying water density in redwood zone	/pat1/apps/hacarray/sideimpact/hexstudy/hexmet/
hexm030	0.65735	0.00049	side	0	0.3	hex	1152	Varying water density in redwood zone	/pat1/apps/hacarray/sideimpact/hexstudy/hexmet/
hexm040	0.65854	0.00050	side	0	0.4	hex	1152	Varying water density in redwood zone	/pat1/apps/hacarray/sideimpact/hexstudy/hexmet/
hexm050	0.66053	0.00049	side	0	0.5	hex	1152	Varying water density in redwood zone	/pat1/apps/hacarray/sideimpact/hexstudy/hexmet/
hexm060	0.66232	0.00049	side	0	0.6	hex	1152	Varying water density in redwood zone	/pat1/apps/hacarray/sideimpact/hexstudy/hexmet/
hexm070	0.66298	0.00050	side	0	0.7	hex	1152	Varying water density in redwood zone	/pat1/apps/hacarray/sideimpact/hexstudy/hexmet/
hexm080	0.66268	0.00049	side	0	0.8	hex	1152	Varying water density in redwood zone	/pat1/apps/hacarray/sideimpact/hexstudy/hexmet/
hexm090	0.66261	0.00049	side	0	0.9	hex	1152	Varying water density in redwood zone	/pat1/apps/hacarray/sideimpact/hexstudy/hexmet/
hexm095	0.66402	0.00050	side	0	0.95	hex	1152	Varying water density in redwood zone	/pat1/apps/hacarray/sideimpact/hexstudy/hexmet/
hexm100	0.66365	0.00049	side	0	1	hex	1152	Varying water density in redwood zone	/pat1/apps/hacarray/sideimpact/hexstudy/hexmet/
hexm100_1	0.65861	0.00050	side	0	1	hex	1152	TB-1s moved 1 cm from flat side of package	/pat1/apps/hacarray/sideimpact/hexstudy/hexmet/
hexm100_2	0.65607	0.00049	side	0	1	hex	1152	TB-1s moved 2 cm from flat side of package	/pat1/apps/hacarray/sideimpact/hexstudy/hexmet/
hexm100_3	0.65325	0.00050	side	0	1	hex	1152	TB-1s moved 3 cm from flat side of package	/pat1/apps/hacarray/sideimpact/hexstudy/hexmet/
hexm100_p5	0.66003	0.00049	side	0	1	hex	1152	TB-1s moved 0.5 cm from flat side of package	/pat1/apps/hacarray/sideimpact/hexstudy/hexmet/
hexs100i01	0.71442	0.00049	side	28.8	1	hex	1152	1% water density between packages	/pat1/apps/hacarray/sideimpact/hexstudy/inter/
hexs100i02	0.71503	0.00050	side	28.8	1	hex	1152	2% water density between packages	/pat1/apps/hacarray/sideimpact/hexstudy/inter/
hexs100i05	0.71569	0.00058	side	28.8	1	hex	1152	5% water density between packages	/pat1/apps/hacarray/sideimpact/hexstudy/inter/
hexs100i10	0.71469	0.00049	side	28.8	1	hex	1152	10% water density between packages	/pat1/apps/hacarray/sideimpact/hexstudy/inter/
hexs100i25	0.71398	0.00057	side	28.8	1	hex	1152	25% water density between packages	/pat1/apps/hacarray/sideimpact/hexstudy/inter/
hexs100i50	0.71610	0.00050	side	28.8	1	hex	1152	50% water density between packages	/pat1/apps/hacarray/sideimpact/hexstudy/inter/
hexs100i75	0.71429	0.00053	side	28.8	1	hex	1152	75% water density between packages	/pat1/apps/hacarray/sideimpact/hexstudy/inter/
hexs100i90	0.71330	0.00050	side	28.8	1	hex	1152	90% water density between packages	/pat1/apps/hacarray/sideimpact/hexstudy/inter/
hexs100i100	0.71491	0.00062	side	28.8	1	hex	1152	100% water density between packages	/pat1/apps/hacarray/sideimpact/hexstudy/inter/
hexsdryi01	0.70379	0.00056	side	28.8	0	hex	1152	1% water density between packages	/pat1/apps/hacarray/sideimpact/hexstudy/inter/
hexsdryi02	0.70389	0.00060	side	28.8	0	hex	1152	2% water density between packages	/pat1/apps/hacarray/sideimpact/hexstudy/inter/
hexsdryi05	0.69864	0.00052	side	28.8	0	hex	1152	5% water density between packages	/pat1/apps/hacarray/sideimpact/hexstudy/inter/
hexsdryi10	0.68545	0.00050	side	28.8	0	hex	1152	10% water density between packages	/pat1/apps/hacarray/sideimpact/hexstudy/inter/

Table 6-17. Tabulation of Calculations Supporting the Analysis of Arrays of Damaged Packages

Case Name	k_{eff}	σ	Package Model Type	H/Pu	Water Density Fraction in Wood Zone	Array Type	Number of Packages	Description	Locations
hexsdryi25	0.65098	0.00049	side	28.8	0	hex	1152	25% water density between packages	/pat1/apps/hacarray/sideimpact/hexstudy/inter/
hexsdryi50	0.62096	0.00053	side	28.8	0	hex	1152	50% water density between packages	/pat1/apps/hacarray/sideimpact/hexstudy/inter/
hexsdryi75	0.60452	0.00050	side	28.8	0	hex	1152	75% water density between packages	/pat1/apps/hacarray/sideimpact/hexstudy/inter/
hexsdryi90	0.59848	0.00050	side	28.8	0	hex	1152	90% water density between packages	/pat1/apps/hacarray/sideimpact/hexstudy/inter/
hexsdryi100	0.59412	0.00050	side	28.8	0	hex	1152	100% water density between packages	/pat1/apps/hacarray/sideimpact/hexstudy/inter/
octmdry	0.66773	0.00049	side	0	0	square	1024	Varying water density in redwood zone	/pat1/apps/hacarray/sideimpact/octstudy/metal/
octm0001	0.66815	0.00050	side	0	0.001	square	1024	Varying water density in redwood zone	/pat1/apps/hacarray/sideimpact/octstudy/metal/
octm0005	0.66646	0.00048	side	0	0.005	square	1024	Varying water density in redwood zone	/pat1/apps/hacarray/sideimpact/octstudy/metal/
octm001	0.66552	0.00049	side	0	0.01	square	1024	Varying water density in redwood zone	/pat1/apps/hacarray/sideimpact/octstudy/metal/
octm002	0.66298	0.00051	side	0	0.02	square	1024	Varying water density in redwood zone	/pat1/apps/hacarray/sideimpact/octstudy/metal/
octm003	0.66009	0.00050	side	0	0.03	square	1024	Varying water density in redwood zone	/pat1/apps/hacarray/sideimpact/octstudy/metal/
octm005	0.65731	0.00049	side	0	0.05	square	1024	Varying water density in redwood zone	/pat1/apps/hacarray/sideimpact/octstudy/metal/
octm010	0.65370	0.00049	side	0	0.1	square	1024	Varying water density in redwood zone	/pat1/apps/hacarray/sideimpact/octstudy/metal/
octm020	0.65596	0.00049	side	0	0.2	square	1024	Varying water density in redwood zone	/pat1/apps/hacarray/sideimpact/octstudy/metal/
octm030	0.65707	0.00049	side	0	0.3	square	1024	Varying water density in redwood zone	/pat1/apps/hacarray/sideimpact/octstudy/metal/
octm040	0.65914	0.00050	side	0	0.4	square	1024	Varying water density in redwood zone	/pat1/apps/hacarray/sideimpact/octstudy/metal/
octm050	0.66046	0.00049	side	0	0.5	square	1024	Varying water density in redwood zone	/pat1/apps/hacarray/sideimpact/octstudy/metal/
octm060	0.66105	0.00049	side	0	0.6	square	1024	Varying water density in redwood zone	/pat1/apps/hacarray/sideimpact/octstudy/metal/
octm070	0.66256	0.00049	side	0	0.7	square	1024	Varying water density in redwood zone	/pat1/apps/hacarray/sideimpact/octstudy/metal/
octm080	0.66262	0.00049	side	0	0.8	square	1024	Varying water density in redwood zone	/pat1/apps/hacarray/sideimpact/octstudy/metal/
octm090	0.66378	0.00049	side	0	0.9	square	1024	Varying water density in redwood zone	/pat1/apps/hacarray/sideimpact/octstudy/metal/
octm095	0.66449	0.00049	side	0	0.95	square	1024	Varying water density in redwood zone	/pat1/apps/hacarray/sideimpact/octstudy/metal/
octm0975	0.66410	0.00048	side	0	0.975	square	1024	Varying water density in redwood zone	/pat1/apps/hacarray/sideimpact/octstudy/metal/
octm099	0.66435	0.00050	side	0	0.99	square	1024	Varying water density in redwood zone	/pat1/apps/hacarray/sideimpact/octstudy/metal/
octm100	0.66424	0.00049	side	0	1	square	1024	Varying water density in redwood zone	/pat1/apps/hacarray/sideimpact/octstudy/metal/
octsdry	0.67719	0.00057	side	28.8	0	square	1024	Varying water density in redwood zone	/pat1/apps/hacarray/sideimpact/octstudy/soln/
octs0001	0.67944	0.00049	side	28.8	0.001	square	1024	Varying water density in redwood zone	/pat1/apps/hacarray/sideimpact/octstudy/soln/
octs0005	0.67808	0.00055	side	28.8	0.005	square	1024	Varying water density in redwood zone	/pat1/apps/hacarray/sideimpact/octstudy/soln/

Table 6-17. Tabulation of Calculations Supporting the Analysis of Arrays of Damaged Packages

Case Name	k_{eff}	σ	Package Model Type	H/Pu	Water Density Fraction in Wood Zone	Array Type	Number of Packages	Description	Locations
octs001	0.67270	0.00059	side	28.8	0.01	square	1024	Varying water density in redwood zone	/pat1/apps/hacarray/sideimpact/octstudy/soln/
octs002	0.65588	0.00053	side	28.8	0.02	square	1024	Varying water density in redwood zone	/pat1/apps/hacarray/sideimpact/octstudy/soln/
octs003	0.64169	0.00049	side	28.8	0.03	square	1024	Varying water density in redwood zone	/pat1/apps/hacarray/sideimpact/octstudy/soln/
octs005	0.62271	0.00056	side	28.8	0.05	square	1024	Varying water density in redwood zone	/pat1/apps/hacarray/sideimpact/octstudy/soln/
octs010	0.60422	0.00050	side	28.8	0.1	square	1024	Varying water density in redwood zone	/pat1/apps/hacarray/sideimpact/octstudy/soln/
octs020	0.61144	0.00055	side	28.8	0.2	square	1024	Varying water density in redwood zone	/pat1/apps/hacarray/sideimpact/octstudy/soln/
octs030	0.63223	0.00053	side	28.8	0.3	square	1024	Varying water density in redwood zone	/pat1/apps/hacarray/sideimpact/octstudy/soln/
octs040	0.65161	0.00053	side	28.8	0.4	square	1024	Varying water density in redwood zone	/pat1/apps/hacarray/sideimpact/octstudy/soln/
octs050	0.66810	0.00063	side	28.8	0.5	square	1024	Varying water density in redwood zone	/pat1/apps/hacarray/sideimpact/octstudy/soln/
octs060	0.68116	0.00050	side	28.8	0.6	square	1024	Varying water density in redwood zone	/pat1/apps/hacarray/sideimpact/octstudy/soln/
octs070	0.69215	0.00050	side	28.8	0.7	square	1024	Varying water density in redwood zone	/pat1/apps/hacarray/sideimpact/octstudy/soln/
octs080	0.70046	0.00059	side	28.8	0.8	square	1024	Varying water density in redwood zone	/pat1/apps/hacarray/sideimpact/octstudy/soln/
octs090	0.70881	0.00053	side	28.8	0.9	square	1024	Varying water density in redwood zone	/pat1/apps/hacarray/sideimpact/octstudy/soln/
octs095	0.71225	0.00050	side	28.8	0.95	square	1024	Varying water density in redwood zone	/pat1/apps/hacarray/sideimpact/octstudy/soln/
octs0975	0.71395	0.00048	side	28.8	0.975	square	1024	Varying water density in redwood zone	/pat1/apps/hacarray/sideimpact/octstudy/soln/
octs099	0.71434	0.00057	side	28.8	0.99	square	1024	Varying water density in redwood zone	/pat1/apps/hacarray/sideimpact/octstudy/soln/
octs100	0.71466	0.00051	side	28.8	1	square	1024	Varying water density in redwood zone	/pat1/apps/hacarray/sideimpact/octstudy/soln/

[a] Limiting cases listed in Table 6-1.

6.9.4.4 Calculations Supporting Single Package Air Transport Analysis

Table 6-18 lists calculations performed to support the analysis of a single package of fissile material intended for air transport.

Table 6-18. Tabulation of Calculations Supporting the Analysis of a Single Package of Fissile Material Intended for Air Transport

Case Name	k_{eff}	σ	g Pu	g H2O	Fissile Radius	H/Pu	Location
sph01	0.65568	0.00050	1300	0	2.501	0	/pat1/apps/hacsp/
sph02	0.64479	0.00050	1300	3	2.544	0.07	/pat1/apps/hacsp/
sph03	0.63394	0.00050	1300	7	2.590	0.15	/pat1/apps/hacsp/
sph04	0.61194	0.00049	1300	16	2.694	0.33	/pat1/apps/hacsp/
sph05	0.59142	0.00049	1300	28	2.817	0.57	/pat1/apps/hacsp/
sph06	0.57162	0.00050	1300	44	2.965	0.89	/pat1/apps/hacsp/
sph07	0.55477	0.00050	1300	65	3.151	1.33	/pat1/apps/hacsp/
sph08	0.54322	0.00049	1300	98	3.394	2.00	/pat1/apps/hacsp/
sph09	0.53893	0.00049	1300	153	3.736	3.11	/pat1/apps/hacsp/
sph10	0.55022	0.00050	1300	262	4.277	5.34	/pat1/apps/hacsp/
sph11	0.60548	0.00050	1300	588	5.388	12.01	/pat1/apps/hacsp/
sph12	0.64898	0.00049	1300	869	6.068	17.74	/pat1/apps/hacsp/
sph13	0.69693	0.00051	1300	1242	6.789	25.36	/pat1/apps/hacsp/
sph14[a]	0.71468	0.00050	1300	1412	7.067	28.78	/pat1/apps/hacsp/
sph15	0.68744	0.00055	1300	1412	7.313	28.78	/pat1/apps/hacsp/
sph16	0.62157	0.00049	1300	1412	8.049	28.78	/pat1/apps/hacsp/
sph17	0.55564	0.00049	1300	1412	9.214	28.78	/pat1/apps/hacsp/
sph18	0.48650	0.00049	1300	1412	11.608	28.78	/pat1/apps/hacsp/
sph19	0.46577	0.00049	1300	1412	13.074	28.78	/pat1/apps/hacsp/
sph20	0.45167	0.00050	1300	1412	14.626	28.78	/pat1/apps/hacsp/
sph21	0.42551	0.00050	1300	1412	19.850	28.78	/pat1/apps/hacsp/
sph22	0.41048	0.00049	1300	1412	25.010	28.78	/pat1/apps/hacsp/
sph23	0.39143	0.00049	1300	1412	31.510	28.78	/pat1/apps/hacsp/

[a] Limiting case listed in Table 6-1.

6.9.5 Sample inputs

This section contains the *csas25* input decks used for the limiting cases shown in Table 6-1 in Section 6.1.2.

6.9.5.1 Input File For cv031.inp

```
=csas25
pat1, single package, case cv031.inp
v6-238
read composition
'4.4327% of MTD Pu = 19.84 g/cm3
pu-239      1 0.879448 300   end
h2o         1 0.955673 300   end
'
h2o         2 1.0 300 end
end composition
read celldata
  multiregion spherical left_bdy=reflected right_bdy=vacuum end
           1        5.4
           2       35.4
      end zone
end celldata
read parameter
 npg=3000
 gen=1050
 nsk=50
 sig=0.0005
 htm=no
end parameter
read geometry
unit 1
com='fuel/moderator region, pu metal/water, sphere'
 cylinder 1 1    5.4     2p8.0680
 cylinder 2 1   35.4     2p38.07
end geometry
end data
end
```

6.9.5.2 Input File for fslsf001.inp

```
=csas25
pat1, 17x17x9 square pitched array, void between drums, water in drum
v6-238
read composition
' 100% of MTD Pu = 19.84 g/cm3
pu-239      1 19.84    300   end
h2o         1 1e-9     300   end
'
' water in TB-1, but outside fuel (rho=0.9982 g/cm3)
h2o         2 1.0       300   end
'
' PH13-8Mo for TB-1 containment vessel
fe          3 0 6.3246E-02 300 end
cr          3 0 1.1430E-02 300 end
ni          3 0 6.3532E-03 300 end
mo          3 0 1.0931E-03 300 end
al          3 0 1.9435E-03 300 end
mn          3 0 8.4843E-05 300 end
'
'replace Redwood with full density water
 h2o         4 1.0       300   end
'
' ss304 for drum body (rho= 7.94 g/cm3)
ss304       5 1.0 300 end
end composition
read celldata
  multiregion spherical left_bdy=reflected right_bdy=vacuum end
           1        2.501
           2        5.4
           3        6.612
           4       28.0289
           5       28.299
           0       29.000
      end zone
end celldata
read parameter
 npg=3000
 gen=1050
 nsk=50
 sig=0.0005
 htm=no
end parameter
read geometry
unit 1
com='fuel/moderator region, pu metal, sphere + x dir'
 sphere       1 1    2.501
 cylinder     2 1    5.4     2p8.07
 cylinder     3 1    6.612   2p9.2815
 cylinder     4 1   28.0289 2p50.368
 cylinder     5 1   28.299  2p50.639
 cuboid       0 1   4p28.3  2p50.639
global unit 2
 array  1  0.0  0.0  0.0
 replicate 2 1  6*30.0  1
```

```
end geometry
read array
 ara=1  nux=17 nuy=17 nuz=9  fill  f1  end fill
end array
read mixt
 eps=1.0
end mixt
end data
end
```

6.9.5.3 Input File for hexs100.inp

```
=csas25
pat1, damaged, hex arrangement
v6-238
read composition
pu-239      1 0.879448 300   end
h2o         1 0.955673 300   end
'
' PH13-8Mo for TB-1 containment vessel
fe          3 0 6.3246E-02 300 end
cr          3 0 1.1430E-02 300 end
ni          3 0 6.3532E-03 300 end
mo          3 0 1.0931E-03 300 end
al          3 0 1.9435E-03 300 end
mn          3 0 8.4843E-05 300 end
'
' water for flooding drum (rho=0.9982 g/cm3)
h2o         4 1.0     300 end
'
' ss304 for drum body (rho= 7.94 g/cm3)
ss304       5 1.0 300 end
'
' water between drum (rho=0.9982 g/cm3)
h2o         6 0.00001 300 end
'
' water reflector around array
' vf = 1 -> rho=0.9982 g/cm3
h2o         7 1.0 300 end
'
'
end composition
read celldata
  multiregion spherical left_bdy=reflected right_bdy=reflected  end
            1        5.4
            3        6.612
            4       37.194
            5       37.465
            6       38
      end zone
end celldata
read parameter
 npg=3000
 gen=1050
 nsk=50
 sig=0.0005
 htm=no
end parameter
read geometry
unit 1
com='fuel/moderator region, pu metal, sphere'
 cylinder   1 1    5.4     2p8.07    origin 0 6.613
 cylinder   3 1    6.612   2p9.2815  origin 0 6.613
 zhemicyl+y 4 1   37.194  2p50.368
 zhemicyl+y 5 1   37.465  2p50.639
unit 2
```

```
com='fuel/moderator region, pu metal, sphere'
 cylinder   1 1    5.4     2p8.07    origin 6.613 0
 cylinder   3 1    6.612   2p9.2815  origin 6.613 0
 zhemicyl+x 4 1   37.194  2p50.368
 zhemicyl+x 5 1   37.465  2p50.639
unit 3
com='fuel/moderator region, pu metal, sphere'
 cylinder   1 1    5.4     2p8.07    origin 0 -6.613
 cylinder   3 1    6.612   2p9.2815  origin 0 -6.613
 zhemicyl-y 4 1   37.194  2p50.368
 zhemicyl-y 5 1   37.465  2p50.639
unit 4
com='fuel/moderator region, pu metal, sphere'
 cylinder   1 1    5.4     2p8.07    origin -6.613 0
 cylinder   3 1    6.612   2p9.2815  origin -6.613 0
 zhemicyl-x 4 1   37.194  2p50.368
 zhemicyl-x 5 1   37.465  2p50.639
unit 5
com='drum steel on flat side of drum on long side'
 cuboid     5 1 0.2708 0 2p37.465 2p50.639
unit 6
com='drum steel on flat side of drum on short side'
 cuboid     5 1  2p37.465 0.2708 0 2p50.639
unit 7
com='fuel/moderator region, pu metal, sphere'
 cuboid     6 1   2p37.737 2p65.1622 2p50.639
   hole     1  0  -64.8914 0
   hole     6  0  -65.1622 0
   hole     2  -37.466 0   0
   hole     5  -37.737 0   0
   hole     3  0   64.8914 0
   hole     6  0   64.8914 0
   hole     4  37.466  0   0
   hole     5  37.466  0   0
global unit 8
com='array of hemicylinder drums'
array 1  0 0 0
reflector 7 1 30 0 30 0 30 0 1
end geometry
read array
 ara=1 nux=4 nuy=3 nuz=3
 fill 36*7  end fill
end array
read bound
  +fc=vacuum  -fc=mirror
end bound
end data
end
```

6.9.5.4 Input File for sph14.inp

```
=csas25
pat1, single package for 10CFR71.55(f) analysis
v6-238
read composition
' 4.4327% of MTD Pu = .879448 g/cm3
pu-239      1 .879448    300   end
h2o         1 .9557     300   end
'
' water outside Pu/water mix
' vf =1.0 ->  rho=0.9982 g/cm3
h2o         2 1.0       300   end
'
end composition
read celldata
  multiregion spherical left_bdy=reflected right_bdy=vacuum end
    1        7.0667
    2       27.0667
     end zone
end celldata
read parameter
 npg=3000
 gen=1050
 nsk=50
 sig=0.0005
 htm=no
end parameter
read geometry
unit 1
com='pu metal/water sphere and 20 cm water reflector'
 sphere    1 1    7.0667
 reflector 2 1   20.0     1
end geometry
end data
end
```

6.9.5.5 USLSTATS Input File for Application cv031

```
tsunami, c(k) vs. keff trend for cv031
0.999  0.950  0.950  0.0  1.0 -1  0.05
0.9659   1.00882   0.0005
0.9602   1.00909   0.0005
0.9604   1.00375   0.0005
0.9454   1.00734   0.0005
0.9481   1.00676   0.0005
0.9455   1.00641   0.0005
0.9454   1.00573   0.0005
0.9456   1.00559   0.0005
0.9455   1.00593   0.0005
0.9513   1.00855   0.0005
0.9521   1.00844   0.0005
0.9531   1.00736   0.0005
0.9536   1.00799   0.0005
0.9535   1.00860   0.0005
0.9545   1.00935   0.0005
0.9490   1.01046   0.0005
0.9509   1.00812   0.0005
0.9528   1.00918   0.0005
0.9543   1.00749   0.0005
0.9503   1.00621   0.0005
0.9521   1.00767   0.0005
0.9533   1.00793   0.0005
0.9542   1.00929   0.0005
0.9474   1.01058   0.0005
0.9507   1.00812   0.0005
0.9528   1.00764   0.0005
0.9525   1.00757   0.0005
0.9542   1.00702   0.0005
0.9544   1.00874   0.0005
0.9546   1.00898   0.0005
0.9458   1.00895   0.0005
0.9486   1.00804   0.0005
0.9455   1.00914   0.0005
0.9458   1.00937   0.0005
0.9458   1.01032   0.0005
0.9461   1.00691   0.0005
0.9472   1.00802   0.0005
0.9458   1.00658   0.0005
0.9455   1.00812   0.0005
0.9457   1.00764   0.0005
0.9458   1.00773   0.0005
0.9458   1.00734   0.0005
0.9455   1.00797   0.0005
0.9456   1.00701   0.0005
0.9459   1.00699   0.0005
0.9455   1.00849   0.0005
0.9453   1.00766   0.0005
0.9455   1.00810   0.0005
0.9455   1.00819   0.0005
0.9457   1.00881   0.0005
0.9455   1.00777   0.0005
0.9601   1.01198   0.0005
0.9603   1.00474   0.0005
```

6.9.6 Considerations for Pu/Be Sources

6.9.6.1 Background: The Need for Pu/Be Source Evaluation

Following completion of work for the revision of Section 6, NCS evaluation of an additional loading of the PAT-1 package was requested. The proposed additional loading includes Pu/Be source items, with the total desired inventory of the sources per PAT-1 package consisting of less than 200 g (0.441 lb) Pu alloy and less than 30 g (0.066 lb) Be metal. Other than the Pu and Be, the proposed loading includes no other neutron-multiplying materials.

Be has several unique properties for interaction with neutrons. It is a neutron-multiplying media; when subjected to high-energy neutrons (such as those from Pu-239 fission), Be can multiply neutrons via (n, 2n) nuclear reactions. In solid form (e.g., as metal parts), Be can be a more effective neutron reflector than water, for either moderated or unmoderated fissile materials.

The preceding sections and analyses of Section 6 do not evaluate presence of Be as an allowable component or material for co-loading with the general-purpose Pu metal loading limit (1300 g [2.87 lb]). If the 1300 g (2.87 lb) Pu limit were to be reevaluated with significant quantities of Be, the reevaluation effort would be substantial and the existing conclusions (e.g., assigned CI value) might require change.

As an alternative approach, it was recognized that if very low loading limits (for both Pu and Be) were accepted as a second (separate) authorized PAT-1 loading, the NCS evaluation work performed for the 1300 g (2.87 lb) general-form Pu metal loading could be demonstrated as clearly bounding the proposed Pu/Be source loading.

6.9.6.2 Basic Comparison Argument for Pu/Be Sources

The basic reason why the proposed Pu/Be source loading limit is bounded by the 1300 g (2.87lb) Pu loading evaluation is that the:

- Permitted Pu loading for the sources is very small (relative to the evaluated 1300 g [2.87 lb] Pu metal loading); and

- Quantity of Be permitted in the source loading (30 g [0.66 lb]) is sufficiently limited to the extent that the beryllium cannot offset the reactivity effect associated with the significant reduction in Pu mass loading.

A simple observation reveals that the impact of the Be presence should be no greater than that resulting from replacement of the Be mass with an equal mass of Pu-239. Using a "mass replacement" basis, it may be asserted that the PAT-1 Pu/Be source loading (200 g [0.441 lb] maximum of Pu alloy plus (30 g [0.066 lb] maximum of Be) is no more reactive than a loading of 230 g (0.507 lb) Pu-239.

The comparison could be done on a more conservative "volume replacement" basis. If theoretical densities of 1.85 g/cm^3 (0.067 lb/in.^{3}) for the Be [Reference 2, page 4-43] and 19.84 g/cm^3 (0.7167 lb/in.^{3}) for the Pu [Reference 2, page 4-83] are assumed, and the 30 g (0.066 lb) of Be is replaced by an equal volume of Pu-239 metal (322 g [0.71 lb] Pu-239), the

resulting idealized package loading (522 g [1.15 lb] Pu-239) remains well below the evaluated general-purpose loading limit of 1300 g (2.87 lb) Pu. If the 200 g (0.441 lb) Pu-239 contained in the sources is considered as the initial (primary) loading constituent, the reactivity effect of adding 30 g (0.066 lb) Be cannot plausibly exceed the reactivity effect due to addition of over 10 times that mass (322 g [0.71 lb]) of Pu-239.

This conclusion that a loading of 200 g (0.441 lb) Pu-239 plus 30 g (0.066 lb) Be is bounded by NCS evaluation of a loading of 1300 g (2.87 lb) Pu-239 holds true for all normal and accident condition models evaluated in Section 6.

6.9.6.3 Supporting Scoping Calculations - Computational Method

For informational purposes only: scoping calculations were performed to augment the comparison argument of Section 6.9.6.2. All inputs and outputs for these calculations are located in the directory tree /pat1/apps/Pu/Be.

The calculations were performed using a quality-assurance-controlled version of SCALE 5.1 similar to that described in Section 6.3.3. The scoping calculations were performed on a cluster of 36 workstations referred to as the *cpile2* cluster and identified as node1 through node36; these workstations all utilized LINUX operating systems. The SCALE 5.1 software used for the scoping calculations was in a directory tree starting at /projects/ymp/scale5.1/ and is under a quality assurance plan, software quality assurance plans, and requirements based on 10 CFR 71 Subpart H.

Although there is no difference in the source SCALE software or data used for other Section 6 calculations and these scoping calculations, the scoping calculations were executed on a different set of workstations, using a different operating system. Thus, as a preliminary action, the benchmark validation set in Table 6-8 was reexecuted on the noted LINUX workstations. For the 125-experiment set, the average of all prior-computed k_{eff} values (as shown in Table 6-8 for the UNIX workstations) is 1.00792; the average of all reexecuted cases (using the LINUX workstations) is 1.00795. This indicates a negligible difference between calculations performed on the LINUX and UNIX computing platforms.

6.9.6.4 Scoping Calculations - Single Packages

Table 6-19 provides scoping calculation results for variant models based on cases *cv001* and *cv031*. The single-package scoping results support that a significant reduction in the neutron multiplication factor is expected from a reduced container loading from 1300 g (2.87 lb) Pu-239 to 200 g Pu-239, and that the inclusion of 30 g (0.066 lb) Be (with the 200 g [0.441 lb] Pu-239 loading) is a negligible positive reactivity effect. These results also support that modeling of the 30 g (0.066 lb) of Be as 30 g (0.066 lb) of Pu-239 is conservative, and that modeling of the 30 g (0.066 lb) of Be as 322 g (0.71 lb) Pu-239 on a volume replacement basis is highly conservative.

Table 6-19. Scoping Calculation Results for Single Packages

Case	$k_{eff} \pm \sigma$ [a]	Notes
cv001 [b]	0.65648 ± 0.00046	Prior UNIX result (see Table 6-1 and Table 6-15): Loading of a 1300 g (2.87 lb) Pu-239 metal sphere in the TB-1 vessel. The remaining TB-1 volume is filled with H_2O in this case, and in all *cv001* variants listed below.
cv001-v0	0.65686 ± 0.00050	Current result; rerun of *cv001* on LINUX workstations.
cv001-v1	0.25956 ± 0.00050	Loading of *cv001* changed to a homogeneous (metal alloy) sphere containing 200 g (0.441 lb) Pu-239 and 30 g (0.066 lb) Be, Be: Pu-239 = 4.0.
cv001-v2	0.36315 ± 0.00048	Loading of *cv001* changed to 200 g (0.441 lb) Pu-239 metal sphere surrounded by a 30 g (0.066 lb) Be metal shell.
cv001-v3	0.35350 ± 0.00050	Loading of *cv001-v2* changed to 200 g (0.441 lb) Pu-239 metal sphere. (The Be volume is modeled as H_2O.)
cv001-v4	0.37073 ± 0.00048	Loading of *cv001-v2* changed to 230 g (0.507 lb) Pu-239 metal sphere. (The Be mass is modeled as Pu-239 metal.)
cv001-v5	0.48962 ± 0.00045	Loading of *cv001-v2* changed to 522 g (1.151 lb) Pu-239 metal sphere. (The Be volume is modeled as Pu-239 metal.)
cv031 [b]	0.70756 ± 0.00055	Prior UNIX result (see Table 6-1 and Table 6-15): The TB-1 vessel is loaded with a homogeneous metal-water mixture containing 1300 g (2.87 lb) Pu-239 metal, and adequate H_2O so as to completely fill the TB-1 volume. H: Pu-239 = 28.8.
cv031-v0	0.70817 ± 0.00051	Current result; rerun of *cv031* on LINUX workstations.
cv031-v1	0.61285 ± 0.00054	Loading of *cv031* changed to a homogeneous mixture of 200 g (0.441 lb) Pu-239 metal, 30 g (0.066 lb) Be metal, and adequate H_2O so as to completely fill the TB-1 vessel. H: Pu-239 = 192.4, Be: Pu-239 = 4.0.
cv031-v2	0.61382 ± 0.00055	Loading of *cv031-v1* changed to a homogeneous mixture of 200 g (0.441 lb) Pu-239 metal and adequate H_2O so as to completely fill the TB-1 vessel. H: Pu-239= 194.5. (Be volume modeled as H_2O.)
cv031-v3	0.62322 ± 0.00051	Loading of *cv031-v1* changed to a homogeneous mixture of 230 g (0.507 lb) Pu-239 metal and H_2O. (Be mass modeled as Pu-239.)
cv031-v4	0.66172 ± 0.00054	Loading of *cv031-v1* changed to a homogeneous mixture of 522 g (1.151 lb) Pu-239 metal and H_2O. (Be volume modeled as Pu-239.)

[a] KENO V.a calculated k_{eff} and standard deviation values.

[b] For *cv001* and *cv031* and variant models, the interior of the TB-1 vessel is fully occupied by the payload material (Pu-239, and Be if modeled), with all remaining volume within the TB-1 vessel volume occupied by H_2O. Structural materials of the TB-1 vessel and the PAT-1 container are not modeled. Instead, the TB-1 payload is centered within a cylinder of water; the water cylinder has the approximate outer dimensions of the PAT-1 container.

6.9.6.5 Scoping Calculations - Normal Condition of Transport Arrays

Table 6-20 provides scoping calculation results for variant models based on cases *fhlsf001* and *fslsf031*. The conclusions are the same as for Table 6-19 single-package results. The computed neutron multiplication constant is significantly reduced by lowering the per-package payload from 1300 g (2.87 lb) Pu-239 to 200 g (0.441 lb) Pu-239, the effect of adding 30 g (0.066 lb) Be

to the 200 g (0.441 lb) Pu-239 loading appears insignificant, and modeling the Be as Pu-239 on mass-replacement or volume-replacement bases is conservative.

Table 6-20. Scoping Calculation Results for Normal Conditions of Transport Arrays

Case	$k_{eff} \pm \sigma$ [a]	Notes
fhlsf001 [b]	0.65094 ± 0.00049	Prior UNIX result (see Table 6-1 and Table 6-16): Each TB-1 vessel is loaded with a 1300 g (2.87 lb) Pu-239 metal sphere. The remaining TB-1 volume is filled with H_2O in this case, and in all *fhlsf001* variants listed below.
fhlsf001-v0	0.65081 ± 0.00050	Current result; rerun of *fhlsf001* on LINUX workstations.
fhlsf001-v1	0.25262 ± 0.00047	Loading of *fhlsf001* changed to a homogeneous (metal alloy) sphere containing 200 g (0.441 lb) Pu-239 and 30 g (0.066 lb) Be.
fhlsf001-v2	0.35924 ± 0.00049	Loading of *fhlsf001* changed to 200 g (0.441 lb) Pu-239 metal sphere surrounded by a 30 g (0.066 lb) Be metal shell.
fhlsf001-v3	0.35163 ± 0.00050	Loading of *fhlsf001-v2* changed to 200 g (0.441 lb) Pu-239 metal sphere. (Be volume modeled as H_2O.)
fhlsf001-v4	0.36844 ± 0.00049	Loading of *fhlsf001-v2* changed to 230 g (0.507 lb) Pu-239 metal sphere. (Be mass modeled as Pu-239.)
fhlsf001-v5	0.48541 ± 0.00050	Loading of *fhlsf001-v2* changed to 522 g (1.151 lb) Pu-239 metal sphere. (Be volume modeled as Pu-239.)
fslsf031 [c]	0.63371 ± 0.00050	Prior UNIX result (see Table 6-1 and Table 6-16): Each TB-1 vessel is loaded with a homogeneous metal-water mixture containing 1300 g (2.87 lb) Pu-239 metal, with adequate H_2O so as to completely fill the TB-1 volume.
fslsf031-v0	0.63336 ± 0.00050	Current result; rerun of *fslsf031* on LINUX workstations.
fslsf031-v1	0.52070 ± 0.00050	Loading of *fslsf031* changed to a homogeneous mixture of 200 g (0.441 lb) Pu-239 metal, 30 g (0.066 lb) Be metal, and H_2O.
fslsf031-v2	0.52248 ± 0.00059	Loading of *fslsf031-v1* changed to a homogeneous mixture of 200 g (0.441 lb) Pu-239 metal and H_2O. (Be volume modeled as H_2O.)
fslsf031-v3	0.53184 ± 0.00050	Loading of *fslsf031-v1* changed to a homogeneous mixture of 230 g (0.507 lb) Pu-239 metal and H_2O. (Be mass modeled as Pu-239.)
fslsf031-v4	0.57872 ± 0.00050	Loading of *fslsf031-v1* changed to a homogeneous mixture of 522 g (1.151 lb) Pu-239 metal and H_2O. (Be volume modeled as Pu-239.)

[a] KENO V.a calculated k_{eff} and standard deviation values.

[b] Close-packed hexagonal-pitch array of 2646 undamaged packages, redwood modeled as H_2O (see Figure 6-2 and Figure 6-10).

[c] Close-packed square-pitch array of 2601 undamaged packages, redwood modeled as H_2O (see Figure 6-2 and Figure 6-8).

6.9.6.6 Scoping Calculations - Hypothetical Accident Condition Arrays

Table 6-21 provides scoping calculation results for hypothetical accident condition arrays. These results further support the conclusions of Sections 6.9.5.4 and 6.9.6.5.

Table 6-21. Scoping Calculation Results for Hypothetical Accident Condition Arrays

Case	$k_{eff} \pm \sigma$ [a]	Notes
hexs100 [b]	0.71538 ± 0.00050	Prior UNIX result (see Table 6-1 and Table 6-17): Each TB-1 vessel is loaded with a homogeneous metal-water mixture containing 1300 g (2.87 lb) Pu-239 metal, with adequate H_2O so as to completely fill the TB-1 volume.
hexs100-v0	0.71491 ± 0.00051	Current result; rerun of *hexs100* on LINUX workstations.
hexs100-v1	0.59043 ± 0.00050	Loading of *hexs100* changed to a homogeneous mixture of 200 g (0.441 lb) Pu-239 metal, 30 g (0.066 lb) Be metal, and H_2O.
hexs100-v2	0.59173 ± 0.00051	Loading of *hexs100-v1* changed to a homogeneous mixture of 200 g (0.441 lb) Pu-239 metal and H_2O. (Be volume modeled as H_2O.)
hexs100-v3	0.60218 ± 0.00049	Loading of *hexs100-v1* changed to a homogeneous mixture of 230 g (0.507 lb) Pu-239 metal and H_2O. (Be mass modeled as Pu-239.)
hexs100-v3a	0.57171 ± 0.00049	Same as *hexs100-v3*, except that the H_2O density in the TB-1 vessel is reduced by 5%.
hexs100-v4	0.65593 ± 0.00054	Loading of *hexs100-v1* changed to a homogeneous mixture of 522 g (1.151 lb) Pu-239 metal and H_2O. (Be volume modeled as Pu-239.)
hexs100-v4a	0.62931 ± 0.00049	Same as *hexs100-v4*, except that the H_2O density in the TB-1 vessel is reduced by 5%.
hexsdry [c]	0.70268 ± 0.00065	Prior UNIX result (see Table 6-1 and Table 6-17): Each TB-1 vessel is loaded with a homogeneous metal-water mixture containing 1300 g (2.87 lb) Pu-239 metal, with adequate H_2O so as to completely fill the TB-1 volume.
hexsdry-v0	0.70344 ± 0.00054	Current result; rerun of *hexsdry* on LINUX workstations.
hexsdry-v1	0.58264 ± 0.00051	Each TB-1 vessel contains a homogeneous metal-water mixture containing 200 g (0.441 lb) Pu-239. A 30 g (0.066 lb) uniform-thickness shell of Be metal lines the interior surface of the TB-1 vessel. All TB-1 volume is filled with either Be metal or the Pu-239-H_2O mixture.
hexsdry-v2	0.57995 ± 0.00055	Loading of *hexsdry* changed to a homogeneous mixture of 200 g (0.441 lb) Pu-239 metal, 30 g Be metal, and H_2O.
hexsdry-v3	0.58414 ± 0.00052	Loading of *hexsdry-v2* changed to a homogeneous mixture of 200 g (0.441 lb) Pu-239 metal and H_2O. (Be volume modeled as H_2O.)
hexsdry-v4	0.59441 ± 0.00048	Loading of *hexsdry-v2* changed to a homogeneous mixture of 230 g (0.507 lb) Pu-239 metal and H_2O. (Be mass modeled as Pu-239.)
hexsdry-v4a	0.56395 ± 0.00052	Same as *hexsdry-v4*, except that the H_2O density in the TB-1 vessel is reduced by 5%.
hexsdry-v5	0.64122 ± 0.00055	Loading of *hexsdry-v2* changed to a homogeneous mixture of 522 g (1.151 lb) Pu-239 metal and H_2O. (Be volume modeled as Pu-239.)
hexsdry-v5a	0.61907 ± 0.00055	Same as *hexsdry-v5*, except that the H_2O density in the TB-1 vessel is reduced by 5%.

[a] KENO V.a calculated k_{eff} and standard deviation values.

[b] Close-packed array of 1152 damaged (side-impact model) packages (see Figure 6-4 and Figure 6-12). The redwood is modeled as full-density water.

[c] Close-packed array of 1152 damaged (side-impact model) packages (see Figure 6-4 and Figure 6-12). The redwood is modeled as void.

The results of cases *hexs100-v3a*, *hexs100-v4a*, *hexsdry-v4a*, and *hexsdry-v5a* all confirm that although the modeled Pu mass (as a homogeneous Pu-239-H_2O mixture) for the Pu/Be cases is significantly less than the general-purpose 1300 g (2.87 lb) Pu load limit, the metal-water mixtures remain under moderated. For each of these four cases, a slight reduction in H_2O content modeled within the TB-1 vessel resulted in a significant reduction in the computed k_{eff} value. A similar effect would be expected for other PAT-1 NCS models, where the TB-1 payload is modeled as a homogeneous mixture of Pu metal and water.

6.9.6.7 Scoping Calculations - Single Package, Air Transport Provision

Table 6-22 provides scoping calculation results for single packages under the air transport accident provision. These results are consistent with conclusions of Sections 6.9.6.4 through 6.9.6.6.

Table 6-22. Scoping Calculation Results for Single Package, Air Transport Accident Provision

Case	$k_{eff} \pm \sigma$ [a]	Notes
sph14 [b]	0.71468 ± 0.00050	Prior UNIX result (see Table 6-1 and Table 6-18): The payload is modeled as a homogeneous metal-water mixture containing 1300 g (2.87 lb) Pu-239.
sph14-v0	0.71540 ± 0.00050	Current result; rerun of *sph14* on LINUX workstations.
sph14-v1	0.62441 ± 0.00056	The central sphere of *sph14* is modeled as two regions: a central sphere contains 200 g (0.441 lb) Pu-239 as a homogeneous metal-water mixture; and an enclosing Be metal shell of mass 30 g (0.066 lb).
sph14-v2	0.62282 ± 0.00051	The fuel sphere of *sph14* is changed to a homogeneous mixture of 200 g (0.441 lb) Pu-239 metal, 30 g (0.066 lb) Be metal, and H_2O.
sph14-v3	0.62457 ± 0.00050	The fuel sphere of *sph14-v2* is changed to a homogeneous mixture of 200 g (0.441 lb) Pu-239 metal and H_2O. (Be volume modeled as H_2O.)
sph14-v4	0.63287 ± 0.00054	The fuel sphere of *sph14-v2* is changed to a homogeneous mixture of 230 g (0.507 lb) Pu-239 metal and H_2O. (Be mass modeled as Pu-239.)
sph14-v5	0.67065 ± 0.00051	The fuel sphere of *sph14-v2* is changed to a homogeneous mixture of 522 g (1.151 lb) Pu-239 metal and H_2O. (Be volume modeled as Pu-239.)

[a] KENO V.a calculated k_{eff} and standard deviation values.

[b] The mixture volume (or mixture volume plus Be shell volume for case *sph14-v1*) equals the internal volume of the TB-1 containment vessel. The containment vessel and remaining structural materials of the PAT-1 container are not explicitly modeled. Instead, the payload volume (1300 g (2.87 lb) Pu-239 as a metal-water mixture) is modeled as a sphere, surrounded by a water reflector providing a reflector thickness of 20 cm (7.87 in.). In all variant cases, a 20 cm–(7.87 in.) thickness of close-fitting water reflector is maintained.

6.9.6.8 Additional Scoping Calculations – Hypothetical Accident Condition Arrays (hexmdry)

In Sections 6.9.6.4 through 6.9.6.7, each limiting-case result in Table 6-1 (see Section 6.1.2) was considered with reduced Pu loadings (200 g [0.441 lb] Pu-239) and various modeling changes to account for the impact of 30 g (0.066 lb) Be.

For all array cases from Table 6-1, water was a dominant factor in controlling neutron moderation and secondary influences on package-to-package interaction. Even for case *hexsdry*, where the only PAT-1 structural materials in the model were the TB-1 vessel and outer drum

steels, water within the fully flooded TB-1 vessel remained a significant neutron moderator. Thus, the potential effects of beryllium to enhance package-to-package interaction effects (in the *hexsdry* scoping calculations of Section 6.9.6.6) are masked by the presence of significant water moderation.

Case *hexmdry* (of Table 6-17) presents the same damaged-container and array models as case *hexsdry*. Case *hexmdry* contains a payload of Pu-239 metal, as was selected as the basis model for Table 6-23 scoping calculations. The purpose of this final set of calculations is to more closely inspect for potential neutron moderating and reflecting effects of the beryllium, for array conditions where the Be surrounds the Pu-239 mass in each package and no H_2O moderator is present outside the TB-1 containment vessel.

The results of Table 6-23 indicate that the effect of the small mass of Be per package (30 g [0.066 lb]) is small compared to the effects of partial or full water flooding internal to the TB-1 vessels.

Table 6-23. Additional Scoping Calculation Results for Hypothetical Accident Condition Arrays

Case	$k_{eff} \pm \sigma$ [a]	Notes
hexmdry [b]	0.67134 ± 0.00049	Prior UNIX result (see Figure 6-17): Each TB-1 vessel is loaded with a 1300 g (2.87 lb) Pu-239 metal sphere, with the remaining volume within the TB-1 vessel being filled with H_2O.
hexmdry-v0	0.67183 ± 0.00050	Current result; rerun of *hexmdry* on LINUX workstations.
hexmdry-v1	0.57556 ± 0.00023	Same loading as *hexmdry* (1300 g (2.87 lb) Pu-239 metal sphere), all H_2O is removed from the TB-1 vessel (the only water in the model is the 30 cm (11.81 in.) thick external array reflector).
hexmdry-v2	0.17899 ± 0.00010	Similar to *hexmdry-v1*, except that the loading per TB-1 vessel has been changed to a homogeneous sphere of Pu-Be metal/alloy, containing 200 g (0.441 lb) Pu-239 and 30 g (0.066 lb) Be.
hexmdry-v3.x	0.30226 ± 0.00049	Similar to *hexmdry-v1*, except that the loading per TB-1 vessel has been changed to a 200 g (0.441 lb) sphere of Pu-239 metal. The k_{eff} increased from case *hexmdry-v2* due to the increased Pu density resulting from removal of the Be.
hexmdry-v3.0	0.31515 ± 0.00049	Similar to *hexmdry-v1*, except that the loading per TB-1 vessel has been changed to a 200 g (0.441 lb) sphere of Pu-239 metal surrounded by a close-fitting 30 g (0.066 lb) shell of Be metal.
hexmdry-v3.10	0.32548 ± 0.00049	Same loading as *hexmdry-v3.0* , a 1.0 cm thick shell of H_2O surrounds the Be/Pu-239.
hexmdry-v3.20	0.33928 ± 0.00048	Same loading as *hexmdry-v3.0* , a 2.0 cm thick shell of H_2O surrounds the Be/Pu-239.
hexmdry-v3.30	0.35326 ± 0.00050	Same loading as *hexmdry-v3.0*, a 3.0 cm thick shell of H_2O surrounds the Be/Pu-239.
hexmdry-v3.f	0.36606 ± 0.00048	Same loading as *hexmdry-v3.0*, the remainder of the TB-1 vessel is completely filled with H_2O.

[a] KENO V.a calculated k_{eff} and standard deviation values.

[b] Close-packed array of 1152 damaged (side-impact model) packages (see Figure 6-4 and Figure 6-12). The redwood is modeled as void.

7. PACKAGE OPERATIONS

This section describes the operations used to load and unload the plutonium metal contents as described in Section 1.2.2 of this addendum. The section includes loading and unloading procedures for the configurations depicted in Figures 1-3 through 1-6; loading the *T-Ampoule Assembly*[A] (designated T-Ampoule) and *Ring, Filler* (designated Ring Filler) in the TB-1 *Containment Vessel* (designated TB-1); loading the TB-1 in the AQ-1 overpack, preparing the package for shipment; and returning or storing the empty packaging.

The PAT-1 package shall be operated in accordance with applicable Nuclear Regulatory Commission (NRC), U.S. Department of Transportation, and other federal, state, and local regulations to protect the health and safety of the public, workers, and the environment. Furthermore, the PAT-1 shall be operated according to a National Nuclear Security Administration (NNSA) approved quality assurance (QA) plan and U.S. Department of Energy (DOE) Order 461.1A[1] requirements.

Specific criteria for operating the PAT-1 package with the plutonium metal content are presented in this section. The package user shall develop detailed site-specific operating procedures based on these criteria and on the NRC-issued certificate of compliance (CoC). Therefore, the operating procedures shall be written in accordance with 10 CFR 71,[2] Subparts A, G, and H. Operational radiation exposures for package operations shall be maintained to as low as reasonably achievable (ALARA), as required by the "Standards for Protection against Radiation" in 10 CFR 20.1101(b).[3]

7.1 Package Loading

The package user shall:

1. Be authorized to acquire, package, transport, or transfer radioactive, fissile, or special nuclear material;

2. Possess a copy of the current NRC PAT-1 CoC, SAR,[4] and this SAR Addendum;

3. Comply with all requirements and restrictions specified in the NRC PAT-1 CoC, SAR,[4] and this SAR Addendum;

4. Be a NRC or DOE, EM-60 registered user; and

5. Perform all PAT-1 operations under a NNSA–approved, site-specific, 10 CFR 71[2] Subpart H–compliant, QA plan.

A cutaway illustration of a PAT-1 package loaded and assembled for shipment is shown in Figure 7-1. The individual part names called out in the procedures are identified in *italics* and drawing numbers are provided in the tables for clarity. Prior to loading the PAT-1 package, verify that the requirements specified in Section 8.0 have been met for the *Overpack, AQ*

[A] The title of the drawing is shown in italics and is used interchangeably with the designated name in this addendum. The drawing number and title information is shown in Section 1.3.2 and Table 7-1, 7-2, 7-3, and 7-4 in this addendum and in Chapter 9 of the SAR.[4] Drawing titles and numbers are used to provide clarity of discussion when specifying components for the procedures.

(designated AQ-1), TB-1, *Ring, Filler, T-Ampoule Assembly*, *Inner Cradle*, and *Sample Container-1 (SC-1) Assembly* (designated SC-1) and *Sample Container-2 (SC-2) Assembly* (designated SC-2). This addendum describes the loading-related preparations, tests, and inspections of the T-Ampoule. It includes inspections performed prior to loading the package, to verify that it is not damaged and radiation and surface contamination levels are within allowable limits.

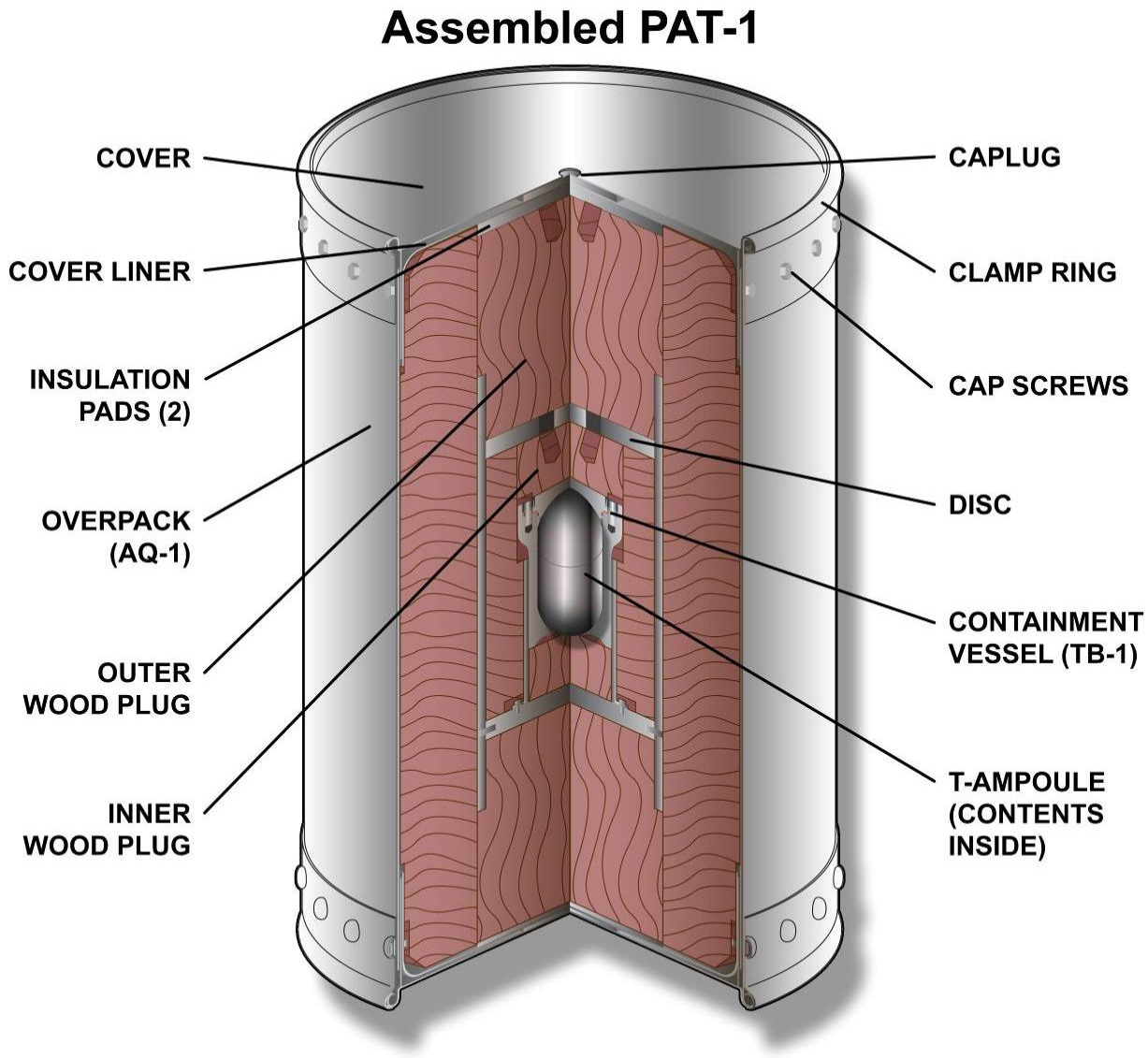

Figure 7-1. Assembled PAT-1 Showing AQ-1, TB-1, and T-Ampoule

7.1.1 Preparation for Loading

The TB-1 *Containment Vessel* (1017) is loaded while outside the *Overpack, AQ* (1002). See Section 1.2.2 of this addendum and the current CoC for the plutonium metal and composite contents.

Detailed, written operating procedures shall be prepared by the user to include, at a minimum, the process steps listed below before the plutonium metal content is placed into the PAT-1 package. These steps, initiated by the operating personnel and their supervisor, ensure that:

(a) All applicable documents have been reviewed by operating personnel and are available for further review, if necessary.

(b) The radioactive materials proposed for shipment are authorized by the CoC, and the use of the package complies with the conditions of the CoC.

(c) The package has been properly maintained and is in an unimpaired condition. All required refurbishment and periodic maintenance shall have been performed and documented within the schedule requirements of the CoC, SAR, SAR Addendum, and maintenance program.

(d) The TB-1 components are visually inspected for defects to include visible damage to the circular knife-edge on both the body and lid. Small nicks (0.079 cm [1/32 in.]) in the knife-edge may be hand-filed to restore contour and verified leak tight using the leakage rate test of 10^{-7} std cm^3/s as described in Section 8.3.1 of the PAT-1 SAR.[4] Larger nicks are not repairable and any leakage rate test of the TB-1 is no longer valid. If the container fails the leakage rate test, it must be scrapped and replaced with a new TB-1.

(e) The used TB-1 *Gasket, Copper* (1019) is replaced with a new undamaged *Gasket, Copper* in usable condition prior to each shipment of a loaded TB-1.

(f) A valid leak-test label must be present on the TB-1 *Containment Vessel* to ensure that the required acceptance, leakage rate test and the annual leakage rate test have been performed.

(g) The *T-Ampoule Assembly* is inspected for any visible damage and replaced if necessary. Per 10 CFR 71.87(b), superficial surface marks are permitted, provided that they fall within part tolerance. The threads and *O-ring* for T-Ampoule groove in the *T-Ampoule Assembly* are inspected for damage. If damage is noted and the container fails a user defined 10^{-3} cm^3 air/sec assembly leakage rate test, the container must be scrapped and replaced with a new *T-Ampoule Assembly*.

(h) The *T-Ampoule Assembly O-ring* is inspected and replaced, if necessary. The O-ring is replaced annually or when damage is discovered.

(i) Verification of a successful *TB-1, T-Ampoule Assembly, SC-1 and SC-2 sample container* required acceptance-, leakage-rate test. See Sections 8.2.2 and 8.3.2 of this Addendum.

(j) The *Ring, Filler* is inspected for damage and replaced if necessary. Per 10 CFR 71.87(b), superficial surface marks are permitted if they fall within the tolerance of the part. A *Ring, Filler* that no longer fits properly on top of the *T-Ampoule Assembly* (form and function not met) is scrapped and replaced.

(k) The *Inner Cradle* for the *Sample Container-1 (SC-1) Assembly* or *Sample Container-2 (SC-2) Assembly* shipping configuration is inspected to ensure that it is appropriate for the planned configuration and free of damage. The *Inner Cradle*, once installed, is not expected to wear, and no periodic tests are required. The *sample containers* must slip freely into and out of the *cradle*. If tightness is noted during *sample container* installation, the distance between the legs of the *cradle* is measured to check for proper gap (7.692 ±0.005 cm [3.030 ±0.002 in.]). If tightness is noted, the *Inner Cradle* components should be inspected for damage. If no damage is located, the parts may be hand adjusted for proper fit.

(l) The *Sample Container-1 (SC-1) Assembly* or *Sample Container-2 (SC-2) Assembly* are inspected for any visible damage and replaced, if necessary. If the threads are damaged on the *sample containers* and closure is not possible, the containers are scrapped.

(m) The package's interior, nonfixed, surface contamination levels cannot significantly contaminate the contents. Nonfixed, surface contamination requirements are specified in 10 CFR 20.1906,[3] 10 CFR 71.87(i),[2] and 49 CFR 173.443,[5] for alpha-, beta-, and gamma-emitting radionuclides.

(n) All closure fasteners are either furnished with the packaging or are certified replacements and acceptable for use.

(o) All required package parts and necessary equipment are available and ready for use.

(p) The weight of the plutonium metal and the overall assembly weight of the *sample container* and *T-Ampoule Assembly* are recorded prior to shipment. The TB-1 contents weight (*Ring, Filler* [2A0262] and *T-Ampoule Assembly* and its contents) shall not exceed 2.1 kg (4.7 lb).

The user may replace the packaging parts listed in Table 7-1 during loading. The certification of all replacement parts must be traceable and recorded by the user. The replacement parts shall be recorded in the QA records with applicable identification information, date of replacement, disposition of the old part, and the name of the individual who performed the replacement, along with the name and signature of the individual who made the entry in the QA records. Records of replacement actions and certifications of completed actions shall be sent to SNL for records management and archiving.

There are two types of facilities that may be used depending on the loading or unloading operation:

- Glove boxes or glove bags, which are used to load and unload the plutonium metal contents into the SC-1 or SC-2 or T-Ampoule. These work spaces have a standard glove box line atmosphere: nitrogen or argon or helium or combination with an oxygen and moisture content not to exceed 100 parts per million. Facilities using the PAT-1 have conduct of operation procedures for glove box/glove bag operations. These procedures address the control and monitoring of oxygen and moisture content and the maintenance of proper atmosphere within the glove boxes. Oxygen and moisture concentrations are monitored during operations in accordance with facility procedures. The procedures to maintain glove box atmospheres are site specific and are intended to maintain product quality of the plutonium material and are not important to the safety the PAT-1 Package.

  The selection of glove box or glove bag is based on organizational preference. Both are operationally acceptable provided the inert atmosphere is adequate for sample integrity. The atmosphere in the glove box/bag for loading and unloading the plutonium metal contents is to be inert with an oxygen and moisture concentration < 100 ppm to maintain product quality and not for safety purposes. There are a number of glove box/bag manufacturers that can meet the inert atmosphere requirements and instrument manufacturers that have hardware that can measure the oxygen and moisture concentration to < 100 ppm within the enclosures.

This is an example glove box (Courtesy of Innovative Technology dclay@innovativetechnologyinc.com).

- Open front hoods and downdraft rooms to load or unload SC-1 or SC-2 *sample containers* with plutonium metal contents into or out of the T-Ampoule. These work spaces do not provide an inert atmosphere. They are open work areas in a standard air atmosphere. Air flow in these work spaces are controlled to draw any potential contamination away from the operators and is exhausted through HEPA filters.

Both work space environments will be used as follows:

- Any *sample container (SC-1* or *SC-2*) or *T-Ampoule Assembly* directly loaded with plutonium will be processed (loaded) in either the glove box or glove bag work space. This will provide the inert atmosphere for the plutonium metal.

- *Sample containers SC-1* or *SC-2* (previously loaded in the glove box or glove bag with an inert atmosphere) will exit the glove box/glove bag and be decontaminated in either the open front hood or downdraft room. The decontaminated *sample containers* will then be placed into a *T-Ampoule Assembly* (previously prepared with the applicable *Inner Cradle).*

Pending facility requirements, the loading of the *T-Ampoule Assembly* with the decontaminated *sample containers (SC-1* or *SC-2)* may or may not be performed in open front hoods or downdraft rooms.

7.1.2 Loading of Contents

The operating procedures for the PAT-1 packaging with *T-Ampoule Assembly* configuration and plutonium metal content shall be specific regarding the handling of all packaging components and clearly state safety aspects or activities such as personnel protection (radiation, chemical, physical); surface contamination or radiation surveys; nuclear criticality safety; and environment temperature.

Table 7-1. Replacement Parts for the PAT-1 Packaging with *T-Ampoule Assembly*

Part Name (ID)	Part Description	Part Material	Drawing/Specification[a]
Gasket, Copper	Copper seal for TB-1	Copper, half hard 110 ETP per QQ-C-576[6]	1019
Ring, Filler	Filler between T-Ampoule and TB-1	Ti-6Al-4V Grade 5	2A0262
T-Ampoule Assembly	Lid and Body of T-Ampoule	Ti-6Al-4V Grade 5	2A0261
O-ring, Viton® A, for T-Ampoule	AS568C-241	100% virgin Viton®A per SAE AMS 7276G, 75 Durometer Shore A	2A0261, Item 3
Sample Container-1 (SC-1) Assembly	Lid and Body of SC-1	Ti-6Al-4V Grade 5	2A0268
Sample Container-2 (SC-2) Assembly	Lid and Body of SC-2	Ti-6Al-4V Grade 5	2A0265
O-ring, Viton® A, for SC-1 and SC-2	AS568C-147	100% virgin Viton®A per SAE AMS 7276G, 75 Durometer Shore A	2A0268, Item 3 2A0265, Item 3
Inner Cradle	Titanium Cradle for SC-1 or SC-2	Ti-6Al-4V Grade 5	2A0385

[a] Drawings are provided in Appendix 1.3.2.

7.1.2.1 Loading the T-Ampoule Assembly

The *T-Ampoule Assembly* has three basic loading configurations (see Section 1.2 for description):

- Plutonium metal hollow cylinder (831 and 731 gram weights)
- *Sample Container-1* in the *Inner Cradle* (3 of these containers)
- *Sample Container-2* in the *Inner Cradle* (2 of these containers)

The process for loading the plutonium metal, hollow cylinder or *sample containers* into the *T-Ampoule Assembly* is expected to proceed under the following conditions:

- The *T-Ampoule Assembly* (2A0261) loading operation with a plutonium metal hollow cylinder is performed in a glove box or glove bag with less than ambient atmospheric air pressure, with adequate exhaust filtration, and with appropriate control of surface cleanliness per established requirements for the glove box or glove bag being used.
- Only one type of plastic bagging or tagging material is permitted in the TB-1 per shipment for use external to the sample containers and for labeling of the T-Ampoule. The plastic material is not to be used directly on the Pu contents. The weight limits are specified below.
    - Polyethylene terephthalate (such as Metalized PET, Mylar™) 6.9 gram
    - Polyethylene (such as HDPE, LDPE) 3.5 gram
    - Polyvinyl chloride (PVC) 12.2 gram
    - Polytetrafluoroethylene (PTFE, such as Teflon™) 12.5 gram

  All previous labels must be removed prior to application of new labels.
- The *SC-1* or *SC-2* sample containers have been leak tested to 10^{-3} atm cc/s per Section 8.2.2.
- The sample container (*SC-1* or *SC-2*) loading operation with plutonium metal is performed in a glove box or glove bag with less than ambient atmospheric air pressure with adequate exhaust filtration, and with appropriate control of surface cleanliness for requirements established for the glove box or glove bag being used. The sample containers with plutonium metal content may be loaded into the *T-Ampoule Assembly* in the glove box or glove bag or in an open front hood or downdraft room.
- If sample containers are used, the *Inner Cradle* (2A0385) is already installed into the *T-Ampoule Assembly*.
- Appropriate processing, handling, and contamination control is implemented to maintain an uncontaminated (≤ free release limits) *T-Ampoule Assembly* and *SC-1* and *SC-2* sample container exterior as required per user facility requirements.

Note: The free release limits are described in Appendix D of 10 CFR Part 835. This information is used to identify the need for posting of contamination and high contamination areas in accordance with §835.603(e) and (f) and identifying the need for surface contamination monitoring and control in accordance with §§835.1101 and 835.1102. DOE Order 5400.5 provides the surface contamination guidelines in Chapter IV, Figure IV-1 for DOE sites. The exterior surface of the containers are decontaminated using industry accepted decontamination procedures and surface measurements performed using standard Health Physics survey measurement equipment per user facility requirements.

- The *T-Ampoule Assembly* shall be serialized, identified, and marked as necessary to identify its contents, and visually inspected to ensure proper assembly and freedom from significant defects. Data is recorded as appropriate.

Steps for loading the *T-Ampoule Assembly*:

1. Visually inspect the parts and materials listed in Table 7-1 for major imperfections,* damage, and cleanliness and ensure that they are ready for loading the specified content.

2. Follow specific content-loading instructions:

   - Plutonium metal hollow cylinder – See Section 7.1.2.1.1

   - *Sample Container-1 (SC-1)* or *Sample Container-2 (SC-2) Assemblies* – See Section 7.1.2.1.2.

3. Visually inspect the *O-ring, Viton® A*, installed in the *Body, T-Ampoule* (2A0259) to ensure that it is properly lubricated and in place. Flood the interior of the T-Ampoule using the tracer gas for the pre-shipment leak test within the facility-approved glove box or glove bag. See Section 7.1.2.2.

4. Engage and tighten the *Lid, T-Ampoule* (2A0260) with strap wrenches until the lid and body flange are fully seated.

   Note: Because the *T-Ampoule Assembly* is designed with a bore seal, a specified torque is not required for proper closure of the *T-Ampoule Assembly*.

5. Verify that the weight of the *T-Ampoule Assembly* with its contents does not exceed 2035 g.

   Note: This total weight does not include the weight of the *Ring, Filler*.

6. Clean and inspect the exterior of the *T-Ampoule Assembly* using standard health physics, swipe tests for plutonium contamination.

* Major imperfections are flaws, imperfections, or faults that will or may compromise the intended functionality of the assembly.

7. Implement appropriate processing, handling, and contamination control to maintain an uncontaminated (i.e., ≤ free release limits) *T-Ampoule Assembly* exterior.

   Note: The *T-Ampoule Assembly* is not a containment boundary. It is used to maintain product quality and to provide a eutectic prevention barrier. The pre-shipment leakage rate test requirement is 10^{-3} atm cc/s. See Sections 8.1.4 and 8.2.2.1.

Table 7-2. Parts List for T-Ampoule Loading

Quantity (each)	Item	Drawing/Specification
1	*T-Ampoule Assembly*	2A0261
	Body, T-Ampoule	2A0259
	Lid, T-Ampoule	2A0260
1	*O-ring, Viton®A*, for T-Ampoule, AS568C-241	2A0261, Item 3
As required for hollow metal cylinder or samples shipped in SC-1 or SC-2 Sample Containers (see below)	Tantalum Foil	0.001- to 0.009-in. thickness, minimum purity ranges - 99.75% (3N5), 99.98% (3N8) to 99.99% (4N)
Lubricant for T-Ampoule, SC-1 and SC-2	Silicone Grease	Dow Corning High Vacuum Grease or equal
For sample shipments, either SC-1 or SC-2 sample containers are used.		
1	*Inner Cradle*	2A0385
3	*Sample Container-1 (SC-1) Assembly*	2A0268
	O-ring, Viton®A, for SC-1, AS568C-147	2A0268, Item 3
	Lid, Sample Container-1 (SC-1)	2A0267
	Body, Sample Container-1 (SC-2)	2A0264
2	*Sample Container-2 (SC-2) Assembly*	2A0265
	O-ring, Viton®A, for SC-2, AS568C-147	2A0265, Item 3
	Lid, Sample Container-2 (SC-2)	2A0269
	Body, Sample Container-2 (SC-2)	2A0266

7.1.2.1.1 Loading the Plutonium Metal, Hollow Cylinder

The plutonium metal, hollow cylinder described in Section 1.2 is may be wrapped with tantalum foil or not wrapped based on operational determination and loaded in the *T-Ampoule Assembly*.

The plutonium metal hollow cylinder is then packed in the *T-Ampoule Assembly* with crushed tantalum foil. There are no positioning requirements for the plutonium metal hollow cylinder.

The process for loading the plutonium metal hollow cylinder should proceed under the following conditions:

- The plutonium metal hollow cylinder loading operation is performed in a glove box with less than ambient atmospheric air pressure, with adequate exhaust filtration, and with

appropriate control of surface cleanliness per established requirements for the glove box or glove bag being used.

- The plutonium metal hollow cylinder may be serialized, identified, and marked as necessary for data recording purposes, per site requirements.
- The plutonium metal hollow cylinder is ready for loading in the glove box or glove bag.
- Tools needed:
  - Strap wrenches – optional
  - User-supplied suction device
  - User-specified gripping tool such as tongs
  - Scale – 1% accuracy

Steps for loading the plutonium metal hollow cylinder into the *T-Ampoule Assembly*:

1. Visually inspect the parts and materials listed in Table 7-2 for major imperfections, damage, and cleanliness, and ensure that they are ready for loading the specified content.
   - Major imperfections of the metal components are cracks, pinholes, dents, deformed threads, and scratches (>0.001 in. deep).
   - Major imperfections of the O-ring are any indication of marring or chafing (i.e., scuff marks), or the O-ring does not have a round cross section.
2. In the glove box, weigh the plutonium metal hollow cylinder and record the weight.
3. Determine whether the plutonium metal hollow cylinder will be wrapped in tantalum foil or not. If the determination is to wrap the cylinder in foil, go to Step 4. If the determination is to leave the cylinder unwrapped, go to Step 5.
4. Wrap the plutonium metal hollow cylinder in tantalum foil and tuck in the foil ends.
5. Determine whether the plutonium metal hollow cylinder will be packed in the T-Ampoule using crushed tantalum foil or no supplemental packing material. If the determination is to pack the hollow cylinder using crushed tantalum foil, go to Step 6. If the determination is to not use packing material, go to Step 7.
6. Add crushed tantalum foil to the open *Body, T-Ampoule*. Go to Step 7.
7. Place the plutonium metal hollow cylinder into the *Body, T-Ampoule*. Add additional crushed tantalum foil as necessary to the sides and top based on operational determination.
8. Install the *Lid, T-Ampoule* and complete loading of the *T-Ampoule Assembly* according to the instructions in Section 7.1.2.1.

9. Weigh the loaded *T-Ampoule Assembly* with contents.

10. Record the weight of the loaded *T-Ampoule Assembly* with contents.

    Caution: The maximum weight of the *T-Ampoule Assembly* with contents and *Ring, Filler* shall not exceed 2.1 kg (4.7 lb).

7.1.2.1.2 Loading the Sample Containers (SC-1 [3 each] or SC-2 [2 each])

The plutonium metal sample contents, either bare or wrapped with tantalum foil, as described in Section 1.2 are packed in the sample containers. The sample containers are positioned and held in place, inside the *T-Ampoule Assembly* using an *Inner Cradle*, as depicted in Figures 1-3 and 1-4. Sample containers (*SC-1* and *SC-2*) shall not be comingled in the same *T-Ampoule Assembly*.

The process for loading plutonium (Pu) samples into the sample containers should proceed under the following conditions:

- The *sample container* loading operation is performed in a glove box or glove bag with less than ambient atmospheric air pressure, with adequate exhaust filtration, and with appropriate control of surface cleanliness per established requirements for the glove box or glove bag being used.

- The plutonium metal samples are properly prepared and ready for loading in the glove box or glove bag.

- The *cradle* is installed in the *T-Ampoule Assembly* per Section 7.1.2.1.3.

- The *sample containers* have been inspected and the *O-rings* properly lubricated and in place.

- Tools needed:

  - Strap wrenches – optional
  - User-supplied suction device
  - User-specified gripping tool such as tongs
  - Scale – 1% accuracy

Steps for loading the sample containers:

1. Visually inspect the parts and materials listed in Table 7-2 for major imperfections, damage, and cleanliness to ensure that they are ready for loading the specified content.

   - Major imperfections of the metal components are cracks, pinholes, dents, deformed threads, and scratches (>0.001 in. deep).
   - Major imperfections of the O-ring are any indication of marring or chafing (i.e., scuff marks), or the O-ring does not have a round cross section.

2. Verify that the *Inner Cradle* components (2A0385) are properly installed in the *T-Ampoule Assembly* (see Section 7.1.2.1.3) and that the *T-Ampoule Assembly* is ready for loading.

3. In the glove box or glove bag, weigh and record the plutonium metal.

4. Determine whether the plutonium metal contents will be wrapped in tantalum foil or not. If the determination is to wrap the contents in foil, go to Step 5. If the determination is to leave the contents unwrapped, go to Step 6.

5. Wrap the contents in tantalum foil.

6. Determine whether the plutonium metal contents will be packed in the *sample container* (*SC-1*, 2A0268 or *SC-2*, 2A0265) using crushed tantalum foil or no supplemental packing material. If the determination is to pack the contents using crushed tantalum foil, go to Step 7. If the determination is to not use packing material, go to Step 8.

7. Add crushed tantalum foil to the open *Body, Sample Container-1*, 2A0264 or *Body, Sample Container 2*, 2A0266. Go to Step 8.

8. Place the plutonium metal contents into the *Body, Sample Container-1*, 2A0264 or *Body Sample Container-2*, 2A0266.

9. Visually inspect the *O-ring, Viton® A*, for *SC-1*, 2A0268, Item 3 or *SC-2*, 2A0265, Item 3 to ensure that it is properly lubricated and in place.

10. Engage and tighten by hand the *Lid, Sample Container (SC-1*, 2A0267 *or SC-2*, 2A0269) until the lid and body flange are fully seated. Hand tightening until seated is only required for proper closure of the *SC-1* or *SC-2*.

11. Weigh the *sample container* and record the weight.

    Note: The maximum weight of the *T-Ampoule Assembly* with contents and *Ring, Filler* should not exceed 2.1 kg (4.7 lb).

12. Lift the *sample container* with a user-supplied suction pickup and place into the *Inner Cradle*.

13. Install the Spacer (2A0385-040 [2 each] for *SC-1* or 2A0385-045 [1 each] for *SC-2*) between the *SC-1s* and *SC-2s* as depicted in Figure 1-4 for the *SC-1s* or in Figure 1-3 for the *SC-2s* in this addendum with a user-specified gripping tool such as tongs. Visually center the Spacer within the *Inner Cradle*.

14. Repeat Steps 3 through 11 until sample containers are in place in the *Inner Cradle*.

    Note: Loading facility personnel have the option of preloading and weighing the contents of the SC-1s and SC-2s (Steps 3-13) and attaching the lid and weighing the *sample container* by repeating Steps 9 and 10.

15. Install the *Lid, T-Ampoule* and complete loading of the *T-Ampoule Assembly* per Section 7.1.2.1.

7.1.2.1.3 Installation and Removal of the Inner Cradle

7.1.2.1.3.1 Installation of the Inner Cradle

For shipment of SC-1 or SC-2 sample containers, an *Inner Cradle* is used to maintain position for normal conditions of transport (NCT). The minimum requirements for cradle installation are presented below; the user site shall prepare detailed installation instructions. Review Drawing 2A0385 (*Inner Cradle*) for assembly view and parts listing. The cradle components are installed as follows:

1. Position *Body, T-Ampoule* (2A0259) so that it is upright. Install Dish in Body (2A0385-020) in *Body, T-Ampoule*. The dish is not indexed.

2. Install four flat *Leg(s)* (2A0385-010) into slots in the Dish in Body. Position the legs so they are flush against the *Body, T-Ampoule* wall sides.

3. Install the *Lock Ring* (2A0385-030) so that it locks into the slots at the top of the leg. The correct assembly of the dish and legs will have the flat legs flush against the *Body, T-Ampoule* wall sides equidistant from each other.

4. Position *Lid, T-Ampoule* (2A0260) so that it is upright. Install the Dish in Lid (2A0383-025) in the *Lid, T-Ampoule*. The dish is not indexed.

5. Install four flat *Leg(s)* (2A0385-015) into slots in the upper dish. Position legs so that they are flush against the *Lid, T-Ampoule* wall sides.

6. Install *Lock Ring* (2A0385-030) so that it locks into the slots at the top of the leg. The correct assembly of the dish and legs will have the flat legs flush against the *Lid, T-Ampoule* wall sides equidistant from each other.

7. Measure distance (7.692 ±0.005 cm [3.030 ±0.002 in.] shown in Drawing 2A0385 of this addendum) between two opposite legs to verify proper gap.

8. Verify that the *Spacer(s)* (2A0385-040 [2 each] for SC-1 or 2A0385-045 [1 each] for SC-2) are available for *sample container* loading operations identified in Section 7.1.2.1.2, Step 11 of this addendum.

9. The installation of the *Spacer(s)* is a step in the *SC-1* and *SC-2* loading procedures.

7.1.2.1.3.2 Removal of the Inner Cradle

Steps for removing the cradle components from the T-Ampoule:

1. Position *Body, T-Ampoule* (2A02659) so that it is upright. Remove Lock Ring from Leg(s).
2. Remove four flat *Leg(s)*.
3. Remove Dish in Body from *Body, T-Ampoule*.
4. Position *Lid, T-Ampoule* (2A0260) so that it is upright. Remove Lock Ring from Leg(s).
5. Remove four *Leg(s)*.
6. Remove Dish in Lid from *Lid, T-Ampoule*.
7. Inspect parts for damage and place all removed parts into labeled container for storage.
8. Verify that the *Spacer(s)* (2A0385-040 [2] for SC-1 or 2A0385-045 [1] for SC-2) are included with the stored items.

   Note: The removal of the Spacer(s) is a step in the SC-1 and SC-2 unloading procedures.

7.1.2.2 Loading the T-Ampoule Assembly into the TB-1 Containment Vessel (1017) and Evacuation and Backfill of TB-1 with Tracer Gas

The parts and materials required for loading the *T-Ampoule Assembly* into the TB-1 are listed in Table 7-3.

During the *T-Ampoule* loading process, the contents are loaded and the *T-Ampoule* is filled with tracer gas such as helium prior to closure, using standard filling techniques. The *T-Ampoule* is then leak tested to 10^{-3} atm cc/s per ANSI N14.5 as described in Section 8.2.2.1.

The Sandia National Laboratories TB-1 Leak Test Requirements document included in Section 8.3.2 and referenced in Section 8.2.2.2 provides guidance for pre-shipment leakage rate testing of the *TB-1* containment vessel. The preferred technique to fill the *TB-1* with tracer gas is evacuate and backfill; the tracer gas concentration is calculated using the partial pressure of the tracer gas. The leak test procedure shall reference ANSI N14.5 – 97 Appendix A Leakage Test Methods and Procedures using Method A.5.4 Evacuated Envelope (Gas Detector); also referred to as a Bell Jar Technique. Detailed leak testing procedures shall be developed by the user facility using the TB-1 Leak Test Requirements document as a guide. Sandia National Laboratories can provide a sample leakage rate test procedure for the preparation and testing of the *TB-1* container upon request. The procedure provided by Sandia is for reference only and all responsibility for performing the leak test remains with the user.

Table 7-3. Parts List for Loading the T-Ampoule into the TB-1

Quantity	Item	Drawing/Specification
1 each	*TB-1 Shipping Vessel Assembly*[a]	2A0263
1 each	*Body, TB*	1022
1 each	*Lid, TB*	1020
1 each	*Gasket, Copper*	1019
12 each	*Bolt, Socket, Head, Special 0.500-20*	1018
1 each	*Sling, Lifting (with Grommets installed)* designated *Lifting Sling*	1017, Item 6
1 each	*T-Ampoule Assembly* loaded with contents and filled with a tracer gas such as helium from Section 7.1.2	2A0261
3 each	Screw, Cap, Hex Head, 0.250-28 × 0.750 in. long	1017, Item 7, MS90726-6
3 each	Washer	1017, Item 8, MS27183-10
1 each	*Ring, Filler*	2A0262
As Required	Silicone grease	General Electric G-624 (MIL-S-8660)[7] or Dow Corning DC-4 (MIL-S-8660)
As Required	Labels, Nuclear Material	See Section 7.1.2.1.
As Required	Labels, Identification	See Section 7.1.2.1.
As Required	System consists of a mass spectrometer type leak detector with suitable test chamber (Bell Jar) that completely encloses the product (TB-1), auxiliary pressurization equipment (Evacuate and Backfill Chamber, certified tracer gas such as helium), instrumentation necessary for performance of the test under specified conditions, Calibrated Leaks, and Handling equipment	Sandia National Laboratories TB-1 Leak Test Requirements (See Section 8.2.2 and 8.3.2.)

[a] This part results from the assembly sequence. See drawing 2A0263 for assembly.

Steps for loading the *T-Ampoule Assembly* into the TB-1 *Containment Vessel* and preparation for tracer gas filling and leakage rate testing:

1. Visually inspect the components of the TB-1 *Containment Vessel* (see Table 7-3) for defects, damage, cleanliness, and for correct part numbers.

   Note: See Section 7.1.1(d) for minor repairs to the knife-edge seal.

2. Use the inspection results in Step 1 and take the necessary steps to ensure that the TB-1 Containment Vessel components are in conditions necessary to ensure that the resultant package meets the requirements specified in 10 CFR 71.87.

3. Perform radiation contamination swipes to verify that nonfixed contamination levels are ALARA and within the specified limits prior to loading into the TB-1.

4. Place the Body, TB (1022) in the Evacuate and Backfill Chamber.

5. Place the tracer gas filled and loaded *T-Ampoule Assembly* into the *Body, TB* (1022).

6. Place and match the *Filler, Ring* into the *T-Ampoule Assembly* curved surface.

7.1.2.3 Tracer Gas Filling and Closing the TB-1 Containment Vessel

Steps for tracer gas filling, closing and leak testing the TB-1:

1. Install an unused *Gasket, Copper* into the seal groove at the top of the *Body, TB.*

   Note: This is a single-use seal.

2. Insert the *Lid, TB* into the *Body, TB,* taking care not to damage the knife-edge seal surfaces.

3. Verify edge of copper gasket is visible through one of the bolt holes.

4. Install cover of Evacuate and Backfill Chamber, tighten fasteners. Complete the following steps to fill TB-1 with tracer gas:

   4.1 Record the atmospheric pressure.

   4.2 Evacuate the TB-1 to less than 1 Torr (or equivalent).

   Note: Reducing the pressure to less than 1 Torr provides a near 100% concentration of tracer gas.

   4.3 Backfill the TB-1 with tracer gas (purge all lines and fitting with tracer gas before assembly) to atmospheric pressure.

4.4 Remove Evacuate and Backfill Chamber cover, install three Bolt, Socket, Head, Special 0.500-20 (1018) designated lid bolt in cover symmetrically (positions 1, 5, and 9) and torque bolts to 14 N-m (10 ft-lb).

4.5 Remove the TB-1 from the Evacuate and Backfill Chamber.

4.6 Flush open lid bolt holes with nitrogen, add remaining lid bolts and torque to 14 N-m (10 ft-lb).

4.7 Remove lid bolts 1, 5, and 9, flush bolt holes with nitrogen.

4.8 Reinstall lid bolts 1, 5, and 9, tighten to 14 N-m (10 ft-lb).

5. Tighten the 12 lid bolts, in two steps, in the following sequence: 1–7, 4–10, 2–8, 11–5, 3-9, 12–6. Tighten all bolts to 68 N·m (50 ft-lb) in the first step and to 102 N·m (75 ft-lb) in the second step.

   Note: Do not use an impact wrench.

6. Determine tracer gas concentration from the evacuate and backfill technique. The tracer gas can be calculated using the partial pressure of the tracer gas.

   % concentration = (tracer gas pressure / total vessel pressure) x 100

7. Attach the *Sling, Lifting* (1017) to the *Lid, TB* using the three Screw, Cap, Hex Head (0.250-28 × 0.750 in.) (1017) and Washers (1017).

8. Place assembled TB-1 with tracer gas into the Bell Jar, remove *Sling, Lifting* and attaching hardware.

9. Place cover of Bell Jar and secure.

10. Perform test using Evacuated Envelope Technique (Bell Jar Technique) under these conditions:

    10.1 The copper seal is in place based on prior verification.

    10.2 The leak rate of the TB-1 container shall be determined by placing a TB-1 and T-Ampoule, which has been properly filled with tracer gas and assembled, into a Bell Jar.

    10.3 The Bell Jar is sealed and connected to a tracer gas leak detector.

    10.4 The Bell Jar shall also contain a second port that allows for a calibration standard to be attached.

    10.5 The tracer gas leak detector shall evacuate the Bell Jar to approximately 1 atm of pressure differential.

10.6 The tracer gas behind the copper seal is limited and the evacuation (evacuation time and test duration) shall be limited.

10.7 After the steady state leak rate is reached, a leak standard with a known leak shall be introduced into the Bell Jar and into the tracer gas leak detector.

10.8 The tracer gas leak detector should respond to the known leak within the amount of time required to reach steady state initially and to the degree equal to the leak rate value of the calibrated leak.

10.9 If the tracer gas detector does not respond in amplitude equal to the leak rate value of the calibrated leak, the final leak rate value shall be corrected using a correction factor as provided below:

$$LRCF = LR_{Std} / (LR_{Std\ Open} - LR_{Std\ Closed})$$

LRCF = Leak Rate Correction Factor
LR_{Std} = The temperature corrected leak rate of the standard leak
$LR_{Std\ Open}$ = The leak detector leak rate reading with the standard leak open
$LR_{Std\ Closed}$ = The leak detector leak rate reading with the standard leak closed

Note: The formula above corrects for any loss of sensitivity that occurs through the test setup, a separate correction factor is required if the trace gas concentration is not 100%).

10.10 The acceptance criterion for the TB-1 containment vessel is an air leak not to exceed a leakage rate of 1 x 10-7 ref. cc/s or equivalent.

10.11 Test Records – Record data as specified in Sandia National Laboratories TB-1 Leak Test Requirements, Section 6.0.

10.12 Remove tested TB-1 with *Sling, Lifting*.

7.1.2.4 Loading the TB-1 / T-Ampoule Shipping Vessel Assembly into the Overpack, AQ

The parts and materials required for loading the *TB-1* / *T-Ampoule Shipping Vessel Assembly* into the *Overpack, AQ* are listed in Table 7-4. These parts are visually inspected for major imperfections, damage, cleanliness, and the presence of the correct part number.

- Major imperfections of the metal components are cracks, pinholes, dents, deformed threads, and scratches (>0.001 in. deep).

- Major imperfections of the *T-Ampoule* and *SC-1* and *SC-2* O-rings are any indication of marring or chafing (i.e., scuff marks), or the O-ring does not have a round cross section.

Use these inspection results and take the necessary steps to ensure that the TB-1 Containment Vessel components are in conditions necessary to ensure that the resultant package meets the requirements specified in 10 CFR 71.87.

The tool list for this procedure includes the following:

- Calibrated hand tools with a tolerance of ±5% for package assembly.

Table 7-4. Parts List for Loading the TB-1 Containment Vessel into the AQ-1 Overpack

Quantity	Item	Drawing Number
1 each	*TB-1 Shipping Vessel Assembly*	2A0263
1 each	*Overpack, AQ*	1002
1 each	*Container Subassembly*	1003
1 each	*Plug, Removable*	1014
1 each	*Disc, Removable*	1002, Item 10
1 each	*Plug, Removable*	1013
1 each	*Cover, Liner*	1007
1 each	*Ring, Clamp, Modified* with 4 in. 304 SST 0.625-11 hex head bolt and 0.625-11 SST hex locking nut supplied as part of drum (Drawing 1004)	1006
1 each	*Cover, Modified*	1005
23 each	Screw Cap, Hexagon Head	1002 Item 10, MS90726-60
1 each	*Pad, Installation*	1027
1 each	*Pad, Installation*	1026
As required	Security wire and seal [This is a tamper indicating device (TID).]	

Steps for loading the *TB-1 Shipping Vessel Assembly* (2A0263) into the *Overpack, AQ* (1002):

1. Perform the required contamination swipes to verify that nonfixed contamination levels are ALARA and within the limits specified in 49 CFR 173.443[5] prior to loading *TB-1 Shipping Vessel Assembly* into the *Overpack, AQ*.

2. Set the *Container Subassembly* (1003) of the *Overpack, AQ* upright prior to loading the *TB-1 Shipping Vessel Assembly*.

3. Visually inspect the removable components of the *Overpack, AQ* (see Table 7-4) for defects, damage, cleanliness, and correct part number.

4. Load the *TB-1 Shipping Vessel Assembly* into the *Overpack, AQ-1* assembly using the *Sling, Lifting* and ensuring that the *TB-1 Shipping Vessel Assembly* is fully seated. This operation is performed manually because the total weight of the TB-1 is less than 22.7 kg (50 lb). A small hoist (453.6 kg [1000 lb] capacity) may be used to lift the TB-1; however, it is not necessary.

   Note: The *Sling, Lifting* remains with the TB-1 during loading into and unloading from the *Overpack, AQ*.

5. Place the smaller inner wooden plug (*Plug, Removable* 1014) on top of the *TB-1 Shipping Vessel Assembly*, aligning the notches in the plug to clear the *Sling, Lifting* cap screws in the TB-1.

6. Insert, in order, the (1) aluminum disk (*Disc, Removable* (1002)), (2) outer wooden plug (*Plug, Removable* 1013), and (3) the inner larger insulation pad (*Pad, Installation* (1026)), which is centered.

7. Insert, in order, (1) the *Cover, Liner* (1007), (2) the outer smaller insulation pad (*Pad, Installation* [1027]), which is centered, (3) the *Cover, Modified* (1005), and (4) the *Ring, Clamp, Modified* (1006).

   Note: During installation, align the index marks on the *Cover, Liner*, the *Cover, Modified*, and the *Ring, Clamp, Modified*, with the index mark on the *Overpack, AQ*-1. A tapered pin is used to line up the holes with the index marks.

8. Install the 23 *screw caps, Hexagon Head* (MS90726-60) (1002), finger tight, through the assembled clamp ring and covers. Start by installing one hexagon head screw into the hole by the index mark, and tighten until finger tight. Install the remaining hexagon head screws one-by-one: one to left of the first screw, then one to the right of the first screw, working back and forth toward the gap in the clamp ring. Use a tapered pin to help line up these holes.

   Note: If some of the screws are faulty and will not screw in, replace them with new certified hexagon head screws.

9. Tighten the 23 hexagon head screws to 20.3 N·m (15 ft-lb).

   CAUTION: Impact wrenches should not be used. For Steps, 8-10, use calibrated hand tools with a tolerance of ±5% for closure of the package.

10. Install the 4-in.-long hexagon head screw in the clamp ring and tighten to 68 N·m (50 ft-lb).

    Note: Impact wrenches should not be used.

11. Install the locking nut on the 4-in.-long screw. Hold a wrench on the screw to keep it from turning, and torque the nut to 41 N·m (30 ft-lb).

A security wire and seal (tamper indicating device [TID]) are installed through the holes provided in the clamp ring lugs.

7.1.3 Preparation for Transport

7.1.3.1 PAT-1 Package Handling

Based on the proposed maximum weight of 1300 g (2.87 lb) plutonium metal, the Criticality Safety Index (CSI) is 0.1.

The PAT-1 package is handled using hoists or forklifts and a strap or specially made drum handling equipment to lift and rotate the package. Operating procedures shall include requirements for safe handling of the package and requirements to limit clamping pressures on the forklift drum handling equipment to prevent damage to the *PAT-1 Assembly* (1001).

7.1.3.2 PAT-1 Package Decontamination

The PAT-1 package may be placed in areas subject to contamination. If the package becomes contaminated, each user shall prepare procedures to decontaminate packages. The procedures should consider, at a minimum, the following:

- Exterior of the package is stainless steel.
- Package vent holes are sealed with plastic plugs.
- Labels and markings on the package must be legible.
- Cleaning solution must be checked for radioactive contamination after use.

7.1.3.3 Requirements Prior to Transport of PAT-1 Package

Prepare the PAT-1 for transport as follows:

1. The onsite movement of this package to storage or to a staging area will be performed in accordance with approved facility procedures.
2. The procedure for loading the PAT-1 package onto the shipping skid is presented below:
    a. Skid – The PAT-1 is loaded on a PAT-1 wooden skid for transportation and handling. ASTM D 3953[8] describes proper strapping of the PAT-1 to the wooden skid. All wooden items (wood crates, shipping containers, dunnage, and pallets) are to conform to the appropriate U.S., United Nations (UN), and European Union (EU) legislation regarding bursaphelenchus xylophilus, commonly known as the pine wood nematode, and are to be marked appropriately. The containers are typically marked with the letters "HT," which means heat treatment and is described on the following website:

http://www.aphis.usda.gov/import_export/plants/plant_exports/wpm/wpm_heat_treatment.shtml. General information discusses the requirement for the wood and is located at the following website: http://www.aphis.usda.gov/import_export/plants/plant_exports/wpm/index.shtml. Procurement documentation for the heat-treated wood shall be retained by SNL. The PAT-1 is steel-banded to the skid that is provided with the AQ-1 overpack for transportation and handling.

b. Lifting Equipment – An overhead hoist of the required capacity with a nylon strap may be used to load the PAT-1 package onto the PAT-1 skid. If a suitable overhead hoist is unavailable, a forklift may be used with a nylon strap attached to the tines. Alternately, a forklift equipped with nonmarring side grippers or a forklift drum lifter/rotator designed for the 24 ½ in. diameter of the PAT-1 with 226.8 kg (500 lb) capacity (with safety factor) can be used. Gripping pressure over a 1 ft^2 area on each side is not to exceed 40 psi (5760 lb). The gripper equipment must meet the requirements of 29 CFR 1910.178.[9]

c. Handling – The PAT-1 is easily hoisted or lowered with a nylon strap attached to midpoint of the upright or horizontal PAT-1, either by the hoist or forklift. For loading onto the skid, the PAT-1 is positioned over the skid and slowly lowered.

d. Transport – The skid mounted PAT-1 may be moved, after being properly secured, with a forklift from one location to another or loaded onto a truck for transport to an aircraft loading facility.

The shipper shall ensure that the quality control requirements of 49 CFR 173.475[5] and the routine determination requirements of 10 CFR 71.87[2] have been satisfied prior to each shipment. The detailed operating procedures of 10 CFR 71.87(f) shall provide evidence that these requirements are met and shall include, at a minimum, the process steps listed below for preparing the PAT-1 for transport:

1. Verify that the package is proper for the content shipped and verified with the appropriate records by the user prior to content loading per 10 CFR 71.87(a).

2. Verify that the package is in an unimpaired physical condition per 10 CFR 71.87(b).

3. Ensure that the package closure devices are properly installed, secured, and free of defects per 10 CFR 71.87(c).

4. Ensure that the containment vessel has been properly loaded and requirements for shipment have been followed, witnessed, checked, and noted in the QA log.

5. Ensure the internal pressure of the containment system does not exceed the design pressure during transportation per 10 CFR 71.85(b); there are no pressure relief devices per 10 CFR 71(e) in the package.

6. Perform surveys for nonfixed surface contamination. The surveys shall be performed in accordance with user facility procedures. The survey shall use criteria derived from the

surface radioactivity guidance of 10 CFR 20.1906,[3] 10 CFR 71.87(i),[2] 49 CFR 173.443,[5] or the user's site-specific criteria, whichever is the most stringent. Surface contamination on any part of the package must not exceed the limits specified in 49 CFR 173.443, Table 9.[5]

7. Perform radiation measurements. Emanations must not exceed the limits prescribed in 49 CFR 173.441.[5] Measuring equipment used for surveys must be calibrated and of sufficient accuracy. The radiation (gamma, neutron) emanating from the package shall be measured before the package is released for transport per 10 CFR 71.47 and 71.87(j).[2] The radiation dose rate is measured at the surface to ensure that it does not exceed the expected or allowable dose rate. It is also measured at 1 meter from the package to determine the package's transportation index (TI).

8. Mark and label the outside of the package in conformance with 49 CFR 172,[10] Sections D and E, 49 CFR 172.310, 172.400, and 172.403 (classified information shall not be revealed).

9. Verify that the package has been properly leak tested and results are noted in the QA log.

10. Ensure all lifting and handling equipment is available and certified for use.

11. Load the PAT-1 on the skid and check strapping for transport.

12. Ensure all loading records for shipment are prepared and maintained.

7.1.3.4 Securing Package to Transport Vehicle

The PAT-1 package shall be secured against movement within the transport vehicle under conditions normally incident to transportation per 49 CFR 177.834[11] and 177.842(d). Detailed securing procedures shall be prepared by the shipper and include these requirements as a minimum. The loading and unloading procedures shall include measures to ensure that:

1. DOE/OST package tie down requirements are met.

2. Only an approved, DOE/OST conveyance is used.

3. All reasonable precautions are employed to prevent motion of the vehicle during loading and unloading.

4. No tampering of packages occurs during transportation.

5. No transport vehicle is loaded or unloaded unless a qualified person, as established according to the loading or unloading procedure, is in attendance, at all times.

7.2 Package Unloading

7.2.1 Receipt of Package from Carrier

Upon receipt of the PAT-1 package from the transport carrier, the following steps must be completed:

1. The consignor (hereafter referred to as the shipper) shall provide any special instructions to the consignee (hereafter referred to as the receiver) to safely open the package per 10 CFR 71.89, including special tools and precautions for handling or unloading. These instructions shall include special actions in the event the tamper indicating device (TID) is not intact, surface contamination is too high, or radiation surveys are too high.

2. The receiver shall accept the package by surveying the conveyance and package surface for contamination and external radiation levels. The receiver's procedures shall clearly indicate that contamination and radiation surveys and inspections shall be conducted upon receipt of the package. The receiver shall, at a minimum, include the following in their procedures in accordance with 10 CFR 71.111:

   - Surveying of the conveyance and package for radioactive contamination and radiation levels.

   - Examining the packaging for surface damage that may have occurred during shipping or handling.

   - Examining the TID to ensure the package has not been tampered with during transport. Reporting when a TID is not intact.

   - Ensuring that all lifting and handling equipment is available and certified for use.

3. All users shall include provisions for reporting safety concerns associated with the packaging or its use. The user shall notify the NRC in accordance with 10 CFR 20.2202, and DOE in accordance with DOE Order 231.1A and 10 CFR 20.2202. Although 10 CFR 20.2202 provides a graduated reporting period based on the severity of the incident, DOE Order 231.1A delineates specific reporting periods in accordance with the category of the occurrence. Incidents that require notification include:

   - Removable radioactive surface contamination in excess of the limits specified in 10 CFR 71.87; and

   - External radiation levels in excess of the limits specified in 10 CFR 71.47.

4. At a minimum, the user shall maintain the records outlined below for the radiation protection program and the dosimetry records of all monitored individuals:

   - ALARA plans and programs and their implementation

   - Individual occupational dose records

   - Monitoring and area control records

   - Monitoring method records

   - Training records of site employees, radiation workers, and radiation safety personnel

- Records of exposure (provided to all workers)

7.2.2 Removal of Contents

This section describes the operations for unloading the contents from the PAT-1 package.

Should the TID be damaged or not intact, verify that there is no leakage of contents. Notify the shipper and the carrier about the TID. Do not proceed until the cause of damage has been determined.

The operational steps include:

1. Remove the PAT-1 from the skid, if not already performed.
2. Inspect for tampering and remove the security wire and seal.
3. Remove the 23 Screw, Cap, and Hexagon Head at the top of the package.
4. Remove the 4-in.-long hex head screw and associated lock nut from the *Ring, Clamp Modified* (1006).
5. Remove the *Ring, Clamp Modified*.
6. Remove the *Cover, Modified* (1005).
7. Remove the outer, smaller insulation pad (*Pad, Insulation* [1027]).
8. Remove the *Cover, Liner* (1007).
9. Remove the inner, larger insulation pad (*Pad, Insulation* [1026]).
10. Remove the outer wood plug (*Plug, Removable* [1013]).
11. Remove the aluminum disc (*Disc, Removable* [1002, Item 10]).
12. Remove the inner smaller wood plug (*Plug, Removable* [1014]).
13. Lift the *TB-1 Shipping Vessel Assembly* (2A0263) out of the *Overpack, AQ* (1002) using the TB-1 *Sling, Lifting*.

    Note: The *Sling, Lifting* remains attached to the TB-1 during loading and unloading into the *Overpack, AQ-1*.

14. Remove the *Sling, Lifting* from the *TB-1 Shipping Vessel Assembly*.

    CAUTION: Pressure relief action may accompany removal of the TB-1 vessel lid. Use the following step to safely release this pressure.

    1. Loosen the TB-1 closure bolts incrementally until any pressure is relieved.

7.2.2.1 Opening the TB-1 and Removing the T-Ampoule Assembly from the TB-1

See discussion in Section 7.1.1 of this addendum for facility requirements for unloading a filled *T-Ampoule Assembly*.

Steps for opening the *TB-1* and unloading the *T-Ampoule Assembly*:

1. Remove the 12 Bolt, Socket, Head (1018) that secures the *Lid, TB* (1020) to the *Body, TB* (1022).

2. Remove the *Lid, TB* from the *Body, TB*. This can be done by reinstalling the 3 screws (1017, Item 7, used for the *Sling, Lifting*) and turning them evenly until the lid releases.

3. Remove *Ring, Filler* (2A0262).

4. Remove the *T-Ampoule Assembly* (2A0261) with contents from the *TB-1*. Unloading of the filled T-Ampoule is performed based on user facility requirements.

5. Reassemble the TB-1, install in the *Overpack, AQ* (1002) and place the PAT-1 package in safe storage.

7.2.2.2 Opening the T-Ampoule Assembly in a Controlled Atmosphere

The receiving facility will develop the necessary detailed procedures for opening the T-Ampoule loaded with a plutonium hollow cylinder or sample containers.

7.2.2.2.1 Unloading a *T-Ampoule Assembly* with Plutonium Metal Hollow Cylinder

The process for unloading the *T-Ampoule Assembly* with plutonium metal hollow cylinders should proceed under the following conditions.

- Unloading the *T-Ampoule Assembly* with plutonium hollow metal cylinder is performed in a glove box with less than atmospheric air pressure, with adequate exhaust filtration, and with appropriate control of surface cleanliness for requirements established for the glove box or glove bag being used.

- Radiation monitoring personnel to check for contamination.

- Tools needed:

  - Strap wrenches
  - User-specified gripping tool such as tongs

Steps for unloading the plutonium metal hollow cylinder from the *T-Ampoule Assembly*:

1. Monitor for contamination before opening the *T-Ampoule Assembly* and when readied for storage.

2. Loosen *Lid, T-Ampoule* and *Body, T-Ampoule* with strap wrenches.

3. Place *T-Ampoule Assembly* upright with *Lid, T-Ampoule* at the top.

   Optional: The *T-Ampoule Assembly* may be placed horizontal for unloading plutonium metal hollow cylinders.

4. Remove the *Lid, T-Ampoule* by hand.

5. Remove plutonium metal hollow cylinder with user specified gripping tool and packing material, if used.

6. Replace *Lid, T-Ampoule* by hand.

7. Clean and inspect the exterior of the *T-Ampoule Assembly* using standard health physics, swipe tests for plutonium contamination.

8. Place *T-Ampoule Assembly* in storage.

7.2.2.2.2 Unloading a T-Ampoule Assembly with Sample Containers

The process for unloading the *T-Ampoule Assembly* with *sample containers SC-1* or *SC-2* should proceed under the following conditions.

- Unloading the *T-Ampoule Assembly* with *Sample Containers* is performed in a glove box or glove bag with less than atmospheric air pressure, with adequate exhaust filtration, and with appropriate control of surface cleanliness for requirements established for the glove box or glove bag being used.

- Radiation monitoring personnel to check for contamination.

- Tools needed:

  - Strap wrenches
  - User specified gripping tool such as tongs
  - User supplied suction device

Steps for unloading the *Sample Containers* from the *T-Ampoule Assembly*:

1. Monitor for contamination before opening the *T-Ampoule Assembly* and when readied for storage.

2. Loosen *Lid, T-Ampoule* and *Body, T-Ampoule* with strap wrenches.

3. Place *T-Ampoule Assembly* upright with *Lid, T-Ampoule* at the top.

4. Remove the *Lid, T-Ampoule* by hand.

5. Remove *Sample Containers* with user supplied suction device or user specified gripping tool. Remove the *Spacer(s)* between the *Sample Containers*.

6. Loosen *Lid, Sample Container* for *SC-1* or *SC-2* by hand or with strap wrenches.

7. Remove contents and packing from the *Sample Container(s).*

8. Replace *Lid, Sample Container* for *SC-1* or *SC-2* by hand.

9. Place empty assembled *Sample Containers* and *Spacers* in *Body, T-Ampoule* using a user supplied suction device or user specified gripping tool.

10. Replace *Lid, T-Ampoule* by hand.

11. Clean and inspect the exterior of the *T-Ampoule Assembly* using standard health physics, swipe tests for plutonium contamination.

12. Place *T-Ampoule Assembly* in storage.

7.3 Preparation of Empty Package for Transport

If the empty PAT-1 package is to be transported, the following procedure shall be employed. Note that the empty PAT-1 package may be shipped without a *T-Ampoule Assembly*. Section 7.3.1 applies when the PAT-1 is shipped with an empty *T-Ampoule Assembly*. Section 7.3.2 applies when the PAT-1 is shipped without a T-Ampoule.

Note: When storing or preparing an empty TB-1 vessel for return shipment, care should be taken to avoid damaging the knife-edges (which engage the copper gasket) on the lid and body of the vessel.

7.3.1 Transporting the PAT-1 Package with an Empty T-Ampoule

1. Ensure that the contents have been removed from the *T-Ampoule Assembly* (2A0261) and that the *T-Ampoule Assembly* is free of contamination.

2. Tighten (hand tight) the *T-Ampoule Assembly* with the existing O-ring.

3. Place the *T-Ampoule Assembly* within the *Body TB* (1022).

4. Place *Lid, TB* (1020) with previously installed copper seal on the body and tighten the 12 cap screws to 34 N·m (25 ft-lb) in the following sequence: 1–7, 4–10, 2–8, 11–5, 3–9, 12–6.

   Note: Prepare a template with the numbering sequence in a clockwise orientation. Arbitrarily define one hole in the TB-1 as "1" and tighten according to the sequence.

5. Visually inspect the *Overpack, AQ* (1002) for damage, defects, and cleanliness.

6. Attach the *Sling, Lifting* on the TB-1 using the three cap screws (0.250-28UNF) and washers.

7. Using the *Sling, Lifting*, place the TB-1 in the *Overpack, AQ* and make sure it is seated.

8. Place the inner wood plug (smaller, [1014]) on top of the TB-1 and align the notches in the plug to clear the lifting screws in the TB-1.

9. Insert, in order, (1) the aluminum disk (1002, Item 10), (2) the outer wood plug (1013), and (3) the inner insulation pad (larger, [1026]).

10. Insert, in order, (1) the cover liner (1007), (2) the outer insulation pad (smaller, 1027), cover (1005), and (3) clamp ring (1006) with the index mark aligned to the index mark on the *Overpack, AQ* (1002).

11. Install the 23 hexagon head bolts through the assembled clamp ring, cover, and cover liner and finger tighten.

12. Tighten the 23 hexagon head bolts to 20 N·m (15 ft-lb).

13. Install the 4-in.-long hexagon head bolt in the clamp ring and tighten to 68 N·m (50 ft-lb).

14. Install the locking nut on the 4-in.-long bolt and tighten to 41 N·m (30 ft-lb).

7.3.2 Transporting an Empty PAT-1 package without a T-Ampoule

1. Place *Lid, TB* (1020) with previously installed copper seal on body and tighten the 12 cap screws to 34 N·m (25 ft-lb).

2. Visually inspect the *Overpack, AQ* (1002) for damage, defects, and cleanliness.

3. Attach the *Sling, Lifting* on the TB-1 lid using the three cap screws (0.250-28UNF) and washers.

4. Place the TB-1 in the *Overpack, AQ* using the *Sling, Lifting*, and make sure it is seated.

5. Place the inner wood plug (smaller, [1014]) on top of the TB-1 and align the notches in the plug to clear the lifting screws in the TB-1.

6. Insert, in order, (1) the aluminum disk (1002, Item 10), (2) the outer wood plug (1013), and (3) the inner insulation pad (larger, [1026]).

7. Insert, in order, (1) the cover liner (1007), (2) the outer insulation pad (smaller, [1027]), (3) the cover (1005), and (4) the clamp ring (1106) with the index mark aligned with the index mark on the *Overpack, AQ*.

8. Install the 23 hexagon head bolts through the assembled clamp ring, the cover, and the cover liner and finger tighten.

9. Tighten the 23 hexagon head bolts to 20 N·m (15 ft-lb).

10. Install the 4-in.-long hexagon head bolt in the clamp ring and tighten to 68 N·m (50 ft-lb).

11. Install the locking nut on the 4-in.-long bolt and tighten to 41 N·m (30 ft-lb).

12. If the package is transported off-site, ensure compliance with 49 CFR 173.443 Table 9, Surface Contamination (at each of the required stages of the packing process), and 49 CFR 172 Sections D & E (49 CFR 172.310, .400 and .403), Marking and Labeling.

The package is now ready for empty transport or storage.

7.3.3 Storage of an Empty PAT-1 Package with or without the TB-1 and Internal Hardware

The PAT-1 packaging, when not in use, shall be stored assembled (with lids in place) inside of a temperature- and humidity-controlled building. The temperature range shall be between 10°C (50°F) and 27°C (80°F), and the relative humidity shall not exceed 60% within the building.

7.4 Other Operations

Through special arrangement with the transport carrier, the shipper shall ensure observance of the operational controls for each air shipment of plutonium, as specified in the package Certificate of Compliance (CoC).

7.5 Appendix

7.5.1 References

1. United States. Dept. of Energy. DOE Order 461.1A, "Packaging and Transfer or Transportation of Materials of National Security Interest." October 2, 1996.

2. United States. Nuclear Regulatory Commission. Code of Federal Regulations, 10 CFR 71. "Packaging and Transportation of Radioactive Material." January 1, 2009.

3. United States. Nuclear Regulatory Commission. Code of Federal Regulations, 10 CFR 20. "Standards for Protection Against Radiation." January 1, 2009.

4. United States. Nuclear Regulatory Commission. NUREG-0361. "Safety Analysis Report for the Plutonium Air Transportable Package, Model PAT-1." Washington, D.C. 1978.

5. United States. Dept. of Transportation. Code of Federal Regulations, 49 CFR 173. "Shippers – General Requirements for Shipments and Packaging." October 1, 2008.

6. QQ-C-576, Federal Specification Copper Flat Products with Slit, Slit and Edge-Rolled, Sheared, Sawed or Machined Edges (Plate, Bar, Sheet, and Strip). July 12, 1961.

7. MIL-S-8660C, Military Specification Silicone Compound, NATO Code Number S-736. September 22, 1983.

8. ASTM D 3953 – 07a. "Standard Specification for Strapping, Flat Steel, and Seals," ASTM International. West Conshohocken, PA. October 1, 2007.

9. United States. Occupational Safety and Health Administration, Labor. Code of Federal Regulations, 29 CFR 1910.178. "Powered Industrial Trucks." July 1, 2008.

10. United States. Dept. of Transportation. Code of Federal Regulations, 49 CFR 172. "Hazardous Materials Table, Special Provisions, Hazardous Materials Communications, Emergency Response Information, and Training Requirements." October 1, 2008.

11. United States. Dept. of Transportation. Code of Federal Regulations. 49 CFR 177. "Carriage by Public Highway." October 1, 2008.

This page intentionally left blank

8. ACCEPTANCE TESTS AND MAINTENANCE PROGRAM

The acceptance tests and maintenance program for the PAT-1 package *Overpack, AQ* (designated AQ-1) and TB-1 *Containment Vessel*[A] (designated TB-1) are described in the SAR[1] (NUREG-0361, Chapter 8). This section describes the acceptance tests and maintenance program for the *Ring, Filler* (Drawing 2A0262, designated Ring Filler)*; T-Ampoule Assembly* (Drawing 2A0261, designated T-Ampoule); *Sample Container-1 (SC-1) Assembly* (Drawing 2A0268, designated SC-1)*; Sample Container-2 (SC-2) Assembly* (Drawing 2A0265, designated SC-2)*;* and *Inner Cradle* (Drawing 2A0385, designated Inner Cradle). Minimum acceptance requirements for fabricating, procuring, and maintaining these components are presented in this section. Detailed procedures shall be developed based on criteria contained herein and on the Certificate of Compliance (CoC)[2]. The fabrication specifications for these components are listed on the fabrication drawings in Section 1.3.2 and Section 1.3.3 of this addendum, respectively.

8.1 Acceptance Tests

This section describes the acceptance tests for the *Ring, Filler*, the *T-Ampoule Assembly*, the *Sample Container-1 (SC-1) Assembly*, the *Sample Container-2 (SC-2) Assembly*, the *Inner Cradle*, and procured components. Note that *SC-1* or *SC-2* is used as the short form of the long drawing name. For this section, these items are grouped as "T-Ampoule components" and are described in Table 8-1.

Table 8-1. T-Ampoule Components

Item	Description	Material	Drawing No.[a]
Ring, Filler	Filler between T-Ampoule and TB-1	Ti-6Al-4V Grade 5	2A0262
T-Ampoule Assembly	Lid and Body of T-Ampoule	Ti-6Al-4V Grade 5	2A0261
O-ring, Viton® A, for T-Ampoule	AS568C-241	O-ring, 100% virgin Viton® A per SAE AMS 7276G, 75 Durometer Shore A	2A0261, Item 3
Sample Container-1 (SC-1) Assembly	Lid and Body of *SC-1*	Ti-6Al-4V Grade 5	2A0268
Sample Container-2 (SC-2) Assembly	Lid and Body of *SC-2*	Ti-6Al-4V Grade 5	2A0265
O-ring, Viton® A, for *SC-1* and *SC-2*	O-ring AS568C147	O-ring, 100% virgin Viton® A per SAE AMS 7276G, 75 Durometer Shore A	2A0268, Item 3 2A0265, Item 3
Inner Cradle	Supports *SC-1* and *SC-2* Sample Containers	Ti-6Al-4V Grade 5	2A0385

[a] A specification on materials is provided in Section 1.3.3, PAT-1040 *Titanium and O-ring Materials and Component Fabrication Specification* in this addendum.

[A] The title of the drawing is shown in italics and is used interchangeably with the designated name in this addendum. The drawing number and title information are shown in Section 1.3.2 and Table 9-3 in this addendum and in Chapter 9 of the SAR.[1] Drawing titles are used to ensure clarity when specifying components.

The package custodian shall determine that the T-Ampoule components listed above have been fabricated in accordance with the approved design and the drawings in Section 1.3.2 of this addendum and inspected for cracks, pinholes, uncontrolled voids, or other defects that could significantly reduce its effectiveness per Title 10, Code of Federal Regulations, Section 71.85 [10 CFR 71.85(c) and (a)].[3]

Requirements are derived from the packaging drawings and specifications and shall be considered as minimum requirements. This information shall be present in the package custodian's fabrication records.

The minimum acceptance inspection and test requirements for the T-Ampoule components are specified in Table 8-2. These requirements must be met prior to the first use of these components per 10 CFR 71.85.

8.1.1 Visual Inspections and Measurements

Visual inspections with the unaided eye of all pertinent features on the T-Ampoule components shall be performed during fabrication. The inspections include markings, surface conditions, and measurements (i.e., toleranced dimensions, positioning, edge breaks, and surface finish). Measurements will be performed by qualified personnel and with calibrated equipment. There is no welding on these components. The required inspections are described in Table 8-2. Failure to meet the acceptance criteria is cause for rejection of the component.

8.1.1.1 Surface Condition

The metal surfaces of the T-Ampoule components shall be visually inspected for penetrations, dents, and corrosion. Any penetrations, dents, and corrosion found, is cause for rejection of the component. The surfaces must be in accordance with the dimensional requirements from the drawings. Per 10 CFR 71.85(a), superficial markings on the surface (scuff marks) are permitted only if they are within the dimensional tolerances for the component.

8.1.2 Weld Examinations

Not applicable: There are no welds in the T-Ampoule components.

8.1.3 Structural and Pressure Tests

Mechanical property tensile tests are required for the T-Ampoule components. The T-Ampoule component vessels listed are not containment boundaries for normal conditions of transport (NCT) and hypothetical accident conditions (HAC), and no credit is taken for pressure retention.

Table 8-2. Acceptance Tests for T-Ampoule Components

Note: The referenced sections and PAT-1040 specification are found in this addendum.

Component	Visual Inspections and Measurements	Structural and Pressure Tests	Leakage Tests[c]	Component and Material Tests	Miscellaneous Tests
Ring, Filler	Visual Inspection and Measurement[b] (Section 8.1.1) Marking (PAT-1040) Surface Condition[d] (Section 8.1.1.1 and PAT-1040	No Structural or Pressure Tests Required	Not Applicable (NA)	Material Certification[a] (PAT-1040) COC[e] (PAT-1040) CMTRs (Sections 8.1.3.1 and 8.1.5.3); and PAT-1040	
T-Ampoule Assembly	Visual Inspection and Measurement[b] (Section 8.1.1) Marking (PAT-1040) Surface Condition[d] (Section 8.1.1.1 and PAT-1040)	No Structural or Pressure Tests Required	Perform leakage rate test – acceptance is less than 10^{-3} atm cc/s	Material Certification[a] (PAT-1040) COC[e] (PAT-1040) CMTRs (Sections 8.1.3.1 and 8.1.5.3); and PAT-1040	Fit and Function (Section 8.1.8) Measurement (Section 8.1.8)
O-ring, Viton® A, for T-Ampoule	Visual Inspection (Section 8.1.5.1 and PAT-1040)	NA	NA	Material Certification (PAT-1040) COC (PAT-1040)	
Sample Container-1 (SC-1) Assembly	Visual Inspection and Measurement[b] (Section 8.1.1, Section 8.1.1.1, and Section 8.1.8) Surface Conditions and Marking (PAT-1040)	No Structural or Pressure Tests Required	Perform leakage rate test – acceptance is less than 10^{-3} atm cc/s	Material Certification[a] (PAT-1040) COC[e] (PAT-1040) CMTRs (Sections 8.1.3.1 and 8.1.5.3); and PAT-1040	Fit and Function (Section 8.1.8)

Table 8-2. Acceptance Tests for T-Ampoule Components (Continued)

Component	Visual Inspections and Measurements	Structural and Pressure Tests	Leakage Tests[c]	Component and Material Tests	Miscellaneous Tests
Sample Container-2 (SC-2) Assembly	Visual Inspection and Measurement[b] (Section 8.1.1, Section 8.1.1.1, and Section 8.1.8) Surface Conditions and Marking (PAT-1040)	No Structural or Pressure Tests Required	Perform leakage rate test – acceptance is less than 10^{-3} atm cc/s	Material Certification[a] (PAT-1040) COC[e] (PAT-1040) CMTRs (Sections 8.1.3.1 and 8.1.5.3); and PAT-1040	Fit and Function (Section 8.1.8)
O-ring, Viton® A, for SC-1 and SC-2	Visual Inspection (Section 8.1.5.1 and PAT-1040) Marking (Section 8.1.5.1) Packing (Section 8.1.5.1)	NA	NA	Material Certification (PAT-1040) COC (PAT-1040)	
Inner Cradle	Visual Inspection and Measurement[b] (Section 8.1.1 and Section 8.1.8) Marking (PAT-1040) Surface Condition[d] (Section 8.1.1.1 and PAT-1040)	No Structural or Pressure Tests Required	NA	Material Certification[a] (PAT-1040) COC[e] (PAT-1040) CMTRs (Sections 8.1.3.1 and 8.1.5.3); and PAT-1040	Fit and Function (Section 8.1.8)

[a] Material certification – Certified quantitative data (physical, mechanical, chemical, and/or visual) in the form of Certified Material Test Reports (CMTRs) demonstrating compliance with the drawing/specification requirements; in particular, stress-strain curves for Ti-6Al-4V Grade 5 material. If applicable, heat treatment information is included in the CMTR.

[b] Measurement – Dimensional inspections; critical dimensions are noted on the drawings.

[c] Leak Test – The vessels listed here are not containment boundaries for normal conditions of transport (NCT) and hypothetical accident conditions (HAC). Leakage rate tests are to demonstrate retention of glovebox atmosphere that is required as part of laboratory support operations to minimize metal contents degradation; the leakage rate acceptance requirements are user defined.

[d] Damage – The components shall be inspected to ascertain that there are no cracks, pinholes, uncontrolled voids, or other defects that could significantly reduce the effectiveness of the packaging (10 CFR 71.85(a)).

[e] COC (Certificate of Conformance) – A document signed or otherwise authenticated by an authorized individual certifying the degree to which items or services meet specified requirements

8.1.3.1 Mechanical Property Tests

Material mechanical property tests shall be performed on Ti-6Al-4V Grade 5 material for T-Ampoule components to assure that higher strength requirements specified in Section 2, *Structural Evaluation*, of this addendum are met for the ASTM B-348, Grade 5 and ASTM B-265, Grade 5 material. The minimum strength requirements specified in this addendum are higher than the minimum strengths specified in the ASTM standards and are 0.2% yield strength (965 MPa [140 ksi]), ultimate tensile strength (1034 MPa [150 ksi]), elongation at tensile failure (10%), and reduction in area at failure (20%). Acceptance criteria are provided in the appropriate material national standards referenced in the specification entitled PAT-1040, *Titanium and Materials and Component Fabrication Specification,* in Section 1.3.3.1 and in the drawings in Section 1.3.2 of this addendum. Failure to meet the acceptance criteria is cause for rejection of the component.

8.1.3.2 Pressure Tests

The *T-Ampoule Assembly*, *Sample Container-1 (SC-1) Assembly*, and *Sample Container-2 (SC-2) Assembly* are not containment vessels and pressure tests are not required for acceptance or maintenance. In accordance with 71.85(b), any new TB-1 *Containment Vessel* shall be pressure-tested in accordance with the regulation.

8.1.4 Leakage Tests

The *T-Ampoule Assembly* is not a containment boundary for NCT and HAC. It serves as a eutectic prevention barrier. The leakage rate test requirement for the *T-Ampoule Assembly*, *Sample Container-1 (SC-1) Assembly*, and *Sample Container-2 (SC-2) Assembly* is 10^{-3} atm cc/s and is for laboratory support operations to maintain product quality.

The TB-1 acceptance tests are referenced in Section 8.2.2.2 and 8.3.2 of this Addendum.

8.1.5 Component and Material Tests

8.1.5.1 O-Ring Tests

O-rings for the *T-Ampoule Assembly*, *Sample Container-1 (SC-1) Assembly*, and *Sample Container-2 (SC-2) Assembly* shall be visually inspected. The O-ring surfaces shall be smooth, nonporous, and free of skin defects. O-rings that do not meet these requirements shall be rejected.

Each O-ring shall be packaged separately to provide traceability. Each O-ring package shall be marked with an O-ring identification number, lot number, cure date, and compound number. These material identification numbers shall be assigned uniquely to each lot and to each size of O-ring. The identifications shall be adequate to trace O-rings to their raw material master batch. Improper packaging, marking, or lack of proper documentation COC is cause for rejection. The shelf life of the O-rings is unlimited per Society of Aerospace Engineers (SAE) issued Aerospace Recommended Practice (ARP) 5316.[4] The shelf life requirement for O-rings of ARP 5316 shall be applied to all organizations handing the O-rings for this package.

8.1.5.2 Titanium Material Property Tests

Material mechanical property tensile tests shall be performed on Ti-6Al-4V Grade 5 material for T-Ampoule components to assure that higher strength requirements specified in Section 2 and PAT-1040 *Titanium and O-Ring Materials and Component Fabrication Specification* of this addendum are met for the ASTM B-348 Grade 5 and ASTM B-265 Grade 5 material. The minimum strengths are 0.2% yield strength (965 MPa (140 ksi)), ultimate tensile strength (1034 MPa (150 ksi)), elongation at tensile failure (10%), and reduction in area at failure (20%). Acceptance criteria are provided in the appropriate material national standards referenced in the PAT-1040 specification in Section 1.3.3 and in the drawings in Section 1.3.2 of this addendum. Failure to meet the acceptance criteria is cause for rejection of the material.

8.1.5.3 Chemical Tests

Tests shall be performed to determine the chemical properties of the T-Ampoule component materials and provided in the Certified Material Test Report (CMTR) as specified in the PAT-1040 *Titanium and O-Ring Materials and Component Fabrication Specification* in Section 1.3.3 and in the drawings in Section 1.3.2 of this addendum. Material that cannot be traced to the mill or heat-treatment lot shall be rejected.

8.1.6 Shielding Tests

No shielding tests are required for the T-Ampoule components. No credit is taken in Section 5 of this addendum for internal shielding within the TB-1.

8.1.7 Thermal Tests

A thermal test is not required for the *T-Ampoule Assembly*, since the maximum heat generation of the payload is the same as that in the SAR.[1]

8.1.8 Miscellaneous Tests

The *Inner Cradle* in the *T-Ampoule Assembly* shall be assembled and checked for function and fit with the *SC-1* or *SC-2*. The clearance gap between the two flat legs of the *Inner Cradle* is 7.692 ±0.005 cm (3.030 ±0.002 in.) and is shown in Drawing Number 2A0385 in this addendum. The *Inner Cradle* Assembly may be hand-smoothed for proper fit and function. Individual components of the *Inner Cradle* will be rejected if fit and function are not met.

8.2 Maintenance Program

When the package is being packed or unpacked, the T-Ampoule components shall be examined to ensure that all components are present and functional. A record of the examination results will be generated and must include the identification and serial numbers of the component examined, the names of the personnel who performed the packing/unpacking and examination, and the date of the activity.

Maintenance on the metal T-Ampoule components shall be performed annually and shall include visual inspection. A record of the maintenance action(s) will be generated. The record must identify maintenance performed, the component(s) on which the maintenance was performed, and the names of the personnel who performed the maintenance.

The TB-1 periodic test and maintenance requirements are referenced in Section 8.2.2.2 and 8.3.2 of this Addendum. Note that for the plutonium metal shipments described in this Addendum, the TB-1 O-ring is not used.

8.2.1 Structural and Pressure Tests

No structural or pressure tests are required for maintenance of the T-Ampoule components.

8.2.2 Leakage Tests

8.2.2.1 T-Ampoule, Sample Container-1 (SC-1), and Sample Container-2 (SC-2)

The *T-Ampoule Assembly* is not a containment boundary for NCT and HAC. The leakage rate test requirement for the *T-Ampoule Assembly*, *Sample Container-1 (SC-1) Assembly*, and *Sample Container-2 (SC-2) Assembly* is 10^{-3} atm cc/s and is for laboratory support operations to maintain product quality. This testing is performed through the use of a test method with sufficient sensitivity such as an evacuated envelope test (Bell Jar) or a pressure change test (A.5.1 Gas pressure drop or A5.2 Gas pressure rise) as described in ANSI N14.5 American National Standard for Radioactive Materials – Leakage Tests on Packages for Shipment, 1997. Note that the test procedure shall demonstrate test sensitivity for pre-shipment as required for ANSI N14.5 97. Since the T-Ampoule is filled with tracer gas, the evacuated envelope technique may be used. It is desirable to have about a 100% concentration of tracer gas within the T-Ampoule, which could be verified using standard techniques such as sampling with an oxygen monitor, flushing/spraying within a glove bag, or closing the T-Ampoule within a glovebox that has a known concentration of helium. The 10^{-3} atm cc/s leakage rate tests shall be performed for fabrication, maintenance, and pre-shipment. Periodic testing is not required.

8.2.2.2 TB-1

The TB-1 is the containment boundary with copper seal, and the TB-1 O-ring is not used for plutonium metal shipments in the PAT-1. The TB-1 leakage rate specification is 10^{-7} std cc/s (air) for Fabrication, Maintenance, Periodic, and Pre-shipment testing. The specification is provided in Section 8.3.2, Leak Testing, and is entitled "Sandia National Laboratories TB-1 Leak Test Requirements." The leak test system consists of a mass spectrometer type leak detector together with a suitable test chamber that will completely enclose the test product, auxiliary pressurization equipment, and instrumentation necessary for performance of the test under the specified conditions. The test procedure that is used to determine the leakage rate of the TB-1 containment vessel shall meet the leak testing requirements of ANSI N14.5 American National Standard for Radioactive Materials – Leakage Tests on Packages for Shipment, 1997.

The following leakage rate tests apply to the TB-1 Containment Vessel:

Fabrication: Fabrication leakage rate testing shall be performed prior to first use.

Maintenance: Maintenance leakage rate testing shall be performed prior to returning a package to service following a maintenance repair.

Periodic: Periodic leakage rate testing shall be performed annually.

Pre-shipment Pre-shipment leakage rate testing shall be performed before each shipment. Before the testing, the contents must be loaded, the T-Ampoule must be filled with tracer gas, and the containment system must be assembled.

When Fabrication, Maintenance or Periodic leak tests are performed, the test shall be completed for the TB-1 without the T-Ampoule installed.

8.2.3 Component and Material Tests

During loading operations, the O-rings for the *T-Ampoule Assembly*, *Sample Container-1 (SC-1) Assembly*, and *Sample Container-2 (SC-2) Assembly* will be inspected for cracks, gouges, or other damage. If any damage is detected, the O-ring must be replaced. The O-rings will be replaced annually.

8.2.4 Thermal Tests

Since the maximum heat generation of the payload is the same as that in the SAR,[1] a thermal test is not applicable for the *T-Ampoule Assembly*.

8.2.5 Miscellaneous Tests

If installation of *Sample Container-1 (SC-1) Assembly* or *Sample Container-2 (SC-2) Assembly* in the *Inner Cradle* becomes difficult after repeated loading and unloading, the *Inner Cradle* must be inspected for damage and for proper clearance between the *Inner Cradle* legs and *SC-1* or *SC-2* sample containers. If damage to the *Inner Cradle* component(s) is discovered, the damaged component(s) will be replaced and the test in Section 8.1.8 of this addendum performed.

The test described in Section 8.1.8 of this addendum is performed annually to ensure that the *Sample Container-1 (SC-1) Assembly* and *Sample Container-2 (SC-2) Assembly* fit and function properly within the *Inner Cradle* of the *T-Ampoule Assembly*. If tightness is observed, inspection and repair as described in Section 8.1.8 shall be performed.

8.3 Appendix

8.3.1 References

1. United States. Nuclear Regulatory Commission. NUREG-0361. “Safety Analysis Report for the Plutonium Air Transportable Package, Model PAT-1.” Washington, D.C. 1978.

2. United States. Nuclear Regulatory Commission. “Certificate of Compliance for Radioactive Material Packages,” Certificate Number 0361, Revision Number 9, Docket Number 71-0361, Package Identification Number USA/0361/B(U)F-96. March 4, 2009.

3. United States. Nuclear Regulatory Commission. Code of Federal Regulations. 10 CFR 71. “Packaging and Transportation of Radioactive Material.” January 1, 2009.

4. Society of Aerospace Engineers (SAE). “ARP 5316 Elastomer Shelf Life Recommendation.” Aerospace Recommended Practice (ARP) 5316, 1998. http://www.oringsusa.com/html/shelf_life.html.

8.3.2 Leak Testing

The leak test requirements for plutonium metal shipments for the TB-1 containment vessel are described in the stand-alone document that follows.

LEAK TESTING SPECIALISTS, INC.
www.leaktestingspec.com
5790 Hoffner Ave. Suite 505 Orlando, FL 32822 Phone (407) 737-6415 Fax (407) 737-6416
Offices in: Washington, DC – Oak Ridge, TN – Orlando, FL

SANDIA NATIONAL LABORATORIES

TB-1 CONTAINMENT VESSEL

LEAK TEST REQUIREMENTS

LTS USE ONLY	
X	Initial Issue
	Issued as a Revision
	Document Change Notice

CLIENT USE ONLY	
X	Approved – Without Comment
	Approved – With Comment
	Not Approved – Comments Attached
	Client Approval Not Required

Signature on file at LTS Aug. 6 2010
LTS - Level III Approval Date

Richard H. Yoshimura 09/01/2010
Client Approval Date

Signature on file at LTS
LTS – QA Approval Date

Richard Yoshimura, SNL 09/01/2010
Reviewer Name & Company Date

Any changes to this document shall void LTS Level III endorsement unless accompanied with a DCN or approved document revision.

This document is approved for use only with the project indentified in the title.

TB-1 Containment Vessel Leak Test Requirements for Plutonium Metal Shipments

1.0 General

1.1 Scope

This specification defines the requirements for the quantitative measurement of the leakage rate of a sealed component for use with plutonium metal shipments of the Plutonium Air Transportable (PAT-1) Package. A mass spectrometer type leak detector is used. The test procedure that is used to determine the leakage rate of the TB-1 Containment Vessel shall meet the leak testing requirements of ANSI N14.5. American National Standard for Radioactive Materials - Leakage Tests on Packages for Shipment.

1.2 Product Description

The item to be leak tested per this specification is the TB-1 Containment Vessel, drawing number 1017, which is a major component of the Plutonium Air Transportable (PAT-1) Package, drawing number 1001. The detail parts of the TB-1 Containment Vessel are:

- TB Body
- TB Lid
- Copper Gasket
- O-Ring (For plutonium metal shipments, the elastomer O-Ring is not used)
- Bolt, Socket Head, Special, 0.500-200NF (12 required)
- T-Ampoule filled with tracer gas is used to provide assurance that gross leaks are detected during TB-1 Containment Vessel leak testing.

1.3 Definitions

1.3.1 Background

Test system background is included in the leakage rate results. This may be spurious output of the leak detector expressed in suitable terms, due to the response to all gases other than the actual leakage of tracer gas from the product being tested and/or the known leak. The background may be inherent in the detector or extraneous, and includes absorbed tracer gas.

1.3.2 Units

1.3.2.1 Pressure Units

a. Millimeter of Mercury (mmHg).
A unit of pressure corresponding to a column of mercury exactly 1 millimeter high at 0°C under standard gravity acceleration of 980.665 cm/sec^2.

b. Micron of Mercury (uHg)
A unit of pressure equal to 1/1000 of millimeter of mercury pressure unit.

c. Torr
A unit of pressure equal to 1/760 of a standard atmosphere; differs by only one part in 7 million from a millimeter of

mercury. Torr is the preferred pressure unit for low pressure (vacuum) measurement.

1.3.2.2 Leakage Rate Units
(cubic centimeter per second, standard temperature and pressure). A flow rate of gas in terms of cubic centimeters per second in which the gas volume is reduced to standard temperature and pressure. 1.0 std cc/sec. = 0.75 Torr-liter/sec. = 1.0×10^{1} Pa m^3/sec. = 1.013 Bar cc^3/sec.

1.3.3 STP (Standard Pressure and Temperature)
Defined as 0^{o} C and 760 Torr.

1.3.4 The K Factor
Equals the Square Root of Molecular weight of helium/Molecular weight of air.

1.3.5 Sealed Product
A product which is capable of maintaining, or of being sealed by special fixtures to maintain, an internal pressure or vacuum.

1.3.6 Tracer Gas
A gas that is used to measure the leakage rate of the product being tested. A tracer of a known concentration shall be used.

1.3.7 Leakage Rate
The quantity of gas flowing in unit time into, or out of, the product under test, reduced to units of volume at standard temperature and pressure.

1.3.7.1 Tracer Gas Leakage Rate
The leakage rate tests results, calculated without application of a K factor, from the leak detector readings.

1.3.7.2 Total Gas Leakage Rate
An estimate of the product leakage rate, obtained by multiplying the tracer gas leakage rate by the specified K factor.

1.3.7.3 Maximum Permissible Leakage Rate
The maximum total gas leakage rate limit allowable for product acceptance.

1.3.8 Known Leak
A calibrated device from which tracer gas is emitted at a known rate.

2.0 Documents
The following documents, of the exact issue shown, form a part of this specification to the extent specified herein.

2.1 NRC Information Notice 97-57 LEAK TESTING OF PACKAGING USED IN THE TRANSPORT OF RADIOACTIVE MATERIAL

3.0 General Requirements

3.1 Equipment Capability

3.1.1 The system shall consist of a mass spectrometer type leak detector together with a suitable test chamber that will completely enclose the product, auxiliary pressurization equipment, and instrumentation necessary for performance of the test under the specified conditions.

3.2 Gases

A tracer gas such as helium shall be used. The concentration of tracer gas shall be known.

3.3 Calibration of Known Leak

The known leaks used shall be calibrated by the Primary Standards Laboratory specified in the contract or purchase order. Calibration shall be performed prior to initial use and at intervals thereafter in accordance with policies established by the Primary Standards Laboratory.

3.4 Personnel

Personnel shall be qualified and certified as Level II in the test method or Level III Leak Testing in accordance with a Written Procedure for the Qualification and Certification of Nondestructive Testing Personnel and the appropriate quality program.

3.5 Test Procedures

The test procedure should reference nationally recognized codes and standards as part of the leak test control of variables and evidence of adequate sensitivity. Examples of national codes and standards are ASME Section V Article 10, ASTM E 493 – 06 Inside-Out Leak Test and ASNT Recommended Practice SNT-TC-1A. The PAT-1 owner can provide a sample test procedure for the preparation and testing of the TB-1 Containment Vessel upon request. The procedure provided is for reference only and all responsibility for performing the leak test remains with the user.

3.6 Test Method

The leak test procedure shall reference ANSI N14.5 – 97 Appendix A Leakage Test Methods and Procedures. The procedure shall specifically reference Method A.5.4 Evacuated Envelope (Gas Detector). The Evacuated Envelope technique (also referred to as a Bell Jar Technique) accurately measures the leakage rate of a vessel or component that has been pre-filled with helium and placed within the evacuated envelope.

3.7 Test Frequency

This test method is intended to meet the Fabrication, Maintenance, Periodic (Annual) and Pre-shipment leakage rate requirements of ANSI N14.5 – 97. The following leak tests apply to the TB-1 Containment Vessel.

3.7.1 Fabrication

Fabrication leakage rate testing shall be performed prior to first use.

3.7.2 Maintenance

Maintenance leakage rate testing shall be performed prior to returning a package to service following a maintenance repair.

3.7.3 Periodic

Periodic leakage rate testing shall be performed annually.

3.7.4 Pre-shipment

Pre-shipment leakage rate testing shall be performed before each shipment, after the contents are loaded and the containment system is assembled.

3.8 Test Sensitivity

The test sensitivity requirement for leakage rate testing shall demonstrate the test can detect a leakage rate of one half of the ref air leakage.

3.9 Tracer Gas Concentration

The leak test requires that the TB-1 Containment Vessel be filled with a tracer gas. The concentration of the tracer gas shall be known and should be 100%; if the tracer gas is less than 100% the final leakage rate shall be corrected to compensate for tracer gas concentration.

3.9.1 The preferred technique to fill the TB-1 Containment Vessel with tracer gas is to evacuate and backfill. The tracer gas concentration can be calculated using the partial pressure of the tracer gas.

% concentration = (Trace gas pressure / total vessel pressure) x 100. This process shall be performed using an absolute pressure gauge.

3.9.1.1 Place the TB-1 Containment Vessel into the pressure chamber.

3.9.1.2 Record the atmospheric pressure.

3.9.1.3 Evacuate the TB-1 Containment Vessel to less than 1 Torr (or equivalent).

3.9.1.4 Backfill the TB-1 Containment Vessel with tracer gas (purge all lines and fitting with tracer gas before assembly) to atm pressure.

3.9.1.5 Remove the TB-1 Containment Vessel from the pressure chamber and secure the lid.

Note: The technique used to fill the TB-1 Containment Vessel with tracer gas and secure the TB-1 Containment Vessel lid shall not compromise the tracer gas concentration.

4.0 General Leak Test Procedure

4.1 Fill the T-Ampoule with tracer gas and secure inside the TB-1 Containment Vessel.

4.2 As part of the final assembly and after the TB-1 Containment Vessel lid is in place verify that the edge of the copper gasket is visible through one of the bolt holes.

4.3 The leakage rate of the TB-1 Containment Vessel shall be determined by placing a TB-1 Containment Vessel that has been properly filled with a tracer gas and assembled, into a bell jar.

4.4 The bell jar is sealed and connected to a tracer gas leak detector.

4.5 The bell jar shall also contain a second port that allows for a calibration standard to be attached.

4.6 The tracer gas leak detector shall evacuate the bell jar to approximately 1 atm of pressure differential.

4.7 The tracer gas behind the copper seal is limited and the evacuation (evacuation time and test duration) shall be limited.

4.8 After the steady state leakage rate is reached, a leak standard with a known leakage rate shall be introduced in the bell jar and into the tracer gas leak detector.

4.9 The tracer gas detector should respond to the known leak within the amount of time required to reach steady state initially and to the degree equal to the leakage rate value of the calibrated leak.

4.10 If the tracer gas detector does not respond in amplitude equal to the leakage rate value of the calibrated leak, the final leakage rate value shall be corrected using a correction factor.

4.11 The Leakage Rate Correction Factor is calculated as follows:

$$LRCF = LR_{Std} / (LR_{Std\ Open} - LR_{Std\ Closed})$$

LRCF = Leakage rate Correction Factor.
LR_{Std} = The temperature corrected leakage rate of the standard leak.
LR_{Std} Open = The leak detector leakage rate reading with the standard leak open.
LR_{Std} Closed = The leak detector leakage rate reading with the standard leak closed.

Note: The formula above corrects for any loss of sensitivity that occurs through the test setup, a separate correction factor is required if the tracer gas concentration is not 100%.

5.0 Acceptance Criteria

5.1 The current requirements for leak testing the TB-1 Containment Vessel is an air leak not to exceed a leakage rate of 1.0×10^{-7} atm cc/sec. or equivalent. The current pre-shipment leakage rate requirements for a one time use seal are the same for all leakage testing for periodic, fabrication and maintenance leakage rate test.

6.0 Test Records

The following information shall be recorded by the testing laboratory. Copies of test records shall be distributed as specified in the contract or purchase order.

6.1 Product part number and serial number.

6.2 Purchase order or contract number.

6.3 Make and model number of leak detector used.

6.4 Value of known leaks used.

6.5 Test pressures (internal and external).

6.6 Tracer gas and concentration used.

6.7 Fill gas used.

6.8 Leak detector output readings.

7.0 References:

7.1 ASTM E 493 Inside-Out Leak Test.

7.2 ASME Section V Article 10 – Boiler & Pressure Vessel Code as applicable.

7.3 ANSI N14.5 1997 – American National Standard for Radioactive Materials - Leakage Tests on Packages for Shipment.

7.4 PAT-1 Safety Analysis Report Addendum.

This page intentionally left blank

9. QUALITY ASSURANCE

This section supplements Chapter 9, *Specifications and Drawings*, of the *Safety Analysis Report for the Plutonium Air Transportable Package, Model PAT-1*, NUREG-0361,[1] and defines the quality assurance (QA) requirements and methods of compliance for requirements associated with the PAT-1 package.

In the late 1970s, Sandia National Laboratories (SNL) developed the PAT-1 under a contract with the Nuclear Regulatory Commission (NRC). The PAT-1 was designed to meet the requirements specified in NUREG-0360, *Qualification Criteria to Certify a Package for Air Transport of Plutonium.*[2] The QA chapter of SAND76-0587 (NUREG/CR-0030)[3] defined the PAT-1 design, procurement, fabrication, testing, and recommended package-user QA requirements. The Department of Energy (DOE) Bendix, Kansas City Plant manufactured 24 PAT-1 packaging systems. SNL used 18 of these 24 packaging systems to perform certification qualification testing, and the remaining packaging systems were made available for use.

The current QA requirements for packaging and transportation of radioactive material are prescribed in Title 10 Code of Federal Regulations Part 71 (10 CFR 71)[4] Subpart H, *Quality Assurance*, as supplemented by DOE orders for DOE organizations/activities. The NRC guidance for establishing QA programs (QAPs) for packaging used in the transport of radioactive material is provided in Regulatory Guide 7.10 (RG 7.10), *Establishing Quality Assurance Programs for Packaging Used in Transport of Radioactive Material*, Revision 2.[5] Each of the requirements specified in Subpart H apply to the PAT-1 activities within the scope of this addendum. While not every Subpart H requirement may be applicable to every activity from design through use of the packaging system (based on the nature of the activity), across all of those activities, each of the Subpart H requirements is applicable at least once. PAT-1 activities shall be performed under QAPs that meet all of the applicable 10 CFR 71 Subpart H and DOE/NNSA QA requirements. National Nuclear Security Administration (NNSA) users of the PAT-1 package must establish and maintain a 10 CFR 71 Subpart H-compliant QAP before designation as an authorized user of the PAT-1 package.

For SNL PAT-1 activities, the *10 CFR 71, Packaging and Transportation of Radioactive Material – Quality Assurance Program Plan*[6] is the applicable QA program plan.

9.1 Organization

SNL is responsible for maintaining PAT-1 QA requirements, developing new QA requirements and/or specifications based on 10 CFR 71 Subpart H requirements, if necessary, and revising the Safety Analysis Report (SAR) QA requirements, if necessary. The NNSA Service Center, Packaging Certification Division is responsible for ensuring NNSA organizations that perform PAT-1 activities establish, maintain, and comply with applicable QA requirements. All SNL PAT-1 activities are conducted under the NNSA-approved SNL corporate QAP, the *Sandia National Laboratories 10 CFR 71, Subpart H Quality Assurance Program Plan (QAPP), AS-PT-PD-04* [6] and associated Quality Assurance Implementing Procedures (QAIPs). The program is implemented using a graded approach, as dictated by the importance to safety of the activity being performed.

The responsible organizations are staffed by technically competent personnel with freedom to make appropriate objective judgments, recommendations, and decisions consistent with delegated authority. The level of authority and independence delegated to the QA function were provided in organization charts that were available when the original set of packages was fabricated.

In this addendum, SNL is the design organization and package custodian and has support from Oak Ridge National Laboratory (ORNL) and Los Alamos National Laboratory (LANL). ORNL provides shielding and criticality analyses for the plutonium metal contents described in Sections 5 and 6 of this addendum. LANL consults with shippers and provides recommendations for the design of the inner packing and proposed plutonium metal contents. LANL also provides technical data on eutectics prevention and estimates of gas generation from volatilization of elastomers at high temperature, in the form of LANL-issued reports or documents.

SNL prepared a Subpart H QAPP that was approved by the DOE/NNSA Packaging Certification Division in 2007.[6] Applicable portions of that plan were extended to ORNL for the shielding and criticality analyses and audits were conducted to ensure compliance.

The SNL Management System Improvement Department provides QA support for the PAT-1 Recertification Project.

See Figure 9-1 for a diagram of the organizational relationships for the PAT-1 Recertification Project.

The users of the PAT-1 package for plutonium metals are contractor organizations within the DOE.

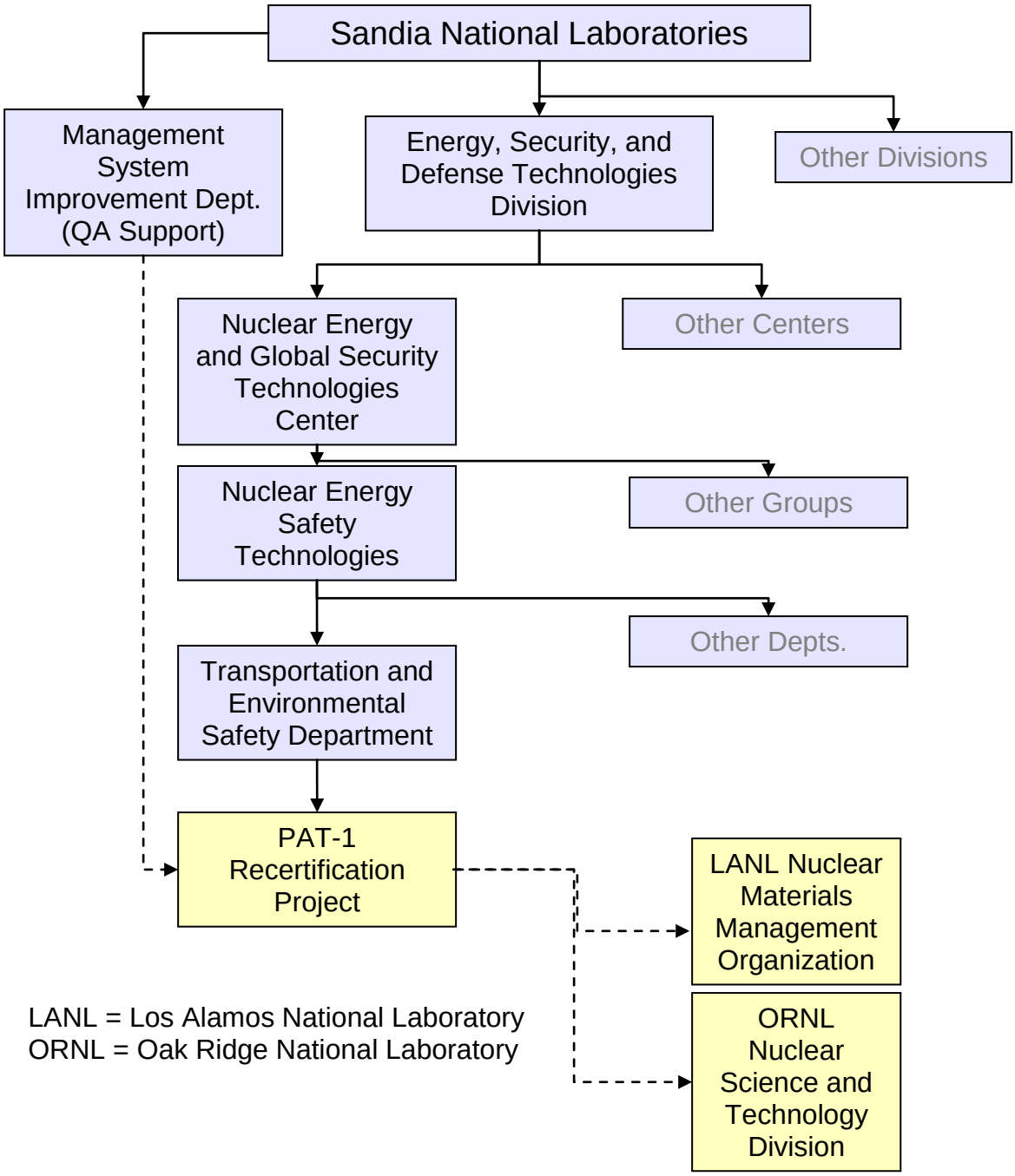

Figure 9-1. Organization Chart for PAT-1 Recertification

9.2 Quality Assurance Program

9.2.1 General

The SNL QAPP is implemented through the use of SNL corporate procedures, where they exist, or the preparation, review, approval, and use of QAIPs for QA controls that are not implemented in the SNL corporate system. These procedures provide a system of checks and balances to ensure a safe, reliable, quality product. Table 9-1 describes the relationship between the

implementing documents and the sections of Subpart H that they implement. The SNL QAP does not apply to PAT-1 packaging system users who use the PAT-1 packaging system to transport materials. These users must have their own NRC- or NNSA-approved 10 CFR 71 Subpart H QAPs.

Table 9-1. Relationship between QA Implementing Documents and Elements of 10 CFR 71, Subpart H

Implementing Document ID	Title	Related Element of Subpart H	Description
AS-PT-PD-04[6]	*Sandia National Laboratories Title 10 CFR 71, Packaging and Transportation of Radioactive Material Quality Assurance Program Plan*	71.103 Organization	Describes the organizational roles, responsibilities, and relationships for activities and projects subject to 10 CFR 71, Subpart H, including packaging system recertification for the PAT-1 system.
AS-PT-PD-04[6]	*Sandia National Laboratories Title 10 CFR 71, Packaging and Transportation of Radioactive Material Quality Assurance Program Plan*	71.105 Quality Assurance Program	Describes the SNL QA program for activities and projects subject to 10 CFR 71, Subpart H, in general.
1071H-QAIP 2-2[7]	*Project Quality Plan Preparation*		Prescribes controls for preparing a Quality Plan specific to an individual project, e.g., PAT-1 Recertification.
1071H-QAIP 3-1[8]	*Design Control*	71.107 Package Design Control	Prescribes design control measures for packaging system items and components.
1071H-QAIP 9-2[9]	*Model Validation*		Prescribes control mechanisms applied to validating mathematical models used for analysis.
1071H-QAIP 9-3[10]	*Analyses and Calculations*		Prescribes controls applied to the conduct of analyses and calculations, including QA controls on software used for those analyses.
SNL Corporate Process Requirement 500.2.1	*Procurement Manual*	71.109 Procurement Document Control	Prescribes controls for preparation, content, and processing of procurement documents at SNL to ensure that applicable regulatory requirements, design bases, technical, and quality requirements are included or referenced in those documents.
1071H-QAIP 4-1[11]	*Control of Procurement Documents and Purchased Material, Equipment, and Services*		Prescribes controls for preparation, content, and processing of procurement documents by procuring organizations other than SNL to ensure that applicable regulatory requirements, design bases, technical, and quality requirements are included or referenced in those documents.

Table 9-1. Relationship between QA Implementing Documents and Elements of 10 CFR 71, Subpart H (Continued)

Implementing Document ID	Title	Related Element of Subpart H	Description
1071H-QAIP 5-1[12]	*Quality Assurance Implementing Procedure Preparation and Content*	71.111 Instructions, Procedures, and Drawings	Prescribes controls specific to the content and processing of documents that establish and implement the QA program.
1071H-QAIP 3-1[8]	*Design Control*		Prescribes controls specific to the content and processing of design drawings and specifications.
1071H-QAIP 6-1[13]	*Document Review and Approval*	71.113 Document Control	Prescribes tools and documentation for review ("inspection") and approval of documents.
1071H-QAIP 6-2[14]	*Document Control*		Prescribes controls for the issuance, use, and revision of documents that, themselves, prescribe processes or specify requirements.
SNL Corporate Process Requirement 500.2.1	*Procurement Manual*	71.115 Control of Purchased Material, Equipment, and Services	Prescribes controls to ensure that materials, equipment, or services procured by SNL conform to requirements specified in the procurement documents.
1071H-QAIP 4-1[11]	*Control of Procurement Documents and Purchased Material, Equipment, and Services*		Prescribes controls to ensure that materials, equipment, or services procured by organizations other than SNL conform to requirements specified in the procurement documents.
1071H-QAIP 8-1[15]	*Identification and Control of Materials, Parts, and Components*	71.117 Identification and Control of Materials, Parts, and Components	Prescribes controls to ensure that only correct and accepted items are used as parts of a packaging system.
1071H-QAIP 9-1[16]	*Control of Special Processes*	71.119 Control of Special Processes	Prescribes controls to ensure that special processes are conducted in a way that ensures their success.
1071H-QAIP 10-1[17]	*Inspection and Identification of Item Status*	71.121 Internal Inspection	Prescribes controls applicable to inspection activities focused on items, components, and assemblies.
1071H-QAIP 9-5[18]	*Technical Products and Deliverable Reports*		Prescribes process for review and approval ("inspection") of technical product documents.
1071H-QAIP 6-1[13]	*Document Review and Approval*		Prescribes tools and documentation for review ("inspection") and approval of documents.
1071H-QAIP 9-5[18]	*Technical Products and Deliverable Reports*		Prescribes process for review and approval ("inspection") of technical product documents.
1071H-QAIP 11-1[19]	*Control of Data Collection and Testing Activities*	71.123 Test Control	Prescribes controls for testing of items, assemblies, or systems to determine whether they meet specified requirements.

Table 9-1. Relationship between QA Implementing Documents and Elements of 10 CFR 71, Subpart H (Continued)

Implementing Document ID	Title	Related Element of Subpart H	Description
SNL Corporate Process Requirement 100.3.1	*Standards and Calibration*	71.125 Control of Measuring and Test Equipment	Prescribes controls applicable to measuring and test equipment used by SNL organizations to ensure validity of data and measurements.
1071H-QAIP 12-1[20]	*Control of Measuring and Test Equipment*		Prescribes controls applicable to measuring and test equipment used by organizations other than SNL to ensure validity of data and measurements.
SNL Corporate Process Requirement 500.2.3	*Property/Assets Management User's Manual*	71.127 Handling, Storage, and Shipping Control	Prescribes controls to be applied at SNL to preclude damage or deterioration of items and materials.
1071H-QAIP 13-1[21]	*Control of Shipping, Handling, Storage, Preservation, and Cleaning*		Prescribes controls to be applied at locations other than SNL to preclude damage or deterioration of items and materials.
1071H-QAIP 10-1[17]	*Inspection and Identification of Item Status*	71.129 Inspection, Test, and Operating Status	Prescribes controls to ensure that the status of items with respect to inspections or tests is indicated.
1071H-QAIP 15-1[22]	*Control of Nonconformances and Corrective Action*	71.131 Nonconforming Materials, Parts, or Components	Prescribes controls to ensure that materials, parts, or components that do not meet requirements are not used or installed.
SNL Corporate Process Requirement 001.3.11	*Corporate Corrective Action Process*	71.133 Corrective Action	Prescribes controls to ensure that conditions adverse to quality are identified and corrected by SNL.
1071H-QAIP 15-1[22]	*Control of Nonconformances and Corrective Action*		Prescribes controls to ensure that conditions adverse to quality are identified and corrected by organizations other than SNL.
SNL Corporate Process Requirement 400.2.20	*Management of Information Throughout its Lifecycle*	71.135 Quality Assurance Records	Prescribes controls for the management of records, including QA records.
SNL Corporate Process Requirement 001.3.5	*Audits*	71.137 Audits	Prescribes policy and controls concerning internal and external audits at SNL.
SNL Corporate Process Requirement 001.3.10	*Corporate Self-Assessment Process*		Prescribes controls for the performance of internal assessments at SNL.

A graded approach is used to selectively apply the QA requirements to the PAT-1 packaging components and related services and activities in accordance with 10 CFR 71.105. The purpose of the graded approach is to select the QA controls and appropriate verifications to the various packaging items, services, and activities consistent with the extent of their importance to health and safety.

The SNL QAP is extended to ORNL through an implementation plan and QAIPs for the shielding and criticality analyses performed for this addendum. LANL provides technical data and reports that are approved under their quality program requirements for unlimited release external reports.

9.2.2 QA Levels

The QA chapter of SAND76-0587 (NUREG/CR-0030)[3] defines the PAT-1 design, procurement, fabrication, testing, and recommended package user QA requirements for the first 24 PAT-1 packaging systems. At that time, there were no defined quality categories.

The tasks performed in support of the PAT-1 with T-Ampoule configuration and plutonium metal content certification effort, and the packaging components for this configuration, are provided in Tables 9-2 and 9-3, respectively. The tasks and packaging components were classified in accordance with the quality categories defined in RG 7.10, Revision 2,[5] Appendix A, and SNL *QAPP, AS-PT-PD-04*[6] based on their importance to safety.

Table 9-4 documents the level of control required for each quality category applicable to the packaging system elements. These defined quality categories consider the impact to safety if the component fails or performs outside of design parameters.

9.2.2.1 Graded Quality Category A Items

These items and tasks are critical to safe operations, and include structures, components, and systems for which a failure or malfunction could directly result in a condition that would adversely affect public health and safety. This includes such conditions as loss of primary containment with subsequent release of radioactive material, loss of shielding, or an unsafe geometry compromising criticality control.

9.2.2.2 Graded Quality Category B Items

These items and tasks have a major impact on safety and includes structures, components, and systems for which a failure or malfunction could indirectly result in a condition that would adversely affect public health and safety. However, an unsafe condition could result only if the primary event occurs in conjunction with a secondary event, or other failure or environmental occurrence.

Table 9-2. Project Tasks and Quality Categories for PAT-1 Addendum

Project Tasks	Quality Category
1. Project Management	None
2. SAR Structural Analysis for T-Ampoule and Contents for NCT, HAC, and Pu Air Transport	Category A
3. SAR Criticality and Shielding Analysis for NCT, HAC and Pu Air Transport	Category A
4. Eutectics Evaluation	Category B
5. Leak Testing for T-Ampoule	Category C
6. SAR Amendment Preparation	None
7. Redesign and Drawings for SAR	Category B
8. SAR Amendment Assembly	None
9. SAR Section Review	None
10. Meeting Preparation	None
11. SAR Revision Based on NRC Comments	None
12. Testing for Model Verification and Margin	Category B
13. Update QA Section 9	None

Table 9-3. QA Categories for Design and Procurement of *T-Ampoule Assembly* and Inner Packing

Component Name	Drawing Number	Quality Category
Ring, Filler	2A0262	A
T-Ampoule Assembly	2A0261	A
O-ring, Viton® for T-Ampoule	2A0261, Item 3	C
Inner Cradle	2A0385	B
Sample Container-1 (SC-1) Assembly	2A0268	B
Sample Container-2 (SC-2) Assembly	2A0265	B
O-ring, Viton for SC-1	2A0268, Item 3	C
O-ring, Viton for SC-2	2A0265, Item 3	C

Table 9-4. Level of QA Control Per QA Element

QA Element	Level of Assurance Effort	Quality Category		
		A	B	C
9.1	Organization – grading not applicable	—	—	—
9.2	Quality Assurance Program – grading not applicable	—	—	—
9.3	Package Design Control ▪ All controls applicable ▪ No controls required	X	X	 X
9.4	Procurement Document Control ▪ Procurement Documents receive management review ▪ Procurement Documents receive technical review ▪ Procurement Documents receive QA review ▪ No review required	X X X	 X X	 X
9.5	Instructions, Procedures, and Drawings – Instructions and procedures (such as QAIPs) are prepared and applied to all quality categories, and design drawings are prepared regardless of the quality category of the subject item. Therefore, grading not applicable for this element.	—	—	—
9.6	Document Control – Document control is applied to <u>all</u> instructions, procedures, and drawings; quality categories are not applicable to those documents. Therefore, grading is not applicable for this element.	—	—	—
9.7	Control of Purchased Material, Equipment, and Services ▪ All controls applicable ▪ No audit/surveillance of supplier required if supplier is qualified; all other controls applicable ▪ Only receipt inspection to verify procurement document requirements met requirements	X	X	X
9.8	Identification and Control of Material, Parts, and Components ▪ Identification by part ID/drawing number and package S/N ▪ Identification by part ID/drawing number only required	X	X	X
9.9	Control of Special Processes ▪ Performed by qualified persons using qualified procedures and equipment ▪ No controls required	X	X	X
9.10	Inspection ▪ All controls applicable – no grading	X	X	X
9.11	Test Control – testing may be performed on assembled components sets of various quality categories; therefore, no grading by quality category is appropriate – all controls applicable.	—	—	—
9.12	Control of Measuring and Test Equipment ▪ All controls applicable – no grading	X	X	X

Table 9-4. Level of QA Control Per QA Element (continued)

QA Element	Level of Assurance Effort	Quality Category		
9.13	Handling, Storage, and Shipping Control ▪ All controls applicable ▪ Instructions, procedures, specifications, or drawings not required to govern handling or storage.	X	X	X
9.14	Inspection, Test, and Operating Status ▪ All controls applicable – no grading	X	X	X
9.15	Nonconforming Materials, Parts, or Components ▪ All controls applicable ▪ Control to ensure item not put in use, dispose without records	X	X	X
9.16	Corrective Action ▪ All controls applicable ▪ Determination of cause of condition and action to preclude recurrence not required	X	X	X
9.17	QA Records – grading not meaningful – all controls applicable	X	X	X
9.18	Audits – grading not applicable	—	—	—

Note: Entries of "grading not applicable" in the above table indicate QAP elements for which a grading scheme for implementing the element is either illogical (i.e., the element is not applied at the individual component level, such as Sections 9.1, 9.2, 9.5, 9.6, 9.11, and 9.18 of this addendum) or where differentiation in the applicability of the element provides no significant value for this project (Sections 9.10, 9.12, 9.14, and 9.17 of this addendum).

9.2.2.3 Graded Quality Category C Items

These items and tasks have only a minor impact on safety, and include structures, components, and systems for which a failure or malfunction would not significantly reduce packaging effectiveness and would be unlikely to create a condition that would adversely affect public health and safety. Examples include dunnage, packaging hardware, security lockwire and seals, etc.

9.3 Package Design Control

Design processes are established and implemented to satisfy the requirements of 10 CFR 71.107. Processes, implemented via procedures, shall ensure that design features of packaging systems are appropriately translated into specifications, drawings, procedures, and instructions. Control measures are established for criticality, shielding, thermal, and structural analyses under both normal and accident condition analyses as defined in applicable Department of Transportation (DOT) and NRC regulations.

The design documents (e.g., drawings and specifications) for Quality Category A and B items (*T-Ampoule Assembly; Ring, Filler; Sample Container-1 (SC-1) Assembly; Sample Container-2 (SC-2) Assembly;* and *Inner Cradle*) are controlled through inclusion in Section 1 of this addendum, and any changes will be reviewed for approval by the NRC. Changes to Category C

items may be approved by NNSA, provided that the applicant demonstrates and documents that the proposed change does not affect safety.

Procedures are established for control design activities to ensure that the following:

- Design activities will be planned, controlled, and documented.
- Regulatory requirements, design requirements, and appropriate quality standards will be correctly translated into specifications, drawings, and procedures.
- Competent engineering personnel, independent of those who produced the design, perform design verification. Verification may include design reviews, alternate calculations, or verification testing. Verification tests are conducted in accordance with test procedures developed, reviewed, approved, and controlled in accordance with this document.
- Design interface controls will be established and adequate.
- Design, specification, drawing, and procedure changes will be reviewed and approved in the same manner as the original issue. Where a proposed design change potentially affects licensed conditions, the QAP shall ensure that licensing considerations have been reviewed and are complied with or otherwise reconciled by amending the license.
- Design errors and deficiencies will be documented, corrected, and corrective action taken to prevent recurrence.

Materials, parts, equipment, and processes essential to the function of items that are important to safety will be selected and reviewed for suitability of application.

9.4 Procurement Document Control

Procurement/acquisition processes and related document control activities shall be established and implemented to satisfy the requirements of 10 CFR 71.109. Processes, implemented via procedures, shall ensure that appropriate levels of quality are achieved for the procurement of material, equipment, and services.

Implementing procedures shall ensure that procurement documents clearly define applicable technical and QA requirements, including codes, standards, regulatory requirements and commitments, and contractual requirements. These documents serve as the principal documents for the procurement of structures, systems, components, and related services for use in the design, fabrication, maintenance and operation, inspection and testing of storage and/or transportation systems. Procedures shall ensure that purchased material, components, equipment, and services adhere to the applicable requirements. Furthermore:

- The assignment of quality requirements through procurement documents is administered and controlled.
- Procurement activities are performed in accordance with approved procedures delineating requirements for preparation, review, approval, and control of procurement documents.
- Procurement documents shall be reviewed and approved by authorized personnel for consistency with these requirements.

- Revisions to procurement documents are reviewed and approved by the same cognizant groups as the original document.
- Quality requirements are included in quality-related purchase orders as applicable to the scope of the procurement referencing 10 CFR 71, Subpart H or other codes and standards, as appropriate. In particular, procuring organizations that do not, themselves, have an NRC-accepted Subpart H QAP must require subcontractors to have such a QAP or recognized equivalent (e.g., a QAP that meets requirements of ANSI/ASME NQA-1, 1983).[23]
- Procurement documents will require vendors to roll-down appropriate QA requirements to sub tier suppliers.
- Audits and/or surveys may be conducted to determine acceptability of proposed vendors based on the quality/performance requirements of the item/activity being purchased. These audits/surveys may be based on one or all of the following criteria: the vendor's capability to comply with the requirements of 10 CFR 71, Subpart H; a review of previous records to establish the past performance of the vendor; and/or a survey of the vendor's facilities and review of the supplier's QAP to assess adequacy and verify implementation of quality controls consistent with the requirements being invoked. Such audits or surveys shall be conducted in accordance with Section 9.18 of this addendum.
- Procurement documents shall specify the right of access to supplier facilities by the procuring entity for performing source surveillance and/or audit activities.
- Periodic surveillance of vendor in-process activities may be performed to verify vendor compliance with the procurement documents. When deemed necessary, the need for surveillance shall be specified in approved procurement documents.
- Procurement documents shall include provisions that suppliers either maintain or supply QA records that provide evidence of conformance to the procurement documents. Additionally, procurement documents shall designate the vendor documents required for submittal to the procuring entity for review and/or approval.

The components procured and fabricated per this addendum include *T-Ampoule Assembly; Ring, Filler; Sample Container-1 (SC-1) Assembly; Sample Container-2 (SC-2) Assembly; Inner Cradle* and *O-rings* for the *T-Ampoule Assembly* and sample containers (*SC-1* and *SC-2*). SNL shall have access to vendor facilities and shall qualify and approve the vendor QAP. The vendor QAP shall describe systems for planning, performing, and assessing work, which ensure materials, systems, results, and personnel meet stated quality objectives. The vendor shall ensure any material suppliers and subcontractors utilized during the performance of the contract meet the vendor's QAP. The vendor QAP shall be submitted to SNL for review and written approval, prior to commencement of any work.

Procurement of consumables and replacement parts will be performed under the SNL Subpart H program in a manner consistent with the quality category assigned to the individual items.

9.5 Instructions, Procedures, and Drawings

As required by 10 CFR 71.111, instructions, procedures, and drawings shall be prepared to prescribe processes or work activities, specify requirements, or establish design. Those

documents shall be used in the performance of the work to which they apply. Processes, implemented via procedures, shall ensure that appropriate levels of quality are achieved in development of those documents.

Implementing procedures shall be established to ensure that methods for complying with each of the applicable criteria of 10 CFR Part 71 for activities affecting quality during design, fabrication, inspection, testing, use, and maintenance are specified in instructions, procedures, and/or drawings.

In addition:

- Instructions, procedures, and drawings shall be developed, reviewed, approved, used, and controlled in accordance with the requirements of approved procedures. These instructions, procedures, and drawings shall include appropriate quantitative and qualitative acceptance criteria.
- Changes to instructions, procedures, and drawings are developed, reviewed, approved, used, and controlled with the same requirements and controls applied to the original documents.
- Compliance with these approved instructions, procedures, and drawings is mandatory.

Specific activities regarding preparation of packaging for use, repair, rework, maintenance, loading contents, unloading contents, and transport must be conducted in accordance with written and approved instructions, procedures, and/or drawings. These documents must identify appropriate inspection and hold points and emphasize characteristics that are important to safety and quality. Transportation package procedures are to be developed and reviewed by technical and quality staff and shall be approved by appropriate levels of management.

9.5.1 Operating Procedures for Preparation and Use of Packaging System

Activities concerning loading and shipping shall be performed in accordance with written operating procedures developed by the user and approved by the package custodian. Packaging first-time usage tests, sequential loading and unloading operations, technical constraints, acceptance limits, and references shall be specified in the procedures.

9.5.2 Operating Procedure Changes

Changes in operating procedures that affect the process must be reviewed and approved in the same manner as the initial issue.

9.6 Document Control

As required by 10 CFR 71.113, documents that prescribe processes or work activities, specify requirements, or establish design shall be controlled to ensure the use of applicable versions of those documents during the performance of activities that affect quality. Controlled documents include, but are not limited to:

- Project Plans
- QAP and QAIPs

- This addendum
- Design specifications
- Design and fabrication drawings
- Design verification test procedures along with the results of these test procedures
- Acceptance and maintenance test plans and test procedures
- Special process specifications and procedures

Documents that prescribe activities affecting quality are to be reviewed and approved for technical adequacy and inclusion of appropriate quality requirements prior to approval and issuance. Changes to documents that prescribe activities affecting quality shall be reviewed and approved by the same organization that performed the initial review and approval or by qualified responsible organizations. Measures are taken to ensure that only current documents are available at the locations where activities affecting quality are performed prior to commencing work.

Package users are responsible for establishing, developing, reviewing, approving, distributing, revising, and retaining their documents. Documents that require control, level of control, personnel responsibilities, and training requirements are to be identified.

Packaging-system-related documents to be controlled include, as a minimum:

- Specifications
- Drawings of packaging and components
- Fabrication records
- Operating procedures
- Maintenance procedures
- Inspection and operational test procedures and resulting data
- Loading and unloading procedures
- Preparation for transport procedures
- Repair procedures

Revisions are processed in the same manner as the original issue and only the latest revisions must be available for use.

Documentation received from the supplier for each package must be filed by package serial number. These documents will be retained at the user facility.

9.7 Control of Purchased Material, Equipment, and Services

As required by 10 CFR 71.115, purchased material, equipment, and services shall be controlled according to applicable procurement requirements. Processes, implemented via procedures, shall

ensure that appropriate levels of quality are achieved. Quality category designations are used to grade the application of QA requirements for procurements.

Control of purchased material, equipment, and services consist of the following activities:

- Implementing procedures shall be established to ensure that purchased material, equipment, and services conform to procurement documents.
- Suppliers are required to provide objective evidence that items or services provided meet the requirements specified in procurement documents. Items shall be properly identified on appropriate records that are available to permit verification of conformance with procurement documents. Any procurement requirements not met by suppliers shall be reported in accordance with Section 9.15, *Nonconforming, Materials, Parts, or Components* of this addendum for control and correction of the condition.
- Performance of source surveillance, test, and shipping and/or receiving inspection activities to verify compliance with approved design and licensing requirements, procurement document requirements, or contract specifications must be performed in accordance with approved procedures.
- For commercial "off-the-shelf" items, where specific quality controls appropriate for nuclear applications cannot be imposed in a practical manner, quality verification shall be performed to verify the acceptability and conformance of an item to procurement document requirements.

9.8 Identification and Control of Material, Parts, and Components

As required by 10 CFR 71.117, activities concerning the identification and control of material, parts, and components of the PAT-1 packaging system to be used for transport of radioactive material shall be controlled. Processes, implemented via procedures, shall ensure that appropriate levels of quality are achieved through the identification and control of those materials, parts, and components.

The requirements for identification and control of material, parts, and components include:

- Implementing procedures shall be established to identify and control materials, parts, and components. These procedures shall ensure identification of items by appropriate means during fabrication, installation, and use of the items, and prevent the inadvertent use of incorrect or defective items.
- Each component, if specified in the drawing, shall be assigned a unique serial number after fabrication or purchase. All documentation associated with subsequent storage, use, maintenance, inspection, acceptance, etc., must refer to the assigned serial number.
- Requirements for identification are established during the preparation of procedures and specifications.
- Methods and location of identification are selected so as not to adversely affect the quality of the item(s) being identified.

- Items with a limited shelf or operating life are controlled to prevent their inappropriate use.
- Control and identification must be maintained either directly on the item or within documents traceable to the item to ensure that only correct and acceptable items are used. When physical identification is not practical, other appropriate means of control must be established, such as bagging, physical separation, or procedural control.

Verification of acceptance status is required prior to use. Items that are not acceptable must be controlled accordingly. Control of nonconforming items is addressed in Section 9.15, *Nonconforming Parts, Materials, or Components*, of this addendum.

Each AQ-1 data plate on the PAT-1 package will be conspicuously and durably marked with information identifying the package owner, model number, unique serial number, and package gross weight, in accordance with 10 CFR 71.85(c) and drawing number 1002.

The *T-Ampoule* will be assigned a unique serial number after fabrication. The vendor shall mark the product, packaging, and accompanying documentation with the item's part number. Laser marking is required on all metal parts (*T-Ampoule Assembly; Ring, Filler; Sample Container-1; Sample Container-2;* and *Inner Cradle*) identified in the engineering drawing set. The laser-produced marking will be a contrasting color on the metal surface, without edges or depth.

Replacement parts must be identified by marking, tagging, or labeling to ensure correct application. Items should be marked based on their quality category. Items such as the O-rings for the TB-1 *Containment Vessel*, *T-Ampoule Assembly*, and *Sample Container-1 (SC-1) Assembly* and *Sample Container-2 (SC-2) Assembly* that are too small or that otherwise do not lend themselves to marking must be individually packaged and the package marked with the material certification, size, cure date, and shelf-life, etc., as appropriate. All replacement fasteners for the AQ-1 and TB-1 as described in NUREG-0361 (Drawing No. 1002, 1003, 1004, 1017, and 1018) must be source traceable, certified, and marked (or in marked packaging) to reflect their identity, and segregated from other similar fasteners to prevent misuse or installation of unacceptable fasteners. Items that have limited calendar-life, operating-life cycles (*Gasket Copper*, Drawing No. 1019), or shelf life (such as the TB-1 *Containment Vessel*, *T-Ampoule Assembly*, and sample container (*SC-1* or *SC-2*) *O-rings*) must be controlled (QAIP 8-1, 13-1) to preclude the use of expired items. Processes (see Section 7 of this addendum) shall be in place to replace aging items prior to failure or expiration.

9.9 Control of Special Processes

As required by 10 CFR 71.119, special processes (QAIP 9-1) used to fabricate or inspect the PAT-1 system or components shall be controlled. The requirements for control of special processes include:

- Implementing procedures shall be established to control special processes used in the fabrication and inspection of storage/transport systems. These processes may include welding, nondestructive examination, or other special processes as identified in procurement documents.
- Special processes shall be performed in accordance with approved procedures.

- Personnel who perform special processes will be trained and qualified in accordance with applicable codes, standards, specifications, and/or other specific requirements. Records of qualified procedures and personnel are to be maintained and kept current by the organization that performs the special processes.
- Equipment used in conduct of special processes must be qualified in accordance with applicable codes, standards, and specifications. Qualification records of special process procedures, equipment, and personnel must be maintained.

Welding shall be performed as specified in PAT-1030. Nondestructive examination personnel (e.g., for visual inspection, penetrant inspection, or leak testing, etc.) shall be qualified at the American Society for Nondestructive Testing (ASNT) Level II or III for the examination technique to be employed. Containment vessel and criticality control component structural welds must be examined using the approved nondestructive method cited on the design drawings.

Fabrication of the *T-Ampoule Assembly; Ring, Filler; Sample Container-1 (SC-1) Assembly; Sample Container-2 (SC-2) Assembly;* and *Inner Cradle* is specified in PAT-1040 *Titanium Material Specification and Fabrication,* Section 1.3.3 of this addendum.

9.10 Internal Inspection

In accordance with 10 CFR 71.121, inspection activities used to ensure that materials, parts, and components of the PAT-1 packaging system for transport of radioactive material shall be controlled. Processes, implemented via procedures, shall ensure that appropriate inspections are performed prior to acceptance or use of the packaging or components.

Requirements for control of inspection activities include:

- Implementing procedures shall be established to ensure that inspection is performed to verify that materials, parts, processes, or other activities affecting quality conform to documented instructions, procedures, specifications, drawings, and/or procurement documents.
- Mandatory hold points, inspection equipment requirements, acceptance criteria, personnel qualification requirements, performance characteristics, variable and/or attribute recording instructions, reference documents, and other requirements are considered and included, as applicable, during inspection and surveillance planning.
- Personnel performing inspection activities shall be trained and qualified in accordance with written, approved procedures.
- Inspections are to be performed by individuals other than those who performed or supervise the subject activities.
- Inspection and process monitoring are both required where either one, by itself, will not provide QA.
- Modifications and/or repairs to and replacement of packaging system components and assemblies are inspected in accordance with the original design and inspection requirements or approved alternatives.

9.10.1 Inspections During Fabrication

Specific inspection criteria are incorporated into the drawings for the PAT-1 packaging. The components fabricated in this addendum include the *T-Ampoule Assembly; Ring, Filler; Sample Container-1 (SC-1) Assembly; Sample Container-2 (SC-2) Assembly;* and *Inner Cradle.* Inspection requirements for fabrication are divided into two areas of responsibility which document that an accepted package conforms to design criteria. These two areas are

- In-process inspections performed by the fabricator pursuant to fabricator's graded QA requirements under the Manufacturing/Fabrication Plan; and
- Independent surveillance of fabrication activities performed by individuals acting on behalf of the purchaser pursuant to graded QA requirements.

The vendor (fabricator) is required to submit a Manufacturing/Fabrication Plan prior to the start of fabrication for approval by SNL. This plan shall be used as a tool for establishing witness and hold points. A review for compliance with procurement documents is normally performed as part of the surveillance function at the vendor facility. The plan shall define how fabrications and inspections are performed, processes are engaged, and the qualification requirements for personnel.

A full-dimensional inspection of manufactured parts shall be performed and documented to ensure adherence to the dimensions and associated tolerances in the engineering drawings. ASME Y14.5M, Dimensioning and Tolerancinf,[24] shall serve as the basis standard for the dimensional inspections.

Inspections must be documented and records delivered in individual data packages accompanying the manufactured parts in accordance with the procurement specification. Vendor inspectors shall be suitably experienced and qualified. Inspectors independent of the operation shall carry out acceptance inspections.

Independent surveillance activities will be performed by qualified personnel selected with SNL approval. SNL reserves the right to have its own qualified inspectors and personnel present during fabrication and inspections activities. Notice of at least five working days is required prior to inspection and testing activities by the vendor so SNL may arrange its staff participation. Hold points may be identified in the schedule for coordination of inspection activities.

Upon delivery of the fabricated components to SNL, the parts will be dimensionally and visually inspected by SNL inspectors as follows:

- Visually inspect components and assemblies for damage.
- Verify that purchase order/job order number is marked on parts, packaging, or accompanying documentation.
- Verify that the Certified Material Test Report (CMTR) contains purchase order/job number, vendor name, and address and is signed by an authorized vendor representative.
- Verify that a Certificate of Conformance (COC) is provided for each lot of components.

- Verify that the COC contains SNL purchase order/job order number, vendor name and address, and is signed by an authorized vendor representative.
- Verify vendor QAP was shipped with components.
- Verify dimensional attributes when established for components or assemblies.

9.10.2 Inspections during Initial Acceptance and during Service Life

Independent inspections shall be performed by SNL upon receipt of the PAT-1 packaging prior to first usage and on an annual basis. Post-loading inspections by the user are also performed prior to shipment. Inspection (by qualified independent inspection personnel) must include the following:

- First-Usage/Annual by SNL – Ensure compliance with procurement documents. As discussed in Section 8 of this addendum, Acceptance Tests and Maintenance Operations, perform first-time-usage inspections. Annually, ensure adequate packaging maintenance to ensure that performance is not impaired, as discussed in Section 8 of this addendum.
- Preshipment by User – Verify proper assembly and that leak testing (if applicable) is carried out as specified in Section 7 of this addendum, Package Operations. Verify proper contents, assembly, marking, shipping papers, and implementation of any special instructions to ensure that each loaded package is ready for delivery to the carrier.

9.11 Test Control

In accordance with 10 CFR 71.123, testing activities, including design verification testing, acceptance testing of fabricated components and assemblies, and operational testing of the PAT-1 system by users, shall be controlled. Processes, implemented via procedures, shall ensure that testing activities are completed as specified in design documentation and this addendum.

Requirements for test control include the following:

- Implementing procedures shall be established to ensure that required acceptance, first-use, preshipment, and annual tests as identified in design or procurement documents are performed and appropriately controlled.
- Test personnel shall have appropriate training and shall be qualified for the level of testing they perform. Personnel shall be qualified in accordance with approved, written instructions, procedures, and/or checklists.
- Tests shall be performed by qualified personnel in accordance with approved, written instructions, procedures, and/or checklists. Test procedures must contain or reference the following information, as applicable:
    - Acceptance criteria contained in the applicable test specifications or design and procurement documents.
    - Instructions for performance of tests, including environmental conditions.
    - Test prerequisites, such as test equipment, instrumentation requirements, personnel qualification requirements, fabrication, or operational status of the items to be tested.

- Provisions for data recording and records retention.

- Test results are to be documented and evaluated to ensure that acceptance criteria have been satisfied.
- Tests for modifications, repairs, or replacements of safety-related and important-to-safety structures, systems, or components are to be performed in accordance with the original design and testing requirements or approved alternatives.

Tests are required when it is necessary to demonstrate that an item or process will perform satisfactorily. Test procedures must specify the objectives of the tests, testing methods, required documentation, and acceptance criteria. Tests conducted by vendors at vendor facilities must be specified in procurement documents. Personnel who conduct tests, test equipment, and procedures must be qualified, and records documenting qualification retained.

9.11.1 Acceptance Tests

The fabricator (vendor) must supply to SNL, QA documentation for the fabrication of each PAT-1 packaging system in accordance with applicable drawings, specifications, and/or other written requirements, including the results of acceptance tests specified in Section 8 of this addendum.

SNL, the package custodian, must ensure required tests for packaging pressure, leakage rate, or others are performed prior to first usage.

9.11.2 Maintenance Tests

Annual maintenance testing will be performed by SNL to ensure the PAT-1 packaging performance has not deteriorated with time and usage. The requirements for the annual tests are documented in the Section 8, *Acceptance Tests and Maintenance Program* of this addendum. The results of these tests are shall be documented and maintained with the specific packaging records.

9.11.3 Preshipment Tests

Preshipment tests, as specified in Section 8, *Acceptance Tests and Maintenance Program* of this addendum and shall be performed and documented by the package user.

9.12 Control of Measuring and Test Equipment

In accordance with 10 CFR 71.125, measuring and test equipment used for inspection and testing activities shall be controlled to ensure their usability, accuracy, and precision as follows:

- Implementing procedures shall be established to ensure that tools, gages, instruments, and other measuring and testing equipment (M&TE) are properly controlled, calibrated and adjusted to maintain accuracy within required limits.
- M&TE are calibrated at scheduled intervals against certified standards with known, valid relationships to national standards. If no national standards exist, the basis for calibration shall be documented. Calibration intervals are based on required accuracy, precision, purpose, frequency of use, stability characteristics, and other conditions that could affect measurement.

- Calibrations shall be performed in accordance with approved, written procedures.
- M&TE shall be identified, labeled, or tagged indicating the next required calibration due date, and traceable to calibration records.
- If M&TE is found to be out of calibration, an evaluation shall be performed and documented regarding the validity of inspections or tests performed and the acceptability of items inspected or tested since the previous acceptable calibration. The current status of M&TE is to be recorded and maintained. Any M&TE that is consistently found to be out of calibration shall be repaired or replaced.

Special calibration and control measures for rules, tape measures, levels, and other such devices are not required when normal commercial practices provide adequate accuracy.

9.13 Handling, Storage, and Shipping Control

In accordance with 10 CFR 71.127, the handling, storage, and shipping activities for materials, parts, and components of the PAT-1 packaging system used to transport radioactive material shall be controlled. Processes, implemented via procedures, shall ensure that such handling, shipping, and storage activities provide adequate control.

Requirements for handling, storage, and shipping control include the following:

- Implementing procedures shall be established to ensure that materials, parts, assemblies, spare parts, special tools, and equipment are handled, stored, packaged, and shipped in a manner to prevent damage, loss, loss of identity, or deterioration.
- When necessary, storage procedures address special requirements for environmental protection, such as inert gas atmospheres, moisture control, temperature levels, etc.

Package users shall ensure that PAT-1 system components and assemblies are controlled to prevent damage or loss, protect against damage or deterioration, and provide for adequate safety of personnel involved with handling, storage, and shipment (outgoing and incoming) operations.

Handling, storage, and shipping must be conducted in accordance with written and approved instructions, procedures, specifications, and/or drawings. These documents must identify appropriate information regarding shelf life, environment, temperature, cleaning, handling, and preservation, as applicable, to meet design, regulatory, and/or DOE shipping requirements which include applicable DOT requirements.

9.14 Inspection, Test, and Operating Status

In accordance with 10 CFR 71.129, the inspection, test, and operating status of materials, parts, and components of the PAT-1 packaging system to be used for transport of radioactive material shall be identified and controlled. Processes, implemented via procedures, shall ensure that appropriate inspections and tests occur prior to acceptance or use of the packaging or component, and identify the status of packaging items, components, etc.

Requirements for identifying inspection, test, and operating status include the following:

- Implementing procedures shall be established to ensure that the inspection and test status of materials, items, structures, systems, and components throughout fabrication, installation, operation, and test are clearly indicated by suitable means, (e.g., tags, labels, cards, form sheets, checklists, etc.).
- Bypassing required inspections, tests, or other critical operations is prevented through the use of approved instructions, procedures, or other controls.
- As appropriate, the operating status of nonconforming, inoperative, or malfunctioning components of a storage/transport system (e.g., valves, switches, etc.) is indicated to prevent inadvertent operation. The application and removal of status indicators are performed in accordance with approved instructions and procedures.
- Any nonconforming items are identified and controlled in accordance with Section 9.15 of this addendum.

Package users shall ensure that the status of inspection and test activities is identified on the item or in documents traceable to the item to ensure that proper inspections or tests have been performed and that those items that do not pass inspection are not used. The status of fabrication, inspection, testing, assembly, and refurbishment activities must be identified in documents traceable to the package components.

Measures established in specifications, procedures, and other instructions shall ensure that the following objectives are met:

- Personnel responsible for oversight of packaging inspections can readily ascertain the status of inspections, tests, and/or operating conditions.
- No controlled items are overlooked.
- Inadvertent use or installation of nonconforming items is prevented.
- Documentation is complete.

9.15 Nonconforming Materials, Parts, or Components

In accordance with 10 CFR 71.131, nonconforming materials, parts, and components of the PAT-1 packaging system used for transport of radioactive material shall be controlled. Processes, implemented via procedures, shall ensure that nonconforming conditions are identified and appropriately dispositioned.

The requirements for nonconforming materials, parts, or components include the following:

- Implementing procedures shall be established to control materials, parts, and components that do not conform to requirements and prevent their inadvertent use during fabrication or service.
- Nonconforming items include those items that do not meet specification or drawing requirements. Additionally, nonconforming items include items not fabricated or tested (1) in accordance with approved written procedures, (2) by qualified processes, or (3) by

qualified personnel where use of such procedures, processes, or personnel is required by the fabrication, test, inspection, or QA requirements.

- Nonconforming items are identified and/or segregated to prevent their inadvertent use until properly dispositioned. Nonconforming items are identified by marking, use of tagout procedures, or other methods that do not adversely affect the end use of the item if the nonconforming item can be restored to the applicable QA requirement. The identification shall be legible and easily recognizable. When identification of each nonconforming item is not practical, the container, package, or segregated storage area, as appropriate, is identified.
- Nonconforming conditions are documented and affected organizations are notified. The nonconformance report (NCR) shall include a description of the nonconforming condition. Nonconforming items shall be dispositioned as Use-As-Is, Reject, Repair, or Rework.
- Acceptability of rework or repair of nonconforming materials, parts, and components is verified through reinspection and/or retesting the item to the original requirements or equivalent inspection/testing methods. Inspection requirements for nonconforming items following rework, repair, or modification shall be detailed in the NCR and approved following determination of the disposition.
- The disposition of nonconforming items as Use-As-Is or Repair shall include technical justification and independent verification to assure compliance with design, regulatory, and contractual requirements.
- NCRs are part of the inspection records and are periodically reviewed to identify quality trends. Unsatisfactory quality trends are documented as detailed in Section 9.16 of this addendum. The results of these reviews are to be reported to management.
- NCRs relating to internal activities are issued to management of the affected organization. The appropriate QA Manager shall approve the disposition and perform follow-up activities to assure proper closure.
- Compliance with the evaluation and reporting requirements of 10 CFR 21 related to defects and noncompliance is controlled by approved procedures.

The components procured and fabricated per this addendum include *T-Ampoule Assembly; Ring, Filler; Sample Container-1 (SC-1) Assembly; Sample Container-2 (SC-2) Assembly; Inner Cradle* and *O-rings* for the *T-Ampoule Assembly,* and sample containers (*SC-1 or SC-2*). Nonconforming items are to be reported as outlined in the vendor's approved QAP, with immediate notification to SNL. NCRs shall be compiled to document the details of the nonconformance. Any nonconforming components shall be clearly identified and segregated. NCRs shall be traceable to the actual component(s) affected.

SNL shall perform corrective action(s) per Section 9.16 of this addendum. SNL shall disposition "Use-As-Is" and "Repair" nonconforming items in writing prior to the vendor proceeding with the next activity or step in the fabrication process. A copy of the completed NCR shall be submitted to SNL by the vendor as part of the manufacturing documentation.

9.16 Corrective Action

As required by 10 CFR 71.133, requirements for corrective action shall be established and implemented. Processes, implemented via procedures, shall ensure that issues associated with transportation and packaging activities are identified and corrected.

Corrective action activities shall be controlled. The requirements for corrective action include the following:

- Implementing procedures shall be established to identify and address conditions adverse to quality.
- Significant and/or repetitive failures, unsatisfactory quality trends, malfunctions, and deficiencies with material, components, equipment, and operations are to be promptly identified, documented, and reported to appropriate management.
- The cause of the condition and corrective action necessary to prevent recurrence are identified, implemented, and followed up to verify corrective action is complete and effective.

9.17 Quality Assurance Records

As required by 10 CFR 71.135, QA records shall be controlled. The QA records system will ensure that documented evidence relative to quality-related activities is maintained and available for use by DOE/NNSA and/or regulatory agencies.

Requirements for QA records include the following:

- Implementing procedures shall be established to assure control of quality records.
- Approved procedures identify the types of documents to be retained as QA records, as well as those to be retained by the originating organization. QA records are retained by the design organization (design, fabrication, and acceptance records) or by the user (use, shipment, inspection, in-use testing, and maintenance records). Records are identified, indexed, and stored in accessible locations.
- QA Records are retained for 3 years after the life of the packaging to which they apply per 10 CFR 71.91(d) to furnish evidence of activities affecting the quality of structures, systems, and components that are safety-related or important to safety. These records include records of design, procurement, fabrication, assembly, inspection, and testing. In addition, 10 CFR 71.135 states that the records shall be retained 3 years beyond the date when the last activity for which the quality program was developed.
- Maintenance records shall include the use of operating logs; results of reviews, inspections, tests, and audits; results from monitoring work performance and material analyses; results of maintenance, modification, and repair activities; qualification of personnel, procedures, and equipment; records of calibration of measuring and test equipment; and related instructions, procedures, and drawings.

- Requirements for indexing, record retention period, storage method(s) and location(s), classification, preservation measures, disposition of nonpermanent records, and responsibility for safekeeping are specified in approved procedures.
- Record storage facilities are established to prevent destruction of records by fire, flood, theft, and deterioration due to environmental conditions (such as temperature, humidity, or vermin). As an alternative, two identical sets of records (dual storage) may be maintained at separate locations.

Sufficient records must be maintained by package users to furnish evidence of item quality and activities affecting quality. QA records that must be retained three years after the life of the packaging to which they apply include:

- Appropriate production-related records that are generated throughout the package manufacturing and fabrication process (design organization).
- QA records are retained by the design organization (design, fabrication, procurement, and acceptance records), by the organization designated by the DOE/NNSA to perform maintenance (inspection, maintenance, procurement and acceptance records) and the users (inspection, use, shipment and in-use testing [leakage rate testing, etc.] records).
- Records documenting repair, rework, and replacement (user) shall be maintained for the lifetime of the package.
- Audit reports and corrective actions.
- Records used as a baseline for maintenance (user).
- Records showing evidence of delivery of packages to a carrier and proof that all DOT requirements were satisfied (user).

QA records shall be:

- Legible
- Completed to reflect the work accomplished and relevant results or conclusions
- Signed (including printed or typed name of the signing individual) and dated or otherwise authenticated by authorized personnel.

QA records should be placed in a records storage area as soon as feasible to avoid loss or damage. Individual QA records must be generated and maintained for each package and include the unique package identifier.

Records are to be available for inspection as per applicable DOE requirements.

9.17.1 Subcontractor/Supplier Submittal Requirements Summary

The components procured and fabricated per in this addendum include *T-Ampoule Assembly; Ring, Filler; Sample Container-1 (SC-1) Assembly; Sample Container-2 (SC-2) Assembly; Inner Cradle* and *O-rings* for the *T-Ampoule Assembly* and sample containers (*SC-1* or *SC-2).* The vendor shall provide a minimum of three copies of all required document submittals, accompanied by official vendor document transmittal forms. Prior to shipment of the above

mentioned components, the vendor shall submit a formal construction report to SNL for review and written approval (see Section 1.3.3 of this addendum).

9.18 Audits

In accordance with 10 CFR 71.137, audit requirements shall be established and implemented. Processes, implemented via procedures, shall ensure that activities pertaining to audits and assessments are controlled.

Requirements for audits and assessments are as follows:

- Implementing procedures shall be established to ensure that periodic audits verify compliance with all applicable requirements of the QAP and determine its effectiveness. Areas and activities to be audited, such as design, procurement, fabrication, inspection, and testing of storage/transportation systems, are to be identified as part of the audit plan.
- Vendor QAPs, procedures, and implementation activities may be audited to evaluate and verify that they are adequate and comply with applicable requirements.
- Audits are planned and scheduled in a manner to provide coverage and coordination with ongoing QAP activities commensurate with the status and importance of the activities.
- Audits are performed by trained and qualified personnel not having direct responsibilities in the areas being audited, and are conducted in accordance with written plans and checklists. Audit results are documented and reviewed by management having responsibility for the area audited. Corrective actions and schedules for implementation are established and recorded. Audit reports include an objective evaluation of the quality-related practices, procedures, and instructions for the areas or activities being audited and the effectiveness of implementation.
- Responsible management shall undertake corrective actions as a follow-up to audit reports when appropriate. The responsible management shall evaluate audit results for indications of adverse trends that could affect quality. When results of such assessments so indicate, appropriate corrective action will be implemented.

The components procured and fabricated per this addendum include *T-Ampoule Assembly; Ring, Filler; Sample Container-1; Sample Container-2; Inner Cradle* and *O-rings* for the T-Ampoule and sample containers. SNL reserves the right to audit and assess the vendor and the vendor subcontractors and supplier to verify conformance to the QAP prior to award of the contract, and at any time during the performance of the contract.

9.19 Appendix

9.19.1 References

1. United States. Nuclear Regulatory Commission. NUREG-0361. “Safety Analysis Report for the Plutonium Air Transportable Package, Model PAT-1.” Washington, D.C. 1978.

2. United States. Nuclear Regulatory Commission. NUREG-0360. “Qualification Criteria to Certify a Package for Air Transport of Plutonium.” Washington, D.C. 1978.

3. United States. Nuclear Regulatory Commission. NUREG/CR-0030. "PARC (Plutonium Accident Resistant Container) Program Research, Design, and Development," (SAND76-0587). Sandia National Laboratories. Albuquerque, New Mexico. Reprinted January 1983.

4. United States. Nuclear Regulatory Commission. Code of Federal Regulations, 10 CFR 71. "Packaging and Transportation of Radioactive Material." January 1, 2009.

5. United States. Nuclear Regulatory Commission. Regulatory Guide 7.10 (RG 7.10). *Establishing Quality Assurance Programs for Packaging Used in Transport of Radioactive Material*, Revision 2. Washington, D.C. March 2005.

6. Sandia National Laboratories. "Title 10 Code of Federal Regulations Part 71 Packaging and Transportation of Radioactive Material – Quality Assurance Program Plan." AS-PT-PD-04. Albuquerque, New Mexico. March 5, 2009.

7. 1071H-QAIP 2-2. "Project Quality Plan." Sandia National Laboratories. Albuquerque, New Mexico.

8. 1071H-QAIP 3-1. "Design Control." Sandia National Laboratories. Albuquerque, New Mexico.

9. 1071H-QAIP 9-2. "Model Validation." Sandia National Laboratories. Albuquerque, New Mexico.

10. 1071H-QAIP 9-3. "Analyses and Calculations," Sandia National Laboratories. Albuquerque, New Mexico.

11. 1071H-QAIP 4-1. "Control of Procurement Documents and Purchased Material, Equipment, and Services," Sandia National Laboratories. Albuquerque, New Mexico.

12. 1071H-QAIP 5-1. "Quality Assurance Implementing Procedure Preparation and Content," Sandia National Laboratories. Albuquerque, New Mexico.

13. 1071H-QAIP 6-1. "Document Review and Approval," Sandia National Laboratories. Albuquerque, New Mexico.

14. 1071H-QAIP 6-2. "Document Control," Sandia National Laboratories. Albuquerque, New Mexico.

15. 1071H-QAIP 8-1. "Identification and Control of Materials, Parts, and Components." Sandia National Laboratories. Albuquerque, New Mexico.

16. 1071H-QAIP 9-1. "Control of Special Processes." Sandia National Laboratories. Albuquerque, New Mexico.

17. 1071H-QAIP 10-1. "Inspection and Identification of Item Status." Sandia National Laboratories. Albuquerque, New Mexico.

18. 1071H-QAIP 9-5. "Technical Products and Deliverable Reports." Sandia National Laboratories. Albuquerque, New Mexico.

19. 1071H-QAIP 11-1. "Control of Data Collection and Testing Activities." Sandia National Laboratories. Albuquerque, New Mexico.

20. 1071H-QAIP 12-1. "Control of Measuring and Test Equipment." Sandia National Laboratories. Albuquerque, New Mexico.

21. 1071H-QAIP 13-1 "Control of Shipping, Handling, Storage, Preservation, and Cleaning." Sandia National Laboratories. Albuquerque, New Mexico.

22. 1071H-QAIP 15-1. "Control of Nonconformances and Corrective Action." Sandia National Laboratories. Albuquerque, New Mexico.

23. American National Standards Institute (ANSI). ANSI/ASME NQA-1-1983. 1983.

24. American Society of Mechanical Engineers. "Dimensioning and Tolerancing." New York: 2009.